Monday July 20th

Opening Ceremony (Main Hall) 10:00 – 10:30

Session Plenary 1,2 (Main Hall) 10:30 – 12:00

PL1 10:30 – 11:15 **David D. Awschalom** (*Center for Spintronics and Quantum Computation, University of California, Santa Barbara, CA 93106 USA*)
Manipulating single spins and coherence in semiconductors

PL2 11:15 – 12:00 **Yoshihisa Yamamoto**[1,2] ([1]*E. L. Ginzton Laboratory, Stanford University, CA, USA,* [2]*National Institute of Informatics, Tokyo, Japan*)
Bose-Einstein condensation and superfluidity of exciton-polaritons

12:00 – 12:15 **Conference Photo**

12:15 – 13:45 **Lunch Break**

Session E1 (Main Hall) 13:45 – 16:00 NEMS and new techniques

E1a 13:45 – 14:15 **Hirosh Yamaguchi** (Invited) (*NTT Basic Research Laboratories, Atsugi, Kanagawa 243-0198, Japan*)
Heterostructure-based Micro/Nanomechanical Systems

E1b 14:15 – 14:30 **A. K. Hüttel**[1,2]**, G. A. Steele**[1]**, B. Witkamp**[1]**, M. Poot**[1]**, L. P. Kouwenhoven**[1]**, H. S. J. van der Zant**[1] ([1]*Kavli Institute of Nanoscience, Delft University of Technology, PO Box 5046, 2600 GA Delft, The Netherlands,* [2]*Institute for Experimental and Applied Physics, University of Regensburg, 93040 Regensburg, Germany*)
Carbon nanotubes as ultra-high quality factor mechanical resonators

E1c 14:30 – 14:45 **A. Mahé**[1]**, F.D. Parmentier**[1]**, J.-M. Berroir**[1]**, G. Fève**[1]**, T. Kontos**[1]**, B. Plaçais**[1]**, D.C. Glattli**[1,2] ([1]*Laboratoire Pierre Aigrain, Ecole Normale Supérieure., 24 ue Lhomond 75005 Paris, France,* [2]*Service de Physique de l'état condensé, CEA Saclay., F-91191 Gif-sur-Yvette, France*)
Ultra sensitive finite frequency noise measurement setup to study the statistical emission noise of an on-demand coherent single electron source

E1d 14:45 – 15:00 **F. Martins**[1]**, B. Hackens**[1]**, L. Gence**[1]**, S. Baltazar**[2]**, M. Pala**[2]**, H. Sellier**[3]**, L. Desplanque**[4]**, X. Wallart**[4]**, S. Huant**[3]**, V. Bayot**[1,3] ([1]*DICE lab, Université Catholique de Louvain, 3 place du levant, Louvain-la-Neuve 1348, Belgium,* [2]*IMEP-LAHC-MINATEC (UMR CNRS/INPG/UJF 5130), Grenoble, France,* [3]*Institut Néel, CNRS, and Université Joseph Fourier, Grenoble, France,* [4]*IEMN, Villeneuve d'Ascq, France*)
Imaging electron transport close to filling factor ν = 2 in a quantum ring

E1e 15:00 – 15:15 **D. Maryenko[1], F. Ospald[1], B. Rosenow[1], H. Lu[2], A. C. Gossard[2], V. Umansky[3], K. von Klitzing[1], J. H. Smet[1]** ([1]*Max-Planck-Institute for Solid State Research, Stuttgart, Heisenbergstr. 1 70569, Germany,* [2]*Materials Department, University of California Santa Barbara, Santa Barbara, California 93106-5050, USA ,* [3]*Department of Condensed Matter Physics, Weizmann Institute, Rehovot, 76100, Israel*)

Ultrafast time-resolved transport studies of a two-dimensional electron system

E1f 15:15 – 15:30 **E. Hoffmann[1], N. Nakpathomkun[1], H. Nilsson[2], A. Persson[1], L. Samuelson[2], H. Linke[1,2]** ([1]*Physics Department and Materials Science Institute, University of Oregon, 1274 University of Oregon, Eugene, Oregon 97403-1274, USA,* [2]*Solid State Physics/The Nanometer Structure Consortium, Lund University, Box 118, S-221 00, Lund, Sweden*)

High-efficiency thermoelectric quantum dots in InAs/InP nanowires

E1g 15:30 – 15:45 **D. Konstantinov, K. Kono** (*Low Temperature Physics Laboratory, RIKEN, 2-1 Hirosawa, Wako, Saitama 3510198, Japan*)

A new type of microwave-induced resistance oscillation observed in a nondegenerate 2DES on liquid helium

E1h 15:45 – 16:00 **Y. Kawano[1,2], K. Ishibashi[1]** ([1]*Advanced Device Laboratory, RIKEN (The Institute of Physical and Chemical Research), 2-1 Hirosawa, Wako, Saitama 351-0198, Japan,* [2]*PRESTO, Japan Science and Technology Agency (JST), 5-3 Yonbancho, Chiyoda-ku, Tokyo, Japan*)

On-chip near-field terahertz detection based on a two-dimensional electron gas

Poster Session Mo-eP (Meeting Room 501, 502) 16:00–18:00

Mo-eP1 **ZS. Tao, ZM. Jiang, F. Lu** (*Department of Physics,Fudan University, No.220 Handan Road 200433, China*)

The properties of Ge quantum dots on strained SiGe layer measured by Photoluminescence and Deep Level Transient Spectroscope

Mo-eP2 **A. A. Sherstobitov[1], G.M. Minkov[1], A.V. Germanenko[2], O.E. Rut[2], I.V. Soldatov[2], B.N. Zvonkov[3]** ([1]*Institute of Metal Physics RAS, Ekaterinburg, Russia,* [2]*Ural State University, Ekaterinburg, Russia,* [3]*University of Nizhnii Novgorod, Nizhnii Novgorod, Russia*)

Probe of the artificial disorder by the capacitance - voltage characteristics

Mo-eP3 **Y. H. Shin[1], Y. H. Park[1], S. J. Noh[1], J. W. Hyun[1], C. H. Perry[2], J. A. Simmons[3], T. Takamasu[4], Yongmin Kim[1,4]** ([1]*Department of Applied Physics, Dankook University, Yongin 448-701, Korea,* [2]*Department of Physics, Northeastern University, Boston, MA 02115, USA,* [3]*Sandia National Laboratories, , Albuquerque, NM 87185, USA,* [4]*National Institute for Materials Science, Tsukuba, Ibaraki 305-0003, Japan*)

Exciton Dynamics in Modulation-doped Asymmetric Double-well Structures in Magnetic Fields

Mo-eP4 **M.V. Entin[1], M.M. Mahmoodian[1,2], L.I. Magarill[1,2]** ([1]*Institute of Semiconductor Physics, Siberian Branch, Russian Academy of Sciences, ,* [2]*Novosibirsk State University,*)

Physical effects in low-dimensional systems subjected to local high-frequency field

Mo-eP5 **E. Räsänen[1,2], S. Pittalis[2], K. Capelle[2,3], C. R. Proetto[2]** ([1]*Nanoscience Center, Department of Physics, University of Jyväskylä, P. O. Box 35, FI-40014 University of Jyväskylä, Finland,* [2]*Institut für Theoretische Physik, Freie Universität Berlin, Arnimallee 14, D-14195 Berlin, Germany,* [3]*Instituto de Física de São Carlos, Universidade de São Paulo, Caixa Postal 369, São Carlos, São Paulo 13560-970, Brazil*)

Lower bounds on the exchange-correlation energy in reduced dimensions

Mo-eP6 **T. Kaizu[1], Y. Imanaka[1], K. Takehana[1], T. Takamasu[1]** ([1]*Quantum Dot Research Center, National Institute for Materials Science, 3-13 Sakura, Tsukuba, Ibaraki 3050003, Japan,* [2]*, ,* [3]*, ,* [4]*,*)

Magnetotransport properties of Ytterbium doped $Al_xGa_{1-x}As$/GaAs two-dimensional electron systems

Mo-eP7 **S. Ono, H. Shima** (*Department of Applied Physics, Hokkaido University, N13, W8, Kita-ku, Sapporo, Hokkaido 060-8628, Japan*)

Low-Temperature Resistivity of Periodic Curved Surfaces

Mo-eP8 **L. M. Thu, O. Voskoboynikov** (*Department of Electronics Engineering, National Chiao Tung University, 1001 Ta Hsueh Rd., Hsinchu. 30010, Taiwan*)

Magneto-optics of two-dimensional arrays of embedded semiconductor quantum dot molecules

Mo-eP9 **A. Fujimoto[1], M. Kitamura[2], H. Kobori[2], A. Yamasaki[2], A. Sugimura[2], A. Ando[3], H. Kawanaka[3], T. Shimizu[3]** ([1]*Nanomaterials Microdevices Research Center, Osaka Institute of Technology, 5-16-1 Ohmiya, Asahi-ward, Osaka,Osaka 535-8585, Japan,* [2]*Department of Physics, Faculty of Science and Engineering, Konan University, 8-9-1 Okamoto, Higashi Nada-ku, Kobe, Hyogo 658-8501, Japan,* [3]*Nanotechnology Research Institute, Advanced Industrial Science and Technology, AIST Tsukuba Central, Tsukuba, Ibaraki 305-8568, Japan*)

Enhancement of negative magnetoresistance due to weak localization in In_2O_3 thin films on Si substrate

Mo-eP10 **V. M. Fomin, P. Kratzer** (*Fachbereich Physik and Center for Nanointegration (CeNiDE), Universität Duisburg-Essen, Duisburg D-47057, Germany*)

Thermoelectric transport in periodic 1D stacks of InAs/GaAs quantum dots

Mo-eP11 **Nafidi** (*GCMP, Ibn Zohr University, Faculty of Sciences, Department of Physics, BP 8106 Hay Dakhla, Agadir 80000, Morocco*)

Band structure and magneto-transport properties in narrow gap, two-dimensional and modulated nano-medium-infrared detector

Mo-eP12 **M. Taut, P. Machon, H. Eschrig** (*Leibniz Institute for Solid State and Materials Research, IFW Dresden, POB 270116, 01171 Dresden, Germany*)

Violation of non-interacting v-representability of the exact solutions of the Schrödinger equation for a parabolic two-electron quantum dot in a homogeneous magnetic field

Mo-eP14 **M. Nishimori[1], S. Sasaki[1], S. Watanabe[2], Y. Hirayama[3,4]** (*[1]Graduate School of Science and Technology, Niigata University, Niigata, Japan, [2]Centre for Advancement of Higher Education, Tohoku University, Sendai, Japan, [3]Graduate School of Science, Department of Physics, Tohoku University, Sendai, Japan, [4]4ERATO Nuclear Spin Project, Sendai, Japan*)

Strains in heterostructures detected by standard NMR

Mo-eP15 **S. Wiedmann[1], N.C. Mamani[2], G.M. Gusev[2], O.E. Raichev[3], A.K. Bakarov[2], J.C. Portal[1]** (*[1]LNCMI-CNRS / INSA, 25 rue des Martyrs, BP 166, Grenoble cedex 9 38042, France, [2]Instituto de Física da Universidade de São Paulo, São Paulo, SP, Brazil, [3]Institute of Semiconductor Physics, NAS of Ukraine, Kiev, Ukraine, [4]Institut Universitaire de France, 103, bd Saint-Michel 75005 Paris, France*)

Integer and fractional microwave induced resistance oscillations in a 2D system with moderate mobility

Mo-eP16 **Ethirajulu Senthamarai Kannan[1], G. H. Kim[1], I. Farrer[2], D. A. Ritchie[2]** (*[1]Sungkyunkwan Advanced Institute of Nanotechnology, Sungkyunkwan University, II Research complex building, 83206 Sungkyunkwan University, Suwon, Gyeonggi-do 440746, South Korea, [2]Cavendish Laboratory, University of Cambridge, Cavendish Laboratory, University of Cambridge, J. J. Thomson Avenue, Cambridge CB3 0HE, UK.*)

Crossover from weak localization to anti-localization in double quantum well system

Mo-eP17 **A. Ganczarczyk[1], S. Voßen[1], M. Geller[1], A. Lorke[1], K. Piegdon[1,2], D. Reuter[1,3], A. D. Wieck[1,3]** (*[1]Experimental Physics and CeNIDE, University Duisburg-Essen, Lotharstr. 1, 47048 Duisburg, Germany, [2]Department of Physics, University of Paderborn, Warburger Str. 100, 33098 Paderborn, Germany, [3]Solid State Physics, Ruhr-Universität Bochum, Universitätsstraße 150, 44801 Bochum, Germany*)

A voltage-tunable self-switching in-plane diode in a 2D-electron system

Mo-eP18 **L. C. Li[1], Y. T. Sung[2], C. W. Chang[3], Y. W. Suen[2,3,4], K. Y. Chen[5], C. T. Liang[5], Y. F. Chen[5], B. C. Lee[6], C. P. Lee[1,6]** (*[1]Center for Nanoscience and Technology, National Chiao Tung University, Hsinchu, Taiwan, R.O.C., [2]National Nano Device Laboratories, Hsinchu, Taiwan, R.O.C., [3]Department of Physics, National Chung Hsing University, Taichung, Taiwan, R.O.C., [4]Institute of Nanoscience, National Chung Hsing University, Taichung, Taiwan, R.O.C., [5]Department of Physics, National Taiwan University, Taipei, Taiwan, R.O.C., [6]Department of Electronics Engineering, National Chiao Tung University, Hsinchu, Taiwan, R.O.C.*)

Microwave-induced DC currents in mesoscopic structures

Mo-eP19 **T. P Martin[1], S. J. MacLeod[1], K. Chan[1], A. R. Hamilton[1], A. See[1], A. P. Micolich[1], M. Aagesen[2], P. E. Lindelof[2]** (*[1]School of Physics, University of New South Wales, Sydney, NSW 2051, Australia, [2]Nano-science center, University of Copenhagen, Universitetsparken 5, DK-2100 Copenhagen, Denmark*)

Re-examination of the single-particle relaxation lifetime for homogeneous background impurities in the two-dimensional electron gas

Mo-eP21 **N. P. Stepina, E.S. Koptev, A.V. Dvurechenskii, A.I. Nikiforov** (*Institute of Semiconductor Physics, 13 Lavrenteva, Novosibirsk 630090, Russia*)

Two-parameter scaling in 2D transport though a Ge/Si quantum dot array

Mo-eP22 **C. R. Proetto**[1], **S. Rigamonti**[2] ([1]*Institut fur Theoretische Physik, Freie Universitat Berlin, Arnimallee 14, Berlin D-14195, Germany,* [2]*Donostia International Physics Center (DIPC), E-20018 San Sebastian, Spain*)

What can we learn on the "universal" exchange-correlation energy of Density Functional Theory from the subband electronic structure of semiconductor quantum wells?

Mo-eP23 **J. Wrobel**[1], **P. Zagrajek**[1], **M. Czapkiewicz**[1], **M. Bek**[2], **K. Fronc**[1], **R. Hey**[3], **K. H. Ploog**[3], **B. Bulka**[2], **T. Dietl**[1,4] ([1]*Instytut Fizyki PAN, Warszawa, Poland,* [2]*Instytut Fizyki Molekularnej PAN, Poznan, Poland,* [3]*Paul Drude Institute, Berlin, Germany,* [4]*Instytut Fizyki Teoretycznej UW, Warszawa, Poland*)

Quantum effects in linear and non-linear transport of three-terminal ballistic junctions

Mo-eP24 **M. Yamaguchi**[1], **S. Nomura**[1,2], **H. Tamura**[1], **T. Akazaki**[1] ([1]*NTT Basic Research Laboratories, 3-1 Morinosato-Wakamiya, Atsugi, Kanagawa 243-0198, Japan,* [2]*University of Tsukuba, 1-1-1 Tennodai, Tsukuba, 305-8571, Japan*)

Photoluminescence spectra of gated undoped quantum well with lateral potential modulation in low electron density

Mo-eP25 **M. S. Fairbanks**[1], **T. P. Martin**[2], **B. C. Scannell**[1], **C. A. Marlow**[1], **H. Linke**[1,3], **R. P. Taylor**[1] ([1]*Department of Physics, University of Oregon, 1371 E 13th Ave. Eugene, Oregon 97403, USA,* [2]*School of Physics, University of New South Wales, Sydney, Australia 2052,* [3]*Division of Solid State Physics, Lund University, Box 118, S-221 00, Sweden*)

Measuring hybridization in GaInAs/InP electron billiard arrays

Mo-eP26 **T. Kubo**[1], **Y. Tokura**[1,2], **T. Hatano**[1], **S. Amaha**[1], **S. Teraoka**[1], **S. Tarucha**[1,3] ([1]*Quantum Spin Information Project, ICORP, JST, Morinosato Wakamiya, Atsugi-shi, Kanagawa 243-0198, Japan,* [2]*NTT Basic Researche Laboratories, NTT Corporation, Morinosato Wakamiya, Atsugi-shi, Kanagawa 243-0198, Japan,* [3]*Department of Applied Physics, University of Tokyo, Hongo, Bunkyo-ku, Tokyo 113-8656, Japan*)

Quantum interference effects in a laterally coupled triple quantum dot containing a quantum dot charge sensor

Mo-eP27 **Y. Imanaka**[1], **K. Takehana**[1], **T. Takamasu**[1], **G. Kido**[1], **G. Karczewski**[2], **T. Wojtowicz**[2], **J. Kossut**[2] ([1]*National Institute for Materials Science, 3-13, Sakura, Tsukuba, Ibaraki 3050003, Japan,* [2]*Institute of Physics, Polish Academy of Sciences, Al. Lotnikôw 32/46, 02-668 Warsaw, Poland*)

Optical detected magnetoplasma effects in CdTe dense two dimensional electron systems

Mo-eP28 **M. Abbarchi**[1], **F. Intonti**[1], **S. Vignolini**[1], **A. Vinattieri**[1], **L. Balet**[2], **L.H.Li**[2], **M. Francardi**[3], **A. Fiore**[4], **M. Gurioli**[1] ([1]*Physics department University of Firenze, Via Sansone 1 50019 , ITALY,* [2]*EPFL, Institute of Photonics and Quantum Electronics, Station 3, CH-1015 Lausanne, Switzerland,* [3]*Institute of Photonics and Nanotechnology, CNR, via del Cineto Romano 42, 00156 Roma, Italy,* [4]*COBRA Research Institute, Eindhoven University of Technology, 5600 MB Eindhoven, The Netherlands*)

Control of the quantum dots angular emission pattern in photonic crystal microcavities

Mo-eP29 **D. Kaewket[1], S. Sanorpim[1], S. Tungasmita[1], R. Katayama[2], K. Onabe[2]** (*[1]Department of Physics, Faculty of Science, Chulalongkorn University, Phayatai Rd., Patumwan, Bangkok 10900, Thailand, [2]Department of Advanced Materials Science, Graduate School of Frontier Sciences, The University of Tokyo, 5-1-5 Kashiwanoha, Kashiwa, Chiba, 277-8561 Japan*)

Band alignment of lattice-matched InGaPN/GaAs and GaAs/InGaPN quantum wells grown by MOVPE

Mo-eP30 **G. Tsuchiya[1], K. Sawano[2], Y. Shiraki[2], K. M. Itoh[1]** (*[1]School of Fundamental Science and Technology, Keio University, 3-14-1 Hiyoshi, Kouhoku-Ku, Yokohama 2238522, Japan, [2]Advanced Research Laboratories, Musashi Institute of Technology, 8-15-1 Todoroki, Setagaya-ku, Tokyo 1580082, Japan*)

Identification of scattering mechanisms limiting the mobility of two-dimensional electron gas in Si/SiGe heterostructures

Mo-eP31 **Y. Lin[1], P.-J. Wu[1], J. C. Chen[1], K. T. Lin[1], D.-S. Luo[1], T. Ueda[2], S. Komiyama[2]** (*[1]Department of Physics, National Tsing Hua University, No. 101, Sec. 2, Kuang-Fu Rd, Hsinchu 30013, Taiwan, [2]Department of Basic Science, University of Tokyo, 3-8-1 Komaba, Meguro-ku, Tokyo, 153-890, Japan*)

Channel Interference on Aharonov-Bohm Effect in a Quasi One-Dimensional Ring

Mo-eP32 **K.M. Liu[1], H.Y. Lin[1], V. Umansky[2], S.Y. Hsu[1]** (*[1]Deptartment of Electrophysics, National Chiao Tung University, 1001 Ta Hsueh Road, Hsinchu 300, Taiwan, [2]Braun center for Submicron Research, Weizmann Institute of Science, Rehovot, 76100, Israel*)

Density influenced electric transport of double quantum point contacts in series

Mo-eP33 **G. M. Gusev[1], Z. D. Kvon[2]** (*[1]Instituto de F ¶ .sica da Universidade de S ao Paulo,, S ao Paulo, SP, Brazil, , [2]Institute of Semiconductor Physics,*)

Magnetic field asymmetry of nonlinear transport in a small ring

Mo-eP34 **S. Wiedmann[1], N.C. Mamani[2], G.M. Gusev[2], A.K. Bakarov[2], J.C. Portal[1,3]** (*[1]LNCMI-CNRS / INSA, 25 rue des Martyrs, BP 166, Grenoble cedex 9 38042, France, [2]Instituto de Física da Universidade de São Paulo, São Paulo, SP, Brazil, [3]Institut Universitaire de France, 103, bd Saint-Michel 75005 Paris*)

Magneto-intersubband oscillations in triple quantum wells

Mo-eP35 **J. L. Movilla, A. Ballester, J. Planelles** (*Departament de Quimica Fisica i Analitica, Universitat Jaume I, Avd. de Vicent Sos Baynat s/n E-12071, Spain*)

Dielectric mismatch effect on coupled donor states in a quantum dot

Mo-eP36 **D. Lin, C. Hung, C. Lu, J. Wu** (*Department of Electronic Engineering, National Changhua University of Education, 1., Jin De Road, Paisha Village, Changhua 500, Taiwan*)

Comparison of two-dimensional electron gas of etched and nonetched InAlAs/InGaAs/InAlAs metamorphic high electron mobility transistor structures

Mo-eP37 **A.L. Vartanian, A.L. Asatryan, K.A. Vardanyan, A.A. Kirakosyan** (*Department of Solid State Physics, Yerevan State University, 1 A. Manoogian St., Yerevan 0025, Armenia*)

Quantum capture of electrons and intradot relaxation by means of Auger processes in quantum dots

Mo-eP38 **Zeng-Ru Zhao, X. X. Liang** (*Department of Physics, Inner Mongolia University, 235 West University Road, Hohhot 010021, China*)
Polaronic effect on an exciton in a cylindrical quantum wire

Mo-eP39 **Hanz Y. Ramirez[1], Chia-Hsien Lin[1], Wen-Ting You[1], Shan-Yu Huang[1], Wen-Hao Chang[1], Sheng-Di Lin[2], Shun-Jen Cheng[1]** ([1]*Department of Electrophysics, National Chiao Tung University, 1001 Ta-Hsueh Road, Hsinchu 300, Taiwan,* [2]*Department of Electronic Engineering, National Chiao Tung University, 1001 Ta-Hsueh Road, Hsinchu, 300 Taiwan*)
Electron-hole symmetry breaking in optical fine structures of single self-assembled quantum dots

Mo-eP40 **T. Moldaschl[1], T. Müller[1], W. Parz[1], S. Golka[2], G. Strasser[2], K. Unterrainer[1,2]** ([1]*Institute of Photonics, Vienna University of Technology, Gusshausstrasse 27-29/387 1040 Vienna, Austria,* [2]*Center for Micro- and Nanostructures, Vienna University of Technology, Floragasse 7, 1040 Vienna, Austria*)
Fine structure of excitons in InAs quantum dots at low magnetic fields

Mo-eP42 **J. Inarrea[1,2], G. Platero[2]** ([1]*Department of Physics. University Carlos III, Avenida de la Universidad. Leganes. Madrid 28760, Spain,* [2]*Instituto de Ciencia de Materiales., Cantoblanco. Madrid*)
Role of an in-plane field in 2D magnetotransport assisted by microwaves

Mo-eP44 **Manvir S. Kushwaha** (*Institute of Physics, University of Puebla, Apdo. Post. J-45, Puebla 72570, Mexico 72570, Mexico*)
How a magnetized quantum wire can act as an active laser medium

Mo-eP45 **M. P. Telenkov, Yu. A. Mityagin** (*P.N. Lebedev Physical Institute, 119991 Leninsky prosp., 53, Moscow, Russia*)
Effect of strong tilted magnetic field on the sequential resonant tunneling in long period GaAs/AlGaAs superlattices

Mo-eP46 **M.B. Santos[1], M. Edirisooriya[1], T.D. Mishima[1], C.K. Gaspe[1], J. Coker[1], R.E. Doezema[1], X. Pan[2], G.D. Sanders[2], C.J. Stanton[2], L.C. Tung[3], Y-J. Wang[3]** ([1]*Department of Physics and Astronomy, University of Oklahoma, 440 West Brooks, Norman OK 73019, USA,* [2]*Department of Physics, University of Florida, P.O. Box 118440, Gainesville, FL 32611-8440, USA,* [3]*National High Magnetic Field Laboratory, Florida State University, 1800 E. Paul Dirac Drive, Tallahassee, FL 32310 - 3706, USA*)
Cyclotron Resonance in 2D Hole Systems in InSb Quantum Wells

Mo-eP47 **S. S. Buchholz[1], S. F. Fischer[1], U. Kunze[1], D. Reuter[2], A. D. Wieck[2]** ([1]*Werkstoffe und Nanoelektronik, Ruhr-Universität Bochum, Universitätstr. 150, 44780 Bochum, Germany,* [2]*Angewandte Festkörperphysik, Ruhr-Universität Bochum, Universitätstr. 150, 44780 Bochum, Germany*)
Aharonov-Bohm phase shift in a multi-terminal asymmetric quantum ring

Mo-eP48 **H. Shima[1], H. Yoshioka[2], J. Onoe[3]** ([1]*Department of Applied Physics, Graduate School of Engineering, Hokkaido University, N13-W8, Kita-ku, Sapporo, Hokkaido 060-8628, Japan,* [2]*Department of Physics, Nara Women's University, Nara 630-8506, Japan,* [3]*Research Laboratory for Nuclear Reactors and Department of Nuclear Engineering, Tokyo Institute of Technology, 2-12-1 Ookayama, Meguro, Tokyo 152-8550, Japan*)
Tomonaga-Luttinger exponent of peanut-shaped hollow nanocylinders

Mo-eP49 **Y. Sakurai[1], S. Nomura[1], Y. Takada[1], K. Shiraishi[1], M. Muraguchi[2], T. Endoh[2], Y. Shigeta[3], M. Ikeda[4], K. Makihara[4], S. Miyazaki[4]** (*[1]Graduate School of Pure and Applied Science, University of Tsukuba, 1-1-1 Tennodai, Tsukuba, Ibadaki 305-8571, Japan, [2]Center of Interdisciplinary Research, Tohoku University, Sendai, 980-8578, Japan, [3]Institute of Picobiology, Graduate School of Life Science, University of Hyogo, Ako, 678-1297, Japan, [4]Graduate School of Advanced Sciences of Matter, Hiroshima University, Higashi-Hiroshima, 739-8530, Japan*)

Anomalous temperature dependence of electron tunneling

Mo-eP50 **Jaeuk U. Kim[1], W.-R. Lee[1], Hyun-Woo Lee[2], H.-S. Sim[1]** (*[1]Department of Physics, Korea Advanced Institute of Science and Technology, 373-1 Guseong-dong, Yuseong-gu, Daejeon 305-701, Republic of Korea, [2]PCTP and Department of Physics, Pohang University of Science and Technology, Pohang, Kyungbuk 790-784, Korea*)

Revival of electron coherence in a Luttinger liquid of finite length

Mo-eP51 **Hitoshi Yoshizumi, Sei-ichiro Suga** (*Department of Applied Physics, Osaka University, 2-1 Yamadaoka, Suita, Osaka 5650871, Japan*)

Multiorbital Kondo effect in quantum dots coupled to ferromagnetic leads

Mo-eP52 **Y. Yamada[1], Y. Tanaka[2], N. Kawakami[1]** (*[1]Department of Physics, Kyoto University, Kitashirakawa, Sakyo, Kyoto 606-8502, Japan, [2]Condensed Matter Theory Laboratory, RIKEN, Wako, Saitama 351-0198, Japan*)

Andreev tunneling through a quantum dot at finite bias

Mo-eP53 **W. Sheng** (*Department of Physics, Fudan University, 220 Handan Road, Shanghai 200433, P.R. China*)

Distribution and Anisotropy of Electron g-factor in Quantum Dots

Mo-eP54 **D. Harbusch[1], H.P. Tranitz[2], W. Wegscheider[2], S. Ludwig[1]** (*[1]Fakultät für Physik, Ludwig-Maximilians-Universität München, Geschwister-Scholl-Platz 1, München 80539, Germany, [2]Institut für Experimentelle und Angewandte Physik, Universität Regensburg, Universitätsstrasse 11, 93040 Regensburg, Germany*)

Interaction between coupled quantum dots and a biased quantum point contact

Mo-eP55 **J.M. Escartín[1], F. Malet Giralt[2], A. Emperador[3], M. Barranco[1], M. Pi[1]** (*[1]Departament ECM, Fac. de Física, and IN2UB, Universitat de Barcelona, Diagonal 647, 08028 Barcelona, Spain, [2] Division of Mathematical Physics, LTH, Lund University, Box 118, Lund , Sweden, [3]Institute for Research in Biomedicine, Parc Científic de Barcelona, Josep Samitier 1-5, 08028 Barcelona, Spain*)

Electron localization in few-electron concentric quantum rings

Mo-eP56 **W.H. Lim[1], H. Huebl[1], F.A. Zwanenburg[1], L.H. Willems van Beveren[1], S. Rubanov[2], P.G. Spizzirri[2], S.J. Angus[2], R.G. Clark[1], A. Morello[1], A.S. Dzurak[1]** (*[1]Centre for Quantum Computer Technology, University of New South Wales, Sydney, Australia, [2]Centre for Quantum Computer Technology, University of Melbourne, Melbourne, Australia*)

Electrostatically-defined quantum dots in silicon

Mo-eP57 **J. W. Song[1], Y. Kawano[2], K. Ishibashi[2], G. Aizin[3], N. Aoki[4], Y. Ochiai[4], J. L. Reno[5], J. P Bird[1,4]** (*[1]Department of Electrical Engineering, University at Buffalo, Buffalo, NY 14260, USA, [2]Advanced Device Laboratory, RIKEN, 2-1 Hirosawa, Wako, Saitama 351-0198, Japan, [3]Department of Physical Sciences, Kingsborough College of the City University of New York, Brooklyn, NY 11235, [4]Graduate School of Advanced Integration Science, Chiba University, 1-33 Yayoi-cho, Inage-ku, Chiba 263-8522, Japan, [5]CINT Science Department, Sandia National Laboratories, P.O. Box 5800, Albuquerque, NM 87185-1303*)

Terahertz Photo-Response of Quantum Point Contacts

Mo-eP58 **C.-T. Liang[1], Tobias Kramer[2,3], Eric J. Heller[3,4], Kuang Yao Chen[1], Robert E. Parrott[5], C. F. Huang[6], Li-Hung Lin[7], Jau-Yang Wu[8], Sheng-Di Lin[8], Han-Chieh Lee[9]** (*[1]Department of Physics, National Taiwan University, Taipei, Taiwan 106, R.O.C., [2]nstitute for Theoretical Physics, University of Regensburg, 93040 Regensburg, Germany, [3]Department of Physics, Harvard University, Cambridge, MA 02138, USA, [4]Department of Chemistry and Chemical Biology, Harvard University, Cambridge, MA 02138, USA, [5]School of Engineering and Applied Science, Harvard University, Cambridge, MA 02138, USA, [6]National Measurement Laboratory, Center for Measurement Standards, Industrial Technology Research Institute, Hsinchu, Taiwan 300, R.O.C., [7]Department of Applied Physics, National Chiayi University, Chiayi, Taiwan 600, R.O.C., [8]Department of Electronics Engineering, National Chiao Tung University, Hsinchu, Taiwan 300, R.O.C., [9]Institute of Physics, National Chiao Tung University, Hsinchu, Taiwan 300, R.O.C*)

The quantum Hall effect beyond linear response

Mo-eP60 **J. C. Chen[1], Yuling Tsai[1], Yiping Lin[1], T. Ueda[2], S. Komiyama[2]** (*[1]Department of Physics, National Tsing-Hua University. Hsinchu, Taiwan, No 101 Sec 2 Kuan Fu Road, Hsinchu, 300, Taiwan, R.O.C., [2]Department of Basic Science, University of Tokyo, Komaba, Tokyo, Japan, 3-8-1 Komaba, Meguro-ku, Tokyo 153-8902, Japan*)

Negative differential conductivity of two-dimensional electron gas layers in high magnetic fields

Mo-eP61 **M. F. Chen[1], Y. C. Huang[2], R. B. Chen[3], C. P. Chang[4]** (*[1]Department of Physics, National Cheng Kung University, Department of Physics, National Cheng Kung University, Tainan, Taiwan, [2]Center for General Education, Kao Yuan University , Center for General Education, Kao Yuan University, Kaohsiung, Taiwan, [3]Center of General Studies, National Kaohsiung Marine University , Center of General Studies, National Kaohsiung Marine University, Kaohsiung, Taiwan, [4]Center of General Education, Tainan University of Technology, 529 Jhongjheng Rd., Yongkang, Tainan 71002, Taiwan*)

Spatially modulated magnetic fields induced modification of magnetic bands of monolayer zigzag graphene ribbon

Mo-eP62 **D. Eksi[1], O. Kilicoglu[1], S. Aktas[1], A. Siddiki[2]** (*[1]Department of Physics, Trakya University, Trakya University, 22030 Edirne, Turkey, [2]Mugla University, Physics Department, Faculty of Sciences and Arts, Mugla University, 48170-Kotekli, Mugla , Turkey*)

The current direction induced rectification effect on the IQHE

Mo-eP63 **M. Hashisaka, Y. Yamauchi, S. Nakamura, K. Chida, S. Kasai, T. Ono, K. Kobayashi** (*Institute for Chemical Research, Kyoto University, Institute for Chemical Research, Kyoto University, Uji, Kyoto 611-0011, Japan*)

Collapse of the Conductance Quantization by the High-frequency Shot Noise in Coupled Quantum Wires

Mo-eP65 **Tsai-Yu Huang[1], C.-T. Liang[1], Gil-Ho Kim[2], C. F. Huang[3], C. P. Huang[1], D. A. Ritchie[4]** (*[1]Department of Physics, National Taiwan University, Taipei 106, Taiwan, , [2]School of Information and Communication Engineering and Sungkyunkwan Advanced Institute of Nanotechnology, Sungkyunkwan University, Suwon 440-746, Republic of Korea, , [3]National Measurement Laboratory, Center for Measurement Standards, Industrial Technology Research Institute, Hsinchu 300, Taiwan, , [4]Cavendish Laboratory, Madingley Road, Cambridge CB3 OHE, United Kingdom,*)

Probing two-dimensional metallic-like and localization effects at low magnetic fields

Mo-eP66 **S. Nomura[1,2], M. Yamaguchi[2], H. Tamura[2], T. Akazaki[2], Y. Hirayama[3,4]** (*[1]Institute of Physics, University of Tsukuba, 1-1-1 Tennoudai, Tsukuba, Ibaraki 305-8571, Japan, [2]NTT Basic Research Laboratories, 3-1 Morinosato-Wakamiya, Atsugi, 243-0198, Japan, [3]Department of Physics, Faculty of Science, Tohoku University, 6-3 Aoba, Aobaku, Sendai, 980-8578, Japan, [4]ERATO-JST, 4-1-8 Honcho, Kawaguchi, 332-0012, Japan*)

Circular polarization reversal of split photoluminescence peaks at ν of slightly less than 1

Mo-eP67 **J. Hayakawa[1], T. Kawamura[1], M. Kuwano[1], K. Onomitsu[2], T. Fujisawa[2], G. Yusa[1,2,3]** (*[1]Department of Physics, Tohoku University, Sendai, 980-8578, Japan, [2]NTT Basic Research Laboratories, NTT Corporation, Atsugi, 243-0198, Japan, [3]PRESTO Japan Science and Technology Agency, Kawaguchi, 331-0012, Japan*)

Optical studies of spin phase transition in the vicinity of ν=2/3 fractional quantum Hall regime

Mo-eP68 **H. Ito[1], D. Fukuoka[1], T. Nagayama[1], K. Oto[1], K. Muro[1], Y. Hirayama[2,4], N. Kumada[3], H. Yamaguchi[3]** (*[1]Graduate School of Science, Chiba University, Chiba, Japan, [2]Graduate School of Science, Tohoku University, Sendai, Japan, [3]NTT Basic Research Laboratories, NTT Corporation, Atsugi, Japan, [4]ERATO Nuclear Spin Electronics Project, Sendai, Japan*)

Sensitive detection of the spin polarization in a quantum Hall regime by a Kerr rotation measurement

Mo-eP69 **Takahiro Morimoto[1], Yasuhiro Hatsugai[2], Hideo Aoki[1]** (*[1]Department of Physics, University of Tokyo, Tokyo, Japan, [2]Institute of Physics, University of Tsukuba, Tsukuba, Japan*)

Optical Hall conductivity in 2DEG and graphene QHE systems

Mo-eP70 **N. Kumada, K. Muraki** (*NTT Basic Research Laboratories, 3-1 Morinosato Wakamiya, Atsugi 243-0198, Japan*)

Spin-pseudospin mixed skyrmion in bilayer ν=1 quantum Hall systems with large tunnel coupling

Mo-eP71 **T. Nakajima, S. Komiyama** (*Department of Basic Science, University of Tokyo, 3-8-1 Komaba, Meguro-ku, Tokyo 153-8902, Japan*)

Lifetime of dissipation-less state of quantum Hall electron systems in the bistable regime

Mo-eP72 **S. P Koduvayur[1], L.P.Rokhinson[1], G.A.Csathy[1], S.Y.Khlebnikov[1], M.J.Manfra[1,2], L.N.Pfeiffer[2], K.W.West[2]** (*[1]Department of Physics, Purdue University , 525 Northwestern Avenue, West Lafayette 47907, USA, [2]Bell Laboratories, Lucent Technologies, Murray Hill, NJ, 07974,USA*)

Effect of strain on nematic phases in two dimensional hole gases

Mo-eP73 **J. Sailer[1], V. Lang[1], A. Wild[1], K. M. Itoh[2], E. E. Haller[3,4], G. Abstreiter[1], D. Bougeard[1]** ([1]*Walter Schottky Institut, Technische Universität München, Am Coulombwall 3, 85748 Garching, Germany,* [2]*Department of Applied Physics and Physico-Informatics, Keio University, 3-14-1, Hiyoshi, Kohoku-ku, Yokohama 223-8522, Japan,* [3]*Lawrence Berkeley National Laboratory, Materials Sciences Division, Berkeley, CA 94720-8197, USA,* [4]*Department of Materials Science and Engineering, University of California at Berkeley, Berkeley, CA 94720-1760, USA*)

Hall resistance overshoot in 2D electron systems in Si/SiGe

Mo-eP74 **P. Plochcocka[1], J. M. Schneider[1], D. K. Maude[1], M. Potemski[1], M. Rappaport[2], V. Umansky[2], I. Bar-Joseph[2], J. G. Groshaus[3], Y. Gallais[3], A. Pinczuk[3]** ([1]*Laboratoire National des Champs Magnètiques Intenses, CNRS, 25, avenue des Martyrs, Grenoble 38042, France,* [2]*Weizmann Institute of Science, Department of Condensed Matter Physics, The Weizmann Institute of Science, Rehovot, Israel,* [3]*Columbia University, Department of Physics and of Appl. Physics and Appl. Mathematics, Columbia University, New York, NY 10027*)

Optical absorption to probe the quantum Hall ferromagnet at ν= 1

Mo-eP75 **J. Kim[1], T. Yoo[1], S. Lee[1], X. Liu[2], J.K. Furdyna[2]** ([1]*Korea University, 5Ga Anamdong, SungbukGu, Seoul 136-701, R. of Korea,* [2]*University of Notre Dame, Notre Dame In 46556 USA*)

Investigation of domain pinning field in GaMnAs using angular dependence of planar Hall effect

Mo-eP76 **T. Matsuda, K. Konishi, K. Yoh** (*Graduate School of Information Science and Technology, Hokkaido University, N13, W8, Kitaku, Sapporo, Hokkaido 060-8628, Japan*)

Possible Sign Reversal of Rashba coefficient in InAs-based Heterostructures

Mo-eP77 **D. A. Vasyukov[1], A. S. Plaut[1], A. H. MacDonald[2], M. Henini[3]** ([1]*Exeter University , School of Physics, Exeter EX4 4QL, England,* [2]*The University of Texas at Austin, Department of Physics, Austin Texas 78712, USA,* [3]*University of Nottingham, School of Physics and Astronomy and Nottingham Nanotechnology and Nanoscience Centre, Nottingham NG7 2RD, UK*)

Measurement of a large hole g-factor in two-dimensional hole gases

Mo-eP78 **P. Vasilopoulos, P. M. Krstaji'c** (*Department of Physics, Concordia University, 7141 Sherbrooke Ouest, Montréal, Québec H4B 1R6, Canada*)

Spin-dependent transport through waveguides with spatially modulated strengths of the Rashba and Dresselhaus spin-orbit interaction terms

Mo-eP79 **R.Z.Vitlina, L.I.Magarill, A. V. Chaplik** (*Institute of Semiconductor PhysicsBranch, Russian Academy of Sciences, Novosibirsk, Russia, 13, prospekt Lavrent'eva, Novosibirsk, 630090, Russia*)

2D magnetoplasmons in systems with spin-orbit interaction (SOI)

Mo-eP80 **P. Kleinert** (*Paul-Drude-Institute for Solid State Electronics, Hausvogteiplatz 5-7 10117-Berlin, Germany*)

Excitation of electric-field-driven spin remagnetization waves on a cylindrical surface with spin-orbit interaction

Mo-eP81 **S. Faniel[1,2], S. Mineshige[3], Y. Sekine[4], T. Koga[1,2]** ([1]*Graduate School of Information Science and Technology, Hokkaido University, N-14, W-9, Kita-ku, Sapporo, Hokkaido 060-0814, Japan,* [2]*Creative Research Initiative , N-21, W-10, Kita-ku, Sapporo, Hokkaido 001-0021, Japan,* [3]*Department of Electronics and Information Engineering, Hokkaido University, N13, W8, Kita-ku, Sapporo, Hohhaido 060-8628, Japan,* [4]*NTT Basic Research Laboratories, NTT Corporation, 3-1, Morinosato-Wakamiya, Atsugi, Kanagawa 243-0198, Japan*)

Spin interference effects in InGaAs/InAlAs rectangular loop arrays

Mo-eP82 **K. Ito[1], A. Narahara[1], H. Akinaga[2], T. Suemasu[1]** ([1]*Institute of Applied Physics, University of Tsukuba, Tsukuba, Ibaraki 305-8573, Japan,* [2]*National Institute of Advanced Industrial Science and Technology (AIST), Tsukuba, Ibaraki 305-8568, Japan*)

Molecular beam epitaxy and magnetoresistance in Fe_4N/MgO/Fe_4N magnetic tunnel junction

Mo-eP83 **S. M. Badalyan[1,2], A. Matos-Abiague[2], G. Vignale[3], J. Fabian[2]** ([1]*Yerevan State University, Yerevan, 375025 Armenia,* [2]*University of Regensburg, 93040 Regensburg, Germany,* [3]*University of Missouri - Columbia, Missouri 65211, USA*)

Spin-orbit interaction induced directional suppression of plasmon propagation

Mo-eP84 **T. Kutsuwa[1], M. Kuwahara[1], K. Ono[2,1], H. Kosaka[3,1]** ([1]*CREST-JST, 2-1-1, Katahira, Sendai 9808577, Japan,* [2]*Low Temperature Physics Laboratory, RIKEN, Saitama, 3510198, Japan,* [3]*Research Institute of Electrical Comminication, Tohoku University, 2-1-1, Katahira, Sendai 9808577, Japan*)

Single electron spin resonance in a g-factor controlled semiconductor quantum dot

Mo-eP85 **S. Ishida[1], T. Manago[1], N. Nishizako[2], H. Geka[2], I. Shibasaki[2]** ([1]*Tokyo University of Science Yamaguchi, Daigakudori 1-1-1, San'yo-Onoda, Yamaguchi 756-0884, Japan,* [2]*Asahi Kasei Corporation, Samejima 2-1, Fuji, Shizuoka 416-8501, Japan*)

Spin-Orbit Interaction and Negative Magnetoresistance for Localized Electrons in InSb Quantum Wells

Mo-eP86 **B. Dai[1], A. Nogaret[1], P. Saraiva[1], F. Nasirpouri[1], J.C.Portal[2], H.E.Beere[3], D.A.Ritchie[3]** ([1]*Department of Physics, University of Bath BA2 7AY, UK,* [2]*Grenoble High Magnetic Field Laboratory, 28 Avenue des Martyrs, Grenoble 38042 France,* [3]*Cavendish Laboratory, University of Cambridge, CB3 0HE UK*)

Electrically detected spin resonance of 'snake' state oscillators

Mo-eP87 **P. Kossacki[1,4], M. Goryca[1,4], T. Kazimierczuk[1], M. Nawrocki[1], A. Golnik[1], J. A. Gaj[1], T. Wojtowicz[2], G. Karczewski[2], J. Cibert[3], S. Tatarenko[3]** ([1]*Institute of Experimental Physics, University of Warsaw, Warsaw, Poland, ul. Hoza 69, 00-681 Warsaw, Poland,* [2]*Institute of Physics, Polish Academy of Sciences, Warsaw, Poland, al. Lotnikow 32/46, 02-668 Warsaw, Poland,* [3]*Institute Neel ,CNRS/UJF, Grenoble, France, 25 rue des Martyrs B.P. 166, 38042 Grenoble cedex 9, France,* [4]*Grenoble High Magnetic Field Laboratory, CNRS, Grenoble, France, 25 rue des Martyrs B.P. 166, 38042 Grenoble cedex 9, France*)

Low field magnetization dynamics in dilute (Cd,Mn)Te

Mo-eP88 **R. Raimondi[1], P. Schwab[2]** ([1]*Department of Physics, Roma Tre University, Via della Vasca Navale 84, Rome I-00146, Italy,* [2]*Institut für Physik, Universität Augsburg, D-86135 Augsburg, Germany*)
Interplay of intrinsic and extrinsic mechanisms to the spin Hall effect in a two-dimensional electron gas

Mo-eP89 **S. H. Lee, C.W. Chiu, M.F. Lin** (*Department of Physics, National Cheng Kung University, No.1, Ta-Hsueh Road, Tainan City 701, Taiwan (R.O.C.)*)
Deformation effects on electronic structures of bilayer graphenes

Mo-eP90 **M. Kida[1], T. Hatori[1], Y. Nakamura[1], Y. Togashi[1], N. Aoki[1], J. P. Bird[2], Y. Ochiai[1]** ([1]*Graduate School of Advanced Integration Science, Chiba University, Yayoi, Inage, Chiba 263-8522, Japan,* [2]*Deapartment of Electrical Engineering, University of Buffalo, SUNY, Buffalo, NY 14260-1900, USA*)
Low temperature magneto-resistance of thin multi-walled carbon nano-tube

Mo-eP91 **Y. Mochizuki, H. Yoshioka** (*Department of Physics, Nara Women's University, Kitauoyanishi-machi, Nara, JAPAN*)
Transport properties of normal metal - graphene nanoribbon - normal metal junctions

Mo-eP92 **T. Maruyama[1], K. Yoshida[2], W. Norimatsu[1], M. Kusunoki[1,2]** ([1]*Nagoya University, Furo-cho, Chikusa-ku, Nagoya, 464-8603 464-8603, Japan,* [2]*Japan Fine Ceramics Center, 2-4-1 Mutsuno, Atsuta, Nagoya, 456-8587, Japan*)
Doping of Si into Aligned Carbon Nanotube Films on SiC

Mo-eP94 **A. A. Kaverzin, F. Withers, A. S. Price, S. M. Strawbridge, A. K. Savchenko, H. Pinto, R. Jones** (*School of Physics, University of Exeter, Stocker Road, Exeter, Devon EX4 4QL, UK*)
Doping of graphene by toluene

Mo-eP95 **S. Park, H.-S. Sim** (*Departmet of Physics, KAIST, 335 Gwahangno, Yuseong-gu, Daejeon 305-701, Republic of Korea*)
Phase jump of the reflection amplitude in bilayer graphene with potential step

Mo-eP96 **Kuang-Yuan Hsu, Chuan-Pu Liu** (*Department of Materials Science and Engineering, National Cheng Kung University, No.1,Ta-Hsueh Road,Tainan,Taiwan,ROC.*)
Molecular beam epitaxy growth of wurtzite GaN nanoislands and nanocolumns

Mo-eP97 **A. Kanda[1,2], H. Goto[1,2], Y. Ootuka[1], K. Tsukagoshi[2,3,4], H. Yoshioka[5], M. Hayashi[6]** ([1]*Institute of Physics and TIMS, University of Tsukuba, 1-1-1 Tennodai, Tsukuba, Ibaraki 305-8571, Japan,* [2]*CREST, JST, Kawaguchi, Saitama 332-0012, Japan,* [3]*MANA, NIMS, Tsukuba, Ibaraki 305-0047, Japan,* [4]*AIST, Higashi, Tsukuba, Ibaraki 305-8568, Japan,* [5]*Department of Physics, Nara Women's University, Nara 630-8506, Japan,* [6]*Faculty of Education and Human Sciences, Akita University, Akita 010-8502, Japan*)
Anomalous temperature dependence of critical supercurrent in multilayer graphene coupled to superconductors

Mo-eP98 **Shao-Pin Chiu[1], Hui-Fang Chuang[2], Ji-Jung Kai[2], Fu-Rong Chen[2], J. Lin[1]** (*[1]National Chiao Tung University, Institute of Physics, National Chiao Tung University, Hsinchu, Taiwan, [2]National Tsing Hua University, Department of Engineering and System Science, National Tsing Hua University, Hsinchu, Taiwan*)

Low-temperature electrical-transport properties of single indium tin oxide nanowires

Mo-eP99 **A. Nath Pal, Arindam Ghosh** (*Department of Physics, Indian Institute of Science, C V Raman Avenue, Bangalore 560012, India*)

Low frequency resistance noise in graphene based field effect devices

Mo-eP100 **W. Norimatsu[1,2], M. Kusunoki[1,2]** (*[1]EcoTopia Science Institute, Nagoya University, Furo-cho, Chikusa-ku, Nagoya-shi, Aichi-ken 464-8603, Japan, [2]Materials Research and Development Laboratory, Japan Fine Ceramics Center, 2-4-1, Mutsuno, Atsuta-ku, Nagoya-shi, Aichi-ken 456-8587, Japan*)

Atomic structures of the interface between homogeneous graphene and 6H-SiC (0001)

Mo-eP101 **P.S. Park[1], S.C. Kim[1], S. Yang[1,2], A.H. MacDonald[3]** (*[1]Department of Physics, Korea university, Seoul , Korea, [2]Korea Institute for Advanced Study, Seoul, Korea, [3]Department of Physics, University of Texas, Austin, TX 78703, USA*)

Interband Conductivity of Neutral Graphene Sheets

Mo-eP102 **S. Weingart[1], C. Bock[1], U. Kunze[1], K.V. Emtsev[2], Th. Seyller[2], L. Ley[2]** (*[1]Werkstoffe und Nanoelektronik, Ruhr-Universität Bochum, Universitätsstr. 150, Bochum 44780 , Germany, [2]Lehrstuhl für Technische Physik, Friedrich-Alexander Universität Erlangen-Nürnberg, Erwin-Rommel-Straße 1, Erlangen 91058, Germany*)

Influence of the growth conditions of epitaxial graphene on the film topography and the electron transport properties

Mo-eP103 **A. B. Dzyubenko[1,2], A. M. Fischer[3], R. A. Römer[3]** (*[1]Department of Physics, California State University Bakersfield, Bakersfield CA 93311, USA, [2]General Physics Institute, Russian Academy of Sciences, Moscow 119991, Russia, [3]Department of Physics and Centre for Scientific Computing, University of Warwick , Coventry CV4 7AL, UK*)

Localized magnetoplasmons in graphene

Mo-eP104 **T. Morinari** (*Yukawa Institute for Theoretical Physics, Kyoto University, Sakyo-ku Kitashirakwa Oiwakecho, Kyoto 6068502, Japan*)

Theory for interlayer magnetoresistance in layered Dirac fermion systems: Application to α-(BEDT-TTF)$_2$I$_3$

Mo-eP105 **J. H. Ho[1,2], S. J. Tsai[1], Y. H. Chiu[1], M. F. Lin[1]** (*[1]Department of Physics, National Cheng Kung University, No.1 University Road, Tainan City 701, Taiwan , [2]Institute of Physics, Academia Sinica, No.128 Academia Road, Section 2, Nankang, Taipei 115, Taiwan*)

Transition of graphene under one-dimensional electric potentials to semimetallic state

Mo-eP106 **A. Toyoda, T. Ando** (*Department of Physics, Tokyo Institute of Technology, 2-12-1 Ookayama, Meguro-ku, Tokyo*)

Resonance scattering by strong and short-range scatterers in graphene

Mo-eP107 **P. Liu[1,2,3], GW. She[2], WS. Shi[2], DM. Chen[1]** ([1]*Institute of Physics, Chinese Academy of Sciences, Beijing, China,* [2]*Technical Institute of Physics and Chemistry, Chinese Academy of Science, Beijing, China,* [3]*Institute Neel, CNRS/UJF, Grenoble, France*)
Polarized memory effect observed in ZnO nanotube point contact system

Mo-eP108 **E.B. Olshanetsky[1], Z.D. Kvon[1,2], M.V. Entin[1], L.I. Magarill[1,2], N.N. Mikhailov[1], I.O. Parm[1], S.A. Dvoretsky[1]** ([1]*Institute of Semiconductor Physics, pr. Lavrentjeva, 13, 630090, Novosibirsk, Russia,* [2]*Novosibirsk State University, 630090, Novosibirsk, Russia*)
Scattering processes in a 2D semimetal

Mo-eP109 **Shao-Pin Chiu[1], Yong-Han Lin[2], Juhn-Jong Lin[1,2]** ([1]*Institute of Physics, National Chiao-Tung University, 1001 Ta Hsueh Road, Hsinchu, 300, Taiwan ROC , Taiwan,* [2]*Department of Electrophysics, National Chiao Tung University, 1001 Ta Hsueh Road, Hsinchu, 300, Taiwan ROC , Taiwan*)
Electrical conduction mechanisms in natively doped ZnO nanowires

Mo-eP110 **R. Yagi[1], S. Fukada[1], H. Kobara[1], N. Ogita[2], M. Udagawa[2]** ([1]*AdSM, Hiroshima University, Kagamiyama 1-3-1, Higashi-Hiroshima, Hiroshima, 739-8530, Japan,* [2]*Graduate School of Integrated Arts and Sciences , Kagamiyama 1-7-1, Higasih-Hiroshima, Hiroshima, 739-8521, Japan*)
Magnetoresistance due to potential fluctuation in monolayer graphene at minimum conductivity point

Mo-eP111 **Yshai Avishai[1,2]** ([1]*Department of Physics, Ben Gurion University, Beer Sheva, Israel,* [2]*Department of Physics, Hong Kong University of Science and Technology, Clear Water Bay, Kowloon, Hong Kong*)
Electron on a Sphere: 2D or not 2D?

Mo-eP112 **M. F. Craciun[1], S. Russo[1,2], M. Yamamoto[1], A. F. Morpurgo[1,3], S. Tarucha[1]** ([1]*Department of Applied Physics, The University of Tokyo, 7-3-1 Hongo, Bunkyo-ku,Tokyo 113-8656, Japan,* [2]*Kavli Institute of Nanoscience, Delft University of Technology, Lorentzweg 1, 2628 CJ, Delft, The Netherlands,* [3]*Department of Condensed Matter Physics, University of Geneva, quai Ernest-Ansermet 24, CH-1211 Geneva 4, Switzerland,* [4]*Quantum Spin Information Project, ICORP, Japan Science and Technology Agency, Atsugi-shi, 243-0198, Japan*)
Contact resistance in graphene-based devices

Mo-eP113 **M. Hayashi[1], H. Yoshioka[1], A. Kanda[1]** ([1]*Faculty of Education and Human Studies, Akita University, 1-1 Tegatagakuen-machi, Akita 0108502, Japan,* [2]*Department of Physics, Nara Women's University, Nara 630-8506, Japan,* [3]*Institute of Physics, University of Tsukuba, Tsukuba 305-8571, Japan*)
Superconducting proximity effect through single-layer and multilayer graphene films

Mo-eP114 **Y. Tomio, H. Suzuura** (*Division of Applied Physics, Graduate School of Engineering, Hokkaido University, Kita 13 Nishi 8, Kita-ku, Sapporo 0608628, Japan*)
Impurity-induced valley mixing of excitons in semiconducting carbon nanotubes

Mo-eP115 **K. Takai, K. Takai, Y. Nishimura, T. Enoki** (*Department of Chemistry, Tokyo Institute of Technology, 2-12-1-W4-1, Ookayama, Meguro, Tokyo, JAPAN*)
Electronic properties of Nanographene

Mo-eP116 **A. Satou[1], A. Satou[1], F. T. Vasko[2], T. Otsuji[3], V. Ya. Aleshkin[4], A. A. Dubinov[4]** (*[1]Computational Nanoelectronics Laboratory, University of Aizu, Aizu-Wakamatsu 965-8580, Japan, [2]Institute of Semiconductor Physics, NAS of Ukraine, Kiev 03028, Ukraine, [3]Research Institute of Electrical Communication, Tohoku University, Sendai 980-8577, Japan, [4]Institute for Physics of Microstructures, RAS, 603950 Nizhny Novgorod, Russia*)

Terahertz/far-infrared lasing by utilization of population inversion in graphene under optical pumping

Mo-eP118 **Kuan-Ting Lin[1], Yiping Lin[1], C. C. Chi[1], J. C. Chen[1], T. Ueda[2], S. Komiyama[2]** (*[1]Department of Physics, National Tsing Hua University, Hsinchu, Taiwan, [2]Department of Basic Science, University of Tokyo, Komaba, Tokyo, Japan*)

Temperature and current-dependent dephasing in an Aharonov-Bohm ring

Mo-eP119 **E. del Valle[1], S. Zippilli[2], A. Gonzalez-Tudela[1], F.P. Laussy[3], G. Morigi[1], C. Tejedor[1]** (*[1]Dept. Fisica Teorica Materia Condensada, Universidad Autonoma de Madrid, Cantoblanco, Madrid 28049, Spain, [2]Dept. Fisica, Universidad Autonoma de Barcelona, Bellaterra, Barcelona 08193, Spain , [3]School of Physics and Astronomy, University of Southampton, , Southampton, UK*)

Two photon laser emission from a quantum dot in a cavity

Mo-eP120 **J. D. Mason[1,3], L. Gaudreau[2,4], S. A. Studenikin[2], A. Kam[2], A. S. Sachrajda[2], J. B. Kycia[1,3]** (*[1]Department of Physics and Astronomy, University of Waterloo, Waterloo, Ontario, Canada N2L3G1, [2]Institute for Microstructural Sciences, National Research Council, Ottawa, Ontario, Canada K1A0R6, [3]Institute for Quantum Computing, University of Waterloo, Waterloo, Ontario, Canada N2L3G1, [4]Régroupement Québécois sur les Matériaux de Pointe, Université de Sherbrooke, Sherbrooke, Québec, Canada J1K2R1*)

A high speed radio-frequency quantum point contact charge detector for time resolved readout applications of spin qubits

Mo-eP121 **Emiliano Cancellieri[1,2], Filippo Troiani[1], Guido Goldoni[3]** (*[1]S3 CNR-INFM, Modena, Italy, Via Campi 213/A, [2]Departamento de Fisica Teorica de la Materia Condensada, Universidad Autonoma de Madrid, C/ Francisco Tomás y Valiente, 7 28049, Spain, [3]Dipartimento di Fisica, Università di Modena e Reggio Emilia, Via Campi 213/A*)

Towards the generation of indistinguishable photons from non-identical artificial molecule

Mo-eP122 **P. K. Pathak[1], Youngnae Lee[2], Kicheon kang[2]** (*[1]Depatment of Physics, Queen's University, Kingston, ON K7L 3N6, Canada, [2]Department of Physics, Chonnam National University, Gwangju 500-757, Republic of Korea*)

High sensitivity charge detection and dephasing in edge state interferometer

Mo-eP123 **C.-W. Sohn[1], T.-U. Rim[1], Y.-H. Jeong[1,2]** (*[1]Department of Electronic and Electrical Engineering, Pohang University of Science and Technology, San 31, Hyoja-Dong, Nam-Gu, Pohang, Gyeongbuk 790-784, Korea, [2]National Center for Nanomaterials Technology, Pohang, Gyeongbuk*)

Two-dimensional device model for staggered-type organic thin-film transistors

Mo-eP124 **A. Kumagai, T. Osada, T. Konoike, K. Uchida** (*Institute for Solid State Physics, University of Tokyo, 5-1-5 Kashiwanoha, Kashiwa, Chiba 277-8581, Japan*)

High-Electric-Field Angle-Dependent Magnetotransport and Electronic Structure in Quasi-Two-Dimensional Conductors

Mo-eP125 **R. Masutomi[1], A. Sekine[1], K. Sasaki[1], K. Sawano[2], Y. Shiraki[2], T. Okamoto[1]** ([1]*Department of Physics, University of Tokyo, 7-3-1, Hongo, Bunkyo-ku, Tokyo 1130033, Japan,* [2]*Research Center for Silicon Nano-Science, Musashi Institute of Technology, 8-15-1 Todoroki, Setagaya-ku, Tokyo, Japan*)
Cyclotron resonance of two dimensional electrons in a Si quantum well

Mo-eP126 **R. Shindou[1], S. Murakami[2]** ([1]*Condensed Matter Theory Laboratory, RIKEN, 2-1 Hirosawa, Wako, Saitama 351-0198, Japan,* [2]*Department of Physics, Tokyo Institute of Technology, 2-12-1 Ookayama Meguro-ku, Tokyo 152-8551 Japan*)
Non-magnetic disorder effect in Z_2 quantum spin Hall systems

Mo-eP128 **L. J. T. Taskinen[1], R. P. Starrett[1], T. P. Martin[1], A. P. Micolich[1], A. R. Hamilton[1], M. Y. Simmons[1], D. A. Ritchie[2], M. Pepper[2]** ([1]*School of Physics, University of New South Wales, Sydney NSW 2052, Australia,* [2]*Cavendish Laboratory, University of Cambridge, Cambridge CB3 0HE, United Kingdom*)
Radio-frequency reflectometry - A fast and sensitive measurement method for 2-Dimensional systems

Mo-eP130 **N. Aoki, K. Matsusaki, T. Yahagi, K. Sudou, Y. Ochiai** (*Graduate School of Advanced Integration Science, Chiba University, 1-33 Yayoi-cho, Inage-ku, Chiba 263-8522, Japan*)
Scanning gate characterization of organic field effect transistor

Mo-eP131 **L. Gaudreau[1,2], S. Studenikin[1], G. Granger[1], J. Kycia[3], P. Mason[3], A. Kam[1], C.Y. Hsieh[1], R. Cheriton[1], M. Korkusinski[1], P.Hawrylak[1], A. Sachrajda[1]** ([1] *Institute for Microstructural Sciences, National Research Council, 1200 Montreal Rd. Bldg. M-50, Ottawa, Ontario K1A 0R6, Canada,* [2]*Physics Department, University of Sherbrooke, Quebec, Canada, J1K 2R1, ,* [3]*Department of Physics and Astronomy, University of Waterloo, Waterloo, Canada, N2L 3G1,*)
Time resolved control of electron tunnelling times and single-shot spin readout in a quantum dot.

Mo-eP132 **L. Smrcka, N. A. Goncharuk** (*Institute of Physics, ASCR, v.v.i., Cukrovarnicka 10, Prague 6, 162 53 , Czech Republic*)
Aperiodic magneto-oscillations in graphite

Mo-eP133 **Z. Wang, P. Gao, X. Bai, D. Chen** (*Beijing National Laboratory for Condensed Matter Physics, Institute of Physics, Chinese Academy of Sciences, Beijing 100080, People's Republic of China*)
An optical and electrical probe inside a TEM

Tuesday July 21st

Session E2 (Main Hall) 9:00 – 10:30 Spin related phenomena

E2a 9:00 – 9:30 **Laurens W. Molenkamp** (Invited) (*Physikalisches Institut (EP3) der Universität Würzburg, Am Hubland, 97074 Würzburg, Germany*)
Spin Hall effects in HgTe Quantum Well Structures

E2b 9:30 – 9:45 **H. Saarikoski**[1,2,3]**, G. E. W. Bauer**[1] ([1]*Kavli Institute of Nanoscience, Delft University of Technology, 2628-CJ Delft, The Netherlands,* [2]*Mathematical Physics, Lund Institute of Technology, SE-22100 Lund, Sweden,* [3] *Helsinki University of Technology, P.O. Box 4100, FI-02015 HUT, Finland*)

Spin accumulation with spin-orbit interaction

E2c 9:45 – 10:00 **D. A. Vasyukov**[1]**, A. S. Plaut**[1]**, A. H. MacDonald**[2]**, M. Henini**[3]**, L. N. Pfeiffer**[4]**, K. W. West**[4] ([1]*Exeter University , School of Physics, Exeter EX4 4QL, UK,* [2]*The University of Texas at Austin, Department of Physics, Austin Texas 78712, USA,* [3]*University of Nottingham, School of Physics and Astronomy and Nottingham Nanotechnology and Nanoscience Centre, Nottingham NG7 2RD, UK,* [4]*Bell Laboratories, Alcatel-Lucent, Murray Hill, New Jersey, 07974, USA*)

Intrinsic photoinduced anomalous Hall effect

E2d 10:00 – 10:30 **D. Chiba**[1,2,3]**, M. Sawicki**[2,4]**, Y. Nishitani**[2]**, Y. Nakatani**[5]**, T. Ono**[3]**, F. Matsukura**[2,1]**, H. Ohno**[2,1] (Invited) ([1]*Semiconductor Spintronics Project, ERATO, Japan Science and Technology Agency, Japan,* [2]*Laboratory for Nanoelectronics and Spintronics, RIEC, Tohoku University, Japan,* [3]*Institute for Chemical Research, Kyoto University, Japan,* [4]*Institute of Physics, Polish Academy of Sciences, Poland,* [5]*University of Electro-communications, Japan*)

Electric-field manipulation of magnetization vector in (Ga,Mn)As

10:30 – 11:00 **Coffee Break**

Session E3 (Main Hall) 11:00 – 12:30 Optical phenomena

E3a 10:30 – 11:15 **Israel Bar-Joseph** (Invited) (*Weizmann Institute of Science, Rehovot 76100, Israel*)

The exciton Mott transition

E3b 11:30 – 11:45 **M. D. Fraser**[1,2,3]**, M. Kuwata-Gonokami**[2]**, S. Höfling**[5]**, A. Forchel**[5]**, Y. Yamamoto**[3,4] ([1]*Institute for Nano Quantum Information Electronics, University of Tokyo, 4-6-1 Komaba, Meguro-ku, Tokyo 153-8505, Japan,* [2]*Department of Applied Physics, University of Tokyo, 7-3-1 Hongo, Bunkyo-ku, Tokyo 113-8656, Japan,* [3]*National Institute of Informatics, 2-1-2 Hitotsubashi, Chiyoda-ku, Tokyo 101-8430, Japan,* [4]*Edward L. Ginzton Laboratory, Stanford University, Stanford, California 94305-4085, USA,* [5]*Technische Physik, Universität Würzburg, Am Hubland, D-97074 Würzburg, Germany*)

Rotation of a two-dimensional exciton-polariton condensate

E3c 11:45 – 12:00 **A. Amo**[1]**, D. Sanvitto**[1]**, F.P. Laussy**[1]**, D. Ballarini**[1]**, E. de. Valle**[1]**, M.D. Martin**[1]**, A. Lemaître**[2]**, J. Bloch**[2]**, D.N. Krizhanovskii**[3]**, M. Skolnick**[3]**, C. Tejedor**[1]**, L. Vina**[1] ([1]*Dept. Fisica de Materiales. Universidad Autonoma de Madrid, C/. Francisco Tomas y Valiente 7 E28049, Spain,* [2]*LPN/CNRS, Route de Nozay, 91460, Marcoussis, France,* [3]*Dep. Physics and Astronomy, Univ. of Sheffield, S3 7RH, Sheffield, U.K.*)

Quantum fluid dynamics of a polariton condensate in a semiconductor microcavity

E3d 12:00 – 12:15 **D. Krizhanovskii[1], K.Lagoudakis[2], A.P.D.Love[1], B.Pietka[2], D.M.Whittaker[1], R.A.Bradley[1], K.Guda[1], S.A. Rizeiqi[1], R.Bouchekioua[1], D.Sanvitto[3], P.R.Eastham[5], M.S.Skolnick[1], M.Wouters[2], B.Deveaud-Pledran[2], M.Richard[4], R.Andre[4], L. S. Dang[4]** (*[1]Sheffield University, Dept. Physics and Astronomy, Sheffield S37RH, UK, [2]Ecole Polytechnique Fédérale de Lausanne, CH-1015 Lausanne, Switzerland, [3]3Dep. Fisica de Materiales, Universidad Autonoma de Madrid, 28049 Madrid, Spain, [4]Institut Néel, CNRS and Université J. Fourier, 38042 Grenoble France, [5]Department of Physics, Imperial College, London SW7 2AZ, UK*)

Intrinsic decoherence mechanisms and formation of coexisting polariton condensates in CdTe microcavities

E3e 12:15 – 12:30 **J. Karch[1], P. Olbrich[1], S.A. Tarasenko[2], T. Schoenberger[1], C. Reitmaier[1], Z.D. Kvon[3], S.D. Ganichev[1]** (*[1]Terahertz Center, University of Regensburg, 93040 Regensburg, Germany, [2]A.F. Ioffe Physical-Technical Institute, Russian Academy of Sciences, 194021 St. Petersburg, Russia, [3]Institute of Semiconductor Physics, Russian Academy of Sciences, 630090 Novosibirsk, Russia*)

Observation of the orbital circular photogalvanic effect in quantum-confined structures

12:30 – 14:00 **Lunch Break**

Session E4 (Main Hall) 14:00 – 16:00 Quantum Hall effect and coherent transport

E4a 14:00 – 14:15 **W. K. Hew[1], K. J. Thomas[2], M. Pepper[1], I. Farrer[1], D. Anderson[1], G. A. C. Jones[1], D. A. Ritchie[1]** (*[1]Cavendish Laboratory, University of Cambridge, J. J. Thomson Avenue, Cambridge CB2 1TP, United Kingdom, [2]Dept. of Electronic and Electrical Engineering, Sungkyunkwan University, Suwon 440-746, South Korea*)

Nascent Wigner lattice in quantum wires of shallow confinement

E4b 14:15 – 14:30 **S. Nakamura, M. Hashisaka, Y. Yamauchi, K. Chida, S. Kasai, T. Ono, K. Kobayashi** (*Institutefor Chemical Research, Kyoto University, Gokasho, Uji, Kyoto 611-0011, Japan*)

Shot Noise in a Quantum Point Contact in High Magnetic Fields

E4c 14:30 – 15:00 **L. Tiemann, Y. Yoon, S. Schmult, M. Hauser, W. Dietsche, K. von Klitzing** (*Max-Planck Institute for Solid State Research, Heisenbergstr. 1, 70569 Stuttgart , Germany*)

New aspects of the total filling factor one state

E4d 15:00 – 15:15 **P. Roulleau[1], F. Portier[1], A. Cavanna[2], G. Faini[2], U. Gennser[2], D. Mailly[2], P. Roche[1]** (*[1] Nanoelectronic group, SPEC, CEA-Saclay, F-91191 Gif-Sur-Yvette, France, [2]Phynano team, CNRS, LPN, Route de Nozay, F-91460 Marcoussis, France*)

Dephasing in the IQHE regime

E4e 15:15 – 15:30 **K. Takashina, K. Nishiguchi, Y. Ono, A. Fujiwara, T. Fujisawa, Y. Hirayama, K. Muraki** (*NTT Basic Research Laboratories, NTT Corporation, 3-1, Morinosato Wakamiya, Atsugi-shi, Kanagawa 243-0198, Japan*)
Electron-hole transport in a 40 nm thick silicon slab

E4f 15:30 – 15:45 **P. Giudici[1,2], N. Kumada[1], K. Muraki[1]** ([1]*NTT Basic Research Laboratories,NTT Corporation, , 3-1Morinosato-Wakamiya,Atsugi 243-0198, Japan,* [2]*Institute of Experimental and Applied Physics, Regensburg University, Universitaetstr. 31 93040 Regensburg, Germany*)
Intrinsic gap of the ν_T= 1 bilayer exciton condensate

E4g 15:45 – 16:00 **A. Croxall, K. Da. Gupta, C. A. Nicoll, I. Farrer, H. E. Beere, D. A. Ritchie, M. Pepper** (*Cavendish Laboratory, University of Cambridge, JJ Thomson Avenue, Cambridge CB3 0HE, UK*)
Towards the ground state of an electron-hole bilayer

Poster Session Tu-eP (Meeting Room 501, 502) 16:00–18:00

Tu-eP1 **K. Yamashita, K, Asano, T. Ohashi, T. Ogawa** (*Department of Physics, Osaka University, 1-1 Toyonaka, Osaka , Japan*)
Quantum Condensation in the electron-hole system with density imbalance

Tu-eP2 **T. Köppen[1], D. Franz[1], A. Schramm[2], Ch. Heyn[1], D. Heitmann[1], T. Kipp[1]** ([1]*Institute of Applied Physics, University of Hamburg, Jungiusstr. 11, 20355 Hamburg , Germany,* [2]*Optoelectronics Research Center, Tampere University of Technology, Korkeakoulunkatu 3, 33720 Tampere, Finland*)
Direct excitation of singlet and triplet states in quantum-dot helium by resonant Raman spectroscopy

Tu-eP3 **J. Wakabayashi, S. Wada, N. Okuda** (*Department of Physics, Chuo University, 1-13-27 Kasuga, Bunkyo-ku, Tokyo 112-8551, Japan*)
Magnetoresisitance of two-dimensional electron systems in random magnetic fields with zero mean

Tu-eP4 **E. Räsänen[1], S. Pittalis[2], M. A. L. Marques[3], C. R. Proetto[2], E. K. U. Gross[2]** ([1]*Nanoscience Center, Department of Physics, University of Jyväskylä, P.O. Box 35, FI-40014 University of Jyväskylä, Finland,* [2]*Institut für Theoretische Physik, Freie Universität Berlin, Arnimallee 14, D-14195 Berlin, Germany,* [3]*CNRS, Université Lyon I, Villeurbanne Cedex, UMR 5586, Domaine scientifique de la Doua, F-69622 Villeurbanne Cedex, France*)
Exchange and correlation in two-dimensional systems: Derivation of accurate and practical density functionals

Tu-eP5 **M. Akabori[1,2], T. Q. Trinh[1], M. Kudo[1], Th. Schäpers[2], H. Hardtdegen[2], T. Suzuki[1]** ([1]*Center for Nano Materials and Technology, Japan Advanced Institute of Science and Technology, 1-1, Asahidai, Nomi, Ishikawa 923-1292, Japan,* [2]*Institute of Bio- and Nanosystems (IBN-1), Research Centre Jülich, D-52425 Jülich, Germany*)
Strain-enhanced electron mobility anisotropy and piezoelectric scattering in InGaAs/InP 2DEGs

Tu-eP6 **B. Kaestner[1], C. Leicht[1], V. Kashcheyevs[2,3], T. Weimann[1], K. Pierz[1], H. W. Schumacher[1]** ([1]*Physikalisch-Technische Bundesanstalt, Bundesallee 100, 38116 Braunschweig, Germany,* [2]*Institute for Solid State Physics, University of Latvia, Riga LV-1063, Latvia,* [3]*Faculty of Physics and Mathematics, University of Latvia, Riga LV-1002, Latvia*)

Magnetic field dependent non-adiabatic quantized charge pumping

Tu-eP7 **C. Faugeras[1], M. Orlita[1], J. Kunc[1], S. Deutschlander[1], G. Martinez[1], M. Potemski[1], P.Y. Yu[2], A. Riedel[3], R. Hey[3], K.J. Friedland[3], G. Karczewski[4], T. Wojtowicz[4]** ([1]*LNCMI-CNRS, BP 166 grenoble cedex 9 38042, France,* [2]*Department of Physics, University of California, Berkeley, CA 94720, USA,* [3]*Paul Drude Institute, Hausvogteiplatz 5-7, D-10117 Berlin, Germany,* [4]*Institute of Physics, Polish Academy of Sciences, Al. Lotnikow 32/46, 02-668 Warsaw, Poland*)

Magneto-polarons in quasi two-dimensional electron systems

Tu-eP8 **J.M.S. Orr[1], K.C. Chuang[1], R.J. Nicholas[1], P.D. Buckle[2]** ([1]*Physics Dept, Oxford University, Clarendon Laboratory, Parks Rd, Oxford, UK.,* [2]*QinetiQ, , Malvern UK*)

Resonant coupling effects in InSb quantum well heterostructures

Tu-eP9 **S. Wiedmann[1], G.M. Gusev[2], O.E. Raichev[3], A.K. Bakarov[2], J.C. Portal[1]** ([1]*LNCMI-CNRS / INSA, 25 rue des Martyrs, BP 166, Grenoble cedex 9 38042, France,* [2]*Instituto de Física da Universidade de São Paulo, São Paulo, SP, Brazil,* [3]*Institute of Semiconductor Physics, NAS of Ukraine, Kiev, Ukraine,* [4]*Institut Universitaire de France, 103, bd Saint-Michel 75005 Paris, France*)

Microwave induced magnetoresistance oscillations and inelastic scattering time in double quantum wells

Tu-eP10 **G.J. Schinner[1], H.P. Tranitz[2], W. Wegscheider[2], J.P. Kotthaus[1], S. Ludwig[1]** ([1]*CeNS and Department of Physics, University of Munich, Geschwister-Scholl-Platz 1, 80539 Muenchen 80539, Germany,* [2]*Institut fuer Experimentelle und Angewandte Physik, University of Regensburg, 93040 Regensburg, Germany*)

Non-equilibrium interaction of electrons and phonons on the nanoscale

Tu-eP11 **B. PIOT[1], D.K. Maude[1], U. Gennser[2], A. Cavanna[2], D. Mailly[2]** ([1]*Laboratoire National des Champs Magnétiques Intenses, Grenoble High Magnetic Field Laboratory, Centre National de la Recherche Scientifique , 25 Avenue des Martyrs, F-38042 Grenoble, France,* [2] *Laboratoire de Photonique et de Nanostructures, Centre National de la Recherche Scientifique, Route de Nozay, 91460 Marcoussis, France*)

A disordered GaAs 2D electron gas in a strong in-plane magnetic field: Interplay between spin, orbital effects and localization

Tu-eP12 **N. A. J. M. Kleemans[1], J. van Bree[1], A. O. Govorov[2], G. J. Hamhuis[1], R. Nötzel[1], A. Yu. Silov[1], P. M. Koenraad[1]** ([1]*Photonics and Semiconductor Nanophysics, Eindhoven University of Technology, Den Dolech 2, Eindhoven 5600 MB, The Netherlands,* [2]*Department of Physics and Astronomy, Ohio University, Athens, USA*)

Observation of the Mahan exciton in shallow quantum dots strongly coupled to an electron reservoir

Tu-eP13 **L. Tung[1], X.-G. Wu[2], L. N. Pfeiffer[3], K. W. West[3], Y-J. Wang[1,1]** ([1]*National High Magnetic Field Laboratory-FSU, A126 NHMFL-FSU, 1800 E. Paul Dirac Dr., Tallahassee, Florida 32304, USA,* [2]*Chinese Academy of Science, Department of Physics, Institute of Semiconductor, Chinese academy of Science, China,* [3]*Bell Laboratorys, Bell Laboratorys, Lucent Technologies, Murray Hill, New Jersey, USA*)

Unusual cyclotron resonance line broadening in ultra-high mobility two-dimensional electron system

Tu-eP14 **S. R McKibbin[1], W. R. Clarke[1], A. Fuhrer[1], T. C. G. Reusch[2], M. Y. Simmons[1,2]** ([1]*School of Physics, University of New South Wales, Sydney, 2052, Australia,* [2]*Australian Research Council Centre of Excellence for Quantum Computer Technology, Sydney, 2052, Australia*)

3D nanoscale control of doping profiles in silicon

Tu-eP15 **Y. Mitsumori[1,2], Y. Miyahara[1], H. Kosaka[1,2], K. Edamatsu[1]** ([1]*Research Institute of Electrical Communication, Tohoku University, 2-1-1 Katahira, Aoba-ku, Sendai, Miyagi 980-8577, Japan,* [2]*CREST, Japan Science and Technology Agency,*)

Coherent manipulation of an exciton in a single quantum dot using a heterodyne pump-probe technique

Tu-eP16 **D. G. Rees, H. Ikegami, K. Kono** (*Low Temperature Physics Group, RIKEN, 2-1 Hirosawa, Wako, Saitama 351-0198, Japan*)

Transport properties of a quasi-one-dimensional electron system on the surface of liquid helium

Tu-eP18 **K. Takehana[1], Y. Imanaka[1], T. Takamasu[1], M. Henini[2]** ([1]*National Institute for Materials Science, 3-13 Sakura, Tsukuba, Ibaraki 3050003, Japan,* [2]*School of Physics and Astronomy, Nottingham Nanotechnology and Nanoscience Centre, University of Nottingham, Nottingham, UK*)

Cyclotron resonance in 2DES incorporating QD layer

Tu-eP19 **U. Wurstbauer[1], S. Knott[1], C. G. Westarp[1], N. Mecking[1], K. Rachor[1], D. Heitmann[1], W. Wegscheider[2], W. Hansen[1]** ([1], , [2],)

Anomalous magnetotransport and cyclotron resonance of high mobility magnetic 2DHGs in the quantum Hall regime

Tu-eP20 **A.A. Greshnov, G.G. Zegrya** (*Ioffe Physico-technical Institute RAS, 26 Polytekhnicheskaya, St Petersburg 194021, Russia*)

Relevant quantum corrections to conductivity in non-zero magnetic field

Tu-eP21 **K. Yoshizawa, K. Takayanagi** (*Department of Physics, Sophia University, 7-1 Kioi-cho, Chiyoda-ku, Tokyo, Japan*)

Spin density wave in integer quantum Hall systems

Tu-eP22 **Z. Kvon[1], E. B.Olshanetsky[1], D. A. Kozlov[1], N. N. Mikhailov[1], I. O. Parm[1], J. C. Portal[2]** ([1]*Institute of Semiconductor Physics, Lavrentyev's street,13 630090 Novosibirsck, Russia,* [2]*GHMF, MPI-FKF/CNRS , BP-166, F-38042, Grenoble, Cedex 9, France*)

Magnetic field induced 2D excitonic insulator in HgTe QWs

Tu-eP23 **M. Hashisaka[1], A. Helzel[2], S. Nakamura[1], L. Litvin[2], T. Ono[1], H.-P. Traniz[2], W. Wegscheider[2], C. Strunk[2], K. Kobayashi[1]** (*[1]Institute for Chemical Research, Kyoto University, Institute for Chemical Research, Kyoto University, Uji, Kyoto 611-0011, Japan, [2]Institut für experimentelle und angewandte Physik, Universität Regensburg, D-93040, Regensburg, Germany*)
Temperature Dependence of the Visibility in an Electronic Mach-Zehnder Interferometer

Tu-eP24 **I.A. Dmitriev** (*Institute of Nanotechnology, Forschungszentrum Karlsruhe, 76021Karlsruhe, Germany*)
A unified description of nonequilibrium magnetooscillations in high Landau levels

Tu-eP25 **S. Nitta, H. K. Choi, S. Yamada** (*Center for Nano Materials and Technology, JAIST, 1-1, Asahidai, Tatsunokuchi, Nomi, Ishikawa 923-1292 Japan*)
In-plane anisotropic transport in 2DEGs having a strong spin-orbit coupling in InGaAs/InALAs hetero-junctions

Tu-eP26 **A. V. Germanenko[1], N. Kozlova[2], G. M. Minkov[3], O. E. Rut[1], A. A. Sherstobitov[3], J. Freudenberger[2]** (*[1]Department of Physics, Ural State University, Lenin St. 51 620083, Russia, [2]Leibnitz Institute for Solid State and Material Research Dresden, IFW Dresden, D-01171 Dresden, Germany, [3]Institute of Metal Physics RAS, 620219 Ekaterinburg, Russia*)
g-Factor of low mobility 2D GaAs electron gas as determined from high magnetic field experiments

Tu-eP27 **N. A. Goncharuk, J. Kucera, L. Smrcka** (*Institute of Physics of the AS CR, v. v. i., Cukrovarnicka 10, Prague 16200, Czech Republic*)
The pre-edge XANES study of substitutional and interstitial Mn impurities in (Ga,Mn)As

Tu-eP28 **R. Shimabukuro, K. Nakamura, T. Akiyama, T. Ito** (*Department of Physics Engineering, Mie University, 1577 Kurima-Machiya, Tsu, Mie 5148507, Japan*)
Electric field effects on magnetocrystalline anisotropy in ferromagnetic monolayers

Tu-eP29 **N. Nishizako[1], T, Manago[1], S. Ishida[1], H. Geka[2], I. Shibasaki[2]** (*[1]Tokyo University of Science, Yamaguchi, 1-1-1 Daigaku-Dori, Sanyo-Onoda, Yamaguchi 756-0884, JAPAN, [2]Asahi Kasei Co., Ltd., 2-1 Samejima, Fuji, Shizuoka*)
Carrier Density Dependence of Spin-Orbit Interaction in InAsSb Quantum Wells

Tu-eP30 **K. Sadakuni[1], T. Harianto[1], H. Akinaga[2], T. Suemasu[1]** (*[1]Institute of Physics, University of Tsukuba, Tsukuba, Ibaraki 305-8573, Japan, [2]National Institute of Advanced Industrial Science and Technology, Tsukuba, Ibaraki 305-8568, Japan*)
Fabrication of $Fe_3Si/CaF_2/Fe_3Si$ ferromagnetic resonant tunneling diodes on Si(111) by molecular beam epitaxy

Tu-eP31 **H. Kumazaki, D. S. Hirashima** (*Department of Physics, Nagoya University, Furo cho, Chikusa ku, Nagoya. Japan*)
Effect of Vacancies on Magnetism in Graphene

Tu-eP33 **Dustin J. Kreft[1], Max Bichler[2], Robert H. Blick[1]** (*[1]Department of Electrical and Computer Engineering, University of Wisconsin - Madison, 1415 Engineering Drive, Madison, WI, USA, [2]Walter Schottky Institut, Technische Universität München, Garching, Germany*)

Electroacoustic excitation of nanomembranes

Tu-eP34 **M. C. Rogge, R. J. Haug** (*Institut für Festkörperphysik, Leibniz Universität Hannover, Appelstr. 2, 30167 Hannover, Germany*)

Triple quantum dots: two path transport and electrostatic stability diagram

Tu-eP35 **L. Gaudreau[1,2], A. Kam[1], P. Zawadzki[1], S. Studenikin[1], G. Granger[1], J. Kycia[3], J. Mason[3], Z. Wasilewski[1], A. S. Sachrajda[1]** (*[1]Institute for Microstructural Sciences, National Research Council, 1200 Montreal Rd. Bldg. M-50, Ottawa, Ontario K1A 0R6, Canada, [2]Physics Department, University of Sherbrooke, Quebec, Canada, J1K 2R1, , [3]Department of Physics and Astronomy, University of Waterloo, Waterloo, Canada, N2L 3G1,*)

Silencing a 'noisy' AlGaAs/GaAs Wafer

Tu-eP36 **K.-D. Hof[1], F.J. Kaiser[2], S. Kohler[2], D. Schuh[3], W. Wegscheider[3], J.P. Kotthaus[1], A. W. Holleitner[4]** (*[1]Center for NanoScience, Ludwig-Maximilians-Universität, Geschwister-Scholl-Platz 1, 80539 München, Germany., [2]Institut für Physik, Universität Augsburg, 86135 Augsburg, Germany, [3]Institut für Angewandte und Experimentelle Physik II, Universität Regensburg, Universitätsstrasse 31, 93040 Regensburg, Germany., [4]Walter Schottky Institut and Physik-Department, Technische Universität München, Am Coulombwall 3, Garching 85748, Germany*)

Optically induced ballistic electron transport across quantum wires

Tu-eP37 **M. Kataoka, H. Kakemoto, R. P. G. McNeil, C. J. B. Ford, C. H. W. Barnes, D. Anderson, G. A. C. Jones, I. Farrer, D. A. Ritchie** (*Cavendish Laboratory, University of Cambridge, Semiconductor Physics Group, Cavendish Laboratory, J J Thomson Avenue, Cambridge CB3 0HE, United Kingdom*)

Quantised charge pumping by submicrosecond surface-acoustic-wave pulse

Tu-eP38 **L. W. Smith[1], W. K. Hew[1], K. J. Thomas[2], M. Pepper[1], I. Farrer[1], D. Anderson[1], G. A. C Jones[1], D. A. Ritchie[1]** (*[1]Department of Physics, University of Cambridge, Cavendish Laboratory, J. J. Thomson Avenue, Cambridge CB3 0HE, United Kingdom, [2]Department of Electronic and Electrical Engineering, Sungkyunkwan University, Suwon 440-746, South Korea*)

Coupled double row formation in a quasi-one-dimensional wire

Tu-eP39 **T. Hatano[1], T. Kubo[1], S. Amaha[1], S. Teraoka[1], Y.Tokura[1,2], S. Tarucha[1,3]** (*[1]Quantum Spin Information Project, ICORP, JST, Atsugi-shi, Kanagawa 243-0198, Japan, [2]NTT Basic Research Laboratories, NTT Corporation, Atsugi-shi, Kanagawa 243-0198, Japan, [3]Department of Applied Physics, Univ. of Tokyo, Hongo, Bunkyo-ku, Tokyo 113-8656, Japan*)

Phases and periods of Aharonov-Bohm oscillations in parallel coupled double quantum dot

Tu-eP40 **O. Göktaş, Jürgen Weis, Klaus von Klitzing** (*Max Planck Institute for Solid State Research, Heisenbergstr. 1, D-70569, Stuttgart , Germany*)

Observation of a zero bias anomaly and single-electron charging in submicron GaAs/AlGaAs Corbino devices

Tu-eP41 **Y. Chen, C. Chao, S. Huang, S. Cheng** (*Department of Electrophysics, National Chiao-Tung University, EF458, Engineering Building VI, No 1001, Ta-Hsueh Rd, Hsinchu , Taiwan*)
Singlet-Triplet Transitions in Highly Correlated Nanowire Quantum Dots

Tu-eP42 **H. Kim, N. Kim** (*Department of Physics, Soongsil University, Sangdo 5 dong, Dongjak-ku, Seoul 156-743, Korea*)
Manipulation of Spin Distribution in a Ferromagnetic/non-Magnetic Hybrid-Double-Quantum-Disk Structure

Tu-eP43 **H. Tamura, S. Sasaki** (*NTT Basic Research Laboratories, 3-1 Morinosato-Wakamiya, Atsugi, Kanagawa, 243-0198, Japan*)
Fano-Kondo effect in side-coupled double quantum dot

Tu-eP45 **J. M Särkkä, A. Harju** (*Department of Applied Physics, Helsinki University of Technology, P.O.B. 4100 FI-02015 TKK, Finland*)
Control of two-electron quantum dot by external fields

Tu-eP46 **S. F. Fischer**[1], **S. S. Buchholz**[1], **U. Kunze**[1], **D. Reuter**[2], **A. D. Wieck**[2], **J. P. Bird**[3], **V. Mitin**[3] ([1]*Electronic Materials and Nanoelectronics, Ruhr-University of Bochum, D-44780 Bochum, Germany* , [2]*Applied Solid State Physics, Ruhr-University of Bochum, D-44780 Bochum, Germany* , [3]*Dep. of Electrical Engineering, University at Buffalo, Buffalo, New York 14260-3000, USA*)
Novel observations of the "0.7"-conductance anomaly in etched quantum point contacts with large subband spacings

Tu-eP47 **A. Tagliacozzo**[1,2], **P. Lucignano**[2,3] ([1]*Università di Napoli Federico II, Dipartimento di Scienze Fisiche, Complesso Universitario Monte S.Angelo, Via Cintia, 80125 Napoli , Italy,* [2]*CNR-INFM Coherentia, via Cintia, 80125 Napoli, Italy,* [3]*Scuola Internazionale Superiore di Studi Avanzati (SISSA) , via Beirut 2, 34014 Trieste, Italy*)
Spin-orbit interaction and quantum transport in a quantum dot in a higher spin state

Tu-eP49 **J. C. H. Chen**[1], **O. Klochan**[1], **A. P. Micolich**[1], **A. R. Hamilton**[1], **D. Reuter**[2], **A. D. Wieck**[2] ([1]*Department of Physics, University of New South Wales, Sydney NSW 2052, Australia,* [2]*Angewandte Festkörperphysik, Ruhr-Universität Bochum, D-44780 Bochum, Germany*)
Zeeman spin-splitting anisotropy in ballistic hole quantum wires fabricated on a (100)-oriented AlGaAs/GaAs heterostructure

Tu-eP50 **R. Takahashi**[1,2], **K. Kono**[1,2], **S. Tarucha**[3,4], **K. Ono**[1,5] ([1]*Low temperature physics laboratory, RIKEN, 2-1 Hirosawa Wako, Saitama 351-0198, Japan,* [2]*Department of Physics, Tokyo Institute of Technology, 2-12-1 O-Okayama, Meguro, Tokyo 152-8551, Japan,* [3]*Department of Applied Physics, University of Tokyo, 7-3-1 Hongo, Bunkyo-ku, Tokyo 113-8656, Japan,* [4]*ICORP-JST, Atsugi-shi, Kanagawa 243-0198, Japan ,* [5]*CREST-JST, 4-1-8 Honcho, Kawaguchi, Saitama 332-0012, Japan*)
Electron spin-nuclear spin interaction in a hetero-g-factor double quantum dot in Spin-Blockade region

Tu-eP51 **F. Sfigakis, C. J. B. Ford, T.-M. Chen, I. Farrer, D. A. Ritchie, M. Pepper** (*Cavendish Laboratory, University of Cambridge, J.J. Thomson Avenue, Cambridge CB3 0HE, United Kingdom*)
Evidence of spin gap physics in fully spin-split quantum wires

Tu-eP52 **H. A. Nilsson[1], P. Caroff[1], C. Thelander[1], M. Larsson[1], J. B. Wagner[2], L-E. Wernersson[1], L. Samuelson[1], H. Q. Xu[1]** (*[1]Solid State Physics, Lund University, Box 118, S-22100 Lund, Sweden, [2]Division of Polymer and Materials Chemistry/nCHREM, Lund University, Box 124, S-22100 Lund, Sweden*)

Giant, level-dependent g-factors and spin correlations in InSb nanowire quantum dots

Tu-eP53 **S. Kalliakos[1], M. Rontani[2], V. Pellegrini[1], C. P. Garcia[1], A. Pinczuk[3,4], G. Goldoni[2,5], E. Molinari[2,5], L. N. Pfeiffer[4], K. W. West[4]** (*[1]NEST, INFM-CNR and Scuola Normale Superiore, Pisa, Italy, [2]S3 INFM-CNR , Modena, Italy, [3]Appl. Phys. and Appl. Math. and Physics, Columbia University, New York, USA, [4]Bell Laboratories, Alcatel-Lucent, Murray Hill, USA, [5]Dipartimento di Fisica, Università degli Studi di Modena e Reggio Emilia, Modena, Italy*)

Observation of the collective modes of an electron molecule in a quantum dot

Tu-eP54 **M. Bukala, M. Galicka, R. Buczko, P. Kacman** (*Institute of Physics, Polish Academy of Sciences, Al. Lotnikow 32/46, Warsaw 02-668 , Poland*)

Stability of III-V and IV-VI Nanowires - a theoretical study

Tu-eP55 **Akira Oguri[1], Yunori Nisikawa[1], Yoichi Tanaka[2]** (*[1]Graduate School of Science, Osaka City University, Sumiyoshi-ku, Osaka 558-8585, Japan, [2]Condensed Matter Theory Laboratory, RIKEN, Wako, Saitama 351-0198, Japan*)

Ground-state properties of a single Anderson impurity coupled to superconductors

Tu-eP56 **Y. Niimi[1,2], Y. Baines[1], T. Capron[1], D. Mailly[1,3], F.-Y. Lo[1], A. D. Wieck[1], T. Meunier[1], L. Saminadayar[1], C. Bäuerle[1]** (*[1]Institut Néel, CNRS and Université Joseph Fourier, 38042 Grenoble, France, [2]Department of Physics, Tohoku University, Sendai, 980-8578, Japan, [3]Laboratoire de Photonique et Nanostructures, 91460 Marcoussis, France, [4]Lehrstuhl für Angewandte Festkörperphysik, Ruhr-Universität, 44780 Bochum, Germany*)

Effect of disorder on the quantum coherence in mesocopic wires

Tu-eP57 **H. Akera** (*Division of Applied Physics, Graduate School of Engineering, Hokkaido University, Kita 13, Nishi 8, Sapporo 0608628, Japan*)

AC quantum Hall effect and the Hall potential distribution

Tu-eP58 **C. Betthausen[1], A. Vogl[1], V. Kolkovsky[2], G. Karczewski[2], T. Wojtowicz[2], D. Weiss[1]** (*[1]Department of Physics, Regensburg University, Universitaetsstr. 31, Regensburg 93040, Germany, [2]Institute of Physics, Polish Academy of Sciences, Al. Lotnikow 32/46, Warsaw 02-668, Poland*)

Fractional Quantum Hall Effect in CdTe and $Cd_{1-x}Mn_xTe$ high electron mobility Quantum Wells

Tu-eP59 **Z. Ge[1,2], W. Pan[2], D.C. Tsui[1], L.N. Pfeiffer[3], K.W. West[3]** (*[1]Department of Electrical Engineering, Princeton University, Princeton, New Jersey 08544, USA, [2]Sandia National Laboratories, Albuquerque, New Mexico 87185, USA, [3]Bell Laboratories, Alcatel-Lucent Inc., Murray Hill, New Jersey 07974, USA*)

Transition from fractional quantum Hall liquid to pinned Wigner solid in two dimensional charge carrier systems

Tu-eP60 **A. Wójs, G. Möller** (*Cavendish Laboratory, University of Cambridge, J J Thomson Avenue, Cambridge CB3 0HE, UK*)
Numerical search for non-Abelian statistics in fractional quantum Hall systems

Tu-eP61 **W. Lee, S.-H. Sim** (*Department of Physics, Korea Advanced Institute of Science and Technology, Natural Science Building #3310, KAIST, Guseong-dong, Yuseong-gu, Daejeon 305-701, Republic of Korea*)
Coulomb Blockade in an Antidot Molecule in the Integer Quantum Hall Regime

Tu-eP62 **A. Endo[1], N. Shibata[2], Y. Iye[1]** ([1]*Institute for Solid State Physics, University of Tokyo, 5-1-5 Kashiwanoha , Kashiwa, Chiba 2778581, Japan,* [2]*Department of Physics, Tohoku University, 6-3 Aoba, Aoba-ku, Sendai, Miyagi 9808578, Japan*)
Collapse of the fractional quantum Hall state by a unidirectional periodic potential modulation

Tu-eP63 **K. Chida[1], M. Hashisaka[1], Y. Yamauchi[1], S. Nakamura[1], T. Machida[2], T. Ono[1], K. Kobayashi[1]** ([1]*Institute for Chemical Research, Kyoto University, Kyoto, Japan,* [2]*Institute of Industrial Science, University of Tokyo, Tokyo, Japan*)
Non-equilibrium Noise Induced by the Breakdown of the Quantum Hall Effect

Tu-eP64 **C. Altimiras, H. le Sueur, A. Cavanna, U. Gennser, D. Mailly, F. Pierre** (*CNRS, Laboratoire de Photonique et de Nanostructures (LPN) - Phynano Team, route de Nozay, 91460 Marcoussis, France*)
Energy relaxation along edge channels in the integer quantum Hall regime

Tu-eP66 **S. Schmult, L. Tiemann, W. Dietsche, K. von Klitzing** (*Max-Planck-Insitute for Solid State Research, Heisenbergstr. 1, Stuttgart 70569, Germany*)
Two-terminal resistance of an electron bilayer system in the strongly correlated total filling factor 1 state

Tu-eP67 **M. V. Yakunin[1], Anne de Visser[2], Gianni Galistu[2]** ([1]*Institute of Metal Physics, RAS, Ural Branch, S.Kovalevskaya Str.,18 620041, Russia,* [2]*Van der Waals - Zeeman Institute, University of Amsterdam, Valckenierstraat 65, 1018 XE Amsterdam, The Netherlands*)
Specific features of InxGa1-xAs/GaAs double quantum well as manifested in the quantum Hall effect under tilted fields

Tu-eP68 **S. Watanabe[1], G. Igarashi[1], K. Hashimoto[1,3], N. Kumada[2], Y. Hirayama[1,3]** ([1]*Tohoku University, Graduate School of Science Department of Physics, Sendai, Japan,* [2]*NTT Basic Research Laboratories, NTT Corporation, Kanagawa, Japan,* [3]*ERATO Nuclear Spin Electronics Project, Sendai, Japan, Sendai, Japan*)
Spectroscopic study of nuclear magnetic resonance mediated by oscillating electron spin domain walls

Tu-eP69 **K. Kobayashi[1], T. Ohtsuki[1], K. Slevin[2]** ([1]*Department of Physics, Sophia University, Tokyo, Japan,* [2]*Department of Physics, Osaka University, Osaka, Japan*)
Spin-Hall conductance fluctuations in quantum spin-Hall network model

Tu-eP70 **D. Fukuoka[1], T. Nagayama[1], K. Oto[1], K. Muro[1], Y. Hirayama[2,4], N. Kumada[3], H. Yamaguchi[3]** (*[1]Graduate School of Science, Chiba University, 1-33 Yayoi, Inage-ku, Chiba-shi, Chiba 263-8522, Japan, [2]Graduate School of Science, Tohoku University, 6-3 Aramaki-Aza-Aoba, Aoba-ku, Sendai 980-8578 Japan, [3]NTT Basic Research Laboratories, NTT Corporation, 3-1 Morinosato Wakamiya Atsugi-shi, Kanagawa 243-0198 Japan, [4]ERATO Nuclear Spin Electronics Project, 6-3 Aramaki-Aza-Aoba, Aoba-ku, Sendai 980-8578 Japan*)

Spin relaxation mechanism in a quantum Hall ferromagnet

Tu-eP71 **S. Teraoka[1], S. Amaha[1], T. Hatano[1], T. Kubo[1], Y. Tokura[1,2], Y. Ohno[3], H. Ohno[3], S. Tarucha[1,4]** (*[1]Quantum Spin Information Project ICORP-JST, 3-1, Morinosato-Wakamiya, Atsugi, Kanagawa 243-0198, Japan, [2]NTT Basic Research Laboratories, NTT Corporation, 3-1, Morinosato-Wakamiya, Atsugi, Kanagawa 243-0198, Japan, [3]Laboratory for Nanoelectronics and Spintronics, Research Institute of Electrical Communication, Tohoku University, Katahira, Aoba-ku, Sendai, Miyagi 980-8577, Japan, [4]Department of Applied Physics, Graduate School of Engineering, The University of Tokyo, 7-3-1, Hongo, Bunkyo-ku, Tokyo 113-8656, Japan*)

Spin resonance of two dimensional hole system

Tu-eP72 **M. V. Yakunin[1], S. M. Podgornykh[1], N.N. Mikhailov[2], S.A. Dvoretsky[2]** (*[1]Institute of Metal Physics, RAS, Ural Branch, S.Kovalevskaya Str.,18, 620041 Ekaterinburg, Russia, [2]Institute of Semiconductor Physics, RAS, Siberian Branch, Lavrentyev ave., 13, 630090 Novosibirsk, Russia*)

Spin splittings in the n-HgTe/Cd$_x$Hg$_{1-x}$Te quantum well with inverted band structure

Tu-eP73 **G. Gamez, K. Muraki** (*NTT Basic Research Laboratories, 3-1 Morinosato-Wakamiya, Atsugi 243-0198, Japan*)

Spin-related origin of the transport feature at filling factor 7/11

Tu-eP74 **K. -S. Park[1], K. S. Yi[1], K. Moon[2]** (*[1]Department of Physics, Pusan National University, Busan 609-735, Korea, [2]Department of Physics, and IPAP, Yonsei University, Seoul 120-749, Korea*)

Manifestations of Topological Phases on Surface States in Topological Insulators

Tu-eP75 **L. Meza-Montes[1], A. H. Rodriguez[2], S. E. Ulloa[3]** (*[1]Instituto de Física Universidad Autónoma de Puebla, Av. 18 Sur y San Claudio, Edif. 14-B, Cd. Universitaria, Puebla, Pue. 72570, Mexico, [2]Universidad Autónoma de la Ciudad de Mexico, Calzada Ermita-Iztalapa s/n Col. Lomas de Zaragoza C.P. 09620 Del. Iztalapa, Mexico, D.F., Mexico, [3]Dept. Phys. and Astron. Ohio University, Clippinger Res. Labs, Athens, OH 45701 USA*)

Dynamical modulation of exchange interaction in two-electron quantum dot molecules

Tu-eP76 **S. Lamari** (*Department of Physics, University Ferhat Abbas, Pole Universitaire EL Bez, SETIF 19000 DZ, Algeria*)

Rashba-Dresselhaus spin orbit effects in quantum wells

Tu-eP77 **M. Niwa[1], M. Kohda[1,2], Y. Kunihashi[1], J. Nitta[1]** (*[1]Department of Materials Science, Tohoku University, 6-6-02, Aramaki-aza Aoba, Aoba-ku, Sendai, Miyagi 9808579, Japan, [2]PRESTO, Japan Science and Technology Agency, 4-1-8, Honcho, Kawaguchi, Saitama 3320012, Japan*)

In-plane anisotropy of spin relaxation under competition between spin orbit interaction and Zeeman effect in InGaAs/InAlAs narrow wire structures

Tu-eP78 **K. Fujii[1], K. Onishi[2], Y. Hachizawa[2], S. Yamada[3]** ([1]*Faculty of Information Science and Technology, Osaka Institute of Technology, Hirakata, Osaka 573-0196, Japan,* [2]*Graduate School of Science, Osaka University, Toyonaka, Osaka 560-0043, Japan,* [3]*Center for Nano Material and Technology, JAIST, Asahidai, Nomi, Ishikawa 923-1292, Japan*)

Suppression of microwave induced magnetic oscillation by Rashba effect in InGaAs/InAlAs heterostructures

Tu-eP79 **T. Yokoyama, M. Eto** (*Faculty of Science and Technology, Keio Univesity , 3-14-1 Hiyoshi, Kohoku-ku, Yokohama, Kanagawa 223-8522, Japan*)

Spin injection using tunable antidot potential in semiconductor heterostructure with spin-orbit interaction

Tu-eP80 **N. Tang[1], B. Shen[1], K. Han[1], Z. X. Qin[1], G. Y. Zhang[1], X. Q. Shen[2], H. Okumura[2]** ([1]*School of Physics, Peking University, No.5.Yiheyuan Street, Haidian district, Beijing, P.R.China 100871, P. R. China,* [2]*Power Electronics Research Center, National Institute of Advanced Industrial Science and Technology (AIST), Umezono 1-1-1, Central 2, Tsukuba-shi, Ibaraki 305-8568, Japan*)

The Spin Splitting of the Two-dimensional Electron Gas in AlxGa1-xN/GaN Heterostructures

Tu-eP81 **N. T. Bagraev[1], N. G. Galkin[1], W. Gehlhoff[2], L. E. Klyachkin[1], A. M. Malyarenko[1], I. A. Shelykh[3]** ([1]*Ioffe Physical-Technical Institute of RAS, Politekhnicheskaya 26, St. Petersburg, 194021, Russia,* [2]*Institut fuer Festkoerperphysik, Technische Universitaet Berlin, D-10623 Berlin, Germany,* [3]*Polytechnical University, St. Petersburg, 195251, Russia*)

Fractional forms of 0.7 feature

Tu-eP82 **J. Li, L. B. Zhang, Kai Chang** (*SKSLM, Institute of Semiconductors, Chinese Academy of Sciences, Tsinghua East Road No. Jia 35, Beijing 100083, China*)

The topological edge states in semiconductors with inverted band structures

Tu-eP83 **R. L. Kallaher[1], J. J. Heremans[1], N. Goel[2], S. J. Chung[2], M. B. Santos[2]** ([1]*Virginia Tech, Department of Physics, Robeson Hall, Blacksburg, Virginia 24061, USA,* [2]*University of Oklahoma, Department of Physics, Norman, Oklahoma 73019, USA*)

Spin and phase coherence in quasi-1D electron systems under strong spin-orbit interaction

Tu-eP84 **T. Kaneko, M. Koshino, T. Ando** (*Department of Physics, Tokyo Institute of Technology, 2-12-1 Ookayama, Meguro-ku, Tokyo , Japan*)

Effect of spin relaxation in Anderson localization in quantum wires

Tu-eP85 **O. Klochan[1], A.P. Micolich[1], L.H. Ho[1], A.R. Hamilton[1], K. Muraki[2], Y. Hirayama[3]** ([1]*School of Physics, University of New South Wales, Sydney NSW 2052, Australia, ,* [2]*NTT Basic Research Laboratories, 3-1 Morinosato Wakamiya, Atsugi, Kanagawa 243-0198, Japan, ,* [3]*Department of Physics, Tohoku University, 6-3 Aramaki aza Aoba, Aobaku Sendai, Miyagi 980-8578, Japan,*)

The interplay between the confinement and crystallographic anisotropy in ballistic hole quantum wires

Tu-eP86 **X.W.He[1], B. Shen[1], Y.H.Chen[2], K.Han[1], C.M.Yin[1], Q.Zhang[1], F.J.Xu[1], N.Tang[1]** (*[1]School of Physics, Peking University, School of Physics, Peking University, Beijing 100873, P.R.China, [2]Laboratory of Semiconductor Materials Science, Institute of Semicoonductrs, CAS, Laboratory of Semiconductor Materials Science, Institute of Semicoonductrs, CAS, Beijing 100083, China*)

Anomalous CPGE of the 2DEG in AlxGa1-xN/GaN heterostructures at room temperature

Tu-eP87 **T. Otsuka, E. Abe, Y. Iye, S. Katsumoto** (*Institute for Solid State Physics, University of Tokyo, 5-1-5 Kashiwanoha, Kashiwa, Chiba 2778581, Japan*)

Detection of spin polarization in a quantum wire

Tu-eP88 **M. Kohda[1,2], J. Nitta[1]** (*[1]Department of Materials Science, Tohokou University, 6-6-02 Aramaki-aza Aoba, Aoba-ku Sendai, Miyagi 9808579, Japan, [2]PRESTO, Japan Science and Technology Agency, 4-1-8 Honcho, Kawaguchi, Saitama 3320012, Japan*)

Spin dependent current induced by spatial gradient of spin orbit interaction in Y-branch shaped narrow wire structures

Tu-eP89 **Maria Busl[1,1], Rafael Sanchez[1,2], G. Platero[1,1]** (*[1]Instituto de Ciencia de Materiales, CSIC, Cantoblanco,Madrid,28049,Spain, [2]Departement de Physique Theorique, Universite de Geneve , CH-1211 Geneve 4, Switzerland*)

Electron Spin Resonance in Triple Quantum Dots

Tu-eP90 **T. Nakanishi[1], T. Ando[2]** (*[1]National Inst. of Advanced Industrial Sci. and Tech., 1-1-1 Higashi, Tsukuba 305-8565, 3058565, Japan, [2]Department of Physics, Tokyo Institute of Technology, 2–12–1 Ookayama, Meguro-ku, Tokyo 152-8551, Japan*)

Conductance images between two STM probes in carbon nanotubes and graphene

Tu-eP91 **S. Miyamoto[1,2], K. Nishiguchi[1], Y. Ono[1], K. M. Itoh[2], A. Fujiwara[1]** (*[1]NTT Basic Research Laboratories, NTT Corporation, 3-1, Morinosato Wakamiya, Atsugi, Kanagawa, 243-0198, Japan, [2]School of Fundamental Science and Technology, Keio University, 3-14-1, Hiyoshi, Kouhoku, Yokohama, 223-8522, Japan*)

Single-electron activation over an oscillating barrier in silicon nanowire MOSFETs

Tu-eP92 **S. Mikhailov** (*Institute of Physics, University of Augsburg, Universitaetsstr. 1, D-86135, Germany*)

Non-linear electrodynamics of graphene

Tu-eP93 **J. Z. Bernad[1], U. Zuelicke[1], K. Ziegler[2]** (*[1]Massey University, Palmerston North 4442, New Zealand, [2]University of Augsburg, Augsburg, Germany*)

AC transport properties of single and bilayer graphene

Tu-eP94 **T. Oshima, K. Matsuno, H. Suzuura** (*Division of Applied Physics, Graduate School of Engineering, Hokkaido University, Kita 8 Nishi 5, Sapporo, Japan 060-8628, Japan*)

Energy splitting between bright and dark excitons in carbon nanotubes

Tu-eP95 **X. R. Wang[1], Wei Zhu[2], Qin Wei Shi[2]** (*[1]Physics Department, The Hong Kong University of Science and Technology, Clear Water Bay, Hong Kong SAR, China, [2]Hefei National Laboratory for Physical Sciences at Microscale, University of Science and Technology of China, Hefei 230026, China*)

Density of states of Landau subbands in disordered graphene

Tu-eP96 **R. Danneau[1,2,3], F. Wu[1], A. Fay[1], M.F. Craciun[4,5], S. Russo[4,5], M.Y. Tomi[1], J.B. Oostinga[4,6], J. Wengler[1], S. Salmilehto[1], A.F. Morpurgo[4,6], P.J. Hakonen[1]** (*[1]Low Temperature Laboratory, Helsinki University of Technology, Finland, [2]Institut für Nanotechnologie, Forschungszentrum Karlsruhe , Germany, [3]Physikalisches Institut, Universität Karlsruhe, Germany, [4]Kavli Institute of Nanoscience, Delft University of Technology, The Netherlands, [5]Department of Applied Physics, University of Tokyo, Tokyo, Japan, [6]Département de Physique de la Matière Condensée, Université de Genève, Switzerland*)

Shot noise and transport in graphene: from large strips to nanoribbons

Tu-eP97 **D. Yoshioka[1], S. Nakakura[1], Y. Nagai[2]** (*[1]Department of Basic Science, The University of Tokyo, 3-8-1 Komaba, Meguro, Tokyo 153-8902, Japan, [2]Department of Physics, The University of Tokyo, 7-3-1 Hongo, Bunkyo, Tokyo 113-0033, Japan*)

Unexpected current distribution in graphene ribbon with zigzag edges

Tu-eP98 **P. Neugebauer, M. Orlita, C. Faugeras, A.-L. Barra, M. Potemski** (*National High Magnetic Field Laboratory, Grenoble, CNRS, 25 rue des Martyrs, BP166, Grenoble Cedex 9 38042, France*)

How ideal can graphene be?

Tu-eP99 **M. Lafkioti, T. Lohmann, B. Krauss, K. v. Klitzing, J. Smet** (*Max Planck Institute for Solid State Research, Heisenbergstr. 1 70569, Stuttgart, Germany*)

Transport properties of graphene prepared on a hydrophobic self-assembled layer

Tu-eP100 **M. Noro, M. Koshino, T. Ando** (*Department of Physics, Tokyo Institute of Technology, 2-12-1 Ookayama, Meguro-ku, Tokyo 152-8551, Japan*)

Screening properties of monolayer and randomly stacked graphenes

Tu-eP102 **M. Koshino, Y. Arimura, T. Ando** (*Department of Physics, Tokyo Institute of Technology, 2-12-1 Ookayama, Meguro-ku, Tokyo 152-8551, Japan*)

Orbital diamagnetism in non-uniform magnetic fields in graphene

Tu-eP103 **F. Molitor, C. Stampfer, A. Jacobsen, J. Güttinger, S. Hellmüller, T. Ihn, K. Ensslin** (*Solid State Physics Laboratory, ETH Zurich, Schafmattstrasse 16, 8093 Zurich 8093, Switzerland*)

Transport gap in graphene constrictions

Tu-eP104 **D. Chae, T. Lohmann, K. von Klitzing, J. H. Smet** (*Max-Planck-Institute for Solid State Research, Stuttgart 70569, Germany*)

Magnetoconductivity in graphene Corbino devices

Tu-eP105 **S. Motooka[1], Y. Ujiie[1], N. Aoki[1], Y. Ochiai[1], D. K. Ferry[2], J. P. Bird[3]** (*[1]Graduate School of Advanced Integration Science, Chiba University, 1-33 Yayoi, Inage, Chiba 263-8522, Japan, [2]Deapartment of Electrical Engineering, Arizona State University, Tempe, Arizona 85287-5706, USA, [3]Department of Electrical Engineering, University at Buffalo, the State university of New York, Buffalo, NY 14260-1920, USA*)

Quasi-Periodic Conductance Fluctuations in Few-Layer Graphene

Tu-eP106 **M. S. Fairbanks[1], T. P. Martin[2], B. C. Scannell[1], C. A. Marlow[1], S. A. Brown[3], R. P. Taylor[1]** (*[1]Department of Physics, University of Oregon, 1371 E 13th Ave. Eugene, Oregon 97403, USA, [2]School of Physics, University of New South Wales, Sydney, Australia 2052, [3]Department of Physics and Astronomy, University of Canterbury, Christchurch, Private Bag 4800, New Zealand*)

Toward chaotic electron transport in bismuth nanocluster wires

Tu-eP107 **S. Ko[1], Y. Y. Lee[1], M. H. Son[1], M. S. Lee[1], J. H. Oh[1], C. Jeon[2], W. Song[2], C. -Y. Park[2], S. -W. Lee[3], B. H. Park[3], D. Ahn[1]** ([1]*Institute of Quantum Information Processing Systems, University of seoul, Seoul, Korea , Korea,* [2]*BK21 Physics research division and CNNC, Sungkyunkwan University, Suwon, Korea,* [3]*Department of Applied Physics, Konkuk University, Seoul, Korea*)

Transport properties of quantum dot with thermally decomposited graphene

Tu-eP108 **V. Ryzhii[1], M. Ryzhii[1], M.S. Shur[2], V. Mitin[3]** ([1]*Computational Nanoelectronics Laboratory, University of Aizu and Japan Science and Technology Agency, Ikki-machi, Aizu-Wakamatsu 965-8580, Japan,* [2]*Department of Electrical, Electronics, and Systems Engineering, Rensselaer Polytechnic Institute, Troy, New York 12180, USA,* [3]*Department of Electrical Engineering, University at Buffalo, Buffalo, New York, 14260, USA*)

Negative terahertz dynamic conductivity in electrically induced

Tu-eP109 **P. Dietl[1], G. Metalidis[1], D. Golubev[2,1], P. San-Jose[3], E. Prada[3], H. Schomerus[3], G. Schoen[1,2]** ([1]*Institut fuer Theoretische Festkoerperphysik and DFG Center for Functional Nanostructures (CFN), University of Karlsruhe, D-76128 Karlsruhe, Germany,* [2]*Forschungszentrum Karlsruhe, Institut fuer Nanotechnologie, 76021 Karlsruhe, Germany,* [3]*Department of Physics, Lancaster University, Lancaster, LA1 4YB United Kingdom*)

Disorder-induced pseudodiffusive transport in graphene nanoribbons

Tu-eP110 **M. Roy, P. A. Maksym** (*Department of Physics and Astronomy, University of Leicester, University Road, Leicester LE1 7RH, UK*)

Interacting electrons in semiconducting carbon nanotube quantum dots: calculation of the excited states by exact diagonalisation

Tu-eP111 **M. Ferrier[1], M. Monteverde[1], C. Ojeda[1], R. Weil[1], S. Gueron[1], H. Bouchiat[1], J.N. Fuchs[1], D. Maslov[1,2]** ([1]*Laboratoire de physique des solides, CNRS UMR 8502, Orsay University, Universite Paris sud 91405, France,* [2]*University of Florida , Gainesville, FL 32611, USA*)

Transport and electron scattering time in single and bilayer graphene as probes of the nature of impurity scattering.

Tu-eP112 **T. Watanabe[1], H. Karasawa[1], T. Komori[1], M. Suemitsu[1,3], V. Ryzhii[2,3], T. Otsuji[1,3]** ([1]*Research Institute of Electrical Communication, Tohoku University, Sendai, Japan,* [2]*Department of Computer Science and Engineering, University of Aizu, Aizu-Wakamatsu, Japan,* [3]*JST-CREST, Tokyo, Japan*)

Observation of carrier relaxation and recombination dynamics in optically pumped epitaxial graphene heterostructures

Tu-eP113 **J. E Matthews[1], E. A. Hoffmann[1], H. A. Nilsson[2], L. A. Samuelson[2], H. Linke[1,2]** ([1]*Department of Physics and Materials Science Institute, University of Oregon, 1274 University of Oregon, Eugene, OR 97403, United States,* [2]*Solid State Physics/The Nanometer Structure Consortium, Lund University, Box 118, S-221 00 Lund, Sweden*)

Phonon-mediated heat flow in heterostructure nanowires via electron-phonon interaction

Tu-eP114 **G. Giavaras[2], P. A Maksym[1], M. Roy[1]** ([1]*Department of Physics and Astronomy, University of Leicester, Leicester LE1 7RH, UK,* [2]*Department of Materials, Oxford University, Oxford OX1 3PH*)

Electron confinement in single layer graphene quantum dots

Tu-eP115 **J. Guettinger, J. Seif, A. Cappelli, C. Stampfer, K. Ensslin, T. Ihn** (*Solid State Physics Laboratory, ETH Zurich, Schafmattstrasse 16, Zurich 8093, Switzerland*)

Time-resolved single-electron counting in a graphene quantum dot

Tu-eP117 **C. Ojeda, M. Ferrier, S. Gueron, H. Bouchiat** (*Laboratoire de physique des solides,CNRS UMR 8502, Orsay University, Universite Paris sud 91405, France*)

Tuning the proximity effect in a superconductor-graphene-superconductor junction

Tu-eP118 **T. Tanamoto[1], K. Maruyama[2], Y.X. Liu[2], X. Hu[3], F. Nori[2,4]** ([1]*Corporate R and D center, Toshiba Corporation, Saiwai-ku, Kawasaki 212-8582, Japan,* [2]*Advanced Science Institute, The Institute of Physical and Chemical Research (RIKEN), Wako-shi, Saitama 351-0198, Japan,* [3]*Department of Physics, University at Buffalo, SUNY, Buffalo, New York 14260-1500,USA,* [4]*Physics Department, Center for Theoretical Physics, Center for the Study of Complex Systems, The University of Michigan, Ann Arbor, Michigan 48109-1040, USA*)

Efficient purification protocols using iSWAP gates in solid-state qubits

Tu-eP119 **A. L Cantone[1], M. R Buitelaar[1], S. J Chorley[1], C. G Smith[1], J. Fransson[3], J. Warner[2], A. A. R Watt[2], K. Porfyrakis[2], G. A. D Briggs[2]** ([1]*Department of Physics, Cavendish Laboratory, Cambridge University, Cavendish Laboratory, J.J Thomson Avenue CB3 0HE, UK,* [2]*Clarendon Laboratory, Oxford University, Parks Road, OX1 3PH, UK,* [3]*Department of Physics and Material Science, Uppsala University, Uppsala, SE-751 05, Sweden*)

Electronic transport characterization of Sc@C_{82} single walled carbon nanotube peapods

Tu-eP120 **L. R. Schreiber[1], T. Meunier[1], V. Calado[1], F. R. Braakman[1], W. Wegscheider[2], L. M. K. Vandersypen[1]** ([1]*Kavli Institute of NanoScience, Delft University of Technology, Lorentzweg 1, Delft 2628 CJ, The Netherlands,* [2]*Institute for Experimental and Applied Physics, University of Regensburg, Universitaetsstr. 31, 93040 Regensburg, Germany*)

Two-electron spin manipulation by photon assisted tunneling

Tu-eP121 **T. Takakura[1], M. Pioro-Ladrière[2], T. Obata[2], Y. -S. Shin[2], R. Brunner[2], K. Yoshida[2], T. Taniyama[3,4], S. Tarucha[1,2]** ([1]*QPEC and Department of Applied Physics, The University of Tokyo, 7-3-1 Hongo, Bunkyo-ku, Tokyo , 113-8656, Japan,* [2]*Quantum Spin Information Project, ICORP, Japan Science and Technology Agency, Atsugi-shi, Kanagawa, 243-0198, Japan,* [3]*Material and Structures Laboratory, Tokyo Institute of Technology, 4259 Nagatsuta, Yokohama, 226-8503, Japan,* [4]*PRESTO, Japan Science and Technology Agency, 4-1-8 Honcho Kawaguchi, Saitama, 332-0012, Japan*)

Triple quantum dots with micro-magnets for implementing three spin qubits

Tu-eP122 **K. D. Petersson, P. Atkinson, D. Anderson, G. A. C. Jones, D. A. Ritchie, C. G. Smith** (*Cavendish Laboratory, JJ Thomson Avenue, Cambridge CB3 0HE, United Kingdom*)

Semiconductor qubit readout using a resonant circuit

Tu-eP123 **J. Sailer[1], V. Lang[1], G. Abstreiter[1], K. M. Itoh[2], E. E. Haller[3,4], S. Ludwig[5], D. Bougeard[1]** ([1]*Walter Schottky Institut, Technische Universität München, Am Coulombwall 3, 85748 Garching, Germany,* [2]*Department of Applied Physics and Physico-Informatics, Keio University, 3-14-1, Hiyoshi, Kohoku-ku, Yokohama 223-8522, Japan,* [3]*Lawrence Berkeley National Laboratory, Materials Sciences Division, Berkeley, CA 94720-8197, USA,* [4]*Department of Materials Science and Engineering, University of California at Berkeley, Berkeley, CA 94720-1760, USA,* [5]*Fakultät für Physik and Center for NanoScience, Ludwig-Maximilians-Universität München, Geschwister-Scholl-Platz 1, 80539 München, Germany*)

Nuclear spin engineering and top-gating of 2DES in Si/SiGe

Tu-eP124 **C. H. Lee[1], W. S. Su[1,2], R. B. Chen[3], M. F. Lin[1]** ([1]*Department of Physics, National Cheng Kung University, 1 Ta-Hsueh Road. Tainan 70101, Taiwan,* [2]*Center for General Education, Tainan University of Technology, 529 Jhongjheng Rd., Yongkang, Tainan 71002, Taiwan ,* [3]*Center of General Education, National Kaohsiung Marine University, 142 Haijhuan Rd., Nanzih District, Kaohsiung City 81143, Taiwan*)

Low-Energy Electronic Properties of Ribbon-Graphene Hybrid Systems

Tu-eP125 **Y. H. Ho[1,2], Y. H. Chiu[2], J. M. Lu[3], M. F. Lin[2]** ([1]*Department of Physics, National Sun Yat-Sen University, No. 70, Lienhai Road, Kaohsiung City 80424, Taiwan,* [2]*Department of Physics, National Cheng Kung University, No. 1, Dasyue Road., Tainan City 70101, Taiwan,* [3]*National Center for High-Performance Computing, No. 28, Nanke 3rd Road., Sinshih Township, Tainan County 74147, Taiwan*)

Low-energy electronic structures of nanotube-graphene hybrid carbon systems

Tu-eP126 **Chiduru Watanabe[1], Yoshiyuki Ono[2]** ([1]*Information Technology Education Center, Tokai University, Hiratsuka, Kanagawa, Japan,* [2]*Department of Physics, Toho University, 2-2-1 Miyama, Funabashi, Chiba 2748510, Japan*)

Phonon softening in Peierls transition in an anisotropic triangular lattice

Tu-eP127 **Sungyoul Choi[1], Bong-Jun Kim[1], Yong Wook Lee[2], Jeongyong Choi[1], Hyun-Tak Kim[1]** ([1]*IT-Convergence and Components Lab., Electronics and Tele-Communications Research Institute (ETRI), Daejeon 305-350, Korea,* [2]*School of Electrical and Control Engineering, Pukyong National University, Busan 608-739, Korea*)

Abrupt current jump of epitaxial p-type GaAs thin film

Tu-eP128 **C. Altimiras, H. le Sueur, A. Cavanna, U. Gennser, D. Mailly, F. Pierre** (*CNRS, Laboratoire de Photonique et de Nanostructures (LPN) - Phynano Team, route de Nozay, 91460 Marcoussis, France*)

Non-equilibrium edge channel spectroscopy in the integer quantum Hall regime

Tu-eP129 **M. Abbarchi[1,2], T. Kuroda[2], C. Mastrandrea[1], A. Vinattieri[1], S. Sanguinetti[3], T. Mano[2], N. Koguchi[3], K. Sakoda[2], M. Gurioli[1]** ([1]*Physics department University of Firenze, Via Sansone 1 50019 , ITALY,* [2]*National Institute for Materials Science, 1-1 Namiki, Tsukuba 305-0044, Japan,* [3]*Dipartimento di Scienza dei Materiali, CNISM, Universit'a di Milano-Bicocca, Via Cozzi 53, 20125 Milano, Italy*)

Poissonian excitonic population of single QDs

Tu-eP130 **R.Brunner[1,2], R. Akis[3], Adam Burke[3], R. Meisels[2], F. Kuchar[2], D. K. Ferry[3]** (*[1]Quantum Spin Information Project, ICORP, JST, Atsugi-shi, Kanagawa, 243-0198, Japan, [2]Institute of Physics, University of Leoben, Franz-Josef Strasse 18, A-8700 Leoben, Austria, [3]Dept. of Electrical Engineering and Center for Solid State Electronics Research ,Arizona State University, Tempe, Arizona 85287,USA*)
Indication for Quantum Darwinism in Electron Billiards

Tu-eP131 **N. Aoki[1], A. M. Burke[2], C. R. da Cunha[3], R. Akis[2], D. K. Ferry[2], Y. Ochiai[1]** (*[1]Graduate School of Advanced Integration Science, Chiba University, 1-33 Yayoi-cho, Inage-ku, Chiba 263-8522, Japan, [2]Department of Electrical Engineering and Center for Solid State Electronics Research, Arizona State University, Tempe, Arizona 85287-5706, USA, [3]Department of Electrical Engineering, Universidade Federal do Rio Grande do Sul, Porto Alegre, Rio Grande do Sul 90035-190, Brazil*)
Scanning gate imaging of quantum point contact

Tu-eP132 **M.V.Entin, L. I. Magarill** (*Institute of Semiconductor Physics, Siberian Branch, Russian Academy of Sciences, Novosibirsk, Russia, 13, prospekt Lavrent,eva, Novosibirsk, Russia*)
Photomagnetic effect caused by spin-orbit interaction in 2D system

Tu-eP134 **S. Sakiroglu[1], U. Erkarslan[2], G. Oylumluoglu[2], A. Siddiki[2], I. Sokmen[1]** (*[1]Physics Department, Dokuz Eylül University, Physics Department, Faculty of Arts and Sciences, Dokuz Eylül University, Izmir 35160, Turkey, [2]Physics Department, Mugla University, Physics Department, Faculty of Arts and Sciences, Mugla University, Mugla 48170, Turkey*)
Microscopic theory of the activated behavior of the quantized Hall effect

Wednesday July 22nd

Session E5 (Main Hall) 9:00 – 10:30 Quantum Hall effect II

E5a 9:00 – 9:30 **Chetan Nayak** (Invited) (*Microsoft Station Q and UC Santa Barbara, USA*)
Topological Quantum Computation in the Quantum Hall Regime

E5b 9:30 – 9:45 **M. A. Zudov[1], A. T. Hatke[1], L. N. Pfeiffer[2], K. W. West[2]** (*[1]School of Physics and Astronomy, University of Minnesota, Minneapolis, Minnesota 55455, USA, [2]Bell Labs, Alcatel-Lucent, Murray Hill, New Jersey 07974, USA*)
Role of $e-e$ interactions in magnetoresistance oscillations in 2DES

E5c 9:45 – 10:00 **O. Dial[1], R. Ashoori[1], L. Pfeiffer[2], K. West[2]** (*[1]Massachusetts Institute of Technology, Cambridge, United States, [2]Alcatel-Lucent Bell Laboratories, Murray Hill, United States*)
Tunneling Spectroscopy of Composite Quasiparticles in the Fractional Quantum Hall Effect

E5d 10:00 – 10:15 **A. Fukuda[1], T. Sekikawa[2], K. Iwata[2], Y. Ogasawara[2], T. Arai[3], Z. F. Ezawa[4], A. Sawada[3]** ([1]*Department of Physics, Hyogo College of Medicine, Mukogawacho 1-1, Nishinomiya, Hyogo 663-8501, Japan,* [2]*Graduate School of Science, Department of Physics, Kyoto University, Kyoto 606-8502, Japan,* [3]*Research Center for Low Temperature and Materials Sciences, Kyoto University, Kyoto 606-8501, Japan,* [4]*Theoretical Physics Laboratory, RIKEN, Saitama 351-0198, Japan*)
Activation Energy Gap of the Layer-Imbalanced Bilayer ν=1/3 Quantum Hall States

E5e 10:15 – 10:30 **T. Kawarabayashi[1], Y. Hatsugai[2], H. Aoki[3]** ([1]*Department of Physics, Toho University, Miyama, Funabashi, 274-8510, Japan,* [2]*Institute of Physics, University of Tsukuba, Tennodai, Tsukuba, 305-8571, Japan ,* [3]*Department of Physics, University of Tokyo, Hongo, Tokyo 113-0033, Japan*)
Landau level broadening in graphene with long-range disorder – Robustness of the n=0 level –

10:30 – 11:00 **Coffee Break**

Session Plenary 3,4 (Main Hall) 11:00 – 12:30

PL3 11:00 – 11:45 **Andre Geim** (*Centre for Mesoscience & Nanotechnology, University of Manchester, Oxford Road, Manchester M13 9PL, UK*)
Outlook over graphene flatland

PL4 11:45 – 12:30 **Leaven M.K. Vandersypen** (*Kavli Institute of Nanoscience, Delft University of Technology, Delft, the Netherlands*)
Coherence and control of single electron spins in quantum dots

12:30 – **Optional Excursion**

18:30- **Banquet at "Kachoen"**

"Kachoen" places in front of "Port Island Minami (South)" station, which is two stops from Shimin-hiroba on Port Liner.

Thursday July 23rd

Session E6 (Main Hall) 9:00 – 11:15 **Graphene**

E6a 9:00 – 9:30 **Michael Fuhrer** (Invited) (*University of Maryland, USA*)
Charge Transport in Graphene

E6b 9:30 – 9:45 **S. Das Sarma, E. H. Hwang** (*Department of Physics, University of Maryland, College Park, Maryland 20723, U.S.A.*)
Screening and its consequences in graphene

E6c 9:45 – 10:00 **A. K. Savchenko, F. V. Tikhonenko, A. A. Kozikov, R. V. Gorbachev** (*University of Exeter, School of Physics, Stocker Rd, Exeter EX4 4QL, UK*)
Weak Localisation and Anti-Localisation in Graphene

E6d 10:00 – 10:15 **M. Orlita, C. Faugeras, J. M. Schneider, G. Martinez, D. K. Maude, M. Potemski** (*National High Magnetic Field Laboratory, Grenoble, CNRS, 25 rue des Martyrs, BP166, Grenoble Cedex 9 38042, France*)
Graphite from the viewpoint of Landau level spectroscopy: An effective graphene bilayer and monolayer

E6e 10:15 – 10:30 **M. Koshino, T. Ando** (*Department of Physics, Tokyo Institute of Technology, 2-12-1 Ookayama, Meguro-ku, Tokyo 152-8551, Japan*)
Parallel and perpendicular optical absorptions in bilayer graphene

10:30 – 11:00 **Coffee Break**

E6f 11:00 – 11:15 **S. Russo**[1,2]**, M. F. Craciun**[1]**, M. Yamamoto**[1]**, J. B. Oostinga**[2,3]**, A. F. Morpurgo**[3]**, S. Tarucha**[1,4] (*[1]Department of Applied Physics, The University of Tokyo, 7-3-1,Hongo,Bunkyo-ku,Tokyo 113-8656, Japan, [2]Kavli Institute of Nanoscience, Delft University of Technology, Lorentzweg 1, 2628 CJ Delft, The Netherlands, [3]Department of Condensed Matter Physics, University of Geneva, quai Ernest-Ansermet 24, CH-1211 Geneva 4, Switzerland, [4]Quantum Spin Information Project, ICORP, Japan Science and Technology Agency, Atsugi-shi, 243-0198, Japan*)
Trilayer graphene: a semimetal with gate-tunable band overlap

Session E7 (Main Hall) 11:15 – 12:30

Coherent manipulation of quantum mechanical freedom

E7a 11:15 – 11:45 **Y. Ohno[1], Y. Kondo[1], M. Ono[1], S. Matsuzaka[1,2], H. Sanada[1], K. Morita[2,1], H. Ohno[1,2]** (Invited) ([1]*Laboratory for Nanoelectronics and Spintronics, Research Institute of Electrical Communication, Tohoku University, 2-1-1 Katahira, Aoba-ku, Sendai 980-8577, Japan,* [2]*ERATO Semiconductor Spintronics Project, Exploratory Research for Advanced Technology, Japan Science and Technology Agency, Sanban-cho 5, Chiyouda-ku, Tokyo 102-0075, Japan*)

Multi pulse operation and optical detection of nuclear spin coherence in a quantum well

E7b 11:45 – 12:00 **H. Kiyama[1], T. Fujita[1], G. Allison[1], T. Asayama[1,2], A. Pioda[1], A. Oiwa[1,3], S. Tarucha[1,3,4]** ([1]*Department of Applied Physics, The University of Tokyo, 7-3-1, Hongo, Bunkyo-ku, Tokyo 113-8656, Japan,* [2]*Advanced Materials Laboratories, SONY Corporation, 4-16-1, Okata, Atsugi-shi, Kanagawa, 243-0021, Japan,* [3]*Quantum Spin Information Project, ICORP, JST, 3-1, MOR3-1, Morinosato-Wakamiya, Atsugi-shi, Kanagawa, 243-0198, Japan,* [4]*Institute for Nano Quantum Information Electronics, The University of Tokyo, 4-6-1, Komaba, Meguro-ku, Tokyo 153-8505, Japan*)

Detection of optically injected single electron charge and spin in a quantum dot using a quantum point contact

E7c 12:00 – 12:30 **Hideo Kosaka[1,2], Hideki Shigyou[1], Takahiro Inagaki[1], Yoshiaki Rikitake[3,2], Hiroshi Imamura[4,2], Yasuyoshi Mitsumori[1,2], Keiichi Edamatsu[1]** (Invited) ([1]*Research Institute of Electrical Communication, Tohoku University, Sendai 980-8577, Japan,* [2]*CREST-JST, Saitama 322-0012, Japan,* [3]*Department of Information Engineering, Sendai National College of Technology, Sendai 989-3128, Japan,* [4]*Nanotechnology Research Institute, AIST, Tsukuba 305-8568, Japan*)

Coherent spin injection and spin state tomography by light in a semiconductor quantum well

12:30 – 14:00 **Lunch Break**

Session E8 (Main Hall) 14:00 – 16:00 Electron-environment interaction

E8a 14:00 – 14:30 **T. Ihn, U. Gasser, S. Gustavsson, T. Müller, B. Küng, T. Choi, M. Studer, R. Leturcq, I. Shorubalko, K. Ensslin** (*Solid State Physics Laboratory, ETH Zurich, CH-8093 Zurich, Switzerland*)

Time-resolved charge detection and back-action in quantum circuits

E8b 14:30 – 14:45 **R. Leturcq[1,2], C. Stampfer[1,3], K. Inderbitzin[1], L. Durrer[3], C. Hierold[3], E. Mariani[4], M. G. Schultz[4], F. von Oppen[4], K. Ensslin[1]** ([1]*Laboratory for Solid State Physics, ETH Zurich, 8093 Zurich, Switzerland,* [2]*IEMN, CNRS-UMR 8520, Department ISEN, Cité Scientifique, Avenue Poincaré BP 60069, 59652 Villeneuve d'Ascq, France,* [3]*Micro and Nanosystems, Department of Mechanical and Process Engineering, ETH Zurich, 8092 Zurich, Switzerland,* [4]*Institut für Theoretische Physik, Freie Universitt Berlin, Arnimallee 14, 14195 Berlin, Germany*)

Franck-Condon blockade in suspended carbon nanotube quantum dots

E8c 14:45 – 15:00 **F. Sfigakis[1], S. Sarkozy[2], K. Das Gupta[1], I. Farrer[1], D.A. Ritchie[1], M. Pepper[1]** ([1]*Cavendish Laboratory, University of Cambridge, J.J. Thomson Avenue, Cambridge CB3 0HE, United Kingdom,* [2]*Northrop Grumman Aerospace Systems, One space park, Redondo beach, California 90278, USA*)

Intrinsic nature of the zero-bias anomaly (ZBA) in quantum point contacts

E8d 15:00 – 15:15 **R. P. G. McNeil, M. Kataoka, C. J. B. Ford, C. H. W. Barnes, D. Anderson, G. A. C. Jones, I. Farrer, D. A. Ritchie** (*Cavendish Laboratory, University of Cambridge, Cavendish Laboratory, JJ Thomson Av., Cambridge CB3 0HE, UK*)

Electron transfer between distant quantum dots by surface acoustic waves

E8e 15:15 – 15:30 **C. Mora[1,2], T. Delattre[1,2], C. Feuillet-Palma[1,2], L.G. Herrmann[1,2], P. Morfin[1,2], J.-M. Berroir[1,2], G. Fève[1,2], B. Plaçais[1,2], D.C. Glattli[1,2,3], M.-S. Choi[4], T. Kontos[1,2]** ([1]*Ecole Normale Supérieure, Laboratoire Pierre Aigrain, 24, rue Lhomond, 75231 Paris Cedex 05,* [2]*CNRS UMR 8551, Laboratoire associé aux universités Pierre et Marie Curie et Denis Diderot, France,* [3]*Service de physique de l'état Condensé, CEA, 91192 Gif-sur-Yvette, France,* [4]*Department of Physics, Korea University, Seoul 136-713*)

Noise in Carbon Nanotubes in the Kondo regime

E8f 15:30 – 15:45 **T. Fujii** (*Institute for Solid State Physics, University of Tokyo, Kashiwanoha 5-1-5, Kashiwa, Chiba, Japan*)

Effect of Coulomb interaction for shot noise in a quantum dot

E8g 15:45 – 16:00 **K. Hitachi[1], A. Oiwa[2], S. Tarucha[2]** ([1]*Department of Physics, University of Tokyo, Hongo, Bunkyo-ku, Japan,* [2]*ICORP-JST and Department of Applied Physics, University of Tokyo, Hongo, Bunkyo-ku, Japan*)

Lifting of Coulomb blockade and Kondo effect in a quantum dot by highly-biased nearby a quantum point contact

Poster Session Th-eP (Meeting Room 501, 502) 16:00–18:00

Th-eP1 **D. G. Austing[1,2], C. Payette[1,2], G. Yu[1], J. A. Gupta[1]** (*[1]Institute for Microstructural Sciences M50, NRC, Ottawa, Ontario K1A 0R6, Canada, [2]Department of Physics, McGill University, Montreal, Quebec H3A 2T8, Canada*)

Hysteretic funnel structures in vertical quantum dot molecules

Th-eP2 **J. Kunc[1,2], P. Plochocka[1], K. Kowalik[1], F. J. Teran[1], R. Grill[2], D. K. Maude[1], M. Potemski[1], T. Wojtowicz[3], G. Karczewski[3]** (*[1]1, Laboratoire National des Champs Magnétiques Intenses, Grenoble High Magnetic Field Laboratory, CNRS, 25 avenue des Martyrs, 38042 Grenoble, France, [2]2, Institute of Physics, Charles University, Prague, Czech Republic, [3]3, IFPAN, Warsaw, Poland*)

Quantum Hall effect in CdTe-based quantum wells

Th-eP3 **Y. Yoon[1], M.-G. Kang[1], T. Morimoto[2], L. Mourokh[3], N. Aoki[4], J. L. Reno[5], J. P Bird[1,4], Y. Ochiai[4]** (*[1]Department of Electrical Engineering, University at Buffalo, the State University of New York, Buffalo, NY 14260-1920, USA, [2]Advanced Device Laboratory, RIKEN, 2-1 Hirosawa, Wako, Saitama 351-0198, Japan, [3]Department of Physics, Queens College of CUNY, 65-30 Kissena Blvd., Flushing, NY 11367, USA, [4]Graduate School of Advanced Integration Science, Chiba University, 1-33 Yayoi-cho, Inage-ku, Chiba 263-8522, Japan, [5]CINT Science Department, Sandia National Laboratories, P.O. Box 5800, Albuquerque, NM 87185-1303*)

Detector Backaction on the Self-Consistent Bound State in Quantum Point Contacts

Th-eP4 **H. Chung[1], M. H. Lee[1], C. C. Chang[1], Y. C. Huang[2], M. F. Lin[1]** (*[1]Department of Physics, National Cheng Kung University, 1 Ta-Hsueh Road, Tainan, Taiwan 70101, Taiwan, [2]Center for General Education, Kao Yuan University, No.1821, Jhongshan Rd., Lujhu Township, Kaohsiung County 821, Taiwan*)

Quasi-Landau levels in bilayer zigzag graphene nanoribbons

Th-eP5 **R.B. Chen** (*Center of General Studies, National Kaohsiung Marine University, Kaohsiung 81143, Taiwan, No. 142, Haijhuan Rd., Nanzih District, Kaohsiung City 81143, Taiwan (R.O.C.)*)

Optical excitations of finite double-walled carbon nanotubes under electric field

Th-eP6 **A.D.Guclu, Pawel Potasz, Oleksandr Voznyy, Marek Korkusinski, Pawel Hawrylak** (*Institute for Microstructural Sciences, National Research Council Canada, bldg M-50, 1200 Montreal Rd, Ottawa, K1A0R6, ON Canada*)

Magnetism and Correlations of Fractionally Filled Zero-energy States in Triangular Graphene Quantum Dots

Th-eP7 **A.V. Smorodin, V. A. Nikolaenko, S. S. Sokolov** (*B.Verkin Institute for Low Temperature Physuics and Engineering of the National Academy of Sciences of Ukraine, Ukraine*)

TRANSPORT OF Q1D SURFACE ELECTRONS OVER LIQUID ELIUM IN DENSE VAPOR

Th-eP8 **K. Nakamura, T. Akiyama, T. Ito** (*Department of Physics Engineering, Mie University, 1577 Kurima-Machiya, Tsu, Mie 5148507, Japan*)

Magnetic anisotropy in single metal-phthalocyanine molecules

Th-eP9 **C. H. Ahn, Y. S. Bae, D. C. Kim, Y. Y. Kim, S. K. Mohanta, H. K. Cho** (*School of Advanced Materials Science and Engineering, Sungkyunkwan University, 300 Cheoncheon-dong, Jangan-gu, Suwon, Gyeonggi-do, 440-746, Korea*)

ZnO nanopencils synthesized by thermal evaporation with controlled working pressure

Th-eP10 **Vassilios Vargiamidis[1], Vassilios Fessatidis[2], Makoto Sawamura[3], Norman J. M. Horing[4]** ([1]*Department of Physics, Aristotle University, GR-54124 Thessaloniki, Greece,* [2]*Department of Physics, Fordham University, Bronx, New York 10458, USA,* [3]*MANA, National Institute for Materials Science, Namiki, Tsukuba, Ibaraki, 305-0044, Japan,* [4]*Department of Physics and Engineering Physics, Stevens Institute of Technology, Hoboken, New Jersey 07030, USA*)

Electric field effect on the Fano resonance in quantum wires

Th-eP11 **D. Takahashi, H. Ikegami, K. Kono** (*Low Temperature Physics Lab., RIKEN, 2-1 Hirosawa, Wako, Saitama 351-0198, Japan*)

Nonlinear transport of two-dimensional positive ions below surface of superfluid 4He

Th-eP12 **A. Castro[1], E. Räsänen[2], C. A. Rozzi[3]** ([1]*Institut für Theoretische Physik and European Theoretical Spectroscopy Facility, Freie Universität Berlin, Arnimallee 14, D-14195 Berlin, Germany,* [2]*Nanoscience Center, Department of Physics University of Jyväskylä, FI-40014 Jyväskylä, Finland,* [3]*CNR-INFM National Research Center S3, via Campi 213a, I-41100 Modena, Italy*)

Exact Coulomb cutoff technique in two dimensions

Th-eP13 **S. J. Angus[1], A. J. Ferguson[2]** ([1]*Department of Physics, University of Melbourne, School of Physics (David Caro Building), The University of Melbourne, VIC 3010, Australia,* [2]*Department of Physics, Cavendish Laboratory, JJ Thomson Ave, Cambridge CB3 0HE, U. K.*)

Single electron detection using the silicon radio-frequency single electron transistor (rf-SET)

Th-eP14 **C. H. Wen[1], J. H. Hsiao[1], T. M. Hong[1], K. T. Lin[1], J. C. Chen[1], T. Ueda[2], S. Komiyama[2]** ([1]*Department of Physics, National Tsing Hua University, Hsinchu 30043, Taiwan, Republic of China,* [2]*Department of Basic Science, University of Tokyo, Komaba 3-8-1, Meguro-ku, Tokyo 1538902, Japan*)

Resonance conductance in a quantum point contact with a tunable barrier potential

Th-eP15 **H. Ikegami, H. Akimoto, K. Kono** (*RIKEN, Wako, Saitama, Japan*)

Crystallization of electrons on liquid helium in channel geometry

Th-eP16 **Fernando Sanchez, V. Sanchez** (*Departamento de Fisica, Facultad de Ciencias, Universidad Nacional Autonoma de Mexico, Apartado Postal 70-542 04510, Mexico*)

Renormalization approach to electrical conductance of two-dimensional aperiodic lattices

Th-eP17 **G. M Minkov[1,2], A.A.Sherstobitov[1,2], A.V.Germanenko[1,2], O.E.Rut[1,2]** ([1]*1,* , [2],)

Renormalization of electron-electron interaction at conductivity decrease in two-dimensional

Th-eP18 **U. Wurstbauer[1], D. Weiss[2], D. Schuh[2], W. Wegscheider[3,2]** ([1]*Institut of Applied Physics, University of Hamburg, Jungiusstraße 9, D-20355 Hamburg D-20355, Germany,* [2]*Institute for Experimental and Applied Physics, University of Regensburg, Universitätsstraße 31, 93040 Regensburg, Germany,* [3]*Solid State Physics Laboratory, ETH Zurich, Schafmattstr. 16, 8093 Zürich , Switzerland*)

From weak to strong localization in a ferromagnetic high mobility 2DHG

Th-eP19 **S. N. Takeda[1], A. Kuwako[1], M. Morita[1], H. Daimon[1], M. Yoshimaru[2], T. Imamura[2]** ([1]*Graduate School of Materials Science, Nara Institute of Science and Technology, 8916-5, Takayama-cho, Ikoma-shi, Nara 630-0192, Japan,* [2]*Semiconductor Technology Academic Research Center (STARC), 3-17-2, Shin Yokohama,Kohoku-ku,Yokohama 222-0033 Japan*)

In-plane anisotropy of hole subbands in Si p-type inversion layers

Th-eP20 **T. Mochizuki, R. Masutomi, T. Okamoto** (*Depertment of Physics, Faculty of Science, University of Tokyo, Tokyo, Japan*)

Hysteresis in magnetoresistance of InAs surface inversion layers covered with submonolayer of Fe films

Th-eP21 **A. Tsukazaki[1,2], M. Nakano[1], S. Akasaka[3], K. Nakahara[3], A. Kamisawa[3], A. Ohtomo[1], M. Kawasaki[1,4,5]** ([1]*Institute for Materials Research, Tohoku University, 2-1-1 Katahira, Aoba, Sendai 980-8577, Japan,* [2]*PRESTO, Japan Science and Technology Agency, Tokyo, Japan,* [3]*Interdisciplinary Technology RandD Center, ROHM Co. Ltd., Kyoto, Japan,* [4]*WPI Advanced Institute for Materials Research, Tohoku University, 2-1-1 Katahira, Aoba, Sendai 980-8577, Japan,* [5]*CREST, Japan Science and Technology Agency, Tokyo, Japan*)

Transistor operation at MgZnO/ZnO interface by Schottky gating with conducting polymer

Th-eP22 **S. Chen[1], C. Liu[1], A. Eliseev[2], K. Napolsky[2]** ([1]*Department of Materials Science and Engineering, National Cheng-Kung University, No.1, University Road, Tainan, Taiwan,* [2]*Department of Materials Science and Engineering, National Cheng-Kung University, MSU, GSP-3, Leninskiye Gory, Moscow, 119899*)

Synthesis and Characterization of Ni Nanowires by Porous Anodic Alumina Oxide Templates

Th-eP23 **Sanjeev Kumar, Young-Gyo Seo, Gil-Ho Kim** (*Department of Electronic and Electrical Engineering and Sungkyunkwan University Advanced Institute of Nanotechnology, Sungkyunkwan University, Suwon 440-746, Korea*)

Photoconductivity characteristics of ZnO nanoparticles assembled in nanogap electrodes for portable ultraviolet photodetector applications

Th-eP24 **C. Eckhardt, W. Brezna, J. Silvano, O. Bethge, E. Bertagnolli, J. Smoliner** (*Department of Solid State Electronics, Vienna University of Technology, Floragasse 7, 1040 Vienna, Austria, EU 1040, Austria*)

Tip Geometry Effects in Scanning Capacitance Microscopy on GaAs Schottky and MOS-Type Junctions

Th-eP25 **M. Sato[1], K. Miura[1], S. Sugawara[2], N. Tajima[3], Y. Nishio[1], K. Kajita[1], K. Murata[4]** ([1]*Department of Physics,Toho University, 2-2-1 Miyama,Funabashi,Chiba 2748510, Japan,* [2]*The Institute for solid Statephysics,Tokyo University, 5-1-5 Kashiwanoha,Kashiwa,Chiba 2778581, Japan,* [3]*RIKEN(The Institute of Physical and Chemical Research), 2-1 Hirosawa,Wako,Saitama 3510198, ,Japan,* [4]*Department of Material Science,Fac.Sci.,Osaka City University, 3-3-138 Sumiyoshi,Osaka 5588585, Japan*)

Interlayer Hall effect of Zero gap conductor

Th-eP27 **I. I Kaya[1], E. Karabudak[1], M. Hauser[2]** ([1]*Sabanci University, 34956 Istanbul, Turkey,* [2]*Max-Planck-Institute FKF, Stuttgart, Germany*)

Current counterflow due to hot electron injection in two dimensional

Th-eP28 **R. Shen[1], E. Kojima[1], R. Akimoto[2], S. Takeyama[1]** ([1]*Institute for Solid State Physics, University of Tokyo, 277-8581, Kashiwa, Japan,* [2]*AIST, Ultrafast Photonics Devices Laboratory, 305-8568, Ibaraki, Japan*)

Anisotropic exciton and charged exciton dichroic photoluminescence in undoped ZnSe/BeTe type-II quantum wells in magnetic fields

Th-eP29 **A. Bertoni[1], G. Cuoghi[1,2], G. Ferrari[1,3], G. Goldoni[1,2]** ([1]*S3 National Research Center, CNR-INFM , Via Campi 213/A Modena 41100, Italy,* [2]*Dipartimento di Fisica, Università di Modena e Reggio Emilia, Modena, Italy,* [3]*CNISM Unità di Ricerca di Modena, Modena, Italy*)

In search for the geometric potential of curved 2DEGs through coherent electron transport.

Th-eP30 **Srijit Goswami[1], Christoph Siegert[1], Arindam Ghosh[2], Michael Pepper[1], Ian Farrer[1], David A. Ritchie[1]** ([1]*Cavendish Laboratory, University of Cambridge, J.J. Thomson Avenue, Cambridge CB3 0HE, United Kingdom,* [2]*Department of Physics, Indian Institute of Science, Bangalore 560 012, India*)

Zero-field colossal thermopower in mesoscopic two-dimensional electron systems

Th-eP31 **A. Harju, E. Tölö** (*Department of Applied Physics and Helsinki Institute of Physics, Helsinki University of Technology, P.O. Box 4100, 02015 Helsinki University of Technology , Finland*)

Quantum dots around ν=5/2

Th-eP32 **N. Kim[1], M. K. Li[2], T. W. Kang[2]** ([1]*Dept. of Physics, Soongsil University, Dongjak-ku Sangdo-dong, Seoul 156-743, Korea,* [2]*Quantum-Functional Semiconductor Research Center, Dongguk University, Seoul 100-715, Korea*)

Spin selector by hybrid triple barrier resonant tunneling diode

Th-eP33 **B. Hong[1], L. Choi[1], K. Song[1], S. Hwang[1], D. Ahn[2], K. Cho[3], K. Yeo[3], D. Kim[3], G. Jin[3], D. Park[3]** ([1]*Research Center for Time domain Nano-functional Devices and School of Electrical Engineering, Korea University, 5-1 Anam, Sungbuk, Seoul 136-701, Korea , Korea,* [2]*Institute of Quantum Information Processing and Systems, Univ. of Seoul, Dongdaemun, Jeonnong, Seoul 130-743, Korea,* [3]*Semiconductor RandD Center, Samsung Electronics Co., Hwaseong-si Gyeonggi-do, 445-701, Korea*)

Few hole quantum dot characteristics of gate-all-around PMOS silicon nanowire field effect transistors

Th-eP34 **L. Gaudreau**[1,2], **S. Studenikin**[1], **G. Granger**[1], **J. Kycia**[3], **P. Mason**[3], **A. Kam**[1], **C.Y. Hsieh**[1], **R. Cheriton**[1], **M. Korkusinski**[1], **P.Hawrylak**[1], **A. Sachrajda**[1] ([1] *Institute for Microstructural Sciences, National Research Council, 1200 Montreal Rd. Bldg. M-50, Ottawa, Ontario K1A 0R6, Canada,* [2]*Physics Department, University of Sherbrooke, Quebec, Canada, J1K 2R1, ,* [3]*Department of Physics and Astronomy, University of Waterloo, Waterloo, Canada, N2L 3G1,*)

Time resolved control of electron tunnelling times and single-shot spin readout in a quantum dot.

Th-eP35 **Y. Utsumi**[1], **D. S. Golubev**[2], **M. Marthaler**[3], **M. Hettler**[2], **G. Schön**[2,3] ([1]*Institute of Solid State Physics, University of Tokyo, Kashiwa, Chiba 277-8581, Japan,* [2]*Forschungszentrum Karlsruhe, Institut für Nanotechnologie, 76128 Karlsruhe, Germany,* [3]*Insitut für Theoretische Festkörperphysik, Universität Karlsruhe, 76021 Karlsruhe, Germany*)

Fluctuation Theorem in Single-Electron Counting

Th-eP36 **Y.-S. Shin**[1], **M. Pioro-Ladrière**[1,2], **T. Obata**[1], **Y. Tokura**[1,3], **R. Brunner**[1], **T. Kubo**[1], **K. Yoshida**[1], **S. Tarucha**[1,4] ([1]*Quantum Spin Information Project, ICORP, JST, Atsugi-shi, Kanagawa, 243-0198, Japan,* [2]*Departement de Physique, Universite de Sherbrooke, Sherbrooke, Quebec, J1K-2R1, Canada,* [3]*NTT Basic Research Laboratories, NTT Corporation, Atsugi-shi, Kanagawa, 243-0198, Japan,* [4]*Department of Applied Physics, University of Tokyo, Hongo, Bunkyo-ku, Tokyo, 113-8656, Japan*)

Single Electron Spin Addressing by Photon-assisted-tunneling for a Double Quantum Dot Integrated with a Micro-magnet

Th-eP37 **Michihisa Yamamoto**[1,2], **Christopher Bäuerle**[1,3], **Seigo Tarucha**[1] ([1]*Department of Applied Physics and QPEC, University of Tokyo, 3-4-1 Hongo, Bunkyo-ku, Tokyo 113-8656, Japan,* [2]*ERATO-JST, Kawaguchi-shi, Saitama 332-0012, Japan,* [3]*Institut Neel, CNRS, 25, rue des Martyrs, BP 166, 8042 Grenoble, France ,* [4]*ICORP-JST, Kawaguchi-shi, Saitama 332-0012, Japan*)

Full control of a flying charge qubit: detection and control of transmission phase shift by Ramsey interference

Th-eP38 **Y. Yamauchi**[1], **M. Hashisaka**[1], **S. Nakamura**[1], **K. Chida**[1], **S. Kasai**[1], **T. Ono**[1], **R. Leturcq**[2], **K. Ensslin**[3], **D. C. Driscoll**[4], **A. C. Gossard**[4], **K. Kobayashi**[1] ([1]*Institute for Chemical Research, Kyoto University, Gokasho Uji Kyoto 611-0011, Japan,* [2]*IEMN - CNRS, Cité Scientifique, Avenue Poincaré BP 60069, Villeneuve d'Ascq, France,* [3]*Solid State Physics Laboratory, ETH Zürich, CH-8093 Zürich, Switzerland,* [4]*Materials Department, University of California, Santa Barbara, California 93106, USA*)

Observation of the "lobe structure"in the ballistic interferometers

Th-eP39 **Y. Utsumi**[1,1], **K. Saito**[1,1,2] ([1]*Institute for Solid State Physics, University of Tokyo, Kashiwanoha 5-1-5, Kashiwa, Chiba 277-8581, Japan,* [2]*Graduate School of Science, University of Tokyo, Tokyo 113-0033, Japan,* [3]*CREST, Japan Science and Technology (JST), Saitama 332-0012, Japan*)

Fluctuation Theorem in a Quantum Dot Aharonov-Bohm Interferometer

Th-eP40 **S. Amaha**[1], **T. Hatano**[1], **H. Tamura**[2], **S. Teraoka**[1], **T. Kubo**[1], **Y. Tokura**[1,2], **D. G. Austing**[3], **S. Tarucha**[1,4] ([1]*Quantum Spin Information Project, ICORP, JST, Atsugi, Kanagawa 243-0198, Japan,* [2]*NTT Basic Research Laboratories, NTT Corporation, Atsugi, Kanagawa 243-0198, Japan,* [3]*Institute for Microstructural Sciences M50, NRC, Ottawa, Ontario K1A 0R6, Canada,* [4]*Department of Applied Physics, School of Engineering, University of Tokyo, Bunkyo, Tokyo 133-8656, Japan*)

Electronic states in laterally coupled vertical triple quantum dots

Th-eP42 **M. Pala[1], F. R Martins[1], B. Hackens[1], S. Baltazar[1], H. Sellier[1], S. Huant[1], V. Bayot[1]** ([1]*IMEP-LAHC (UMR 5130), INP, Grenoble, France,* [2]*DICE lab, Université Catholique de Louvain, 3 place du levant, Louvain-la-Neuve 1348, Belgium,* [3]*Institut Néel, CNRS, and Université Joseph Fourier, Grenoble, France*)

Scanning gate microscopy on quantum rings: influence of the magnetic field and of charged defects

Th-eP43 **R. Koushik[1], Matthias Baenninger[1,2], Arindam Ghosh[1], H.E.Beere[2], David A.Ritchie[2], Michael Pepper[2]** ([1]*Department of Physics, Indian Institute of Science, Bangalore-560012, Karnataka, India,* [2]*Cavendish Laboratory, University of Canbridge, J.J.Thomson Avenue, Cambridge, UK*)

Differential resistivity noise in low density mesoscopic two-dimensional electron system

Th-eP44 **J. R Prance, C. G. Smith, J. P. Griffiths, S. J. Chorley, D. Anderson, G. A. C. Jones, I. Farrer, D. A. Ritchie** (*Cavendish Laboratory, University of Cambridge, Semiconductor Physics group, Cavendish Laboratory, J. J. Thomson Ave., Cambridge CB3 0HE, UK*)

Cooling a 2D electron gas using quantum dots

Th-eP45 **B. Kueng[1], O. Pfaeffli[1], S. Gustavsson[1], T. Ihn[1], M. Reinwald[2], W. Wegscheider[1], K. Ensslin[1]** ([1]*Solid State Physics Laboratory, ETH Zurich, Zurich , Switzerland,* [2]*Institut fuer Experimentelle und Angewandte Physik, Universität Regensburg, Regensburg, Germany*)

Time-resolved charge detection with cross-correlation techniques

Th-eP46 **Y. F. Lai[1], Y. H. Su[1], C. P. Liu[1], Y. W. Yang[2], L. J. Fan[2]** ([1]*Department of Materials Science and Engineering and Center for Micro/nano Science and Technology, National Cheng Kung University, No.1, Dasyue Rd., East District, Tainan City 701, Taiwan (R.O.C.) , Taiwan,* [2]*National Synchrotron Radiation Research Center, 101 Hsin-Ann Road, Hsinchu, Taiwan 30077*)

Enhanced efficiency in natural dye-sensitized solar cells with surface plasmon resonance by incorporating Au nanoparticles

Th-eP47 **C. Yang, J. Kim, U. Sim, J. Lee, E. Yoon** (*Department of Materials Science and Engineering, Seoul National University, RM 105, Research Institute of Advanced Materials, Seoul National University, Gwanak-gu, Seoul 151-742, Republic of Korea*)

Competitive growth mechanisms of the InAs quantum dots on the $In_xGa_{1-x}As$ layer during the post growth interruption

Th-eP48 **Keun Wook Shin, Hyun-Woo Kim, Euijoon Yoon** (*Seoul National University, RM208 BN104 Shinlim9dong Gwankgu Seoul, South Korea , South Korea*)

The influences of the thickness of low temperature Ge layers on a two-step Ge growth on a Si(100) using UHV-CVD

Th-eP49 **R. Yoshii, M. Eto** (*Fuculty of Science and Technology, Keio University, 3-14-1 Hiyoshi, Kohoku-ku, Yokohama, Kanagawa 223852, Japan*)

Ring-size dependence of Kondo effect in quantum dot embedded in Aharonov-Bohm ring

Th-eP50 **S. Kirino, T. Fujii, K. Ueda** (*Institute for Solid State Physics, University of Tokyo, Kashiwanoha 5-1-5, Kashiwa, Chiba 277-8581, Japan*)

Time-dependent DMRG study on nonlinear transport through quantum dot

Th-eP52 **R. Sakano[1], S. Tarucha[1,2], N. Kawakami[3]** ([1]*Department of Applied Physics, University of Tokyo, 7-3-1, Hongo, Bunkyo, Tokyo 1130033, Japan,* [2]*ICORP JST, Kanagawa, Japan,* [3]*Department of Physics, Kyoto University, Kyoto, Japan*)

Enhanced thermoelectric power of single quantum dot systems at low temperatures: Exact solution analysis

Th-eP53 **Y. Hamamoto, T. Kato** (*Institute for Solid State Physics, University of Tokyo, Kashiwanoha 5-1-5, Kashiwa, Chiba 277-8581, Japan*)

Monte Carlo study of resonant tunneling in a Tomonaga-Luttinger liquid

Th-eP55 **Y. Fu[1], S. Lin[1], M. Tsai[1], H. Lin[2], C. Lin[2], S. Wang[2], S. Cheng[2], W. Chang[2]** ([1]*Department of Electronics Engineering, National Chiao Tung University, 1001 Ta-hsueh road, Hsinchu 300, Taiwan,* [2]*Department of Electrophysics, National Chiao Tung University, 1001 Ta-hsueh road, Hsinchu 300, Taiwan*)

Diamagnetic shift of exciton complexes in InAs quantum dots

Th-eP56 **Masao Arai[1], Yasuhiro Hatsugai[2]** ([1]*Computational Materials Science Center, National Institute for Materials Science, 1-1 Namiki, Tsukuba, Ibaraki 3050031, Japan,* [2]*Institute of Physics, University of Tsukuba, Tsukuba, Ibaraki, 3058571, Japan*)

Numerical study of quantum Hall effects in two-dimensional multi-band system: single- and multi-layer graphene

Th-eP57 **N. Shibata, K. Nomura** (*Department of Physics, Tohoku University, Aoba, Aoba-ku, Sendai 980-8578, Japan*)

Fractional quantum Hall states in single-layer and bilayer graphene

Th-eP58 **E. A. Henriksen[1], P. Cadden-Zimansky[2,3], Z. Jiang[4], L.-C. Tung[2], M. E. Schwartz[3], Y.-J. Wang[2], P. Kim[3], H. L. Stormer[3,5]** ([1]*California Institute of Technology, Pasadena, California, U.S.A.,* [2]*National High Magnetic Field Laboratory, Tallahassee, Florida, U.S.A.,* [3]*Columbia University, New York, New York, U.S.A.,* [4]*Georgia Institute of Technology, Atlanta, Georgia, U.S.A.,* [5]*Bell Labs, Murray Hill, New Jersey, U.S.A.*)

Cyclotron Resonance in Graphene

Th-eP59 **E. Cicek[1], A. I. Mese[1], D. Eksi[1], M. Ulas[1], A. Siddiki[2]** ([1]*Department of Physics, Faculty of Art and Science, Trakya University, Edirne 22030, Turkey,* [2]*Physics Department, Faculty of Arts and Science, Mugla University, Mugla-Kotekli 48170, Turkey*)

Spatial distribution of the incompressible strips at Aharonov-Bohm interferometer

Th-eP60 **N. Paradiso[1], S. Heun[1], S. Roddaro[1], L. N. Pfeiffer[2], K. W. West[2], F. Beltram[1]** ([1]*NEST, CNR-INFM and Scuola Normale Superiore, Piazza San Silvestro 12, Pisa 56127 , Italy,* [2]*Bell Laboratories, Alcatel-Lucent, Murray Hill, New Jersey 07974, USA*)

Selective control of edge channel trajectories by SGM

Th-eP61 **A. Helzel, L. V. Litvin, H. P. Tranitz, W. Wegscheider, C. Strunk** (*Institute for experimental and applied physics, Universitiy of Regensburg, Universitätsstr. 31, 93040 Regensburg , Germany*)

Finite bias visibility and phase in an electronic Mach-Zehnder interferometer

Th-eP62 **K. Slevin[1], T. Ohtsuki[2]** ([1]*Department of Physics, Graduate School of Science, Osaka University, 1-1 Machikaneyama, Toyonaka-shi, Osaka-fu 560-0043, Japan,* [2]*Department of Physics, Sophia University, Kioi-cho 7-1, Chiyoda-ku, 102-8554, Tokyo, Japan*)

Finite size scaling analysis of the Chalker-Coddington model

Th-eP64 **K. Oto[1], R. Inaba[1], T. Yamada[1], Y. Saisyu[1], T. Matsuda[1], K. Muro[1], Y. Hirayama[2,3], N. Kumada[4], H. Yamaguchi[4]** ([1]*Department of Physics, Graduate School of Science, Chiba University, 1-33 Yayoi, Inage, Chiba 263-8522, Japan,* [2]*Graduate School of Science, Tohoku University, Sendai, Miyagi 980-8577, Japan,* [3]*ERATO Nuclear Spin Electronics Project, Miyagi 980-8578, Japan,* [4]*NTT Basic Research Laboratories, NTT Corporation, Atsugi, Kanagawa 243-0198, Japan*)

Imaging of local filling factor in current flowing ν=1 quantum Hall state by scanning Kerr microscope

Th-eP65 **H. Kamata[1,2], T. Ota[1], K. Muraki[1], T. Fujisawa[2]** ([1]*NTT Basic Research Laboratories, 3-1 Morinosato-Wakamiya, Atsugi, Kanagawa 243-0198, Japan,* [2]*Research Center for Low-Temperature Physics, Tokyo Institute of Technology, 2-12-1 Ookayama, Meguro, Tokyo 152-8551, Japan*)

Voltage controlled group velocity of edge magnetoplasmon in the quantum Hall regime

Th-eP66 **K. Ikushima[1,2], D. Asaoka[3], S. Komiyama[3], T. Ueda[3], K. Hirakawa[4]** ([1]*Department of Applied Physics, Tokyo University of Agriculture and Technology, 2-24-16 Naka-cho, Koganei-shi, Tokyo 184-8588, Japan,* [2]*PRESTO, JST, 4-1-8 Honcho Kawaguchi, Saitama, Japan,* [3]*Department of Basic Science, University of Tokyo, Tokyo, Japan,* [4]*Institute of Industrial Science, University of Tokyo, Tokyo, Japan*)

Manipulating terahertz photons on a quantum Hall effect device

Th-eP67 **Ugur Erkarslan, Gorkem Oylumluoglu, Afif Siddiki** (*Department of Physics, Mugla University, Faculty of Arts and Sciences, Kotekli, Mugla, 48170, TURKEY*)

Edge to bulk transition of the IQHE at cleaved edge overgrown samples: an interaction based experimental proposal

Th-eP68 **G. Bilgec[1], H. Toffoli[2], A. Siddiki[3], I. Sokmen[1]** ([1]*Dokuz Eylül University, Physics Department, Dokuz Eylül University,Physics Department, Faculty of Arts and Sciences, Izmir 35100, Turkey,* [2]*Middle East Technical University, Physics Department, Middle East Technical University, Physics Department, Ankara, 06531, Turkey,* [3]*Mugla University, Physics Department, Mugla University, Physics Department, Faculty of Arts and Sciences, 48170-Kotekli, Mugla, Turkey*)

Calculation of odd integer quantized Hall plateaus due to exchange enhancement of Landé g* factor under experimental conditions

Th-eP70 **K. Fujita, A. Endo, S. Katsumoto, Y. Iye** (*Institute for Solid State Physics, University of Tokyo, 5-1-5 Kashiwanoha, Kashiwa, Chiba 2778581, Japan*)

Measurement of diffusion thermopower in the quantum Hall systems

Th-eP71 **Y.Yoon, L.Tiemann, S. Schmult, M. Hauser, W. Dietsche, K. von Klitzing** (*Max-Planck-Institute for Solid State Physics, Heisenbergstr. 1 70569, Germany*)

Importance of interlayer tunneling in Quantum Hall Bilayers at ν_T= 1

Th-eP72 **K. Sasaki[1], R. Masutomi[1], K. Toyama[1], K. Sawano[2], Y. Shiraki[2], T. Okamoto[1]** ([1]*Department of Physics, University of Tokyo, 7-3-1, Hongo, Bunkyo-ku, Tokyo 113-0033, Japan,* [2]*Research Center for Silicon Nano-Science, Musashi Institute of Technology, 8-15-1, Todoroki, Setagaya-ku, Tokyo 158-0082, Japan*)

Landau level crossing and pseudospin phase transitions in Si quantum wells

Th-eP73 **E. Vernek[1,2], N. Sandler[2], S. E. Ulloa[2]** ([1]*Instituto de Fisica, Universidade Federal de Uberlandia, Uberlandia, 38400-902, MG - Brazil,* [2]*Department of Physics and Astronomy, Ohio University, Athens, Ohio 45701, USA*)

Spin filtering in Kondo quantum dots and spin-orbit interaction

Th-eP74 **Y.H. Chen, C.G.Tang, Y. Liu, Z.G.Wang** (*Key Lab. of Semiconductor materials Science, Institute of Semiconductors, Chinese Academy of Sciences, P.O.Box.912, Beijing, P.R.China 100083, P.R.China*)

Anomalous circular photogalvanic effect in GaAs/AlGaAs two-dimensional electron gas

Th-eP75 **K. Hamaya[1,2,3], K. Shibata[1], K. Hirakawa[1,2,5], S. Ishida[6], Y. Arakawa[1,2,6], T. Machida[1,2,5]** ([1]*Institute of Industrial Science, University of Tokyo,, Tokyo, Japan,* [2]*Institute for Nano Quantum Information Electronics, University of Tokyo, Tokyo, Japan,* [3]*Department of Electronics, Kyushu University, Fukuoka, Japan,* [4]*Japan Science and Technology Agency, PRESTO, Kawaguchi, Japan,* [5]*Japan Science and Technology Agency, CREST, Kawaguchi, Japan,* [6]*Research Center for Advanced Science and Technology, University of Tokyo, Tokyo, Japan*)

Electron transport in a Semiconductor-Quantum-Dot Spin Diode

Th-eP77 **Y. Kunihashi[1], M. Kohda[1,2], J. Nitta[1]** ([1]*Department of Materials Science, Tohoku University, Sendai, Japan,* [2] *PRESTO Japan Science and Technology Agency, Saitama, Japan*)

Suppression of spin relaxation due to dimensional confinement and resonant spin-orbit interaction effect

Th-eP78 **S. Z. Denega[1], T. Last[1], J. Liu[1], A. Slachter[1], P. J. Rizo[1], B. J. van Wees[1], D. Reuter[2], A. D. Wieck[2], P. H. M. van Loosdrecht[1], C. H. van der Wal[1]** ([1]*Zernike Institute for Advanced Materials, University of Groningen, Nijenborgh 4, Groningen 9747AG, The Netherlands,* [2]*Laboratory for Solid State Physics, Ruhr-University Bochum, D-44780 Bochum, Germany*)

Anisotropy for spin dephasing in quasi-1D electron ensembles in a GaAs/AlGaAs heterostructure

Th-eP79 **M. Kawamura[1,2,3], M. Ono[1], Y. Hashimoto[4], S. Katsumoto[4,5], T. Machida[1,5]** ([1]*Institute of Industrial Science, University of Tokyo, 4-6-1 Komaba, Meguro, Japan,* [2]*RIKEN, 2-1 Hirosawa, Wako, Japan,* [3]*PRESTO, Japan Science and Technology Agency, 4-1-8 Kawaguchi, Japan,* [4]*Institute for Solid State Physics, University of Tokyo, 5-1-5 Kashiwanoha, Kashiwa, Japan,* [5]*Institute for Nano Quantum Information Electronics, University of Tokyo, 4-6-1 Komaba, Meguro, Japan*)

Nuclear spin polarization in the breakdown regimes of integer and fractional quantum Hall states

Th-eP80 **K. Hosono, A. Takeuchi, G. Tatara** (*Department of Physics, Tokyo Metropolitan University, Minamiohsawa 1-1, Hachioji-shi,Tokyo 192-0397, JAPAN*)

Charge conservation in dynamic inverse spin Hall effect

Th-eP81 **M. Kawamura[1,2,3], T. Yamashita[1], H. Takahashi[1], S. Masubuchi[1], Y. Hashimoto[4], S. Katsumoto[4,5], T. Machida[1,5]** (*[1]Institute of Industrial Science, University of Tokyo, 4-6-1 Komaba, Meguro, Japan, [2]RIKEN, 2-1 Hirosawa, Wako, Japan, [3]PRESTO, Japan Science and Technology Agency, 4-1-8 Kawaguchi, Japan, [4]Institute for Solid State Physics, University of Tokyo, 5-1-5 Kashiwanoha, Kashiwa, Japan, [5]Institute for Nano Quantum Information Electronics, University of Tokyo, 4-6-1 Komaba, Meguro, Japan*)

Strain-induced enhamcement of electric quadrupole splitting in resistively detected NMR spectrum in quantum Hall systems

Th-eP82 **Y. Tokura[1,2], T. Kubo[2], Y. -S. Shin[2], K. Ono[2,3], S. Tarucha[2,4]** (*[1]NTT Basic Research Laboratories, NTT Corporation, 3-1 Wakamiya, Morinosato, Atsugi 2430198, Japan, [2]Quantum Spin Information Project, ICORP, JST, 3-1 Wakamiya, Morinosato, Atsugi 2430198, Japan, [3]Low Temperature Physics Laboratory, RIKEN, Wako-shi, Saitama, 3510198, Japan, [4]Department of Applied Physics, University of Tokyo, Bunkyo-ku, Tokyo 1138656, Japan*)

Quantum spin transport in magnetic-field-engineered nano-structures

Th-eP83 **S. Watanabe[1], S. Sasaki[2], S. Sato[2], M. Nishimori[2], N. Isogai[3], Y. Matsumoto[3]** (*[1]Centre for Advancement of Higher Education, Tohoku University, Japan, [2]Graduate School of Science and Technology, Niigata University, Niigata, Japan, [3]Department of Applied Physics and Physico-Informatics, Keio University, Yokohama, Japan*)

Nuclear-spin detection of magnetic-field gradient in nanostructures

Th-eP84 **R.Brunner[1], M. Pioro-Ladrière[1,2], Y. Tokura[1,3], T. Obata[1], Y.-S. Shin[1], T. Kubo[1], K. Yoshida[1], T. Taniyama[4,5], S. Tarucha[1,6]** (*[1]Quantum Spin Information Project, ICORP, JST, Atsugi-shi, Kanagawa, 243-0198, Japan, [2]Departement de Physique, Universite de Sherbrooke, Sherbrooke, Quebec, J1K-2R1, Canada, [3]NTT Basic Research Laboratories, NTT Corporation, NTT Corporation, Atsugi-shi, 243-0198, Japan, [4]Materials and Structures Laboratory, Tokyo Institute of Technology, 4259 Nagatsuta, Yokohama, 226-8503, Japan, [5]PRESTO, Japan Science and Technology Agency, 4-1-8 Honcho Kawaguchi, Saitama 332-0012, Japan, [6]Department of Applied Physics, University of Tokyo, Hongo, Bunkyo-ku, Tokyo, 113-8656, Japan*)

Coherent Single Electron Manipulation in a Double Quantum Dot Specially Designed for Scalable Qubits

Th-eP86 **J. Swiebodzinski[1], A. L. Chudnovskiy[1], A. Kamenev[2]** (*[1]I. Institut für Theoretische Physik, Universität Hamburg, Jungiusstrasse 9, D-20335 Hamburg, Germany, [2]Department of Physics, University of Minnesota, Minneapolis, Minnesota 55455, USA*)

Spin torque shot noise

Th-eP87 **T. Yoshida, K. Oto** (*Department of Physics, Graduate School of Science, Chiba University, 1-33, Yayoi, Inage, Chiba 263-8522, Japan*)

Graphene-like magneto-oscillations in graphite capacitor

Th-eP88 **K. Bennaceur, F. Portier, P. Roche, C. GLATTLI** (*CEA Saclay, Nanoelectronics Group, SPEC, CEA Saclay, Gif-sur-Yvette F-91191, France*)

Quantum Hall effect in Graphene at large bias current.

Th-eP89 **T. Fukuzawa, M. Koshino, T. Ando** (*Department of Physics, Tokyo Institute of Technology, 2-12-1 Ookayama, Meguro-ku, Tokyo 152-8551, Japan*)
Weak-field Hall effect in graphene calculated in self-consistent Born approximation

Th-eP90 **E. V. Kurganova[1], A. J. M. Giesbers[1], U. Zeitler[1], L. A. Ponomarenko[2], K. S. Novoselov[2], A. K. Geim[2], J. C. Maan[1]** ([1]*IMM, High Field Magnet Laboratory, Radboud University Nijmegen, Toernooiveld 7 , Nijmegen 6525 ED, The Netherlands,* [2]*Department of Physics, University of Manchester, Manchester M13 9PL, United Kingdom*)
Quantum Hall activation gaps in bilayer graphene

Th-eP91 **K. Asano[1], T. Ando[2]** ([1]*Department of Physics, Osaka University, 1-1 Machikaneyama, Toyonaka, Osaka , Japan,* [2]*Department of Physics, Tokyo Institute of Technology, 2-12-1 O-Okayama, Meguro, Tokyo, Japan*)
Approximate validity of Kohn's theorem in cyclotron resonance in graphene

Th-eP92 **J. M. Schneider, M. Orlita, M. Potemski, D. K. Maude** (*Grenoble High Magnetic Field Laboratory, 25 rue des Martyrs, Grenoble 38042 , France*)
Low temperature magneto-transport in graphite interpreted using the Slonczewski–Weiss–McClure band structure calculations

Th-eP93 **J. Guignard[1], W. Poirier[1], F. Schopfer[1], D. C. Glattli[2]** ([1]*Quantum Metrology Group, Laboratoire National de Metrologie et d'Essais (LNE), 29, avenue Roger Hennequin, Trappes 78197, France,* [2]*Service de Physique de l'Etat Condense, CEA, Orme des Merisiers, Gif-sur-Yvette 91191 France*)
Towards quantum Hall effect quantization tests in graphene

Th-eP94 **T. Higashi, N. Shibata** (*Department of Physics, Tohoku University, Aoba, Aoba-ku, Sendai 980-8578, Japan*)
Ground state phase diagram of graphene in a high Landau level

Th-eP95 **K. Shizuya** (*Yukawa Institute for Theoretical Physics, Kyoto University, Kitashirakawa, Sakyo-ku, Kyoto 606-8502, Japan*)
Pseudo-zero-mode Landau levels and pseudospin waves in bilayer graphene

Th-eP96 **K. Nomura[1], S. Ryu[1], M. Koshino[1], C. Mudry[1], A. Furusaki[1]** ([1]*Department of Physics, Tohoku university, Aoba, Aoba-ku, Sendai 980-8578 , Japan,* [2]*Department of Physics, University of California, Berkeley, Berkeley, CA, 94729, USA,* [3]*Department of Physics, Tokyo Institute of Technology, Meguro-ku, Tokyo 152-8551, Japan,* [4]*Condensed Matter Theory Group, Paul Scherrer Institute, CH-5232 Villigen PSI,,* [5]*Condensed Matter Theory Laboratory, RIKEN, Wako, Saitama 351-0198, Japan*)
Quantum transport of massless Dirac fermions in graphene

Th-eP97 **M. Ezawa** (*Department of Applied Physics, University of Tokyo, Hongo 7-3-1, Tokyo, Japan*)
Generation and Manipulation of Spin Current in Graphene Nanodisks

Th-eP98 **A. Secchi[1], M. Rontani[2]** ([1]*CNR-INFM S3 and Dipartimento di Fisica, Università degli Studi di Modena, Modena, Italy,* [2]*CNR-INFM Research Center S3, Modena, Italy*)
Coulomb versus spin-orbit interaction in carbon-nanotube quantum dots

Th-eP99 **S. Masubuchi[1], M. Ono[1], T. Machida[1,2]** ([1]*Institute of Industrial Science, University of Tokyo, 4-6-1 Komaba, Meguro-ku, Tokyo, 153-8505 Japan,* [2]*Institute for Nano Quantum Information Electronics, University of Tokyo, 4-6-1 Komaba, Meguro-ku, Tokyo, 153-8505 Japan*)
Gate-controlled magnetoresistance effect in graphene spin-valve devices

Th-eP100 **Mehdi Zarea, N. P Sandler** (*Dept. of Physics and Astronomy, and Nanoscale and Quantum Phenomena Inst., Ohio University, Clippinger Laboratory, Athens. OH 45701*)
Spin-orbit interactions in graphene and zigzag ribbons

Th-eP101 **S. J. Chorley, M. R. Buitelaar, A. L. Cantone, G. A. C. Jones, C. G. Smith** (*Cavendish Laboratory, University of Cambridge, Cavendish Laboratory, J J Thomson Avenue, Cambridge, CB3 0HE. England*)
Spin blockade and Kondo physics in a carbon nanotube double quantum dot

Th-eP102 **J. Chaste[1], G. Feve[1], T. Kontos[1], J.-M. Berroir[1], D. C. Glattli[1,1], B. Placais[1]** ([1]*Laboratoire Pierre Aigrain, Ecole Normale Superieure, 24, rue Lhomond, Paris 75005, France,* [2]*Servie de Physique de l'Etat Condense, CEA-Saclay, F-91191 Gif-sur-Yvette, France*)
Dynamical properties of single carbon nanotube transistors

Th-eP103 **J. Hwang[1], H. T. Kim[1], D. Ahn[2], S. W. Hwang[1]** ([1]*TiNa and School of Electrical Engineering, 5-1 Anam, Sungbuk, Seoul 136-701, Korea,* [2]*iQUIPS and School of Electrical and Computer Engineering, 90 Jeonnong, Dongdaemoon, Seoul 130-743, Korea*)
Transport properties of guanine nucleotide-conjugated single-wall carbon nanotube field-effect transistor

Th-eP104 **Dong Chan Kim, Cheol Hyoun Ahn, Bo Hyun Kong, Hyung Koun Cho** (*School of Advanced Materials Science and Engineering, Sungkyunkwan University, Korea, 300 Cheoncheon-dong, Jangan-gu, Suwon, Gyeonggi-do*)
Epitaxial growth of vertically aligned MgZnO nanowire/nanowall network structures by MOCVD

Th-eP105 **T. Schuettfort, A. Nish, R.J. Nicholas** (*Physics Department, Oxford University, Clarendon Laboratory, Parks Rd, Oxford OX1 3PU, UK*)
Observation of type II excitons in carbon nanotubes

Th-eP106 **H. Miyazaki[1,2], K. Tsukagoshi[1,2,3], A. Kanda[2,5]** ([1]*AIST, 1-1-1 Higashi, Tsukuba, Ibaraki 305-8562, Japan,* [2]*CREST, JST, Kawaguch, Japan,* [3]*MANA, NIMS, Tsukuba, Japan,* [4]*RIKEN, Wako, Japan,* [5]*Inst. of Physics and TIMS, Univ. of Tsukuba, Tsukuba, Japan*)
Tunable semiconducting state in bilayer graphene

Th-eP108 **J. Berezovsky, R. M. Westervelt** (*Department of Physics, and School of Engineering and Applied Sciences, Harvard University, 9 Oxford St., Cambridge MA 02138, United States*)
Low temperature scanning probe imaging of electronic transport in graphene nanostructures

Th-eP109 **L. Prechtel[1,2], L. Song[2], S. Manus[2], D. Schuh[3], W. Wegscheider[3], A.W. Holleitner[1,2]** ([1]*Walter Schottky Institut and Physik-Department, Technische Universitaet Muenchen, Am Coulombwall, 85748 Garching, Germany,* [2]*Center for NanoScience (CeNS), Ludwig-Maximilians-University, Geschwister-Scholl-Platz 1, 80539 Munich, Germany,* [3]*Institut fuer Angewandte und Experimentelle Physik II, University Regensburg, Universitaetsstrasse 31, 93040 Regensburg, Germany*)
Picosecond Photocurrent Spectroscopy of Carbon Nanotubes

Th-eP110 **C. Faugeras[1], M. Orlita[1], M. Potemski[1], R.R. Nair[2], A. Geim[2]** (*[1]LNCMI-CNRS, BP 166 grenoble cedex 9 38042, France, [2]School of Physics and Astronomy, Schuster Building, University of Manchester, Oxford Road, Manchester M13 9PL, UK*)

Thermal conductivity of a large graphene membrane

Th-eP111 **H.M. Dong[1], W. Xu[1,2], Z. Zheng[1]** (*[1]Key Laboratory of Materials Physics, Institute of Solid State Physics, Chinese Academy of Sciences, Hefei 230031, P.R. China, P.O.Box 1129, Hefei ,Anhui, P.R.China 230031, China, [2]Department of Physics, Yunnan University, Kunming, China, Department of Physics, Yunnan University, Kunming, China*)

Photo-excited carriers and optical conductance and transmission in graphene in the presence of phonon scattering

Th-eP112 **Y. C. Wang[1], Q. Y. Kuo[1], J. M. Lu[2], C. C. Hwang[3]** (*[1]Department of Civil Engineering, National Cheng Kung University, No.1, University Rd., East District, Tainan City 70101, Taiwan, [2]National Center for High-Performance Computing, No. 28, Nanke 3rd Rd., Sinshih Township, Tainan County 74147, Taiwan, [3]Department of Engineering Science, National Cheng Kung University, No.1, University Rd., East District, Tainan City 70101, Taiwan*)

Molecular dynamics study of multi-walled carbon nanotubes under uniaxial loading

Th-eP113 **H. Schmidt, T. Lüdtke, P. Barthold, R. J. Haug** (*Institut für Festkörperphysik, Leibniz Universität Hannover, Appelstr. 2, Hannover 30167, Germany*)

Temperature Dependent Measurements on Two Decoupled Graphene Monolayers

Th-eP114 **T. Lüdtke, R. J. Haug** (*Abteilung Nanostrukturen, Institut für Festkörperphysik, Universität Hannover, Appelstr. 2, Hannover , Germany*)

Local gating of decoupled graphene monolayers

Th-eP115 **K. Sakai, K. Takai, K. Fukui, T. Enoki** (*Department of Chemistry, Tokyo Institute of Technology, 2-12-1, Meguro, Tokyo 152-8552, Japan*)

Investigation of the local electronic structure in the vicinity of the graphene edge by means of scanning tunneling microscopy

Th-eP116 **G. Giavaras[1], J. Wabnig[1], B. W. Lovett[1], J. H. Jefferson[2], G. A. D. Briggs[1]** (*[1]Department of Materials, University of Oxford, Parks Road, Oxford OX1 3PH, UK, [2]QinetiQ, St. Andrews Road, Malvern WR14 3PS, UK*)

A double quantum dot as a magnetic field and spin detector

Th-eP117 **S. Kawabata[1], Y. Asano[2], Y. Tanaka[3], S. Kashiwaya[1]** (*[1]National Institute of Advanced Industrial Science and Technology (AIST), Tsukuba, Japan, [2]Department of Applied Physics, Hokkaido University, Sapporo, Japan, [3]Department of Applied Physics, Nagoya University, Nagoya, Japan*)

Atomic-scale 0-π transition in Josephson junctions through spintronics nanostructures

Th-eP119 **N. Mizuochi[1,2], P. Neumann[3], F. Rempp[3], K. Nakamura[4], H. Watanabe[5], S. Yamasaki[6], F. Jelezko[3], J. Wrachtrup[3]** (*[1]Graduate School of Library, Information and Media Studies, University of Tsukuba, 1-2 Kasuga, Tsukuba-City 305-8550, Japan, [2]PRESTO, JST, 4-1-8 Honcho kawaguchi, Saitama, Japan, [3]Physikalisches Institut, Universität Stuttgart, Pfaffenwaldring 57, D-70550 Stuttgart, Germany, [4]Tokyo Gas Co., Ltd., 3-13-1, Minamisenju, Tokyo, 116-0003, Japan, [5]Diamond Research Center, AIST, Tsukuba Central 2, Tsukuba, 305-8568, Japan, [6]Nanotechnology Research Institute AIST, Tsukuba Central 2, Tsukuba, 305-8568, Japan*)

Coherence of single electron and nuclear spins in Diamond

Th-eP120 **G. L. Khym, K. Kang** (*Department of Physics, Chonnam National University, Gwangju 500-757, Korea*)

Conditional evolution of a charge qubit coupled to a quantum point contact detector

Th-eP121 **T. Osada, S. Sugawara, D. Nakahara, H. Imamura, T. Konoike, K. Uchida** (*Institute for Solid State Physics, University of Tokyo, 5-1-5 Kashiwanoha, Kashiwa, Chiba 277-8581, Japan*)

Negative Interlayer Magnetoresistance and Dirac Fermion Nature in an Layered Organic Conductor and Multilayer Graphite

Th-eP123 **A. Mobius** (*Leibniz Institute for Solid State and Materials Research IFW Dresden, POB 270116, D-01171 Dresden , Germany*)

Indications for a line of continuous phase transitions at finite temperatures connected with the apparent metal-insulator transition in two-dimensional disordered systems

Th-eP124 **A. P Micolich[1], L.H. Ho[1], A.R. Hamilton[1], W.R. Clarke[1], R. Danneau[1], O. Klochan[1], M.Y. Simmons[1], M. Pepper[2], D.A. Ritchie[2]** (*[1]School of Physics, University of New South Wales, Sydney NSW 2052, Australia, [2]Cavendish Laboratory, University of Cambridge, Cambridge CB3 0HE, United Kingdom*)

Ground-plane screening as a probe of the role of long-range Coulomb interactions in the metallic state of a 2D hole system

Th-eP125 **J. Huang[1], J. S. Xia[2], D. C. Tsui[3], L. N. Pfeiffer[3], K. West[3]** (*[1]Taylor University, Department of Physics, Upland, Indiana 46989, USA, [2]University of Florida, Department of Physics, Gainsville, FL, USA, [3]Princeton University, Department of Electrical Engineering, Princeton, NJ 08544, USA*)

Possible Finite Temperature Phase Transition in Strongly Correlated GaAs Two-dimensional Holes in Zero Field

Th-eP127 **P. Liu[1,2], ZZ. Wang[1], WW. Cai[1], DM. Chen[1]** (*[1]Institute of Physics, Chinese Academy of Sciences, Beijing, China, [2]Institute Neeel, CNRS/UJF, Grenoble, France*)

Dielectrophoresis-scanning tunneling microscopy method for electron transport measurement of individual nanowires

Th-eP128 **M. Abbarchi[1,2], T. Kuroda[2], C. Mastrandrea[1], A. Vinattieri[1], S. Sanguinetti[3], T. Mano[2], N. Koguchi[3], K. Sakoda[3], M. Gurioli[1]** (*[1]Physics department University of Firenze, Via Sansone 1 50019 , ITALY, [2]National Institute for Materials Science, 1-1 Namiki, Tsukuba 305-0044, Japan, [3]Dipartimento di Scienza dei Materiali, CNISM, Universit'a di Milano-Bicocca, Via Cozzi 53, 20125 Milano, Italy*)

Fine structure splitting of quantum dot excitons: role of geometry and environment

Th-eP129 **Z. F. Ezawa[1], G. Tsitsishvili[2]** (*[1]Theoretical Physics Laboratory, RIKEN, Saitama 351-0198, Japan, [2]Department of Theoretical Physics, A. Razmadze Mathematical Institute, Tbilisi, 380093 Georgia*)

Skyrmion and Bimeron Excitations in Bilayer Quantum Hall Systems

Th-eP130 **G.M. Gusev[1], S. Wiedmann[2], A.K. Bakarov[3], J.C. Portal[2]** (*[1]Instituto de Fisica da Universidade de São Paulo, São Paulo, SP, Brazil, [2]LNCMI-CNRS / INSA, 25 rue des Martyrs, BP 166, Grenoble cedex 9 38042, France, [3]Institute of Semiconductor Physics, Novosibirsk, Russia, [4]Institut Universitaire de France, 103, bd Saint-Michel 75005 Paris, France*)

Fractional quantum Hall effect in trilayer systems in a tilted magnetic field

Th-eP131 **K. D. Moiseev[1], V. A. Berezovets[1,2], M. P. Mikhailova[1], V. I. Nizhankovskii[2], R. V. Parfeniev[1]** (*[1]Ioffe Physical-Technical Institute RAS, 26 Politekhnicheskaya street, St Petersburg 194021, Russia, [2]International Laboratory of High Magnetic Fields and Low Temperatures, Wroclaw, Poland*)

Spin-related electron transport in a single type II broken-gap heterojunction doped with Mn

Th-eP132 **T. Kato, S. Onari, J. Inoue** (*Department of Applied Physics, Nagoya University, Furo-cho, Chikusa-ku, Nagoya , Aichi 4648603, Japan*)

Spin Hall effect in a curved graphene with spin-orbit interaction

Th-eP133 **T. Inagaki[1], H. Kosaka[1,2], Y. Rikitake[3,2], H. Imamura[4,2], Y. Mitsumori[1,2], K. Edamatsu[1]** (*[1]Research Institute of Elecrtical Communication, Tohoku University, Sendai, Japan, [2]CREST-JST, Saitama, Japan, [3]Department of Information Engineering, Sendai National College of Technology, Sendai, Japan, [4]Nanotechnology Research Institute, AIST, Tsukuba, Japan*)

Optical measurement of electron spin coherence in a semiconductor quantum well

Th-eP134 **E. Alcobi, Y. Oreg** (*Department of condensed matter physics, Weizmann Institute of Science, Rehovot Israel 76100*)

Decoherence in adiabatic passage

Th-eP135 **Z. L. Liao, Z. Z. Wang, D. M. Chen** (*Institute of Physics, Chinese Academy of Sciences, China*)

Categorization of Resistive Switching of Metal-$Pr_{0.7}Ca_{0.3}MnO_3$-Metal Devices

Th-eP136 **J. Guettinger[1], C. Stampfer[1], F. Libisch[2], T. Frey[1], J. Burgdoerfer[2], T. Ihn[1], K. Ensslin[1]** (*[1]Solid State Physics Laboratory, ETH Zurich, Schafmattstrasse 16, 8093 Zurich, Switzerland, [2]Institute for Theoretical Physics, Vienna University of Technology, Wiedner Hauptstrasse 8-10/136, 1040 Vienna, Austria*)

Electron-hole crossover in graphene quantum dots

Friday July 24th

Session E9 (Main Hall) 9:00 – 10:30 Quantum transport

E9a 9:00 – 9:30 **M. Pioro-Ladriere[1,2], R. Brunner[1], Y. Tokura[1,3,1], T. Obata[1], Y.-S. Shin[1], T. Kubo[1], K. Yoshida[1], T. Taniyama[4], S. Tarucha[5,6]** (Invited) ([1]*Quantum Spin Information Project, ICORP-JST, Atsugi-shi, Kanagawa, 243-0198, Japan,* [2]*Departement Physique,, Universite de Sherbrooke, Sherbrooke, Quebec, J1K-2R1, Canada,* [3]*NTT Basic Research Laboratories, NTT Corporation, Atsugi-shi, 243-0198, Japan,* [4]*Materials and Structures Laboratory, Tokyo Institute of Technology, 4259 Nagatsuta, Yokohama, 226-8503, Japan,* [5]*PRESTO, 4-1-8 Honcho Kawaguchi, Saitama 332-0012, Japan,* [6]*Department of Applied Physics, University of Tokyo, Hongo, Bunkyo-ku, Tokyo, 113-8656, Japan*)

Manipulating single electron spins with micro-magnets

E9b 9:30 – 9:45 **C. Fricke[1], F. Hohls[1], C. Flindt[2], R. J. haug[1]** ([1]*Institut für Festkörperphysik, Leibniz Universität Hannover, Appelstr. 2, 30167 Hannover, Germany,* [2]*Department of Physics, Harvard University, 17 Oxford Street, Cambridge, MA 02138, USA*)

High cumulants in the counting statistics measured for a quantum dot

E9c 9:45 – 10:00 **R.S. Deacon[1], Y. Tanaka[2], A. Oiwa[1,3,4], R. Sakano[1], K. Shibata[5], K. Hirakawa[5,4,6], S. Tarucha[1,3,6]** ([1]*Department of Applied Physics and QPEC, University of Tokyo,* [2]*Condensed matter theory lab, RIKEN,* [3]*ICORP JST, Japan,* [4]*JST CREST, Japan,* [5]*IIS, University of Tokyo,* [6]*INQIE, University of Tokyo,*)

Andreev localized states and Kondo effect in InAs quantum dots contacted with superconducting and normal electrodes

E9d 10:00 – 10:15 **Seok-Chan Youn[1], Hyun-Woo Lee[2], H.-S. Sim[1]** ([1]*Department of Physics, Korea Advanced Institute of Science and Technology, 335 Gwahangno, Yuseong-gu, Daejeon 305-701, Republic of Korea,* [2]*PCTP and Department of Physics, Pohang University of Science and Technology, Pohang, Kyungbuk 790-784, Korea*)

Nonequilibrium Dephasing in an Electronic Mach-Zehnder Interferometer

E9e 10:15 – 10:30 **S. Sasaki[1], H. Tamura[1], S. Miyashita[2], T. Maruyama[2], T. Akazaki[1], T. Fujisawa[3]** ([1]*NTT Basic Research Laboratories, 3-1, Morinosato-Wakamiya, Atsugi, Kanagawa 243-0198, Japan,* [2]*NTT Advanced Technology Corporation , 3-1, Morinosato-Wakamiya, Atsugi, Kanagawa 243-0198, Japan,* [3]*Tokyo Institute of Technology, 2-12-1, Ookayama, Meguro, Tokyo 152-8550, Japan*)

Fano-Kondo interplay in a side-coupled double quantum dot

10:30 – 11:00 **Coffee Break**

Session Plenary 5,6 (Main Hall) 11:00 – 12:30

PL5 11:00 – 11:45 **Susumu Noda** (*Department of Electronic Science and Engineering, Kyoto University, Kyoto 615-8510, Japan*)
Manipulation of Photons by Photonic Crystals

PL6 11:45 – 12:30 **Moty Heiblum** (*Braun Center for Sub Micron Research, Dept. of Condensed Matter Physics, Weizmann Institute of Science, Rehovot 76100, Israel*)
Physics observed through shot noise measurements

12:30 – 13:00 **Closing**

July 20 (Monday)

10:30 – 12:00

Plenary Session 1, 2

Main Hall

EP2DS-MSS Joint session

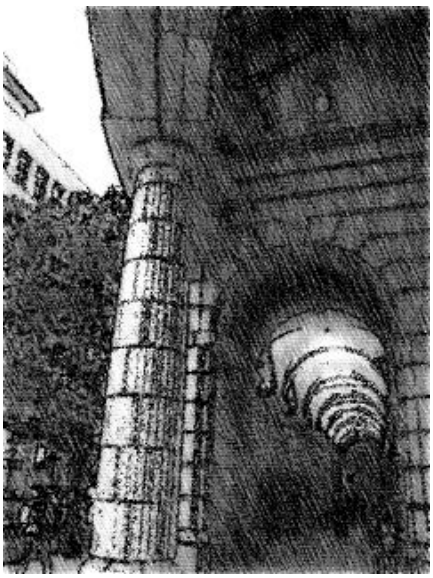

Kobe Daimaru Department Store

Manipulating single spins and coherence in semiconductors

David D. Awschalom

Center for Spintronics and Quantum Computation, University of California, Santa Barbara, CA 93106 USA

Keywords: spintronics, quantum information, quantum dots, diamond

Over eighty years since luminaries such as Pauli and Dirac developed the theory of electron spin, contemporary information technology still relies largely on classical electronics: the charge of electrons for computation and ferromagnets for permanent storage. With the advent of "semiconductor spintronics" and the discovery of long-lived spin coherence in solid state materials, new scientific and technological opportunities have emerged for quantum computing by combining elements of standard electronics with spin-dependent interactions between electrons, nuclei, electric and magnetic fields.

Research at the frontiers of this field includes both optical and electrical schemes to generate, manipulate, and transport coherent spin states in crystalline films and nanometer-scale structures. Moreover, the coupling of spins and photons in the solid state offers natural avenues for integrating quantum computing and communication. While many of these fundamental issues have been addressed using spin ensembles, we discuss recent developments aimed at controlling single spin states using a combination of optical and electrical techniques in a variety of semiconductor systems. The last few years have witnessed extraordinary progress in the ability to create and address single electron, nuclear, and magnetic ion spins by exploiting advances in highly sensitive experimental probes and sophisticated materials synthesis techniques [1].

A semiconductor quantum dot offers an ideal platform for isolating and probing a single electron spin. By placing an electrically-gated quantum dot into an integrated optical cavity, the spin in the quantum dot may be initialized, controlled, and read-out using both optical and electronic means. The non-destructive detection and dynamical observation of single electron spins in these quantum dots is demonstrated using a magneto-optical Kerr rotation measurement [2]. This technique provides a means to directly probe a spin off-resonance, thus minimally disturbing the system. By extension into the time domain, it allows for the direct observation of the coherent evolution of a single electron spin state (figure 1) [3]. The measurements reveal information about the relevant spin decoherence mechanisms, while also providing a sensitive probe of the local nuclear spin environment.

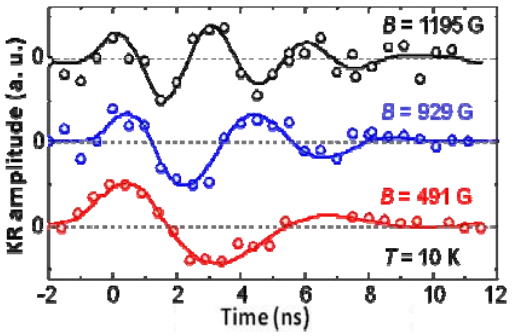

Figure 1. Time-resolved single electron spin precession within an electrically-gated quantum dot at different magnetic fields.

Within the limits of decoherence, practical quantum information processing schemes require fast single-qubit operations. For spin-based qubits, this involves performing arbitrary coherent rotations of the spin state on timescales much faster than the spin coherence time. A scheme for gigahertz all-optical

control of the spin state allows for ultrafast manipulation of a state through arbitrary angles [4]. These results represent progress toward the control and coupling of single spins and photons for quantum information processing as well as quantum non-demolition measurements of a single spin.

While these advanced materials provide exciting new avenues for quantum information processing primarily at low temperatures, spin qubits that operate at room temperature have appeared in the most unexpected of places: diamond – a material that has had a prominent place in the non-scientific world for generations. The electron spins of individual nitrogen-vacancy color centers can be imaged, initialized and manipulated at room temperature with coherence times sufficiently long that quantum error correction may be within reach [5]. There remain significant challenges, however, both in understanding the physics of these defects as well as the development of technologies based on their quantum properties.

Using magneto-optical imaging, photon antibunching, and pulsed electron spin resonance techniques, we describe gigahertz coherent control of isolated single spins (Figure 2) as well as their coupling to nearby nitrogen dopants [6]. The mechanisms of decoherence are explored with measurements probing the fundamental coherent dynamics of a central spin coupled to an adjustable bath of spins. The interactions can be continuously tuned with an applied magnetic field, allowing access to regimes with surprisingly different behavior [7], yielding insights into the loss of coherence for future quantum information processing systems. Combining these elements with precise implanting techniques [8], knowledge of the spin structure of the orbital excited state [9], and the fabrication of diamond microcavities [10] paves the way towards future spin-based quantum devices.

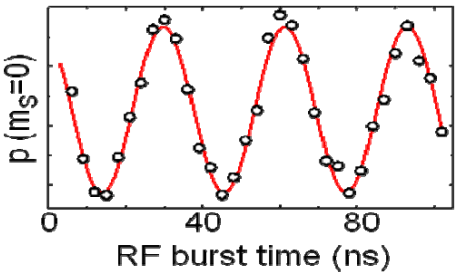

Figure 2. Electrically-driven single spin Rabi oscillations at GHz frequencies under ambient conditions.

References

1. R. Hanson and D. D. Awschalom, Nature **453**, 1043 (2008).
2. J. Berezovsky, M.H. Mikkelsen, O. Gywat, N.G. Stoltz, L.A. Coldren, D.D. Awschalom, Science **314**, 1916 (2006).
3. M. H. Mikkelsen, J. Berezovsky, N.G. Stoltz, L.A. Coldren, D.D. Awschalom, Nature Physics **3**, 770 (2007).
4. J. Berezovsky, M.H. Mikkelsen, N.G. Stoltz, L.A. Coldren, D.D. Awschalom, Science **320**, 349 (2008).
5. D.D. Awschalom, R.J. Epstein, R. Hanson, Scientific American **297**, 84 (2007).
6. R. Hanson, F.M. Mendoza, R.J. Epstein, D.D. Awschalom, Phys. Rev. Lett. **97**, 087601 (2006).
7. R. Hanson, V.V. Dobrovitski, A.E. Feiguin, O. Gywat, D.D. Awschalom *et al.*, Science **320**, 352 (2008).
8. C. D. Weis *et al.*, J. Vac. Sci. Tech. B **26**, 2596 (2008).
9. G. D. Fuchs, V. V. Dobrovitski, R. Hanson, A. Batra, C. D. Weis, T. Schenkel, D. D. Awschalom, *Phys. Rev. Lett*. **101**, 117601 (2008).
10. C.F. Wang *et al.*, Appl. Phys. Lett. **91**, 201112 (2007).

P12
E1
MoP
E2
E3
E4
TuP
E5
P34
E6
E7
E8
ThP
E9
P56

Bose-Einstein condensation and superfluidity of exciton-polaritons

Yoshihisa Yamamoto

E. L. Ginzton Laboratory, Stanford University, CA, USA

National Institute of Informatics, Tokyo, Japan

Keywords: exciton-polariton, Bose-Einstein condensation, superfuidity, microcavity

Particle-particle interaction and peculiar excitation spectra are keys for understanding BEC and superfluidity physics. A quantum field-theoretical formulation for a weakly interacting Bose condensed system was developed by Bogoliubov in 1947, which predicted the phonon-like excitation spectrum in the low-momentum regime. Exciton-polaritons in a semiconductor microcavity, which are elementary excitations created by strong coupling between quantum-well excitons and microcavity photons, were proposed as a new BEC candidate in solid-state systems [1]. Recent experiments with exciton-polaritons have demonstrated several standard but convincing signatures for supporting the polariton condensation, such as the polariton-bunching effect at above the condensation threshold [2], spontaneous spin polarization [3], formation of the long range spatial coherence [4], quantum degeneracy at thermal equilibrium conditions [5] and dynamical condensation in excited p-orbital states [6]. The particle-particle interaction, the Bogoliubov excitation spectrum and the quantized vortices are at the heart of BEC and superfluidity physics, but have only been studied theoretically for exciton-polaritons until very recently. In this talk, we also report the recent observation of interaction effects on the exciton-polariton condensate, such as the linear excitation spectra [7] and the vortex-antivortex pairs [8].

Reference

1. Atac Imamoglu et al., Phys. Rev. A **53**, 4250-4253 (1996).
2. H. Deng et al., Science **298**, 199-202 (2002).
3. H. Deng et al., PNAS **100**, 15318-15323 (2003).
4. H. Deng et al., Phys. Rev. Lett. **99,** 126403 (2007).
5. H. Deng et al., Phys. Rev. Lett. **97**, 146402 (2006).
6. C.W. Lai et al., Nature **450**, 529 (2007).
7. S. Utsunomiya et al., Nature Physics **4**, 700-705 (2008).
8. G. Roumpos et al., submitted for publication.

July 20 (Monday)

13:45 – 16:00

Session E1

NEMS and New Techniques

Main Hall

EP2DS-MSS Parallel session

Himeji Castle

Heterostructure-based Micro/Nanomechanical Systems

Hiroshi Yamaguchi

** NTT Basic Research Laboratories, Atsugi, Kanagawa 243-0198, Japan*

Keywords: NEMS/MEMS, parametric resonators, mechanical devices, nonlinear dynamics

The use of compound semiconductor heterostructures allows us to fabricate micro/nanoelectromechanical systems (MEME/NEMS) with new functionalities. In this talk, I present the experimental results that we have recently obtained from our investigations of electromechanical resonators fabricated from compound semiconductor heterostructures.

The mechanical resonance characteristics can be controlled by the photon-carrier interaction in a dynamical way. The generation of electron-hole pairs by laser light illumination can modify the internal friction in the mechanical systems. What is remarkable is that the quality factor can not only be decreased but also increased by appropriately choosing the wavelength and the cantilever orientation. When the photon energy is close to the band gap, the electron-hole pair is generated selectively depending on the cantilever deflection, leading to the control of resonance characteristics. We demonstrated vibration amplification, damping, and self-oscillations in micromechanical resonators by opto-mechanical coupling through carrier excitation [1,2].

Piezoelectricity has been playing an important role in micro- and nano-electromechanical devices, where it makes possible the highly efficient transduction of mechanical motion into electric signals. Compound semiconductors are piezoelectric materials and highly functional micro- and nano-electromechanical devices can therefore be integrated with electronic architectures. We have fabricated micro-electromechanical parametric resonators based on the piezoelectricity in GaAs/AlGaAs modulation-doped heterostructures. We demonstrate the possible applications of the parametric resonator for signal amplification [3], sensitive charge detection [4], and the logic data storage [5].

The Superconducting quantum interference devices (SQUIDs) are the most sensitive detectors of magnetic flux. Using InAs-based heterostructures, a novel class of devices that incorporate micromechanical resonators into SQUIDs was fabricated to achieve sensitive motion detection of the resonators. I also briefly show the results demonstrating the detection of a 2MHz flexural resonator obtained from the collaboration with Technical University of Delft [6]. The resonator's thermal motion at millikelvin temperatures was measured, achieving an amplifier-limited displacement sensitivity of 10 fm $Hz^{-1/2}$ and a position resolution that is 36 times the quantum limit.

References

1. H. Okamoto, D. Ito, K. Onomitsu, T. Sogawa, and H. Yamaguchi, Appl. Phys. Express. 2, 035001 (2009).
2. H. Okamoto, D. Ito, K. Onomitsu, H. Sanada, H. Gotoh, T. Sogawa, and H. Yamaguchi, unpublished.
3. I. Mahboob and H. Yamaguchi, Appl. Phys. Lett. 92, 173109 (2008).
4. I. Mahboob and H. Yamaguchi, Appl. Phys. Lett. 92, 253109 (2008).
5. I. Mahboob and H. Yamaguchi, Nature Nanotechnol. 3, 275 (2008).
6. S. Etaki, M. Poot, I. Mahboob, K. Onomitsu, H. Yamaguchi, and H.S.J. van der Zant, Nature Phys. 4, 785 (2008).

Carbon nanotubes as ultra-high quality factor mechanical resonators

A. K. Hüttel*, G. A. Steele, B. Witkamp, M. Poot, L. P. Kouwenhoven, and H. S. J. van der Zant
Kavli Institute of Nanoscience, Delft University of Technology,
PO Box 5046, 2600 GA Delft, The Netherlands
**Present Address: Institute for Experimental and Applied Physics, University of Regensburg,*
93040 Regensburg, Germany

Keywords: nanotube, quantum dot, nano-electromechanical system, resonator

High quality factors of nano-mechanical resonators are an important prerequisite for many advanced experiments. We present observations of the transversal vibration mode of suspended carbon nanotubes at device temperatures in the millikelvin range [1]. The nanotubes act as doubly-clamped beam resonator, driven by a radio-frequency signal. Measuring the single electron tunneling current through the embedded quantum dot, the mechanical resonance becomes visible as a sharp current feature.

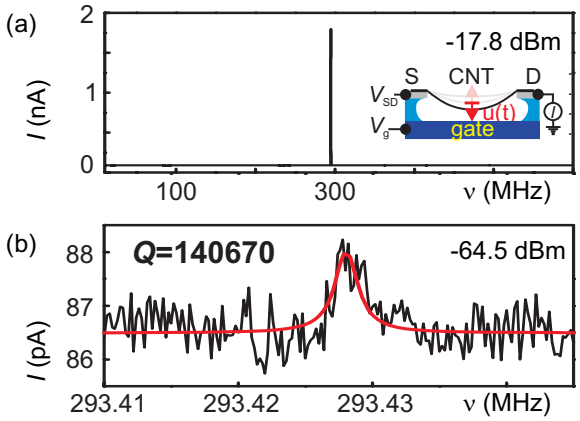

Figure 1: Mechanical resonance visible in the single-electron tunneling current of a suspended carbon nanotube quantum dot (see inset), at (a) high and (b) low RF driving power. Gate voltage V_g and bias voltage V_{sd} are kept constant while sweeping the driving frequency ν and measuring the tunnel current.

Fig. 1 exemplarily shows two measurements at (a) high and (b) low driving power. We obtain a mechanical quality factor of up to $Q \gtrsim 10^5$, much higher than previously reported results, and a tunable resonance frequency of $120\,\mathrm{MHz} \leq \nu \leq 360\,\mathrm{MHz}$.

As expected for a very high quality factor, we find that the resonator can easily be driven into the non-linear regime at increased driving power. Here, the typical hysteretic behaviour and frequency pulling is observed, see Fig. 2(a).

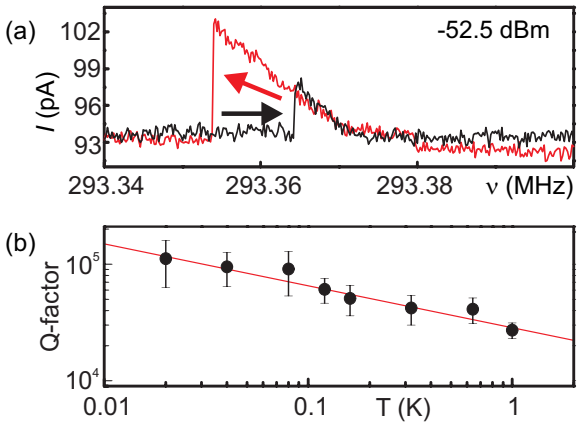

Figure 2: (a) Exemplary measurement of hysteretic resonator behaviour at high driving power. Tunnel current I at fixed V_g and V_{sd}, for a frequency up-sweep (black) and down-sweep (red) of the driving signal. (b) Temperature dependence of the observed quality factor. The solid line corresponds to a $T^{-0.36}$ power law.

The measured magnitude and temperature dependence of the Q-factor, plotted in Fig. 2(b), shows a remarkable agreement with the intrinsic damping for a suspended carbon nanotube, as predicted by molecular dynamics simulations [2].

References

[1] A. K. Hüttel, G. A. Steele, B. Witkamp, M. Poot, L. P. Kouwenhoven, and H. S. J. van der Zant, submitted to Nano Letters (2009).

[2] H. Jiang, M.-F. Yu, B. Liu, and Y. Huang, Phys. Rev. Lett. 93, 185501 (2004).

Ultra sensitive finite frequency noise measurement setup to study the statistical emission noise of an on-demand coherent single electron source.

A. Mahé*, F. D. Parmentier*, J.-M. Berroir*, G. Fève*, T. Kontos*, B. Plaçais*, D. C. Glattli*,**

*Laboratoire Pierre Aigrain, Ecole Normale Supérieure, 24 rue Lhomond, 75005 Paris, France

** Service de Physique de lEtat Condensé, CEA Saclay, F-91191 Gif-sur-Yvette, France

Keywords: shot noise, coherent transport, quantum dot, edge states.

The recent realization of an on demand single electron source [1] opens the way to the implementation of so called quantum electron optics experiment involving single electrons emitted in ballistic quantum conductors. Typical examples of such experiments are the electronic analog of the Hanbury-Brown and Twiss experiment, where a single electron is partitioned by an electronic beam-splitter, or the Hong-Ou-Mandel experiment, where two indistinguishable electrons collide on the beam-splitter. In these experiments, deviations from classical partitioning are expected to show up in the correlations of the output currents. With this in mind, it is highly important to characterize the nature of the quantum state generated by the single electron source and the charge fluctuations resulting from the emission process. These questions have stimulated many recent theoretical works [3, 4].

The first step towards an accurate description of the emitted state is to characterize the current noise of the electron source. First of all, the noise of the emission process appears as a figure of merit of the single electron emitter. Furthermore, being able to measure current noise on single electron states is a requirement to perform any quantum electron optics experiment (and in particular those mentioned above).

In our device, single electron emission is generated by the periodic emission and absorption on subnanosecond timescales of a single charge by a quantum dot (see figure 1). Quantization of the emitted charge reflects in the observation of a quantized ac current in units of the driving frequency f: I=2ef (see figure 1). Measuring the charge noise in such a process amounts to measure current noise at GHz frequency. For such frequencies, current noise is converted to voltage noise through the low 50 Ohms impedance of the RF transmission lines which makes noise measurements highly challenging. Indeed, the expected noise variations of the source brought to 50 Ohms correspond to an equivalent noise temperature of a few tens of microKelvins.

After a review of the observation of a quantized ac current demonstrating the controlled emission of quantized charges, we will present a GHz noise measurement setup that we have realized which reaches this noise sensitivity. This setup is currently used to characterize the emission noise of the single electron source.

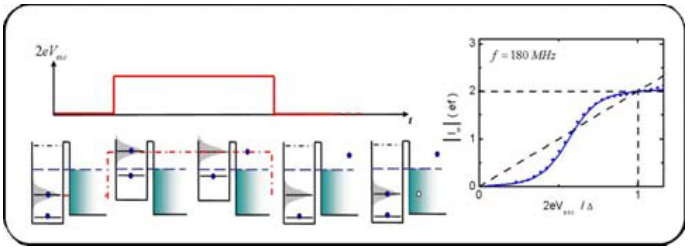

Figure 1: Left: Principle of single charge emission. A sudden variation of the internal potential of a quantum dot of amplitude $2eV_{exc}$ comparable with the dot level spacing Δ brings a single energy level above the Fermi energy. A single electron is then emitted on a subnanosecond timescale. The potential is brought to its initial value leading to the emission of a hole. Right:Periodic emission of single electron and holes reflects in the observation of a quantized ac current I=2ef.

References

[1] Fève G. et al., Science **316**, 1169-1172 (2007).

[2] Ol'khovskaya S et al., Phys. Rev. Lett. **101**, 166802, (2008).

[3] Moskalets M et al., Phys. Rev. Lett. **100**, 086601 (2008).

[4] Keeling J et al., Phys. Rev. Lett. **101**, 196404 (2008).

Imaging electron transport close to filling factor $\nu = 2$ in a quantum ring

F. Martins*, B. Hackens*, L. Gence*, S. Baltazar**, M. Pala**,
H. Sellier***, L. Desplanque****, X. Wallart****, S. Huant*** and V. Bayot*,***
**DICE lab, Université catholique de Louvain, Belgium*
*** IMEP-LAHC-MINATEC (UMR CNRS/INPG/UJF 5130), Grenoble, France*
**** Institut Néel, CNRS, and Université Joseph Fourier, Grenoble,*
*****IEMN, Villeneuve d'Ascq, France*

Keywords: SGM, Quantum Rings, Aharonov-Bohm effect, Quantum Hall effect

Probing electron transport at the local scale inside buried mesoscopic electron systems has been a subject of intense activity in the last few years. To get an access to local information in such systems, one possibility consists in recording the resistance of the system as the electrically biased tip of an atomic force microscope scans over it. The local perturbation induced by the biased tip alters electron transport through the device, and therefore changes its resistance. In previous works, we showed that this method (namely the Scanning Gate Microscopy - SGM) yields resistance maps which can be correlated to the local density of states (LDOS) of the electrons inside mesoscopic devices [1].

Here, we extend our range of investigations to the high magnetic field (B) regime. We measured the quantum ring (QR) shown in Fig. 1a (inset), patterned from an InGaAs/InAlAs heterostructure and equipped with two lateral gates. At low temperature T =90 mK, the QR magnetoresistance exhibits plateaus of quantized resistance at high B, corresponding to the Quantum Hall (QH) regime, as shown in Fig. 1a. Between the plateaus, the magnetoresistance fluctuates, due to electron interferences.

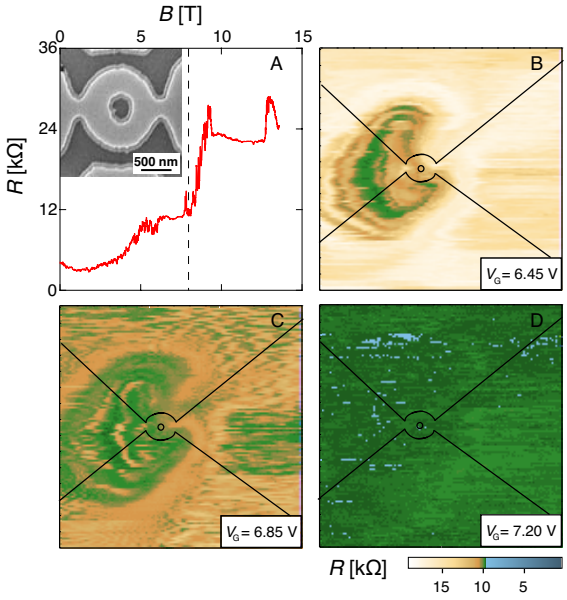

Figure 1: (a) Magnetoresistance of the quantum ring, at V_G= 5.5 V. The inset shows an electron micrograph of the quantum ring. (b-d) SGM resistance maps at B= 8 T and V_G = 6.45 V, V_G = 6.85 V = and V_G = 7.2 V, respectively.

We performed SGM measurements at B = 8 T, between the plateaus at $\nu = 1$ and $\nu = 2$, and changed the lateral gate voltage V_G. In this way, we tune the electron density within and very near the QR, which, in turn, shifts the position of the plateaus and oscillations observed in the magnetoresistance. Close to V_G = 7 V, narrow concentric resistance fringes appear in the SGM map on Fig. 1b. We analyse these features in terms of electron interference phenomena visible in the magnetoresistance between the QH plateaus. We also note that the fringe pattern is asymmetric, and its center is shifted with respect to the QR center. We discuss this observation relying on the electron potential landscape, to which SGM mapping is particularly sensitive in the vicinity of QH plateaus. Finally, increasing V_G, we observe a smooth increase of the lateral extent of the fringe pattern, but no qualitative change of its shape (Fig. 1c). At even larger V_G, electron transport enters in the QH regime, and current through the device is carried by edge states. It thus becomes insensitive to local variations of potential caused by the tip (Fig. 1d), which illustrates the robustness of the QH state.

References

[1] B. Hackens et al., Nature Phys. **2**, 826 (2006); F. Martins et al., Phys. Rev. Lett. **99**, 136807 (2007).

Ultrafast time-resolved transport studies of a two-dimensional electron system

D. Maryenko*, F. Ospald*, B. Rosenow*, H. Lu**, A. C. Gossard**, V. Umansky***, K. von Klitzing* and J. H. Smet*

**Max-Planck-Institute for Solid State Research, D-70569 Stuttgart, Germany*

*** Materials Department, University of California-Santa Barbara, Santa Barbara, California 93106-5050, USA*

****Department of Condensed Matter Physics, Weizmann Institute, Rehovot, 76100, Israel*

Keywords: non-equilibrium phenomenon, time-resolved transport, two-dimensional plasmons, terahertz physics.

The excitations in the two-dimensional electron system have been investigated previously with conventional spectroscopy tools. Here, we have used time-dependent transport experiments instead. A Fourier analysis of the time domain data does not only provide the amplitude of the spectral excitation components across the full experimental bandwidth (up to a THz), but also their relative phase. These experiments were carried out with the help of two fiber coupled photoconductive switches, which are part of a coplanar waveguide structure and are triggered with a femtosecond laser source. The short electrical pulses, generated by one switch, propagate through the AlGaAs/GaAs 2D electron system, which is part of the central conductor of the waveguide, and is subsequently detected with a second switch. The time-resolution of the experiment is limited by the pulse dispersion across the coplanar waveguide connecting both switches. The time domain output of such an experiment for a 140 μm long and 20 μm wide stripe as a function of a perpendicular magnetic field is depicted in Fig. 1.

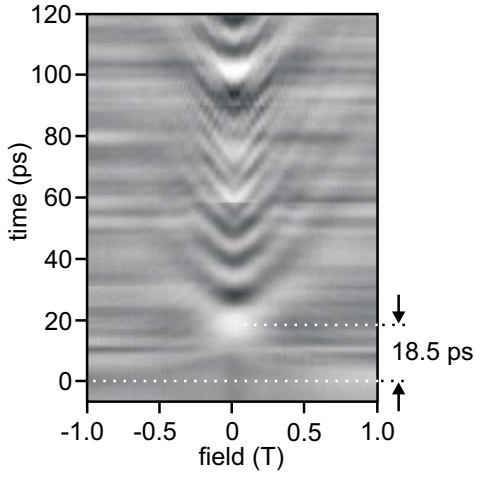

Figure 1: Time-domain response to a short pulse excitation of a stripe of a 2D electron system.

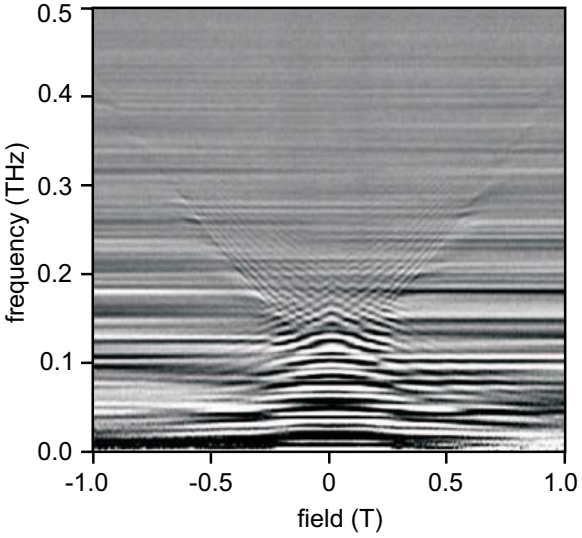

Figure 2: Real part of the Fourier transformation of time domain data shown in Fig. 1.

At zero magnetic field the pulse excitation propagates in the 2DEG at a velocity of 140 μm/18.5 ps = $7.5 \cdot 10^6$ m/s, much larger than the Fermi velocity of $1.5 \cdot 10^5$ m/s at the density $1 \cdot 10^{11}$ cm^{-2} of the experiment. It confirms the collective nature of the excitations making up the pulse. The real part of the Fourier spectrum of the time domain data in Fig. 1 is shown in Fig. 2. The spectrum is composed of excitation modes whose frequency either drops (edge magnetoplasmons) or increases with magnetic field (bulk magnetoplasmons). Multiple modes of each type are visible. We will demonstrate that the phase information contained in the Fourier transform of the time domain is very instrumental in the proper identification and assignment of the wavevector of each mode.

High-efficiency thermoelectric quantum dots in InAs/InP nanowires

E. A. Hoffmann[1], N. Nakpathomkun[1], H. Nilsson[2], A. I. Persson[1], L. Samuelson[2], and H. Linke[1,2]
[1]*Physics Department and Materials Science Institute, University of Oregon, Eugene, Oregon 97403-1274, USA*
[2]*Solid State Physics/The Nanometer Structure Consortium, Lund University, Box 118, S-221 00, Lund, Sweden*

Keywords: thermoelectrics, quantum dots

The field of thermoelectrics benefits from recent advances in nanoscale device engineering, which offers a means to filter electrons by energy using reduced dimensionality and band gap manipulation. The electronic efficiency of such a thermoelectric device outperforms bulk thermoelectric materials and can in principle operate arbitrarily close to the theoretical maximum efficiency, Carnot efficiency[1]. We present experimental results demonstrating the predicted highly efficient conversion of heat energy to electrical energy via a quantum dot (QD) embedded in an InAs nanowire, and we show that such devices typically display strong nonlinear thermoelectric behavior.

The InAs nanowire includes two thin InP regions between which defines an InAs QD whose quantized energy states effectively filter electrons by energy. If the energy states are separated by much more the kT, where T is the background cryostat temperature, electron filtering can be tuned to encourage charge transport at only the exact energy which does not increase the system's entropy.

To measure efficiency, we use the well-established thermoelectric performance metric, ZT, which is typically on the order of $0.1 - 1$. With our QD devices, we have measured values of $ZT \gg 1$ if phonons are neglected. This demonstrates a heat engine operating near Carnot efficiency, making it perhaps the most efficient heat engine ever realized. This achievement is a capstone of many theoretical and experimental developments.

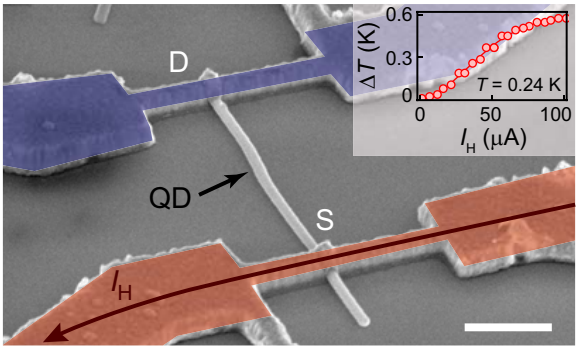

Figure 1: An SEM image of an InAs nanowire device. The QD between the source (S) and drain (D) is not resolved at this magnification. The scale bar is 500 nm. The inset shows the relationship between ΔT and I_H.

QD devices demonstrate nonlinear current-voltage behavior. In the context of thermal biasing rather than electrical biasing, the relationship analogous to Ohm's law is $V_{th} = S\Delta T$, where V_{th} is the thermovoltage established by an applied temperature difference, ΔT, and S is the thermopower. This linear relationship holds in bulk systems, but our highly energy-sensitive mesoscopic devices demonstrate a V_{th} that is nonlinear in ΔT. Surprisingly, we have seen nonlinear behavior when $\Delta T/T$ is as small as 10%. We demonstrate here that the same physical mechanisms responsible for the strong energy filtering and high efficiency are also responsible for strong nonlinear thermoelectric behavior.

The InAs/InP heterostructure nanowires are grown via chemical beam epitaxy and have a diameter of 55 nm and InP barriers 4 to 7 nm in width defining QDs 15 to 150 nm in width. The nanowires are placed on a thin, insulating SiO_x surface under which lies an n-doped Si wafer serving as a back-gate. Metallic Au/Ni leads are patterned using electron beam lithography to define Ohmic source and drain contacts to the nanowire. ΔT is applied across the nanowire by electrically (Joule) heating the metallic source contact with a heating current, I_H. Recently developed quantum-dot thermometry[2, 3] is used to determine the relationship between I_H and ΔT (see Fig. 1).

References

[1] Humphrey and Linke, Phys. Rev. Lett. **89**, 116801 (2002).
[2] Hoffmann *et al*. Appl. Phys. Lett. **91**, 252114 (2007).
[3] Hoffmann *et al*. Nano Lett. **9**, 779 (2009).

A new type of microwave-induced resistance oscillation observed in a nondegenerate 2DES on liquid helium

D. Konstantinov and K. Kono
Low Temperature Physics Laboratory, RIKEN, Japan

Keywords: nondegenerate 2DES on helium, magneto-oscillations, microwave resonance, correlation effects

Recentely, there has been a remarkable discovery of microwave-induced resistance oscillations and zero resistance states in a degenerate 2DES in GaAs/AlGaAs heterostructure devices.[1] Here, we report the observation of a new type of magneto-resistance oscillation induced by microwave resonance in a nondegenerate 2DES bound to a liquid helium surface.

In a strong magnetic field $B_\perp$ applied perpendicular to the helium surface, the energy spectrum of electron motion is fully quantized. Each energy level is labeled by (n, l), where n and l are the quantum number of transverse quantum states and lateral Landau states, respectively. In our experiment, we excite $n = 1 \rightarrow 2$ transition by irradiating the 2DES with resonant microwaves at frequency ω (see inset of Fig. 1), and measure the magneto-resistance using a Corbino disk. We find that the Corbino resistance R_C under radiation differs from that without radiation, and the difference ΔR_C depends on the electron surface density and magnetic field $B_\perp$. The plots of ΔR_C versus $B_\perp$ for several densities are shown in Fig. 1. At large densities, ΔR_C is positive, that is the resistance increases with excitation. We explain this result by many-electron effects in the strongly correlated 2DES heated by the microwave radiation.[2] At reduced densities, we observe that (i) ΔR_C changes sign as $B_\perp$ increases, and (ii) the application of resonant microwaves induces resistance oscillations. We explain the first phenomenon by the interplay between many-electron effects and the effects of Landau quantization on the electron scattering. As for the oscillations, our analysis reveals that they are periodic in $B_\perp^{-1}$, and, at the resistance minima, $B_\perp$ satisfies the condition $j = \omega/\omega_c$, where $\omega_c = eB_\perp/m_0$ is the cyclotron frequency and j is an integer number. All our measurements carried out at different values of the resonant frequency ω are consistent with the above result.

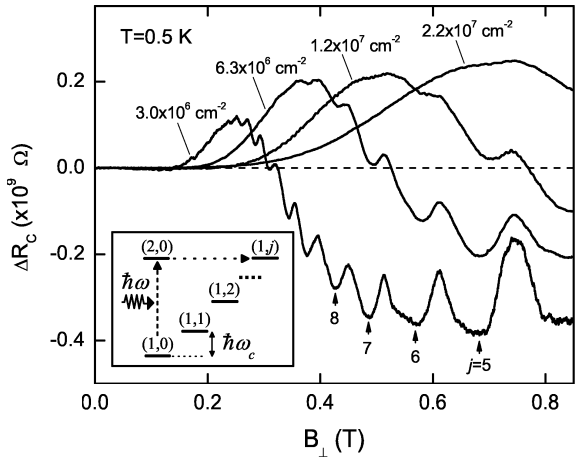

Figure 1: The change in the Corbino resistance R_C of nondegenerate 2DES on liquid ^{3}He as a result of irradiation with microwaves at $\omega/2\pi = 97$ GHz plotted verses applied magnetic field $B_\perp$. The electron density is indicated for each curve. Inset: a schematic energy diagram for an electron in a quantizing magnetic field as explained in the text. The microwave excitation of $n = 1 \rightarrow 2$ transition (dashed arrow) and a subsequent decay into a Landau level of index $l = j$ (dotted arrow) are also indicated.

Under our experimental conditions, the electron resistivity is determined by quasi-elastic scattering from the helium vapor atoms, which act as impurities in this system. We elucidate that the observed oscillations originate from the microwave excitation and a subsequent scattering-induced decay of electrons into a Landau level with a higher index l. In particular, when an integer number j of Landau levels are commensurate with photon energy $\hbar\omega$, the excited electron decays quickly into the Landau level of index $l = j$ (see inset of Fig.1) producing the observed minimum in the resistance (arrow marks in Fig.1).

References

[1] M. A. Zudov *et al*, Phys. Rev. B **64**, 201311 (2001), R. G. Mani *et al*, Nature **420**, 646 (2002)

[2] D. Konstantinov *et al*, Phys. Rev. Lett. **98**, 235302 (2007).

On-chip near-field terahertz detection based on a two-dimensional electron gas

Y. Kawano*,** and K. Ishibashi*

* *Advanced Device Laboratory, RIKEN, 2-1 Hirosawa, Wako, Saitama 351-0198, Japan*

** *PRESTO, Japan Science and Technology Agency (JST), 5-3 Yonbancho, Chiyoda-ku, Tokyo, Japan*

Keywords: Two-dimensional electron gas; Carbon nanotube; Terahertz; Near-field imaging

Terahertz (THz) wave imaging is expected to be used as a powerful tool in various fields. Nevertheless, a much longer wavelength of the THz wave, compared to the visible light, hampers obtaining a high-resolution image. A promising approach for achieving high resolution is to utilize near-field imaging (NI) technique. Contrary to the situations in the microwave and visible light regions, the development of NI in the THz region has not been well established, and hence has attracted much attention.

In this work, we have developed a new device for THz-NI in which all components: an aperture, a probe, and a detector are integrated on one semiconductor (GaAs/AlGaAs) chip [1]. This scheme does not need any optical alignments. As depicted in Fig. 1, the presence of the probe changes the distribution profile of the evanescent field, enhancing the coupling of the evanescent field to the 2DEG THz detector.

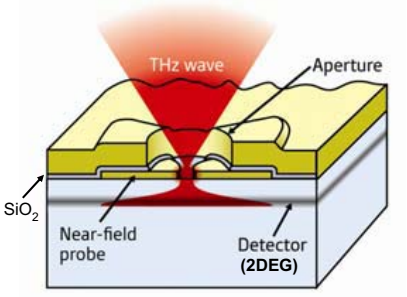

Fig.1 Schematic representation of the THz-NI device.

We measured the THz transmission profile by scanning the device across a sample. For comparison, we used two kinds of THz-NI devices; the aperture plus the probe and the aperture alone. Figure 2 shows that in the former case, a clear profile is seen, whereas in the latter case, no signal is observed. These results provide clear evidence of significant enhancement in the detection sensitivity of the THz evanescent field due to the existence of the planar probe. From signal decay, we obtain a resolution of 9μm. The resolution: (i) does not depend on the wavelength of the incident THz wave [1], (ii) almost matches the aperture diameter of 8μm, and (iii) corresponds to λ/24 for the wavelength λ=214.6μm. These facts clearly demonstrate that the present device properly functions as a THz-NI probe.

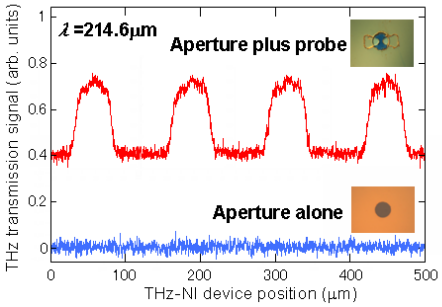

Fig.2 THz signal versus the THz-NI device position.

We are currently trying to utilize a carbon nanotube THz detector [2]. Compared to the 2DEG detector, the carbon-nanotube detector exhibits much higher sensitivity and has a much smaller sensing area (~200nm). This detector, integrated with an aperture and a probe, would show ultra-high sensitivity and a sub-μm resolution simultaneously. We further expect that application of such a near-field THz detector will allow more detailed investigation into various nano-devices, compared to a solid immersion THz lens [3].

References

1. Y. Kawano *et al.*, Nature Photonics **2**, 618 (2008).
2. Y. Kawano *et al.*, J. Appl. Phys. **103**, 034307 (2008); also in V. J. Nano. Sci. Tech. **17**, (2008).
3. Y. Kawano *et al.*, Phys. Rev. B **70**, 081308(R) (2004); Phys. Rev. Lett. **95**, 166801 (2005).

July 20 (Monday)

16:00 – 18:00

Poster Session Mo-eP

Meeting Room 501, 502

EP2DS-MSS Parallel session

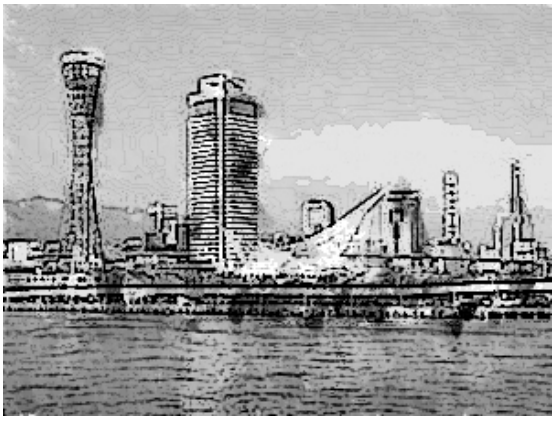

"Meriken" park and Kobe tower

The properties of Ge quantum dots on strained SiGe layer measured by Photoluminescence and Deep Level Transient Spectroscope

Zhensheng Tao, Zuimin Jiang, Fang Lu

Surface Physics Laboratory, Laboratory of Advanced Materials, Fudan University, Shanghai 200433, China

Keywords: quantum dot, SiGe, PL, DLTS

Systematic studies of Ge quantum dots (QDs) grown on strained $Si_{0.3}Ge_{0.7}$ layer have been carried out by photoluminescence (PL) and deep level transient spectroscope (DLTS). The samples are grown on P-type Si (001) substrates by solid source molecular beam epitaxy (MBE), Ge QDs were grown on strained $Si_{0.7}Ge_{0.3}$ layer to obtain small sized QDs with high density. Two types of islands, small hut-shaped and large dome-shaped dots, are observed by AFM. The huts are ~20nm wide and 2.1nm high, the domes are ~50nm in diameter and ~8.7nm in height. The density of the huts and the domes are 1×10^{11} and 6×10^{9} cm^{-2}, respectively.

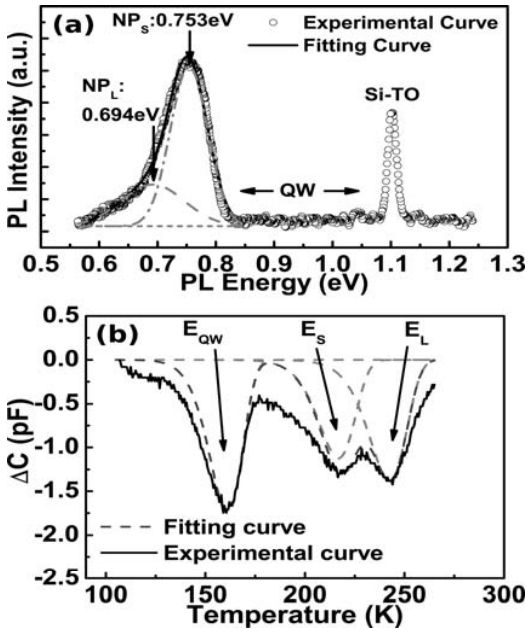

Fig.1. (a) Full PL spectrum at 14K with excitation laser power 50mW/mm^2. (b) Full DLTS spectrum with pulse width t_p=3ms.

The PL spectra shows two peaks around 0.7eV (1770nm) are distinguished for two types of QDs, large blue shifts with increasing excitation laser power are explained by band bending effects typically for type-II band alignment. In DLTS measurements, three peaks are observed, including one related to SiGe layer and two originated from QDs. Experiments under different pulse width enable us to obtain the shift of hole energy levels due to Coulomb charging energy for both types of QDs with the increase of hole density. The energy difference between PL blue shifts and the shift of hole energy levels is expected to be the charging energy of electrons confined in the tensile strained Si around QDs. By combining the PL and DLTS measurements together, we get a complete picture of the band alignment and a comprehensive knowledge of the properties of Ge QDs grown on strained SiGe layer.

References

1. D.N. Lobanov, A.V. Novikov, N.V. Vostokov, Y.N. Drozdov, A.N. Yablonskiy, Z.F. Krasilnik, M. Stoffel, U. Denker, O.G. Schmidt, Optical Materials 27, 818 (2005)

2. B. Ismail, M. Descoins, A. Ronda, and F. Bassani, G. Brémond, H. Maaref, I. Berbezier, J. Vac. Sci. Technol. B 23, 242 (2005)

Probe of the artificial disorder by the capacitance – voltage characteristics

A.A. Sherstobitov*, G.M. Minkov*, A.V. Germanenko**, O.E. Rut**, I.V. Soldatov** and B.N. Zvonkov***

* *Institute of Metal Physics RAS, Ekaterinburg, Russia*

** *Ural State University, Ekaterinburg, Russia*

*** *University of Nizhnii Novgorod, Nizhnii Novgorod, Russia*

Keywords: compressibility, controlled disorder, weak to strong localization

Due to weak screening the inhomogeneities play an important role in two dimensional systems with low electron density. They can be studied by the analysis of the dependence of capacitance between the gate electrode and the electron gas on gate voltage [1]. We report the result of such research on the conventional 2D structures and structures with artificial disorder.

The conventional n – GaAs 2D structures have concentration $(5\text{-}15)\times10^{11}$ cm^{-2} and mobility (3000-20000)cm^2/Vs. The artificial disorder was made on the same structures by the electron beam lithography and the subsequent etching of the surface of two the dimensional structure (fig. 1).

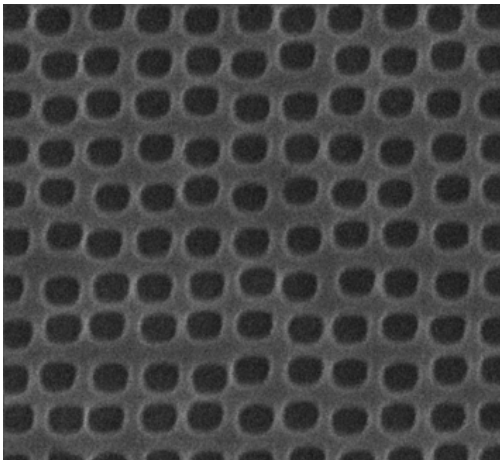

Fig.1 The SEM image of the surface of patterned structure. Dark places are etched on the half of cap layer. The average distance between dots is 1mkm.

On all investigated structures we have found the similar dependencies of the capacitance versus gate voltage. Initially, with the decreasing of the concentration, the capacitance is practically independent on the gate voltage, then it rapidly decrease towards zero. The similar dependence was obtained previously on high mobility structures [2], what is usually ascribed to arising of droplet structure in electron gas.

It was ascertained that in our homogeneous structures The whole the capacitance drop is concerned with the effect of increasing resistance of 2d gas only. In the structures with artificial disorder the C-V curves has similar shape but can not be described by the effect of serial resistance of 2d gas. From that difference we can estimate some parameters of disorder.

Work was supported by the RFBR grants N 08-02-00662, 07-02-00528, 08-02-91962.

References

1. Michael M. Fogler, PRB **69** 121409 (2004).
2. G. Allison, E. A. Galaktionov, A. K. Savchenko, S. S. Safonov, M. M. Fogler, M.Y. Simmons, and D. A. Ritchie PRL **96** 216407 (2006)

Exciton Dynamics in Modulation-doped GaAs/AlGaAs Asymmetric Double-well Structures in Magnetic Fields

Y. H. Shin[1], Y. H. Park[1], S. J. Noh[1], J. W. Hyun[1], C. H. Perry[2], J. A. Simmons[3], T. Takamasu[4], and Yongmin Kim[1,4]

[1]*Department of Applied Physics, Dankook University, Yongin 448-701, Korea*

[2]*Department of Physics, Northeastern University, Boston, MA 02115, USA*

[3]*Sandia National Laboratories, Albuquerque, NM 87185, USA*

[4]*National Institute for Materials Science, Tsukuba, Ibaraki 305-0003, Japan*

Keywords: double quantum well, magnetic field, photoluminescence, quantum Hall effect

We present optical transitions performed on a series of GaAs/AlGaAs asymmetric coupled double quantum well structures (ACDQW, Fig. (a)) in magnetic field (∼45 T). The conduction band in such ACDQW structures has symmetric (E1) and antisymmetric (E2) subbands located energetically in close proximity through a tunneling gap (Δ_{SAS}). The valence band on the other hand has only one heavy hole level because the valence band quantum well on the substrate side is unbound.

In Fig. (b), we tried to plot Landau pans for P3 transition. Cross markers and straight solid lines are experimental and calculated Landau levels, respectively. At ν <2 the lowest Landau level (LLL) transition undergoes free carrier to exciton transitions. The fitted data (thick dotted curve) matches well with experimental 0-0 transition at ν <2 for excitonic diamagnetic shift. One important thing of note is 1-1 and 2-2 Landau transitions also show non-linear behavior when magnetic field sweeps ν=4 and ν=6, respectively. This is possibly due to the complicated Coulomb interactions generated by Landau level mixing of E1 and E2 energy levels.

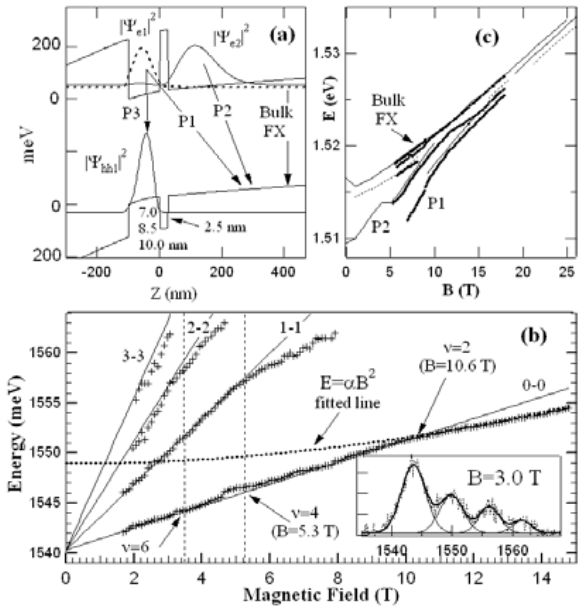

Figure 1: (a) Sample structure used for this study. (b) Landau pan diagram of P3 interband transition in single quantum well side. (c) Magnetic field vs transition energy for single heterojunction and bulk GaAs side.

We would like to discuss two PL transition behaviors of single heterojunction side displayed in Fig. (c); 1) as soon as both P1 and P2 transitions approach to the GaAs FX, they show changeover behavior from free carrier to exciton transitions. This means that P1 and P2 run parallel with GaAs FX. 2) When P1 and P2 transitions become excitons, tunneling gap collapses.

Collapsing Δ_{SAS} may due to the charge fluctuation effect.[1] When the conduction electrons in symmetric (P1) and antisymmetric (P2) bands become excitons, due to the dipole-dipole repulsive interaction, an electron distributed unevenly through tunneling confines in each well. This means that electron in E1 level stays in SQW side and E2 level stays in SHJ side. Therefore, this charge confinement similar to Ref.[1] is the plausible reason that Δ_{SAS} collapses in magnetic fields.

This work was supported by the Korea Science and Engineering Foundation (KOSEF) grant funded by the Korea government (MEST) (R01-2008-000-10212-0).

References

[1] G. S. Boebinger, H. W. Jiang, L. N. Pfeiffer, and K. W. West, Phys. Rev. Lett. **64**, 1793 (1990).

Physical effects in low-dimensional systems subjected to local high-frequency field

M.V. Entin[1], M.M. Mahmoodian[1,2] and L.I. Magarill[1,2]
[1] *Institute of Semiconductor Physics, Siberian Branch, Russian Academy of Sciences, Novosibirsk, Russia*
[2] *Novosibirsk State University, Novosibirsk, Russia*

Keywords: curved quantum wires, photocurrent, quantum pumps, high-frequency blockade

Usually optical fields acting on solids are treated as homogeneous what is argued by large ratio of velocities of light and electrons at comparable energies. Therefore, if the system scale is of order or less than the electron wavelength, it obviously less than the wavelength of photons, with which this electron interacts. However, it is possible to create the systems where the alternating field has spatial scale, comparable with electrons wavelength. This is the topic of the present study.

Let us imagine curved low-dimensional system placed in a homogeneous high-frequency field. The system shape dictates spatial scale of an effective high-frequency field which becomes comparable or smaller than electron wavelength. Presence of high spatial harmonics in a high-frequency field leads to kinematic ability of absorption of the electromagnetic field by free electrons. The absorption can be accompanied by the photo-EMF if the system possesses asymmetry. In such system the local field acts as a "pump" which transfers charge between contacts.

We have studied photo-EMF in curved quantum wires. In particular, specific shapes were under consideration: spiral and planar curves: "angle", "omega"-shaped curve, "opened book" [1]. The effects were studied on the basis of the classical kinetic equation. Besides, quantum consideration of a problem is carried out when frequency of light is comparable with the Fermi energy.

If the value of a high-frequency local field is large its influence cannot be reduced to square-law response to the field. We considered a one-dimensional quantum wire with local (sharp or smooth) vibrating potential and a chain of quantum dots, the level of one of which oscillates. Strong enough field changes electron spectrum giving rise new unusual types of electron states [2], namely, high-frequency blockade states, wave functions of which contain no transmitted wave. Other unusual states are localized states in presence of alternating signal, quasistationary states with the large relaxation time and reflectionless states.

We investigated stationary responses of the systems to the high-frequency field, including conductance and pump effect. The spatial system was mapped on the one-dimensional model with local vibrating potential. The Figure illustrates one of such models: a step-like potential with vibrating delta-function $U(x,t) = V_0\theta(x) + (u + v\cos(\omega t))\delta(x)$ together with the dependence of the stationary conductance on parameters. The blockade states are represented by valleys bottoms tangent to the zero plane.

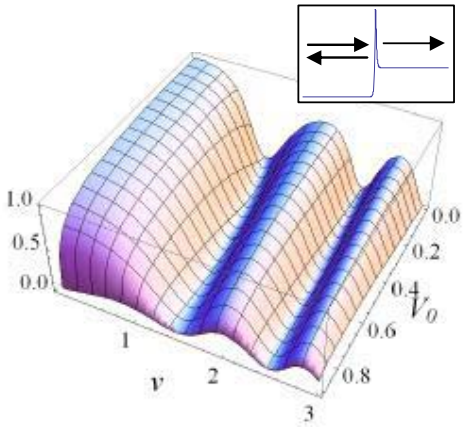

Stationary conductance of the system with potential $U(x,t)$ (insert) *versus* potential gap V_0 and amplitude of oscillating barrier v at u=0, E_F=0.9ω. We set $\hbar = m = \omega = 1$.

References

[1] M.V. Entin, L.I. Magarill. Phys. Rev. B **79**, 075434 (2009).
[2] M.V. Entin and M.M. Mahmoodian. Europhys. Lett. **84**, 47008 (2008).

Lower bounds on the exchange-correlation energy in reduced dimensions

E. Räsänen*,**, S. Pittalis**, K. Capelle**,*** and C. R. Proetto**
*Nanoscience Center, Department of Physics, University of Jyväskylä, Finland
** Institut für Theoretische Physik, Freie Universität Berlin, Germany
*** Instituto de Física de São Carlos, Universidade de São Paulo, São Carlos, Brazil

Keywords: Lieb-Oxford bound, exchange-correlation energy, reduced dimensions

In 1979 Lieb [1] planted a landmark in quantum many-body physics by proving the existence of a lower bound on the indirect part of the Coulomb interaction. The bound is of inmediate relevance to such fundamental questions as the stability of matter [2]. For quantitative calculations, however, the mere existence of a bound is not enough – it should be as tight as possible. A tighter version of the bound, known as the Lieb-Oxford (LO) bound [3], is used as a key constraint in the construction of many modern density functionals for exchange and correlation [4, 5]. In turn, these functionals are routinely used in electronic-structure calculations of atoms, molecules, solids, and nanoscale systems.

In connection with broad advances in low-dimensional physics it is relevant to ask whether LO-like bounds exist and can be formulated also in two and one dimensions (2D and 1D). For a general D-dimensional system, the bound can be expressed in terms of the indirect part of the interaction energy,

$$W_{xc}[\Psi] \equiv \left\langle \Psi | \hat{V}_{ee} | \Psi \right\rangle - U[n] \geq - C_D \int d^D r \, n^\alpha(\mathbf{r}), \quad (1)$$

where $\hat{V}_{ee} = \sum_{i>j} |\mathbf{r}_i - \mathbf{r}_j|^{-1}$ is the (Coulombic) electron-electron (e-e) interaction operator, $n(\mathbf{r})$ is the density, and $U[n]$ is the classical Hartree energy. We note that the *existence* of a bound of this form has been rigorously proven only in 3D and 2D, and that the tighest possible form, i.e., the smallest possible value of $C_D > 0$, is unknown in *all* dimensions [6].

In this presentation we will (i) show that the exponents of n are consequences of universal scaling properties of the e-e interaction; (ii) present the exponent of a possible 1D bound; (iii) provide the tightest estimate to date of the numerical prefactor C_3 and C_2, and the first proposal for C_1; (iv) discuss unexpected parameter independence and universality of the bound with respect to the model chosen for e-e interactions in 1D; and (v) show results for the 1D and 2D bounds against analytic and numerically exact data for various low-dimensional systems [7].

References

[1] E. H. Lieb, Phys. Lett. **70A**, 444 (1979).

[2] L. Spruch, Rev. Mod. Phys. **63**, 151 (1991).

[3] E. H. Lieb and S. Oxford, Int. J. Quantum Chem. **19**, 427 (1981).

[4] J. P. Perdew, K. Burke, and M. Ernzerhof, Phys. Rev. Lett. **77**, 3865 (1996).

[5] J. P. Perdew *et al.*, J. Chem. Phys. **120**, 6898 (2004).

[6] M. M. Odashima and K. Capelle, J. Chem. Phys. **127**, 054106 (2007); ibid. **108**, 2428 (2008).

[7] E. Räsänen, S. Pittalis, K. Capelle, and C. R. Proetto, submitted (arXiv: 0902.1416).

Magnetotransport properties of Ytterbium doped $Al_xGa_{1-x}As$/GaAs two-dimensional electron systems

T. Kaizu, Y. Imanaka, K. Takehana and T. Takamasu
Quantum Dot Research Center, National Institute for Materials Science, Tsukuba, Japan

Keywords: two-dimensional electron system, rare-earth doping, magnetotransport, electron trap

Rare-earth (RE) doped semiconductors are attractive materials for optical device applications such as semiconductor lasers, because the RE ions show sharp and temperature-stable luminescence due to the intra-4*f*-shell transitions. So far, photoluminescence properties of various combinations of RE ions and semiconductor hosts have been studied and it has been suggested that isoelectronic traps formed by the RE ions play a key role in the luminescence mechanism. For Ytterbium (Yb) doped $Al_xGa_{1-x}As$, photo-luminescence due to Yb intra-4*f*-shell transitions have been observed in the thin film and superlattice samples with Al composition of x≥0.3, which were grown by molecular beam epitaxy (MBE) [1, 2]. However, the Yb-related trap state in $Al_xGa_{1-x}As$ is not well understood yet. In this study, we fabricated Yb-doped $Al_xGa_{1-x}As$/GaAs two dimensional electron systems (2DES) by MBE and investigated the magneto-transport properties. Analysis of the transport property of 2DES with an adjacent Yb-doped layer is an effective approach to find out the Yb-related trap state because 2DES is sensitive to ionized impurity scattering.

$Al_xGa_{1-x}As$:Yb/GaAs 2DES samples with two different Al composition, x=0.3 and 1, were grown. Their magnetotransport measurements were performed under dark and light-illumination conditions. Magnetic field was applied up to 15 T at 1.6 K. Figure 1 shows the magnetic field dependence of the longitudinal magnetoresistance, ρ_{xx}, of $Al_{0.3}Ga_{0.7}As$:Yb/GaAs (a) and AlAs:Yb/GaAs (b) 2DES samples under light-illumination conditions. The photo energies are $h\nu$ = 1.54 and 1.95 eV, which almost correspond to the band gap energies of GaAs and $Al_{0.3}Ga_{0.7}As$, respectively. In the $Al_{0.3}Ga_{0.7}As$:Yb sample, Shubnikov-de Haas (SdH) oscillations are clearly observed at both excitation energies, which is similar to the result of the non-doped sample. In contrast, the AlAs:Yb sample shows a SdH oscillation only at $h\nu$ = 1.95 eV. At $h\nu$ = 1.54 eV, ρ_{xx} first increases and then decreases with increasing magnetic field, peaking at about 7 T. These results show that Yb ions act as electron traps only in AlAs layer. In addition, in order to investigate the Yb-related electron trap levels in detail, we measured the excitation energy dependence of ρ_{xx} and calculated the energy band structures of the samples. As the results, it has been found that the Yb levels in $Al_{0.3}Ga_{0.7}As$ and AlAs are located above and below the conduction band edge of GaAs, respectively, and the difference in the location of Yb levels according to the energy band structure of $Al_xGa_{1-x}As$ host affects the transport property of 2DES.

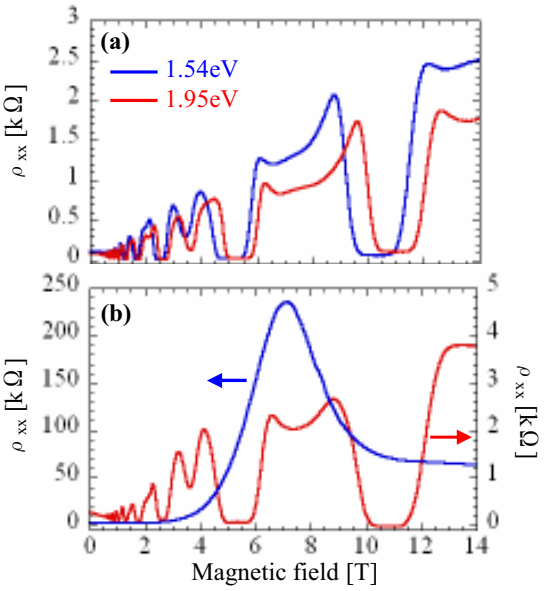

Fig.1 Magnetic field dependence of the longitudinal magnetoresistance of $Al_{0.3}Ga_{0.7}As$:Yb/GaAs (a) and AlAs:Yb/GaAs (b) 2DES samples for $h\nu$ = 1.54 and 1.95 eV

References

[1] K. Sato, T. Takamasu and G. Kido, J. Appl. Phys. **95** 2924 (2004).
[2] K. Sato, T. Takamasu and G. Kido, J. Super-conductivity **18** 127 (2005).

Low-Temperature Resistivity of Periodic Curved Surfaces

Shota Ono and Hiroyuki Shima
Department of Applied Physics, Graduate School of Engineering, Hokkaido University, Sapporo, Japan

Keywords: surface curvature, electron-electron Umklapp scattering, low-temperature resistivity

The purpose of our study is quantitative determination of curvature effects on the electrical resistivity of periodically curved surfaces. Nanostructures with curved geometry have been attracting interest in the last years [1, 2], since their electronic properties are markedly affected by curvature-induced potential [3, 4]. Especially intriguing are low-dimensional systems having periodically curved geometry; in those systems, periodic potential induced by curvature modulation results in energy band gaps [5, 6], which may enhance the contribution of electron-electron Umklapp scattering process (U-process) to the resistivity. This implies a sizable increase in the resistivity due to surface curvature modulation, whereas such phenomena remain unexploited so far. To make clear the point, we calculate the low-temperature resistivity of two-dimensional periodic curved surfaces given by $z = f(x, y) = a\cos(\gamma x)$, where a is the corrugation amplitude and $2\pi/\gamma$ is the period of corrugation. The electrical resistivity is represented by $\rho = \rho_c \left(\frac{k_B T}{E_F}\right)^2 \frac{h}{e^2}$, where ρ_c is a dimensionless coefficient depending on a and the Fermi energy E_F. Figure 1 shows a-dependence of ρ_c for several E_F, where γ=0.15 and material constants of GaAs/Al_xGa_{1-x}As heterostructures are employed. As a increases, ρ_c shows a sudden jump (at a=5nm for E_F=10meV, for instance) followed by a shoulder behavior. We have found that this sudden jump of ρ_c results from significant contribution of U-processes illustrated in Fig. 2. In fact, specific values of a which gives rise to the jump of ρ_c corresponds to those of a just above which gaps open at given E_F. This is because the U-process involving the states in the vicinity of gaps makes ρ_c so large, and then leading to the jump of ρ_c at the specific a. Detailed mechanism will be given in the session.

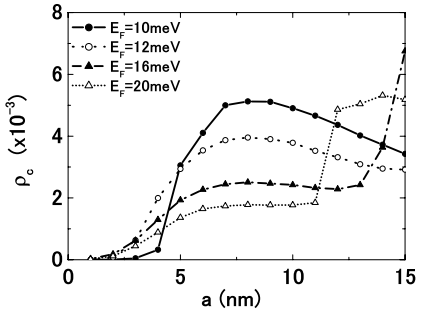

Figure 1: Dependence of ρ_c on the corrugation amplitude a. Sudden jumps of ρ_c appearing in the regions of $a \lesssim$5nm and $a \gtrsim$10nm are, respectively, due to the contribution of 1st- and 2nd-order Umklapp processes.

References

[1] G. Ferrari and G. Cuoghi, Phys. Rev. Lett **100**, 230403 (2008), and references therein.

[2] H. Shima, H. Yoshioka, and J. Onoe, arXiv:0903.0798

[3] R. C. T. da Costa, Phys. Rev. A **23**, 1982 (1981).

[4] M. Ikegami and Y. Nagaoka, Prog. Theor. Phys. **106**, 253 (1991).

[5] H. Aoki, M. Koshino, D. Takeda, and H. Morise, Rhys. Rev. B **65**, 035102 (2001).

[6] N. Fujita, J. Phys. Soc. Jpn. **73**, 3115 (2004)

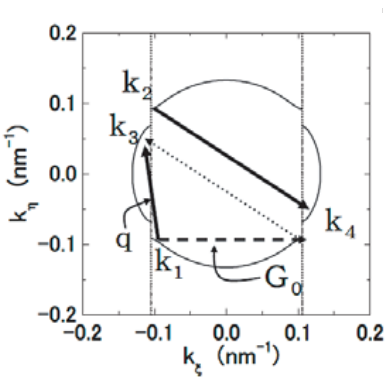

Figure 2: Sketch of U-process arising on the Fermi surface. The presence of gaps enhances the contribution of U-process to ρ_c.

Magneto-optics of two-dimensional arrays of embedded semiconductor quantum dot molecules

L. M. Thu and O. Voskoboynikov

Department of Electronics Engineering, National Chiao Tung University, 1001 Ta Hsueh Road, Hsinchu 30010, Taiwan

Keywords: Quantum dot molecule, Magneto-optics, Discrete dipole

In this study we implement our computational hybrid model [1] to simulate the magneto-optics of two-dimensional arrays of semiconductor double quantum dot molecules (QDMs) embedded in a host material. In the model each QDM is presented by a single discrete dipole and characterized by a bare excess polarizability. This polarizability includes a static part, determined electromagnetically and dynamic part determined quantum mechanically. Using this we obtain the collective electromagnetic response (reflectance, transmittance, and absorbance) of a two-dimensional array of the dipoles.

The simulation has been performed for arrays of asymmetrical InAs QDMs embedded into GaAs matrix. We use the same sizes and material parameters, as used in Ref. 2. The tunnel coupling between dots and non-uniformity of the QDM's geometry generates upon the magnetic field application non-uniform diamagnetic shifts for the lowest electronic energy states (see [2]) and the non-uniform diamagnetic shifts for corresponding energies of the allowed transitions in the molecules. At the same time the electronic and hole wave functions are redistributing within the molecule. This coherent manipulation of the quantum mechanical states obviously changes the overlap integrals for the corresponding optical transitions. The QDM's polarizability and then the collective magneto-optical response of the array of the QDMs reflect this clear quantum mechanical effect. In Fig. 1 we present our results for the absorbance of the system. The s-polarized light beam incidence angle is 60^0. The damping constant was taken as 0.5meV, distance between dots in the molecule is 20nm, and the inter-molecular distance in the array is 100nm. Clearly the coherent transformation of the electronic wave functions in QDMs can be observed by means of the modern magneto-optics (modern magneto-ellipsometry).

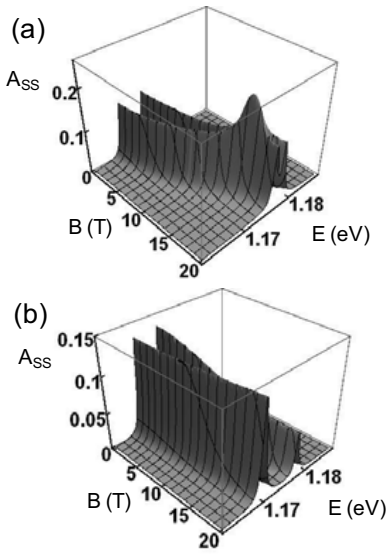

Fig.1 Absorbance of the two-dimensional array of InAs/GaAs QDMs. Magnetic field is: (a) parallel and (b) perpendicular to the system growth direction.

References

1. C. M. J. Wijers et al.,Phys. Rev. B **74**, 035323 (2006).
2. O. Voskoboynikov, Phys. Rev. B **78**, 113310 (2008).

Enhancement of negative magnetoresistance due to weak localization in In_2O_3 thin films on Si substrate

A. Fujimoto*, M. Kitamura**, H. Kobori**, A. Yamasaki**, A. Sugimura**,
A. Ando***, H. Kawanaka*** and T. Shimizu***

** Nanomaterials Microdevices Research Center, Osaka Institute of Technology, Osaka, Japan*
*** Department of Physics, Faculty of Science and Engineering, Konan University, Kobe, Japan*
****Nanotechnology Research Institute, Advanced Industrial Science and Technology, Tsukuba, Japan*

Keywords: In_2O_3, RF-magnetron sputtering, magnetoresistance, weak localization

Indium tin oxide (ITO) has been widely used as a transparent conductor in electronic devices. Recently, Indium oxide (In_2O_3) has attracted many researchers, since the new oxide-based ferromagnetic semiconductor produced by doping various transition-metals has been reported to realize spintronics devices [1]. However, there are fewer reports on solid state properties of In_2O_3 itself compared with those of ITO. Indium oxide has a lot of inherent oxygen vacancies, which are believed to behave as double-donors and be responsible for the electrical conductivity. In this study, In_2O_3 thin films on Si (100) single crystal and a-SiO_2 glass substrates were prepared by using RF-magnetron sputtering method. The In_2O_3 thicknesses are 20, 50 and 100 nm. The purpose of this study is to investigate the substrate dependence of weak localization (WL) regarding In_2O_3 thin films.

Fig.1(a) shows X-ray diffraction (XRD) spectra of In_2O_3 films with thickness of 20 nm on Si and a-SiO_2 substrates. (222) diffraction peak of In_2O_3 on Si was clearly observed, on the other hand, there was no (222) diffraction peak from the film on a-SiO_2. In addition, by means of atomic force microscope (AFM) observation, we found that the In_2O_3 film on Si had granular structures with a size of tens of nm, but, there was no granular structure for the one on a-SiO_2. We consider that In_2O_3 film with thickness of 20 nm on Si has better crystallinity than that on a-SiO_2. In fact, the carrier concentration of the film on a-SiO_2 is $1.3 \times 10^{15} cm^{-2}$ at low temperatures (LT), which is about four times as many as that of the one on Si. The electrically metallic In_2O_3 film on a-SiO_2 is transparent and the surface does not have metallic luster. Amorphous-like In_2O_3 film is considered to be grown on a-SiO_2.

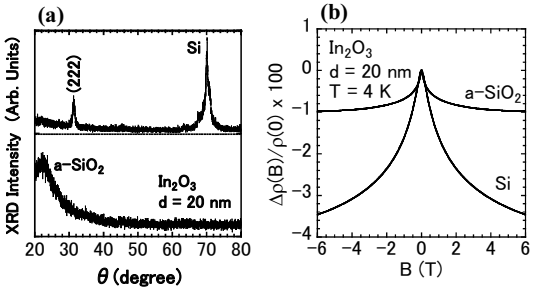

Fig.1 (a) XRD spectra from In_2O_3 films with thickness of 20 nm on Si substrate (upper panel) and a-SiO_2 one (lower panel). (b) Transverse MR under perpendicular magnetic field at 4 K.

Fig.1(b) shows transverse magnetoresistance (MR) under the magnetic field perpendicular to the film surface up to 6 T at 4 K. Negative MR caused by WL was observed for both samples. The negative MR of the film on Si is 3.5 times larger than that of the one on a-SiO_2 at 6 T. The WL effect becomes more remarkable in use of Si substrate. The negative MR data are in agreement with the two dimensional WL theory [2] using the parameter τ_i (inelastic scattering time). The result of the analysis shows that τ_i of the film on Si is much larger than that of the one on a-SiO_2 at 4 K. Since the inelastic scattering predominantly occurs at crystal defects of In_2O_3 film at LT, the larger negative MR of In_2O_3 film on Si is concluded to originate in better crystallinity.

References

1. T. Ohno *et al*., Jpn. J. Appl. Phys. **45**, L957 (2006).
2. S. Hikami *et al*., Prog. Theor. Phys. **63** 707 (1980).

P12
E1
MoP
E2
E3
E4
TuP
E5
P34
E6
E7
E8
ThP
E9
P56

Thermoelectric transport in periodic 1D stacks of InAs/GaAs quantum dots

V. M. Fomin* and P. Kratzer*

* *Fachbereich Physik and Center for Nanointegration (CeNiDE), Universität Duisburg-Essen, Duisburg, Germany*

Keywords: InAs/GaAs quantum dots, 1D superlattices, relaxation time, thermoelectric transport

Nanostructured semiconductors offer new possibilities, due to the quantum confinement of electrons and phonons, to fabricate thermoelectric devices with an improved figure-of-merit. A narrow distribution of the energy of the carriers participating in the transport process is needed for maximum thermoelectric efficiency. Of interest for possible thermoelectric applications are 1D, 2D and 3D superlattices of quantum dots (QDs), in which strong coupling between dots leads to the formation of minibands.

We investigated electron and phonon states and thermoelectric transport due to the electron-phonon interaction in a periodic 1D stack of disk-shaped InAs QDs in GaAs, which can be produced by self-assembly. Electron minibands for a 3D array of InAs/GaAs QDs calculated using the tight-binding approach [1] are adequately represented within the Kronig-Penney model of a periodic 1D stack of QDs. Solution of the dispersion relation for acoustic phonons reveals that an effective medium approximation can be applied with a good accuracy. The relaxation time is calculated using the Boltzmann transport equation. The relaxation time significantly increases at the center and at the boundaries of the first Brillouin zone (Fig. 1). From the numerical analysis of the electric and thermal conductivities, the Seebeck coefficient S (Fig. 2) and the figure-of-merit, we conclude that a 1D stack of QDs could achieve a geometry-controlled enhanced efficiency as a thermoelectric converter.

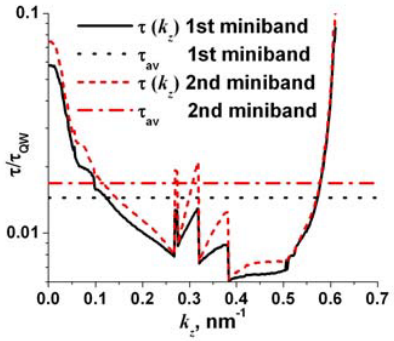

Fig. 1 The relaxation time for two minibands in a periodic stack of InAs/GaAs QDs with height 1.473 nm, period 5.13 nm, radius 5.00 nm and the conduction band offset 1.03 eV. Dotted and dash-dotted lines indicate the average values of the relaxation time τ_{av} for two minibands. τ_{QW} is the relaxation time of a quantum well with the same geometric parameters.

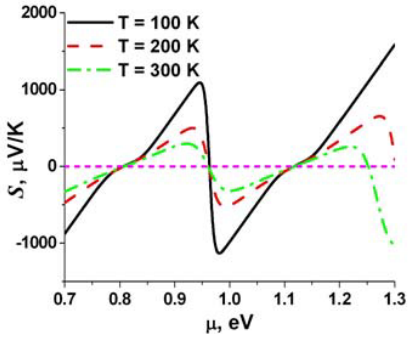

Fig. 2 The Seebeck coefficient calculated using three minibands for a periodic stack of InAs/GaAs QDs as a function of the Fermi energy.

The support from DFG under SPP 1386 is acknowledged. V.F. has been supported by the ESF through Exchange Grant No. 2157 within the activity *'Arrays of Quantum Dots and Josephson Junctions*'.

Reference

1. R. Santoprete, B. Koiller, R. B. Capaz, P. Kratzer, Q. K. K. Liu, and M. Scheffler, Phys. Rev. B **68**, 235311 (2003)

Band structure and magneto-transport properties in narrow gap, two-dimensional and modulated nano-medium-infrared detector

A. Nafidi *

** Group of Condensed Matter Physics, Faculty of Sciences, Department of Physics, B.P 8106 Hay Dakhla, Ibn Zohr University, 80000 Agadir, Morocco*

Keywords: Band structure in envelope function formalism, Magneto transport properties, narrow gap and two-dimensional nano- semiconductor, II-VI medium-infrared detector HgTe/CdTe superlattice

The work of Essaki and Tsu in 1970 [1] caused a big interest to the study of superlattices made from alternating layers of two semiconductors. The development of molecular beam epitaxy (MBE) was successfully applied to fabricate different quantum wells and superlattices. Among them, III-V superlattices ($Ga_{1-x}Al_xAs$-GaAs-type I), IV-IV (InAs/GaSb - type II) and later II-VI superlattice (HgTe/CdTe - type III). The later has been predicted as a stable alternative for application in infrared optoelectronic devices than the $Hg_{1-x}Cd_xTe$ alloys. Especially in the region of second atmospheric window (around 10 μm) witch is of great interest for communication

HgTe is a zero gap semiconductor when it is sandwitched between the wide gap semiconductor CdTe (at 4.2 K) layers yield to a small gap HgTe/CdTe superlattice witch is the key of an infrared detector.

We report here carrier's magneto-transport properties and band structure results for II-IV nanostructured semiconductor. HgTe is a zero gap semiconductor when it is sandwiched between CdTe layers yield to a small gap HgTe/CdTe superlattice witch is the key of an infrared detector. Our sample, grown by MBE, had a period $d=d_1+d_2$ (90 layers) where d_1(HgTe)=5.6 nm and d_2(CdTe)= 3 nm. Calculations of the specters of energy $E(d_2)$, $E(k_z)$ and $E(k_p)$, respectively, in the direction of growth and in plane of the superlattice; were performed in the envelope function formalism [1]. The energy $E(d_2, \Gamma, 4.2\ K)$, shown that for each d_1/d_2, when d_2 increase the gap E_g decrease to zero at the transition semiconductor to semimetal conductivity behavior and become negative accusing a semimatallic conduction. At 4.2 K, the sample exhibits p type conductivity with a Hall mobility of 8200 cm^2/Vs [2]. This allowed us to observe the Shubnikov-de Haas effect with p = 1,80 10^{12} cm^{-2}. Using the calculated effective mass (m^*_{HH} = 0,297 m_0) of the degenerated heavy holes gas, the Fermi energy (2D) was E_F=14 meV in agreement with 12 meV of thermoelectric power α. In intrinsic regime, $\alpha \sim T^{-3/2}$ and $R_H\ T^{3/2}$ indicates a gap $E_g = E_1\text{-}HH_1$= 190 meV in agreement with calculated $E_g(\Gamma, 300\ K)$ =178 meV.

The formalism used here predicts that this sample is a narrow gap, two-dimensional modulated nanostructure and medium-infrared detector. Note that we had observed a p- type, semi metallic and quasi-two-dimensional conduction in the far-infrared detector HgTe/CdTe (18 nm / 4.4 nm) [3].

References

1. L. Essaki and R. Tsu, IBM, J. Res. Develop., 14 (1970)

2. A. Nafidi, et al, Proc. Inter. Conf. on theoretical Physics, Paris, France 22-27 July, 274 (2002).

3. A. Nafidi et al, AIP Conference Proceedings 772, pp.1001-1002,, (2005)..

4. A. El Abidi, A. Nafidi et al, Proc. of SPIE, Vol. 7055, 70550C (2008), DOI:10.1117/12.803320

Violation of non-interacting v-representability of the exact solutions of the Schrödinger equation for a parabolic two-electron quantum dot in a homogeneous magnetic field

M.Taut, P.Machon and H.Eschrig
Leibniz Institute for Solid State and Materials Research, IFW Dresden, POB 270116, 01171 Dresden, Germany

Keywords: Current density functional theory, quantum dots

In density functional theory it can be shown that the electron density of the ground state (GS) can be calculated from a model system of non-interacting particles in a properly chosen external potential, the Kohn-Sham (KS) system. This property is called non-interacting v-representability (NIVR). It follows from the fact that all mutual mappings between the external potential, many body wave function (WF) and electron density of the GS are invertible [1].

In the basic work on (non-relativistic) current density functional theory (CDFT) [2] NIVR of both densities (charge- and the paramagnetic current density) has been tacitly assumed, because the invertibility of the mapping of the external potentials (scalar- and vector potential) on the wave function has never been proven. In the contrary, in [3] has been shown, that different external potentials can provide the same WF. This rules the invertibility of the above mentioned mapping out, but does not say anything about NIVR.

We have shown by means of the exact solutions for the two-electron system in a parabolic confinement and a homogeneous magnetic field [4] that the exact densities are not always NIVR, or equivalently, that an exact KS system does not always exist. Whether it exists depends on the total angular momentum of the GS. (It is well known that the modulus of the orbital angular momentum L of the GS grows step-wise with increasing magnetic field connected with singlet-triplet oscillations.)

If the GS is a singulet (L is even) both densities are NIVR if the vorticity of the exact solutions vanishes. For L=0 this is trivially guaranteed because the paramagnetic current density vanishes in this state. (The gauge invariant mechanical current density does not vanish, though.) Fig.1 shows, that the vorticity based on the exact solutions for the higher L does not vanish, in particuler for small r.

If the GS is a triplet (L is odd) we can show, that there is no circular symmetric KS system which can provide the exact densities, except for L= – 1. Therefore, in this case NIVR cannot be ruled out in general, but it has been shown that common practise in self-consistent CDFT computations, where NIVR with a circular symmetcc KS system is assumed on the basis of the circular symmetry of the real system, is not rigorously justified. However, this does not mean, that all these results are completely wrong.

References

[1] P.Hohenberg, W.Kohn, Phys. Rev. **136B**, 864 (1964)

[2] G.Vignale, M.Rasolt, Phys. Rev. B **37**, 10685 (1988)

[3] K.Capelle, G.Vignale, Phys. Rev. B **65**, 113106 (2002)

[4] M. Taut, J. Phys. A **27**, 1045 (1994) and 4723 (1994)

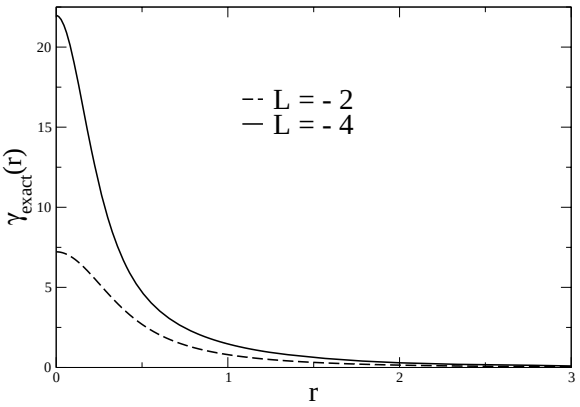

Figure 1: Vorticity for exact singlet states for effective confinement frequency (see [4]) =1 and total orbital angular momenta L= – 2 and L= – 4.

Strains in heterostructures detected by standard NMR

M. Nishimori[1], S. Sasaki[1], S. Watanabe[2] and Y. Hirayama[3, 4]

[1]*Graduate School of Science and Technology, Niigata University, Niigata, Japan*

[2]*Centre for Advancement of Higher Education, Tohoku University, Sendai, Japan*

[3]*Graduate School of Science, Department of Physics, Tohoku University, Sendai, Japan*

[4]*ERATO Nuclear Spin Project, Sendai, Japan*

Keywords: strain, heterostructure, GaAs, standard NMR

Around the interface of heterostructured GaAs, it had been believed that nanoscale strains should exist due the lattice mismatch between the AlGaAs and GaAs layers. In principle, nuclear magnetic resonance (NMR) [1] could be one of the most suitable methods to observe the strains. However, this has been believed to be next to impossible totally due to the insufficient sensitivity in standard NMR.

Recently, instead of the standard NMR, Ota and his collaborators have succeeded in direct observation of the interface strain by employing a newly developed method, resistivity-detected NMR (RDNMR) in a quantum Hall state, to a nanoscale region around the split gates [2]. Moreover, RDNMR has been employed to observe strain in the breakdown regime of a quantum Hall state of heterostructured GaAs [3]. However, the RDNMR method can be applied only to a sample in a quantum Hall state.

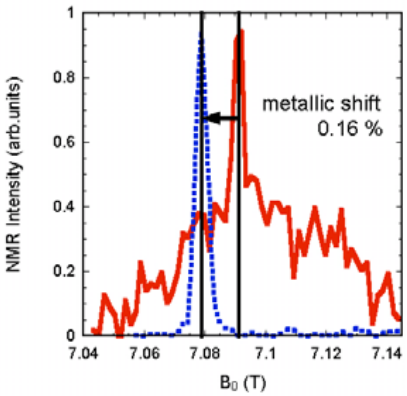

Fig.1 Al-NMR spectra of 2-dimensional $Al_{0.3}Ga_{0.7}As$/GaAs heterotructured sample (solid curve) and a bulk Al metal (dotted curve).

Here we report that, by developing the sensitivity of our custom-made spectrometer, we have succeeded, for the first time, in standard-NMR detection of the strains around the interface through the Al nuclear spins that are embedded in neither the substrate nor the GaAs layer [4].

Figure 1 shows field (B_0)-swept Al-NMR spectra of the $Al_{0.3}Ga_{0.7}As$/GaAs and a bulk Al metal. The single line shape of the dotted curve clearly indicates that the Al nuclear spins in the bulk metal feel no strains. Since the shifted value of 0.16 % is the same as the Al-metal Knight shift [5], it is very likely to say that the Al nuclear spins in the $Al_{0.3}Ga_{0.7}As$/GaAs are surely in a nonmetallic state, and that the broad structure cannot be ascribed to the distribution of the metallic shifts but to the distribution of the electric field gradient (EFG) which Al nuclear spins feel. More detailed discussion on the EFG values will be given by referring the values from refs. 2 and 3.

References

1. C. P. Slichter, *Principles of Nuclear Magnetic Resonance* (Springer, Berlin, 1989).

2. T. Ota, N. Kumada, G. Yusa, S. Miyashita and Y. Hirayama, Phys. Sta. Sol. (c) **4**, 1759 (2007).

3. T. Yamashita, H. Takahashi, M. Kawamura, Y. Hashimoto, S. Katsumoto and T. Machida, to be submitted.

4. M. Nishimori, S. Sasaki, M. Kudo, S. Watanabe and Y. Hirayama, to be submitted.

5. E. R. Andrew, W. S. Hinshaw and P. S. Tiffen, Phys. Lett. **46A**, 57 (1973).

Integer and fractional microwave induced resistance oscillations in a 2D system with moderate mobility

S. Wiedmann*, N. C. Mamani**, G. M. Gusev**, O. E. Raichev***, A. K. Bakarov** and J. C. Portal*,****

*LNCMI-CNRS, BP 166, 38042 Grenoble and INSA, 31077 Toulouse, France

** Instituto de Física da Universidade de São Paulo, São Paulo, SP, Brazil

*** Institute of Semiconductor Physics, NAS of Ukraine, Kiev, Ukraine

**** Institut Universitaire de France, 75005 Paris, France

Keywords: 2D system, microwave excitation, microwave induced resistance oscillations

Microwave induced resistance oscillations (MIROs) which occur by irradiating a two dimensional (2D) system with a continuous microwave irradiation governed by the ratio ϵ between irradiation frequency ω and cyclotron resonance ω_c have attracted much interest in both experimental and theoretical studies [1]. Remarkably, at very high microwave power, fractional MIROs or FMIROs appear at ϵ = 1/2, 3/2, 1/3,... . Several FMIROs have already been observed in [2] and theory offers actually two possibilities to explain this high power phenomenon [3][4].

First, FMIROs were ascribed to a multi-photon process [3] and second, a stepwise absorption of single photons where the commensurability effect between n Landau energy gaps and the energy of a subsequent absorption of m photons ($m \cdot \omega = n \cdot \omega_c$) lead to oscillations of the electron distribution function, and via the inelastic mechanism to oscillations in magnetoresistance [4]. In contrast to previous experiments with low density and ultrahigh mobility [2], we have carried out MIRO and FMIRO studies in samples with high density and moderate mobility ($< 2 \cdot 10^6$ cm^2/Vs), especially at high temperatures (up to 10 K) where both MIRO and FMIRO survive while Shubnikov-de Haas oscillations are almost suppressed. We obtain FMIRO features ϵ = 1/2, 1/3, 1/4, 1/5, 1/6, 1/7, 1/8 at 6.5 K. The FMIRO features are well developed, especially for odd fractions (see Figure 1). We focus on different properties of MIRO and FMIRO:

- Temperature dependence: Both, MIRO and surprisingly FMIRO survive at high temperatures
- Power dependence: MIROs occur in the linear regime whereas FMIRO is a nonlinear phenomenon
- Threshold frequency: MIROs are quenched at ≈200 GHz while for FMIROs we observe a threshold frequency $f_{th} \approx 85$ GHz, independent of the fractional value.

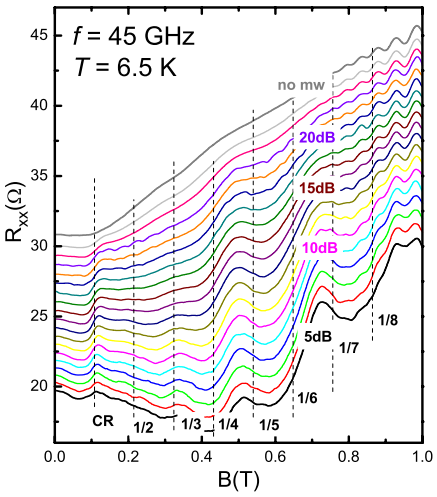

Figure 1: FMIRO features at 6.5 K under a microwave irradiation of 45 GHz.

References

[1] M. A. Zudov *et al.*, Phys. Rev. B **64**, 201311(R) (2001), R. G. Mani *et al.*, Nature **420**, 646 (2002), I. A. Dmitriev *et al.*, Phys. Rev. B **71**, 115316 (2005).

[2] M. A. Zudov *et al.*, Phys. Rev. Lett. **90**, 046807 (2003), S. I. Dorozhkin *et al.*, arXiV:cond-mat/0608633.

[3] I. A. Dmitriev *et al.*, Phys. Rev. Lett. **99**, 206805 (2007).

[4] I. V. Pechenezhskii *et al.*, JETP Letters **85**, 86, (2007).

Crossover from weak localization to anti-localization in double quantum well system

E. S. Kannan*, G. H. Kim*, I. Farrer** and D. A. Ritchie**

** School of Information and Communication Engineereing, Sungkyunkwan Univeristy, Suwon 440746, Korea and SKKU Advanced Institute of Nanotechnology, Sungkyunkwan University, Suwon 440746, Korea.*

*** Cavendish Laboratory, University of Cambridge, J. J. Thomson Avenue, Cambridge CB3 0HE, UK.*

Keywords: Double quantum well, Weak localization, Two dimensional electron gas, and Magnetoresistance

In a system with disorder, weak localization decreases the conductance of the system due to the quantum interference of time reversed path of the electron wavefunction. Applying a magnetic field breaks the time reversal symmetry and delocalizes the electrons which enable them to contribute towards conduction. It has been suggested that a crossover from weak localization to antilocalization could occur at high carrier densities when the second sub-band is occupied by the two dimensional electron gas (2DEG). Till date such crossovers were observed only in systems with strong spin orbit (SO) interaction [1].

The aim of this present work is to investigate the possibility of observing the crossover from localization to antilocalization in system with weak SO interaction. For this study, two GaAs/AlGaAs double quantum well (DQW) samples with different starting disorder were fabricated by molecular beam epitaxy on a GaAs substrate. Sample A consisted of two GaAs quantum wells with a width of 180 Å separated by a 100 Å AlGaAs barrier. The electrons were provided by the Si doping layer on each side of the quantum wells. The doping layers were separated from the quantum wells by AlGaAs layers with a thickness 500 Å. Sample B have the same structure as sample A, however self-assembled InAs quantum dots were embedded in the upper well at a distance of 40 Å from the barrier. The quantum dots acts as strong short range scattering center and hence the sample B is more disordered than sample A. Magnetoresistance measurements were taken in the four terminal configurations as a function of the gate voltage using the standard lock-in detection technique at 1.5 K. The slope of the longitudinal resistivity (ρ_{xx}) at near zero fields were calculated for sample A and B and shown in Fig. 1. At lower gate voltages, sample A exhibit weak localization effect indicated by the negative slope of ρ_{xx}. The crossover from localization to anti-localization occurs at 0.3 V, when the 2DEG densities in neighbouring wells are sufficiently off balanced. In this scenario electrons in DQW were able to screen the disorder potential and inter-well scattering becomes the dominant scattering mechanism. However in the case of sample B, no such crossover is observed due to the presence of strong disorder.

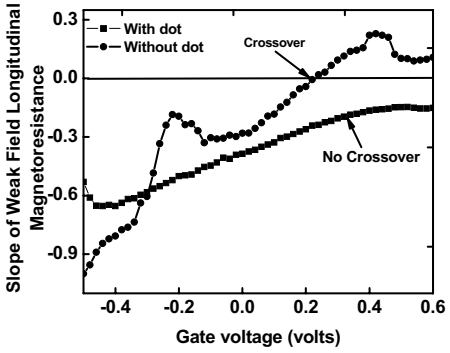

Fig.1 Slope of longitudinal magnetoresistance as a function of gate voltage for sample A and B.

References

1. Takayuki Nihei, Yoshifumi Suzuki, Makoto Kohda, and Junsaku Nitta, Phys. Stat. Sol (c) **3**, 4239 (2006).

A voltage-tunable self-switching in-plane diode in a 2D-electron system

A. Ganczarczyk*, S. Voßen*, M. Geller*, A. Lorke*, K. Piegdon**, D. Reuter*** and A. D. Wieck***
*Experimental Physics and CeNIDE, University Duisburg-Essen
**Department of Physics, University of Paderborn
*** Solid State Physics, Ruhr-Universität Bochum

Keywords: tunable rectification, nonlinear transport, two-dimensional electron gas, self-switching effect

The characteristic of a conventional semiconductor rectifier is mainly given by the properties of the materials at the interface. The turn-on voltage of a Schottky diode e. g. depends on the metal used and the doping level in the semiconductor. In contrast we present here a tunable in-plane diode in a nanoscale two-dimensional electron system, whose functionality is mainly determined by the sample geometry. The I(V)-characteristic of this rectifier can be widely tuned by an applied voltage at two in-plane side gates [1], as opposed to the fixed I(V)-characteristic of a p-n or Schottky diode.

The fabricated sample structure contains a 400 nm wide channel in a two-dimensional electron gas defined by etched insulating trenches (see inset of Fig. 1). As the gate voltage is defined with respect to the drain contact, the applied source-drain voltage will cause an asymmetry in the lateral depletion region of the narrow channel. The working principle is based on the lateral pinch off effect, which modulates the width of the depletion zones of the narrow etched channel. Depending on the orientation of the source-drain voltage, the channel will be populated with electrons (the channel opens) or depleted (it closes), which results in the diode-like I(V)-characteristic.

An in-plane diode based on this effect without two side gates has previously been presented by Song et al. [2]. However, we demonstrate here the voltage-tunability of the self-switching device (SSD) achieved by two additional in-plane side gates (see inset of Fig. 1), which modulate the width of the depletion zones of the electron channel. Therefore, the non-linear diode characteristic of the SSD can be controlled by the bias V_G applied to the side gate contacts, seen in Fig.1. For instance, we find that the on-voltage of the diode depends linearly on the side gate voltage V_G and can be tuned from about -0.15 V up to -0.70 V, which is in contrast to a fixed on-voltage of a conventional p-n diode, where the on-voltage depends mainly on the material properties.

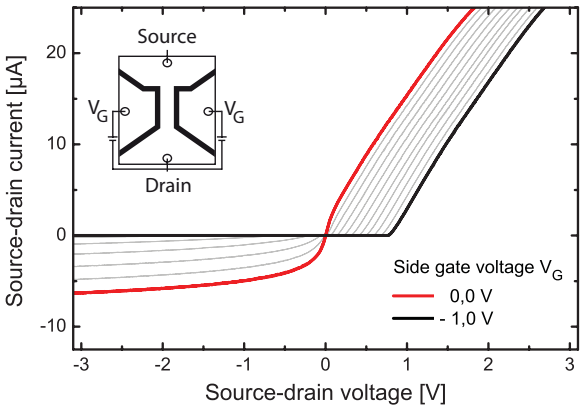

Figure 1: I(V)-characteristic of the voltage-tunable self-switching in-plane diode for different side gate voltages. Inset: Schematic picture of the device.

An applied sine-wave to the source-drain contacts demonstrates a rectification of the device up to the cut-off frequency of about 25 kHz, at the moment limited by the parasitic RC element. An on-voltage in the same range as in the dc case is measured and the rectifier behaves like a half-wave rectifier. For frequencies above 25 kHz the half-wave rectifier gradually changes itself into a constant-current rectifier, which exhibits a DC output current up to frequencies of at least 200 MHz.

References

[1] A. D. Wieck and K. Ploog, Appl. Phys. Lett. 56, 928-930 (1990).

[2] A. M. Song, M. Missous, P. Omling, A. R. Peaker, L. Samuelson, and W. Seifert, Appl. Phys. Lett. 83, 1881-1883 (2003).

Microwave-induced DC currents in mesoscopic structures

L. C. Li[a], Y. T. Sung[b], C. W. Chang[c], Y. W. Suen[b,c,d], K. Y. Chen[e], C. T. Liang[e], Y. F. Chen[e], B. C. Lee[f], and C. P. Lee[a,f]

[a] *Center for Nanoscience and Technology, National Chiao Tung University, Hsinchu, Taiwan, R.O.C.*

[b] *National Nano Device Laboratories, Hsinchu, Taiwan, R.O.C.*

[c] *Department of Physics, National Chung Hsing University, Taichung, Taiwan, R.O.C.*

[d] *Institute of Nanoscience, National Chung Hsing University, Taichung, Taiwan, R.O.C.*

[e] *Department of Physics, National Taiwan University, Taipei, Taiwan, R.O.C.*

[f] *Department of Electronics Engineering, National Chiao Tung University, Hsinchu, Taiwan, R.O.C.*

Keywords: mesoscopic, microwave-induced, photocurrent, magnetic field

We report on the power (P) and also the magnetic-field (B) dependence of microwave (MW)-induced photocurrents (I_{ph}) in mesoscopic structures. The samples were fabricated from two-dimensional electron gases (2DEGs) embedded in GaAs/AlGaAs heterostructures with areal density of 1.9×10^{11} cm^{-2} and low-T (1.4 K) mobility of 2.4×10^{5} cm^2/Vs. Two crossing 1-μm-wide channels were defined by e-beam lithography and wet mesa etching. The MW signal (500 MHz ~ 18 GHz) was fed onto the sample through a 3-mm-diameter loop antenna placed about 5 mm above the sample. I_{ph} was measured from a pair of ohmic contacts (their linearity was carefully checked) connected to the channels.

In the frequency (f) range we have studied, I_{ph} does not exhibit a simple behavior against the change of the magnitude (V_{ac}) of MW signal. Figure 1 (a) gives an example for f = 3 GHz: I_{ph} even decreases with increasing V_{ac} The details of the I_{ph}-V_{ac} curve are very sensitive to f. We also found that this behavior is not very sensitive to T between 1.4 and 4.2 K. By contrast, the data for a standard macroscopic Hall bar sample did not show this non-monotonous behavior, suggesting that such a behavior may relate to the boundaries or some specific impurities of the mesoscopic channels. Further scrutinizing the low-power data as shown in Fig. 1(b), we found that I_{ph} is roughly proportional to P (or V_{ac}^2); this dependence is quite universal for data at different f and has been predicted for diffusion-limited electron transport in mesoscopic systems [1].

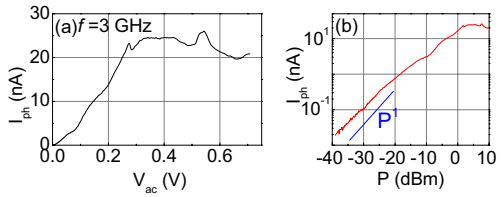

Fig. 1 (a) I_{ph} vs. V_{ac} for f = 3 GHz at T = 1.4 K. (b) I_{ph} vs. P. V_{ac} and P are the nominal output voltage and the power of the microwave signal generator respectively.

We also investigated the B-dependence of I_{ph}. Figure 2 (a) shows a typical sweep for both directions of B. Apparently the data are not symmetric against reversal of B direction. We can separate the symmetric part from the anti-symmetric part via I_{sym} = [$I_{ph}(B)$+ $I_{ph}(-B)$]/2 and $I_{antisym}$ = [$I_{ph}(B)$-$I_{ph}(-B)$]/2 as shown in Fig. 2(b). I_{sym} and $I_{antisym}$ should originate from scattering mechanisms with different time-reversal symmetric properties [2].

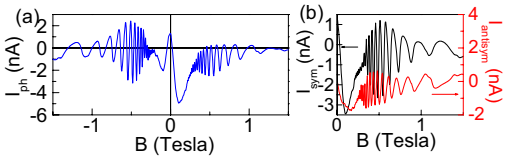

Fig. 2 (a) I_{ph} vs B for f = 15.13 GHz and P = -5 dBm at T = 1.4 K. (b) I_{sym} and $I_{antisym}$ vs B.

References

1. V. Falko, Europhysics Letts. **8**, 785 (1989)

2. M. L. Polianski and M. Büttiker, Phys. Rev. B **76**, 205308 (2007)

Re-examination of the single-particle relaxation lifetime for homogeneous background impurities in the two-dimensional electron gas

T. P. Martin*, S. J. MacLeod*, K. Chan*, A. R. Hamilton*, A. See*, A. P. Micolich*, M. Aagesen**, and P. E. Lindelof**

* *School of Physics, University of New South Wales, Sydney NSW 2052, Australia*

** *Nano-science center, University of Copenhagen, Universitetsparken 5, DK-2100 Copenhagen, Denmark*

Keywords: quantum lifetime, homogeneous background impurities, impurity scattering, multiple-scattering

Charged Coulomb impurities in the lattice of a crystal, known as homogeneous background impurities, are present in every semiconductor device. Background impurity scattering can limit the mobility at low temperatures where phonon scattering has been suppressed, particularly in the cleanest devices where charge carriers are introduced by remote donors, or electrostatically by a gate electrode. High-mobility applications in two-dimensional electron systems (2DES), such as topological quantum computation using non-Abelian quarter-charge states [1,2], have brought about renewed interest in understanding and reducing scattering mechanisms that limit the mobility in high-quality heterostructures.

A comparison between the quantum τ_q and transport τ_t lifetimes can give an indication of the dominant scattering mechanism in a 2DES [3,4]. A small ratio τ_t/τ_q indicates that large-angle scattering events, often a result of background impurities close to the plane of conduction, dominate the transport. Comparing this analysis with theory has traditionally been problematic because the quantum lifetime for background impurities is divergent in the lowest order theory [3].

In this work we derive a non-divergent τ_q for finite thickness heterostructures, both in the lowest order theory and using the more sophisticated multiple-scattering approach [3,4]. We present the first comparison of theoretical results for τ_q and τ_t with measurements of an accumulation mode 2DES, which operates in the absence of remote doping. We obtain good agreement between our theory and the experiment, and are able to use the theory to extract the background impurity density in the different layers of the measured heterostructure.

Finally, we find that the correct rule for determining the dominant scattering mechanism in a 2DES should be $\tau_t/\tau_q \lesssim 10$ for background impurities and $\tau_t/\tau_q \gtrsim 10$ for remote ionized impurities, which departs from previous suggestions that the ratio should be order 1 for background impurity scattering [5].

References

1. S. Das Sarma, M. Freedman, and C. Nayak, Phys. Rev. Lett. **94**, 166802 (2005).
2. M. Dolev *et al.*, Nature **452**, 829–834 (2008).
3. A. Gold, Phys. Rev. B **38**, 10798–10811 (1988).
4. S. J. MacLeod *et al.*, Proc. SPIE **6800**, 68001L (2007).
5. For example, see S. Das Sarma and F. Stern, Phys. Rev. B **32**, 8442–8444 (1985).

Two-parameter scaling in 2D transport though a Ge/Si quantum dot array

N.P. Stepina, E.S. Koptev, A.V. Dvurechenskii and A.I. Nikiforov
Institute of Semiconductor Physics, Novosibirsk, Russia

Keywords: 2D quantum dots, localization, scaling, hopping,

To describe the transport behavior of disordered systems, the authors [1] proposed a one-parameter scaling theory in which the disorder parameter Z [2] determining the system state was found to coincide with the non-dimensional (in units of e^2/h) conductance G. However, the authors [3] showed theoretically that two-, instead of one-parameter scaling defines the system state in 2D systems, with one scaling variable being governed by disorder, and the other, by the electron-electron (e-e) interaction. For such evidence to be gained, the e-e interaction and the disorder have to be varied independently. However, in the majority of reported studies, the transport behavior was analyzed while varying just one parameter, the carrier concentration N_e, affecting both the disorder and the interaction.

In the present study, the scaling hypothesis was scrutinized when studying the conductance behavior in 2D tunnel-coupled Ge quantum dots in Si at different correlations between the disorder and e-e interaction. Three ways to vary the disorder, the hopping integral, and the interaction force, were proposed and realized in this work. First, the average number of holes in QD was varied by the boron concentration in the δ-doped Si layer inserted 5 nm below the QD layer. Second, to enhance the hopping integral and the interaction without significant change of structural disorder, the QD array density value was varied by changing the growth regimes. Third, annealing at $T = 480 - 625$°C was employed to modify the size and composition of the Ge islands, which was expected to enhance the overlap of carrier wave functions without seriously affecting the e-e interaction in the system. To reveal the influence which the e-e interaction has on the transport behavior of the QD systems under study, we used samples in which the long-range Coulomb potential was screened with a metal plane located close to the QD layer.

The conductance mechanism has been thoroughly examined when analyzed the conductance nonlinearity and the temperature dependence of conductance within the strong- and weak-localization approaches. As a result, we identified a transition from hopping to diffusion transport, and the range of intermediate conductance values was found to be ($0.4e^2/h \geq G \geq 10^{-2}e^2/h$).

When checking the scaling hypothesis for our samples, we found that both the interaction and the disorder determine the transport mode of the system and the transition from strong to weak localization. With the interaction force changing insignificantly, data taken from samples with different QD array densities and from samples annealed at different conditions can be described with one-parameter scaling practically for all used dot filling factors ν. The only sample in which the interaction reaches a maximum value (ν=2), exhibited an upward shift of the Gell-Mann-Low function [1] from the common curve for all other samples, suggesting that the interaction is the second parameter determining the system state. The role of the long-range Coulomb interaction is definitely confirmed by the observation of downward shift of the universal scaling curve in the case when the interaction is screened by the metal plane located nearby of the QDs plane. This result is the direct indication that not only disorder but also interaction determine the system behavior and confirms two-parametric scaling in the interacting 2D systems. Independent contribution of these parameters into scaling has never been observed experimentally before.

References

[1] E. Abrahams, P.W. Anderson, D.C. Licciardello, T.V. Ramakrishnan. Phys. Rev. Lett. **61**, 673 (1979).

[2] Anderson P.W. Phys. Rev. **109**, 1492 (1958).

[3] A.Punnose and A.M. Finkelstein, Science **310**, 289 (2005).

What can we learn on the "universal" exchange-correlation energy of Density Functional Theory from the subband electronic structure of semiconductor quantum wells?

C. R. Proetto*, and S. Rigamonti**

* *Institute für Theoretische Physik, Freie Universität Berlin, Berlin, Germany*

** *Donostia International Physics Center (DIPC), San Sebastian, Spain*

Keywords: DFT, exchange-correlation energy, quantum wells, inter-subband transitions

Density Functional Theory (DFT) has become the standard calculation tool in quantum chemistry and physics for the study of atomic, molecular, and solid state systems. The key ingredient of any DFT code is the exchange-correlation (*xc*) component of the total energy functional (E_{xc}), for which DFT itself does not give any clue and should be necessarily approximated. In this talk, recent results will be discussed concerning the presence of striking many-body induced discontinuities in the electronic spectra of semiconductor quantum wells (QW), as the number of occupied subbands changes from N to $N + 1$. These novel results have been obtained through the development of a new DFT accurate calculation method, specially designed for the treatment of strongly correlated and inhomogeneous low-dimensional systems. The potentiality of the method has been already demonstrated at the *x*-only level (i.e., neglecting correlation) [1]. The new key ingredient from which the discontinuities are derived is the use of an *ab-initio* generated functional for E_{xc} which includes *exchange exactly*, and *correlation* in an *exact partial* way [2]. The discontinuities will be transparently exemplified by the detailed study of the QW inter-subband transition energies. As the QW chemical potential touches the bottom of the second subband, the ground state – first excited inter-subband transition energy suffers an abrupt renormalization, as a result of the competing effects of exchange, which induces a positive jump, and correlation, which induces also a discontinuous change but with the opposite sign. Interestingly, correlation overcomes exchange, being this crucial for obtaining an excellent qualitative and quantitative agreement with available experimental data. Continuum approximations to *xc* functionals, including all currently widely used LDA's and GGA's, fail to reproduce the correct discontinuities. It is expected that this *ab-initio* generated functional will be very valuable for the study of confined electron gases in 2D and 1D, leading to a rich interplay between theory and experiment. Given the "universal" character of the *xc* functional, its "characterization" through calculations and experiments in QW's may be important in other fields of physics. As an example of this, and building on the unique knowledge gained is the semiconductor QW system, I will discuss a deep and fruitful connection between these discontinuities, and the long-standing puzzle of the severe underestimation of the fundamental band gap for all semiconductors by current available approximations for bulk DFT functionals.

References

1. C. M. Horowitz, S. Rigamonti, and C. R. Proetto, Phys. Rev. Lett. **97**, 026802 (2006).

2. S. Rigamonti and C. R. Proetto, Phys. Rev. Lett. **98**, 066806 (2007).

Quantum effects in linear and non-linear transport of three-terminal ballistic junctions.

J. Wróbel*, P. Zagrajek*, M. Czapkiewicz*, M. Bek**,
K. Fronc*, R. Hey***, K. H. Ploog***, B. Bułka**, T. Dietl*,****
*Instytut Fizyki PAN, Warszawa, Poland
** Instytut Fizyki Molekularnej PAN, Poznań, Poland
***Paul Drude Institute, Berlin, Germany
****Instytut Fizyki Teoretycznej, Uniwersytet Warszawski, Warszawa, Poland

Keywords: quantum transport, three-terminal branch switches, linear and nonlinear effects.

Recently, the so-called tree-terminal ballistic junctions (TBJs) are seriously considered as the next-generation nanoelectronic devices. Such structures consist of three quantum wires connected via a ballistic cavity to form a Y-shaped or T-shaped current splitter which in principle can operate at high speed with a very low power consumption. The interesting and unexpected nonlinear transport characteristics of TBJs are intensively investigated due to possible applications of such devices in logic circuits. Large number of new phenomena, which are theoretically proposed and experimentally demonstrated for Y-branch (or T-branch) switches [1], originate from the ballistic motion of charge carriers and from the self–consistent nature of a one-dimensional potential profile.

In this work we report on fabrication and low temperature transport measurements of T-shaped tree-terminal devices, based on a high mobility GaAs/AlGaAs:Si heterostructure with electron concentration $n_{2D} = 2.3 \times 10^{11}$ cm^{-2} and carrier mobility $\mu = 1.8 \times 10^6$ cm^2/Vs. The interconnected wires of length $L = 0.6$ μm and lithographic width $W_{lith} = 0.4$ μm are patterned by *e*-beam lithography and shallow-etching techniques to form a T-shaped nanojunction. The physical width of all branches is controlled by means of a top metal gate which is evaporated over the entire structure. The differential conductances G_{ij} have been measured in a He-3/He-4 dilution refrigerator, by employing a standard low-frequency lock-in technique, here $i, j = 1, 2, 3$ enumerate all distinct terminals of the device (e.g. $i = 1$ corresponds to the lower part of the letter T). In particular, data shows that G_{23} is quantized as a function of gate voltage, whereas G_{12} (or G_{13}) oscillates strongly. Such observations indicate that transport through the junction area is ballistic, however, in the central part of the device a certain asymmetry is present. The bend resistance of such asymmetric TBJ is modeled using a recursive Green function technique and the results are compared with experimental data.

We have also studied the non-linear transport in the typical for TBJs, the so-called *push-pull* bias regime, when equal but opposite in sign dc voltages are simultaneously applied to the left (2) and right (3) input terminals. The usage of modulation technique has enabled to measure the output voltage (V_1) at small bias regions i.e. for $|V_2| = |V_3| < 10$ mV. For the first time we have shown that output voltage can assume either negative or positive values as a function of Fermi energy. This behavior was predicted theoretically in [2] for Y-shaped device and is attributed to the formation of quasibound states in the junction cavity region. Our calculations for symmetric and non-symmetric TBJs show that for such geometry it is in fact the bend resistance effect, which is responsible a positive value of the output voltage.

We acknowledge the support by the European Science Foundation EUROCORES Programme FoNE by funds from the Ministry of Science and Higher Education and EC Project SPINTRA (contract N.ERAS-CT-2003-980409) and also Semiconductor Spintronics ERATO project by JST.

References

[1] Hongqi Xu, Nature Mat., **4**, 649 (2005).

[2] D. Csontos and Hongqi Xu, Phys. Rev. B **67**, 235322 (2003).

Photoluminescence spectra of gated undoped quantum well with lateral potential modulation in low electron density

M. Yamaguchi*, S. Nomura*,**, H. Tamura*, and T. Akazaki*

** NTT Basic Research Laboratories, NTT Corporation, 3-1 Morinosato-Wakamiya, Atsugi, 243-0198, Japan.*
*** Institute of Physics, University of Tsukuba, 1-1-1 Tennodai, Tsukuba, 305-8571, Japan.*

Keywords: charged exciton, photoluminescence, modulation potential

We present an observation of the change of photoluminescence (PL) intensity ratio of neutral (X_0) and charged (X^-) excitons near the onset of two-dimensional electron system (2DES) formation with lateral potential modulations. Under optical excitation, the patterned-gate bias is expected to modulate the photo-created-hole distribution in 2DES regime and the binding energies of X_0 and X^- below the onset of the 2DES formation, which can be detected by PL. The PL measurement is advantageous for studying the low electron density regimes and particularly interesting for the properties near the onset of 2DES formation [1]. Our gated undoped GaAs QWs are advantageous for controlling the electron density precisely and achieving a high mobility at low electron density, enabling us to observe interesting many-body phenomena [2]. In addition, it is possible to control the electrostatic potential independently from the electron density by means of the front and back gates.

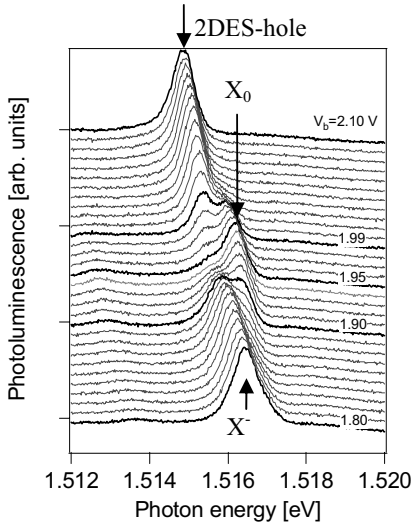

Fig. 1. PL spectra of the sample with 500-nm square mesh at 2 K for different gate voltages.

In this paper, we present the results of a low temperature PL measurement on a 250-nm-deep 20-nm GaAs back-gated QW with semi-transparent square mesh surface gates. The mesh spacing are 1000, 500, 400, and 300-nm with 100-nm-width metallic lines of a 0.5-mm-square in size.

We observed an abrupt enhancement of the X_0 peak in between the transition from X^- to 2DES-hole peaks as shown in Fig. 1, which was absent in QWs without lateral modulation potential where the X^- peak continuously changes to the 2DES-hole peak while X_0 peak is monotonically weakened by electron accumulation [3,4]. This enhancement was reproduced in all five samples with mesh surface gates we measured, although there were some variations in the bias voltage dependence of the PL intensities and the energy. This enhancement was not observed for a sample with a flat surface gate. The change from X_0 to 2DES-hole peaks corresponded to the onset of the 2DES formation detected by capacitance measurements between the back gate and 2DES. One possible explanation of the X_0 enhancement is the diffusion of the photo-created holes into the lower potential region, which is the void in the electron sea. The mesh surface gate plays an essential role in producing such an enhancement near the onset of the 2DES.

This work was partly supported by KAKENHI No. 20104005.

References

1. M. Yamaguchi *et al*., Phys. Rev. Lett. **101**, 207401 (2008).
2. S. Nomura *et al*., Phys, Rev. B. **76**, R201306(2007).
3. G. Finkelstein *et al.,* Phys. Rev. Lett. **74**, 976(1995).
4. M. T. Portella-Oberli *et al.*, Phys. Rev. Lett. **102**, 096402 (2009).

Measuring hybridization in GaInAs/InP electron billiard arrays

M. S. Fairbanks[1], T. P. Martin[2], B. C. Scannell[1], C. A. Marlow[1], H. Linke[1,3] and R. P. Taylor[1]

[1] *Department of Physics, University of Oregon, Eugene OR, USA*

[2] *School of Physics, University of New South Wales, Sydney, Australia*

[3] *Division of Solid State Physics, Lund University, Lund, Sweden*

Keywords: electron billiards, transport, hybridization

Arrays of electron billiards are of interest to fundamental (e.g. quantum coherence [1]) and applied (e.g. quantum computing [2] and spintronics [3]) research. Generally, understanding how individual array elements combine and interact is of crucial importance in developing circuits and hence more complex functionality. Work in the 'open' regime (where no tunneling is required for transport) is mostly limited to the canonical $Al_xGa_{1-x}As/GaAs$ heterostructure, where devices are defined via patterned surface gates [5]. However, etched $Ga_xIn_{1-x}As$ heterostructures have recently been used in the fields of quantum coherence [6] and engineered conductance asymmetry [7] because of their reduced effective mass (~ 0.04 – 0.05m_e compared to 0.067m_e for GaAs) and steeper confinement potentials.

We use the $Ga_{0.25}In_{0.75}As/InP$ heterostructures to address the question of how the energy level spectrum of open arrays evolves with the number of elements in the arrays and their coupling strength. We develop a novel metrology technique for measuring average energy level spacing (ΔE_s) based on magnetoconductance fluctuations (MCF). We apply this technique to two array devices, consisting of one and two billiards coupled by quantum point contacts. The presence of hybridization between array elements is demonstrated by a distinct reduction of ΔE_s between the single and double element arrays (Fig. 1). Fourier decomposition and variance analysis of the MCF in the universal regime lend further support to our conclusion.

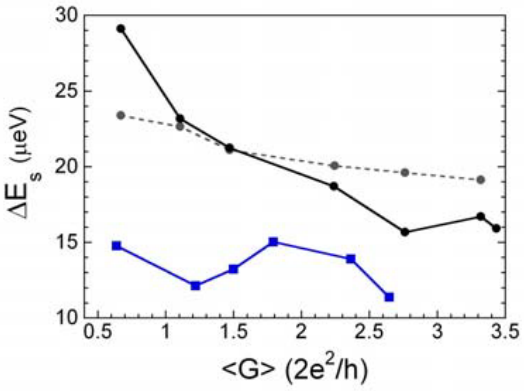

Figure 1. The average energy level spacing in the arrays vs. the coupling strength. One (black circles) and two (squares) element arrays are shown. The one element ΔE_s estimated from lithographic area is shown in gray as a baseline.

References

1. R. H. Blick, D. Pfannkuche, et al., Phys. Rev. Lett. **80**, 4032 (1998).

2. P. Zanardi and F. Rossi, Phys. Rev. Lett. **81**, 4752 (1998).

3. E. A. Laird, J. R. Petta, A. C. Johnson et al., Phys. Rev. Lett. **97**, 056801 (2006).

5. M. Elhassan, J.P. Bird, et al., Phys. Rev. B **64**, 085325 (2001).

6. B. Hackens, S. Faniel, et al., Phys. Rev. Lett. **94**, 146802 (2005).

7. C. A. Marlow, R. P. Taylor, et al., Phys. Rev. Lett. **96**, 116801 (2006).

Quantum interference effects in a laterally coupled triple quantum dot containing a quantum dot charge sensor

T. Kubo[1], Y. Tokura[1,2], T. Hatano[1], S. Amaha[1], S. Teraoka[1] and S. Tarucha[1,3]
[1]*Quantum Spin Information Project, ICORP, JST, Atsugi-shi, Kanagawa, Japan*
[2]*NTT Basic Research Laboratories, NTT Corporation, Atsugi-shi, Kanagawa, Japan*
[3]*Department of Applied Physics, University of Tokyo, Hongo, Bunkyo-ku, Tokyo, Japan*

Keywords: laterally coupled triple quantum dot, charge sensing, Aharonov-Bohm effect, Schwinger-Keldysh nonequilibrium perturbative approach

Particle-wave duality is one of the most essential concepts in quantum theory and provides perhaps the most vivid illustration of Bohr's complementarity principle [1]. The wave-like property occurs only when the different possible paths a particle can take are indistinguishable, even in principle. The introduction of a which-path detector [2] for determining the actual path taken by the particle inevitably involved coupling the particle to a measuring environment, which in turn results in dephasing. In other words, simultaneous observation of particle and wave behaviors is prohibited.

Mesoscopic systems can be often used to study the interplay between interference and dephasing of electrons. Nano-fabrication and low-temperture measuring techniques using semiconductors have enabled us to observe a variety of coherent effects of electrons such as Aharonov-Bohm (AB) [3], Fano, and Kondo effects.

In this work, we investigate the effects of observation on quantum interference in a laterally coupled double quantum dot (DQD) due to a coupling with a quantum dot charge sensor as shown in Fig. 1. We employ the nonequilibrium Green's function method based on the Schwinger-Keldysh formalism [4, 5]. We consider the inter-dot Coulomb interactions V_{inter}, V_S, xV_S as perturbations, where V_S is the sensing interaction strength, and $0 < x \leq 1$. In particular, we introduce the notion of the coherent indirect coupling, which characterizes the strength of the coherent indirect coupling between two quantum dots via the reservoirs [6]. For the tunneling process from ith QD to jth QD via the reservoir ν, we take into account the propagation process of electrons in the reservoir. In general, the coherent indirect coupling parameter is a function of the propagation length s_{ij}^{ν} in the reservoir $\nu(= S, LD)$ shown in Fig. 1. The coherent indirect coupling plays an important roll on the quantum interference effects such as AB effects. We show that the visibility of AB oscillations for the tunneling current through a DQD not only decreases but also increases, according to the situations, by a charge sensing.

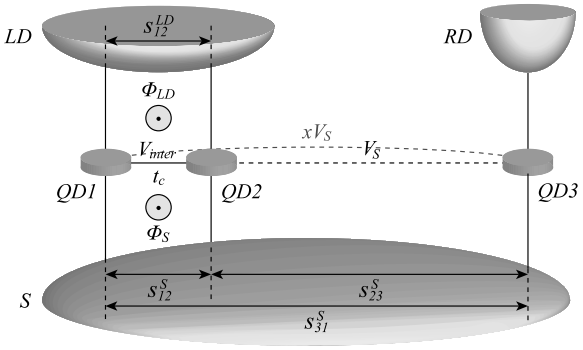

Figure 1: Schematic diagram of a laterally coupled double quantum dot (QD1, QD2) with a capacitively coupled quantum dot charge sensor (QD3). V_{inter} and V_S are inter-dot Coulomb interaction and capacitive coupling energy of the charge sensor, respectively.

References

[1] N. Bohr, Nature **121**, 580 (1928).

[2] E. Buks, R. Schuster, M. Heiblum, D. Mahalu, and V. Umansky, Nature **391**, 871 (1998).

[3] T. Hatano, M. Stopa, W. Izumida, T. Yamaguchi, T. Ota, and S. Tarucha, Physica E **22**, 534 (2004).

[4] J. Schwinger, J. Math. Phys. **2**, 407 (1961).

[5] L. V. Keldysh, Sov. Phys. JETP **20**, 1018 (1965).

[6] T. Kubo, Y. Tokura, T. Hatano, and S. Tarucha, Phys. Rev. B **74**, 205310 (2006).

Optical detected magnetoplasma effects in CdTe dense two dimensional electron systems

Y. Imanaka*, K. Takehana*, T. Takamasu*, G. Kido*, G. Karczewski**, T. Wojtowicz** and J. Kossut**
*National Institute for Materials Science, Tsukuba, Ibaraki, Japan
** Institute of Physics, Polish Academy of Sciences, Warsaw, Poland

Keywords: Cyclotron resonance, quantum oscillation, II-VI semiconductor, high magnetic field

Among polar materials, II-VI semiconductors are the one of good candidates for studying the polaron effects through cyclotron resonance (CR) in high magnetic fields. CR is the most direct method to study the effective mass of semiconductors, and the larger polaron mass can be observed in II-VI compounds around a LO phonon energy as the resonant polaron effect.

Recent progresses of epitaxial growth techniques enable us to study the quantum Hall effect even in CdTe two dimensional electron systems (2DES). We have been studying the THz CR in the CdTe and CdMnTe 2DES at high magnetic fields up to 18T [1, 2]. However, in GaAs heterostructures with a dense 2 dimensional electron gas (2DEG), the resonant polaron effect was found to be suppressed because of the occupation effect of the Landau levels [3]. Magneto transmission, CR spectra are strongly affected by the carrier density of samples.

In this study, we have investigated the carrier density dependence of the CR in the CdTe quantum Hall systems in order to study polaron and magnetoplasma effects. For the wide range of the CR experiments between 40GHz to a THz region, we used a Fourier transform infrared spectrometer and a vector network analyzer with a superconducting magnet up to 15T. The substrate of samples was wedged to avoid interference effects.

Figure 1 shows typical CR spectra in a sample with high carrier density at 43.44 GHz. In addition to the CR absorption at lower fields, the periodic oscillation of the magneto transmission is observed at higher magnetic fields. The inset shows the plot of the transmission against the filling factor of Landau levels, which is calculated with n=4.4$\times 10^{11}$cm^{-2}. The obtained carrier concentration is in good agreement with the data from transport measurements in the same sample [2]. The optical detected quantum oscillation in the 2DES is due to a magnetoplasma effect in the sample which have relatively high carrier concentration and mobility.

We have also observed the suppression of the resonant polaron effect in the magnetic field dependence of the CR for samples having the carrier density more than 3×10^{11}cm^{-2}. We have already studied the CR in several samples, and the magnetic field dependence of the polaron mass will be discussed for the wide range of the carrier concentration between 1-6$\times 10^{11}$cm^{-2}.

References

[1] Y. Imanaka et. al., Physica B **298**, 392 (2001).

[2] G. Karczewski et. al., phys. stat. sol. (b) **229**, 597 (2002).

[3] X. G. Wu et. al., Phys. Rev. Lett. **84**, 4934 (2000).

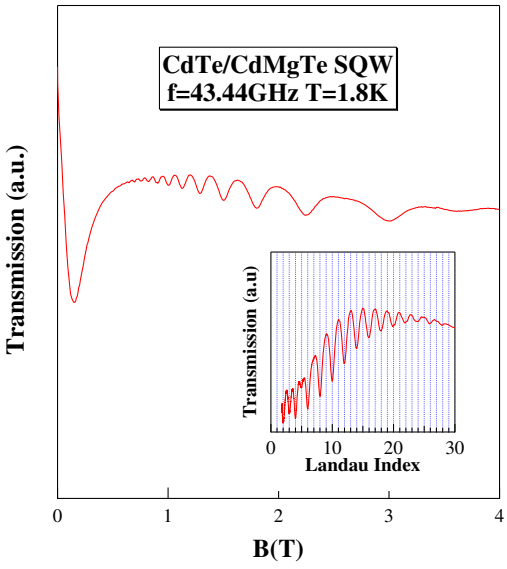

Figure 1: Magneto transmission spectrum in a CdTe quantum Hall system at f=43.44GHz. The transmission is oscillated against integer filling factors clearly.

Control of the quantum dots angular emission pattern in photonic crystal microcavities

M. Abbarchi*, F. Intonti *, S. Vignolini*, A. Vinattieri*, L. Balet**, L.H.Li**, M. Francardi***, A. Fiore****, and M. Gurioli*

*Physics department University of Firenze, Via Sansone 1, 50019 Sesto Fiorentino (Firenze), Italy

**EPFL, Institute of Photonics and Quantum Electronics, Station 3, CH-1015 Lausanne, Switzerland

***Institute of Photonics and Nanotechnology, CNR, via del Cineto Romano 42, 00156 Roma, Italy

****COBRA Research Institute, Eindhoven University of Technology, 5600 MB Eindhoven, The Netherlands

Keywords: Photonic crystal, microcavity, quantum dots

Optical microcavity (MC) can be created by introducing a structural defect into a perfect photonic crystal (PhC) and this opened the way to control the flow of light in unprecedented ways. Among different structures and geometry, a major role is played by slab structures processed with standard fabrication processes [1]. After the pioneering work on the PhC-MC laser [1], several cavity structures have been demonstrated, showing rich characteristics, in particular high Q/V value [2]. For technological application, an important aspect is the out-coupling into a single mode fiber using conventional optics, therefore the far-field of the PhC resonator should be well directed and the forward emission optimized [3]. In this contribution, we experimentally demonstrate the success of a simple design for finely controlling the vertical angular emission pattern out-coupling of PhC light emitters. Angularly resolved photoluminescnece spectroscopy is employed to characterize the angular pattern of a series of samples. The devices investigated are made of a slab of GaAs with embedded InAs quantum dots. A hexagonal lattice of holes has been patterned into the slab to form the photonic crystal. The cavity itself is formed by a single missing air-hole in a two dimensional triangular lattice (H1 PhC-MC). This cavity has been chosen for its small size to facilitate a high spontaneous emission enhancement. Geometry changes have been applied to the holes adjacent to the defect, as originally suggested by Akahane et al. [2]. The holes have been modified by resizing and radially moving each of them by the same value to preserve the hexagonal symmetry. We experimentally observe that the angular pattern can be tailored and controlled by small changes in the radius and position of the modified hole. Typical angular patterns of the fundamental optical mode of two different modified H1 cavities are reported in Fig.1.

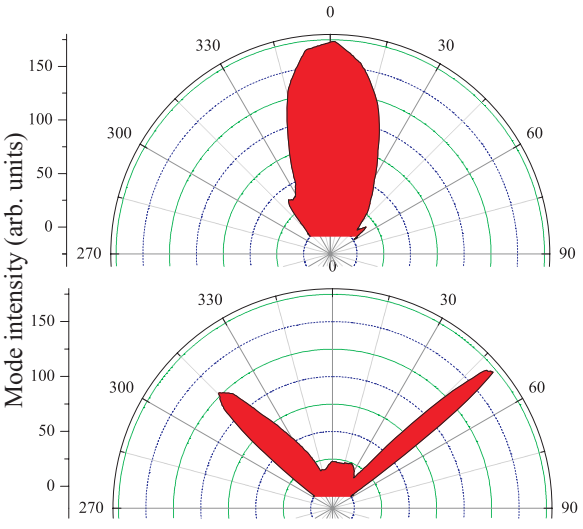

Figure 1: Typically angular pattern of the fundamental optical mode of two different modified H1 PhC-MC, with slight variations of the radius and position of the modified hole

References

[1] O. Painter, et al. , Science 284, 1819 (1999).

[2] Y. Akahane, et al. , Nature 425, 944 (2003).

[3] S.H.Kim et al Phys. Rev. B 73, 235117 (2006).

Band alignment of lattice-matched InGaPN/GaAs and GaAs/InGaPN quantum wells grown by MOVPE

D. Kaewket*, S. Sanorpim*, S. Tungasmita*, R. Katayama** and K. Onabe**

** Department of Physics, Faculty of Science, Chulalongkorn University, Bangkok, Thailand*

*** Department of Advanced Materials Science, The University of Tokyo, Chiba, Japan*

Keywords: InGaPN, band alignment, quantum well, MOVPE

InGaPN, which is the material in the group of dilute nitrides, can be lattice-matched to the GaAs and GaP substrate materials [1]. Its potential applications conclude of optoelectronic and electronic devices such as light emitting diodes, laser diodes and heterojunction bipolar transistors [2]. Moreover, it has potential to become a part of important development of sustainable energy. It is well known that the incorporation of N drastically reduces the bandgap energy [3]. The bandgap and lattice parameter engineering with controlling of In and N concentrations are interested for photovoltaic applications. Moreover, its corrosion resistance property is suitable for photoelectrochemical applications which produce H_2 for fuel cells [4]. The band alignment of two contact interface becomes crucial with those applications. The one approach to observe this effect is studying of quantum well (QW) structures which are simple for fabricating and understanding. Until now, there have been only few reports on InGaPN/GaAs both bulk and QW structures.

In this work, we will present the report on lattice-matched $In_{0.53}Ga_{0.47}P_{0.98}N_{0.02}$/GaAs bulk film, $In_{0.53}Ga_{0.47}P_{0.98}N_{0.02}$/GaAs and GaAs/$In_{0.53}Ga_{0.47}P_{0.98}N_{0.02}$ single quantum wells (SQWs) grown by metal-organic vapor phase epitaxy (MOVPE). High-resolution x-ray diffraction (HRXRD) and temperature dependent (10 – 300K) photoluminescence (PL) were performed. PL emission observed from all samples can be divided into high (1.4 – 2.0 eV) and low (1.0 -1.5 eV) energy regions. The evidences are clarified as follows: (i) for high energy range, $In_{0.53}Ga_{0.47}P_{0.98}N_{0.02}$/GaAs bulk layer and GaAs/$In_{0.53}Ga_{0.47}P_{0.98}N_{0.02}$ SQW exhibit red emission at 1.73 eV related to the InGaPN emission, but no emission at 1.73 eV was observed for $In_{0.53}Ga_{0.47}P_{0.98}N_{0.02}$/GaAs SQW; (ii) for low energy range, broad peak at energy around 1.32 eV was observed for all samples. In addition, extra peaks appeared at higher-energy side of the broad peak were observed at 1.35 eV and 1.36 eV for GaAs/$In_{0.53}Ga_{0.47}P_{0.98}N_{0.02}$ and $In_{0.53}Ga_{0.47}P_{0.98}N_{0.02}$/GaAs SQWs, respectively. All evidences indicate that $In_{0.53}Ga_{0.47}P_{0.98}N_{0.02}$/GaAs heterostructure is type II band alignment. The valence band offset and conduction band offset estimated from the luminescence of these two SQWs are around 450 meV and 150 meV, respectively.

References

1. K. Onabe, T. Kimura, N. Nakadan, J. Wu, Y. Ito, S. Yoshida, J. Kikawa and Y. Shiraki, presented at ICCG-13/ICVGE-11, Kyoto, 2001.

2. Y. G. Hong, R. Andre, C. W. Tu, J. Vac. Sci. Technol. B. **19**, 1413 (2001)

3. M. Kondow, K. Uomi, A. Niwa, T. Kitatani, S. Watahiki, Y. Yazawa, Jpn. J. Appl. Phys. **35**, 1273 (1996)

4. T. G. Deutsch, J. L. Head, and J. Turner, J. Electrochem. Soc. **155**, B903 (2008)

Identification of scattering mechanisms limiting the mobility of two-dimensional electron gas in Si/SiGe heterostructures

G. Tsuchiya*, K. Sawano**, Y. Shiraki**, and K. M. Itoh*
** School of Fundamental Science and Technology, Keio University, Yokohama 223-8522, Japan*
*** Advanced Research Laboratories, Musashi Institute of Technology, Setagaya-ku, Tokyo 158-0082, Japan*

Keywords: 2DEG, Si/SiGe heterostructures, intervalley scattering, mobility

It is not straight forward to properly probe the carrier density and mobility of two-dimensional electron gas (2DEG) in modulation-doped structures due to presence of other parallel conduction paths such as three-dimensional conduction in doped layers and bulk substrates. As we will show, these parallel paths can interfere severely in the standard efforts (e.g., Hall effect measurement) to investigate physics of 2DEG properties. In order to overcome this challenge, we have developed maximum-entropy mobility spectrum analysis (ME-MSA) method [1]. This method allows us to obtain the density and mobility of each conduction path for a given temperature. This work presents temperature dependence of the electron density and mobility of the 2DEG layer without contribution of other parallel paths in Si/SiGe heterostructures. Such experimental results are compared directly with numerical calculation of mobility to identify dominant scattering mechanisms limiting the electron mobility of 2DEG in Si/SiGe heterostructures.

A sample is composed of a 15 nm strained-Si channel layer surrounded by $Si_{0.7}Ge_{0.3}$ layers and a Sb-doped layer placed 20 nm away from the channel. Fig. 1 shows the temperature dependence of 2DEG mobility obtained by ME-MSA (●). It shows room temperature mobility of 2780 cm^2/Vs, which is close to the record mobility 2900 cm^2/Vs so far reported for strained Si [1]. On the other hand, mobility obtained by Hall effect measurement (×) is much lower and is only 1070 cm^2/Vs at room temperature due to the parallel conduction through the Sb-doped layer. ME-MSA successfully obtains the mobility of the Sb-doped layer (▲). When both conductions (● and ▲) are added properly, we obtain □ which agrees very well with the result of Hall effect measurement (×) as we expected. This confirms the reliability of ME-MSA method to separate the transport properties of different layers.

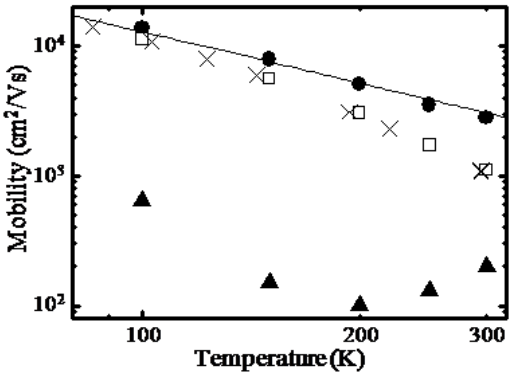

Fig. 1 Temperature dependence of 2DEG mobility obtained by ME-MSA, Hall effect measurement, and numerical calculation. See text for details.

The mobility calculation was performed including acoustic phonon and intervalley g-process scatterings based on self-consistent calculation of Poisson's and Schrödinger's equations. The parameters of phonon energy and deformation potential were taken from Ref. 2, i.e., there is no adjustable parameter. The intervalley f-process scattering is ignored due to large splitting (~200 meV) between twofold and fourfold degenerate valleys. The calculated results (solid curve in Fig. 1) shows excellent agreement with our measurement (●) demonstrating for the first time that acoustic phonon and intervalley g-process scatterings are the dominant scattering mechanisms limiting the mobility for this temperature range.

This work was supported by Grant-in-Aid for Scientific Research #18001002, Special Coordination Funds for Promoting Science and Technology, JST-DFG Strategic Cooperative Program on Nanoelectronics, and Grant-in-Aid for the Global Center of Excellence at Keio University.

1. M. Myronov, K. Sawano, K. M. Itoh, and Y. Shiraki, Appl. Phys. Exp. **1**, 021402 (2008).
2. C. Canali, C. Jacoboni, F. Nava, G. Ottaviani, and A. Alberigi-Quaranta, Phys. Rev. B **12**, 2265 (1975).

Channel Interference on Aharonov-Bohm Effect in a Quasi One-Dimensional Ring

Yiping Lin*, Pei-Jung Wu*, J. C. Chen*, Kuan. Ting. Lin*, Dong-Sheng Luo*, T. Ueda** and S. Komiyama**

**Department of Physics, National Tsing-Hua University. Hsinchu, Taiwan*

***Department of Basic Science, University of Tokyo, Komaba, Tokyo, Japan*

Keywords: Quantum interference, Aharonov-Bohm effect, Quasi one-dimensional system

The importance of the multi- or inter-channel scatterings in the Aharonov-Bohm (AB) interference has been revealed in numerous experiments [1, 2]. Especially in the ballistic narrow wire with few transverse modes comprising the annulus, the inter-channel scatterin is expected to be crucial to the oscillation amplitude. Despite of these impressive experimental studies, the effects of the transverse modes in AB interference have not been satisfactorily clarified. It is mainly because most of these experiments are performed in multi-mode regimes and the channel numbers cannot be globally tuned and decisively known.

In the present paper, we have implemented an AB interferometer with a pair of the side gates to separately tune the mode numbers in each branch of the ring. Unlike previous approaches, the global side gates can be uniformly squeeze the channel width and by monitoring the conductance steps with the gating voltages we are able to identify the channel numbers involving AB interference. In this design, we concern the variations of the amplitude and phase of AB oscillations resulted from the inter-channel scattering.

Our device consists of four arcs gates and a dot was defined by electron beam lithography, followed by a shallow wet etching and then the deposition of Cr/Au as gate metal (see the inset in Fig.1). Each arc gate can be separately biased to uniformly squeeze the channel width of electrons, thereby externally tuning the transverse modes in the interference paths.

The oscillatory magnetoconductance of the device is systematically studied by varying the number of channels in each path. We have observed the evidence of phase shifts in the magnetoconductance oscillations due to the suppression of the mode numbers on the ring path. Though the periodicity is not well resolved, qualitatively our data support the random phase shifts between the successive modes (see Fig. 2).

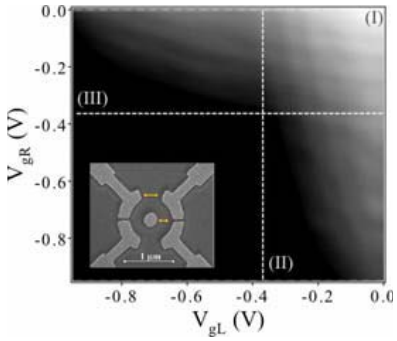

Fig. 1 Conductance image plot as a function of two gate voltages, V_{gL}(left) and V_{gR} (right), at 0.3 K. The visible strips correspond to the channel modes in both paths. The inset illustrates the active region of our device.

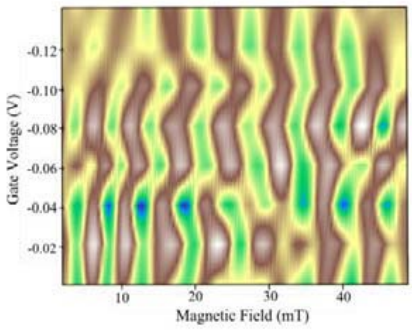

Fig. 2 Conductance image plot of Aharonov-Bohm oscialltions by changing both gate voltages ($V_g = V_{gR} = V_{gL}$) at 0.3K.

References

1. S. Washburn, H. Schmid, D. Kern, and R. A. Webb, Phys.Rev. Lett. **59**, 1791 (1987).

2. P. G. N. de Vegvar, G. Timp, P. M. Mankiewich, R. Behringer, and J. Cunningham, Phys. Rev. B **40**, 3491 (1989).

Density influenced electric transport of double quantum point contacts in series

K.M. Liu*, H.Y. Lin*, V. Umansky**, and S.Y. Hsu*

* *Department of Electrophysics, National Chiao Tung University, Hsinchu 300, Taiwan*

** *Braun center for Submicron Research, Weizmann Institute of Science, Rehovot, 76100, Israel*

Keywords: Quantum transport, Quantum wire

In high mobility $Al_xGa_{1-x}As/GaAs$ heterostructures, a negative bias on surface split gates above 2DEG can be used to make constrictions with lengths less than carrier's mean free path as called "quantum point contact". The conductance of such a device is known to be quantized in units of $2e^2/h$. With increasing interest in nanostructures and their scope for novel functionality, the study of the ballistic and coherent natures of transmission through these gated nanostructures is important. Here, we have measured the electric transport of double quantum point contacts (QPCs) in series at low temperatures to investigate the transmission coefficient T_d which represents the portions of electrons travelling ballistically from one QPC to the other.

Electron beam lithograph was used to pattern numerous pairs of split gates to define one dimensional wires in 2DEG. Different configurations were chosen to have a variety of edge-to-edge separation distance L between two pairs of identical split gates. Isolated from an insulating layer, a top gate was also fabricated on top of the quantum wires to modify the electron densities in the wires and the two dimensional electron gas as well. The transport is characterized by the direct transmission coefficient T_d. Based on theoretical work by Bennakker and Houten[1], the conductance through the serial QPCs can be written as $G_{series} = \frac{1}{2}\left(G + \frac{2e^2}{h}T_d\right)$.

As shown in Fig.1 for a device with L=0.6μm, T_d decreases continuously from 0.5 to 0.1 with decreasing top gate voltage (carrier density) when both QPCs are confined with only one 1D channel (n=1). The transport is partially adiabatic in high electron densities and transits to nearly complete ohmic (T_d~0) in low densities. When both QPCs are confined with more than one 1D channel (n>1), T_d is smaller than that for n=1, but seems to be insensitive to n for n=2, 3, and 4. Moreover, T_d saturates at positive top gate voltages. The behaviour of T_d will be described in terms of the carrier density dependent mean free path and coherence length in the electron gas[2].

This project is financially sponsored by National Science Council in Taiwan (grand no. NSC 96-2112-M-009-030-MY3) and MOE ATU program.

References

1. C.W. J. Beenakker and H. van Houten, Phys. Rev B **39,** 10445 (1989).
2. B.E. Kane *et al*., Appl. Phys. Lett. **72**, 3506 (1998).

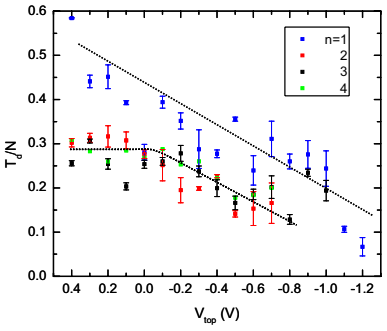

Fig.1 Transmission coefficient T_d versus top gate voltage for QPCs of different confined sub-band index n. Lines are guides to the eye.

Magnetic field asymmetry of nonlinear transport in a small ring

G.M.Gusev*, Z. D. Kvon**

* *Instituto de F¶.sica da Universidade de S~ao Paulo,, S~ao Paulo, SP, Brazil*
** *Institute of Semiconductor Physic, Novosibirsk, Russia*

Keywords: Aharonov-Bohm effect, semiconductor ring

We report study of Aharonov-Bohm oscillations in small (effective radius r_{ef} = 80 nm) ring in strong nonlinear regime. The ring interferometer investigated in this paper has been produced on the basis of the AlGaAs/GaAs heterostructures with a shallow two-dimensional electron gas (2DEG) confined at the heterointerface, which is 25 nm below the sample surface. The electrons supplied by a Si-doped plane 7.5 nm remote from the heterointerface. The electron mobility in the initial heterostructure was $\mu = 10^5$ *Vs/cm*^{2} at T=4.2 K and density $n_s = 5 \cdot 10^{11}$, which corresponds to the electron mean free path *l* = 1:2 *μm*. The Aharonov-Bohm ring was fabricated by means of a high resolution electron beam lithography followed by a fast plasma etching in the center of the Hall bar structure The ring was connected with two dimensional electron gas in Hall bar through two point contacts, and effective two-terminal measurements was performed. The structure was entirely covered by *TiAu* gate. The longitudinal resistance was measured using AC current of 10^{-8} A at a frequency 6.1 Hz with four-probe Hall bar setup in the linear regime. Direct electric current I_{DC} was applied simultaneously with DC excitation through the same current leads. Measurements have been performed in magnetic fields up to 1.5 T and in the temperature range1.5-4.2K. The main results are the following: 1. As expected for two-terminal mesoscopic nonlinear transport the magnetic field symmetry of Aharonov-Bohm oscillations is broken. Due to the small size of the ring we justied the violation of the Onzager relation for conditions, when the value of asymmetry is comparable with amplitude of Aharonov-Bom oscillations. Moreover the effect of practically complete suppression of these oscillations for one direction of the magnetic field while for the opposite direction of magnetic field there is the quite pronounced oscillations is observed (fig. 1).

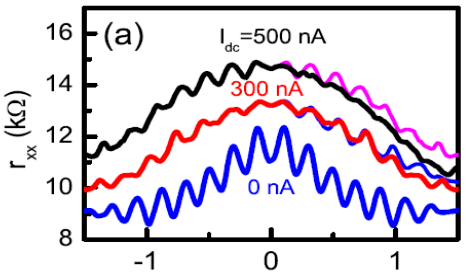

Fig. 1. Ring resistance for both direction of magnetic field at different values of DC current through the ring.

2. We independently measured the Thouless energy, energy level spacing and capacitance energy in our ring and using recently advanced theory [1] determined the interaction strength constant, which is responsible for asymmetric nonlinear conductance in mesoscopic system. This coefficient is consistent with value derived from comparison of the B asymmetric AB oscillations and theory. The phase rigidity of the AB oscillations in the nonlinear regime is unexpectedly broken and the phase jump with magnetic field sweep has been found.

References

1. M.L.Polianski, M.Buttiker, Phys. Rev. Lett. 96, 156804 (2006); Physica E 40, 67 (2007).

Magneto-intersubband oscillations in triple quantum wells

S. Wiedmann*, N. C. Mamani**, G. M. Gusev**, A. K. Bakarov** and J. C. Portal*,***

LNCMI-CNRS, BP 166, 38042 Grenoble and INSA, 31077 Toulouse, France

** Instituto de Física da Universidade de São Paulo, São Paulo, SP, Brazil*

*** Institut Universitaire de France, 75005 Paris, France*

Keywords: triple quantum wells, magnetotransport, intersubband oscillations

A two-dimensional (2D) electron system in a perpendicular magnetic field shows magnetoresistance oscillations, known as Shubnikov-de Haas oscillations (SdH) originating from the sequential passage of Landau levels through the Fermi level. If more than one subband is occupied the possibility of intersubband transitions start to occur and leads to another kind of magnetoresistance oscillation.

These oscillations, called magneto-intersubband oscillations (MIS) have been studied in single quantum wells with two occupied subbands [1] and recently in a double quantum well (DQW) system [2]. MIS oscillations appear if Landau levels of different subbands are aligned sequentially (see bottom inset in Figure 1) and offer new possibilities in transport measurements, e.g. the determination of quantum lifetimes in regions where SdH oscillations are completely suppressed at high temperatures [2]. A triple quantum well system consists of three quantum wells separated by thin barriers where electrons occupy three 2D subbands coupled by tunneling. Our samples are coupled GaAs triple quantum wells (TQWs) with a central well width of 200 nm and lateral well widths of 140 nm separated by a 1.4 nm barrier in a 2D electron gas with a mobility of $5 \cdot 10^5$ cm^2/Vs. The barrier widths are 1.4 nm and 2 nm, respectively. We have carried out transport measurements in a wide temperature range in order to study MIS phenomena in these coupled systems (see Figure 1). The alignment of Landau levels leads to well pronounced MIS oscillations which survive at high temperatures. By analyzing MIS amplitude, we are able to extract quantum lifetime of electrons in triple quantum well systems.

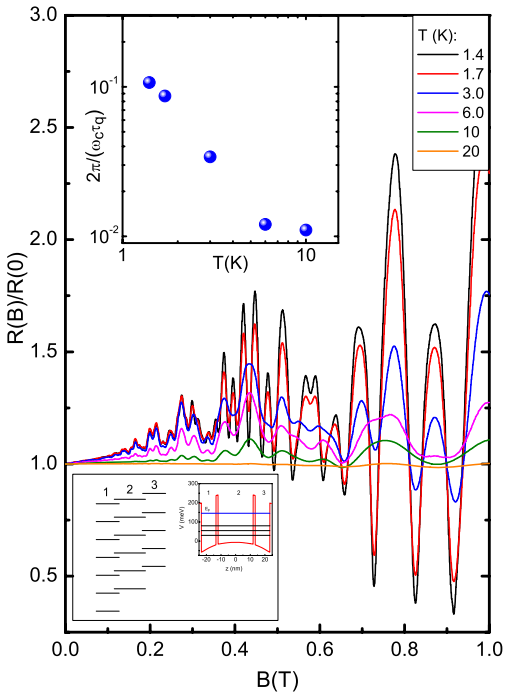

Figure 1: MIS oscillations in a TQW system for different temperatures. From amplitude one can obtain information about the quantum lifetime of electrons even when SdH oscillations are already vanished for high temperatures (see inset). The staircase of Landau levels is shown in the bottom inset.

References

[1] see ,e.g.,V. Polyanovsky, Fiz. Tekh. Poluprovodn., S.-Petersburg **22**, 2230 (1988).

[2] N. C. Mamani *et al.*, Phys Rev. B **77**, 205327, (2008).

Dielectric mismatch effect on coupled donor states in a quantum dot

J. L. Movilla, A. Ballester and J. Planelles
Departament de Química Física i Analítica, Universitat Jaume I, Box 224, E-12080, Castelló, Spain

Keywords: quantum dot, coupled impurities, dielectric confinement

The system built of two coupled semiconductor quantum dots (QDs) containing electrons, holes, or an exciton, constitutes one of the simplest solid structures proposed as the functional part in a wide range of device applications, including spintronics, optoelectronics, photovoltaics, and quantum information technologies. The widespread interest in this system relies on the ability to manipulate conveniently its molecular properties, such as the energy splitting between the bonding (nodeless) and antibonding (noded) lowest-lying molecular-like states or the spatial distribution of carriers in the system[1, 2].

Advances in single-dopant fabrication[3] and charge detection[4] have led atomic scale electronics (particularly the field of quantum computing) to pear increasing attention to another molecular system. Namely, the D_2^+ system, i.e., the system built of two coupled donor impurities in a semiconductor host in which one of the two excess electrons has been ionized. This system encodes the logical information either on the spin or on the charge of the remaining excess electron[5, 6].

The electronic structure and related properties of single shallow donors in nanoscale semiconductor heterostructures have been widely studied in the last two decades[7, 8]. In addition to the well-known quantum size effect, the influence on the donor levels of the dielectric confinement (coming from the different dielectric response of the QD and the surrounding medium) has been revealed as a noticeable effect in colloidal quantum dots, as they are usually synthesized in media with a dielectric response rather different to that of the dot material[8].

In this contribution, we present a theoretical study on the molecular properties of a D_2^+ system confined in a spherical quantum dot. Spatial and dielectric confinement modulation of electron density distributions, splitting energies, and spontaneous emission rates involving the bonding and anti-bonding lowest-lying molecular states is investigated within the framework of the effective-mass envelope function approximation. The results indicate that the donor molecule behaves as heteropolar when the spatial confinement breaks the inversion symmetry, which is paralleled by a strong reduction of the excited state radiative lifetime. Dielectric confinement, acting on a larger length scale than spatial confinement, may recover the bulk-like homopolar character when the dot is embedded in a low dielectric constant medium. In the weak spatial confinement regime, dielectric effects can increase the corresponding bulk radiative lifetimes significantly, and simultaneously modulate the charge density distribution.

References

[1] B. Bayer, P. Hawrylak, K. Hinzer, S. Fafard, M. Korkusinski, Z.R. Wasilewski, O. Stern, and A. Forchel, Science **291**, 451 (2001).

[2] S.A. Wolf, D.D. Awschalom, R.A. Buhrman, J.M. Daughton, S. von Molnár, M.L. Roukes, A.Y. Chtchelkanova, and D.M. Treger, Science **294**, 1488 (2001).

[3] T. Shinada, S. Okamoto, T. Kobayashi, and L. Ohdomari, Nature (London) **437**, 1128 (2005).

[4] A. Aassime, G. Johansson, G. Wendin, R.J. Schoelkopf, and P. Delsing, Phys. Rev. Lett. **86**, 3376 (2001).

[5] M.J. Calderón, B. Koiller, X. Hu, and S. Das Sarma, Phys. Rev. Lett. **96**, 096802 (2006).

[6] L.C.L. Hollenberg, A.S. Dzurak, C. Wellard, A.R. Hamilton, D.J. Reilly, G.J. Milburn, and R.G. Clark, Phys. Rev. B **69**, 113301 (2004).

[7] B. Li, A.F. Slachmuylders, B. Partoens, W. Magnus, and F.M. Peeters, Phys. Rev. B **77**, 115335 (2008).

[8] J.L. Movilla and J. Planelles, Phys. Rev. B **71**, 075319 (2005).

Comparison of two-dimensional electron gas of etched and nonetched InAlAs/InGaAs/InAlAs metamorphic high electron mobility transistor structures

J. S. Wu, C. C. Hung, C. T. Lu, D. Y. Lin

Department of Electronic Engineering, National Changhua University of Education, Changhua, Taiwan

Keywords: 2DEG, photoluminescence, Hall, photo-Hall

We present the studies of two-dimensional electron gas (2DEG) in two (etched and nonetched) InGaAs/InAlAs/InGaAs metamorphic high electron mobility transistor (mHEMT) structures using photoluminescence (PL) [1], photoconductivity (PC)[2], Hall and photo-Hall measurements. These two samples were grown by molecular beam epitaxy (MBE) on semi-insulating GaAs substrate and were designated as A (etched) and B (nonetched). Sample A has the same layer structure with sample B but its Si doping cap layer has been etched. In the PL spectra, two optical features are observed, and they are identified to be the 11H and 21H transitions localized in the channel layer. It can be used to estimate related information about the energy positions of electron quantization levels, and Fermi level by fitting the PL spectra, and then the carrier concentration can be estimated at various temperatures. Comparison with Hall measurement, the PL measurement is a nondestructive technique, so the ohmic contact fabricating is unnecessary. Furthermore, the effect of Si doping cap layer can be avoided because only the carriers localized in the conduction channel are concerned. We also performed the Hall measurements at various temperatures. Comparing the Hall data (including carrier concentration and mobility) of samples A and B, two conduction channels, the high mobility 2DEG channel and the low mobility capping channel, are observed. We also presented the PC and photo-Hall spectra, the intersubband transitions and the carrier concentration induced by photo illumination were observed. Absorption coefficient of the channel layer can be estimated from the photo-Hall spectra.

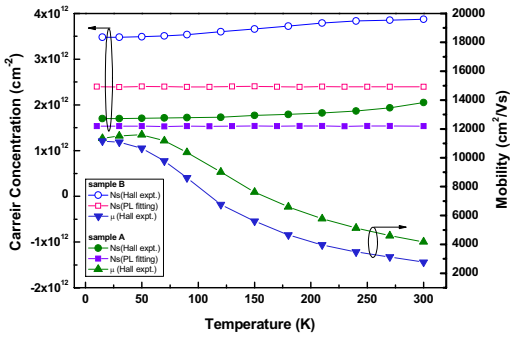

Fig.1 Carrier concentration and mobility measured by Hall and PL measurements at various temperatures.

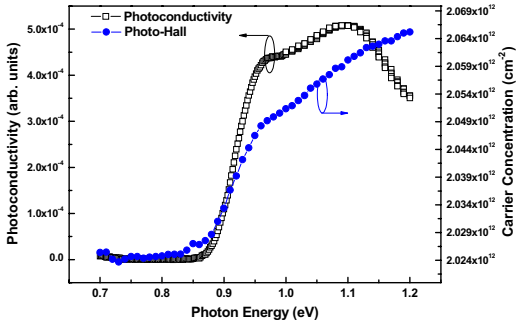

Fig.2 Photoconductivity and photo-Hall spectra of sample A measured at room temperature. .

References

1. D.Y. Lin, Y.S. Huang, T.S. Shou, K.K. Tiong, Fred H. Pollak, J. Appl. Phys. Vol.90, 6421 (2001).
2. F. Schuermeyer, D. Cheskis, R. S. Goldman, H. H. Wieder, IEEE International Symposium on Compound Semiconductors, 303-306 (1997)

Quantum capture of electrons and intradot relaxation by means of Auger processes in quantum dots

A.L. Vartanian, A.L. Asatryan, K.A. Vardanyan and A.A. Kirakosyan

Department of Solid State Physics, Yerevan State University, 1 A. Manoogian St., Yerevan 0025, Armenia

Keywords: dot, capture, Auger process

The nature of carrier relaxation mechanisms in semiconductor quantum dots has attracted much attention during the last decade, since it is of particular scientific interest and central for the development of efficient and fast optoelectronic devices such as quantum dot (QD) laser diodes. In QD lasers, the carriers are injected into the barriers embedding the QDs. After energy dissipation processes, the carriers are captured by the QDs and then relax to the fundamental lasing state. The efficiency of the relaxation cascade directly affects the device performances, such as threshold current, temperature stability, and so on. The achievement of a very fast capture rate is therefore a relevant aspect of the device optimization study.

Ferreira and Bastard [1] theoretically considered the problem of carrier capture and relaxation in QDs. They discussed the capture of pairs photocreated in the wetting-layer continuum into excited dot levels, assisted by the emission of one LO phonon, and considered the intra-dot relaxation due to Auger processes, which become possible when two or more carriers are trapped in the excited dot levels.

However, the picosecond time resolved photoluminescence measurements of $GaAs/GaAlAs$ quantum-dot structures grown by modified droplet epitaxy, where no wetting layer is connecting the dots, show a fast carrier relaxation time (30 ps) to the dot ground state, which becomes even faster for increasing the photogenerated carrier injection [2]. This shows that the two-dimensional character of the wetting layer is not relevant in determining the QD capture, in contrast with the conclusion of [3].

Therefore in this work we consider theoretically the problem of LO phonon-assisted capture and intradot Auger relaxation dynamics in $GaAs$ QDs embedded in three-dimensional $GaAlAs$ barriers. The average capture velocity is investigated as a function of the QD diameter and the electron temperature of the injected electrons using different models for the polar optical phonons in QD structure. The results show that the capture efficiency increases with the carrier concentration in the three-dimensional barrier.

The carrier scattering mechanism we investigate is a sequential one where two carriers, initially captured in dot excited states, undergo an irreversible Auger scattering to final states where one particle remains bound in the dot with a lower energy while the other has been ejected from the dot in a three-dimensional barrier continuum state. The two-electron initial state in QD includes Pauli correlations both in the wave function and in the energy. Singlet states and triplet states are considered.

We have estimated the importance of various Auger processes and found characteristic relaxation times depending on barrier carrier density and on dot diameter. Our calculated $P \to S$ Auger decay liftimes compare well with data in $GaAs/GaAlAs$ QDs [2].

References

1. R.Ferreira, and G.Bastard, Appl. Phys. Lett. **74**, 2818 (1999).

2. S.Sangunetti, K.Watanabe, T.Tateno, M.Wakaki, N.Koguchi, T.Kuroda, F.Minami, and M.Gurioli, Appl. Phys. Lett. **81**, 613 (2002).

3. D.Morris, N.Perret, and S.Fafard, Appl. Phys. Lett. **75**, 3593 (1999).

Polaronic effect on an exciton in a cylindrical quantum wire with an electric filed

Zeng-Ru Zhao and X. X. Liang

Department of Physics, Inner Mongolia University, Hohhot 010021, China

Keywords: Excitons; Quantum wires; Electron-phonon interaction; Stark effect

The behaviour of excitons in quantum wires has been extensively investigated [1-2]. The results show that the binding energies in quantum wires are much larger than those in quantum wells [1]. The electron-phonon interaction [3,4] and the Stark effect [5] on the exciton states have also been studied, respectively. However, the phonon effects on the exciton states in quantum wires with an electric field have rarely been discussed in previous literatures.

In this work, we use the variational solution to investigate the binding energies and the Stark shift of an exciton in a cylindrical quantum wire (CQW) with an external electric field perpendicular to the wire axis. The exciton-phonon interactions including both the confined bulk longitudinal-optical (LO) and interface-optical (IO) phonon contributions are taken into account in the calculations.

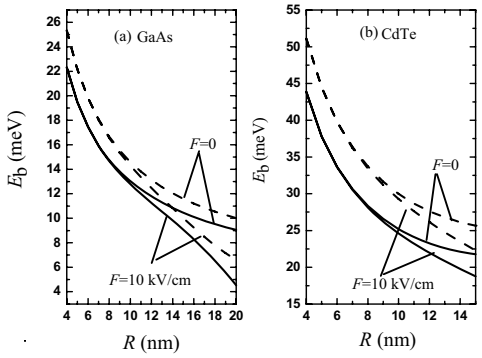

Fig.1. The binding energies E_b as function of the wire radius with (solid lines) and without (dashed lines) exciton-phonon interaction for the electric field of F = 0 and 10kV/cm in GaAs (a) and CdTe (b) quantum wires.

The numerical results for the binding energies of excitons as functions of the wire radius with different electric field strengths for the GaAs and CdTe CQWs are given in Fig. 1. It is seen that the exciton binding energies increase monotonically with decreasing the wire radius. As expected, the applied electric field lowered the binding energies because it pushes the electron and the hole to the opposite directions. The results indicate that the exciton-phonon coupling reduces both the exciton binding energies and Stark shifts by screening the Coulomb interaction, and can not be neglected. The energy dropped by phonon field in the quantum wire of the II-VI compound CdTe is much larger than that of the III-V compound GaAs due to the stronger polarity in the former.

Project was supported partly by the National Natural Science Foundation of China (No 10764003).

References

1. J. B. Xia and K. W. Cheah, Phys. Rev. B **55**, 1596 (1997).

2. J.Costa e Silva, Andrey Chaves, J. A. K. Ferire, V. N. Freire, and G. A. Farias, Phys. Rev. B **74**, 085317 (2006).

3. M. H. Degani and O. Hipólito, Phys. Rev. B **35**, 9345 (1987)

4. R. A. Escorcia, C. Riva and I. D. Mikhailov, Solid state commun. **131,** 365 (2004).

5. E. Kasapoglu, H. Sari, M. Bursal and I. Sökmen, Physica E **16**, 237 (2003).

Electron-hole symmetry breaking in optical fine structures of single self-assembled quantum dots

Hanz Y. Ramirez[1], Chia-Hsien Lin[1], Wen-Ting You[1], Shan-Yu Huang[1], Wen-Hao Chang[1], Sheng-Di Lin[2] and Shun-Jen Cheng[1]

[1] *Department of Electrophysics, National Chiao Tung University, Hsinchu, 300 Taiwan*
[2] *Department of Electronic Engineering, National Chiao Tung University, Hsinchu, 300 Taiwan*

Keywords: fine structure splitting, electron-hole exchange interaction, self-assembled quantum dot.

Fabricating self-assembled semiconductor quantum dots (QDs) as efficient entangled photon pair emitters has remained a challenge for a long time because of the inherent fine structure splittings (FSS's) of excitons (X's) in solids [1]. The FSS's have been established as a consequence of electron-hole (e-h) exchange interactions that are closely associated with the inevitable symmetry breaking of dot structures and the extents of e- and h- wave functions. Our recent magneto-photoluminescence (M-PL) studies of single dots have revealed the significant asymmetry of e- and h- wave functions existing in highly quantized small InGaAs/GaAs dots [2]. In this work, we further, experimentally and theoretically, study the effects of e-h symmetry breaking on the optical FSS's of the individual InGaAs/GaAs QDs.

Figure 1 shows the measured FSS's of single spin X's versus the emission energies in different individual InGaAs/GaAs QDs. Theoretically, the magnitudes of the FSS's were shown to be inversely proportional to QD size [3]. Thus, the measured FSS's are anticipated to increase with the emission energy. However, the measured zero field-FSS's show an opposite behavior to the expectation.

To understand such a physical feature, a theory based on a 3D asymmetric parabolic model of QD for the e-h exchange interactions of spin excitons in QDs was developed. The developed theory provides explicit expressions for the FSS of a spin exciton in an asymmetric QD in terms of the mean extents (*le*, *lh*) of the e- and h-wave functions. The values of the parameters, *le* and *lh,* were provided by 3D finite difference simulations for the electronic structures of truncated pyramid shaped InGaAs/GaAs QDs with the consideration of strain and Ga-diffusion. The calculated FSS's of the QDs with 10% lateral deformation and various extents of Ga-diffusion are shown in Fig.1 (squares), showing an agreement with the experimental results. The reduced FSS's in the high emission energy regime are attributed to the significant e-h symmetry breaking and the formation of the electronic quasi-bound states in small and Ga-rich dots, which reduce the strength of e-h Coulomb interactions and undo the asymmetry of dot structure, respectively.

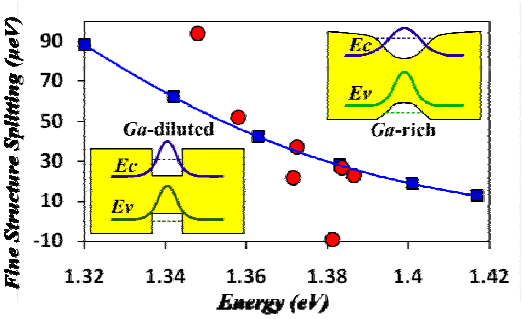

Fig.1 Calculated (Squares) and measured (diamonds) fine structure splittings between single exciton spin states of single InGaAs/GaAs QDs as a function of the single exciton energies.

References

1. R. M. Stevenson, R. J. Young, P. Atkinson, K. Cooper, D. A. Ritchie and A. J. Shields, Nature **439**, 179 (2006).
2. Ming-Fu Tsai, Hsuan Lin, Chia-Hsien Lin, Sheng-Di Lin, Sheng-Yun Wang, Ming-Cheng Lo, Shun-Jen Cheng, Ming-Chih Lee and Wen-Hao Chang, Phys. Rev. Lett. **101**, 267402 (2008).
3. Takagahara, Phys. Rev. B **62,** 16840 (2000).

Fine structure of excitons in InAs quantum dots at low magnetic fields

T. Moldaschl*, T. Müller*, W. Parz*, S. Golka**, G. Strasser** and K. Unterrainer*, **

* *Institute of Photonics, Vienna University of Technology, Austria*

** *Center for Micro- and Nanostructures, Vienna University of Technology, Austria*

Keywords: quantum dots, exciton fine structure, spectral hole burning

The excitonic fine structure of self – assembled quantum dots, specifically the origins of it, have been subject to fundamental investigations lately [1]. The effects of magnetic fields are especially capable to reveal many aspects of the fine structure, like the polarization change of photons emitted from the excitons [2], which in return reveal the change of the polarization states of the excitons themselves. Most of these works have been focused on photon emission in high magnetic fields, whereas there is only little work on absorption effects [3], but also focused on higher magnetic fields. In this work femtosecond spectral hole burning spectroscopy (SHB) [4] is employed on an ensemble of self-assembled InAs / GaAs QDs in weak magnetic fields in the Faraday configuration up to 150 mT.

Excitons in self- assembled QDs exhibit a linear polarization in zero magnetic fields, due to an intermixing of the original circular eigenstates. When a magnetic field is applied in the Faraday geometry, i. e. in the growth direction of the QD sample, the Zeeman interaction can be used to counteract the effects of the fine structure coupling that cause the intermixing. This leads to the observation of an increased degree of circular polarization in the luminescence of the QDs, indicating a change of the oscillator strength in the circular and linear polarization bases. This fact can be seen directly in the transmission change of the SHB spectra. Fig 1 shows a measured spectrum with distinct magnetic field dependencies. The increased oscillator strength corresponds to an increased differential transmission signal in the weak absorber limit. Furthermore, the lifetime of a state is inversely proportional to the oscillator strength of its optical transition, which can directly be seen from the time-resolved differential transmission data, where increased signal strengths and decreased lifetimes have been observed simultaneously with clear dependencies on the magnetic field.

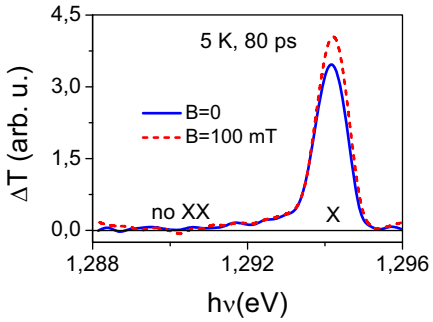

Fig.1 SHB spectra for orthogonal linear pump and probe polarizations (no biexciton XX [4]). For magnetic fields as low as 100 mT an 18 % signal change of the differential transmission is visible.

Acknowledgements:

This work was supported by the Austrian "Fond zur Förderung der wissenschaftlichen Forschung"
(SFB IR-ON, CoQuS)

References

1. G. Bester, A. Zunger and D. Vanderbilt, Phys. Rev. B **74**, 081305 (2006)

2. M. Bayer, G. Ortner and A. Forchel, Phys. Rev. B **65**, 195315 (2002)

3. G. Chen, E. T. Bateh and D. S. Katzer, Phys. Rev. B **68**, 115303 (2003)

4. T. Müller, G. Strasser and K. Unterrainer, Appl. Phys. Lett., **88**, 192105 (2006)

Role of an in-plane field in 2D magnetotransport assisted by microwaves

Jesus Inarrea* and Gloria Platero**
*Department of Physics, University Carlos III, Madrid. Spain.
** Instituto de Ciencia de Materiales. CSIC. Madrid. Spain.

Keywords: Microwave-induced resistance oscillations, in-plane magnetic field, 2D electron system

In recent years, with the rise of Nanotechnology, a lot of effort has been devoted to the study and research of physics of nano-devices, from theoretical, experimental and application perspectives. In particular the response of such systems to external, time-dependent or stationary, fields is receiving much attention from the scientific community. The potential applications of these results to design and build a broad spectrum of nanoscale devices will become increasingly important in the forthcoming years. A remarkable example is the recently obtained microwave- (MW-) induced resistance oscillations (MIRO) and zero resistance states (ZRS)

In this work we present a theoretical approach to study the effect of an in-plane (parallel) magnetic field on the microwave-assisted transport properties of a two-dimensional electron system. Previous experimental evidences show that microwave-induced resistance oscillations and zero resistance states are differently affected depending on the experimental set-up: two magnetic fields (two-axis magnet)[1] or one tilted magnetic field [2]. In the first case, experiments report a clear quenching of resistance oscillations and zero resistance states. In a tilted field, one obtains oscillations displacement and quenching but the latter is unbalanced and less intense. When a 2DES is illuminated with MW radiation, electronic orbits are forced to move back and forth, oscillating harmonically at the frequency of MW radiation and with an amplitude proportional to the MW electric field[3]. MIRO are proportional to the magnitude of this amplitude and any variation of it, is finally reflected on MIRO. In their MW-driven orbits motion, electrons interact with the lattice ions being damped and producing acoustic phonons. According to our model, the presence of $B_{||}$ imposes an extra harmonically oscillating motion in the z-direction enlarging the electrons trajectory in their orbits. This would increase the interactions with the lattice making the damping process more intense and reducing the amplitude of the orbits oscillations[4]. Eventually MIROs are progressively quenched (see Fig.1).

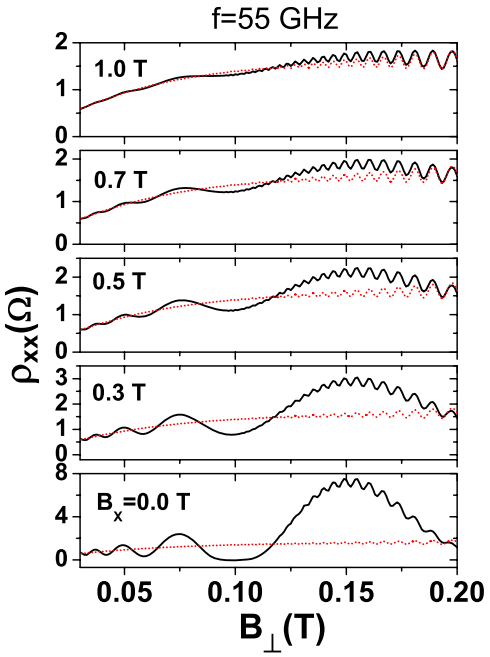

Figure 1: ρ_{xx} vs $B_\perp$ for different values of $B_x(B_{||})$ from 0.0 T to 1.0 T. $B_\perp$ and B_x are independent. Single lines correspond with MW on, and dotted lines with MW off. We observe a progressive quenching of ρ_{xx} oscillations as B_x increases.

References

[1] C. L. Yang, R. R. Du, L. N. Pfeiffer and K. W. West, Phys. Rev. B, **74**, 045315, (2006).

[2] R. G. Mani, Phys. Rev. B, **72**, 075327, (2005); R.G. Mani, Appl. Phys. Lett, **92**, 102107, (2008).

[3] J. Iñarrea and G. Platero, Phys. Rev. Lett. **94** 016806, (2005).

[4] J. Iñarrea and G. Platero, Phys. Rev. B **78** 193310, (2008).

How a magnetized quantum wire can act as an active laser medium

Manvir S Kushwaha*

**Institute of Physics, University of Puebla, Puebla, Mexico*

Keywords: Quantum wire, intersubband excitations, magnetorotons, laser medium

We report on the theoretical investigation of magnetoplasmon excitations in a quantum wire characterized by a confining harmonic potential and in the presence of a perpendicular magnetic field. The problem involves two length scales: $l_0 = \sqrt{\hbar/m^*\omega_0}$ and $l_c = \sqrt{\hbar/m^*\omega_c}$, which characterize the relative strengths in the interplay of confinement and the magnetic field. We embark on the charge-density excitations within a two-subband model in the framework of Bohm-Pines' random-phase approximation. The main focus of our study is the (intersubband) magnetoroton excitation which changes the sign of its group velocity twice before merging with the respective single-particle continuum. We analyze the terms and conditions within which the magnetoroton excitation persists in the quantum wires. It is suggested that the electronic device based on such magnetoroton modes can act as an *active* laser medium.

The most interesting aspect of the excitation spectrum (Fig. 1) is the existence of this intersubband collective (magnetoplasmon) excitation (henceforth referred to as the magnetoroton). Notice that the magnetoroton (MR) changes its group velocity twice before merging with the respective single-particle excitation. At the origin, the energy difference between the intersubband CME and SPE is a manifestation of the many-body effects such as depolarization and excitonic shifts[1].

The group velocity of the MR becomes negative between the maxon maximum and roton minimum. An interesting feature of this aspect is that it leads to tachyon-like (superluminal) behavior without one's having to introduce negative energies. The interest in the negative group velocity is based on anomalous dispersion in a gain medium, where the sign of the phase velocity is the same for incident and transmitted waves and energy flows inside the gain medium in the opposite direction to the incident energy flow in vacuum. The insight is that demonstration of negative group velocity is possible in media with inverted populations, so that gain instead of absorption occurs at the frequencies of interest. A medium with an inverted population has the remarkable ability of amplifying a small optical signal of definite wavelength, i.e., it can serve as an *active* laser medium. The situation is analogous to the superlattices where the crystal can exhibit a negative resistance: it can refrain from consuming energy like a resistor and instead feed energy into an oscillating circuit.

References

[1] M.S. Kushwaha, Phys. Rev. B **78**, 153306 (2008).

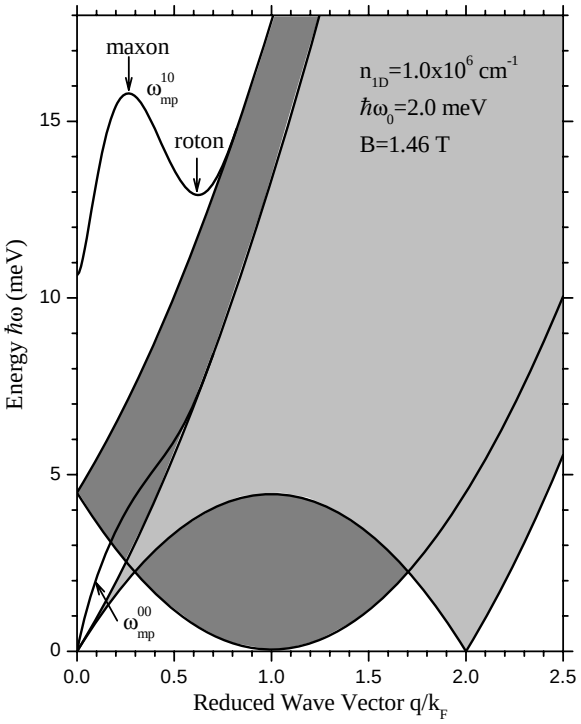

Figure 1: Magnetoplasmon dispersion for a quantum wire within a two-subband model in the framework of full RPA. The light (dark) shaded region refers, respectively, to the intrasubband (intersubband) SPE. The bold solid curve marked as ω_{mp}^{00} (ω_{mp}^{10}) is the intrasubband (intersubband) CME. The parameters are as given inside the picture.

Effect of strong tilted magnetic field on the sequential resonant tunneling in long period GaAs/AlGaAs superlattices

M. P. Telenkov, Yu.A. Mityagin
P.N. Lebedev Physical Institute, Moscow, Russia

Keywords: superlattice, magnetic field, resonant tunneling

The effect of strong tilted magnetic field (B=0-7T) on the sequential resonant tunneling in n-type long period (well width 25 nm, barrier width 10 nm, 30 periods, doping density $N_d = 1.8 \cdot 10^{10}$ cm^{-2}) MBE-grown $GaAs/Al_{0.3}Ga_{0.7}As$ superlattices (SL) was investigated both theoretically and experimentally over the whole tilting angle region. The static and time-averaged current-voltage characteristics were measured in tilted magnetic fields at 4.2K. At zero magnetic field the samples revealed several plateau regions with a sawtoothlike structure caused by the electric field domain formation and domain boundary shift across the SL.

In a magnetic field orientation close to perpendicular to layers (tilting angle $\theta<20^0$) no significant effect of magnetic field on I-V characteristics of investigated SLs was detected, the electric field distribution remained determined by subband spacing rather than by cyclotron energy of electrons. This results from the selection rule $\Delta n=0$ for tunneling transition between Landau levels in neighboring quantum wells due to the in-plane orthogonality of Landau states.

But at higher θ ($\theta>30^0$) the observed I-V curves start to be strongly affected by magnetic field. With increasing B the NDC structure in each of the plateau decreased in amplitude and gradually disappeared at higher B. The fast shift at higher B of the plateau position to higher voltage values was also observed (Fig.1).

A detailed experimental study of static I-V characteristics of the SLs were carried out in the whole interval of tilting angles. Using the previously suggested model [1,2] the resonant tunneling profiles as well as I-V characteristics of the superlattice in a tilted magnetic field were calculated and compared with experimental ones. The calculated results revealed a good overall agreement with the experimental data (Fig.2).

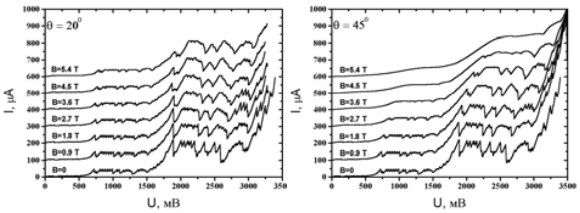

Fig1 Measured I-V characteristics of superlattices in tilted magnetic field for $\theta=20^0$ and $\theta=45^0$

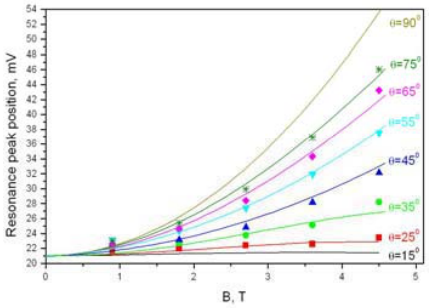

Fig.2 Calculated(solid lines) and measured(points) resonant peak positions corresponding tointerwell tunneling transitions from 1-st to 2-nd subbands.

References

1. M.P.Telenkov, Yu.A.Mityagin, JETP **103** (3), 426 (2006).
2.M.P.Telenkov, Yu.A.Mityagin, International Journal of Modern Physics B **21** (8-9), 1594 (2007).

Cyclotron Resonance in 2D Hole Systems in InSb Quantum Wells

M.B. Santos*, M. Edirisooriya*, T.D. Mishima*, C.K. Gaspe*, J. Coker*, R.E. Doezema*, X. Pan**, G.D. Sanders**, C.J. Stanton**, L.C. Tung***, and Y-J. Wang***

* *Homer L. Dodge Department of Physics & Astronomy, University of Oklahoma, Norman, Oklahoma, USA*

** *Department of Physics, University of Florida, Gainesville, Florida, USA*

*** *National High Magnetic Field Laboratory, Florida State University, Tallahassee, Florida, USA*

Keywords: Molecular Beam Epitaxy, Magneto-optics, Narrow Gap Semiconductors

In order to realize high-performance CMOS circuits, both *n*-type and *p*-type quantum-well (QW) transistors with high room-temperature mobility are necessary. Some III-V QW materials, including GaAs and $In_xGa_{1-x}As$ QWs, exhibit high electron mobilities, but have low hole mobilities that are comparable to Si. In principle, the hole mobility can be increased through compressive strain and by using a material, such as InSb, that has a narrower band gap. InSb *n*-type field-effect transistors (FETs) have already exhibited higher switching speeds and lower power consumption than other III-V FETs [1].

We report on a study of two-dimensional hole systems in InSb QWs with $Al_{0.20}In_{0.80}Sb$ barriers doped with Be [2]. The heterostructures were grown by molecular beam epitaxy on GaAs (001) substrates. The room-temperature hole mobility (700 cm^2/Vs) is higher than others have observed in *p*-type $In_xGa_{1-x}As$ or GaAs QWs. Manipulation of the structural parameters to increase the strain in the QW is expected to substantially lower the effective mass for holes and, consequently, increase the hole mobility.

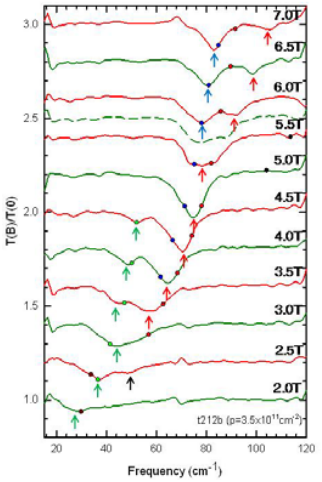

Fig.1 Normalized transmission through a *p*-type InSb QW as a function of photon frequency for different applied magnetic fields. The arrows mark the positions of observed cyclotron resonances.

The effective mass of the holes was characterized through cyclotron resonance experiments (see Fig. 1) in applied magnetic fields up to 17.5T, at a temperature of 4.2K. At low temperatures, the hole mobility is ~50,000 cm^2/Vs. At fields less than 4T, we deduce a hole effective mass of 0.04 to 0.1m_o for densities of 2 to $5\times10^{11}cm^{-2}$, which is up to a factor of 5 larger than observed in $In_xGa_{1-x}As$ QWs and suggests that higher hole mobilities are possible. At higher fields, we observe separate features for different spin-conserving transitions between neighboring Landau levels. The energies of the features depend on the levels' spin index and Landau level indices. The energies and intensities are explained by a modified Pidgeon-Brown model (See Fig. 2) that explicitly incorporates pseudomorphic mechanical strain.

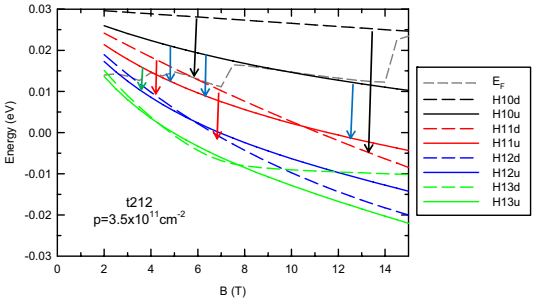

Fig.2 Calculated Landau-level fan diagram for holes in an InSb QW. Spin-conserving cyclotron transitions are indicated by arrows.

References

1. S. Datta *et al.*, Proc. IEEE IEDM (2005) 763.

2. M. Edirisooriya *et al.*, J. Crystal Growth (in press).

Aharonov-Bohm phase shift in a multi-terminal asymmetric quantum ring

S.S. Buchholz*, S.F. Fischer*, U. Kunze*, and D. Reuter **, A.D. Wieck**
**Werkstoffe und Nanoelektronik, Ruhr-Universität Bochum, 44780 Bochum, Germany*
*** Angewandte Festkörperphysik, Ruhr-Universität Bochum, 44780 Bochum, Germany*

Keywords: Aharonov-Bohm ring, phase rigidity, ballistic transport, nonlocal resistance

The Aharonov-Bohm (AB) effect enables to monitor both the coherence (AB amplitude) and phase in ballistic quantum rings. However, in order to determine the phase evolution it is necessary to overcome phase rigidity and realize a multi-terminal ring geometry: In a two-terminal interference device the AB phase is restricted to 0 or π. Schuster *et al.* [1] realized a multi-terminal open geometry to investigate the phase evolution of electron transmission through a quantum dot in a nonlocal measurement setup. Kobayashi *et al.* [2] have shown that nonlocal measurements in a four-terminal geometry allow for the observation of a gradual phase shift.

In this work, we demonstrate a four-terminal quantum ring for which all measurement configurations prove to be free of phase rigidity. We investigate ballistic transport and quantum interference in a quantum wire loop fabricated from a high mobility GaAs/AlGaAs field-effect heterostructure. Two equally wide electron waveguides orthogonally intersect twice forming an asymmetric ring structure (inset of Fig.1) which is covered with an Au gate. Transport measurements were performed at temperatures between $T_{\mathrm{base}} = 23$ mK and $T = 2$ K.

Remote bend resistance as a function of DC bias is visible as a clear signature of inertial ballistic transport [3]. In magnetic fields AB resistance oscillations prove coherence and show equal amplitudes in the local ($R_{14,32} = V_{14}/I_{32}$), the nonlocal ($R_{34,21}$) and the crosslocal ($R_{24,13}$) measurement setups. We attribute this observation to the symmetry of the orthogonal cross junctions. It is well described within the Landauer-Buttiker formalism [3].

The gate voltage allows to modulate the phase of the interference electrostatically by changing the electrons' Fermi wavelength along the unequal paths. We observe phase shifts with gate voltage in all four-terminal measurement configurations. Fig.1 shows the interference pattern in the magnetic field for several gate voltages ranging from 680 mV to 725 mV (5 mV steps) in the nonlocal configuration. The phase shifts gradually as indicated by arrows. The right inset of Fig.1 displays the phase evolution as the magnetic field position of two maxima / minima (phase jump of π considered) for the applied gate voltages.

This demonstrates that narrow etched electron waveguides are applicable for phase sensitive interferometric measurements.

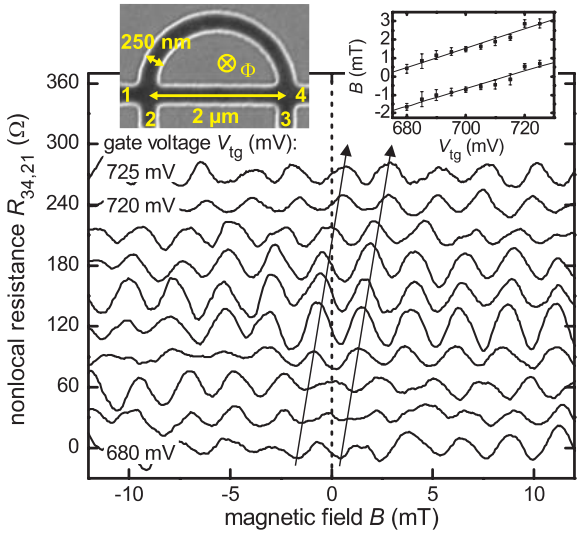

Figure 1: AB component of the nonlocal resistances $R_{34,21}$ for several gate voltages after substraction of background (at $T_{\mathrm{base}} = 23$ mK). Curves are offset for clarity. The left inset shows a scanning electron micrograph of the ring structure. The right inset displays the B-position of two AB maxima for the different gate voltages applied.

References

[1] R. Schuster *et al.*, Nature **385**, 417 (1997).

[2] K. Kobayashi *et al.*, J. Phys. Soc. Jap. **71**, 2094 (2002).

[3] S.S. Buchholz *et al.*, Appl. Phys. Lett. **94**, 022107 (2009).

Tomonaga-Luttinger exponent of peanut-shaped hollow nanocylinders

Hiroyuki Shima*, Hideo Yoshioka** and Jun Onoe***

*Dept. of Applied Physics, Graduate School of Engineering, Hokkaido University, Sapporo 060-8628, Japan

** Dept. of Physics, Nara Women's University, Nara 630-8506, Japan

*** Research Laboratory for Nuclear Reactors and Dept. of Nuclear Engineering, Tokyo Institute of Technology, 2-12-1 Ookayama, Meguro, Tokyo 152-8550, Japan

Keywords: surface curvature effect, Tomonaga-Luttinger liquid, peanut-shaped fullerene polymer

When a quantum particle is confined to a thin curved layer, geometric surface curvature of the layer produces an effective "force" exerting on the particle, and then yielding spatial modulation of the wavefunction amplitude purely induced by nonzero surface curvature of the system [1]. Such the geometric curvature effect on quantum mechanics was originally brought up several decades ago [2]. Still, it has focused renewed attention in the last years due to technological progress that enables to fabricate low-dimensional nanostructures with complex geometry. Many intriguing phenomena associated with curved geometry have been suggested so far [3], while most of them considered non-interacting electron systems; little attempt has been done for interacting electrons and their collective excitations. The latter issue should be important particularly when studying quasi-one dimensional systems, in which the Fermi liquid theory breaks down and the system goes to Tomonaga-Luttinger (TL) liquid states. In TL liquids, physical quantities often exhibit power-law anomalies stemming from the absence of single-particle excitations near the Fermi energy [4]. This context naturally poses a question about how geometric perturbation affects TL behaviors of quasi-one dimensional curved systems. Peanut-shaped C_{60} polymers [5] are exemplary materials to be considered; they are thin long hollow tubules whose radius are periodically modulated along the tube axis. Hence, periodic surface curvature intrinsic to the systems will provide sizeable effects on their TL properties, though details are largely unknown.

In this project, we consider geometric perturbation effects on TL liquid states in long thin hollow cylinders with periodically varying radius [6]. We reveal that the presence of curvature-induced potential can yield a significant increase in the power-law exponent α of the single-particle density of states $n(\omega)$ near the Fermi energy E_F, *i.e.*, $n(\omega) \propto |\hbar\omega - E_F|^{\alpha}$. Geometric conditions for the cylinders to observe the shift in α are within the realm of laboratory experiments, implying the verifiability of our predictions via existing materials. Further strikingly, our results signal that nonzero surface curvature yields diverse alterations in TL liquid behaviors characterized by power-law singularities, bearing in mind that various kinds of power-law exponents observed in TL liquids depends on the exponent α we have considered.

[Corresponding author: shima@eng.hokudai.ac.jp]

References

[1] R. C. T. da Costa, Phys. Rev. A **23** (1982) 1981.

[2] B. De Witt, Phys. Rev. **85** (1952) 635.

[3] H. Taira and H. Shima, Surf. Sci. **601** (2007) 5270, and references therein.

[4] For reviews see, J. Voit, Rep. Prog. Phys. **57** (1994) 977, T. Giamarchi, *Quantum Physics in One Dimension* (Oxford University Press, 2004).

[5] J. Onoe, T. Nakayama, M. Aono and T. Hara, Appl. Phys. Lett. **82** (2003) 595; J. Onoe, T. Ito, S. Kimura, K. Ohno, Y. Noguchi and S. Ueda, Phys. Rev. B **75** (2007) 233410.

[6] H. Shima, H. Yoshioka and J. Onoe, arXiv:0903.0798.

Anomalous temperature dependence of electron tunneling between a two-dimensional electron gas and Si dots

Y. Sakurai,[*] S. Nomura,[*] Y. Takada,[*] K. Shiraishi,[*] M. Muraguchi,[**] T. Endoh,[**]
Y. Shigeta,[***] M. Ikeda,[****] K. Makihara[****] and S. Miyazaki[****]
[*]*Graduate School of Pure and Applied Science, University of Tsukuba, Tsukuba, 305-8571, Japan.*
[**]*Center of Interdisciplinary Research, Tohoku University, Sendai, 980-8578, Japan.*
[***]*Institute of Picobiology, Graduate School of Life Science, University of Hyogo, Ako, 678-1297, Japan.*
[****]*Graduate School of Advanced Sciences of Matter, Hiroshima University, Higashi-Hiroshima, 739-8530, Japan.*

Keywords: tunneling, quantum dot, Monte-Carlo simulation

We present our observation of an anomalous temperature dependence of electron tunneling between a two-dimensional electron gas (2DEG) and Si dots in the direct tunneling mode, where no temperature dependence should be present. The experimental results are reproduced by a theory based on our proposal that the wave-packet-like temporal and spatial modification of the initial state electrons is important to satisfy the geometrical matching of electron wave functions, implicitly assuming that tunneling should occur within a finite experimental measurement time.

Electron tunneling modes are classified into Fowler-Nordheim tunneling, resonant tunneling (trap assisted tunnelling), and direct tunneling modes. It has been well accepted that the direct tunneling mode has no temperature dependence as long as the barrier height is much higher than the thermal energy. Conductance peaks as a function of gate voltage in single electron transistors showed absence of peak shift with temperature [1-3].

We have studied the electron tunneling in a LPCVD grown sample, where Si dots with 5.1 nm height is weakly coupled to 2DEG through a 3.5-nm thick SiO_2 barrier [4], as schematically shown in Fig. 1 (a). The density of the Si dots was estimated to be $1.7\times10^{11}cm^{-2}$. Displacement current (I) originating from the change in the charge distribution in the MOS capacitor was measured as a function of the gate voltage (V) between the gate electrode and the Si substrate by varying the temperature in a He flow-type cryostat.

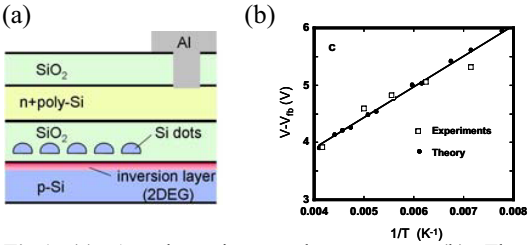

Fig.1 (a) A schematic sample structure. (b) The observed and calculated temperature dependence of effective gate voltage necessary for electron tunneling from 2DEG to Si dots.

Peaks were observed in the I-V curves when the gate voltage was swept from negative to positive direction. The peaks in I-V curves appear as a result of charging of Si dots. We have found that the gate voltages necessary for the electron injection to Si dots shift toward the higher voltage side with an increase in temperature as shown in Fig. 1 (b).

The electron tunneling is conventionally treated as a one-dimensional overlap integral between initial and final state wave functions, implying that both wave functions and a potential barrier infinitely extend in the direction perpendicular to the propagation direction. However, the experimental results are explained by a Monte-Carlo simulation, in which thermal fluctuation of the wave-packet-like modification of the initial state electrons in 2DEG is considered as shown in Fig. 1 (b). This indicates that the geometrical matching of initial and final state electron wave functions plays a crucial role for electron tunneling between 2DEG and Si dots.

This work was partly supported by KAKENHI No. 18063003.

References

1. Y. Takahashi, *et al*., IEEE Trans. Electron Device, **43**, 1213 (1996).
2. M.A. Kastner, Rev. Mod. Phys., **64**, 849 (1992).
3. D.G. Austing, T. Honda, and S. Tarucha, Solid-State Electronics, **40**, 237 (1996).
4. S. Miyazaki, Y. Hamamoto, E. Yoshida, M. Ikeda, and M. Hirose, Thin Solid Films, **369,** 55 (2000).

Revival of electron coherence in a Luttinger liquid of finite length

Jaeuk U. Kim*, W.-R. Lee*, Hyun-Woo Lee**,and H.-S. Sim*
*Department of Physics, Korea Advanced Institute of Science and Technology, Daejeon 305-701, Korea
** PCTP and Department of Physics, Pohang University of Science and Technology, Pohang, Kyungbuk 790-784, Korea

Keywords: Quantum interference, Dephasing, Electron fractionalization

Electron dephasing, the decay of electron coherence is one of the central issues in mesoscopic physics. At low temperature, electron-electron interaction is a dominant source of the dephasing, and it generates nontrivial effects. For instance, when an electron is injected to an infinitely long one-dimensional wire, the interaction splits it into two fractional charges[1]. The charge fractionalization causes the decay of electron coherence in the infinite wire[2]. Note that the charge fractionalization was experimentally detected very recently[3].

We investigate the spatial decay of electron coherence in a disorder-free quantum wire of finite length[4]. Using the bosonization technique, we show that the coherence length characterizing the exponential decay of the coherence can vary from region to region, and that the coherence can even revive after the decay. This counterintuitive behavior, which is in clear contrast to the conventional exponential decay with single coherence length, is due to the effects of electron interaction, the fractionalization of an electron and the finite-size-induced recombination of the fractions.

References

[1] K.-V. Pham, M. Gabay, and P. Lederer, Phys. Rev. B 61, 16397 (2000).

[2] K. Le Hur, Phys. Rev. Lett. 95, 076801 (2005).

[3] H. Steinberg et al., Nature Phys. 4, 116 (2008).

[4] Jaeuk U. Kim, W.-R. Lee, Hyun-Woo Lee, and H.-S. Sim, Phys. Rev. Lett. 102, 076401 (2009).

Multiorbital Kondo effect in quantum dots coupled to ferromagnetic leads

Hitoshi Yoshizumi and Sei-ichiro Suga
Department of Applied Physics, Osaka University, Suita, Osaka 565-0871, Japan

Keywords: orbital Kondo effect, quantum dot, ferromagnetic leads

In recent years, the Kondo effect in multiorbital quantum dot (QD) systems such as vertical QD and carbon nanotube QD have attracted a lot of attention both theoretically and experimentally. In these systems, the orbital Kondo effect comes into existence. Fascinating aspects of the multiorbital Kondo effect have been revealed. On the other hand, the QD coupled to ferromagnetic leads is actively investigated [1,2,3,4]. The spin-polarized QD system can be a potential candidate of a novel spintronics application such as a gate-tunable spin memory. For a parallel magnetic configuration of the ferromagnetic leads the Kondo resonance splits into two peaks, while the Kondo resonance for an antiparallel magnetic configuration is the same as for the case of nonmagnetic leads [1]. For multiorbital QD systems coupled to ferromagnetic leads, the effects of ferromagnetic leads may be different between the spin and orbital degrees of freedom, thus yielding possibly interesting behavior for the multiorbital Kondo effects.

In this study, we investigate the two-orbital Kondo effect in a QD coupled to ferromagnetic leads. The model is described by the following Hamiltonian,

$$\begin{aligned} H &= \sum_{k,l,\sigma} \epsilon_{k\sigma} c^\dagger_{kl\sigma} c_{kl\sigma} + \sum_{l,\sigma} \epsilon_{l\sigma} d^\dagger_{l\sigma} d_{l\sigma} \\ &+ \sum_{k,l,\sigma} (V_{kl\sigma} c^\dagger_{kl\sigma} d_{l\sigma} + h.c.) \\ &+ U \sum_{l} n_{l\uparrow} n_{l\downarrow} + U' \sum_{\sigma\sigma'} n_{l\sigma} n_{\bar{l}\sigma'}, \end{aligned} \quad (1)$$

where, $c^{(\dagger)}_{kl\sigma}$ annihilates (creates) a conduction electron with wave number k, spin σ and orbital l in the ferromagnetic leads. $d^{(\dagger)}_{l\sigma}$ annihilates (creates) a localized electron with spin σ and orbital l in the QD, and $n_{l\sigma} = d^\dagger_{l\sigma} d_{l\sigma}$. Intraorbital and interorbital Coulomb interactions are expressed by U and U', which are assumed to be very large. The spin polarization of the ferromagnetic leads is given by $p = (\rho_\uparrow - \rho_\downarrow)/(\rho_\uparrow + \rho_\downarrow)$, where ρ_σ is the density of states (DOS) for spin σ in the ferromagnetic leads. The DOS are assumed to be independent of the orbital l.

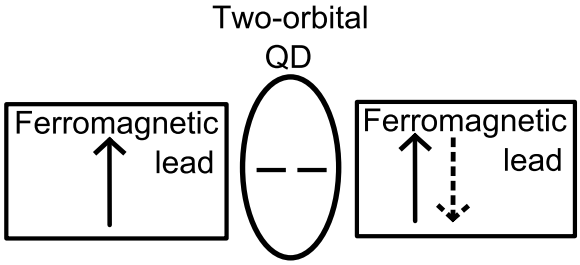

Figure 1: A two-orbital QD system coupled to ferromagnetic leads.

We calculate the single-particle excitation spectra of the localized electron in the QD using an equation of motion method. The splittings of the Kondo resonance are investigated by changing the spin polarization p for parallel and antiparallel magnetic configurations. The splittings of the Kondo resonance are also studied complementarily using a poor man's scaling method. Both results are compared and qualitative features are discussed.

References

[1] J. Martinek *et al.*, Phys. Rev. Lett. **91**, 127203 (2003).
[2] D. Matsubayashi and M. Eto, Phys. Rev. B **75**, 165319 (2007).
[3] P. Simon *et al.*, Phys. Rev. B **75**, 045310 (2007).
[4] A. N. Pasupathy *et al.*, Science **306**, 86 (2004).

Andreev tunneling through a quantum dot at finite bias

Y. Yamada*, Y. Tanaka** and N. Kawakami*
*Department of Physics, Kyoto University, Kyoto, Japan
** Condensed Matter Theory Laboratory, RIKEN, Wako, Saitama 351-0198, Japan

Keywords: quantum dot, Andreev reflection, Kondo effect, nonequilibrium transport

Recent developments in the nanotechnology make it possible to fabricate mesoscopic systems that consist of a quantum dot (QD) and superconducting leads. Since an intriguing interplay is expected between the Andreev reflection and the electron correlation effects like the Kondo effect, these systems have attracted much attention and a lot of investigations have been done so far. Among them, recent experimental studies show that the nonequilibrium transport strongly depends on the total spin at the QD, which implies that the Kondo effect plays the essential role in the transport of these systems at finite bias [1-3]. To address this problem, we investigate the Andreev tunneling through a QD coupled to the normal and superconducting leads (N-QD-S) [4-5] at finite bias. Using an improved second-order perturbation theory in the Keldysh Green's function formalism, we calculate the density of states (DOS) at the QD and the current due to the Andreev reflection.

Figure 2 shows the DOS at the QD for various applied voltages. In the equilibrium case ($eV = 0$), we can see a double-peak structure in the DOS, which means that the superconducting correlation is dominant at the QD. The two peaks are little influenced by a small applied bias voltage ($eV = 0.015$). On the other hand, a sufficiently large bias voltage ($eV = 1$) collapses the double-peak structure and instead creates a new sharp peak at the Fermi surface of the normal lead ($\omega = eV$). This means that the applied bias voltage weakens the superconducting correlations at the QD, which in turn revives the Kondo effect competitive to the above superconducting correlations.

More detailed analyses of the DOS and also the transport properties will be presented at the symposium.

Fig.1

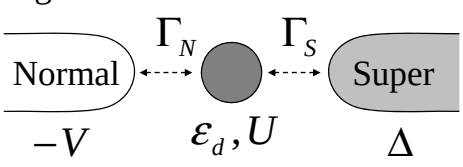

Figure 1: Schematic diagram of the N-QD-S system. V,$\Gamma_{N(S)}$,ϵ_d,U,Δ mean the applied bias voltage, resonance width between the QD and normal (superconducting) lead, the energy level of the QD, the Coulomb interaction at the QD and superconducting gap, respectively.

References

[1] A. Eichler *et. al.*, Phys. Rev. Lett. **99**, 126602 (2007).

[2] T. Sand-Jespersen *et. al.*, Phys. Rev. Lett. **99**, 126603 (2007).

[3] C. Buizert *et. al.*, Phys. Rev. Lett. **99**, 136806 (2007).

[4] Y.Tanaka *et. al.*, J. Phys. Soc. Jpn. **76**, 74701 (2007).

[5] Y.Yamada *et. al.*, Physica E **40**, 265 (2007).

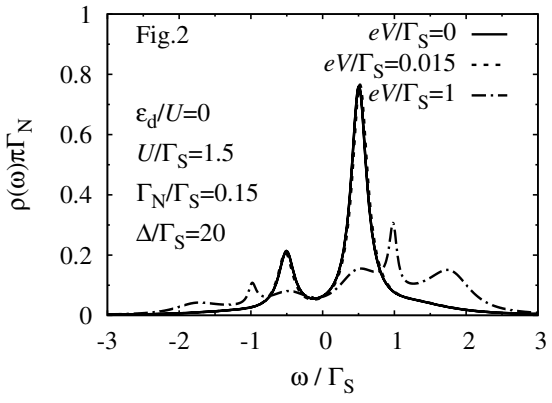

Figure 2: Density of states at the quantum dot for various applied voltages.

Distribution and Anisotropy of Electron g-factor in Quantum Dots

Weidong Sheng
Department of Physics, Fudan University, Shanghai 200433, P.R. China

Keywords: g-factor, anisotropy, quantum dot

A good understanding of properties of an electron spin in quantum dots, in particular its control and engineering, is key to the success of their perspective applications in spintronics. As one of the most important property of an electron spin, electron g-factor measures the Zeeman splitting of an electron state in a magnetic field and is determined by both the spin and orbital motion of the electron. In self-assembled quantum dots, complicated environment like strong quantum confinement and inhomogeneous strain field makes electron g-factors greatly different from those values in the bulk.

Presented in this work is a systematical study of the electron g-factor tensor in InAs/GaAs self-assembled quantum dots. A tight-binding approach is applied to calculate g-factors of electronic states in quantum dots. Figure 1 plots the longitudinal electron g-factors calculated as a function of the height of the dots. It is noticed that the modulus of the electron g-factor slightly decreases with the increasing height for all the structures except for the pure InAs dots. The electron g-factor shows a very small variation of less than 15% as the height varies from 3.0 nm to 6.0 nm in $In_{0.8}Ga_{0.2}As$ and $In_{0.6}Ga_{0.4}As$ dots. Although the lateral dimension of these dots is smaller than that of the larger ones by more than 40% and the volume by almost 100%, the difference in the electron g-factors is only about 10%. The insensitive dependence of the electron g-factor on the size fluctuation of the quantum dots agrees well with the experiment [1].

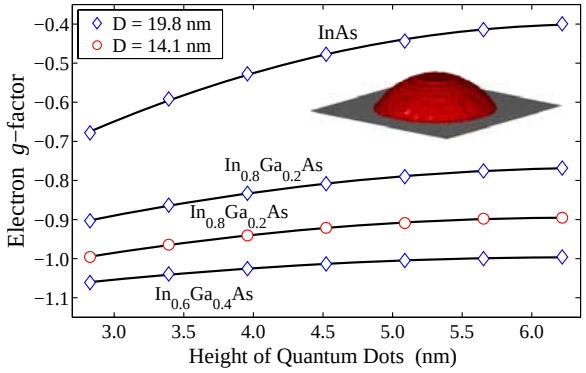

Figure 1: Electron g-factors calculated as a function of the height of the dots.

Figure 2 plots the electron g-factor calculated as the applied magnetic field changes from Faraday to Voigt configuration. In the pure InAs dot, the g-factor is seen to become larger in amplitude as the magnetic field is tilted from the growth direction to the quantum-dot plane, i.e., $|g_\perp| < |g_\parallel|$. While in the highly intermixing structure such as the $In_{0.6}Ga_{0.4}As$ dot, the opposite trend, i.e., $|g_\perp| > |g_\parallel|$, is observed. Between the two distinct kinds of behavior, the electron g-factor in the moderately intermixing $In_{0.6}Ga_{0.4}As$ dot is noticed to be almost independent on the direction of the applied magnetic field. Hence, the electron g-factor is found to be sensitive to the chemical composition instead of the aspect ratio of the structures of quantum dots.

References

[1] W. Sheng et at, Phys. Rev. B **77**, 241307(R) (2008).

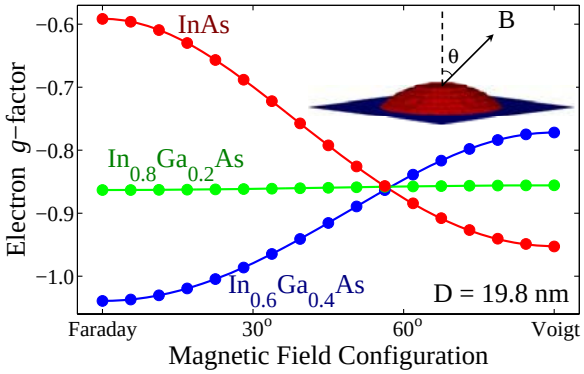

Figure 2: Electron g-factor as a function of the tilt angle of the applied magnetic field, calculated for a lens-shaped $In_xGa_{1-x}As$/GaAs dots with various chemical composition.

Interaction between coupled quantum dots and a biased quantum point contact

D. Harbusch*, H.P. Tranitz**, W. Wegscheider** and S. Ludwig*
* *Fakultät für Physik, Ludwig-Maximilians-Universität, München, Germany*
** *Institut für Experimentelle und Angewandte Physik, Universität Regensburg, Regensburg, Germany*

Keywords: back–action, quantum dots, quantum point contact, charge detection

Biased quantum point contacts (QPC) are commonly employed to detect the charge states of qubits composed of coupled quantum dots (QD) [1]. Such charge detection is an essential technique to read out quantum states in solid state based quantum information processing schemes. Although a biased QPC can be a very sensitive charge detector, it emits energy that can be reabsorbed by the nearby QDs and thereby cause unwanted decoherence [2, 3, 4]. We investigate the back–action of such a charge detector on coupled QDs.

Our nano-devices are defined by means of Schottky gates on the surface of a GaAs/AlGaAs heterostructure containing a two-dimensional electron system (2DES). All measurements are performed in a dilution refrigerator at its base temperature of $T \simeq 20\,\mathrm{mK}$.

In our experiments the back–action becomes directly visible in the charge stability diagram of a serial double QD that is measured using a biased QPC which at the same time causes the back–action. We operate the double QD in a configuration with very asymmetric coupling to the leads, i. e. one of the QDs is essentially charged via the other QD. Such a configuration allows for strong modifications of charging rates under absorption of energy quanta originating from a non-equilibrium source.

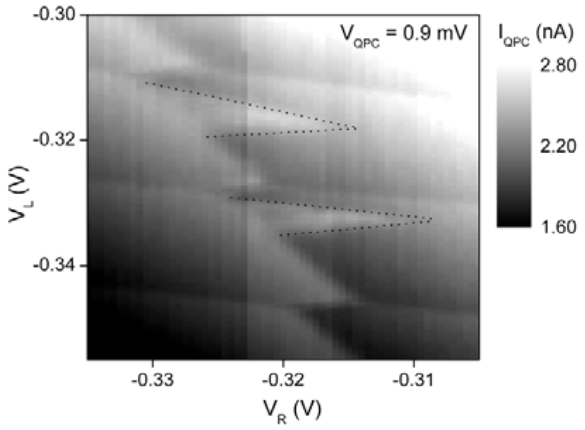

Figure 1: Charge stability diagram of a double QD. The grey scale displays the current through the QPC detector as a function of plunger gate voltages of the two QDs. The dotted lines are a guide to the eye.

Figure 1 shows a stability diagram of such an asymmetrically coupled double QD. Displayed is the dc–current through a nearby QPC that is almost pinched off and biased with $V_{\mathrm{QPC}} = 0.9\,\mathrm{mV}$. Two approximately triangular shaped shaded regions (dotted lines in figure 1 are a guide to the eye) correspond to non–equilibrium charge occupancies of the double QD. These regions are a direct manifestation of the back–action of the biased QPC. We study the size and substructure of the triangles as a function of external parameters like V_{QPC} or the power emitted by the QPC in order to learn about the coupling mechanisms that lead to the observed back–action. While a counting statistics experiment is very powerful in determining the relevant relaxation and tunneling rates [3], our dc–measurements are not bandwidth limited and allow us to investigate the regime of extremely small powers. Based on our results we optimize the charge detector for minimal back–action while keeping its sensitivity high.

References

[1] Elzerman et al., Phys. Rev. B **67**, 161308 (2003)

[2] V.S. Khrapai, S. Ludwig, J.P. Kotthaus, H.P. Tranitz and W. Wegscheider, Phys. Rev. Lett. **97**, 176803 (2006)

[3] S. Gustavsson, M. Studer, R. Leturcq, T. Ihn, and K. Ensslin, Phys. Rev. Lett. **99**, 206804 (2007)

[4] D. Taubert, M. Pioro-Ladrière, D. Schröer, D. Harbusch, A.S. Sachrajda, and S. Ludwig, Phys. Rev. Lett. **100**, 176805 (2008)

Electron localization in few-electron concentric quantum rings

J. M. Escartín*, F. Malet**, A. Emperador***, M. Barranco*, and M. Pi*
*Departament ECM, Fac. de Física, and IN^{2}UB, Universitat de Barcelona, Diagonal 647, 08028 Barcelona, Spain
**Mathematical Physics, LTH, Lund University, Box 118, 22100 Lund, Sweden
***Institute for Research in Biomedicine, Parc Científic de Barcelona, Josep Samitier 1-5, 08028 Barcelona, Spain

Keywords: Quantum rings, electron localization, infrared absorption.

Using an exact diagonalization technique [1], we show that few-electron concentric double quantum rings, experimentally realized a few years ago [2], and theoretically modeled within the effective mass approximation by the two-dimensional circularly symmetric potential

$$V_{\rm conf}(r) = \frac{m}{2}\,\min\left\{\omega_1^2\,(r-R_1)^2,\ \omega_2^2\,(r-R_2)^2\right\}\ ,$$

display *radial and azimuthal* localized electronic states in the presence of a perpendicularly applied magnetic field. These states are the quantum analog of the classical few-electron equilibrium configurations arising in one-dimensional concentric rings. The fingerprint of their appearance is a very soft mode in the dipole infrared response at an energy that roughly corresponds to the absorption of a photon by a rigidly rotating N-electron molecule.

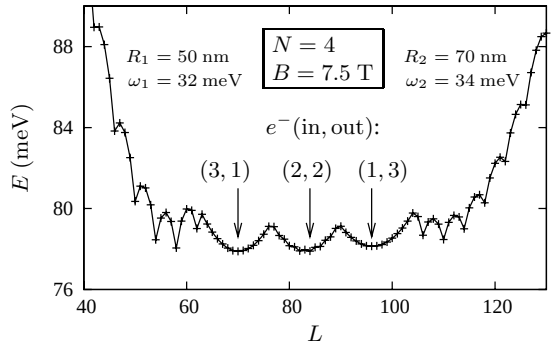

Figure 1: Yrast line (minimum state energy as a function of the total angular momentum) for two concentric quantum rings hosting four fully polarized electrons. Single ring behaviour [3] is observed for large and small angular momenta, whilst for intermediate L values a distinct structure, made of "yrast traps", shows up associated to the simultaneous occupation of both rings.

Two-particle density and dipole infrared absorption spectrum are discussed for highly symmetric configurations made of $N = 4$ and 6 electrons. A comparison with the results obtained within density functional theory is also presented.

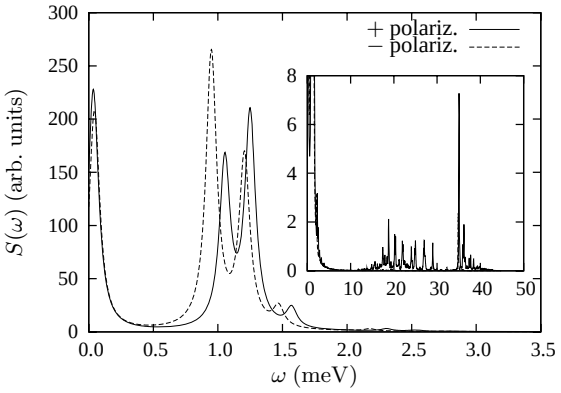

Figure 2: Infrared absorption spectrum for the ground state, $L = 70$ configuration, displayed in Figure 1 (inset). The very low energy peaks arise at nearly the same frequency as the dipole excitation of a rigid rotor.

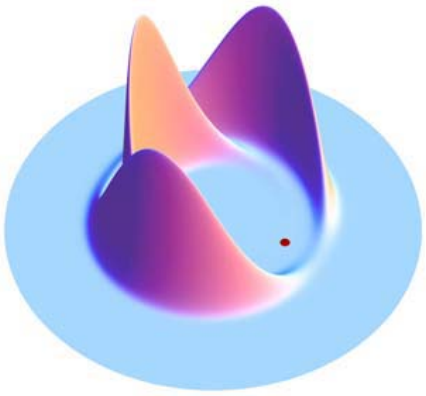

Figure 3: Two-particle density for the $L = 84$ configuration in Figure 1. The position of one of the electrons is fixed at the marked point (at $r = 50$ nm).

References

[1] A. Emperador, E. Lipparini, and F. Pederiva, Phys. Rev. B **72**, 033306 (2005).

[2] T. Mano *et al.*, Nanoletters **5**, 425 (2005); A. Mühle *et al.*, Appl. Phys. Lett. **91**, 133116 (2007).

[3] S. Viefers, *et al.*, Physica E **21**, 1 (2004).

Electrostatically-defined quantum dots in silicon

W.H. Lim*, H. Huebl*, F.A. Zwanenburg*, L.H. Willems van Beveren*, S. Rubanov**, P.G. Spizzirri**, S.J. Angus**, R.G. Clark*, A. Morello* and A.S. Dzurak*

** Centre for Quantum Computer Technology, University of New South Wales, Sydney, Australia*

*** Centre for Quantum Computer Technology, University of Melbourne, Melbourne, Australia*

Keywords: silicon, quantum dot, FastCap, MOSFET

Electrostatically-defined single and double quantum dot (QD) systems in GaAs/AlGaAs heterostructures [1,2] are the benchmark with regards to the implementation of DiVincenzo's criteria using semiconductor qubits [3-5]. Although nuclear spins inherently present in GaAs provide a fast decoherence mechanism, this drawback has been partly overcome recently [6]. Silicon has a natural advantage in this respect since the only stable isotope with a nuclear spin is ^{29}Si. The 4.7% abundance of this isotope in natural Si can be reduced by isotopic purification, resulting in nearly nuclear-spin-free crystals. This should, in principle, increase the coherence time of electron-spin qubits in silicon [7].

In this work, we report the fabrication and milli-kelvin electrical measurement of nano-structured (i) double QDs [8] and (ii) a single QD dot with a charge detector. These two devices are based upon recently developed double-gated silicon QDs [9].

Fig. (a) shows the scanning electron micrograph (SEM) of the silicon metal-oxide-semiconductor (MOS) double QD. The morphology of the device is investigated using cross sectional transmission electron microscopy (TEM) analysis. Transport spectroscopy demonstrates the ability to tune the double dot from the weakly-coupled to strongly-coupled regime. In the weakly-coupled regime (fig. b) extracted capacitances of the system show good quantitative agreement with simple modelling using FastCap [8].

Fig. (c) shows the SEM of a single QD capacitively coupled, via an Al wire of ~1 μm long, to a single electron transistor (SET) or charge detector. In this design, the QD and SET are made of 3 Al layers, where the first layer provides the barrier gates, second layer provides contact to source and drain and the third layer independently controls the island. Preliminary measurement data shows formation of a single QD as evidenced by regular closed Coulomb diamonds (fig. d). We have also measured the cross capacitances from the charge detector gates to the dot and the results are promising for charge sensing experiments.

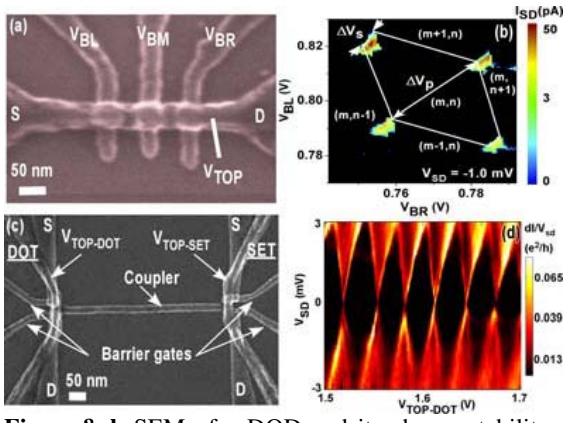

Fig. a & b SEM of a DQD and its charge stability diagram in the weakly-coupled regime. Clear honeycomb and bias triangles are observed. **Fig. c & d** SEM of a single QD with a SET and the bias spectroscopy performed on the QD. Regular closed Coulomb diamonds are observed in the many-electron regime.

These Si MOS-based QDs have excellent potential for the investigation of the spin-based qubits in silicon.

References

1. I.H. Chan, et. al., Nanotechnology **15**, 609 (2004).
2. W.G. van der Wiel, et.al., Rev. Mod. Phys. **75**, 1 (2002).
3. D. Loss and D.P. DiVincenzo, Phys. Rev. A **57**, 120 (1998).
4. J.R. Petta, et. al., Science **309**, 2180 (2005).
5. F.H.L. Koppens, et. al., Nature **442**, 766 (2006).
6. D.J. Reilly, et. al., Science **321**, 817 (2008).
7. C. Tahan, et. al., Phys. Rev. B **66**, 035314 (2002).
8. W.H. Lim, et. al., arXiv: 0904.0311v1, (2009).
9. S.J. Angus, et. al., Nano Lett. **7**, 7 (2007).

Terahertz Photo-Response of Quantum Point Contacts

J. Song[1], Y. Kawano[2], K. Ishibasi[2], G. Aizin[3], N. Aoki[4],
Y. Ochiai[4], J. L. Reno[5], and J. P. Bird[1,4]

1 *Department of Electrical Engineering, University at Buffalo, the State University of New York, Buffalo, NY 14260-1920, USA*

2 *Advanced Device Laboratory, RIKEN, 2-1 Hirosawa, Wako, Saitama 351-0198, Japan*

3 *Department of Physical Sciences, Kingsborough College of the City University of New York, Brooklyn, NY 11235*

4 *Graduate School of Advanced Integration Science, Chiba University, 1-33 Yayoi-cho, Inage-ku, Chiba 263-8522, Japan*

5 *CINT Science Department, Sandia National Laboratories, P.O. Box 5800, Albuquerque, NM 87185-1303*

Keywords: Terahertz, quantum point contacts, rectification

A focus of terahertz (THz) research concerns the applications of quantum-effect semiconductor devices, whose characteristic energies lie in the THz (i.e. meV) range. Quantum point contacts (QPCs) are an important example of such devices, and their natural tunability is of interest for frequency-sensitive THz detection. While rectification of THz fields by QPCs has been discussed in terms of the effective coupling of the THz to the QPC source-drain bias, another possibility is that this field can modulate the QPC gate voltage (V_g). Such a mechanism is, in fact, desirable, since the gate characteristic of QPCs should show ranges of V_g for which the photo-response is strongly pronounced. These are the transition regions between quantized plateaus, where a small modulation of V_g should cause a large photo-signal. In this report, we provide evidence of such a mechanism, demonstrating a clear THz response in multi-mode QPCs at 1.4 & 2.5 THz. This response is inconsistent with a bolometric effect, but is instead excellently described by a classical model of gate rectification. In our presentation, we discuss how this effect is distinct from the rectification mechanisms that have been invoked previously, being determined by the phase-dependent interference of the source-drain and gate-voltage modulations induced by the THz field.

In other experiments, we investigate the photo-response of QPCs to THz irradiation under conditions where the QPCs are pinched off and an energy barrier of controllable height impedes current flow. In this regime, we observe a clear THz photoresponse in the sub-threshold current that appears to be primarily of bolometric origin. The sensitivity of this photocurrent to heating may allow QPCs to function as sensitive THz detectors.

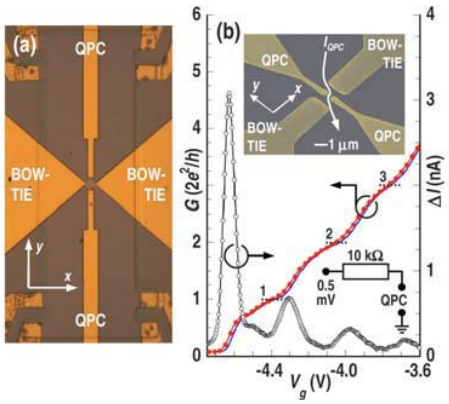

(a) Optical image of QPC device with integrated antenna. (b) The left axis shows the QPC conductance measured at 2.5 K, with (line with symbols) and without THz. The right axis shows the current change induced by the THz [1].

References

1. J. W. Song *et al*. Appl. Phys. Lett. **92**, 223115 (2008).

The quantum Hall effect beyond linear response

C.-T. Liang[1], Tobias Kramer[2,3], Eric J. Heller[3,4], Kuang Yao Chen[1], Robert E. Parrott[5], C. F. Huang[6], Li-Hung Lin[7], Jau-Yang Wu[8], Sheng-Di Lin[8], and Han-Chieh Lee[9]

[1]Department of Physics, National Taiwan University, Taipei, Taiwan 106, R.O.C.

[2]Institute for Theoretical Physics, University of Regensburg, 93040 Regensburg, Germany

[3]Department of Physics, Harvard University, Cambridge, MA 02138, USA

[4]Department of Chemistry and Chemical Biology, Harvard University, Cambridge, MA 02138, USA

[5]School of Engineering and Applied Science, Harvard University, Cambridge, MA 02138, USA

[6]National Measurement Laboratory, Center for Measurement Standards, Industrial Technology Research Institute, Hsinchu, Taiwan 300, R.O.C.

[7]Department of Applied Physics, National Chiayi University, Chiayi, Taiwan 600, R.O.C.

[8]Department of Electronics Engineering, National Chiao Tung University, Hsinchu, Taiwan 300, R.O.C.

[9]Institute of Physics, National Chiao Tung University, Hsinchu, Taiwan 300, R.O.C

Keywords: two-dimensional electron system, quantum Hall effect, current injection, beyond linear response

The quantum Hall effect observed in two-dimensional electron systems (2DESs) is important to both the metrological application [1] and fundamental physics [2-4]. The accurate Hall plateaus have been taken as the primary resistance standard [1], and the transitions separating different states in such an effect provide good examples of quantum phase transitions [2]. However, more studies are still necessary to understand the QHE beyond linear response limit. The cyclotron emission image [3] shows the importance of the current injection points with increasing the current I while the conventional theory focuses on the bulk region including the edge channels. Such points, in fact, are crucial to the formation of the Hall voltage [4].

Here we report a study on the QHE beyond linear response limit. Plateau-like structures can be observed as the filling factor ν~2.5 and 3.5 with increasing I, and Fig. 1 (a) and (b) show the theoretical and experimental curves $d\rho_{xy}/dB$-B, where B denotes the perpendicular magnetic field. We can see the consistency from the valley at ν~2.5 and 3.5 [4], and some predicted structures in ν=4-6 survives experimentally. Our study shows the transport contributions of the current injection points, where Landau-level addition transformation is invalid.

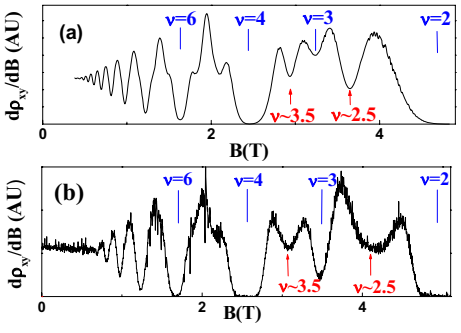

Fig.1 (a) and (b) shows the theoretical and experimental curves $d\rho_{xy}/dB$-B. at I=1.25 μA.

References

[1] F. Delahaye and B. Jecklmann, Metrologia **40**, 217 (2003).

[2] D. Shahar *et al.*, Phys. Rev. Lett. **79**, 479 (1999).

[3] Y. Kawano and T. Okamoto, Phys. Rev. Lett. **95**, 166801 (2005).

[4] T. Kramer *et al.*, arXiv:0811.3572 (2008).

Negative differential conductivity of two-dimensional electron gas layers in high magnetic fields

J. C. Chen*, Yuling Tsai*, Yiping Lin*, T. Ueda**, and S. Komiyama**

*Department of Physics, National Tsing-Hua University. Hsinchu, Taiwan
**Department of Basic Science, University of Tokyo, Komaba, Tokyo, Japan

Keywords: two-dimensional electron gas, negative differential conductivity, quantum Hall effect, Hall angle

It is well known that the negative differential conductivity (NDC) occurs if $\partial J/\partial E<0$, or the current density J decreases as the electric field E increases. However, Kurosawa and his co-workers [1] pointed out more than three decades ago that this is not a necessary condition for NDC if $\boldsymbol{J}$ is not parallel to $\boldsymbol{E}$. They argued that the generalized condition is that $\Delta\boldsymbol{J}\cdot\Delta\boldsymbol{E}<0$ in some direction of $\Delta\boldsymbol{E}$; That is, a fluctuation in charge distribution, causing $\Delta\boldsymbol{E}$, induces current $\Delta\boldsymbol{J}$ that amplifies the original fluctuation (Fig 1(b)). Reference [1] showed that this generalized condition of NDC is expressed as

$$D = \beta^2\tan^2\psi + 2\alpha(2-\beta)\tan\psi + \alpha^2 - 4(1-\beta) > 0 \quad (1)$$

in terms of the non-linear parameters $\alpha = \partial\psi/\partial\log E$ and $\beta = 1-(\partial\log J/\partial\log E)$ with ψ being the angle between $\boldsymbol{J}$ and $\boldsymbol{E}$. The generalized NDC is of particular importance in strong magnetic fields with $\psi \approx \pi/2$ because $\tan\psi \approx \infty$ and $D < 0$ ($\Delta\boldsymbol{J}\cdot\Delta\boldsymbol{E}<0$) readily holds with extremely small nonlinearities.

Here we study nonlinear coefficients, α and β, along with ψ against E in Hall bar devices (two standard GaAs/AlGaAs heterostructure crystals) at ν=2 and 4 quantum Hall plateaus at temperatures of 4K<T<44K. In all the devices, we find instability to take place above the critical current (E) (indicated by arrows in Fig.2 (a)), at which generalized NDC is predicted (Relation (1)). We will emphasize that the NDC here takes place with $\partial J/\partial E>0$ ($\beta<1$), show detailed experimental results and argue that the NDC here is a general and intrinsic property of 2DEG layers at high magnetic fields.

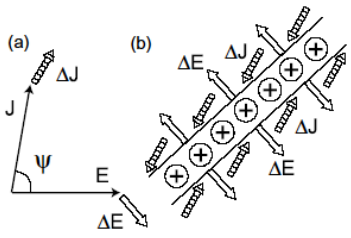

Fig.1 (a) $\Delta\boldsymbol{J}\cdot\Delta\boldsymbol{E}$ can be negative even if $\boldsymbol{J}\cdot\boldsymbol{E}>0$. (b) Growth of a space-charge sheet when $\Delta\boldsymbol{J}\cdot\Delta\boldsymbol{E}<0$.

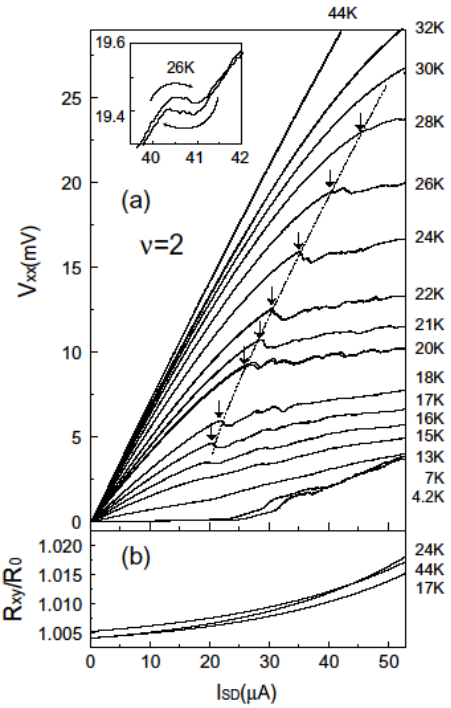

Fig.2 (a) Longitudinal voltage V_{xx} against the current for ν =2 QHE plateau (5.9T). (b) The Hall resistance R_{xy} as a function of the current.

References

1.T.Kurosawa, H. Maeda, & H. Sugimoto, *JPhysSocJapan*,**36**,491(19)

Spatially modulated magnetic fields induced modification of magnetic bands of monolayer zigzag graphene ribbon

M. F. Chen*, Y. C. Huang**, R. B. Chen***, and C. P. Chang****

*Department of Physics, National Cheng Kung University, Tainan, Taiwan

**Center for General Education, Kao Yuan University, Kaohsiung, Taiwan

***Center of General Studies, National Kaohsiung Marine University, Kaohsiung, Taiwan

****Center of General Education, Tainan University of Technology, Tainan, Taiwan

Keywords: Graphene ribbon, spatially inhomogeneous magnetic field, magnetic bands

The Peierls-coupling tight-binding model is employed to investigate the modification of magnetic bands of the hydrogen-terminated monolayer zigzag graphene ribbon resulting from the spatially inhomogeneous magnetic field (B_{inhom}). B_{inhom}, causing a new boundary condition (magnetic potential), can change band shapes, alter band curvature, shift band edge states, and hybridize parabolic bands and partial Landau levels. Density of states, e.g., the position, height and the number of dominant strong peaks, feature such interesting characteristics.

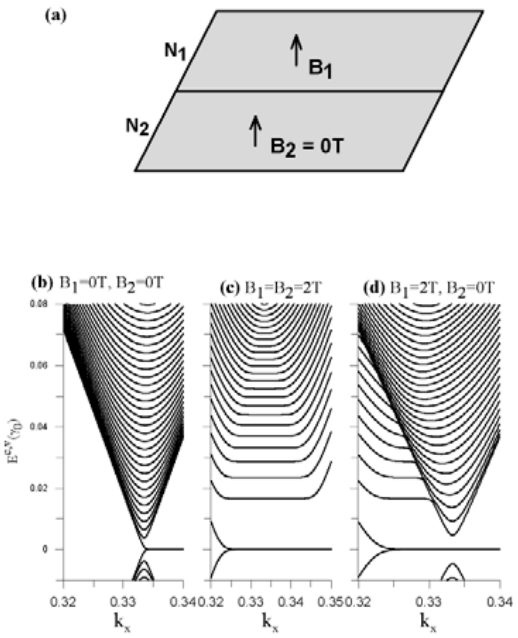

Figure 1: The geometrical structure of the system. N_1=N_2=600 denotes the zigzag lines along the y-axes[2]. The magnetic bands of (b) B_1= 0 and B_2=0, (b) B_1= 2 T and B_2=2 T, and (c) B_1= 2 T and B_2=0.

While the band shape is chiefly dominated by the ribbon width (W) and the spatial distribution (D) of Landau wave functions[1, 2], the application of a uniform perpendicular magnetic field to one monolayer zigzag graphene ribbon can induce the Landau flat band and Hall edge states [Fig. (c)]. As D $<$ W, the Landau states form and so arise the partial flat bands. With the Landau wave function once touching one of the ribbon edges, it will be too modified to meet the boundary condition. Thus, the partial flat bands are destroyed and the Hall-edge states happen [Fig. (c)].

The properties of the magnetic bands are very sensitive to the boundary conditions. The spatially inhomogeneous magnetic field B_{inhom} leads to a new magnetic potential[3], modifying the magnetic bands of zigzag graphene ribbons. The findings show that B_{inhom} induces the composites of the parabolic bands, partial Landau levels, and Hall edge states [Fig. (d)], which are quite different from the original parabolic bands at B=0 [Fig. (b)] and B_{hom}=2 T [Fig. (c)]. The effect of strength of modulated field (B1 and B2) and the different period (N_1 and N_2) on the magnetoelectronic properties (magnetic bands and DOS) will also be explored.

References

[1] Y. C. Huang, C. P. Chang, and M. F. Lin, Nanotechnology **18**, 495401 (2007).

[2] Y. C. Huang, C. P. Chang, and M. F. Lin, J. of Appl. Phys. **103**, 073709 (2008).

[3] S. Park and H. -S. Sim, Phys. Rev. B **77**, 075433 (2008).

The current direction induced rectification effect on the IQHE

D. Eksi*, O. Kilicoglu*, S. Aktas* and A. Siddiki**

* *Trakya University, Department of Physics, 22030 Edirne, Turkey*

** *Mugla University, Physics Department, Faculty of Arts and Sciences, 48170-Kotekli, Mugla, Turkey*

Keywords: Quantum Hall effect; Screening, current

The phenomenon of the integer quantized Hall effect (IQHE) [1] continuous to hold interest as newer and newer types of structures are developed [2]. It is known that the widths of the QHP depend on the electron density, mobility, temperature and the amplitude of the applied current. However, the direction of the applied current is not considered to be influencing the plateau widths. The early attempts to explain the IQHE, like the bulk [3] or the edge [4] pictures, considers electron-electron (e-e) interactions to be irrelevant. Here, we show that the widths of QHPs depend on the current intensity and the existence of the incompressible strips (ISs). We obtain the QHPs from a model which is purely based on the e-e interactions, supported by the local Ohm's law [5,6]. We solve the Schrödinger equation within a Hartree type mean field approximation [6], where it was shown that, if there exists an IS somewhere in the sample the system is in a QHP. When a DC current is imposed in the +y direction, due to the tilting of the Landau levels, the IS at the right hand side enlarges, whereas, the IS on the left hand side (LHS) shrinks. Fig. 1c, depicts such a situation under potential bias. Now if we start with a narrow IS on the LHS, it is possible to achieve equi-width ISs on both sides, by applying a certain current regardless of the donor inhomogeneity, Fig. 1d. As a result, we conclude that the widths of the QHPs also should depend on the applied current direction [7].

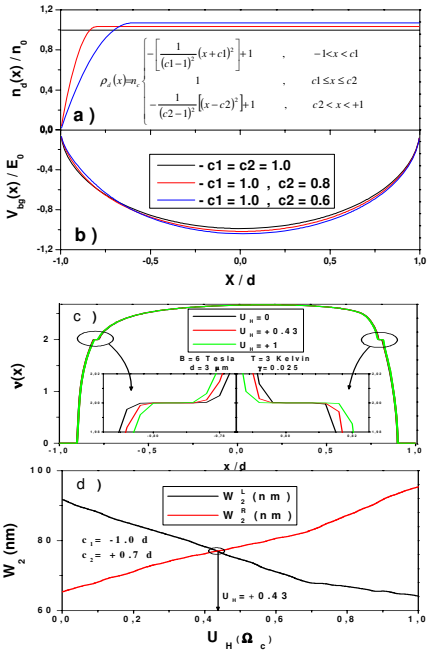

Figure: (a) The cross section of the donor layer considering for two values of steepness parameter (c1 left and c2 right). b) The corresponding potential. c) The electron density as a function of lateral coordinate normalized with the sample width, for three selected current amplitudes (U_H). d) The widths of the ISs as a function of U_H.

References

1. K. v. Klitzing, *et. al.* , Phys. Rev. Lett. **45**, 494 (1980)
2. J. Horas, *et al.*, Physica E **40,** 1130 (2008)
3. R. B. Laughlin, Phys. Rev. B **23**, 5632 (1981)
4. M. Büttiker, Phys. Rev. Lett. 57, 1761 (1986).
5. K. Güven, *et al.,* Phys. Rev. B **67**, 115327 (2003).
6. A. Siddiki and R. R. Gerhardts, Phys. Rev. B **70**, 195335 (2004).
7. A. Siddiki, Unpublished (2009).

Collapse of the Conductance Quantization by the High-frequency Shot Noise in Coupled Quantum Wires

M. Hashisaka*, Y. Yamauchi*, S. Nakamura*, K. Chida*, S. Kasai*, T. Ono* and K. Kobayashi*

** Institute for Chemical Research, Kyoto University, Kyoto, Japan*

Keywords: shot noise, edge current, quantum Hall effect, quantum interference

Interference of electrons has been the central issue in mesoscopic physics. Recent experiments on the electronic Mach-Zehnder interferometer (MZI) have clarified that the dephasing is induced by the environmental fluctuation such as the shot noise [1]. As the MZI relies on the edge transport in quantum hall regime, it is important to evaluate how the edge state is affected by the environmental disturbance.

Here, we present the experimental evaluation of the stability of the quantized conducting channel in edge transport regime exposed to the high-frequency shot noise. In capacitively coupled mesoscopic systems, the shot noise in one device (noise source) disturbs the electronic environment at another nearby device (noise detector) [2]. In Fig. 1, we show the electron scanning microscope image of our sample and the measurement setup. The sample was fabricated on the GaAs/AlGaAs 2DEG (electron density 2.3×10^{11} cm^{-2} and mobility 1.1×10^{6} cm^2/Vs) by the split-gate-method. These quantum wires (QW1 and QW2) are decoupled to each other by the center-gate electrode for DC current, whereas the high-frequency (~ GHz) noise can be transferred through the capacitive coupling. We injected DC current into the QW1 to generate the shot noise while QW2 kept unbiased. We measured the conductance and the noise of these wires to evaluate how the quantized channel in QW2 is stable against the shot noise coming from QW1.

Figure 2 shows the conductance of the QW2 as a function of the gate voltage at 4.0 T magnetic field. The conductance shows clear conductance plateau of e^2/h without the shot noise radiation from QW1. The conductance at the e^2/h plateau, however, gradually decreases when the current is injected to the QW1 to cause the shot noise. Through the noise measurement (See inset in Fig. 2.), we found that the observed collapse of the conductance quantization is not simply due to the Joule heating, but due to the exposure to the high-frequency shot noise. By analyzing the energy scale of the collapse, the stability of the edge current against the shot noise is estimated quantitatively.

References

1. F. Marquardt and C. Bruder, Phys. Rev. Lett., **92**, 056805 (2004).

2. M. Hashisaka *et al*., Phys. Rev. **B 78**, 241303(R), (2008).

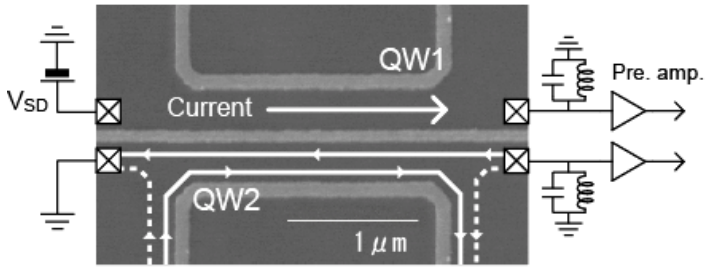

Fig.1 Scanning electron microscope image of the sample and the schematic diagram of the measurement setup.

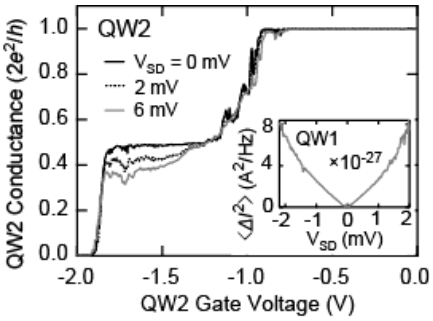

Fig.2 Conductance of the wire2 as a function of the gate voltage at 4.0 T magnetic field. (Inset) Measured current noise in QW1.

Probing two-dimensional metallic-like and localization effects at low magnetic fields

Tsai-Yu Huang[1], C.-T. Liang[1], Gil-Ho Kim[2], C. F. Huang[3], Chao-Ping Huang[1], and D. A. Ritchie[4]

[1]Department of Physics, National Taiwan University, Taipei 106, Taiwan

[2]School of Information and Communication Engineering and Sungkyunkwan Advanced Institute of Nanotechnology, Sungkyunkwan University, Suwon 440-746, Republic of Korea

[3]National Measurement Laboratory, Center for Measurement Standards, Industrial Technology Research Institute, Hsinchu 300, Taiwan

[4]Cavendish Laboratory, Madingley Road, Cambridge CB3 OHE, United Kingdom

Keywords: two-dimensional electron system, quantum Hall effect. insulator, metallic effects

It has attracted much attention how metallic-like regimes appear in two-dimensional electron systems (2DESs). While metallic-like behaviors described by Shubnikov-de Haas formula (SdH) are observed in most 2DESs, the metallic regimes are unstable with respect to the disorder. [1] It is well-known how the disorder-induced localization results in the quantum Hall (QH) liquid and insulator in the infinite noninteracting 2DES. Experimentally, however, only finite 2DESs are available, and the electron-electron (e-e) interaction can induce the metallic phase [2]. Therefore, more studies are still necessary to understand the metallic-like and localization effects, especially at low magnetic fields where the effective sample size becomes smaller than the localization length.

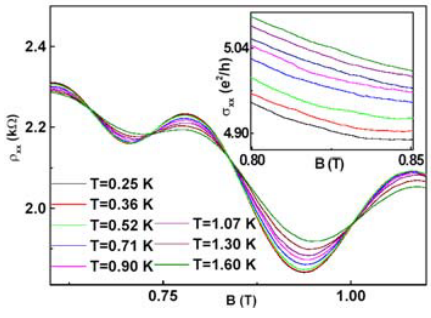

Fig.1 Multiple crossing points in ρ_{xx} in the crossover from the low-field insulator to quantum Hall liquid. The inset shows the corresponding curves of σ_{xx} near a crossing point.

Recently, our group [3] reported the existence of the metallic-like regime following SdH formula in the crossover from the low-field insulator to QH liquid. As shown in Fig. 1, multiple crossing points exist in the longitudinal resistivity ρ_{xx} in such a regime while only single point is allowed between the insulating and QH states in the infinite noninteracting 2DES. By converting ρ_{xx} to the longitudinal conductivity σ_{xx}, the crossing points disappear because σ_{xx} does not equal the Hall conducrivity σ_{xy} [4] under the *T*-dependent Hall resistivity due to the e-e interaction [5]. The inset to Fig. 1 shows the corresponding curves of σ_{xx} near a crossing point in ρ_{xx}. Our study shows that such an interaction is important not only to the zero-field metallic phase, but also to the metallic-like regime under localization effects.

References

[1] S. Kivelson, D.-H. Lee, and S. C. Zhang, Phys. Rev. B **46**, 2223 (1992)

[2] S. V. Kravchenko *et al.,* Phys. Rev. B **50**, 8039 (1994).

[3] T.-Y. Huang *et al.,* Phys. Rev. B **78**, 113305 (2008).

[4] S. S. Murzin, private communications.

[5] M. Y. Simmons *et al.,* Phys. Rev. Lett. **84**, 2489 (2000) and references therein.

Circular polarization reversal of split photoluminescence peaks at ν of slightly less than 1

S. Nomura,[*,**] M. Yamaguchi,[**] H. Tamura,[**] T. Akazaki,[**] and Y. Hirayama[***,****]

[*]*Institute of Physics, University of Tsukuba, 1-1-1 Tennodai, Tsukuba, 305-8571, Japan.*

[**]*NTT Basic Research Laboratories, 3-1 Morinosato-Wakamiya, Atsugi, 243-0198, Japan.*

[***]*Department of Physics, Faculty of Science, Tohoku University, 6-3 Aoba, Aobaku, Sendai, 980-8578, Japan.*

[****]*ERATO-JST, 4-1-8 Honcho, Kawaguchi, 332-0012, Japan.*

Keywords: quantum Hall, photoluminescence, skyrmion

We report our findings of two distinct photoluminescence (PL) peaks with remarkably different circular polarization properties at ν of slightly less than 1. Our results are explained by two branches: a spin polarized state and a spin unpolarized skyrmion state at around $\nu = 1$.

The PL spectra exhibit characteristic features originating from the electron-electron (e-e) and electron-hole (e-h) interactions in the quantum Hall regime [1]. The PL at around ν=1 is particularly interesting because of the existence of a spin texture called "skyrmion". Previously, a low-energy tail of a PL peak was attributed to be evidence of a skyrmionic exciton state [2]. However, numerical calculations based on the exact diagonalization of the Hamiltonian have indicated that the PL spectra consist of several peaks due to different initial and final state spins and that the polarization of the ground state depends sensitively on the ratio of e-h to e-e interactions [3]. To date, there has been no report of observations of polarization reversal of two distinct PL peaks.

We used a gated relatively wide single 50 nm GaAs quantum well (QW). One of the advantages of the sample is low disorder in the low electron density regime due to the lack of a donor layer [4]. The electron density is tuned by applying a bias voltage between an ohmic contact to the QW and the thick *n*-type GaAs buffer layer. The circular polarization-resolved PL measurements were performed at T~100 mK in magnetic fields.

At ν>1, an asymmetric peak with a tail in the lower energy side is observed in both σ^+ and σ^- polarizations. Opening of the quantum Hall energy gap at ν=1 suppresses the electron screening, which leads to a strong reduction of the PL intensity [5]. At ν<1 the PL in σ^- polarization split into two peaks, accompanied by discontinuous lower energy shifts. The lower energy peak is polarized to σ^- and depolarizes with decreasing ν. In contrast, the higher energy peak is weakly polarized to σ^-. The polarization becomes higher with decreasing ν and eventually exceeds the polarization of the lower energy peak. Electron-density-dependence measurements reveal that the two distinct peaks are observed only in the case of relatively large d/l_B, where d is e-h separation and l_B is the magnetic length. Our results are qualitatively explained by a theory that predicts a spin maximally polarized ground state and low-spin higher energy states at ν=1 and a spin singlet ground state and high-spin higher energy states at $\nu = 1^-$ [3].

This work was partly supported by KAKENHI No. 20104005.

References

1. L. Gravier, M. Potemski, P. Hawrylak and B. Etienne, Phys. Rev. Lett. **80**, 3344 (1998).

2. J.L. Osborne *et al*., Phys. Rev. B **58**, R4227 (1998).

3. K. Asano, J. Phys. Soc. Jpn. **72**, 1260 (2003).

4. M. Yamaguchi *et al*., Phys. Rev. Lett. **101**, 207401 (2008).

5. S. Nomura *et al*., Phys. Rev. B **76**, R201306 (2007).

Optical studies of spin phase transition in the vicinity of ν=2/3 fractional quantum Hall regime

J. Hayakawa*, T. Kawamura*, M. Kuwano*, K. Onomitsu**, T. Fujisawa**, G. Yusa*,***,****

* *Department of Physics, Tohoku University, Sendai, Japan*

** *NTT Basic Research Laboratories, NTT Corporation, Atsugi, Japan*

*** *PRESTO Japan Science and Technology Agency, Kawaguchi, Japan*

Keywords: fractional quantum Hall effect, charged exciton, photoluminescence, quantum well

Nuclear spin is one of the most promising candidates for qubit because of their very long coherence time. The ability to measure and manipulate nuclear spins coherently is vital in the ongoing effort to achieve quantum computing. We have demonstrated multiple quantum coherences of nuclear spins using novel NMR technique [1]. This is based on the resistance changes of a quantum well (QW) in the fractional quantum Hall (FQH) regime at ν=2/3 phase transition point, where spin polarized and unpolarized state are degenerate. The detailed mechanism is, however, not unveiled yet.

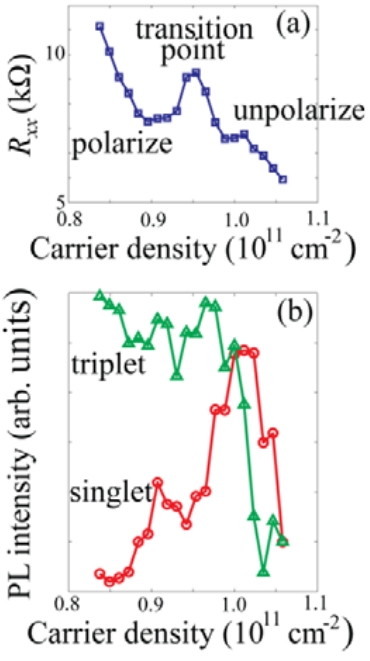

Fig.1 Simultaneously measured (a) R_{xx} and (b) PL intensity originated from charged excitons in the vicinity of ν=2/3 spin transition point at B=7.3 T.

In contrast with standard resistance measurement, optical measurement can reveal local configurations of electron and nuclear spins with a micron order spatial resolution. In this presentation, we focus on the ν=2/3 FQH system. We measured circularly polarized photoluminescence [2] from a 20 nm QW and longitudinal resistance simultaneously at 150 mK. The electron density can be controlled by a bias voltage between a semi-transparent front gate and an ohmic contact connected to the QW.

We compared the PL peak intensity originated from charged excitons and longitudinal resistance (R_{xx}) as the function of the carrier density in the vicinity of ν=2/3. R_{xx} peak corresponds to the phase transition point between spin polarized and unpolarized regions. From simultaneous measurement, we found by decreasing carrier density the peak intensity of singlet charged exciton tends to increase until the transition point. Beyond this point, however, it tends to decrease. Whereas the peak intensity of triplet charged exciton tends to monotonically increase. This behavior is consistent with the transition between two possible ground states of electron spins at ν=2/3. Therefore charged exciton intensity can be probe of electron spins polarization. This technique enable us to image the spatial distribution of electron and nuclear spins at ν=2/3 phase transition point.

References

1. G. Yusa, K. Muraki, K. Takashina, K. Hashimoto, Y. Hirayama, Nature **434**, 1001 (2005).

2. I. V. Kukushkin, K. von Klitzing, and K. Eberl, Phys. Rev. B **60**, 2554 (1999).

High sensitive measurement of Kerr rotation spectra of quantum Hall states

H. Ito*, D. Fukuoka*, T. Nagayama*, K. Oto*, K. Muro*,
Y. Hirayama**,****, N. Kumada***, and H. Yamaguchi***

* *Graduate School of Science, Chiba University, Chiba, Japan*
** *Graduate School of Science, Tohoku University, Sendai, Japan*
*** *NTT Basic Research Laboratories, NTT Corporation, Atsugi, Japan*
**** *ERATO Nuclear Spin Electronics Project, Sendai, Japan*

Keywords: quantum Hall effect, Skyrmion, Kerr effect

Quantum Hall systems present a variety of spin related states such as quantum ferromagnet and Skyrmion. Kerr rotation measurement is an effective method to study the spin polarization and the spin dynamics [1]. We have developed a novel multi-channel measurement system for magneto-optical Kerr rotation spectrum by using super-luminescent diode and optical phase modulation. Adjusting the central phase, we can selectively pick up Kerr rotation and magnetic dichroism (MD) signals. MD is caused by the difference of the absorption intensity between the left (σ^-) and right (σ^+) circular polarizations and directly relates with the spin polarization of the system.

Figure 1 shows a grey-scale plot of the MD spectrum between 0 and 7 T at 1.5 K. The spectrum is significantly modified from the standard Landau fan due to electron-electron interactions in quantum Hall states. Peaks become sharper at integer filling factors and additional peaks appear at higher field side [2].

In Fig. 2, MD spectra around Landau filling factor ν = 1 are extracted. At the filling factor slightly away from ν=1, σ^- component appears on the low energy side of the transition from the heavy hole band to the lowest Landau level (HH→N = 0), indicating the existence of unoccupied of spin-up level at N = 0. Spin polarization can be determined by integrating the MD spectra across the specific optical transition. The obtained spin polarization is reduced rapidly when filling factor deviates from ν=1. This can be explained by Skyrmion excitation. Similar depolarization is also observed ν=3. Details of filling factor dependence of spin polarization will be presented.

References

[1] D. Fukuoka *et al*. Phys.Rev.B **78**, 041304(R) (2008)
[2] P.Plochocka-Polack *etal*. Phys.Rev.Lett. **98**, 186810 (2007).

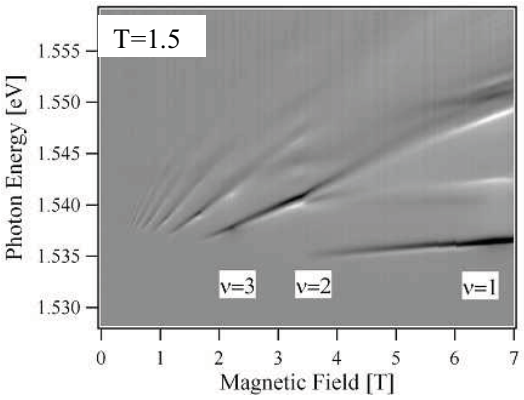

FIG 1: Grey-scale plot of MD spectra.

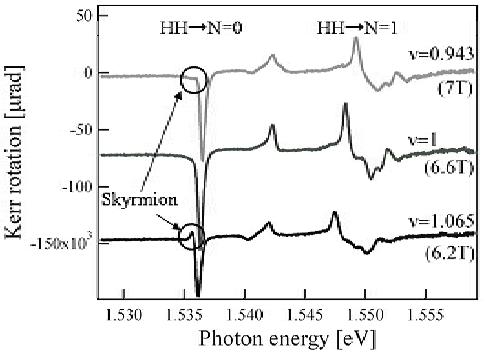

Fig 2: Magnetic dicroic spectra observed around ν=1 at 1.5K.

Optical Hall conductivity in 2DEG and graphene QHE systems

Takahiro Morimoto*, Yasuhiro Hatsugai** and Hideo Aoki*
*Department of Physics, University of Tokyo, Tokyo, Japan
** Institute of Physics, University of Tsukuba, Tsukuba, Japan

Keywords: quantum Hall effects, optical Hall conductivity, Faraday rotation, graphene

While the quantum Hall effect(QHE) is a static property of 2D electron systems(2DEG) in magnetic fields, recent experimental advances in optics begin to make spectroscopic measurements (e.g., Faraday rotation in magnetic fields) for QHE systems in the THz regime a reality[1, 2]. Theoretically, we pose here a fundamental question of how QHE evolves into the *optical Hall conductivity*, especially in the THz regime which is the scale of the cyclotron energy.

Motivated by this, we have theoretically calculated the optical Hall conductivity $\sigma_{xy}(\omega)$ in the quantum Hall regime with the Kubo formula for both the ordinary 2DEG and graphene, where the effect of disorder is taken into account with the exact diagonalization method[3]. If we first look at the result for 2DEG, we can see that (i) cyclotron resonances, usually discussed for $\sigma_{xx}(\omega)$, are seen for the optical Hall $\sigma_{xy}(\omega)$ (Fig.1(a)). (ii) The plateaus in $\sigma_{xy}(\omega)$, although not quantized, are unexpectedly robust in the optical (THz) region as far as the disorder is not too strong (Landau level broadening $\Gamma < \hbar\omega_c$) (Fig.1(b)), which we interpret as a localization effect.

If we turn to the optical Hall conductivity $\sigma_{xy}(\omega)$ in the graphene QHE system (Fig.2), the cyclotron resonance structure now reflects the graphene Landau levels that are not equally spaced for the massless Dirac band. The optical Hall palteaus are again retained in the THz regime.

The optical Hall effect should be observable as a Faraday rotation angle, $\Theta_H \sim [1/(n_0+n_s)c\epsilon_0]\sigma_{xy}(\omega)$ (with the refractive indices of air and substrate). Thus the step structure in $\sigma_{xy}(\omega)$ should be measured as steps in the Faraday rotation, for which we can estimate $\Theta_H \sim \alpha \sim 10$ mrad, which is well within the experimentally resolution [2] and may be called the fine-structure constant α seen as a rotation, while α has been visualized from transmission in [4].

We shall further discuss the effect of range of random potential on the plateau structure in relation with disorder (ripples) in graphene.

References

[1] H. Sumikura et al., JJAP **46**, 1739 (2007).
[2] Y. Ikebe and R. Shimano, APL **92**, 012111 (2008).
[3] T. Morimoto, Y. Hatsugai and H. Aoki, unpublished.
[4] R. R. Nair et al., Science **320**, 1308 (2008).

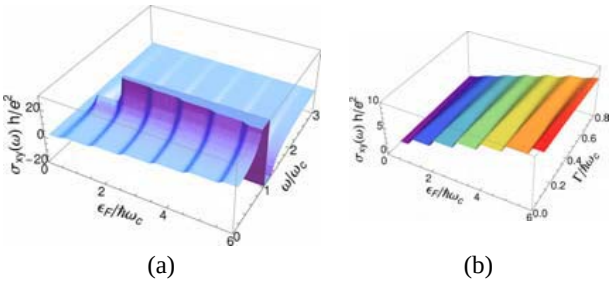

Figure 1: (a) Optical Hall conductivity $\sigma_{xy}(\omega)$ against the Fermi energy ε_F and the frequency ω for $\Gamma = 0.2\hbar\omega_c$. (b) $\sigma_{xy}(\omega)$ against ε_F and the disorder Γ for $\omega = 0.4\omega_c$.

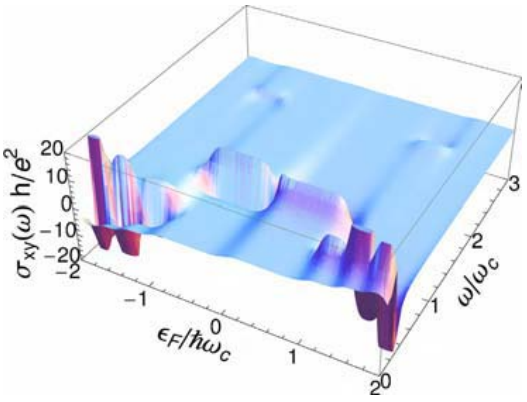

Figure 2: Optical Hall conductivity $\sigma_{xy}(\omega)$ for the graphene QHE system against ε_F and ω for $\Gamma = 0.2\hbar\omega_c$.

Spin-pseudospin mixed skyrmion in bilayer $\nu = 1$ quantum Hall systems with large tunnel coupling

Norio Kumada and Koji Muraki

NTT Basic Research Laboratories, NTT Corporation, Atsugi, Japan

Keywords: quantum Hall effect, bilayer system, skyrmion, NMR

In a bilayer quantum Hall (QH) system at total filling factor $\nu = 1$, both spins and pseudospins are polarized ferromagnetically, where pseudospin denotes the layer degree of freedom. It is believed that, when the tunnelling energy gap $\Delta_{\rm SAS}$ acting as a pseudospin Zeeman energy is negligibly small, the charged quasiparticle in the QH state is a pseudospin skyrmion (or bimeron). On the other hand, in the limit of large $\Delta_{\rm SAS}$, the quasiparticle should be a skyrmion of real spin as in a single-layer system. At intermediate $\Delta_{\rm SAS}$, spin-pseudospin mixed skyrmions, called CP^3 skyrmions, that interpolate the two types of skyrmions are theoretically predicted [1,2].

In this work, we investigate the spin properties of the quasiparticles in GaAs/AlGaAs double-quantum-well systems with various $\Delta_{\rm SAS}$ (= 11, 15, and 29 K) by a current-pump and resistively detected NMR [3]. We measured the spin polarization through the Knight shift as a function of the filling factor at a fixed magnetic field of 6 T, that is, with the fixed Zeeman energy $\Delta_{\rm Z} = 1.9$ K (Fig. 1). When $\Delta_{\rm SAS}$ (= 29 K) is dominant over $\Delta_{\rm Z}$ (= 1.9 K), spin polarization decreases rapidly on both sides of $\nu = 1$ as in a single-layer system, suggesting that the quasiparticle is a spin skyrmion. From the slope, the number of flipped spins in the spin skyrmion is estimated to be $N_s \sim 4$. The spin component in the quasiparticle decreases with decreasing $\Delta_{\rm SAS}$ and becomes $N_s \sim 1$ when $\Delta_{\rm SAS} = 11$ K. Since a pure spin skyrmion with smaller $N_s < 4$ is energetically unfavorable, the quasiparticle in the samples with smaller $\Delta_{\rm SAS}$ should be the CP^3 skyrmion involving not only spin but also pseudospin.

The nuclear spin relaxation rate $1/T_1$, which probes low-frequency spin fluctuations, reinforces the Knight shift data (Fig. 2). In the sample with $\Delta_{\rm SAS} = 11$ K, the contribution of the quasiparticles to $1/T_1$ is weak, consistent with the small N_s. As $\Delta_{\rm SAS}$ is increased, $1/T_1$ increases gradually and approaches the value for the single-layer spin skyrmion system. Our results provide information on the evolution between the spin and pseudospin skyrmions via the CP^3 skyrmion.

[1] Z. F. Ezawa and G. Tsitsishvili, Phys. Rev. B **70** 125304 (2004).

[2] R. Côté *et al*., Phys. Rev. B **76** 125320 (2007).

[3] N. Kumada, K. Muraki, and Y. Hirayama, Phys. Rev. Lett. **99**, 076805 (2007).

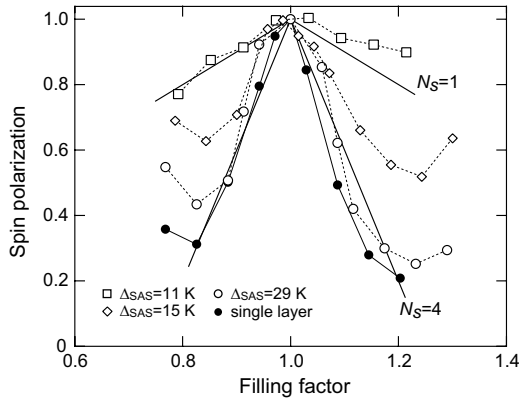

Figure 1: Spin polarization at 55 mK around $\nu = 1$ for bilayer systems (open symbols), and a single-layer system (solid circles). For comparison, lines for $N_s = 1$ and 4 are included.

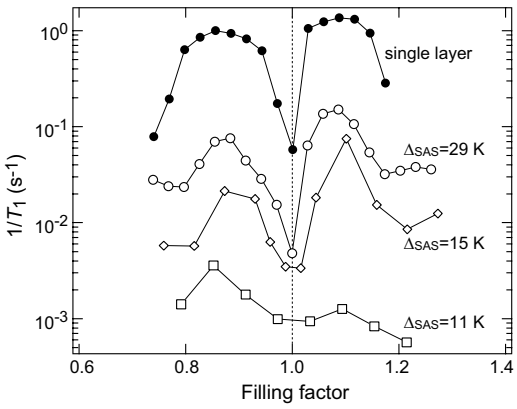

Figure 2: Nuclear spin relaxation rate $1/T_1$ at 55 mK around $\nu = 1$ for bilayer systems (open symbols) and a single-layer system (solid circles).

Lifetime of dissipation-less state of quantum Hall electron systems in the bistable regime

T. Nakajima and S. Komiyama

** Department of Basic Science, University of Tokyo, Komaba, Tokyo, Japan*

Keywords: quantum Hall effect, current-induced breakdown, bistability, thermal noise/fluctuation

The longitudinal resistance of electron systems in the quantum Hall effect (QHE) regime abruptly increases above a critical current density (or the electric field E) [1,2]. This breakdown phenomenon is frequently accompanied by a bistability in the electron temperature T_e (Fig.1) [3]. However, interpretation of the breakdown is made somewhat ambiguous by different views to the bistability. For instance, ref.[4] assumes that the transition between the dissipation-less state and the breakdown state, $T_{LS}\rightarrow T_{HS}$ ($T_{LS}\leftarrow T_{HS}$), takes place only when the upper (lower) critical field E_{UC} (E_{LC}) is reached with increasing (decreasing) E, whereas ref. [5] clearly sees the switching processes between the two states in a finite range of E bounded by the two critical fields.

Here, to shed more light to the bistability, we scan the current I passing through 100μm-wide GaAs/AlGaAs Hall bars (ν=2 QH plateaus, B=5.6T & T=0.3K) at different rates ($\partial I/\partial t$ = 0.16mA/s~5.2mA/s) in the form of saw-tooth. The critical current I_c is found to fluctuate from one scan to another at all the scan rates (upper right inset of Fig.2), yielding broadened histogram of the probability, $P(I)dI$, that the transition occurs in the interval I~$I+dI$ (inset of Fig.2). In contrast, the histogram is a sharp peak for ν=4, where bistability is absent. The rate of escape from the dissipation-less T_{LS}-state is derived from $P(I)$ as

$$1/\tau(I) = (\partial I/\partial t)\cdot P(I)/\{1-\int_0^I P(u)du\}\ . \quad (1)$$

The derived values of 1/τ (Fig.2) are substantially independent of $\partial I/\partial t$ and increase sharply as I increases.

The experiments thus provide a consistent picture of the QHE breakdown, where the dissipation-less T_{LS}-state is of a finite lifetime τ and gets less likely with increasing E in the bistable region. We will argue that the transition $T_{LS}\rightarrow T_{HS}$ is triggered by thermal fluctuation (Fig.1) as in many bistable systems [6,7].

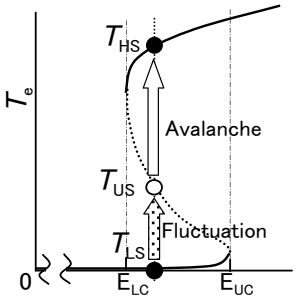

Fig.1 T_e versus E: In the bistable range, $E_{LC}<E<E_{UC}$, a low-T_e stable state (T_{LS}), an intermediate-T_e unstable state (T_{US}) and a high-T_e stable state (T_{HS}) coexist.

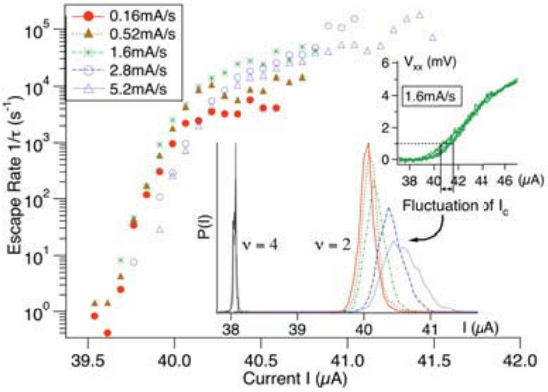

Fig.2 Escape rate 1/τ against I for ν=2, derived from the histograms of I_c in the lower inset.

References

1. G. Ebert et al., J. Phys. C **16**, 5441 (1983),
2. E. Cage et al., Phys. Rev. Lett. **51**, 1374 (1983).
3. S. Komiyama et al., Solid State Commun. **54**, 479 (1985), S. Komiyama & Y. Kawaguchi, Phys. Rev. B **61**, 2014 (2000).
4. A. Buss et al., Phys. Rev. **B 71**, 195319 (2005).
5. J. Ahlerst et al., Semicond. Sci. & Technol. **8,** 2062 (1993).
6. R. Landauer, Phys. Today **31** (11), 23 (1978),
7. T. A. Fulton & L. N. Dunkleberger, Phys. Rev. B **9**, 4760 (1974)

Effect of strain on nematic phases in two dimensional hole gases

Sunanda Koduvayur*, Leonid Rokhinson*, Gabor Csathy*, Sergei Khlebnikov*, Michael Manfra*†, Loren Pfeiffer † and Ken West†

**Department of Physics, Purdue University, West Lafayette,USA*

†*Bell Laboratories, Lucent Technologies, New Jersey, USA*

Keywords: Quantum Hall Effect, anisotropic magnetoresistance, charge density wave

Ground state of a two dimensional electron gas (2DEG) in weak magnetic fields is unstable against the formation of a charge density wave (CDW). At exactly half-filled Landau Levels (LLs) CDW is expected to form a unidirectional stripe phase[1, 2]. Observation of anisotropic magnetoresistance confirmed the theoretical prediction in high mobility 2D electron[3, 4] and hole[5] gases. The puzzling experimental feature which is yet to be understood is the preferential orientation of the stripes along [110] crystallographic direction in a variety of structures. The isotropic nature of electronic states in a cubic crystal does not account for this preferential orientation. Anisotropic piezoelectric interactions in GaAs break the rotational symmetry and the electrostatic energy is minimized if CDW is oriented along $[110]$ or $[1\bar{1}0]$ axes[6]. However, the electrostatic model cannot differentiate between $[110]$ and $[1\bar{1}0]$ directions. In 2DHG anisotropic magnetoresistance is found to exist at even lower filling factors than in electron samples, which can be attributed to the warping of the Fermi contour for holes or to the strong spin-orbit interactions. We try to understand some of these puzzles by using a controllable experimental knob, viz. uniaxial strain. For holes, strain deforms the Fermi contours, thereby altering the exchange interactions. Moreover, strain couples to the spin, both directly and via spin-orbit terms.

We study samples fabricated in the Van der Pauw geometry from C-doped GaAs/AlGaAs 2DHG grown on (001) substrate. We apply uniaxial strain along the two orthogonal directions $[110]$ and $[1\bar{1}0]$ and study the transport properties in a perpendicular field at 10mK. The major result is summarized in Fig. 1: strain switches the hard and easy transport axes. We also see that strain induces stripe phases at filling fractions of $\nu = 5/2$ and $9/2$, which are isotropic in unstrained samples. We further study the effect of in-situ strain modulation on these states and observe different strain response of the resistances along $[110]$ and $[1\bar{1}0]$. We try to understand the role of piezoelectricity by incorporating uniaxial strain in an extended electrostatic model. We are also working on separating effects related to the spin-orbit interactions from effects related to the anisotropy of electronic states.

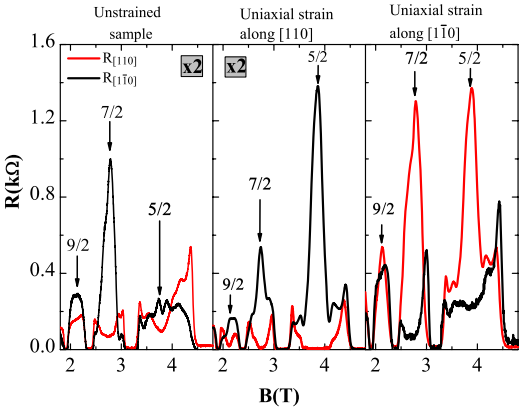

Figure 1: Magnetoresistance along $[110]$(red) and along $[1\bar{1}0]$ for (a) Unstrained, (b) Uniaxially strained along $[110]$ and (c) Uniaxially strained along $[1\bar{1}0]$ sample. Data in (a) and (b) are multiplied by a factor of 2.

References

[1] M.M. Fogler et al. *Phys. Rev. B*, 54(3):1853 – 71, 1996/07/15.

[2] A.A. Koulakov et al. *Phys. Rev. Lett.*, 76(3):499 –, 1996.

[3] M.P. Lilly et al. *Phys. Rev. Lett.*, 82(2):394 –, 1999.

[4] R.R. Du et al. *Physica E*, 6(1):36 – 39, 2000.

[5] M.J. Manfra et al. *Phys. Rev. Lett.*, 98(20):206804 –, 2007.

[6] D.V. Fil. *Physica E*, 14(4):355 – 60, 2002/07/.

Hall resistance overshoot in 2D electron systems in Si/SiGe

J. Sailer*, V. Lang*, A. Wild*, K. M. Itoh**, E. E. Haller***,****, G. Abstreiter* and D. Bougeard*

** Walter Schottky Institut, Technische Universität München, 85748 Garching, Germany*

*** Department of Applied Physics and Physico-Informatics, Keio University 3-14-1, Hiyoshi, Kohoku-ku, Yokohama 223-8522, Japan*

**** Lawrence Berkeley National Laboratory, Materials Sciences Division, Berkeley, CA 94720-8197, USA*

***** Department of Materials Science and Engineering, University of California at Berkeley, Berkeley, CA 94720-1760, USA*

Keywords: Quantum Hall effect, Hall resistance overshoot, 2-dimensional electron system, Si/SiGe

In this contribution we report on unusual phenomena observed in magneto-transport experiments with narrow Hall bars of 2DES in strained Si.

Strain in Si/SiGe heterostructures leads to a lifting of the six-fold degeneracy of the conduction band minimum in Si. Two-dimensional electron systems (2DES) can be confined in the resulting type-II band offset between Si and SiGe. In addition and similar to Si MOSFETs, the energetically lower lying valleys exhibit a low effective transport mass giving rise to high mobilities, which opens up the path to study various transport phenomena in the Si/SiGe material system.

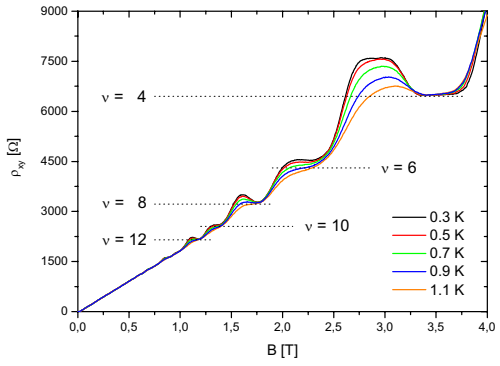

Fig.1 Temperature dependence of the Hall resistance overshoot. The overshoot increases with decreasing temperature.

Independent of the contacts and the magnetic field polarity we interestingly observe a pronounced Hall resistance overshoot which is exemplarily shown in Fig. 1: in the transition region between quantized Hall plateaus the Hall resistance increases to higher values thus overshooting before falling back to the exact quantized value.

This phenomenon occurs at even Hall plateaus up to filling factor 4 but not for filling factor 2. The overshoot depends strongly on the width of the Hall bar, the 2D sheet carrier density and the temperature. It becomes stronger with decreasing width of the Hall bar, increasing 2D sheet carrier density and decreasing temperature.

Additionally, there is a strong dependence on the excitation current. At higher excitation currents, the Hall resistance overshoot is completely suppressed while still maintaining exact quantization of the Hall plateaus.

Our investigations suggest that this phenomenon can be explained by a complex interplay between compressible and incompressible strips [1, 2] taking place at the Hall-bar edges.

References

1. Chklovskii et al., Phys. Rev. B 47, 12605 (1993)
2. Siddiki and Gerhardts, Phys. Rev. B 70, 195335 (2004)

Optical absorption to probe the quantum Hall ferromagnet at $\nu = 1$

P. Plochocka*, J. M. Schneider*, D. K. Maude*, M. Potemski*, M. Rappaport**, V. Umansky**, I. Bar-Joseph**, J. G. Groshaus***, Y. Gallais*** and A. Pinczuk***

*Laboratoire National des Champs Magnètiques Intenses, CNRS, 25 avenue des Martyrs, 38042 Grenoble, France

** Department of Condensed Matter Physics, The Weizmann Institute of Science, Rehovot, Israel

*** Department of Physics and of Appl. Physics and Appl. Mathematics, Columbia University, New York, NY 10027

Keywords: Quantum Hall Ferromagnet

Electron-electron interactions in two dimensions can dominate over the single particle physics leading to new collective ground states of the system. This is particularly true in GaAs due to the small value of the single particle Zeeman energy. The physics in the vicinity of filling factor $\nu = 1$ is particularly rich. At exactly $\nu = 1$, the predicted ground state is an itinerant quantum Hall ferromagnet [1], while on either side of $\nu = 1$ the system depolarizes more rapidly than predicted by the single particle picture, due to the formation of spin textures (Skyrmions or anti-Skyrmions) in the ground state.

Here we report on optical absorption (transmission) measurements in a high mobility GaAs quantum well to directly probe the subtle physics of the $n = 0$ Landau level (LL) via the spin polarization of the system. The optical dichroism (spin polarization) is calculated from the integrated intensity of the absorption measured for both σ^+ and σ^- polarizations (Fig.1). We find that full spin polarization does indeed occur, but only at exactly filling factor $\nu = 1$ and at very low (40 mK) temperatures. A small change in filling factor ($\delta\nu \approx \pm 0.01$) leads to a significant depolarization of the system (Fig.2(a)). This, together with the temperature dependence (Fig.2(b)), suggest that the itinerant quantum Hall ferromagnet at $\nu = 1$ is not robust, and collapses, whenever possible, to a lower energy ground state with a large number of reversed spins [2].

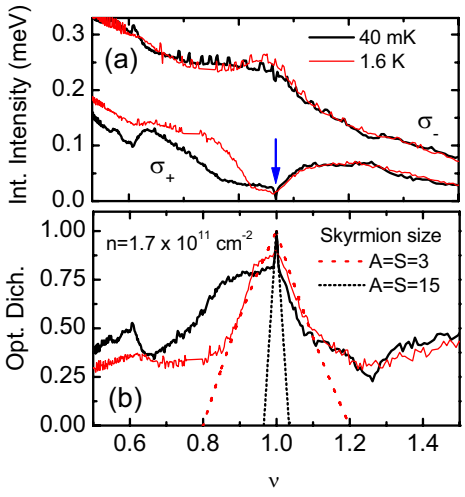

Figure 1: (a) Integrated intensity of the absorption to the $n = 0$ LL measured for both σ^+ and σ^- polarizations as a function of filling factor. (b) optical dichroism (spin polarization).

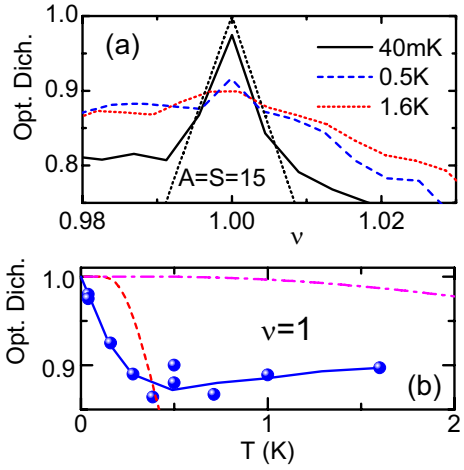

Figure 2: (a) Spin polarization (optical dichroism) near $\nu = 1$. (b) Temperature dependence of the spin polarization at exactly $\nu = 1$. The predicted temperature dependence is shown for a spin wave excitation (dash-dot line) and a single particle excitation (dashed line).

References

[1] M. Kasner and A. H. MacDonald, Phys. Rev. Lett. **76**, 3204 (1996).

[2] P. Plochocka *et al.* arXiv:0901.3959 (2009) Accepted Phys. Rev. Lett.

Investigation of domain pinning field in GaMnAs using angular dependence of planar Hall effect

Jungtaek Kim*, Taehee Yoo, Sanghoon Lee*, X. Liu** and J. K. Furdyna**

* *Department of Physics, Korea University, Seoul, Korea*

** *Department of Physics, University of Notre Dame, Notre Dame, IN 46556, USA*

Keywords: GaMnAs, domain pinning field,

Recently, a GaMnAs ferromagnetic semiconductor has received a great deal of attention due to simultaneous presence of magnetic order and of semiconducting properties. The magnetic domain pinning field, which determines magnetization reversal process in the GaMnAs thin film, was studied by transport measurements [1,2]. In those studied, however, many field scan measurements of planar Hall effect (PHE) at different magnetic field angles is required to plot a relation between switching fields and applied field angles, from which the domain pinning field is obtained.

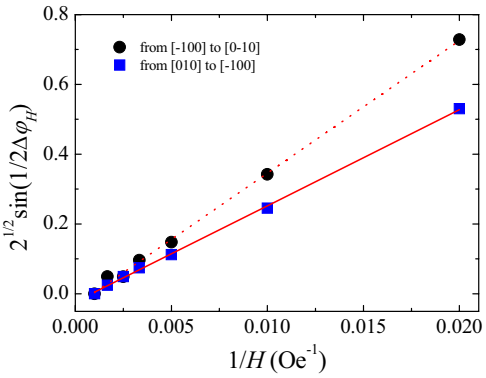

Fig.1 Plot of $\sqrt{2}\sin(1/2\Delta\varphi_H)$ as a function of $1/H$. Solid and dot lines are best linear fitting result. Slopes represent domain pinning fields.

In this study, we develops a new method, which is much more simple and elegant, to obtain domain pinning fields of GaMnAs film.

A ferromagnetic GaMnAs thin film was grown in a molecular beam epitaxy (MBE) machine. Hall bar of 1500 × 300 μm^2 was patterned on the film for magnetotransport measurement. The PHE was measured as a function of applied magnetic field angle while the field strength H was kept constant. All experimental data were taken at 13 K.

In the field region smaller than magnetic anisotropy fields, the planar Hall resistance (PHR) changes abruptly as the magnetization switches between the two crystallographic directions. The energy difference between the two magnetization direction (i.e., **M**||[100] and **M**||[010]) is given as $\Delta E = \sqrt{2}MH\sin(1/2\Delta\varphi_H)$, where **M** is magnetization, H is external magnetic field, and $\Delta\varphi_H$ is width of the hysteresis. The values of $\sqrt{2}\sin(1/2\Delta\varphi_H)$ can be plotted as function of $1/H$ at several magnetic fields as shown in Fig. 1. The data can be fitted with the relation obtained from the magnetic free energy formula, in which the slope $\Delta E/M$ is the pinning field. Experimental data and fitting results are shown in Fig. 1. The best fitting results provide domain pinning fields as $\Delta E_{[\bar{1}10]}/M$ =38.0±0.7 Oe and $\Delta E_{[\bar{1}\bar{1}0]}/M$ =27.5±0.3 Oe for the two directions. The domain pinning fields of $\Delta E_{[\bar{1}10]}/M$ =37.0±0.3 Oe and $\Delta E_{[\bar{1}\bar{1}0]}/M$ =27.2±0.3 Oe are also obtained from the the method used by Shin *et al*. in Ref. [2]. The pining fields are in good agreement in the two methods indicating usefulness of our new approach to obtain the pinning fields.

References

1. K. Hamaya, T. Taniyama, Y. Kitamoto, R. Moriya, and H. Munekata, J. Appl. Phys. **94**, 7657 (2003).
2. D. Y. Shin, S. J. Chung, S. Lee, X. Liu, and J. K. Furdyna, IEEE Trans. Magn. **43**, 3025 (2007).

Possible Sign Reversal of Rashba Coefficient in InAs-based Heterostructures

Takashi Matsuda and Kanji Yoh

Graduate School of Information Science and Technology, Hokkaido University, Sapporo, Japan

Keywords: Rashba effect, spintronics

The estimation and control of the spin transport property have been of significant importance to attain intended functionality of spintronic devices. Particularly, spin-orbit interaction (SOI) in two-dimensional electron gases (2DEG) has been getting much attention because this is believed to open up the way to manipulate the spin degree of freedom of the conducting electrons without external magnetic field.

The origin and controllability of SOI are not quite certain, though band gap engineering seems to work also to control the strength of Rashb effect[1]. In Ref. 1, authors presented that the strength of Rashba effect can be estimated from the sum of the weighted strength of the electric field by probability distribution of electrons in quantum well (QW). This result, tells entire structure contributes to Rashba effect, settled the long confusion about the exact origin of Rashba effect[2], yet assuming one uncertain concept, negative Rashba coefficient. It is tradition to treat the sign of Rashba coefficient α as a arbitral parameter. One reason could be that in conventional theoretical estimation only one part in a QW, either the band off-set or bottom, over where the electric field has same sign, has been treated. And in ex-perimental point of view, positive and negative α both result in the same energy shift which is usually examined to estimate α. It would be quite interesting if we can successively flip the direction of the electric field in a QW and observe how α actually develops.

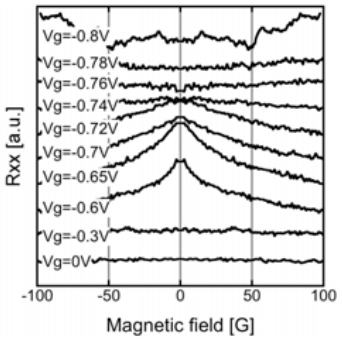

Fig.1 Weak antilocalization effect measured at various negative gate bias.

We have fabriated a psuedomorphic InGaAs/InAlAs HEMT structure described in Ref. 1 to examine the above-mentioned sign flip. It has a 50A-thick inserting $In_{0.9}Ga_{0.1}As$ layer in the middle of the InGaAs channel layer. Mobility and carrier concentration of the sample were 76000cm^2/Vs, 1.6x$10^{12}$$cm^{-2}$, respectively at 3.8K.

Rashba coefficient, evaluated from Shubnikov de Haas oscillations, at zero gate bias was 52x10^{-12}eVm. We have assigned the Rashba effect originating from the electric field pointing (00-1) direction positive. Weak antilocalization effect was examined at various negative gate biases (Fig.1). The suppression and revival of WAL over the gate modulation impliy that successful reduction of α due to the shift of electron probability distribution, yet not entirely, from a front side band off-set of QW which cause positive α to back side one which causes negative α. The positive α still is dominant in the sample, however, farther optimization of structure and gate bias will lead to the appearance of pure negative Rashba coefficient.

Acknowledgement

The authors are grateful to K. Konishi for technical help. This work was partly supported by Grant-in-Aid for Scientific Research from the Japanese Ministry of Education, Culture, Sports, Science and Technology.

References

1. T. Matsuda *et al.*, J. Ele. Matt., **37**, 1806 (2008).
2. E. A. de Andrada et Silva *et al.*, Phys. Rev. B, **55**, 16293 (1997)

Measurement of a large hole g-factor in two-dimensional hole gases

D. A. Vasyukov,[1] A. S. Plaut,[1] A. H. MacDonald[2] and M. Henini[3]

[1] *School of Physics, Exeter University, Exeter EX4 4QL, UK*
[2] *Department of Physics, The University of Texas at Austin, Austin, Texas 78712, USA*
[3] *School of Physics & Astronomy and Nottingham Nanotechnology & Nanoscience Centre, University of Nottingham, Nottingham NG7 2RD, UK*

Keywords: circular photogalvanic effect, g-factor, spintronics

The circular photogalvanic effect (CPGE) [1] is one amongst a number of recently-discovered striking spin-transport effects that have attracted attention due to their potential spintronic applications. This effect is observed only in two-dimensional (2D) systems grown along low-symmetry directions in crystals with broken inversion symmetry.

Here we present the first spectral study in perpendicular magnetic field (B) of the CPGE in a high-mobility, Si-doped, (311)A-grown GaAs/AlGaAs quantum well illuminated with circularly polarized light at 350 mK to create a non-equilibrium spin population. Under such conditions the spin-orbit coupling tends to drive charge carriers with different spin orientation to opposite sides of the sample in certain crystallographic directions. This spin current can be measured as an open-circuit voltage, V_{CPGE}.

We have found that the smooth dependence of V_{CPGE} on energy at B = 0, splits, in magnetic field, into a series of maxima and minima on either side of zero voltage. We show, for the first time, that the sign of the voltage is spin sensitive and that these maxima and the minima correspond to opposite hole spin orientations. Plotting the energy positions of these peaks and troughs against B produces a fan-chart (Fig. 1).

The average Zeeman splitting of neighbouring peaks and troughs has been found to be 1.2 ± 0.3 meV/T, which corresponds for heavy holes ($m_j = 3/2$) to a Landé g-factor of ~7. This experimentally-determined value agrees extremely well with the value of ~7.2 predicted theoretically for these quantum wells [2].

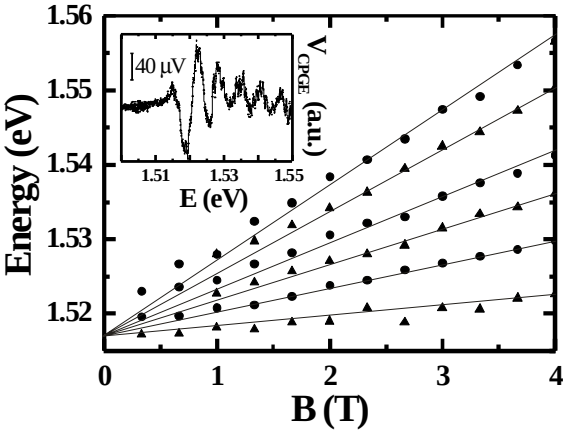

Fig. 1 Energy positions of the maxima (circles) and minima (triangles) in V_{CPGE} as a function of magnetic field. The lines are guides for the eye. Inset: The spectral dependence of V_{CPGE} at B = 1.67 T.

Thus we have measured for the first time the hole g-factor in low-symmetry quantum wells and have found, as predicted by theory [2] that it is significantly enhanced over that for (100)-grown quantum wells [3].

References

1. S. D. Ganichev *et al.*, Phys. Rev. Lett. **86**, 4358 (2001)
2. R. Winkler *et al.*, Phys. Rev. Lett. **85**, 4574 (2000)
3. M. J. Snelling *et al.*, Phys. Rev. B **45**, 3922 (1992)

Spin-dependent transport through waveguides with spatially modulated strengths of the Rashba and Dresselhaus spin-orbit interaction terms

P. Vasilopoulos and P. M. Krstajić

Concordia University, Department of Physics, 7141 Sherbrooke Ouest, Montréal, Québec H4B 1R6, Canada

Keywords: spintronics, spin-orbit interaction, waveguides

We evaluate the electron transmission T through waveguides (WGs) in which the strengths of the Rashba (α) and Dresselhaus (β) terms of the spin-orbit interaction (SOI) are simultaneously present and vary periodically in space. For sufficiently narrow WGs, with negligible transverse subband mixing, the transmission exhibits a spin-transistor behavior as a function of α or β and of α/β or β/α. In addition, T shows *longitudinal* resonances, as a function of the length of a SOI-free region separating two regions with SOI present, which become sharper when the length of the latter is increased and are most pronounced for $\alpha = \beta$. The sign of ϕ strongly affects the spin-up and spin-down transmissions. The influence of mixing between the lowest two subbands is mainly to shift the transmission resonances and to decrease the relative contribution of the spin down states. For $\beta = 0$ the results agree with those of Ref. [1]. The results indicate that a realistic spin transistor is possible.

In a WG along the y axis the electron energy spectrum is given by $E^{\pm} = E_n + \lambda k_y^2 \pm [\alpha^2 + \beta^2]^{1/2} k_y$, E_n being the n-th subband due to confinement along the x axis. The eigenvectors of the E^+ and E^- branches are $|\pm\rangle = e^{ik_y y}(1, \pm\exp(i\phi))^T/\sqrt{2}$, T denotes the transpose, and $\tan\phi = -\beta/\alpha$. We plot this spectrum vs k_y in Fig. 1 (b).

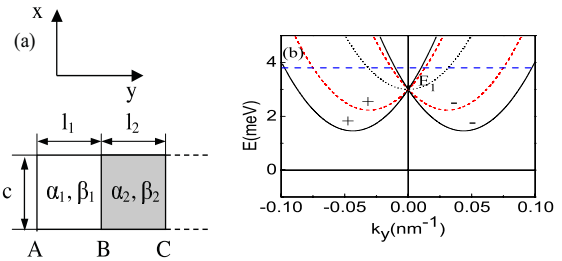

Figure 1: (a) Schematics of the periodically repeated WG unit. (b) Dispersion relation. The solid, dashed, and dotted curves are, respectively, for $\alpha = \beta = \alpha_0 = 5\times10^{-11}$ eVm, $\alpha = \alpha_0$, $\beta = 0$, and $\alpha = \beta = 0$. The dashed blue curve shows the Fermi level and only the lowest subband E_1 is occupied.

We obtain the transmission T by matching the wave functions and the flux at all interfaces between different strengths. In Fig. 2 we plot T through two WG segments, with SOI , vs ℓ_{sep}, the length of the SOI-free region separating them. Subband mixing is present ($\delta \neq 0$) or absent ($\delta = 0$). The total T is independent of the sign of β.

In Fig. 3 we plot T through 3 units vs ℓ_2, the length of the shaded segments with SOI present, with the mixing between the lowest two subbands present in (a) and absent in (b) for $\alpha = \alpha_0$ and various values of β. The solid (dashed) curve shows the total (spin-down) transmission.

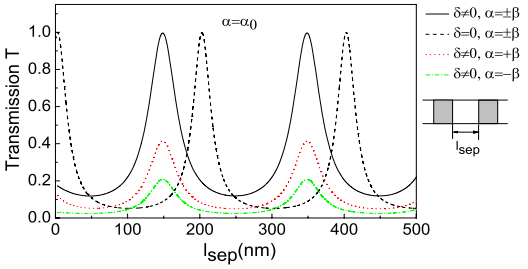

Figure 2: Transmission through two WG segments vs the length ℓ_{sep} of the SOI-free region that separates them for $\ell_2 = 100$nm and $E = 0.2$ meV. The solid (dashed) curve shows the total transmission when subband mixing is present (absent). The dotted (dash-dotted) curves show the spin-down transmission for $\alpha = +\beta$ ($\alpha = -\beta$).

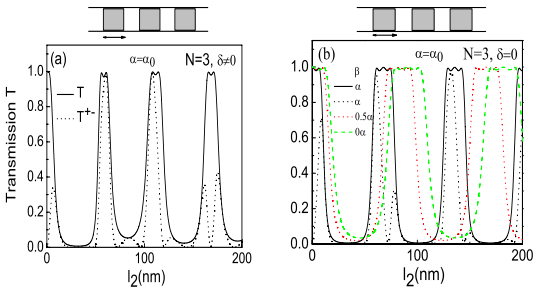

Figure 3: Transmission through 3 units vs ℓ_2 for $\ell_1 = 100$nm and $E = 0.2$ meV, see Fig. 1. Subband mixing is present in (a), absent in (b). The solid, dashed (dotted) curves show the total (spin-down) transmission.

References

[1] X. F. Wang *et al.* Appl. Phys. Lett. **83**, 940 (2003).

2D magnetoplasmons in systems with spin-orbit interaction (SOI)

R.Z.Vitlina, L.I. Magarill, and A.V.Chaplik
Institute of Semiconductor Physics, Siberian Branch, Russian Academy of Sciences, Novosibirsk, Russia

Keywords: 2D system, Rashba interaction, plasmon spectrum

We investigate the eigenmodes of 2D plasma with accounting for SOI of electrons taken in the form of the Rashba term. The dispersion equation of plasmons has the form

$$1+\frac{2\pi e^2}{\varepsilon q}(\Pi_1+\Pi_2)=0, \qquad (1)$$

where Π_1 and Π_2 are the diagonal and off-diagonal in chirality contributions to the polarization operator, correspondingly. The quantity $\Pi_2(\omega,q)$ (ω is the frequency, q is the wave number of a plasmon) vanishes when the SOI coupling constant α tends to zero and eq. (1) gives in this case the well-known Bernstein modes. Each of these modes can be attributed to a certain pole of $\Pi_1(\omega,q)$ as a function of ω. Accounting for SOI leads to two results:

i) the poles of Π_1 are split and form doublets; the splitting is small for weak SOI;

ii) the poles of Π_2 generate new branches of the plasmon spectrum – spin-plasmon oscillations. If the quantity $z=\sqrt{1+(2\alpha p_0/\hbar\omega_c)^2}$ is not close to an integer or half-integer the poles of Π_1 and Π_2 are well separated; here p_0 is the Fermi momentum, ω_c is the cyclotron frequency. As SOI is weak one can find the dispersion law of each branch by keeping only one pole term in the eq.(1). For example, at $1<z<3/2$ and in the quasi-classical limit $\hbar\omega_c \ll \varepsilon_F$ we have the spin-plasmon mode

$$\omega^2=(z\omega_c)^2+\frac{2\alpha^2 q}{a_B}\frac{J_1^2(X)}{1+\frac{2}{qa_B}F(z)},$$

where J_1 is the Bessel function, v_0 is the Fermi velocity, $X=qv_0/\omega_c$, a_B – effective Bohr radius;

$$F(z)=\frac{1}{1-\gamma^2}-\frac{\pi z}{2}\left(\frac{J_{z_+}(X)J_{-z_+}(X)}{(1+\gamma)^{3/2}\sin(\pi z_+)}+\right.$$
$$\left.+\frac{J_{z_-}(X)J_{-z_-}(X)}{(1-\gamma)^{3/2}\sin(\pi z_-)}\right),$$

where $\gamma=4m\alpha^2/z\omega_c$, $z_\pm=z/\sqrt{1\pm\gamma}$.

The second situation corresponds to converging of poles in Π_2 (z is close to an half-integer). Then the magnetic dispersion of two branches looks like anti-crossing with the minimal splitting proportional to α^2.

At last, the third case is possible. For z close to an integer we deal with converging of four poles: a doublet pole of Π_1 and m-th and m'-th poles in Π_2, where $m+m'=$ even. In principle, 4 branches should interact but as a rule the coefficient at one of two Π_2-pole-terms turns out extremely small. For example, at $z\approx3$ we have $m=0$, $m'=6$ and the pole residue for $m'=6$ is around 5 orders of magnitude smaller than the one for $m=0$. The plasmon spectrum for this situation is illustrated in the Fig.1.

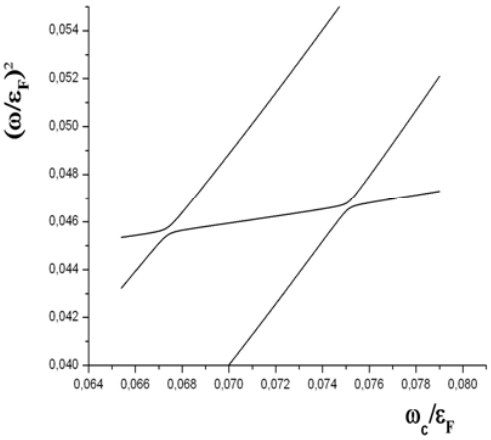

Fig. 1. Magnetic dispersion of plasmons for $n_s=3\cdot10^{11}$ cm^{-2}, $m=0.055m_0$, $\alpha=1.44\cdot10^6$ cm/s, $q=4\cdot10^4$ cm^{-1}.

Excitation of electric-field-driven spin remagnetization waves on a cylindrical surface with spin-orbit interaction

P. Kleinert*

**Paul-Drude-Institute for Solid State Electronics, Berlin, Germany*

Keywords: spin-orbit interaction, spin remagnetization waves, cylindrical surface, electric field

The generation and manipulation of a spin polarization by an electric field has become a main subject in the emerging field of spintronics. The proposal of a spintronic device that operates in the non-ballistic regime has received considerable interest, since spin randomization is a major issue for the device development. Due to the existence of an exact spin-rotation symmetry, the spin relaxation is strongly suppressed in a two-dimensional electron gas (2DEG) with definite spin-orbit coupling (SOC) constants. This persistent spin mode exists also in inhomogeneous systems, in which spin and charge degrees of freedom are coupled to each other so that spin remagnetization modes exist[1]. The character of this mode can be modified by an in-plane electric field. Exploiting the physics of space-charge waves in crystals, we study field-dependent spin remagnetization waves by optical generation of an oscillating interference pattern that matches the wavelength of the excitation.

As the details of the SOC strongly depend on the curvature of the surface, novel spin effects are expected to occur in systems with a nontrivial geometry or topology. This expectation is confirmed by a rigorous spin-density matrix approach, from which coupled spin-charge drift-diffusion equations are systematically derived. The theory is applied to a cylindrical 2DEG, whose radius is much larger than the lattice constant. From the exact analytical solution of these equations, the dispersion relations of the field-dependent spin eigenmodes are obtained. There are three damped spin excitations, whose character is determined by the coupling constants of the Rashba and Dresselhaus SOC. For the Rashba model, however, we identify a robust field-dependent persistent spin mode on a cylindrical surface, whose radius R matches the quantity $\hbar/2m^*\gamma$ with γ being the Rashba SOC constant. This long-lived spin mode has no counterpart in a planar 2DEG. The excitation of the novel spin-charge coupled eigenmode is likewise possible by optically generating a definite photo-injected spin or charge pattern. We consider the photogeneration via an oscillating interference pattern, which induces a current in the outer circuit. Sharp resonances appear in the steady-state current, which are due to weakly damped spin remagnetization waves of the 2DEG on a cylindrical surface.

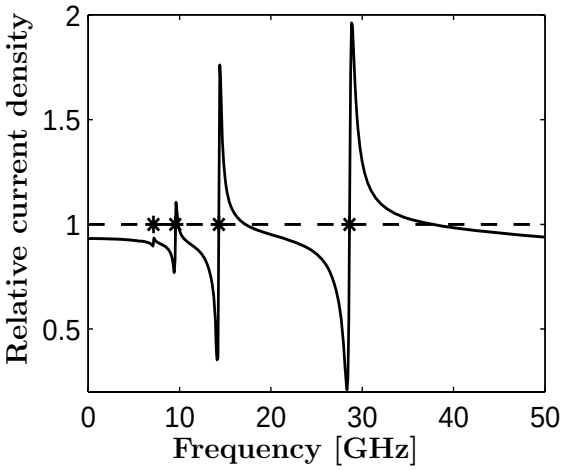

Figure 1: Induced relative stationary current density as a function of the frequency of the oscillating interference pattern for $R = \hbar/(2m^*\gamma)$ (solid curve) and $R = 5\mu$m (dashed curve). Resonance frequencies are indicated by $(*)$. Parameters refer to the InAs-based system.

A numerical example is shown in Figure 1. Pronounced resonances are due to oscillations of free carriers that are a mixture of space-charge waves and long-lived spin excitations. Experimental and theoretical studies of these novel eigenmodes in planar and curved 2DEGs with SOC profit from the well established physics of space-charge waves.

References

[1] V.V. Bryksin, H. Böttger, and P. Kleinert, Phys. Rev. B **74**, 235302 (2006).

Spin interference effects in InGaAs/InAlAs rectangular loop arrays

S. Faniel[1,2], S. Mineshige[3], Y. Sekine[4] and T. Koga[1,2]
[1]*Graduate School of Information Science and Technology, Hokkaido University, Sapporo, Japan*
[2]*Creative Research Initiative "Sousei", Hokkaido University, Sapporo, Japan*
[3]*Department of Electronics and Information Engineering, Hokkaido University, Sapporo, Japan*
[4]*NTT Basic Research Laboratories, NTT Corporation, Atsugi, Japan*

Keywords: spin-orbit interaction, quantum interference, InGaAs

We report experimental investigation of spin interference in InGaAs/InAlAs rectangular loop arrays. Magnetotransport measurements, in such loop array systems, exhibit Alt'shuler-Aronov-Spivak (AAS) oscillations stemming from interference between closed loop trajectories propagating in clockwise and counterclockwise directions. Moreover, in InGaAs devices, which show a large Rashba spin-orbit (SO) interaction [1], the spin precession along these closed eletectronic trajectories can be tuned by means of a front gate voltage, leading to a modulation of the spin interference (SI) and, consequently, of the AAS oscillations' amplitude [2].

In this work, we investigate the anisotropic interplay between the Rashba and the Dresselhaus contributions to the SO interaction. In this context, we note that, along the [110] and the [1$\bar{1}$0] crystallographic directions, the Rashba and the Dresselhaus effective magnetic fields are expected to be aligned together and the associated SO parameters to be added or subtracted to/from each other, respectively [3]. To probe this anisotropy, we study rectangular loop arrays whose sides are aligned along these two particular crystallographic directions (as schematically illustrated in the inset of Fig. 1).

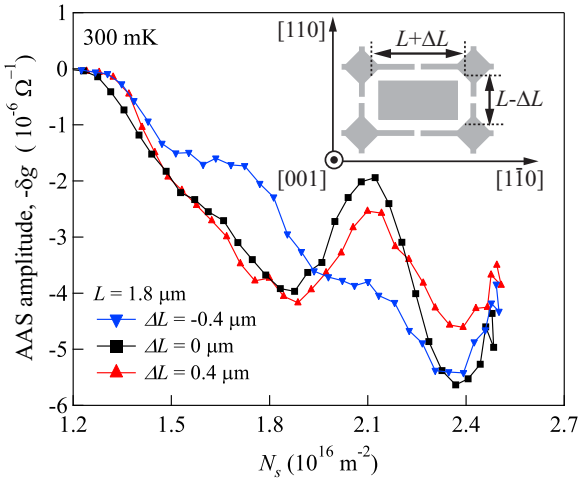

Figure 1: Amplitude of the AAS $h/2e$ oscillations as a function of the electronic density for 3 devices with different aspect ratios. The devices were made from sample 1 in Ref. [1]. Inset: schematic representation of the loops' geometries. The orientation of the devices with respect to the crystal axes is also shown.

The amplitude of the AAS $h/2e$ oscillations as a function of the electronic density (referred to as the SI pattern) obtained for devices with different aspect ratios is shown in Fig. 1. The measured SI patterns are qualitatively different among devices with different aspect ratios. We find that this behavior is consistent with the predictions of the one-dimensional spin interferometer model [4] that has been extended to account for the rectangular shape of the loops and the coexistence of the Rashba and Dresselhaus SO interactions. While the spin interferometer model successfully describe the oscillating part of the SI patterns, our results also indicates that a negative monotonic background, that is likely generated by the SI from complex trajectories within the loops, is superimposed on the traces.

This work is supported by KAKENHI, Grant-in-Aid for Young Scientists (A), No. 19684009.

References

[1] T. Koga *et al.*, Phys. Rev. Lett. **89**, 046801 (2002).

[2] T. Koga *et al.*, Phys. Rev. B **74** 041302(R) (2006); Bergsten *et al.*, Phys. Rev. Lett. **97**, 196803 (2006).

[3] R. Winkler, *Spin-Orbit Coupling Effects in Two-Dimensional Electron and Hole Systems* (Springer-Verlag, Berlin/Heidelberg, 2003).

[4] T. Koga *et al.*, Phys Rev. B **70**, 161302(R) (2004).

Molecular beam epitaxy and magnetoresistance in $Fe_4N/MgO/Fe_4N$ magnetic tunnel junction

K. Ito*, A. Narahara*, H. Akinaga** and T. Suemasu*

* *Institute of Applied Physics, University of Tsukuba, Tsukuba, Japan*

** *National Institute of Advanced Industrial Science and Technology (AIST), Tsukuba, Japan*

Keywords: MTJ, MR, Fe_4N, MBE

In recent years, magnetic tunnel junctions (MTJs) composed of ferromagnet/insulator/ferromagnet structures have been extensively studied for the application of spintronic devices such as MRAM and magnetic head sensors for hard disk drives. We have paid special attention to Fe_4N as spintronic materials since highly spin-polarized transport has been theoretically predicted in γ'-Fe_4N [1]. There have been only a few reports thus far on the MTJs using Fe_4N such as $Fe_4N/Cu_3N/Fe_4N$ and Fe_4N/MgO/CoFeB MTJs [2,3]. In the Fe_4N/MgO/CoFeB MTJs, an inverse tunnel magnetoresistance (TMR) effect was reported, and this result was explained by dominant minority-spin electrons at the Fermi level of Fe_4N. However, the number of reports on the TMR effect in Fe_4N has been very limited. Very recently, we have succeeded the formation of highly *a*-axis-oriented Fe_4N/MgO/Fe MTJs on MgO(001) substrates by molecular beam epitaxy (MBE) [4]. In this study, we reported the current-voltage (*J-V*) characteristics and the MR ratios of these MTJs at room temperature (RT).

MgO(1 nm)/Fe(100 nm) structures were grown on MgO(001) substrate by RF magnetron sputtering. Then, Fe(7 nm) was grown using $Fe(CO)_5$, and the Fe_4N(75 nm) top ferromagnetic layer was formed by supplying simultaneously the $Fe(CO)_5$ and ECR-N_2* on the Fe layer. Detailed growth procedures were reported in Ref. [4]. The mesa-isolated diode structures with an area ranging from 30×30 to 30×60 μm^2 were fabricated by photolithography, selective wet chemical etching, and a lift-off process using sputtered SiO_2 layers.

Formation of *a*-axis-oriented MTJs was confirmed by θ-2θ XRD patterns. The magnetization versus magnetic field (*M-H*) curve with *H* parallel to the sample surface at 280K showed a two-step hysteresis loop. The coercive fields were 40 and 200 Oe. The symmetric *J-V* characteristics were obtained at RT as shown in Fig. 1. The barrier height, estimated from the Simmons' equation to the experimental results was 0.51±0.07 eV. The thickness of the MgO barrier layer was approximated to be 0.44 nm, but differed among samples. Figure 1 shows typical examples of *J-V* characteristics. The MR curve shown in the inset shows scattering; however, the MR ratio can be estimated at least more than 30%. This value is the highest in the MTJs using Fe_4N. From the θ-2θ XRD patterns, symmetric *J-V* characteristics and normal TMR effect, we speculate that the upper region of the 100-nm-thick α-Fe layer was likely to transform into γ'-Fe_4N, indicating the probable formation of $Fe_4N/MgO/Fe_4N$ MTJ. In our previous paper [5], we have reported similar phenomena in the growth of Fe_3N/AlN(2 nm)/Fe_4N MTJ. When the same Fe and N sources were supplied to form ε-Fe_3N layers on the AlN(2 nm)/Fe(30 nm) structure, Rutherford backscattering spectroscopy measurements revealed that the α-Fe layer was nitrided to form γ'-Fe_4N through the 2-nm-thick AlN barrier layer during growth of the ε-Fe_3N layers.

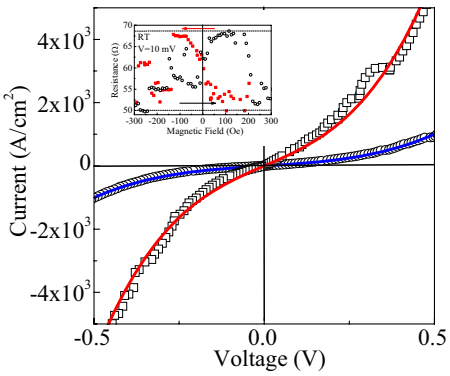

Fig. 1 *J-V* characteristics measured at RT. The inset shows the MR curve at RT with *H* parallel to the sample.

[1] S. Kokado, N. Fujima, K. Harigawa, H. Shimizu and A. Sakuma, Phys. Rev. B **73**, 172410 (2006).

[2] D. M. Borsa, S. Grachev, C. Presura and D. O. Boerma, Appl. Phys. Lett. **80**, (2002) 1823.

[3] K. Sunaga, M. Tsunoda, K. Komagaki, Y. Uehara and M. Takahashi, J. Appl. Phys. **102**, 013917 (2007).

[4] A. Narahara, K. Ito and T. Suemasu, J. Cryst. Growth in press (doi:10.1016/j.jcrysgro.2009.01.115).

[5] A. Narahara and T. Suemasu, Jpn. J. Appl. Phys. **46**, L892 (2007).

Spin-orbit interaction induced directional suppression of plasmon propagation

S. M. Badalyan[*,**], A. Matos-Abiague[**], G. Vignale[***], and J. Fabian[**]
*Department of Radiophysics, Yerevan State University, Yerevan, 375025 Armenia
** Department of Physics, University of Regensburg, 93040 Regensburg, Germany
***Department of Physics and Astronomy, University of Missouri - Columbia, Missouri 65211, USA

Keywords: spin-orbit interaction, anisotropy, plasmon filtering

We investigate the effect of structure-induced spin-orbit interactions on the density oscillations (plasmons) of a two-dimensional electron gas in zincblende semiconductor nanostructures. The anisotropy of single-particle spectrum, induced by interplay of linear Bychkov-Rashba and Dresselhaus spin-orbit interactions, is reflected in the anisotropy of the plasmon dispersion, which we calculate in the random phase approximation, together with the damping rate and the dynamical structure factor. Based on these calculations we predict the existence of specific directions along which the propagation of plasmons is suppressed, due to strong Landau damping, and argue that this plasmon filtering effect can be exploited in the construction of spintronic and plasmonic devices. Remarkably, our calculations show that all the traces of the linear spin-orbit coupling in the collective response disappear when the strengths of the two interactions are equal.

Recently several many-body effects important for semiconductor spintronics have been studied in two-dimensional electron systems (2DES). One of the key phenomena due to spin-orbit interaction (SOI) in many-spin systems is the generation of the inter-chirality-subband electron-hole continuum. However, the dispersive and dissipative modifications, induced by individual (Bychkov-Rashba or Dresselhaus) SOI, are difficult to observe in experiment – their effect is isotropic and proportional to the small SOI coupling. In real samples the interplay of different SOI mechanisms takes place and as we show here, it results in the striking anisotropy effect on the spectral properties of collective excitations in 2DES. This qualitatively strong effect can serve as a valuable tool to facilitate the observation and exploitation of usually weak SOI effects on many-body properties of 2DES.

An important outcome of our theory is the prediction of plasmon directional filtering: the interplay of the spin-orbit couplings leads to plasmon overdamping (blocking) in certain special directions of propagation and for certain magnitudes of the wave vector. This may be surprising at first sight, given that the spin-orbit effects on the plasmon dispersion and on the electron-hole excitation energies are in themselves quite small. However even small energy shifts are sufficient, at these special wave vectors, to move the plasmon in or out of resonance with electron-hole excitations, thus producing a large effect on the plasmon damping.

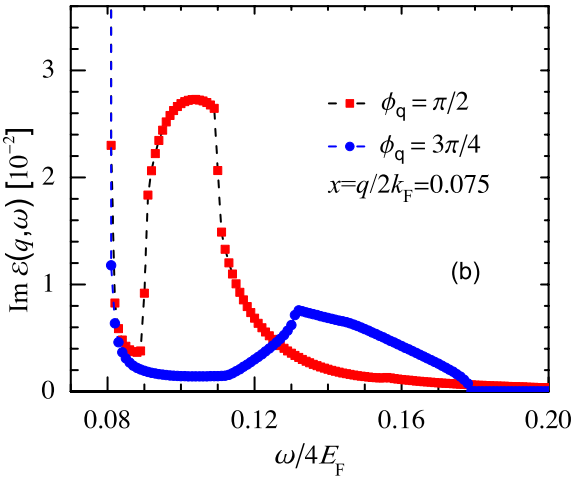

Figure 1: The imaginary part of the dielectric function vs energy for the fixed momentum magnitude $q = 0.15k_F$ and for $\phi_{\mathbf{q}} = \pi/2$ and $3\pi/4$, shown as square and round symbols, respectively.

This effect is illustrated in the figure, which shows the imaginary part of the dielectric function vs the energy for the fixed momentum magnitude and different orientations of plasmon propagation. As seen, the SOI induced dissipation properties *within EHC* are strongly anisotropic. In the region near the plasmon energy, $\omega/4E_F \approx 0.1$, the imaginary part for $\phi_{\mathbf{q}} = 3\pi/4$ is strongly suppressed with respect to its value for $\phi_{\mathbf{q}} = \pi/2$.

Single Electron spin resonance in a g-factor controlled semiconductor quantum dot

Takeshi Kutsuwa[1], Makoto Kuwahara[1], Keiji Ono[2, 1], Hideo Kosaka[3, 1]

[1]*CREST-JST, Kawaguchi, Saitama 332-0012, Japan*
[2]*Low Temperature Physics Laboratory, RIKEN, Saitama 351-0198, Japan*
[3]*Research Institute of Electrical Communication, Tohoku University, Sendai 980-8577, Japan*

Keywords: Quantum dot, electron spin resonance, g-factor, coherent control, spin coherence

Single spin coherent rotation in a semiconductor quantum dot has been demonstrated by applying the electron spin resonance (ESR) technique based on on-chip coils [1], spin-orbit coupling [2], and micro magnets [3]. It will enable two-spin basis exchange needed for the full Bell-state measurement with the help of singlet detection based on the Pauli spin blockade in a double quantum dot (DQD) [4]. However, the g-factor of electrons in those demonstrations is fixed at relatively high value ($g \approx 0.4$), which does not meet with the spin degeneracy condition ideal for the quantum state transfer from a photon to an electron spin [5, 6]. The degenerated spin is also favourable to keep the spin coherence longer because it is robust against the magnetic field fluctuations. Here we demonstrate ESR of a single electron in a DQD which has a nearly-zero g-factor. quantum well (QW) and the gate voltage [7, 8].

The DQD device was fabricated on a 6-nm-thick modulation-doped GaAs/$Al_{0.3}Ga_{0.7}As$ QW. We applied fast gate pulse (100 kHz) and RF to one side of the plunger gates to drive the ESR. The RF electric fields in the QD generate effective alternative magnetic field (f_{ac}) via the spin-orbit interaction [2]. We monitored the leakage current though the DQD under the Pauli spin blockade condition as a function of an in-plain external magnetic field as shown in Fig. 1(a). A current increase was observed around the ESR condition ($B_{ext}=hf_{ac}/g_e\mu_B$). The relatively broad ESR resonance width may result from the increase in the effective magnetic field cause by nuclear spins due to the reduced g-factor. From the resonant peaks measured over a wide magnetic field range as shown in Fig. 1(b), we determined an electron g-factor of $|g_e| \approx 0.05$, which agrees with the value ($|g_e| < 0.08$) obtained in the same QW structure measured by using the time-resolved Kerr rotation method [5].

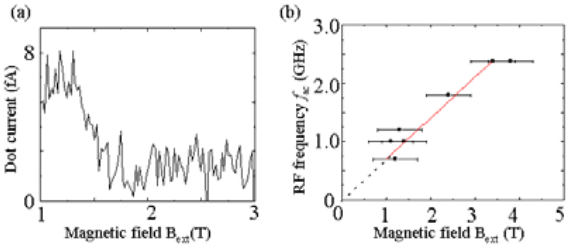

Fig.1 (a) Current measured through a DQD in the spin blockade regime with RF field (f_{ac}=1.20GHz) as a function of magnetic field. (b) Plot of the resonance magnetic field as a function of RF frequency.

This demonstration implies that we can coherently control the electron spin state even with a nearly-zero g-factor. With this device structure we have a possibility to operate the full Bell-state measurement needed for building a quantum repeater.

This work was supported by CREST-JST, SCOPE-MIC, ERATO-JST.

References

[1] F. H. L. Koppens et al., Nature **442**, 766 (2006).
[2] K. C. Nowack et al., Science **318**, 1430 (2007)
[3] M. Pioro-Ladriere et al., nature physics **4**, 776 (2008).
[4] K. Ono, et al,. Science **297**, 1313 (2002).
[5] H. Kosaka et al., Nature **457**, 702 (2009).
[6] H. Kosaka et al., Phys. Rev. Lett. **100**, 096602 (2008).
[7] H. W. Jiang and E. Yablonovitch, Phys. Rev. B **64**, 041307(R) (2001).
[8] G. Salis et al., Nature **414**, 619-622 (2001).

Spin-Orbit Interaction and Negative Magnetoresistance for Localized Electrons in InSb Quantum Wells

S. Ishida*, T. Manago*, N, Nishizako*, H. Geka** and I. Shibasaki**

** Tokyo University of Science Yamaguchi, San'yo-Onoda, Yamaguchi 756-0884, Japan*

***Asahi Kasei Corporation, Samejima, Fuji, Shizuoka 416-8501, Japan*

Keywords: spin-orbit interaction, variable-range hopping, weak anti-localization, InSb quantum well

Considerable attention has been paid to the role of spin-orbit interaction (SOI) in magnetoresistance (MR) due to the quantum interference (QI) for both weakly and strongly localized (WL and SL) 2DEGs. In the WL regime, the low-field negative MR is modified into the positive one by the weak anti-localization (WAL) depending on the strength of the SOI. In the SL regime, where the transport mechanism is via variable-range hopping (VRH), both theories and experiments established a singular negative MR, $\delta R(B) \propto -B$, in the absence of SOI. A question in controversy was whether the negative MR survives the SOI in the SL regime or not, and it was theoretically suggested that the low-field hopping MR remains negative regardless of the strength of the SOI [1]. However, no further experiment has been reported to solve the question, and the controversy is still unsettled.

The 2DEG in InSb quantum wells (QWs) shows strong SOI, and it is known that there exists accumulation layer composed of the localized states at heterointerface. This is suitable system to investigate the SOI in the SL regime. In this paper, we study the SO effect in both regimes of SL and WL in the accumulation layer of $Al_xIn_{1-x}Sb$/InSb QWs (x=0.1), examining in particular the low-field hopping MR. AlInSb(50nm)/InSb(L_w=15~100nm) /AlInSb(700nm) QWs were grown on GaAs (100) substrates by MBE. The lattice mismatch between the QW and the barriers is 0.5%.

Fig. 1 shows the sheet resistance ρ (T) in unit of h/e^2 (=25.9 kΩ), at various electron densities with n_s = 0.3~6.3×10^{11}cm^{-2}. At low Ts, samples with $\rho > \rho_c \sim h/e^2$ exhibit VRH, while those with $\rho < \rho_c$ exhibit WL, where ρ_c corresponds to the critical sheet resistance at the MI transition in 2DEGs. As shown in the inset, the WAL in the presence of SOI is clearly observed in the WL regime. In contrast, the low-field hopping MR remains entirely negative surviving the SOI. These results support the prediction that the hopping MR due to the QI is completely negative regardless of the SOI [1].

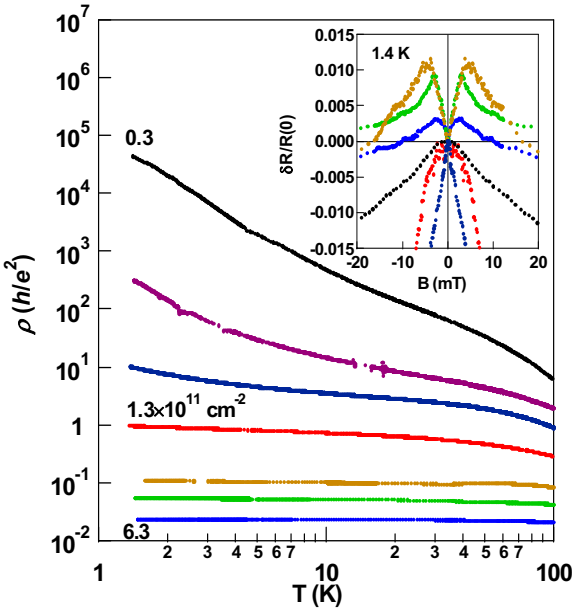

Fig.1 Sheet resistance ρ (T) in unit of h/e^2. Inset: Low-field MR (T=1.4 K) characterized by WAL in the WL regime and negative MR in the SL regime.

Reference

1. T. V. Shahbazyan and M. E. Raikh, Phys. Rev. Lett. **73**, 1408 (1994), and references there in.

Electrically detected spin resonance of 'snake' state oscillators

B.Dai*, A.Nogaret*, P.Saraiva*, F.Nasirpouri*, J.C.Portal**, H.E.Beere***, D.A.Ritchie***

* *Department of Physics, University of Bath, Bath BA2 7AY, UK*

** *High Magnetic Field Laboratory, 25 Avenue des Martyrs, 38042 Grenoble, France*

*** *Cavendish Laboratory, University of Cambridge, Cambridge CB3 0HE, UK*

Keywords: Electron spin resonance, Magnetic field gradient, Snake states, Overhauser coupling

We report the observation of electrical detection of spin resonance in a gradient of magnetic field. Two dimensional electrons modulated by a gradient of magnetic field are known to oscillate in 'snake' orbits which spontaneously undergo spin resonance when the oscillator frequency equals the Larmor frequency [1]. The Larmor frequency is varied by applying a homogeneous magnetic field *in the plane* of the 2DEG [1]. The gradient of magnetic field is obtained by means of Samarium-Cobalt finger gates fabricated at the surface of a GaAs/AlGaAs HEMT structure. The structure was then plunged in the parallel magnetic field to vary the Larmor frequency but also to maintain a pure 1D magnetic modulation with zero average modulation field. Under microwave irradiation, the magnetoresistance reveals a rich spectroscopic probe of spin resonant phenomena in the 2DEG - a typical magnetoresistance trace being shown in Fig.1.

At 10T, one observes a microwave induced peak (arrows) which moves to higher B linearly as a function of the microwave frequency. The Landé g-factor is g=0.38 (GaAs |g|=0.44). This ESR peak arises from spin resonance within 'snake' orbits. We establish this by tilting the magnetization of the finger gates from the short in-plane axis to the long axis direction and observing the extinction of the ESR peak. This occurs because no magnetic modulation is produced when the finger gates are magnetized parallel to the fingers. Among other notable features, the ESR peak is shifted by $5.2T \pm 0.6T$ depending on the direction and rate of magnetic field sweep – see Fig.1. The offset and the high field magnetic hysteresis are explained by the dynamic nuclear polarization. The saturation of spin resonance dynamically polarizes the nuclear spins which in turn bias the ESR line via the Overhauser interaction of electron and nuclear spins.

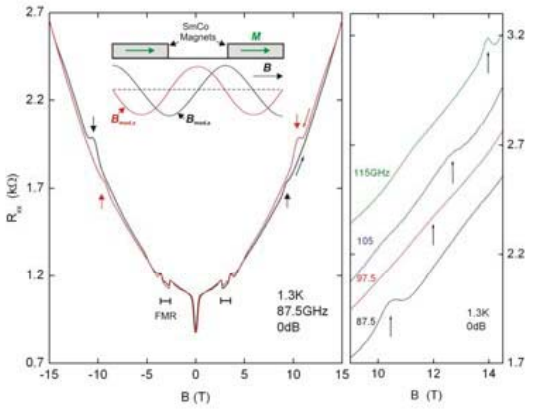

Fig.1 Longitudinal resistance of a magnetically modulated 2DEG. The magnetic field, B, is **in the plane** of the 2DEG to vary the Larmor frequency. Vertical arrows show the spin resonance of electron oscillators in the magnetic field gradient. Ferromagnetic resonance is also seen at low B.

At low magnetic field (3T), the 2DEG also detects the ferromagnetic resonance (FMR) of the finger gates. High frequency switching of the magnetization causes high frequency oscillations of the magnetic modulation giving the observed dip in the resistance. In summary, we have demonstrated the resonant absorption of electromagnetic radiation by snake orbits at frequencies near their cut-off frequency [1]. The mechanism allowing the electrical detection of ESR is the difference in conductivities [2] of the initial and final spin states in the magnetic field gradient (not heating).

References

1. A.Nogaret Phys.Rev.Lett **94**, 147207 (2005); A.Nogaret and F.M.Peeters, Phys.Rev.B **76**, 075311 (2007); ibid **76,** 075312 (2007)

2. D.Stein, K. von Klitzing and G.Weimann, Phys.Rev.Lett. **51**, 130 (1983)

Low field magnetization dynamics in dilute (Cd,Mn)Te

P. Kossacki[1,4], M. Goryca[1,4], T. Kazimierczuk[1], M. Nawrocki[1], A. Golnik[1], J. A. Gaj[1], T. Wojtowicz [2], G. Karczewski[2], J. Cibert[3] and S. Tatarenko [3]

[1] *Institute of Experimental Physics, University of Warsaw, Warsaw, Poland*

[2] *Institute of Physics, Polish Academy of Sciences, Warsaw, Poland*

[3] *Institute Neel ,CNRS/UJF, Grenoble, France*

[4] *Grenoble High Magnetic Field Laboratory, CNRS, Grenoble, France*

Keywords: spin relaxation, spin memory, quantum well, diluted magnetic semiconductor

A nanostructure containing one or a few magnetic ions is a simple, but very interesting quantum system. CdTe based structures with Mn ions are particularly suitable for studies of low dimensional structures. This is due to the isoelectronic character of Mn in CdTe, offering the possibility of modulation doping and electrical biasing of nanostructures, and the broad range of optical methods, which yield direct information on the magnetic configuration of the Mn system through the so called giant Zeeman effect.

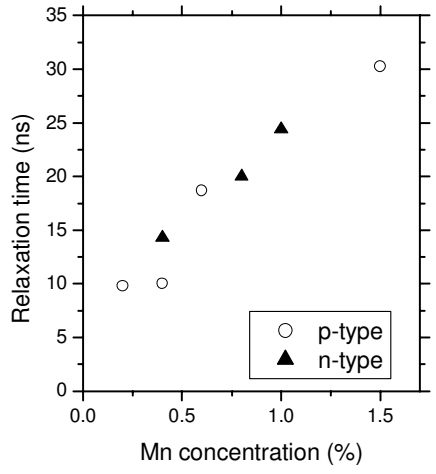

Fig.1 Magnetization relaxation time determined for different (Cd,Mn)Te/(Cd,Mg)Te quantum wells. Measurements were done after short pulses of magnetic field at 1.5K.

From the point of view of possible applications in spintronics one of the most important features is the spin relaxation in zero external magnetic field. We developed a method to measure the evolution of the magnetization in (Cd,Mn)Te based heterostructures after a short pulse of magnetic field [1]. It was applied for quantum wells with very low Mn concentration and variable carrier density. It was shown that the spin dynamics of a dilute magnetic ion system in a quantum well is of the nanosecond scale in absence of magnetic field. The zero-field magnetization relaxation is up to three orders of magnitude faster than that measured previously in magnetic field. To describe this fast dynamics two mechanisms were proposed: the hyperfine interaction with the nuclear spin and the anisotropy due to the strain in the epitaxial structure.

In the present paper we present a more detailed study of the dependence of the fast relaxation on the manganese ion concentration in the quantum well material. We show that the relaxation is slowed down with increase of the concentration of magnetic ions. This observation is explained as resulting from a competition between the hyperfine interaction and exchange interaction with more distant Mn ions.

References

1. M. Goryca *et al.*, Phys. Rev. Lett. **102**, 046408 (2009).

Interplay of intrinsic and extrinsic mechanisms to the spin Hall effect in a two-dimensional electron gas

R. Raimondi* and P. Schwab**

*CNISM and Dipartimento di Fisica, Università Roma Tre, Via della Vasca Navale 84, 00146 Roma, Italy

** Institut für Physik, Universität Augsburg, D-86135 Augsburg, Germany

Keywords: spin Hall effect, spin-orbit interaction, spin relaxation, spintronics

Spin-orbit interaction in semiconductors, which has been studied for more than fifty years, has attracted in recent years a renewed attention due to its potential for controlling the spin degrees of freedom with electric fields. In this respect, the spin Hall effect, where a pure transverse spin current is generated by an applied electric field, appears as one of the most promising paradigm's for developing a new generation of spintronics devices.

It has become conventional to distinguish between extrinsic and intrinsic mechanisms for the spin Hall effect, depending whether the spin-orbit interaction originates from impurity and structure potential, respectively. In a two-dimensional electron gas, the intrinsic spin Hall effect due to the structure inversion asymmetry (Rashba term) has been intensively studied and it has been established that there is no spin Hall current as long as the static limit in the bulk is considered. The case is different when extrinsic and intrinsic effects are both present. Our contribution provides a theory for this situation.

The problem of the interplay of extrinsic and intrinsic spin Hall effects has already been analyzed in the literature, although the answers provided are contradictory [1, 2, 3] and show some non analytic features, which are puzzling from the physical point of view. In this paper, we clarify the origin of the above problems.

The key physical observation is that a correct evaluation of the spin current requires the consideration of the spin relaxation due to both extrinsic and intrinsic spin-orbit scattering. This is made transparent in our approach, where we derive coupled kinetic equations for charge and spin densities. These latter are obtained in terms of the quasiclassical Green function, satisfying an Eilenberger-like equation, which in the case of only intrinsic spin-orbit interaction was derived previously[4].

More in detail, we provide the drift-diffusion equations for the spin-current and solve them to obtain the electric-field induced in-plane spin polarization and spin current with out-of-plane spin polarization. These show that the effects of extrinsic and intrinsic spin-orbit interaction mechanisms are not additive. First, the classical result by Edelstein[5] for the in-plane spin polarization is strongly modified by the presence of the extrinsic spin-orbit interaction. Second, the spin current is written as a sum of three sources. Two of them can be associated to the well known mechanisms of side-jump and skew-scattering due to the extrinsic spin-orbit interaction. The third one is an intrinsic spin-orbit contribution. Our expression for the spin current correctly reproduces the known limits, where one of the two spin-orbit interaction is absent, and agrees with Ref. [1] in the limit when spin relaxation due to extrinsic spin orbit scattering is negligible. Finally, we point out that our analysis has been extended to finite frequencies as well.

References

[1] Wang-Kong Tse and S. Das Sarma, Phys. Rev. B **74**, 5 (2006).

[2] Liangbin Hu, Zhian Huang, Shejun Hu, Phys. Rev. B **73**,235314 (2006).

[3] E. M. Hankiewicz and G. Vignale, Phys. Rev. Lett. **100**, 4 (2008).

[4] R. Raimondi, C. Gorini, P. Schwab, and M. Dzierzawa, Phys. Rev. B **74**, 035340 (2006).

[5] V. M. Edelstein, Solid State Commun. **73**, 233 (1990).

Deformation effects on electronic structures of bilayer graphenes

S.H. Lee, C.W. Chiu and M.F. Lin

Department of Physics, National Cheng Kung University, Tainan, Taiwan

Keywords: monolayer graphene, deformation, electronic property

The deformation effects on the electronic properties of AA- and AB-stacked bilayer graphenes are explored through the tight-binding model. The mechanical deformation of graphene lattices are based on the elasticity theory [1]. The intralayer and interlayer hopping integrals strongly depend on the deformed C-C bond lengths. In the presence of the uniaxial stress, both the interlayer interaction and the stacking sequence have strong effects on the low-energy properties, such as energy dispersions, and density of states [D(ω)].

In this work, the stacking sequence causes important differences between AA- and AB-stacked bilayer graphenes. The latter owns the more asymmetric energy bands. At the low energy, the former and the latter own, respectively, the linear and the parabolic bands (the inset of Fig. 1). As regard to the deformed effects, they include the shifts of Fermi momenta, the modifications of energy dispersions, and the variations of band width.

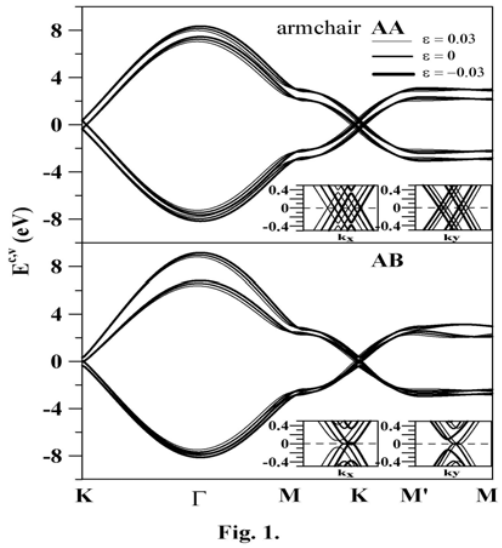

Fig. 1.

Fig.1 The π-electronic structures at $\varepsilon = 0.03$, 0, -0.03.

The above band structures would reflect on the density of states. For the AB-stacked bilayer graphene, D(ω) exhibits more asymmetric between ±ω, much smaller near ω=0, and larger range of frequency (Fig. 2). In the presence of the uniaxial stress, it varies the range of frequency, and doubles the peak structures near ω=±2.6 eV. Furthermore, the semimetal-semiconductor transition might occur in the AB-stacked bilayer graphene. Such features are due to the changes of energy dispersions. The predicted electronic properties could be verified by the scanning tunneling spectroscopy.

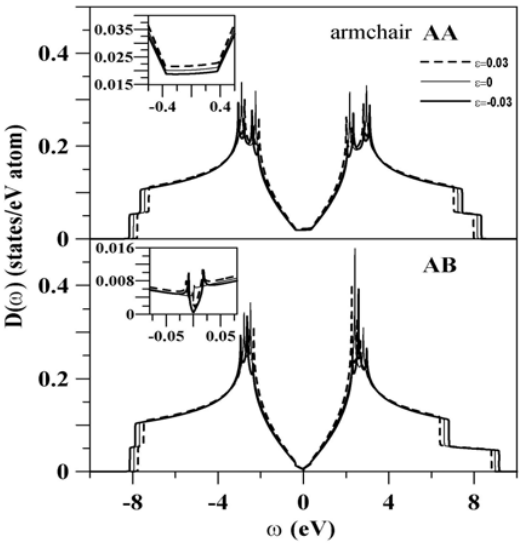

Fig. 2.

Fig.2 Density of states at different ε's

References

1. B. T. Kelly, Physics of graphite. Applied Science: London, Englewood, N. J. (1981)

Low temperature magneto-resistance of thin multi-walled carbon nano-tube

M. Kida*, T. Hatori*, Y. Nakamura*, Y. Togashi*, N. Aoki*, J. P. Bird**
and Y. Ochiai*

** Graduate School of Advanced Integration Science, Chiba University, Yayoi, Inage, Chiba263-8522, Japan*

*** Department of Electrical Engineering, University at Buffalo, SUNY, NY 14260-1900, USA*

Keywords: multi-walled carbon nano-tube, magneto-resistance, quantum interference

In order to determine the quantum phase interference in thin multi-walled carbon nanotube (MWNT), the low temperature magneto-resistance (MR) has been studied. From prior works on the magneto-transport experiments of MWNT, metallic conduction and a weak localization (WL) peak near zero magnetic field have been expected to arise from conduction via the outermost surface layer of the tube [1]. Nanoscale confinement of electrons in such curved spaces should strongly and coherently influence the WL-MR behavior. In our study, AB type oscillations are observed in the low-temperature MR of MWNTs, in spite of their multi layer structure.

In order to clarify the effect of the lead contact to the MWNT, two kinds of metallic leads (Au/Ti or Pd), have been employed for four-terminal resistance measurements. The contact resistance of the Pd metal shows to be much lower than that of the Au/Ti ones. In previous analysis of the phase coherence of the electron transport of the MWNT, various phase breaking behaviors have been expected and observed to show a clear dependence on both the magnitude and angular orientation of the applied field [2]. Therefore, we must clarify the origin of the WL peak and the flux cancellation in the parallel field layout into the direction of the axis of the MWNT [3, 4].

Among these phase breaking processes, one is found to be temperature dependent, while another is almost independent of temperature. These processes can be ascribed to different origins of phase breaking, for example, due to the intrinsic nature of the tube, to local effects at the lead contacts, or to thermal related processes. It can be determined that the phase coherence of the electron almost spreads over the whole region of the MWNT sample between the voltage leads. Also, a large, a few hundred percent larger height, MR can be observed for the case of the Pd metal contacts then we can expect to observe a clear distinguish behavior for the Pd- or Au-contact lead metal. In order to clarify the surface transport mechanisms in the outmost layer of the MWNT, the angular dependence of the MR is important and useful. In order to determine the phase coherent behavior, it is very important to discuss on the phase braking behaviors, especially comparing with the theoretical calculation such as on impurity scattering in the metallic wires [5].

References

1. T. Mihara et al., Superlattices & Microstructures, 34, 383 (2003).
2. M. Kang et al., Phys. Rev., B77, 113408 (2008).
3. A. Fujiwara et al., Phys. Rev., B60, 13492 (1999).
4. T. Ando, J. Phys. Soc. Jpn., 74, 777 (2005).
5. T. Nakanishi et al. J. Phys. Soc. Jpn., 74, 3027 (2005).

Transport properties of normal metal - graphene nanoribbon - normal metal junctions

Y. Mochizuki and H. Yoshioka
Department of Physics, Nara Women's University, Nara, Japan

Keywords: Graphene nanoribbon, Transport properties, Zigzag edges, Klein edges

A graphene nanoribbon (GNR), which is a nano-meter size graphene fragment, is known to have a remarkable property that the band structure strongly depends on the shape of edges [1, 2]. For example, the GNR with the armchair shaped edges has a metallic or an insulating band depending on the width N. In the case with $N = 2$ mod 3, there is no gap at the Fermi energy, whereas the gap opens for the other cases. On the other hand, the GNR with the zigzag shaped edges has a metallic band structure irrespective of the width N. The energy dispersion is, however, quite different from that of the regular square lattices, especially near the Fermi energy. The asymptotic behavior near the Fermi energy is written as $E(k) \propto \pm|k - k_{\rm F}|^N$ where $k_{\rm F} = \pi/a$ is the Fermi wavenumber with a being the lattice spacing and then the Fermi velocity becomes zero. The states near the Fermi energy have localized nature near the zigzag edges.

Transport properties of GNR with spatial dependent external potential have been investigated theoretically [3, 4, 5, 6, 7], and the remarkable properties depending on the parity of the width N have been found in the case of zigzag shaped edges. Note that such a parity effect is also observed in the persistent currents of the isolated ring [8]. However, the junctions composed of the GNR and the normal metal have not been discussed. In the present work, we investigate the transport properties of normal metal - GNR - normal metal junctions as is schematically shown in Figure 1. Here, the GNR with the width N and the length $2N_L$ and the normal metal expressed by the regular square lattices are illustrated by the thick and thin lines, respectively. In the GNR region, the electron hopping at the bond expressed by the solid line and that by the dotted one are given by t and $c \times t$ with $0 \leq c \leq 1$, respectively. So, the case with $c = 1$ ($c = 0$) corresponds to the zigzag (Klein) edges. The conductances as a function of the length N_L and of the Fermi energy are discussed for several choices of c. We can tune effects of the localized states near the zigzag edges on the transport properties by changing the value of c.

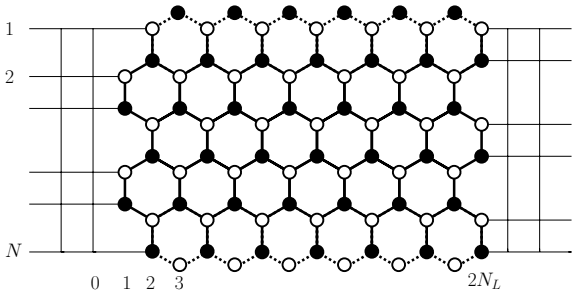

Figure 1: Schematic representation of normal metal - GNR - normal metal junctions where the filled and open circles express the A and B sublattices, respectively. Here, the GNR has the width N and the length $2N_L$, and the electron hopping at the bond expressed by the solid line and that by the dotted one are expressed by t and $c \times t$ ($0 \leq c \leq 1$), respectively.

References

[1] M. Fujita, K. Wakabayashi, K. Nakada and K. Kusakabe, J. Phys. Soc. Jpn. **65**, 1920 (1996).

[2] K. Nakada, M. Fujita, G. Dresselhaus and M. S. Dresselhaus, Phys. Rev. B **54**, 17954 (1996).

[3] K. Wakabayashi and T. Aoki, Int. J. Mod. Phys. B **16**, 4897 (2002).

[4] A. Rycerz, J. Tworzydło and C. W. J. Beenakker, Nat. Phys. **3**, 172 (2007).

[5] A. R. Akhmerov, J. H. Bardason, A. Rycerz and C. W. J. Beenakker, Phys. Rev. B **77**, 205416 (2008).

[6] A. Cresti, G. Grosso and G. P. Parravicini, Phys. Rev. B **77**, 233402 (2008).

[7] J. Nakabayashi, D. Yamamoto and S. Kurihara, Phys. Rev. Lett. **102**, 066803 (2009).

[8] H. Yoshioka and S. Higashibata, arXiv:0807.3999, to be published in J. Phys. Conf. Ser.

Doping of Si into Aligned Carbon Nanotube Films on SiC

T. Maruyama[1], K. Yoshida[2], W. Norimatsu[1], M. Kusunoki[1 2]

[*] *Nagoya University, Nagoya, Japan*

[**] *Japan Fine Ceramics Center, Nagoya, Japan*

Keywords : Carbon nanotube

Carbon nanotube (CNT) has attracted a great attention for various applications based on its specific properties since its discovery. However, applying CNTs to nanodevices, it is important to control their electrical properties as a semiconductor. Theoretical calculation indicates the possibility that when another element is inserted into the CNT lattice, CNTs would exchange its physical and electrical properties dramatically[1]. And some groups reported about characterization of doped CNTs with some kinds of elements [2].

We have reported that well-aligned CNTs are formed all over the SiC surface by selecting evaporation of Si atoms due to surface decomposition of SiC in vacuum at high temperature.[3] Here we report the results about Si-doping of the aligned CNT films formed by the SiC surface decomposition, using a conversion method aimed to control its electric property.

Firstly, CNTs 230 nm long oriented on SiC substrates were prepared by heating SiC(0001) surface to 1700 ℃ and held at the temperature for 0.5 h. (Figure 1) These were located with SiO_2 and C powders in carbon crucible. The crucible was heated to 1500-1600 ℃ and held at these temperatures for 0.5 h in vacuum around 3.0 x 10^{-4} Torr in the electronic furnace. The microstructure observation and EELS analysis were carried out using TEM (JEOL 2010-DM, 200kV) and EF-TEM (tecnai 30F, 300kV).

Figure 2 shows Si element mapping of the CNT films (a) before and (b) after the present reaction at 1500 ℃ by EELS. These results revealed that a little amount of Si atoms were doped into the pure CNTs without any change of CNT morphology. After the reaction over 1515 ℃, SiC single crystals started to grow at the CNT caps having orientation relationship with the CNT axis direction.

References

1. R. J. Baierle, Solange. B. Fagan, R. Mota, Antonio J. R. da Silva, A. Fazzio Phys. Rev. B, **64**, 085413 (2001).
2. X. H. Sun, C. P. Li, W. K. Wong, N. B. Wong, C. S. Lee, S. T. Lee, B. K. Teo, J. Am. Chem. Soc., **124**, 14464 (2002).
3. M. Kusunoki, T. Suzuki, T. Hirayama and N. Shibata, Appl. Phys., Lett. **77**, 531 (2000).

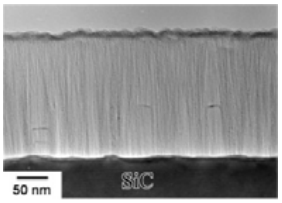

Fig. 1 Well-aligned CNT film on SiC (000$\bar{1}$)

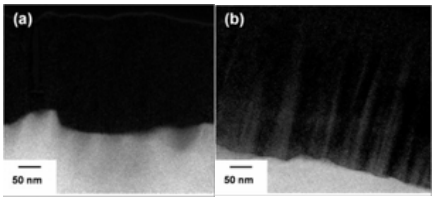

Fig. 2 Si element mappings of the CNT film (a) before and (b) after the present reaction

Doping of graphene by toluene

A. A. Kaverzin, F. Withers, A. S. Price, S. M. Strawbridge, A. K. Savchenko, H. Pinto, R. Jones

School of Physics, University of Exeter, Stocker Road, Exeter, EX4 4QL, UK

Keywords: graphene doping sensors mobility

It has been shown that the carrier concentration in graphene can be changed by chemical doping, and that graphene devices can allow for the detection of individual molecules [1], indicating the great potential for future ultra-sensitive graphene-based detectors. The ability to detect organic molecules would be of particular interest to many applications. We report the observation of doping by electrons of graphene due to the addition of an organic molecule, Toluene ($C_6H_5CH_3$). This is detected as a shift of the resistance peak $R(V_G)$ to negative values of the gate voltage (see figure). Surprisingly, the addition of toluene is seen to be accompanied by an increase of the mobility of carriers in graphene, in contrast to the result of doping by simple chemical species, where the mobility either is unaffected by doping [2] or is decreased [3].

Our experiments are complemented by density functional calculations order to determine the doping effect of toluene on graphene-based transistors.

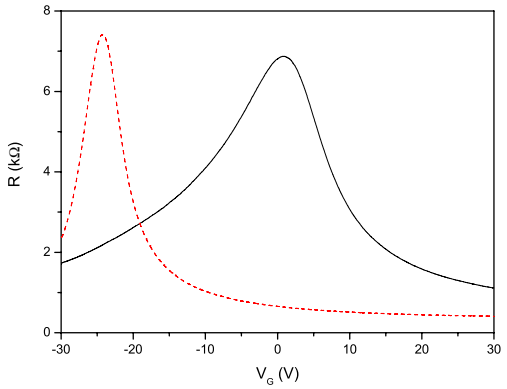

Fig. 1: Resistance as a function of gate voltage before addition of toluene (black solid) and after exposing graphene to toluene for 3 hours (red dashed).

References

[1] F. Schedin *et al*, Nature Materials **6**, 652 (2007).
[2] T. O. Wehling *et al*, Nano Letters **8**, 173 (2008).
[3] J. H. Cheng *et al*, Nature Physics **8**, 377 (2008).

Phase jump of the reflection amplitude in bilayer graphene with potential step

Sunghun Park[1], H.-S. Sim[1]

1*Department of Physics, Korea Advanced Institute of Science and Technology, Daejon 305-701, Korea*

Keywords: Bilayer graphene, Electronic transport.

Bilayer graphene has attracted recently due to the potential application of its electronic properties to nanodevices. One unusual feature of the bilayer graphene is a pseudospin degree of freedom of a charge carrier in low-energy limit, which represents the two sublattice sites in each layer [1]. We theoretically investigate the electronic transport properties related to the pseudospins of charge carriers in the bilayer graphene in the presence of an electrostatic potential step; $V(x) = V_0$ for $x < 0$, and $V(x) = V_1$ for $x > 0$, based on a non-interacting electron approach. For simplicity, we assume that the length scale of spatial variation of the potential is much longer than the lattice constant of the graphene.

We focus on the phase of the reflection amplitude with varying incidence angle θ of a plane wave. The phase of the reflection amplitude is found to strongly depend on the height of the potential step. When V_0 is nearly same as V_1, the phase of the reflection amplitude shows a jump by π at $\theta = \pi/4$ measured relative to the normal incidence angle; see Fig.1. This behavior is a consequence of a symmetry of the bilayer Hamiltonian, which is invariant under a transformation from $(\vec{q}, \vec{\sigma})$ to $(-\vec{q}, -\vec{\sigma})$. Here, $\vec{q} \equiv (-p_x^2 + p_y^2, -2p_x p_y)$, $\vec{p} = (p_x, p_y)$ is the momentum of the electron in bilayer graphene, and $\vec{\sigma}$ is the pseudospin operator. On the other hand, the symmetry becomes broken when the difference between V_0 and V_1 becomes large, because of waves localized at the boundary $(x = 0)$ [1]. This causes a smooth change of the reflection phase, rather than the sharp jump, with respect to the angle θ around $\pi/4$. The properties of the reflection phase to the angle θ manifest the coupling between the momentum and the pseudospin in the bilayer graphene, and can be observed in an interferometry setup.

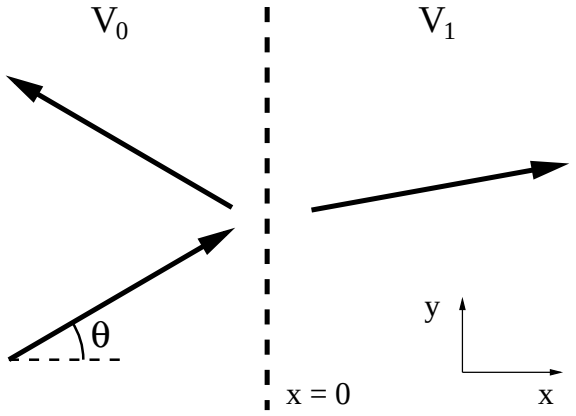

Figure 1: Schematic diagram for the reflection of the wave with incidence angle θ at the potential step in a bilayer graphene sheet. The constant potential V_0 is applied for $x < 0$ and V_1 for $x > 0$.

References

[1] M. I. Katsnelson, K. S. Novoselov, and A. K. Geim, Nature phys. **2**, 620 (2006).

Molecular beam epitaxy growth of wurtzite GaN nanoislands and nanocolumns

Kuang-Yuan Hsu , Chuan-Pu Liu

Department of Materials Science and Engineering, National Cheng Kung University, Tainan, Taiwan

Keywords: GaN, nanoislands, nanocolumns, quantum well

In this study, we report on the direct growth and optical properties of InGaN/ GaN multiple quantum wells (MQW) grown on GaN nanoisland and nanocolumn arrays by molecular beam epitaxy. Due to the lack of defects and the large surface areas provided by the sidewalls of nanoislands and nanocolumns, we expect to enhance both internal and extraction efficiencies significantly. The nanoisland growth requires special conditions in the V/III ratio and substrate temperature as shown in Fig. 1. The insertion of a nitrided Ga layer may effectively improve the GaN island size uniformity, as shown in Fig. 1 (b). Furthermore, an increase of the N flux will lead to a higher density of GaN nanoislands, as shown in Fig. 1 (c). Figures 2 (a) and (b) show SEM images in the plan and cross-sectional view, respectively, for the GaN nanocolumns. The nanocolumns were grown by MBE on Si (111) at 750^{o}C for 3 hours. The growth of the GaN nanocolumns can be explained by the diffusion-induced (DI) mechanism [1], where the adatoms diffuse to the column apex from its lateral sides driven by a lower chemical potential at the top surface.

From the RT μ-PL spectra as shown in Fig. 3, the InGaN/GaN MQW grown on nanoislands exhibit better optical property with narrower FHWM and higher In content due to the lower density of threading dislocations and the large surface areas compared to that grown on flat MOCVD GaN template. The InGaN/GaN MQW embedded in GaN nanocolumns also exhibits a superior luminescence property. The GaN nanoislands and nanocolumns can serve as ideal templates for further growth of high efficient and bright light-emitting devices.

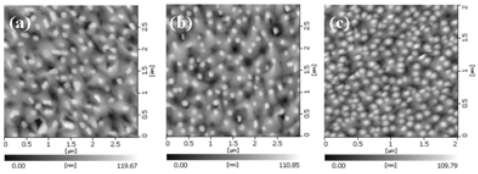

Fig. 1: AFM images of GaN islands grown by MBE at 750 ^{o}C for 3 hours: (a) directly on c-sapphire, V/III= 30; (b) on Ga-buffered c-sapphire, V/III= 30; (c) on Ga-buffered c-sapphire, V/III= 40.

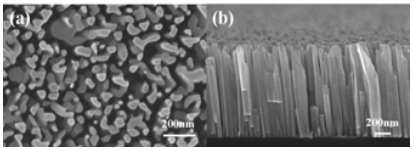

Fig.2: (a) Plan view and (b) cross-section view of FESEM images of the vertically aligned GaN nanocolumns grown on Si (111) by MBE.

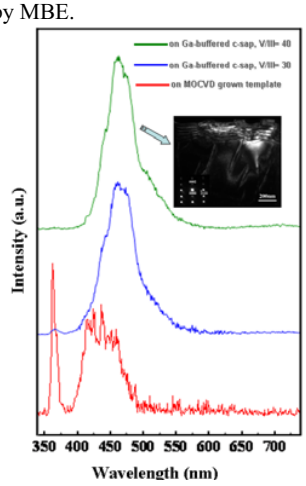

Fig. 3: RT μ-PL spectra of InGaN/GaN MQW grown on GaN nanoislands and MOCVD grown GaN template. The inset shows cross-sectional TEM image of InGaN/GaN MQWs grown on GaN nanoislands.

Reference
1. R. K. Debnath, R. Meijers, T. Richter, T. Stoica, R. Calarco, and H. Luth, Appl. Phys. Lett. 90, 123117 (2007).

Anomalous temperature dependence of critical supercurrent in multilayer graphene coupled to superconductors

A. Kanda[A,B], H. Goto[A,B], Y. Ootuka[A], K. Tsukagoshi[B,C,D], H. Yoshioka[E], and M. Hayashi[F]

[A]*Institute of Physics and TIMS, University of Tsukuba, Tsukuba, Japan*

[B]*CREST, JST, Kawaguchi, Japan*

[C]*MANA, NIMS, Tsukuba, Japan*

[D]*AIST, Tsukuba, Japan*

[E]*Department of Physics, Nara Women's University, Nara, Japan*

[F]*Faculty of Education and Human Sciences, Akita University, Akita, Japan*

Keywords: graphene, superconducting proximity effect

Graphene is not only a promising candidate for the future nanoelectronics element, but also is an attractive material for the mesoscopic physics. Up to now, single layer and bilayer has mainly been studied due to their characteristic band structures, resulting in chiral nature of carriers. Here, we demonstrate a new kind of transport phenomena observed in multilayer graphene (MLG) which come from a nonuniform distribution of charge carriers due to the finite interlayer screening length λ_{SC} = 1.4 nm of the gate electric field [1].

Our sample is a superconducting field effect transistor (SFET), in which a couple of superconducting electrodes (Ti/Al or Pd/Al) with a gap d = 0.2 - 0.5 μm were deposited on MLG (thickness: 4 - 10 nm) placed on a highly-doped Si/SiO_2 substrate. The substrate was used as a back gate. At temperatures well below T_c of the electrodes, clear proximity-induced supercurrent was observed for large gate voltages, but with anomalous temperature dependence of the critical supercurrent I_C. An example is shown in Fig. 1, in which the second derivative of I_C as a function of temperature is positive. This temperature dependence of I_C is well fitted by the formula, $I_C \propto \exp(-(T/T_0)^2)$, where T is temperature and T_0 is a constant around 0.5 K. This bahavior was observed in all MLG-SFETs and for all gate voltages which gives relatively large I_C at low temperatures. This behavior cannot be explained by the conventional theories for the proximity effect.

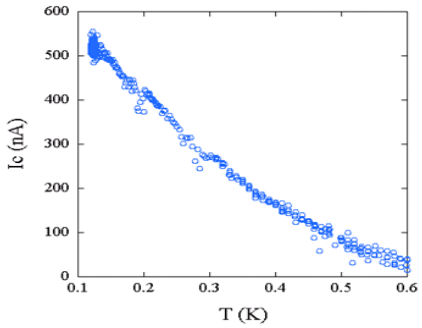

Fig.1 Temperature dependence of I_C of a MLG-SFET.

As a control experiment, we also measured the critical supercurrent of SFETs of single layer graphene. In this case, $d^2I_C/dT^2 < 0$ and I_C is explained with the conventional theory for short junctions in the dirty limit, i.e., mean free path << d << coherence length [2].

There are two possible origins for the anomalous behaviour observed in MLG-SFET. One is the successive superconducting transition of the graphene layers and the other is the decrease in the interlayer resistance of MLG with decreasing temperature. Both are closely related to the fact that the supercurrent is confined to the bottom layers close to the back gate when large V_g is applied. Detailed discussion will be given in the presentation.

References

1. H. Miyazaki et al., Appl. Phys. Express **1**, 034007 (2008).

2. I. O. Kulik and A. N. Omel'yanchuk, JETP Lett. **21**, 96 (1975).

Low-temperature electrical-transport properties of single indium tin oxide nanowires

Shao-Pin Chiu*, Hui-Fang Chuang**, Ji-Jung Kai**, Fu-Rong Chen** and Juhn-Jong Lin*

* *Institute of Physics, National Chiao Tung University, Hsinchu, Taiwan*

** *Department of Engineering and System Science, National Tsing Hua University, Hsinchu, Taiwan*

Keywords: indium tin oxide nanowires, low-temperature resistivities, dynamic structural defects

Single-crystalline indium tin oxide (ITO) nanowires (NWs) were grown by the thermal evaporation method. The as-grown NWs were typically 100–300 nm in diameter and a few μm long. Four-probe submicron Ti/Au electrodes on individual NWs were fabricated by the electron-beam lithography technique. The resistivities of several single NWs have been measured from 300 down to 1.5 K. The results indicate that the as-grown ITO NWs are metallic, but disordered.

Figure 1 shows the normalized resistivities of four ITO NWs between 1.5 and 300 K, where ρ_{min} is the minimum resistivity measured for each NW. The room temperature resistivities of these NWs fall in the range 140–300 $\mu\,\Omega$ cm. This figure indicates that, at temperatures above a few tens of K, the resistivities decrease with reducing temperature. That is, the electrical-transport characteristic is metallic, suggesting a good quality of our NWs. What is more interesting is that, at lower temperatures, the resistivities increase with decreasing temperature, and they vary approximately with the square root of temperature. The amounts of the resistivity rises (especially those in the ITO-j1 and ITO-l1 NWs) are of the order of 1% or larger. Quantitative estimates indicate that such resistivity rises are more than one order of magnitude as would be expected from the weak-localization and electron-electron interaction effects which are usually responsible for low-temperature resistivity corrections in metals in the diffusive regime [1].

The low-temperature resistivity rises are found to originating from the scattering of electrons off *dynamic*, rather than *static*, structural defects. The electron–dynamic defect scattering can be described in terms of the nonmagnetic two-channel Kondo effect which causes a resistivity correction given by [1]

$$\Delta\rho_{2CK} \approx -A\sqrt{T/T_K}\ , \qquad (1)$$

where A is a prefactor containing material properties (e.g., the concentration of dynamic defects, electronic density of states, etc.), and T_K is a characteristic Kondo temperature. A comparison of our measured resistivity rises with Eq. (1) suggests a typical dynamic defect concentration of ~ 10^{23} – 10^{25} m^{-3} in our NWs. Thus, this experiment clearly demonstrates that the as-grown single-crystalline ITO NWs contain numerous dynamic structural defects. Similar phenomenon has also been found in metallic RuO_2 NWs. The dynamic defects are likely associated with the huge amounts of point defects which inevitably exist in many kinds of as-grown NWs.

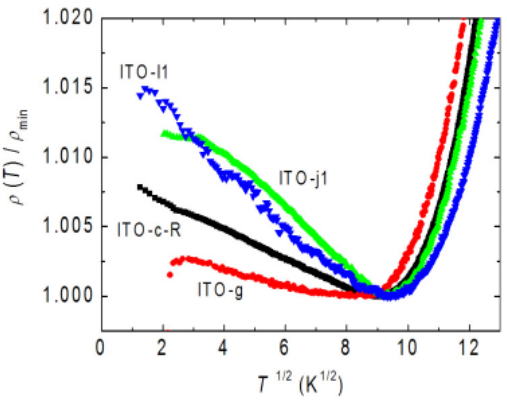

Fig.1 Normalized resistivities as a function of the square root of temperature for four ITO NWs.

References

1. S. P. Chiu, H. F. Chuang, Y. H. Lin, J. J. Kai, F. R. Chen and J. J. Li, Nanotechnology **20**, 105203 (2009).

Low frequency resistance noise in graphene based field effect devices

Atindra Nath Pal and Arindam Ghosh
Department of Physics, Indian Institute of Science, Bangalore 560 012, India

Keywords: bilayer graphene, conductivity noise, band gap

Graphene, a single sheet of carbon atoms, has become a potential candidate for future electronics. In particular, interest in bilayer graphene (BLG) is fueled by the ability to control the energy gap between its valence and conduction bands through external means. The Bernal stacking of graphene layers in BLG leads to four orbitals, but strong interlayer coupling between the adjacent sites results in splitting to two high energy bands, leaving two low-lying states that form a zero gap semiconductor with quadratic dispersion. However, both chemical doping and transverse electric field have been shown to open a band gap at the Fermi energy in a controllable manner, making BLG particularly attractive for nanoelectronic applications.

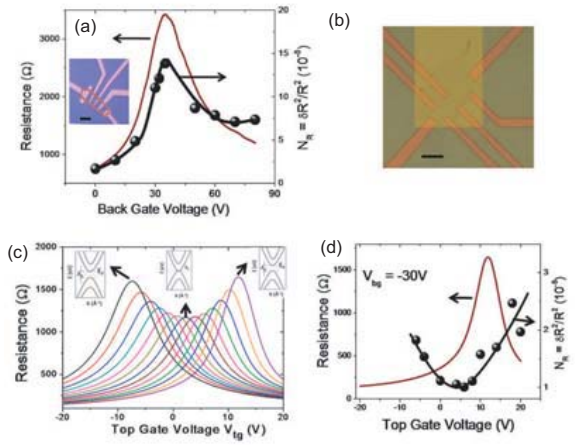

Figure 1: (a) The resistance and the normalized noise power spectral density (N_R) as functions of back gate voltage for a single layer device at 100K. Inset shows the optical micrograph of the device. The scale bar is 5 μm. (b) Optical micrograph of the dual gated BLG device. The scale bar is 10 μm. (c) Resistance versus topgate voltage, at 107 K, for various back gate voltages, ranging from 30 V to -30 V (left to right) with an interval of 5 V. Insets show schematics of corresponding band structures. (d) The resistance and the normalized noise power spectral density (N_R) as functions of top gate voltage, at a fixed back gate voltage of -30V, for BLG device at 107K.

Here, we present the low-frequency resistance noise measurements in both monolayer and bilayer graphene field effect devices. For BLG, we have used a double-gated FET devices to tune the zero gap and charge neutrality points independently, which offers a unique mechanism to investigate the low-energy band structure, charge localization and screening properties of bilayer graphene. The graphene films were prepared on top of an n++ doped Si substrate covered with $\approx$ 300 nm layer of SiO_2 by the usual mechanical exfoliation technique, and FET devices were made using standard electron beam lithography. Noise in these devices were measured in low-frequency ac four-probe method, as well as in a five probe technique. Fig. 1a shows that, for a backgated single layer graphene (SLG) device, the noise magnitude decreases with gate voltage in both side of the charge neutrality point, which can be well explained by the effective screening of the trap potentials by the mobile charges [1]. Conversely, for the dual gated BLG device (Fig. 1b) our experiments show that noise in BLG *increases* with increasing n, thereby forming a minimum around $n = 0$ (Fig. 1d). This can be explained by the diminished ability of BLG to screen the external potential fluctuations in presence of finite bandgap (Δ_g) [1, 2]. Also, a further analysis indicate that multiple processes involving the charge traps are active in producing the resistance noise which is intimately connected to the BLG band structure, being minimum at $\Delta_g = 0$ [2] even if it corresponds to a nonzero n.

References

[1] Y. Lin and Phaedon Avouris, Nano Lett. **8**, 2119 (2008).

[2] Atindra Nath Pal and Arindam Ghosh, Phys. Rev. Lett. (2009) (in press).

Atomic structures of the interface between homogeneous graphene and 6H-SiC (0001)

W. Norimatsu, and M. Kusunoki

EcoTopia Science Institute, Nagoya University, Nagoya, Japan

Materials Research and Development Laboratory, Japan Fine Ceramics Center, Nagoya, Japan

Keywords: graphene, interface structure, transmission electron microscopy

Graphene is a one-atom-thick carbon material, with carbon atoms packed densely in a hexagonal honeycomb lattice. Few-layer graphene on the SiC substrate is one of the promising materials for device integration. The opening of a gap in few-layer graphene due to the interaction with the SiC substrate is also an advantage in switching-device application. For detailed understanding of the electronic state due to the interaction between graphene and the SiC substrate, it is important to observe the cross-section directly from a perspective parallel to the interface. In this study, high-resolution transmission electron microscopic (TEM) cross-sectional observations were performed to investigate the interface structure between graphene and 6H-SiC (0001). A first principles calculation combined with high-resolution TEM allowed us to understand the interface structures together with their electronic states.

Graphene-on-SiC samples were prepared by annealing Si-terminated 6H-SiC single crystals. SiC substrates were cleaned using HF solution and then annealed at different temperatures, ranging from 1350 to 1500 ºC, in a vacuum furnace. Thin specimens for TEM observation were prepared by Ar-ion thinning method. Cross-sectional observation of the interface structure was carried out using a JEM-2010-type TEM with an accelerating voltage of 200 kV.

Our observations revealed the presence of a metastable transitional structure formed by decomposition of a single SiC bilayer as well as fully-packed honeycomb graphene as the interface structure [1]. Figure 1 shows two types of the interface structure. Structure type-(a) is characterized by graphene layer 1 which contains the atomic displacement toward the SiC substrate. In the structure type-(b), there exists graphene layer 0 having less C atom density. The results of our calculation clarified that the difference in the interface structures should strongly influence the electronic state. The obtained results of our observations and calculations will be reported in the conference.

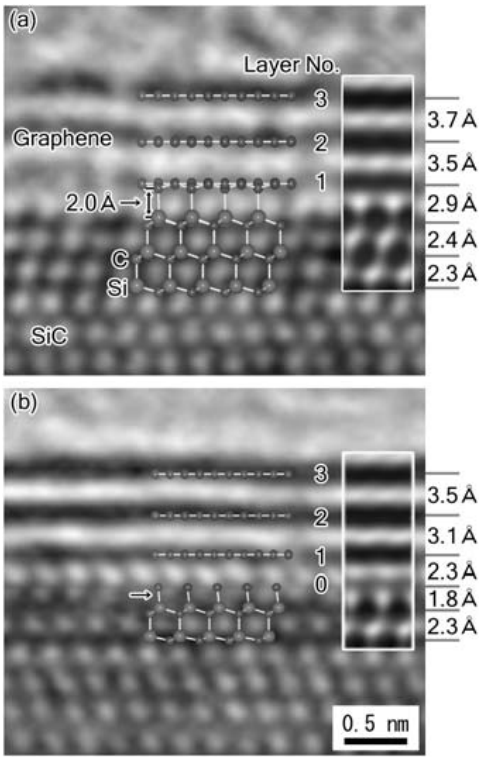

Fig.1 Two-types of the interface structure between graphene and SiC. Both images were obtained from different areas of the same sample annealed at 1450 ºC.

References

1. W. Norimatsu and M. Kusunoki, Chem. Phys. Lett. **468**, 52 (2009).

Interband Conductivity of Neutral Graphene Sheets

P.S.Park[1], S.C. Kim[1], S.-R. Eric Yang[1,2], and A.H. MacDonald[3]
1*Physics Department, Korea University, Seoul, Korea*
2*Korea Institute for Advanced Study, Seoul, Korea*
3*Department of Physics, University of Texas, Austin, TX 78703, USA*

Keywords: graphene, optical conductivity

The optical properties of graphene have recently attracted both experimental and theoretical attention. The interband conductivity of graphene is unusual because the material is two-dimensional, because it is gapless, and because its envelope function theory does not conserve electron-hole pair (exciton) number. Moreover, the Fermi surface of a neutral graphene sheet consists of single Dirac points, and the Fermi wavelength diverges at these points. Optical absorption in graphene has an unusually strong dependence on electronic gating in both infrared and visible regimes which is potentially attractive for optoelectronic applications Gate voltages can vary the density of Dirac fermions in graphene from 0 to $\sim 10^{13} cm^{-2}$. This density change corresponds to an interband absorption threshold shift of ~ 0.3 eV, roughly two orders of magnitude larger than the maximum shift possible in semiconductor-quantum-well quasi-two dimensional systems. There is also fundamental interest in the optical properties of graphene sheets because of subtle and incompletely understood many-body effects on which our work focuses. According to perturbative RG calculations in a neutral graphene layer with no disorder the static conductivity is given by a universal constant, independent of electron-electron interactions

$$\sigma_{uni} = \frac{\pi}{2}\frac{e^2}{h}. \tag{1}$$

In these theories the optical conductivity increases with frequency from this universal value when electron-electron interactions are present. In this work we report on an envelope-function theory of the $T = 0$ conductivity of clean graphene sheet which accounts accurately for the competition between self-energy and vertex-correction interaction effects. We find that the low-frequency conductivity depends on a delicate balance between an upward shift in excitation energies, which tends to lower the conductivity, and a shift in oscillator strength to low-energies which tends to enhance the conductivity. Our results show that these two effects do not cancel in general and suggest that the interband conductivity can be strongly influenced by interactions.

Influence of the growth conditions of epitaxial graphene on the film topography and the electron transport properties

S. Weingart*, C. Bock*, U. Kunze*, K.V. Emtsev**, Th. Seyller**, and L. Ley**
*Werkstoffe und Nanoelektronik, Ruhr-Universität Bochum, Germany
** Lehrstuhl für Technische Physik, Friedrich-Alexander Universität Erlangen-Nürnberg, Germany

Keywords: epitaxial graphene, magnetotransport, charge carrier mobility, charge carrier density

In this work we report on temperature-dependent magnetotransport measurements on epitaxial graphene grown on silicon faced SiC under different annealing conditions. Compared to UHV-grown epitaxial graphene [1] graphene samples annealed in Ar atmosphere [2] exhibit an improved topography with step widths of about 2 – 3 μm. We demonstrate that the improved topography is accompanied by an increased electron mobility. The temperature dependency of the charge carrier mobility and density clearly depends on the growth conditions.

Two samples are prepared, which are *ex-situ* annealed in Ar atmosphere at different process pressures and temperatures [2]. The graphene film of sample A is grown at 2123 K in an Ar atmosphere at 450 mbar. On sample B graphene is formed at 1923 K close to atmospheric pressure. Figure 1 shows atomic force micrographs which demonstrate an enlarged step width (about 2 μm) and height (2 – 4 nm) found for sample B.

The mobility μ and the charge carrier density n are determined by Hall-effect measurements at temperatures between 1.5 K and 300 K. As shown in Figure 2 the mobility (charge carrier density) of sample A decreases (increases) with rising temperature. In contrast for sample B a nearly constant carrier mobility for low temperatures

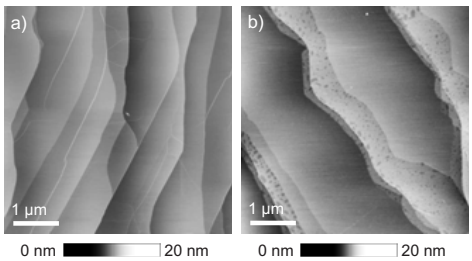

Figure 1: Top-view atomic force micrographs of (a) sample A with a step height of 1 – 2 nm, and (b) sample B with a step height of 2 – 4 nm.

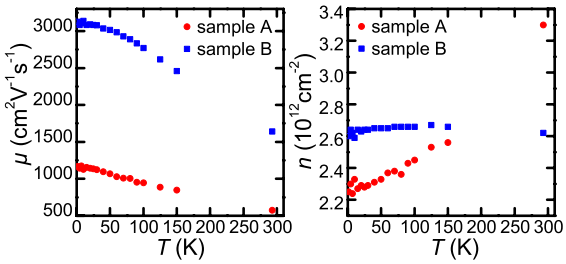

Figure 2: Temperature dependency of the mobility and charge carrier density of sample A (●) and sample B (■).

($T < 30$ K) and a roughly linear decrease for higher temperatures is observed. The carrier density of sample B is constant in the whole temperature range. Up to now the reason for the different temperature dependencies of μ and n is unclear. A possible explanation is a reduced defect density of the substrate under the graphene film for samples annealed in Ar atmosphere close to atmospheric pressure and at lower temperature.

Additionally the electron density, quantum scattering time τ_q and effective mass m^* are determined from Shubnikov-de Haas (SdH) oscillations in magnetic fields up to 15 T. At 4.2 K from sample A only one SdH oscillation period can be resolved which yields to a carrier density of $1 \cdot 10^{12}$ cm^{-2} and an effective mass of $0.05 \cdot m_0$. For sample B a carrier density of $2.5 \cdot 10^{12}$ cm^{-2}, a quantum scattering time of 36 ps and an effective mass of $0.04 \cdot m_0$ are found. The effective mass well agrees with the data for a monolayer of exfoliated graphene [3].

References

[1] T. Ohta *et al.*, New J. Phys. **10**, 023024 (2008).
[2] K.V. Emtsev, *et al.*, Nature Mater. **8**, 203 (2009).
[3] Y. Zhang *et al.*, Nature **438**, 197 (2005).

Localized magnetoplasmons in graphene

Alexander B. Dzyubenko,*,** Andrea M. Fischer*** and Rudolf A. Römer***

*Department of Physics, California State University Bakersfield, Bakersfield, CA 93311, USA

**General Physics Institute, Russian Academy of Sciences, Moscow 119991, Russia

*** Department of Physics and Centre for Scientific Computing, University of Warwick, Coventry CV4 7AL, UK

Keywords: graphene, collective excitations, magnetooptics

We consider collective excitations in graphene with filled Landau levels (LL's) in the presence of an external potential due to a single charged donor D^+ or acceptor A^-. We demonstrate that localized collective modes split off the magnetoplasmon continuum and, in addition, quasibound states are formed within the continuum. As an example, Fig. 1a shows the spectra of magnetoplasmons bound on the D^+ at filling factor $\nu = 1$ (see the inset). We label excitations by angular momentum M_z and give their energies in units of $E_0 = (\pi/2)^{1/2} e^2/\varepsilon l_B$, which is the characteristic energy of Coulomb interactions in strong fields, l_B is the magnetic length. The shaded area of width $0.75E_0$ represents the continuum of extended magnetoplasmons. Quasibound states within the continuum are not shown. Energies are given relative to the cyclotron energy $\hbar\widetilde{\omega}_c = \hbar\omega_c + \delta\hbar\omega_c$, which is renormalized in graphene by Coulomb electron-electron interactions with $\delta\hbar\omega_c \simeq 0.92\, E_0 \sim \sqrt{B}$. We demonstrate that, because of the electron-hole symmetry in graphene, the spectra of collective excitations exhibit the symmetry $D^+ \leftrightarrow A^-$, $M_z \leftrightarrow -M_z$ and $\nu \leftrightarrow 4 - \nu$.

A study of the evolution of the strengths and energies of magneto-optical transitions is performed for integer filling factors $\nu = 1, 2, 3, 4$ of the lowest LL's in two circular polarizations $\sigma^{\pm}$. The states optically active in the σ^- are shown in Fig. 1b by circles with sizes proportional to dipole transition matrix elements $|d_\nu^-|^2$; the diamonds represent optically dark states. We predict, therefore, impurity absorption peaks above as well as below the cyclotron resonance. We show that the single-particle electron-hole symmetry of graphene shows up as a set of the D^+ and A^- magneto-absorption peaks having same energies, but active in *different* circular polarizations. Our work establishes the spectra and the symmetries of collective excitations bound on defects with axial symmetry in graphene in magnetic fields. The results demonstrate the breaking of particle-hole symmetry in a sample with predominantly positively or negatively charged impurities.

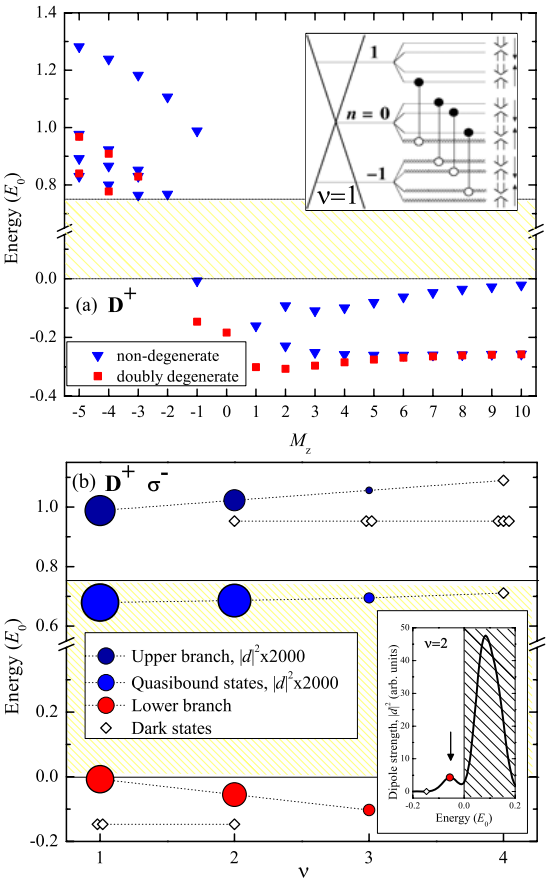

Figure 1: (a) Magnetoplasmons bound on a charged donor D^+ at $\nu = 1$. Inset: four branches of resonantly mixed inter-LL transitions conserving spin and pseudospin. (b) Evolution with ν of energies and optical strengths of magnetoplasmons bound on the D^+ in the σ^- polarization. The dotted lines are guides to the eye. Inset: Dipole strength $|d_\nu^-|^2$ vs energy for $\nu = 2$. The spectra were convoluted with a Gaussian of width $0.03E_0$. The arrow indicates an impurity-related feature below $\hbar\widetilde{\omega}_c$ (below energy zero in the Figure).

Theory for interlayer magnetoresistance in layered Dirac fermion systems: Application to α-(BEDT-TTF)$_2$I$_3$

T. Morinari

Yukawa Institute for Theoretical Physics, Kyoto University, Kyoto, Japan

Keywords: Dirac fermions, interlayer magnetoresistance, α-(BEDT-TTF)$_2$I$_3$

Since the discovery of half-integer quantum Hall effect in graphene[1,2], Dirac fermions in condensed matter systems attract much attention. Although graphene is a purely two-dimensional system, a massless Dirac fermion spectrum is also realized in an organic layered compound, α-(BEDT-TTF)$_2$I$_3$. From tight-binding model calculations, Kobayashi *et al*. [3,4] suggested the presence of a massless Dirac fermion spectrum in this system. The presence of the massless Dirac fermion sepectrum is confirmed by first principle calculations[5]. Experimentally Tajima *et al*. observed [6] that the carrier density varies as the square of temperature, which is consistent with such the spectrum. In addition, negative interlayer magnetoresistance is observed experimentally[7]. The origin of the negative magnetoresistance is associated with the Dirac fermion's zero-energy Landau level as theoretically explained by Osada[8].

For the study of Dirac fermions, α-(BEDT-TTF)$_2$I$_3$. has several advantages. In the ambient pressure, the system is charge-ordered insulator below 135K. The Dirac fermion spectrum is realized under pressure above 2GPa[9]. Because of the presence of the charge-ordered state, electron correlations are important. Furthermore, the system is controlled by pressure. In Dirac fermion systems, there are two Dirac points. In α-(BEDT-TTF)$_2$I$_3$ the distance between these Dirac points are controlled by pressure[4]. Another feature of the Dirac fermion spectrum is large anisotropy because of the tilt of the Dirac cone[10]. On the other hand, there are some disadvantages. Since α-(BEDT-TTF)$_2$I$_3$ is an organic compound, angle resolved photoemission spectroscopy is not applicable to study Dirac fermion spectrum. Shubnikov-de Haas oscillation has not been observed because the Fermi energy is fixed to the Dirac point, and gate voltage control of the chemical potential has not been successful.

In this paper, I propose that the interlayer magnetoresistance is used to determine the parameters characterizing the anisotropic Dirac fermion spectrum. According to the strength of the applied magnetic field perpendicular to the layers, there are two regimes: One is the negative magnetoresistance regime[11] and the other is the positive magnetoresistance regime. Theoretical formulae are derived for both cases, and we discuss applications of the formulae to determine the parameters of the system.

References

1. K. S. Novoselov *et al*., Nature **438**, 197 (2005).
2. Y. B. Zhang *et al*., Nature **438**, 201 (2005).
3. A. Kobayashi *et al*., J. Phys. Soc. Jpn. **73**, 3135. (2004).
4. S. Katayama, A. Kobayashi, and Y. Suzumura: J. Phys. Soc. Jpn. **75**, 054705 (2006).
5. H. Kino and T. Miyazaki: J. Phys. Soc. Jpn. **75**, 034704 (2006).
6. N. Tajima *et al*., J. Phys. Soc. Jpn. **69**, 543 (2000).
7. N. Tajima *et al*., arXiv:0812.0857 (2008).
8. T. Osada: J. Phys. Soc. Jpn. **77**, 084711 (2008).
9. N. Tajima *et al*., J. Phys. Soc. Jpn. **75**, 051010 (2006).
10. A. Kobayashi *et al*.,J. Phys. Soc. Jpn. **76**, 034711 (2007).
11. T. Morinari, T. Himura, and T. Tohyama, J. Phys. Soc. Jpn. **78**, 023704 (2009).

Transition of graphene under one-dimensional electric potentials to semimetallic state

J. H. Ho [1,2], S. J. Tsai [1], Y. H. Chiu [1] and M. F. Lin [1]

1 *Department of Physics, National Cheng Kung University, Tainan, Taiwan*

2 *Institute of Physics, Academia Sinica, Nankang, Taipei, Taiwan*

Keywords: graphene, one-dimensional electric potentials, semimetallic transition

Graphene is an emerging material with promise for developing the next-generation nano devices [1]. In this work, we employ the tight-binding model to study the low-energy electronic structure of graphene under one-dimensional periodic potentials with cosine-type profile. Remarkably, it is found that semiconducting graphene can be made semi-metallic as long as the period is longer enough. Such a transition also accompanies drastic change in energy bands close to the Fermi level (E_F). The originally light-cone structure is replaced with two distinct kinds of valley structures with highly anisotropic energy dispersion.

The particle-hole symmetry is still preserved under 1D modulated potentials, so we illustrate the contour plots of the first conduction band near E_F (Figs. 1(a)-1(d)). The energy dispersion around the Dirac point shows that the group velocity of quasiparticles is strongly renormalized perpendicular to the modulation direction (x) whereas is not renormalized at all parallel to the modulation direction, as shown in Figs. 1(a) and 1(b) [2]. It should be noted that new band crossings occur far away from the Dirac point (Figs. 1(c) and 1(d)), which demonstrate opposite behaviour against the quasiparticles around the Dirac point.

The non-zero density of states at E_F, in connection with the degree of band overlap between conduction and valence bands, serves as an indicator of the semimetallic transition. Referring to Fig. 2(a), $D(\omega=E_F)$ shows a nearly linear variation with the potential strength. On the other hand, a threshold is observed in Fig. 2(b) for the period dependence of $D(\omega=E_F)$.

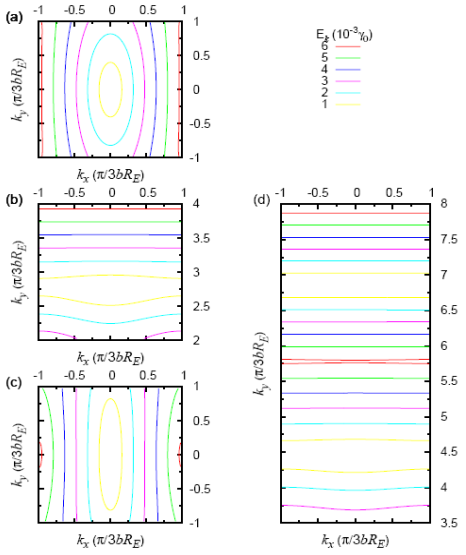

Fig.1 The considered modulated electric potentials are $V_0 = 0.025\ \gamma_0$ and $R_E = 250$ in (a) and (b); and $V_0 = 0.05\ \gamma_0$ and $R_E = 250$ in (c) and (d) , with V_0 being the potential strength and R_E being the period. $\gamma_0 \approx 3$ eV is the nearest hopping integral. The origin of coordinate is

References

1. K. S. Novoselov et al., Science 306, 666 (2004).
2. C.-H. Park et al., Nature Phys. 4, 213 (2008).

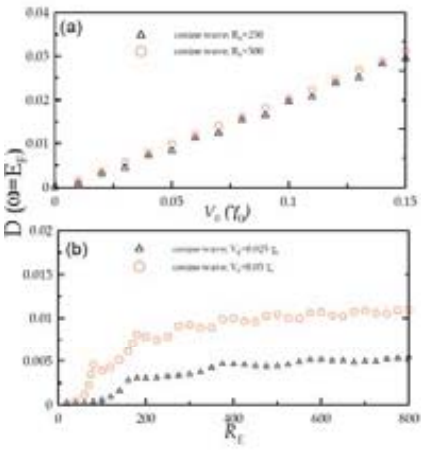

Fig.2 The density of states at E_F versus (a) the potential strength at $R_E = 250$ and 500, and versus (b) the period at $V_0 = 0.025\ \gamma_0$ and $0.05\ \gamma_0$.

Resonance scattering by strong and short-range scatterers in graphene

Atsushi Toyoda and Tsuneya Ando

Department of Physics, Tokyo Institute of Technology,
2–12–1 Ookayama, Meguro-ku, Tokyo 152-8551, Japan

Keywords:graphene, strong, short-range, scattering

Recently direct and clear evidences for the presence of atomic defects in graphene layers were experimentally obtained [1]. The electron scattering by such localized defects in graphene is quite interesting. In fact, the scattering of electrons by vacancies was studied in carbon nanotubes both in a tight-binding model and in an effective-mass approximation and was shown to depend critically on the difference in the number of impurities at A and B sublattices when the strength of the potential is sufficiently large [2, 3, 4, 5]. In this paper effects of impurities with a strong and short-range potential are studied in graphene within a $\mathbf{k}\cdot\mathbf{p}$ scheme.

When the potential strength at each site is much smaller than the width of the π band, effects are described simply by assuming a scattering Hamiltonian obtained by the sum of the potential for A sites located at a certain average A site position and by that for B sites located at an average B site position. Such a scheme has been previously proposed in carbon nanotubes [6]. The situation changes dramatically when the potential becomes stronger, however, and scattering effects depend sensitively on the difference in the number of A and B impurity sites.

For the demonstration, for example, we can consider the electron scattering by a single short-range impurity and an A-B pair of double short-range impurities and show that the feature similar to that in nanotubes is present in graphene. In fact, when the impurity potential becomes sufficiently strong, the scattering strength of a single impurity increases considerably, but the scattering strength of an A-B pair impurity saturates to a small value after taking a resonance enhancement when the potential strength is of the order of the π-band width (see Fig. 1). Similar analysis can be extended to the case of several impurities, giving results with features strongly dependent on the difference in the number of sublattice sites with impurity. This interesting behavior can manifest itself in fluorine or hydrogen-adsorbed graphenes giving rise to a strong local potential.

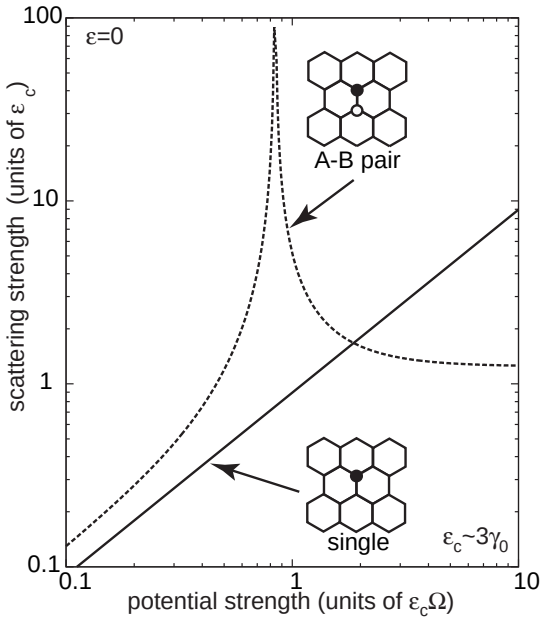

Figure 1: Effective scattering strength of a single impurity and A-B pair impurities as a function of the potential strength.

References

[1] A. Hashimoto, K. Suenaga, A. Gloter, K. Urita, and S. Iijima, Nature **430**,870.(2004).

[2] T. Ando, T. Nakanishi, and M. Igami, J. Phys. Soc. Jpn. **68**, 3994 (1999).

[3] M. Igami, T. Nakanishi, and T. Ando, J. Phys. Soc. Jpn. **68**, 716 (1999).

[4] M. Igami, T. Nakanishi, and T. Ando, J. Phys. Soc. Jpn. **68**, 3146 (1999).

[5] M. Igami, T. Nakanishi, and T. Ando, J. Phys. Soc. Jpn. **70**, 481 (2001).

[6] T. Ando and T. Nakanishi, J. Phys. Soc. Jpn. **67**, 1704 (1998).

Polarized memory effect observed in ZnO nanotube point contact system

P.Liu*,**, G.W.She**, W.S.Shi** and D.M.Chen*
*Institute of Physics, Chinese Academy of Sciences, Beijing, China
**Technical Institute of Physics and Chemistry, Chinese Academy of Science, Beijing, China

Keywords: polarized memory effect, ZnO, nanotube, point contact

In this abstract, we will report the first observation of polarized memory effect (the memory in which switching between ON and OFF states depends on the polarity of the bias voltage)[1] in ZnO nanotube (ZNT) point contact system, with STM technique[2].

Fig.1(A) displays the *I-V* characteristics when sweeping voltage: $0\text{V} \rightarrow +10\text{V} \rightarrow -10\text{V} \rightarrow 0\text{V}$. Initially, from 0 to below 4.03V (O $\rightarrow$ A), the device is in a high resistance (HR) state. At 4.03V, the device promptly switches to a low resistance (LR) state and remains in that state when voltage ramped from 4.03 to 10V (A $\rightarrow$ C). On the return sweep (C $\rightarrow$ O), the device switches back to the HR state at a bias of 0.40V (E). This HR states persists when the bias polarity is changed and only when the amplitude is raised to -0.6V (O $\rightarrow$ F), and the resistance state will switch to LR state and remain so from -0.6V to -10V (F $\rightarrow$ H). On the return sweep (H $\rightarrow$ O), the device switches back to the HR state at a bias of -3.42V (J), exhibiting a hysteresis loop.

Fig.1(B) records a detailed study of the AC switching behavior. We first ramp the voltage from 0 to 5V and the device is in a HR state (black squares in the RHS panel). Next, a 10ms, -10V pulse is applied and the *I-V* curve shows a very small change indicated by the red circles. However, when a 10ms, $+10\text{V}$ pulse is applied, the system switches to a LR state indicated by the green triangles. This effect is independent of measurement polarity, as shown in the LHS panel. That is, a positive (negative) bias pulse leads to LR (HR) states. Thus the AC switching yields the same results as the DC switching.

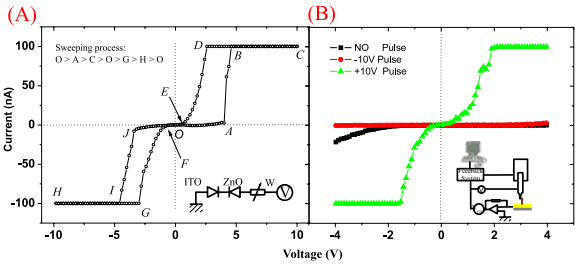

Figure 1: (A) DC switching behavior of ZNT point contact system; inset, equivalent circuit. (B) AC switching behavior; inset, schematic of measurement setup. The flat in $\pm 100nA$ is due to saturation of current amplifier.

In general, the ZNT point contact system can be represented by an equivalent circuit shown in the inset of Fig.1(A). That is, two back-to-back diodes serially connected to a 'resistor' element that can be switched ON/OFF by positive/negative bias. In LR state, the system is two back-to-back diodes with a small 'resistor'. In HR state, most of the voltage is dropped across the 'resistor'.

The switching of the 'resistor' is associated with two important factors. First, this behavior is only found when the probe-ZNT is set to a point contact. Second, the switching is unipolar which suggests that it is a charge related phenomenon. It is therefore reasonable to speculate that the switchable 'resistor' is formed at the probe-ZNT junction. The weak probe-ZNT coupling allows a large electrical filed be established at the junction, which in turn attract or repel charges from some defect states that would move defect levels away or towards the conduction band, respectively. Alternatively, the applied voltage might change the effective width of the barrier layer located at the metal-ZNT interface, *i.e.*, the positive/negative pulses might reduce/increase the barrier layer thickness. The detail nature of these defect states requires further investigation.

References

[1] T. Matsushita, T. Yamagami and M. Okuda: *Jpn. J. Appl. Phys.* **11** 1657 (1972)

[2] P. Liu, GW She, ZL Liao, Y. Wang, ZZ Wang, WS Shi, XH Zhang, ST Lee and DM Chen: *Appl. Phys. Lett.* **94**, 063120 (2009).

Scattering processes in a 2D semimetal

E.B. Olshanetsky*, Z.D. Kvon**, M.V. Entin*, L.I. Magarill**, N.N. Mikhailov*, I.O. Parm*, S.A. Dvoretsky*

* *Institute of Semiconductor Physics, 630090, Novosibirsk, Russia*

***Novosibirsk State University, 630090, Novosibirsk, Russia*

Keywords: HgTe quantum wells, 2D semimetal

It has recently been shown [1] that in undoped HgTe quantum wells with the surface orientation (013) and an inverted structure of the energy bands there exists a two-dimensional semimetal. It has been proposed that this semimetal is formed due to an overlap (by about 10 meV) of the conduction band minimum in the center of the Brilluin zone with two symmetric valence band maxima located off center in the direction [031]. The structures studied in [1] did not have an electrostatic gate and so they were not suitable for the investigation of the properties of a 2D semimetal for various ratios between the electron and hole densities. In the present work using the technology of a low temperature growth of SiO_2 and Si_3N_4 layers on the top of the structures that serve as an insulating layer for the subsequent metallic gate deposition we have been able to fabricate gated samples where by tuning the gate voltage it is possible to study the properties of a 2D semimetal at almost any ratio of electron and hole densities. Some new transport properties of a 2D semimetal have been observed including those associated with the interaction of 2D electrons and 2D holes.

In particular it has been shown that the 2D semimetal resistance temperature dependence at B=0 depends drastically on the presence of 2D holes in the quantum well. Fig.1a shows the temperature dependence of ρ as the gate voltage is swept from 3 to –3 V. One can see that for positive V_g when there are no holes in the QW but only electrons ρ is practically T-independent. At $V_g \leq +0.5$V when the QW begins to be populated with holes ρ becomes T-dependent. This T-dependence was explained as resulting from mutual scattering of electrons and holes in the QW and a corresponding theory is proposed.

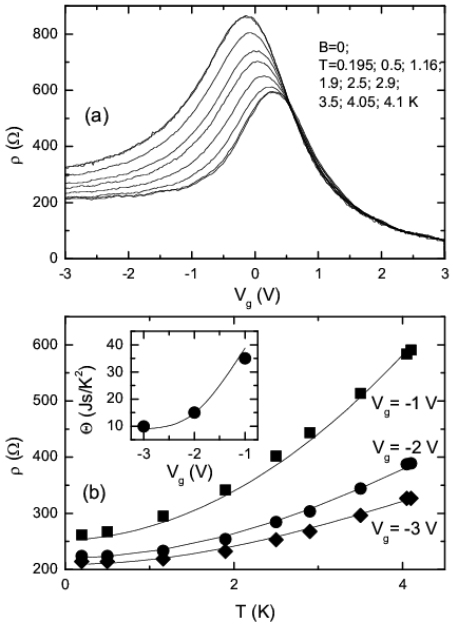

Fig.1 (a)-ρ(V_g) at B=0 and for temperatures in the range T=0.2-4.1 K (temperature increasing from the lower to the upper curve). (b)- Black symbols show the ρ(V_g) dependences obtained from the curves in Fig.1(a) for V_g=-1;-2;-3 V. Black curves are the theory fitting. The insert shows the gate voltage dependence of the fitting parameter Θ (the symbols – experiment, the lines – theory).

References

1. Z.D. Kvon, E.B. Olshanetsky, D.A. Kozlov, N.N. Mikhailov, and S.A. Dvoretskii, JETP Lett., Vol.87, 502 (2008).

Electrical conduction mechanisms in natively doped ZnO nanowires

Shao-Pin Chiu*, Yong-Han Lin** and Juhn-Jong Lin*,**

* *Institute of Physics, National Chiao Tung University, Hsinchu, Taiwan*

** *Department of Electrophysics, National Chiao Tung University, Hsinchu, Taiwan*

Keywords: Zinc oxide nanowires, impurity band conduction, metal-insulator transition

Single-crystalline zinc oxide (ZnO) nanowires (NWs) with diameters of 90–200 nm were synthesized by the thermal evaporation method. Four-probe Ti/Au electrodes were made by the electron-beam lithography technique. Figure 1 shows the intrinsic resistivities, $\rho(T)$, of four individual NWs measured over a wide range of temperature from 300 down to 0.25 K. Between 300 and 5 K, the measured $\rho(T)$ reveals that the intrinsic electrical-transport mechanisms are due to a combination of the thermal activation conduction and the nearest-neighbor hopping conduction processes. Three distinct activation and hopping contributions with discrete characteristic activation energies are observed. Above about 100 K, the charge transport mechanism is dominated by the conduction electrons thermally activated from the Fermi level, E_F, to the conduction band. Between approximately 20 and 100 K, the charge transport mechanism is due to the activation of electrons from E_F to the upper impurity (D^-) band. Between approximately 5 and 20 K, the charge transport mechanism arises from the nearest-neighbor hopping conduction within the lower impurity (D) band. Such unique electrical conduction behaviors can be explained in terms of the intricate material properties (in particular, the presence of moderately high concentrations of n-type defects accompanied with a slight self-compensation) in natively doped ZnO NWs [1]. In one heavily doped NW, a surface-related conduction process manifesting the two-dimensional attributes of quantum-interference (weak-localization) transport phenomena is observed. The carrier concentrations in our NWs have been estimated, and they were found to lie close to the critical concentration for the Mott metal–insulator transition. This work provides for the first time a meaningful explanation for the long-standing and puzzling electronic conduction mechanisms in the academic and industrial alluring ZnO NWs [1].

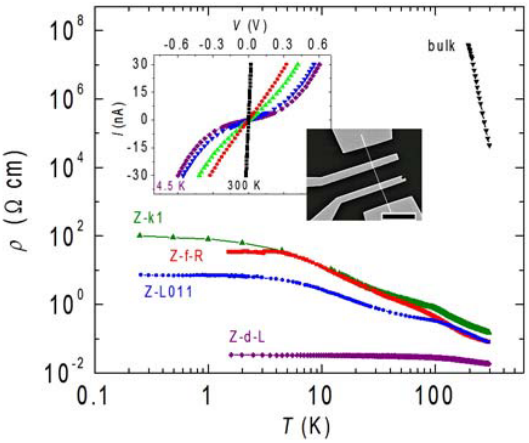

Fig.1 Variation of resistivity with temperature for four ZnO NWs and a bulk ZnO single crystal. The inset shows the current–voltage curves for the Z-k1 NW at 300, 30, 20, 10 and 4.5 K. Also shown is a SEM image for a four-probe NW device fabricated with electron-beam lithography. The scale bar is 5 μm.

References

1. S. P. Chiu, Y. H. Lin and J. J. Lin, Nanotechnology **20**, 015203 (2009).

Magnetoresistance due to potential fluctuation in monolayer graphene at minimum conductivity point

R. Yagi*, S. Fukada*, H. Kobara*, N. Ogita** and M. Udagawa**
*AdSM, Hiroshima University, Higashi-Hiroshima, Japan
** Graduate School of Integrated Arts and Sciences, Hiroshima University, Higashi-Hiroshima, Japan

Keywords: monolayer graphene, magnetoresistance, electron-hole puddles

Magnetotransport at the minimum conductivity point is one of the most interesting issues in monolayer graphene. Lifting of spin and valley degeneracy[1] in high magnetic field, and positive classical magnetoresistance in low magnetic field [2] has been reported. In this work we studied negative magnetoresistance appearing in moderately high magnetic field after the classical positive magnetoresistance disappeared.

Figure 1 shows B- dependence ρ_{xx} at the minimum conductivity point. Negative magnetoresistance appeared above B =2.5 T following positive classical magnetoresistance. The shape of the magnetoresistance was qualitatively different from those for the gate voltages not at the vicinity of the minimum conductivity point. Detailed measurement of V_g- and B- dependence of ρ_{xx} showed that above $B = 2.5$ T Shubnikov-de Haas oscillation for Landau levels $n = 0$ and $n = 1$ could be de clearly observed in V_g- dependence of ρ_{xx} so that transport at the minimum conductivity point is principally due to Landau level with $n = 0$.

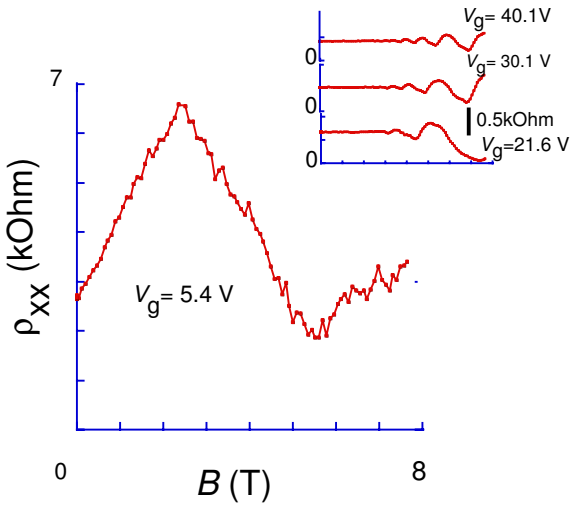

Figure 1: B-dependence of ρ_{xx} of monolayer graphene at the minimum conductivity point. Inset is for gate voltages not at the vicinity of the minimum conductivity point.

A possible origin of the negative magnetoresistance is intrinsic conductance of the Landau level with $n = 0$. Diagonal conductivity for Landau level with $n = 0$ is given in Ref.[3] in self-consistent Born approximation. The theory predicts that the conductance of Landau level with n=0 exhibits B-dependence except at exact Dirac point: the conductance increases with magnetic field and saturates at high field limit. Real graphene devices are in strong influence of local potential fluctuation due to electron-hole puddles created by ionized impurity potential.[4] The local potential fluctuation should result in distribution of energy of Landau levels with $n = 0$. We estimated magnitude of the local potential fluctuation to be about $\pm$20 meV, which is about 40 percent of the energy between Landau levels with $n = 0$ and ± 1 at $B = 2.5$ T where negative magnetoresistance appears.

All the samples that we measured exhibited negative magnetorsistance: large negative magnetoresistance was observed in low mobility samples. This fact is consistent with that the observed phenomenon arises from the inhomogeneity possibly due to the electron-hole puddles.

References

[1] Y. Zhang, Z. Jiang, et al., Phys. Rev. Lett. **96**, 136806 (2006).

[2] S. Cho and M. S. Fuhrer et al., Phys. Rev. B **77**, 081402 (2008).

[3] N. H. Shon and T. Ando, J. Phys. Soc. Jpn. **67**, 2421 (1998).

[4] S. Adam and S. D. Sarma, Solid State Commun, **146**, 356 (2008).

Electron on a Sphere: 2D or not 2D?

Yshai Avishai[1,2]

[1] *Department of Physics, Ben-Gurion University, Beer Sheva 84105, Israel*

[2] *Department of Physics, Hong Kong University of Science and Technology*

Keywords: Electron on a sphere, Tight binding, Topology, Spectrum, Symmetries

In most cases, electron states in two dimensions are subject to periodic boundary conditions, which imply a torus geometry (a genus 1 in the language of Topology). However, two dimensional systems can be realized also in other geometries, such as a sphere (a genus 0). This is not just an academic anecdote, since such a system is realizable e.g by letting an electron hop on the carbon sites of a Fullerene. In what way the pertinent physical results depend on the topology of the two-dimensional system? Moreover, is a system of electron on a sphere should be considered as two dimensional or zero dimensional? These and other questions are studied in the present work, where we analyze a tight binding model for electron on a sphere subject to electric and magnetic fields.

In the first part, calculation of the spectrum in the presence of central magnetic charge g is studied. It should take into account the fact that g is quantized as $g = (hc/2e)n$ where n is the monopole number. This restriction requires a meticulous determination of the phase factors appearing in the hopping matrix elements. Having solved this mathematical problem, the spectrum of the symmetric polytopes (tetrahedron, cube, octahedron, dodecahedron and icosahedron) is calculated analytically and shown to display a beautiful pattern, which is entirely distinct from that of the Hofstadter butterfly. The pattern of level degeneracy is also rather intriguing and poses some challenges to to the theory of point symmetry groups. We also calculate the spectrum of an electron hopping on the sites of the Fullerene, and compare it with the pertinent spectrum of an electron in graphene.

In the second part, the electron spectrum in the central field of an electric charge Q is calculated. The radial electric field induces Rashba type spin-orbit interaction on the hopping electron. In order to construct the Hamiltonian we establish the tight-binding form of the familiar atomic $\mathbf{L}\cdot\mathbf{S}$ interaction. The spectra for the five symmetric polytopes and the Fullerene are calculated as function of the (dimensionless) spin-orbit strength μ and display rich and beautiful patterns with some unexpected symmetries. In particular, if A, B are two adjacent sites on a sphere centered at O and $\Theta = \widehat{AOB}$ then all the energies $E_n(\mu)$ are symmetric with respect to $\mu = \frac{\Theta}{2}$.

Finally, we expose a remarkable relation between the two seemingly distinct physical problems: The spectrum of the second system (electron in the field of central electric charge inducing spin-orbit interaction) at the symmetry point $\mu = \frac{\Theta}{2}$ is found to be identical with the spectrum of the first system (electron in the field of magnetic monopole) at $n = 1$. This means that it is principally possible to test the spectrum of an experimentally inaccessible system (magnetic monopole) in terms of an experimentally accessible one (electron subject to spin-orbit force induced by central electric charge).

Contact resistance in graphene-based devices

M. F. Craciun*, S. Russo*,**, M. Yamamoto*, A. F. Morpurgo*** and S. Tarucha*,****

* *Department of Applied Physics, The University of Tokyo, Tokyo, Japan*

** *Kavli Institute of Nanoscience, Delft University of Technology, Delft, The Netherlands*

*** *Department of Condensed Matter Physics, University of Geneva, Geneva, Switzerland*

**** *Quantum Spin Information Project, ICORP, Japan Science and Technology Agency, Atsugi, Japan*

Keywords: graphene layers, contact resistance

The versatility of graphene-based materials illustrated by the large variety of novel electronic phenomena recently discovered in these systems [1, 2] together with their high carrier mobility makes them promising candidates for electronic applications. Whereas considerable work has focused on the electronic properties of bulk graphene, virtually no experiments have addressed the properties of metal/graphene interfaces. This is somewhat surprising, since these interfaces will unavoidably be present in future electronic device, and may crucially affect their performance. In recently demonstrated single-molecule sensors, for instance, graphene trilayers have been claimed to be better suited than single-layers because of a lower contact resistance, leading to a higher device sensitivity (the measurements of the values of contact resistance, however, were not discussed in any detail - see Ref. [3] and related online supporting material). Not only in the realm of electronic applications, but also for many transport experiments of fundamental interest, the quality of graphene/metal contacts is of crucial importance. For instance, the simplest shot-noise measurements require the use of a two terminal configuration, and it was recently argued that properly taking into account the quality of the contacts is essential to interpret the experimental data correctly [4].

In order to better understand the influence of the contacts we have performed a series of measurements of the contact resistance present at the interface between Ti/Au electrodes and graphene layers of different thickness (single, double and triple layer). The Ti/Au bilayer was chosen because, together with Cr/Au, it is most commonly used as electrode. In addition, in contrast to the Cr interlayer, Ti/graphene interface gives highly transmissive contacts, as demonstrated by the large probability for Andreev reflection reproducibly observed in Josephson junctions with Ti/Al [4].

Our work is based on transport measurements performed on graphene flakes of different thickness on which different kinds of devices were fabricated. Using these devices we succeeded in extracting the value of contact resistance as a function of charge density, using three different methods: through scaling as a function of device length, of device width, and by comparing the resistance values measured in a two and four terminal device configuration. We find that the contact resistance is quantitatively the same for single, double and triple layer graphene (~ 800 Ωμm), and is in all cases independent of charge density and temperature. We argue that the observed behavior is due to charge transfer from the metal, causing the Fermi level in the graphene region under the contacts to shift far away from the charge neutrality point.

References

1. A. K. Geim and K. S. Novoselov, Nature Materials **6**, 183 (2007).
2. K. S. Novoselov, et al., Nature **438**, 197 (2005).
3. F. Schedin, et al., Nature Materials **6**, 652 (2007).
4. J. Cayssol, B. Huard, and D. Goldhaber-Gordon, preprint at http://arxiv.org/abs/0810.4568 (2008).
4. H. H. Heersche, et al, Nature **446**, 56 (2007).

Superconducting proximity effect through single-layer and multilayer graphene films

M. Hayashi*, H. Yoshioka** and A. Kanda***

*Faculty of Education and Human Studies, Akita University, Akita 010-8502, Japan

** Department of Physics, Nara Women's University, Nara 630-8506, Japan

***Institute of Physics, University of Tsukuba, Tsukuba305-8571, Japan

Keywords: graphene, superconductivity, proximity effect

We discuss the superconducting proximity effect in graphite films (or graphene) by studying the critical current through superconductor-graphite film (or graphene)-superconductor Josephson junction. The two leads are assumed to be conventional s-wave superconductors. We especially pay attention to the dispersions of electrons in graphite films: because of the delicate band structure of graphite, the electron dispersion in the film, which undergoes the effects of various external factors such as leads, gate electrodes and sample inhomogeneities, can show a wide variety. We introduce several models for electrons in the film: 1) graphene-like (Fermi points), 2) zero-gap semiconductor (graphen double layers), and 3) gapped semiconductor. The superconducting critical current I_c through the junction can be estimated from the coupling energy of two superconducting leads,

$$F_J = -2t^4 T (N_F S)^2 \times \mathrm{Re}\left[\frac{(\pi\Delta)^2 e^{-i\theta}}{(\pi T)^2+\Delta^2}\left\{|J(i\pi T)|^2 + |J(-i\pi T)|^2\right\}\right]$$

where t and T are tunneling matrix element between film and leads and temperature, respectively. N_F, Δ and θ are the density of states at Fermi energy, the gap, and the phase difference of two superconductors. S is the area of the film. The critical current is usually expressed as $I_c \propto \exp\{-d/\xi(T)\}$, where d is the distance between two leads and $\xi(T)$ is the proximity length. We show that the temperature dependence of $\xi(T)$ is largely affected by the band structure of the graphite film and by examining this dependence some insight into the electronic properties of the graphite film can be obtained.

In case of single layer graphen (Fermi point dispersion), we obtain,

$$|J(i\pi T)|^2 \propto K_0(\pi T d/C)^2 \sim \exp(-2\pi T d/C)$$

($d \to \infty$) where $K_0(z)$ is the modified Bessel function and we have assumed the dispersion at the Fermi point to be $\varepsilon = C|\vec{l}|$, where C is a constant and $\vec{l}$ is the wave vector measured from the Fermi point. Here $\xi(T) \propto 1/T$ which coincide with the case of the normal-metal proximity effect.

In case of the zero-gap semiconductors, the behavior of $|J(i\pi T)|$ as a function of d and T is rather complicated and sometimes shows oscillating behavior as one can see from the numerical estimation shown in Fig. 1.

I case of the gapped semiconductors, the coherence length saturates $\xi(T) < \infty$ even at $T \to 0$.

We also discuss how these phenomena can be observed in actual experiments.

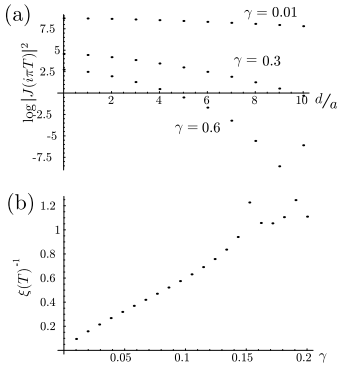

Figure 1: (a) $\log|J(i\pi T)|^2$ of the zero-gap semiconductor case (a is the lattice spacing and $\gamma = \pi T/C'$ where C' is the curvature at Fermi point) (b) $\xi(T)^{-1}$ as a function of γ.

References

[1] Masahiko Hayashi, Hideo Yoshioka and Akinobu Kanda, Journal of Physics: Conference Series **109**, 012014 (2008).

Impurity-induced valley mixing of excitons in semiconducting carbon nanotubes

Yuh Tomio and Hidekatsu Suzuura
Division of Applied Physics, Graduate School of Engineering, Hokkaido University, Sapporo, Japan

Keywords: carbon nanotube, exciton, effective mass theory, impurity scattering

Carbon nanotubes (CN's) have attracted much attentions for their unique physical properties [1, 2] since the discovery, and therefore many experimental and theoretical studies have been dedicated from viewpoints of both fundamental and applied science. Optical properties of CN's, particularly, are interesting because of the strong enhancement of exciton effects arising from the Coulomb interaction and the one-dimensional nature. The main aim of our study is to examine effects of local potential such as defects and impurities on optical spectra in semiconducting CN's. We clarify how energy levels of optically active (bright) and inactive (dark) excitons are split by an impurity scattering within the effective-mass approximation and perturbation theory for the local potential.

In the $\boldsymbol{k}\cdot\boldsymbol{p}$ approximation, the exciton state is expressed by $|\mathrm{K_1K_2}\rangle_q = \sum_{n,k}\psi_n^{\mathrm{K_1K_2}}(k)c^{\mathrm{K_1}\dagger}_{+,n,k+q/2}c^{\mathrm{K_2}}_{-,n,k-q/2}|g\rangle$ where $\mathrm{K_1, K_2}$ = K or K′, $c^{\mathrm{K_1}\dagger}_{+,n,k}$ ($c^{\mathrm{K_2}}_{-,n,k}$) is the electron creation (annihilation) operator in the conduction (valence) band specified by the index n of the $\mathrm{K_1}$ ($\mathrm{K_2}$) valley with the wave vector k in the axis direction, and $|g\rangle$ is the ground state wave function. The excitons $|\mathrm{KK}\rangle_0$ and $|\mathrm{K'K'}\rangle_0$ can be coupled to photons because of momentum conservation. Therefore, only bonding state $|b1\rangle_0 = (|\mathrm{KK}\rangle_0 + |\mathrm{K'K'}\rangle_0)/\sqrt{2}$ is optically active and all the others, $|b1\rangle_{q\neq 0}$, $|a1\rangle_q = (|\mathrm{KK}\rangle_q - |\mathrm{K'K'}\rangle_q)/\sqrt{2}$, $|b2\rangle_q = (|\mathrm{KK'}\rangle_q + |\mathrm{K'K}\rangle_q)/\sqrt{2}$ and $|a2\rangle_q = (|\mathrm{KK'}\rangle_q - |\mathrm{K'K}\rangle_q)/\sqrt{2}$, are optically inactive in the absence of a magnetic flux. These exciton states are generally split into several levels due to the Coulomb exchange interaction.

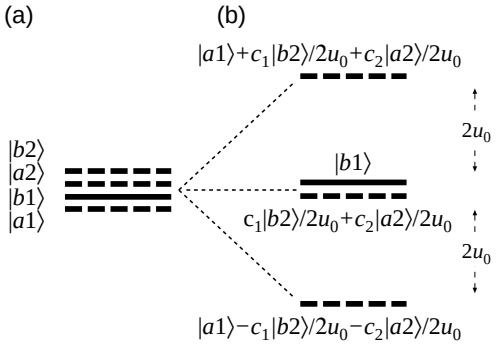

Figure 1: Schematic of exciton energy levels for $q = 0$ or $n = 0$, (a) without impurity scattering and (b) with impurity scattering, where $c_1 = 2u_0\cos(2\pi/3+\eta)$, $c_2 = -2iu_0\sin(2\pi/3+\eta)$. Note that a shift of the whole energy levels is subtracted in (b).

Now we shall introduce an impurity potential $U(\boldsymbol{r})$ whose range is smaller than the lattice constant, which makes inter-valley electron scattering between the K and K' valleys dominant [2], and hence gives rise to mixing between KK/K′K′ and KK′/K′K excitons. If $U(\boldsymbol{r})$ is described by the delta function $u_0\delta(\boldsymbol{r})$ located at a carbon B site at the origin and has an isotropic symmetry, the matrix elements are, e.g., given by ${}_q\langle b2|\hat{U}|b1\rangle_0 = 2u_0\cos(2\pi/3+\eta)\sum_{n,k}[\psi_n^{\mathrm{KK'}}(k-q/2)\psi_n^{\mathrm{KK}}(k) - \psi_n^{\mathrm{KK'}}(k+q/2)\psi_n^{\mathrm{K'K'}}(k)]$ with η being the chiral angle, etc. These provide the following two key insights within the lowest order perturbation theory: (i) The inter-valley KK′/K′K exciton may become optically allowed for $q \neq 0$ and $n \neq 0$, while it remains inactive for the lowest optical transition (E_{11}) because there is no coupling to $|b1\rangle_0$ (resulting from $\psi_0^{\mathrm{KK'}}(k) = \psi_0^{\mathrm{KK}}(k)$), as shown in Fig. 1. (ii) The potential anisotropy also may allow the KK′/K′K exciton to be optically observed even for $q = 0$ or E_{11} transitions.

The absorption spectra including the effects of impurities will be discussed on the basis of the above considerations, as well as the higher order contribution and anisotropy of impurity scattering.

References

[1] R. Saito, *et al.*, *Physical Properties of Carbon Nanotubes* (Imperial College Press, London, 1998).

[2] T. Ando, J. Phys. Soc. Jpn. **74**, 777 (2005).

Electronic properties of Nanographene

Kazuyuki Takai, Ken-ichi Sakai, Yasuyuki Nishimura, and Toshiaki Enoki

Department of Chemistry, Tokyo Institute of Technology, Meguro-ku, Japan

Keywords: graphene edge, nano-lithography, edge state, magnetotransport

Like other materials, nano-size effect is interesting on graphene. Indeed, nano-sized graphene (nanographene) has been known to have enhanced magnetism in spite of its non-magnetic nature in its bulk form [1, 2, 3]. When a graphene sheet is cut along the zigzag direction, strongly spin-polarized non-bonding π-state (edge state) with flat band dispersion appears along the created edges, in spite that cutting along the armchair direction produces no such state. Meantime, the presence of edges gives graphene the potential to control its electronic properties through the chemical modification. Here, I present the novel magnetic and magnetotransport properties of nanographene and its assembly systems, and tuning its electronic properties though chemical modification. For fabricating single nanographene sample, the nano-patterned gold mask was fabricated on graphene sample prepared by cleaving method, where oxygen plasma was used for etching process. Through this process, nanographene sample (ribbons, grids, dots) with the size down to 50 nm was successfully fabricated. On the other hand, magnetism of graphene and its chemical modification effect was examined by using nanographene network material (activate carbon fibers; ACFs).

The magnetotransport measurement reveals the electronic structure of nanographe similar to bulk graphene through SdH oscillation analysis far from the Dirac point. However, in the vicinity of the Dirac point, SdH signal is much modified and indicates the presence of the large Fermi surface, suggesting the significant influence of the edge states on the electronic strucuture nanographene at the Dirac point. Magnetic susceptibility of nanographene with 2 -3 nm shows localized spin magnetism feature with Curie-Weiss type temperature dependence, which is attributed to the edge-state spin [2, 3]. On the other hand, the orbital diamagnetism is much suppressed by the reduction in size of systems, which is major feature of the magnetism of bulk graphene

The chemical modification features the peculiar character of the edge-state spin magnetism well. In the lower fluorine concentration of F/C~0.4, the reaction with fluorine atoms takes place mainly around the edges of nanographene due to its chemical activity, resulting in the decreasing in the concentration of edge state spins. The spin polarization of the edge state is suppressed through bending of the flat band of edge state caused by electron nature of fluorine terminating the edge sites. The chemical modification of the nanographene edge by bromine gives other interesting aspect of the edge-state spin magnetism. By terminating the edge of nanographene with bromine, the edge-state slightly hybridizes with the bromine orbital as suggested by the hyper fine broadening in the ESR line width, followed by the gradual reduction in the g-value as bromine content increases [6]. This suggests the tunable nature of the spin-orbit coupling in nanographene by the chemical modification.

The present study is partially supported by by MEXT Nanotechnology Network Project in the Tokyo Institute of Technology.

References

[1] M. Fujita, K. Wakabayashi, K. Nakada, and K. Kusakabe, J. Phys. Soc. Jpn. 65, 1920 (1996).

[2] T. Enoki, K. Takai, "Unconventional magnetic properties of nanographite" (Carbon-based magnetism, p. 397, ed. F. Palacio and T. Makarova, Elsevier, Amsterdam, 2006).

[3] T. Enoki, K. Takai, Dalton Trans., 3773 (2008)

[4] K. Kusakabe and M. Maruyama, Phys. Rev. B67, 092406 (2003).

[5] K. Takai, H. Sato, T. Enoki, N. Yoshida, F. Okino, H. Touhara, and M. Endo, J. Phys. Soc. Jpn., 70, 175 (2001).

[6] K. Takai, H. Kumagai, H. Sato, and T. Enoki, Phys. Rev. B 73, 035435 (2006)

Terahertz/far-infrared lasing by utilization of population inversion in graphene under optical pumping

A. Satou*, V. Ryzhii*, F. T. Vasko**, T. Otsuji***, V. Ya. Aleshkin****, and A. A. Dubinov****
*Computational Nanoelectronics Laboratory, University of Aizu, Aizu-Wakamatsu 965-9580, Japan
** Institute of Semiconductor Physics, NAS of Ukraine, Kiev 03028, Ukraine
*** Research Institute of Electrical Communication, Tohoku University, Sendai 980-8577, Japan
**** Institute for Physics of Microstructures RAS, 603950 Nizhny Novgorod, Russia

Keywords: Graphene, population inversion, terahertz, lasing

The features of the dynamics of electrons and holes in different graphene-based structures (graphene, graphene nanoribbons, and graphene bilayer) are of great interest for device applications. In particular, their peculiar energy spectrum can be utilized in novel optoelectronic devices in terahertz (THz)/far-infrared (IR) range [1, 2, 3]. It has been suggested recently that the optical pumping of graphene and graphene bilayer by mid-IR/near-IR light can result in the population inversion and, consequently, can lead to THz/far-IR lasing [1, 2, 4, 5]. Under the optical pumping, photoexcited carriers in graphene immediately emit cascade of optical phonons with energy $\hbar\omega_o \simeq 198$ meV, and they are accumulated near the Dirac point if the pumping photon energy is close to even multiple of $\hbar\omega_o$. Since the value of carrier distribution functions at the Dirac point in intrinsic graphene in equilibrium is one half, the pumping can easily give rise to the population inversion.

In this paper, we consider the carrier distributions in graphene under the optical pumping in two limiting cases: (1) carrier-carrier collisions are dominant and (2) these collisions are relatively ineffective. For the first case, those collisions establish the Fermi distributions of carriers with nonzero Fermi energy determined by the pumping power. For the second case, we solve numerically the kinetic equation for the distributions which accounts for the energy relaxation due to scattering on quasi-elastic acoustic phonon process and thermal radiative generation and recombination processes. In both cases, we show that the optical pumping results in the population inversion in THz/far-IR range. The carrier distributions in the case (2) with the lattice temperature $T = 77$ K, the pumping energy $\hbar\Omega = 830$ meV, and with several values of pumping power S are shown in Fig. 1.

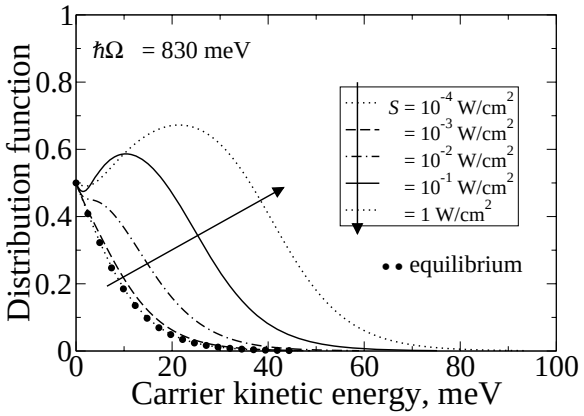

Figure 1: Distribution function of carriers in graphene under optical pumping.

We also calculate the dynamic conductivity taking into account both inter and intraband (Drude-like) absorption of pumping photons and show that the dynamic conductivity can be negative due to the population inversion. We assess the feasibility of the lasing by considering the energy loss of generated electromagnetic waves by media surrounding the graphene layer.

References

[1] V. Ryzhii, M. Ryzhii, and T. Otsuji, J. Appl. Phys. **101**, 083114 (2007).

[2] F. Rana, IEEE Trans. Nanotechnol. **7**, 91 (2008).

[3] V. Ryzhii, V. Mitin, M. Ryzhii, N. Ryabova, and T. Otsuji, Appl. Phys. Express **1**, No. 6 (2008).

[4] A. Satou, F. T. Vasko, and V. Ryzhii, Phys. Rev. B **78**, 11531 (2008).

[5] V. Ya. Aleshkin, A. A. Dubinov, and V. Ryzhii, JETP Lett. **89**, 70 (2009).

Temperature and current-dependent dephasing in an Aharonov-Bohm ring

Kuan-Ting Lin*, Yiping Lin*, C. C. Chi*, J. C. Chen*, T. Ueda** and S. Komiyama**

** Department of Physics, National Tsing Hua University, Hsinchu, Taiwan*

*** Department of Basic Science, University of Tokyo, Komaba, Tokyo, Japan*

Keywords: Aharonov-Bohm ring, dephasing mechanism, Landauer-Büttiker formula

We report an experimental observation of how the temperature T and the driven current I affect the dephasing rate in a multi-mode ballistic Aharonov-Bohm (AB) ring defined on a GaAs/AlGaAs heterostructure with a two-dimensional electron gas. The main dephasing sources in ballistic conductors are attributed to thermal averaging effect and electron-electron (e-e) interactions. Recent studies reveal that the internal potential fluctuations induced by the charge fluctuation between the metal gate and the arms of the ring play a dominated role in dephasing [1,2]. Consequently, the dephasing rate τ_ϕ^{-1} is linear in temperature and depends on the probe configurations.

To investigate the intrinsic dephasing mechanism, we fabricated a ballistic AB ring without the external gates in situ the ring as shown in Fig. 1. The salient feature of our device is the contact leads are made such that the device size (~15μm) is less than the phase coherence length l_ϕ.

Fig. 2(a) shows that $\tau_\phi^{-1} \propto T$ in different probe configurations consisted with previous experiments. In contrast, the dephasing rate is found insensitive to the measurement circuits. It suggests that $\tau_\phi^{-1} \propto T$ is the nature dephasing behaviour. The slope (~0.7 K^{-1}) of the fit line in Fig. 2(a) is within the thermal broadening range. Fig. 2(b) shows that the increasing of applied current strongly reduces AB signals; intriguingly τ_ϕ^{-1} increases in the larger I and still linear to T. Moreover, the saturation is still there. Our findings can be interpreted by including nonlinear transport in the thermal averaging effect. We will emphasize that beyond the low temperature saturation region the thermal averaging effect is the major dephasing source in a ballistic conductor.

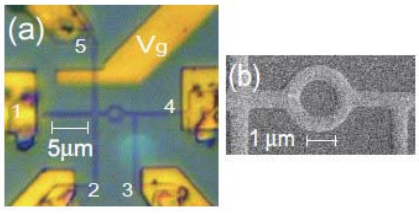

Fig.1 (a) An optical micrograph of one of the devices used in the experiment. (b) SEM picture of the ring structure.

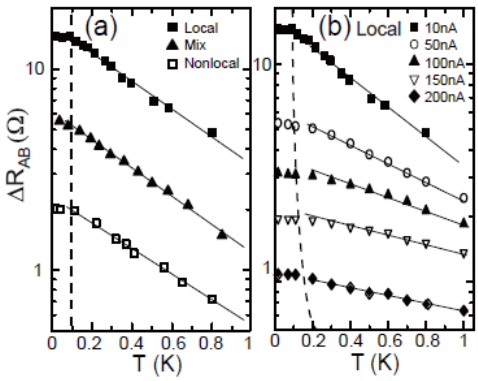

Fig.2 Temperature dependence of the AB amplitude ΔR_{AB} for (a) various probe configurations. (b) various biasing currents in local configuration. The solid lines are the results of the fitting to the exponential decay of temperatures. The dash line indicates the border of ΔR_{AB} saturation..

References

[1] Seelig, G. and Pilgram, S. and Jordan, A. N. and Büttiker, M., Phys. Rev. B **68**, 161310 (2003).

[2] K. Kobayashi, H. Aikawa, S. Katsumoto, and Y. Iye, J. Phys. Soc. Jpn **71**, 2094 (2002).

Two photon laser emission from a quantum dot in a cavity

E. del Valle*, S. Zippilli**, A. Gonzalez-Tudela*, F.P. Laussy***, G. Morigi**, C. Tejedor*

* *Departamento Fisica Teorica Materia Condensada, Universidad Autonoma Madrid, Madrid, Spain*

** *Departament Fisica, Universidad Autonoma Barcelona, Barcelona, Spain*

*** *School of Physics and Astronomy, University of Southampton, Southampton, UK.*

Keywords: Laser emission, Quantum dots, Optical cavity.

We use a generalized Jaynes-Cummings Hamiltonian [1] to study the two photon (2P) versus one photon (1P) lasing emission from a semiconductor microcavity containing one quantum dot (QD) in strong coupling with one of the photonic modes. In this system, a 2PR can be induced when the cavity energy ω_a is half the biexciton total energy, $\omega_B \cong 2\omega_a$. At the same time, in order to suppress one photon processes, the single exciton energies should be greatly detuned from the cavity mode. This is possible experimentally thanks to the biexciton binding energy. In such a configuration there is no destructive interference between the two 2P emission processes. Second order resonant 2P Rabi oscillations can become much larger than the first order off-resonance 1P oscillations as detuning is increased. We analyze this competition by deriving the effective Hamiltonian at large detuning and finding the 1P and 2P resonances. We study this system in the steady state under a continuous incoherent pump of the QD. This pumping mechanism, corresponding to carrier excitation at high energies with subsequent incoherent relaxation into the dot, is the one most widely applied in semiconductors experiments. In order to characterize the emission properties in the steady state and compare the 1P and 2P resonance situations, we must adapt all the proposals made in atomic physics to our system. We discuss the change in the intensity of the cavity emission when the cavity mode is tuned in and out the 1P and 2P resonances, and the effect on the QD level populations. Finally, we compute exactly first and second order correlations functions and the luminescence spectrum, applying master equation techniques and the quantum regression theorem [1]. By Fourier-transforming the first order correlation function we get spectra as that shown in figure 1.

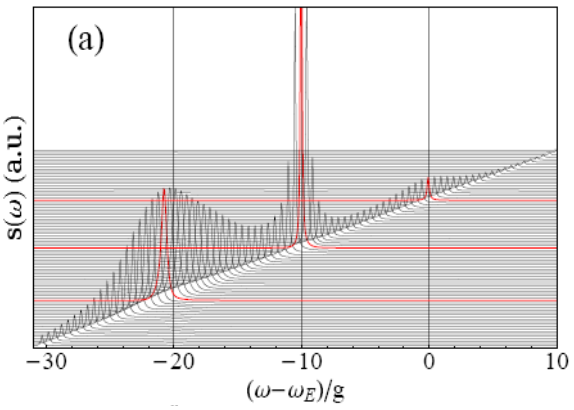

Fig.1 Set of cavity spectra for a typical set of parameters with a pumping rate equal to the coupling between excitons and cavity modes. The cases corresponding to the three resonances are highlighted in thick red (from top to bottom): $\Delta = 0$ (1PR), $\Delta = 20g$ (2PR) and $\Delta = 40g$ (1PR).

In order to characterize 2P laser as different from the 1P one, we use either the so-called *differential correlation function* at zero delay, $C^{(2)}$, or the *Fano factor* which are variations of the second order correlation function $g^{(2)}$.

References

[1] E. del Valle, S. Zippilli, A. Gonzalez-Tudela, F.P. Laussy, G. Morigi, C. Tejedor, to be published.

A high speed radio-frequency quantum point contact charge detector for time resolved readout applications of spin qubits

J.D. Mason[1,3], L. Gaudreau[2,4], S.A. Studenikin[2], A. Kam[2], A.S. Sachrajda[2], J.B. Kycia[1,3]

[1]*Department of Physics and Astronomy, University of Waterloo, Waterloo, Ontario, Canada*

[2]*Institute for Microstructural Sciences, National Research Council, Ottawa, Ontario, Canada*

[3]*Institute for Quantum Computing, University of Waterloo, Waterloo, Ontario, Canada*

[4]*Régroupement Québécois sur les Matériaux de Pointe*, *Université de Sherbrooke, Québec, Canada*

Keywords: spin qubit, readout, quantum point contact, quantum dot

Time resolved charge detection is one of the most important tools for measuring spin qubits [1]. Standard systems, for example, measuring changes in the current through a quantum point contact, operate successfully down to about 20 microseconds. To be able to approach timescales shorter than the T2 decoherence time, one needs other approaches. We are implementing a radio-frequency quantum point contact (rf-QPC) charge detector which measures reflected power from a resonant tank circuit [2, 3]. This scheme utilizes an LC resonator to transform the resistance of the QPC to a value close to the 50 ohm cable impedance. In this way, radio-frequency components can be used which allow the resolution of changes in charge at a 50 nanosecond timescale. We determine the state of the quantum dot system by measuring the signal reflected off of the circuit composed of the QPC resistance and the LC resonator. This present circuit has a resonance frequency of 1 GHz allowing the use of an isolator which reduces the influence of the HEMT amplifier noise on the quantum dot system. A lithographically patterned LC resonator reduces the parasitic capacitance allowing optimal impedance transformation. A push to even higher frequencies is being made allowing small microwave components to be used in the cryostat. A detailed description of the measurement configuration and the preliminary measurements of the rf-QPC coupled to a quantum dot device will be presented.

References

1. J. M. Elzerman, R. Hanson, L. H. Willems van Beveren, B. Witkamp, L. M. K. Vandersypen, L. P. Kouwenhoven, Nature **430**, 431 (2004).

2. R. J. Schoelkopf, P. Wahlgren, A. A. Kozhevnikov, P. Delsing, D. E. Prober, Science **280**, 1238 (1998).

3. D. J. Reilly, C. M. Marcus, M. P. Hanson, A. C. Gossard, Appl. Phys. Lett. **91**, 162101 (2007).

Towards the generation of indistinguishable photons from non-identical artificial molecules

E. Cancellieri[1,2], F. Troiani[1] and G. Goldoni[3]

[1] *S3 CNR-INFM, Modena, Italy*

[2] *Departamento de Fisica Teorica de la Materia Condensada, Universidad Autonoma de Madrid*

[3] *Dipartimento di Fisica, Università di Modena e Reggio Emilia, Modena, Italy*

Keywords: Quantum Dots, Indistinguishable Photons, Quantum Information

Single-photon sources (SPSs) are fundamental building blocks of quantum communication and linear-optics quantum computation. A SPS, essentially, consists of an atomic-like system that can be deterministically excited and thus triggered to emit single-photons wave-packets into a preferred mode. In addition, all photons have to be emitted in the same quantum state in order to make two-photon interference possible. Antibunched emission has been recently observed in solid-state systems, based on the use either of vacancies, molecules, or mesoscopic heterostructures. The latter, specifically consisting in semiconductor quantum dots (QDs), are particularly attractive due to the increasing degree of accuracy whit which they can be coupled to different kinds of optical microcavities, thus forming monolithic and in principle scalable arrays. As a major downside, however, self-assembled QDs come with a finite dispersion in terms of size, shape, and composition. This results in spectral inhomogeneities in the meV range. i.e., orders of magnitude larger than the homogeneous linewidth of the lower exciton transitions: photons emitted by different QDs thus tend to be distinguishable which severely limits the source scalability.

In this contribution we show that in devices based on cavity-coupled QDs, photons indistinguishability can be greatly improved with respect to current upper bounds [1,2,3]. We simulate the time evolution of the dot-cavity system and compute the coherence functions of the emitted light by means of a density-matrix approach. The emitted photon indistinguishability is quantified by the coincidence probability in a Hong-Ou-Mandel setup, and maximized by optimizing the driving fields, through an evolutionary programming approach [4]. In particular we consider the case where each photon source is represented by two vertically stacked self-assembled QDs (often referred to as *artificial molecules*).

We find that the use of virtual Raman transition together with the optimization of the external driving fields increases the tolerance to spectral inhomogeneity to the meV energy range. A trade-off however emerges between photon indistinguishability and efficiency in the photon-generation process. Linear (quadratic) dependence of the coincidence probability is found with respect to dephasing (non-radiative relaxation) rate in the artificial molecule. Possible implications for the entanglement of spins in remote (and non-identical) dots are discussed.

References

1. C. Santori, D. Fattal, J. Vuckovic, G. Solomon, and Y. Yamamoto *Nature* **419**, 594 (2002).
2. A. Kiraz, M. Atature, and A. Imamoglu, *Phys. Rev. A* **69**, 32305 (2004).
3. F. Troiani, I. Wilson-Rae, and C. Tejedor, *Appl. Phys. Lett* **90**, 140103 (2007).
4. Z. Michalewicz, *Genetic Algorithms + Data Sturctures = Evolutionary Programming* (Springer-Verlag, Berlin, 1992).

High sensitivity charge detection and dephasing in edge state interferometer

P. K. Pathak*, Youngnae Lee** and Kicheon Kang**

**Department of Physics, Queen's University, Kingston, ON K7L 3N6, Canada*

*** Department of Physics, Chonnam National University, Gwangju 500-757, Republic of Korea*

Keywords: mesoscopic systems, transport and tunneling

Measurement of the charge-state of a mesoscopic system has generated lot of interest in recent years [1, 2]. Mesoscopic devices such as quantum point contact (QPC) and single electron transistor (SET) have been widely used as the charge detectors. These detectors do not perform instantaneous measurement, but the measurement is performed as a sequence of continuous weak measurements [3]. The quantum mechanical complementarity establishes a trade-off between acquisition of information about the state of the system and the back-action dephasing. A detector is called quantum-limited if the dephasing occurred in the measured system is only due to the acquisition of information by the detector [4]. The improvements in measurements can be accomplished by developing methods that rely on properties like entanglement [5].

We propose an interferometry model of a high sensitivity charge detector in the integer quantum Hall regime. Our model is an electronic analog of Fabry-Perot interferometer. We show that the charge sensitivity of our model is higher than a two-path interferometer due to multiple reflections of electrons at QPCs. We report the possibility of tuning the interferometer for quantum limited measurement for $R_a < R_b$, where R_a (R_b) is reflection probability of quantum point contact QPC$_a$ (QPC$_b$) (cf.Fig.1). For $R_a > R_b$, dephasing rate is always larger than the measurement rate. On the other hand, for $R_a < R_b$, the measurement rate is equal to the dephasing rate at $\Phi_0 \simeq \pm\cos^{-1}\sqrt{R_a/R_b}$, where Φ_0 is phase difference between two possible paths of electron in the interferometer. These points are symmetrically placed on both sides of resonance.We note that, two-path interferometer with edge channel has been realized [6], which is an electronic analogue of the optical Mach-Zehnder interferometer.

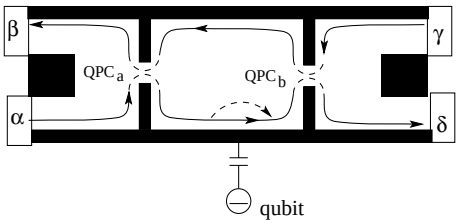

Figure 1: The schematic arrangement for measurement of charge qubit. Two spatially separated point contacts form the Fabry-Perot interferometer. The qubit is capacitively attached in one arm of the interferometer.

Next, we discuss improvement in sensitivity using quantum entanglement. For our purpose we consider spin entangled singlet pairs injected through identically biased input terminals α and γ. For input entangled singlet state, electrons show bunching behavior and the current shot noise in the interferometer is enhanced [7]. Electron bunching, in turn, leads to improvement in sensitivity. We find that the charge sensitivity (per electron) of the interferometer is enhanced by a factor of two, and argue that it originates from the entanglement.

References

[1] S. A. Gurvitz, Phys. Rev. B **56**, 15215 (1997); A. N. Korotkov, *ibid.* **60**, 5737 (1999).

[2] D.-I. Chang *et al.*, Nature Physics **4**, 205 (2008).

[3] A. N. Korotkov and D. V. Averin, Phys. Rev. B **64**, 165310 (2001).

[4] D. V. Averin and E. V. Sukhorukov, Phys. Rev. Lett. **95**, 126803 (2005).

[5] Y. Lee, G. L. Khym, and K. Kang, J. Phys.: Condens. Matter **20**, 395212 (2008).

[6] Y. Ji, *et al.*, Nature(London) **422**, 415 (2003); I. Neder, *et al.*, Nature(London) **448**, 333 (2007).

[7] G. Burkard *et al.*, Phys. Rev. B **61**, R16 303 (2000).

Two-dimensional device model for staggered-type organic thin-film transistors

C.-W. Sohn*, T.-U. Rim* and Y.-H. Jeong*, **

* *Department of Electronic and Electrical Engineering, Pohang University of Science and Technology, Korea*

** *National Center for Nanomaterials Technology (NCNT), Pohang, Gyeongbuk, Korea*

Keywords: Current crowding, organic thin film transistor, space charge limited conduction, staggered type, two dimensional model, variable range hopping

Organic thin-film transistors (OTFTs) have been studied for various applications such as electrophoretic display (EPD), radio frequency identification (RFID) tags, and large-area sensors. Even though much improvement is accomplished in the aspect of electrical performance, stability, and processing technology, device physics of OTFTs is not fully understood, i.e., the carrier transport mechanism in OTFTs, the charge injection process between metal and organic materials, etc. Applying a model without physical basis may result in misleading the experimental analysis.

In this paper, we propose a device model for staggered-type OTFTs, in which the source-drain contact is placed on the opposite side to the insulator-semiconductor interface. By the nature of current flow, the device is divided into three regions: source, channel, and drain (see inset of Fig. 1). Current-voltage equation for channel region is simply derived from the variable range hopping (VRH) theory [1]. In the theory, charge carriers transport by thermally activated tunnelling between localized states of which distribution is assumed to be spatially uniform and energetically exponential. Current-voltage equations for source and drain regions are derived by coupling two orthogonal currents with the current crowding model. While the current parallel to the interface still follows the VRH theory, the current density perpendicular to the interface may be described as either ohmic behaviour or space-charge-limited conduction (SCLC) with or without traps [2]. Those current-voltage equations are solved simultaneously by the circuit analysis program to yield the same current.

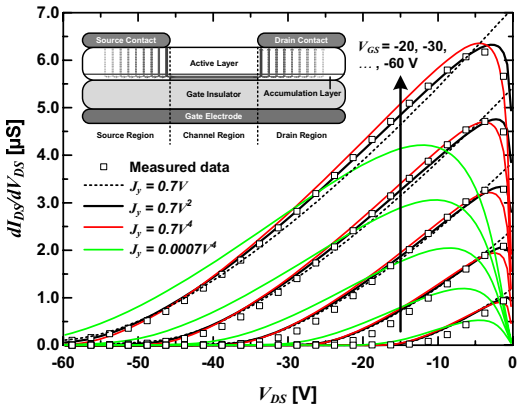

Fig.1 Comparison of the simulation results with the measured data in the differential conductance from output characteristics. The inset shows a schematic diagram of staggered-type device.

Our model is validated by comparing the simulation results with the measured data as shown in Fig.1. In the differential conductance from output characteristics, a presence of peak at small V_{DS} represents a nonlinear behaviour of the contact region. If we consider the channel region only or the contact region with the ohmic behaviour, the differential conductance will monotonically decrease with increasing $|V_{DS}|$. From simulation results, we conclude that the vertical current in the contact region follows SCLC without traps or with very low density of traps.

References

1. E. Calvetti, L. Colalongo, and Z. M. Kovacs-Vajna, Solid State Electron. **49**, pp. 567-577 (2005).

2. R. R. Troutman, and A. Kotwal, IEEE Trans. Electron Devices. **36**, no. 12, pp. 2915–2922, (1989).

High-Electric-Field Angle-Dependent Magnetotransport and Electronic Structure in Quasi-Two-Dimensional Conductors

A. Kumagai, T. Osada, T. Konoike, and K. Uchida

Institute for Solid State Physics, University of Tokyo, 5-1-5 Kashiwa, Chiba 277-8581, Japan

Keywords: organic conductors, magnetotransport, AMRO, Lebed resonance

It has been known that interlayer magnetoresistance in quasi-two-dimensional (Q2D) conductors shows angle-dependent oscillatory or resonant phenomena as a function of the magnetic field orientation. The typical examples are the angle-dependent magnetoresistance oscillation (AMRO) in Q2D systems with a cylindrical Fermi surface (FS) and the Lebed resonance in the highly anisotropic Q2D systems with a pair of sheetlike FSs. These phenomena have been explained by the Boltzmann magnetotransport theory based on electron orbital motion on the FS. So far, they have been used as experimental tools to study the FS shape of novel layered organic or oxide conductors.

The electric field effects on these angle-dependent magnetotransport phenomena have been studied by the Boltzmann theory and electron orbital motion under the tilted magnetic field and the interlayer electric field. In Q2D systems with a cylindrical FS, the interlayer current normalized by the additional electric field, j_z/E_z, shows the resonant increase (Stark cyclotron resonance: SCR) when $\omega_B=p\omega_c$ (p: integer) is satisfied, where $\omega_B=ceE_z/\hbar$ and $\omega_c=eB_z/m^*$ are the Bloch frequency and the cyclotron frequency, respectively. The amplitude of SCR shows angle-dependent oscillation with shifted pattern from the conventional AMRO. Therefore, it is possible to estimate the effective mass m^* if the SCR with shifted AMRO pattern is identified.

In highly anisotropic Q2D systems with sheetlike FSs, the Lebed resonance splits into two resonances under additional electric fields. Each resonance satisfies the condition $B_y/B_z=p(b/c)\pm(E_z/v_FB_z)$, where p is an integer, and b and c are lattice constants. Therefore, it is possible to estimate the Fermi velocity v_F along the most conducting axis if the double-splitting of the Lebed resonance is observed.

In order to confirm experimentally the above theoretical predictions, we have carried out the angle-dependent magnetotransport measurements on organic conductors α-(BEDT-TTF)$_2$NH$_4$Hg(SCN)$_4$ and α-(BEDT-TTF)$_2$KHg(SCN)$_4$. In the former compound having a cylindrical FS, we have successfully observed the shift of angle-dependent pattern from the AMRO to the angle-dependent modulation of SCR under electric fields. In the latter compound having a pair of sheetlike FSs, we have successfully observed double splitting of Lebed resonance under electric fields. The estimated values of the effective mass and the Fermi velocity are consistent with those evaluated by other methods.

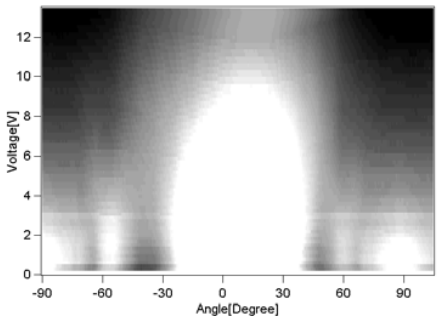

Fig.1 Voltage-dependent shift of AMRO peaks in α-(BEDT-TTF)$_2$NH$_4$Hg(SCN)$_4$.

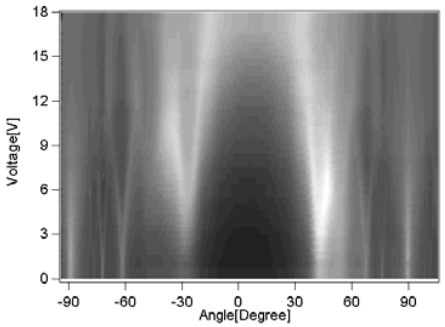

Fig.2 Voltage-driven splitting of the Lebed resonance in α-(BEDT-TTF)$_2$KHg(SCN)$_4$.

Cyclotron resonance of two dimensional electrons in a Si quantum well

R. Masutomi*, A. Sekine*, K. Sasaki*, K. Sawano**, Y. Shiraki** and T. Okamoto*
*Department of Physics, University of Tokyo, Tokyo, Japan
** Research Center for Silicon Nano-Science, Musashi Institute of Technology, Tokyo, Japan

Keywords: Cyclotron resonance, Si/SiGe

A metal-insulator transition (MIT) in two dimensional electron systems (2DESs) has attracted much attention because it conflicts with the scaling theory of localization in two dimensions[1]. The metallic behavior of the resistivity is studied in a variety of semiconductor systems. However, its origin remains unclear and controversial. In this work, we report cyclotron resonance (CR) measurements on two dimensional electrons in a Si quantum well. The scattering time τ_c obtained from the CR signal is compared with the transport scattering time.

We used a heterostructure sample with a 20-nm-thick strained Si channel sandwiched between relaxed $Si_{0.8}Ge_{0.2}$ layers[2]. The 2DES has a high mobility of 43 (16) m^2/Vs at electron concentration $N_s = 2.3\ (1.2) \times 10^{15}\ m^{-2}$. The sample was mounted inside a wave-guide with a 6 mm bore inserted into a pumping ^{3}He cryostat. The oscillation frequency of the microwave was 40 GHz. The cyclotron resonance signal was detected by a carbon bolometer immersed in liquid ^{3}He.

Fig. 1(a) shows a CR signal observed in our silicon 2DES at $N_s = 2.3 \times 10^{15}\ m^{-2}$ and $T = 0.6$ K. The resonance magnetic field B_c agrees well with the value given by $B_c = m^*\omega_c/e = 0.27$ T, where m^* is the effective mass ($m^* = 0.19m_0$) and ω_c is the cyclotron frequency. The τ_c is estimated to be 22 psec from the full width at half maximum of the CR signal. Plotted in Fig. 1(b) are the temperature dependences of τ_c and τ_t at $N_s = 1.2 \times 10^{15}\ m^{-2}$. Here, τ_t is the transport scattering time related to the zero-field conductivity σ_0 ($\tau_t = m^*\sigma_0/e^2N_s$). Both τ_c and τ_t exhibit a metallic temperature dependence. Systematic measurements for various N_s and T will be reported in the presentation.

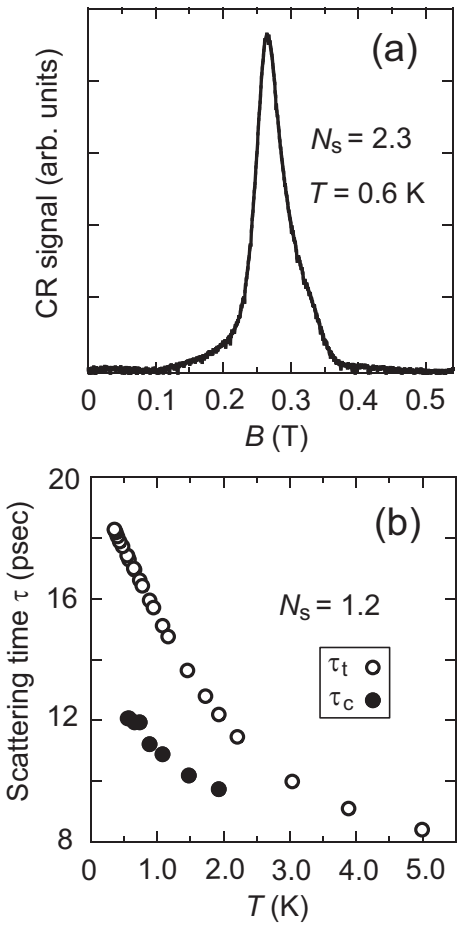

Figure 1: (a) CR signal at $N_s = 2.3 \times 10^{15}\ m^{-2}$ and $T = 0.6$ K. (b) Temperature dependence of τ_c and τ_t at $N_s = 1.2 \times 10^{15}\ m^{-2}$.

References

[1] E. Abrahams *et al.*, Phys. Rev. Lett. **42**, 673 (1979).

[2] A. Yutani and Y. Shiraki, Semicond. Sci. Technol. **11**, 1009 (1996); J. Cryst. Growth **175/176**, 504 (1997).

[3] B. Das *et al.*, Phys. Rev. B **47**, 9650 (1993).

Non-magnetic disorder effect in Z_2 quantum spin Hall systems

Ryuichi Shindou*, Shuichi Murakami**

* *Condensed Matter Theory Laboratory, RIKEN, 2-1 Hirosawa, Wako, Saitama 351-0198, Japan*

** *Department of Physics, Tokyo Institute of Technology, 2-12-1 Ookayama Meguro-ku, 152-8551, Japan*

Keywords: Anderson localization, topological insulator, relaxation time, topological quantum critical point

The Z_2 quantum spin Hall insulator (Z_2 QSHI) is a new topological state of matter, in a sense that it cannot be decomposed into the two copies of the quantum Hall states. Between such a time-reversal invariant topological insulator and a conventional insulator, one can also expect a new type of the topological quantum critical point (TQCP), which is essentially distinct from those TQCPs intervening two neighbouring quantum Hall plateaus. Namely, such time-reversal invariant TQCPs are expected to be robust against non-magnetic disorders, provided that the helical edge (or surface) state by itself is stable under them.

In this paper, we study non-magnetic disorder effects onto the effective continuum model of this TQCP, only to uncover its several nontrivial features. That is, we performed (a) the self-consistent Born calculation, (b) the weak-localization calculation based on the Kubo formula and (c) the mean-field calculation for the diffusion constant based on the mode coupling theory. Armed with these analyses, we then discuss a possible microscopic mechanism of how the criticality (i.e. "extended" character) of the TQCP is stabilized against non-magnetic disorders.

More specifically, we first observe that, near the TQCP, the diffuson is composed of two degenerate low-energy modes. The first mode participates in the usual charge diffusion mode, and therefore always carries the diffusion pole. The other low-energy mode, however, becomes massless only at the TQCP, while, otherwise, it is generally truncated by the finite infrared cutoff τ^{-1}_{topo}.

Physically speaking, this second mode describes the diffusion of the party density degree of freedom, which becomes a conserved quantity only at the TQCP. Namely, it turns out to be the case that the parity-density correlation function exhibits the diffusion pole structure at the critical point, while it suffers from a finite relaxation time, τ_{topo}, once a system enters either the Z_2 QSHI side or an ordinary insulator side. Consequently, the diffuson mentioned above acquires additional low-energy mode, into which this novel behaviour of the parity density correlation function is separately encoded.

When the hole-line of the diffuson time-reversed, the two mode feature around the TQCP is transcribed into that of the Cooperon: the Cooperon thus obtained is also composed of two (quasi-)degenerate dominant contributions. We next show that, precisely at the TQCP, these two contributions bring about the same magnitude of the anti-weak-localization (AWL) corrections to the electric conductivity. When a system is off the TQCP, however, the Cooperon originated from the parity mode channel becomes ineffective, since its backward scattering behaviour is truncated by the finite relaxation time τ_{topo}. In other words, the AWL correction generally becomes precisely doubled, when a system is fine-tuned to the TQCP. ("quantum conductivity correction doubling").

In terms of this behaviour of the parity diffusion mode and its corresponding AWL correction, we will finally argue a possible microscopic mechanism of how the extended character of the TQCP is stabilized. More specifically, we discuss that the parity diffusion mode becomes generally massless, when a system transit form the Z_2 QSHI side to an ordinary insulator side. Based on this surmise, we will ascribes the stability of the critical nature of the TQCP to the AWL correction obtained from the parity diffusion channel

References

1. R. Shindou and S. Murakami, Phys. Rev. B **79**, 045321(2009)

Radio-frequency reflectometry - A fast and sensitive measurement method for 2-Dimensional systems

L.J. Taskinen*, R.P. Starrett *, T.P. Martin*, A.P. Micolich*, A.R. Hamilton*, M.Y. Simmons*, D.A. Ritchie** and M. Pepper**

*School of Physics, University of New South Wales, Sydney NSW 2052, Australia

** Cavendish Laboratory, University of Cambridge, Cambridge CB3 0HE, United Kingdom

Keywords: radio frequency reflectometry, 2 Dimensional hole systems

There is a growing interest in studying non-equilibrium and noise properties of 2D systems, e.g., in context of the still controversial metal insulator transition [1] and glassy dynamics [2]. These studies would benefit from sensitive large bandwidth measurement methods, such as the rf reflectometry widely used with mesoscopic devices such as single electron transistors and quantum point contacts [3]. Initially one would expect that it is not possible to use the rf reflectometry technique with large area gated 2D systems because the large capacitance results in a negligible sensitivity at high resistances. However, our experimental results and a simple model show that rf reflectometry is a sensitive method to measure the device resistance up to several hundreds of k$\Omega/\Box$ with a bandwidth up to tens of MHz [4].

To test how rf reflectometry works with large area devices we embedded a 2D hole system (2DHS) in an AlGaAs/GaAs heterostructure (a Hall bar with a 80μm$\times 800$ μm metal top gate) into an impedance matching LC circuit that terminates a transmission line, and used rf reflecetometry to measure temporal changes in the resistance of the device at mK temperatures. In Figure 1 we show the measured reflectance, $S11$, versus the carrier frequency at a few different resistances ρ_{xx} of the 2DHS. At low ρ_{xx} the resonance is very shallow. The matching point, where the impedance of the LC circuit is 50 Ω, is at ρ_{xx} $\approx$7 k$\Omega/\Box$. At the matching point the resonance frequency is 328 MHz and the width of the resonance, roughly the bandwidth of the circuit, is $\sim$ 10 MHz. The reflectance at the resonance frequency changes by 75 dB when ρ_{xx} is increased to 100 k$\Omega/\Box$. We also show that it is possible to tune the resistance range where the sensitivity is largest by changing the device geometry and tank circuit parameters.

Our method enables rapid measurements of 2D systems, e.g., fast mapping of the Landau level evolution in a 2DHS as a function of magnetic field and gate voltage [4]. We have also used rf reflectometry to study non-equilibrium relaxation processes in AlGaAs/GaAs heterostructures by measuring 2DHS resistance changes with sub-millisecond time resolution.

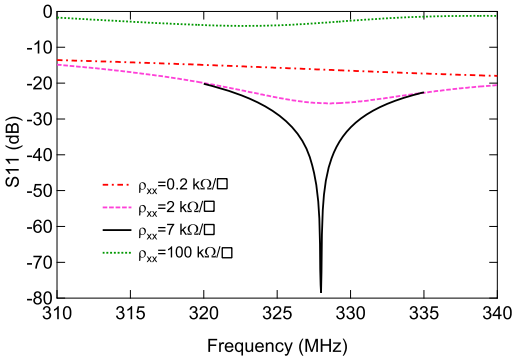

Figure 1: (a) Reflectance (S11) measured at different carrier densities. T=100 mK.

References

[1] S. V. Kravchenko and M. P. Sarachik, Rep. Prog. Phys. **67**, 1, (2004).

[2] J. Jaroszyński and D. Popović, Phys. Rev. Lett. **96**, 037403, (2006).

[3] R. J. Schoelkopf , P. Wahlgren, A. A. Kozhevnikov, P. Delsing and D. E. Prober, Science **280**, 1238, (1998).

[4] L. J. Taskinen, R. P. Starrett, T. P. Martin, A. P. Micolich, A. R. Hamilton, M. Y. Simmons, D. A. Ritchie and M. Pepper, Rev. Sci. Inst. **79**, 123901, (2008).

Scanning gate characterization of organic field effect transistor

N. Aoki*, K. Matsusaki, T. Yahagi, K. Sudou and Y. Ochiai

Graduate School of Advanced Integration Science, Chiba University, Chiba, Japan

Keywords: SGM, organic semiconductor, FET, CuPc, Schottky barrier

There has been great interest in organic semiconductor as a key technology for new device applications, such as organic electro-luminescent display, and their drive transistors. However, there still exist many questions regarding the transport characteristics of these materials. For example, how the interface between the organic film and the metal electrode is connected electrically, or where the carrier transport is restricted in the device. Such information is very important to understand the characteristics of the device. However the use of a global back gate, which covers the device entirely, is not sufficient to reveal the local phenomena. In this study, we have therefore applied a conductive SPM cantilever as a "movable point gate" in an organic thin-film field effect transistor (OFET). This technique of SGM has recently been used widely to study many kinds of semiconductor nano-structure. We have applied the technique to the study of a two-dimensional OFET for the first time, and successfully obtained SGM images of the Schottky barriers in the device [1].

The sample consists of thin Au electrodes having 15 nm thick with a gap of 10 μm on SiO_2/Si substrate. A copper phthalocyanine (CuPc) films are deposited 17 nm thick for a thinner sample and 50 nm thick for a thicker one, respectively. A PtIr coated cantilever is then made to approach the structure in ambient atmosphere, and to scan above the channel. Dc voltage ($V_{tip\text{-}dc}$) and ac modulation voltage ($V_{tip\text{-}ac}$) are coupled and applied to the tip during interleave-mode operation with lifting up the tip 30 nm high above the surface. The modulated channel current is measured by a lock-in amplifier, and stored in a SPM controller simultaneously. The use of the lock-in amp has successfully improved signal/noise ratio of the SGM response. Consequently, the SGM image has mapped out clear peaks of scanning gate response along the edge of Au electrodes as shown in Fig. 1. It indicates that the electric field from the tip could modulate the Schottky barrier at the CuPc/Au interface and that the barrier strongly restricts the carrier (hole) injection into the CuPc channel. Moreover, a large voltage drop was confirmed at the interface from the potential mapping evaluated by electrostatic response during the SGM observation. The intermittent SGM peaks indicate that the hole injection does not occur uniformly at the CuPc/Au interface in the thinner sample due to a physical disconnection in a bottom-contact configuration. Moreover, it was revealed that each injection points have different threshold voltage and transconductance. On the other hand, continuous SGM response was observed along the interface in the thicker sample. However, an edge effect which is current concentration at the edge of the channel is visualized in the SGM image. These characteristics are never revealed by a conventional back gate operation.

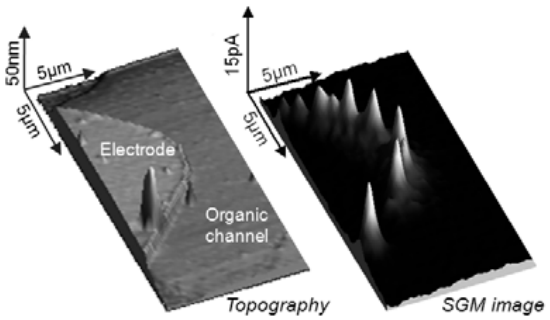

Fig.1 Topography of the OFET (left) and the corresponding ac-modulated SGM image (right).

References

1. N. Aoki, *et al*., Appl. Phys. Lett. **91**, 192113 (2007).

Time resolved control of electron tunnelling times and single-shot spin readout in a quantum dot.

L. Gaudreau[*,**], S. Studenikin[*], G. Granger[*], J. Kycia[***], P. Mason[***], A. Kam[*], C.Y. Hsieh*, R. Cheriton*, M. Korkusinski*, P.Hawrylak* and A. Sachrajda[*]

Institute for Microstructural Sciences, National Research Council, Ottawa, Canada, K1A 0R6

** *Physics Department, University of Sherbrooke, Quebec, Canada, J1K 2R1*

*** *Department of Physics and Astronomy, University of Waterloo, Waterloo, Canada, N2L 3G1*

Keywords: Quantum dot, Coulomb blockade, Charge detection, Electron spin relaxation

Since the first report of a few electron lateral quantum dot about 10 years ago [1], there has been much focus on the application of these systems as spin qubits. A crucial technique for read-out of spin qubits has been the time resolved charge detection. In particular, emphasis has been placed on the DiVincenzo criteria and their individual demonstration. A crucial technique for this research has been the time resolved charge detection. This enabled, for example, single-shot single spin read out by Elzerman et al [2]. Surprisingly, to our knowledge, this important scheme has not yet been reproduced.

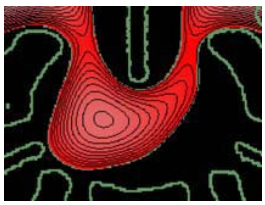

Fig.1 Calculated potential profile of a single quantum dot in a triple quantum dot device.

In this paper we reproduce this Delft protocol for single-shot single spin readout on one quantum dot within a triple quantum dot device (Fig.1) in a GaAs-AlGaAs heterostructure with neighbouring quantum point contacts as charge detectors, and extract the T_1 values at different magnetic fields, e.g., ~300μs at 10T (see Fig. 2).

To enable such investigations, it is important to extract and control the tunnel times for different device gate voltage settings. We achieve this using two techniques : (i) A statistical approach for which the chemical potential of the dot is aligned with the reservoirs and (ii) An averaged gate pulsing scheme in

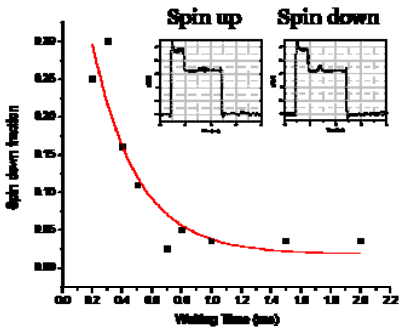

Fig.1 Spin relaxation time extraction from single-shot spin readout experiments as a function of the waiting time in which the electron is held in the dot before measuring its spin state. Each point represents a series of 200 single-shot measurements from which we extract the fraction in which the spin was measured to be down. Inset: two examples of a spin-up and a spin-down measurement.

which the N=0 to N=1 to N=0 transitions are induced by pulses. The first approach results in tunnel in and out times being approximately equal whereas (ii) results in very different times for tunnelling in and out due to the energy dependence of the tunnel barriers. Experimental results are compared with calculated spin relaxation times due to phonons [3], nuclear spins and electrons in leads.

References

1. Ciorga *et al.,* Phys. Rev. B **61**, R16315 (2000).
2. J. M. Elzerman *et al.*, Nature **430**, 431 (2004).
3. M.Florescu *et al.* Physica **E 22**, 41

Aperiodic magneto-oscillations in graphite

L. Smrčka and N. A. Goncharuk
Institute of Physics, ASCR, v. v. i., Prague, Czech Republic

Keywords: graphite, graphene, phase of magneto-oscillations, Dirac fermions

Electrons in graphene obey a linear energy dependence on the wave-vector k, and behave like massless relativistic particles – Dirac fermions (DFs). Shubnikov-de Haas (SdH) magneto-oscillations (MOs) in graphene were found periodic in an inverse magnetic field $1/B$, similarly as in the case of 2D gas of massive Schrödinger fermions (SFs), but with the phase shifted by π. Also, the anomalous quantum Hall effect with half-integer instead of an integer quantization was observed, which is the most direct evidence of Dirac fermions in graphene.

The spectral analysis of SdH and de Haas-van Alphen (dHvA) MOs, including the determination of the phase factor, was used to investigate to what extent the phase of DFs is preserved in bulk graphite. We analyzed the problem theoretically and found this approach inadequate, as the MOs in graphite are not periodic and, therefore, have no specific phase at all.

The energy spectra of 2D SFs and DFs in zero magnetic field can be written as

$$E^{SF}(k) = \frac{\hbar^2 k^2}{2m^*}, \quad E^{DF}(k) = \pm \hbar v_F k. \qquad (1)$$

Here m^* is the effective mass and v_F is the Fermi velocity. In a magnetic field the spectra are quantized, ω_c is the cyclotron frequency, $n = 0, 1, 2, \ldots$:

$$E_n^{SF} = \hbar\omega_c \left(n + \frac{1}{2}\right), \; E_n^{DF} = \pm\sqrt{2\hbar|e|v_F^2 B n}. \quad (2)$$

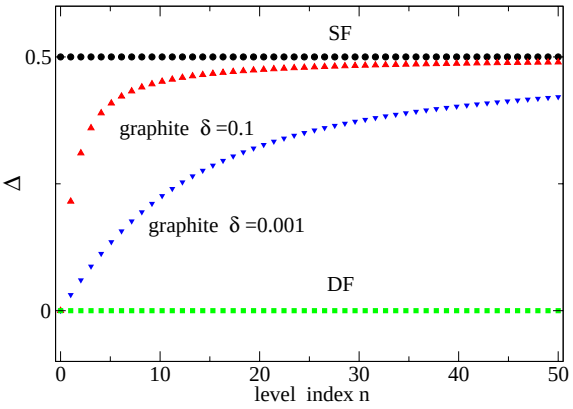

Figure 1: Example of the differences Δ between $1/B$ dependences of graphite, SF and DF, assuming unit-frequencies.

MOs observed in SdH and dHvA effects are controlled by MOs of the density of states (DOS). The DOS reaches maxima when the Landau levels cross the Fermi energy E_F. A plot of the corresponding inverse magnetic fields as a function of the level index, n, is used to determine the period and phase of MOs. For the SFs and DFs, described by Eq. (2), we have

$$\frac{B^{SF}}{B} = n + \frac{1}{2}, \quad \frac{B^{DF}}{B} = n, \qquad (3)$$

where $B^{SF} = m^* E_F/(\hbar|e|)$ and $B^{DF} = E_F^2/(2\hbar|e|v_F^2)$ are the frequencies of periodic MOs. The phase shift is π, i.e., a half of the period.

An expression similar to Eq. (3) can be obtained also for the k_z-dependent cross-sections of the 3D graphite Fermi surface. Starting from the Slonczewski, Weiss and MacClure (SWM) model, and the secular equation as published in the MacClure's paper, [1] we derived a formula for the inverse magnetic field as a function of n:

$$\frac{B^G(k_z)}{B} = \frac{n + \frac{1}{2} \mp \sqrt{\frac{1}{4} + n(n+1)\delta(k_z)}}{1 \mp \sqrt{\delta(k_z)}}. \qquad (4)$$

Here $B^G(k_z)$ and $\delta(k_z) \geq 0$ were obtained from parameters of the SWM model and depend also on E_F. The k_z--dependence originates from $\cos(k_z c/2)$ which appears in the inter-layer tight-binding SWM parameters, $c/2$ is the inter-layer distance in graphite. Obviously, $B^G(k_z)/B$, as given by Eq. (4), is not periodic in $1/B$, except of the case of vanishing inter-layer interaction $k_z \to \pi/c$, $\delta(k_z \to 0)$. The expression (4) becomes only asymptotically periodic in the case of the quasi-classical limit $\sqrt{n(n+1)} \to n + 1/2$, with the phase of SFs.

References

[1] J. W. McClure, Phys. Rev.**119**, 606 (1960).

An optical and electrical probe inside a TEM

Zhenzhong Wang, Peng Gao, Xuedong Bai, Dongmin Chen*

** Beijing National Laboratory for Condensed Matter Physics, Institute of Physics, Chinese Academy of Sciences, Beijing 100080, People's Republic of China*

Keywords: nanoprobe, TEM, electromechanical resonance, optical stimulation

In this abstract, we report an optical and electrical probe technique inside a TEM for optical tuning of a nanomechanical resonator, which is consisted by a Cadmium Sulfide (CdS) nanowire.

The experimental setup is based on our home-made TEM-SPM system, in which a 3-dimensional nano-manipulator is embedded in a TEM sample rod, as show in Fig. 1(a). A multi-mode fiber with diameter is used for feeding light into TEM via a home-made vacuum feedthrough. CdS nanowires were attached to a Pt/Ir tip by silver epoxy with a good electric contact, which in turn is fixed onto the nano-manipulator. The output end of the fiber with a grounded gold electrode is fixed in front of Pt/Ir tip, as show in Fig. 1(b). The nanowire was navigated under the TEM to a position about 5 μm away from the grounded golden electrode, as show in Fig. 1(c). Then an alternating current (AC) voltage was applied on the nanowire, so a time-dependent electrical force was induced in the nanowire and caused it to vibrate accordingly.

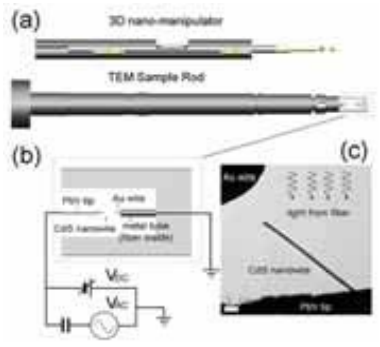

Fig.1 (a) Home-made nano-manipulator inside TEM. (b) Optical nanomechanical resonator based on a CdS nanowire. (c) Pt/Ir tip with CdS nanowires is driven by nano-manipulator to approach the golden tip.

Figure 2(a) shows a TEM image of a vibrating CdS nanowire being excited by an AC voltage. Interestingly, when a 403 nm light with 3 μW power is turned on, nanowire's amplitude of vibration decreases, as shown in Fig. 2(b). The changing of the vibration amplitude with/without the light exposure can be well repeated, as shown in Fig. 2(c). Figure 2(d) shows the frequency response of the nanowire to the driving AC voltage for both on the dark and light conditions. The resonance frequency of the nanowire shifted toward lower frequency under the light exposure.

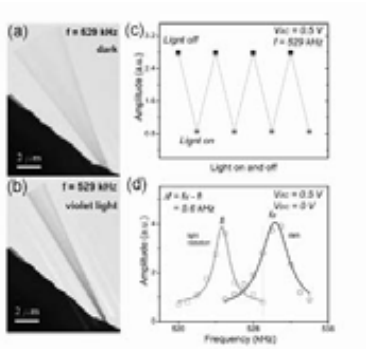

Fig.2 (a) A vibrating CdS nanowire. (b) Vibration amplitude decreased. (c) The amplitude of vibration changed with the exciting light on and off for several circles. (d) The dependence of vibration amplitudes with frequency of V_{AC} were fitted by Lorentzian curves both for dark and light radiation status.

The amount of frequency shift strongly depended on the wavelength of the light. According to photoluminescence and static electrical field analyses, the frequency-shift behavior was caused by the decrease of elastic coefficient, which is induced by the damping of electric fields caused by the increasing of photoelectrons.

July 21 (Tuesday)

9:00 – 10:30

Session E2

Spin Related Phenomena

Main Hall

EP2DS-MSS Parallel session

Kobe Portpia Hotel

Spin Hall effects in HgTe Quantum Well Structures

Laurens W. Molenkamp

Physikalisches Institut (EP3) der Universität Würzburg, Am Hubland, 97074 Würzburg, Germany
E-mail: laurens.molenkamp@physik.uni-wuerzburg.de Phone:+49-931-8884925 Fax:+49-931-8885142

Spin-orbit interaction in semiconductors causes many interesting and potentially useful transport effects, such as e.g. the presently very topical spin-Hall effect[1]. So far no direct evidence for a ballistic, intrinsic SHE (i.e. resulting from the band structure) has been obtained by transport experiments. Here, we demonstrate that in specially designed nanostructures[2], which are based on narrow gap HgTe type-III (a.k.a. inverted) quantum wells, a detection of the spin signal is possible via non-local voltage measurements.

Recently, it was pointed out that such inverted HgTe structures are topologically non-trivial insulators[3], in which the quantum spin Hall insulator state[4] should occur. In this novel quantum state of matter, a pair of spin polarized helical edge channels develops when the bulk of the material is insulating, leading to a quantized conductance. I will present transport data provide very direct evidence for the existence of this third quantum Hall effect: when the bulk of the material is insulating, we observe a quantized electric conductance[5].

Finally, we demonstrate how a combination of the techniques used in the above experiments allows us to verify that the transport in the quantum spin Hall insulator state indeed occurs through spin-polarized helical edge channels.

[1] S. Murakami et al., Science 301 (2003) 1348; J. Sinova et al., Phys. Rev. Lett. 92 (2004) 126603; Y. Kato et al., Science 306 (2004) 1910 – and many more.
[2] E.M. Hankiewicz, et al., Phys. Rev. B 70 (2004) 241301(R).
[3] B.A. Bernevig et al., Science 314 (2006) 1757.
[4] C.L. Kane and E.J. Mele, Phys. Rev. Lett. 95 (2005) 146802.
[5] M. König et al., Science 318, 766 (2007).

Spin accumulation with spin-orbit interaction

Henri Saarikoski[1,2,3], and Gerrit E. W. Bauer[1]
[1]*Kavli Institute of Nanoscience, Delft University of Technology, 2628-CJ Delft, The Netherlands*
[2]*Mathematical Physics, Lund Institute of Technology, SE-22100 Lund, Sweden*
[3] *Helsinki University of Technology, P.O. Box 4100, FI-02015 HUT, Finland*

Keywords: spin-orbit coupling, spintronics, Rashba 2DEG, spin transistor

Spin accumulation is a crucial but imprecise concept in spintronics. In metal-based spintronics it is characterized in terms of semiclassical distribution functions. In semiconductors with a strong spin-orbit coupling the spin accumulation is interpreted as a superposition of coherent eigenstates. We show that both views can be reconciled by taking into account the electron-electron interaction: a sufficiently strong self-consistent exchange field reduces a spin accumulation to a chemical potential difference between the two spin bands even in the presence of spin-orbit coupling. We demonstrate the idea on a clean two-dimensional electron gas (2DEG) by showing how the exchange field protects a spin accumulation from dephasing and introduces an easy-plane anisotropy [1].

Metal-based spintronics [2] has evolved into a mature field in which spin phenomena are routinely exploited in versatile applications. However, integration of spin-based functionalities into semiconductor circuits is still a pressing challenge. Much of recent research in this area has been motivated by device concepts, such as the seminal Datta-Das transistor [3], which requires injection and detection of spins by ferromagnetic contacts to a narrow channel of a two-dimensional electron gas with gate-controlled spin-orbit interaction (SOI). In spite of progress to inject, modulate, transport, and detect spin polarization all-electrically [4] as well as evidence that the SOI can indeed be tuned by external gates [5], the route to a working spin transistor appears to be still full of obstacles. In the meantime, many insights have been obtained on the spin accumulation and its dynamics by optical methods, especially time-dependent Kerr and Faraday rotation spectroscopy.

Spin can be injected either adiabatically, *e.g.* by a ferromagnetic contact with small electric bias, or diabatically, *e.g.* by pulsed optically induced excitation. We discuss spin-accumulation eigenstates that are accessible by adiabatic excitation as well as spin accumulation dynamics of rapidly excited states. We illustrate the general ideas at the hand of a 2DEGs with Rashba SOI (Fig. 1), in which the disorder-scattering lifetime broadening is much smaller than the spin-orbit splitting at the Fermi-level.

References

[1] H. Saarikoski and G. E. W. Bauer, Phys. Rev. Lett. (to be published) (2009), arXiv:0810.3386.

[2] I. Žutić, J. Fabian, and S. Das Sarma, Rev. Mod. Phys. **76**, 323 (2004).

[3] S. Datta and B. Das, Appl. Phys. Lett. **56**, 665 (1990).

[4] X. Lou *et al.*, Nature Phys. **3**, 197 (2007).

[5] J. Nitta *et al.*, Phys. Rev. Lett. **78**, 1335 (1997).

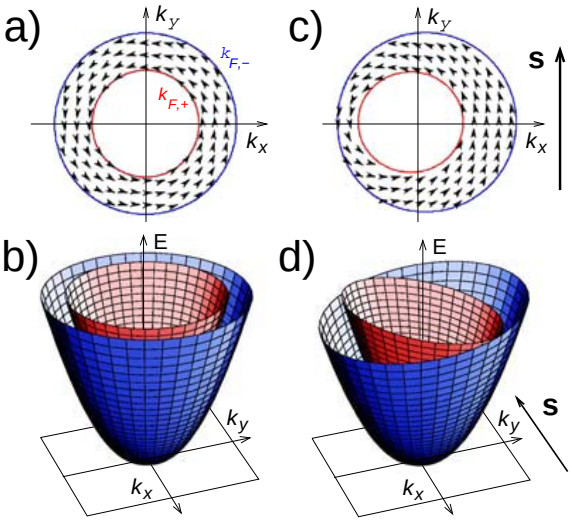

Figure 1: Spins (a) and energies (b) of the ground-state spin-split bands in a non-interacting Rashba 2DEG. (c-d) Modulation of the electronic structure in the presence of an in-plane spin accumulation s by its the exchange field.

Intrinsic photoinduced anomalous Hall effect

D.A. Vasyukov,[1] A.S. Plaut,[1] A.H. MacDonald,[2] M. Henini,[3] L.N. Pfeiffer[4†] and K.W. West[4†]

[1] *School of Physics, Exeter University, Exeter EX4 4QL, UK*
[2] *Department of Physics, The University of Texas at Austin, Austin, Texas 78712, USA*
[3] *School of Physics & Astronomy and Nottingham Nanotechnology & Nanoscience Centre, University of Nottingham, Nottingham NG7 2RD, UK*
[4] *Bell Laboratories, Alcatel-Lucent, Murray Hill, New Jersey 07974, USA*

Keywords: spin Hall effect, anomalous Hall effect, spintronics

Spin effects in semiconductors have attracted huge attention lately due to their potential applications in spintronic devices. In particular the spin Hall effect (SHE) [1] and the circular photogalvanic effect (CPGE) [2] have been shown to exist in samples without crystal inversion symmetry. The intrinsic anomalous Hall effect (AHE) [3], like the SHE, is exhibited in crystals with spin-orbit (SO) interaction which tends to drive charge carriers with different spin orientation to opposite sides of the sample. If one spin orientation predominates then a voltage ($V_{PI\text{-}AHE}$) is measurable transverse to the current applied.

In our experiments we create a non-equilibrium spin population in very high-mobility, Si-doped (311)A-grown symmetric and asymmetric GaAs/AlGaAs quantum wells (QWs) by illuminating them with circularly polarized light at 350 mK. We have measured the photoinduced-AHE (PI-AHE) as a function of the applied current, magnetic-field, temperature, polarisation of the incident light and its photon energy. In the case of the latter we observe Landau levels in finite magnetic field.

Such ultra-high mobility two-dimensional (2D) hole systems ensure that the effect that we measure is almost certainly intrinsic in nature, unlike previous reports of the PI-AHE in the literature, all of which had extrinsic origins [4]. Figure 1 shows that in our case $V_{PI\text{-}AHE} \propto$ hole mobility (μ), whereas for extrinsic skew-scattering $V_{PI\text{-}AHE} \propto 1/\sqrt{\mu}$ [4].

We have found that the intrinsic PI-AHE requires perpendicular magnetic field to be observed. The magnetic field, we believe, spatially separates the photoexcited electrons and holes, similarly to the function of the p-n junction in Ref. 4. The magnetic field also decreases the spin relaxation rate, thereby increasing the voltage signal [5].

While the two symmetries of the QWs allow investigation of the effect of Rashba SO coupling, we have been unable to detect the PI-AHE in similar measurements in C-doped (100)-grown QWs. In such high-symmetry 2D hole systems the Dresselhaus SO coupling is not as large as in (311)A-grown QWs.

These measurements constitute the first measurement of the intrinsic PI-AHE.

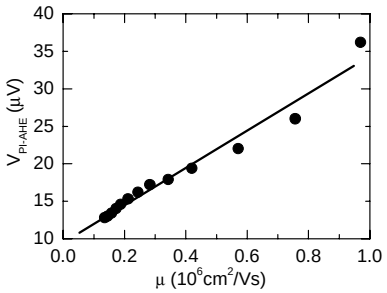

Fig. 1 $V_{PI\text{-}AHE}$ versus hole mobility. The line is a guide for the eye.

† Present address: PRISM, Princeton University, Princeton, NJ 08544, USA

References

1. J. Wunderlich *et al.*, Phys. Rev. Lett. **94**, 047204 (2005)
2. S.D. Ganichev *et al.*, Phys. Rev. Lett. **86**, 4358 (2001)
3. T. Jungwirth, Q. Niu, A.H. MacDonald, Phys. Rev. Lett. **88**, 207208 (2002); and references therein
4. J. Wunderlich *et al.* arXiv:0811.3486v1 [cond-mat.mes-hall]; and references therein
5. G.E. Pikus and A.N. Titkov in *Optical Orientation*, [Ed.: F. Meier and B.P. Zakharchenya, North Holland, 1984]

Electric-field manipulation of magnetization vector in (Ga,Mn)As

D. Chiba,[1,2,3] M. Sawicki,[2,4] Y. Nishitani,[2]
Y. Nakatani,[5] T. Ono,[3] F. Matsukura,[2,1] and H. Ohno[2,1]

[1]*Semiconductor Spintronics Project, ERATO, Japan Science and Technology Agency, Japan*
[2]*Laboratory for Nanoelectronics and Spintronics, RIEC, Tohoku University, Japan*
[3]*Institute for Chemical Research, Kyoto University, Japan*
[4]*Institute of Physics, Polish Academy of Sciences, Poland*
[5]*University of Electro-communications, Japan*

Keywords: Electric-field, Magnetization direction, (Ga,Mn)As

Ferromagnetic properties in III-V ferromagnetic semiconductors are electrically tunable by control of their carrier concentration. We have shown in the past that Curie temperature and coercivity can be manipulated by applying electric-fields.[1,2] Here, we show that electric-field manipulation of magnetic anisotropy, and thus magnetization vector direction, is possible in (Ga,Mn)As.[3]

The basic idea is to control the density of carrier (hole) on spin-split anisotropic valence bands that governs the magnetic anisotropy, which should result in the change of the direction of magnetization. In order to measure the magnetic anisotropies of (Ga,Mn)As thin film under the electric-fields, a capacitance structure consists of (Ga,Mn)As / insulator / gate electrode from the bottom was prepared. We used the anisotropic magnetoresistance and the planar Hall effect to detect the magnetization direction of the (Ga,Mn)As channel. We first applied magnetic field perpendicular to the sample, which has an in-plane easy axis, to measure the hard axis anisotropy. It was found that the hard axis anisotropy, in terms of anisotropy field, increased as carrier concentration increased by applying electric-field to the channel. This finding is consistent with the p-d Zener model calculation.[4] We next turned to the in-plane anisotropies. The planar Hall effect was measured as a function of the angle of in-plane magnetic field. Analyses showed that there are biaxial as well as uniaxial anisotropies; the latter changed its magnitude and sign as the carrier concentration was reduced. From the electric-field dependent anisotropy fields determined from the experiment, one can show that the angle of the magnetization direction in the absence of magnetic fields is modulated. We believe that this opens up a new and unique opportunity for manipulating magnetization direction solely by electronic means, not resorting to magnetic-field, spin-current, mechanical stress, nor multiferroics. The conditions for switching the magnetization direction will also be discussed.

Fig. 1 Schematic of magnetization vector manipulation by electric-field.

References

1. H. Ohno, *et al. Nature* **408**, 944 (2000).
2. D. Chiba, *et al. Science*, **301**, 943 (2003).
3. D. Chiba, *et al. Nature* **455**, 515 (2008).
4. T. Dietl *et al. Phys. Rev. B* **63**, 195205 (2001).

July 21 (Tuesday)

11:00 – 12:30

Session E3

Optical Phenomena

Main Hall

EP2DS-MSS Parallel session

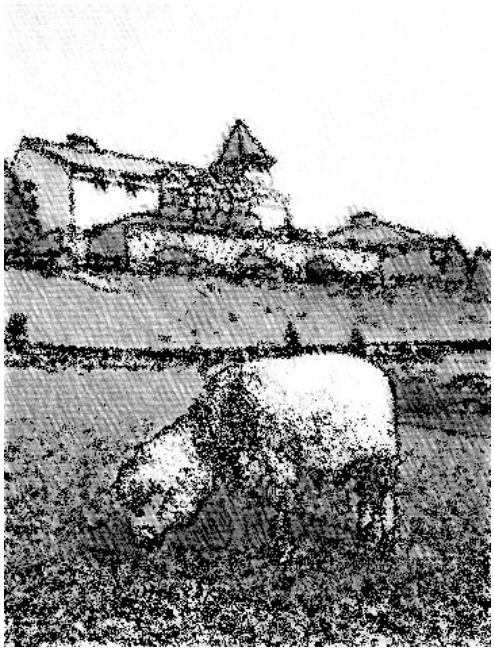

Rokko farm

Rotation of a two-dimensional exciton-polariton condensate

M. D. Fraser[a,b,c], M. Kuwata-Gonokami[b], S. Höfling[e], A. Forchel[e] and Y. Yamamoto[c,d]

a *Institute for Nano Quantum Information Electronics, University of Tokyo, 4-6-1 Komaba, Meguro-ku, Tokyo 153-8505, Japan*

b *Department of Applied Physics, University of Tokyo, 7-3-1 Hongo, Bunkyo-ku, Tokyo 113-8656, Japan*

c *National Institute of Informatics, 2-1-2 Hitotsubashi, Chiyoda-ku, Tokyo 101-8430, Japan*

d *Edward L. Ginzton Laboratory, Stanford University, Stanford, California 94305-4085, USA*

e *Technische Physik, Universität Würzburg, Am Hubland, D-97074 Würzburg, Germany*

Keywords: exciton-polariton, Bose-Einstein condensation, quantized vortex

Quantized vortices are metastable excitations of a spatially phase-coherent system, and in a Bose-Einstein condensate (BEC) become stable under the application of a rotating potential. The lowest energy configuration of a multi-vortex superfluid system is an Abrikosov lattice, which has been previously observed in rotating atomic condensates [1]. A BEC-like state can also be created in microcavity exciton-polaritons, the strong coupling of the quantum well exciton and cavity photon modes [2]. While the atomic condensate is a relatively clean system (non-dissipative, simple interactions), condensates of polaritons decay in a short time scale (compared with dynamical evolution) and posses number non-conservation due to continuous stimulated scattering into the condensate and loss of photons from the cavity.

Single quantized vortices [3] and single vortex-anti vortex pairs [4] have recently been observed in polariton condensates due to non-equilibrium dissipative dynamics of polaritons in a disordered landscape and spontaneous thermal fluctuations respectively. The formation of a controlled stable vortex ensemble is however considerably more difficult requiring ultra-high quality cavities, spatial confinement and the application of a rotating potential. This work explores the stimulated scattering from, and interaction with appropriately phase engineered orbital angular momentum (OAM) states to directly rotate the polariton condensate. It is well established that optical Laguerre-Gauss (LG) modes can posses a non-zero quantized orbital angular momentum and while single-shot excitation with an LG mode cannot be used to form stable multi-vortex arrays due to dissipation, the ability to continuously pump a polariton condensate allows evolution on long time scales.

The rapid rotation of exciton-polariton condensates is particularly relevant to investigation of new phases resembling those of 2D electronic systems in high magnetic fields [5], notably a possible fractional quantum Hall-like regime. Exciton-polaritons occupy a unique position in the condensate parameter space and with a highly variable but light effective mass are found to be theoretically more applicable than atomic condensates in this context to the observation of these phases which occur at much higher particle numbers.

In this presentation we report on the experimental and theoretical implementation of effective rotating potentials for an exciton-polariton condensate and the progress in pushing this system towards novel phases at high vortex count.

This work is supported by JST/SORST and the Special Coordination Funds for Promoting Science and Technology in Japan and the DARPA-MTO QuEST program.

References

[1] J.R. Abo-Shaeer, C. Raman, J.M. Vogels and W. Ketterle, Science **292**, 476–479 (2001).

[2] H. Deng, G. Weihs, C.Santori, J. Bloch and Y. Yamamoto, Science **298**, 199–202 (2002).

[3] K.G. Lagoudakis, M. Wouters, M. Richard, A. Baas, I. Carusotto, R. André, L.S. Dang and B. Deveaud-Plédran, Nature Physics **4**, 706–710 (2008).

[4] G. Roumpos, M.D. Fraser, S. Höfling, A. Forchel and Y. Yamamoto, In preparation (2009).

[5] T.L. Ho, Physical Review Letters **87**, 60403 (2001).

Quantum fluid dynamics of a polariton condensate in a semiconductor microcavity

A.Amo*, D. Sanvitto*, F.P. Laussy*, D. Ballarini*, E. del Valle*, M.D. Martin*, A. Lemaître**, J Bloch**, D.N. Krizhanovskii†; M.S. Skolnick†, C. Tejedor* and L.Viña*

* *SEMICUAM. Universidad Autónoma. E-28049 Madrid. Spain*

** *LPN/CNRS, Route de Nozay, 91460, Marcoussis, France.*

† *Dep. Physics & Astronomy, Univ. of Sheffield, S3 7RH, Sheffield, U.K.*

Keywords: Superfluidity, Bose-Einstein condensation, polaritons, semiconductor microcavities

We study the hydrodynamics of a coherent polariton fluid lasting for hundreds of picoseconds and moving inside of a semiconductor microcavity. Making use of intrinsic structural defects, we observe unique behaviours due to the quantum nature of the polariton states. Amongst the observation of quantum reflection, diffusionless motion and formation of Ĉerenkov-like supersonic waves, we have been able to observe typical signatures of superfluid behaviour. The experiments have been realised making use of a new technique for the detection of images simultaneously resolved in time, energy and real- or reciprocal- space [1].

Our sample is a λ/2 AlAs microcavity with a 20 nm GaAs QW at its centre. Due to their very short lifetime, polaritons dwell in the cavity only a few ps hindering the observation of dynamical phenomena, like superfluidity. To observe condensed polaritons during a sizeable amount of time, we have used a combination of a continuous-wave (CW) pump and a pulsed probe to trigger an optical parametric scattering process in a given state along the polariton dispersion. Using ultrafast detectors, it is possible to follow the dynamics of the condensates for hundreds of ps. The CW pump feeds the stimulated scattering process even after the pulsed probe has disappeared. In this way a coherent signal polariton state can be observed moving inside of the cavity, enabling the study of its dynamics resolved in time and either in real- or k-space.

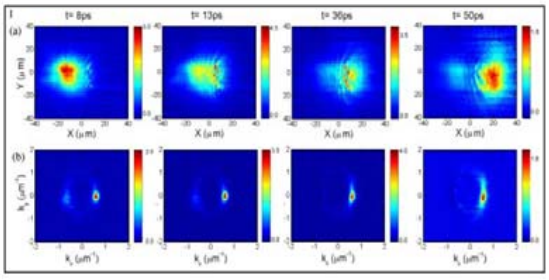

Fig.1 False-colour images of a polariton droplet colliding against a native defect. The position of the obstacle is revealed, in real space (a), by Ĉerenkov waves caused by the pump polaritons (travelling at a supersonic speed). However, the signal polaritons pass through the defect in a superfluid fashion without changing direction or scattering against the obstacle. This fact is confirmed by the images taken at the same times in momentum space (b).

The polariton dispersion, deformed by the strongly occupied pump state, is linear and asymmetric (typical of superfluid systems). Due to the linear dispersion, the dimension of the condensate wave packet does not increase significantly when travelling (Fig.1a). Moreover, the coherent polariton signal, during its motion, is peaked at a k-vector, which is maintained throughout the travelling even when running against obstacles (Fig.1b), demonstrating superfluid-like, friction-less motion. However, Cherenkov shock waves are generated on the pump state due to its supersonic speed. This work opens the way to the investigation of new phenomenology of out-of-equilibrium condensates.

(1 blank line)

References

1. A. Amo, *et al.*,Nature **457**, 291 (2009).

Intrinsic decoherence mechanisms and formation of coexisting polariton condensates in CdTe microcavities

D.N. Krizhanovskii[1], K.G.Lagoudakis[2], A. P. D. Love[1] , B.Pietka[2], D.M. Whittaker[1], R.A. Bradley[1], K. Guda[1], S. Al Rizeiqi[1], R Bouchekioua[1], D.Sanvitto[3], P. R. Eastham[5], M.S. Skolnick[1], M.Wouters[2], B. Deveaud-Pledran[2], M Richard[4], R.Andre[4] and Le Si Dang[4]

[1]*Department of Physics & Astronomy, University of Sheffield, Sheffield S3 7RH, United Kingdom.*
[2] *Ecole Polytechnique Fédérale de Lausanne (EPFL), Station 3, CH-1015 Lausanne, Switzerland*
[3]Dep. Fisica de Materiales, Universidad Autonoma de Madrid, 28049 Madrid, Spain
[4]*Institut Néel, CNRS and Université J. Fourier, 38042 Grenoble France*
[5]*Department of Physics, Imperial College, London SW7 2AZ, UK*

Keywords: polariton, Bose-Einstein condensation, coherence

The recent observations[1] of polariton condensation in semiconductor microcavities have provided a new solid state system for the study of non-equilibrium Bose-Einstein Condensate (BEC)-related phenomena. We show that the polariton BEC is able to reveal new physics of interacting BECs, not accessible so far for the case of atom condensates.

Here we investigate fundamental quantum properties of the CdTe polariton BEC,[1] such as temporal and spatial coherence. Above threshold, the observed polariton emission consists of several narrow lines. The peaks exhibit superlinear behaviour with power, which indicates the formation of coexisting condensates with different energies. The lower energy modes usually consist of 1-2 maxima in real space and arise from polariton localisation on the disorder potential. Higher energy condensates (E>0.5 meV) are extended over 10-20 μm and have spatial coherence length comparable to their size. These modes are delocalised and have well-defined k-vectors (Fig.1), which are determined by the local potential landscape.

We provide a theoretical model based on nonlinear Gross-Pitaevskii equations coupled to a rate equation for the exciton reservoir. Qualitative agreement between experiment and theory is obtained. A peak of delocalised condensed modes at momentum **+k** is frequently accompanied by a weaker satellite at **–k**, consistent with coherent backscattering at these k-vectors in the photonic disorder potential. The backscattering minimizes in-plane losses at particular k-vectors, leading to triggering of condensation.

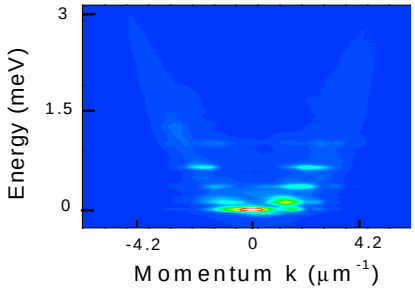

Fig 1 Image of polariton condensate emission above threshold in energy-momentum (E-k) space

We observe coherence times[2] of the individual modes of τ~100-200 ps for both the $g^{(1)}$ phase correlation function and the second order intensity correlation function, $g^{(2)}$. $g^{(1)}$ has a Gaussian (Lorentzian) shape if its decay time is shorter (longer) than 150 ps. In the limit of slow decay of $g^{(2)}$ just above threshold the interactions in the polariton system cause spontaneous number fluctuations, which translate into random energy variations, leading to decoherence and hence fast (τ<150 ps) Gaussian decay of $g^{(1)}$. These decoherence processes would occur in a true equilibrium system. By contrast, the number fluctuations are averaged out in case of fast decay of $g^{(2)}$, which occurs well above threshold. This results in a longer Lorentzian decay of $g^{(1)}$.

[1] J.Kasprzak et al, Nature 443, 409-414 (2006)
[2] A.P.D. Love et all, Phys. Rev. Lett. **101**, 067404 (2008)

Observation of the orbital circular photogalvanic effect in quantum-confined structures

J. Karch*, P. Olbrich*, S.A. Tarasenko**, T. Schoenberger*, C. Reitmaier*, Z.D. Kvon*** and S.D. Ganichev*

** Terahertz Center, University of Regensburg, 93040 Regensburg, Germany,*

*** A.F. Ioffe Physical-Technical Institute, Russian Academy of Sciences, 194021 St. Petersburg, Russia*

**** Institute of Semiconductor Physics, Russian Academy of Sciences, 630090 Novosibirsk, Russia*

Keywords: Photocurrents, Quantum interference, Silicon-based quantum-confined structures

Here we report on the observation of the photocurrent caused by transfer of photon angular momenta to free carriers in silicon metal-oxide-semiconductor field-effect-transistors (Si-MOSFETs) [1]. The photocurrent is excited by circularly or elliptically polarized terahertz radiation and reverses its direction upon switching the sign of circular polarization of the radiation. So far such a circular photogalvanic effect (CPGE) has been detected only in materials with strong spin-orbit coupling and attributed to spin-dependent processes occurring due to the absorption of circularly polarized light [2]. In silicon, spin-orbit coupling is weak, therefore, such mechanisms of the CPGE get ineffective and can not account for the observed photocurrent. We show that the circular photocurrent in Si-MOSFETs originates from the quantum interference of different pathways contributing to the absorption of monochromatic radiation. This pure orbital (spin-unrelated) mechanism of the CPGE describes well all features observed in experiment.

The experiments are carried out on Si-MOSFETs with electron channels fabricated on (001) and (111) as well as miscut surfaces. In (001)- and (111)-oriented structures the circular photocurrent is detected only at oblique incidence of the radiation while in MOSFETs on miscut surfaces the photocurrent is also observed in the geometry of normal incidence, which is in accordance with the theory of the CPGE. For excitation we use terahertz radiation of a molecular optically-pumped laser operating in the wavelength range between 77 and 280 μm. Depending on the temperature and gate voltage, which varies the separation between size-quantized subbands, the radiation induces intrasubband (Drude-like) or direct intersubband optical transitions. We detect the CPGE photocurrent in the spectral ranges of both type of the transitions and study it as a function of the radiation polarization, wavelength, temperature and gate voltage.

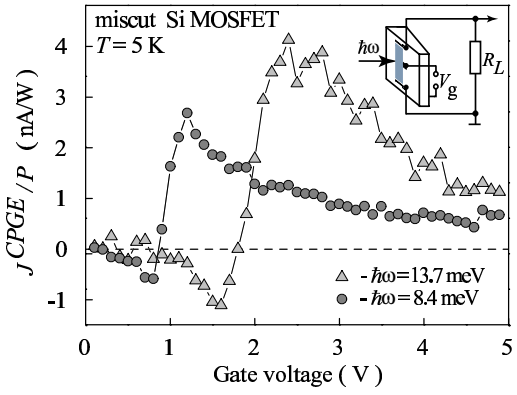

Figure 1: Gate voltage dependence of the circular photocurrent in Si-MOSFET on miscut surface.

Figure 1 presents the gate voltage dependence of the circular photocurrent measured in Si-MOSFET on miscut surface at low temperature. The dependence is non-monotonous: The CPGE photocurrent changes its sign upon variation of the gate voltage and vanishes at the voltage where the energy spacing between the subbands corresponds to the photon energy. Such a behavior is in accordance with the microscopic theory of the orbital CPGE, which predicts spectral inversion of the photocurrent at the point of the intersubband resonance.

References

[1] P. Olbrich, S.A. Tarasenko, C. Reitmaier, J. Karch, D. Plohmann, Z.D. Kvon, and S.D. Ganichev, Phys. Rev. B **79**, 121302(R) (2009)

[2] E.L. Ivchenko and S.D. Ganichev, *Spin Photogalvanics* in *Spin Physics in Semiconductors*, ed. M.I. Dyakonov (Springer 2008) pp. 245-278

P12
E1
MoP
E2
E3
E4
TuP
E5
P34
E6
E7
E8
ThP
E9
P56

July 21 (Tuesday)

14:00 – 16:00

Session E4

Quantum Hall Effect and Coherent Transport

Main Hall

EP2DS-MSS Parallel session

Night view of port Kobe

Nascent Wigner lattice in quantum wires of shallow confinement

W. K. Hew, K. J. Thomas*, M. Pepper, I. Farrer, D. Anderson, G. A. C. Jones and D. A. Ritchie
Cavendish Laboratory, University of Cambridge, Cambridge CB3 0HE, United Kingdom
** Dept. of Electronic and Electrical Engineering, Sungkyunkwan University, Suwon 440-746, South Korea*

Keywords: quantum wire, electron-electron interaction, Wigner crystal, quasi-1D electron transport

Electrons in a quantum wire are predicted to relax laterally as the 1D confinement is weakened, separating initially into two rows, and then progressively more, until the system approaches a regular 2D lattice. Experimental evidence for such a bifurcation is reported here.

We present low-temperature transport measurements of a top-gated split-gate quantum wires[1], the carrier density and the shape of the transverse confinement potential well of which can be independently controlled. Such wires proven fruitful for investigating strong-interaction effects, e.g., the spin-incoherent Luttinger liquid[2].

As the confinement of a quantum wire weakens, we observe in Fig. 1 (right to left across the plot) the suppression of the $G_0 = 2e^2/h$ plateau of ballistic 1D transport, which falls to e^2/h before disappearing entirely, whereupon the conductance jumps directly to $4e^2/h$ when the wire populates. That the conductance here is twice G_0 reflects the bifurcation of the electrons into a double wire, the manifestation of which is confirmed by magnetic-field measurements[3], which show the two lowest 1D subbands merging to form a level that is four-fold degenerate (at $B = 0$ T) as the confinement is weakened. At high magnetic fields, the mixing of spin-aligned levels gives rise to interesting, more complex states.

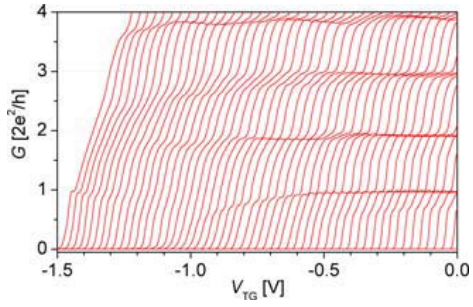

Figure 1: Conductance traces taken by sweeping the top-gate ($V_{\rm TG}$) at various fixed split-gate voltages $V_{\rm SG} = -0.52 \rightarrow -2$ V right-to-left, corresponding to a widening of the quantum wires as confinement weakens. The double-row formation, marked by a jump to $4e^2/h$, is observed in near $V_{\rm TG} \approx -1$ V.

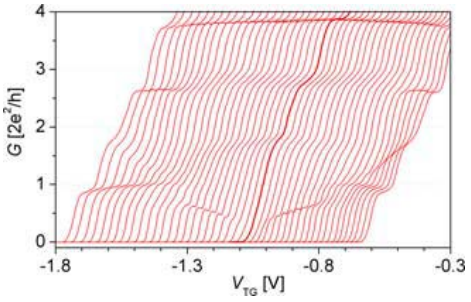

Figure 2: Laterally shifting the channel by applying a differential bias to the split gates. The symmetry of the characteristics about the central (bold) trace attests the cleanliness of the channel and its freedom from random impurities and disorder.

The theoretical literature supports our conclusions, for classical and quantum calculations[4, 5] both predict that a system of electrons thus confined to 1D will divide as the confinement weakens, initially staggering into a zigzag before splitting into two or more distinct rows.

Although reproducible across devices, the double-row formation is somewhat fragile, stable only within a critical intermediate range of densities. Unsurprisingly, this state is sensitive to confinement symmetry, as its response to differential split-gate bias in Fig. 2 reveals.

This is the first time double-row transport has been observed in quantum wires, pressing further into the quasi-1D régime, where the standard sub-band model begins to break down. The formation of two rows is a necessary first and most important step towards a more complex lattice, its significance underpinned by theoretical work predicting the formation of a staggered Wigner crystal.

References

[1] W. K. Hew et al., *Physica E* **40**, 1645 (2008).
[2] W. K. Hew et al., *Phys. Rev. Lett.* **101**, 036801 (2008).
[3] W. K. Hew et al., *Phys. Rev. Lett.* **102**, 056804 (2009).
[4] G. Piacente et al., *Phys. Rev. B* **69**, 045324 (2004).
[5] A. Klironomos et al., *Phys. Rev. B* **76**, 75302 (2007).

Shot Noise in a Quantum Point Contact in High Magnetic Fields

S. Nakamura, M. Hashisaka, Y. Yamauchi, K. Chida, S. Kasai, T. Ono and K. Kobayashi

Institute for Chemical Research, Kyoto University, Uji, Japan

Keywords: shot noise, quantum point contact, 0.7 anomaly

The quantum point contact (QPC) whose conductance is quantized by the unit of $2e^2/h$ is one of the ideal stages to investigate the quantum transport. Beyond the free electron picture, however, QPC often shows the "anomaly" in the last conducting channel. Recently it has been reported that the shot noise is reduced from the expected value at the conductance anomaly [1,2,3]. It directly indicates that the spin degree of freedom is lifted due to the many body effect. Therefore, it is of great interest to investigate how the conductance anomaly behaves in high magnetic field by the shot noise measurement.

Here, we report the shot noise measurement in a QPC in high magnetic fields. We fabricated gate electrodes on a GaAs/$Al_xGa_{1-x}As$ 2DEG by using electron beam lithography and evaporation. Figure 1 (a) shows the sample image of the scanning electron micrograph and our measurement setup. We changed the electric potential of the QPC by applying different voltages on the two gate electrode [3]. The shot noise was measured in the magnetic fields parallel to the 2DEG between 0 T and 8 T at the electron temperature of 125 mK.

First, we measured the shot noise when the gate voltages were tuned so that the QPC had a quantized plateau in $0.5\times2e^2/h$ at 8 T. The Fano factor is close to zero at ~$0.5\times2e^2/h$ being consistent with previous report[1][2]. Second, we tuned this QPC so that it had an anomaly at $0.25\times2e^2/h$ at 8 T as shown in the upper panel of Fig. 2. Surprisingly, the Fano factor is reduced at ~ $0.25\times2e^2/h$. The differential conductance measurement clearly shows that this anomaly is related to the spin subband (Fig. 2). Recent theoretical work suggests that the Fano factor decreases at $0.25\times2e^2/h$ if the conduction is performed by the spin singlet [4]. The present result may indicate that a similar many-body spin state is formed around the QPC in spite of the high magnetic field.

References

1. Roche *et al*., PRL **76,** 116602 (2004).
2. Dicarlo *et al*., PRL **97,** 36810 (2006).
3. Nakamura *et al*., ArXiv: 0901.3178v1
4. Jeffersoon *et al.,* J.Phys.: **20,** 164206 (2008).

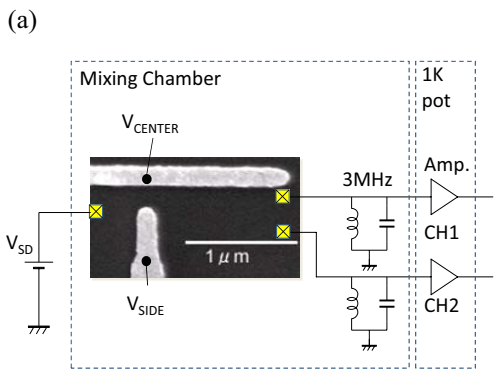

Figure 1 The scanning electron micro graph of the sample and the set up for the noise measurement

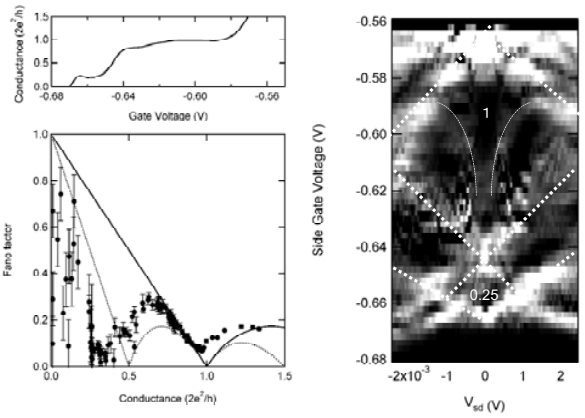

Figure 2 The Fano factor and the differential conductance of the QPC which is quantized in $0.25\times2e^2/h$ anomaly

New aspects of the total filling factor one state

L. Tiemann*, Y. Yoon*, S. Schmult*, M. Hauser*, W. Dietsche* and K. von Klitzing*
**Max-Planck Institute for Solid State Physics, Heisenbergstr. 1, 70569 Stuttgart, Germany*

Correlation effects between two closely-spaced two-dimensional electron systems at a total filling factor of one ($\nu_{tot} = 1$) may spontaneously lead to interlayer phase coherence. One of the most fascinating properties of this quantum coherence is the prediction of a Josephson-effect-like phenomenon [1, 2]. We will give a brief overview of the most compelling experimental signatures of this state and report on more recent developments.

While the single particle tunnel splitting $\Delta_{S,AS}$ for standard double layer systems is indeed small ($\approx$ 100 μK), the tunneling probability itself can increase enormously due to the interlayer coherence when reaching a total filling factor of one. Yet, magneto transport experiments at $\nu_{tot} = 1$ generally disregarded the relevance of interlayer tunneling for transport. Contrary to the common belief we suggest that tunneling may play a rather significant role in transport as well. We will show that the magnitude of the transport current I_D determines whether tunneling is large or small. The value of I_D which separates the strongly from the weakly tunneling case can be found in DC tunneling experiment [3] which will be discussed in detail. By comparing the tunneling data with the data from a counterflow configuration (i.e., where both layers are connected in series), an intriguing new aspect of the total filling factor one state is revealed.

References

[1] Z. F. Ezawa and A. Iwazaki, Phys. Rev. B **47**, 7295 (1993); Z. F. Ezawa, Phys. Rev. B **51**, 11152 (1995).

[2] X. G. Wen and A. Zee, Phys. Rev. Lett. **69**, 1811 (1992).

[3] L. Tiemann, W. Dietsche, M. Hauser and K. von Klitzing, New J. Phys. **10**, 045018 (2008).

Measurement of the coherence length in the integer quantum Hall regime

P. Roulleau*, F. Portier*, A. Cavanna**, G. Faini**, U. Gennser**, D. Mailly** and P. Roche*
*Nanoelectronic group, CEA Saclay, SPEC, F-91191 Gif-Sur-Yvette, France
** Phynano team, CNRS, LPN, Route de Nozay, F-91460 Marcoussis, France

Keywords: Quantum Hall regime, Quantum Coherence, Electronic interferometer

The edge states of the integer Quantum Hall regime (IQHE) are ballistic chiral wires which allow to realize the electronic counter parts of experiments usually done in quantum optic. One of the most promising is the possibility to violate Bell's inequalities [1], using two coupled Mach-Zehnder interferometer [2] and cross correlated noise measurements [3]. However, one of the major limitation for such kind of experiment is the so-called coherence length l_φ which represents the typical length on which a quasi-particle exchanges information with the surrounding environment, loosing by the way his phase memory.

Surprisingly, before our work [4], very little was known about the actual coherence length and on its temperature dependence in the IQHE regime. To determine a coherence length one needs to observe quantum interferences and to vary the length on which these interferences occur. Unfortunately, Fabry-Perot (FP) interferometers, easily obtained with dots, have a phase which depends on the energy. As a consequence FP interferometers are sensitive to the spectral width of the source (the temperature) preventing any direct determination of the coherence length. It is only recently that the improvement of nano-fabrication technics has allowed to realize electronic Mach-Zehnder Interferometers (MZI) which can be designed such that the phase of interferences is energy independent. This is achieved when the two arms of the MZI are of equal length L. Thus, MZIs provide a way for a direct determination of the coherence length when measuring the interferences amplitude. The normalized amplitude of the interferences $\mathcal{V}$ (called the visibility) varies with l_φ like $\mathcal{V} = \mathcal{V}_B \exp(-L/l\varphi(T))$, where $\mathcal{V}_B$ is the base temperature visibility [4].

We present here the very first determination of the coherence length and its temperature dependence, in the IQHE regime at filling factor 2, by measuring the visibility of interferences on three MZIs with sizes scaling up by a factor $\sqrt{2}$ (see Fig. 1). We have shown that l_φ varies like $1/T$ [4, 5], where T is the temperature, and that the coherence length reaches a maximum near the center of the quantum Hall resistance plateau, with a value of 20 μm at 20 mK.

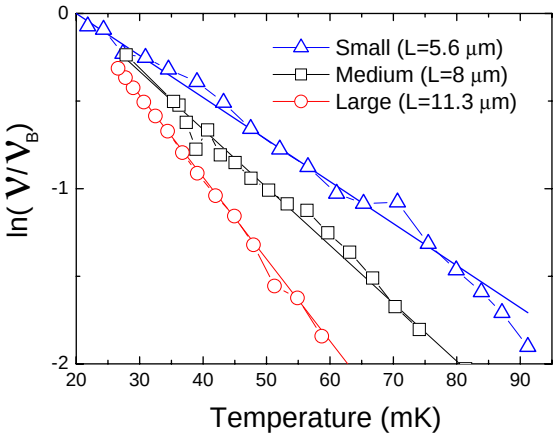

Figure 1: Logarithm of the normalized interferences visibility $\mathcal{V}/\mathcal{V}_B$ versus temperature T for the three interferometers of arm lengths L (from Fig.(3) of ref. [4]). $\ln(\mathcal{V}/\mathcal{V}_B)$ is shown to be a linear function of $-L \times T$.

References

[1] P. Samuelsson, E. V. Sukhorukov, and M. Büttiker, Phys. Rev. Lett. **92**, 026805 (2004).

[2] Y. Ji *et al.*, Nature **422**, 415 (2003).

[3] I. Neder *et al.*, Nature **448**, 333 (2007).

[4] P. Roulleau *et al.*, Phys. Rev. Lett. **100**, 126802 (2008).

[5] P. Roulleau *et al.*, Phys. Rev. Lett. **101**, 186803 (2008).

Electron-hole transport in a 40 nm thick silicon slab

K. Takashina*, K. Nishiguchi*, Y. Ono*, A. Fujiwara*, T. Fujisawa**,
Y. Hirayama*** and K. Muraki*

** NTT Basic Research Laboratories, NTT Corporation, Atsugi-shi, Kanagawa 243-0198, Japan*

Keywords: electron-hole, silicon, drag

Electron-hole bilayers in which a two-dimensional electron gas (2DEG) and a two-dimensional hole gas (2DHG) coexist in close proximity have received considerable interest owing to the possibility of their hosting a condensation of indirect dipolar excitons [1]. Here, we present low temperature transport measurements of a device in which electrons and holes are simultaneously generated but separately contacted [2] based on a 40 nm thick layer of silicon.

The device consists of a Silicon-On-Insulator transistor [Fig. 1(a)] in which the front- and back-gates allow sufficient electric field in the silicon quantum well to overcome the band-gap so that a 2DEG and 2DHG can be generated simultaneously at opposite sides of the well. The device is cut into a Hall-bar where each of the arms is terminated by *p*- and *n*-type contacts [Fig. 1(b)] made by ion implantation of B and P respectively [3]. The *n*-contacts (*p*-contacts) connect to the 2DEG (2DHG) but the *p*-contacts (*n*-contacts) do not due to the depletion regions formed at each junction between the 2DEG (2DHG) and the *p*-contacts (*n*-contacts) leading to independent contacts.

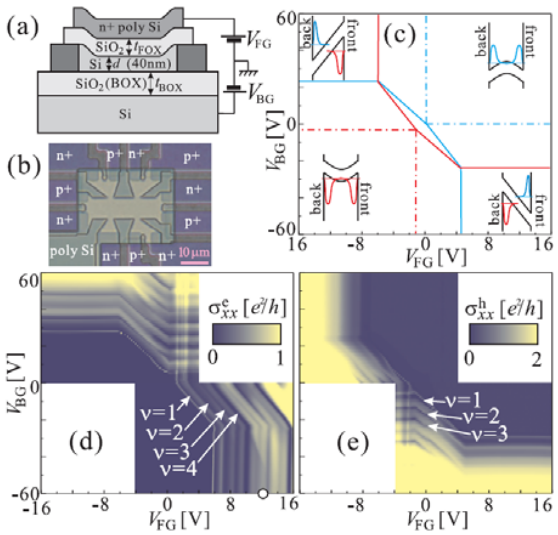

Fig.1 (a) A schematic diagram of the device. (b) An optical micrograph of a Hall bar. The voltage probes are terminated by *n*- and *p*-type contacts. (c) Schematics of the confinement potential in different regions of (V_{FG}, V_{BG}) for data shown in (d) and (e). (d) and (e) show conductivity at B = 15 T, T~250 mK taken using *n*- and *p*-type contacts respectively with an interlayer bias voltage of 0.6 V.

Low temperature measurements of Shubnikov de Haas oscillations [Fig. 1(d) and Fig. 1(e)] show that the charge carriers are generated at the expected positions in the structure [Fig. 1(c)] and that their densities can be controlled by an interlayer bias applied between the 2DEG and 2DHG in addition to the gate voltages. This allows the electric field (confinement potential) to be tuned in the quantum well, and in turn allows the physical properties of the carriers such as the strength of disorder and electronic valley splitting to be controlled [4]. We confirm that drag measurements are possible with the structure.

References

** *Now at Tokyo Institute of Technology, Japan.*

*** *Now at Tohoku University and ERATO Nuclear Spin Electronics Project, Japan*

1. Y.E. Lozovik and V.I. Yudson, JETP Lett. **22**, 556 (1975).

2. U. Sivan, P.M. Solomon and H. Shtrikman, Phys. Rev. Lett. 68, 1196 (1992)

3. K. Takashina et al, Extended Abstracts of the 2006 International Conference on Solid State Devices and Materials, Yokohama 2006, pp.830-831, K. Takashina et al, Jpn. J. Appl. Phys. **46**, 2596 (2007), M. Prunnila et al, Appl. Phys. Lett. **93**, 112113 (2008)

4. K. Takashina et al, Phys. Rev. Lett. **96**, 236801 (2006)

Intrinsic gap of the $\nu_{\mathrm{T}} = 1$ bilayer exciton condensate

P. Giudici[1,2], N. Kumada[1] and K. Muraki[1]

[1] *NTT Basic Research Laboratories, NTT Corporation, 3-1 Morinosato-Wakamiya, Atsugi 243-0198, Japan*

[2] *Institut für Experimentelle und Angewandte Physik, Universität Regensburg, 93040 Regensburg, Germany*

Keywords: QH effect, bilayers, many-body effects

Bilayer electron systems at total filling factor $\nu_{\mathrm{T}} = 1$ presents a new class of purely many-body quantum Hall (QH) state that emerges in the limit of strong interlayer interactions, distinguished by possessing spontaneous interlayer phase coherence and a gap that opens at the Fermi level. Upon increasing the effective interlayer distance d/ℓ_B, the system undergoes a phase transition to a compressible state, characterized by the individual layer filling $\nu = 1/2$. Recently, we have shown that, in the standard experimental conditions, the compressible state is only partially spin polarized, so that the position of the phase boundary strongly depends on the Zeeman energy [1]. This suggests that the behavior of the $\nu_{\mathrm{T}} = 1$ QH state in the vicinity of the phase transition reported thus far may not represent the intrinsic property of the system.

Here we report on the investigation of the quasiparticle energy gap Δ through activation measurements in a tilted magnetic field. The sample consists of a double quantum well with an interlayer distance d ~28 nm and negligible interlayer tunneling. When the Zeeman energy is increased by tilting the sample, we observe that the gap first increases with tilt reflecting the shift of the phase boundary and then saturates at large tilt (Fig. 1a). As a consequence, when the gap is plotted as a function of d/ℓ_B, all data in this saturation region, align on a single curve representing the intrinsic behavior of the gap, solely governed by d/ℓ_B (Fig. 1b). Furthermore, a simple mean-field model based on exciton formation provides, without adjustable parameters, an excellent description of the measured gap (solid line in Fig. 1b).

Our results present the first experimental observation of the intrinsic transition only dependent on d/ℓ_B, as discussed in theory for the spinless system. Furthermore, the remarkable agreement between the measured gap and the model in the Bose-Einstein condensation picture demonstrates that the QH state is being continuously constructed from the compressible state through exciton formation upon decreasing d/ℓ_B. Connections to a theoretical scenario for the continuous transition [2] and implications on the character of the QH state are discussed.

References

[1] P. Giudici, K. Muraki, N. Kumada, Y. Hirayama, and T. Fujisawa, Phys. Rev. Lett. **100**, 106803 (2008).

[2] S. H. Simon, E. H. Rezayi, and M. V. Milovanovic, Phys. Rev. Lett. **91**, 046803 (2003).

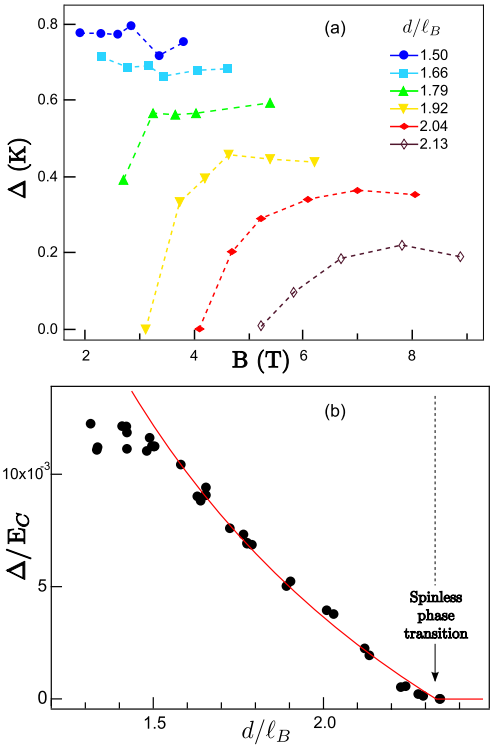

Figure 1: Quasiparticle gap Δ, measured at the tilt angles $\theta = 0°$, 33°, 42°, 48°, 55°, 61° and 65° (symbols). a) Δ plotted as a function of the total magnetic field. The values at the saturation region are plotted in b) as a function of d/ℓ_B. The solid line was obtained from the the exciton condensation model.

P12 E1 MoP E2 E3 E4 TuP E5 P34 E6 E7 E8 ThP E9 P56

Towards the ground state of an electron-hole bilayer

A. F. Croxall, K. Das Gupta, C. A. Nicoll, I. Farrer, H. E. Beere, D. A. Ritchie and M. Pepper
Cavendish Laboratory, University of Cambridge, JJ Thomson Avenue, Cambridge, CB3 0HE, UK

Keywords: electron-hole bilayer, Coulomb drag, exciton, charge density wave

We have fabricated independently contacted electron-hole bilayer (EHBL) devices, where 2-dimensional electron and hole gases are separated by a 10nm $Al_{0.9}Ga_{0.1}As$ barrier. This is close to the excitonic Bohr radius in GaAs ($a_B \approx$10nm). Three decades ago excitonic phases in such a system were predicted [1], but experimental realisation has proven to be extremely difficult. Only recently have transport measurements been possible in a regime where exciton formation is considered likely [2, 3]. At the lowest densities we can reach, the intra-layer particle separation is larger than the inter-layer separation.

We probe the inter-layer scattering rate using the Coulomb drag technique. Current is passed in one layer and the momentum transferred to the other layer is detected as an open circuit voltage. The low temperature data (T<1K) cannot be explained within the Fermi-liquid picture, where an approximate T^2 dependence is expected. We see an upturn in the drag (Fig.1) that indicates the emergence of a new scattering mechanism [4]. In some cases the upturn in the Coulomb drag is followed by a downturn or even a sign reversal at the lowest temperatures. The anomalous drag resistivity when measured on the electron or hole layer disagrees at the lowest temperatures. At matched densities the effect is either absent or weaker in the drag measured on the electrons. This appears to contradict Onsager's reciprocity theorem when applied to four-terminal measurement of resistance. We do not find any non-linearities in our measurements on either the electron or hole layer.

For devices with the thinnest barriers (10nm), we find the presence of the electrons induces a strongly insulating state ($d\rho/dT > 0$) in the single layer resistivity of the holes, in the same temperature range where the anomalous drag is seen [5]. Insulating behaviour in both layers is seen in a regime where $\rho << h/e^2$ and $k_F l > 500$, very far from where the 2D metal-insulator transition is expected. When the electron layer is not present the holes become metallic ($d\rho/dT < 0$), if $\rho < h/e^2$. Thus we can attribute the insulating state to the electron-hole interaction as opposed to background disorder. Similar to the anomalous drag, the insulating state is not very sensitive to matching the densities (n=p). We consider the possibility that a charge density wave phase, indicated by a divergence in the eigenvalues of the bilayer susceptibility matrix [6], may be competing with an excitonic phase.

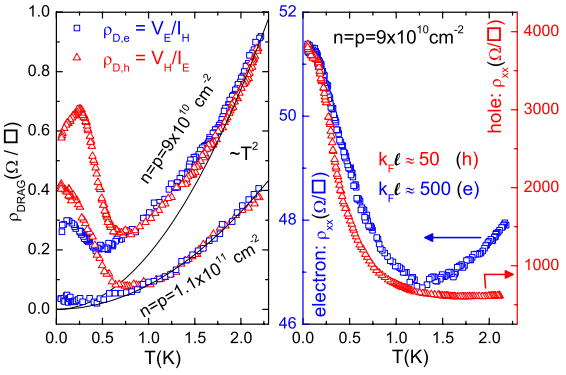

Figure 1: Coulomb drag (left) and single layer resistivities (right) in an EHBL with 10nm $Al_{0.9}Ga_{0.1}As$ barrier. For $n = p = 9\times10^{10}\mathrm{cm}^2$ at 1.5K the mobilities are $\mu_h = 1.1 \times 10^5\mathrm{cm}^2\mathrm{V}^{-1}\mathrm{s}^{-1}$ and $\mu_e = 1.5 \times 10^6\mathrm{cm}^2\mathrm{V}^{-1}\mathrm{s}^{-1}$.

References

[1] Yu. E. Lozovik and V. I. Yudson, Sov. Phys. J.E.T.P. **44**, 389 (1976)

[2] A. F. Croxall *et al.*, Phys. Rev. Lett. **101**, 246801 (2008)

[3] J. A. Seamons *et al.*, Phys. Rev. Lett. **102**, 026804 (2009), C. P. Morath *et al.*, Phys. Rev. B **79**, 041305 (2009)

[4] G. Vignale and A. H. MacDonald, Phys. Rev. Lett. **76**, 2786 (1996)

[5] A. F. Croxall *et al.*, arXiv:0812.3319v1

[6] Lerwen Lui *et al.*, Phys. Rev. B **53** 7923 (1996)

P12
E1
MoP
E2
E3
E4
TuP
E5
P34
E6
E7
E8
ThP
E9
P56

July 21 (Tuesday)

16:00 – 18:00

Poster Session Tu-eP

Meeting Room 501, 502

EP2DS-MSS Parallel session

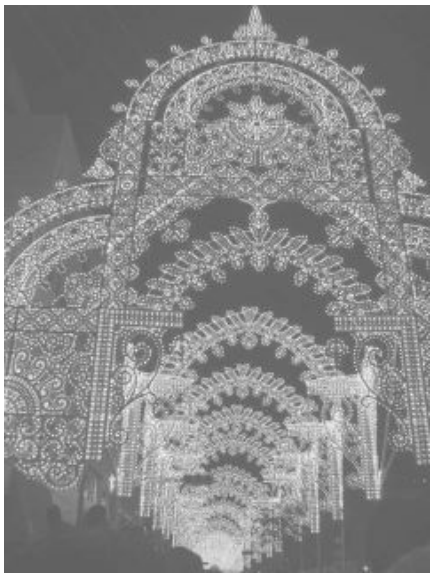

Kobe luminarie
(December)

Quantum Condensation in the electron-hole system with density imbalance

K. Yamashita, K. Asano, T. Ohashi and T. Ogawa
Department of Physics, Osaka University, Toyonaka, Japan

Keywords: phase diagram, FFLO phase, exciton, coupled quantum well, quantum condensation

The electron-hole (e-h) systems in the photo-excited semiconductors or semimetals have been extensively investigated for several decades, and expected to exhibit various phases: e-h plasma, exciton gas, e-h pair condensations, and so on. Recently, the e-h bilayers realized in Type II quantum wells (QWs) attract attention both experimentally and theoretically, where the electrons and holes can have a long radiation lifetime due to the spatial separation between the electron and hole layers. So far, the e-h pair condensation phases on such systems are mainly studied for the "balanced" case, where the electrons and holes have the same density. In the present paper, we consider the "imbalanced" systems with different electron and hole densities, and explore the possibility of the exotic quantum condensation phases at absolute zero temperature.

Besides the e-h systems, the quantum condensation in two-component fermion systems with density imbalance have already been studied for more than 40 years in various fields of physics: in the superconductivity under a magnetic field, in the heavy-fermion physics, in the organic superconductors, in the ultra cold atoms, and in the color superconductivities in quantum chromodynamics. In these studies, two exotic condensation phases are proposed. Those are the Fulde-Ferrel-Larkin-Ovchinnikov (FFLO) and Sarma (breached-pair) phases characterized by the e-h pairs with and without the center-of-mass momentum, respectively. Recently, Pieri et al.[1] suggest that these two phases can also appear in imbalanced e-h bilayer systems. However, their calculations are insufficient to determine the phase diagram, because only the Sarma phase of s-wave pairing, and its instability towards the FFLO phase are investigated.

Our model is same as that used in Ref. 1, where electrons and holes are confined in the different layers, and attract with each other through the long-range Coulomb interaction. However, we estimate the ground energy of the system using the Bardeen-Cooper-Schrieffer (BCS) trial wave functions, in which the center-of-mass momentum of the e-h pairs are taken into account. In this way, we can compare the thermodynamic stability of the Sarma and FFLO phases on an equal footing.

The phase diagram is drastically changed from that shown in Ref. 1. We find that the FFLO phase is fairly stable in the high-density regime. On the other hand, the Sarma phase found in Ref. 1 almost vanishes showing higher energies than those of FFLO phase. It is also turned out that the FFLO phase is stabilized by the continuous deformation of the e-h pair wave function, which is accompanied by lose of its s-wave symmetry. In fact, the FFLO phase is strongly suppressed for the short-range e-h interaction which allows only the s-wave pairing.

References

[1] P. Pieri, D. Nelson, and G. C. Strinati, Phys. Rev. **B75**, 113301 (2007).

Direct excitation of singlet and triplet states in quantum-dot helium by resonant Raman spectroscopy

T. Köppen*, D. Franz*, A. Schramm**, Ch. Heyn*, D. Heitmann*, and T. Kipp*
*Institute of Applied Physics, University of Hamburg, Germany
** Optoelectronics Research Center, Tampere University of Technology, Tampere, Finland

Keywords: quantum dots, optical properties, electronic properties

Semiconductor quantum dots (QDs) containing two electrons, also called artificial quantum-dot helium atoms, are model structures to investigate the most fundamental many-particle states induced by Coulomb interaction. Here, we report on direct excitation into singlet and triplet states in InGaAs quantum-dot helium investigated by resonant Raman spectroscopy in magnetic fields up to $B = 6.5$ T. Importantly for our highly resonant experiments, the QD ground state transition energy matches with both the sensitivity range of our detector and the emission energy of our laser which we achieve by rapidly thermally annealing of the samples. This leads to strong Raman excitations and sharp Raman resonances. The occupation of the QDs with electrons can be controlled and monitored by applying a voltage between a back contact and a gate and by measuring the capacitance. In particular, we can apply a gate voltage so that about 95 % of the QDs are filled with exactly two electrons.

In Fig. 1 measurements varying the exciting laser energy between 1.306 eV and 1.380 eV in steps of ≈ 3 meV at a magnetic field of $B = 4.5$ T are shown. The energy axis is given in Raman depiction, i. e. as the difference between the exciting laser energy E_{L} and the detection energy E_{det}. The spectra are vertically shifted and multiplied by a factor of 9 for Raman shifts smaller than 25 meV.

We observe several sharp peaks resonantly occuring at different excitation energies. By investigating their magnetic field dispersion and by a comparison with numerically exact two electron calculations, these peaks can be assigned to transitions from the ground state into excited singlet and triplet states provoked by both resonant Raman (S_-, T_+, and T_-) and resonant photoluminescence processes (S_+^{PL}, S_-^{PL}, T_+^{PL}, and T_-^{PL}). Furthermore, transitions between excited triplet and singlet (TS) states and, for finite magnetic fields, transition between different angular momentum singlet (Q_2) or triplet (Q_1) states are detected. The experimental observed resonances are totally different if we charge the QDs with exactly one electron, demonstrating the unique and fundamental many body interaction in the two electron case, i. e. the ortho- and para-quantum-dot He.

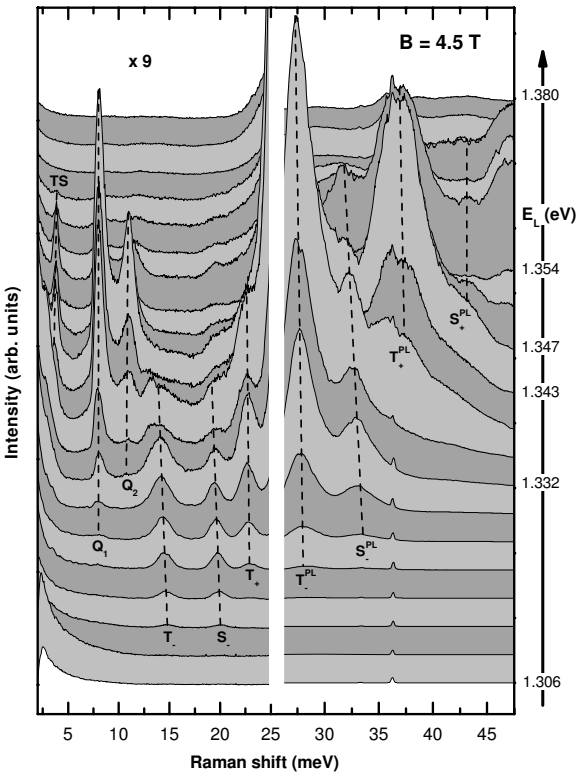

Figure 1: Emission spectra of QDs in He configuration varying the excitation energy E_{L} for a magnetic field of $B = 4.5$ T at $T = 9$ K.

This project is supported by the Deutsche Forschungsgemeinschaft via SFB 508 “Quantenmaterialien”.

Magnetoresistance of two-dimensional electron systems in random magnetic fields with zero mean

J. Wakabayashi, S.Wada and N. Okuda
Department of Physics, Chuo University, 1-13-27 Kasuga, Bunkyo-ku, Tokyo 112-8551, Japan

Keywords: magnetoresistance, random magnetic field, zero mean field, snake orbit

Transport properties of a two-dimensional electron system (2DES) in a spatially random magnetic field (RMF) are classified in two cases according to the type of the RMF, i.e., RMF with zero mean and that with a finite mean value. In the former case and when the RMF is strong, electron transport in 2DES is supposed to be governed by 'snake orbit' formed along $B = 0$ line. In a recent paper[1], the origin of the magnetoresistance of 2DES in RMF with zero mean has been attributed to the 'snake orbit'. When the strength of RMF is weak, on the other hand, the transport is treated semiclassically and the magnetoresistance arises from scattering by RMF.[2] In this paper, we report recent results of magnetoresistance in RMF having several amplitudes with zero mean.

Samples used are Hall bars whose channel width and length are 20 μm and 220 μm, respectively. The channel area was covered by 50 nm thick Au gate electrode. Cobalt disks with a diameter of 1.5 μm were deposited randomly onto the half of the Au gate electrode covering 30% of the area. The thickness of the cobalt disks is 50nm, 70nm, 100nm, 120nm, and 150nm for samples A to E, respectively. We apply an external magnetic field parallel to the 2DES in the direction of the channel. The resultant fringing fields emanating from the cobalt disks with the saturated magnetization produce RMF at 2DES with the amplitude B_0 of 100mT, 136mT, 171mT, 194mT, and 233mT for samples A to E, respectively.

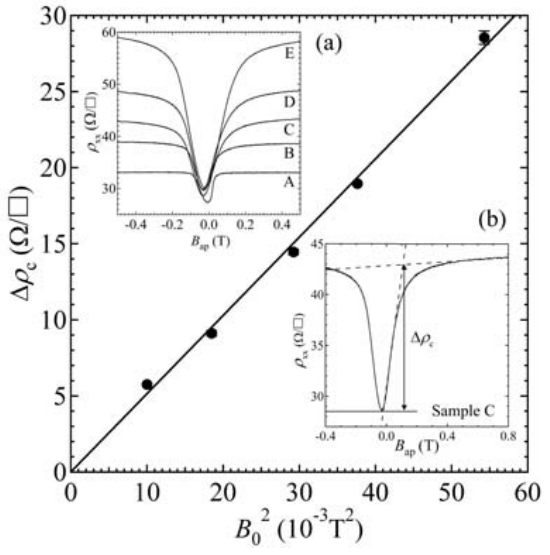

Figure 1: Inset(a): Resistivity ρ_{xx} vs. applied magnetic field B_{ap} for samples A to E. Inset(b): Definition of $\Delta\rho_c$. Main panel: $\Delta\rho_c$ vs. the square of the amplitude of the random magnetic field B_0.

The inset (a) in Fig.1 shows the applied field dependence of resistivity ρ_{xx} of samples A to E at $n_s = 3.8 \times 10^{15}\mathrm{m}^{-2}$ and $T \approx 80$ mK. Near zero field, the resistance increases rapidly as the magnetic field increases giving rise to a cusp structure. Outside of the cusp structure, resistance saturates and we define the magnitude of the cusp, $\Delta\rho_c$, as shown in the inset (b). The obtained $\Delta\rho_c$ for each sample is plotted against B_0^2 in Fig.1, which clearly shows linear dependence. The square dependence of the magnetoresistance on B_0 is theoretically predicted assuming electron scattering by weak RMF. [2]

We have also measured magnetoresistance of samples A to E at several gate voltages. The $\Delta\rho_c$ of each sample has shown a power-law dependence against the electron density (n_s) as n_s^{-k} with $k \simeq 1.5$ in the region $n_s \gtrsim 2.5 \times 10^{15}\mathrm{m}^{-2}$. The value of 1.5 for the exponent is predicted by the theory[2] assuming that the transport is governed by electron scattering due to weak RMF.

Our present results of the square dependence on the amplitude B_0 and the power low dependence on n_s indicate that the magnetoresistance is dominated by electron scattering due to RMF in the present system.

References

[1] A. W. Rushforth et. al. : Phys. Rev. B **70**(2004) 193313.

[2] F. Evers et. al. : Phys. Rev. B **60**(1999) 8951.

Exchange and correlation in two-dimensional systems: Derivation of accurate and practical density functionals

E. Räsänen*, S. Pittalis**, M. A. L. Marques***, C. R. Proetto** and E. K. U. Gross**
*Nanoscience Center, Department of Physics, University of Jyväskylä, Finland
** Institut für Theoretische Physik, Freie Universität Berlin, Germany
*** CNRS, Université Lyon I, Villeurbanne Cedex, France

Keywords: density-functional theory, exchange, correlation, quantum dot

Practical success of density-functional theory depends on finding good approximations for exchange and correlation. So far, most density functionals have been developed in three dimensions (3D) with a view to studying the properties of atoms, molecules, and solids. Such efforts for two-dimensional (2D) systems have been relatively scarce despite the rapidly increasing theoretical, experimental, and technological interest in 2D structures such as semiconductor layers and surfaces, quantum-Hall systems, graphene, and various types of quantum dots.

Here we present our very recent advances in the development of non-empirical 2D density functionals for both exchange and correlation [1, 2, 3, 4, 5]. For finite, inhomogeneous 2D systems, all these functionals lead to considerably more accurate results than the commonly used 2D local spin-density approximation (LSDA).

For the exchange, adapting the strategy of Becke and Roussel [6] to 2D, and thus modeling the cylindrical average of the exchange hole, we derive both implicit and explicit 2D density functionals for the exchange energy [1]. Both functionals lead to accurate results when compared with exact reference data for the uniform 2D electron gas (2DEG) and few-electron quantum dots, respectively. Further generalization of the functional to ring topology leads to accurate description of the electronic exchange in quantum rings, even in the quasi-1D limit, where the (2D) LSDA is explicitly shown to fail [2]. Parallel to this approach, we have also derived a more standard generalized gradient approximation for the 2D exchange, which reduces the error of the LSDA by a factor of four [3].

For the correlation, which is of extraordinary importance in low-dimensional systems, we have developed two functionals [4, 5]. The first one [4] is based on modeling of the correlation-hole functions satisfying a set of exact properties [7]. Excellent performance is obtained in comparison with numerically accurate quantum Monte Carlo data for quantum dots in magnetic fields, as well as for the 2DEG. Our second correlation functional [5] originates from an extension of the Colle-Salvetti approach [8] to 2D, supplemented by a Gaussian approximation for the pair density. The resulting local approximation for the correlation energy broadly outperforms the LSDA, and it is very straightforward to implement.

References

[1] S. Pittalis, E. Räsänen, N. Helbig, and E. K. U. Gross, Phys. Rev. B **76**, 235314 (2007).

[2] E. Räsänen, S. Pittalis, C. R. Proetto, and E. K. U. Gross, Phys. Rev. B, Rapid Comm. (in print).

[3] S. Pittalis, E. Räsänen, J. G. Vilhena, and M. A. L. Marques, Phys. Rev. A **79**, 012503 (2009).

[4] S. Pittalis, E. Räsänen, C. R. Proetto, and E. K. U. Gross, Phys. Rev. B **79**, 085316 (2009).

[5] S. Pittalis, E. Räsänen, and M. A. L. Marques, Phys. Rev. B **78**, 195322 (2008).

[6] A. D. Becke and M. R. Roussel, Phys. Rev. A **39**, 3761 (1989).

[7] A. D. Becke, J. Chem. Phys. **88**, 1053 (1988).

[8] R. Colle and O. Salvetti, Theor. Chim. Acta **37**, 329 (1975); ibid. **53**, 55 (1979).

Strain-enhanced electron mobility anisotropy and piezoelectric scattering in InGaAs/InP 2DEGs

M. Akabori*,**, T. Q. Trinh*, M. Kudo*, Th. Schäpers**, H. Hardtdegen**, T. Suzuki*

* *Center for Nano Materials and Technology, Japan Advanced Institute of Science and Technology, Japan*
** *Institute of Bio- and Nanosystems (IBN-1), Research Centre Jülich, Germany*

Keywords: InGaAs/InP, electron mobility anisotropy, piezoelectric scattering

2DEGs in InGaAs with high indium contents have been obtained by means of metamorphic (MM) growth on GaAs or lattice-matched/pseudomorphic (LM/PM) growth on InP. In MM InGaAs on GaAs(001), the electron mobility anisotropy, highest along the [1-10] direction and lowest along [110], is often observed. While the anisotropy had been attributed to anisotropic lattice relaxation, or interface roughness due to anisotropic cross-hatch morphology (ACHM), it has been claimed that indium composition modulation due to ACHM is the most important mechanism for the anisotropy [1]. However, sometimes there is no mobility anisotropy even in MM InGaAs with ACHM. Moreover, PM InGaAs on InP(001), which of course has neither lattice relaxation nor cross-hatch morphology, also exhibits the anisotropy [2]. These indicate a different origin of the anisotropy. The purpose of this work is to investigate and elucidate the anisotropic electron transport using 2DEGs with high mobility in InGaAs quantum well (QW) obtained by InP-LM or PM growth.

Three modulation-doped structures for 2DEGs, 30nm-InP/10nm-n-InP/20nm-InP/10nm-InGaAs/300nm-InP/InP(001) substrate, were grown by metal-organic vapor phase epitaxy with N_2 carrier gas at 670°C. By using X-ray diffraction we confirmed indium content x = 0.53, 0.62, and 0.75; the $In_xGa_{1-x}As$ QW of x = 0.53 is lattice-matched, while those of x = 0.62 and 0.75 are compressively strained. As shown in Fig. 1, atomic force microscope images of sample surfaces exhibit very smooth morphologies with step-flows. We fabricated 6-terminal Hall-bars (50-µm-width and 200-µm-length) with several current-flowing directions as shown in Fig. 1, [1-10], [100], and [110], whose angles from [1-10] are 0°, 45°, and 90°, respectively. Hall-bar measurements show sheet electron concentrations ~6-8×10^{11} cm^{-2}, and, as shown in Fig. 2, very high mobilities and their systematic anisotropy even in the case of x = 0.53. The data suggests that the anisotropy is enhanced by the strain of QWs. In real strained QWs with imperfection, there are non-vanishing shear strains, which are proportional to average normal strains and cause the piezoelectric (PE) scattering dominating the electron mobility at low temperatures [3]. The anisotropy enhanced by the strain suggests the anisotropy of the PE scattering associated with the shear strains. In the LM case (x = 0.53), interface imperfection due to As-P exchange can induce small strains as well as small anisotropy. We consider that the anisotropy of the electron transport is closely related to the strain and the PE scattering.

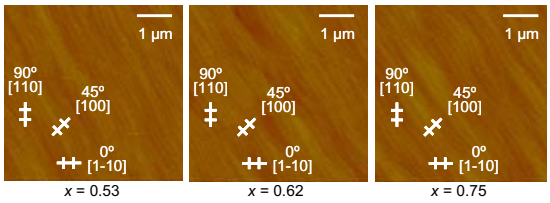

Fig. 1. Surface morphology of the samples and the Hall-bar geometries.

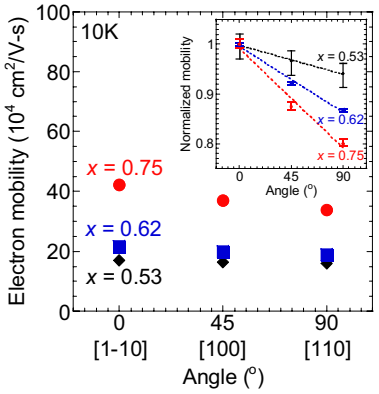

Fig. 2. Electron mobility as a function of angles.

References

[1] D. Ercolani *et al.*, Phys. Rev. B **77**, 235307 (2008).
[2] P. Ramvall *et al.*, Appl. Phys. Lett. **68**, 1111 (1996).
[3] D. N. Quang *et al.*, Phys. Rev. B **68**, 195316 (2003).

Magnetic field dependent non-adiabatic quantized charge pumping

B. Kaestner*, C. Leicht*, V. Kashcheyevs**,***, T. Weimann*, K. Pierz*, and H. W. Schumacher*
*PTB, 38116 Braunschweig, Germany
** Institute for Solid State Physics, University of Latvia, Riga LV-1063, Latvia
***Faculty of Physics and Mathematics, University of Latvia, Riga LV-1002, Latvia

Keywords: single-electron pump, few-electron quantum dot, single-charge tunneling

Quantum dots (QD) connected to leads have been a standard model system for many years to study single charges in so called artificial atoms. Dynamic QDs, which are repeatedly formed and manipulated by time-varying confining potentials appear, for instance, in structures for quantum information processing [1], single-electron [2] or single-photon sources [3], but the understanding of the transport mechanism is limited.

Here we study a periodically formed semiconductor QD leading to non-adiabatic quantized charge pumping, and investigate the magnetic field dependence. The employed QD is defined between two top gates in an $\mathrm{AlGaAs/GaAs}$ heterostructure, where application of an oscillating voltage to one of the gates leads to pumped current plateaus in the gate charactersitic (see Figure). We use a universal decay cascade model introduced in Ref. [4] to describe the transport process, where the current plateaus are related to the confining potential via a fixed sequence of decay rate ratios $\Gamma_n/\Gamma_{n-1} = e^{\delta_n}$, one rate per each QD occupation number n. In the limit of $\Gamma_n/\Gamma_{n-1} \gg 1$, δ_n determines the distance between the n-th and $n-1$-st steps.

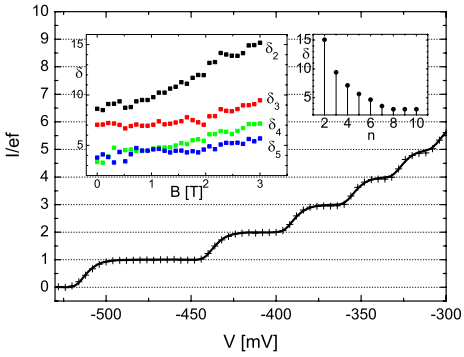

Figure: Pumped current I normalized by the pumping frequency f and the elementary charge e as function of control gate voltage V. A perpendicular-to-plane magnetic field of $B = 3\,\mathrm{T}$ was applied. Crosses correspond to the measured current while the solid line represents the fit to the model. The fitting parameters, δ_n, are plotted in the insets: the right inset shows the case for $B = 3\,\mathrm{T}$, while in the left inset the evolution of $\delta_{2\ldots5}$ can be seen when the magnetic field is increased from $B = 0$ to $3\,\mathrm{T}$.

In the second part the dependence of the plateau characteristic on perpendicular-to-plane magnetic field will be investigated [5]. The aim is to manipulate these tunnel couplings owing to the magnetic field influence on the wave function and the corresponding rearrangement of electrons between quantum states. By fitting to the model we extract information on the tunnel couplings of different few-electron states to the leads from the plateau structure, as shown in the right inset of the Figure. The left inset shows how these decay rate ratios evolve with magnetic field. The decay rates Γ_n seem to be affected differently depending on the occupation number n. In general we find that in magnetic field the current quantization may be improved, i.e. the value of δ_n increases, and that quantization is sustained up to magnetic fields where full spin polarization of the device can be expected.

References

[1] C. H. W. Barnes, J. M. Shilton, and A. M. Robinson, Phys. Rev. B **62**, 8410 (2000).

[2] B. Kaestner *et al.*, Phys. Rev. B **77**, 153301 (2008).

[3] J. R. Gell *et al.*, Appl. Phys. Lett. **89**, 243505 (2006).

[4] V. Kashcheyevs and B. Kaestner, arXiv:0901.4102 [cond-mat.mes-hall] (2009).

[5] B. Kaestner *et al.* Appl. Phys. Lett. **94** 012106 (2009).

Magneto-polarons in quasi two-dimensional electron systems

C. Faugeras*, M. Orlita*, J. Kunc*, S. Deutschlander*, G. Martinez*, M. Potemski*, P.Y. Yu**, A. Riedel***, R. Hey***, K-J. Friedland***, G. Karczewski****, T. Wojtowicz****

** LNCMI-CNRS, Grenoble, France*

***University of California,Berkley, USA*

**** Paul Drude Institute, Berlin, Germany*

***** Institute of Physics, Polish Academy of Science, Warsaw, Poland*

Keywords: Magneto-polaron, FIR magneto-transmission, 2DEG

The electron-optical phonon interaction is the relevant property of polar semiconductors, leading among other things to the formation of quasi-particles known as polarons. Despite many experimental approaches, over last 30 years, no clear evidence of polaronic effects in a free quasi two dimensional electron gas with weak disorder has been reported so far. In contrast, these effects are clear for excitations of electrons which are localised on impurities or laterally confined in quantum dots.

Our previous studies on highly doped samples revealed no signs of interaction with the bare LO phonon but rather with the TO phonon [1,2]. This was later described as being the resonant magneto-polaron effect of a high density polaron gas [3,4]. In this communication, we present absolute magneto transmission experiments performed for magnetic fields up to 33T on single quantum wells (QW) doped at a lower level and we show that they exhibits a pronounced resonant polaron effect and new unexpected features not seen in higher doped samples. The QWs are based on 2 different material systems:

- two single CdTe QWs with a width of 20 nm and 30 nm and doping of $4.2x10^{11}$ cm^{-2} and $3.4x10^{11}$ cm^{-2} respectively, with mobilities up to 240000 $cm^2.V^{-1}.sec^{-1}$.

- a series of single GaAs QWs with a width of 13nm, doped at a level Ns ranging from 2 to $7.5x10^{11}$ cm^{-2} and mobilities exceeding 10^6 $cm^2.V^{-1}.sec^{-1}$.

The analysis of the spectra is done with a multi-layer dielectric model which allows extracting the imaginary part of the electronic dielectric function, the damping parameter. Its variations are characteristic of any interaction mechanism.

For the CdTe QWs grown within a structure such that the reststrahlen band (RB) is not fully developed and the resonant condition can be investigated, we observe a pinning of the cyclotron resonance (CR) line at the CdTe LO phonon energy and, at higher fields, a new CR line appears at higher energy with a reduced effective mass together with a large increase of the damping parameter. This behaviour is characteristic of polaronic interaction involving the bare LO phonon of the QW.

For the GaAs quantum wells, the LO phonon range of energy is obscured by the substrate and we thus focus on energies above the RB. The line width of the CR line exhibits different features for cyclotron energies higher than the bare LO phonon energy. For the lower doped samples, the field dependence of the damping parameter shows a pronounced increase when the energy exceeds the longitudinal optical phonon energy characteristic of polaronic effects. At higher fields this parameter increases once more resonantly showing a new interaction. For densities higher than $6x10^{11}$ cm^{-2}, only this new interaction is clearly visible though its amplitude decreases when increasing the doping. We will discuss the origin of this new interaction which is very likely related to mechanisms involving phonons.

References

1.A.J.L. Poulter *et al*, Phys. Rev. Lett. **86**, 336, (2001).
2.C. Faugeras *et al*, Phys. Rev. Lett. **92**, 107403, (2004)
3.S. Klimin *et al.*, Phys Rev. B **68**, 45303, (2003)
4.S. Klimin *et al.*, Phys. Rev. B **77**, 205311, (2008)

Resonant coupling effects in InSb quantum well heterostructures

J. M. S. Orr*, K.-C. Chuang*, R. J. Nicholas* and P. D. Buckle**

** Clarendon Laboratory, University of Oxford, Oxford, UK, ** QinetiQ, Malvern, UK*

Keywords: Cyclotron resonance, polaron coupling, narrow bandgap

We report spin-resolved cyclotron resonance (CR) measurements in InSb/AlInSb-on-GaAs quantum well (QW) heterostructures in which the cyclotron effective mass was deduced and resonant coupling phenomena were observed. Unlike GaAs-based heterostructures the dissimilar 2DEG and substrate materials in these samples allow the observation of resonant coupling effects outside the substrate restrahlen band.

InSb quantum well heterostructures are able to achieve high room temperature mobility [1]. Their narrow bandgap leads to strong non-parabolicity effects which can be observed in both the effective mass and Landé g-factor making it an ideal system in which to detect spin-resolved transitions. Spin-resolved CR is detected at fields as low as 2.2T in these samples, which is significantly lower than in comparable InAs-based systems. Figure 1 shows the experimental CR energies as a function of magnetic field up to 11.5T obtained using a FTIR spectrometer. The transitions were identified by comparison to an 8-band **k.p** model (solid lines).

Resonant coupling was observed in the data via a characteristic anti-crossing of the CR transitions (see figure 1), due to resonant subband-Landau level coupling (RSLC) and resonant magnetopolaron coupling (RMPC). RSLC was observed at small and zero tilt angles, giving subband energies consistent with modelling. According to a single band approach the subbands are decoupled while the field remains perpendicular to the 2DEG, however a more careful multi-band treatment reveals that such coupling is allowed, and is enhanced in narrowgap materials such as InSb. This allows the electron motion in the 2DEG plane to couple to motion in the z-direction. In bulk materials RMPC occurs when $\hbar\omega_c \approx \hbar\omega_{LO,}$ however in a 2DEG the resonance energy is modified by coupling between the LO phonon and the intersubband plasmon [2]. Resonant coupling of the CR to this mode is allowed in perpendicular field as a result of the z-(x,y) decoupling induced by the non-parabolicity. Strong RMPC can be observed in these samples because it occurs outside the substrate restrahlen band. RMPC was seen to occur just below the InSb LO phonon energy to a hybrid intersubband plasmon-LO phonon mode, indicating a small contribution from the 2DEG plasmon.

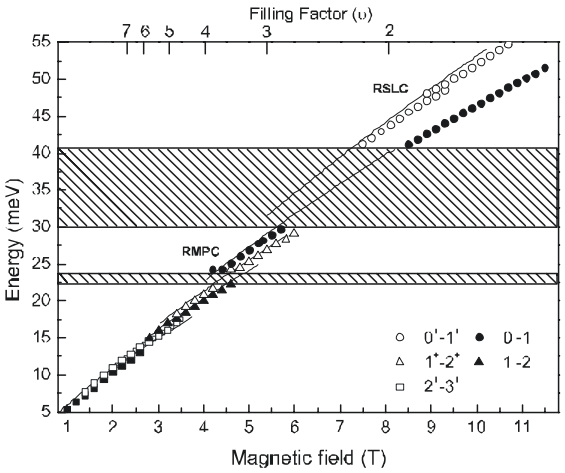

Fig 1. CR energies for InSb quantum well heterostructures measured in the perpendicular Faraday geometry.

References

[1] J.M.S. Orr *et al.* Phys. Rev. B **77** 165334 (2008)

[2] C.Faugeras *et al.* Phys. Rev. Lett. **92** 107406 (2004)

Microwave induced magnetoresistance oscillations and inelastic scattering time in double quantum wells

S. Wiedmann*, G. M. Gusev**, O. E. Raichev***, A. K. Bakarov** and J. C. Portal*,****
*LNCMI-CNRS, BP 166, 38042 Grenoble and INSA, 31077 Toulouse, France
** Instituto de Física da Universidade de São Paulo, São Paulo, SP, Brazil
*** Institute of Semiconductor Physics, NAS of Ukraine, Kiev, Ukraine
**** Institut Universitaire de France, 75005 Paris, France

Keywords: double quantum wells, magnetotransport, microwave excitation, inelastic scattering time

Transport properties in two-dimensional electron systems (2D) irradiated by a continuous microwave irradiation have recently attracted much interest in experimental and theoretical studies [1]. The so-called microwave induced resistance oscillations (MIROs) which evolve into Zero Resistance States (ZRS) for ultrahigh mobility and high microwave power are governed by the ratio of the radiation frequency ω and the cyclotron resonance ω_c.

Double quantum wells (DQWs) with two occupied subbands indicate new transport features know as magneto-intersubband oscillations (MIS) due to a periodic modulation of the probability of intersubband transitions in the magnetic field [2]. These MIS oscillations illustrate a strongly different picture under microwave irradiation compared to QWs. In DQWs groups of MIS peaks are continuously enhanced or inverted for different frequencies (see Figure 1). The theoretical model for this two-subband system is based on the inelastic mechanism (see [3] and references therein) which explains the experimental results very well for low temperatures.

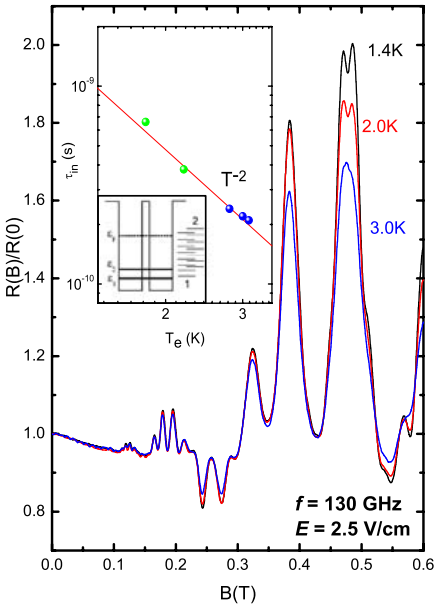

Figure 1: Magnetotransport in a DQW under a continuous microwave irradiation of 130 GHz at different temperatures. The inelastic scattering time is extracted from theory [3] and plotted as a function of electron temperature T_e (see inset with a sketch of a DQW system with two occupied subbands).

We have performed measurements in double quantum wells, separated by a barrier of 1.4 nm with a subband energy of Δ_{12} = 3.67 meV in the temperature range between 1.4 K and 3.5 K under a continuous microwave irradiation from 35 to 170 GHz. In order to extract inelastic scattering time τ_{in}, we fit experimental data with the theoretical model in [3] for different temperatures at a fixed microwave electric field. Temperature dependent transport time τ_{tr} and quantum lifetime τ_q, we extract from traces without microwave irradiation. We confirm that the inelastic scattering event (inelastic mechanism) explains well data in this temperature range.

References

[1] M. A. Zudov *et al.*, Phys. Rev. B **64**, 201311(R) (2001), R. G. Mani *et al.*, Nature **420**, 646 (2002), I. A. Dmitriev *et al.*, Phys. Rev. B **71**, 115316 (2005).

[2] N. C. Mamani *et al.*, Phys Rev. B **77** 205327, (2008).

[3] S. Wiedmann *et al.*, Phys. Rev. B **78**, 121301(R), (2008).

Non-equilibrium interaction of electrons and phonons on the nanoscale

G. J. Schinner*, H. P. Tranitz**, W. Wegscheider**, J. P. Kotthaus*, S. Ludwig*
*Center for NanoScience and Fakultät für Physik, Ludwig-Maximilians-Universität, Geschwister-Scholl-Platz 1, 80539 München, Germany
** Institut für Experimentelle und Angewandte Physik,Universität Regensburg, 93040 Regensburg, Germany

Keywords: back–action, electron–electron–interaction, phonon–spectroscopy, non–equilibrium

Interactions between nanoscale devices is a key component for solid–state–based quantum information processing. E. g. the capacitive coupling between a biased quantum point contact (QPC) and quantum dots (QD) is utilized for charge detection of a qubit. In this context, the back–action of a QPC is often associated with Coulomb–forces between fluctuating charges [1].

We have performed experiments demonstrating that interface phonons, emitted by non–equilibrium electrons, can dominate such back–action [2]. Our setup combines a hot electron transfer amplifier (HETA) [3] device with phonon spectroscopy within the two–dimensional electron system (2DES) of a high mobility GaAs/AlGaAs–heterostructure. The layout of our sample displayed in the electron micrograph in Figure 1 contains a Hall–bar connected to eight ohmic contacts. QPCs can be electrostatically defined at the two ends of the Hall–bar. In its center region three gates, spanning the entire bar, are negatively biased to define and control barriers (B1, B2, B3) for electrons.

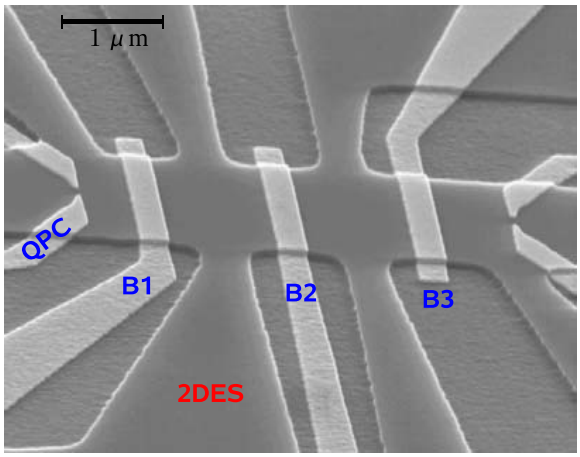

Figure 1: Scanning electron micrograph showing the sample layout. Elevated dark–gray areas contain a 2DES. Light–gray areas are metal top–gates.

In our measurements one barrier (e. g. B2) is always adjusted to be completely opaque for electrons, separating an emitter circuit from an unbiased detector circuit. We show conclusively that interface acoustic phonons emitted by a biased QPC (all other ohmic contacts are grounded) transport energy across the opaque barrier. Part of these phonons, moving in the plane of the 2DES, are reabsorbed by electrons, giving rise to a current across an unbiased detector barrier (B3) adjusted to be just high enough to prevent linear response current. Tuning this barrier we perform energy spectroscopy of the electrons excited in the detector circuit. We find an upper bound for the energy absorbed by electrons corresponding to back–scattering of cold electrons by interface phonons.

In addition to phonon spectroscopy the emitter circuit can be adjusted to resemble a HETA, using B1 as tunable barrier, while B2 is always opaque for electrons. B2 separates the HETA from the phonon–detector circuit as above. Hot electrons emitted by the QPC to the left of B1 loose part of their energy by electron–electron scattering thereby multiplying the number of electrons excited above the Fermi–level. Adjusting the transmission of barrier B1 this three terminal device can result in a current–amplification, i. e. the current flowing across B1 can be enhanced compared to the current originally emitted at the QPC. In our setup we combine the two techniques, HETA and phonon–spectroscopy, to study the interplay of electron–electron and electron–phonon interactions.

References

[1] E. Onac, et al., Phys. Rev. Lett. **96**, 176601 (2006).

[2] G. J. Schinner, H. P. Tranitz, W. Wegscheider, J. P. Kotthaus, S. Ludwig, arXiv:0901.3520 (2009).

[3] M. Heiblum, Solid-State Electronics **24**, 343 (1981).

A disordered GaAs 2D electron gas in a strong in-plane magnetic field: Interplay between spin, orbital effects and localization

B.A. Piot*, D. K. Maude*, U. Gennser**, A. Cavanna**, and D. Mailly**

*Laboratoire National des Champs Magntiques Intenses, Grenoble High Magnetic Field Laboratory, Centre National de la Recherche Scientifique, 25 Avenue des Martyrs, F-38042 Grenoble, France

** Laboratoire de Photonique et de Nanostructures, Centre National de la Recherche Scientifique, Route de Nozay, 91460 Marcoussis, France

Keywords: spin polarization - electron electron interactions - localization - GaAs

An in-plane magnetic field couples to the spins of a 2D system, and can thus be used to probe the impact of many body effects on the ground state of the 2D electron gas (2-DEG). For example, the longitudinale resistance under parallel magnetic field generally exhibits a saturation or a kink for a magnetic field B = Bp signaling the complete spin polarization of the 2D system [1].

In this work, we report on the particularly rich parallel field physics occurring in 2D electron gas in GaAs, revealing an interplay between these spin effects, disorder, and orbital effects. The magneto resistance kink usually associated with the 2-DEG complete spin polarization is observed up to B_p ~30T, and shifts down continuously on more than 20 T as the electron density (and mobility) is lowered in the sample (see Fig.1), consistent with the predicted electron-electron interaction enhancement of the spin susceptibility at low density. However, the absolute value of B_p remains 2-3 times smaller than the one calculated at T = 0K for a disorder-free system. We argue this offset is due to the localization of electrons which are subsequently subtracted from the total free carrier density. In this situation the Fermi sea appears effectively smaller and less magnetic field is required to fully polarize the system. This approach is motivated by the strong mobility drop measured as the electron density is decreased in this region and confirmed by the temperature dependence of B_p corresponding to the polarization of an effectively smaller Fermi sea. From this temperature behavior, a density of delocalized electron can be estimated, and used to re-plot the experimental B_p of Fig.1.b. (triangles), giving a better quantitative agreement with theory

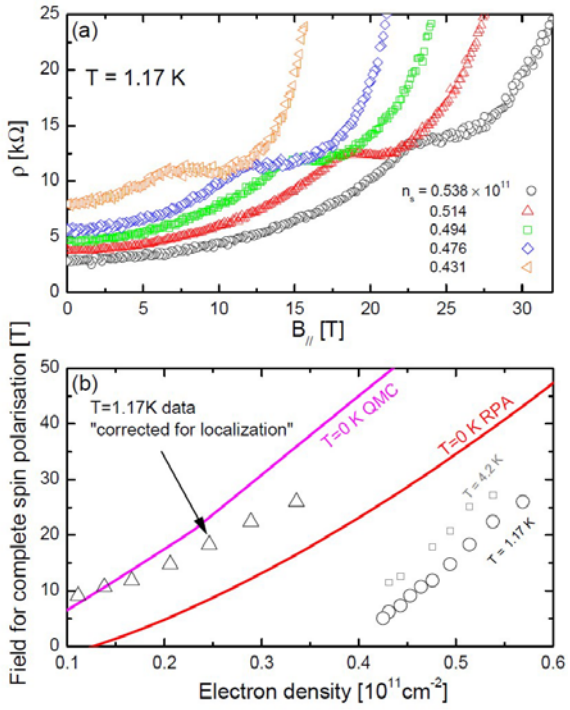

Figure 1: (a) Magneto resistance for different electron densities. (b) Field associated with the complete spin polarization Bp as a function of the electron density (circles and squares), and as a function of the " corrected " electron density (triangles). Theoretical T = 0K calculations of the magnetic field for full spin polarization including many-body effects: RPA [2], and QMC [3].

References

[1] T. Okamoto, K. Hosoya, S. Kawaji, and A. Yagi, Phys. Rev. Lett. **82**, 3875 (1999).

[2] Y. Zhang and S. D. Sarma, Phys. Rev. Lett. **96**, 196602 (2006).

[3] A. L. Subasi and B. Tanatar, Phys. Rev. B **78**, 155304 (2008).

Observation of the Mahan exciton in shallow quantum dots strongly coupled to an electron reservoir

N. A. J. M. Kleemans*, J. Van Bree*, A. O. Govorov**, G. J. Hamhuis*, R. Nötzel*, A. Yu. Silov* and P. M. Koenraad*

*Photonics and Semiconductor Nanophysics, COBRA, Eindhoven University of Technology, The Netherlands

** Department of Physics & Astronomy, Ohio University, Athens, USA

Keywords: self-assembled quantum dots, hybridization, Mahan exciton, photoluminescence

Charge-tuneable shallow self-assembled InAs/GaAs quantum dots (QDs) interacting with a Fermi sea of electrons in the back contact are investigated. We report the strong coupling of the QD excitonic states to the electron reservoir. The tunnel coupling of electrons between the n-doped back contact and the QDs results in the hybridization of the final states of the negatively charged exciton X^- [1]. This gives rise to non-Lorentzian line shapes and an unusual voltage dependence of the emission energy of the X^-.

We demonstrate that strong coupling of the back contact to the excitonic states in shallow QDs gives rise to new excitonic states. The photoluminescence (PL) of individual dots as function of the gate voltage is analyzed. For large negative gate voltages we observe that the emission energy of several exciton complexes are strongly dependent on the gate voltage (see Figure 1). These lines are labeled by X^n_M, where n corresponds to the charged state of the exciton. Analysis of the voltage dependence shows that the emission energy reflects the lever arm of our device and is directly related to the Fermi energy in the back contact. These lines result from the recombination of an electron present in the back contact and a hole residing in the QD. The line shapes resemble the Fermi edge singularity in modulation-doped quantum wells [2]. This type of exciton is known as the Mahan exciton [3], and has up till now never been observed in QDs.

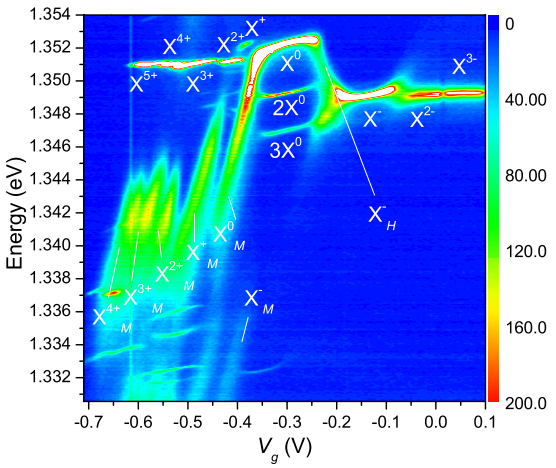

Figure 1: The measured PL spectrum of a shallow QD strongly coupled to the electron reservoir in the back contact as function of the gate voltage V_g. The scale bar relates to the detector counts. The different exciton complexes are indicated. The recombination lines of the Mahan exciton complexes are labeled as X^n_M.

Furthermore, we observe the transition of the neutral exciton (X^0) plateau to the X^- plateau, indicated by X^-_H in Figure 1. The transition region can be described by a hole and an electron residing in the QD and a second electron being in a hybridized QD-continuum state. The X^-_H feature can be well understood using a model based on the Anderson Hamiltonian, which includes the tunnel coupling between an electron reservoir and the electron energy level in the QD [4]. Magneto-luminescence experiments show that the hybridization of the X^0 plateau gives rise to a change of the exciton g-factor up to 10 percent over the length of the plateau.

References

[1] P. A. Dalgarno *et al.*, Phys. Rev. Lett. **100**, 176801 (2007).

[2] M. S. Skolnick *et al.*, Phys. Rev. Lett. **58**, 2130 (1987).

[3] G. D. Mahan, Phys. Rev. B **21**, 1421 (1980).

[4] A. O. Govorov *et al.*, Phys. Rev. B **67**, 241307(R) (2003).

Unusual cyclotron resonance line broadening in ultra-high mobility two-dimensional electron system

L.-C. Tung*, X.-G. Wu**, L. N. Pfeiffer***, K. W. West*** and Y.-J. Wang *

* *National High Magnetic Laboratory, Tallahassee, Florida, USA*

** *Department of Physics, Institute of Semiconductor, Chinese academy of Science, China*

*** *Bell Laboratorys, Lucent Technologies, Murray Hill, New Jersey, USA*

Keywords: cyclotron resonance line shape, ultra-high mobility two dimensional electron system

A systematic infrared optical study has been carried out on a set of ultra high mobility (>10^7cm²/Vs) GaAs/$Ga_{0.7}Al_{0.3}As$ samples at 4K to study the line width of electron cyclotron resonance (CR). In Faraday geometry, the observed CR line width (half width half maximum) remains around the resolution limits used in the measurements at low fields. (<20T) Then the line width grows rapidly with increasing magnetic field, reaching over 10 cm^{-1} at 33T, as shown in Fig. 1. This behaviour is uniquely found in all three heterojunctions (HJs) studied, but not in the quantum well samples with comparable mobility and carrier density. At the same time, transport measurements show no signs of dropping mobility, manifested by the clear observation of the fractional quantum Hall states for both types of samples.

When a HJ sample is tilted from the normal field direction, an anti-level crossing at 100cm^{-1} is observed and the CR starts to become broad near the crossing point. Although the level crossing can be attributed to the resonant subband-Landau-level coupling, [1] the line width broadening is very unusual. The width continues to grow with increasing magnetic field, even when the CR energy is far away the subband separation energy. As the tilting angle is increased, the point where the line begins to grow moves to lower energy. When the angle is 35°, the integrated intensity begins to decrease around ω_c= 80cm^{-1} and the CR completely disappears at about ω_c= 90cm^{-1}, the entire upper branch of the anti-level crossing can no longer be observed. Our similar tilting measurements on the quantum well samples show no measurable CR line broadening near the subband-Landau-level crossing, and HJs with ordinary mobility only exhibit line broadening near the anti-level crossing. [1] Our observed CR line width does not follow $\sqrt{B}$ asymptotically, predicted by Ando *et. al.* [2] for short-range scattering. And there is no sign of narrowing down at highest reachable magnetic fields, observed in the past for samples with ordinary mobility. [3]

The origin of this novel behaviour is not yet understood, and we hope that our presentation will stimulate the interests among theorists for this subject.

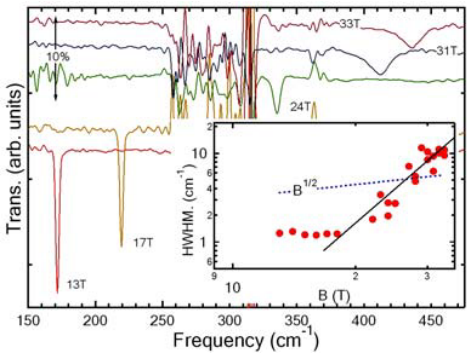

Fig.1 The magneto-IR spectra at several selected magnetic fields. Inset: CR line width as a function of the magnetic field B. The dashed line demonstrates $\sqrt{B}$-behavior in the log-to-log plot.

References

1. Z. Schlesinger, J. C. Hwang and S. J. Allen, Jr., Phys. Rev. Lett. **50**, 2098 (1983)
2. T. Ando and y. Murayama, J. Phys. Soc. Jpn. **54**, 1519 (1985).
3. B. A. Wilson, S. J. Allen. Jr. and D. C. Tsui, Phys. Rev. B **24**, 5887 (1981)

3D nanoscale control of doping profiles in silicon

Sarah R. McKibbin*, Warrick R. Clarke*, A. Fuhrer*, T. C. G. Reusch** and Michelle Y. Simmons*,**
*School of Physics, University of New South Wales, Sydney, 2052, Australia
**Australian Research Council Centre of Excellence for Quantum Computer Technology

Keywords: STM, 3D, multi-layer, δ-doping.

Scanning tunneling microscopy (STM) has been shown to provide atomic precision control of doping profiles in silicon down to the level of single atoms[1]. In combination with molecular beam epitaxy (MBE) this technology has the potential to realise atomic level control of doping in all three dimensions, thus providing a mechanism to investigate further miniaturization of silicon transistors.[2]

STM lithography on H:Si(100) with PH_3 gas has shown that we can laterally confine P dopants on one atomic plane[3] to produce nanowires, tunnel junctions and quantum dots.[4, 5, 6]. In this presentation we discuss the adaptation of this technology towards 3D devices by STM-patterning multiple layers vertically. We present three sets of results: the first is the optimisation of the encapsulation of the first active layer to form the starting surface for the second active layer. Here we demonstrate the importance of the growth conditions to achieve full electrical activation whilst minimising vertical dopant diffusion and provide an optimal starting surface for the second active layer, see Figure 1. Secondly we present a study of 2D bilayers of delta-doped P:Si, to highlight the presence this first layer has on the electrical activation of the second layer. Finally we will present results from the first 3D patterned devices where we have investigated the ability to vertically gate wires and junctions with nanometer dopant control, see Figure 2. This is the first time that fully 3D control of dopant profiling in silicon has been achieved with nanometer precision.

References

[1] S. R. Schofield, Phys. Rev. Lett. **91**, 136104 (2003).

[2] V. V. Zhirnov, IEEE Trans. Semicond. Manuf. **15**, 157-168 (2002).

[3] J. W. Lyding, J. Vac. Sci. Technol., B **12**, 3735 (1994).

[4] F. J. Ruess, Nano Lett. **4**, 1969-1973 (2004).

[5] W. Pok, IEEE Trans. Nanotechnol. **6**,213 (2004).

[6] A. Fuhrer, Nano Lett. **9**, 707-710 (2009).

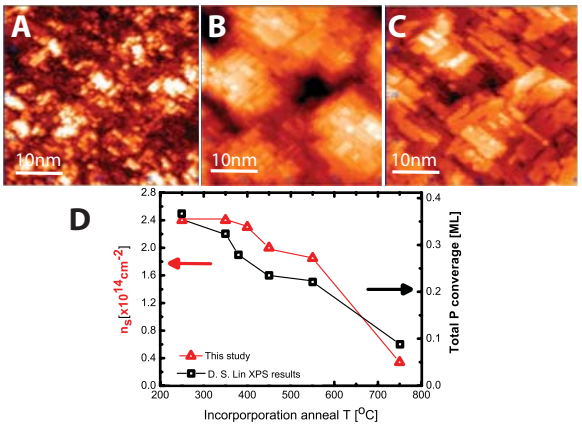

Figure 1: STM images of the regrowth surface after PH_3 incorporation at (a) 350°C, (b) 450°C (c) 550°C (d) Corresponding activation of the Si:P δ-layer as a function of incorporation temperature.

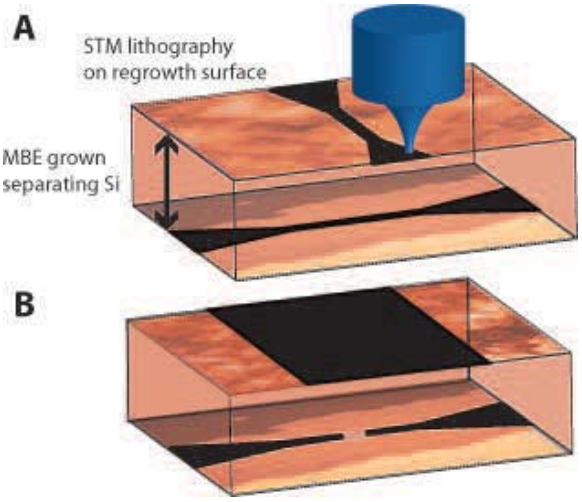

Figure 2: A schematic of two different 3D STM-patterned devices made to date where the first active layer is made on the Si(001)2×1 surface and the second active layer is made on a regrowth surface. (a) Crossbar wire, (b) Gated nano-gap.

Coherent manipulation of an exciton in a single quantum dot using a heterodyne pump-probe technique

Yasuyoshi Mitsumori*,**, Yuki Miyahara*, Hideo Kosaka*,** and Keiichi Edamatsu*

* *Research Institute of Electrical Communication, Tohoku University, Japan*

** *CREST, Japan Science and Technology Agency, Japan*

Keywords: quantum dot, Rabi oscillations, heterodyne

Exciton in semiconductor quantum dot with the discrete energy structure and long coherence time is extensively studied to develop quantum computation devices controlled by light. In typical experiments to study transient optical properties of a single quantum dot, strong scattered light from pump pulses prevents the direct probing of the excited exciton state. Because of this difficulty, many experiments are performed by monitoring indirect states, such as luminescence from a lower exciton state relaxed from the upper excited state [1] or an orthogonally polarized state using cross-polarized pump and probe beams [2]. Here, we propose and demonstrate the application of a heterodyne detection technique to coherent manipulation of an exciton in a transient micro-pump-probe spectroscopy. This technique provides direct monitoring of the excited state even in the presence of strong pump pulses.

The sample in this work is a pyramidal dot in a single GaAs/GaAlAs quantum well [3]. Optical pulses from a ps-Ti:sapphire laser are divided into three beams for preparing the pump, probe and reference pulses. The probe pulse, whose frequency is shifted by 21 MHz by an acoustic optical modulator (AOM), and the pump pulse without the frequency shift are collinearly fed into an objective lens and focused on the sample. The probe pulse reflected from the sample is mixed with the reference pulse, whose frequency is shifted by 20 MHz, to obtain a heterodyne signal. A beating signal with the frequency difference (1 MHz) of the probe and reference pulses is monitored in combination with a lock-in technique.

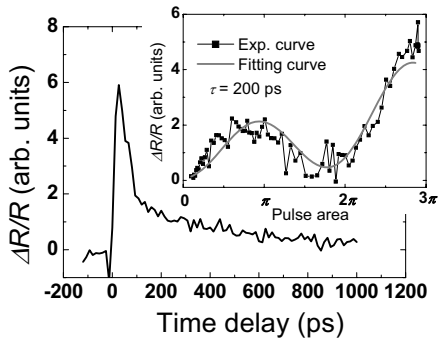

Fig.1 *ΔR/R* vs. time delay. Inset shows *ΔR/R* at 200 ps as a function of the pump pulse area.

Figure 1 shows the pump-induced change in the reflectivity (*ΔR/R*) as a function of the time delay between the pump and probe pulses at 4K. The clear decay profile of the signal represents the successful elimination of the influence of the pump pulse. The decay time constant, which corresponds to the lifetime of the exciton in the single quantum dot, is estimated to be 500 ps. As shown in inset in Fig. 1, the *ΔR/R* exhibits oscillation structure as a function of the pump pulse area; the behavior can be understood as the Rabi oscillations. The oscillatry behavior can be reproduced by a fitting, in which we assume at least two quantum states responsible for resonant and non-resonant Rabi oscillations. Our results suggest that the heterodyne technique is a powerful tool for transient optical studies and coherent manipulation of an exciton in a single quantum dot.

References

1. H. Htoon, *et al.,* Phys. Rev. Lett. **88**, 087401 (2002).
2. T. H. Stievater, *et al.*, Phys. Rev. Lett. **87**, 133603 (2001).
3. K. Edamatsu, *et al.*, J. Lumin. **94-95**, 143 (2001).

Transport properties of a quasi-one-dimensional electron system on the surface of liquid helium

D.G.Rees, H. Ikegami and K. Kono

Low Temperature Physics Group, RIKEN, Wako, Japan

Keywords: Quasi-one-dimensional Surface Electron Qubit

Electrons on the surface of liquid helium form an almost ideal two-dimensional electron system in which the essentially unscreened Coulomb force between charges gives rise to strongly correlated electron effects and, at low temperatures, the formation of the 2D Wigner crystal [1]. Recently, advances in microfabrication technology have allowed the construction of microchannel devices for the manipulation of small numbers of electrons and single-electron traps [2]. Here we present experimental results from a new microchannel device in which the transverse confinement potential is, for the first time, controlled by a pair of 'split-gate' electrodes.

The new devices (Fig 1) were fabricated on a boron-doped (p-type) silicon wafer. A small microchannel of width 10 μm, length 20 μm and depth 2μm separated two larger arrays of channels, which acted as electron reservoirs. Electrodes underneath these reservoirs were insulated from the upper Guard electrode. Along the base of the central channel was a thin electrode of width 2 μm, flanked on either side by the exposed wafer surface, which acted as a split-gate when a DC bias V_{SG} was applied to the silicon substrate.

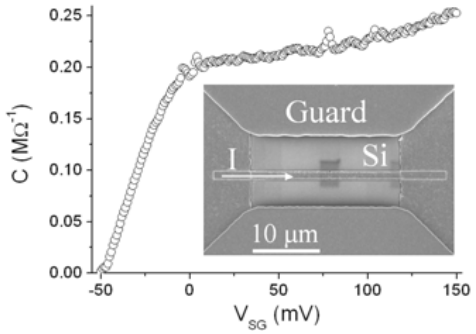

Fig.1 The conductance through the central channel decreased to zero as the split-gate voltage V_{SG} was swept negative. Inset: an SEM image of the small central channel one of the devices. The silicon substrate acts as a split-gate (see text).

Helium was condensed into the experimental cell until the bulk liquid surface was approximately 0.5 mm below the sample; below 2.2 K the microchannel array then filled with helium due to the capillary action of the superfluid. The helium surface was charged by heating a small tungsten filament above the sample whilst applying a bias voltage of 0.5 V between the Guard and Reservoir electrodes. The conductance of the electron system passing through the central channel was then measured, as a function of V_{SG} and temperature, by applying a small AC voltage to the left reservoir electrode and measuring the current induced in the right reservoir electrode with a lock-in amplifier.

The conductance through the central channel decreased to zero as V_{SG} was swept negative and the quasi-one-dimensional electron system above the central electrode was depleted (Fig 1). With decreasing temperature a step-like decrease in the conductance was observed, which may be related to Coulomb crystallisation effects. Our results will be discussed in the context of recent proposals that such surface state electrons may be suitable as qubits for quantum computation [3].

References

1. H. Ikegami et al, Phys. Rev. Lett **102**, 046807 (2009)
2. G. Papageorgiou et al, Appl. Phys. Lett. **86** 153106 (2005).
3. P. M. Platzman and M. I. Dykman, Science **284**, 1967 (1999)

Cyclotron resonance in 2DES incorporating QD layer

K. Takehana*, Y. Imanaka*, T. Takamasu* and M. Henini**

* *National Institute for Materials Science, Tsukuba, Japan*

** *School of Physics and Astronomy, Nottingham Nanotechnology and Nanoscience Centre, University of Nottingham, Nottingham, UK*

Keywords: two-dimensional electron system, quantum dots, quantum Hall effect, cyclotron resonance

Few studies have been performed to investigate how the self-assembled quantum dots (QDs) affect on the properties of a nearby two-dimensional electron system (2DES) in quantum Hall regime, despite of its great fundamental interests.

In our previous study, we have investigated the transport property of the 2DES separated by a thin barrier from a layer of InAs QDs in high magnetic fields. Clear features of both integer QHE and fractional QHE were observed despite the proximity of the QD layer to the 2DES. Only at the filling factor, $\nu < 1$, a well-defined hysteresis loop was found on the traces of both the magnetoresistance (ρ_{xx}) and Hall resistance (ρ_{xy}) when the gate voltage, Vg, was swept, and both ρ_{xx} and ρ_{xy} were suppressed when a positive Vg was applied [1]. We attributed this to the charging effect of the nearby QD layer.

In this study, we have performed the cyclotron resonance (CR) measurements on the same sample with the magnetic fields fixed, in order to investigate further the electron state of the system.

Figure shows the transmission spectra normalized by the spectrum at B = 0 T in the far-infrared region under high magnetic fields. Two resonances were observed; one is a sharp line, and the other is a broad absorption. The former exhibits linear magnetic field dependence. Therefore, it was assigned to CR of 2DES. The latter, on the other hand, was found to be described as CR of localized electron confined in a random potential of a quasi-two-dimensional system [2]. Both CRs were assigned to be originated from the electrons confined in the GaAs quantum well, according to their estimated effective mass. A similar observation was reported in Ref. [3]. As the result of the Vg dependence, absorption intensity of the broad CR change steeply versus the gate voltage around Vg = 0 V. On the other hand, that of the sharp one changes weekly against Vg. Our previous study indicates that the charge state changes around Vg = 0 V [1]. Therefore, the broad CR corresponds to the electrons which are strongly affected by the charge state of the nearby QD layer and that the sharp CR does to the electrons relatively free from the influence of the QD layer. We will discuss more detailed properties of this system according to the systematic studies of the transport and optical measurements.

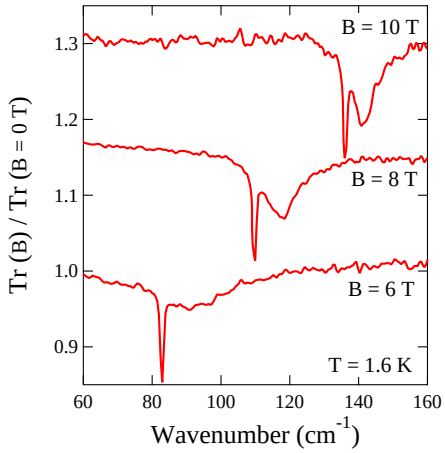

Figure Normalized transmission spectra of the 2DES sample incorporating QD layer in the far-infrared region under high magnetic fields. Two modes of CR can be seen clearly.

References

1. K. Takehana, T. Takamasu and M. Henini, J. Phys. Soc. Jpn **75,** 114713 (2006).
2. U. Merkt, P Phys. Rev. Lett., **76**, 1134 (1996).
3. Y. Vasilyev et al., Appl. Phys. Lett., **75**, 2942 (1999).

Anomalous magnetotransport and cyclotron resonance of high mobility magnetic 2DHGs in the quantum Hall regime

U. Wurstbauer*, S. Knott*, C. G. Westarp*, N. Mecking*, K. Rachor*, D. Heitmann*, W. Wegscheider**, and W. Hansen*

** Institute for Applied Physics,University of Hamburg, Hamburg, Germany*

*** Solid State Physics Laboratory, ETH Zurich, Zurich, Switzerland*

Keywords: quantum Hall effect, magnetic two-dimensional hole system (M2DHG), effective mass m*

High-mobility two-dimensional hole gases (2DHG) in the presence of local magnetic ions feature intriguing localization phenomena. We investigate magnetic manganese (Mn) or nonmagnetic carbon (C) modulation doped two-dimensional hole gases (2DHGs) with low-temperature magnetotransport in tilted fields and microwave (MW) as well as far-infrared (FIR) spectroscopy.

The 2DHGs are confined in a 20 nm thick InGaAs QW containing a 4 nm thick InAs channel. The InGaAs QW is embedded in modulation-doped InAlAs. The QWs are additionally co-doped with few Mn ions supplying 5/2 moments that interact with the spins of the free holes [1, 2].

Low-temperature magnetotransport experiments reveal pronounced Shubnikov-de Haas (SdH) oscillations in the longitudinal resistance and well developed Hall-plateaus in the Hall resistance as demonstrated in Fig.1 for a Mn-modulation and Mn co-doped QW structure. The data demonstrate that the Hall resistance neither rises linearly nor monotonously. Furthermore, an unusual filling factor dependence is found. We point out that the vanishing longitudinal resistance at higher magnetic fields exclude a parallel conducting layer to be responsible for these effects.

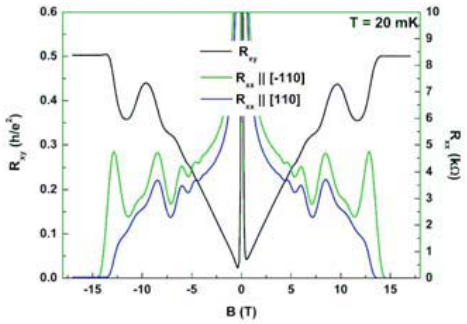

Fig.1 Anisotropic longitudinal resistance traces along the [-110] (green) and [110] (blue) directions, Hall resistance (black) of a magnetic Mn modulation and Mn co-doped 2DHG at T = 20 mK with p = $5 \cdot 10^{11}$ cm^{-2}. In the Hall resistance unusual minima appear in the quantum Hall effect. Around B = 0 strong localization dominates the transport.

In a nonmagnetic modulation-doped, Mn co-doped 2DHG, the even filling factor 2 is absent, but the odd filling factors 3 and 1 are well pronounced. In contrast, no anomalous high field transport behaviour is observed in magnetic modulation doped QW without Mn in the QW [2]. This indicates that the anomalies observed in the transport behaviour are caused by the interaction of the spins of itinerant holes with the localized moments of 5/2.

In order to gain information about the complex valence band structure in the strained QWs, the effective hole masses *m** were determined from the temperature dependent damping of the SdH oscillations. The values for *m** vary from about 0.1 m_e to about 0.3 m_e in different samples. The values indicate mixing of heavy- and light-hole bands enhanced by the strain. From FIR and microwave spectroscopy with perpendicular applied magnetic fields well pronounced cyclotron resonance with nonparabolic effective masses similar to the transport masses were observed at high B. Additional resonances are found that exhibit an anticrossing with the cyclotron resonance.

References

1. U. Wurstbauer et al., Physica E **40**, 1563 (2008).
2. U. Wurstbauer et al., J. Cryst. Growth, In Press, (2008), doi:10.1016/j.jcrysgro.2008.10.004.

Relevant quantum corrections to conductivity in non-zero magnetic field

A. A. Greshnov* and G. G. Zegrya*
Ioffe Physico-technical Institute RAS, St. Petersburg, Russia

Keywords: weak localization, unitary localization length, integer quantum Hall effect

Relevant quantum corrections to conductivity (i.e. divergent at $\omega = 0$) play a key role in the scaling theory of localization [1]. Quantum correction of the first order in $(k_F l)^{-1}$ is due to Cooperon channel [2], $\delta\sigma_1(\omega) = 1/\pi \ln(\omega\tau)\, e^2/h$. This determines value of the so-called ortogonal localization length, $\xi_o = l\exp(\pi g/2)$ [1], where $g = k_F l$ is Drude conductivity in the units of e^2/h. However, the first-order correction ceases to diverge in non-zero magnetic field due to magnetic length cut-off giving rise to negative magnetoresistivity [1]. In the present study we consider intermediate range of magnetic fields where Cooperon channel is already suppressed but Landau quantization still can be neglected therefore quantum correction to conductivity of the second order in $(k_F l)^{-1}$, $\delta\sigma_2(\omega)$, comes to the front.

We apply usual short-range impurity diagram technique at $T = 0$ and pick out relevant diagrams of the second order in $(k_F l)^{-1}$ following Refs. [2],[3],[4] (Fig. 1). As it was first stated if Ref. [2] all terms containing $\ln^2(\omega\tau)$ cancel out up to the second order in $(k_F l)^{-1}$. In Ref. [3] and Ref. [4] the problem was treated using diffusive non-linear σ-model and mutually contradictory answers for $\ln(\omega\tau)$ prefactor were obtained. However, so-called diffusion approximation adopted in Refs. [3],[4], i.e. substitution of exact Diffuson

$$D(k) = \frac{1}{\sqrt{(1 - i\omega\tau)^2 + (kl)^2} - 1} \qquad (1)$$

by the approximate expression $[(kl)^2/2 - i\omega\tau]^{-1}$ is obviously incorrect for arbitrary values of k resulting in convergent answer for $\delta\sigma_2(\omega = 0)$ in line with Ref. [3].

Correct evaluation of the diagrams depicted in Fig. 1 requires accurate taking into account of ballistic contributions (e.g. small k, arbitrary q and vice versa for the diagrams a-d) and results in the following answer:

$$\delta\sigma_2(\omega) = \frac{\Sigma}{\pi^2}\frac{\ln(\omega\tau)}{k_F l}\frac{e^2}{h}, \qquad (2)$$

$$\Sigma = a + .. + m = \frac{11}{12} + 3\ln 2 \approx 2.996. \qquad (3)$$

So-called unitary localization length is related to Σ via

$$\xi_u = l\exp\left(\frac{\pi^2 g^2}{2\Sigma}\right). \qquad (4)$$

Previously it was argued [5] that $\xi_u = l\exp(\pi^2 g^2)$ corresponding to $\Sigma = 0.5$. We have shown that the actual value of Σ is almost one order of magnitude higher. Let us estimate ξ_u in the limit of high magnetic field using SCBA σ_{xx} peak values due to Ando, $g_n = (2n+1)/\pi$,

$$\xi_0 \approx 1.2a_H,\ \xi_1 \approx 4.5a_H,\ \xi_2 \approx 65a_H. \qquad (5)$$

These estimations confirm reliability of the linear growth of σ_{xx} peaks with Landau level number n in the integer quantum Hall effect regime stated in Ref. [6].

A.A. Greshnov is grateful to V.Yu. Kachorovskii, I.S. Burmistrov and A.D. Mirlin for valuable discussions.

References

[1] P.A. Lee, T.V. Ramakrishnan, Rev. Mod. Phys. **57**, 287 (1985).
[2] L.P. Gor'kov et al., JETP Lett. **30**, 248 (1979).
[3] K.B. Efetov et al., JETP **52**, 568 (1980).
[4] S. Hikami, Phys. Rev. B **24**, 2671 (1981).
[5] B. Huckestein, Rev. Mod. Phys., **67**, 357 (1995).
[6] A.A. Greshnov, G.G. Zegrya, Physica E **40**, 1185 (2008); A.A. Greshnov, G.G. Zegrya, E.N. Kolesnikova, JETP **107**, 491 (2008).

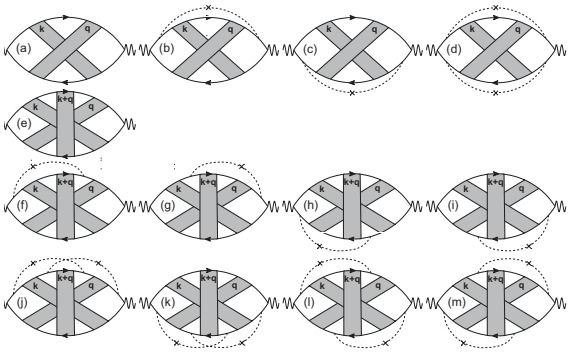

Figure 1: Diffuson-type corrections to Drude conductivity of the second order in $(k_F l)^{-1}$.

Spin density wave in integer quantum Hall systems

Kanako Yoshizawa and Kazuo Takayanagi
Department of Physics, Sophia University, 7-1 Kioi-cho, Chiyoda-ku, Tokyo 102, Japan

Keywords: integer quantum Hall system, spin instability, spin density wave, phase diagram

Recent theoretical and experimental investigations have suggested that it is quite likely that the spin density wave (SDW) can be the ground state of integer quantum Hall systems [1, 2, 3, 4, 5]. In this work we adopt the time-dependent Hartree-Fock (TDHF) and the Hartree-Fock (HF) theories to determine the ground state of the systems in a tilted magnetic field. For each value of the integer filling factor ν $(= 1, 2, \cdots)$, the results can be presented as a phase diagram in the (r_s, E_Z) plane, where r_s is the Wigner-Seitz parameter and E_Z is the Zeeman energy. In this work, we report for the first time the complete phase diagram that shows explicitly the existence of the SDW ground state.

We briefly explain our study for the $\nu = 2$ system with $E_Z = 0$. Here the paramagnetic state $|\mathrm{P}\rangle$ ($\nu_\uparrow = \nu_\downarrow = 1$) and the ferromagnetic state $|\mathrm{F}\rangle$ ($\nu_\uparrow = 2, \nu_\downarrow = 0$) are the trivial HF ground states. We first perform the TDHF calculations for these two systems in the spin density excitation (SDE) channel to find the onset of spin instabilities. We have found that $|\mathrm{P}\rangle$ ($|\mathrm{F}\rangle$) is stable against the formation of the SDW only for $r_s < 2.01$ ($2.15 < r_s$). Then we perform the HF calculation for $2.01 < r_s$ starting from $|\mathrm{P}\rangle$, to obtain the SDW ground state $|\mathrm{SDW(P)}\rangle$ that is expressed as a condensate of the SDW Boson on $|\mathrm{P}\rangle$. In the same way, we obtain the SDW ground state $|\mathrm{SDW(F)}\rangle$ for $r_s < 2.15$. By comparing energies of the four HF ground state, $|\mathrm{P}\rangle$, $|\mathrm{F}\rangle$, $|\mathrm{SDW(P)}\rangle$, and $|\mathrm{SDW(F)}\rangle$, we have found that the ground state for $E_Z = 0$ is $|\mathrm{P}\rangle$ for $r_s < 2.01$, $|\mathrm{SDW(P)}\rangle$ for $2.01 < r_s < 2.15$, and $|\mathrm{F}\rangle$ for $2.15 < r_s$. The calculation for $E_Z \neq 0$ proceeds in the same way, and leads us to the phase diagram in Fig. 1, which is in accordance with existing experimental and theoretical information [5]. Two points should be noted here; first, $|\mathrm{SDW(P)}\rangle$ is the ground state of the system for $E_Z < 0.06\hbar\omega_c$ and $r_s \sim 2$, and second, the boundary between $|\mathrm{P}\rangle$ and $|\mathrm{F}\rangle$ is of first order.

We have examined systems with $\nu \neq 2$ in the same way as for the $\nu = 2$ system. In this work we discuss the phase diagram for integer quantum Hall systems in detail on the basis of our TDHF and HF calculations.

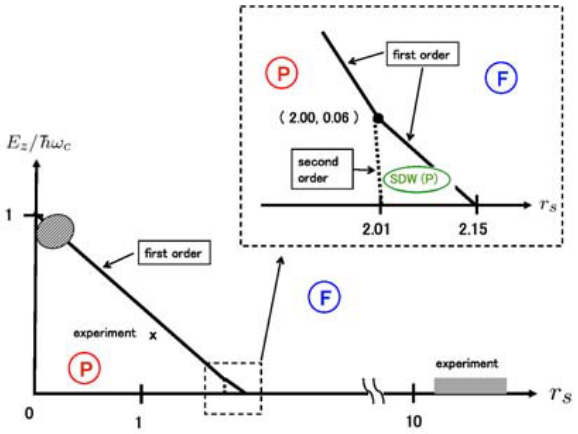

Figure 1: Magnetic phase diagram. Three phases, $|\mathrm{P}\rangle$ $|\mathrm{F}\rangle$, and $|\mathrm{SDW(P)}\rangle$, are shown with their boundaries. In the hatched region, a first order transition between $|\mathrm{P}\rangle$ and $|\mathrm{F}\rangle$ is expected theoretically [6]. The cross at $(r_s \sim 1.1, E_Z \sim 0.37\hbar\omega_c)$ indicates the first order transition observed experimentally [7]. Empirical SDE energy is expected to vanish in the shaded area $(11 \lesssim r_s \lesssim 14, E_Z \sim 0)$ [1].

References

[1] M. A. Eriksson, A. Pinczuk, B. S. Dennis, S. H. Simon, L. N. Pfeiffer, and K. W. West, Phys. Rev. Lett. **82**, 2163 (1999).

[2] C. Kallin and B. I. Halperin, Phys. Rev. B **30**, 5655 (1984).

[3] A. H. MacDonald, J. Phys. C **18**, 1003 (1985).

[4] K. Yoshizawa and K. Takayanagi, Phys. Rev. B **76**, 155329 (2007).

[5] K. Yoshizawa and K. Takayanagi, Phys. Rev. B **79**, in press (2009).

[6] G. F. Giuliani and J. J. Quinn, Phys. Rev. B **31**, 6228 (1985).

[7] S. Koch, R. J. Haug, K. v. Klitzing, and M. Razeghi, Phys. Rev. B **47**, 4048 (1993).

Magnetic field induced 2D excitonic insulator in HgTe QWs

Z. D. Kvon*, E.B.Olshanetsky*, D. A. Kozlov*, N. N. Mikhailov*, I. O. Parm*, and J.C.Portal**

* *Institute of Semiconductor Physic, Novosibirsk, Russia*
** *GHMF, MPI-FKF/CNRS, BP-166, F-38042, Grenoble, Cedex 9, France*

Keywords: electron and holes, exciton, semimetal, excitonic insulator

Two-dimensional (2D) excitonic insulator (EI) state induced by magnetic field is found in undoped HgTe quantum wells (QW). It arises in the magnetic fields range (1.5 – 2) T between electron-like and hole-like quantum Hall liquid states at and in the vicinity of the gate voltage where the electron and hole densities become equal ($N_s = P_s$). It is shown that the transition metal – EI is similar to the normal metal - superconductor transition and described by BCS-scenario: up to a critical temperature $T_c \approx 1$ K no temperature dependence of the transport and capacitance response of the system is observed but just below this temperature a strong insulator behavior appears characterized by a gap of about a few K. The samples studied were 2D semimetal recently discovered in undoped HgTe QW with (013) surface orientation [1]. This semimetal is the result of size quantization of (013) surface oriented QW with inverted band structure having the thickness 18-21 nm. It was shown that in such QWs a simultaneous existence on 2D electrons and holes with quite low carriers densities (less than 10^{11} cm^{-2}) and high mobility of both 2D electrons $\mu_n = (3\text{-}6)\cdot 10^5$ cm^2/Vs and 2D holes $\mu_p = (3\text{-}10)\cdot 10^4$ cm^2/Vs can be realized. It was established that the energy spectrum of this system is determined by the overlapping (about 10 meV) of electron energy dispersion curve with a minimum in the centre of the Brillouin zone and the valence band with two maxima in [0-31] direction. Using gate voltage allows to obtain any ratio between N_s and P_s including the most interesting point of equal densities and so to perform a detailed study of the transition from $N_s \neq P_s$ to $N_s = P_s$.

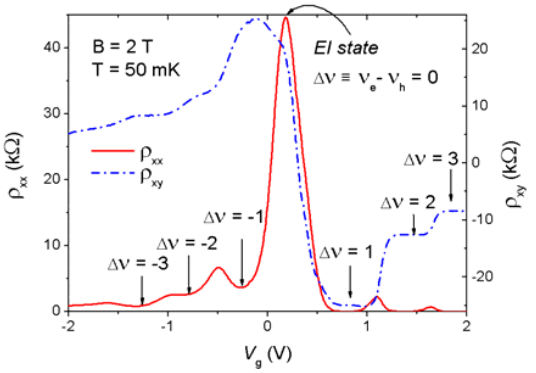

Fig.1 Gate voltage dependences $\rho_{xx}(V_g)$ and $\rho_{xy}(V_g)$ of 2D semimetal in undoped HgTe QW in magnetic field.

he main result is shown in the figure where the gate voltage dependences of dissipative $\rho_{xx}(V_g)$ and Hall $\rho_{xy}(V_g)$ components of the resistivity tensor at magnetic field B = 2 T are presented. Between the electron and hole-like QHE one can see in the vicinity of the point $N_s = P_s$ that $\rho_{xx}(V_g)$ has a maximum and $\rho_{xy}(V_g)$ is close to zero. It was suggested that these features are a signature of the formation of excitonic insulator state induced by magnetic field. Capacitance measurements support this assumption. Moreover they have demonstrated a critical behavior of the transition similar to the normal metal-superconductor transition: up to a critical temperature $T_c \approx 1$ K there is no gap in the spectrum of 2D semimetal but as soon as this temperature becomes lower there appears a gap with of few K.

References

1. Z. D. Kvon, E.B.Olshanetsky, D. A. Kozlov, N. N. Mikhailov, S.A.Dvoretsky, JETP Lett. **62**, (2008).

Temperature Dependence of the Visibility in an Electronic Mach-Zehnder Interferometer

M. Hashisaka*†, A. Helzel**†, S. Nakamura*, L. Litvin**, T. Ono*,
H.-P. Tranitz**, W. Wegscheider**, C. Strunk**, and K. Kobayashi*

** Institute for Chemical Research, Kyoto University, Kyoto, Japan*

*** Institut für experimentelle und angewandte Physik, Universität Regensburg, Germany*

Keywords: Mach-Zehnder interferometer, quantum interference, electron temperature, visibility

The electronic Mach-Zehnder interferometer (MZI), which was recently realized experimentally [1] – [3], is a promising system to promote our understanding on the electron coherence in ballistic systems. Large visibilities of the interference in the MZI were observed as a direct result of the quasi-one-dimensional transport in the edge channel in the quantum hall regime. Here, we present an experimental work on the dependence of the visibility in the MZI on the electron temperature. The reduction of the visibility as function of electron temperature should provide an evidence for the relevant dephasing mechanism in the edge states.

In Fig. 1, the schematic geometry of the electric MZI is shown. The MZI was fabricated on the GaAs/AlGaAs two-dimensional electron gas system (2DEG: electron density 2.0×10^{11} cm^{-2} and mobility 2.06×10^{6} cm^2/Vs). The arm-length of the MZI estimated from the Aharonov-Bohm oscillation is around 6.7 μm. We measured the visibility of the MZI ($\nu \equiv (I_{max}-I_{min}) / (I_{max}+I_{min})$. Here I indicates the current that flows from the source S1 to the drain D2). The electron temperature was determined by measuring the Nyquist noise.

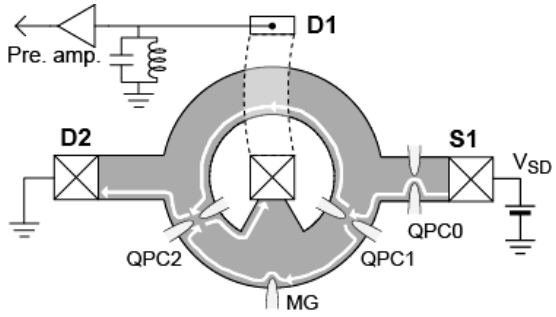

Fig.1 The electron MZI and the measurement setups.

Figure 2 shows the visibility of the interferometer as a function electron temperature, measured at two magnetic fields 4.5 T and 5.0 T. The inset of Fig. 2 shows the oscillation of the D2 current as a function of the modulation gate (MG) voltage measured at 20 mK, showing $\nu \sim 0.5$. Experimentally, we observed a signature of the possible saturation of the visibility at low temperatures (< 50 mK), while the visibility exponentially decreases with increasing the temperature above 80 mK. This method allows a reliable determination of the electron phase coherence length vs. temperature.

† These Authors contributed equally to this work.

[1] Y. Ji, Y. Chung, D. Sprinzak, M. Heiblum, D. Mahalu, and H. Shtrikman, Nature **422**, 415 (2003).
[2] P. Roulleau, F. Portier, P. Roche, A. Cavanna, G. Faini, U. Gennser and D. Mailly, Phys. Rev. Lett. **100**, 126802 (2008)
[3] L. Litvin, A. Helzel, H.-P. Tranitz, W. Wegscheider, and C. Strunk, Phys. Rev. **B 78**, 075303, (2008).

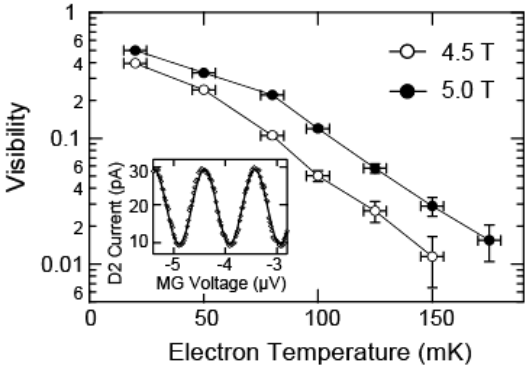

Fig.2 Electron temperature dependence of the visibility. (Inset) The oscillating current flowing to D2 as a function of the MG voltage.

A unified description of nonequilibrium magnetooscillations in high Landau levels

I.A. Dmitriev

Institute of Nanotechnology, Forschungszentrum Karlsruhe, 76021Karlsruhe, Germany

Keywords: nonequilibrium magnetooscillations

We propose a unified quantum kinetic description of a family of nonequilibrium magnetooscillations observed in high mobility quantum Hall structures under microwave [1] and dc [2] excitations, or in presence of phonons [3]. The magnetoresistivity in these structures is governed by spectral and spatial resonances set by the cyclotron frequency and the cyclotron diameter in various combinations with the parameters of the external fields.

We treat these effects on equal footing using quantum kinetic equation recently derived for the case of generic disorder potential [4]. Previous studies [5,6] of the microwave-induced resistance oscillations (MIRO) have shown that in the case of smooth disorder the effect is dominated by nonequilibrium changes in the electron distribution function ("inelastic" mechanism [6]). Our analysis [7] shows that in the presence of sufficient amount of short-range disorder the "displacement" mechanism, related to modification of the scattering integral, can provide the leading contribution to the MIRO in a certain temperature window, consistent with recent experiments [8]. The short-range component of disorder is also responsible for the resonant backscattering leading to the Hall-field induced resistance oscillations (HIRO) [2] and for a nontrivial interplay of the MIRO and HIRO [9].

Quite interestingly, microwave-induced photocurrent or photovoltage oscillations were observed also in absence of the dc driving [10]. The effect is due to band bending in the vicinity of highly resistive internal contact. Application of the quantum kinetic approach to this spatially inhomogeneous case [11] shows that, in contrast to electrical current, the microwave radiation barely affects the diffusion flow against the electron density gradient. Such a nonequilibrium violation of the Einstein relation between electrical current and diffusion explains the observation of Ref. 10.

Further, the quantum kinetic approach has been generalized to include the interaction with phonons [12]. Using this approach, we show that the phonon –induced resistance oscillations [3] (PIRO) are due to resonant backscattering of electrons mediated by phonons having a multiple of the cyclotron energy.

References

1. Zudov et al, PRB 64, 201311(R) (2001); PRL 90, 046807 (2003). Mani et al, Nature 420, 646 (2002).
2. Yang et al, PRL 89, 076801 (2002).
3. Zudov et al, PRL 86, 3614 (2001).
4. Khodas and Vavilov, PRB 78, 245319 (2008).
5. Vavilov and Aleiner, PRB 69, 035303 (2004).
6. Dmitriev et al, PRL 91, 226802 (2003); PRB 71, 115316 (2005); PRB 75, 245320 (2007).
7. I.A. Dmitriev, M. Khodas, A.D. Mirlin, D.G. Polyakov, and M. G. Vavilov, to be published.
8. Hatke et al, PRL 102, 066804 (2009).
9. Zhang et al, PRL 98, 106804 (2007). Hatke et al, PRB 77, 201304(R) (2008).
10. Dorozhkin et al, PRL 102, 036602 (2009).
11. I.A. Dmitriev, S.A. Dorozhkin, and A.D. Mirlin, to be published.
12. I.A. Dmitriev and M.G. Vavilov, to be published.

In-plane anisotropic transport in 2DEGs having a strong spin-orbit coupling in $In_{0.75}Ga_{0.25}As$/ $In_{0.75}Al_{0.25}As$ hetero-junctions

S. Nitta, H. K. Choi and S. Yamada

Center for Nano Materials and Technology, Japan Advanced Institute of Science and Technology

1-1, Asahidai, Nomi, Ishikawa, 923-1292, Japan

Keywords: InGaAs/InAlAs hetero-junction, Rashba SOI (spin-orbit interaction), anisotropic in-plane

Two-dimensional electron gas (2DEG) formed at high In-content InGaAs/InAlAs hetero-junction interface is one of the most promising candidate for realizing various spintronics devices utilizing the Rashba type spin-orbit interaction (SOI), since it reveals high electronic quality (low temperature mobility of ~$2x10^5$ cm^2/Vsec) as well as a very large spin-orbit coupling constant of ~20×10^{-12} eVm [1]. We describe in this paper the results of the in-plane anisotropic transport of the 2DEG, mobility anisotropy as well as possible SO coupling constant anisotropy, obtained recently in the high quality inverted InGaAs/InAlAs HEMT structures.

Those structures were grown by standard molecular beam epitaxy (MBE) on (100) semi-insulating GaAs substrates via metamorphic buffers. The $In_{0.75}Ga_{0.25}As$ surface channel of $t_{channel}$ ~ 40 or 60 nm was adopted and the thickness of the topmost InAlAs cap is varied within t_{cap} ~ 0 – 10 nm.

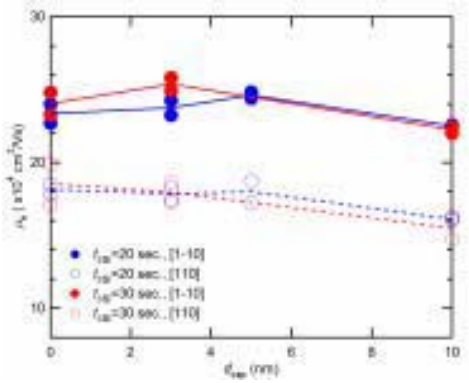

Fig. 1 In-plane mobility anisotropy in the 2DEGs in a variety of $In_{0.75}Ga_{0.25}As$/ $In_{0.75}Al_{0.25}As$ i-HEMTsamples..

Figure 1 shows the low temperature 2DEG mobilities (μ_es) in the $t_{channel}$ ~ 60 nm samples with various t_{cap}s. For all the samples, clear and big mobility anisotropies, μ_e [1-10] / μ_e [110] ~ 1.3, were observed [2]. In all the samples, we have confirmed cross-hatch patterns in the surface morphology analysis by atomic force microscope (AFM) and found the difference of the undulation period spectrum such as λ [1-10]> λ [110] ~ 200 nm. This may partly responsible to the in-plane mobility anisotropy.

Furthermore, SO coupling constant, α, deduced from the low field 2DEG SdH oscillations revealed possible in-plane anisotropy, α [1-10] / α [110] ~ 1.1 in $t_{channel}$ ~ 40 nm samples. This seems unexpected, since α is determined from the difference of the electron densities between the two spin sub-bands. However, since the cross-hatch pattern itself suggests the strain relaxation anisotropy, residual strain at the 2DEG interface might reveal some kind of in-plane anisotropy. And if the α includes some contributions from the Dresselhaus term [3], strain-related α anisotropy could appear.

We now consider this problem also from the view point of detailed XRD analysis, which can estimate the in-plane lattice constants of the sample surfaces.

References

1. H. K. Choi, et al, Physica E40 (2008) 2823-2828.
2. M. Rosini et al, Physica E40, (2008) 1392-1394.
3. Koga, private communication.

g-Factor of low mobility 2D GaAs electron gas as determined from high magnetic field experiments

A. V. Germanenko*, N. Kozlova†, G. M. Minkov**, O. E. Rut*, A. A. Sherstobitov** and J. Freudenberger†
*Ural State University, 620083 Ekaterinburg, Russia
†Leibnitz Institute for Solid State and Material Research Dresden, IFW Dresden, D-01171 Dresden, Germany
**Institute of Metal Physics RAS, 620219 Ekaterinburg, Russia

Keywords: spin phenomena, transport

One of the widely used method for determining the value of *g*-factor in two-dimensional (2D) systems is the study of the Shubnikov-de Haas (SdH) oscillations in the tilted magnetic field. The method is based on the fact that the spin splitting of the Landau levels is controlled by the total magnetic field (B) while the orbit quantization is sensitive only to the normal component of B. The *g*-factor determining the conduction band spin splitting can be found by rotating the sample in the magnetic field to identify the angle angle between the magnetic field and the direction normal to the 2D plane at which the spin splitting is equal to the half of the cyclotron energy. When the sample is in such a position, the SdH oscillations amplitude passes through zero. Once, such orientation angle, θ_0, is found, the effective *g*-factor can be determined as

$$g = \frac{e\hbar}{2\mu_B m}\cos\theta_0 \qquad (1)$$

provided that the effective mass m is known for the same sample. This method works well for the high-mobility systems, in which the oscillations are observed starting from the very low magnetic fields, and for the systems with the relatively high value of *g*-factor. In the dirty systems with low mobility and/or with small value of *g*-factor the vanishing of the oscillations amplitude is not observed under usual experimental conditions, and more delicate approach is needed.

We report the results of the experimental study of the 2D GaAs electron system in the tilted magnetic field up to 45 T. The electron density and mobility are 1.8×10^{16} m^{-2} and 1.5 m^2/(Vs), respectively. The measurements have been performed using the DC technique in the Laboratory for pulsed high magnetic fields of the Institute for Metallic Materials, IFW Dresden.

To obtain experimentally the value of *g*-factor we have analyzed the magnetic field dependence of the SdH oscillations measured for different θ. Theoretically, the amplitude of the s-th harmonic of the oscillations measured in tilted magnetic field is connected with that measured at $\theta = 0$ via the simple expression

$$\frac{A_s(\theta)}{A_s(0)} = \cos\left(\frac{\pi s}{2}\frac{g}{\cos\theta}\frac{m}{m_0}\right)\Big/\cos\left(\frac{\pi s}{2}g\frac{m}{m_0}\right). \qquad (2)$$

As seen the $A_s(\theta)$ to $A_s(0)$ ratio should not depend on the magnetic field, and its angle dependence is fully determined by the value of *g*-factor. In Fig. 1, the experimental data for the 1st harmonic are compared with the expression (2). The best agreement is achieved for $|g| = 0.9 \pm 0.1$. This value is significantly larger than that calculated theoretically and observed in optical experiments for the bottom of the conduction band: $g = -0.15$. At the Fermi energy, $E_F \simeq 25$ meV, the theoretical value is still less due to nonparabolicity of the conduction band, it can be estimated as $g \simeq 0 \pm 0.05$. Possible physical reasons for this discrepancy will be discussed.

This work has been supported in part by the RFBR (Grant 08-02-91962) and DFG (Grant KO 3743/1-1).

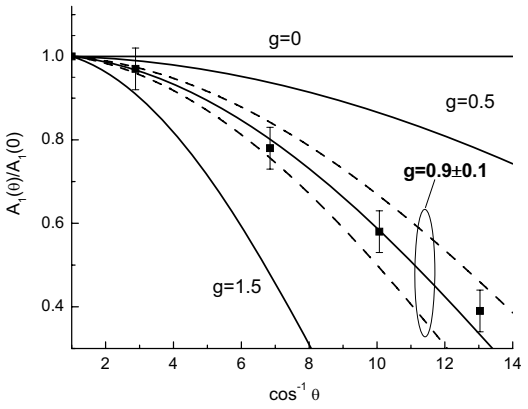

Figure 1: The $A_1(\theta)$ to $A_1(0)$ ratio as a function of $1/\cos\theta$. Symbols are the data, the lines are calculated from (2) with $m = 0.067m_0$.

The pre-edge XANES study of substitutional and interstitial Mn impurities in (Ga,Mn)As

Nataliya A. Goncharuk, Jan Kučera and Ludvík Smrčka
Institute of Physics of the AS CR, v.v.i., Prague, Czech Republic

Keywords: (Ga,Mn)As magnetic semiconductor, X-ray absorption near-edge structure, defect

The Mn-doped GaAs magnetic semiconductors are promising materials for potential applications in spintronic technology. The main motivation behind the preparation and investigation of these materials is the combination of both semiconducting/semimetallic and ferromagnetic properties in one physical system.

There are several possibilities for a Mn atom to be embedded in GaAs. Three of them have a comparable energy [1]: the substitutional Mn atoms, Mn_{Ga}^{sub}, occupying Ga sites, and the Mn atoms in two tetrahedral interstitial positions, surrounded by either As or Ga atoms, Mn_{As}^{int} and Mn_{Ga}^{int}. The substitutional Mn atoms act as hole-producing acceptors which contribute to ferromagnetism. The Mn interstitials are electron-producing double donors which destroy ferromagnetic states. Each interstitial Mn compensate two Mn_{Ga}^{sub} acceptors, reducing the number of holes [2].

The X-ray absorption near-edge structure (XANES) at the Mn K-edge in (Ga,Mn)As was simulated using the full potential linearized augmented plane wave method including the core-hole effect [3]. The spin-polarized calculations were performed in the 64-atom supercell scheme for Mn_{Ga}^{sub}, Mn_{As}^{int} and Mn_{Ga}^{int}. The spectra of different Mn impurity types were simulated by separate calculations, considering always only one Mn atom inside each supercell. Thus, the supercells represent GaAs doped with ~ 3 atomic percent of Mn impurities.

The self-consistent final state calculations were carried out with one core electron removed from the Mn $1s$ level and an additional valence electron placed at the bottom of the conduction band to fill the lowest unoccupied $4p$ orbital. In the dipole approximation, the absorption spectrum is obtained as a product of the transition probability, calculated from $1s$-$4p$ dipole matrix elements, which is a smooth function increasing with energy, and the local partial density of states of $4p$-states above the Fermi energy in the Mn muffin-tin sphere, obtained from the final state calculation.

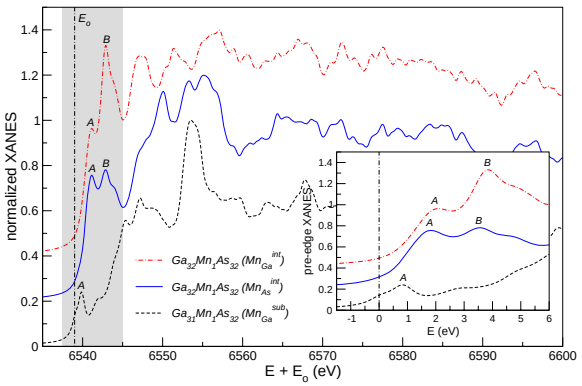

Figure 1: Normalized ab-initio Mn K-edge XANES spectra simulated including the core-hole effect in the 64-atom (Ga,Mn)As supercell for Mn_{Ga}^{sub}, Mn_{As}^{int} and Mn_{Ga}^{int}. Energies of spectra are shifted by the experimental transition energy of a Mn atom, $E_{\circ}$=6539 eV. The grey region indicates the pre-edge part of absorption spectra (peaks A and B), which is shown in detail in the insert.

The resulting pre-edge absorption structures show clear distinction between the spectra simulated for the substitutional and interstitial Mn defects (Fig. 1). A single feature is obtained for the substitutional Mn impurity, whereas two peaks appear for both types of interstitial defects. The difference between simulated spectra is determined mainly by the second nearest neighbor ligands.

References

[1] J. Mašek, F. Máca, Phys. Rev. B **69**, 165212 (2004).

[2] T. Jungwirth, J. Sinova, J. Mašek, J. Kučera, A. H. MacDonald, Rev. Mod. Phys. **78**, 809 (2006).

[3] P. Blaha, K. Schwarz, G. K. H. Madsen, D. Kvasnicka, J. Luitz, WIEN2k, *An Augmented Plane Wave plus Local Orbitals program for calculating crystal properties*, edited by K. Schwarz, Techn. Univ. Wien, Austria, 2007, ISBN 3-9501031-1-2.

Electric field effects on magnetocrystalline anisotropy in ferromagnetic monolayers

Riki Shimabukuro, Kohji Nakamura, Toru Akiyama, Tomonori Ito
Department of Physics Engineering, Mie University,Tsu,Mie514-8507,Japan

Keywords: magnetocrystalline anisotropy, electric field effect, ferromagnetic film, first principles calculations

Controlling magnetic properties by an external electric field is one key challenge in modern magnetic physics and technology. Very recently, in ferromagnetic metallic films (PtFe and PbFe) with liquid interfaces, a modification in the coercitivity [i.e., the magnetocrystalline anisotropy (MCA)] with application of an external electric field has been experimentally observed.[1] Motivated by this finding, we here present first principles results of the MCA change induced by an electric field in transition-metal monolayers and reveal the electric field effect. Moreover, we predict the MCA change in an Fe(001) monolayer sandwiched by ceramics such as MgO.

Self-consistent calculations are carried out based on the local spin density approximation by means of the film full-potential linearized augmented plane-wave (FLAPW) method,[2,3] in which a static external electric field is applied along the surface normal. The MCA energy, E_{MCA}, which is defined as the energy eigenvalue difference for the magnetization oriented along the in-plane [100] and out-of-plane [001] directions, is determined by the force theorem.[3,4]

First, we considerer simple systems of free-standing Fe(001), Co(001), and Ni(001) monolayers. Our calculations demonstrate that when an external electric field is introduced, a remarkable MCA change in the Fe(001) monolayer is observed, in which the E_{MCA} has a positive value of 0.19 meV/atom in zero field but it becomes a negative value as the electric field is larger than 1 V/Å. Thus, the MCA can be controlled by the electric field so as to change the magnetization orienting from the out-of-plane direction to the in-plane direction. In contrast, no change in the MCA in the Co(001) and Ni(001) monolayers is found. By analyzing the band structures, we find that small components of the *p* orbitals near Fermi level, which are coupled to the *d* states, play a key role to determine the MCA change. Also, a reasonable origin of the MCA change among the Fe, Co, and Ni systems is obtained from a band filling analysis.

In the case of the Fe monolayer sandwiched by MgO, when an electric field of 1 V/Å is introduced, the E_{MCA} is found to increase by 0.1 meV/atom compared to that in zero field. Within a rigid band model, furthermore, we analyze the behavior of the E_{MCA} with respect to an assumed variation of the number of valence electrons, N, and find that a maximum change of the E_{MCA}, by about 0.5 meV/atom, is achieved at N=8.4〜8.5.

References

[1] M. Weisheit et.al., Science **315**, 349 (2007).
[2] E. Wimmer et.al., Phys. Rev. B **24**, 864 (1981); Phys. Rev. B **26**, 4571 (1982).
[3] K. Nakamura et.al., Phys. Rev. B 67, 014420 (2003).
[4] C. Li.al., Phys. Rev. B. **42**, 5433 (1990)

Carrier Density Dependence of Spin-Orbit Interaction in InAsSb Quantum Wells

N. Nishizako*, T. Manago*, S. Ishida*, H. Geka** and I. Shibasaki**

** Tokyo University of Science, Yamaguchi, San'yo-Onoda, Yamaguchi 756-0884, JAPAN*

*** Asahi Kasei Co., Ltd., Samejima 2-1, Fuji, Shizuoka 416-8501, JAPAN*

Keywords: spin-orbit interaction, weak anti-localization, InAsSb quantum well

Spin-orbit interaction (SOI) in two dimensional electron systems of semiconductors has been investigated intensively in recent years for spintronic applications. One of the popular methods for spin control is using Rashba SOI caused by structural inversion asymmetry (SIA) in a quantum well (QW). InAsSb has a great potential because it has a smaller band-gap than that of other narrow-gap semiconductors. In our previous report, the SOI in undoped InAsSb QWs was investigated using weak anti-localization analysis in low magnetic field. It is expected that the SIA changes with the doping level in an uniformly doped QW layer because the potential gradient changes in the QW layer. In the present work, we investigated the SOI in uniformly doped InAsSb QWs, and compare them with the undoped QWs.

The structure is GaAs (6.5 nm) cap / $Al_{0.1}In_{0.9}Sb$ (50 nm) / Sn-doped $InAs_{0.1}Sb_{0.9}$ QW (30 nm) / AlInSb (700 nm). The magneto-resistance was measured in a magnetic field perpendicular to the QW plane below 4.2 K. The carrier densities of the samples were 1.9×10^{11}(undoped), 2.8×10^{11}, 3.6×10^{11} and 4.5×10^{11}cm^{-2}.

Fig.1 shows the magnetic field dependence of conductivity at 1.4 K. Solid curves are fitting curves by ILP theory, which is in good agreement with the experimental data in low magnetic-field. The inelastic scattering time (τ_i) decreases with increasing doping level. The τ_i dependence indicates that increasing electron-electron scattering by increase of the carrier density. The spin splitting energy (Δ_0) increases with carrier density. The calculation results of band alignment suggest that the potential gradient at the QW interface decreases with increasing carrier density. Therefore decrease of the Rashba SOI is expected. However, the carrier density dependence of the Δ_0 shows opposite results. In recent research, it was reported that the Dresselhaus SOI is also important even in narrow-gap systems and the contribution of the Dresselhaus SOI to the spin-splitting is opposite sign from the Rashba SOI [1]. Our results indicated that the Dresselhaus contribution is larger than the Rashba one, and the decrease of the Rashba contribution caused the increase of the net spin-splitting. It supports that the Dresselhaus term is not negligible in InSb alloy systems.

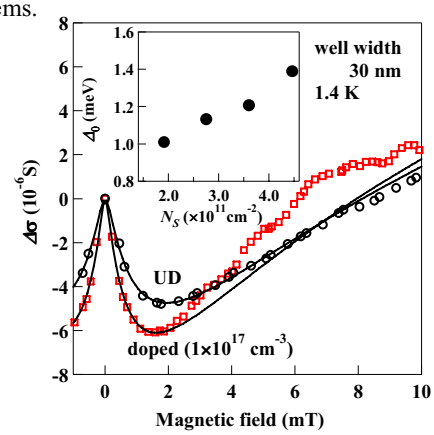

Fig.1 Magneto-conductance $\Delta\sigma(B)(=\sigma(B)-\sigma(0))$ at 1.4 K. The inset shows the sheet carrier density dependence of Δ_0.

References

1. M. Akabori et al., Phys. Rev. B **77**, 205320 (2008)

Fabrication of $Fe_3Si/CaF_2/Fe_3Si$ ferromagnetic resonant tunneling diodes on Si(111) by molecular beam epitaxy

K. Sadakuni, T. Harianto, H. Akinaga*, and T. Suemasu
Institute of Physics, University of Tsukuba, Tsukuba, Japan
** National Institute of Advanced Industrial Science and Technology (AIST), Tsukuba, Japan*

Keywords: ferromagnetic, RTD, Fe_3Si, CaF_2

Numerous different types of half metals and hetero junctions have been studied extensively to realize ferromagnetic electrodes with highly spin-polarized electrons. We have been paying attention to Fe_3Si/CaF_2 heterostructures to realize resonant tunneling diodes (RTDs) working as a very sharp spin filter as well as an energy filter.[1] Both ferromagnetic Fe_3Si and insulator CaF_2 are nearly lattice-matched to Si. We have developed a technique of epitaxial growth of $Fe_3Si/CaF_2/Fe_3Si$ magnetic tunnel junctions (MTJs) on CaF_2/Si(111) substrates.[2-3] The current-voltage (*J-V*) characteristics of the MTJs measured at room temperature (RT) were well fitted to Simmons' equation, and the barrier height for electrons in the Fe_3Si to tunnel through the CaF_2 barrier was found to be approximately 2.4 eV.[3] In this paper, we have fabricated $CaF_2/Fe_3Si/CaF_2$ RTDs by molecular beam epitaxy (MBE), and realized negative different resistance (NRD) in the *J-V* characteristics at RT.

Fe_3Si(10 nm)/CaF_2(5 nm)/Fe_3Si(4 nm)/CaF_2(5 nm) hetero structures were grown on n^+-Si (111) by MBE. The mesa-isolated diode structures with an area ranging from 6×6 to 30×30 μm² were fabricated by conventional photolithography and wet etching.

In the magnetization versus magnetic field curves at RT, a two-step hysteresis loop was clearly observed. Figure 1 shows an example of *J-V* characteristics at RT. The positive bias voltage, *V*, is defined as that applied to the top Fe_3Si(10 nm) layer. The *J-V* characteristics were asymmetric due to the asymmetric structure of the RTD. The NRD region was observed at around 2-3 V under positive bias, while it was not observed under negative bias. The peak-to-valley current ratio of NDR reached as large as approximately 1000 at V=3.2 V. Examples of the d^2I/dV^2-V characteristics were shown in Fig. 2(a). The peak positions correspond to the voltages where resonant tunneling occurred.[4] Fig. 2(b) shows the distribution of the peak voltage, V_p, in the d^2I/dV^2-V characteristics obtained for 36 RTDs. The distribution in V_p is probably caused by the deviation in layer thickness, and is divided into two parts, that is 0.6-0.8 and 2.2-2.8 V. The energy separation between the two quantized levels above the Fermi level in the 4--nm-thick Fe_3Si was approximately 1 eV from free-electron approximation using Tsu-Esaki formula.[5] Thus, the obtained *J-V* characteristics were well explained by the resonant tunneling.

1) T. Hayashi, M. Tanaka and A. Asamitsu: J. Appl. Phys. **87** (2000) 4673.
2) K. Kobayashi, T. Sunohara, M. Umada, H. Yanagihara, E. Kita, H. Akinaga and T. Suemasu: Thin Solid Film **508** (2006) 78.
3) T. Harianto, K. Sadakuni, H. Akinaga and T. Suemasu: Jpn. J. Appl. Phys. **47** (2008) 6310.
4) M. Tsuchiya, and H. Sakaki :Jpn. J. Appl. Phys. **30** (1991) 1164.
5) R. Tsu, and L. Esaki : Appl Phys Lett. **22** (1973) 56.

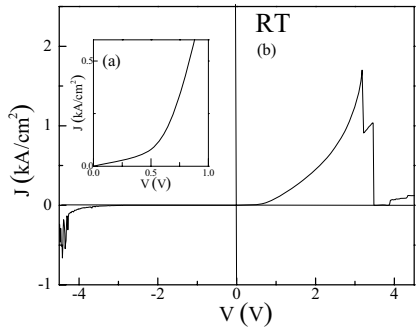

Fig.1 (a) *I-V* characteristics of RTD measured at RT, and (b) magnified *J-V* characteristics.

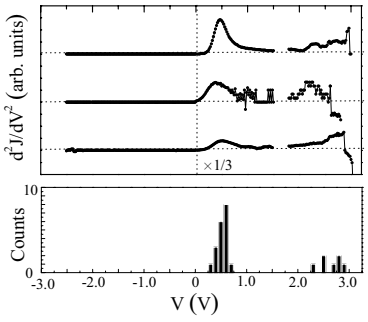

Fig.2 (a) Examples of d^2I/dV^2-V characteristics measured at RT. (b) Distribution of the peak voltage in the d^2I/dV^2-V characteristics.

Effect of Vacancies on Magnetism in Graphene

H. Kumazaki and D. S. Hirashima

Department of Physics, Nagoya University, Nagoya, Japan

Keywords: graphene, magnetism, vacancy, edge

Graphene, mono-layer graphite, has attracted much experimental and theoretical attention because of their interesting physical properties since it was fabricated. Graphene is a two-dimensional sheet of sp^2-bonded carbon atoms densely packed in honeycomb lattice, and the itinerant π-*e*lectrons on form unique band structure called Dirac cone.

Because of its small spin-orbit interaction, graphene is thought to be an ideal material of spintronics. Therefore magnetic properties of graphene are worth studying. In nanoscale graphenes (nanographenes), their physical properties are strongly dependent on the size and the geometric structure of edge [1]. Besides we think that strong defects such as vacancies have a similar effect of edges on graphene. So we focus the effect of vacancies on graphene and nanographene.

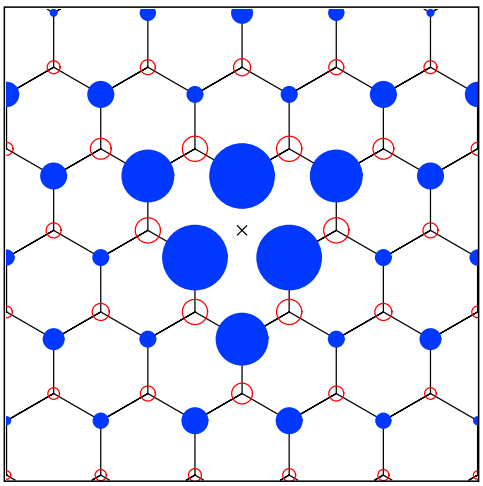

Fig.1 Spin density around a vacancy site at U=1.0t. Area of each circle is proportional to the magnitude of the spin density at each lattice point. Open circles represent positive magnetic moments and filled circles negative magnetic moments.

We describe the π-*e*lectrons on a honeycomb lattice of graphene by a Hubbard model, and resort to a mean field approximation. Furthermore, we introduce vacancies as strong short-range scattering potentials. By diagonalizing self-consistently, we obtain the density of π-electrons on each lattice point.

In previous results, we found that a quasilocalized stare is induced around a vacancy at Fermi level, and this state forms ferromagnetic moments around vacancy [2] (**Fig. 1**). These results are similar to ones from the same calculation of graphene nanoribbons (GNRs) with the zigzag edge. We think that one edge of graphene can be generated by introducing vacancies continuously, and characterized by the sublattice sequence of nearest vacant sites (NVS's) [3].

In this presentation, we show the relativeness between vacancy and edge, and the effect on magnetism from them. In addition, we refer to spin-polarized currents of GNRs [4] with vacancies.

References

1. M. Fujita, K. Wakabayashi, K. Nakada and K. Kusakabe: J. Phys. Soc. Jpn. **65**, 1920 (1996).
2. H. Kumazaki and D. S. Hirashima: J. Phys. Soc. Jpn. **76**, 064713 (2007).
3. H. Kumazaki and D. S. Hirashima: J. Phys. Soc. Jpn. **77**, 044705 (2008).
4. M. Wimmer, I. Adagideli, S. Berber, D. Tomanek and K. Richter: Phys. Rev. Lett. **100**, 117207 (2008).

Electroacoustic excitation of nanomembranes.

Dustin J. Kreft*, Max Bichler** and Robert H. Blick*

*Electrical and Computer Engineering, University of Wisconsin-Madison, Madison, Wisconsin, USA.

**Walter Schottky Institut, Technische Universität München, Garching, Germany.

Keywords: *2DEG, phonon cavity, electron-phonon coupling*

Circuit Quantum-Electrodynamics (cQED) by now is within reach for superconducting circuitry [1]. For low-dimensional electron systems a similar approach can be taken if dissipation, or more specifically the electron-phonon interaction, can be reduced. The required tailoring of the phonon density of states (DOS) is achieved when thin semiconductor slabs (nano-membranes) are suspended. The DOS of such a phonon cavity will reveal van Hove singularities [2], which in turn can be brought into or out of resonance with electronic energy states. Placing a two-dimensional electron gas (2DEG) within the membrane enables such a detailed study of the electron-phonon interaction.

Here we realized a quantum point contact (QPC) on a 2DEG in a large suspended AlGaAs nanomembrane using top gates. The large membrane size gives rise to large Q-values, i.e. a large number of phonons can be excited in vibrational modes. To excite the phonon system out of equilibrium we generate surface acoustic waves (SAWs) through the use of patterned interdigitated transducers (IDTs) on top of the nanomembrane, see Fig. 1. The two IDTs will be used to create a standing wave pattern, which drives an electroacoustic current [3,4]. Our work has the potential to test squeezed phonon states, as has been shown by theory [5].

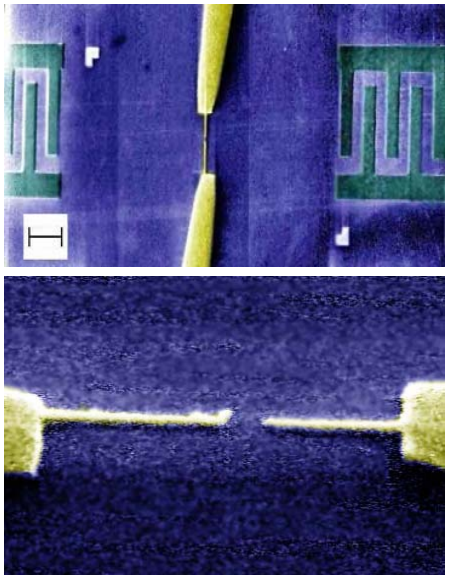

Figure 1. Colorized SEM images of a quantum point contact (golden) on top of a GaAs mesa with embedded 2DEG (purple). The transducers left and right (green) operate at 1 GHz. The scale bar in the top figure is 2 µm and the gap of the quantum point contact is 200 nm.

References

1. R.J Schoelkopf and S.M. Girvin, Nature **451**, 664 (2008).

2. S. Debald, T. Brandes, and B. Kramer, Phys. Rev. B **66**, 041301(R) (2002).

3. F.W. Beil, R.H. Blick, A. Wixforth, W. Wegscheider, D. Schuh, and M. Bichler, Europhysics Letters **76**, 1207 (2006).

4. F.W. Beil, A. Wixforth, W. Wegscheider, D. Schuh, M. Bichler, and R.H. Blick, Phys. Rev. Lett. **100**, 026801 (2008).

5. X. Hu and F. Nori, Phys. Rev. Lett. **79**, 4605 (1997).

Triple quantum dots: two path transport and electrostatic stability diagram

M. C. Rogge and R. J. Haug
Institut für Festkörperphysik, Leibniz Universität Hannover, Appelstr. 2, 30167 Hannover, Germany

Keywords: electronic transport, triple quantum dots, stability diagram, quadruple points

We investigate electronic transport on a lateral triple quantum dot with a special two path geometry. The device is prepared using local anodic oxidation on a GaAs/AlGaAs heterostructure such that three coupled dots are connected to three leads. The configuration allows two transport paths with two dots in each path and a common dot being part of both paths. The simultaneous measurements along both paths can thus be interpreted not only in terms of a triple dot but also in terms of two double quantum dots. This becomes obvious in a novel analysis method. The two conductances via the two double dots in both paths can be used to extract a hypothetic conductance via the three dots coupled in serie. This calculated conductance shows finite values only at the so called quadruple points, when all three dots are in resonance. Thus quadruple points can be identified although the single paths show transport off the quadruple points as well. Therefore the evolution from double dots to triple dots can be analyzed in detail.

The results are illustrated in comparison with an electrostatical model showing the structure of the three dimensional stability diagram of triple quantum dots. This model shows that stability diagrams of triple quantum dots contain six quadruple points in general. However it depends on the device geometry, which points are visible in transport.

References

[1] M. C. Rogge and R. J. Haug, Phys. Rev. B **77**, 193306 (2008).

[2] M. C. Rogge and R. J. Haug, Physica E **740**, 1656 (2008).

[3] M. C. Rogge and R. J. Haug, Phys. Rev. B **78**, 153310 (2008).

[4] A. Vidan, R. M. Westervelt, M. Stopa, M. Hanson, and A. C. Gossard, Appl. Phys. Lett. **85**, 3602 (2004).

[5] L. Gaudreau, S. A. Studenikin, A. S. Sachrajda, P. Zawadzki, A. Kam, J. Lapointe, M. Korkusinski, and P. Hawrylak, Phys. Rev. Lett. **97**, 036807 (2006).

[6] D. Schröer, A. D. Greentree, L. Gaudreau, K. Eberl, L. C. L. Hollenberg, J. P. Kotthaus, and S. Ludwig, Phys. Rev. B **76**, 075306 (2007).

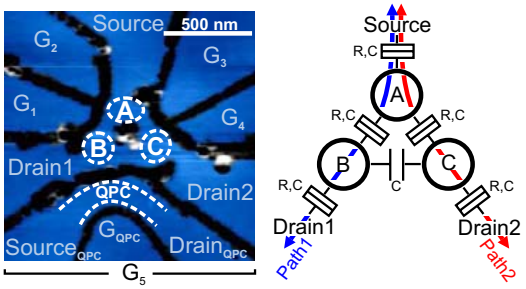

Figure 1: AFM-image of the lateral triple quantum dot with the three dots A, B and C (left) and capacitance model showing the two transport paths (right).

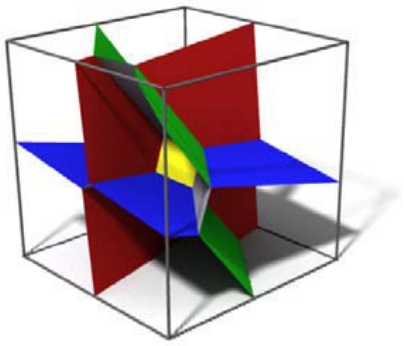

Figure 2: Three dimensional stability diagram of a triple quantum dot.

Silencing a 'noisy'AlGaAs/GaAs Wafer

L. Gaudreau*,**, A. Kam*, P. Zawadzki*, S. Studenikin*, G. Granger*, J. Kycia***, J.Mason***, Z. Wasilewski* and A. S. Sachrajda*

*Institute for Microstructural Sciences, National Research Council, Ottawa, Canada, K1A 0R6

** Physics Department, University of Sherbrooke, Quebec, Canada, J1K 2R1

*** Department of Physics and Astronomy, University of Waterloo, Waterloo, ON N2L 3G1 Canada

Keywords: Telegraphic noise, Schottky barrier, Leakeage current

One of the most important hurdles to be overcome before the routine application of lateral 2DEG nanostructures in quantum information circuits such as spin qubits, is the common prevalence of time fluctuations usually referred to as telegraph or switching noise in these devices. Whilst the origin of these fluctuations is certainly wafer related in the sense that a rare number of wafers do exist in which the noise is absent, we recently demonstrated that one necessary condition for these time fluctuations to exist is an interrupted leakage current into the semiconductor arising at the submicron gate/semiconductor interface[1]. Two strategies have been adopted in the field with partial success to minimize the leakage current and hence reduce the noise; (i) bias cooling and (ii) the use of a global gate[2]. Both of these realize the noise reduction using the same principle. Specifically, they achieve a reduction in the operating voltage of the nanostructure defining gates which thereby increases the tunnel barrier at the metal-semiconductor interface and hence reduces the leakage current.

In this paper we take this approach to the limit by exploring the possibility of eliminating the metal semiconductor interface all together through the use of a MOS (metal-oligomer-semiconductor) architecture. We successfully demonstrate how this approach can actually transform old 'noisy' AlGaAs/GaAS wafers into 'quiet' wafers. Metallic gates are defined not on top of the semiconductor surface as usual but on top of a 40nm thick intermediate insulator. For our experiments, we use an AlGaAs/GaAs wafer which historically has produced only devices plagued by significant telegraphic noise. Two sorts of devices were defined, quantum point contacts and few electron quantum dots. In each case, telegraphic noise issues were almost completely eliminated when the intermediate insulator layer was used. This directly confirms the important role that the metal-semiconductor interface plays in the origin of telegraph noise. We find that a monotonic drift towards more negative device operating voltages occurs in these devices. We will discuss the strategies that we find need to be adopted to eliminate this drift.

References

[1] M. Pioro-Ladriere *et al*., Phys. Rev. B **72**, 115331 (2005).

[2] C. Buizert *et al*., Phys. Rev. Lett. **101**, 226603 (2008).

Optically induced ballistic electron transport across quantum wires

K.-D. Hof*, F.J. Kaiser**, S. Kohler**, D. Schuh***, W. Wegscheider***, J.P. Kotthaus*, and A.W. Holleitner****

** Center for NanoScience, Ludwig-Maximilians-Universität, Geschwister-Scholl-Platz 1, 80539 München, Germany.*

*** Institut für Physik, Universität Augsburg, 86135 Augsburg, Germany.*

**** Institut für Angewandte und Experimentelle Physik II, Universität Regensburg, Universitätsstrasse 31, 93040 Regensburg, Germany.*

***** Walter Schottky Institut and Physik-Department, Technische Universität München, 85748 Garching, Germany.*

Keywords: Ballistic quantum transport, nanoscale optoelectronics.

Recent interest in the optoelectronic properties of one-dimensional quantum wires is spurred by their possible application as THz detectors [1]. Generally, we study the transport phenomena of an optically induced, non-equilibrium charge population in the diffusive and the ballistic regime at the transition from a two-dimensional to a one-dimensional electron system [2,3]. In particular, we present optoelectronic experiments, where we locally excite charge carriers in a GaAs-AlGaAs quantum well at a specific distance to lithographically defined quantum wires and measure the photo-induced current across the quantum wires. On one hand, we observe a photoconductive gain effect, by which the one-dimensional subbands of the quantum wires can be detected [4,5]. On the other hand, we resolve the ballistic transport of photo-excited charge carriers across the quantum wires. By scanning the excitation spot across the samples, we acquire photocurrent images of the mesoscopic circuits. Hereby, we gain insight into the ballistic trajectories of optically excited charge carriers. These photocurrent images can be compared to recent spatially resolved conductance experiments without laser excitation [6,7]. In addition, the setup allows us studying the optoelectronic dynamics in the mesoscopic circuit as a function of the excitation distance, photon wavelength, source-drain voltage, and a gate voltage applied to the plunger gate of the quantum wires. We discuss effects of excess charge tunneling, electron/hole pair recombination, and non-equilibrium transport dynamics in the mesoscopic circuits.

We gratefully acknowledge financial support from BMBF via nanoQUIT, the DFG (Ho 3324/4), the Center for NanoScience (CeNS), and the German excellence initiative via the "Nanosystems Initiative Munich (NIM)".

References

1. J. W. Song, N. A. Kabir, Y. Kawano, K. Ishibashi, G. R. Aizin, L. Mourokh, J. L. Reno, A. G. Markelz, and J. P. Bird, Appl. Phys. Lett. 92, 223115 (2008).

2. A.W. Holleitner, V. Sih, R.C. Myers, A.C. Gossard, D.D. Awschalom, Phys. Rev. Lett. 97, 036805 (2006).

3. A.W. Holleitner, V. Sih, R.C. Myers, A.C. Gossard, D.D. Awschalom, New J. of Phys. 9, 342 (2007).

4. C. Rossler, K.-D. Hof, S. Manus, S. Ludwig, J.P. Kotthaus, J. Simon, A.W. Holleitner, D. Schuh, W. Wegscheider, Appl. Phys. Lett. 93, 071107 (2008).

5. K.-D. Hof, C. Rossler, S. Manus, J.P. Kotthaus, A.W. Holleitner, D. Schuh, W. Wegscheider, Phys. Rev. B 78, 115325 (2008).

6. M.A. Topinka, et al. Science 289, 2323 (2000).

7. M.A. Topinka, et al. Nature 410, 183 (2001).

Quantised charge pumping by submicrosecond surface-acoustic-wave pulse

M. Kataoka, H. Kakemoto, R. P. G. McNeil, C. J. B. Ford, C. H. W. Barnes, D. Anderson, G. A. C. Jones, I. Farrer, and D. A. Ritchie

Cavendish Laboratory, J J Thomson Avenue, Cambridge CB3 0HE, United Kingdom

Keywords: single electron, surface acoustic wave, current quantisation, quantum dot

Gigahertz electrostatic potential waves accompanying surface acoustic waves (SAWs) have been used to transport electron-hole pairs [1] or quantised numbers of electrons [2] in semiconductor quantum transport and optoelectronic devices. One inherent problem with such experiment has been unintentional microwave radiation from the RF circuit, causing unwanted interference with the SAW potential [2]. Past experiments had extreme difficulty in completely eliminating crosstalk interference even though care was taken in the circuit design to screen microwave radiation.

Here, we demonstrate that such interference can be completely removed from a SAW charge-pump device using pulse-modulation technique [3]. Because SAWs travel relatively slowly (~ 3000 ms^{-1}) compared to free-space travelling microwave, switching off the microwave power applied to the transducer before SAWs arrive at the depleted one-dimensional channel would avoid microwave radiation while the SAWs carry electrons through the channel. The difficulty in implementing this technique in a SAW charge pump was caused by the large Q ($\sim 10^3$) of typical transducers [Fig. 1(b) and (c), top panels]. Since the distance between the transducer and the channel is typically a few millimeters [see Fig. 1(a)], the microwave pulse needs to be submicrosecond, for which the transducer generates broadened SAW pulses, leading to degradation of current quantisation [4].

In order to maintain a top-hat pulse shape, we have deliberately used an inefficient transducer design with $Q \sim 50$ [Fig. 1(b) and (c), bottom panels]. The split-gate channel was fabricated on a mesa containing a two-dimensional electron gas in a GaAs/AlGaAs heterostructure. We show that crosstalk interference is absent for pulse width $<$ 350 ns. Good acoustoelectric current quantisation (pulse duty ratio 1:30) was observed down to 100 ns [Fig. 1(d)]. We also present a method to reconstruct the amplitude of the SAW pulse from the Fourier analysis of crosstalk interference between short microwave and SAW pulses [Fig. 1(e)].

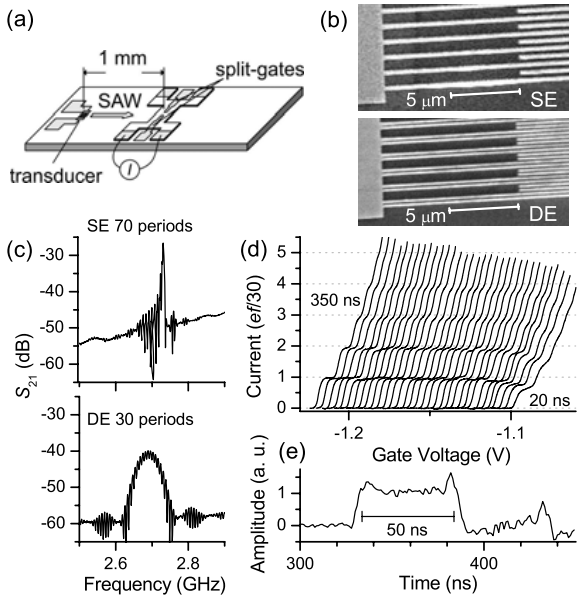

Figure 1: (a) Sample schematic. (b) SEM micrographs of single-electrode (top) and double-electrode (bottom) transducers. (c) Transmittance characteristics of 70-period single-electrode (top) and 30-period double-electrode (bottom) transducers. (d) Dependence of acoustoelectric current on pulse width . (e) SAW pulse amplitude obtained from Fourier analysis.

References

[1] J. A. Stotz *et al.*, Nature Material **4**, 585 (2005).

[2] J. M. Shilton *et al.*, J. Phys.:Condens. Matter **8**, L531 (1996).

[3] J. Heil *et al.*, J. Phys. C **17**, 2433 (1984).

[4] M. Kataoka *et al.*, J. Appl. Phys. **100**, 063710 (2006).

Coupled double row formation in a quasi-one-dimensional wire

L. W. Smith*, W. K. Hew*, K. J. Thomas**, M. Pepper*, I. Farrer*, D. Anderson*, G. A. C. Jones*, and D. A. Ritchie*

** Cavendish Laboratory, University of Cambridge, Cambridge, United Kingdom*

*** Department of Electronic and Electrical Engineering, Sungkyunkwan University, Seoul, Korea*

Keywords: Semiconductor, One-dimensional, Coupled quantum wires

It is well known that split gate devices, defined above a two-dimensional electron gas, can be used to form a quasi-one-dimensional channel, giving rise to quantized conductance. Split gate devices with an additional top gate, as used by Hew *et al.* [1], have made it possible to study various confinement regimes. The weak-confinement regime has proved very interesting, exhibiting spin-incoherent transport [2] and the formation of a double row of electrons [1]. This regime has also attracted much theoretical attention, with predictions of a zigzag formation of electrons [3] and Wigner crystallisation [4].

We present evidence of coupling between the two rows of electrons which form in weakly confined 1D channels, and report the appearance of hybrid states [5]. In Fig. 1(a), the first quantized plateau disappears as the electrostatic confinement weakens (from right to left), indicating that two parallel conducting rows exist. The greyscale plot in Fig. 1(b) shows that this disappearance occurs at the anticrossing of the first two energy levels. As the gap between the energy levels decreases, the wavefunctions hybridize, forming bonding and antibonding states (shown in inset). Up to three bonding-antibonding states have been observed in another device.

At high dc source-drain bias, the coupled double row gives rise to a structure at $0.5(2e^2/h)$, in addition to the 0.25 structure expected for a single row. We will show experimental evidence of un-coupled double rows in a 1D channel, which only exhibit a single structure at $0.5(2e^2/h)$ in high dc bias. The dc bias results are intriguing and may shed light on the origin of the 0.25 structure.

Since our measurements are performed in the regime for which a zigzag electron formation is predicted, the observed anticrossing behaviour and hybridization of states is likely to be the signature of such electronic configurations.

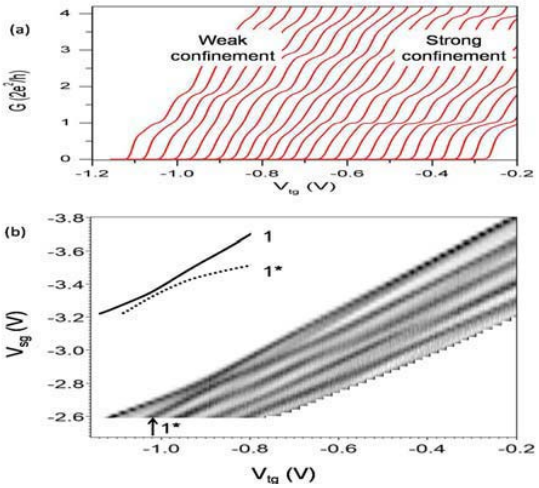

Fig.1 (a) Conductance traces sweeping top gate voltage (V_{tg}) for fixed split gate voltage (V_{sg}), V_{sg} incremented negatively between traces. (b) Grey scale (dG/dV_{tg}) plot as a function of V_{tg} and V_{sg}, black and white regions correspond to risers and plateaux respectively. The inset shows the first bonding (1) and antibonding (1*) states.

References

1. W. K. Hew *et al.*, Phys. Rev. Lett. **102**, 056804 (2009)

2. W. K. Hew *et al.*, Phys. Rev. Lett. **101**, 036801 (2008)

3. A. D. Klironomos *et al.*, Phys. Rev. B **76**, 075302 (2007)

4. J. S. Meyer, and K. A. Matveev, arXiv:0808.2076 (August 2008)

5. K. J. Thomas *et al.* Phys. Rev. B **59**, 12252 (1999)

Phases and periods of Aharonov-Bohm oscillations in parallel coupled double quantum dot

T. Hatano[1], T. Kubo[1], S. Amaha[1], S. Teraoka[1], Y. Tokura[1,2] and S. Tarucha[1,3]

[1]*Quantum Spin Information Project, ICORP, JST, Atsugi-shi, Kanagawa 243-0198, Japan*
[2]*NTT Basic Research Laboratories, NTT Corporation, Atsugi-shi, Kanagawa 243-0198, Japan*
[3]*Department of Applied Physics, Univ. of Tokyo, Hongo, Bunkyo-ku, Tokyo 113-8656, Japan*

Keywords: Aharonov-Bohm oscillation, bonding and antibonding states

Double quantum dots (DQDs) are fundamental elements of quantum computation with quantum bits made out of charge states as well as spin states. Quantum coherence between dots is the important prerequisite for realizing qubit gates. Aharonov-Bohm (AB) oscillation is the most typical phenomenon of quantum interference. For an AB ring with a QD embedded in one of the ring arms, phase effect associated with the transport through the dot states has been well studied [1]. For a DQD with one QD in each AB ring arm, AB oscillations can reflect intrinsic phase, depending on the tunnel coupling and exchange coupling. However, there have been only a few experimental studies [2,3] reported on AB oscillations with DQDs.

In this work we use a parallel coupled DQD (Fig.1(a)) with a common source and drain to study the phase and period of AB oscillations associated with the bonding and anti-bonding states. Figure 1(b) schematically shows the electron path between the source and drain contacts in the DQD device. When the two dots are coupled quantum mechanically, two current loops are formed through the source, and through the drain, respectively. These loops enclose approximately the same area for magnetic flux. We initially observed bonding and anti-bonding states in the excitation spectrum of the DQD charging diagram, and then measured the current through the respective state as a function of magnetic field. We observed periodic oscillations or AB oscillations of current flowing through the bonding, and anti-bonding state, respectively. Particularly for the AB oscillations associated with the anti-bonding state, we observed clearly that the phase changed by π, and the period became about double, respectively, depending on the center gate voltage. To account for these findings, we consider the coherent path via the reservoirs between the two QDs [4]. This coherence loop depends on the electron propagation in the two reservoirs, and therefore, can be varied by the center gate voltage. Note the center gate can work to modulate the path in the reservoirs. From theoretical calculation, we actually find that the periods and phases of the two-terminal AB oscillations between the source and drain can be modulated to reproduce the experiment by taking into account the interference between the AB oscillations for the two loops.

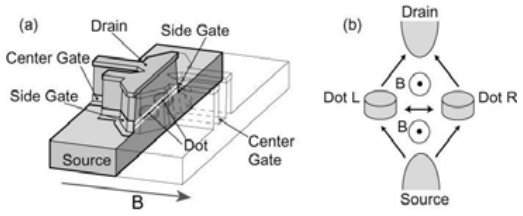

Fig.1 (a) Structure of double dot device. (b) Schematic representation of double dot device.

References

1. A. Yacoby, et al., Phys. Rev. Lett. **74**, 4047 (1995).
2. A. W. Holleitner, et al., Phys. Rev. Lett. **87**, 256802(2001).
3. T. Hatano, et al., Physica E **22**, 534 (2004).
4. T. Kubo, et al., Phys. Rev. B **74**, 205310 (2006).

Observation of a zero bias anomaly and single-electron charging in submicron GaAs/AlGaAs Corbino devices

Oktay Göktaş, Jürgen Weis and Klaus von Klitzing
Max-Planck-Institut für Festkörperforschung, Heisenbergstr. 1, Stuttgart, Germany

Keywords: quantum Hall effect, weak localization, single-electron charging, Corbino device

In this work we have prepared Corbino devices of submicron diameter in a two-dimensional electron system (2DES) embedded in an AlGaAs/GaAs heterostructure. The inner contact diameter ranges between 0.2 μm to 0.5 μm and the outer contact diameter between 0.6 μm to 0.9 μm. Au/Ge/Ni is alloyed as ohmic contacts. An SEM image of one of these devices is shown in Fig.1 (a).

The mean free path is larger than the device size, therefore transport is ballistic. At 4 K a usual linear current-voltage characteristic is measured. However, at 50 mK a zero bias anomaly is observed - a huge dip in the differential conductance versus bias voltage curve centered at zero bias as shown in Fig.1 (b). The amplitude of zero bias dip can be as large as 7 e^2/h which is usually 85% of the total conductance in the device. As the temperature raises the effect is less pronounced. Applying a small perpendicular magnetic field partly suppresses the observed zero bias anomaly. That is, the conductance increases with the applied magnetic field strongly up to 20 mT then gradually increases and saturates at around 200 mT, as shown in Fig.1 (c). The saturation value is smaller than the high temperature (or large bias voltage) differential conductance (the dashed line in Fig.1 (c)). At finite magnetic fields where magneto conductance is already saturated, a zero bias anomaly is still present with a smaller amplitude. This suggests that there are actually two different effects determining the overall conductance of the device. The effect has been reproduced in several devices.

Weak localization is a possible candidate for such an effect. Due to partial depletion in front of ohmic contacts, reflection at the contact/2DES is expected [1]. For the reflected electrons the system is similar to ballistic cavities. Reflected electrons can result in coherent backscattering for the time reversal paths. The area enclosed by time reversal paths can be extracted from the FWHM of the magneto conductance dip according the theory of weak localization in ballistic cavities [2]. The radius of the circle enclosing the area is generally comparable or slightly larger than the inner radius of the Corbino device. In ballistic cavities the amplitude of the magneto conductance dip is around 0.1 e^2/h whereas in our Corbino devices it can be as large as 6 e^2/h. Such a large amplitude for weak localization has not been reported.

Recent experiments on Hall bars and Corbino devices show that incompressible (IC) stripes exists not only at the edges of the 2DES but also in front of the ohmic contacts [1]. For a region of magnetic field a compressible (C) island in the device can be separated from the contacts by IC stripes. Therefore, single-electron charging play a role since the device size is small. We have observed single-electron charging at high magnetic field which we explain with the existence of C and IC regions in the depletion region of 2DES. The properties of electron transport in Corbino devices in ballistic regime and under high magnetic field will be discussed on this contribution.

References

[1] E. Ahlswede *et. al* Physica E **12**, 165 (2002).

[2] H. U. Baranger *et. al* PRL **70**, 3876 (1993).

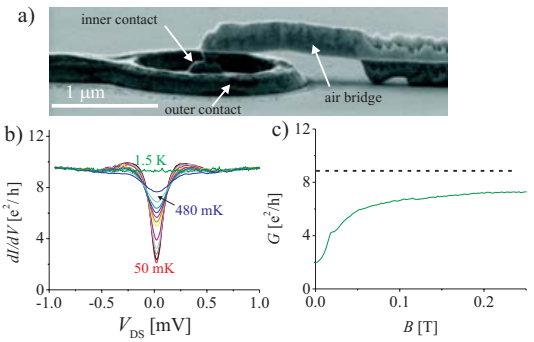

Figure 1: (a) An SEM image of a submicron Corbino device. (b) Differential conductance versus bias voltage at different temperatures at zero magnetic field. (c) Conductance versus magnetic field.

Singlet-Triplet Transitions in Highly Correlated Nanowire Quantum Dots

Yan-Ting Chen, Chian-Jen Chao, Shang-Yu Huang, and Shun-Jen Cheng*

Department of Electrophysics, National Chiao-Tung University, Hsinchu 300, Taiwan

Keywords: Nanowire quantum dot, many body physics, correlation, singlet-triplet transition

The fabrication of quantum dots formed in electrically gated nanowires or nanowire heterostructure has been successfully demonstrated recently [1,2]. Such nanowire quantum dots (NWQDs) are advantageous in the control of aspect ratio, and provide an unique playground for studying the many-body physics in quasi-0D and finite 1D systems. In this work, we present theoretical studies of the singlet-triplet (S-T) transitions in two-electron (2e) charged NWQDs by exact diagonalization techniques. A configuration interaction (CI) theory based on an asymmetric 3D parabolic model was developed for few-electron NWQDs with arbitrary aspect ratios. The validity of the solvable 3D parabolic model was confirmed by full 3D finite difference simulations.

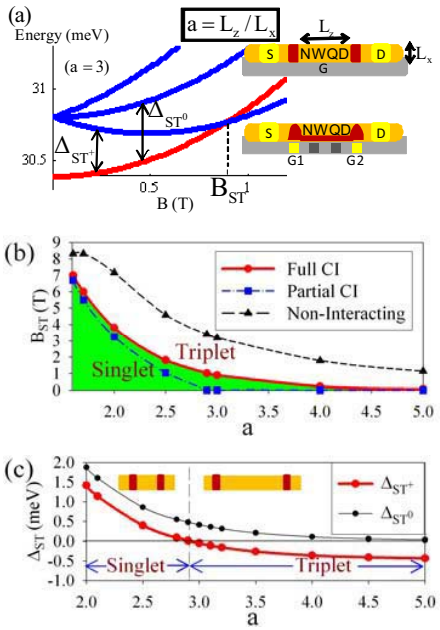

Fig.1 (a) The calculated energy spectrum vs. magnetic field of two electrons in a NWQD of radius 25nm and aspect ratio a=3 (b) The critical magnetic field B_{ST} for the S-T transitions vs. the tunable aspect ratio of the NWQD. (c) The energy separation between the S and T states, Δ_{ST}, of two electrons in the NWQD at fixed field B=1T as function of the tunable aspect ratio of the dot.

The underlying physics of the S-T transitions in InAs NWQDs in magnetic fields is associated with the competing effects of large spin Zeeman energies, exchange and correlation energies. First, the spin Zeeman splittings lower the energies of the T states and push the critical field B_{ST} for the S-T transitions down to only few Tesla. The Coulomb exchange interactions in the T states further decrease the B_{ST}. However, the electron correlations stabilize the S states and increase B_{ST} again. Comparing the results obtained by the lowest-order partial CI calculations with those by the full CI method, the highly correlated natures of few electrons in long NWQDs with aspect ratios a>3 are identified. The electron correlations lead to nearly degenerate S and T states, Δ_{ST} ~0, at zero field and make B_{ST} extremely small in very long NWQDs (Fig.1(b)). The energy separation (Δ_{ST}) between the S- and T- states of a NWQD reverses its sign at the critical aspect ratio value a~3 [Fig.1(c)], suggesting the possibility of electrical (rather than magnetic) control of spin (S or T) states of 2e in a gate-defined NWQD by electrically varying the aspect ratio of the dot.

References

1. M. T. Bjork *et al.*, Nano Lett. **4**, 1621 (2004).
2. C. Fasth *et al.*, Phys. Rev. Lett. **98**, 266801 (2007)

Manipulation of spin distribution in a ferromagnetic/non-magnetic hybrid-double-quantum-disk structure

Heesang Kim and Nammee Kim
Department of Physics, Soongsil University, Seoul, 156-743 Korea

Keywords: Magnetic Semiconductor, Hybrid Quantum Structure, Spin devices

One of the main purposes of spintronic nano-devices is to control the spin states of nano-sized quantum structures [1, 2, 3, 4]. A ferromagnetic/non-magnetic hybrid-double-quantum-disk (HDQD) structure is proposed, which is capable of manipulating distribution of the spin polarization of the system by changing external magnetic field[5]. The schematic diagram of the HDQD structure, we propose, is shown in Fig. 1 (a) and the carrier's potential profile with zero bias voltage is shown in Fig. 1 (b). The thicker disk(W_1) is diluted magnetic semiconductor (DMS) and the narrow disk(W_2) is non-magnetic semiconductor (NMS). We choose asymmetric size of the disks in order to design proper energy levels in the device.

Carrier's spin distribution in the system is studied within a qualitative effective mass Hamiltonian framework[4]. The distribution of the spin polarization strongly depends on the external magnetic field and the barrier's thickness. Since a DMS has a giant Zeeman effect, there exists a energy-level crossing in the DMS disk at a certain magnitude of the external magnetic field. Here, the field is denoted by B_c, the critical field. Owing to the energy-level crossing, which originates from the giant Zeeman splitting of the DMS disk, and owing to the exchange of the carriers between the disks, distribution the spin polarization in the system changes drastically by modulating the external magnetic field around the critical value B_c. Due to such a characteristics, the HDQD structure we propose can be applied to spin devices such as memory devices.

References

[1] J. R. Petta, A. C. Johnson, J. M. Taylor, E. A. Laird, A. Yacoby, M. D. Lukin, C. M. Marcus, M. P. Hanson, and A. C. Gossard, Science **309**, 2180 (2005).

[2] N. Kim, S. J. Lee, T. W. Kang, and H. Kim, Phys. Rev. B **69**, 115308 (2004).

[3] J. I. Climente, M. Korkusiński, P. Hawrylak and J. Planelles, Phys. Rev. B **71**, 125321 (2005).

[4] N. Kim, H. Kim, and T. W. Kang, Appl. Phys. Lett. **91**, 113504 (2007).

[5] S. N. Yi, Jong H. Na, Kwan H. Lee, Anas F. Jarjour, Robert A. Taylor, Y. S. Park, T. W. Kang, S. Kim and D. H. Ha, Appl. Phys. Lett. **90**, 101901 (2007)

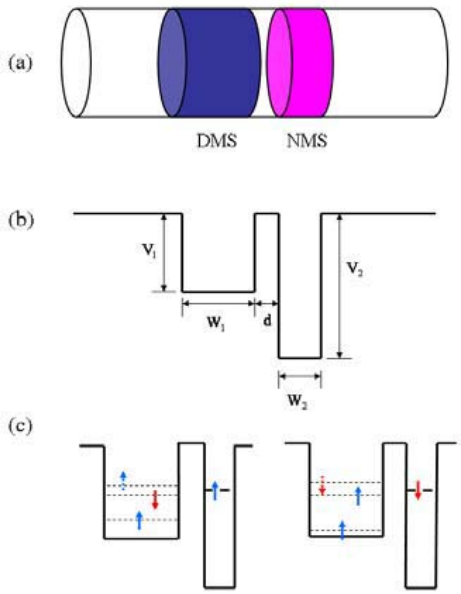

Figure 1: (a) Schematic diagram of the DMS/NMS HDQD. (b)The z-axis potential profile for a carrier in the HDQD, where $V_1 = -0.105$eV, $V_2 = -0.166$eV, $w_1 = 40$nm, $w_2 = 9$nm, and $d = 6$nm. (c) Energy levels and corresponding spin states of the HDQD without coupling between the disks. The left-hand-side one is for high external magnetic field being below the critical value, while the right-hand-side one is for the field above the critical value.

Fano-Kondo effect in side-coupled double quantum dot

H. Tamura and S. Sasaki

NTT Basic Research Laboratories, NTT Corporation, Atsugi, Kanagawa, 243-0198, Japan

Keywords: Fano resonance, Kondo effect, quantum dot

The Kondo effect in a quantum-dot device is produced when a localized electron with spin strongly interacts with conduction electrons. A localized single-particle-level in a quantum dot also acts as a resonant center when it is connected to continuum states, which is known as the Fano effect. In a recent experiment [1], low temperature transport characteristics of the side-coupled double QD fabricated in a two dimensional electron system have revealed novel Fano resonances which arise from interference between the Kondo enhanced conductance in dot 1 and discrete levels in dot 2. It is quite interesting to investigate theoretically how this interference effect appears when the side QD is *not* directly connected to the continuum states of leads.

In this paper, we simulate the Kondo effect in an embedded QD which is coupled to a side QD in the tight-binding model schematically shown in Fig. 1. The embedded QD-1 between 1D conduction leads has the single-particle energy ε_1 and the on-site Coulomb energy U_1 and induces the Kondo effect. The side QD-2 with the energies ε_2 and U_2=0 is coupled to QD-1. The effect of the Coulomb interaction in QD-1 is taken into account by the slave-boson mean field approximation. The conductance through QD-1 is calculated from the transmission probability which is obtained by the S-matrix formalism. The Fano parameter q and the level broadening Γ are analytically evaluated from the conductance formula and are related to the tight-binding parameters t_1 and t_d.

Figure 2 shows the calculated conductance as functions of single-particle levels ε_1 and ε_2 for U_1=4, t_1=0.45, t_d=0.23 in units of t_0. When ε_2 is away from the Fermi level E_F=0, the conductance shows an ordinary Kondo enhanced resonance. As ε_2 is closer to E_F=0, two asymmetric peaks appear at ε_1=0 and -4 and the peak at ε_1=-4 shifts towards the lower energy. This result shows the Fano anti-resonance strongly suppresses the Kondo resonance even when the side QD is not directly coupled to the continuum leads.

This work was supported by the Next Generation Supercomputing Project, Nanoscience Program, MEXT, Japan.

References

1. S. Sasaki, H. Tamura, S. Miyashita, T. Maruyama, T. Akazaki and T. Fujisawa, submitted to EP2DS-18.

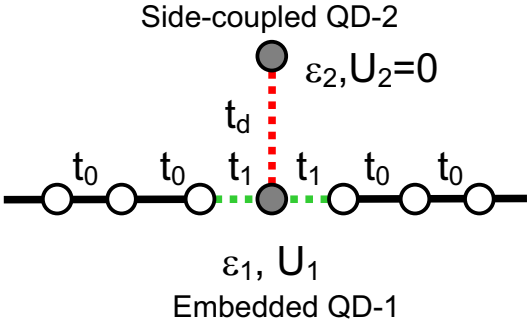

Fig.1 The tight-binding model for the side-coupled double QD.

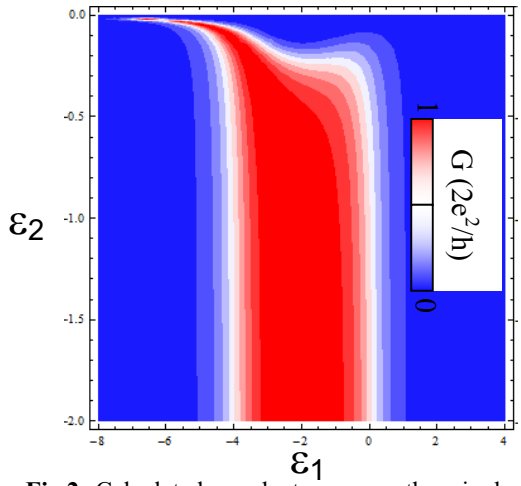

Fig.2 Calculated conductance vs. the single-particle energies ε_1, ε_2.

Control of two-electron quantum dot by external fields

J. Särkkä and A. Harju
Helsinki Institute of Physics and Department of Applied Physics, Helsinki University of Technology, Espoo, Finland

quantum dots, quantum state engineering

Electron spin is one of the most promising realizations of a qubit. A setup of two electrons confined in a double quantum dot (DQD) and coupled through the exchange interaction has been investigated experimentally during last few years. The control of the quantum states of the DQD, singlet and triplet states, has been shown experimentally by adjusting the exchange energy using gate voltage[1, 2]. The dominant decoherence mechanism in a GaAs DQD is the hyperfine interaction between electrons in the quantum dot and the surrounding nuclei.

We have calculated numerically, using exact diagonalization and perturbation theory, the time-dependent singlet probability and its variance in the setup of Laird et al.[2]. We obtained results which are in agreement with the experiments[3] (see Fig. 1). For the asymptotic value of the singlet probability and its variance, we obtained exact analytical formulae. We have also analyzed the effect of the hyperfine spin polarization on the singlet-triplet decoherence[4], calculating numerical results for the spin state evolution and analytical expressions for the asymptotic singlet probability and variance. The polarization does not have a considerable effect on the oscillations of the singlet probability. We showed that the ratio of the mean and variance of the hyperfine field may be deduced from the experimental measurements of the singlet probability and variance.

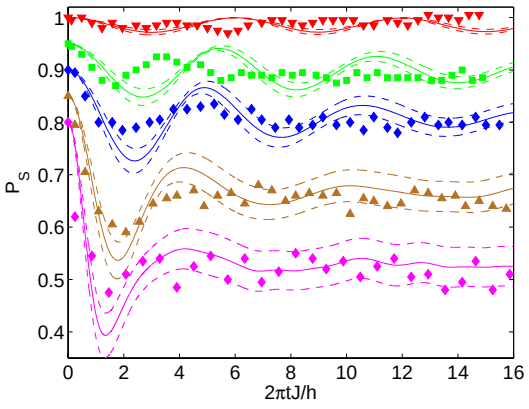

Figure 1: Singlet probabilities as a function of time for different exchange energies, compared with data of Laird et al. [2]

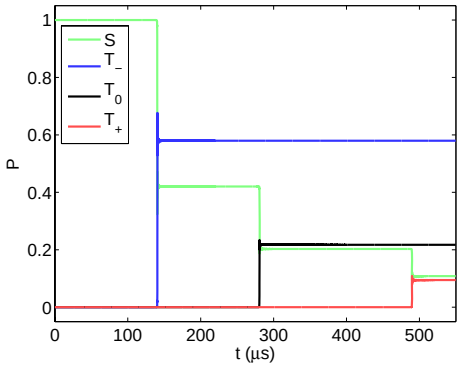

Figure 2: Probabilities of the singlet and triplet states as a function of time. Magnetic field is changed so that all singlet-triplet crossings are passed.

Another way to control the DQD could be the use of time-dependent magnetic field. For certain magnetic field values the singlet and triplet states become degenerate, which enables transitions to triplet states (see Fig. 2). The probabilities of the three triplet states depend strongly on the velocity of the magnetic field sweeping. The calculated results are in agreement with the Landau-Zener formula for nonadiabatic transitions. Thus, a diverse manipulation of the quantum states of the DQD may be realized using external magnetic field.

References

[1] J.R. Petta et al., Science **309**, 2180 (2005).

[2] E.A. Laird et al., Phys. Rev. Lett. **97**, 056801 (2006).

[3] J. Särkkä and A. Harju, Phys. Rev. B **77**, 245315 (2008).

[4] J. Särkkä and A. Harju, Phys. Rev. B **79**, 085313 (2009).

Novel observations of the "0.7"-conductance anomaly in etched quantum point contacts with large subband spacings

S.F. Fischer*, S.S. Buchholz*, U. Kunze*, D. Reuter**, A.D. Wieck**, J.P. Bird+, V. Mitin+

* *Electronic Materials and Nanoelectronics, Ruhr-University of Bochum, D-44780 Bochum, Germany*

** *Applied Solid State Physics, Ruhr-University of Bochum, D-44780 Bochum, Germany*

+ *Dep. of Electrical Engineering, University at Buffalo, Buffalo, New York 14260-3000, USA*

Keywords: quantum point contacts, quantized conductance, 0.7-anomaly, persistent recharging

The noninteger plateau-like feature near 0.7x2e^2/h in the linear conductance of quantum points contacts (QPCs) has been observed consistently for many years but no conclusive picture on it is available. This "0.7-anomaly" is widely discussed as a many-body state, possibly involving spontaneous spin polarization and/or Kondo phenomena. Recently, an unusual resonant enhancement of the nonlinear conductance was observed in split-gated long QPCs [1], and it was suggested to be associated with the formation of a correlated state near pinch-off.

Here, we investigate etched QPCs (120-150 nm wide, 100 nm long) fabricated from a high-mobility GaAs/AlGaAs field-effect heterostructure with large subband spacings of about 10 meV. The population of electrons in the one-dimensional (1D) subbands is increased by increasing top gate voltage. In most cases a small dc bias does not enhance the conductance before the onset of the first quantized plateau at about 30 mK, Fig. 1(a). However, as in [1] we also observe a resonantly enhanced conductance *above* the first plateau (see Fig. 1(b)). This occurs for about one third of the investigated QPCs which were all processed simultaneously. As the QPCs are only 100 nm in length, hence much shorter than in [1], this is in contrast with the assumption that elongated quantum wires are required to observe such a conductance enhancement.

Additionally, we report on a strong effect of cooling the QPCs under a top gate bias from room temperature to 4.2 K on the 0.7-feature. A top gate bias while cooling is well-known to vary the confining potential of etched QPCs by a persistent recharging of the doping layer and is known to affect the lateral 1D confinement such that the subband spacings can be reduced by several meV [2]. We find that the pronounced evolution of the "0.7"-feature in magnetic field up to 8 T (see Fig. 1(c)) is fully suppressed after cooling under top gate bias (see Fig. 1(d)). Hence, variations in the 1D confinement originating from a persistent recharging of the donors strongly influence the sub-single mode transport properties of QPCs.

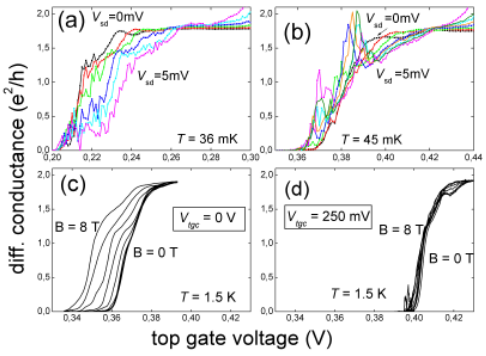

Fig.1 Differential conductance (not corrected for series resistance) at small dc drain bias (ranging from 0 to 5 mV) of etched QPCs: Examples for (a) no enhancement, (b) enhancement. The magnetic field evolution of the 0.7-feature at zero dc drain bias: (c) after cooling under zero top gate bias, and (d) after cooling under a top gate bias of +250 mV.

References

1. T. Morimoto, M. Henni, R. Naito, K. Tsubaki, N. Aoki, J. P. Bird, Y. Ochiai, Phys. Rev. Lett **97**, 096801 (2006).
2. S.F. Fischer, G. Apetrii, S. Skaberna, U. Kunze, D. Reuter, A.D. Wieck, Appl. Phys. Lett. **81**, 2779, (2002).

Spin-orbit interaction and quantum transport in a quantum dot in a higher spin state

A.Tagliacozzo ° *, P.Lucignano*§

° *Universita'di Napoli "Federico II Monte S.Angelo, via Cintia, 80125 Napoli, Italy*

* *CNR-INFM Coherentia, via Cintia, 80125 Napoli, Italy*

§ *Scuola Internazionale Superiore di Studi Avanzati (SISSA), via Beirut 2, 34014 Trieste, Italy*

Keywords: Quntum dot, Quantum transport, Kondo effect, Spin-Orbit coupling

Gate-controlled semiconductor Quantum Dots (QDs) enable manipulation of the quantum states down to the single electron level. In the recent past we have explored the quantum coherent properties of spin degrees of freedom in QDs with few electrons. The Coulomb interaction is usually strong with respect to the single particle energy spacing, therefore exact diagonalization calculations are needed.

By increasing the magnetic field B orthogonal to the plane of a parabolically confined vertical QD, the total spin increases, up to full spin polarization (FSP). The Rashba spin-orbit interaction tilts the spin polarization at the border of the dot toward a radial in plane direction. We have recognized that the lowest lying excitation of a FSP QD is a collective spin mode with the spin density reversed at the centre of the dot, healing back to the ground state polarization at the boundary, in analogy to what happens in the Quantum Hall Ferromagnet, whose first excited state is a skyrmion.

We have found that the rise in intensity with B of the far-infrared absorption peak due to the appearance of this mode marks the crossover to the FSP state. The total absorption satisfies the optical sum rule, giving direct information on the total number of electrons inside the dot and on the nature of the spin-orbit interaction.

By attaching leads to the QD, transport affects its local magnetic properties and, vice versa, its magnetic properties inprint the current response with a zero bias anomaly. At zero magnetic field a QD with four electrons is in a triplet spin state, due to Hund's rule. Still, the magnetic moment is influenced by the coupling to the leads. The Kondo screening competes with the Hund's ferromagnetic exchange interaction if the coupling to the leads is strong enough. A novel Kondo physics with an even number of electrons on the QD can emerge, as we show on Anderson-like models using a Numerical Renormalization Group approach to the quantum transport. Rashba and Dresselhaus spin orbit interactions, by breaking the spin symmetry, provide changes in the conduction properties of such device.

References

1. P.Lucignano, B.Jouault, A. Tagliacozzo, Phys. Rev. B75, 153310 (2007).
2. P.Lucignano, B.Jouault, A.Tagliacozzo and B.L. Altshuler, Phys.Rev. B71,121310(R)(2005)

Zeeman spin-splitting anisotropy in ballistic hole quantum wires fabricated on a (100)-oriented AlGaAs/GaAs heterostructure

J.C.H. Chen*, O. Klochan*, A.P. Micolich*, A.R. Hamilton*, D. Reuter** and A.D. Wieck**

* *School of Physics, University of New South Wales, Sydney NSW 2052, Australia*

** *Angewandte Festkörperphysik, Ruhr-Universität Bochum, D-44780 Bochum, Germany*

Keywords: holes, quantum wires, Zeeman spin-splitting, GaAs

Holes in an AlGaAs/GaAs heterostructure have strong spin-orbit coupling, which introduces the possibility of manipulating spins with an electric field. In addition to this possibility, holes have spin 3/2, which show different behaviour compared to electrons with spin 1/2. This was demonstrated by Winkler *et al*., [1] who observed a g-factor anisotropy in 2DHGs. The observation of this anisotropy has led to the study of holes in 1D wires [2, 3] because by measuring in the 1D regime, we can measure the g-factor quantitatively.

In previous studies [2, 3], hole 1D wires were fabricated on wafers grown in the (311) plane with wires aligned along the [-233] and [01-1] directions. By applying an in-plane magnetic field, either parallel or perpendicular to the wire, the *g*-factor in each direction can be extracted. In Refs [2, 3], the results were complicated because it was unclear whether the g-factor anisotropy was due to the 1D confinement of the wire or the underlying 2D crystallographic anisotropy. In order to eliminate the 2D crystallographic effect, we have used wafers with high crystallographic symmetry. Winkler *et al*. [3] calculated that the 2D in-plane *g*-factor should be zero in high symmetry systems such as wafers grown in the (100) direction. Therefore the interplay between the 2D g-factor anisotropy and 1D confinement should be eliminated for a quantum wire on a (100)-oriented AlGaAs/GaAs heterostructure.

In this work, we present measurements of 1D hole wires fabricated on a (100)-orientated AlGaAs/GaAs heterostructure. The device used in this measurement was an 'induced' quantum wire device [4] with a C-doped GaAs cap layer wet-etched to define metal gates for inducing the 2DHG and depopulate the 1D wires. Two wires were oriented along [011] and [01-1] on the same hall bar. This enabled us to measure wires in different crystallographic directions in the same cool down to minimize uncertainties introduced from thermal cycling. Clear conductance quantization in units of $2e^2/h$ was observed in both crystal directions. Strong Zeeman spin-splitting anisotropy due to the 1D confinement was also observed. Our data shows that when the field is aligned along the wire then the Zeeman spin-splitting is turned on, when the field is aligned across the wire, the spin-splitting is turned off, irrespective of the orientation of the wire with respect to the host crystal.

References

1. R. Winkler, S. J. Papadakis, E. P. de Poortere and M. Shayegan, Phys. Rev. Lett. **85**, 4574 (2000).
2. S.P. Koduvayur, L.P. Rokhinson, D.C. Tsui, L.N. Pfeiffer and K.W. West, Phys. Rev. Lett. **100**, 126401 (2008).
3. O. Klochan, A. P. Micolich, L. H. Ho, A. R. Hamilton, K. Muraki and Y. Hirayama, arXiv:0809.0969 (2008).
4. O. Klochan, W.R. Clarke, R. Danneau, A.P. Micolich, L.H. Ho, A.R. Hamilton, K. Muraki and Y. Hirayama, Appl. Phys. Lett. **89,** 092105 (2006).

Electron spin-nuclear spin interaction in a hetero-g-factor double quantum dot in Spin-Blockade region

R. Takahashi[1,2], K. Kono[1,2] S. Tarucha[3,4] and K. Ono[1,5]
[1]*Low temperature physics laboratory, RIKEN, Saitama, Japan*
[2]*Department of Physics, Tokyo Institute of Technology, Tokyo, Japan*
[3]*Department of Applied Physics, University of Tokyo, Tokyo, Japan*
[4]*ICORP-JST, Kanagawa, Japan,* [5]*CREST-JST, Saitama, Japan*

Keywords: semiconductor quantum dot, electron spin g-factor, nuclear spin, hyperfine interaction

We studied an electron−nuclear spin interaction using a vertical double quantum dot (DQD) device. Spin-Blockade (SB) state [1] in the DQDs with same g-factor systems, where two quantum well layers made of the same material, e.g. two GaAs or two InGaAs has been used. However their response to magneic field is identical in these systems. In order to study more detail, a device with different g-factor layers is used in this study.

We made the DQD consisting of GaAs and InGaAs (Fig.1 (a)) and measured a leakage current in SB state at various source drain voltage and magnetic field at 1.5K

We observed two types current steps and hysteresis in the leakage current in SB region. One of the steps shifted to lower magnetic field side with increasing source drain voltage (energy difference between two dots, detuning) (Fig.1 (b) line I), and this feature is similar to those were observed in the same g-factor DQDs [2, 3]. Another type shifted toword higher field side with increasing detuning (Fig.1 (b) line II). This behavior has not been observed in the same g-factor DQDs.

From these behaviors, it is found that the current step (plotted as a line I in Fig.1 (b)) occurs at the point where the high energy level of triplet states crosses (1, 1) singlet state (Fig.2 (a) point A). On the other hand, the step on line II occurs where the lower energy level of triplet state crosses (0, 2) singlet state (Fig.2 (a) point B).

We estimated DQD parameters from a Coulomb diamond (see Fig.2) and calculated the energy difference between triplet states and singlet states based on Hubbard model and spin pairs model with different g-factors. Although using no fitting parameters, the result (Fig.2 (b)) is quite similar to the experiment data (Fig.1 (b)). From this result, it is suggested that nuclear polization direction is different on each line and the electrical control of nucler spin bipolar is possible.

[1] K. Ono *et al.*, Science. **297**, 1313 (2002).
[2] K. Ono *et al.*, Phys. Rev. Lett. **92**, 256803 (2004).
[3] J. Baugh *et al.*, Phys. Rev. Lett. **99**, 096804 (2007).
[4] S. M. Huang *et al.*, to be submitted.

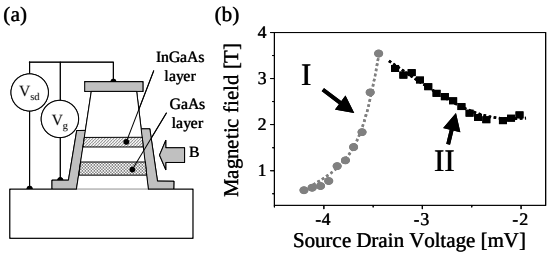

Figure 1: (a) Schematic of the device and measurement setup. From a previous study, it is found that g-factor of GaAs and InGaAs are -0.33, -0.89 respectively [4]. (b) Step position and source drain voltage relation for various magnetic fields. The step on line I shifts toward lower magnetic field side with increasing the voltage and another step on line II shifts to higher field side.

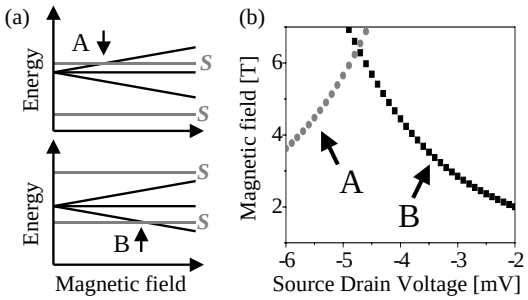

Figure 2: (a) Crossing of triplets and singlets. Upper singlet is (1, 1) and lower is (0, 2). (b) Calculated energy difference using parameters from Coulomb diamond, onsite (interdot) Coulomb energy = 3.59 meV (2.69 meV), energy offset at zero sourec drain voltage = 0.90 meV, tunnel coupling = 134 μeV and voltage drop raito for three barriers are 0.40, 0.20 and 0.40.

Evidence of spin gap physics in fully spin-split quantum wires

F. Sfigakis, C. J. B. Ford, T.-M. Chen, I. Farrer, D.A. Ritchie and M. Pepper
Cavendish Laboratory, University of Cambridge, United Kingdom

Keywords: Kondo effect, 0.7 structure, spin polarization, quantum wire

The quantization of the differential conductance $G = dI/dV_{\rm sd}$ in units of $2e^2/h$ in ballistic quantum wires is well understood in terms of non-interacting electrons. However, a conductance feature near at $0.7(2e^2/h)$, the so-called 0.7 anomaly or 0.7 structure [1], cannot be explained in such terms. The discovery of "0.7 analogs" at Zeeman crossings [2], where Zeeman-split 1D subbands of opposite spins become degenerate in energy, initially suggested that the physical mechanism of the 0.7 structure becomes manifest whenever two levels of opposite spin become degenerate in energy. Despite considerable attention, both theoretical and experimental, the physical origins of the 0.7 structure/analogs are still unclear. Models based on spin polarization (with an energy gap, also referred to as a "spin gap", opening between spin-split subbands) and on Kondo physics (involving a quasi-bound state in the 1D channel) can describe most – but not all – of the phenomenology associated with the 0.7 structure/analogs. One cannot always resolve which model best fits the data.

Transport in an in-plane magnetic field $B_{\|}$, where spin-split 1D subbands are equidistant in energy, allows the properties of spin-down (defined as the spin type lowest in energy in finite magnetic field) and spin-up subbands to be studied *separately*. We show that many-body effects are not restricted merely to regimes of near-degeneracy between electrons of opposite spin [3, 4]. Our experimental results in non-equilibrium transport and temperature dependence are not consistent with Kondo physics, "spin incoherence", or purely pinning of the spin-up subband near a chemical potential. In contrast, our results are consistent with a phenomenological model where a spin gap affects *both* spin-up and spin-down subbands.

References

[1] K.J. Thomas *et al.*, Phys. Rev. Lett **77**, 135 (1996).

[2] A. C. Graham *et al.*, Phys. Rev. Lett **91**, 136404 (2003).

[3] F. Sfigakis *at al.*, arXiv:0903.2538.

[4] T.-M. Chen *et al.*, Phys. Rev. B **79**, 081301(R) (2009).

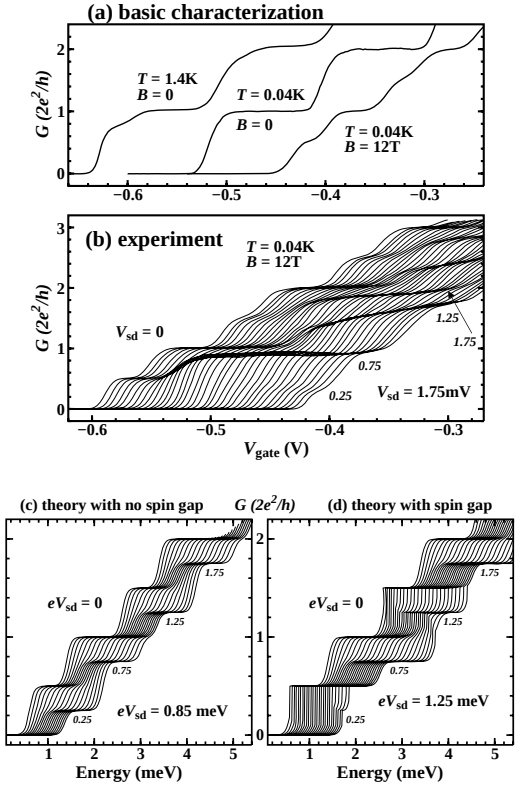

Figure 1: (a) Measured conductance traces at equilibrium in three different regimes (traces offset laterally). (b) Non-equilibrium conductance in magnetic field from $V_{\rm sd} = 0$ to $V_{\rm sd} = +1.75$ mV in 0.05 mV steps (traces offset laterally). Note the evolution from half-integer plateaus to quarter-integer plateaus as $V_{\rm sd}$ increases. Calculated conductance traces for a fixed source-drain bias V_{sd} for a 1D channel with: (c) non-interacting electrons, and (d) interacting electrons. Source-drain bias $V_{\rm sd}$ is increased in 0.05 meV steps from left to right (traces offset laterally). Note the late onset of the $0.25\,G_0$ and $1.25\,G_0$ quarter-integer plateaus in (d) compared to (c).

Giant, level-dependent g-factors and spin correlations in InSb nanowire quantum dots

Henrik A. Nilsson*, Philippe Caroff*, Claes Thelander*, Marcus Larsson*, Jakob B. Wagner**, Lars-Erik Wernersson*, Lars Samuelson* and H. Q. Xu*

** Division of Solid State Physics, Lund University, Box 118, S-22100 Lund, Sweden*

***Division of Polymer and Materials Chemistry/nCHREM, Lund University, Box 124, S-22100 Lund, Sweden*

Keywords: InSb, quantum dot, magnetotransport, spin physics

Bulk InSb is a narrow band gap (E_g = 170 meV) semiconductor with high electron mobility (μ_n=77 000 cm^2/Vs) and is therefore of relevance for low power and high speed electronics applications. It also has a small electron effective mass ($m_e^* = 0.015m_e$) and a very large electron g-factor |g| = 51 which are of interest for studies of quantum and spin physics. In this work, we report on the observation of giant, level-dependent electron g-factor and the studies of spin physics in few-electron spin configurations in InSb quantum dots.

Our InSb quantum dots were made from high crystalline-quality InSb nanowires. The nanowires were grown by metalorganic vapour phase epitaxy from 40 nm Au aerosol seed particles deposited on a (111)B InAs substrate, where the growth was initiated by a 100 nm InAs segment.[1] The grown InSb nanowires were then transferred to degenerately doped, SiO_2 capped, Si substrates. After locating the wires, Ti/Au contacts were made by electron beam lithography. At low temperatures the contact metal/semiconductor nanowire interfaces form potential barriers for the electrons, thereby creating a quantum dot in the InSb nanowire. By varying the spacing of the metal contacts quantum dots with different electron occupation number ranging from the many-electron down to the few-electron regime can be achieved.

Electron transport measurements on the fabricated InSb nanowire quantum dots were performed at T=300 mK in a ^{3}He cryostat. The measured differential conductance as a function of the source-drain bias and the Si-substrate back gate voltage (charge stability diagram) shows a typical shell structure of a few-electron quantum dot. The measured evolution of the zero-bias conductance peaks with increasing magnetic field allows us to extract the g-factors of quantum levels in the quantum dots. The results show that the quantum levels in the few-electron InSb quantum dots have giant g-factors with absolute values up to 68, the largest value ever observed for semiconductor quantum dots. We have also observed that the g-factors are strongly level dependent. The appearance of these giant, level-dependent g-factors in the few-electron InSb quantum dots allows to tune the quantum dots to different spin configurations and to study few-electron spin physics in the regimes which could not be accessible otherwise. We are able to observe a series of stripes of high differential conductance at small source-drain bias inside the Coulomb-blockade regions. These stripes are split by an applied magnetic field and can be attributed to the normal S = 1/2 Kondo effect in the InSb quantum dots. We are also able to demonstrate Zeeman-induced integer-spin Kondo effect in the few-electron regime at weak magnetic fields. In contrast to previous works on a many-electron system or in the Landau quantization limit, we can identify the orbital configurations of the Zeeman-induced integer-spin Kondo peaks. We are now studying novel spin correlation physics in other few-electron spin configurations. We have also investigated the magnetic-field evolution of the excited states of the InSb nanowire quantum dots at given electron occupations and have deduced spin-orbit coupling strengths in the InSb nanowire quantum dots.

References

1. P. Caroff *et al.*, Small **4**, 878 (2008).

Observation of the collective modes of an electron molecule in a quantum dot

S. Kalliakos[1], M. Rontani[2], V. Pellegrini[1], C. P. Garcia[1], A. Pinczuk[3,4], G. Goldoni[2,5], E. Molinari[2,5], L. N. Pfeiffer[4] and K. W. West[4]

[1]*NEST, INFM-CNR and Scuola Normale Superiore, Pisa, Italy*

[2]*S3 INFM-CNR, Modena, Italy*

[3]*Appl. Phys. & Appl. Math. and Physics, Columbia University, New York, USA*

[4]*Bell Laboratories, Alcatel-Lucent, Murray Hill, USA*

[5]*Dipartimento di Fisica, Università degli Studi di Modena e Reggio Emilia, Modena, Italy*

Keywords: Electron molecule; quantum dot; inelastic light scattering; configuration interaction

Electron states in semiconductor quantum dots are largely affected by electron-electron interaction. At sufficiently low density the Coulomb interaction is expected to give rise to a "molecule" made of electrons, whose mutual distances are rigidly fixed like those of nuclei in conventional molecules -the confined counterpart of the electron solid. This fundamental quantum state of matter has remained elusive so far.

Here we report the first observation of the molecular roto-vibrational modes of electrons confined in quantum dots which turn out to be fully developed at experimentally attainable low densities, at which localization in space of the electron wave function is not yet fully achieved [1]. We have accomplished this by means of a joint experimental and theoretical investigation of the evolution of few-body charge and spin excitations of four electrons confined in nanofabricated AlGaAs/GaAs quantum dots as a function of magnetic field.

In the low-density molecular limit, the excitations are quantized normal modes of roto-vibration, with either a rigid-rotor or a relative-motion character. In the regime of weak correlation, on the contrary, the Coriolis force mixes the rotational and vibrational motions. We find unambiguous evidence of molecular-type excitations of the electronic system by means of inelastic light scattering measurements of the collective spin excitations in these low-density nanofabricated quantum dots with four electrons, in which Coulomb correlations beyond mean-field are significant [2]. The key finding is that the observed spectra of low-energy excitations associated to changes of the relative-motion wave function –the analogues of the vibration modes of a conventional molecule- do not depend on the rotational state, represented by the ground-state total spin which is controlled by the application of a weak magnetic field. This result is the hallmark of the molecular excitations. Theoretical predictions obtained via the full configuration interaction method [3] allow for unambiguous assignement of the observed excitations and highlight that such roto-vibrational modes develop at the onset of short-range correlation.

References

1. S. Kalliakos, M. Rontani, V. Pellegrini, C. P. García, A. Pinczuk, G. Goldoni, E. Molinari, L. N. Pfeiffer, and K. W. West, Nature Phys. **4,** 467-471 (2008).

2. C. P. García, V. Pellegrini, A. Pinczuk, M. Rontani, G. Goldoni, E. Molinari, B. S. Dennis, L. N. Pfeiffer, and K. W. West, Phys. Rev. Lett. **95,** 266806 (2005).

3. M. Rontani, C. Cavazzoni, D. Bellucci, and G. Goldoni, J. Chem. Phys. **124,** 124102 (2006).

Stability of III-V and IV-VI Nanowires - a theoretical study

M. Bukala, M. Galicka, R. Buczko, and P. Kacman
Institute of Physics PAS, Al. Lotnikow 32/46, 02-668 Warsaw, Poland

Keywords: nanowires, crystallographic structure, *ab initio* methods

Using *ab initio* methods based on the density functional theory, we study the properties and the stability of III-V (GaAs, InAs) and IV-VI (PbTe) nanowires (NWs). The mutual stability of the wires have been studied by the comparison of their free energy calculated per atomic pair. Only very thin NWs (with diameters up to 5nm) has been studied by this method. The model NWs were constructed along various crystallographic directions using bulk atomic positions of either zinc-blende or wurtzite structures in the case of III-V compounds and rock-salt or CsCl structures in the case of PbTe,. For each of the initial structures the minimum energy atomic positions have been determined with the reconstruction of the NW surfaces and relaxation of the unit cell dimension in the growth direction allowed. Our calculations were performed for zero pressure and zero temperature. We have also assumed that the surface atoms are not saturated by foreign, e.g. hydrogen atoms.

In the case of III-V NWs we have found that the most stable wires adopt the wurtzite structure along (0001) direction, even though the bulk crystallographic structure of the studied compounds is zinc-blende. Among zinc-blende NWs the ones grown in (111) direction have the lowest energy. The free energy of zinc-blende NWs along any crystallographic axis is, however, always larger than that of the wurtzite NWs grown in (0001) direction. This results from the higher energy of lateral surfaces for the zinc-blende NWs and from the presence of side atoms with additional dangling bonds. The surface contribution to the total energy of the NW diminishes with the wire diameter and so does the free energy difference between the NWs in wurtzite and zinc-blende structures. Extrapolating the results obtained for very thin wires, we predict that for diameters larger than about 10-15 nm this difference should drop to about 5 meV, i.e., to values which do not lead to stabile crystallographic structure. This was indeed confirmed by experimental observations of perfect wurtzite structure in both InAs and GaAs NWs with diameters smaller than 10 nm and occurrence of stacking faults in as grown NWs with higher diameters. The theoretical result that very thin NWs adopt purely wurtzite structure has been exploited for obtaining (via lateral growth with thin wires as a core) thicker wires with the number of stacking faults considerably suppressed [1].

In contrast to the case of III-V NWs, the most stable PbTe NWs for all studied diameters have the same crystallographic structure (rock-salt) as the bulk crystal. Moreover, the PbTe NWs grow always along (001) direction. In our studies we found that this is connected with the fact that the side surfaces of such wires are mainly of the (100) type, which has the lowest energy among all possible surfaces of rock salt structure, due to the smallest number of dangling bonds. The energy difference between the NWs grown in (100) direction and those with the next lowest free energy, i.e., grown along (111) axis, is for the wires with diameter about 3 nm as big as 50 meV. Although the role of surface diminishes with the radius of the wire, this difference will be always present and can explain the observed tendency of the PbTe wires to grow along the (100) axis. Moreover, the energy cost of adopting by the wire a different (e.g., CsCl) structure would be higher by few hundred of meV per atomic pair, what makes PbTe wires of another crystallographic structure or any stacking faults unlikely to occur.

References

[1] H. Shtrikman, et al." Suppression of Stacking Faults in Wurzite III-V Nanowires" - NanoLetters 2009 (in print).

Ground-state properties of a single Anderson impurity coupled to superconductors

Akira Oguri*, Yunori Nisikawa* and Yoichi Tanaka**
**Graduate School of Science, Osaka City University, Sumiyoshi-ku, Osaka 558-8585, Japan*
*** Condensed Matter Theory Laboratory, RIKEN, Wako, Saitama 351-0198, Japan*

Keywords: Quantum dot, Kondo effect, Superconductivity, Andreev bound state

We study the low-energy properties of a single Anderson impurity coupled to BCS hosts (Fig. 1), as a model for a quantum dot connected to superconducting (SC) leads on the left (L) and right (R). The system shows a quantum phase transition (QPT) between a nonmagnetic singlet and a magnetic doublet ground states, and it depends on the parameters such as the SC gaps $\Delta_{L/R}$, the hybridization energy scale $\Gamma_{L/R}$, the impurity level ϵ_d, and Coulomb interaction U [1–4]. The competition between the magnetic fluctuation of the local moment and the SC proximity effect determines the ground state, and it also affects substantially the transport properties. For instance, the Josephson current shows a dicontinuous jump at QPT. Furthermore, when one of the leads is in the normal (N) state, the Andreev transport through a S-dot-N junction is enhanced at the corresponding crossover point [5, 6].

The variety in the tunable parameters causes some qualitatively different regimes in the singlet ground state. For instance, even in the particle-hole symmetric case, not only the Kondo and mixed valence regimes, but also a singlet which can be characterized by a local Cooper pairing in the impurity site becomes the ground state for $|\Delta_{L/R}| \gtrsim U$. The essential feature of this regime can be described by a fixed point Hamiltonian in the limit of $|\Delta_{L/R}| \to \infty$ [2]. To our knowledge, despite the model itself has been studied intensively so far, still not all the regimes have been fully investigated in detail with accurate theoretical approaches.

In this work we calculate the ground-state phase diagram and some correlation functions, using the Wilson numerical renormalization group (NRG), for a junction with finite Josephson phase $\phi \equiv \theta_R - \theta_L$. Specifically, we study precisely the crossover between the local Cooper-pairing regime and the Kondo regime where the one parameter scaling by T_K/Δ works. Here, T_K is the Kondo temperature and Δ is the amplitude of the smaller SC gap.

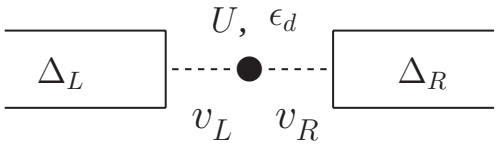

Figure 1: Anderson impurity (●) coupled the two leads: $v_{L/R}$ is the tunneling matrix element, and $\Gamma_{L/R} \equiv \pi\rho\, v_{L/R}^2$ with ρ the density of states of the leads. It describes a Josephson junction with finite phase difference $\phi \equiv \theta_R - \theta_L$, where $\Delta_{L/R} = |\Delta_{L/R}|\, e^{i\theta_{L/R}}$, and also a S-dot-N junction when one of the SC gaps is zero.

References

[1] A. Oguri, Yoshihide Tanaka and A. C. Hewson, J. Phys. Soc. Jpn. **73**, 2494 (2004).

[2] Yoshihide Tanaka, A. Oguri, and A. C. Hewson, New J. Phys. **9**, 115 (2007); Errata *ibid*, **10**, 029801 (2008).

[3] J. Bauer, A. Oguri, and A. C. Hewson, J. Phys.: Condes. Mat. **19**, 486211 (2007).

[4] C. Karrasch, A. Oguri, and V. Meden, Phys. Rev. B **77**, 024517 (2008).

[5] Yoichi Tanaka, N. Kawakami, and A. Oguri, J. Phys. Soc. Jpn. **76**, 074701 (2007).

[6] Yoichi Tanaka, N. Kawakami, and A. Oguri, Phys. Rev. B **78**, 035444 (2008).

Effect of disorder on the quantum coherence in mesocopic wires

Y. Niimi[1,2], Y. Baines[1], T. Capron[1], D. Mailly[3], F.-Y. Lo[4], A. D. Wieck[4], T. Meunier[1], L. Saminadayar[1] and C. Bäuerle[1]

[1]*Institut Néel, CNRS and Université Joseph Fourier, 38042 Grenoble, France*

[2]*Department of Physics, Tohoku University, Sendai, 980-8578 Japan*

[3]*Laboratoire de Photonique et Nanostructures, 91460 Marcoussis, France*

[4]*Lehrstuhl für Angewandte Festkörperphysik, Ruhr-Universität, 44780 Bochum, Germany*

Keywords: quantum coherence, weak localization, disorder

The time τ_ϕ over which an electron can maintain its phase coherence at low temperatures is one of the fundamental concepts in mesocopic systems. It is closely related to the lifetime of a quasiparticle in the Fermi liquid theory and sets a limit to the observability of many quantum interference phenomena. A profound understanding of the limitation of the phase coherence of electrons at low temperatures is hence of importance. According to the Fermi liquid theory, the phase coherence time τ_ϕ diverges when reducing temperature as the phase space available for electron diffusion crunches to zero [1]. An alternative theory, however, predicts a saturation of τ_ϕ at T = 0 K due to electron-electron interactions in the ground state of the Fermi liquid [2]. These two theories predict different diffusion coefficient dependencies on τ_ϕ at very low temperatures which could be tested experimentally. In metallic systems, however, the accessible range of diffusion coefficients is relatively limited [3-5].

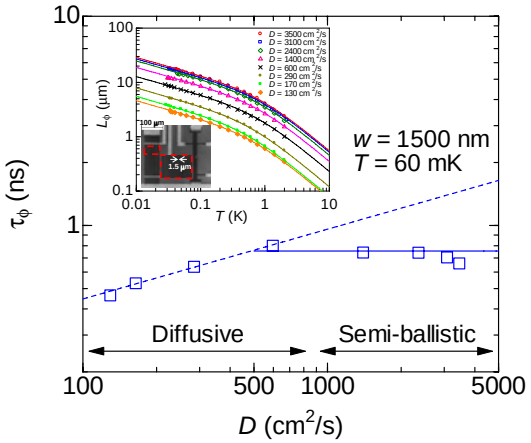

Figure 1: Phase coherence time τ_ϕ as a function of diffusion coefficient D. Inset: Phase coherence length as a function of temperature for wires with various diffusion coefficients.

Here, we present phase coherence time measurements in quasi one-dimensional mesoscopic wires made from a high mobility two dimensional electron gas. Using an original ion implantation technique, we are able to change the intrinsic disorder felt by the electrons and allows us to probe the disorder dependence of the above theories on decoherence.

We show that in the diffusive limit, the phase coherence time τ_ϕ follows a power law as a function of the diffusion coefficient, D^α, with α close to $1/3$ [see Fig. 1]. This result is quantitatively consistent with the "standard" model of decoherence proposed in Ref. [1]. On the other hand, when the disorder is low enough so that the samples are semi-ballistic, we observe a new and unexpected regime in which τ_ϕ is independent of the disorder. Moreover, for all the samples the temperature dependence of τ_ϕ follows a power law down to the lowest temperature without any sign of saturation (see inset of figure 1) [6]. This strongly suggests that the frequently observed low temperature saturation is *not* intrinsic.

References

[1] B. L. Altshuler, A. G. Aronov, and D. E. Khmelnitzky, J. Phys. C **15**, 7367 (1982).

[2] D. S. Golubev and A. D. Zaikin, Phys. Rev. Lett. **81**, 1074 (1998).

[3] P. Mohanty, E. M. Q. Jariwala, and R. A. Webb, Phys. Rev. Lett. **78**, 3366 (1997).

[4] F. Pierre *et al.*, Phys. Rev. B **68**, 085413 (2003).

[5] C. Bäuerle *et al.*, Phys. Rev. Lett. **95**, 266805 (2005).

[6] Y. Niimi *et al.*, ArXiv:0809.1381 (2008).

AC quantum Hall effect and the Hall potential distribution

H. Akera
Division of Applied Physics, Graduate School of Engineering, Hokkaido University, Sapporo, Japan

Keywords: quantum Hall effect, dynamics, theory

The Hall potential distribution in a long rectangular sample fabricated from a two-dimensional electron system (2DES) has been studied since the discovery of the quantum Hall effect [1]. Theoretically in the absence of diffusion ($\sigma_{xx} = 0$) the Hall field in a uniform sample has been shown to be enhanced near edges [2], while nonzero diffusion ($\sigma_{xx} \neq 0$) makes them uniform [3]. An experiment [4] has found a crossover from the distribution enhanced near edges to the uniform one with the increase of diffusion (by increasing the temperature or by changing the filling factor). This is seemingly a paradox because any real systems have nonzero diffusion. This discrepancy between the theory and the experiment may be due to the difference in the frequency f of the applied current: the two theories are for $f = 0$, while the experiment has been done using a lock-in technique with $f = 235$Hz. In this paper we study AC response of quantum Hall systems at even-integer filling factors ν, and show that the AC response is a function of a normalized angular frequency

$$\tilde{\omega} = \frac{\omega \sigma_{yx}}{\omega_{\mathrm{c}} \sigma_{xx}}$$

with ω_{c} the cyclotron frequency and $\sigma_{yx} = \nu e^2/h$, and that the crossover of the Hall potential distribution occurs around $\tilde{\omega} = 1$ when the frequency ω or the diffusion σ_{xx} is changed (such a crossover has been suggested to occur when the time interval, in which the current is applied, is equal to the relaxation time [5]).

We consider an infinitely long sample with the width W in $|y| < W/2$ with the magnetic field applied along z. The current is applied along x and the Hall field $E_y(y,t)$ is induced. The Hall field is produced by the charge density in the sample, which consists of two components. One is the polarization component which comes from the Landau-level mixing in wave functions due to $\partial E_y/\partial y$. The other is the diffusion component which comes from hoppings between localized states. The ratio between the two components is shown to be $\tilde{\omega}$, and the polarization component is dominant in the high-frequency region or in the low diffusion regime. We have calculated $E_y(y,t)$ in the case of screened Coulomb interaction which is expected to model the Coulomb interaction in the presence of the gate electrode above 2DES. The amplitude of the Hall field $E_y(y,t)$ is the highest at edges ($y = \pm W/2$) and decays in the bulk. The decay length λ is given by

$$\lambda = \lambda_\infty \left(1 + \tilde{\omega}^{-2}\right)^{1/4}$$

where λ_∞ is the decay length at $\tilde{\omega} \to \infty$ and is determined solely by the polarization component. This equation shows that in the limit of low frequency ($\tilde{\omega} \to 0$) the decay length becomes infinite and the Hall field becomes uniform. The crossover from the polarization-dominant region to the diffusion-dominant region occurs around $\tilde{\omega} = 1$. We will also discuss the case of unscreened Coulomb interaction as well as the phase difference between the Hall field and the current.

References

[1] K. von Klitzing, G. Dorda and M. Pepper, Phys. Rev. Lett. **45**, 494 (1980).

[2] A.H. MacDonald, T.M. Rice and W.F. Brinkman, Phys. Rev. B **28**, 3648 (1983).

[3] D.J. Thouless, J. Phys. C **18**, 6211 (1985).

[4] P.F. Fontein, P. Hendriks, F.A.P. Blom, J.H. Wolter, L.J. Giling and C.W.J. Beenakker, Surface Science **263**, 91 (1992).

[5] A. Cabo and A. González, Revista Mexicana de Física **40**, 71 (1994).

Fractional Quantum Hall Effect in CdTe and $Cd_{1-x}Mn_xTe$ high electron mobility Quantum Wells

C. Betthausen*, A. Vogl*, V. Kolkovsky**, G. Karczewski**, T. Wojtowicz** and D. Weiss*

* *Department of Physics, Regensburg University, Regensburg, Germany*

** *Institute of Physics, Polish Academy of Sciences, Warsaw, Poland*

Keywords: Fractional Quantum Hall Effect; CdTe; CdMnTe; Quantum Well

Heterostructures made of CdTe and $Cd_{1-x}Mn_xTe$ are interesting material systems as they allow combining magnetic properties (by incorporation of spin 5/2 Manganese ions) with the physics of low dimensional electron systems. $Cd_{1-x}Mn_xTe$ belongs to the class of diluted magnetic semiconductors and has thoroughly been investigated in the past [1,2].

Over the years electron mobilities in modulation doped $Cd_{1-x}Mn_xTe$ based quantum structures could be steadily increased [3]. This allowed a number of new discoveries [4,5], mainly exploiting the giant spin splitting – arising due to the interaction of highly mobile carriers with the localized magnetic moments (sp-d exchange interaction). Only very recently mobilities have reached a level which is comparable to the one of the first GaAs/AlGaAs samples displaying the Fractional Quantum Hall Effect.

Here we have studied the Fractional Quantum Hall Effect (FQHE) in high mobility CdTe and $Cd_{1-x}Mn_xTe$ heterostructures. Fig. 1 shows magnetotransport data collected for a 30 nm wide CdTe (Fig. 1a) and a 20 nm wide $Cd_{1-x}Mn_xTe$ quantum well with $x \sim 0.3$ % (Fig. 1b). Both samples have $Cd_{1-x}Mg_xTe$ barriers. After illumination with a yellow LED, electron mobilities are 400 000 cm^2/Vs and 170 000 cm^2/Vs, respectively, with carrier concentrations in the range of $3 - 4 \cdot 10^{11}$ cm^{-2}. These values correspond to electron mean free paths between 1.5 µm and 4 µm. Fig. 1a displays clear plateaus at $\upsilon = 5/3$ and $\upsilon = 4/3$, so far not observed in II-VI materials. Fractional quantized steps in the Hall resistance can also be resolved in the $Cd_{1-x}Mn_xTe$ quantum well (Fig. 1b) – which is the very first observation of FQHE in a diluted magnetic semiconductor. In these preliminary experiments on $Cd_{0.997}Mn_{0.003}Te$ heterostructures, plateaus corresponding to $\upsilon = 6/5$ and $\upsilon = 4/3$ are well resolved. The incorporation of magnetic ions into the quantum well therefore does not inhibit the formation of FQH states.

An interesting question to be addressed in future experiments is how the spin 5/2 Manganese ions interact with the many particle FQH states.

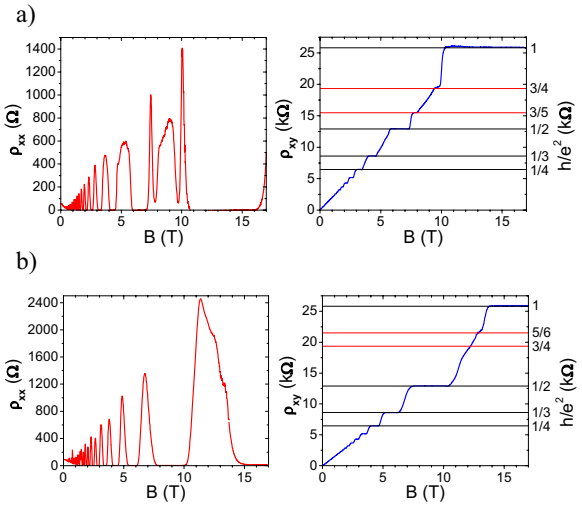

Fig. 1 Magnetotransport data for (a) 30 nm wide CdTe and (b) 20 nm wide $Cd_{0.997}Mn_{0.003}Te$ quantum well. In each case the temperature is 100 mK and magnetic field is applied perpendicular to the quantum well.

References

1. T. Wojtowicz *et al.*, J. Cryst. Growth **214/215**, 378 (2000).
2. J. Gaj *et al.*, Phys. Rev. B **50**, 5512 (1994).
3. G. Karczewski *et al.*, J. Cryst. Growth **184/185**, 814 (1998).
4. J. Jaroszynski *et al.*, Phys. Stat. Sol. B **241**, 712 (2004).
5. F. Teran *et al.*, Phys. Rev. Lett. **88**, 186803 (2002).

Transition from fractional quantum Hall liquid to pinned Wigner solid in two-dimensional charge carrier systems

Zhiguo Ge*, †, W. Pan†, D.C. Tsui*, L.N. Pfeiffer#, and K.W. West#
* *Department of Electrical Engineering, Princeton University, Princeton, New Jersey 08544, USA*
† *Sandia National Laboratories, Albuquerque, New Mexico 87185, USA*
# *Bell Laboratories, Alcatel-Lucent Inc., Murray Hill, New Jersey 07974, USA*

Keywords: Fractional quantum Hall effect, Wigner solid, 2DES, phase transition

It has been demonstrated that in a two-dimensional hole system (2DHS), upon changing r_s (the Coulomb interaction energy in unit of the Fermi energy) by adjusting carrier density [1] or by introducing in-plane magnetic field (B_{ip}) [2], there exists a transition from the fractional quantum Hall (FQH) liquid state to a pinned Wigner solid (WS) state at the Landau level filling ν=1/3. A more recent work [3] shows that in a 2D electron system (2DES) with a large quantum well (QW) width, the B_{ip} induced transition can also occur at ν=1/5.

So far, previous measurements have been done through magnetoresistivity (ρ_{xx}) and its temperature dependent measurements. The identification of the phase boundary, based on whether ρ_{xx} was over h/e^2 or the activation energy became zero in the Arrhenius plot, can be equivocal. On the other hand, it is known that the method of I-V (or dV/dI) measurement can identify the liquid to solid transition rather precisely [4]. In this paper, we will present results of such measurements in mapping the transition from the FQH liquid state to the pinned WS state in 2DHS at ν=1/3 and in 2DES at ν=1/5.

Our 2D hole specimen is a 30nm QW grown on {311} GaAs substrate. It has a low temperature density $p=1.7\times10^{10}cm^{-2}$ and mobility $\mu\sim6\times10^5 cm^2/Vs$. The 2D electron specimen is a 40nm QW with $n=1.1\times10^{11}$ cm^{-2} and $\mu\sim10\times10^6$ cm^2/Vs. In Fig. 1(a), we show the magnetoresistance R_{xx} as a function of perpendicular magnetic field (B_{perp}) at various tilt angles (θ) for the 2DHS. The curves are aligned to each other according to the position of R_{xx} minima at ν=2/3. Fig. 1(b) shows the dV/dI data as a function of the DC bias current (I_{dc}). At θ=0, dV/dI displays a strong minimum at I_{dc}=0, the signature of a FQH liquid. At θ=68.3°, dV/dI at the zero bias is a maximum, the characteristic of a pinned WS state [4]. At $\theta\sim44°$, dV/dI is flat, indicating the separatix between the FQH liquid phase and the pinned WS phase. More dV/dI measurements have been carried out at different 2DHS densities by applying a gate bias and at various Landau level fillings (e.g., in the re-entrant insulator regime between ν=1/3 and 2/5). These results will be presented and discussed.

In our 2DES, the transition from the ν=1/5 FQH liquid state to the pinned WS solid state was also observed upon tilting, similar to previous work [3]. At high tilt angles, a strong peak was observed in dV/dI at the zero bias, corroborating the formation of the pinned WS phase.

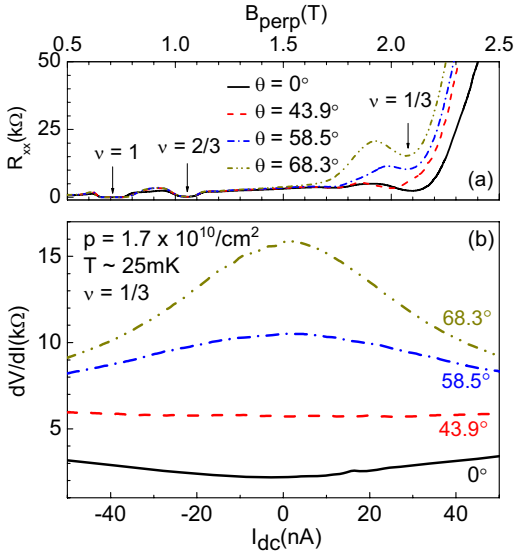

Fig. 1. (a) R_{xx} vs. B_{perp} for the 2DHS; (b) dV/dI vs. DC bias current at various tilt angles at ν=1/3.

References

1. G. A. Csáthy, *et.al.*, PRL **94**, 226802 (2005).
2. W. Pan, *et.al.*, PRB **71**, 035302 (2005).
3. B. A. Piot, *et.al.*, Nature Physics **4**, 936 (2008).
4. J. Yoon, *et.al.*, PRL **82**, 1744 (1999).

Numerical search for non-Abelian statistics in fractional quantum Hall systems

A. Wójs and G. Möller

TCM Group, Cavendish Laboratory, University of Cambridge, Cambridge, UK

Keywords: fractional quantum Hall effect, non-Abelian statistics

Fractional quantum Hall systems, especially some of the experimentally confirmed incompressible quantum liquids in the second Landau level, are among the most promising candidates for the physical realization of the hypothetical non-Abelian quantum statistics in 2D [1]. In this communication, we report the extensive studies involving large-scale exact numerical diagonalization (for Hamiltonian dimensions nearing 1 billion), carried out in the search of signatures of non-Abelian statistics in the second Landau level of either electrons (LL_1) or composite fermions (CF-LL_1).

Spin-polarized states in LL_1: We have modeled a general short-range repulsive interaction by the Haldane pseudopotential with arbitrary three leading coefficients U_1, U_3, and U_5 (and $U_{m>5} = 0$), and studied the phase diagram at different filling factors ν (e.g., the excitation gap in Fig. 1). We demonstrate adiabatic connection of the ν=1/2 and 1/3 Coulomb ground states in LL_1 to the Moore-Read (pfaffian) and Laughlin wave functions, and perform detailed analysis of their excitation spectra

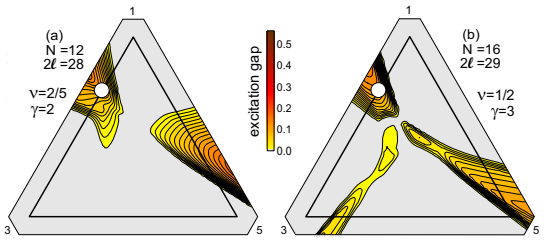

Fig.1 Ternary contour plots of neutral excitation gaps for N fermions in a partially filled Landau level with shell angular momentum ℓ, interacting via U_m (corners of the big triangles correspond to $U_m = \delta_{m,\mu}$ with μ = 1, 3, 5, as marked). White circles mark positions relevant for LL_1; ν is the filling factor; $\gamma = N/\nu - 2\ell$ is the "shift".

(e.g., suggesting novel quasiparticles at ν=1/3). For the ν=2/5 ground state in LL_1, we investigate competition of the universality classes of Jain (noninteracting CFs), Read-Rezayi (parafermion), and Bonderson-Slingerland states [2] (the latter two obeying non-Abelian statistics) as a function of the quasi-2D layer width. Finally, we demonstrate the validity of the four-flux noninteracting CF model at ν<1/3 in LL_1 (→ e.g., Abelian ν=2/7 state).

Spin-unpolarized states in LL_1: The comparison of pair and triplet Coulomb pseudopotentials in different LLs suggests relatively robust spin polarization in LL_1. Nevertheless, we observe that finite layer width allows (in the absence of a large Zeeman gap) depolarization at some filling factors. The most intriguing case of ν=1/2 (e.g., puzzling experimental/theoretical gap discrepancy was raised recently [3]) will be addressed in some detail.

'Second-generation' states in CF-LL_1: The unique short-range interaction in CF-LL_1 precludes description of the ν=1/3 and 1/2 incompressible states of the CFs (i.e., the ν=4/11 and 3/8 states of the electrons) by the Laughlin or Moore-Read wave functions. We propose a flux-attachment procedure (similar to Jain's mean-field CF transformation) generating the family of condensed CF states identified in the numerics. Remarkably, the calculated degeneracy of the quasihole spectra for some of these states appears to preclude Abelian statistics.

References

1. C. Nayak et al., Rev. Mod. Phys. **80**, 1083 (2008).
2. P. Bonderson and J.K. Slingerland, Phys. Rev. B **78**, 125323 (2008).
3. C.R. Dean et al., Phys. Rev. Lett. **100**, 146803 (2008).

Coulomb Blockade in an Antidot Molecule in the Integer Quantum Hall Regime

W.-R. Lee* and H.-S. Sim*
*Department of Physics, Korea Advanced Institute of Science and Technology, Daejeon 305-701, Korea

Keywords: Coulomb blockade; Quantum Hall effect; Aharonov-Bohm interference; Antidot

Lots of studies have focused on the role of electron-electron interaction in an antidot system in the integer quantum Hall regime [1]. For the simplest case of a single antidot, the interaction causes interesting phenomena such as $h/2e$ Aharonov-Bohm (AB) oscillations [2] and Kondo effects [3]. Such phenomena can be explained by a model based on capacitive interaction between excess charges around the antidot [4]. It would be interesting to find interaction effects in more general antidot systems.

An antidot molecule was experimentally studied in the integer quantum Hall regime [5]. The antidot molecule has two types of bound states, atomic states enclosing a single antidot and molecular states enclosing both the antidots; see Fig. 1. In this setup, the AB resonances due to the molecular state may be expected to dominantly appear in conductance signals, because the molecular state couples to extended edge channels more strongly than the atomic states. However, the period of the observed AB resonances corresponds to the area enclosed not by the molecular state but by the atomic state. The molecular state, which does not seem to participate in the AB resonances, is called as a spectator mode. The mechanism of the spectator mode still remains unclear.

In this work, we theoretically study the mechanism of the spectator mode, taking the capacitive coupling between the molecular state and the atomic states into account. It is found that the appearance of the AB resonances by the molecular state depends on the strength of the capacitive coupling. In a weak coupling regime, both the molecular state and the atomic states give rise to the AB resonances, as expected in the noninteracting limit. On the other hand, in a strong coupling regime, the resonant tunneling into the molecular states can be Coulomb-blockaded. As a result, the period of the AB resonances is modified, and the molecular states show the spectator behavior. Our result is in good agreement with the observation in Ref. [5]. More studies on antidot molecule systems will be useful for understanding of interaction effects in the integer quantum Hall regime.

References

[1] H.-S. Sim, M. Kataoka, and C. J. B. Ford, Phys. Rep. **456**, 127 (2008).

[2] C. J. B. Ford *et al.*, Phys. Rev. B **49**, 17456 (1994).

[3] M. Kataoka *et al.*, Phys. Rev. Lett. **89**, 226803 (2002).

[4] H.-S. Sim *et al.*, Phys. Rev. Lett. **91**, 266801 (2003).

[5] C. Gould *et al.*, Phys. Rev. Lett. **77**, 5272 (1996).

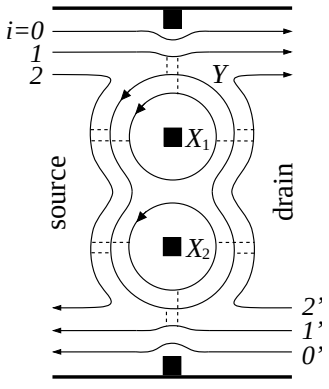

Figure 1: Schematic view of an antidot molecule in the integer quantum Hall regime with filling factor 4. The molecule has two types of bound states, molecular state (Y) and atomic states (X_1 and X_2). The solid lines represent spin-unresolved edge states, while the dashed lines indicate electron tunnelings between the edge states.

Collapse of the fractional quantum Hall state by a unidirectional periodic potential modulation

A. Endo*, N. Shibata** and Y. Iye*
*Institute for Solid State Physics, University of Tokyo, Kashiwa, Japan
** Department of Physics, Tohoku University, Sendai, Japan

Keywords: fractional quantum Hall effect, stripe phase, unidirectional periodic potential modulation, DMRG

We have studied experimentally the effect of a unidirectional periodic potential modulation on the fractional quantum Hall states (FQHS) located between the filling factors ν=1 and 2. A modulation $V(x)=V_0\cos(2\pi x/a)$ with a small amplitude and period (V_0=0.05 meV, a=115 nm) is found to exert minimal effect on FQHS, simply to slightly reduce the activation energies. Introduction of a larger amplitude modulation (V_0=0.3 meV, a=184 nm), by contrast, profoundly alters the FQHS. As shown in Fig. 1, the resistivity minimum at ν=5/3 FQHS (equivalent to ν=1/3=2 − 5/3 by particle-hole symmetry) gives way to a peak that develops with decreasing temperature, while the ν=4/3 FQHS (corresponding to ν=2/3) survives albeit with a much reduced activation energy. More generally, we find, after improving the sample mobility by illumination, that FQHS with odd numerator (ν=7/5, 11/7) are suppressed, while an even numerator state (ν=8/5) is enhanced, by the modulation.

In the vicinity of ν=5/3, an oscillatory feature appears in the Hall resistivity by the introduction of the modulation, as seen in Fig. 2. The "period" of the oscillation ΔB is found to gradually increase with increasing electron density n_e, from $\Delta B\sim$0.04 T at n_e=2.1×10^{15} m^{-2} to ∼0.1 T at n_e=2.5×10^{15} m^{-2}, and the oscillation disappears for larger n_e.

The effect of the modulation on ν=1/3 FQHS is theoretically examined by the density matrix renormalization group (DMRG) method. The calculation shows that the energy gap $\Delta_{1/3}$ decreases with increasing V_0 and disappears at $V_0\simeq\Delta_{1/3}(V_0=0)$, consistent with the experimental behavior of the ν=5/3 FQHS with differing V_0 described above. Moreover, the calculation reveals the V_0-induced transition from FQHS to a stripe phase; a unidirectional charge-density-wave state having a period ∼4l (with $l=(\hbar/eB)^{1/2}$ the magnetic length), reminiscent of the stripe phase in higher Landau levels [1], emerges accompanying the disappearance of $\Delta_{1/3}$. We discuss the emergence of a peak at ν=5/3 in ρ_{xx} and the oscillatory feature in ρ_{xy} in terms of the stripe phase.

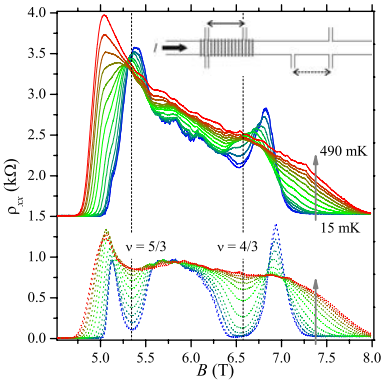

Figure 1: Longitudinal resistivity (T = 15−490 mK) between ν = 1 and 2 for the modulated (top, offset by 1.5 kΩ) and the pristine (bottom) section of a 2DEG sample schematically depicted in the inset. n_e = 2.1×10^{15} m^{-2}.

References

[1] A. A. Koulakov, M. M. Fogler and B. I. Shklovskii., Phys. Rev. Lett. **76**, 499 (1996).

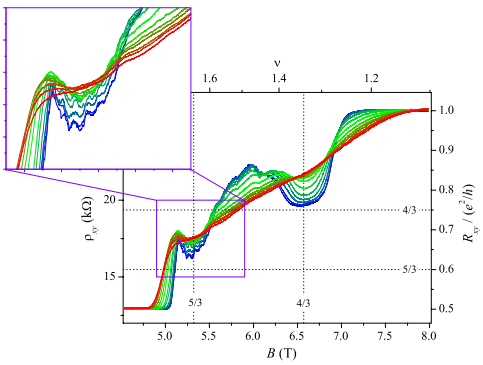

Figure 2: Hall resistivity (T = 15−490 mK) between ν = 1 and 2 for the modulated section. n_e = 2.1×10^{15} m^{-2}.

Non-equilibrium Noise Induced by the Breakdown of the Quantum Hall Effect

K. Chida*, M. Hashisaka*, Y. Yamauchi*, S. Nakamura*, T. Machida**, T. Ono*, K. Kobayashi*

* *Institute for Chemical Research, Kyoto University, Kyoto, Japan*

** *Institute of Industrial Science, University of Tokyo, Japan*

Keywords: shot noise, edge current, quantum Hall effect, breakdown

The quantum Hall effect (QHE) is a phenomenon peculiar to the two-dimensional electron gas (2DEG) systems, where the longitudinal resistance vanishes with the quantized Hall resistance. The dissipationless state of 2DEG in the QHE, however, breaks down when the device current exceeds a critical value [1, 2]. Although the breakdown has been extensively studied, its mechanism has not yet been fully understood.

Here we report the experiment to measure the non-equilibrium noise induced by the breakdown in a quantum wire (QW) fabricated on the GaAs/AlGaAs 2DEG (electron density 2.3×10^{11} cm^{-2} and mobility 1.1×10^{6} cm^2/Vs). Figure 1 shows the schematic picture of the QW whose length and width are ~ 2 μm and 370 nm, respectively. The small width favours the breakdown at a small injected current. At the electron temperature as low as 20 mK, we simultaneously measured the conductance and the noise of the QW [3], when the filling factors in the bulk and in the QW was tuned to 2 and 1 by the magnetic field and the gate voltages, respectively.

As shown in Fig. 2, the zero-bias conductance of the QW is e^2/h, while it rapidly decreases when the injected current exceeds ±2 nA and takes its minimum around ±5 nA as a clear signature of the breakdown of the QHE. The present breakdown occurs through the excitation between the spin-splitting Landau levels due to the high current injection. The voltage noise across the QW is superposed in Fig. 2. Around 0 nA, the noise is very close to zero, reflecting the dissipationless state of the QHE. When the breakdown occurs, the voltage noise starts to increase and peaks at the conductance dip around ±5 nA. At higher currents, the noise increases almost linearly with the current.

To the best of our knowledge, the present work is the first experimental attempt for the breakdown of the QHE probed by the noise measurement, which is a powerful tool to address the non-equilibrium state of the electrons.

References

1. G. Ebert *et al.*, J. Phys. C **16**, 5441 (1983).
2. M. E. Cage *et al.*, PRL **51**, 1374 (1983).
3. M. Hashisaka *et al.*, PRB **78,** 241303(R) (2008).

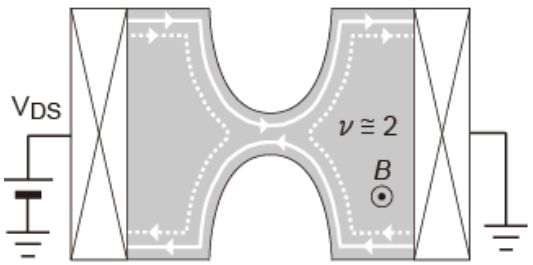

Figure 1: Schematic picture of the QW device for the breakdown measurement.

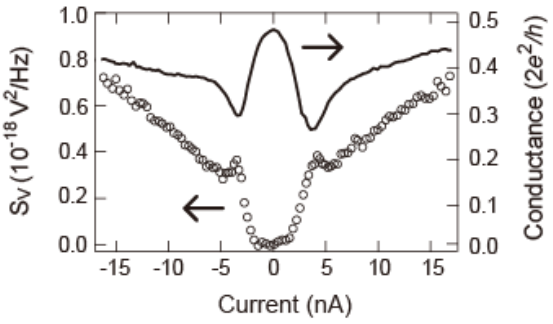

Figure 2: The differential conductance and the voltage noise of the QW as a function of the injection current to the QW.

Energy relaxation along edge channels in the integer quantum Hall regime

C. Altimiras, H. le Sueur, A. Cavanna, U. Gennser, D. Mailly and F. Pierre

CNRS, Laboratoire de Photonique et de Nanostructures (LPN), route de Nozay, 91460 Marcoussis, France

Keywords: Quantum Hall effect, Edge channels, energy exchanges

We report on measurements of energy relaxation along edge channels (EC) driven out of equilibrium in the quantum Hall regime at filling factor ν=2. We identify a strong coupling between adjacent ECs of same chirality as the main mechanism for energy exchanges. This finding provides crucial information in the context of the active ongoing debate to interpret the recent Mach-Zehnder interferometer experiments [1]. Finally, we demonstrate that it is possible to strongly reduce the energy redistribution between EC by changing the geometry. This method can be directly transposed to increase the phase coherence length.

We drive out of equilibrium an EC using a voltage biased QPC and measure, after different propagation lengths (Fig. 1a), the derivative of the energy distribution $\partial f(E)/\partial E$ using a quantum dot (QD) as an energy filter [2].

First we drive out of equilibrium the outer EC with a QPC transmission of 0,5 and a QPC bias difference of 36μV. For a propagation length of 0,8μm, we observe a double dip in the QD conductance (Fig. 1b), which is the derivative of a double step f(E) as injected by the QPC. For longer propagation lengths, the double dip converges towards a single broad dip corresponding to a temperature close to $T_{HOT}/\sqrt{2}$, with T_{HOT} the expected temperature for full energy redistribution within the outer EC. The measured limit would be expected for an energy redistribution among both ECs. To demonstrate this is the case, we inject the non-equilibrium f(E) in the inner EC and probe the outer one (Fig. 1c). The outer EC heats up as the propagation length increases and converges to the same temperature limit $T_{HOT}/\sqrt{2}$ at the same propagation length of 10μm.

By closing the inner EC on itself, we discretize its density of states (DOS). Energy relaxation measurements on the outer EC show that energy exchanges decrease drastically. Our experiment demonstrates that this constraint on the inner EC DOS suppresses efficiently the inter edge coupling.

References

1. Y. Ji *et al.*, Nature **422**, 415 (2003)
2. See poster of C. Altimiras

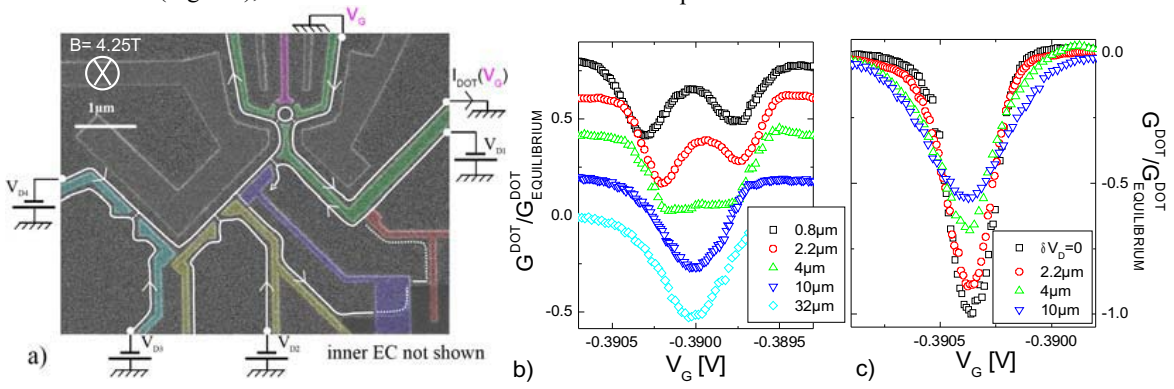

Fig.1 a Sample micrograph. **b&c** QD conductance (proportional to the outer EC $\partial f(E)/\partial E$) measurement for different propagation lengths: **b** outer EC driven out of equilibrium **c** inner EC driven out of equilibrium.

Two-terminal resistance of an electron bilayer system in the strongly correlated $\nu_{Total} = 1$ state

S. Schmult*, L. Tiemann*, W. Dietsche* and K. von Klitzing*

* *Max-Planck-Institute for Solid State Research, Stuttgart, Germany*

Keywords: Electron bilayers, Total filling factor One, Bose-Einstein condensation, Quantum Hall Effect

A two-terminal resistance close to h/e^2 is determined for an electron bilayer system at total filling factor one ($\nu_{Total} = 1$), strongly indicating that the two layers become indistinguishable beyond the phase transition into this correlated quantum Hall state. Two-terminal measurements became possible due to a modified sample preparation technique that allows for directly contacting the $\nu_{Total} = 1$ state.

The $\nu_{Total} = 1$ state of two closely-spaced two-dimensional electron layers is obtained when the lowest Landau levels of both layers are half filled. It is an startling example of correlated electron phenomena as it shows strong indications of exciton superfluidity which had been previously predicted [1]. Despite extensive experimental work carried out for more than a decade [2] it has not been possible to measure the resistance between source and drain directly to determine its two-terminal value. This is due to the fact that the $\nu_{Total} = 1$ state existed only in gated regions which are linked to the contacts via quantum Hall systems adding magnetic field dependent contributions to the overall resistance. Using separate contacts to the two layers, we find that the Hall resistance of one of the two layers is h/e^2. For two quantized Hall systems connected in parallel one would expect half of this value for both, the Hall and the two-terminal resistance. On the other hand both Hall-drag and tunneling data imply that in the $\nu_{Total} = 1$ state the current flow cannot be separated [3] leading to the prediction of a Hall resistance of h/e^2 in the parallel connected layers.

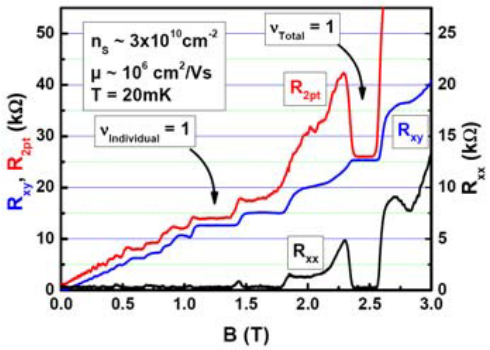

Fig.1 Comparison between the 4-terminal resistances R_{xy} and R_{xx} and the two-terminal resistance R_{2pt} at 20mK. The contacts connect both 2D layers; R_{xy} reads 12.9kΩ at individual filling factors 1, since two layers (having R_{xy} = 25.8kΩ each) are in parallel.

In this paper we present results of both the two- and four-terminal resistances (measured simultaneously) of both layers in the $\nu_{Total} = 1$ state at dilution refrigerator temperatures. These measurements are made possible by directly contacting the bilayer system at its physical edges while it exhibits the fragile $\nu_{Total} = 1$ state. Both layers are characterized by densities and mobilities of ~$3x10^{10}$ cm^{-2} and ~10^6 cm^2/Vs respectively. The d/l_B value of our system is ~1.8. The measured two-terminal resistance at $\nu_{Total} = 1$ is about 26 kΩ (see Fig. 1). This value contains contributions of contact resistances which can be determined from deviations of the two-terminal resistances at integer filling factors in the individual layers. Contact resistances of ~1 kΩ lead to a two-terminal resistance of h/e^2 for the $\nu_{Total} = 1$ state, which supports the picture of indistinguishable layers.

References

[1] H.A. Fertig, Phys. Rev. B **40**, 1087 (1989)

[2] J.P. Eisenstein and A.H. MacDonald, Nature **432**, 691(2004)

[3] L.Tiemann et al., New J. Phys. **10**, 045018 (2008)

Specific features of $In_xGa_{1-x}As/GaAs$ double quantum well as manifested in the quantum Hall effect under tilted fields

M.V. Yakunin*, Anne de Visser** and Gianni Galistu**

** Institute of Metal Physics, RAS, Ural Branch, Ekaterinburg, Russia*

*** Van der Waals – Zeeman Institute, University of Amsterdam, Amsterdam, The Netherlands*

Keywords: double quantum well, quantum Hall effect, tilted fields, InGaAs/GaAs heterosystem

A variety of intriguing phenomena revealed in the GaAs/AlGaAs double quantum wells (DQW) stimulates expanding the researches onto DQW created in other heterosystems, particularly those with greater bulk *g*-factors that promises new aspects of many-body phenomena due to realization of a spin degree of freedom, in addition to the pseudospin one.

We study the quantum Hall effect (QHE) in the symmetric $In_xGa_{1-x}As/GaAs$ DQW under magnetic fields tilted a set of angles θ from the sample normal. Among the strongest peculiarities observed are: sharp transformations in the structure of some QH features within narrow ranges of angle and field; nonmonotonous development of the feature for magnetic level filling factor $\nu = 3$ (fig.1, inset); considerable shifts of some features along the axis of perpendicular field component $B_\perp$ with tilt. To explain these the quasiclassical approach in the calculations of DQW magnetic levels under tilted field [1,2] is insufficient so we used a quantum calculation [2]. In the magnetic level pattern calculated (fig.1), the pseudogaps within upper levels oscillate with field and the nodal points move to lower $B_\perp$ with increased θ. Sharp transformations of QH features observed are quantitatively explained in terms of the Fermi level passing through the nodal points. The lowest pseudogap decreases monotonously with parallel field component (i.e. with $B_\perp$ at a fixed θ or with θ at $B_\perp$ fixed), and while at lower θ the $\nu = 3$ feature is connected with the spin gap in the lowest asymmetric Landau level, so it increases with θ since the total field increases, the lowest asymmetric and symmetric Landau sublevels start to interfere at some critical θ and the nature of $\nu = 3$ gap changes from the spin to a pseudospin one. The latter decreases with θ that explains the observed nonmonotony. But to reconcile the behavior of $\nu = 3$ feature with the slowly damping $\nu = 2$ one it is necessary to suppose that the spin gap is locally enhanced by the exchange interaction.

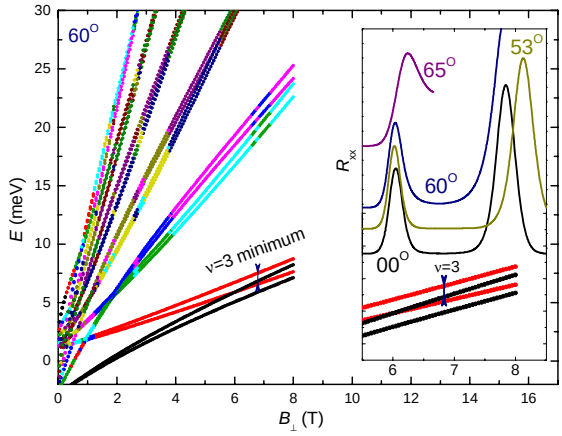

Fig.1. Magnetic level pattern at 60^O tilt and the nonmonotonous evolution of $\nu = 3$ minimum (inset).

The slowly approaching and interfering levels in a DQW create new conditions for the overlap of their tails of localized states and delocalized levels causing the shifts of QH features from the half-integer ν values. We show that the observed shifts and their development with θ could indeed be induced by this overlap for reasonable sample parameters.

References

1. N.E. Harff *et al.*, Phys. Rev. B **55**, 13405 (1997); M.V. Yakunin *et al.*, Physica E **40**, 1451 (2008); JETP **105**, 214 (2007).
2. J. Hu and A.C. MacDonald, Phys. Rev. B **46**, 12554 (1992)

Spectroscopic study of nuclear magnetic resonance mediated by oscillating electron spin domain walls

S. Watanabe[1], G. Igarashi[1], K. Hahimoto[1,3], N. Kumada[2] and Y. Hirayama[1,3,]

[1] *Graduate School of Science, Department of Physics, Tohoku University, Sendai, Japan*

[2] *NTT Basic Research Laboratories, NTT Corporation, Kanagawa, Japan*

[3] *ERATO Nuclear Spin Electronics Project, Sendai, Japan*

Keywords: Nuclear spin, Domain wall, Quantum Hall state, 2DEG

Recently, resistively detected (RD) nuclear magnetic resonance (NMR) has been exploited to study electronic spin properties in two dimensional electron systems with high sensitivity [1]. In this study, we report characteristics of a recently-developed novel RD-NMR, called the nuclear electric resonance (NER) [2]. We use a radio frequency (RF) electric field to oscillate electron spin domain walls, which have an in-plane component of the hyperfine field (B_x^{HF}) perpendicular to the external magnetic field, resulting in relaxation of nuclear spins. The sample, which consists of a 20-nm GaAs quantum well, was processed into 50-μm wide Hall bar. The density can be controlled using an n^+-GaAs substrate acting as a back gate. The longitudinal resistance (R_{xx}) was measured by a standard low-frequency lock-in technique. After the dynamic nuclear spin polarization by current flow, an RF electric field is applied to the gate through a bias-tee with time duration of 5 sec. Measurements were performed at the magnetic field of 7.7 T and temperature at around 300 mK.

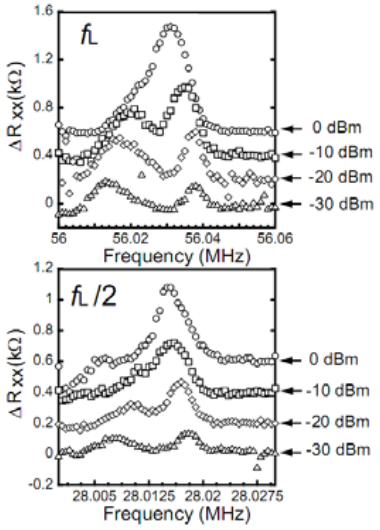

Fig.1 Bias power dependence of ^{75}As-NER spectrum around the Larmor frequency of ^{75}As nuclei f_L and $f_L/2$.

Fig. 1 shows the NER spectrum recorded in two different ranges of frequency, around the Larmor frequency of ^{75}As nuclei f_L = 56.03 MHz and $f_L/2$. The NER signal appears not only at f_L but also at $f_L/2$. The resonance strength at $f_L/2$ is comparable to that at f_L. These results indicate that the time evolution of B_x^{HF} at the nuclear sites contains large amount of harmonics, reflecting the oscillations of electron spin domain walls. It should be noted that when RF magnetic field is applied through a surrounding coil like a standard RD-NMR, the resonance at $f_L/2$ does not occur.

We also demonstrate that the NER spectral shape depends on a bias power of the RF electric field. Two peaks observed at a week power (P = -30 dBm) change into a single peak at a strong power (P = 0 dBm). The similar behaviour appears in the data set around $f_L/2$. These results give us a hint to analyze a spatial distribution of nuclear spin polarization and electron spin domain motion under the inhomogeneous nuclear spin polarization.

References

1. K. Hashimoto, *et al*. Phys. Rev. Lett. **88**, 17660 (2002).

2. N. Kumada, *et al*. Phys. Rev. Lett. **101**, 137602 (2008).

Spin-Hall conductance fluctuations in quantum spin-Hall network model

K. Kobayashi*, T. Ohtsuki* and K. Slevin**
*Department of Physics, Sophia University, Tokyo, Japan
** Department of Physics, Osaka University, Osaka, Japan

Keywords: quantum spin-Hall effect, universal spin-conductance fluctuation

The universal conductance fluctuation is one of the most important transport properties in mesoscopic systems. The value of the universal conductance fluctuation is determined by the universality class and the shape. Recently, the universal fluctuation was also found in spin-Hall conductances [1].

In this paper, we discuss the spin-Hall conductances and their fluctuations in quantum spin-Hall systems. The quantum spin-Hall effect (QSHE) [2, 3, 4] is the novel quantum transport that has been attracting a lot of attentions. The QSHE occurs in some systems that have strong spin-orbit interactions and the time-reversal symmetry.

The simplest model assumes no spin-flipping where we have spin conservation (Kane-Mele model without Rashba term [2] or Obuse *et al.*'s model [5] without spin-flipping). In this case, we observe the quantization of spin-Hall conductance $G_{\rm sH} = 1$ in units of $e/2\pi$, where we define

$$G_{\rm sH} = (I_2^{\uparrow} - I_2^{\downarrow})/(\mu_1 - \mu_3), \qquad (1)$$

μ_i being the chemical potential in the probe i and $I_2^{\uparrow,\downarrow}$ the spin-currents in the probe 2 (see Fig. 1).

Here, we numerically calculate the spin-Hall conductances in the quantum spin-Hall network model [5] with four-terminal structures (Fig. 1). At the critical point of the Anderson transition (i.e. transition from $G_{\rm sH} = 0$ to 1), we found the universal spin-Hall conductance fluctuation (see Fig. 2). We compare the spin-Hall conductance fluctuations in quantum spin-Hall network models with the universal fluctuation in the conventional spin-Hall systems. We also study the effect of spin-flipping (say, Rashba interaction) on the spin-Hall conductance. The structure dependence of the spin-Hall conductance will also be discussed.

References

[1] W. Ren, Z. Qiao, J. Wang, Q. Sun, and H. Guo, Phys. Rev. Lett. **97**, 066603 (2006).

[2] C. L. Kane and E. J. Mele, Phys. Rev. Lett. **95**, 226801 (2005); **95**, 146802 (2005).

[3] L. Sheng, D. N. Sheng, C. S. Ting, and F. D. M. Haldane, Phys. Rev. Lett. **95**, 136602 (2005).

[4] B. A. Bernevig and S. C. Zhang, Phys. Rev. Lett. **96**, 106802 (2006).

[5] H. Obuse, A. Furusaki, S. Ryu, and C. Mudry, Phys. Rev. B **76**, 075301 (2007).

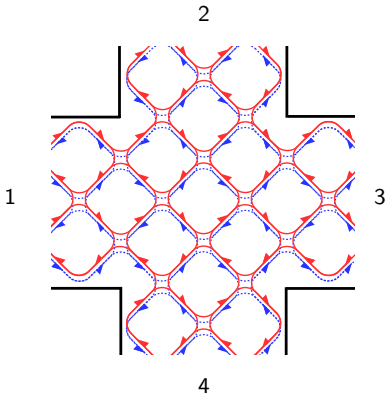

Figure 1: Schematic of quantum spin-Hall network model with four-terminal structure. The solid (broken) arrows indicate the flow of current with up- (down-) spin. We apply current from lead 1 to 3, and the spin-current is induced from lead 4 to 2.

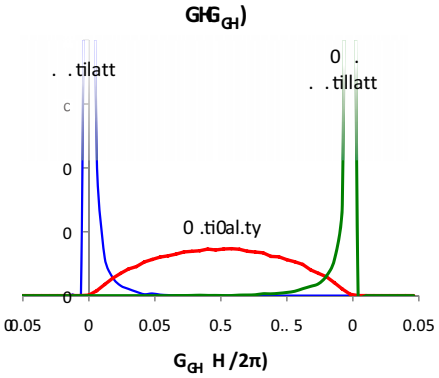

Figure 2: Probability distribution functions $P(G_{\rm sH})$. At criticality, $G_{\rm sH}$ broadly distributes between zero and unity with mean $\langle G_{\rm sH}\rangle = 0.50$ and ${\rm sdv}(G_{\rm sH}) = 0.23$ independent of the system size.

Spin relaxation mechanism in a quantum Hall ferromagnet

D. Fukuoka[*], T. Nagayama[*], K. Oto[*], K. Muro[*],
Y. Hirayama[**,****], N. Kumada[***], and H. Yamaguchi[***]

[*] *Graduate School of Science, Chiba University, Chiba, Japan*
[**] *Graduate School of Science, Tohoku University, Sendai, Japan*
[***] *NTT Basic Research Laboratories, NTT Corporation, Atsugi, Japan*
[****] *ERATO Nuclear Spin Electronics Project, Sendai, Japan*

Keywords: spin dynamics, quantum Hall ferromagnet, Skyrmion, time-resolved Kerr rotation

We have applied the time-resolved Kerr rotation (TRKR) measurement to high mobility 2D electrons to investigate the spin dynamics in quantum Hall systems. The TRKR measurement has revealed the intrinsic spin-flip energy and the transverse spin relaxation time (T_2^*). In the quantum Hall regime, T_2^* strongly depends on the Landau filling factor and presents peaks at odd filling factors (ν = 9, 7, 5). This enhancement of the spin relaxation time can be explained by the long-lived spin wave in the quantum Hall ferromagnet. However, at ν = 1 and 3, T_2^* shows a sharp dip instead of the peak [1].

In this work, we investigate the origin of the suppression of the spin coherence at ν = 1 and 3 by means of a two-color pump-probe TRKR technique with narrow band spectral filter. In this technique, the probe beam is fixed to the transition from the heavy hole band to the Landau level N = 0 while the pump beam is tuned to the individual absorption lines.

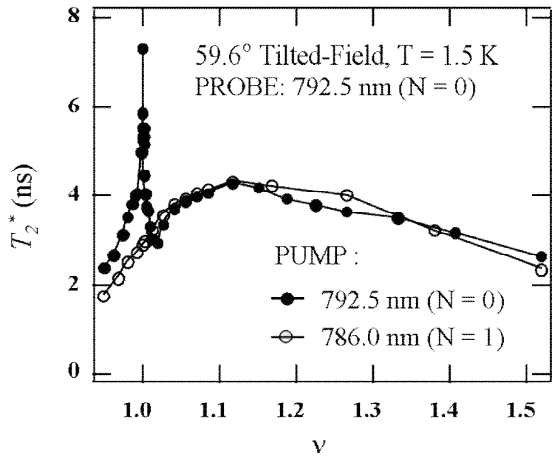

Fig.1: Filling factor dependence of T_2^* obtained by the TRKR measurement with two-color pump-probe technique in 59.6° tilted-field at 1.5 K. Filled and opened circles are obtained by the pumping to the Landau level at N = 0 and N = 1, respectively.

Figure 1 shows the filling factor dependence of T_2^* at 1.5 K. Filled and opened circles are obtained by choosing the pump beam for the transition from the heavy hole band to the Landau level at N = 0 and N = 1, respectively. When electrons are pumped to the N = 1 level, T_2^* does not present peak at ν = 1, similar to the data obtained by a broad band beam [1]. On the other hand, for the pumping to the N = 0 level, T_2^* presents a very sharp peak at ν = 1. The difference in the behaviour of T_2^* is ascribed to the optical generation of Skyrmion and anti-Skyrmion pairs under the pumping to the higher Landau level; when electron-hole pairs are generated, electrons relax to the N = 0 level through the phonon scattering and then Skyrmion and anti-Skyrmion pairs are formed. Spatial spin inhomogeneity induced by Skyrmions and anti-Skyrmions dephases the spin dynamics and suppresses T_2^*. On the other hand, under the pumping to the N = 0 level, spin excitons with long coherence time are observed.

The rapid decrease in T_2^* on both sides of the ν = 1 peak for the pumping to the N = 0 level indicates that very small number of Skyrmions or anti-Skyrmions is enough to suppress the spin coherence. Complete understanding of this sharp feature requires further experimental and theoretical studies.

References

1. D. Fukuoka, T. Yamazaki, N. Tanaka, K. Oto, K. Muro, Y. Hirayama, N. Kumada, and H. Yamaguchi Phys. Rev. B **78**, 041304(R) (2008).

Spin resonance of two dimensional hole system

S. Teraoka[*], S. Amaha[*], T. Hatano[*], T. Kubo[*], Y. Tokura[*,**],
Y. Ohno[***], H. Ohno[***], and S. Tarucha[*,****]

[*] *Quantum Spin Information Project, ICORP-JST Atsugi, Kanagawa, 243-0198, Japan*

[**] *NTT Basic Research Laboratories, NTT Corporation, Atsugi, Kanagawa 243-0198, Japan*

[***] *Laboratory for Nanoelectronics and Spintronics, Research Institute of Electrical Communication Tohoku University, Katahira, Aoba-ku, Sendai, Miyagi 980-8577, Japan*

[****] *Department of Applied Physics, Graduate School of Engineering, The University of Tokyo, Bunkyo-ku, Tokyo, 113-8656, Japan*

Keywords: Two dimensional hole system, Spin decoherence, Hyperfine interaction, Spin-orbit interaction

Regarding quantum information processing, intensive efforts have been devoted in recent years to implement electron spin as a quantum bit. In case of confined electrons in GaAs based quantum dots, spin dephasing caused by the hyperfine interaction of the electron spin with the randomly fluctuating nuclear spins in host crystal is an emerging problem [1]. One alternative to the electron spin is the hole spin for implementing spin qubits with least influence of nuclear spin. It has often been stated holes have negligible interaction with nuclear spins, because the valence band has p-like atomic states, which have no direct cross-section with nuclei. However, neither spin resonance, which is one of the bases of the spin qubit operations, nor the influence of nuclear hyperfine field has been studied yet for holes in GaAs.

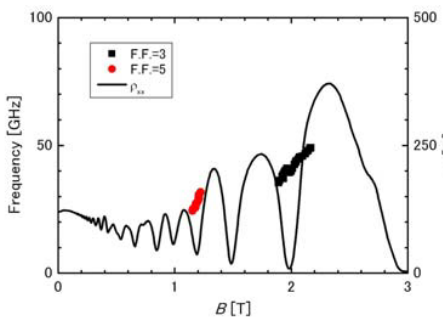

Fig.1 Resonance frequency vs magnetic field (■ and ●) and Shbunikov de-Haas oscillation (solid line) observed for the two-dimensional hole gas. The observed $\rho_{xx}(B)$ trace shows beat in the low magnetic field region, indicating zero field spin splitting due to spin-orbit interaction.

In this work we use a two-dimensional hole gas at a p-AlGaAs/GaAs heterostructure grown on GaAs(311)A substrate to study hole spin resonance and the effect of hyperfine coupling observed as Overhauser shift. The resonance was observed at around the filling factor 3 and 5 (Fig.1). The resonance frequency significantly deviates from the linear relation to external magnetic field, reflecting the strong spin-orbit coupling of this system. We try to interpret this non-linear relation due to contributions from both Zeeman splitting and zero field spin splitting, which arises from inversion asymmetry in this system. We evaluate the lower bound for spin decoherence time T_2^* = 0.18 ns from the line width $\Delta\omega$ equivalent to the observed resonance peak width ΔB. The main contribution to this linewidth would be the shorter hole spin lifetime T_1^h due to the strong spin-orbit interaction. Note that T_1^h is expected to become longer for quantum dots [2]. In contrast to spin resonance observed for a two-dimensional electron gas [3], we did not observe any Overhauser shift of the resonance peak or any indication of dynamical nuclear spin polarization.

References

1. W.A. Coish and D. Loss, cond-mat 0606550.
2. D. Heiss *et.al*, Phys. Rev. B **76**, 241306(R) (2007)
3. S.Teraoka *et.al* PhysicaE **21**, 928 (2004).

Spin splittings in the *n*-HgTe/$Cd_xHg_{1-x}Te$ quantum well with inverted band structure

M.V. Yakunin*, S.M. Podgornykh*, N.N. Mikhailov** and S.A. Dvoretsky**

** Institute of Metal Physics, RAS, Ural Branch, Ekaterinburg, Russia*

*** Institute of Semiconductor Physics, RAS, Siberian Branch, Novosibirsk, Russia*

Keywords: HgTe quantum well, quantum Hall effect, tilted fields, effective *g*-factor

A property of the $Cd_xHg_{1-x}Te$ solid solution to transform its band diagram from the gapless to a gapped one with growing x causes a unique energy structure of the quantum well created in the HgTe/$Cd_xHg_{1-x}Te$ heterosystem: it is inverted when the HgTe well width d_w is greater than the critical value of ~6.3nm so that the conduction band is formed of the *p*-like wave function. Its properties are expected and found to differ from the ones of a traditional conduction band formed by functions of *s*-like character.

We study the quantum Hall effect (QHE) in the HgTe/$Cd_xHg_{1-x}Te$ (113) oriented quantum well, x = 0.6÷0.73, d_w= 20.3nm, doped on both sides with ~10nm spacers, electron density $1.5\times10^{15}m^{-2}$ and mobility $20m^2/V\cdot s$. Along with the study of magnetoresistivities $\rho_{xx,xy}$ under perpendicular field, $B = B_\perp$, our specific technique of sample rotation [1] is used to get the most detailed picture on the influence of field component $B_\parallel$ parallel to the layers, either in the form of $\rho_{xx,xy}(B_\perp,B_\parallel)$ surface functions of two variables or of their maps projected onto the $(B_\perp,B_\parallel)$ plane (fig.1). This allows to get the full picture of magnetic level coincidences within the whole segment of reachable field component values and to trace the evolution with $B_\parallel$ of the spin and cyclotron gaps in the magnetic level spectrum.

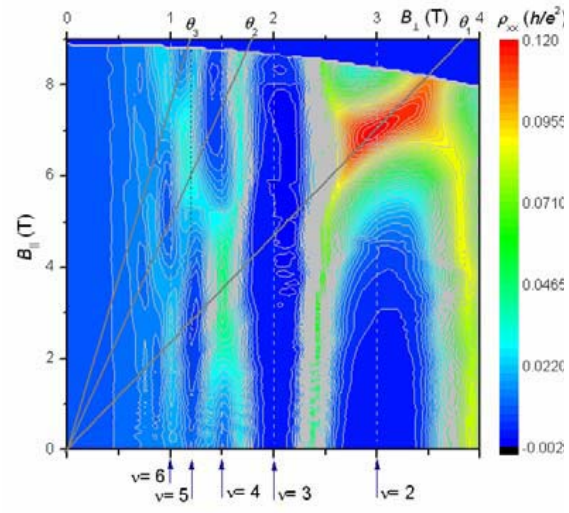

Fig.1. Diagonal magnetoresistivity $\rho_{xx}(B_\perp,B_\parallel)$ and the coincidence angles $\theta_{1,2,3}$.

As obtained from the $\rho_{xx,xy}(B_\perp,B_\parallel)$ maps measured, the positions of points for the locally closed gaps are well described within the traditional coincidence effect for the spin/cyclotron gaps relation r = 1 and 2. But it yields the value of $gm^*/m_0 = 2\cos\theta_1 = 0.8$ (*g*-factor; m^* and m_0 – the effective and free electron masses) while it should be within $1 < gm^*/m_0 < 2$ to describe the observed QHE structure under the perpendicular field configuration with odd-numbered features prevailing over the even ones. The higher value, $gm^*/m_0 = 1.38$, is obtained from a comparison of the fields corresponding to onsets of oscillations and of their splittings. On the other hand, much lower value, $gm^*/m_0 = 0.19$, is deduced from the observed evolution with $B_\parallel$ of the gaps between levels.

To resolve the discrepancies found the following things should be taken into account: (i) zero field spin splittings that might be considerable in the band of *p*-states [2]; (ii) quasi-two-dimensional character of spin splittings in this type of a band [3]; (iii) the level widths influence the obtained absolute values of the gaps.

References

1. M.V. Yakunin, S.M. Podgornykh, V.N. Neverov, JETP **105**, 214 (2007).
2. X.C. Zhang *et al.*, Phys. Rev. B **63**, 245305 (2001).
3. R.W. Martin *et al.*, Phys. Rev. B **42**, 9237 (1990).

Spin-related origin of the transport feature at filling factor 7/11

Gerardo Gamez and Koji Muraki

NTT Basic Research Laboratories, NTT Corporation, 3-1 Morinosato-Wakamiya, Atsugi 243-0198, Japan

Keywords: Magnetotransport, fractional quantum Hall effect, composite fermion, spin

In the composite-fermion picture, the fractional quantum Hall effect (FQHE) of strongly interacting electrons can be described as the integer quantum Hall effect (IQHE) of non-interacting quasi-particles, termed composite fermions (CFs), which can be viewed as electrons carrying an even number of flux quanta. Albeit experiments carried out on high-mobility two-dimensional electron systems in the 1990's had already hinted the existence of an additional magnetoresistance minimum between $\nu = 2/3$ and 3/5, corresponding to IQHE of CFs at filling 2 and 3, respectively, it was not until a recent experiment was performed on an ultra-high-mobility sample that this feature at $\nu = 7/11$ was identified as a FQHE of CFs, with its origin ascribed to interactions between CFs [1]. It was also reported that the R_{xx} minimum at $\nu = 7/11$ disappears with the application of an in-plane magnetic field, suggesting an incomplete spin polarization of the 7/11 state [1]. However, conclusive experiment clarifying the origin of the 7/11 structure is still lacking.

Here, we report a magnetotransport study performed on modulation-doped 30-nm-wide GaAs quantum wells as a function of density, temperature, and tilt angle, in the filling factor range around $\nu = 7/11$. We observe a minimum in R_{xx}, accompanied by a plateau-like structure in R_{xy}, around $\nu = 7/11$, at a magnetic field of 11.4 T, which is significantly higher than the previously reported value of 6.4 T [1]. At such a high fields, the spin degree of freedom is believed to be frozen. Indeed, density-dependent transport and angle-dependent activation gap measurements confirm that both of the FQHE states flanking $\nu = 7/11$, namely the $\nu = 2/3$ and 3/5 states, are fully spin polarized, with their spin transitions located at magnetic fields far below (4.3 and 5.1T, respectively). Nevertheless, upon tilting the sample we observe that the dip at 7/11 weakens and then disappears at a certain critical angle (Fig. 2). Using a model based on the CF picture, we show that even at high magnetic fields where both 2/3 and 3/5 FQHE states are fully spin polarized, the spin degree of freedom may not be completely frozen in the transition region between them. Systematic temperature- and density-dependent experiments reveal that the exact filling-factor position of the 7/11 feature depends on the density and tilt angle, which can also be explained by the model. We also show that our experiment and model can account for the different behavior of $\nu = 7/11$ and its electron-hole counterpart, $\nu = 4/11$ [1].

References

1. Pan *et al.,* Phys. Rev. Lett. **90**, 016801 (2003)

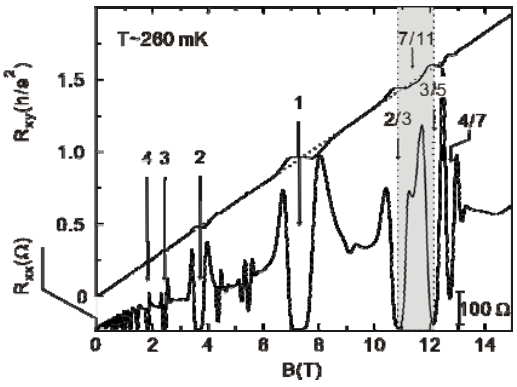

Fig.1 R_{xx} and R_{xy} at $T = 260$ mK.

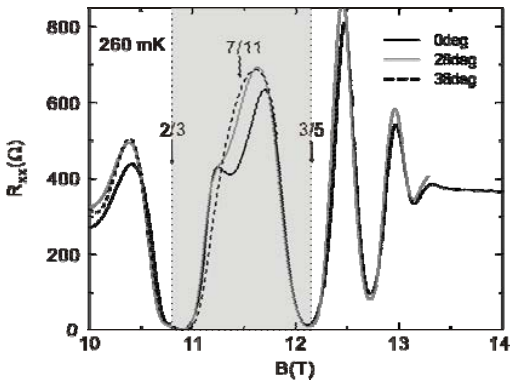

Fig.2 R_{xx} around $\nu = 7/11$ at three tilt angles.

Manifestations of Topological Phases on Surface States in Topologigal Insulators

K-S. Park*, K.-S. Yi* and K. Moon**
*Department of Physics, Pusan National University, Busan 609-735, Korea; email: kspark@pusan.ac.kr
** Department of Physics, and IPAP, Yonsei University, Seoul 120-749, Korea

Keywords: Dirac Fermion, Charge Fractionalization, Topological Phase, Surface State, Topological Insulator.

We study exotic phases of surface states emerging from topological insulators [1, 2] in (3+1) spacetime dimensions. A spin-statistics theorem of quantum field theory says that the total wave function of any many-body object can be identified as bosons and fermions under a statistical transmutation between two objects in (3 +1) dimensions. But in (2 + 1) dimensions, when interchanging a pair of two objects, they have unusal quantum statistics of anyons revealing a complex phase angle different from 0 or π. There is a dynamical realization of anyons in terms of flux and charge under a topological interaction. When moving around a flux Φ, an object or a family of objects with charge nq can have an extra phase factor $e^{(i \oint d\vec{r}.\vec{A})} = e^{i\Phi nq}$. Consequently composites or a family of objects with flux and charge would generally exhibit nontrivial topological phases of anyonic objects on a 2-dimensional membrane like suspended graphene embedded on topological insulators in 3-spatial dimensions.

In this work, as a generalization of graphene modeled by relativistic massless Dirac fermions and exploited by index theorem in (2+1) space-time dimensions [3], we investigate topological phases of surface states on topological insulators in (3 + 1) space-time dimensions. Assume that topological surface states are composed of n quasiparticles in a suspended graphene, which is placed on the surface of a magnetic layer deposited over a topological insulator. Then, the exotic phase of the topological surface state can elegantly be described by the Atiyah-Patodi-Singer index theorem. Employing the index theorem, we can obtain

$$\prod_{i=1}^{N}\left(\mathrm{Pfaff}(\mathrm{D}(C_i))e^{i\{(\frac{q_i}{2\pi}\oint_{C_i}A_{q_i})+(\frac{\theta_i}{2\pi}\frac{\alpha}{2\pi}\oint_{C_i}A_{g_i})\}}\right)$$
$$= e^{i\sum_i^N[q_i\mathrm{Ind}(\mathrm{D_i})+\{\frac{\theta_i}{2\pi}\frac{\alpha}{4\pi}\int d^3x_i dt\partial^\mu(\epsilon_{\mu\nu\rho\lambda}A_i^\nu\partial^\rho A_i^\lambda)\}]}$$

where $\mathrm{Pfaff}(\mathrm{D}(C_i))$ is a pfaffian of a Dirac operator $\mathrm{D}(C_i)$ on C_i which is a curve i on a 3-dimensional manifold. Here A_{q_i} indicates a vector potential of differential form for an electric charge q_i while A_{g_i}, that of magnetic flux g_i. α is a fine-structure constant of $\frac{e^2}{\hbar c}$. Provided that $\theta_i = (2l_i + 1)\pi$, with l_i an integer, θ_i gives rise to a quantized Hall conductance of $\sigma_{x_iy_i} = (l_i + \frac{1}{2})\frac{e^2}{h}$ [2]. One has a constrain of $\sum_i^N n_i = n$ for arbitrary N loops. And $\mathrm{Ind}(\mathrm{D_i})$ (i. e., the number of zero modes of the Dirac operator $\mathrm{D_i}$) indicates the index theorem associated with the total flux emerging out of the surface. The index theorem enables one to have charge fractionalization which is usually related to the fractional quantum Hall effect. The charge fractionalization results from the topological property of realizing anyons which exhibit fractional statistics. An electric charge near the topological surface state may give rise to a magnetic monopole charge due to the electro-magnetic dual effect in the topological insulator. It is proposed how to manifest topological phases for a gas of quantum dyons with fractional statistics, made up of the bound states of the electric charge and the magnetic monopole one.

References

[1] Observation of Unconventional Quantum Spin Textures in Topological Insulators, D. Hsieh, et al., Science 323, 919 (2009).

[2] Inducing a Magnetic Monopole with Topological Surface States; X.-L. Qi, et al., Science 323, 1184 (2009).

[3] Unconventional Quantum Hall effects, Index Therem and Supersymmetry in Graphene, K.-S. Park and K. S. Yi, accepted for publication in Int. J. Mod. Phys. B, April (2009); Supersymmetric Quantum Mechanics in Graphene; K.-S. Park and K. S. Yi, J. Korean Phys. Soc. 50, 1678 (2007).

Dynamical modulation of exchange interaction in two-electron quantum dot molecules

L. Meza-Montes*, A. H. Rodríguez** and S. E. Ulloa***
*Instituto de Física, Universidad Autónoma de Puebla, México
**Universidad Autónoma de la Ciudad de México, México
***Dept. of Phys. and Astron., Ohio University, Athens, OH, USA

Keywords: Quantum dot, spin-orbit, exchange, harmonic field

Following the suggestion of using electronic spins in coupled quantum dots as qubits [1] we explore the possibility of modulating them in quantum dots molecules by means of applied fields and the spin-orbit effect. The artificial hydrogen molecule of InSb is studied under magnetic and harmonic electric fields. A six-level Floquet formalism [2] is used to study the time evolution of the system.

While the perpendicular magnetic field allows to modify the spin-orbit interaction and to control whether the initial ground state is a singlet or a triplet state [3], the in-plane electric field deals with the dot occupancies, and the spin-orbit effect plays an important role through spin flips. In contrast with the single-electron case where dynamical localization and spin flips are easily identified [4], the dynamical symmetries of the two-electron system cause the quasi-energy spectra to have a pattern of crossings and anticrossings which reflect complex admixtures of the singlet-triplet subspaces.

We study the occupancy and time evolution of exchange interaction through the probability densities. They show an oscillatory behavior and spin flips can be detected for proper values of Ω and F, the frequency and intensity of the electric field, respectively, at a given magnetic field B. In Fig. 1 we plot the probability $P^{RL}(s_1,s_2;t)$ of finding at time t one electron in right dot while the other is in left dot, with same ($\uparrow\uparrow$) or different spins ($\uparrow\downarrow$). For the chosen magnetic field B = 1.4 T, the initial state is predominantly T_+ triplet.

We notice that for a short time, which is a small fraction of the field period, $P^{RL}(\uparrow\downarrow) > P^{RL}(\uparrow\uparrow)$, indicating a spin-flip which is caused by the spin-orbit coupling. We present a full analysis of the dynamics for different parameter values, analyzing the interplay between spin-orbit coupling, Zeeman effect, Coulomb exchange interaction, and interdot coupling.

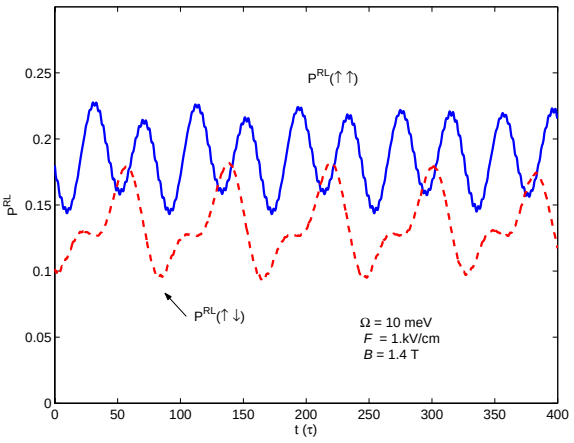

Figure 1: Probability of finding the electrons in the dots with same or different spins as a function of time. Time unit is the electric field period τ. Parameters of the applied fields are shown.

Partially supported by CONACyT-Mexico.

References

[1] D. Loss, D. P. DiVincenzo, Phys. Rev. A **57** 120 (1998).

[2] Arezky H. Rodríguez, L. Meza Montes, C. Trallero Giner, and S. E. Ulloa, Phys. Rev. B **77**, 235405 (2008).

[3] L. Meza-Montes, Carlos F. Destefani, and Sergio E. Ulloa, Phys. Rev. B **78**, 205307 (2008).

[4] L. Meza-Montes, Arezky H. Rodrguez, and S. E. Ulloa, Physica E **40**, 1226 (2008).

Rashba-Dresselhaus spin orbit effects in quantum wells

Saadi Lamari*

Department of Physics, Faculty of Sciences, University Ferhat Abbas Setif 19000 DZ, Algeria

Keywords: Rashba effect, Dresselhaus term, Spin Orbit, Quantum Wells

Following the seminal paper of Datta and Das [1] many years ago where a new kind of device called the spin polarized field effect transistor was introduced for the first time, and in which current flow between source and drain is spin dependent, the study of spin-orbit effects in semiconductor research both by experimentalists and theoreticians has grown tremendously in the last few years thus giving rise to the emerging field of spintronics where the new nano-devices exploit the spin degree of freedom on a large scale. In their original proposal, using a simple model capturing the essential physics Datta and Das show that provided a phenomenological constant α called the Rashba parameter can be tuned by a gate voltage Vg, spin related current modulation follows and a thorough understanding of this parameter was therefore more than necessary.

In the present work and as a follow up to our recent contributions [2], for heterostructures made of semiconductors with wide to medium size gaps we numerically investigate with the help of our self consistent electronic structure calculation codes the relative importance of the main spin orbit mechanisms known as Rashba and Dresselhaus. We also monitor their variations with the applied gate voltage and pay particular attention to their interesting interference effects. In an effort to gain more control on spin orbit effects in heterostructures, we furthermore carry out a detailed study of the intricate effects of the interfaces and the barriers and how these together combine to yield the well width dependence of the spin orbit splitting. We also suggest ways to enhance or supress the latter and also study additional effects of an external magnetic field.

References

1. S. Datta and B. Das, Appl. Phys. Lett. 56, p.665 (1990).

2. S. Lamari, Phys. Rev. B 75, 155302 (2007).

In-plane anisotropy of spin relaxation under competition between spin orbit interaction and Zeeman effect in InGaAs/InAlAs narrow wire structures

M. Niwa*, M. Kohda*, **, Y. Kunihashi*, and J. Nitta*

* *Department of Materials Science, Tohoku University, Sendai, Japan*

** *PRESTO, Japan Science and Technology Agency, Kawaguchi, Japan*

Keywords: Spin orbit interaction, two dimensional electron gas, narrow wire structure

In narrow gap III-V semiconductors, dominant contribution for spin relaxation originates from the spin orbit interaction (SOI). Momentum-dependent effective magnetic field due to SOI randomizes the spin precession axis. SOI yields the spin relaxation, while the Zeeman effect tends to align the spin precession axis along the applied magnetic field direction. Since electron momentum is confined one direction in semiconductor narrow wires, uniaxial alignment of the effective magnetic field is competitive with the external magnetic field depending on their relative angles. Thus, we investigated in-plane anisotropy of spin relaxation by applying magnetic field with respect to the direction of the effective magnetic field in InGaAs based narrow wire structures.

$In_{0.7}Ga_{0.3}As$ / $In_{0.53}Ga_{0.47}As$ / $In_{0.52}Al_{0.48}As$ two dimensional electron gas was grown by metal organic chemical vapor deposition. The epitaxial wafer was processed into 120 parallel wire structure by electron beam lithography and reactive ion etching. The wire widths are set to w = 450, 670, and 1000 nm, while the wire length is fixed to 600 μm. Longitudinal direction of the wire is along [100] direction. We measured magneto-conductance at T = 1.7 K to analyze the weak antilocalization (WAL). WAL is observed around zero magnetic fields in all the wire structures. We evaluated the spin relaxation length l_{SO} by fitting the data with the quantum correction of conductivity for a wire structure developed by Kettemann [1] and found that the one dimensional confinement, *i.e.* $l_{SO} > w$, is achieved in 450 nm-width wire. Thus, we applied in-plane magnetic field $B_{//}$ for different angles with respect to the longitudinal direction of the wire. Figure 1 (a) shows the magneto-conductance with θ = 0 º, 39 º, 90 º, and 129º under $B_{//}$ = 0.3 T. WAL is only observed in θ = 0º, while weak localization is dominant for the magneto-conductance in the other $B_{//}$ directions. This indicates that the anisotropic spin relaxation is induced by the relative angle between magnetic fields induced by SOI and by Zeeman effect. We then fit the data with Ketteman model and Fig. 1 (b) shows the angle dependence of extracted l_{SO} for $B_{//}$ = 0 and 0.3 T. In $B_{//}$ = 0 T, the identical spin relaxation lengths are obtained. However, in $B_{//}$ = 0.3 T, minimum and maximum l_{SO} are observed in θ = 0º and 90º, respectively. Since $B_{//}$ with θ = 90º is almost parallel to the effective magnetic field direction, uniaxial alignment of the total magnetic field is conserved. It suppresses the randomization of the spin precession axis and yields longer spin relaxation length. Thus, we can detect the effective magnetic field direction through the angle dependent WAL analysis.

Reference

[1] S. Kettemann *et al.*, Phys. Rev. Lett. **98**, 176808 (2007).

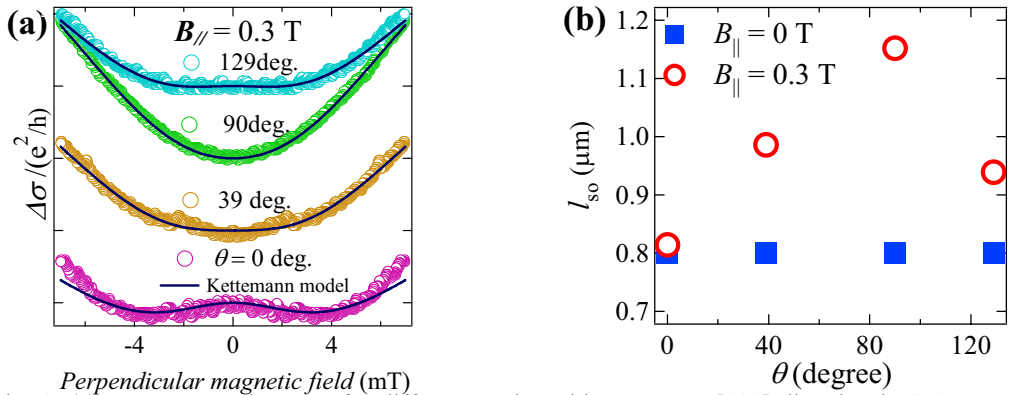

Fig. 1. (a) Magneto-conductance for different angles with respect to [100] direction in 450 nm-width wire measured at T = 1.7 K and (b) Angle-dependent spin relaxation lengths in $B_{//}$ = 0 and 0.3 T.

Suppression of microwave induced magnetic oscillation by Rashba effect in InGaAs/InAlAs heterostrucutures

K. Fujii*, K. Onishi**, Y. Hachizawa** and S. Yamada***

*Faculty of Information Science and Technology, Osaka Institute of Technology, Hirakata, Osaka 573-0196, Japan

** Graduate School of Science, Osaka University, Toyonaka, Osaka 560-0043, Japan

***Center for Nano Material and Technology, JAIST, Asahidai, Nomi, Ishikawa 923-1292, Japan

Keywords: Rashba effect; MIMO; InGaAs/InAlAs heterostructure

We observed microwave induced magnetic oscillation (MIMO) in InGaAs/InAlAs heterostructures and the large spin-orbit interaction of the heterostructures affects on MIMO signals. Since the fast and independent observation by Mani *et al.*[1] and Zudov *et al.*[2], the MIMO has been studied extensively mainly in extreamly high mobility GaAs/AlGaAs heterostructures, because of an appearance of zero-resistance states.

Electronic states in the InGaAs/InAlAs heterostructure are strongly affected by Rashba effect, which gives a strong spin-orbit interaction due to the structure inversion asymmetry of the heterostructure and the small effective mass. Because of the Rashba effect, large zero-field spin-splitting was observed in InGaAs/InAlAs heterostructures. We investigate the spin states of the InGaAs/InAlAs heterostructure by means of microwave modulated photoconductivity measurements.

In the measurement, we applied the microwaves with the wavelength between 35 GHz and 140 GHz. The microwave power generated by Gunn oscillators was between 10 and 100 mW. The measurement was carried out at 4.2 and 1.7 K. We employed two InGaAs/InAlAs heterostructures, sample-A and sample-B. The density of the 2 dimensional electron gas (2DEG) is $5 \times 10^{11}\mathrm{cm}^{-2}$ in both samples. From Shubnikov de-Haas (SdH) oscillation and far-infrared (FIR) magneto-optical absorption measurements, the zero-field spin-splitting energy is estimated as 9 meV for sample-A. While clear zero-field spin-splitting was not observed in sample B.

In the microwave modulated photoconductivity measurement, a clear SdH oscillation was observed in both samples. Below the onset field of the SdH oscillation, several peaks were observed in sample-B. The peaks are caused by the microwave irradiation and observed at the magnetic fields corresponding to the cyclotron resonance (CR) and its harmonics. The origin of the peaks may be same as that of the MIMO. In sample-A, however, only one peak was observed at CR field. The harmonics of the CR could not be observed. By considering the difference of the spin splitting energy between sample A and B, the suppression of the appearance of the MIMO peaks in sample A is due to the magnetic filed parallel to the 2DEG plane induced by Rashba effect[3] . This fact is the evidence that the strong spin-orbit interaction exists. In addition, the reduction of the resistance at zero magnetic field by the microwave irradiation was observed. This reduction of the resistance is considered as the change in the ant-localization due to spin orbit interaction by the microwave irradiation. We will discuss the mechanism of the reduction.

[1] R. G. Mani *et al.*, Nature **420** 646 (2002).

[2] M. A. Zudov *et al.* PRB. **64** 201311 (2001).

[3] C. L. Yang *et al.*, PRL **91** 06803 (2003).

Spin injection using tunable antidot potential in semiconductor heterostructure with spin-orbit interaction

T. Yokoyama and M. Eto
Faculty of Science and Technology, Keio University, Yokohama, Japan

Keywords: spin-orbit interaction, spin Hall effect, antidot, resonant scattering

The spin injection into semiconductors is an important issue for the application to spin-based electronics, "spintronics." The spin Hall effect is one of the phenomena which generate the spin current without using a magnetic field nor ferromagnetic materials. A three-terminal spin filter has been proposed by an extrinsic spin Hall effect due to the scattering at a repulsive antidot potential [1]. The potential created by antidot, STM tip, etc., is artificially tunable and even may be attractive. In this work, we show that the spin Hall effect is significantly enhanced when the attractive potential is tuned to the resonance [2] and that multi-terminal devices including an antidot could realize the spin injection of more than 50%.

First, we consider an axially symmetric potential $V(r)$ in two-dimensional electron gas in the xy-plane. The spin-orbit (SO) interaction is given by

$$H_{\rm SO} = \frac{\lambda}{\hbar}\boldsymbol{\sigma}\cdot(\boldsymbol{p}\times\boldsymbol{\nabla}V) = -\lambda\frac{2}{r}\frac{dV}{dr}l_z s_z,$$

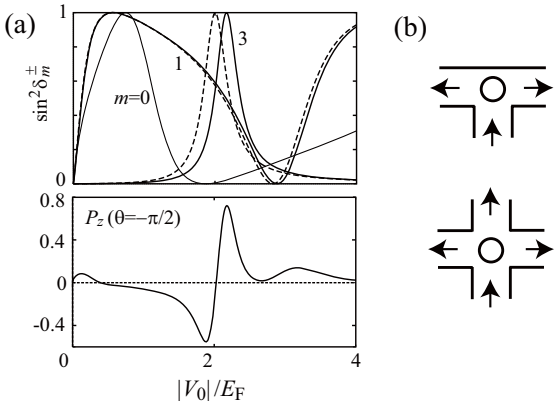

Figure 1: (a) The scattering probability of each partial wave $\sin^2\delta_m^{\pm}$ (solid and broken lines for $s_z = \pm 1/2$; $\delta_m^{\pm} = \delta_{-m}^{\mp}$) and spin polarization P_z at $\theta = -\pi/2$ in the scattering by a potential well [$V(r) = V_0 < 0$ $(r < R_0)$ and 0 $(r > R_0)$], as functions of depth of the well. $E_{\rm F}$ is the Fermi energy and θ is the angle between the wave vectors of incident and scattered waves. $R_0 = 2/k_{\rm F}$, where $k_{\rm F}$ is the Fermi wave number. $\lambda/R_0^2 = 0.01$. (b) Three- and four-terminal devices adopted for numerical study.

with λ being the strength of SO interaction. The Rashba and Dresselhaus SO interactions are neglected. We formulate the spin Hall effect using a partial wave expansion, in which the scattering amplitude and spin polarization P_z are expressed in terms of phase shifts $\delta_m^{\pm}$ for partial waves with $l_z = m$ and $s_z = \pm 1/2$. For a potential well, Fig. 1(a) shows the scattering probability of each partial wave and P_z of the scattered wave in $-\pi/2$ direction, as functions of the well depth $|V_0|$. The resonant scattering takes place ($\delta_m^{\pm} = \pi/2$) when V_0 is tuned properly. Around the resonance with $m \neq 0$, the difference of $\delta_m^{\pm}$ remarkably enhances the spin polarization (only with odd m in the case of $\theta = -\pi/2$).

Next, we numerically examine the spin injection in three- and four- terminal devices in the presence of an antidot [Fig. 1(b)]. We assume a hard-wall potential for the leads and a smooth potential well for the antidot. The conductance $G_{\pm}$ for $s_z = \pm 1/2$ is evaluated using the recursive Green's function method on the tight-binding model of a square lattice [1]. We find that (i) the spin polarization of the current to the drain on the right side, $P_z = (G_+ - G_-)/(G_+ + G_-)$, is enhanced to more than 50% when the potential well is tuned to the resonance, (ii) the spin polarization qualitatively agrees with the analysis by the partial wave expansion shown in Fig. 1(a), and (iii) the calculated results are almost the same for three- and four-terminal devices.

References

[1] M. Yamamoto and B. Kramer, J. Appl. Phys. **103**, 123703 (2008).

[2] A. Fert and O. Jaoul, Phys. Rev. Lett. **28**, 303 (1972); A. Fert *et al.*, J. Magn. Magn. Mater. **24**, 231 (1981).

The Spin Splitting of the Two-dimensional Electron Gas in $Al_xGa_{1-x}N$/GaN Heterostructures

N. Tang*, B. Shen*, K. Han*, Z. X. Qin*, G. Y. Zhang*, X. Q. Shen** and H. Okumura**

** State Key Laboratory of Artificial Microstructure and Mesoscopic Physics, School of Physics, Peking University, Beijing 100871, China*

*** Power Electronics Research Center, National Institute of Advanced Industrial Science and Technology (AIST), Umezono 1-1-1, Central 2, Tsukuba-shi, Ibaraki 305-8568, Japan*

Keywords: $Al_xGa_{1-x}N$/GaN heterostructures; two-dimensional electron gas; spin

$Al_xGa_{1-x}N$/GaN heterostructures are the new low-dimensional semiconductor material system with large conduction-band offset and strong polarization-induced electric field. In comparison with $Al_xGa_{1-x}As$/GaAs heterostructures, $Al_xGa_{1-x}N$/GaN ones have the characteristics of much larger band offset and much stronger polarization effects, which induce a two-dimensional electron gas (2DEG) with the sheet carrier concentration as high as 10^{13} cm^{-2}. This makes a large difference in the spin properties between the two kinds of heterostructure systems. Making a detail study on the spin properties of the 2DEG in $Al_xGa_{1-x}N$/GaN heterostructures has the important meaning in the development of the low-dimensional semiconductor physics.

Beating patterns in the oscillatory magnetoresistance in $Al_xGa_{1-x}N$/GaN heterostructures, which are attributed to the zero-field spin splitting of the 2DEG, have been investigated by means of Shubnikov-de Haas (SdH) measurements. The zero-field spin splitting energy is determined to be 2.5 meV, and the spin-obit coupling parameter is determined to be 2.2×10^{-12} eVm in $Al_{0.11}Ga_{0.89}N$/GaN heterostructures. Despite the energy bandgap in GaN is very large, the zero-field spin splitting is still observed in our study, which is due to a strong polarization-induced electric field and high 2DEG density in the heterostructures. It is also found that the spin-orbit coupling parameter can be tuned by the polarization-induced electric field.

Beating patterns in the oscillatory magnetoresistance have been investigated by means of SdH measurements under illumination. It is observed that the beating nodes shift to lower magnetic fields after the illumination. Therefore, the spin splitting energy decreases after the illumination. The illumination decreases the electric field at the $Al_xGa_{1-x}N$/GaN heterointerface. Based on the fact that the electric field changes the spin splitting energy, it is suggested that the zero-field spin splitting of the 2DEG in $Al_xGa_{1-x}N$/GaN heterostructures mainly arises from the Rashba effect. The $Al_xGa_{1-x}N$/GaN heterostructure is one of the promising materials for the spin-polarized field effect transistor.

References

1. N. Tang, B. Shen, K. Han, et al., Phys. Rev. B **79**, 073304 (2009).
2. N. Tang, B. Shen, K. Han, et al., Appl. Phys. Lett. **93**, 172113 (2008).
3. N. Tang, B. Shen, X. W. He, et al., Phys. Rev. B **76**, 155303 (2007).
4. N. Tang, B. Shen, M. J. Wang, et al., Appl. Phys. Lett. **88**, 172112 (2006).

Fractional forms of 0.7 feature

N. T. Bagraev*, N. G. Galkin*, W. Gehlhoff**, L. E. Klyachkin*,
A. M. Malyarenko* and I. A. Shelykh***

** Ioffe Physical-Technical Institute, St. Petersburg, 194021, Russia*

*** Institut fuer Festkoerperphysik, Technische Universitaet Berlin, D-10623 Berlin, Germany*

**** Polytechnical University, St. Petersburg, 195251, Russia*

Keywords: 0.7 feature, quantum conductance, silicon quantum well, ring

We present the first findings of the spin transistor effect caused by the Rashba gate-controlled ring embedded in the p-type self-assembled silicon quantum well (SQW) that is prepared on the Si (100) surface using the planar diffusion CVD technology. The parameters of the SQW that contains the high mobility 2D gas of holes were defined by the SIMS, STM, cyclotron resonance (CR) and EPR methods. The one-dimensional ring embedded in SQW, R=2500 nm, contains the source and drain constrictions that represent quantum point contacts (QPCs). The quantum conductance staircase caused by the QPC inserted within one of the arms of the one-dimensional ring was controlled by varying the split-gate voltage. The first quantum step of this staircase is found to reveal the $0.7(2e^2/h)$ feature that is caused by the spin interference in the QPC. Then, the coherence and phase sensitivity of the spin-dependent transport of holes are studied by varying the value of the external magnetic field and the top gate voltage that are perpendicular to the plane of the three-terminal ring. By varying the top gate voltage at the fixed value of the split-gate voltage, the transition from the positive magnetoresistance to the negative magnetoresistance is observed in very weak magnetic field, 0.005 mT thereby verifying a crossover from the weak antilocalization to the weak localization following the changes of the sheet density of the 2D holes. Firstly, the amplitude of the $0.7(2e^2/h)$ feature fixed by the split-gate voltage is demonstrated to exhibit the Aharonov-Casher (AC) conductance oscillations by varying the top gate voltage, which are due to the Rashba spin-orbit interaction SOI. The phase variations of the $0.7(2e^2/h)$ feature revealed by the Aharonov-Bohm (AB) and the AC oscillations are shown to be caused by the scattering on the QPCs inside the three-terminal ring Secondly, the amplitude of the $0.7(2e^2/h)$ feature is found to take in the fractional form with both plateuax and steps in the range from the $0.7(2e^2/h)$ to $0.7(e^2/h)$ and $1.5(e^2/h)$ values by varying respectively the forward and reverse p^+n junction bias applied to the top gate. The oscillations of the positions of the $0.7(2e^2/h)$ fractions seem to be due to the interplay of the AB and AC effects (Fig.1). Finally, at low positive top gate voltage, the large decrease of the amplitude of the $0.7(2e^2/h)$ feature is observed, which appears to result from the spontaneous spin polarization of heavy holes in the SQW that is created by decreasing of the sheet density.

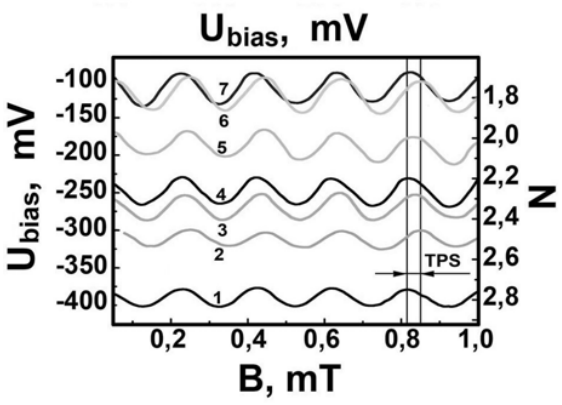

Fig.1 The U_{bias}-B plots of the positions of the $0.7(2e^2/h)$ fractions, $\nu\cdot(e^2/h)$, that exhibit the plateaux (2,3,5,6) and steps (1,4,6,7) with the transmission phase shift: 1-ν=7/4, 2-12/7, 3-22/13, 4-17/10, 5-5/3, 6-8/5, 7-13/8. N is the number of holes in one-dimensional channel.

The topological edge states in semiconductors with inverted band structures

J. Li, L. B. Zhang, and Kai Chang *

* SKLSM, *Institute of Semiconductors, Beijing,China*

Keywords: Topological insulator, Edge state, Quantum phase transition, Spin transport

Topological insulator is a very recent discovery[1,2,3]. The topological insulators, e.g., Graphene[1], HgTe[2,3] quantum wells, etc, show a topological edge states crossing the bulk gap. The topological edge states can lead to the Quantum spin Hall effect and provide us a new way to realize spin transport in semiconductors. Very recently it was demonstrated that external electric field can induce a very strong intrinsic spin Hall effect in HgTe quantum wells. [5]

In this work, we investigate theoretically the topological edge states in HgTe quantum wire and the effect of external electric field based on the eight-band Kane model. The edge states can be found in HgTe quantum wire structures and the gap between edge states can be tuned by adjusting the thickness and width of HgTe quantum wire. Interestingly, the electric field can induce a quantum phase transition between the band insulator and topological insulators. The spin transport through the topological edge states is studied numerically using the scattering matrix theory. A perfect transmission is found in the bulk gap of topological insulator, which is caused by the transport in the topological edge channel. Utilizing the split-gate technique, we can find an interesting focusing in HgTe quantum wires.

In summary, we investigate theoretically that topological edge states and transport property in semiconductor quantum wires with inverted bandstructures. The theoretical results could provide us more realistic understanding about topological edge states and is helpful for potential application of spintronic devices.

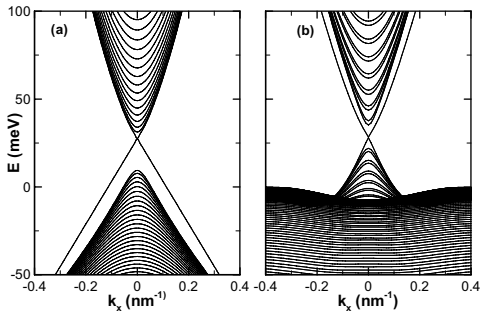

Fig.1 The band structures of HgTe quantum wires obtained from the four-band nodel[2] (a) and the eight-band Kane model[5] (b). The width of the quantum wire d=500nm, the thickness of quantum wire is 7nm

References

1, C. L. Kane and E. J. Mele, Phys. Rev. Lett. 95, 146802 (2005); 95, 226801 (2005);

2, B. A. Berneveg, T. L. Hughes, and S. C. Zhang, Science 314, 1757 (2007).

3, M. Konig et al., Science 318, 766 (2007).

4, S. Murakami, Phys. Rev. Lett. 97, 236805 (2006).

5, W. Yang, Kai Chang and S. C. Zhang, Phys. Rev. Lett. 100, 056602(2008).

Spin and phase coherence in quasi-1D electron systems under strong spin-orbit interaction

R. L. Kallaher*, J. J. Heremans*, N. Goel**, S. J. Chung** and M. B. Santos**

* *Department of Physics, Virginia Tech, Blacksburg, VA, USA*

** *Department of Physics, University of Oklahoma, Norman, OK, USA*

Keywords: InSb, spin coherence, antilocalization, 1D wire

We present measurements of antilocalization (AL) in quasi-1D lithographic wires on narrow-bandgap InSb/InAlSb heterostructures. AL allows a study of spin and phase coherence of carriers with strong spin-orbit interaction, here in confined geometries. Interaction of carriers with device boundaries offers opportunities to manipulate spin states for spintronics devices [1], and also affects spin coherence lengths. The latter aspect, important in the context of spintronics devices, we explore here. Confined geometries restrict the phase space for scattering, and the literature [2] and our experiments on InSb/InAlSb indeed show the influence of quasi-1D geometries on electron spin coherence.

AL results from quantum interference between electrons, and under spin-orbit interaction causes a sharp positive magnetoresistance (MR) around zero magnetic field, crossing over to negative MR at higher fields. Spin and phase coherence times can be extracted from the MR. Quasi-1D wires of conducting widths 130-530 nm were fabricated from MBE-grown InSb/InAlSb heterostructures with InSb quantum wells of density ≈ 5.5 x 10^{15} m^{-2}, and mobility ≈ 10 m^2/Vs. Measurements over 0.4-15 K on unpatterned InSb/InAlSb and on quasi-1D wires are compared. The positive MR is substantially larger in the quasi-1D wires than in the unpatterned sample, due to a flux-cancellation effect. Also, Aharonov-Bohm type periodic modulation in the MR is observed in the wires. Apart from these observations, within the limits of AL theory and fitting the MR to a quasi-1D theory [3,4] with spin-orbit interaction, the wire-width dependence and temperature dependence of the spin and phase coherence times can be extracted. The data shows an increase in the spin coherence time at reduced wire widths, consistent with optical experiments on InGaAs wires [2] and with theory [4]. As expected, the conducting widths of the wires substantially affects the temperature dependence of AL: the effect is still strong at an unusually high 15 K in wide wires (530 nm), but disappears above 5 K in narrower channels (130 nm), whereas AL is very weak at 15 K in the unpatterned sample. The temperature and width dependence of the observed AL and the conclusions from the data will be presented in detail.

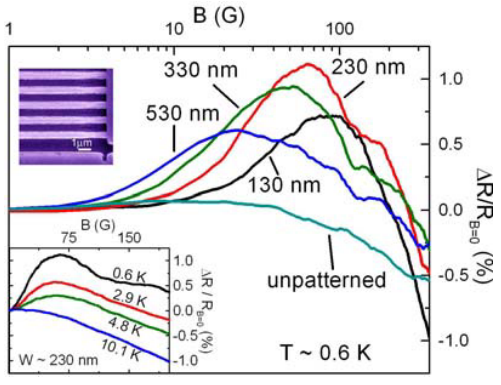

Fig.1 Low field MR for wires of different widths. Upper inset: Example of SEM image of wires fabricated from an InSb/InAlSb heterostructure. Lower inset: MR at different temperatures for wires of width ≈ 230 nm.

References

1. Hong Chen et al., Appl. Phys. Lett. **86**, 032113 (2005).
2. A. W. Holleitner et al., Phys. Rev. Lett. **97**, 036805 (2006).
3. C.W.J. Beenakker et al., Phys. Rev. B **38**, 3232 (1988).
4. S. Kettemann, Phys. Rev. Lett. **98**, 176808 (2007).

Effect of spin relaxation in Anderson localization in quantum wires

Tomoaki Kaneko, Mikito Koshino, and Tsuneya Ando
Department of Physics, Tokyo Institute of Technology, Tokyo, Japan

Keywords: Quantum wire, Spin relaxation length, Localization length, Symmetry crossover

The goal of spintronics is to utilize the spin degree of freedom in electronics devices. In a semiconductor nano-structure, structure inversion asymmetry and spin orbit interaction cause spin splitting even in the absence of a magnetic field [1, 2]. This spin splitting behaves as an effective magnetic field and noncommutativity of spin precession around the effective magnetic field leads spin relaxation by spin independent scattering [3]. In a quantum wire with spin splitting, the spin relaxation is considerably suppressed due restriction of spin precession axis [4]. In this paper, the spin relaxation length is shown to determine the effective systems size for which the symmetry crossover takes place in the Anderson localization.

In disordered systems, the symmetry such as translational and rotational symmetry is broken and the remaining symmetry related to time and spin plays important role. According to the Random matrix theory, we can classify the system into three universality classes. In the presence of both time reversal and spin rotational symmetry, the system belongs to the orthogonal class. When spin rotational symmetry is broken by spin-orbit interaction, the universality class becomes symplectic. In the quantum wire with channel number N, localization length ξ is approximately given by $\xi \simeq \beta N \Lambda$, where Λ is mean free path and β is symmetry factor with $\beta = 1$ for orthogonal and 4 for symplectic. Therefore, the localization length is strongly affected by the symmetry.

In this study, a tight binding model is used to numerically calculate transmission coefficients [5], spin relaxation length, and localization length. Figure 1 shows calculated localization length ξ (solid lines) and spin relaxation length Λ_S (dashed lines) as a function of the mean free path for wires with $N = 7$. In this figure, δ represents the strength of the spin-orbit interaction, defined as the ratio of the spin splitting at the Fermi level to the Fermi energy. The localization length for $\delta = 0.5$ (fully symplectic) is approximately 4 times as large as that of $\delta = 0$ (perfectly orthogonal), showing the consistency with the symmetry change. In this figure, Λ_S for $\delta = 0.02$ is much larger than corresponding ξ due to the strong suppression of the spin relaxation and ξ is almost independent of δ in regime $\delta \leq 0.02$. On the other hand, for $\delta = 0.05$, ξ starts to increase faster than that for $\delta = 0$ or 0.02 with Λ once Λ_S becomes smaller than ξ. The same conclusion is obtained for wires with different N's. This shows that the spin relaxation length gives an effective system size determining the symmetry crossover.

References

[1] F. J. Ohkawa and Y. Uemura, J. Phys. Soc. Jpn. **37**, 1325 (1974).
[2] Yu. A. Bychkov and E. I. Rashba, J. Phys. C, **17**, 6039 (1984).
[3] M. I. Dyakonov and V. I. Perel, Zh. Eksp. Teor. Fiz. **60**, 1954 (1971). [Sov. Phys. JETP **33**, 1053 (1971)].
[4] T. Kaneko, M. Koshino, and T. Ando, Phys. Rev. B **78**, 245303 (2008) and references cited therein.
[5] T. Ando, Phys. Rev. B **44**, 8017 (1991).

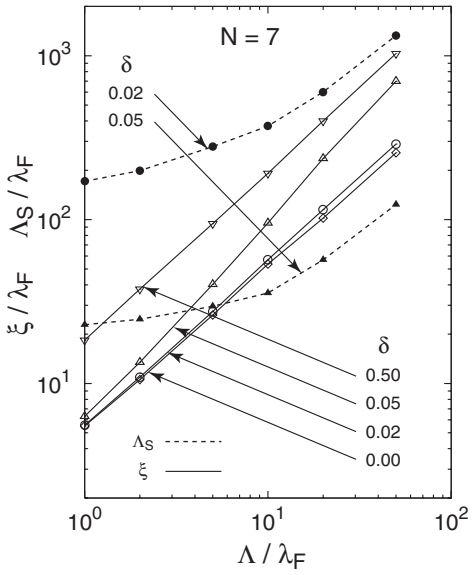

Figure 1: Calculated localization length (solid lines) and spin relaxation length (dashed lines) as a function of mean free path Λ for $N = 7$. For $\delta = 0.05$, ξ starts to increase faster with Λ when corresponding Λ_S becomes shorter than ξ, corresponding to the symmetry crossover.

The interplay between the confinement and crystallographic anisotropy in ballistic hole quantum wires

O. Klochan*, A.P. Micolich*, L.H. Ho*, A.R. Hamilton*, K. Muraki**, and Y. Hirayama***

** School of Physics, University of New South Wales, Sydney NSW 2052, Australia*

*** NTT Basic Research Laboratories, 3-1 Morinosato Wakamiya, Atsugi, Kanagawa 243-0198, Japan*

**** Department of Physics, Tohoku University, 6-3 Aramaki aza Aoba, Aobaku Sendai, Miyagi 980-8578, Japan*

Keywords: ballistic transport, holes, GaAs, Zeeman splitting.

Holes attract a lot of scientific interest due to their unique spin properties – holes are spin 3/2 particles whereas electrons are spin 1/2 particles. The non-zero orbital angular momentum for holes results in a strong interaction between the hole's orbital and spin angular momenta, known as spin-orbit coupling. This means that hole spins can be manipulated not only by a magnetic field but also by other means (e.g. an electric field). For this reason, holes hold considerable promise for spintronics applications [1].

The spin-orbit coupling in hole systems can be studied by measuring the response of a system to an external magnetic field *B*. Strong spin-orbit coupling leads to an pronounced anisotropy of the response of the hole spins to this applied field. Confining the holes to lower dimensions adds another level of control over their spin properties.

Previous studies of two dimensional (2D) systems [2] have revealed a complex interplay of the spin-orbit coupling, crystallographic anisotropy of the host crystal, and the confinement on the spin properties of holes. For example, it has been shown that the Zeeman splitting in 2D hole systems grown on (311) A oriented heterostructures is highly anisotropic due to low symmetry of the host crystal [3]. In contrast, previous results on [-233] oriented one dimensional (1D) hole wires revealed enhanced anisotropy of the Zeeman splitting, which was attributed to 1D confinement [4]. This situation raises a very interesting question: "Is the Zeeman splitting in 1D hole wires affected by its crystallographic orientation?"

We answer this question by investigating two one-dimensional hole wires fabricated along orthogonal crystallographic directions ([-233] and [01-1]) on a (311)A oriented heterostructure. The two wires exhibit different behaviour in an in-plane magnetic field. The Zeeman splitting of the 1D subbands shows a strong dependence on the orientation of the magnetic field relative to both the wire and the underlying crystal axis. When the magnetic field is applied along the [01-1] axis, the 1D subbands only show a Zeeman splitting when *B* is parallel to the wire. However when the field is applied along the [-233] axis the situation is much more complex, due to an interplay between crystallographic and 1D confinement effects [5].

References

1 I. Žutić *et al.*, *Rev. Mod. Phys.* **76**, 323 (2004).

2 R. Winkler, *Spin-Orbit Coupling Effects in Two-Dimensional Electron and Hole Systems* (Springer, Berlin, 2003).

3 S.J. Papadakis *et al.*, *Phys. Rev. Lett.* **84**, 5592 (2000).

4 R. Danneau *et al.*, *Phys. Rev. Lett.* **97**, 026403 (2006).

5 O. Klochan *et al.*, arXiv:0809.0969 (2008).

Anomalous CPGE of the 2DEG in $Al_xGa_{1-x}N$/GaN heterostructures at room temperature

X.W.He[1], B.Shen[1, a)], Y.H.Chen[2], K.Han[1], C.M.Yin[1], Q.Zhang[1], F.J.Xu[1], N.Tang[1]

[1]*State Key Laboratory of Artificial Microstructure and Mesoscopic Physics, School of Physics, Peking University, Beijing 100871, China*

[2]*Laboratory of Semiconductor Materials Science, Institute of Semicoonductrs, CAS, Beijing 100083, China*

Keywords: Anomalous Circular Photogalvanic Effect, Reverse spin Hall effect, Spin transverse force

In this study, we report on an anomalous circular photogalvanic effect (CPGE) observed in the two dimensional electron gas (2DEG) in $Al_{0.25}Ga_{0.75}N$/GaN heterostructures which firstly indicates that there are close relationships between the CPGE and the reverse spin Hall effect (RSHE) [1]

Theoretically, the CPGE current should be zero for the 2DEG in $Al_xGa_{1-x}N$/GaN heterostructures under normal incidence. However, we found it is not zero through changing the position of the light spot

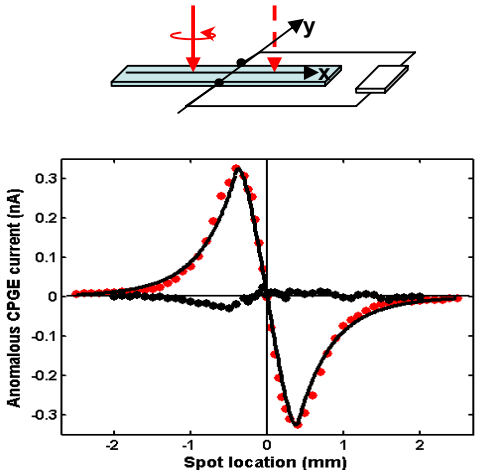

Fig. 1 The anomalous CPGE current as a function of the light spot location for normal incidence with the wavelength of 1064 nm

From Fig. 1, it can be found that the current signal increases remarkably when the light spot deviates from the center point of two electrodes, and reverses the sign from the left to right side of the electrodes. The experimental result suggests that a current is swirling over the edge of the light spot. We name it anomalous CPGE current.

This anomalous CPGE current is the transfer of photon angular momentum into the rotational motion of electrons which is realized by RSHE. The spin dependent chemical potential provided by the light spot drives a radial spin current on the 2DEG, this radial spin current is converted into a swirly charge current via spin transverse force. Considering the 2DEG as an ideal two-dimensional conductor, by fitting the experimental data, we obtained the spin transverse force acting on a single electron and the Hall voltage for a light spot with given size are 2.4x10-19 N and 2.4 μV, respectively.

We believe that the anomalous CPGE is a universal phenomenon for the transport of electrons in various semiconductors and suggests an experimental way to study the RSHE on the macroscopic scale and at room temperature

References

1. X.W. He, Bo. Shen, Y.H. Chen et al, Phys. Rev. Lett, **101**, 147402 (2008)

Email: a) bshen@pku.edu.cn

Detection of spin polarization in a quantum wire

T. Otsuka, E. Abe, Y. Iye and S. Katsumoto

Institute for Solid State Physics, University of Tokyo, 5-1-5 Kashiwanoha, Kashiwa, Chiba 277-8581, Japan

Keywords: quantum dot, quantum wire, spin polarization

Detection of spin polarization generated in non-magnetic semiconductors is one of the key technologies in the development of spintronics. We propose a detection method utilizing a side coupled quantum dot (QD) with advantage of small disturbance to the target. We apply the method to the polarization detection in a quantum wire (QW) and confirm its work.

Figure (a) shows a scanning electron micrograph of the device. With in-plane magnetic field of 14 T, spin split conducting channels are formed in QW and we control the spin polarization P by changing the number of transmitting channels with wire gate voltage V_W. QD tunnel-couples to QW with a single connection, and works as a spin polarization detector. The tunnelling of an electron between QW and QD is monitored by the conductance through a nearby quantum point contact (QPC). The net current through QD is zero, which leads to the detection with small disturbance.

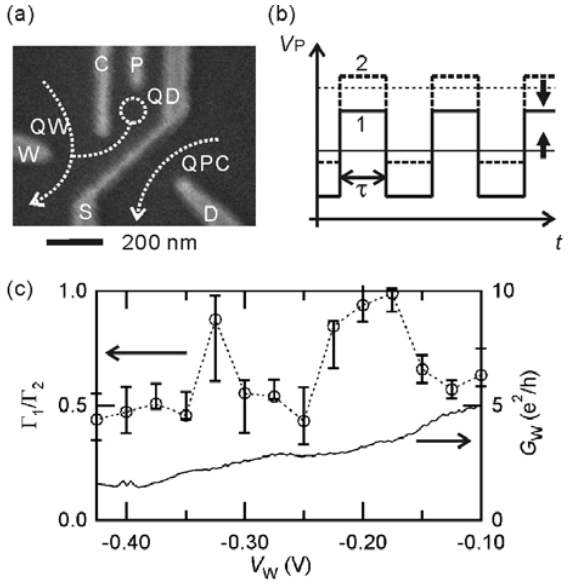

Figure (a) Scanning electron micrograph of the device. (b) Wave form of V_P to detect spin polarization. (c) Γ_1/Γ_2 and G_W as a function of V_W.

For the detection, we apply square wave voltage V_P on the plunger gate as shown in Fig. (b). Under the magnetic field, the spin states in QD are split by the Zeeman energy. When V_P crosses only the up-spin state (thick solid line 1), an up-spin electron can shuttle between QW and QD in phase with V_P. On the other hand, when V_P crosses up- and down-spin states (thick broken line 2), both of the spins can shuttle. We evaluate effective tunnelling rate in the former (latter) condition Γ_1 (Γ_2) from the lock-in detection of QPC conductance in phase with V_P [1]. If $P = 0$, both up- and down-spin electrons exist in QW and this makes $\Gamma_1/\Gamma_2 = 0.5$. If $P = 1$, there are only up-spin electrons and $\Gamma_1/\Gamma_2 = 1$. From Γ_1/Γ_2, we get the information of P.

The obtained Γ_1/Γ_2 as a function of V_W is shown in Fig. (c). Γ_1/Γ_2 oscillates with the change of V_W. Near the narrow plateaus of the conductance through QW G_W ($P > 0$), Γ_1/Γ_2 is around 1. Near the wide plateaus ($P = 0$), Γ_1/Γ_2 is fixed around 0.5. These results show that the system works as a spin polarization detector.

Γ_1/Γ_2 takes large value even when many channels open in QW. This is the result of larger coupling between QW and QD in the higher channel because of the larger overlap of their wave functions. The change of the coupling strength is confirmed experimentally from the analysis of Γ with changing V_W. This supports that the detection is sensitive to the higher channel in the case of QW.

A similar pulsed gating detection method using two-electron singlet and triplet states in QD can be applicable even in the zero magnetic field. This is promising for the detection of the spin polarization created by the spin-orbit interaction or spin Hall effect.

References

1. J. M. Elzerman *et al*., Appl. Phys. Lett. **84**, 4617 (2004).

Spin dependent current induced by spatial gradient of spin orbit interaction in Y-branch shaped narrow wire structures

M. Kohda*, ** and J. Nitta*

* *Department of Materials Science, Tohoku University, Sendai, Japan*

** *PRESTO, Japan Science and Technology Agency, Kawaguchi, Japan*

Keywords: Spin orbit interaction, two dimensional electron gas, narrow wire structure

In III-V semiconductor two dimensional electron gas (2DEG), Rashba spin orbit interaction induces an effective magnetic field due to structural inversion asymmetry, and it enables us to manipulate electron spin precession through gate bias voltages [1,2]. Recently, spin filter effect and generation of spin current are theoretically predicted in 2DEGs without any ferromagnetic electrodes due to spin dependent force generated by spatially modulated and time-dependent spin orbit interactions, respectively [3,4]. Since the spin orbit interaction allows us not only to manipulate electron spin precession, but also to generate electron spin polarization by electrical means, we can integrate electrical spin generation [3], manipulation [2], and detection [4] through the use of spin orbit interaction. Here, we investigated spin dependent current induced by the spatial gradient of spin orbit interaction in Y-branch shaped narrow wire structures.

$In_{0.7}Ga_{0.3}As$ / $In_{0.53}Ga_{0.47}As$ 2DEG was grown by metal organic chemical vapor deposition. The epitaxial wafer was processed into Y-branch shaped narrow wire structures. Wire width and length were designed to 0.7 μm and 5.6 μm, respectively. At Y-branch junction, Cr / Au side gate electrodes, V_{gL} and V_{gR}, were deposited on Al_2O_3 gate insulator for controlling the strength of Rashba spin orbit interaction. Scanning microscope image of the fabricated sample is shown in Fig. 1 (a). We applied an in-plane magnetic field perpendicular to the direction of wire length to generate spin polarized electrons due to the Zeeman effect, and measured the spin dependent current with different side gate voltages at T = 4.0 K. Figure 1 (b) shows the left gate bias dependence of the separated branch currents with fixed right gate bias of V_{gR} = -6.0 V at $B_{//}$ = -15, 0, and +15 T. At $B_{//}$ = 0 T, the measured current increases and decreases in right and left branches, respectively, as the left gate voltage increases. However, separated branch currents show different values from V_{gL} = 0 V to +4.0 V at $B_{//}$ = ±15 T, which indicates the generation of spin dependent current due to the relative strength of right and left side gate voltages. Since different V_{gR} and V_{gL} yield spatial gradient of the spin orbit interaction in 2DEG underneath the gate region, it provides spin dependent force for electrons resulting in the different branch currents depending on the injected spin direction.

References

[1] J. Nitta *et al*., Phys. Rev. Lett. **78**, 1335 (1997).
[2] T. Bergsten *et al*., Phys. Rev. Lett. **97**, 196803 (2006).
[3] J. Ohe *et al*., Phys. Rev. B **72**, 041308 (R) (2005).
[4] A. G. Malshukov *et al*., Phys. Rev. B **68**, 233307 (2003).

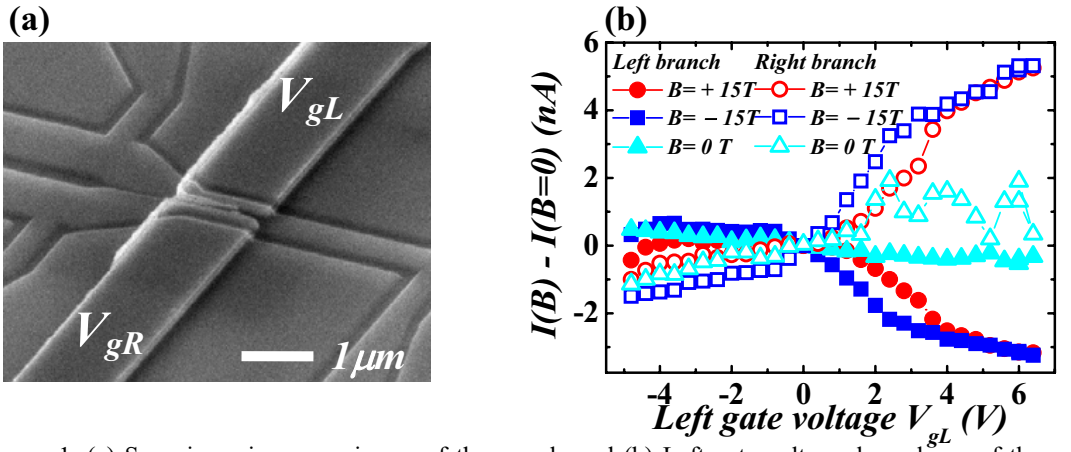

Figure. 1. (a) Scanning microscope image of the sample and (b) Left gate voltage dependence of the separated branch currents at $B_{//}$ = -15, 0, and +15 T at T = 4.0 K.

Electron Spin Resonance in Triple Quantum Dots

M. Busl*, R. Sanchez** and G. Platero*
* *Instituto de Ciencia de Materiales, CSIC, Cantoblanco,Madrid,28049,Spain*
** *Departement de Physique Théorique, Université de Genève, CH-1211 Genève 4, Switzerland*

Two-level-system formed by electron spin-up and down states in a QD is one of the most promising candidates for a qubit [1]. Coherently controlling of these electron spin states therefore is of great importance. In the last few years experimental [2] and theoretical [3] effort has been devoted to describe electron spin resonance (ESR) in double quantum dots. There, crossed DC and AC magnetic fields with a frequency resonant to the Zeeman energy splitting in the dots drive electrons to perform spin coherent rotations.

In the last few years, Triple Quantum Dots (TQDs) in a linear o triangular configuration have been investigated intensively both experimentally [4] and theoretically [5]. TQDs have been proposed as solid-state-entanglers [6] or charging rectifiers. TQDs also motivate fundamental research, because their electronic properties present a rich variety of new physical phenomena, concerning quantum interference effects, spin blockade or electron spin resonance. In TQDs, it was shown that the closed loop configuration of the TQD (triangular configuration) leads to quantum interference and, in the presence of a magnetic field, to Aharonov-Bohm (AB) oscillations [7][8].

In the present work, we analyze the interplay of the AB-phase and coherent spin rotations induced by crossed dc and ac magnetic field in a DC biased TQD in a triangular configuration, filled with one and two extra electrons. We investigate different sample configurations, i.e. equal or different Zeeman splittings within the three dots. We discuss how coherent population trapping, which occurs in a TQD filled with one electron [7], is affected by the AC field. We will show, that in this case the electron is forced to perform single electron spin rotations induced by the AC magnetic field. These spin rotations are stable against decoherence coming from the leads, once the electron drops in the so-called dark state.
The presence of a second extra electron in the TQD leads to new interesting features in the spin dynamics due to the interplay between spin blockade, AB-interference and coherent spin rotations induced by the ac magnetic field. Current through the system can be blocked either by coherent population trapping or by spin blockade. We will discuss how electron spin resonance induced by a time dependent magnetic field modifies the spin dynamics in both cases. We will discuss as well how it depends on the magnetic flux through the sample induced by the dc field. Finally, we predict that, for certain sample configurations, bichromatic magnetic fields are able to induce electron coherent trapping in the TQD [9]. Our results indicate that not only electron spin coherence but also electron spin rectification properties in transport can be tuned with ac and dc magnetic fields.

[1] F.H.L. Koppens *et al.*, Nature 442, 766 (2006).
[2] J.R. Petta *et al.*, Science 309, 2180 (2005), M. Pioro-Ladrière *et al.*, Nature Physics 4, 776 - 779 (2008), K. C. Nowack *et al.*, Science 318, 1430 (2007).
[3] R. Sánchez *et al.*, Phys. Rev. B 77, 165312 (2008).
[4] M. C. Rogge *et al.*, Phys. Rev. B 78, 153310 (2008), Phys. Rev. B 77, 193306 (2008), D. Schröer *et al.*, Phys. Rev. B 76, 075306 (2007), L. Gaudreau it et al., Phys. Rev. Lett. 97, 036807 (2006).
[5] M. Korkusinski *et al.*, Phys. Rev. B 75, 115301 (2007).
[6] D. S. Saraga and D. Loss, Phys. Rev. Lett. 90, 166803 (2003), A. Vidan *et al.*, Appl. Phys. Lett. 85, 3602 (2004).
[7] C. Emary, Phys. Rev. B 76, 245319 (2007).
[8] F. Delgado *et al.*, Phys. Rev. Lett. 101, 226810 (2008).
[9] M. Busl *et al.*, submitted.

Conductance images between two STM probes in carbon nanotubes and graphene

Takeshi Nakanishi* and Tsuneya Ando**
*Nanotube Research Center, AIST, 1–1–1 Higashi, Tsukuba 305-8565, Japan
** Department of Physics, Tokyo Institute of Technology, 2–12–1 Ookayama, Meguro-ku, Tokyo 152-8551, Japan

Keywords: graphite, carbon nanotube, STM, Kekulé-type pattern

The scanning-tunneling-microscopy (STM) is a powerful technique for directly viewing electronic wave functions at the atomic level. Quite recently multi-probe STM was developed. In this paper the conductance image between two STM probes is calculated in carbon nanotubes and graphene within a tight-binding model and a realistic model for STM probes [1]. We show that a Kekulé-type pattern usually appears due to interference of states at K and K' points except in special cases.

The STM probes have been modeled with sp Slater-Koster hopping terms. The conductance is given by Landauer's formula and transmission probabilities between these two STM probes are numerically calculated by the use of Green's function according to a lattice model at the charge neutrality point. Because the coupling between STM probes and graphene is sufficiently weak, we approximately take into account only the lowest order of couplings.

In the calculation, a left STM probe is fixed at several points and a right probe is continuously swept over the wide region. An example of calculated conductance in graphene is shown in Fig. 1 by the density as a function of the right-probe position. The position of the left probe is denoted by an open circle, but its actual position is shifted by $(-102,\ 0)a$ in the coordinate system (x, y) with a lattice constant $a = |\mathbf{a}|$ and therefore is quite far from the right-probe position. The Kekulé-type pattern peak usually appears in the calculated conductance in graphene and carbon nanotubes. Its basis vectors can be chosen as $\tilde{\mathbf{a}} = -\mathbf{a} - 2\mathbf{b}$ and $\tilde{\mathbf{b}} = 2\mathbf{a} + \mathbf{b}$ as shown in Fig. 1, for example, and therefore the lattice constant is $\sqrt{3}a$ and the area is three times as large as the unit-cell area determined by basis vectors $\mathbf{a}$ and $\mathbf{b}$.

For carbon nanotubes, the Kekulé-type pattern disappears in special cases where an electron is injected into a single propagating state classified by the parity in the effective-mass scheme. This is possible because there are only two modes propagating in one direction and the amplitude of one of the modes vanishes for a certain ratio of the injection from neighboring A and B sites. This also makes the STM image very sensitive to the left-tip position.

In graphene, on the other hand, there are propagating modes in all directions because of the two-dimensional nature and therefore the vanishing amplitude for a certain mode with a specific direction does not give rise to any visible effect. As a result, the STM images become robust for the change in the left-tip position. This allows us the observation of interference effects sensitive to intrinsic scatters such as ripples and point defects in graphene, avoiding ambiguity in the tip position.

References

[1] T. Nakanishi and T. Ando, J. Phys. Soc. Jpn. **77**, 024703 (2008); phys. stat. sol. (b) **245**, 2173 (2008).

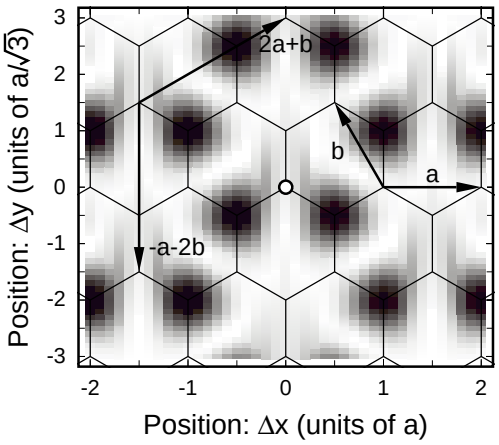

Figure 1: Calculated conductance in a graphene as a function of right STM tip position for the left-tip position fixed on a carbon atom. The larger conductance is shown by the darker color.

Single-electron activation over an oscillating barrier in silicon nanowire MOSFETs

S. Miyamoto*,**, K. Nishiguchi*, Y. Ono*, K. M. Itoh**, and A. Fujiwara*
*NTT Basic Research Laboratories, NTT Corporation, Kanagawa, Japan
**School of Fundamental Science and Technology, Keio University, Yokohama, Japan

Keywords: Single-electron transfer dynamics, resonant activation, silicon nanowire MOSFETs

Single-electron (SE) transfer is investigated based on metrological motivation to establish ultra-highly-accurate current standards. A gigahertz clock high-frequency transfer was recently demonstrated in a novel SE ratchet scheme [1]. By utilizing the SE ratchet, the escape dynamics of SEs from a potential well were investigated in detail. The results suggested that thermal activation is a dominant process around 20 K [2]. The SE system in the classical regime is well suited to verifying the theoretical prediction of resonant activation of a particle over a fluctuating barrier [3, 4]. Such resonance takes place when the oscillation frequency satisfies the condition of scale matching with the average rate of the particles crossing the barrier. In this investigation, we address the resonant activation of SEs over a barrier weakly modulated by RF signals. The measured device is a 30-nm wide silicon nanowire with multiple finger gates fabricated on a silicon-on-insulator wafer. The SE transfer is performed at 16 K with the clock frequency of f_c =16.7 MHz. During th ejection time, t_e, which is a part of the transfer cycle, $1/f_c$, a SE is thermally activated from a potential well as illustrated in Fig. 1(a). We obtain the average number of escaping SE, $\langle n_t \rangle$, (less than one) by normalizing the SE transfer current by ef_c. Figure 1(b) shows the t_e dependence of $\langle n_t \rangle$ as a function of the applied RF frequency, f_{RF}. Enhancement of the SE escape can be observed around several tens of megahertz. We note that a wide 0.5 plateau appears in the lower-frequency regime where the escaping SEs experience two-height barriers slowly fluctuating between high and low states with the ratio of 1/2. This results in a double-exponential decay of the SE survival probability, $P_s = 1 - \langle n_t \rangle$ [inset to Fig. 1(c)]. As f_{RF} increases, the SE dynamics undergo a gradual transition to a single-exponential behavior, which reflects the fact that an effective barrier for SEs has a single height in the higher-frequency regime. In Fig. 1(c) the average escape times, τ_{avg}, determined by exponential fitting to the time-domain data are plotted as a function of the RF frequency. V_e is the voltage parameter used to change the order of τ_{avg}. As indicated by the dotted line in Fig. 1(c), τ_{avg} manifests a minimum that is correlated to the corresponding f_{RF}. This indicates that SEs can preferentially cross the low-state barrier formed at least once within the measurement window ($0 < t_e < 50$ ns). Hence, the signature of the resonant activation was observed in the silicon-based SE transfer device, which well-embodies the universal problem of particle activation.

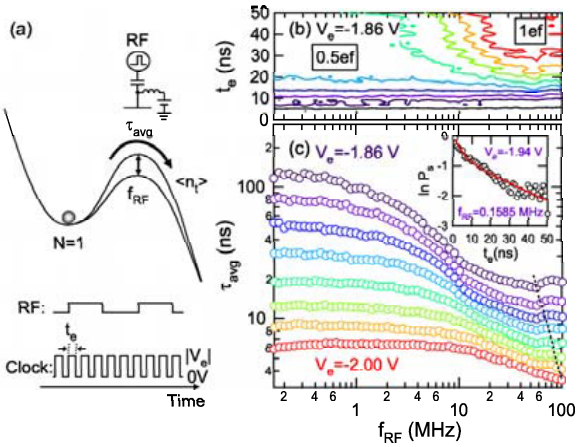

Figure 1: (a) Thermally-activated transfer of SEs over a barrier weakly modulated by RF signals. V_e is the ejection voltage applied to a transfer gate (not shown) with the duration of t_e [2]. (b) Time-resolved measurements of escaping SEs as a function of the applied RF frequency, f_{RF}. (c) Variations in the average escape time, τ_{avg}, at different V_e. The inset shows the survival probability, P_s, measured in the lower-frequency regime together with the best fit.

References

[1] A. Fujiwara *et al.*, Appl. Phys. Lett. **92**, 042102 (2008).
[2] S. Miyamoto *et al.*, Appl. Phys. Lett. **93**, 222103 (2008).
[3] C. R. Doering *et al.*, Phys. Rev. Lett. **69**, 2318 (1992).
[4] M. Bier *et al.*, Phys. Rev. Lett. **71**, 1649 (1993).

Non-linear electrodynamics of graphene

S. A. Mikhailov
Institute of Physics, University of Augsburg, D-86135 Augsburg, Germany

Keywords: Graphene, electromagnetic response, non-linear cyclotron resonance, chaos.

The linear energy dispersion of graphene quasiparticles results in the strongly non-linear electromagnetic response of this material. If the external magnetic field is zero and the amplitude of the incident electromagnetic wave E_0 satisfies the condition $eE_0V/\omega\mu \gtrsim 1$, graphene can generate higher harmonics [1] at $\Omega = n\omega$ with $n = 3, 5, \ldots$; here ω is the frequency of the incident electromagnetic wave, $V = 10^8$ cm/s is the velocity of quasi-particles in graphene, and μ is the chemical potential counted from the Dirac points. The radiative decay and the response to a pulse excitation in graphene also substantially differ from those in conventional semiconductor 2D electron systems [2].

In the finite external magnetic field $\mathbf{B}$ the graphene response is non-linear *even in the weak external electric fields* $eE_0V/\omega\mu \ll 1$ [3]. The cyclotron frequency of a particle with the linear spectrum $\mathcal{E} = V|\mathbf{p}|$ depends on the energy, $\omega_c = eBV^2/\mathcal{E}c$. As a consequence, its cyclotron motion under the action of the external electromagnetic wave is accompanied by the energy oscillations $\mathcal{E}(t)$ and by the generation of many different (higher and lower) frequency harmonics [3], Figure 1. Such an unusual response in weak electric fields shows that graphene radically differs from other materials in view of its electrodynamic properties.

Our findings have several important consequences. First, the linear response theoretical approaches based on the linearization of the classical or quantum kinetic equations (e.g. the Kubo formalism) are not appropriate for graphene in finite magnetic fields. Instead, one should use the methods of non-linear dynamics and the theory of chaos. Second, due to the harmonics generation the cyclotron resonance line can be substantially broadened even in the system without disorder, only due to the massless spectrum of graphene quasi-particles [3]. Third, measuring the electromagnetic response of standard materials one implicitly relies on the validity of the linear relation $j_\omega \propto E_\omega$ and uses either a narrow-band source of radiation and a broad-band detector, or a broad-band source and a narrow-band detector. In graphene, in order to get full information on its response, one has to use *both* a narrow-band source *and* a narrow-band detector. Finally, the ability of graphene to transform the frequency spectra and generate harmonics may be used for the creation of new devices for microwave, terahertz and far-infrared optoelectronics.

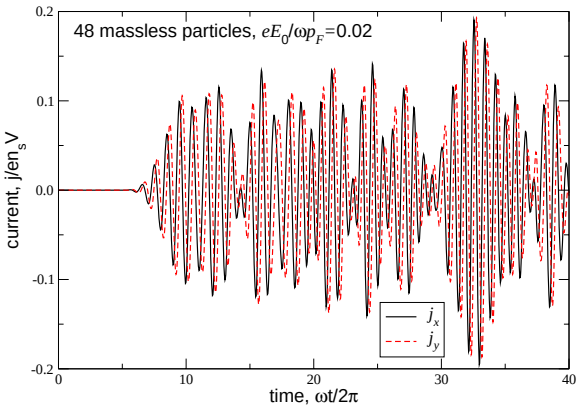

Figure 1: Time dependence of the current j in a system of 48 massless quasiparticles at the harmonic excitation of the system by the field $E_0 \cos\omega t$. It is assumed that the particles are Fermi-distributed in the $\mathbf{p}$-space at $t = 0$ and that the electric field is zero at $\omega t/2\pi < 5$ and smoothly grows up to a constant value at $5 < \omega t/2\pi < 10$. The frequency of the external field corresponds to the cyclotron resonance condition $\omega = eBV^2/\omega\mu$.

Graphene opens up a lot of interesting opportunities in both the fundamental and applied electrodynamics.

References

[1] S. A. Mikhailov, Europhys. Lett. **79**, 27002 (2007).

[2] S. A. Mikhailov and K. Ziegler, J. Phys. Condens. Matt. **20**, 384204 (2008).

[3] S. A. Mikhailov, arXiv:0812.0855.

AC transport properties of single and bilayer graphene

J. Z. Bernad*, U. Zülicke* and K. Ziegler**
*Institute of Fundamental Sciences and MacDarmid Institute for Advanced Materials and Nanotechnology, Massey University (Manawatu Campus), Palmerston North, New Zealand
** Institut für Physik, Universität Augsburg, Augsburg, Germany

Keywords: optical conductivity of graphene, trigonal warping, dephasing from continuous quantum measurement

We present a theoretical study of electronic transport in single and bilayer graphene based on the standard Kubo formalism [1, 2] and continuum-model descriptions of the graphene band structure. We are focusing especially on the interband (i.e., Zitterbewegung) contribution to the optical conductivity $\sigma(\omega)$. Analytical results are obtained for a variety of situations, which allow clear identification of features in $\sigma(\omega)$ that are associated with relevant electronic energy scales such as inter-layer hopping and voltage bias (for a bilayer), and trigonal warping (for the single-layer case). See Figs. 1 and 2 for an illustration. Our work extends previous numerical studies [3] and elucidates ways to infer electronic properties of graphene samples from optical-conductivity measurements [4].

Motivated by recent interest in mesoscopic-transport effects in graphene samples, we have developed a theory of how a continuous quantum measurement of electrical current affects the conductivity of single-layer graphene. Generalizing standard methods in the field [5], we find that the coupling to a quantum current detector induces a finite conductivity in the dc limit. Based on this result, we suggest that intrinsic quantum dephasing can be the origin of a nonuniversal minimal conductivity in graphene.

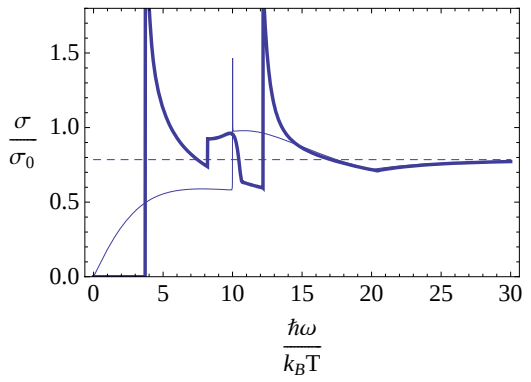

Figure 1: Optical conductivity $\sigma(\omega)$ of clean bilayer graphene with chemical potential at the symmetry point and a finite bias voltage between the layers (thick solid curve). The zero-bias case is shown as the thin solid curve. The dashed line indicates the value $\pi/4$.

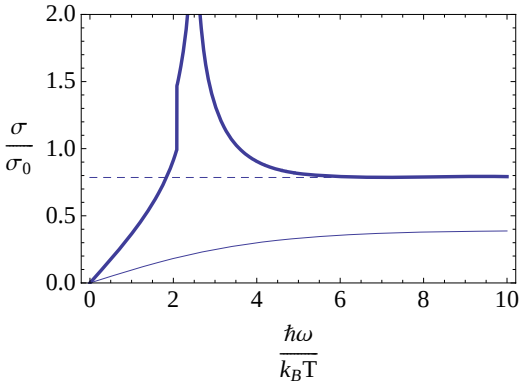

Figure 2: $\sigma(\omega)$ of clean single-layer graphene with chemical potential at the symmetry point and trigonal warping (thick solid curve). The Dirac-model case is shown as the thin solid curve, and the dashed line indicates $\pi/4$.

References

[1] See, e.g., O. Madelung, *Introduction to Solid-State Theory* (Springer, Berlin, 1978).

[2] S. Ryu *et al.*, Phys. Rev. B **75**, 205344 (2007); K. Ziegler, *ibid.* 233407 (2007).

[3] N. M. R. Peres, F. Guinea, and A. H. Castro Neto, Phys. Rev. B **73**, 125411 (2006); E. J. Nicol and J. P. Carbotte, *ibid.* **77**, 155409 2008); J. Nilsson *et al.*, *ibid.* **78**, 045405 (2008).

[4] Z. Q. Li *et al.*, Nat. Phys. **4**, 532 (2008); Phys. Rev. Lett. **102**, 037403 (2009); F. Wang *et al.*, Science **320**, 206 (2008).

[5] K. Jacobs and D. A. Steck, Contemp. Phys. **47**, 279 (2006).

Energy splitting between bright and dark excitons in carbon nanotubes

T. Oshima, K. Matsuno and H. Suzuura
Division of Applied Physics, Graduate School of Engineering, Hokkaido University, Sapporo, Japan

Keywords: carbon nanotubes, bright and dark excitons

Photophysics of carbon nanotubes have attracted a great deal of attention, where the excitons play a dominant role reflecting one-dimensionality[1]. What characterizes the unique physical properties in graphenes and carbon nanotubes is the electronic state described by the massless Dirac particle and its valley degeneracy also generates a rich variety of physics. From the viewpoint of optical properties, the degeneracy causes the fine structure of excitons which should be determined in detail to understand optical responses. In this paper, we have studied the structure dependence of the energy splitting between bright and dark excitons in semiconducting carbon nanotubes.

Short-range part of the Coulomb interaction gives rise to the valley mixing and, as a result, four spin-singlet states are split into one bright and three dark excitons. Two of the dark states consist of electron-hole pairs created by inter-valley transitions. We only focus on the bright exciton and the other dark one, that is to say, the bonding and anti-bonding states of two intra-valley excitons belonging to the K and K' points. Recent experimental studies have revealed that the energy of the bright exciton for the lowest-subband transitions (which we call E_{11} transitions) is higher than that of the dark exciton[2, 3], while a theoretical study on the valley mixing by Ando indicates that the small energy splitting compared to that of the excitons is highly sensitive to the model for the interaction potential between electrons and holes and that the two energy positions of the bright and dark excitons can be interchanged by controlling the parameter in the model potential[4]. Actually, it is still an open problem whether the bright exciton for higher-subband transitions (E_{22}, E_{33}, and so on) should also have higher energy than the dark one does or not.

First, we have theoretically studied exciton states and calculated absorption spectra for semiconducting zigzag nanotubes by using the simplest tight-binding model for π-electrons within the Hartree-Fock approximation. In a similar manner to previous studies, we adopt the Ohno potential for the interaction

$$V(\boldsymbol{R}) = \frac{e^2}{4\pi\varepsilon\sqrt{|\boldsymbol{R}|^2 + (e^2/4\pi\varepsilon U)^2}}$$

where U is the cut-off energy for short-range distance. It is certain that the energy of the bright exciton is higher than that of the dark exciton in the large U limit, while the energy splitting monotonically decreases and becomes negative for smaller U, or the former energy can be lower than the latter. This behavior basically agrees with that in the previous study on the E_{11}-excitons by using the effective-mass equations[4] and our calculations have shown that this is the case with the excitons for higher-subband transitions.

What should be stressed here is that the sign of the bright-dark splitting in E_{11}-excitons can be different from that in E_{22}-excitons in a certain range of U dependent on the nanotube structure. Furthermore, we have found that this sign changes can be classified into two types and that what we call family pattern can clearly explain such a classification. On the assumption that the bright exciton is higher than the dark one for E_{11}-transitions, the bright exciton can be lower than the dark one for E_{22}-transitions in nanotubes of one family type, while that cannot be the case with the other family. We also discuss the family pattern in the bright-dark splitting with the effective-mass equations taking the effect of trigonal warping into account in order to clarify the mechanism.

References

[1] T. Ando, J. Phys. Soc. Jpn. **66**, 1066 (1997).

[2] B. Mortimer and R. J. Nicholas, Phys. Rev. Lett. 98, 027404 (2007).

[3] R. Matsunaga et al., Phys. Rev. Lett. 101, 147404 (2008).

[4] T. Ando, J. Phys. Soc. Jpn. **75**, 024707 (2006).

Density of states of Landau subbands in disordered graphene

X. R. Wang[1], Wei Zhu[2] and Qin Wei Shi[2]

[1] Physics Department, The Hong Kong University of Science and Technology, Clear Water Bay, Hong Kong SAR, China
[2] Hefei National Laboratory for Physical Sciences at Microscale, University of Science and Technology of China, Hefei 230026, China

The shape of the density of states (DOS) of Landau subbands of a disordered 2D Schrödinger electron gas in a strong magnetic field is a well-studied subject both theoretically and experimentally for a long time. Based on the self-consistent Born approximation (SCBA), the shape of the DOS was argued to be the well-known semi-circular form. Later, Wegner predicted that the shape of the lowest LL is Gaussian-like in the strong-field limit and with white-noise random potential. The supersymmetry method reaches similar conclusions. However, the shape of disorder-broadened Landau subbands for Dirac electrons is less well studied because the Dirac electrons are thought for long time irrelevant to condensed matter physics. The situation changed when graphene became accessible experimentally. This is because Dirac electrons emerges from the ordinary Schrödinger electrons near the two inequivalent corners K and K' of the first Brillouin zone in graphene, owing to the linear dispersion spectrum.

Similar to the 2D Schrödinger electrons, 2D Dirac electron states in a perpendicular uniform magnetic field B also form highly degenerated discrete Landau levels (LLs). Instead of the equally spaced LLs found with the Schrödinger electrons, the LLs of 2D Dirac electrons are unevenly distributed. Due to electron-hole symmetry, the LLs are symmetrically distributed above and below zero energy that is also one of the LLs. Similar to the Schrödinger electrons, each LL broadens into a Landau subband in the presence of disorders. Based on a tight t the tight-binding formulation for the pi-electrons of a graphene, we shown numerically that LLs are indeed unevenly distributed around zero energy according to the spectrum of a Dirac electron. In order to obtain an accurate averaged DOS, the system size should be large enough so that the Lanczos recursive method is used. The averaged DOS can be evaluated by

$$\rho(E) = \mathrm{Im}\overline{\left\langle \psi \left| \frac{1}{E - H + i\nu} \right| \psi \right\rangle},$$ where

$|\psi\rangle$, H, and ν are electron state, the system Hamiltonian and an infinitesimal positive number, respectively. The bar denotes the ensemble average. In the presence of disorders, we show numerically that the zero-energy Landau subband has a Gaussian shape. The width and the peak height depend on both the strength of the disorder and magnetic field. Not surprisingly, the width is proportional to randomness while the peak is inversely proportional to the randomness. Surprisingly, both the width and the peak are proportional to the square root of the magnetic field. Furthermore, they do not depend on the band index. The Wegner-type calculation is used to understand our simulation results.

References

[1] W. Zhu, Q.W. Shi, X.R. Wang, J. Chen, J.L. Yang, and J.G. Hou, Phys. Rev. Lett. 102, 056803 (2009).

Shot noise and transport in graphene: from large strips to nanoribbons

R. Danneau[*,†,‡], F. Wu[*], A. Fay[*], M. F. Craciun[♭,♮], S. Russo[♭,♮], M. Y. Tomi[*], J. B. Oostinga[♭,♯], J. Wengler[*], J. Salmilehto[*], A. F. Morpurgo[♭,♯] and P. J. Hakonen[*]

[*] *Low Temperature Laboratory, Helsinki University of Technology, Finland*

[†] *Institut für Nanotechnologie, Forschungszentrum Karlsruhe, Germany*

[‡] *Physikalisches Institut, Universität Karlsruhe, Germany*

[♭] *Kavli Institute of Nanoscience, Delft University of Technology, The Netherlands*

[♮] *Department of Applied Physics, University of Tokyo, Tokyo, Japan*

[♯] *Département de Physique de la Matière Condensée, Université de Genève, Switzerland*

Keywords: Shot noise, Graphene, Evanescent waves, Electron-phonon coupling, Nanorribons

We have investigated shot noise in graphene strips with large width over length ratio as well as graphene etched nanoribbons in the temperature range of 4.2–30 K at low frequency (f = 600–850 MHz). We measured gate dependent current fluctuations in short graphene strips with large and small W/L. At the Dirac point, i.e. where the conduction and the valence band touch, we observed that for large W/L both minimum conductivity and Fano factor reach universal values of $\frac{4e^2}{\pi h}$ and 1/3, respectively [1]. For W/L smaller than 3, the Fano factor is lowered and the minimum conductivity increases. These findings are well explained by the evanescent wave theory describing transport at the Dirac point in perfect graphene [2, 3]. We observed that the effect of the disorder increases the minimum conductivity and lowers the Fano factor [4] which is in a good agreement with [5]. At large bias, both conductivity and the Fano factor are reduced which may be due to optical phonon-electron coupling [6].

By reducing the width of a graphene sheet to form a constriction or a nanoribbon, one may open a energy gap [7]. Experiments demonstrate that a gap appears in graphene nanoribbons (GNR), however its physical origin remains unclear.

We also performed shot noise measurements in etched GNR. We observed a Fano factor very close to zero and nearly-independent of the carrier density. This is the value expected for ballistic systems but also when the scattering length is much shorter than the length of the sample. In etched GNRs, edges are not perfect and the dangling bonds may lead to magnetic state which should lower the Fano factor. It has been seen that shot noise can be reduced by inhomogeneities in hopping transport [8]. We analyze our findings within this frame. Our results are consistent with a model with localized states presumably arising from rough edges and adsorbed molecules [9].

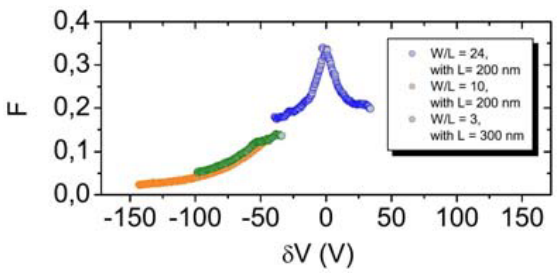

Figure 1: Fano factor versus $\delta V = V_{gate} - V_{Dirac}$ for three different samples with large W/L.

References

[1] R. Danneau *et al.*, Phys. Rev. Lett. **100**, 196802 (2008).

[2] M.I. Katsnelson, Eur. Phys. J. B **51**, 157 (2006).

[3] J. Tworzydło *et al.*, Phys. Rev. Lett. **96**, 246802 (2006).

[4] R. Danneau *et al.*, J. Low Temp. Phys. **153**, 374 (2008).

[5] P. San-Jose *et al.*, Phys. Rev. B, **76** 195445 (2007).

[6] A. Fay *et al.*, to be published.

[7] K. Nakada *et al.*, Phys. Rev. B **54**, 17954 (1996).

[8] V.V. Kuznetsov *et al.*, Phys. Rev. Lett. **85**, 397 (2000).

[9] R. Danneau *et al.*, to be published.

Unexpected current distribution in graphene ribbon with zigzag edges

D. Yoshioka*, S. Nakakura* and Y. Nagai**
*Department of Basic Science, The University of Tokyo, Tokyo, Japan
** Department of Physics, The University of Tokyo, Tokyo, Japan

Keywords: graphene, edge state, electric current

Graphene is a zero gap semiconductor. It is well known that the dispersoin around the Fermi level has a form of massless Dirac fermion; the density of states vanishes at $E = 0$, the band center. However, at the zigzag edge of a sample, there appears electric states localized there with energy $E = 0$[1], and for a sample with finite width, a peak in the density of states appears at $E = 0$. These states localized around edges (edge states) contribute mainly to electric conduction, when the Fermi level is at $E = 0$.

Since the edge states are localized around edges, it may be expected that the current due to these states also flow near the edges. However, it has been shown that the current actually flows in the entire sample, the current density showing maximum at the center of the ribbon[2]. In this paper we clarify the reason for this current distribution. In this paper we consider single electron states, and neglect electron correlation effects, which can be quite important for actual systems.

We consider the electronic states of graphene π-band by a tight binding model, in which only nearest neighbor hopping is taken into account. We consider a ribbon that extends in the x-direction and has a finite width in the y-direction, which is bordered by zigzag edges parallel to the x-direction. We consider this system as collection of zigzag chains. On each chain A and B sublattices alternate. The amplitude of wave function on A and B sublattice in the m-th chain at x is written as $A_m \exp(\mathrm{i}kx)$ and $B_m \exp(\mathrm{i}kx)$, respectively, k being wave number. We consider a lattice in which B sublattice in the m-th chain is connected with A sublattice in the $m+1$-th chain. Then the tight binding equations for this system are

$$ctA_m + tA_{m+1} = EB_m \quad (1)$$

$$tB_m + ctB_{m+1} = EA_{m+1} \quad (2)$$

where $c = 2\cos(ka/2)$, t is the hopping parameter, a is lattice constant, and E is the energy eigenvalue.

When the width is infinitely wide, this equation have solutions at $E = 0$ for $(2\pi/3) < ka \leq \pi$. One of the solution has $A_m = [-2\cos(k/2)]^{m-1}A_0$, and $B_m = 0$. This is the edge state localized around the lower edge. Similar edge states at the upper edge exists in which only $B_m \neq 0$. For a finite width ribbon, symmetric and anti-symmetric combinations of these edge states are the approximate eigenstates with energy $E(k) \simeq \pm tc^w(1-c^2)$.

The current flowing along the m-th chain is given by

$$j_m = \frac{2et}{\hbar} A_m B_m \sin(ka/2) \quad (3)$$

For any eigen states we obtained the following relation between j_m's using eqs.(1) and (2):

$$j_{m+1} - j_m = \frac{eE}{\hbar}(A_{m+1}^2 - B_m^2) \quad (4)$$

For the edge states, $A_m > B_m$ ($B_m > A_m$) in the lower (upper) half of the ribbon, this equation shows that the current has maximum value at the center of the ribbon. From this equation we also notice that the current becomes uniform as $E \to 0$, or $k \to \pi/a$. This uniform current distribution is also understood from the wave function. At $k \to \pi/a$, the coupling between the edge states becomes small, thus $A_m = (-c)^{m-1}A_0$, and $B_m = \pm(-c)^{w-m}A_0$ is a good approximation to the wave function. Then $j_m = (2et/\hbar)A_0^2 c^{w-1}\sin(ka/2)$ is independent of m. This result clarifies the reason for uniform current. The wave function of the edge state has large value only on one of the sublattices, and current is given by the product of large and small amplitudes.

In summary we have shown that the current due to the edge state flows in the bulk of the ribbon, and clarified the reason.

References

[1] M. Fujita, K. Wakabayashi, K. Nakada and K. Kusakabe: J. Phys. Soc. Jpn. **65**, 1920 (1996).

[2] L.P. Zârbo and B.K. Nikolić. EPL, **80** (2007) 47001.

How ideal can graphene be?

P. Neugebauer, M. Orlita, C. Faugeras, Anne-Laure Barra, and M. Potemski
National High Magnetic Field Laboratory - Grenoble, CNRS, France

Keywords: Graphene, graphite, Landau level spectroscopy

Fabrication of graphene structures has triggered vast research efforts focused on the properties of 2D systems with massless Dirac fermions. Nevertheless, further progress in exploring this quantum electrodynamics system in solid-state laboratories seems to be limited by insufficient electronic quality of manmade structures and the crucial question arises whether existing technologies have reached their limits or major advances are in principle possible. Here we show that graphene in a significantly purer state can be found in nature on the surface of bulk graphite, in form of flakes decoupled from the substrate material. Probing such flakes with Landau level (LL) spectroscopy in the THz range at very low magnetic fields, we demonstrate a superior electronic quality of these ultra low density layers ($n_0 \approx 3 \times 10^9$ cm^{-2}) expressed by the carrier mobility in excess of 10^7 cm^2/(V.s). This finding represents an important challenge for further improvements of current graphene technologies.

A typical example of our experimental finding is illustrated in Fig. 1a, where the derivative of the magneto-absorption spectrum of decoupled graphene on the surface of a natural graphite specimen at $T = 25$ K, measured as a function of the magnetic field at a fixed microwave frequency. The interpretation is schematically illustrated in part (b). The observed spectral lines are assigned to cyclotron resonance transitions between adjacent LLs with energies: $E_n = \mathrm{sign}(n)\tilde{c}\sqrt{2e\hbar B|n|}$, characteristic of massless Dirac fermions in graphene sheets with an effective Fermi velocity $\tilde{c}$. This velocity is the only adjustable parameter required to match the energies of the observed and calculated CR transitions and reaches $\tilde{c} = (1.00 \pm 0.02) \times 10^6$ m.s^{-1}.

Since the well-defined LL quantization in our graphene flakes is observed down to $|B| = 1$ mT we obtain via the semi-classical LL quantization condition $\mu B > 1$ the carrier mobility $\mu > 10^7$ cm^2/(V.s), almost two orders of magnitude higher in comparison to any other reported values. The scattering time $\tau \approx 20$ ps derived from the typical CR width in our spectra also significantly exceeds values reported in any kind of graphene samples. This scattering time gives an independent estimation for the mobility $\mu = e\tau\tilde{c}^2/E_F \approx 3 \times 10^7$ cm^2/(V.s) in good agreement with the estimate above.

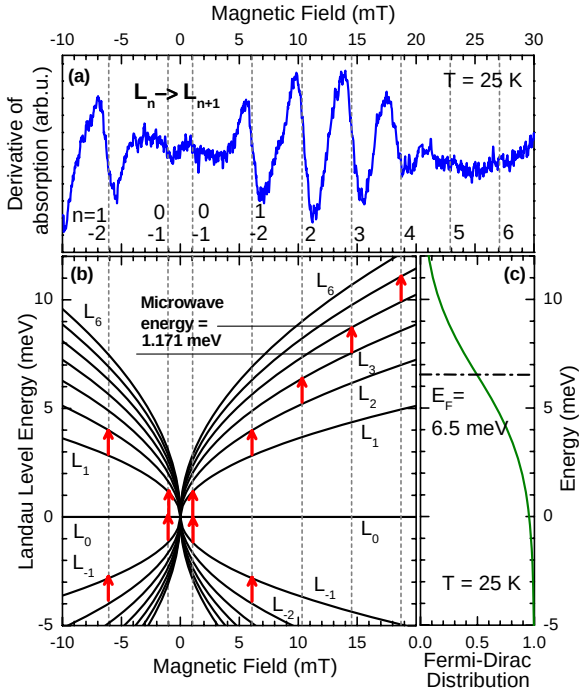

Figure 1: Derivative of magneto-absorption spectrum measured at $T = 25$ K and microwave frequency $\hbar\omega = 1.171$ meV (a) in comparison with the LL fan chart (b), where the observed CR transitions are shown by arrows. The occupation of individual LLs is given by the Fermi-Dirac distribution plotted in the part (c). The dashed lines show positions of resonances assuming $\tilde{c} = 1.00 \times 10^6$ m.s^{-1}.

Transport properties of graphene prepared on a hydrophobic self-assembled layer

M. Lafkioti , T. Lohmann, B. Krauss, K. v. Klitzing, J. H. Smet

Max Planck Institute for Solid State Research, Stuttgart, Germany

Keywords: Graphene, QHE, doping, hydrophobic self-assembled layer

Graphene has attracted considerable interest since its isolation by Novoselov *et al*. in the year 2004 [1]. A large part of this interest stems from the Dirac particle behaviour of the charge carriers and the unusual quantum Hall effect (QHE) occurring even at room temperature [2]. However, the properties of graphene prepared by micromechanical cleavage on SiO_2 appear to be highly dependent on the ambient conditions. Measurements on free-hanging graphene and theoretical studies have suggested that the substrate as well as adsorbates such as water are pivotal for the final sample properties [3, 4].

Obtaining a chemically well-defined template with low adsorbate concentration is therefore a key to achieve better and more reproducible quality in graphene. Here, we have deposited a hydrophobic self-assembled layer (SAL) on top of an oxidized Si substrate. The SAL inhibits the organization or clustering of dopants, especially water molecules, on the substrate and hence should provide a high quality template for graphene deposition.

Room temperature field effect measurements indeed confirm a considerable reduction of the influence of ambient conditions on the sample properties. Using these templates, we reproducibly obtain low doping, typically a factor of 10 lower than for graphene prepared on untreated substrates. A further important indicator for the presence of adsorbed water molecules is hysteresis in the field effect data at room temperature. This has been known from the studies of carbon nanotubes [5]. Graphene samples prepared on SiO_2 indeed show hysteresis, but hysteresis is absent for graphene deposited on top of the hydrophobic SAL (s. Fig.1). Furthermore the transport properties are evidently improved. The carrier mobility is on average higher and we observe a substantial gain in the quality

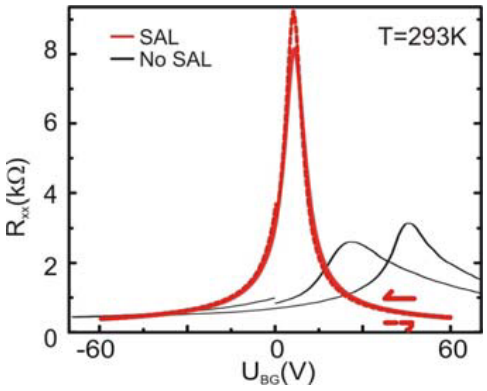

Fig.1 Room temperature field effect data for graphene on SiO_2 with (red curve) and without (black curve) a hydrophobic template.

of the Shubnikov-de Haas (SdH) and QHE data recorded at T = 1.7 K. SdH oscillations can be observed up to filling factors as large as 50. This corroborates that water significantly influences the transport properties of graphene samples and thus reducing its adsorption consistently improves their quality.

References

1. K. S. Novoselov, A. K. Geim, S. V. Morozov, D. Jiang, Y. Zhang, S. V. Dubonos, I. V. Grigorieva, and A. A. Firsov, Science 306, 666 (2004)
2. K. S. Novoselov, Z. Jiang, Y. Zhang, S. V. Morozov, H. L. Stormer, U. Zeitler, J. C. Maan, G. S. Boebinger, P. Kim, A. K. Geim, Science 315, 1379 (2007)
3. K. I. Bolotin, K. J. Sikes, Z. Jiang, M. Klima, G. Fudenberg, J. Hone, P. Kim, H. L. Stormer, Solid State Communications 146, 351 (2008)
4. T. O. Wehling, M. I. Katsnelson and A. I. Lichtenstein, Appl. Phys. Lett. 93, 202110 (2008)
5. W. Kim, A. Javey, O. Vermesh, Q. Wang, Y. Li, H. Dai, Nanoletters 3, 193 (2003)

Screening properties of monolayer and randomly stacked graphenes

Masaki Noro, Mikito Koshino, and Tsuneya Ando
Department of Physics, Tokyo Institute of Technology, 2–12–1 Ookayama, Meguro-ku, Tokyo 152-8551, Japan

Keywords: graphene, dielectric screening, image effect, perfect screening

In an effective-mass approximation, an electron in a graphite monolayer or graphene is described by Weyl's equation for a massless neutrino. Transport properties in such an exotic electronic structure are quite intriguing and have theoretically been investigated for some time [1], demonstrating that the system exhibits various characteristic behaviors different from conventional two-dimensional systems. Quite recently, this single layer graphene was fabricated using the so-called scotch-tape technique and the magnetotransport was measured including the integer quantum Hall effect, demonstrating the validity of the neutrino description of the electronic states. In this paper, we show that atomically thin graphene works as a dielectric shield that strongly screens external potential.

In previous papers, the dielectric screening of monolayer graphene has been studied within the effective-mass approximation [2], and the screening has been shown to exhibit behavior significantly different from that in conventional two-dimensional systems. In fact, the polarization function for vanishing Fermi wave vector k_F is proportional to wave vector q and its effect can be incorporated as an effective dielectric constant as large as ~ 6 [2]. For nonzero k_F, the polarization function for small q becomes nonzero and independent of q up to $\sim 2k_F$, giving rise to relatively small corrections.

As a result, graphene works as a strong dielectric shield where the field produced by a charged object placed above is always screened by a constant factor ~ 6 on the other side of graphene. Further, the object is attracted by an image force as if there exists its mirror image on the other side of graphene. For the demonstration we consider the potential distribution of a point charge with $+e$ placed on graphene with distance d, for example. The calculated potential distribution is shown in Fig. 1 as a function of the vertical position.

In multi-layer graphenes with incommensurate lattice orientations such as those fabricated on SiC substrates [3], direct interaction between adjacent layers is negligible because of cancellation [4]. In this case, the dielectric screening in monolayer graphene can directly be applicable for calculations of the potential distribution. The results shown in Fig. 1 show clearly that the external potential is screened almost completely by a few layers of graphenes. This is quite analogous to self-consistent results for multi-layer graphenes with a commensurate lattice structure [5].

References

[1] T. Ando, Physica E **40**, 213 (2007) and references cited therein.
[2] T. Ando, J. Phys. Soc. Jpn. **75**, 074716 (2006).
[3] J. Hass et al., Phys. Rev. Lett. **100**, 125504 (2008).
[4] S. Uryu and T. Ando, Phys. Rev. B **72**, 245403 (2005).
[5] F. Guinea, Phys. Rev. B **75**, 235433 (2007).

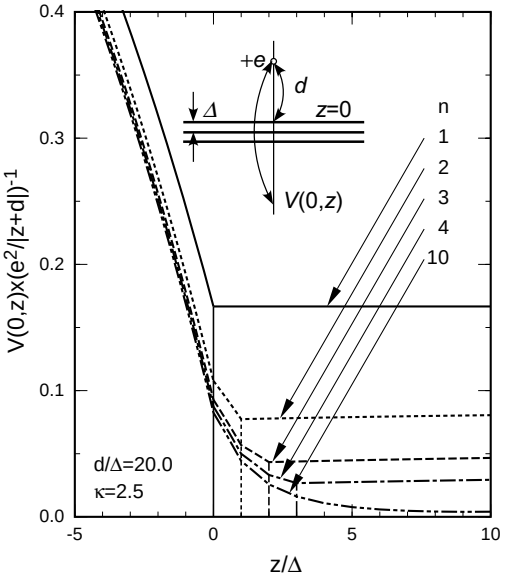

Figure 1: Calculated potential distribution in the vertical direction when a charge $+e$ is placed on top of graphene with distance $d/\Delta = 20$ for different layer numbers n, where Δ is the distance between adjacent monolayer graphenes. The potential at each point is normalized by that in the absence of graphene. $k_F = 0$.

Orbital diamagnetism in non-uniform magnetic fields in graphene

Mikito Koshino, Yasunori Arimura, and Tsuneya Ando
Department of Physics, Tokyo Institute of Technology, Tokyo, Japan

Keywords: graphene, diamagnetism

Graphene, an atomic sheet of graphite, has a peculiar electronic structure analog to a relativistic particle, and its unique properties have been of great interest. In a uniform magnetic field, it is known that graphene exhibits a huge and singular diamagnetic susceptibility due to the orbital motion of electrons, which is quite different from the conventional Landau diamagnetism [1, 2].

In this paper, we present a theoretical study of the electronic response in the presence of a spatially varying magnetic field. Using the effective mass approximation and the perturbation theory, we calculate the electric current induced by an external magnetic field with wavenumber q, to obtain susceptibility $\chi(q)$. We apply the result to arbitrary geometries where a certain magnetic object is located above graphene, and estimate the response current induced on graphene, as well as the diamagnetic repulsive force which works between graphene and the magnetic object.

For $k_F = 0$, in particular, we have $\chi(q) \propto q^{-1}$. Surprisingly, for nonzero q, the susceptibility suddenly starts from zero at $q = 2k_F$ and rapidly approaches the curve for $k_F = 0$. This shows that no electric current is induced when the external field is smooth enough compared to the Fermi wavelength. As a function of Fermi energy ε_F at fixed q, it is nonzero only in a finite region satisfying $|\varepsilon_F| < \hbar v q/2$ with v being the electron velocity, and its integral over ε_F becomes a constant. This agrees with the susceptibility against uniform magnetic field [1, 2].

We find that, unlike the conventional two-dimensional electron system, graphene with small Fermi wave number k_F works as a magnetic shield where the field produced by a magnetic object placed above graphene is always screened by a constant factor on the other side of graphene. The object is repelled by a diamagnetic force from the graphene, as if there exists its mirror image with a reduced amplitude on the other side of graphene. The magnitude of the force is incomparably greater than that of conventional two-dimensional system. The effect disappears with the increase of k_F.

References

[1] J. W. McClure, Phys. Rev. **104**, 666 (1956).

[2] M. Koshino and T. Ando, Phys. Rev. B **75**, 235333 (2007).

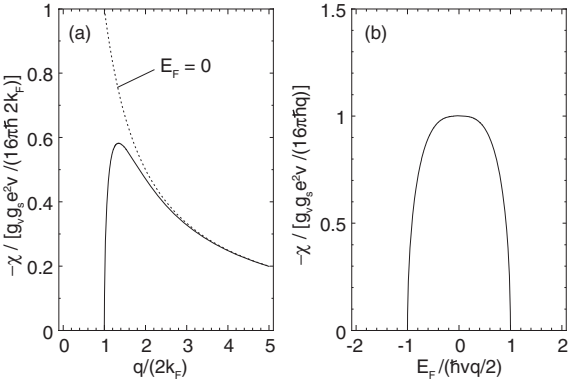

Figure 1: Magnetic susceptibility $\chi(q\,;\varepsilon_F)$ in graphene plotted against (a) q with fixed Fermi energy ε_F, and (b) ε_F with fixed q.

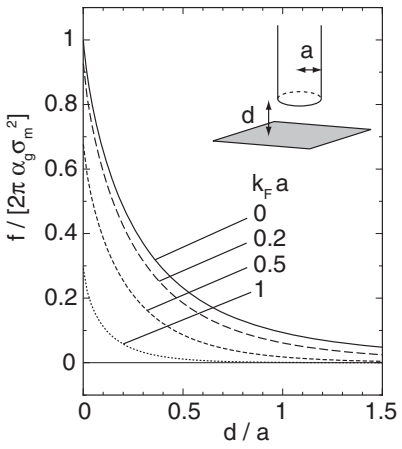

Figure 2: Diamagnetic force per unit area of a semi-infinite magnet cylinder with radius a as a function of the distance d from the tip to graphene.

Transport gap in graphene constrictions

F. Molitor, C. Stampfer, A. Jacobsen, J. Güttinger, S. Hellmüller, T. Ihn and K. Ensslin

Solid State Physics Laboratory, ETH Zurich, 8093 Zurich, Switzerland

Keywords: Graphene nanostructures, constrictions

We present transport measurements on side gated graphene constrictions of different sizes. We distinguish two different energy scales characterizing the transport gap: its extension in back gate voltage $\Delta V_{gap,BG}$ and the extension in bias direction $E_{gap.}$, and show a linear dependence between the two parameters. We present a model explaining the origin of the gap. Finally we show that high side gate voltage lift the complete suppression of the current in the gap, and show the presence of edge states in the constriction in high magnetic fields.

Fig. 1(a) shows a typical conductance measurement as a function of applied back gate and bias voltage. A diamond-shaped region of suppressed conductance, the so-called transport gap, can be seen. It can be characterized by two parameters: its extension in back gate voltage, $\Delta V_{gap,BG}$, and the extension in bias direction $-eV_{bias}=E_{gap}$. The back gate voltage can be converted to energy using a plate capacitor model and the graphene density of states. The bias voltage is a direct measure of the internal energy scale of the system. These two energy scales differ by more than one order

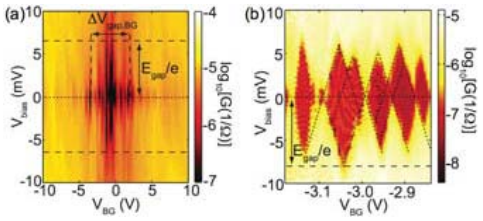

Fig.1 Conductance as a function of bias and back gate voltage for a constriction of width W=85 nm and length L=500 nm.

of magnitude. A closer look at the region of suppressed conductance shows that it consists of individual diamond-shaped regions, sometimes overlapping as in the case of Coulomb blockade (Fig. 1(b)).

Fig. 2(a) shows $\Delta V_{gap,BG}$ as a function of the constriction width. It decreases for increasing width or decreasing length. A negative value of $\Delta V_{gap,BG}$ results from the way of defining the gap size, and means that the conductance is not completely suppressed. Fig. 2(b) displays the gap size in bias direction E_{gap} as a function of $\Delta V_{gap,BG}$. E_{gap} increases linearly with $\Delta V_{gap,BG}$. The

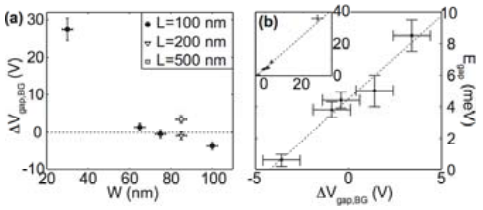

Fig.2 (a) $\Delta V_{gap,BG}$ as a function of the constriction width. (b) E_{gap} as a function of $\Delta V_{gap,BG}$.

formation of the transport gap, and its different energy scales, can be explained by a model taking into account disorder and a quantum confinement gap in the constriction. This is expected to lead to the formation of electron and hole puddles, separated by real tunnel barriers instead of Klein tunnelling. Within this model, $\Delta V_{gap,BG}$ is related to the region in Fermi energy where the transport at the Fermi energy is governed by localization, and is a measure for the amplitude of the potential fluctuations due to disorder. E_{gap} is related to the charging energy of the individual islands, and therefore to their size.

Further we show that the application of a high side gate voltage (about 15 V) lifts the complete suppression of the current in the gap.

Finally, we study the effect of an applied magnetic field and show the presence of edge states in the constriction.

References

1. F. Molitor et al., Phys. Rev. B **79**, 075426 (2009)
2. C. Stampfer et al., Phys. Rev. Lett. **102**, 056403 (2009)

Magnetoconductivity in graphene Corbino devices

Dong-Hun Chae, Timm Lohmann, Klaus von Klitzing and Jurgen H. Smet

Max-Planck-Institute for Solid State Research, Stuttgart, Germany

Keywords: Graphene, Corbino, Scattering mechanism, PN-junction

We present a study of the magnetoconductivity of graphene as a function of the carrier density in the Corbino geometry. Far away from the charge neutrality point, current is carried by a single charge carrier type (holes or electrons). The inverse of the conductivity measured in this annular geometry then exhibits a quadratic magnetic field dependence as in conventional 2D electron systems with a single carrier type, for which the Drude description holds. Using the Drude formula, the transport relaxation time is extracted as a function of gate voltage. The carrier density dependence of the transport relaxation time implies that long-range Coulombic disorder may not be the prime source of scattering far away from the neutrality point. This fuels the controversial debate on the importance of long range Coulomb scattering in graphene [1].

Motivated by the work on lateral graphene pn-junctions [2-4], graphene bipolar junctions were also fabricated in the edgeless Corbino geometry. The ``fractional'' conductance plateaus observed in lateral bipolar junctions at high magnetic fields can be explained in terms of edge channel equilibration near the junction [2,3]. Such measurements do not reveal intrinsic properties of the junction itself. The electronic transport in Corbino devices is not expected to be dominated by edge channel equilibration. Here we have studied this case where the two regions have different carrier densities and/or carrier types.

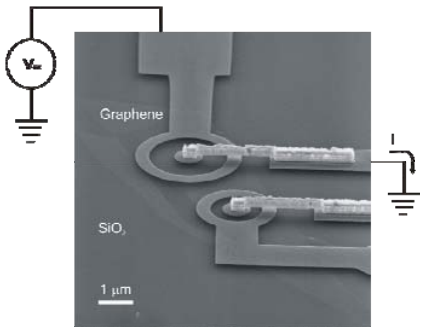

Fig.1 Scanning electron microscope image of a graphene Corbino device with a central contact connected through an airbridge.

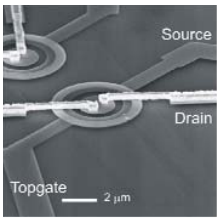

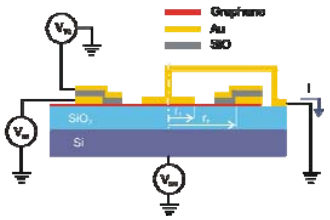

Fig.2 Top-gated graphene Corbino device. A schematic cross-section is shown on the right.

Reference

[1] Y.W. Tan, Y. Zhang, K. Bolotin, Y. Zhao, S. Adam, E.H. Hwang, S. Das Sarma, H.L. Stormer, and P.Kim, Phys. Rev. Lett. 99, 246803 (2007)

[2] J.R.Williams,L. DiCarlo, and C.M. Marcus, Science, 317, 638 (2007)

[3]B.Oezyilmaz,P.Jarillo-Herrero,D.Efetov,D.A.Abanin, L.S. Levitov, and P.Kim, Phys. Rev. Lett., 99, 166804 (2007)

[4] B.Huard, J.A. Sulpizio, N. Stander, K.Todd, B.Yang, and D. Goldhaber-Gordon, Phys. Rev. Lett., 98, 236803 (2007)

Quasi-Periodic Conductance Fluctuations in Few-Layer Graphene

S. Motooka[1], Y. Ujiie[1], N. Aoki[1], Y. Ochiai[1], D. K. Ferry[2] and J. P. Bird[3]

[1]*Graduate School of Advanced Integration Science, Chiba University, 1-33 Yayoi-cho, Inage-ku, Chiba 263-8522, Japan*

[2]*Department of Electrical Engineering and Center for Solid State Electronics Research, Arizona State University, Tempe, Arizona 85287-5706, USA*

[3]*Department of Electrical Engineering, University at Buffalo, the State University of New York, Buffalo, NY 14260-1920, USA*

Keywords: Graphene, quantum dots, conductance fluctuations

Quantum transport behaviour has long been of basic interest, and, most recently, electrical transport in graphene has been reported and noted for its elementary transport properties that are strongly influenced by the linear energy spectrum and the chirality of its charge carriers. Among the studies, there have been reports of using magneto-transport measurements to probe the chiral carriers, for example in studies of the quantum Hall effect [1, 2], weak localization [3], universal conductance fluctuations [4] and the Aharonov-Bohm (AB) effect [5].

In this study, we report on the low-temperature magneto-transport in a sub-micron sized few-layer graphene sample. At temperatures below a degree of Kelvin, as shown in Fig. 1, the graphene exhibits quasi-periodic conductance fluctuations across a wide range of magnetic field. The periodic nature is confirmed by their Fourier power spectra which consist of well-pronounced peaks at a few isolated magnetic frequencies. These observations are in marked contrast to the behavior expected for the universal conductance fluctuations [4], in which strongly aperiodic fluctuations yield a dense series of overlapping Fourier peaks [6]. The quasi-periodic fluctuations should not be related to the AB effects [5], since our device does not feature a ring-like geometry.

We show that there could exist a small number of periodic orbits in the graphene [7], which give rise to the quasi-periodic fluctuations by means of dynamical tunneling [8]. Furthermore, in our graphene quantum dot, the contact channel between the lead metal and the few-layer graphene should serve as an important region. Our studies therefore point to the need to clarify the origin of the electron inlet and outlet channels, so as to allow their practical device applications, and to also provide an understanding of the role of contact effects in carbon nanotubes.

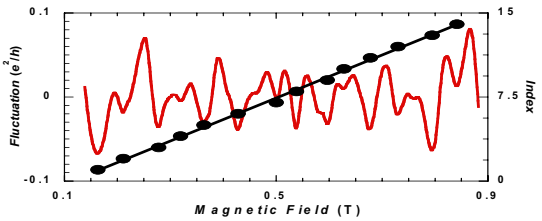

Fig. 1. Spacing of the successive minima in the fluctuations.

References

1. K. S. Novoselov, et al., Nature, 438, 197 (2005).
2. Y. Zhang, et al., Nature 438, 201 (2005).
3. S. V. Morozov, et al., Phys. Rev. Lett., 97, 016801 (2006).
4. N. E. Staley, et al., Phys. Rev., B77, 155429 (2008).
5. S. Russo, et al., Phys. Rev., B77, 085413 (2008).
6. R. P. Taylor, et al., Surf. Sci., 196, 52 (1988).
7. R. Akis, et al., Appl. Phys. Lett., 81, 129 (2002).
8. A.P.S. de Moura, et al., Phys. Rev. Lett., 88, 236804 (2002)

Toward chaotic electron transport in bismuth nanocluster wires

M. S. Fairbanks[1], T. P. Martin[2], B. C. Scannell[1], C. A. Marlow[1], S. A. Brown[3] and R. P. Taylor[1]

[1] *Department of Physics, University of Oregon, Eugene OR, USA*

[2] *School of Physics, University of New South Wales, Sydney, Australia*

[3] *Department of Physics and Astronomy, University of Canterbury, Christchurch, New Zealand*

Keywords: chaos, electron transport, bismuth, nanoclusters

Future generations of nanoscale electronic devices will require both new approaches to fabrication and new models of transport physics at the nanometer scale. One novel fabrication technology is the deposition of nanoscale metallic or semiconducting clusters formed by inert gas aggregation. This versatile "self-assembly" fabrication technique can be used to create electronic circuits and devices from the 'bottom-up' in contrast to traditional 'top-down' lithography [1].

Here we consider bismuth nanoclusters, where the 5nm thickness is smaller than the Fermi wavelength (~10nm) [2], such that transport is expected to be confined to a 2D plane. By depositing into etched grooves in the substrate, the clusters can be further confined to wires with widths as low as the cluster diameter. In contrast to the straight walls of wires defined by traditional lithography techniques, a key characteristic of these self-assembled wires is the significant variation of the wire width along the wire's length (see Figure 1).

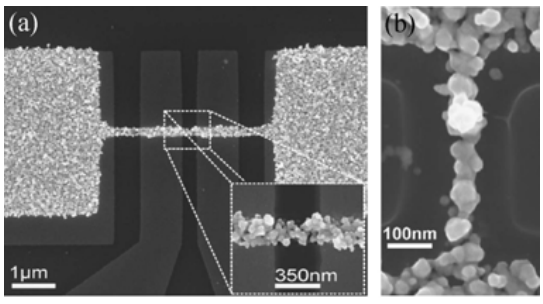

Figure 1. Two examples of bismuth nanocluster wires. (a) shows a wire contacted by a 4-terminal configuration of Ti/Au contacts. (b) demonstrates a narrower wire in a 2-terminal configuration.

We present a generic electron transport model for self-assembled wires, in which this intrinsic variation in width produces an array of connected cavities. Based on previous experiments performed on micron-scale 2D cavities [3], scattering sites in the material are expected to act as Sinai diffusers that induce chaotic dynamics in the electron trajectories. The role of the cavity walls is to reflect the trajectories repeatedly through these scatterers, generating a fractal behavior in the semi-classical wave interference. This manifests itself as a power-law spectral density in the magnetoconductance fluctuations.

Whereas observation of these fractal fluctuations have been limited to temperatures below 100K for micron-sized systems, we show that the material parameters of the smaller (30 - 50nm) cavities lead to the prediction that fluctuations will be observed at significantly higher temperatures approaching room temperature for the self-assembled wires. We discuss the potential consequences of realizing this inherently quantum phenomenon at high temperatures for applications related to quantum coherent devices.

References

1. J. G. Partridge, D. M. A. Mackenzie, et al., Microelect. Eng. **83**, 1460 (2006); R. Reichel, J. G. Partridge, et al., Appl. Phys. Lett. **89**, 213105 (2006).

2. B. Hackens, J. P. Minet, et al., Phys. Rev. B **67**, 121403(R) (2003).

3. C. A. Marlow, R. P. Taylor, et al., Phys. Rev. B **73**, 195318 (2006).

Transport properties of quantum dot with thermally decomposited graphene

S. N. Ko*, Y. Y. Lee*, M. H. Son*, M. S. Lee*, J. H. Oh*, C. Jeon**, W. Song**, C.-Y. Park**, S.-W. Lee***, B. H. Park***, and D. Ahn*

* *Institute of Quantum Information Processing Systems, University of Seoul, Seoul, Korea*

** *BK21 Physics research division & CNNC, Sungkyunkwan University, Suwon, Korea*

*** *Department of Applied Physics, Konkuk University, Seoul, Korea*

Keywords: epitaxial graphene, quantum dot, transport property, Raman spectroscopy

Recently, graphene has been intensively studied as a potential candidate for the next generation of silicon based device. Unlike the conventional semiconductor materials, graphene has no band gap, called Dirac point, and unique properties like electron-hole degeneracy and vanishing electron mass at the charge neutral point. Most of the studies on graphene reported so far were using exfoliated graphene from highly ordered pyrolytic graphite (HOPG). However, the method has drawbacks such as its low yield in exfoliating single layer graphene and difficulty in to obtaining a large area graphene. Recently, thermal decomposition of SiC substrate growth of graphene was proposed in order to obtain large area graphene layer with reproducibility [1].

In this work, we have investigated transport properties of graphene quantum dot structure. The mono- and bi- layer graphene has been synthesized on (0001) semi-insulating 6H-SiC substrate by heating up to 1200 ^{o}C in UHV chamber. The size of the synthesized graphene layer was 2x7 mm^2.

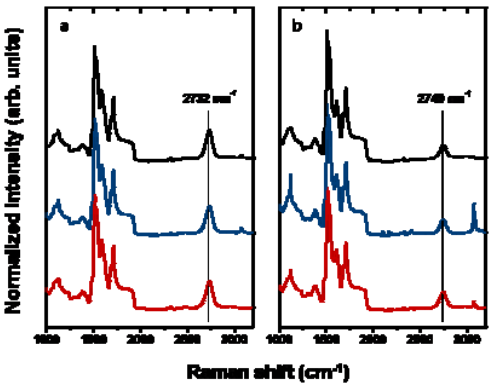

Fig. Raman spectra of epitaxial graphene with mono-layer (a) and bi-layer (b) epitaxial graphene on silicon carbide substrate measured at room temperature.

The synthesized graphene layers were investigated using micro-Raman spectroscopy at room temperature. Figure (a), (b) shows Raman spectra of the mono-layer and bi-layer graphene layers measured at 3 different places, respectively. As Ferrari *et al.* mentioned in order to distinguish mono-, bi-, and few-layer, it is important to focus on 2D Raman peak which stems from electron-phonon double resonance scattering process [2]. The 2D Raman peaks shows the different intensity between mono- and bi-layer graphene. Furthermore, the 2D peaks are well isolated from the SiC peaks and exist at around 2730-2750 cm^{-1}.

For the fabrication of the graphene quantum dot structure, a standard photolithography and electron-beam lithography were used to construct desired pattern followed by oxygen plasma etching to isolate the path of the electron or hole [3-5]. And then we will discuss on low temperature transport properties of graphene dot structure on SiC substrate.

References

1. C. Berger *et al.*, Science **312**, 1191 (2006).
2. A. C. Ferrari *et al.*, Physical Review Letters **97**, 187401 (2006).
3. X. Lu *et al.*, Applied Physics Letters **75**, 193 (1999).
4. S. Schnez *et al.*, Applied Physics Letters **94**, 012107 (2009)
5. C. Berger *et al.*, Science **312**, 1191 (2006).

Negative terahertz dynamic conductivity in electrically induced lateral p-i-n junction in graphene

V. Ryzhii*, M. Ryzhii*, M. S. Shur**, and V. Mitin***
*Computational Nanoelectronics Laboratory, University of Aizu, Aizu-Wakamatsu and Japan Science and Technology Agency, Tokyo, Japan
**Department of Electrical, Electronics, and Systems Engineering, Rensselaer Polytechnic Institute, Troy, USA
***Department of Electrical Engineering, University at Buffalo, Buffalo, USA

Keywords: Graphene, tunneling, transit-time effect, terahertz,

We propose a device based on a gated graphene structure with electrically induced lateral p-i-n juction - graphene tunneling transit-time diode (GT-diode) and study its high-frequency characteristics. The GT-diode under consideration utilizes the interband tunneling and the pertinent generation of electrons and holes in the i-section of the gapless graphene channel. The GT-diode structure and its band diagram are shown in Fig. 1. The structure consists of a graphene layer (channel) supplied with the source and drain contacts. The bias voltages of different polarity , $V_p < 0$ and $V_n > 0$, provide in the formation of the p- and n-sections, respectively, with the i-section in between. The electric field in the latter section results in the interband tunneling producing electrons and holes propagating across the i-section and inducing the transient currents in highly conducting p- and n-sections.

We demonstrate that due to the electron and hole transit-time effects in the i-section, the dynamic conductivity can

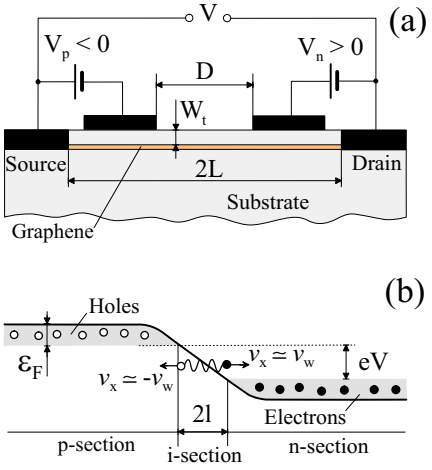

Figure 1: Schematic view of a GT-diode (a) and its band diagram under applied bias voltages (b).

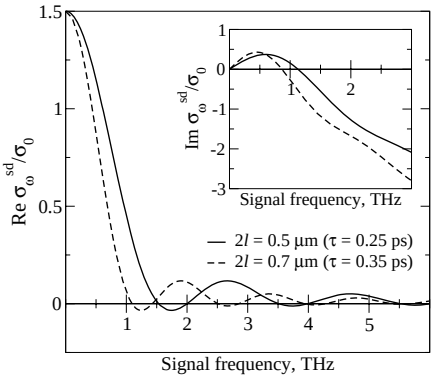

Figure 2: Real part and imaginary part (inset) of the GT-diode dynamic conductivity σ_ω^{sd}.

be negative in the THz range of frequencies. Indeed, the source-drain (terminal) dynamic conductivity as a function of the signal frequency ω calculated using the developed GT-diode model is given by

$$\sigma_\omega^{sd} = \frac{3\sigma_0}{2}\left[\frac{e^{i\omega\tau}\mathcal{J}_0(\omega\tau) - 1}{i\omega\tau}\right] - i\omega\, C, \qquad (1)$$

where σ_0 is the dc conductivity, C is the lateral p-i-n junction capacitance, $\mathcal{J}_0(\xi)$ is the Bessel function, τ is the electron and hole transit time across the i-section. As seen from this equation, both the real and imaginary parts of σ_ω^{sd} have different signs in certain frequency ranges. Examples of the Reσ_ω^{sd} and Imσ_ω^{sd} frequency dependences for different lengths of the i-section $2l$ (different electron and hole transit times) are shown in Fig. 2.

The GT-diode can work as an active element of a THz oscillator with a complementary resonant cavity. It also can generate THz radiation owing to the self-excitation of the plasma oscillations (plasma instability) in the gated p- and n-sections. In the latter case, the two-dimensional electron and hole plasmas in these section play the role of the resonant cavities.

Disorder-induced pseudodiffusive transport in graphene nanoribbons

P. Dietl*, G. Metalidis*, D. Golubev*,**, P. San-Jose***, E. Prada***, H. Schomerus***, G. Schön*,**
*Institut für Theoretische Festkörperphysik and DFG Center for Functional Nanostructures (CFN), Universität Karlsruhe, D-76128 Karlsruhe, Germany
**Forschungszentrum Karlsruhe, Institut für Nanotechnologie, 76021 Karlsruhe, Germany
***Department of Physics, Lancaster University, Lancaster, LA1 4YB United Kingdom

Keywords: graphene, adsorbates, pseudodiffusive transport

We study the transition from ballistic to diffusive and localized transport in graphene nanoribbons in the presence of binary disorder, which can be generated by chemical adsorbates or substitutional doping [1]. We base our investigation on the following tight-binding Hamiltonian,

$$H = -t \sum_{\langle i,j \rangle} c_i^\dagger c_j + \sum_i v_i c_i^\dagger c_i. \qquad (1)$$

The first term describes clean graphene with hopping between nearest neighbors on the hexagonal lattice. The second term describes disorder, generated by onsite energies v_i which take values $v_i = V_0$ with probability p, and $v_i = 0$ with probability $1 - p$.

Utilizing the numerical recursive Green's function technique, we show that the interplay between the induced average doping (arising from the non-zero average of the disorder) and impurity scattering modifies the traditional picture of phase-coherent transport. Close to the Dirac point, intrinsic evanescent modes localized around impurities dominate transport at short lengths, giving rise to a new regime analogous to pseudodiffusive transport in clean graphene [2]. The conductivity of a sufficiently wide sample aquires the universal value $2e^2/\pi^2\hbar$ in this regime. The intrinsic pseudodiffusive regime precedes the traditional ballistic, diffusive and localized regimes. The last two regimes exhibit a strongly modified effective number of propagating modes, and a mean free path which becomes anomalously large close to the Dirac point.

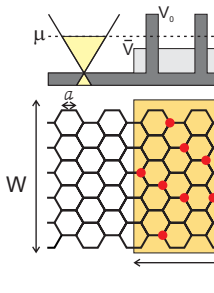

Figure 1: Schematic view of an armchair ribbon with width W. Disorder is introduced in a region of length L by adding a potential V_0 to a percentage p of lattice sites. Disorder sites are depicted by red dots. The induced local doping, due to the non-zero average of the disorder, is effectively described by a barrier of height $\bar{V} = pV_0$.

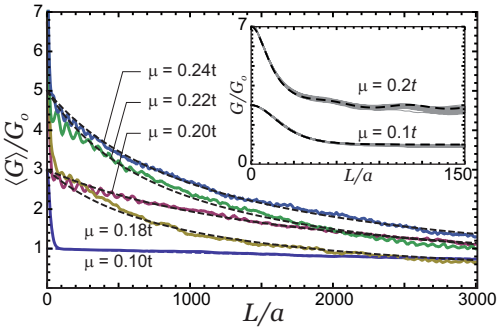

Figure 2: Averaged conductance $\langle G \rangle$ (in units $e^2/\pi\hbar$) of an armchair ribbon of width $W = 103\sqrt{3}a/2$ ($a = 1.49$ Å is the length of C-C bond) as a function of the length of the disordered region for different chemical potentials. The parameters of the binary disorder are $p = 0.4$, $V_0 = 0.25t$. Dashed curves are fits to the formula $G = G_0/(1 - L/l_m)$ with l_m as a fit parameter. Inset: Pseudodiffusive regime zoom-in. Good agreement is obtained with the ballistic conductance through a square potential barrier of height $\bar{V}$, shown in dashed black.

References

[1] Petra Dietl, Georgo Metalidis, Dmitri Golubev, Pablo San-Jose, Elsa Prada, Henning Schomerus, Gerd Schn, arXiv:0902.1928.

[2] J. Tworzydlo, B. Trauzettel, M. Titov, A. Rycerz, and C. W. J. Beenakker, Phys. Rev. Lett. **96**, 246802 (2006).

Interacting electrons in semiconducting carbon nanotube quantum dots: calculation of the excited states by exact diagonalisation.

Mervyn Roy and P. A. Maksym
Department of Physics and Astronomy, University of Leicester, Leicester, LE1 7RH, United Kingdom.

Keywords: nanotubes, quantum dots

Semiconducting nanotube (SNT) dots are very different to traditional semiconductor quantum dots and we investigate the quantum states of these novel, quasi-1D, systems computationally. We calculate the states of a few interacting electrons by exact diagonalisation of a new 2-band effective mass Hamiltonian and investigate the previously unstudied electronic excitations in detail. We find evidence for quasi-1D strongly correlated electron behaviour in a surprisingly wide range of SNT dots.

Our model is based on a gated SNT dot that has been studied experimentally [1]. In our model, electrons are confined electrostatically near the tube centre and the 1D confinement is harmonic. We describe the states of such a dot with an effective mass theory and there are new features that arise from the SNT band structure. We derive our SNT states from a basis of the 2-component graphene Bloch states and this introduces additional terms into our effective mass theory for interacting electrons in a SNT dot. The net result is a one dimensional 2-band Hamiltonian with a modified effective Coulomb interaction.

We calculate the states of 2 to 6 interacting electrons by exact diagonalisation of this Hamiltonian. We investigate the ground and excited states for a wide range of dots with different physical parameters and find that, in a large proportion of these dots, the electrons are strongly correlated. In the strongly correlated regime we can describe the electron states with a simple molecular approximation in which each electron is strictly localised on its own Wigner lattice site: we separate the Hamiltonian into centre of mass (CM) and relative motion (RM) parts and expand the relative motion potential to second order about its minimum. Within this approximation the RM excitations should all be equally spaced in energy and, in the strongly correlated regime, we find that this is the case to within a few percent. For example in a 10,0 SNT dot with a harmonic confinement energy $\hbar\omega = 2.0$ meV and dielectric constant $\epsilon_r = 4.1$ (see Fig. 1) the 2-electron ground state energy and first 3 RM excitations are given to within 4.6% by the molecular approximation.

The degeneracy of the levels and relative ordering of the excitations is also interesting. If we ignore the very weak interaction between electrons in different bands the levels become multi-degenerate due to the equivalence of the spin and band quantum numbers. In this case, for example, all the levels in a 2-electron dot are 4-fold degenerate. In the strongly correlated regime these sets of 4 levels are arranged in pairs that are close in energy, but are split due to tunnelling between the Wigner lattice sites. We estimate the tunnelling probability within the molecular model with the WKB approximation and find this is small (< 0.01 for the 2 electron ground state) in a surprisingly large range of SNT dots. Here, the molecular model is accurate to within a few % and the electrons in the SNT dot behave like quasi-1D Wigner-molecules.

References

[1] P. Jarillo-Herrero, *et al*, Nature **429**, 389 (2004).

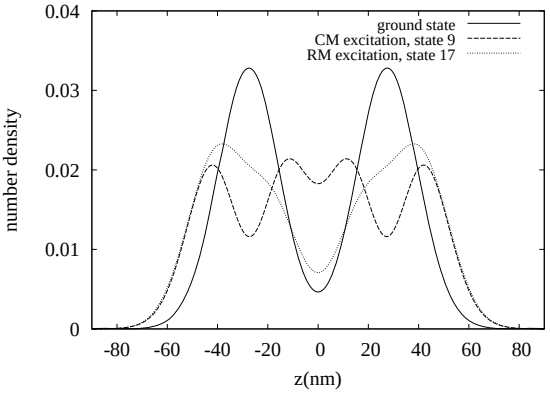

Figure 1: Exact 2-electron number density in a 10,0 SNT dot ($\hbar\omega = 2.0$, $\epsilon_r = 4.1$). Ground state and first CM and RM excitations are shown: states 1 ($E_1 = 10.2$ meV), 9 ($E_9 = 15.1$ meV), and 17 ($E_{17} = 16.7$ meV).

Transport and electron scattering time in single and bilayer graphene as probes of the nature of impurity scattering.

M. Ferrier*, M. Monteverde*, C. Ojeda*, R.Weil*, S. Gueron*, H. Bouchiat*, J.N. Fuchs*, D. Maslov*,**
* Univ. Paris-Sud, CNRS, UMR 8502, F-91405 Orsay Cedex, France
** University of Florida Gainesville, FL 32611, USA

Keywords : graphene, quantum transport

Both transport τ_{tr} and elastic scattering times τ_e are experimentally determined from the carrier density dependence of the magnetoconductance of monolayer and bilayer graphene. Both times and their dependences in carrier density are found to be very different in the monolayer and the bilayer. However their ratio is found to be of the order of 1.5±0.1 in both systems and independent of the carrier density. These measurements give insight on the nature (neutral or charged) and spatial extent of the scattering centers. Comparison with theoretical predictions yields that the main scattering mechanism in our graphene samples could be due to strong scatterers of short range inducing resonant scattering; the most likely candidate being vacancies.

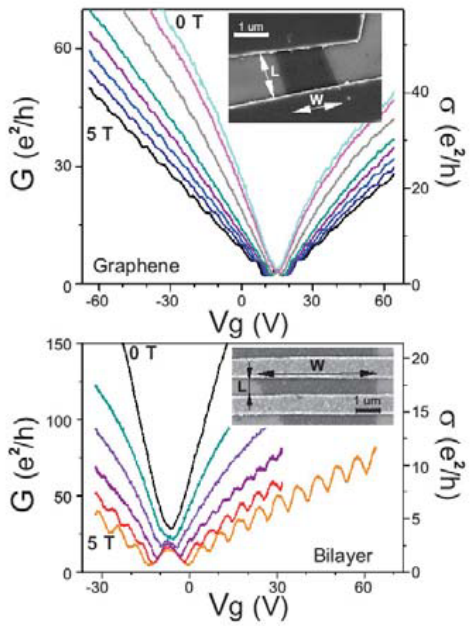

Gate voltage dependence of the conductance measured for several values of magnetic field spaced by 0.5 T. The contact resistances have been subtracted. Top panel: monolayer. Bottom panel: bilayer. the insets are electron micrographs of the measured samples.

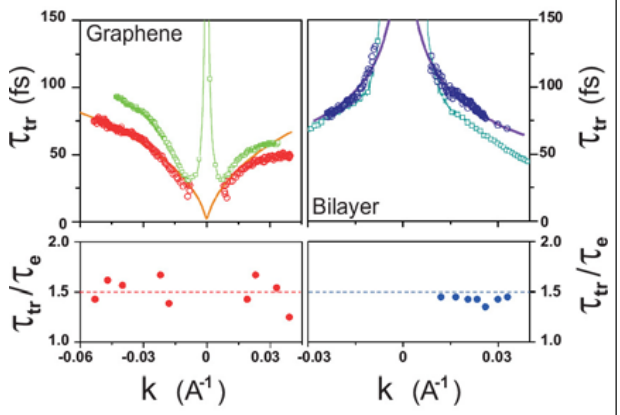

Fermi wavevector dependence of τ_{tr} extracted from the B^2 dependence of the low field quadratic magnetoresistance (dark circles) in comparison with the value τ_{tr} extracted from the sole zero field Drude conductivity (light circles). The continuous lines are the fits according to the resonant impurity model. Left panel: monolayer. Right panel: bilayer. Upper curves: ratio τ_{tr} / τ_e deduced from the low temperature exponential decay of the SdH oscillations.

Observation of carrier relaxation and recombination dynamics in optically pumped epitaxial graphene heterostructures

T. Watanabe*, H. Karasawa*, T. Komori*, M. Suemitsu***, V. Ryzhii****, T. Otsuji***

** Research Institute of Electrical Communication, Tohoku University, Sendai, Japan*
*** Department of Computer Science and Engineering, University of Aizu, Aizu-Wakamatsu, Japan*
**** JST-CREST, Tokyo, Japan*

Keywords: graphene, carrier, relaxation, population inversion

Linear dispersion relations for the electron/hole energy spectra with zero energy band gap in graphene [1] provide nontrivial features like negative-dynamic conductivity in far infrared and terahertz (THz) spectral ranges [2]. Due to ultrafast optical phonon emission $\tau_0 \approx 10^{-12}$s , the photogeneration of electrons/holes leads to the emission of a cascade of optical phonons, so that the photoelectrons and photoholes occupy the states with the energies close to $\varepsilon_N = \hbar(\Omega/2 - N\omega_0) < \hbar\omega_0$, where $\hbar\Omega$ the pumping photon energy, $\hbar\omega_0$ the optical phonon energy, and N the number of emitted optical phonons. As a consequence, photoelectrons/holes recombine to radiate THz photons with the energy $\hbar\omega = 2\varepsilon_N$ (inset in Fig. 1(a)) [1]. The incident photon spectra will reflect on the THz photoemission spectra as a proof of occurrence of such a cascading process.

We observed the carrier relaxation and recombination dynamics in optically pumped epitaxial graphene heterostructures using THz emission spectroscopy. An ultra-thin graphene layer was grown by the thermal decomposition of an 80-nm-thick 3C-SiC film heteroepitaxially grown on a B-doped Si(110) substrate [3]. Its 2D-band Raman spectra proven the existence of mono- and bilayer of graphene, and the G-band spectra at 1595 cm^{-1} corresponds to the optical phonon energy of 198 meV [3]. A 1550-nm, 20-MHz, 80-fs pulsed fibre laser beam (Fig. 1) was impinged to the sample (normal to the surface).

Time-resolved electric-field intensity originated from the THz photon emission was electrooptically sampled in total-reflection geometry [4]. Measured temporal profile (inset in Fig. 2) exhibited frequency-up/down chirped relaxation oscillation, and was damped in an exponential decay on the order of ~10 ps corresponding to the relaxation of radiative electron-hole recombination. Its Fourier spectra roughly trace the pumping photon spectra (Fig. 2). The spectral drop below 2 THz in the lower side-lobe might be caused by the band-gap opening due to existing bilayer graphene with the built-in vertical potential slope arisen at the heterointerface.

In summary, we experimentally observed the fast relaxation and relatively slow recombination dynamics of photogenerated electrons/holes in an epitaxial graphene heterostructure. The result supports the occurrence of negative dynamic conductivity leading to the population inversion for a new type of THz lasers.

References

1. K.S. Novoselov, A.K. Geim, S.V. Morozov, D. Jiang, M.I. Katsnelson, et al., Nature **438**, 197 (2005).
2. V. Ryzhii, M. Ryzhii, and T. Otsuji, J. Appl. Phys. **101**, 083114 (2007).
3. M. Suemitsu, Y. Miyamoto, H. Handa, and A. Konno, e-J. Surface Sci. and Nanotech. (in press).
4. T. Otsuji, Y.M. Meziani, M. Hanabe, T. Nishimura, and E. Sano, Solid State Electron. **51**, 1319 (2007).

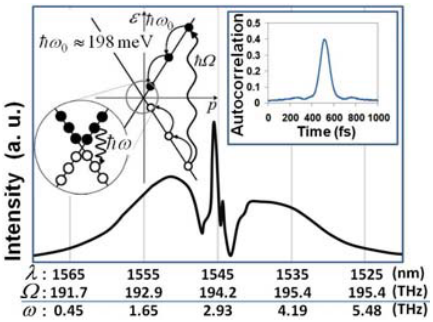

Fig. 1 Carrier relaxation/recombination in optically pumped graphene. Pumping laser profiles are shown.

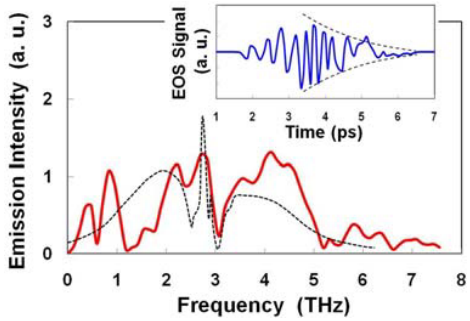

Fig. 2 Measured temporal profile (inset) and its Fourier spectrum. Dashed line is for pumping laser.

Phonon-mediated heat flow in heterostructure nanowires via electron-phonon interaction

J. E. Matthews*, E. A. Hoffmann*, H. A. Nilsson†, L. A. Samuelson†, H. Linke*†

*Department of Physics and Materials Science Institute, University of Oregon, Eugene, OR 97403, USA

†Solid State Physics/The Nanometer Structure Consortium, Lund University, Box 118, S-221 00 Lund, Sweden

Keywords: electron-phonon, phonon-mediated, nanowire

For research and applications dependent on controlling heat flow in nanowires, e.g. thermoelectrics and thermal management in electronics, the mechanisms capable of adding and removing heat from an electron reservoir must be understood. One such mechanism capable of doing both is electron-phonon (e-ph) interaction. The literature on e-ph interaction in nanowires, however, is limited[1,2]. Here we study the effects of e-ph interaction on the flow of heat in heterostructure nanowires.

Quantum dot thermometry experiments were first carried out using the technique developed in Ref [3] – see figure 1 for a device schematic. In our experiments, the electron temperature rises, ΔT_s and ΔT_d, were measured in the vicinity of a quantum dot. Based on concurrent measurements showing low electrical conductance, and hence low electronic thermal conductance via the Wiedemann-Franz Law, a naïve model would predict $\Delta T_s \approx \Delta T_{HC}$ and $\Delta T_d \approx \Delta T_{DC} \approx 0$. However measurements show $\Delta T_s \approx c\Delta T_d$, where c is of the order 2. Thus a mechanism other than diffusive electronic heat flow is heating the drain electrons.

To understand this rise in ΔT_d, we use finite element analysis to model the experimental system. Of the heat flow mechanisms considered, we show that phonon-mediated heat flow between the source and drain electron reservoirs via e-ph interaction is the dominant contributor to heat flow into the drain electron reservoir. Using this model, we obtain qualitative agreement between simulations and experiments by tuning the model parameters. The two results in conjunction then have the ability to predict quantitative information about e-ph interaction in nanowires.

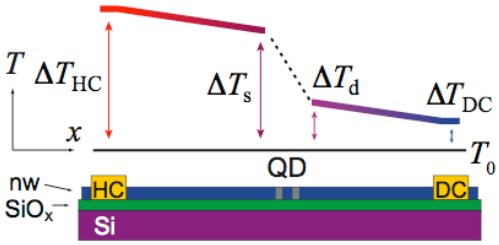

Fig.1 Schematic of the heterostructure nanowire with contacts and electron temperature profile. The nanowire (nw) is comprised of InAs with two InP barriers defining a quantum dot (QD). Electrical measurements are made using the heating (HC) and drain (DC) contacts. The heating contact is also used to apply a temperature gradient along the nanowire. The source and drain electron temperature rises, ΔT_s and ΔT_d respectively, are measured using the thermometry technique developed in Ref [3].

References

1. Sugaya T. et al., Appl. Phys. Lett., **81**, 727 (2002)
2. Vartanian A.L. et al. Phys. Stat. Sol. (b) **245**, 963 (2008)
3. Hoffmann, E. A. et al., Nano Lett. **9**, 779 (2009)

Electron confinement in single layer graphene quantum dots

G. Giavaras**, P. A. Maksym*, and M. Roy*
*Department of Physics and Astronomy, University of Leicester, Leicester LE1 7RH, UK
**Department of Materials, Oxford University, Oxford OX1 3PH, UK

Keywords: Graphene, Quantum Dot

The quantum states of electrons in a graphene quantum dot are investigated theoretically. The dot is formed from an external potential applied to a graphene sheet in the presence of a perpendicular magnetic field. Because the graphene charge carriers are massless the behaviour of this system is completely different from that of a conventional electrostatic dot: both confined (Fig. 1, right) and deconfined (Fig. 1, left) 2-component states occur *at similar energies* [1]. The conditions for each type of state are given and states are computed for model potentials and a realistic device model. The physics of these states corresponds to the quantum Klein paradox.

Here the unusual quantum physics of graphene charge carriers is related to the unusual classical dynamics of massless, charged particles which move at constant speed c. There is an exact correspondence between the classical motion (insets to Fig. 1) and the quantum states: confined states correspond to bounded classical orbits and deconfined states correspond to a situation where bounded and open orbits occur at the *same energy*. This is in complete contrast to the classical Kepler case where bounded and open orbits have *different energies*. The form of the orbits depends on the angular momentum, $m\hbar$. Unusual, nearly closed orbits occur when $m < 0$ (insets to Fig. 2).

The classical calculations give a good prediction of the regions where the quantum states are large. This insight into the physics is used to develop a semi-classical approximation to the energy levels of the confined states. In many cases, the approximation agrees well with the numerically computed quantum states and explains the node distributions found in the numerical data. The semi-classical approach also gives simple analytic formulas for the energy levels which agree with the numerical data to within a few % or better (Fig. 2).

The experimental consequences of the theory are that specific conditions must be satisfied to confine electrons in a graphene dot. Since these conditions depend on the strength of the potential and the magnetic field, it is possible to fabricate a dot where the form of the states can be changed at will by adjusting the potential or magnetic field. A dot design suitable for this experiment is presented and ways of probing the state character via transport or STM are discussed. These experiments would give insight into the unique physics of classical massless, charged particles, which do not occur naturally, as well as insight into the unique quantum states of graphene dots.

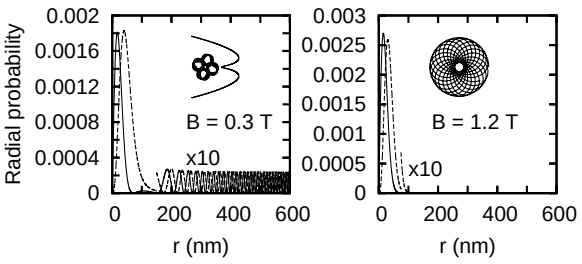

Figure 1: 0.3 T: deconfined state, bounded orbit and unbounded orbit. 1.2T: confined state and bounded orbit. Orbits scaled and shifted for clarity.

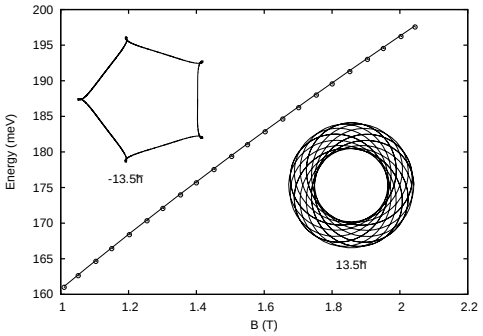

Figure 2: Exact (line) and approximate (circles) energies for $m = 10$. Insets: orbits for negative and positive m.

References

[1] G. Giavaras, P. A. Maksym and M. Roy, J. Phys. Condens. Mat. **21**, 102201 (2009).

Time-resolved single-electron counting in a graphene quantum dot

J. Güttinger, J. Seif, A. Capelli, C. Stampfer, K. Ensslin, T. Ihn
Solid State Physics Laboratory, ETH Zurich, Switzerland

Keywords: graphene, quantum dots, charge detection

We present low-temperature time-resolved charge counting experiments on a graphene quantum dot coupled capacitively to a graphene charge detector (see Fig. 1 for an image of the sample). The quantum dot is connected to a source and a drain contact and shows a typical Coulomb-blockade addition spectrum when single electrons are added with increasing plunger gate (pg) voltage. In our experiments the tunneling coupling to the drain contact is unmeasurably small and only tunneling between the source contact and the dot is relevant. The charge detector is a narrow graphene constriction [1] which exhibits broad conductance resonances as a function of the constriction gate (cg). The detector is sensitive to the addition of individual electrons to the quantum dot on the slopes of these resonances. A single quantum dot electron changes the conductance of the detector by about 20 percent. Close to the degeneracy of a quantum dot level with the electrochemical potential in the source contact we observe single-electron tunneling events between the dot and the lead in real time using the charge detector (Fig. 2). The statistical analysis of such random telegraphic signals allows us to determine the tunneling rates, the occupation statistics of the lead states, and the tunneling coupling strength between dot and source contact.

We find that the decay of each of the two charge states follows an exponential law as expected for a quantum tunneling process. The measured occupation statistics of the leads resembles the Fermi-distribution function within measurement accuracy and allows us to extract the electronic temperature of the source electrons. The results are of particular relevance for the current discussion about the nature of electron transport through narrow constrictions and the related energy scales.

The results are comparable to well controlled quantum dot systems with integrated charge read-out in GaAs heterostructures [2]. The results pave the way to a whole class of new experiments in graphene, for example, to the realization of a single-shot charge read-out for future graphene-based qubits, and for measurements of the full counting statistics of transport through graphene quantum dots.

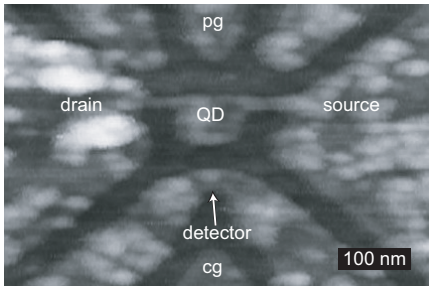

Figure 1: Scanning force microscope image of the all-graphene structure. Dark gray regions correspond to etched trenches, brighter regions are on the graphene surface which is partially covered by processing residues. The quantum dot (QD) is connected to a source and a drain contact via narrow and long constrictions in order to keep the tunneling rates low. The detector consists of a graphene constriction coupled capacitively to the quantum dot.

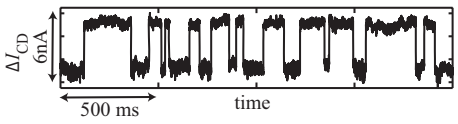

Figure 2: Change in charge detector current measured as a function of time in a situation where the quantum dot level is nearly resonant with the electrochemical potential in the source contact. The two distinct current levels correspond to the two charge states of the quantum dot.

References

[1] J. Güttinger, C. Stampfer, S. Hellmüller, F. Molitor, T. Ihn, K. Ensslin, Appl. Phys. Lett. **93**, 212102 (2008).

[2] R. Schleser, E. Ruh, T. Ihn, K. Ensslin, D.C. Driscoll, A.C. Gossard, Appl. Phys. Lett. **85**, 2005 (2004) .

Tuning the proximity effect in a superconductor-graphene-superconductor junction

C. M. Ojeda-Aristiz`abal, M. Ferrier, S. Gueron and H. Bouchiat

Laboratoire de Physique des Solides, Univ. Paris-Sud, CNRS, UMR 8502, F-91405, Orsay, France

Keywords : graphene, proximity effect

We have tuned in situ the proximity effect in a single graphene layer coupled to two Pt/Ta superconducting electrodes.
The superconductor-graphene-superconductor junction (SGS) was fabricated with exfoliated graphene deposited on a doped silicon substrate with a 285 nm thick oxide, which allows the visual detection with an optical microscope, while providing a capacitively coupled gate electrode. Raman spectroscopy confirmed that the sample was made of a single layer graphene. The leads, a Pt/Ta/Pt trilayer of thicknesses 3 nm/70 nm/3 nm, were made using standard electron beam lithography and lift-off. The distance between the electrodes L is about 330 nm, and the width of the junction W is 2.7μm. The critical temperature of the Ta leads is 2.5 K, and the critical field is 2 Tesla.
An annealing current through the device changed the transmission coefficient of the electrode/graphene interface, increasing the probability of multiple Andreev reflections (MAR). Repeated annealing steps improved the contact sufficiently for a Josephson current to be induced in graphene.
The Dirac point was not sufficiently well defined in that state to check the predicted original properties of the proximity effect in S-graphene-S junctions. A promising possibility would be to perform this kind of annealing on suspended sample, to improve the sample mobility and the homogeneity of doping.

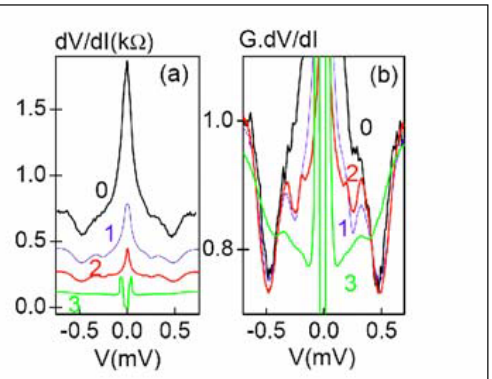

(a) Differential resistance versus bias voltage as a function of annealing steps.
(b) Differential resistance normalized to the 0.75 meV value, zoom around the MAR region. A supercurrent appears after the third annealing step (curve 3). The MAR structures demonstrate the fact that the interface transparency is not perfect, and that it improves with annealing.

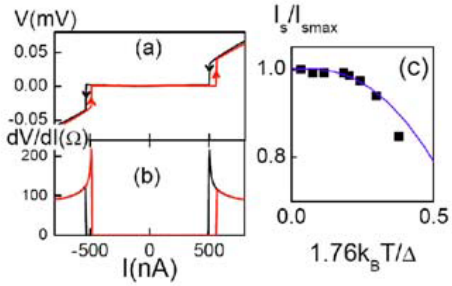

Full proximity effect induced in graphene after the third annealing step. (a) I-V curve and (b)dV/dI(I) of the SGS junction taken at 60 mK: a zero resistance state prevails at bias currents below a switching current of 600 nA. (c) The temperature dependance of the switching current (data points) follows a Kulik-Omelyanchuk law (continuous line) typical of short SNS junctions, see text. We have used the gap 250 μV deduced from the MAR features.

Efficient purification protocols using iSWAP gates in solid-state qubits

T. Tanamoto[1], K. Maruyama[2], Y.X. Liu[2], X. Hu[3] and F. Nori[2,4]
[1]*Corporate R & D center, Toshiba Corporation, Kawasaki, Japan*
[2]*Advanced Science Institute, The Institute of Physical and Chemical Research (RIKEN), Saitama, Japan*
[3]*Department of Physics, University at Buffalo, SUNY, Buffalo, New York, USA*
[4]*Physics Department, Center for Theoretical Physics, Center for the Study of Complex Systems, The University of Michigan, Michigan, USA*

Keywords: qubit, purification, quantum computing, quantum communication

The entanglement purification protocols proposed by Bennett *et al.* [1] and Deutsch *et al.* [2] are not only important contributions to the theory of quantum information, but also essential ingredients to applications such as quantum communications. In the purification protocols, the two parties (Alice and Bob) repeat a process in which, after choosing two shared entangled pairs in mixed states, they bilaterally apply controlled-NOT (CNOT) gates to their two local qubits that belong to the shared pairs, and measure one of the pairs. However, for most solid-state qubits, two-qubit interactions are quite delicate and are difficult to control without error and decoherence. In addition, when a CNOT gate is constructed using the XY interaction which frequently appears in solid-state qubits [3, 4], *at least twice* the number of two-qubit interactions have to be invoked with complicated pulse sequences.

Here, we show how to reduce the use of iSWAP gate in purification protocols, and we show that the bilateral CNOT gate (BCNOT) can be replaced by a bilateral iSWAP gate (BiSWAP) in the XY model. The XY model is expressed by the Hamiltonian $H_{xy} = \sum_{i<j} J(\sigma_i^x \sigma_j^x + \sigma_i^y \sigma_j^y)$, where σ_i^α $(\alpha = x, y, z)$ are the Pauli matrices acting on the i-th qubit. Then the iSWAP gate is obtained when $t = \tau_{\rm iswap} \equiv \pi/(4J)$ such that $|00\rangle \rightarrow |00\rangle$, $|11\rangle \rightarrow |11\rangle$, $|01\rangle \rightarrow -i|10\rangle$ and $|10\rangle \rightarrow -i|01\rangle$.

The basic relationship between the CNOT gate and the iSWAP gate is derived by the property between qubits '1' and '2' given by $U_{\rm iswap} = U_{\rm swap}{\rm diag}(1, -i, -i, 1)$.

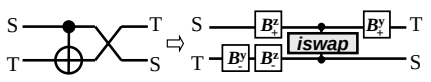

Figure 1: Replacement of a bilateral CNOT (BCNOT) gate by a bilateral iSWAP (BiSWAP) gate for one of the parties. $B_\pm^x$, $B_\pm^y$ and $B_\pm^z$ are bilateral single-qubit $\pm\pi/2$ rotations for Alice and Bob about the x, y and z axes.

Using Hadamard matrices (H_1 and H_2), and $\pi/2$ rotations ($P_{1+}$and P_{2+}), we have the main equation [5]:

$$U_{\rm swap}U_{\rm cnot} = H_1 U_{\rm iswap} P_{1+} P_{2+} H_2. \qquad (1)$$

By bilaterally applying this equation to the two parties, we can replace the BCNOT by BiSWAP gates (Fig.1): In step (i), the B_-^y mapping is applied only to the target qubits. In step (ii), the B_+^z mapping is applied to the source qubits, and the B_-^z mapping is applied to the target qubits. In step (iii), the BiSWAP gate is applied between the source pair and the target pair. Finally, in step (vi), the B_+^y mapping is carried out on the source pair. If we apply to the Deutsch protocol, the time $\tau_{\rm puri}^{\rm biswap}$ for each purification process is given by $\tau_{\rm puri}^{\rm biswap} \approx 4\tau_{\rm rot} + \tau_{\rm iswap}$, ($\tau_{\rm rot}$ is a typical time for a qubit rotation) which is faster than the Deutsch protocol using the conventional CNOT gate, with the time advantage $\Delta\tau_{\rm puri}^{\rm adv}$ given by

$$\Delta\tau_{\rm puri}^{\rm adv} = \tau_{\rm puri}^{\rm bcnot} - \tau_{\rm puri}^{\rm biswap} \approx \tau_{\rm rot} + \tau_{\rm iswap} \qquad (2)$$

In summary, we have constructed an efficient adaptation of the entanglement purification protocols for qubits with XY interactions. Our simplification of the gate pulse sequence reduces the time for entanglement purification and increases the robustness of the protocols.

References

[1] C.H. Bennett *et al*., Phys. Rev. Lett. **76**, 722 (1996).
[2] D. Deutsch *et al*., Phys. Rev. Lett. **77**, 2818 (1996).
[3] J.Q. You and F. Nori, Phys. Today **58** (11), 42 (2005).
[4] T. Tanamoto *et al*., to appear in Phys. Rev. Lett.
[5] T. Tanamoto *et al*., Phys. Rev. A **78**, 062313 (2008).

Electronic transport characterization of Sc@C_{82} single walled carbon nanotube peapods

A.L. Cantone*, M.R. Buitelaar*, S.J. Chorley*, C.G. Smith*, J. Fransson***, J. Warner**, A.A.R. Watt**, K. Porfyrakis** and G.A.D. Briggs**

**Cavendish Laboratory, Cambridge University, Cambridge, UK*

*** Clarendon Laboratory, Oxford University, Oxford, UK*

**** Department of Physics and Materials Science, Uppsala University, Uppsala, Sweden*

Keywords: Nanotube, peapods, quantum information, Spin blockade

Recent investigations into carbon materials has raised the possibility of measuring and manipulating spin interactions, in particular for quantum computing processing. We present the electrical transport and on individual single-wall nanotubes filled with paramagnetic metallofullerenes Sc@C_{82}. Metallofullerenes such as Sc@C_{82}, Y@C_{82} and La@C_{82} have hybridized orbitals between the metal dopant and the fullerene cage and this leads to an unpaired electron primarily delocalized across the C_{82} cage with a long spin coherence time [1]. This is why single wall carbon nanotubes encapsulating paramagnetic endohedral fullerenes are also of fundamental interest for the possibility to investigate one-dimensional (1D) spin chains which might have quantum information processing (QIP) applications [2].

Here we show that there is a marked difference between the room-temperature gate characteristics of filled and unfilled nanotubes which is tentatively interpreted as the result of bandstructure modification of the nanotube by the Sc@C_{82} molecules. Of importance for QIP applications is our observation that despite the strong effect on the room-temperature characteristics, the metallofullerenes do not introduce strong backscattering in the nanotubes and, at low-temperatures, transport is found to be phase coherent over extended distances[4] as shown in figure 1 from the presence of the Kondo effect. Pauli spin blockade in a carbon nanotube double quantum dot defined by tunnel barriers at the contacts and a structural defect in the nanotube is also reported[3]. The measured differential conductance agrees well with a theoretical model of a double quantum dot system in the spin-blockade regime, which allows us to estimate the occupation probabilities of the relevant singlet and triplet states. This work shows that effective spin-to-charge conversion in nanotube quantum dots is feasible and opens the possibility of single-spin readout in a material that is not limited by hyperfine interaction with nuclear spins.

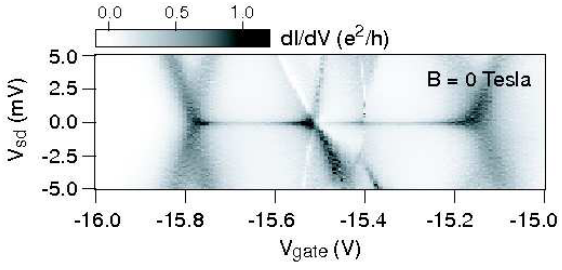

Figure 1: Grey scale representation of the differential conductance (dI/dV) as a function of source drain (V_{sd}) and gate voltage (V_g) of an Sc@C_{82}@SWNT peapod measured at $T = 50$ mK and $B = 0$ T. The high-conductance ridges at $V_{sd} = 0$ mV are a manifestation of the Kondo effect.

References

[1] G.W. Morley, B.J. Herbert, S.M. Lee et al. **16**, 2469 (2005).

[2] S.C. Benjamin, A. Ardavan, G.A.D. Briggs et al. J. Phys. Cond. Matter **18**, S867 (2006).

[3] M. R. Buitelaar, J. Fransson, A. L. Cantone et al. Phys. Rev. B **77**, 245439 (2008).

[4] A. L. Cantone, M. R. Buitelaar, C. G. Smith et al. J. Appl. Phys **104**, 083717 (2008).

Two-electron spin manipulation by photon assisted tunnelling

L. R. Schreiber*, T. Meunier*, V. Calado*, F. R. Braakman*, W. Wegscheider**
and L. M. K. Vandersypen*

** Kavli Institute of NanoScience, Delft University of Technology, The Netherlands*

*** Institute for Experimental and Applied Physics, University of Regensburg, Germany*

Keywords: QuBit, electron spin manipulation, photon assisted tunnelling, (Al,Ga)As 2DEG

Electron spins in a gate-defined double quantum dots formed in a GaAs/(Al,Ga)As 2DEG are promising candidates for quantum information processing as coherent single spin rotation [1,2] and spin swap [3] has been demonstrated recently.

In this system we investigate the two-electron spin dynamics in the presence of microwaves (5 GHz to 20 GHz) applied to one side gate. The charge state of the zero-biased double quantum dot is read out by a nearby quantum point contact (QPC). During microwave excitation we observe characteristic photon assisted tunnelling (PAT) peaks in the QPC current close to the (1,1) to (0,2) double dot charge transition. We analyse the PAT pattern as a function of the detuning of the double dot potential, of the microwave frequency and of the in-plane magnetic field (0 T to 5 T).

Most of the PAT peaks can be attributed to multi-photon tunnelling events between the singlet S(0,2) and the singlet S(1,1) state. Some PAT peaks, however, stand out by a different magnetic field dependence. These peaks result from tunnelling between a S(0,2) and a triplet T+(1,1) state. Therefore, the electron spin is flipped during the tunnel process. The underlying mechanism for the spin flip could be spin orbit interaction or the inhomogeneous magnetic field of a Co micro magnet placed next to the electric gates.

References

1. F. H. L. Koppens *et al.*, Nature 442, 766 (2006)
2. K. C. Nowack *et al.*, Science 318, 1430 (2007)
3. J. R. Petta *et al.*, Science 309, 2180 (2005)

Triple quantum dots with micro-magnets for implementing three spin qubits

T. Takakura[1], M. Pioro-Ladrière[2], T. Obata[2], Y. –S. Shin[2], R. Brunner[2], K. Yoshida[2], T. Taniyama[3, 4] and S. Tarucha[1, 2]

[1] *QPEC and Department of Applied Physics, The University of Tokyo, Bunkyo-ku, Tokyo, Japan*

[2] *Quantum Spin Information Project, ICORP, Japan Science and Technology Agency, Atsugi, Kanagawa, Japan*

[3] *Materials and Structures Laboratory, Tokyo Institute of Technology, Yokohama, Kanagawa, Japan*

[4] *PRESTO, Japan Science and Technology Agency, Kawaguchi, Saitama, Japan*

Keywords: Quantum dots, Micro-magnets, Spin qubits, Quantum information processing

Since the proposal [1] of electron-spin-based quantum computation, many experimental challenges have been performed to coherently manipulate electron spins in quantum dots (QDs). Electron spin resonance (ESR) is the most fundamental technique to realize qubit operation and has been demonstrated in several ways. We have recently proposed and demonstrated a new technique of electrical ESR using a micro-magnet (MM) [2,3]. An a.c. magnetic field for ESR is generated by electrical oscillation of an electron in a QD under a gradient of the *out-of-plane* stray field, which is imposed by a MM located above. This technique has the advantage to address single spins in multiple QDs with ESR at different resonance frequencies, which has already been demonstrated for double QDs (DQDs) [3]. In this work we further extend the technique to triple QDs (TQDs) for making three spin qubits. There are just a few previous reports on TQDs because of the difficulty in fabrication. We have initially fabricated a relevant TQD and observed the stability diagram with tunable number of electrons in each dot. We have designed a split-type MM Based on this device geometry to optimise the stray field distribution in realizing three-qubit operation.

We prepared a TQD with two quantum point contacts as charge sensors made in a 2DEG by Schottky gates (Fig.1), and measured the stability diagrams of charge states as a function of side gate voltages to two QDs on both ends with plunger gate voltage to the central QD as a parameter. We observed that the number of electrons in each QD and tunnel couplings between QDs can be independently varied with gate voltages (Fig.2). To address each QD with ESR, a sufficiently large difference in the *in-plane* stray field between the QDs is necessary as well [3]. We found that this requirement is met by the split-type MM designed here (Fig.3), from simulation of the stray field distribution across the TQD.

References

1. D. Loss and D. P. DiVicenzo, Phys. Rev. A **57**, 120 (1998).
2. Y. Tokura et al., Phys. Rev. Lett. **96**, 047202 (2006).
3. M. Pioro-Ladrière et al. Nature Physics **4**, 776 (2008).

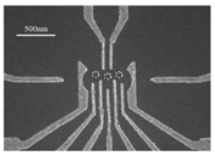

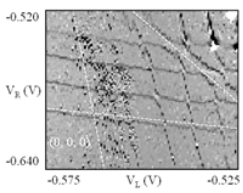

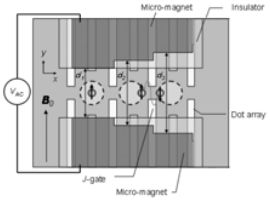

Fig.1 SEM micrograph of the TQD device without micro-magnets. **Fig.2** Stability diagram of the TQD device probed by charge sensing. Three different slopes of dark lines represent respective charging of three QDs. **Fig.3** Schematic of split-type MM to achieve addressable ESR for three QDs.

Semiconductor qubit readout using a resonant circuit

K. D. Petersson, P. Atkinson, D. Anderson, G. A. C. Jones, D. A. Ritchie and C. G. Smith
Cavendish Laboratory, JJ Thomson Road, Cambridge CB3 0HE, United Kingdom

Keywords: quantum dots, quantum information processing

State readout is a key requirement for a quantum information processor. Recently non-invasive fast charge detection for semiconductor quantum dot devices has been realised by embedding an adjacent quantum point contact (QPC) in a radio frequency resonant circuit [1, 2].

In this work, we demonstrate a dispersive readout scheme where a low-Q resonant circuit, operating at 385 MHz, is directly coupled to an AlGaAs/GaAs few-electron double quantum dot device. We then measure the state of the double quantum dot in an isolated regime by detecting a change in capacitance that depends on its polarizability [3], as shown in Fig. 1. This non-invasive readout scheme eliminates the need for a mesoscopic charge detector and has the potential to greatly simplify the complexity of semiconductor qubit devices.

We compare this detection signal with the average charge signal from a proximal rf-QPC embedded in a second frequency multiplexed resonant circuit and also with direct transport measurements through the double dot. We then show how this measurement technique can be used to distinguish the singlet and triplet spin states of a pair of electrons confined to the double dot.

Finally, we discuss what currently limits the detection sensitivity and how it could be improved to approach the predicted quantum limit [4].

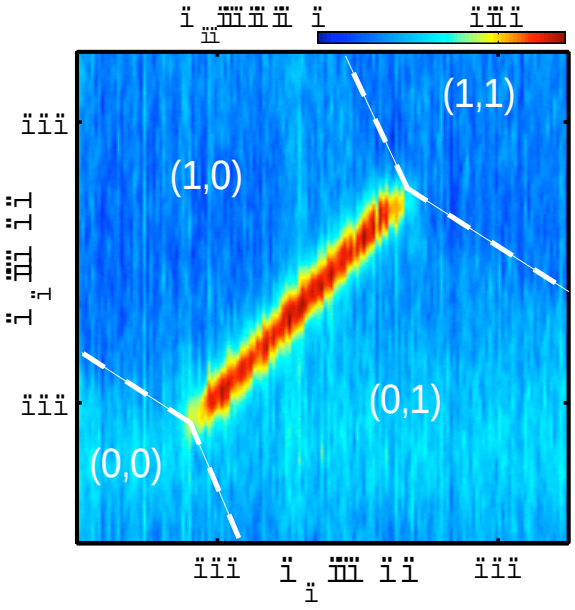

Figure 1: Demodulated response of the resonant circuit as a function of the left and right gates voltages of the double quantum dot. Absolute electron numbers for the left and right dots are indicated in brackets.

References

[1] M. C. Cassidy et al., App. Phys. Lett. **91**, 222104 (2007).

[2] D. J. Reilly et al., Appl. Phys. Lett. **91**, 162101 (2007).

[3] T. Duty et al., Phys. Rev. Lett. **95**, 206807 (2005).

[4] G. Johansson, L. Tornberg, and C. M. Wilson, Phys. Rev. B **74**, 100504(R) (2006).

Nuclear spin engineering and top-gating of 2DES in Si/SiGe

J. Sailer*, V. Lang*, G. Abstreiter*, K. M. Itoh**, E. E. Haller***,****, S. Ludwig***** and D. Bougeard*

** Walter Schottky Institut, Technische Universität München, 85748 Garching, Germany*

*** Department of Applied Physics and Physico-Informatics, Keio University 3-14-1, Hiyoshi, Kohoku-ku, Yokohama 223-8522, Japan*

**** Lawrence Berkeley National Laboratory, Materials Sciences Division, Berkeley, CA 94720-8197, USA*

***** Department of Materials Science and Engineering, University of California at Berkeley, Berkeley, CA 94720-1760, USA*

****** Fakultät für Physik and Center for NanoScience, Ludwig-Maximilians-Universität München, Geschwister-Scholl-Platz 1, 80539 München, Germany*

Keywords: nuclear spin free, Si/SiGe, conductance quantization, electrostatically defined double quantum dot

Si/SiGe is an attractive material system for quantum dot based applications in quantum information processing. It is characterized by a weak spin-orbit interaction and the availability of isotopes which do not carry a finite nuclear spin, promising long coherence times for spin qubits. On the other hand, two-dimensional electron systems (2DES) in Si/SiGe are also characterized by the valley splitting of the multiple equivalent conduction band minima in bulk Si. The impact of this valley splitting and intervalley interactions as scattering on decoherence times has seldom been studied.

We present an evaluation of this materials system through the study of top-gated 2DES devices in a quasi nuclear spin free $^{28}Si/^{28}Si^{70}Ge$ environment [1] as well as in Si/SiGe structures with natural isotopic composition.

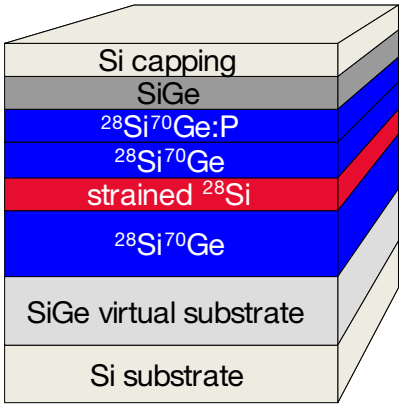

Fig.1 Layer structure of an isotopically engineered $^{28}Si/^{28}Si^{70}Ge$ heterostructure. The 2DES forms in the nuclear spin free strained ^{28}Si layer.

The valley- and spin-degeneracy in 2DES is studied through split gate quantum point contacts formed by means of e-beam lithography and subsequent Pd deposition as Schottky top-gates. A lifting of the degeneracy impedes valley interference effects and thereby is expected to have a positive effect on spin decoherence times.

The feasibility of a single electron device and the influence of the nuclear spins on the device is currently studied on electrostatically defined double quantum dots with engineered nuclear spin content.

References

1. J. Sailer et al., Phys. status solidi RRL 3, 61 (2009)

Low-Energy Electronic Properties of Ribbon-Graphene Hybrid Systems

C. H. Lee, W. S. Su, R. B. Chen, and M.F. Lin

Department of Physics, National Cheng Kung University, Tainan 701, Taiwan
Center for General Education, Tainan University of Technology, Tainan 710, Taiwan
Center of General Education, National Kaohsiung Marine University, Kaohsiung 811, Taiwan

Keywords: Graphene ribbon, monolayer graphene, electronic properties

Few-layer graphene is one of the most interesting materials, which has been extensively studied since Novoselov et al. first succeeded in fabricating it in 2004 [1]. In this work, the $2p_z$ tight-binding model is applied to investigate the electronic properties of zigzag ribbon-graphene hybrid systems. We mainly focus on the modification of linear bands from the corresponding monolayer graphene in this hybrid system. The interlayer interactions as well as the effects of ribbon with various widths and periods will be taken into account. The present study shows that the stacking type of the hybrid system is a key factor in dominating the two type band structures in the low-energy region.

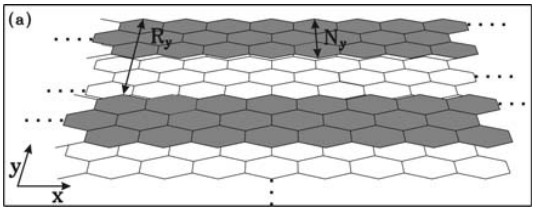

Fig.1 The geometric structure of zigzag ribbon-graphene hybrid system. N_y and R_y represent the ribbon width and period, respectively.

The geometric structure of zigzag ribbon-graphene hybrid system is sketched in Fig. 1. The ribbons with a width N_y are aligned on the graphene with a period R_y along the y-axis, where N_y and R_y denote the numbers of the zigzag lines. The C-C bond length is b=1.42Å. The interlayer distance between ribbon and graphene is assumed to be 3.35 Å, which is the same as that of the graphite. The unit cell of such a system, whose periodical lengths along the x-axis and y-axis are $I_x=(3)^{1/2}b$ and $I_y=(3b/2)R_y$, respectively, has $(2N_y+2R_y)$ carbon atoms.

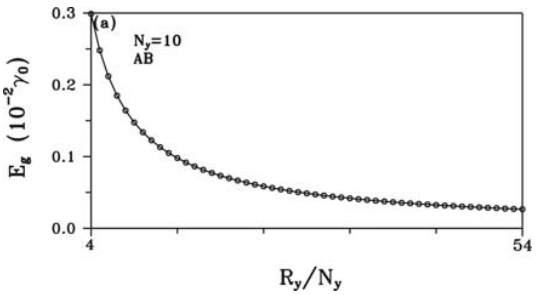

Fig.2 The R_y-dependent energy gaps of the hybrid system with N_y=10.

Figure 2 shows E_g of the AB-stacked hybrid system against R_y/N_y with N_y=10. The energy gap has strong dependence on ribbon period R_y. As R_y increases, E_g sharply decreases at first and slightly reduces later. For such a case, E_g occurs at $k_x=2/3I_x$ and k_y=0 where linear bands intersect without the interlayer interactions. Moreover, the expansion of the ribbon period would lead to various influence on the two parabolic bands near E_F=0. As a result, the energy gap could be effectively modulated by the width and period of the ribbon.

References

1. K. S. Novoselov, A. K. Geim, S. V. Morozov, D. Jiang, Y. Zhang, S. V. Dubonos, I. V. Grigorieva, and A. A. Firsov, Science **306,** 666 (2004).

Low-energy electronic structures of nanotube-graphene hybrid carbon systems

Y. H. Ho*,**, Y. H. Chiu**, J. M. Lu***, and M. F. Lin**
*Department of Physics, National Sun Yat-Sen University, Kaohsiung, Taiwan
**Department of Physics, National Cheng Kung University, Tainan, Taiwan
***National Center for High-Performance Computing, Tainan, Taiwan

Keywords: graphene, carbon nanotube, electronic structure

Physical properties of carbon nanotubes would be substantially influenced by the substrate, such as the formation of chemical bonds, the transfer of carrier concentration, and the deformation of atomic configurations[1, 2]. In this work, we mainly focus on the nanotube-graphene hybrid systems with periodic alignment. The Lennard-Jones potential is used to estimate the weak van der Waals interactions between the two subjects and determine the optimal interfacial geometry[3]. The low-energy subbands are calculated by the tight-binding model[4]. The periodic alignment of nanotubes on graphene would result in the quasi-one-dimensional physical phenomena. The interlayer atomic hoppings remarkably cause the subband coupling of nanotube and graphene, as shown in Fig. 1(b)-(c). The way they destroy the band degeneracy and induce new band-edge states is based on how the nanotubes are adsorbed on graphene sheet. The energy gaps strongly rely on the nanotube sizes and the alignment periods, as illustrated in Fig. 1(d). The composite systems might be direct or indirect semiconductors. The main characteristics of electronic structures are directly reflected in density of states. The interlayer interactions would bring about many minor peaks near Fermi level. The predicted results could be verified by the experimental measurements from the scanning tunneling spectroscopy.

References

[1] S. Berber, A. Oshiyama, Phys. Rev. Lett. **96**, 105505 (2006).

[2] T. Hertel, R. E. Walkup, Ph. Avouris, Phys. Rev. B **58**, 13870 (1998).

[3] R. Saito, R. Matsuo, T. Kimura, G. Dresselhaus, M. S. Dresselhaus, Chem. Phys. Lett. **348**, 187 (2001).

[4] Y. H. Ho, G. W. Ho, S. C. Chen, J. H. Ho, M. F. Lin, Phys. Rev. B **76**, 115422 (2007).

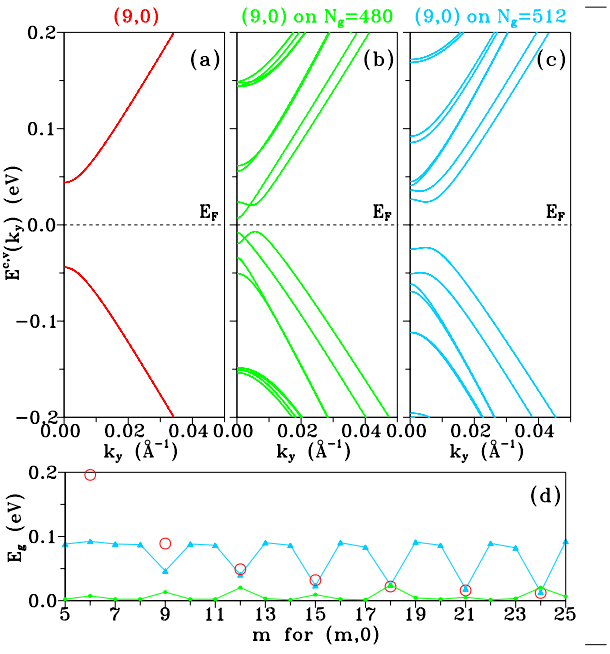

Figure 1: Low energy subbands of (a) (9,0) zigzag carbon nanotubes, and nanotube-graphene composite systems with (b) 480 and (c) 512 atoms in a graphene unit cell. (d) The dependence of energy gaps on nanotube size for non-interacting zigzag nanotubes and interacting nanotube-graphene hybrid systems.

Phonon softening in Peierls transition in an anisotropic triangular lattice

C. Watanabe*, and Y. Ono**
*Information Technology Education Center, Tokai University, Hiratsuka, Kanagawa, Japan
** Department of Physics and RCMIP, Toho University, Funabashi, Chiba, Japan

Keywords: 2D multimode Peierls transition, phonon softening, anisotropic triangular lattice

In recent numerical studies on 2D electron systems with square lattice structure[1, 2] indicate that a rich variety of distortion patterns can be expected in the 2D Peierls transition in contrast to the 1D Peierls system. This 2D Peierls state is called the multimode Peierls (MMP) state because it involves distortion Fourier components not only with the nesting vector $\boldsymbol{Q} = (\pi, \pi)$ or $\overline{\boldsymbol{Q}} = (-\pi, \pi)$ of the Fermi line in the square lattice with a half-filled electronic band, but also with fractional wave vectors of $\boldsymbol{Q}$; here the lattice constant is set to be unity. Different combinations of the fractional wave vectors result in different distortion patterns. In the case of the isotropic square lattice, those different distortion patterns are found to yield the same total energy (i.e. the sum of electronic and lattice energies). This degeneracy is shown to be lifted by introducing anisotropy within the square lattice structure[3]. More recently Horita and Ono[4] studied the stable Peierls state in a modified square lattice where the electronic transfer across one of the diagonal directions of the square lattice is introduced. As long as the transfer in the diagonal direction is sufficiently weak, the MMP state is found to be the ground state, although the aforementioned degeneracy is lifted by the diagonal transfer.

In the present paper, the 2D Peierls transition in the modified square lattice or the anisotropic triangular lattice is discussed from the view point of the phonon softening[5], which is useful when we consider the transition from the metallic to the Peierls state at a finite temperature. We perform the standard phonon softening study[5] which is nothing but the lattice normal mode analysis in the presence of the electron-lattice coupling. In the metallic phase, there is no static distortion, and the normal mode analysis reduces to the eigenvalue problem of 2×2 matrices for fixed phonon wave vectors.

An example of results is shown in Fig. 1 where the temperature dependence of the square frequencies of transverse modes for several wave vectors parallel to $\boldsymbol{Q}$ or $\overline{\boldsymbol{Q}}$. Here λ is the dimensionless electron lattice coupling and γ indicates the relative strength of the electronic transfer in the diagonal direction compared to the transfer in the perpendicular directions. The system is assumed to have a size $N \times N = 8 \times 8$ with periodic boundary conditions. This result means that, as long as γ is small, we may expect a multimode type transition from the metallic to the Peierls phase. Although the data is omitted here, the result for larger $\gamma(\simeq 0.7)$ indicates that the first softened mode is the transverse mode with $\boldsymbol{Q}/2$, which is consistent with the result at absolute zero[4].

References

[1] YO, T. Hamano, J. Phys. Soc. Jpn. **69**, 1769 (2000).
[2] T. Hamano, YO, J. Phys. Soc. Jpn. **70**, 1849 (2001).
[3] CW, S. Chiba, YO, AIP Conf. Pro. Ser. **850**, 1321 (2006).
[4] Y. Horita, YO, J. Phys. Soc. Jpn. **78**, 024711 (2009).
[5] S. Chiba, YO, J. Phys. Soc. Jpn. **72**, 1995 (2003).

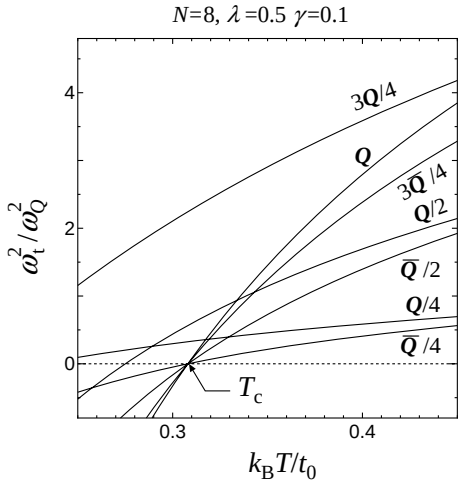

Figure 1: The temperature dependence of eigenfrequencies of transverse modes for different wave vectors.

Abrupt current jump of epitaxial p-type GaAs thin film

(1 blank line)

Sungyoul Choi*, Bong-Jun Kim*, Yong Wook Lee**, Jeongyong Choi*, and Hyun-Tak Kim*

** IT-Convergence & Components Lab.,Electronics and Tele-Communications Research Institute (ETRI), Daejeon 305-350, Korea*

*** School of Electrical and Control Engineering, Pukyong National University, Busan 608-739, Korea*

Keywords: *metal-insulator transitions*

In recent years much attention has been given to the theory of the abrupt first-order metal-insulator transition. It shows the abrupt and/or discontinuous current jump without phase transition. It argues much theory and experimental results about phase transition temperature on external electric field. The abrupt first-order metal-insulator transition (MIT) not accompanied with a structural phase transition, the abrupt Mott MIT as a current jump, was first proved experimentally in VO_2 [1]. We predicted that the abrupt MIT would occur even in some p-type semiconductors having an energy gap less than 2 eV as well as Mott insulators [2]. We noticed that p-type GaAs thin films with lower hole doping concentrations exhibited a thermally activated semiconduction, while those thin films with higher doping concentrations showed the metallic conduction at room temperature.

We grew Be-doped p-type GaAs thin films on GaAs(001) substrates at a substrate temperature of T_s=560 °C by molecular beam epitaxy (MBE). The growth velocity was 2.5 Å/sec. The thin film thicknesses were approximately 150 nm. The hole doping concentration in the GaAs was in the ranging from $n_p \approx 3.3 \times 10^{15}$ cm^{-3} to 1.6×10^{16} cm^{-3}. These concentrations were estimated at room temperature by Hall measurements. The Ni source electrode was fabricated using RF sputtering and channel intervals between electrodes were 3~30 μm. Electrical characteristics of the devices were measured by a precision semiconductor parameter analyzer. To protect devices from excess current, the maximum current was limited to compliance current.

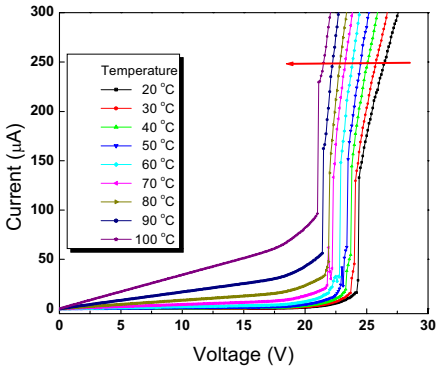

Fig. 1 The temperature dependence of I-V curve measured using epitaxial p-type GaAs thin film with a hole doping concentration of $n_p \approx 3.0 \times 10^{16}$ cm^{-3}.

In figure 1, we observed that the abrupt current jump of epitaxial p-type GaAs thin film showed temperature dependent behaviours. In this paper, we report on abrupt current jump of a two terminal device fabricated by using p-type (Be-doped) GaAs thin film grown by molecular beam epitaxy (MBE), and discuss the difference in the abrupt current jump and avalanche breakdown.

References

1. H. T. Kim, B. G. Chae, D. H. Youn, S. L. Maeng, G. Kim, K. Y. Kang, and Y. S. Lim, New J. Phys. **6**, 52 (2004).
2. H. T. Kim, B. G. Chae, D. H. Youn, G. Kim, K. Y. Kang, and Y. S. Lim, Appl. Phys. Lett. **86**, 242101 (2005).

Non-equilibrium edge channel spectroscopy in the integer quantum Hall regime

C. Altimiras, H.le Sueur, A. Cavanna, U. Gennser, D. Mailly and F. Pierre

CNRS, Laboratoire de Photonique et de Nanostructures (LPN), route de Nozay, 91460 Marcoussis, France

Keywords: Quantum Hall effect, quantum dots, quantum point contacts, edge channels

We demonstrate a new scheme to measure and tune the energy distribution of electrons f(E) in low dimensional systems. We implement it in the ν=2 quantum Hall regime to test whether the complex edge structure [1] for realistic edges [2] shows up in energy resolved experiments. We find that energy transport through a quantum point contact (QPC) and along short propagation distances in an edge channel (EC) are quantitatively described by the scattering approach for 1 D chiral fermions. The spectroscopy technique demonstrated here opens the path to energy transport measurements and to probe the inelastic mechanisms at low magnetic fields, in the integer and in the fractional quantum Hall regime.

A QPC of transmission τ is used to generate a tunable non-equilibrium f(E) by combining two incoming ECs of different electrochemical potential. Mapping EC into 1D chiral fermions, the scattering approach predicts that f(E) resembles a double step resulting from the weighted sum of two Fermi functions. We probe f(E) 0,8μm downhill the QPC (Fig. 1c) using the discrete levels of a quantum dot (QD) as energy filters (Fig. 1a). The probed energy is tuned with the voltage applied to a plunger gate coupled to the QD. Raw data are $\partial I_{dot}/\partial V_G$ variations of the QD current with the voltage applied to the plunger gate. It is proportional to $\partial f(E)/\partial E$ (Fig. 1a&b).

First, the gate voltage to energy conversion is calibrated from standard measurements of Coulomb diamonds and $\partial I_{dot}/\partial V_G$ temperature dependence. Second, we fix the bias voltage δV across the QPC, while its transmission τ is varied (Fig. 1e). Measured $\partial I_{dot}/\partial V_G$ show two dips separated by a fixed voltage whose relative weights follow the measured τ. Third, we fix τ while δV is changed (Fig. 1f). The single equilibrium dip of $\partial I_{dot}/\partial V_G$ splits into two similar dips separated by a gate voltage proportional to δV, in quantitative agreement with the QD calibration.

References

1. I.L. Aleiner and L.I. Glazman, Phys. Lett **72**, 2935 (1994).

2. D.B. Chklovskii *et al.*, Phys. Rev. B **46**, 4026 (1992).

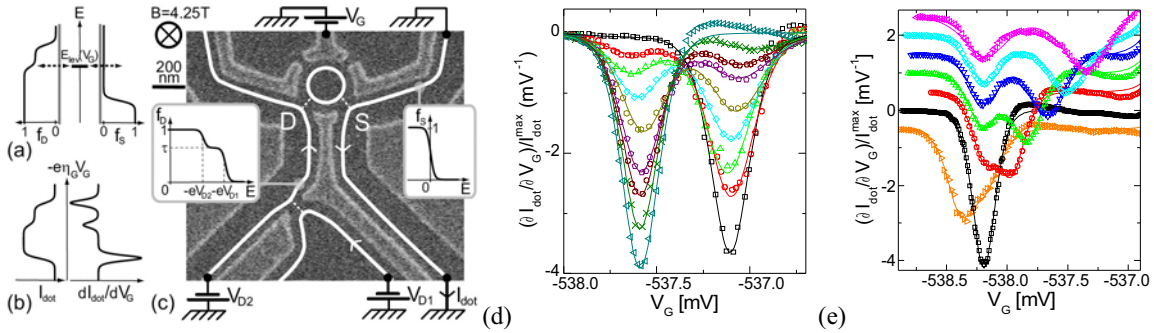

Fig.1 a, Schematic illustration of energy filtering. **b**, I_{dot} ($\partial I_{dot}/\partial V_G$) is proprtionnal to f(E) ($\partial f(E)/\partial E$). **c**, Sample micrograph **d**, $\partial I_{dot}/\partial V_G$ measured for fixed QPC bias δV=36μV and different transmissions τ ∈ [0, 1]. **e**, $\partial I_{dot}/\partial V_G$ measured for fixed transmission τ≈0,5 and different QPC biases δV∈ [-18μV, +54μV] (vertical offset for clarity)

Poissonian excitonic population of single QDs

M. Abbarchi*,**, T. Kuroda**, C. Mastrandrea*, A. Vinattieri*, S. Sanguinetti***, T. Mano**, N. Koguchi***, K. Sakoda** and M. Gurioli*

*Dipartimento di Fisica, CNISM, Università di Firenze and European Laboratory for Non-Linear Spectroscopy, Via Sansone 1, 50019 Sesto Fiorentino (Firenze), Italy

**National Institute for Materials Science, 1-1 Namiki, Tsukuba 305-0044, Japan

***Dipartimento di Scienza dei Materiali, CNISM, Universit di Milano-Bicocca, Via Cozzi 53, 20125 Milano, Italy

Keywords: quantum dot, power dependence, random population

As a consequence of Pauli's principle, level filling can be easily realized in quantum dots (QDs) and multi excitons complexes can be generated much before the saturation of the fundamental excitonic transition. This effect can be understood in terms of the random population theory [1]. This theory was introduced for quantitatively explaining the recombination spectra, transients, and gain of quantum dots ensemble [1] and it has been used for studying two state lasing in QDs [2] and for interpreting the role of p–doping in QD amplifiers [3]. Much less it has been reported on the recombination kinetics of single QDs. The model has been also applied for discussing the photon statistics [4] and to explain the exciton saturation under optical pumping [5]. The random population idea has been implemented by a 9 microstate master equation model [5] and can be applied to both steady state and time resolved excitation. However is quite complicated and requires many fitting parameters and a truncation procedure. Here we propose an analytical solution of the random population theory for steady state conditions, in terms of the simple picture of Poissonian excitonic population of the QDs. The model predictions are compared with the experimental data obtained GaAs/AlGaAs QDs grown by modified droplet epitaxy (MDE). Photoluminescence spectroscopy is employed to characterize the excitons (X) and biexcitons (XX) lines. The power dependence of the X and XX lines are quantitatively fitted by Poissonian P(1) and P(2) functions as shown in Fig.1 (with $P(n) = \langle n \rangle^n exp(-\langle n \rangle)/n!$ being $\langle n \rangle$ average number of excitons in the QDs). The simple model explains saturation and quenching of both X and XX emission. In addition it gives information on the dependence of the average number of excitons on the excitation power, and allows us to estimate the capture volume of a single QD, highlighting the relaxation and capture mechanisms.

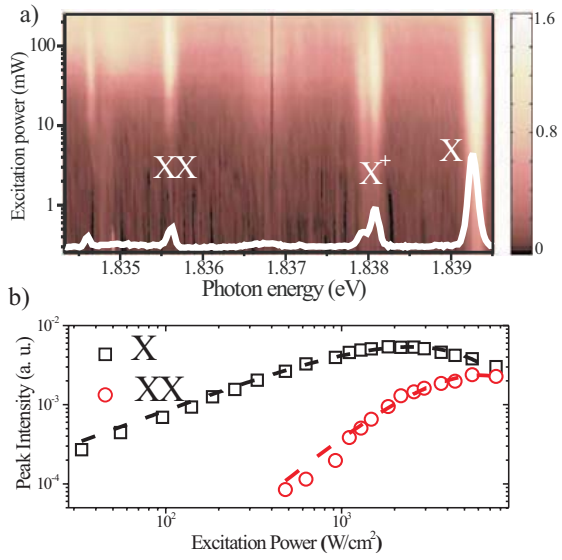

Figure 1: Power dependence of X and XX lines (squares and circles respectively), together with the corresponding poissonian fit (dashed lines)

References

[1] M. Grundmann et al, Phys. Rev. B 55, 9740 (1997)

[2] A. Markus, et al. Appl. Phys. Lett. 82 1818 (2003)

[3] V. Cesari, et al. Appl. Phys. Lett. 94, 041110 (2009)

[4] M.H. Bayer et al. Phys. Rev. B 73, 205321 (2006)

[5] G. Munoz Matutano et al. Physica E 40, 2100 (2008)

Indication for Quantum Darwinism in Electron Billiards

R. Brunner[1,2], R. Akis[3], Adam Burke[3], R. Meisels[2], F. Kuchar[2], D. K. Ferry[3]

1. Quantum Spin Information Project, ICORP, JST, Atsugi-shi, Kanagawa, 243-0198, Japan

2. Institute of Physics, University of Leoben, Franz-Josef Strasse 18, A-8700 Leoben, Austria

3. Dept. of Electrical Engineering and Center for Solid State Electronics Research ,Arizona State University, Tempe, Arizona 85287,USA

Keywords: Electron Billiards, open quantum system, Quantum Darwinism

The disturbance of open quantum systems due to a coupling to the environment or a measuring process has been a main topic since the advent of quantum theory [1]. It is also a basic ingredient in quantum information processing. Of significant importance is the border where the two worlds of classical and quantum mechanics meet. It has been shown by Zurek [2] that in an open system the environment imposes so-called superselection rules leading to environment-induced superselection (einselection). This means that a set of preferred states (pointer states) survive the coupling with the environment. They are characterized by their robustness and their ability to create offspring. This ability of the pointer states to advertise information about themselves makes it possible for different observers to measure the same information. The natural promotion of certain information in a quantum system is known as quantum Darwinism [2]. The "fitness" in the Darwinian sense of the selected states is essentially a measure of their classicality. Therefore, in order to measure a quantum system objectively it has to be designed in such a way that the transition between the classical and quantum world is observable.

We demonstrated in [3] that in open quantum dots this pointer states corresponds to regular orbits within the individual dots.

In this contribution we show (1) that beside the "regular" (single dot) pointer states a new type of einselected states arise, the bipartite pointer state.

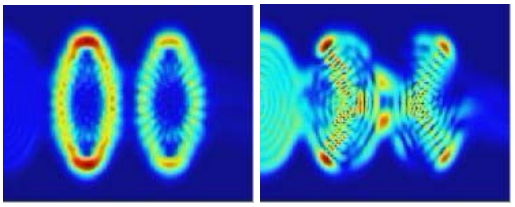

Fig. 1. Left: probability density at B=0.2 T and E=8.63 meV for a two dot array showing the single dot pointer states. Right: The bipartite pointer state at 0.2 T and 8.70 meV.

This new type of states cannot be presented by a linear combination of pointer states of the individual dots [4]. (2) We show that identical wave-function imprint is present in several current carrying modes at the same energy, i.e. they contain identical information. We interpret this as the propensity of the new type of einselected states to produce offspring indicating that quantum Darwinism is in action in the array of electron billiards. (3) Finally, we show preliminary experimental results which can be connected to this concept of quantum Darwinism.

References

[1] E. Schroedinger, Naturwissenschaften **48**, 807; **49**, 823; **50**, 844 (1935).

[2] W. H. Zurek, Rev. Mod. Phys. **75**, 715 (2003).

[3] R. Brunner et al. PRL **98**, 204101 (2007).

[4] R. Brunner et al. PRL **101**, 024102 (2008).

Scanning gate imaging of quantum point contact

N. Aoki*, A. M. Burke**, C. R. da Cunha***, R. Akis**, D. K. Ferry** and Y. Ochiai*

**Graduate School of Advanced Integration Science, Chiba University, Chiba, Japan*

***Department of Electrical Engineering and Center for Solid State Electronics Research, Arizona State University, USA*

****Department of Electrical Engineering, Universidade Federal do Rio Grande do Sul, Brazil*

Keywords: SGM, QPC, low temperature, quantum transport, localized spin

Quantum point contacts (QPCs) have been studied using scanning gate microscopy (SGM) at low temperature. In contrast to the SGM images of an InGaAs-QPC [1], those of a GaAs-QPC are seemingly trivial since no quantum fluctuations have been observed due to the sample's characteristic high mobility. However, interesting transport phenomena based on many body effects, such as the Kondo effect and the 0.7 structure, are reported in the GaAs-QPC system. It can be expected that such transport features can be visualized as a real-space image using the SGM technique. In this study, we have observed ring shape structures and their evolutions around the center of the QPC for the first time in SGM images and they appeared in two different samples [2].

The QPC was fabricated on an AlGaAs/GaAs hetero-structure using a wet etching method, which allowed us to scan the entire surface with minimum tip lift height (~50 nm) and to apply in-plane gate voltage to squeeze the QPC without the danger of shorting the tip that a metal gate system would risk. The carrier density and the mobility are 4.7×10^{11} /cm^2 and 4.2×10^{15} cm^2/Vs, respectively, and the mean free path is 4.7 μm. The SGM observations were performed at 300 mK with a piezoelectric self-sensing cantilever.

The ring structures were first observed in a SGM conductance image located at one of QPC constrictions of an open quantum dot as shown in Fig. 1. When the conductance of the QPC (base conductance) is squeezed lower than 0.8 G_0 ($G_0 = 2e^2/h$), a single ring began to appear and the diameter increased up to ~500 nm with decreasing base conductance. The diameter depends not only on the side gate bias but also upon magnetic field. Similar rings have been observed in the other QPC sample. The mechanism of the ring structure has not yet been clarified. However, when the biased tip comes close to the constriction, it locally reduces the carrier density in the QPC. This would manipulate a certain energy level within a QPC. This ring could be indicative of a spin related level or its confinement potential because it appears at conductance of lower than $2e^2/h$. Also, the rings might be related to the manipulation of an ionized donor level or an impurity level within the QPC.

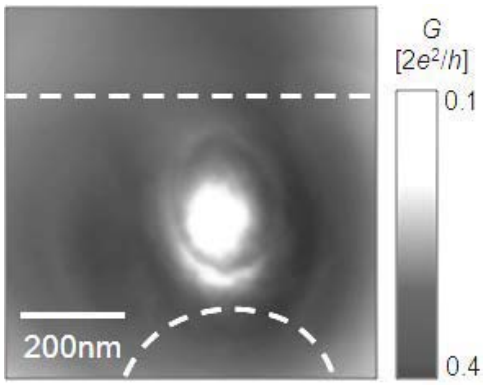

Fig. 1 The ring structure observed in a SGM image. The color bar indicates conductance variation in the image. The broken lines indicate physical edges of the wet-etched region forming an asymmetric QPC.

References

1. N. Aoki, C. R. da Cunha, R. Akis, D. K. Ferry, and Y. Ochiai, Appl. Phys. Lett. **89**, 212109 (2005).

2. N. Aoki, A. Burke, C. R. da Cunha, R. Akis, D. K. Ferry, and Y. Ochiai, J. of Phys: Conference Series **38**, 79 (2006).

Photomagnetic effect caused by spin-orbit interaction in 2D system

M.V. Entin and L.I. Magarill
Institute of Semiconductor Physics, Siberian Branch, Russian Academy of Sciences, Novosibirsk, Russia

Keywords: 2D system, Rashba interaction, photocurrent

We consider 2D system placed in the in-plane magnetic field **B** and external RF field $\mathbf{E}=\mathbf{n}E\cos\omega t$ along the system normal **n**. The Hamiltonian of the system contains the Rashba spin-orbit interaction [1]. The purpose of the paper is calculation of the stationary photocurrent which flows along the direction [**Bn**] (see Fig.1).

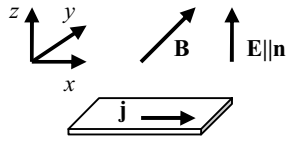

Fig. 1. Sketch of considered system.

In bulk semiconductors this geometry corresponds to the known photomagnetic effect, caused by the Hall deflection of photoexcited flow of electrons. However, in quantized systems, where the vertical flow is forbidden, the photocurrent has different nature: combined effect of Zeemann and Rashba splitting that causes asymmetry of the excitation.

We deal with strict 2D system with the Hamiltonian

$$H=\frac{p^2}{2m}+\alpha[\boldsymbol{\sigma},\mathbf{p}]\mathbf{n}+\frac{1}{2}g\mu_B\boldsymbol{\sigma}\mathbf{B}. \qquad (1)$$

Here **p** is 2D momentum, μ_B is the Bohr magneton, **σ** are the Pauli matrices, α is the effective parameter of spin-orbit coupling. Equation (1) formally does not contain the vertical electric field. To couple alternating field with electrons the modulation of coefficients of the Hamiltonian (namely, g-factor [2,3] and α) by E should be taken into account. This results in the transitions between spin subbands. Here the modulation of the parameter α: $\alpha(E)\approx\alpha_0(1+\gamma E)$ is assumed arising from the variation of asymmetry of the potential well. The parameter γ has the order of α_0/E_0, where E_0 is the vertical electric field built in the 2D channel. The asymmetry of unperturbed spectrum $\varepsilon_{\mathbf{p}\pm}=p^2/2m\pm\sqrt{(\alpha_0 p_x+g\mu_B B/2)^2+\alpha_0^2 p_y^2}$ leads to the asymmetry of excitation with respect to p_x and, hence, to the photocurrent.

We have found the absorption of external RF field and the stationary current caused by it. Assuming that the spin splitting is less than the Fermi energy the stationary current reads $j=-C(E\gamma)^2R(y,t)$, where $C=\mu n_e|\alpha_0|^3m^2/8\hbar$, $R(t,y)=(y^2+t^2-1)(ty)^{-1}\times\sqrt{4t^2-(t^2+1-y^2)^2}$, μ is the mobility, n_e is the electron concentration, $y=\hbar\omega/2|\alpha_0|p_F$, $t=g\mu_B B/2\alpha_0 p_F$ (here CGSE unites are utilized).

The function $R(y,t)$ which reflects the dependencies of the current on frequency and magnetic field is depicted in the Fig. 2. The current changes sign and grows with magnetic field. It exists in narrow "windows", of intersubband transitions. The estimates yield j~15 μA/cm for GaAs parameters at n_e= $5\cdot10^{11}$ cm^{-2}, μ=10^6cm^2/Vs, R=1 and γE=10^{-1}.

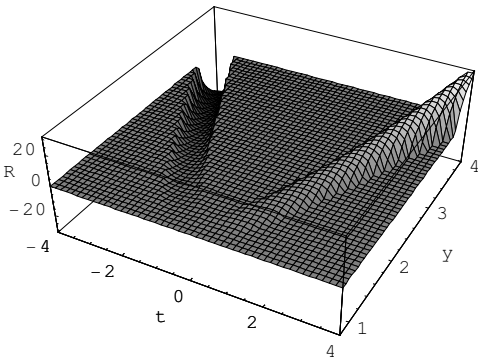

Fig. 2. Stationary current as a function of frequency and magnetic field.

References

[1] Yu.A. Bychkov and E.I. Rashba, JETP Lett., **39**, 78 (1984).
[2] Y. Kato *et al.*, Science **299**, 1201 (2003).
[3] E.I. Rasba and Al.L. Efros, PRL, **91**, 126405 (2003).

Microscopic theory of the activated behavior of the quantized Hall effect

S. Sakiroglu*, U. Erkarslan**, G. Oylumluoglu**, A. Siddiki** and I. Sokmen*
*Physics Department, Faculty of Arts and Sciences, Dokuz Eylül University, 35160 İzmir, Turkey
** Physics Department, Faculty of Arts and Sciences, Muğla University, 48170 Muğla, Turkey

Keywords: thermally activated conduction, longitudinal resistance

We study the thermally activated behavior [1] of narrow gate defined Hall bars by analyzing the existence of the incompressible strips [2] within Hartree-type approximation [3]. We investigate the variation of the activation energy depending on the width of samples in the range of $2d \sim [1-10]\,\mu$m.

The temperature dependence of the longitudinal and the Hall resistances obtained from the position dependent two-dimensional resistivity tensor [4] is studied within integer Hall plateau in magnetic fields around the centers of the highest mobility samples corresponding to filling factor $\nu = 2$. In this work we consider the extremely clean GaAs/(AlGa)As heterostructures where local DOS is almost a delta function and no long-range potential fluctuations exist. 2DES is populated by ionized Si-donors which are distributed homogeneously in the same plane with the 2DES. Quantized resistance values are obtained by self-consistent calculations. We use the local version of the conventional transport theory, i.e. Ohm's law, which takes into account the peculiar screening effects in 2DES under the high magnetic fields, however avoids any localization assumptions. The nonlocal effects on the conductivity along the incompressible strips are simulated by a suitable averaging procedure.

Results of our microscopic theory for the high-mobility samples presents strong deviations from the single-particle theories [5, 6]. We demonstrate that without any localization assumptions, our microscopic theory explains the enormous experimental reproducibility of the quantized resistance values. At low currents, thermally activated resistance is investigated by the Arrhenius plot at the relevant magnetic field values. For relatively wide samples, higher activation energy is obtained at the high field edge of Hall plateau whereas for the narrower samples activation energy is higher at the low field edge. The activation energies obtained by fitting the data to the Arrhenius law, which exceeds half of the cyclotron energy of the interval between adjacent Landau levels, are in good agreement with the experimental results [7].

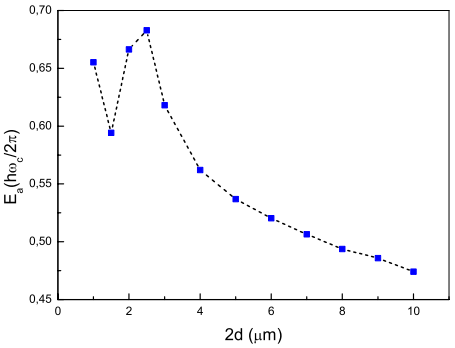

Figure 1: Dependence of the activation energy of the $\nu = 2$ Hall plateau on the width of the samples.

References

[1] J. Matthews and M. E. Cage, J. Res. Natl. Inst. Stand. Technol. **110**, 497–510 (2005).

[2] D. B. Chklowski, B. I. Schklowskii and I. I. Glazman, Phys. Rev. B. **46**, 4026–4034 (1992).

[3] A. Siddiki and R. R. Gerhardts, Phys. Rev. B **70**, 195335 (2004).

[4] T. Ando, A. B. Fowler and F. Stern, Rev. Mod. Phys. **54**, 437–672 (1982).

[5] M. Büttiker, Phys. Rev. B **38**, 9375–9389 (1988).

[6] R. B. Laughlin, Phys. Rev. B **23**, 5632–5633 (1981).

[7] J. Horas, A. Siddiki, J. Moser, W. Wegscheider and S. Ludwig, Physics E **40**, 1130–1132 (2008).

July 22 (Wednesday)

9:00 – 10:30

Session E5

Quantum Hall effect II

Main Hall

EP2DS-MSS Parallel session

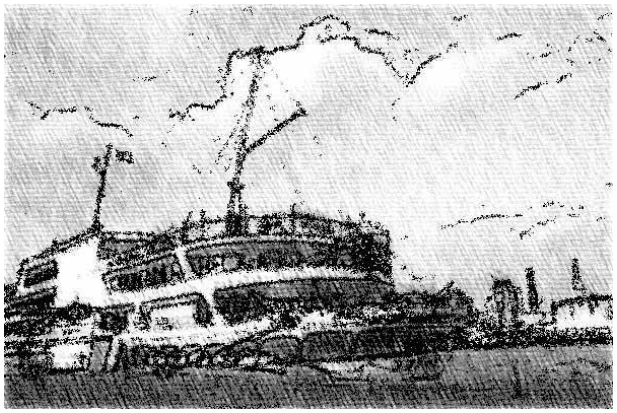

Kobe harbor cruise

Role of e-e interactions in magnetoresistance oscillations in 2DES

M. A. Zudov,* A. T. Hatke,* L. N. Pfeiffer,** and K. W. West**
*School of Physics and Astronomy, University of Minnesota, Minneapolis, Minnesota 55455, USA
** Bell Labs, Alcatel-Lucent, Murray Hill, New Jersey 07974, USA

Keywords: microwave photoresistance, electron-electron interactions

When a clean 2D electron system (2DES) is subject to a magnetic field and microwave radiation, the resistance will oscillate dramatically [1], depending on the ratio of microwave to cyclotron frequencies, $\epsilon_{ac} = \omega/\omega_c$. Remarkably, at the minima of these microwave-induced resistance oscillations (MIRO) the resistance can virtually vanish forming exotic zero-resistance states [2, 3].

MIRO were discussed in terms of the "displacement" model [4], which is based on the impurity scattering, and the "inelastic" model [5], stepping from the oscillatory electron distribution function. The correction to the resistivity due to either mechanism can be written as [5]:

$$\delta\rho \propto -\epsilon_{ac}\bar{\tau}\delta^2 \sin(2\pi\epsilon_{ac}), \qquad (1)$$

where $\delta = e^{-\pi/\omega_c\tau_q}$ is the Dingle factor. In the "displacement" model $\bar{\tau} = 3\tau_q^{im}$ (impurity quantum lifetime) and in the "inelastic" model $\bar{\tau} = \tau_{in} \propto T^{-2}$ (inelastic time). One can favor the "inelastic" mechanism over the "displacement" because, usually, $\tau_{in} \gg \tau_q^{im}$, and because it naturally explains the high temperature decay of MIRO.

In this work [6] we experimentally find that MIRO decay exponentially with temperature, as $\exp(-\alpha T^2)$, where α scales with the inverse magnetic field. This observation indicates that the temperature dependence originates *primarily* from the modification of τ_q, which we attribute to the electron-electron interaction effects.

Fig. 1 (a) shows exponential dependence of the normalized MIRO amplitude $\delta\rho/\epsilon_{ac}$ on $1/B$ for $T = 1, 2, 3$ and 4 K indicating that τ_q decreases with T. At the same time our data show no considerable temperature dependence of the prefactor, such as $\bar{\tau}$ in (1). Fig. 1 (b) shows quadratic temperature dependence of $1/\tau_q$ over the whole temperature range, signaling important contribution from electron-electron scattering, $1/\tau_q^{ee} \propto T^2$.

This talk will further discuss relative contributions from both mechanisms, roles of electron-phonon scattering and short-range disorder, as well as our recent studies [7, 8] of the temperature evolution of phonon- [9] and Hall field-induced resistance oscillations [10]. Taken together, our experiments suggest that sensitivity to electron-electron interactions is a generic property of magnetoresistance oscillations appearing in the second order of the Dingle factor. This is in contrast to Shubnikov oscillations where the Dingle factor does not contain the $1/\tau_q^{ee} \propto T^2$ term [11].

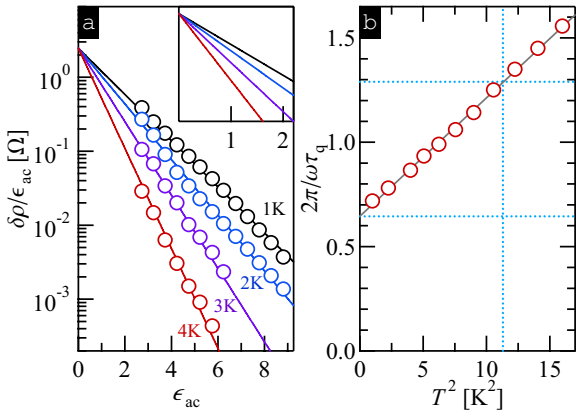

Figure 1: (a) "Dingle" plots for $T = 1, 2, 3, 4$ K. (b) Temperature dependence of the extracted scattering rate.

References

[1] Zudov *et al*, PRB **64**, 201311(R) (2001).
[2] Mani *et al*, Nature **420**, 646 (2002).
[3] Zudov *et al*, PRL **90**, 046807 (2003).
[4] Vavilov and Aleiner, PRB **69**, 035303 (2004).
[5] Dmitriev *et al*, PRB **71**, 115316 (2005).
[6] Hatke *et al*, PRL **102**, 066804 (2009).
[7] Hatke *et al*, PRL **102**, 086808 (2009).
[8] Hatke *et al*, submitted (2009).
[9] Zudov *et al*, PRL **86**, 3614 (2001).
[10] Yang *et al*, PRL **89**, 076801 (2002).
[11] Martin *et al*, PRB **68** 241309(R) (2003).

Tunneling Spectroscopy of Composite Quasiparticles in the Fractional Quantum Hall Effect

O. E. Dial*, R. C. Ashoori*, L. N. Pfeiffer** and K. W. West**
*Massachusetts Institute of Technology, Cambridge, United States
** Alcatel-Lucent Bell Laboratories, Murray Hill, United States

Keywords: Composite Fermions, Spectroscopy, Fractional Quantum Hall Effect

Using time domain capacitance spectroscopy, we measure the tunneling density of states of a two dimensional electron system (2DES). The resulting spectra have quantitatively accurate and undistorted energy and density axes. Within these spectra, individual quasiparticles can be seen as sharp features in the tunneling density of states and identified by their evolution with changing 2DES density and magnetic field. Improvements in the technique have allowed measurements at increased magnetic fields, making visible new features within the Landau level closest to the Fermi surface.

We identify these features as Landau fans of composite quasiparticles. These features have energies that vary linearly with density, and can be divided into families by the filling factor at which their energies extrapolate to zero. This filling factor is used to identify the flux attachment of the associated quasiparticles. The first family (green arrows) is identified with ^{2}CF composite Fermions (CFs). We measure the CF effective mass by measuring the cyclotron splitting in the spectra, and we find masses significantly smaller than those measured using thermally activated transport. These masses appear more consistent with theoretical predictions of cyclotron masses.

The second family (blue arrows) can be explained as resulting from a composite particle with only a single flux quantum attached. This is not expected within the CF picture; only attachment of an even number of flux quanta guarantees that the resulting quasiparticle is a fermion. Explanations for this unexpected flux attachment include non-trivial spin structure in the excitation, the formation of a composite boson, or the quasiparticle may be one of the unusual types proposed for the $\nu = 5/2$ Hall plateau. We also see this "^{1}C" family of states centered about $\nu = 3$. If these states are not merely excited states near $\nu = 3$, but part of the ground state, a naive interpretation of this single flux attachment leads to the expectation of Hall plateaus at $\nu = 5/2$ and $\nu = 7/2$. While at 80 mK, our experiment is too warm for the $\nu = 5/2$ plateau to appear, the underlying excitations may already be present in the excited state spectrum. Measurements of these spectra at lower temperatures may answer the open question of the nature of the $\nu = 5/2$ fractional quantum Hall plateau.

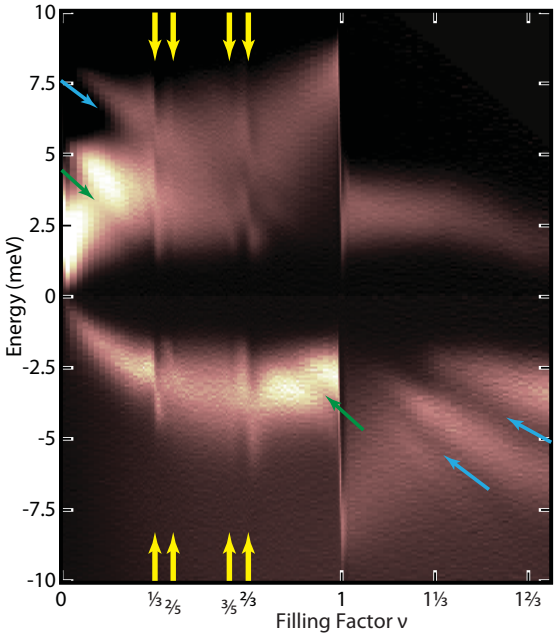

Figure 1: A tunnel density of states spectrum of a 2DES acquired at 13.5 Tesla. The horizontal axis of the spectrum is density, with the fully depleted well at the left edge, and the quantum well near $\nu = 2$ at the right edge. The vertical axis is energy, with the Fermi energy at $E = 0$. Bright regions correspond to high density of states. A dark tunneling pseudogap is expected at the energies of the CF, bounded by a bright region of enhanced tunneling at higher energies. Features identified with a ^{2}CF fan are indicated with green arrows centered about $\nu = 1/2$, while those identified with the unexpected ^{1}C fan are indicated with blue arrows about $\nu = 1$. Chemical potential jumps associated with several fractions are indicated with yellow arrows.

Activation Energy Gap of the Layer-Imbalanced Bilayer $\nu = 1/3$ Quantum Hall States

A. Fukuda*, T. Sekikawa**, K. Iwata**, Y. Ogasawara**, T. Arai***, Z. F. Ezawa**** and A. Sawada***
*Department of Physics, Hyogo College of Medicine, Nishinomiya 663-8501, Japan
** Graduate School of Science, Department of Physics, Kyoto University, Kyoto 606-8502, Japan
*** Research Center for Low Temperature and Materials Sciences, Kyoto University, Kyoto 606-8501, Japan
**** Theoretical Physics Laboratory, RIKEN, Saitama 351-0198, Japan

Keywords: Fractional quantum Hall state, Bilayer, Activation energy, Layer imbalance

The single-layer fractional quantum Hall state (FQHS) at Landau level filling factor $\nu = 1/3$ is interpreted as the $\nu = 1$ integer quantum Hall state (IQHS) of composite fermions (CFs); one composite fermion consists of one electron and two flux quanta. On the other hand, the bilayer $\nu = 1$ IQHS, where the layer degree of freedom (pseudospin) plays an essential role, supports the interlayer phase coherence[1]. When an in-plane magnetic field $B_{||}$ is applied, the bilayer $\nu = 1$ system undergoes the commensurate (C) - incommensurate (IC) phase transition[1]. Recently we reported the existence of a new class of quantum phase called "pseudospin soliton lattice" between the C and IC phases in the balanced $\nu = 1$ bilayer IQHS[2]. To clarify the similarity of the bilayer $\nu = 1/3$ FQHS to the $\nu = 1$ IQHS and the applicability of the CF model even in the in-plane magnetic fields, the possible existence of the soliton lattice in the bilayer $\nu = 1/3$ FQHS attracts our interests. We already reported the preliminary results in the balanced $\nu = 1/3$ FQHS[3]. The effects of the layer imbalance in the bilayer $\nu = 1$ IQHS are also investigated[2]. Therefore, not only the existence of soliton lattice but also the effects of the layer imbalance on the C-IC phase transition in the bilayer $\nu = 1/3$ FQHS is worth investigating.

In this report, we carried out the detailed magneto-transport experiments of the bilayer layer-imbalanced $\nu = 1/3$ FQHS. We used the GaAs/AlGaAs double-quantum-well sample with the tunneling energy 11 K, provided by NTT basic research laboratory. Activation energy Δ is derived from the temperature T dependence of magnetoresistance $R_{xx} \propto \exp(-\Delta/2kT)$. $B_{||}$ is applied by rotating the sample *in situ* in the magnetic fields $B_{\rm tot}$ with tilting angle $\theta = \sin^{-1}(B_{||}/B_{\rm tot})$. In Fig. 1, we show Δ in the $\nu = 1/3$ bilayer FQHS as a function of θ for various layer imbalance parameter $\sigma \equiv (n_{\rm f} - n_{\rm b})/(n_{\rm f} + n_{\rm b})$ where $n_{\rm f}$ and $n_{\rm b}$ are the electron density in the front and back layer, respectively. The total density $n_{\rm T}$ is fixed at $0.6 \times 10^{11}{\rm cm}^{-2}$. At small σ (0 and 0.2), Δ steeply degreases as increasing θ and FQHSs collapse above the critical tilting angle $\theta_{\rm C}$. These behaviors at $\theta < \theta_{\rm C}$ are similar to the C phase in the bilayer $\nu = 1$ IQHS. At large σ (0.3 and 0.4), as increasing θ, Δ drops initially. However, Δ stays finite even above $\theta_{\rm C}$, which means the IC-like phase appears in the $\nu = 1/3$ layer-imbalanced bilayer FQHS. In the conference, we will report the transition from the C-like phase to the IC-like phase of the $\nu = 1/3$ layer-imbalanced bilayer FQHS in detail.

References

[1] S. Q. Murphy, *et al.*, Phys. Rev. Lett. **72**, 728 (1994).

[2] A. Fukuda, *et al.*, Phys. Rev. Lett. **100**, 016801 (2008).

[3] A. Fukuda, *et al.*, Physica E **40**, 1261 (2008).

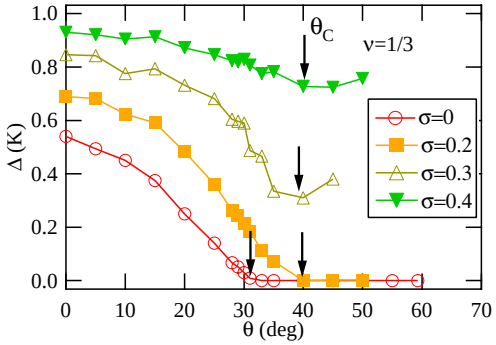

Figure 1: Activation energy Δ as a function of tilting angle θ for various σ in the $\nu = 1/3$ bilayer FQHS. $n_{\rm T}$ is fixed at $0.6 \times 10^{11}{\rm cm}^{-2}$.

Landau level broadening in graphene with long-range disorder — Robustness of the $n = 0$ level—

T. Kawarabayashi*, Y. Hatsugai** and H. Aoki***
*Department of Physics, Toho University, Funabashi, Japan
** Institute of Physics, University of Tsukuba, Tsukuba, Japan
***Department of Physics, Univeristy of Tokyo, Hongo, Tokyo, Japan

Keywords: graphene, Landau level broadening, correlated disorder

After the discovery of a characteristic quantum Hall effect (QHE) in graphene, interest have been shifted towards the effect of disorder on the Landau levels and QHE in graphene. Specifically, sensitivity of the electronic structure in a honeycomb lattice on the range of disorder (short-ranged vs long-ranged), bond disorder vs site disorder, and the bond disorder in phase vs magnitude. In the case of the correlated bond disorder in magnitude, which can be related to ripples in graphene, we have shown[1] that the broadening of the $n = 0$ Landau level becomes anomalously small when the correlation length exceeds the lattice constant. For this problem we have to go back to the honeycomb lattice (rather than the Dirac model), since the chiral (A-B sublattice) symmetry and the associated valley degeneracy are crucial[2], and discuss the effect of the range of disorder, which controls the strenght of the inter-valley (K $\leftrightarrow$ K') scattering.

In addition to the bond disorder in magnitude[1], here we consider the long-ranged disordered magnetic field (disorder in phases) which describes ripples when the model is reduced to a single Dirac cone. We then find that the $n = 0$ Landau level is also robust against the disordered magnetic field, if the range of disorder exceeds several lattice constants. Namely, the density of states, shows that the $n = 0$ Landau level at $E = 0$ is anomalously sharp for finite spatial correlation in disordered magnetic field (figure 1). Note that it is considerably sharper than the uncorrelated case. It is rather remarkable that this occurs even when the fluctuation of the magnetic field is strong, for which $n \neq 0$ Landau levels are smeared out. No such a sharp peak at $E = 0$ appears for the correlated site disorder (figure 2). All these results confirm that for the honeycomb lattice, the robustness of the $n = 0$ Landau level is generic to the bond disorder with a longer range than the lattice constant, being consistent with the topological stability of the zero-energy modes.

References

[1] T. Kawarabayashi, Y. Hatsugai, and H. Aoki, in preparation.

[2] Y. Hatsugai, T. Fukui, and T. Aoki, Phys. Rev. B74, 205414 (2006).

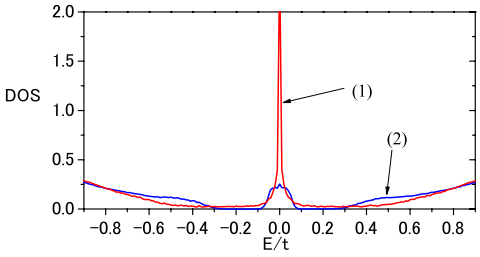

Figure 1: Density of states around $E = 0$ for a random magnetic field. Fluxes per hexagon are distributed in the range $[-0.2 + (1/41), 0.2 + (1/41)]$ in units of (h/e). The mean value $\phi_{\rm mean} = 1/41$ is much smaller than the fluctuation ± 0.2. The cases with (1) and without (2) spatial correlation are presented. The system has 82×5000 sites.

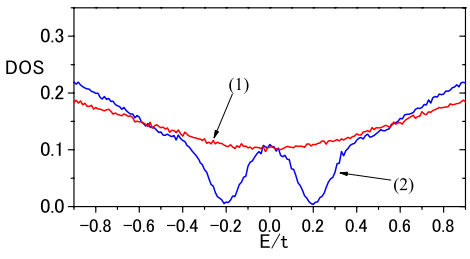

Figure 2: Density of states around $E = 0$ for a random site potential with $\phi_{\rm mean} = 1/41$. Site energies are distributed in the range $[-1, 1]$ in units of the transfer integral. The cases with (1) and without (2) spatial correlation are presented. The system has 82×5000 sites.

July 22 (Wednesday)

11:00 – 12:30

Plenary Session 3, 4

Main Hall

EP2DS-MSS Joint session

Ikuta shrine

Outlook over graphene flatland

A. K. Geim*

**Centre for Mesoscience & Nanotechnology, University of Manchester, Oxford Road, Manchester M13 9PL, UK*

Keywords: graphene

Graphene is a wonder material with many superlatives to its name [1-3]. It is not only a new 2D electronic system but the first truly 2D crystal. It is the thinnest material in the universe and the strongest one ever measured. Charge carriers in graphene exhibit the highest known intrinsic mobility, have the smallest effective mass (it is zero) and can travel the longest (micron) distances without scattering at room temperature. Graphene can sustain the highest current densities (million times higher than copper), shows record thermal conductivity and stiffness, is impermeable and reconciles such conflicting qualities as brittleness and ductility. Electron transport in graphene is described by a Dirac-like equation (rather than the standard Schrödinger equation) allowing the investigation of relativistic quantum phenomena in a bench-top experiment.

I will overview our experimental work on graphene concentrating on its fascinating electronic and optical properties and speculate about future applications.

References

1. A. H. Castro Neto, F. Guinea, N. M. R. Peres, K. S. Novoselov, A. K. Geim. The electronic properties of graphene. *Rev. Mod. Phys.* **81**, 109 (2009).

2. A. K. Geim, K.S. Novoselov. The rise of graphene. *Nature Mat.* **6**, 183 (2007).

2. A. K. Geim, A.H. MacDonald. Graphene: Exploring carbon flatland. *Physics Today* **60**, 35 (2007).

Coherence and control of single electron spins in quantum dots

L.M.K. Vandersypen

* Kavli *Institute of Nanoscience, Delft University of Technology, Delft, the Netherlands*

Keywords: electron spin, quantum dots, quantum coherence

Individual electron spins isolated in semiconductor quantum dots are natural two-level quantum systems that could form the basis of a quantum information processor. Using a fully electrical approach, it is now possible to initialize, coherently manipulate and read out the spin state of a single electron in a quantum dot, and to couple it coherently to the spin of an electron in a neighbouring dot. Furthermore, we have come to a quantitative understanding of the timescales and mechanisms by which the spin loses phase coherence. Ongoing work focuses on integrating all buildings blocks in a single experiment, and on either control or elimination of the electron spin environment, in particular the nuclear spins in the quantum dot host material. This should permit using entangled spins as a new resource for quantum information processing.

References

[1] R. Hanson, L.P Kouwenhoven, J.R. Petta, S. Tarucha, and L.M.K. Vandersypen, *Spins in few-electron quantum dots*, Reviews of Modern Physics 79**,** 1217 (2007)

[2] I. T. Vink, K. C. Nowack, F. H. L. Koppens, J. Danon, Yu. V. Nazarov, and L. M. K. Vandersypen, Locking electron spins into magnetic resonance by electron-nuclear feedback, arXiv:0902.2659

[3] F.H.L. Koppens, K.C. Nowack, and L.M.K. Vandersypen, *Spin echo of a single electron spin in a quantum dot*, Phys. Rev. Lett. 100, 236802 (2008)

[4] K.C. Nowack, F.H.L. Koppens, Yu.V. Nazarov and L.M.K. Vandersypen, *Coherent control of a single electron spin with electric fields*, Science 318, 1430 (2007)

[5] F.H.L. Koppens, C. Buizert, K.J. Tielrooij, I.T. Vink, K.C. Nowack, T. Meunier, L.P. Kouwenhoven, and L.M.K. Vandersypen, *Driven coherent oscillations of a single electron spin in a quantum dot*, Nature 442, 766-771 (2006)

July 23 (Thursday)

9:00 – 11:15

Session E6

Graphene

Main Hall

EP2DS-MSS Parallel session

Kobe “Ijinkan”

Screening and its consequences in graphene

S. Das Sarma and E. H. Hwang
Condensed Matter Theory Center, Department of Physics, University of Maryland, College Park, Maryland 20742-4111

Keywords: Screening, Collective mode, Thermopower, Transport in spin polarization.

We present the dynamical dielectric function of graphene at arbitrary wave vector q and frequency ω, $\epsilon(q,\omega)$. [1] As a direct consequences of the dynamical dielectric function, we provide the long-wavelength plasma oscillation of a collection of charged massless Dirac particles interacting via the long-range Coulomb interaction [2]. We find that the long-wavelength plasmon frequency in such a doped massless Dirac plasma is explicitly non-classical in all dimensions with the plasma frequency being proportional to $1/\sqrt{\hbar}$. We also show that the long wavelength plasma frequency of the D-dimensional superlattice made from such a plasma does not agree with the corresponding $D+1$ dimensional bulk plasmon frequency. We compare and contrast such Dirac plasmons with the well-studied regular palsmons in metals and doped semiconductors which manifest the usual classical long wavelength plasma oscillation.

As consequences of static screening function we provide the temperature and spin-polarization dependent transport in graphene. We calculate the temperature dependent conductivity and thermopower of graphene in the presence of randomly distributed Coulomb impurity charges arising from the temperature dependent screening of the Coulomb disorder. We find that the calculated temperature dependent conductivity is non-monotonic, decreasing with temperature at low temperatures, and increasing at high temperatures as observed in experiments. [3] The calculated thermopower [4] behaves as $1/\sqrt{n}$ at high densities, but saturates at low densities. We also find that the thermopower scales with normalized temperature T/T_F and does not depend on the impurity densities, but strongly depends on the fine structure constant r_s and the location of the impurities. We use an effective medium theory to calculate thermopower at low carrier density regimes where electron-hole puddles dominate. We also consider the transport of graphene in the presence of in-plane magnetic field (B). [5] We take into account the magnetic field induced spin polarization. We find $\sigma \propto B^2$ for intrinsic graphene, but for extrinsic graphene the change of the screening behavior due to the polarization of the carriers gives rise to the positive magnetoresistance.

This work is supported by U.S. ONR.

References

[1] E. H. Hwang and S. Das Sarma, Phys. Rev. B **75**, 205418 (2007).

[2] S. Das Sarma and E. H. Hwang, arXiv:0902.3822 (2009).

[3] K. I. Bolotin *et al.*, Phys. Rev. Lett. **101**, 096802 (2008).

[4] E. H. Hwang, E. Rossi, and S. Das Sarma, arXiv:0902.1749 (2009).

[5] E. H. Hwang and S. Das Sarma, arXiv:0812.0403 (2008).

Weak Localisation and Anti-Localisation in Graphene

A. K. Savchenko, F. V. Tikhonenko, A. A. Kozikov, R. V. Gorbachev

School of Physics, University of Exeter, Exeter EX4 4QL, UK

Keywords: graphene, quantum interference, weak antilocalisation

It has recently become clear that quantum interference in graphene is very different from that in conventional 2D systems. It was predicted that it is controlled not only by inelastic scattering, which is responsible for the phase breaking, but also by a number of elastic scattering processes [1, 2]. This prediction has been confirmed in experiments on mechanically exfoliated [3] and epitaxial [4] graphene structures, where the characteristic elastic times important for the manifestation of weak localisation have been determined: the time of intra-valley suppression of quantum interference, τ^*, and inter-valley scattering time, τ_i. These times play different roles in the quantum interference of the chiral carriers in graphene: whilst small τ^* suppresses quantum interference, small τ_i restores its manifestation, which is seen in the temperature dependent magneto-conductance.

It was expected that in defect-free graphene (large τ^* and τ_i) the quantum correction to the conductance at zero magnetic field would have a positive sign (weak antilocalisation) accompanied by a negative low-field magneto-conductance. However, in the experimental systems studied before [3,4], the low-field magnetoconductance always had a positive sign, indicating weak localisation at B = 0.

In this work we study the magnetoconductance of graphene flakes on Si/SiO_2 substrates and determine the characteristic times involved in the quantum interference at different temperatures T and different carrier densities n. We show that in mechanically exfoliated samples one can achieve both weak localisation and antilocalisation, by varying T and n. By changing the experimental conditions we indeed observe the transition between these two regimes of quantum interference, which is detected as a transition from positive to negative low-field magneto-conductance.

We also show that quantum interference in graphene can be seen at unusually high temperatures, up to T~110 K. We discuss the origin of this behaviour and determine the mechanisms of electron dephasing in graphene in a broad range of temperatures: from 40 mK to 110 K.

References

1. E. McCann et al., Phys. Rev. Lett. **97**, 146805 (2006); K. Kechedzhi et al., Phys. Rev. Lett. **98**, 176806 (2007).
2. A. F. Morpurgo, and F. Guinea, Phys. Rev. Lett. **97**, 196804 (2006).
3. R. V. Gorbachev et al., Phys. Rev. Lett. **98**, 176805 (2007); F. V. Tikhonenko et al., Phys. Rev. Lett. **100**, 056802 (2008).
4. X. Wu et al., Phys. Rev. Lett. **98**, 136801 (2007).

Graphite from the viewpoint of Landau level spectroscopy: An effective graphene bilayer and monolayer

M. Orlita, C. Faugeras, J. M. Schneider, G. Martinez, D. K. Maude, and M. Potemski
National High Magnetic Field Laboratory - Grenoble, CNRS, France

Keywords: Dirac fermions, graphite, Landau level spectroscopy

We describe an infrared transmission study of a thin layer of bulk graphite in magnetic fields up to $B = 34$ T. Two series of absorption lines whose energy scales as $\sqrt{B}$ and B are present in the spectra and identified as contributions of massless holes at the H point and massive electrons in the vicinity of the K point, respectively. We show that infrared magneto-absorption spectra of graphite, measured over a wide range of the energy and magnetic field, can be interpreted in a very simple, transparent and elegant manner. Our results confirm, in agreement with recent theoretical considerations [Koshino and Ando, Phys. Rev. B 77, 115313 (2008)], that graphite can be viewed as an effective graphene monolayer and bilayer, see Fig. 1. This theoretical picture is derived using a drastically simplified SWM model, which includes only two parameters γ_0 and γ_1, describing the intra- and inter-layer tunneling, respectively.

In this simplified picture, the dominant contribution to the optical response is provided by the H point, where electron states closely resemble graphene but with an additional double degeneracy, and by the K point, where the energy spectrum resembles a graphene bilayer, but with an effective coupling of $2\gamma_1$, twice enhanced compared to a real bilayer system. Remarkably, using this simple graphene monolayer plus bilayer view of graphite, we are able to correctly reproduce the magnetic field evolution of all observed inter-LL transitions using only the SWM parameters γ_0 and γ_1, with values which perfectly match those derived from studies of real graphene monolayer and bilayer systems. Interestingly, the electronic states at K point of graphite are found to mimic those of the graphene bilayer, but with a doubled value of the effective mass, so that they might be useful to further explore the interesting physics of massive Dirac fermions.

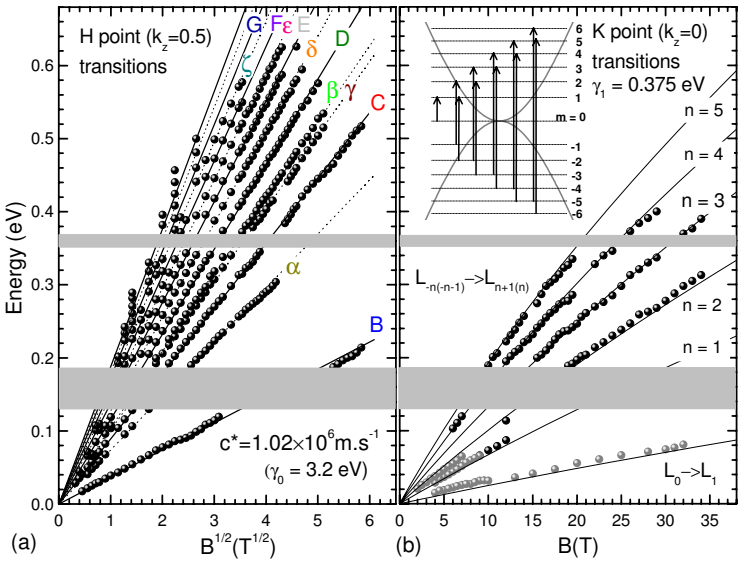

Figure 1: (a): Positions of the absorption lines related to the H point as a function of $\sqrt{B}$. The solid and dashed lines represent expected positions of absorption lines for $\tilde{c} = 1.02 \times 10^6$ m/s ($\gamma_0 = 3.2$ eV). (b): K point related absorption lines as a function of B. The solid lines show expected dipole allowed transitions in a graphene bilayer with an effective coupling $2\gamma_1$ for $\gamma_0 = 3.2$ eV and $\gamma_1 = 0.375$ eV. The inset schematically shows the observed interband transitions in the effective bilayer.

Parallel and perpendicular optical absorptions in bilayer graphene

Mikito Koshino and Tsuneya Ando
**Department of Physics, Tokyo Institute of Technology, Tokyo, Japan*

Keywords: graphene, bilayer graphene, conductivity, optical absorption

Graphene bilayer, which was recently found in experiments [1], was shown to have a unique band structure distinct from monolayer graphene, where the conduction and valence bands with quadratic dispersion touch at zero Fermi energy [2, 3]. A unique property of bilayer graphene is that an electric-field applied perpendicularly to the layers modifies its low-energy band structure by opening an energy gap between the electron and hole bands [4, 5, 6].

In this paper, we study the optical response of bilayer graphene to light polarized perpendicular and parallel to graphene layers. We consider the effect of the top and bottom gates attached to the sample, which control the electron concentration as well as the perpendicular electric field. The effective electric-field giving rise to the gap is self-consistently calculated. For the perpendicular polarization, in particular, the effective dynamical conductivity giving the absorption is calculated with inclusion of the depolarization effect associated with induced charge redistribution between two layers.

Spectral features, characterized by peaks and edges associated with specific transitions between subbands, are quite different between perpendicular and parallel polarizations, since each of transitions can be allowed or prohibited depending on the polarization direction. For the perpendicular light, the absorption energy is considerably shifted by the dynamical screening effect, while that is absent for parallel polarization.

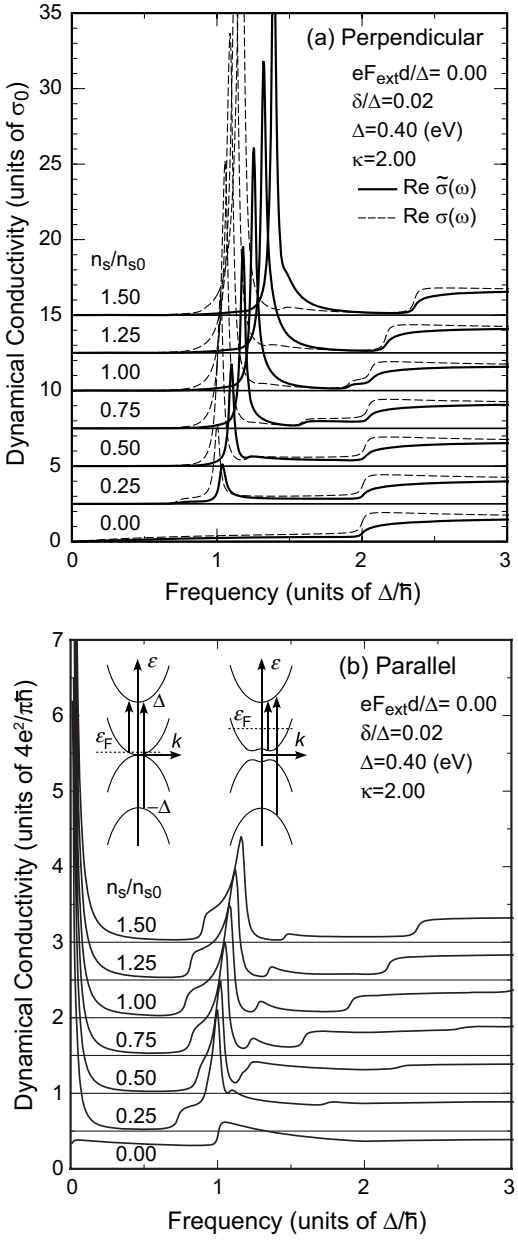

Figure 1: Optical absorption in bilayer graphene for (a) perpendicular and (b) parallel polarizations, with several electron concentration n_s. In (a), the dashed lines represent results neglecting the dynamical screening effect. The electron concentration when the Fermi level touches the bottom of the first excited conduction band is denoted by n_s^0 ($\approx 2.5 \times 10^{13}$ cm^{-2}).

References

[1] K. S. Novoselov, A. K. Geim, S. V. Morozov, D. Jiang, M. I. Katsnelson, I. V. Grigorieva, S. V. Dubonos, and A. A. Firsov, Nature **438**, 197 (2005).
[2] E. McCann and V. I. Fal'ko, Phys. Rev. Lett. **96**, 086805 (2006).
[3] M. Koshino and T. Ando, Phys. Rev. B **73**, 245403 (2006).
[4] E. McCann Phys. Rev. B **74**, 161403(R) (2006).
[5] J. B. Oostinga, H. B. Heersche, X. Liu, A. F. Morpurgo and L. M. K. Vandersypen, Nat. Mat. **7**, 151 (2008).
[6] T. Ando and M. Koshino, J. Phys. Soc. Jpn. **78**, 034709 (2009).

Trilayer graphene: a semimetal with gate-tunable band overlap

S. Russo*,**, M. F. Craciun*, M. Yamamoto*, J. B. Oostinga**,***, A. F. Morpurgo*** and S. Tarucha*,****

** Department of Applied Physics, The University of Tokyo, Tokyo, Japan*

*** Kavli Institute of Nanoscience, Delft University of Technology, Delft, The Netherlands*

**** Department of Condensed Matter Physics, University of Geneva, Geneva, Switzerland*

***** Quantum Spin Information Project, ICORP, Japan Science and Technology Agency, Atsugi, Japan*

Keywords: trilayer graphene, electronic transport

Graphene-based materials are promising candidates for nano-electronic applications, ranging from high-speed circuits to single-molecule sensors [1-3]. One of the remarkable aspects of graphene, important for possible electronic applications, is the very high carrier mobility that can be achieved without the use of sophisticated material preparation techniques [1]. However, the carrier mobilities reported for single-layer and bilayer graphene are still less than those reported for graphite crystals at low temperatures, and it is currently unclear which layer thickness may be more suitable for a given application. For the optimization of future devices, it is important to understand how the electronic properties of graphene based materials evolve from Dirac massless particles, in single layer graphene [3], to massive particles in bulk graphite.

We experimentally address this question by investigating trilayer graphene, which is the thinnest few layer graphene based system with a tight-binding Hamiltonian that includes all the transfer integrals that are needed to describe the band structure of graphite. Our study is based on charge transport through trilayers graphene as a function of carrier density, temperature, and perpendicular electric field, which is generated using a double-gated device. Contrary to single layer and bilayer graphene (which are both zero gap semiconductors), we find that trilayer graphene is a semimetal with a finite overlap of conduction and valence bands (see Fig.1). We show that the low energy band structure of trilayer graphene can be tuned by a large amount by means of an external perpendicular electric field, achieving 100% change in band overlap a property not known to occur in any other semimetal [4]. The quantitative analysis of the data further allows the determination of the carrier effective mass, which accounts for large part of the observed evolution of the carrier mobility with layer thickness.

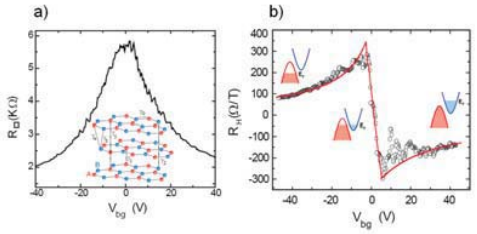

Fig.1 (a) Square resistance and (b) the Hall coefficient measured as a function of the voltage applied to the back gate for trilayer graphene. A perpendicular magnetic field of 9T is applied in (b). The inset in (a) shows the crystal structure of a trilayer graphene. The continuous curve in (b) is the fitted $R_H(V_{bg})$ assuming that trilayer graphene is a semimetal with a band overlap of 28meV. The three insets in (b) schematically depict the position of the Fermi level at different values of V_{bg}.

References

1. K. S. Novoselov et al., Science **306**, 666 (2004).
2. A. K. Geim and K. S. Novoselov, Nature Materials **6**, 183 (2007).
3. K. S. Novoselov et al., Nature **438**, 197 (2005).
4. M. F. Craciun, S. Russo, M. Yamamoto, J. B. Oostinga, A. F. Morpurgo and S. Tarucha, to appear in Nature Nanotechnolgy (2009).

July 23 (Thursday)

11:15 – 12:30

Session E7

Coherent manipulation of quantum mechanical freedom

Main Hall

EP2DS-MSS Parallel session

Kobe port tower 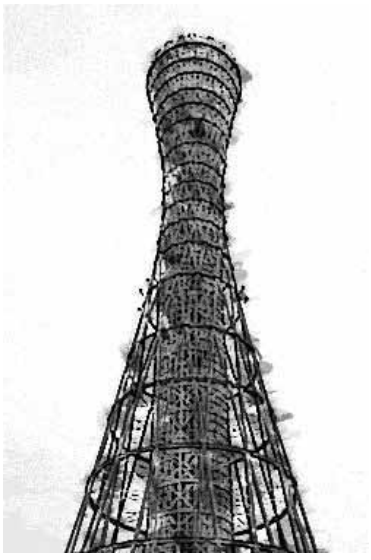

Multi pulse operation and optical detection of nuclear spin coherence in a quantum well

Y. Ohno[*], Y. Kondo[*], M. Ono[*], S. Matsuzaka[*,**], H. Sanada[*], K. Morita[**,*], and H. Ohno[*,**]

[*]*Laboratory for Nanoelectronics and Spintronics, Research Institute of Electrical Communication, Tohoku University, 2-1-1 Katahira, Aoba-ku, Sendai 980-8577, Japan*

[**]*ERATO Semiconductor Spintronics Project, Exploratory Research for Advanced Technology, Japan Science and Technology Agency, Sanban-cho 5, Chiyouda-ku, Tokyo 102-0075, Japan*

Keywords: semiconductor spintronics, nuclear magnetic resonance, GaAs, quantum well

A new class of nuclear magnetic resonance (NMR) with high-sensitivity and high-spatial resolution has become important tool to investigate spin-related physics in semiconductor nanostructures. In our previous work, we have developed a time-resolved Faraday rotation (TRFR) magnetometry to readout the coherent dynamics of nuclear polarization [1], in which spin precession of electrons monitors the nuclear polarization via hyperfine interaction. In this work, we show the manipulation of the phase coherence in nuclear spin ensemble in a GaAs/AlGaAs single quantum well (QW) by employing multi pulse sequence that is identical to the quantum gate operation for preparation of superposition as well as the Bell states of (virtual) 2-qubit states, i.e. Hadmard (H-) and controlled-NOT (CNOT) gates based on classical rf-pulse NMR technique [2].

The sample studied here is a single, 8.5 nm-wide GaAs/$Al_{0.3}Ga_{0.7}As$ quantum well (QW) with 5×10^{17} cm^{-3} Si donor concentration. The eigenstates of spin-3/2 ^{75}As, i.e., $|m\rangle = |-3/2\rangle, |-1/2\rangle, |1/2\rangle$, and $|3/2\rangle$ are taken as basis of virtual two-qubit system $|11\rangle$, $|10\rangle$, $|01\rangle$, and $|00\rangle$. The evolution of the density matrix $\boldsymbol{\rho}_j$ after the application of rf magnetic field $\mathbf{B}_{rf}$ pulses can be evaluated by measuring the change of Faraday rotation angle θ_F at fixed time delay Δt (labeled as $\Delta\theta_F$).

The inset of Fig. 1 shows the cw-NMR spectrum for ^{75}As detected by TRFR. Three distinct resonance lines are resolved, corresponding to (I) $|3/2\rangle\leftrightarrow|1/2\rangle$, (II) $|-1/2\rangle\leftrightarrow|1/2\rangle$, and (III) $|-3/2\rangle\leftrightarrow|-1/2\rangle$ transitions, respectively. Figure 1 shows $\Delta\theta_F$ measured as a function of the width τ of a single-square-shaped pulse $\mathbf{B}_{rf}$, that corresponds to the evolution of $\langle I_z\rangle \equiv \mathrm{tr}(\boldsymbol{\rho}_{As}\mathbf{I}_z)$ (Rabi oscillation). By fitting, we found T_{2Rabi} of the I and II transitions to be 0.9 ms and 2.1 ms, respectively.

Starting from the initial population of the nuclear spin states under optical pumping, we generated the pseudo-pure state (pps), $|00\rangle_{pps}$, which is represented by $\Delta\boldsymbol{\rho}_{As}(|00\rangle) = \mathrm{diag}([1/2, 1/2, 1/2, -3/2])$. $|00\rangle_{pps}$ is generated by applying two sine-shaped pulses. Next we generated a superposition of two states by

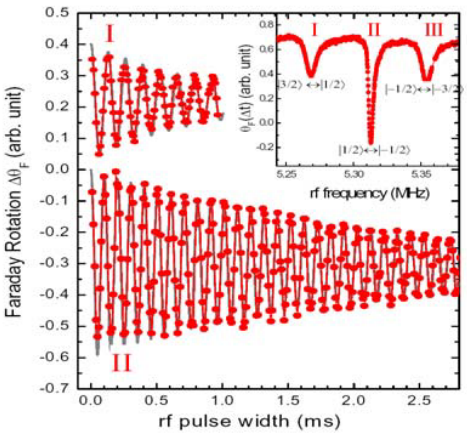

Fig. 1 Rabi oscillations for I (upper) and II (lower) transitions are shown. $\Delta\theta_F$ reveals the change of the nuclear polarization after application of a single-square $\mathbf{B}_{rf}$ pulse. The inset is a cw-NMR spectrum of ^{75}As.

applying Hadmard (H-) gate upon the pseudo-pure state $|00\rangle_{pps}$, and then the Bell state by applying CNOT-gate upon the superposition state. For $I = 3/2$ two-qubit spin systems, H-gate can be constructed by two successive pulses with different phases, a $\pi/2$-pulse at ω_I with $\varphi = 90°$ (labeled by $Y(\pi/2)_I$) and a π-pulse at ω_I with $\varphi = 0°$ (labeled by $X(\pi)_I$), that turns $|00\rangle$ into a superposition $(|00\rangle+|01\rangle)/\sqrt{2}$. The Bell state $(|00\rangle+|11\rangle)/\sqrt{2}$ is then generated by operating CNOT-gate, which consists of three π-pulses $Y(\pi)_{II}$-$Y(\pi)_{III}$-$X(\pi)_{II}$. These protocols are schematically shown in Fig. 2(a). In Fig. 2(b), the NMR spectra for the initial pseudo-pure state (labeled by $|00\rangle$), the superposition $(|00\rangle+|01\rangle)$, and the Bell state $(|00\rangle+|11\rangle)$ are shown: The baseline of the NMR curves amount to the averaged nuclear polarization $\langle I_z\rangle$, and the peak and dip in NMR spectra indicate the population difference between two states. For comparison, simulation results of $\langle I_z\rangle$ for each state are plotted in Fig. 2(c) as a function of $\Delta\omega_{rf} = \omega_{rf} - \omega_{II}$. The experimental NMR spectra agree quite well with the simulations, indicating that the population of each state is controlled by these gate operations.

In order to probe the coherence of the system, we examined the off-diagonal components of $|00\rangle+|11\rangle$ by measuring the populations (diagonals) after a three-pulse sequence of the quantum state tomography (QST) that is composed of $Y(\pi/2)_{III}$-$Y(\pi/2)_{II}$-$Y(\pi/2)$. The experimental NMR spectrum of the QST is also shown in Fig. 2(b) (labeled by "QST"). For comparison, we calculated the NMR spectra as a function of the off-diagonal value α (–1, –0.5, and 0) and plotted in Fig. 2(c). The position of the baseline ($\langle I_z\rangle$) and the negative peak at ω_{II} seen in the experimental curve are close to the calculated QST curve with finite phase coherence ($\alpha = -0.5$). This appears to show that the phase coherence is partially retained after the gate operations, in spite of the fact that the total time of the pulse sequences is 400~500 μs, which is 1/2 ~ 1/4 of T_{2Rabi} and comparable to the intrinsic spin coherence time T_2 ~ 600 μs (370 μs) for transition-II (I).

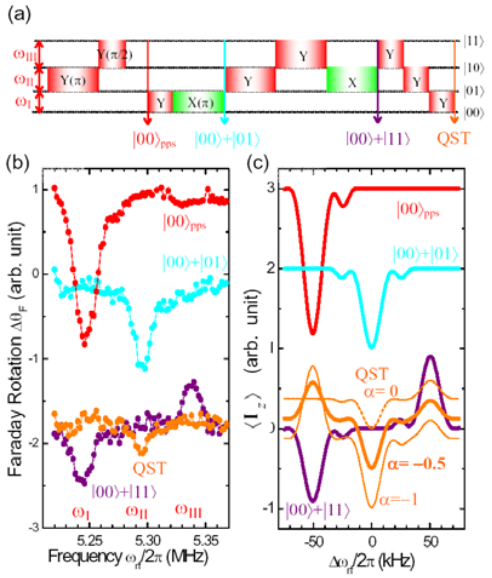

Fig. 2 (a) The schematic diagram of the multipulse sequence. (b)(c) The experimental and simulation results of NMR spectra for $|00\rangle_{pps}$, $|00\rangle+|01\rangle$, $|00\rangle+|11\rangle$, and the QST are shown.

We believe that the present optical approach is useful not only for studying phase coherence in quantum states and nuclear spin dependent physics in semiconductor nanostructures but also read-out of a quantum information stored in multi-level nuclear spins in dense memory devices.

References

[1] H. Sanada et al. Phys. Rev. Lett.**96**, 067602 (2006).

[2] Y. Kondo et al., Phys. Rev. Lett. **101**, 207601 (2008).

Detection of optically injected single electron charge and spin in a quantum dot using a quantum point contact

H. Kiyama*, T. Fujita*, G. Allison*, T. Asayama*,**, A. Pioda*, A. Oiwa*,†, and S. Tarucha*,†,‡

* *Department of Applied Physics and QPEC, The University of Tokyo*

** *Advanced Materials Laboratories, SONY Corporation*

†*Quantum Spin Information Project, ICORP, JST*

‡*Institute for Nano Quantum Information Electronics, The University of Tokyo*

Keywords: Quantum dot, Photon- electron conversion, Spin read-out

Photons, and electron spins in a semiconductor quantum dot (QD) are leading candidates for implementing qubits in information transmission, and computing, respectively. Therefore, quantum media conversion (QMC) between them is a key technology for a comprehensive quantum network.

The first step toward QMC is the conversion of single photon to single electron charge. We successfully demonstrated it using a lateral QD quantum point contact (QPC) as a charge sensor, all made on a GaAs/AlGaAs heterostructure. The measurements were performed at 1.5 K. Incident single photons with photon energy of 1.59 eV are absorbed in the GaAs buffer layer and the photo-electrons are only trapped in the QD. The time evolution of QPC current with a pulsed single photon irradiation shows a distinctive up-step of 0.8 nA superposed on a gradually-decaying background (Fig. 1 (a)). The step height matches that typically observed for one-electron tunnelling out of QD in the transport regime. We stress that the trapped electron can be ejected from the QD in a controlled manner within a time scale faster than the typical spin flip time.

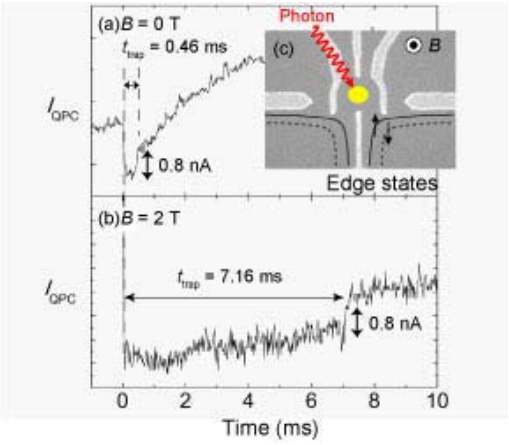

Fig.1 Time evolution of QPC current at (a) B = 0 and (b) B = 2 T. (c) SEM image of the device and schematic diagram of the spin–polarized edge states.

The second step is the conversion of circularly polarized single photon to single electron spin. Prior to this, we examined a scheme combining the single photon detection with tunnel-rate selective spin readout using spin-resolved quantum Hall edge states formed in the 2DEG reservoirs (Fig 1(c)). The spatial difference between the edge states causes the difference in the dot-lead tunnel rate between up and down spin [1]. We measured the QPC current with unpolarized light, which creates equal numbers of up and down spin electrons in the QD. The observed photo-electron trapping time t_{trap} was sometimes much longer for magnetic field B exceeding 1.5 T than at B = 0 T (Fig. 1). Observation of long t_{trap} at the high magnetic field indicates that the dot-lead tunnel-rate is much longer for up-spin electrons than for down-spin electrons, as expected. This result ensures that the present scheme will hold for the angular momentum transfer between single photon and single electron spin.

References

1. M. Ciorga *et al*., Appl. Phys. Lett. **80**, 2177 (2002)

Coherent spin injection and spin state tomography by light in a semiconductor quantum well

H. Kosaka[1,2], H. Shigyou[1], T. Inagaki[1], Y. Rikitake[3,2], H. Imamura[4,2], Y. Mitsumori[1,2], K. Edamatsu[1]

[1] Research Institute of Electrical Communication, Tohoku University, Sendai, Japan
[2]CREST-JST, 4-1-8 Honcho, Kawaguchi, Saitama, Japan
[3]Department of Information Engineering, Sendai National College of Technology, Sendai, Japan
[4] Nanotechnology Research Institute, AIST, Tsukuba, Japan

Key words: quantum interface, quantum state transfer, photon polarization, electron spin

We demonstrate that the polarization coherence of light can be coherently transferred to the spin coherence of electrons in a semiconductor quantum well [1], and the prepared coherence of the electron spin can also be coherently read out with light by the developed tomographic Kerr rotation method [2].

Spin is a fundamental property of electrons and plays an important role in information storage. For spin-based quantum information technology, preparation and readout of the electron spin state are essential functions. Since coherence of the spin state is the manifestation of quantum nature, both the preparation and readout should be spin coherent. However, a traditional spin injection based on optical selection rule and spin measurement based on Kerr rotation, basically prepare and read out the up or down projective spin states, which do not carry the spin coherence. Here we show schemes of coherence transfer and measurement by generalizing the traditional optical selection rule and the Kerr rotation method to directly prepare and readout the electron spin coherence with light independent on the basis selection. Both of the developed spin coherence transfer and the tomographic Kerr rotation (TKR) method utilize the light-hole excitons under in-plane magnetic field in a g-factor controlled semiconductor quantum wells.

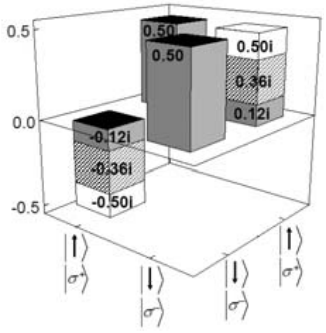

Fig. 1, A reconstructed density matrix of the optically injected electron spin state measured by the developed tomographic Kerr rotation method (dark bars). Shaded bars show the calibrated amplitudes. White bars are the density matrix of the pump light with the D^+ polarization.

Figure 1 shows a density matrix of the electron spin state reconstructed from the measured TKR amplitudes with and without calibration (shaded and dark bars) together with that of the pump light state as a reference (white bars). We assumed that the initial degree of polarization of the electron spin created by a circularly polarized light is unity owing to the optical selection rule of the well-defined LH excitons. By comparing those two density matrices (shaded and white bars), we estimate that the fidelity of the spin coherence transfer from photons to electrons in the maximally superposed case is 0.86±0.03, which is close to unity. The fidelity degradation is due to spin decoherence after the initial preparation originating in the electron-hole exchange interaction.

The spin coherence transfer and the spin state tomography demonstrated here will be applicable to the transfer of a single-particle quantum state and a two-particle entangled state, which is the kind of transfer needed for quantum information technology. The developed scheme offers a tool for performing basis-independent preparation and readout of a spin quantum state in a solid-state device for quantum cryptography and quantum distributed computing.

This work was supported by CREST-JST, ERATO-JST, SCOPE-MIC, MEXT and NEDO.

References

[1] Kosaka, H. *et al*. ***Phys. Rev. Lett.*** **100**, 096602 (2008).
[2] Kosaka, H. *et al*. ***Nature*** **457**, 702 (2009).

July 23 (Thursday)

14:00 – 16:00

Session E8

Electron-environment interaction

Main Hall

EP2DS-MSS Parallel session

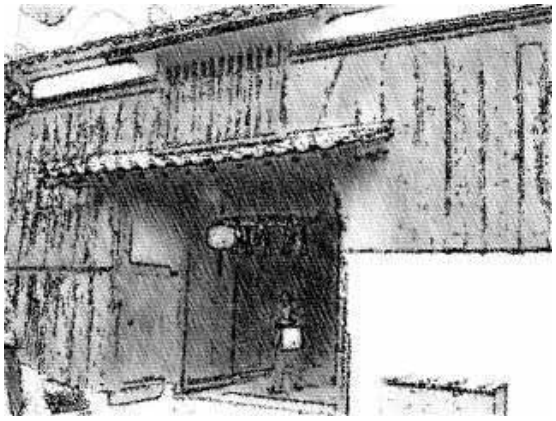

Nada “sake” brewery

Time-resolved charge detection and back-action in quantum circuits

T. Ihn, U. Gasser, S. Gustavsson, T. Müller, B. Küng, T. Choi, M. Studer, R. Leturcq, I. Shorubalko, and K. Ensslin
Solid State Physics Laboratory, ETH Zurich, CH-8093 Zurich, Switzerland

Keywords: double quantum dots, quantum point contacts, charge-detection, back-action

The detection of quantum dot charge states using a quantum point contact charge detector has opened a new exciting route for the investigation of quantum circuits [1]. In particular, time-resolved charge detection allowed the precise measurement of quantum dot shot noise at sub-femtoampere current levels, and the full counting statistics of the current. The technique has been applied to different material systems, such as dots in Ga[Al]As, InAs quantum wires, and even graphene. It holds promise for the future application in quantum dot-based quantum information processing implementations. Scientists are challenged by the perspective to push the technique to bandwidths at which quantum time scales become relevant [2].

Quantum point contacts Coulomb-coupled to double quantum dots are of particular interest. For example, an appropriately placed charge detector can distinguish, which of the two dots an excess electron occupies. Also the coupling strength of all tunneling barriers can be directly measured in a time-resolved fashion. In addition, the charge detector can provide insights into cotunneling processes occurring in the double quantum dot device off resonance [3]. Shot noise induced spectral shifts have been measured as well [4]. It has been proposed theoretically that such systems are predestined to be used for weak measurements [5].

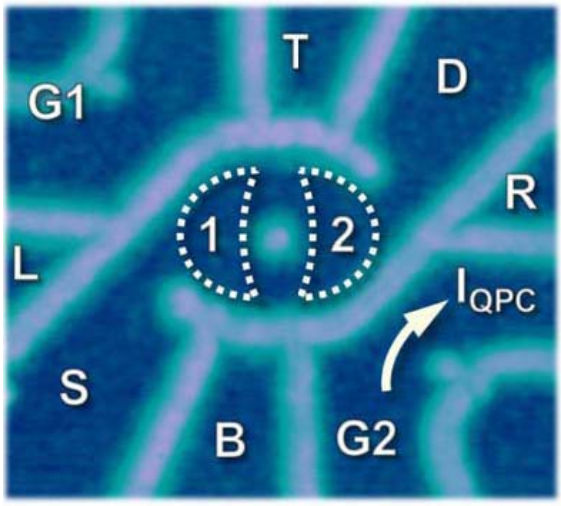

Figure 1: Double quantum dot system based on a Ga[Al]As heterostructure with a two-dimensional electron gas 34 nm below the surface. Lateral pattening was performed by standard photolithography and local anodic oxidation of the semiconductor surface with a scanning force microscope. The two quantum dots labeled 1 and 2 are connected to source (S) and drain (D) contacts. Charge detection is achieved by driving a current I_{QPC} through the quantum point contact (G2). Regions L, R, T, and G1 are used as in-plane gates.

It is a property of all quantum measurements that the detector unavoidably disturbs the measured system, a phenomenon called detector back-action. An equivalent way of looking at the same effect is to exchange the role of the measured system and the detector. We therefore address the question, in which way double quantum dots (or single dots) can detect electrons traversing a quantum point contact. It has been established in previous experiments that the shot noise of the quantum point contact current can couple into a system with coherent dynamics and act as a source for decoherence [6]. We have performed complementary experiments using double quantum dot devices as a frequency selective detector to observe the shot noise in the quantum point contact [7], as well as current induced heating of the phonon bath [8]. These experiments demonstrate the use of double quantum dots as a spectroscopic tool with excellent energy resolution for the study of non-equilibrium bosonic environments. At the same time they open the perspective to use double quantum dots themselves as ultrasensitive charge detectors, as it has been recently suggested theoretically [9].

References

[1] for a review, see: T. Ihn, S. Gustavsson, U. Gasser, B. Küng, T. Müller, R. Schleser, M.

Sigrist, I. Shorubalko, R. Leturcq, K. Ensslin, arXiv:0905.3398v1(2009).

[2] T. Müller, K. Vollenweider, T. Ihn, R. Schleser, M. Sigrist, K. Ensslin, M. Reinwald, and W. Wegscheider, CP893, Physics of Semiconductors, 28th Int. Conf., edited by W. Jantsch and F. Schäffler, American Institute of Physics, 2007; D.J. Reilly, C.M. Marcus, M.P. Hanson, and A.C. Gossard, Appl. Phys. Lett. **91**, 162101 (2007); M.C. Cassidy, A.S. Dzurak, R.G. Clark, K.D. Petersson, I. Farrer, D.A. Ritchie, and C.G. Smith, Appl. Phys. Lett. **91**, 222104 (2007); M. Thalakulam, W.W. Xue, F. Pan, Z. Ji, J. Stettenheim, L. Pfeiffer, K.W. West, and A.J. Rimberg, arXiv:0708.0861 (2007).

[3] S. Gustavsson, M. Studer, R. Leturcq, T. Ihn, and K. Ensslin, D.C. Driscoll, A.C. Gossard, Phys. Rev. B **78**, 155309 (2008).

[4] B. Küng, S. Gustavsson, T. Choi, I. Shorubalko, T. Ihn, S. Schön, F. Hassler, G. Blatter, K. Ensslin, arXiv:0904.3656v1 (2009).

[5] A. Romito, Y. Gefen, Ya.M. Blanter, Phys. Rev. Lett. **100**, 056801 (2008); see also: A.N. Jordan, B. Trauzettel, G. Burkard, Phys. Rev. B **76**, 155324 (2007).

[6] E. Buks, R. Schuster, M. Heiblum, D. Mahalu, V. Umansky, Nature **391**, 871 (1998); D. Sprinzak, E. Buks, M. Heiblum, H. Shtrikman, Phys. Rev. Lett. **84**, 5820 (2000); I. Neder, F. Marquardt, M. Heiblum, D. Mahalu, and V. Umansky, Nature Physics **3**, 534 (2007).

[7] S. Gustavsson, M. Studer, R. Leturcq, T. Ihn, K. Ensslin, D.C. Driscoll, A.C. Gossard, Phys. Rev. Lett. **99**, 206804 (2007); S. Gustavsson, I. Shorubalko, R. Leturcq, T. Ihn, K. Ensslin, S. Schön, Phys. Rev. B **78**, 035324 (2008).

[8] U. Gasser, S. Gustavsson, B. Küng, K. Ensslin, T. Ihn, D.C. Driscoll, and A.C. Gossard, Phys. Rev. B **79**, 035303 (2009).

[9] T. Gilad, S.A. Gurvitz, Phys. Rev. Lett. **97**, 116806 (2006); T. Geszti, Z. Bernád, Phys. Rev. B **73**, 235343 (2006).

Franck-Condon blockade in suspended carbon nanotube quantum dots

R. Leturcq[1,2], C. Stampfer[1,3], K. Inderbitzin[1], L. Durrer[3], C. Hierold[3], E. Mariani[4], M. G. Schultz[4], F. von Oppen[4] and K. Ensslin[1]

1 *Laboratory for Solid State Physics, ETH Zurich, Zurich, Switzerland*

2 *IEMN, CNRS-UMR 8520, Department ISEN, Villeneuve d'Ascq, France*

3 *Micro and Nanosystems, Department of Mechanical and Process Engineering, ETH Zurich, Zurich, Switzerland*

4 *Institut für Theoretische Physik, Freie Universitt Berlin, Berlin, Germany*

Keywords: transport in carbon nanotubes; semiconductor quantum dots; nanoelectromechanical systems

Measurements through nanoelectromechanical systems and single-molecule junctions have shown that electronic transport is strongly influenced by the mechanical motion, leading to transport assisted by emission of vibrons. Furthermore, a strong electron-vibron coupling is expected to lead to a suppression of transport through the vibronic ground state, known as Franck-Condon blockade [1].

Here we report on transport in a quantum dot formed in a suspended carbon nanotube device (inset of Fig. 1) [2]. The data show Coulomb diamonds with a clear four-fold degeneracy (Fig. 1) and allows us to make a quantitative comparison between experiment and theory (Fig. 2). We observe a strong suppression of electron transport through the vibronic ground state, and give an equivocal confirmation of Franck-Condon blockade in suspended nanostructures [3]. Furthermore, we show vibron absorption processes, and we present an explanation and estimates for the surprisingly strong electron-vibron coupling in carbon nanotubes. The strong negative differential conductance observed ubiquitously remains to be understood.

References

[1] J. Koch and F. von Oppen, Phys. Rev. Lett. **94**, 206804 (2005).

[2] C. Stampfer, A. Jungen, R. Linderman, D. Obergfell, S. Roth and C. Hierold, Nano Lett. **6**, 1449 (2006).

[3] R. Leturcq, C. Stampfer, K. Inderbitzin, L. Durrer, C. Hierold, E. Mariani, M. G. Schultz, F. von Oppen, K. Ensslin, Nature Physics (in press).

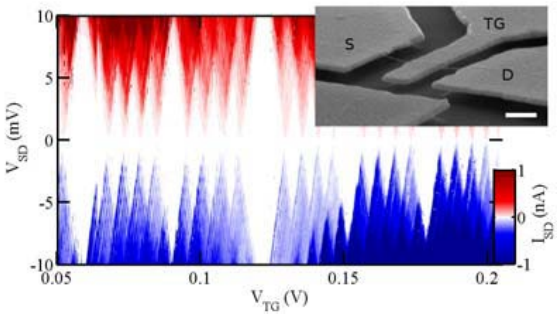

Figure 1: Map of the source-drain current vs. bias and gate voltages. Inset: Scanning electron microscope micrograph of the suspended carbon nanotube sample, with source (S) and drain (D) contact, and a suspended top-gate (TG). The white scale bar is 200 nm.

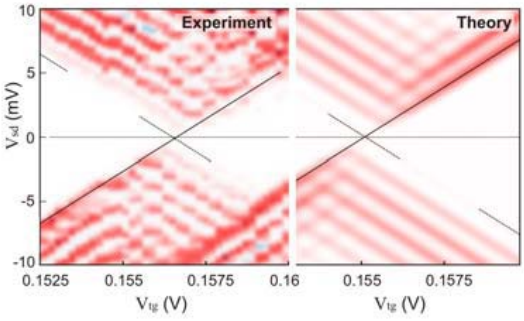

Figure 2: Map of the differential conductance dI_{DS}/dV_{DS} vs. bias and gate voltages from the experiment (left) and simulated (right), showing that both the excited vibronic states and the suppression of the transport at low bias voltage are very well reproduced by the Franck-Condon blockade theory [1].

Intrinsic nature of the zero bias anomaly (ZBA) in quantum point contacts

F. Sfigakis, S. Sarkozy*, K. Das Gupta, I. Farrer, D.A. Ritchie and M. Pepper
Cavendish Laboratory, University of Cambridge, United Kingdom
**Currently with Northrop Grumann Aerospace Systems, California, USA*

Keywords: zero bias anomaly, Kondo, quantum point contact

Quantisation of conductance in units of $2e^2/h$ is the best known signature of ballistic transport through quantum point contacts (QPC), as described by the picture of transmission of non-interacting electrons through a saddle point potential. Yet, in nanoelectronic devices (of which QPCs are building blocks), the channel is generally biased such that the conductance $G \leqslant 2e^2/h$. In this regime, the 0.7 structure and a Kondo-like zero bias anomaly (ZBA) [1] are observed, and cannot be explained within a non-interacting picture. Since the Kondo effect requires a bound state for which there is no obvious origin (other than an unintentional impurity), the ZBA in QPCs is an intriguing effect. In this paper, we describe experiments designed to answer two specific questions: (i) "What happens to the ZBA if the number of charged impurities in the channel is reduced in a quantifiable way?", and (ii) "Is the ZBA related to the 0.7 structure?".

QPCs were fabricated on undoped GaAs/AlGaAs heterostructures, and consisted of two levels of gates separated by a layer of insulating polyimide [2]. Undoped heterostructures enabled a high mobility to be obtained at very low densities – this is crucial if the conductance regime near pinch-off is to be studied. Modulation-doped 2-dimensional electron gases (2DEG) with very high mobilities at high carrier densities rapidly lose mobility as the carrier density is lowered, due to remote ionised impurity scattering. In undoped heterostructures, the only source of scattering is the unintentional background doping (N_B). From our density-mobility curves, we experimentally determine an average $\overline{N_B} = 1.2{\times}10^{14}\mathrm{cm}^{-3}$ in our wafers. Thus our 2DEG (extending 20 nm) has a sheet impurity density of $N_A = 2{\times}10^{16}\mathrm{cm}^{-2}$. If the lithographic area of the QPC is $W = 0.4\mu m \times 0.7\mu m$, then the classical probability $P = 1 - e^{-N_A W}$ of a random impurity occupying the channel is less than $\sim$0.4. Such a regime is very difficult to achieve using high mobility delta-doped or modulation-doped 2DEGs.

Our main finding is that the ZBA in clean QPCs can be traced reproducibly over five orders of magnitude in conductance from $G \sim 2e^2/h$ down to $10^{-5} \times 2e^2/h$ [3], deep in the tunneling regime. Thus its origin must be very distinct from the 0.7 structure, which occurs only in ballistic transport with at least one fully transmitting spin subband. We also find that the ZBA splits in magnetic field with a variable effective g-factor, which is very small near pinch-off and increases as the channel is opened up. Our data strongly suggests that the ZBA is an intrinsic feature in QPCs and its origin cannot be due to a random nearby impurity coupling to conduction electrons.

References

[1] K.J. Thomas *et al.*, Phys. Rev. Lett **77**, 135 (1996). S. Cronenwett *et al.*, Phys Rev. Lett. **88**, 226805 (2002).

[2] S. Sarkozy *et al.*, Appl. Phys. Lett. (accepted).

[3] S. Sarkozy *at al.*, Phys. Rev. B (Rapid), (accepted).

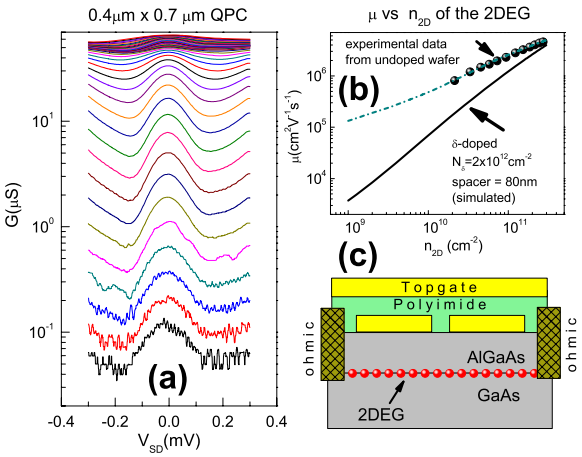

Figure 1: (a) An example of ZBA traced down to G< $0.1\mu S$. (b) The advantage of undoped 2DEGs over doped 2DEGs becomes important at low densities. (c) A schematic of the 2-level gating method used.

Electron transfer between distant quantum dots by surface acoustic waves

R. P. G. McNeil, M. Kataoka, C. J. B. Ford, C. H. W. Barnes, D. Anderson, G. A. C. Jones, I. Farrer and D. A. Ritchie.

Cavendish Laboratory, University of Cambridge, Cambridge CB3 0HE, United Kingdom

Keywords: quantum dot, dynamic quantum dot, quantum point contact, surface acoustic wave

Quantum dots (QDs) provide a useful tool for studying confined systems [1]. Tunnelling of electrons between double quantum dots [2] has been demonstrated but over micron distances a tunnel barrier is inadequate. We demonstrate the transfer of single electrons over micron distances from one quantum dot to another through a depleted one dimensional channel using a surface acoustic wave (SAW) pulse. This technique may allow the movement of quantum information between distant quantum dots.

The device consist of two QDs (RQD & LQD) connected by a 4 μm long channel all defined by surface gates [Fig. 1(a)], on a GaAs/AlGaAs heterostructure with a 2DEG 90nm below the surface. A transducer is placed 1 mm to the right. The number of electrons a dot can hold is controlled by the barrier and plunger gates. Electrons trapped in the RQD are raised above the Fermi energy by plunger and barrier gate sweeps where these non-equilibrium electrons can be held for several seconds [3]. Having set the RQD (full) and LQD (empty) a SAW pulse is sent. If the RQD potential is set near that of the depleted channel, the SAW potential will lift an electron from the right dot and carry it towards the left dot. The electron is then trapped in the left dot by a large voltage on the barrier gate. Changes in the occupation of the QDs are monitored by quantum point contacts [Fig 1(c)]. We will explain how the QDs can be set up with extra electrons, [Fig. 1(b)(inset)] and how the SAW pulses depopulate the RQD [Fig. 1(b)]. A 'full' QD may be initialised and depopulated with a reliability of 97% and the 'empty' state with near complete reliability. Figure 1(d) shows how the capture of electrons by the LQD varies with barrier gate voltage and initial RQD state with increasingly reliability in the range -0.9 to -1.2 V. We currently see capture rates up to 60% limited by the maximum voltage we could apply to the barrier gate before the device becomes unstable. We believe this problem can be easily resolved and a larger barrier bias would further increase the success rate.

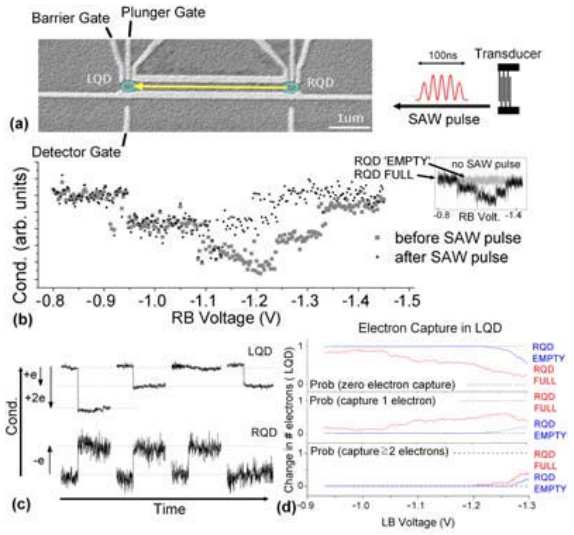

Figure 1: (a) SEM of device. Arrow shows electron transfer between QDs (outlined) due to SAW pulse from the right. (b) Mean conductance before and after SAW pulse for 'full' RQD. Above -1.1V SAW pulse partially or fully depopulates the RQD. (inset) RQD set 'empty'(grey) or with extra electrons(black). (c) QPC conductance traces during SAW (de)population of (LQD)RQD. (d) Probability of capturing 0, 1 or ≥ 2 electrons depends on left barrier voltage and initial state of RQD.

References

[1] R. Hanson *et. al.,* Rev. Modern Phys. **79**, 1217 (2007).

[2] T. Hayashi *et. al.,* Phys. Rev. Lett. **91**, 226804 (2003).

[3] M. Kataoka *et al.,* Phys. Rev. Lett. **98**, 046801 (2007).

Noise in Carbon Nanotubes in the Kondo regime

C. Mora*,**, T. Delattre*,**, C. Feuillet-Palma*,**, L.G. Herrmann*,**, P. Morfin*,**, J.-M. Berroir*,**, G. Fève*,**, B. Plaçais*,**, D.C. Glattli*,**,***, M.-S. Choi**** and T. Kontos*,**

*Ecole Normale Supérieure, Laboratoire Pierre Aigrain, 24, rue Lhomond, 75231 Paris Cedex 05, France

**CNRS UMR 8551, Laboratoire associé aux universités Pierre et Marie Curie et Denis Diderot, France

***Service de physique de l'état Condensé, CEA, 91192 Gif-sur-Yvette, France

****Department of Physics, Korea University, Seoul 136-713

Keywords: Kondo effect, Carbon Nanotube Quantum Dot, current noise measurements.

The Kondo effect is a very active subject in condensed matter physics and a paradigm for strongly correlated electronic systems. It arises as a resonant antiferromagnetic coupling between the spin of an impurity with the spin of the conduction electrons in the host matrix. In nanoscale conductors like carbon nanotube devices, the spin impurity is formed in a strong Coulomb blockade region where charge is quenched. Such artificial impurities offer new perspectives for the study of the Kondo effect, in particular in out-of-equilibrium situations. We report here on *current noise* measurements in a carbon nanotube quantum dot tuned to the Kondo regime. A strong enhancement of the current noise is observed within the Kondo resonance compared to simple non-interacting theories. While the measured conductances come close to the unitary limit $2e^2/h$, the noise is not suppressed as in a coherent conductor but remains sizeable. This effect can not be accounted for, either by a resonant level model, or by a simple SU(2) Kondo model. This emphasizes the importance of the doubly degenerate orbital degree of freedom (in addition to the spin degeneracy) in the dot related to clockwise and counterclockwise motion around the nanotube. Moreover, the addition of this orbital pseudo-spin with the true spin could lead to Kondo screening with an enhanced SU(4) symmetry. In fact, using an interacting slave-boson mean field (SBMFT) approach with SU(4) symmetry to describe the Kondo effect, we can account [1] for both conductance and noise measurements with a rather good agreement.

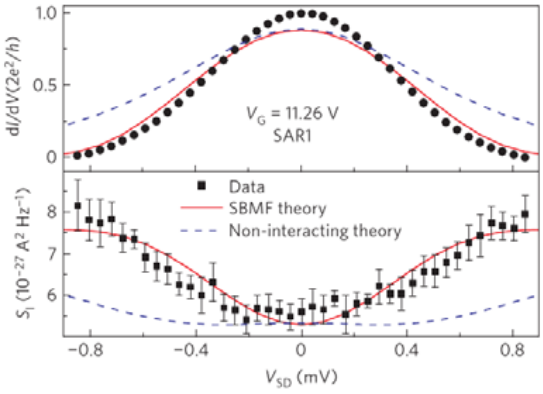

Figure 1: Conductance and noise measurements (black circles and black squares respectively) compared to the SU(4) SBMFT calculation (solid line). A resonant (non-interacting) model is shown in dashed lines for comparison.

We also discuss theoretically [4] the computation of current and noise in the Fermi liquid regime, *i.e.* for energies much smaller than the Kondo temperature. We focus in particular on the definition and calculation of universal effective charges [2, 3] which characterize the current fluctuation, for instance the shot noise. In the case of the Kondo effect with an extended SU(4) symmetry, a universal charge $e^* = 0.300\,e$ is predicted. The importance of temperature and asymmetric coupling to the electrodes is also emphasized.

References

[1] T. Delattre et al., Nature Physics 5, 208 (2009).

[2] E. Sela, Y. Oreg, F. von Oppen, J. and Koch, Phys. Rev. Lett. **97**, 086601(2006).

[3] O. Zarchin et al., Phys. Rev. B **77**, 241303 (2008).

[4] C. Mora, X. Leyronas, and N. Regnault, Phys. Rev. Lett. **100**, 036604 (2008).

Effect of Coulomb interaction for shot noise in a quantum dot

T. Fujii
*Institute for Solid State Physics, University of Tokyo, Kashiwa, Chiba, Japan

Keywords: Kondo effect, quantum dot, shot noise, nonequilibrium Kubo formula

Advance of nanotechnology has allowed us to address the correlated transport in mesoscopic devices. Kondo effect in a quantum dot is one of fascinating examples. Recently shot noise in the Kondo regime has been studied. Especially in Refs.[1, 2], the Fermi-liquid nature has been reexamined. They have shown that the current close to the unitarity limit is given by $I = 2e^2V/h - I_b$ using "the backscattering current" I_b. Here $I_b \equiv -e\partial_t(N_{LH}(t) - N_{RH}(t))$ gives a reduction from the perfect transmission for the $\pi/2$ phase shift. H is the fixed point Hamiltonian. Therefore noise power is defined by only the backscattering current. This fact has thus stimulated to estimate an effective charge for the backscattering current. They have shown that the Fano factor $F_b = S/2eI_b$ results in a universal fractional value $5/3$ up to $\mathcal{O}(V^3)$. This universal feature has stimulated further studies. A shot-noise measurement has been reported on $F_b = 5/3$ close to the unitarity limit at low bias voltages[3]. In the context of the full counting statistics[4] this result has been reproduced and an expression in any strength of Coulomb interaction has been conjectured .

Here we prove the conjectured result in any strength of Coulomb interaction by using the renormalization perturbation theory(RPT). As shot noise, we use a new formula of shot noise S_h in the following discussion.

Recently we have deeply analyzed the density matrix of the Keldysh formalism applied for mesoscopic systems. The resulting density matrix enables us to obtain an expression of differential conductance: $G = \beta S/4 - \beta S_h/4$, where S is the current-current correlation function, and S_h is the non-trivial current-charge correlation function and $\beta = 1/k_{\rm B}T$[5, 6]. We have called it the *nonequilibrium Kubo formula*. The nonequilibrium Kubo formula is written into $S_h = S - 4k_{\rm B}TG$. At zero temperature S_h equals the conventional shot noise S. In the linear response regime S_h is proven to vanish, and the Nyquist-Johnson relation is reproduced. Furthermore in noninteracting systems $S^0 - 4k_{\rm B}TG^0$ expresses shot noise. Therefore we have proposed that S_h gives a definition of shot noise at any temperature in correlated systems. Thus theoretically calculated S_h can be compared with $S - 4k_{\rm B}TG$ using S and G measured in experiments. Therefore, the nonequilibrium Kubo formula enables us to address shot noise at any temperature in correlated systems[5].

Appling S_h to a quantum dot at zero temperature, the Fano factor $F_b = S_h/2eI_b$ is calculated using the RPT, and shown as

$$F_b = 1 + \frac{4(R-1)^2}{1+5(R-1)^2}, \tag{1}$$

where R is the Wilson ratio. Using limiting values of the Wilson ratio R, F_b yields

$$F_b = \begin{cases} \frac{5}{3} & U \to \infty \quad R = 2 \\ \\ 1 & U \to 0 \quad R = 1 \end{cases} \tag{2}$$

F_b indeed reproduces the universal fractional value of $F_b = 5/3$ derived in the s-d limit, and a naively expected value $F_b = 1$ for a noninteracting system. Therefore eq.(1) indeed gives the general expression in any Coulomb interaction strength[6].

References

[1] E. Sela, Y. Oreg, F von Oppen, and J. Koch, Phys. Rev. Lett. **97**, 086601 (2006).

[2] A. Golub, Phys. Rev. B **73**, 233310 (2006); A. Golub, ibid. **75**, 155313 (2007).

[3] O. Zarchin, M. Zaffalon, M. Heiblum, D. Mahalu, and V. Umansky, Phys. Rev. B **77**, 241303(R) (2008).

[4] A. O. Gogolin and A. Komnik, Phys. Rev. Lett. **97**, 016602 (2006).

[5] T. Fujii, J. Phy. Soc. Jap. **76**, 44709 (2007).

[6] T. Fujii, arXiv:08074869v1.

Lifting of Coulomb blockade and Kondo effect in a quantum dot by highly-biased nearby a quantum point contact

K. Hitachi*, A. Oiwa** and S. Tarucha**

** Department of Physics, University of Tokyo, Hongo, Bunkyo-ku, Japan*

*** ICORP-JST & Department of Applied Physics, University of Tokyo, Hongo, Bunkyo-ku, Japan*

Keywords: Quantum dot, quantum point contact, Kondo effect, photon-assisted tunneling

Electron spin in quantum dots (QDs) is a robust quantum number, and has been studied for application to quantum information processing. A quantum point contact (QPC) capacitively coupled to a QD has been used as a charge sensor to the dot and also to read out the spin state. On the other hand, application of a large excitation voltage to the QPC can induce fluctuation of charge states in the QD due to emission of photons from the QPC. Inter-dot photon-assisted tunneling [1] and photon-assisted excitation of an excited state in a QD [2] were observed. In addition, lifting of the Kondo effect was observed, although the underlying physics was not fully understood [3].

In this work we studied the influence on the Coulomb blockade and Kondo effect in a QD by a nearby QPC when highly biased. We found that Coulomb blockade is partially, asymmetrically lifted, depending on the way of coupling of photons emitted from the QPC to the leads and also that the Kondo effect is lifted by electron heating via photon absorption in the leads.

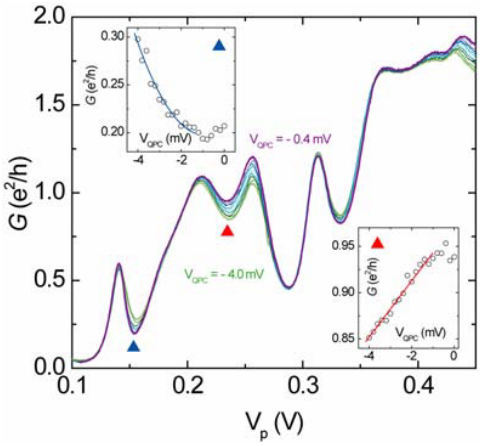

Fig.1 Coulomb oscillations in G vs. V_p for V_{QPC} = -0.4mV (purple) to -4.0mV (green). Top, and bottom insets show G vs. V_{QPC} at Coulomb and Kondo valley, respectively.

We prepared a QD with a nearby QPC in a GaAs/AlGaAs heterostructure. For a QD with a small dot-lead coupling, we observed excess current due to lifting of Coulomb blockade. This current polarity is different between to the left and right of Coulomb peaks. It also depends on the QPC bias (V_{QPC}) polarity. These results are consistently explained by predominant photon coupling to one of the leads. We also found that the photon absorption accompanies local electron heating, from measurement of Coulomb peak width.

For the large dot-lead tunnel coupling, we observed increased conductance of Coulomb valley and decreased conductance of Kondo valley for the large $|V_{QPC}|$ (> 1 mV) (Fig. 1). By analyzing the $|V_{QPC}|$ dependence of electron temperature, we could assign the decreased Kondo conductance to the increased electron temperature. Note this is the first experimental clarification for the decreased Kondo conductance for the large $|V_{QPC}|$. In contrast, for the small $|V_{QPC}|$ (< 1 mV), no increase of electron temperature and therefore, no decrease of Kondo conductance was observed. This means that Kondo coherence is not affected by QPC at the small $|V_{QPC}|$ as used for charge sensing to QDs.

References

1. E. Onac *et al*., Phys. Rev. Lett. **96**, 176601 (2006).
2. S. Gustavsson *et al*., Phys. Rev. Lett. **99**, 206804 (2007).
3. M. Avinun-Kalish *et al*., Phys. Rev. Lett. **92**, 156801 (2004).
4. D. Goldhabor-Goldon *et al*., Phys. Rev. Lett. **81**, 5225(1998).

July 23 (Thursday)

16:00 – 18:00

Poster Session Th-eP

Meeting Room 501, 502

EP2DS-MSS Parallel session

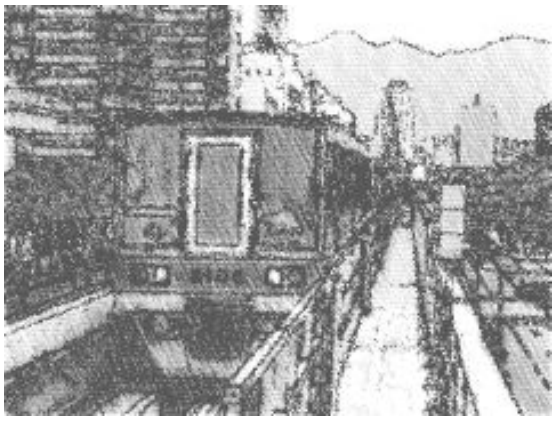

Port liner

Hysteretic funnel structures in vertical quantum dot molecules

D. G. Austing[1,2], C. Payette[1,2], G. Yu[1] and J. A. Gupta[1]

[1]*Institute for Microstructural Sciences M50, NRC, Ottawa, Ontario K1A 0R6, Canada*

[2]*Department of Physics, McGill University, Montreal, Quebec H3A 2T8, Canada*

Keywords: Coupled quantum dots, Transport properties, Hyperfine interaction, Hysteresis

Recently funnel-like structures have been reported in the transport properties of weakly coupled quantum dot systems in relation to (actual or effective) two-electron singlet and triplet state physics. These systems include lateral GaAs quantum dots [1-5]; InAs quantum dots in a nanowire [6]; and ^{13}C quantum dots in a carbon nanotube [7]. When in or near the spin-blockade regime, close to 0 T, the funnel-like structures may exhibit hysteresis either on sweeping the generally weak (<0.2 T) magnetic (B-) field through 0 T [1,6,7] or sweeping a voltage at fixed B-field [6]. The hysteresis is attributed to the electron-spin nuclear-spin (hyperfine) interaction (dynamic nuclear polarization).

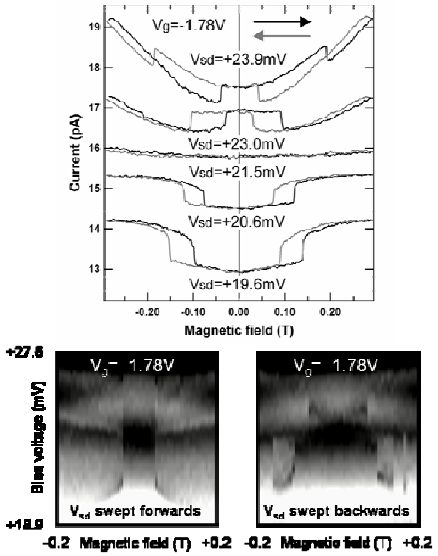

Fig.1 Funnel in regime II. Top: Current at fixed gate voltage (V_g) on sweeping the magnetic field up and down for different high bias voltages (V_{sd}). Bottom: Differential conductance at fixed gate voltage on sweeping the high bias voltage up and down and stepping the B-field.

Weakly coupled vertical dots in the spin-blockade regime [8,9] or at high bias [10] also show hysteretic behaviour generally for B-fields exceeding 200 mT but funnel-like structures close to 0 T have not previously been reported.

Here, we describe the appearance and properties of hysteretic funnel-like structures in the tunnelling current in the vertical double dot system on application of a B-field parallel to the current in two regimes: I and II (in two different devices).

Regime I: In the N=2 spin-blockade region, over a wide range of gate voltage, on sweeping the bias voltage up and down at fixed B-field, the region of hysteresis forms a funnel located symmetrically around 0 T between -45 mT and +45 mT (not shown).

Regime II: At high bias (~20 mV), well outside the spin-blockade regime, on sweeping the B-field up and down at fixed bias or on sweeping the bias voltage up and down at fixed B-field, a funnel is located symmetrically around 0 T between -200 mT and +200 mT (Fig. 1). Note the intriguing inversion of hysteresis on stepping the bias through ~21.5 mV (top panel).

References

1. F. H. L. Koppens et al, Science **309**, 1346 (2005).
2. J. R. Petta et al, Science **309**, 1346 (2005).
3. E. A. Laird et al, Phys. Rev. Lett. **99**, 246601 (2007).
4. J. R. Petta et al, Phys. Rev. Lett. **100**, 067601 (2008).
5. S. Foletti et al, arXiv:cond-mat/0604008 v.
6. A. Pfund et al, Phys. Rev. Lett. **99**, 036801 (2007).
7. H. O. H. Churchill et al, arXiv:0811.3236v1.
8. K. Ono and S. Tarucha, Phys. Rev. Lett. **92**, 256803 (2004).
9. J. Baugh et al, Phys. Rev. Lett. **99**, 096804 (2007).
10. D. G. Austing et al, Physica E **40**, 1118 (2008).

Quantum Hall effect in CdTe-based quantum wells

J. Kunc[1,2], P. Plochocka[1], K. Kowalik[1], F. J. Teran[1], R. Grill[2], D. K. Maude[1], M. Potemski[1], T. Wojtowicz[3] and G. Karczewski[3]

[1] Laboratoire National des Champs Magnétiques Intenses, *Grenoble High Magnetic Field Laboratory, CNRS, 25 avenue des Martyrs, 38042 Grenoble, France*

[2] *Institute of Physics, Charles University, Prague, Czech Republic*

[3] *IFPAN, Warsaw, Poland*

Keywords: II-VI quantum wells, 2DEG, FQHE, magneto-optics

We present magneto-transport and magneto-optical study of CdTe/CdMgTe quantum wells (QW) grown by molecular beam epitaxy. Our structures are one-side I-doped QWs with electron concentration of about $4.5x10^{11}cm^{-2}$. QWs are 20 nm wide and they exhibit relatively high electron mobility of ~300 000 cm^2/Vs. In addiiton to the integer quantum Hall effect (IQHE) we present the observation of well developed fractional quantum Hall effect (FQHE) (see Fig.1). Plateau in Hall resistance R_{xy} and zero longitudinal resistance R_{xx} at magnetic fields of 11.2 T and 14.0 T are identified as fractional filling factors ν = 5/3 and 4/3, respectively.

The polarisation resolved emission from the n=0 Landau level (LL) was recorded at filling factors $\nu \geq 3$ when the n=0 LL is well below the Fermi energy. The energetic separation of the emission lines in $\sigma^+$and σ^- polarisations gives a direct measure of the enhanced spin gap of the n=0 LL. A strong spin gap enhancements at odd filling factors is observed (see Fig. 2) which we assign to the exchange interaction of electrons in the n = 0 LL with electrons in the partially occupied Landau level at the Fermi energy. Thus, in contrast to transport measurements which are only sensitive to what is happening at the Fermi energy, optics can probe the exchange driven spin gap enhancement for electrons in completely occupied Landau levels well below the Fermi energy.

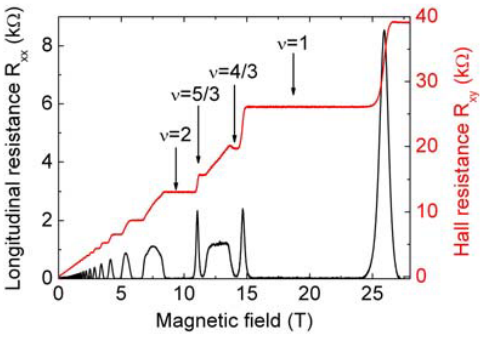

Fig.1 Fractional filling factors 5/3 and 4/3 can be clearly seen in both longitudinal and Hall resistance of 20 nm CdTe/CdMgTe quantum well at 40 mK.

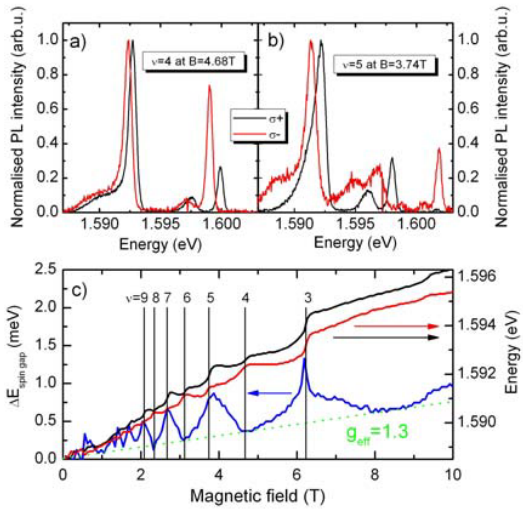

Fig.2 (a-b) Polarisation resolved PL at even odd filling factor. (c) Energy of the n=0 LL PL line in $\sigma^+$and σ^- polarisations and the spin gap (difference in energy of PL lines) vs magnetic field.

Detector Backaction on the Self-Consistent Bound State in Quantum Point Contacts

Y. Yoon[1], M.-G. Kang[1], T. Morimoto[2], L. Mourokh[3], N. Aoki[4], J. L. Reno[5], J. P. Bird[1,4], and Y. Ochiai[4]

1 *Department of Electrical Engineering, University at Buffalo, the State University of New York, Buffalo, NY 14260-1920, USA*

2 *Advanced Device Laboratory, RIKEN, 2-1 Hirosawa, Wako, Saitama 351-0198, Japan*

3 *Department of Physics, Queens College of CUNY, 65-30 Kissena Blvd., Flushing, NY 11367, USA*

4 *Graduate School of Advanced Integration Science, Chiba University, 1-33 Yayoi-cho, Inage-ku, Chiba 263-8522, Japan*

5 *CINT Science Department, Sandia National Laboratories, P.O. Box 5800, Albuquerque, NM 87185-1303*

Keywords: 0.7 feature, Fano resonance, detector backaction, quantum measurement

The manner in which a measurement affects a quantum system is central to philosophical discussions of quantum theory. Mesoscopic devices are well adapted to study this issue, since their properties are sensitive to their mutual coupling. Quantum dots and quantum point contacts (QPCs) have been used, for example, as capacitively-coupled charge detectors, to count electrons on a nearby, electrically-isolated, dot. A general problem with such schemes, however, arises from the *back-action* of the detector, the shot-noise in whose current can induce undesirable transitions in the system under study.

Inter-device coupling has also been used to study spin transport in QPCs, which are thought to spontaneously spin polarize near pinch-off. The spin polarization has been attributed to the ability of the QPC to function as a single-spin trap that confines an electron to a bound state (BS), formed by Friedel oscillations in the QPC potential. Evidence of this spin binding has been provided by studying the conductance of a (detector) QPC in close proximity to another (swept QPC) [1,2]. A resonance that occurs in the detector conductance when the swept QPC pinches off has been attributed [3] to an unusual Fano resonance, due to the wavefunction overlap between the BS and the detector. This coherent tunnel correlation arises between the QPCs, with electrons continuously being swapped between them, when the BS is driven through the Fermi level by the swept-QPC gate voltage.

While the use of QPCs as an all-electrical single-spin system could have important applications, realizing these will require a full understanding of how the bound spin is influenced by the coupling to its detector. For capacitive charge sensing, the backaction is due to multi-electron shot-noise. The spin-binding resonance, on the other hand, has been attributed to *single-particle* interference, arising from the wavefunction overlap of the QPCs. We show here that this results in an unusual backaction, in which increasing the wavefunction overlap, which we quantify via the Fano q-parameter, dramatically suppresses the resonance [4]. This behavior is shown to be inconsistent with shot noise, and is argued to arise instead from a weakening of the confinement of the BS due to its increased overlap with the detector. Our results thus demonstrate how the formation of BSs in QPCs is sensitive to their local environment, an important finding for discussions of the 0.7 feature, and the use of QPCs as a single-spin system.

References

1. J. P. Bird and Y. Ochiai, Science **303**, 1621 (2004).
2. Y. Yoon *et al*., Phys. Rev. Lett. **99**, 136805 (2007).
3. V. I. Puller *et al*., Phys. Rev. Lett. **92**, 096802 (2004).
4. Y. Yoon et al., Phys. Rev. B, Rapid Comm., *in press*.

Quasi-Landau levels in bilayer zigzag graphene nanoribbons

H. C. Chung*, M. H. Lee*, C. C. Chang*, Y. C. Huang**, and M. F. Lin*

*Department of Physics, National Cheng Kung University, Tainan, Taiwan

**Center for General Education, Kao Yuan University, Kaohsiung, Taiwan

Keywords: graphene, Landau level, density of states

The 1D AB-stacked bilayer zigzag graphene nanoribbons are investigated for the magnetoelectronic properties by the Peierls tight-binding model [1]. They exhibit rich energy spectra, mainly owing to the perpendicular uniform magnetic field (B), quantum confinement effects (finite widths), and interlayer interactions. The calculated energy bands and density of states (DOS) could be verified by the experimental measurements on absorption spectra, scanning tunnelling currents, and transport conductance.

A perpendicular magnetic field would induce the dispersionless Landau levels (LL's) in a 2D monolayer graphene. The quantum confinement effects in 1D graphene nanoribbons make them change into the composite energy bands. Such bands, as shown in Fig.1, are composed of the flat quasi-Landau levels (QLL's) and the parabolic energy bands. Two groups of QLL's, which are caused by the interlayer interactions, occur at E_F=0 and $E^{c,v}$=±0.36eV. The first and second groups include the unoccupied (c) and occupied (v) QLL's. They are not symmetric to each other about the Fermi level E_F=0. Moreover, they would gradually disappear as the state energy $|E^{c,v}|$ grows.

The main features are directly reflected on DOS. There exist a lot of symmetric prominent peaks. They come from the 1D composite energy bands. The heights, frequencies, and number of pronounced peaks are determined by the field strength, ribbon width, and interlayer interactions. DOS is closely related to the available channels in optical excitations and transport properties.

Reference

1. M. F. Lin et al., Phys. Rev. B **77,** 085426 (2008).

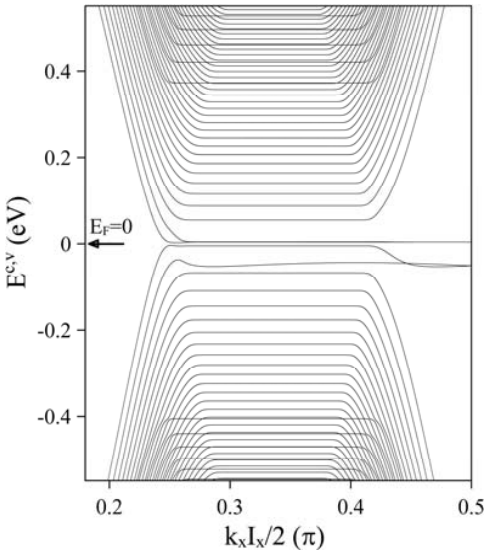

Fig.1 The magnetoelectronic structure of the AB-stacked bilayer zigzag nanoribbons with width W=1596Å at B=20T. The Fermi level is E_F=0.

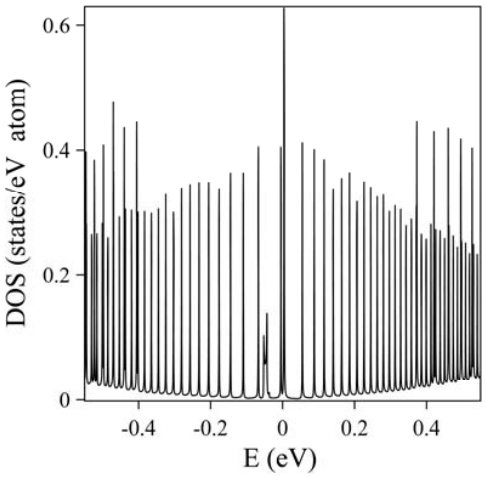

Fig.2 The low-frequency density of states.

Optical excitations of finite double-walled carbon nanotubes under electric field

R. B. Chen*

**Center of General Studies, National Kaohsiung Marine University, Kaohsiung 81143, Taiwan*

Keywords: Carbon nanotubes, Optical properties, Electric field

Double-walled carbon nanotubes (DWCNTs) with strong covalent bonds between carbon atoms in intratube and weak van der Waals forces between the intertubes. By cutting a very long CNT into a shorter one, a quasi-zero-dimensional finite CNT is obtained [1]. The reductions in length and in dimensionality exhibit special physical properties [2]. Each wall finite CNT is characterized by $(m, n; N_A)$. (m, n) corresponds to radius, and the total atom number N_A is proportional to length $N_z = N_A/2m$. The $(5, 5; 90)@(10, 10; 180)$ finite armchair DWCNT, inner and outer nanotubes, respectively, correspond to the heavy and light solid curves. The electronic states are evaluated by the tight-binding model. In the absence of electric field, for the S_5 symmetry, the discrete states are shown in Fig. 1(a). Electronic states are characterized by the angular momentum J=$(1, 2, \cdots, m)$. That is a narrow-gap semiconductor with energy gap $\sim 0.15\,\gamma_0$. The exhibits asymmetric energy dispersions about Fermi level with an J. The application of transverse electric field $\mathbf{E}_\perp$ can drastically modulate the discrete state energies [Fig. 1(b)]. State energies would become large (or small) with an increase in field strength, and exist state crossings at large field strength.

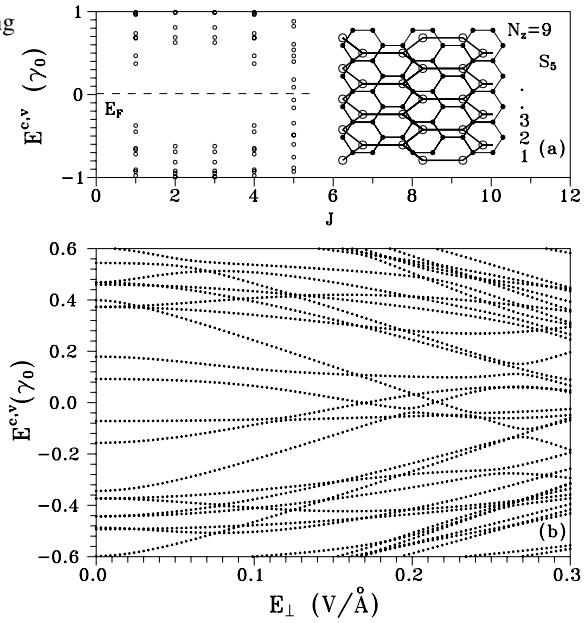

Figure 1: The (5,5;90)@(10,10;180) DWCNT for S_5 (a)electronic states; (b)energy spectra versus $E_\perp$.

The optical spectrum is mainly determined by the number of excitation channels and the dipole matrix element. The former is associated the density of states (DOS). In the absence of intertube interactions, the optical spectra $A(\omega)$ exhibits three prominent peaks at different electric field directions [no shown], since most the excitation channels are closed by the vanishing dipole matrix elements. They all present delta-function-like peaks, which are the characteristics of the finite systems. The threshold excitation energy is not equal to the band gap. Apparently, the intertube atomic hoppings have changed the excitation energies and the carrier distribution. Thus, both three prominent peaks and the weaker peaks separate into two or three absorption peaks. Besides, the direction of electric field plays an important role on $A(\omega)$, it would make the weaker peaks exhibit obviously energy different.

References

[1] L.C. Venema, J.W.G. Wildoer, H.L.J.T. Tuinstra, C. Dekker, A.G. Rinzler, and R.E. Smalley, Appl. Phys. Lett. **71**, 2629(1997).

[2] R.B. Chen, C.H. Lee, C.P. Chang, and M.F. Lin, Nanotechnology **18**, 075704(2007).

Magnetism and Correlations of Fractionally Filled Zero-energy States in Triangular Graphene Quantum Dots

A. D. Güçlü, Pawel Potasz, Oleksandr Voznyy, Marek Korkusinski and Pawel Hawrylak
Institute for Microstructural Sciences, National Research Council Canada, Ottawa, Canada

Keywords: graphene, quantum dots

Graphene quantum dots are atomically thick nanometer-scale islands etched out of a single graphene sheet. In this work, we focus on electronic and magnetic properties of triangular dots with zig-zag edges. Strikingly, such structures were suggested[1, 2] to lead to a band of degenerate zero-energy states at the Fermi level (Dirac point). Therefore, electrons in the zero energy band (shell) can be expected to form a strongly correlated electronic system, in analogy with the fractional quantum Hall effect.

In this work we present new results demonstrating the important role of electronic correlations, beyond the Hubbard model[1, 2], on the ground state and excitation spectra of triangular graphene quantum dots as a function of dot size and filling fraction of the band of zero-energy states. The interactions are treated by a combination of DFT, tight-binding, Hartree-Fock and configuration interaction methods (tb-HF-CI). In addition to the on-site interaction term, all scattering and exchange terms within second nearest neighbors, and all direct interaction terms are included in the calculations. Our model also includes the effect of next nearest neighbor hopping term, positive background charge, and charge induced on the gate.

Fig.1 shows the self-consistent single particle states close to the Fermi level for an island of 33 Carbon atoms, obtained from LDA and tight-binding/Hartree-Fock approaches. Consistent with previous calculations, there are 3 nearly degenerate levels, one of which is strongly localized on the edge of the island. In a second step, CI calculations were performed for a given number of electrons within the nearly degenerate band . The spin of the ground state as a function of shell filling obtained using tb-HF-CI method is shown in Fig.2, together with results obtained using tb-CI calculation with only Hubbard term included. Both models lead to fully spin polarized island at filling factor 1/2. However, Hubbard model enhances the ferromagnetism, forcing the ground state to be maximally polarized for all filling fractions. On the other hand, the full tb-HF-CI calculation shows that correlations lower the total spin of graphene quantum dot for filling fractions of 1/3 and 2/3.

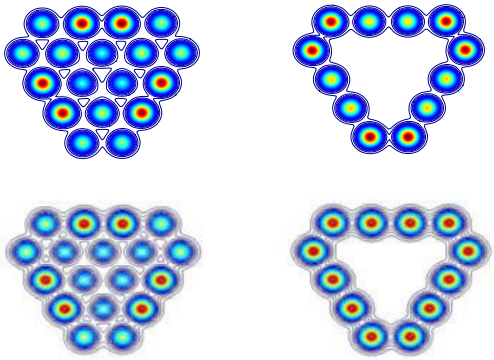

Figure 1: Densities of the 3 zero-energy levels obtained from LDA (top panel) and tight-binding/Hartree-Fock (bottom panel) approaches

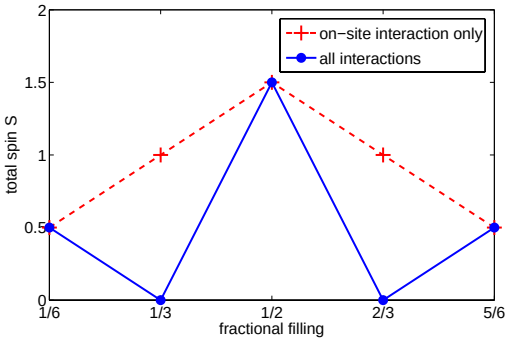

Figure 2: Total spin of the zero-energy energy electrons obtained from configuration interaction method

References

[1] J. Fernandez-Rossier and J.J. Palacios, Phys.Rev.Lett. **99**, 177204 (2007)

[2] M. Ezawa, Phys.Rev.B, **77**, 155411 (2008)

TRANSPORT OF Q1D SURFACE ELECTRONS OVER LIQUID ELIUM IN DENSE VAPOR

A.V. Smorodin, V. A. Nikolaenko, and S. S. Sokolov

B.Verkin Institute for Low Temperature Physuics and Engineering of the National Academy of Sciences of Ukraine

Keywords: surface electrons, liquid helium, dense gas

The behavior of electron in a dense inert gas calls a large attention. Especially attractive is helium where, due to a small mass, an electron obtains large energy of zero oscillations. As a result electron can be localized in a cavity (bubble) in a dense gas forming a specific particle - surface cation (also called bubblon). The interaction of 3D electron with helium gas leads to the bubble formation at gas density 10^{27} m^{-3} with bubble size of about 2×10^{-7} cm. The formation of a bubblon is accompanied by a strong change of electron conductivity. The study of the 3D electron transport in helium gas was carried out by the time-of-fight method /Levin and Sanders, 1967/. It was shown that at vapor density 2×10^{27} m^{-3} (the temperature was about 3.2 K) one observes a sharp decrease (jump) of electron conductivity. For 2D electrons over helium, the jump of conductivity is also observed but at lower temperature (about 3 K). In present work, we study the conductivity of surface electrons in helium localized in the system of Q1D channels. The substrate is formed by glass fibers (diameter 125 μm). The surface density of electrons was 10^9 cm^{-2} and temperature range was 1.3 - 2.5 K. As is seen in the Figure, the conductivity decreases exponentially with temperature and falls sharply near two orders at T = 2.43 - 2.46 K (curve 1). If one decreases temperature, the conductivity increases inthat range but only one order (curve 2). Probably such an asymmetry is connected with partial localization of electrons on the substrate roughness. We suppose that the change of electron conductivity at$T$ = 2.44 K is caused by a localization electron in dense vapor with formation of one-electron cations (bubblons). Note that drastic change in electron conductivity is observed in temperature range lower than that in 2D. We attribute such a difference with restricted nature of electron motion in Q1D conducting channel.

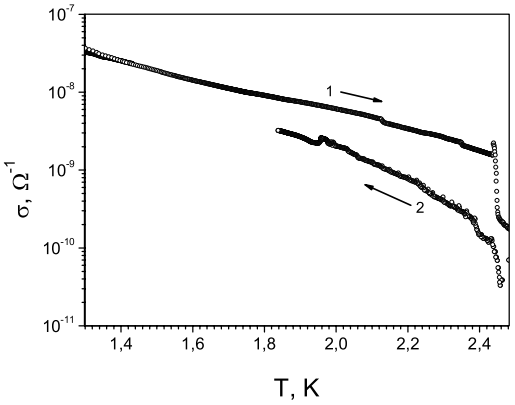

Figure 1:

Magnetic anisotropy in single metal-phthalocyanine molecules

Kohji Nakamura, Toru Akiyama and Tomonori Ito
Department of Physics Engineering, Mie University, Tsu, Mie 514-8507, Japan

Keywords: magnetic anisotropy, metal-phthalocyanine, first principles calculations

Interest in nanomagnetism has increased because of the potential importance in both basic and applied science, in which challenges now extend to treat an extreme limit of single atoms and molecules. So far many candidates of magnetic molecules — so-called single molecule magnets (SMMs) — are synthesized experimentally, and new and exotic features including their rich quantum behaviors are discovered. Generally, magnetic anisotropy in SMMs, which allows spin-magnetization orientation to maintain along the magnetic easy axis, may be enhanced due to a breaking of symmetry and an enhanced spin-orbit coupling (SOC) arising from the reduced dimensionality. Indeed, recent experiments found a large magnetic anisotropy in single atoms and molecules,[1, 2] which would represents a breakthrough in advancing magnetic molecular technology. From a theoretical point of view, however, little is known quantitatively about the detailed complexity in the magnetic anisotropy, and therefore it is desirable to understand it from highly precise first principles calculations.

In the present work, metal-phthalocyanines are focused as prototype molecules, in which a substitution of row transition-metals in the host molecule leads to a variety in electronic structures. Calculations are carried out by means of the film full-potential linearized augmented plane-wave (FLAPW) method[3, 4, 5] in the scalar relativistic approximation (SRA) for the conduction electrons, *i.e.*, without the SOC, and fully relativistically for the core electrons. The LAPW basis with a cutoff of $|\mathbf{k}+\mathbf{G}| < 3.6$ a.u.$^{-1}$ and muffin-tin (MT) sphere radii of 2.3 a.u. for transition-metals, and 1.2 a.u. for N and C, and 0.8 a.u. for H are used; lattice harmonics with angular momenta up to $\ell = 8$ for transition-metals, 6 for N and C, and 4 for H are employed to expand the charge and spin density, the potential, and eigenvectors. To determine the magnetic anisotropy, the second variational method[5] for treating the SOC is performed by using the calculated eigenvectors in the SRA, and the magnetic anisotropy energy, $E_{\rm MA}$, is determined by the force theorem,[6] which is defined as the energy eigenvalue difference for the magnetization oriented along the in-plane and out-of-plane directions with respect to the molecular plane.

As a first, here, results for a Cu-phthalocyanine are presented, where a β-phase structure consisted of 57 atoms are employed by assuming the experimental structural parameters. The calculated magnetic moment integrated in the central Cu MT sphere results in 0.53 $\mu_{\rm B}$, being responsible to the $d_{x^2-y^2}$ orbitals, and a large moment of 0.06 $\mu_{\rm B}$ at the nearest-neighbor Ni atoms is induced. The calculated $E_{\rm MA}$ has a positive value of 0.14 meV, indicating that the magnetization energetically favors pointing in the out-of-plane direction. Within a rigid electric structure analysis, furthermore, the Cu d-electron states are found to play a key role to determine the $E_{\rm MA}$. Detailed electronic and magnetic structures, as well as for another transition-metal-phthalocyanines, will be presented.

References

[1] C. F. Hirjibehedin et. al., Science **317**, 1199 (2007).

[2] M. Mannini et. al., Nature Mater. **8**, 194 (2009).

[3] E. Wimmer et. al., Phys. Rev B. **24**, 864 (1981).

[4] M. Weinert et. al., Phys. Rev. B. **26**, 4571 (1982).

[5] K. Nakamura et. al., Phys. Rev. B **67**, 014420 (2003).

[6] G. H. O. Daalderop et. al., Phys. Rev. B **41**, 11919 (1990).

ZnO nanopencils synthesized by thermal evaporation with controlled working pressure

Cheol Hyoun Ahn, Young Sook Bae, Dong Chan Kim, Young Yi Kim, Sanjay Kumar Mohanta and Hyung Koun Cho*

* *School of Advanced Materials Science and Engineering, Sungkyunkwan University, Korea*

E-mail: chohk@skku.edu

Keywords: Nanopencils, Field emission, catalyst free

ZnO based materials have attracted extensive attention in the application of optoelectronic devices, chemical sensors, nanogenerators due to their superior emission, electronic, chemical and piezoelectric properties. In particular, vertically well-aligned one-dimensional (1D) ZnO nanostructures are of special interest for optoelectronic devices such as light emitting diodes (LED), laser diodes, and field emission displays [1, 2]. Recently, several groups have investigated field emission properties of various 1D ZnO nanostructures with tetrapoded-like, tip-like, and nanopencils-like shapes. Moreover, wide band gap and large exciton binding energy of ZnO was very useful for field emitter because of thermal stability and oxidation resistance [3, 4]. In this study, we investigated the synthesis and characterization of ZnO nanorods and nanopencils fabricated by thermal evaporation.

The synthesis process was based on thermal evaporation of Zn source in a 3 inch quartz tube at a temperature of 700 ^{o}C. The synthesis time was held for 30 min with an injected O_2 flow rate of 30 sccm. The ZnO nanorods were prepared at various working pressure in the range from 7 ~ 9 Torr. The synthesis of ZnO nanopencils were performed through two-step process by controlling the working pressures at 9 (20 min) and 7 (10 min) Torr for each step, respectively. Figures 1(a-c) shows the SEM images of ZnO nanorods synthesized by thermal evaporation at various working pressures. The aspect ratio of ZnO nanorods was shown to increase with decreasing working pressure. The ZnO nanopencils were completely synthesized by changing working pressure, as shown Fig. 1(e).

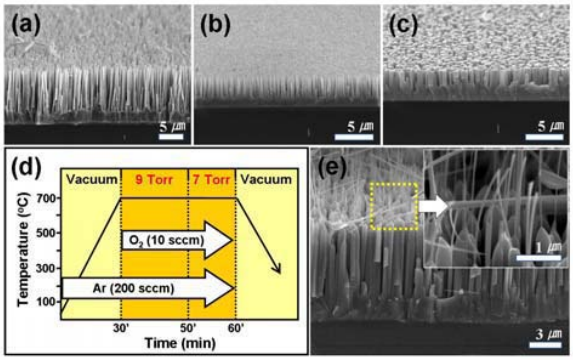

Fig. 1. SEM images of ZnO nanorods grown by thermal evaporation with various working pressure; (a) 7 torr, (b) 8 Torr, and (c) 9 Torr. (d) Schematic diagram of two-step process and (e) SEM images of ZnO nanopencils synthesized by thermal evaporation using two-step process.

References

1. G. C. Yi, C. Wang, W II Park, Semicond. Sci. Tecjnol. 20, S22-S34, (2005)
2. J. Zhou, P Fei, Y. Gao, Y. Gu, J. Liu, G. Bao, and Z. L. Wang, Nano Lett., 8, 2725-2730, (2008)
3. Q. Zhao, H. Z. Zhang, Y. W. Zhu, S. Q. Feng, X. C. Sun, J. Xu, and D. P. Yu, A.P.L. 86, 203115 (2005)
4. B. Debasish, S. H. Jo, D. R. Zhi, Adv. Mater, 16, 2028-2032, (2004)

Electric field effect on the Fano resonance in quantum wires

Vassilios Vargiamidis,[1*] Vassilios Fessatidis,[2]
Makoto Sawamura[3] and Norman J. M. Horing[4]
[1]*Department of Physics, Aristotle University, GR-54124 Thessaloniki, Greece*
[2]*Department of Physics, Fordham University, Bronx, New York 10458, USA*
[3]*MANA, National Institute for Materials Science, Namiki, Tsukuba, Ibaraki, 305-0044, Japan*
[4]*Department of Physics and Engineering Physics, Stevens Institute of Technology, Hoboken, New Jersey 07030, USA*

Electronic transport through a straight parabolically confined quantum wire with an attractive impurity and a transverse electric field is investigated via the Feshbach coupled-channel theory [1]. The impurity is modeled by a δ-function potential in the propagation direction while it is Gaussian in the transverse direction. In the presence of an impurity, the transmission probability of the wire may exhibit resonances of the Fano type [1-4] (which is the result of the interference between background transmission and transmission via a quasibound state created in the impurity). It is shown here that increasing the field strength causes displacement of the confining potential, thereby inducing a "shifting" of the impurity across the channel and therefore influencing the resonance structure. As the impurity center approaches the center of the confining potential, the coupling of the (first) propagating state with the quasibound state of the second channel gradually decreases, resulting in a decrease of the resonance width. For a particular value of the field strength the resonance width shrinks to zero and the Fano profile collapses. The resonance energy is also examined as a function of the electric field strength.

References:

[1] J. U. Nöckel and A. D. Stone, Phys. Rev. B **40**, 17415 (1994).
[2] C. S. Kim, A. M. Satanin, Y. S. Joe, and R. M. Cosby, Phys. Rev. B **60**, 10962 (1999).
[3] V. Vargiamidis and H. M. Polatoglou, Phys. Rev. B **71**, 075301 (2005).
[4] J. Y. Vaishnav, A. Itsara, and E. J. Heller, Phys. Rev. B 73, 115331 (2006).

Nonlinear transport of two-dimensional positive ions below surface of superfluid ^{4}He

D. Takahashi, H. Ikegami and K. Kono
Low Temperature Physics Lab., RIKEN, 2-1 Hirosawa, Wako, Saitama 351-0198, Japan

Keywords: two-dimensional ions, superfluid, critical velocity

It is possible to create positively or negatively charged ions in liquid He. The positive ion called snowball is a sphere of solid He bound around a $^4He_2^+$ ion caused by the enhancement of the local pressure by electrostriction. In contrast, a negative ion consists of an electron trapped in an empty bubble formed in liquid He. The radius is around 6 Å for the snowball and 17 Å for the bubble[1]. Such ions provide the only means of studying the Landau critical velocity for emission of rotons and the mechanism of quantum vortex ring creation when they are accelerated to high velocity. In the case of the electron bubble, the creation of vortex rings and the emission of rotons have extensively investigated by the time of flight (TOF) method at low pressure and high pressure of liquid He, respectively. The mechanism of the quantized vortex ring creation is understood as a macroscopic quantum tunneling process below ∼0.2 K, above which temperature the vortex rings are created by thermally activated process[2].

Ions trapped a few hundred Å below a free He surface form a two-dimensional ion layer. The velocity of ions can be controlled by continuous variation of the electric field along the surface unlike with the TOF method. Therefore, it has an advantage to observe the critical velocity (v_c) associated with both roton emission or vortex ring creation. Here we present transport properties of a two-dimensional snowball system under a high driving electric field.

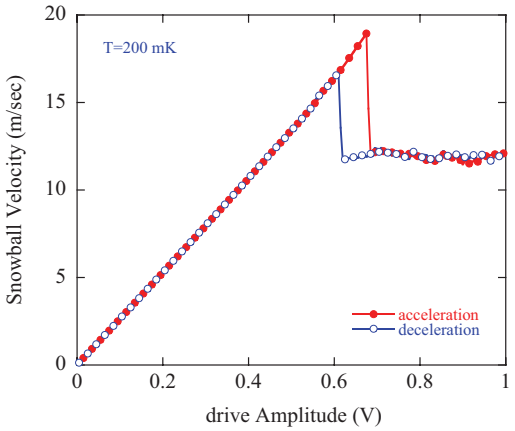

Figure 1: Drive voltage dependence of the snowball velocity at 200 mK. The dot and circle indicate the increasing and decreasing of the drive amplitude, respectively.

We measure the I-V characteristic of the two dimensional snowball system by means of the Sommer-Tanner method with corbino electrodes. The snowball density (n_i) is $\sim 6.6 \times 10^{11}$ /m^2, as determined by the plasma resonance frequency. The velocity (v_i) is derived from the detected current with $v_i = i/2\pi r_i n_i e$, where r_i and e are the inner corbino radius and elementary charge respectively. As shown in the figure, v_i increases proportionally with the driving voltage at low driving voltage following Ohm's law. Then v_i decreases abruptly at a certain threshold voltage and shows non-linear behavior above the threshold. The transition between the linear and non-linear state shows hysteresis. We found that the temperature dependence of v_c is quite unique; v_c at 450 mK is ∼31 m/sec, and it decreases with decreasing temperature. However, it is independent of temperature at a value of ∼18 m/sec below 200 mK.

The observed non-linear transport indicates that a new dissipation mechanism arises at v_c. v_c is sufficiently small ($\sim$ 60%) compared to Landau critical velocity for roton emission. The creation of vortex rings could be the origin of the nonlinear behavior. We discuss the details of the experimental procedure and possible explanations for the results.

References

[1] K. W. Schwarz, Adv. Chem. Phys., **33**, 1 (1975).

[2] P. C. Hendry *et al.* , Phys. Rev. Lett., **60**, 604 (1988).

Exact Coulomb cutoff technique in two dimensions

A. Castro*, E. Räsänen** and C. A. Rozzi***

*Institut für Theoretische Physik and European Theoretical Spectroscopy Facility, Freie Universität Berlin, Germany

**Nanoscience Center, Department of Physics, University of Jyväskylä, Finland

***CNR-INFM National Research Center S3, Modena, Italy

Chain of semiconductor quantum dots, supercell technique

We present a reciprocal space technique for the calculation of the Coulomb integral in two dimensions in systems with reduced periodicity, i.e., finite systems, or systems that are periodic only in one dimension. The technique consists in cutting off the long-range part of the interaction by modifying the expression for the Coulomb operator in reciprocal space. The physical result amounts in an effective screening of the spurious interactions originated by the presence of ghost periodic replicas of the system. This work extends a previous report [1], where three-dimensional systems were considered. We show that the use of the cutoffs dramatically enhances the accuracy of the calculations for a given supercell size, and it allows to describe two-dimensional systems of reduced periodicity with substantially less computational effort. Our technique does not depend on the choice of the basis set, and, as well as its 3D counterpart, it is exact for a particular choice of the supercell size.

We exemplify our approach by utilizing density functional theory (DFT), although the method we propose can also be useful in different fields. In particular we consider semiconductor quantum-dot arrays, having potential applications in quantum information technology [2]. We show that the inclusion of the truncated Coulomb interaction greatly improves the convergence of the band structure (Fig. 1), and it gives an insight about the role of inter-chain interaction in determining the conductive or insulating character of the ground state (Fig. 2).

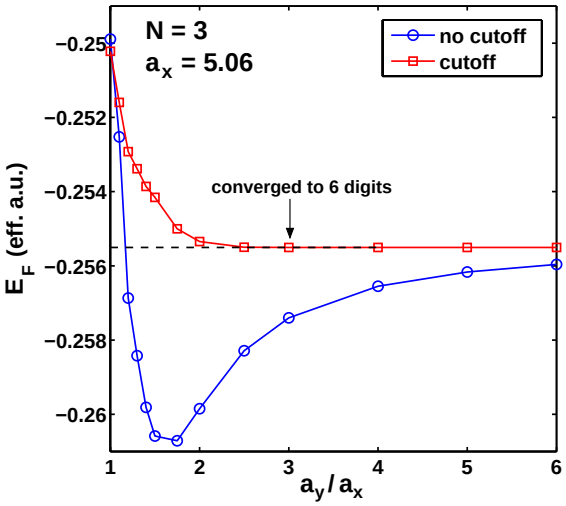

Figure 1: (Color online) Fermi energy of a quantum-dot chain with three electrons per dot as a function of the supercell size perpendicular to the chain.

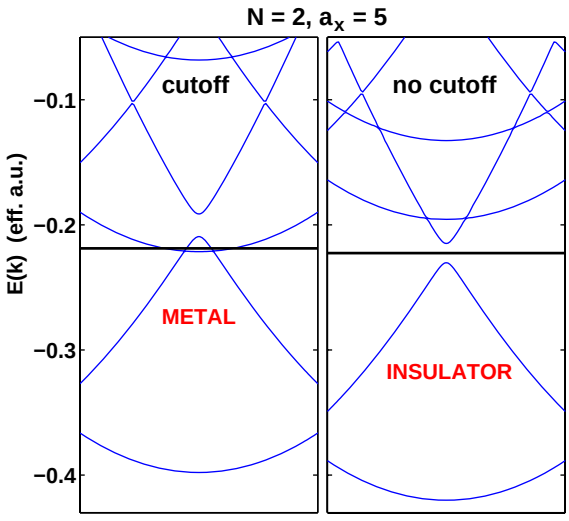

Figure 2: (Color online) Band structure at a lattice constant $a_x = 5$ for a quantum-dot chain with two electrons in each dot. The left and right panels show the results with and without the cutoff procedure, leading to to metallic and insulating band structures, respectively. In the latter case, the parallel chains are located at $a_y = na_x$, $n = \pm 1, \pm 2, \ldots$.

References

[1] C. A. Rozzi, D. Varsano, A. Marini, E. K. U. Gross, and A. Rubio, Phys. Rev. B **73**, 205119 (2006)

[2] K. Shiraishi, H. Tamura, and H. Takayanagi, Appl. Phys. Lett. **78**, 3702 (2001).

Single electron detection using the silicon radio-frequency single electron transistor (rf-SET)

S. J. Angus* and A. J. Ferguson**
*School of Physics, The University of Melbourne, Melbourne, Australia
** Cavendish Laboratory, University of Cambridge, Cambridge, United Kingdom

Keywords: silicon rf-SET, quantum dot

We report the detection of individual electron transfers onto a silicon quantum dot using the silicon radio-frequency single electron transistor. This represents the first single electron detection using the silicon rf-SET.

Silicon quantum dots are an attractive system for quantum computation because of the expected long electron spin coherence time.

We have developed a technique to define tunable silicon quantum dots in a double-gated metal oxide semiconductor (MOS) structure [1], and we have utilised this technique to demonstrate the first silicon rf-SET [2].

We report here the use of the silicon rf-SET as a sensitive charge detector coupled to a silicon quantum dot. The rf-SET and quantum dot were fabricated using the double-gated MOS technique (see Figure 1).

Radio-frequency reflectometry revealed the Coulomb blockade oscillations of the silicon rf-SET, as shown in Figure 2(a).

Individual electrons are added to the silicon dot by sweeping its top-gate. These electron transfers are observed as sawtooth steps in the reflected signal of the rf-SET, as illustrated in Figure 2(b). Each sawtooth step represents the addition of a single electron onto the silicon dot (situated 200nm away) and is equivalent to 2% of an electron on the rf-SET island ($\Delta q = 0.02e$).

These results constitute an important step toward the realisation of single spin manipulation and measurement in silicon quantum dots.

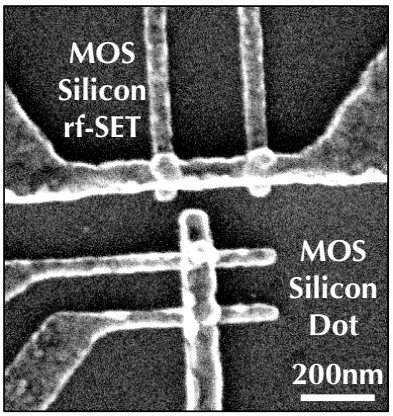

Figure 1: Scanning electron microscope image illustrating the silicon rf-SET coupled to a silicon double quantum dot.

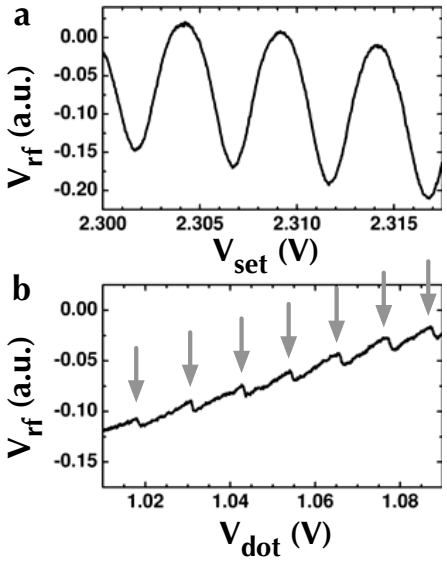

Figure 2: (a) Coulomb blockade oscillations in the radio-frequency reflectometry response of the silicon rf-SET. (b) Addition of individual electrons detected by the silicon rf-SET. Each sawtooth indicated by an arrow represents the addition of a single electron onto the nearby silicon dots.

References

[1] S. J. Angus, A. J. Ferguson, A. S. Dzurak and R. G. Clark, Nano Lett. **7**, 2051 (2007).

[2] S. J. Angus, A. J. Ferguson, A. S. Dzurak and R. G. Clark, Appl. Phys. Lett. **92**, 112103 (2008).

Resonance conductance in a quantum point contact with a tunable barrier potential

C. H. Wen*, J. H. Hsiao*, T. M. Hong*, K. T. Lin*, J. C. Chen*,
T. Ueda** and S. Komiyama**

*Department of Physics, National Tsing Hua University, Hsinchu 30043, Taiwan, Republic of China
**Department of Basic Science, University of Tokyo, Komaba 3-8-1, Meguro-ku, Tokyo 1538902, Japan

Keywords: Quantum point contact, one-dimensional quantum wire, resonance conductance

One of the hallmarks of mesoscopic physics is the quantization effect in ballistic transport of electrons through a narrow constriction between two reservoirs. It is known that the quantized features on the conductance G is sensitive to the process of how the electrons are injected and emitted through the constricted channels [1,2]. Here we demonstrated the appearance of resonance conductance in a controllable manner on the quantized G plateaus in a quantum point contact (QPC).

The device consists of a QPC and a top cross gate, as displayed in Fig. 1. By positively or negatively biasing the cross gate, the confining potential profile of the channel can be deform locally and become attractive-like well or repulsive-like barrier respectively.

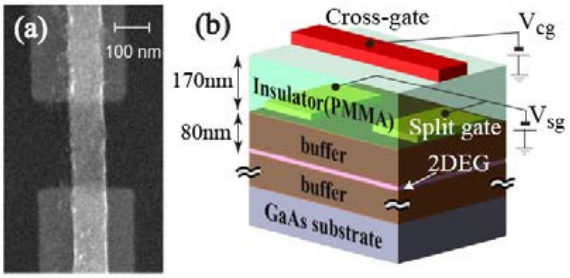

Fig.1: (a) Scanning electron microscope image of the device. (b) Schematic diagram illustrating of a cross-sectional view of our device. A QPC is defined by a pair of the split metal gates in a GaAs/AlGaAs two-dimensional electron gas. A cross gate is implemented on top of the QPC channel separated by an insulating layer.

Fig. 2 shows the evolution of G as a function of the split gate V_{sg} and cross gate V_{cg} voltages at temperature T=0.3K. As the cross gate is more negatively biased, the quantized G is suppressed from the idea case. In contrast, while V_{cg} becomes more positive, an oscillatory structure rises up on the G steps. Furthermore, the quantized G values recover as a magnetic field B is applied up to 1T regardless the sign of V_{cg}.

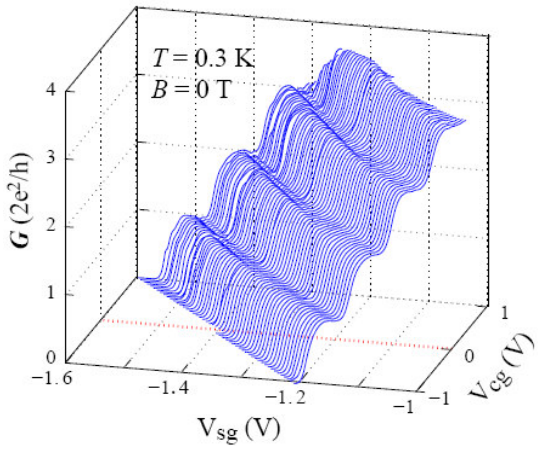

Fig.2: Conductance G versus split gate voltage V_{sg} for different cross gate voltage V_{cg}.

To investigate the origin of the structures in the steps, numerical simulation of the potential profile has been performed. It is found that the occurrence of oscillations is related to the aspects ratio of the channel, consisted with the theories [1,2]. We conclude that the observed conductance features are resulted from the resonance effects, which is very responsive to the shape of the local potential in the channel.

References

1. Aaron Szafer and A. Douglas Stone, Phys. Rev. Lett. **62**, 300 (1989)
2. G. Kirczenow, Phys. Rev. B **39**, 10452 (1989)

Crystallization of electrons on liquid helium in channel geometry

Hiroki Ikegami, Hikota Akimoto, and Kimitoshi Kono

RIKEN, Wako, Saitama, Japan

Keywords: electron on helium, Wigner crystal, quasi-one-dimensional system

Electrons trapped on the surface of liquid helium form a classical two-dimensional electron system with a density of ~10^{12} m^{-2}. The ground state of these electrons is the Wigner solid due to the predominance of the Coulomb interaction over the kinetic energy. The melting of the Wiger solid is driven by the dissociations of dislocation pairs as originally proposed by Kosterlitz and Thouless [1]. The properties of the melting should be strongly affected when the dimension of the system is comparable to the characteristic length of dislocations i.e. electron spacing (~1 μm). Here we present the study of the melting of electrons confined in quasi-one-dimensional channels with a width of 5, 8, and 15 μm by transport measurements.

In our previous study, we found that the Wigner solid shows the peculiar nonlinear transport [2]. Especially at a small excitation, the mobility in the Wigner solid phase exhibits the significant decrease due to the resonant scattering of surface waves called the Bragg-Cherenkov scattering. Because the Bragg-Cherenkov scattering occurs only in the Wigner solid phase, the mobility measurement is very useful to investigate the crystallization transition.

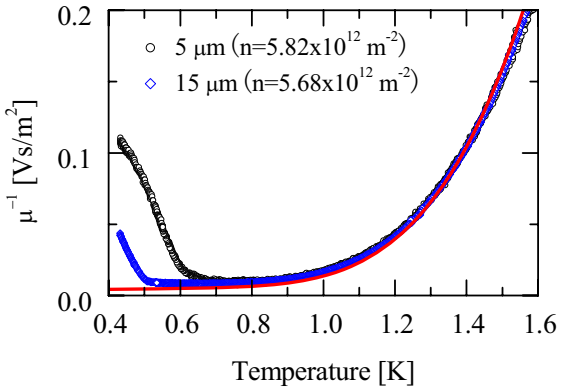

Fig.1 Temperature dependence of inverse of mobility (μ^{-1}) of the 5 and 15 μm-wide channels for similar electron densities. Solid line is the theoretical mobility in electron gaseous regime [3].

Temperature dependences of inverse of mobility (μ^{-1}) of electrons confined in the 5 and 15 μm-wide channels are shown in Fig. 1 for similar electron densities. At high temperatures, μ^{-1} decreases with decreasing temperature because of the reduction of the scattering rate with helium vapor atoms and surface waves. The theoretical mobility calculated for these scatterings [3] well reproduces the experimental behavior in electron gaseous phase. Decreasing temperature further, μ^{-1} turns to increase at a certain temperature. The increase of μ^{-1} is caused by the crystallization of electrons accompanied by the Bragg-Cherenkov scattering [2]. The most striking feature found in Fig. 1 is the higher crystallization temperature for the 5 μm-wide channel.

We investigated the crystallization temperature for three channel-widths by systematically changing the electron density. We found that the crystallization temperature is higher for a narrower channel at a same density, that is, the transition into the Wigner occurs at a higher temperature for a fewer electrons in the lateral direction. This increase of the transition temperature is understood by the finite size effect on the Kosterlitz and Thouless mechanism.

References

1. J. M. Kosterlitz and D. J. Thouless, J. Phys. C **6**, 1181 (1973); B. I. Halperin and D. R. Nelson, Phys. Rev. Lett. **41**, 121 (1978); A. P. Young, Phys. Rev. B **19**, 1855 (1979).

2. H. Ikegami, H. Akimoto, and K. Kono, Phys. Rev. Lett. **102**, 046807 (2009).

3. M. Saitoh, J. Phys. Soc. Jpn. **42**, 201 (1977).

Renormalization approach to electrical conductance of two-dimensional aperiodic lattices

Fernando Sanchez and Vicenta Sanchez

Departamento de Fisica, Facultad de Ciencias, Universidad Nacional Autonoma de Mexico, Apartado Postal 70-542, 04510, D.F., MEXICO

Keywords: Renormalization method, Electronic transport and Aperiodic systems.

The fabrication of two-dimensional (2D) electronic high-mobility GaAs-AlGaAs heterostructures has enabled the experimental study of ballistic transport in 2D systems, finding a quantization of the conductance in units of $g_0=2e^2/h$ [1,2]. On the other hand, the electronic conduction in 2D aperiodic lattices is an interesting but not thoroughly understood subject, since the quantum transport and macroscopic-scale aperiodic system both *per se* are not easy topics. Nowadays, there is a consensus that in quasiperiodic systems the electronic wave functions are critical and the corresponding eigenvalue spectra are singular continuous [3]. The transport properties of these critically localized states are a fascinating and still unclear theme. In this work, we report an extension of a previously developed renormalization plus convolution method [4] to other aperiodic systems, such as Thue-Morse and period-doubling ones [5]. For 2D periodic lattices, the conductance spectrum shows a uniform structure of steps and a fractal distribution of these steps when the arrangement of atoms in the perpendicular direction becomes aperiodic.

In figure 1, the spectrally averaged conductance <g> [4] is shown for 2D periodic, Fibonacci, period-doubling and Thue-Morse lattices. Observe a clear power-law decay of <g> as the system length grows for both Fibonacci and period-doubling systems, and a beyond power-law behaviour is noted in the Thue-Morse case. For all these cases, <g> is neither constant as in periodic systems nor exponential decays occurred in randomly disordered lattices, revealing the peculiar localization nature in aperiodic lattices. Finally, the transition of conductivity from one- to two-dimensional behaviour will also be analyzed.

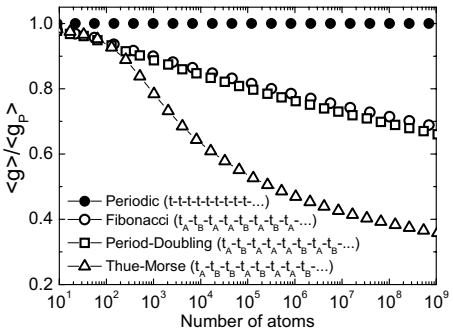

Fig.1 Spectral average of the 2D conductance (<g>) versus the system length, for periodic (solid circles), Fibonacci (open circles), period-doubling (open squares) and Thue-Morse (open triangles).

References

1. B.J.van Wees, et.al., Phys. Rev. Lett. 60, 848 (1988).
2. R. de Picciotto, et.al., Nature 411, 51 (2001).
3.- A. Süto, in Beyond Quasicrystals, Ed. By F. Axel and D. Gratias, Les Editions de Physique, 483 (1994).
4. V. Sanchez and C. Wang, Phys. Rev. B **70**, 144207 (2004).
5. L. Kroon and R. Riklund, J. Phys. A: Math. Gen. 36, 4519 (2003).

Renormalization of electron-electron interaction at conductivity decrease in two-dimensional structures

G. M. Minkov*, A. A. Sherstobitov*, A. V. Germanenko ** and O. E. Rut **
*Institute of Metal Physics RAS, 620219 Ekaterinburg, Russia
** Institute of Physics and Applied Mathematics, Ural State University, 620083 Ekaterinburg, Russia

Keywords: e-e interaction, RG theory

The analysis of the electron-electron (e-e) interaction contribution within the framework of the theory of the renormalization group (RG)[1] shows that the reduction of the temperature and/or conductivity would lead to the renormalization of the Fermi liquid amplitude γ_2 and thus to crossover to the metallic-like behavior of the conductivity. The RG equations have been successively used for interpretation of the temperature dependence of the conductivity and metal-insulator transition in Si-MOSFETs [2]. However, we believe that the analysis of the temperature dependence of the conductivity at $B = 0$ alone is not reliable way to understand the role of the renormalization of e-e interaction because there are a lot of effects, such as the weak localization and antilocalization, the ballistic contribution of the e-e interaction, the temperature dependent disorder and so on, which govern the temperature dependence of the conductivity.

The reliable results can be obtained only from simultaneous analysis of the data obtained at zero, low and high magnetic fields. Such analysis was not carried out even for simplest 2D systems with the single valley isotropic spectrum, in the deeply diffusion regime for which the RG-equation was derived. Therefore the range of the parameters where 1-loop RG-equation is valid remains unknown up to now.

We have experimentally studied the evolution of the diffusion part of the interaction correction to the conductivity in a n-type 2D system (GaAs/In$_x$Ga$_{1-x}$As/GaAs with $x \approx 0.2$) within the conductivity range from $\sigma_0 \simeq 150\,G_0$ to $\sigma_0 \simeq 5\,G_0$ ($G_0 = e^2/\pi h$) at the temperatures where the ballistic contribution of the e-e interaction is negligible.

To separate out the interaction contribution to the conductivity we have used the unique property of the e-e interaction in the diffusion regime, namely, the fact that it contributes to the diagonal component of the conductivity tensor, σ_{xx}, only. The simultaneous analysis of weak localization magnetoresistance, temperature dependence of σ_{xx} and conductivity at $B = 0$ allows us to determine the conductivity dependence of the Fermi liquid amplitude γ_2 (that controls the e-e interaction in the triplet channel). The experimental results are presented in Figure together with theoretical conductivity dependence of γ_2. One can see that above the conductivity of $15G_0$ the renormalization of γ_2 is well described by 1-loop approximation of RG. However at lower conductivity RG predicts significantly larger γ_2 gain. We have concluded that at $\sigma < 15G_0$ the 2-loop terms and interplay of WL and interaction should be taken into account.

References

[1] Alexander Punnoose, Alexander M. Finkel'stein, Phys. Rev. Lett. **88**, 016802 (2001).

[2] S. Anissimova, S. V. Kravchenko, A. Punnoose, A. M. Finkel'stein, and T. M. Klapwijk, Nat. Phys. **3**, 707 (2007).

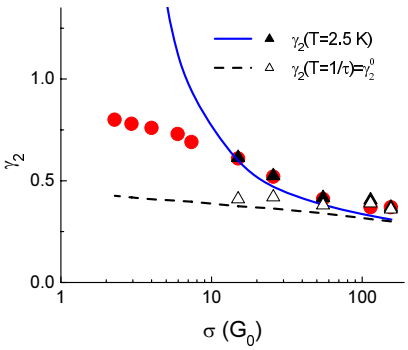

Figure 1: The conductivity dependence of interaction amplitude γ_2. Points are the experimental data. The dashed line is the result of perturbative theory; the solid line is calculated from 1-loop RG equations.

From weak to strong localization in a ferromagnetic high mobility 2DHG

U. Wurstbauer*, D. Weiss**, D. Schuh**, and W. Wegscheider***

* *Institute for Applied Physics,University of Hamburg, Hamburg, Germany*

** *Institute for Experimental and Applied Physics, University of Regensburg, Regensburg, Germany*

*** *Solid State Physics Laboratory, ETH Zurich, Zurich, Switzerland*

Keywords: quantum Hall effect, metal-insulator transition, weak antilocalization, ferromagnetic 2DHG

We have investigated ferromagnetic high mobility two-dimensional hole gases (2DHG) in manganese (Mn) doped strained InAlAs/InGaAs/InAs quantum well structures by magnetotransport experiments. The samples were grown on strain-relaxed metamorphic buffers on GaAs substrates by molecular beam epitaxy. The active layer consists of a 20 nm InGaAs QW with an inserted 4 nm InAs channel and a 7 nm thick Mn doped InAlAs layer that is 5 nm spaced from the QW. The Mn acceptor concentration is less than $2 \cdot 10^{20}$ cm^{-3}.

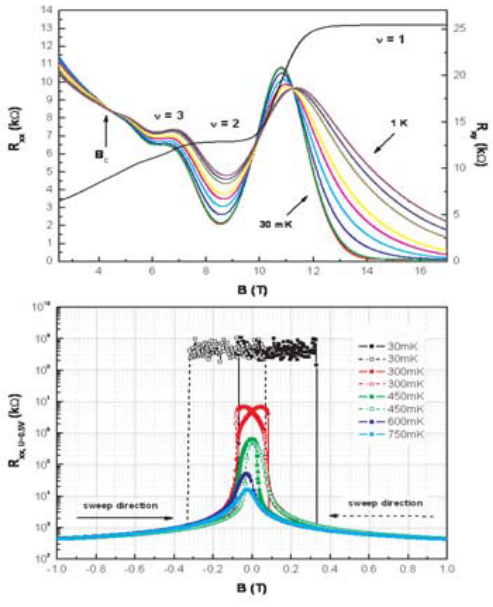

Fig.1 Upper panel: Temperature dependence of the Shubnikov-de Haas oscillations and Hall resistance trace at T = 30 mK for a Mn codoped 2DHG in the high-field region. Lower panel: Temperature dependence of hysteretic metal-insulator transition in the low field region of the ferromagnetic Mn codoped 2DHG.

Mn ions play a dual role and provide itinerant holes in the QW, bound holes in the InAlAs:Mn layer and localized spins of 5/2 [1].

Below 700 mK a transition from a paramagnetic to a ferromagnetic phase is reflected by a hysteretic behaviour in the longitudinal resistance and a superposition of normal, anomalous and planar Hall effects in the Hall resistance in the low-field region [2]. In the high-field region Shubnikov-de Haas oscillations and quantum Hall plateaus are observable in the longitudinal and Hall resistance, respectively.

Samples without Mn in close proximity to the QW reveal a weak anti-localization effect indicating strong spin orbit coupling [2]. At temperatures below the Curie temperature T_C it is superimposed by additional hysteretic maxima. Additive Mn co-doping in close proximity to the itinerant holes of the 2DHG leads to strong localization effects depending on the ratio between localized Mn ions and itinerant holes [1]. Below T_C hysteretic behaviour and insulating states appear with abrupt changes in the resistivity over more than 6 orders of magnitude up to several 10^{11} Ohms in the low field region as shown in the lower panel of Fig. 1. A perpendicular applied magnetic field drives the system back into a metallic phase where SdH-oscillations in the longitudinal resistance and quantum Hall-plateaus in the Hall resistance are observable, as demonstrated in the upper panel of Fig.1 .

References

1. U. Wurstbauer et al., J. Cryst. Growth, In Press, (2008), doi:10.1016/j.jcrysgro.2008.10.004.

2. U. Wurstbauer et al., submitted to Phys. Rev. B. (2009).

In-plane anisotropy of hole subbands in Si p-type inversion layers

S. N. Takeda, A. Kuwako, M. Morita, H. Daimon, M. Yoshimaru*, and T. Imamura*
Nara Institute of Science and Technology (NAIST), Nara, Japan
* *Semiconductor Technology Academic Research Center (STARC), Yokohama, Japan*

Keywords: hole, subband, dispersion, Si

In contrast to ideal 2-dimensional electrons(2DEs), 2DEs in crystals show anisotropic behaviors due to periodic potentials given by arrangements of atoms. Dispersion structures of subbands reflect the anisotropy arising from the crystal structures. Thus, determinations of the subband dispersion structures has been required to understand transport and optical properties of 2DEs.

In recent years, we have developed an experimental method for the determination of dispersion structures of hole subbands in semiconductor inversion layers[1, 2]. In this presentation, we will show the anisotropy of valence subband dispersions in Si inversion layers.

In this experiments, Schottkey barriers induced by atomic metal layers were used as inversion layers. The measurements of subband dispersion were done by high-energy-resolution angle-resolved photoelectron spectroscopy (ARPES). Fig. 1 shows the experimental geometry in this study. In-plane directions in the dispersion measurement could be changed by sample rotation along the z axis.

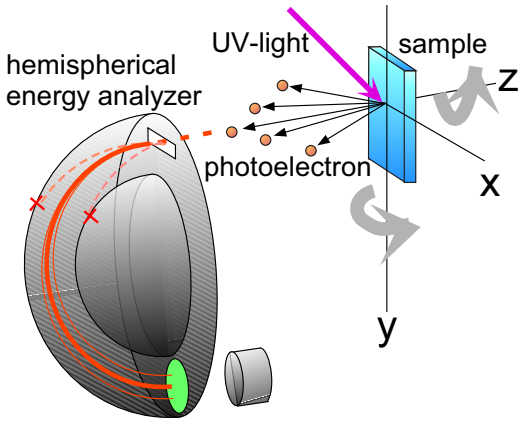

Figure 1: Experimental geometry of ARPES measurements in this study.

By measuring dispersion curves of subbands along various in-plane directions, equienergy lines of the subbands could be obtained. Fig.2 shows an equienergy lines of subbands for Si(111) in the $k_x - k_y$ plane. In contrast to the isotropic light hole subbands, heavy hole subbands were found to be highly anisotropic. The anisotropy of heavy hole subbands were found to be different from the anisotropy of the bulk effective mass calculated by k · p approximation using Luttinger's parameters.

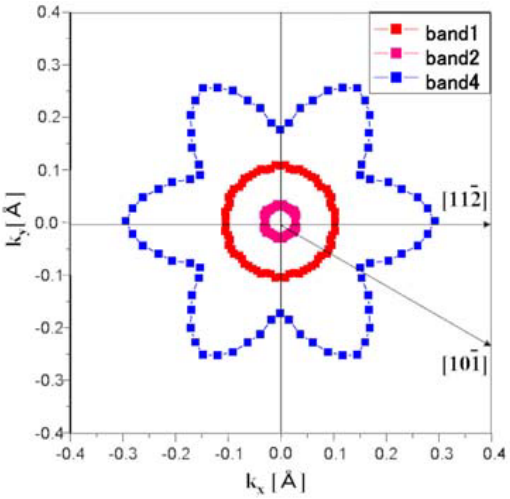

Figure 2: Equienergy lines of of measured subbands for Si(111) in the $k_x - k_y$ plane. The energy is 0.35eV below the E_F.

References

[1] S. N. Takeda and N. Higashi and H. Daimon, Phys. Rev. Lett. **94**, 037401 (2005).

[2] M. Morita and S. N. Takeda and M. Yoshikawa and A. Kuwako and Y. Kato ad H. Daimon, Appl. Surf. Sci. **254**, 7872 (2008).

Hysteresis in magnetoresistance of InAs surface inversion layers covered with sumonolayer Fe films

T. Mochizuki*, R. Masutomi* and T. Okamoto*
*Department of Physics, Faculty of Science, University of Tokyo, Tokyo, Japan

Keywords: Magnetotransport, Hystertesis, Spin-glass, InAs

It is well known that a two-dimensional electron gas (2DEG) can be easily formed at the surfaces of InAs and InSb by deposition of other materials. In our previous works, magnetotransport measurements have been performed on inversion layers formed at cleaved surfaces of *p*-type InAs and InSb covered with submonolayers of Ag or alkali metals [1, 2, 3]. The observed coverage dependence of the Hall mobility indicates that adatoms strongly affect electron scattering in the inversion layer.

In this work, we extend the study to 2DEGs formed at InAs surfaces covered with submonolayer Fe films. Hysteresis in the magnetoresistance is found in a narrow coverage range. At a coverage of $\Theta = 0.42$ monolayer (ML), the resistivity is significantly reduced during the initial magnetic field cycle $0\ \mathrm{T} \rightarrow 9\ \mathrm{T} \rightarrow 0\ \mathrm{T}$ (Fig. 1 (a)). The reduction of resistance shows a clear difference between zero-field-cooling (ZFC) procedures and field-cooling (FC) procedures (Fig. 1 (b)). It also exhibits a dependence on the direction of the applied magnetic field which corresponds to Ising-like anisotropy of the Fe film. A long-time relaxation behavior is observed after a magnetic field sweep (Fig. 1 (c)). The results demonstrate that the 2DEG is useful to study the magnetic state of adsorbed Fe films, and strongly suggest that the 2D spin-glass ordering occurs at $\Theta = 0.42$ML [4].

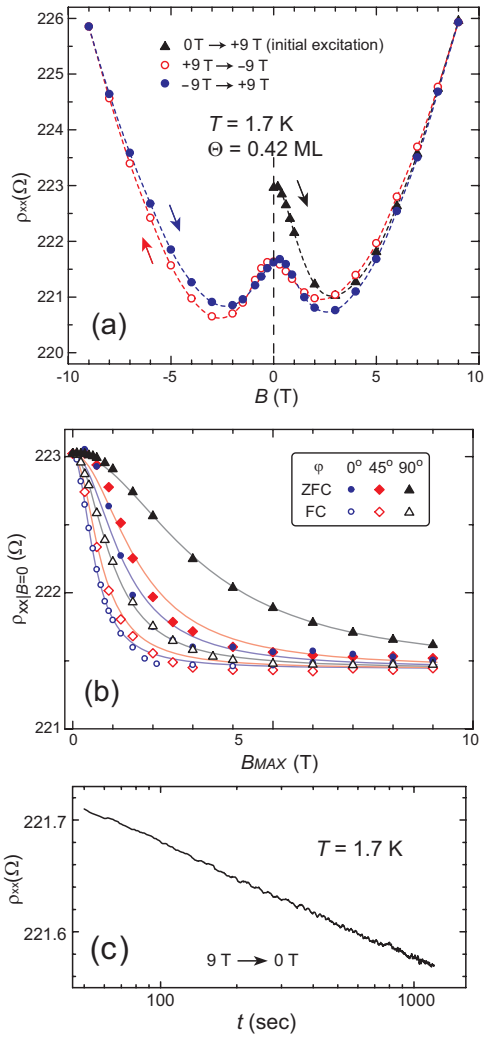

Figure 1: (a) In-plane magnetic field dependence of ρ at $T = 1.7$ K for $\Theta = 0.42$ ML. Solid triangles represent the data obtained during the initial excitation up to $+9$ T. Open (solid) circles represent the data obtained during subsequent sweeps from $+9$ T (-9 T) to -9 T ($+9$ T). (b) Remanent magnetoresistivity at $B = 0$ T and $T = 1.7$ K for FC and ZFC procedures. The magnetic field was applied at different angles of $\varphi = 0°$ (circles), $45°$ (diamonds), and $90°$ (triangles) with respect to the surface normal. (c) Example of time evolution of ρ after magnetic field sweep at $\varphi = 90°$.

References

[1] Y. Tsuji, T. Mochizuki and T. Okamoto, Appl. Phys. Lett. **87**, 062103 (2005)

[2] R. Masutomi, M. Hio, T. Mochizuki and T. Okamoto, Appl. Phys. Lett. **90**, 202104 (2007)

[3] M. Minowa, R. Masutomi, T. Mochizuki and T. Okamoto, Phys. Rev. B **77**, 233301 (2008)

[4] T. Mochizuki, R. Masutomi and T. Okamoto, Phys. Rev. Lett. **101**, 267204 (2008).

Transistor operation at MgZnO/ZnO interface by Schottky gating with conducting polymer

A. Tsukazaki[1,2], M. Nakano[1], S. Akasaka[3], K. Nakahara[3], A. Kamisawa[3], A. Ohtomo[1] and M. Kawasaki[1,4,5]

1 *Institute for Materials Research, Tohoku University, Sendai, Japan*

2 *PRESTO, Japan Science and Technology Agency, Tokyo, Japan*

3 *Interdisciplinary Technology R&D Center, ROHM Co. Ltd., Kyoto, Japan*

4 *WPI Advanced Institute for Materials Research, Tohoku University, Sendai, Japan*

5 *CREST, Japan Science and Technology Agency, Tokyo, Japan*

Keywords: ZnO, two-dimensional electron gas, field-effect transistor,

We have shown that MgZnO/ZnO interfaces accumulate high mobility two-dimensional electron gas (2D) due to the mismatch in electric polarization of constituent piezoelectric materials [1,2]. Quantum Hall effect (QHE) was readily observed and the mobility exceeds 20,000 $cm^2V^{-1}s^{-1}$. However, we could so far control the 2DEG density only by the built-in Mg composition or donor concentration. In view of future challenges, we need to develop a technique that enables us to control 2D transport by electric field in a field-effect transistor (FET) geometry. In this study, a conducting polymer, PEDOT:PSS, was utilized as Schottky gate electrode with respect to control 2D transport at MgZnO/ZnO interface. Recently, we have reported excellent Schottky properties for PEDOT:PSS/ZnO junctions as characterized by current-voltage, capacitance-voltage, and photo response characteristics[3,4].

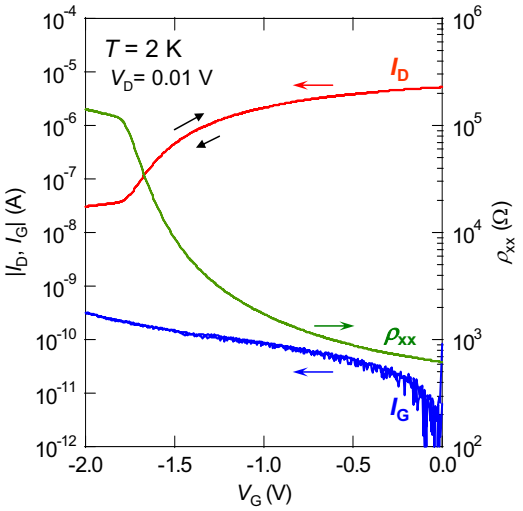

Fig. 1 Transfer property and leakage current of the device at 2 K. ρ_{xx} was systematically varied with gate bias.

The MgZnO/ZnO heterostructures were grown on Zn-polar ZnO single crystal substrates by molecular beam epitaxy. The materials were processed into standard Hall-bar geometry by dry etching, followerd by a spin-coating of 50-nm-thick PEDOT:PSS as a Schottky gate electrode and an evaporation of an 100-nm Au capping layer. Transport properties were characterized below 20 K to eliminate the parasitic conduction in the ZnO substrate. Fig. 1 shows transfer curve (I_D-V_G) and leakage current (I_G) at 2 K. 2DEG transport could be systematically controlled by applying gate bias via Schottky electrode. We discuss quantum transport phenomena under controlled 2DEG density and magnetic field.

References

1. A. Tsukazaki *et al.*, Science **315**, 1388 (2007).
2. A. Tsukazaki *et al.*, Appl. Phys. Express **1**, 055004 (2008).
3. M. Nakano *et al.*, Appl. Phys. Lett. **91**, 142113 (2007).
4. M. Nakano *et al.*, Appl. Phys. Lett. **93**, 123309 (2008).

Synthesis and Characterization of Ni Nanowires by Porous Anodic Alumina Oxide Templates

Shu-Fang Chen*, Chuan-Pu Liu*, A. A. Eliseev** and K. S. Napolsky**

** Department of Materials Science and Engineering, National Cheng-Kung University, Tainan, Taiwan*

*** Department of Materials Science, Moscow State University, Moscow,, Russian Federation*

Keywords: Magnetic, nanowire, AAO, TEM

Ferromagnetic nanowires have attracted great attention owing to their potential applications in magnetic recording media, sensors and other devices [1].

In this work, we studied the arrays of Ni nanowires synthesized by electro-deposition using AAO templates with different growth potential ranging from -1V to -3V. The pore size and the interpore distance of AAO templates are 50 nm and 100nm, respectively.

Figure 1(a) is the TEM image of Ni nanowires grown at potential of -1V, showing that the nanowires are cylindrical with diameter around 50nm. The Ni nanowire is single crystalline with FCC structure and the growth direction is along (110) as revealed by the electron diffraction shown in the inset of Fig. 1(a).

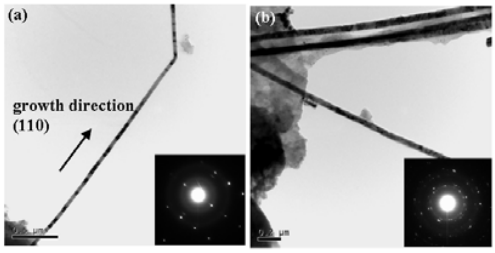

Fig. 1 TEM images of Ni nanowires with different growth potential. (a) -1V (b) -2V

In Fig. 1(b), with the increasing growth potential, the nanowires are grown into polycrystalline caused by the higher growth rate.

The single crystalline Ni nanowires have easy axis along the wire axis (~95% squareness) due to large shape anisotropy as shown in Fig. 2(a). However, polycrystalline samples do not have a preferential magnetic orientation and the squareness decreases to 52% (Fig. 2(b)). Furthermore, the coercive field is found to decrease with the increasing growth potential, which results from the transformation of domain structures.

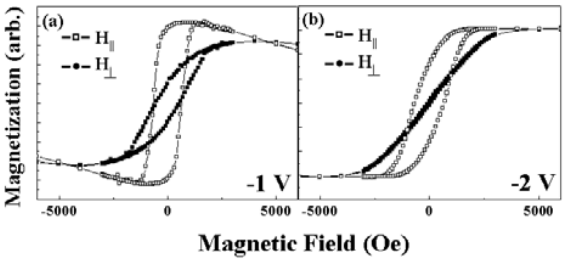

Fig. 2 M-H loops of Ni nanowires with applied magnetic both parallel and perpendicular to the wire axis. (a) -1V (b) -2V

References

[1] G. J. Strijkers, J. H. J. Dalderop, M. A. Abroeksteeg, H. J. M. Swagten, and W. J. M. de Jonge, J. Appl. Phys. **86**, 5141 (1999).

Photoconductivity characteristics of ZnO nanoparticles assembled in nanogap electrodes for portable ultraviolet photodetector

Sanjeev Kumar, Young-Gyo Seo, and Gil-Ho Kim*

Department of Electronic and Electrical Engineering and Sungkyunkwan University Advanced Institute of Nanotechnology, Sungkyunkwan University, Suwon 440-746, Korea

Detection of ultraviolet (UV) radiation is becoming an important area of research and has taken special consideration from material scientists. Many materials have been investigated for designing UV sensors based on thin films and nanostructures but could not hold interest either due to limit of responsivity or complexity of design of such sensors. Out of the various studied materials, Zinc oxide (ZnO) has drawn broad attention due to its remarkable features such as good UV photoconductivity, resistance to radiation hardness, established growth techniques in thin film form or nanostructures. It is well known fact that sensor responsivity depends on electrodes configuration and surface to volume ratio of the sensing material. Miniaturized devices consisting of UV sensing materials in nanogap electrodes would be of interest to study in realizing future functional sensors.

In the present work, ZnO nanoparticles of size ~ 9 nm, grown by sol gel process, have been assembled by optimized dielectrophoresis (DEP) process on the prefabricated nanogap electrodes (20-110 nm). The fabricated ZnO nanoparticles based device was studied for its I-V characteristic and typical non-linear semiconducting behavior was observed. When illuminated with UV radiation of wavelength 365 nm, a tremendous change in conductivity of one order of magnitude was observed indicating a high sensitivity of the fabricated miniaturized device. Temporal photoresponse characteristics were studied at different levels of UV illumination intensities and quick rise and recovery time (under 10 ms) were observed. The photoresponse curve exhibited a perfect rise and recovery without any slow component and the change in photocurrent with UV illumination exhibited a linear variation. Absence of any slow component in the photoresponse characteristics indicated that shallow trapping centers were inactive and the photoresponse is mainly due to either transitions through deep centers or band-to-band transition. Furthermore, this also infers that fabricated ZnO nanoparticles based miniaturized device is suitable for quick sensing of UV radiation and finds applications as portable UV-meter for layman use, fire-alarm sensors, and sensors use for in military appliances.

*Corresponding author: ghkim@skku.edu

Tip Geometry Effects in Scanning Capacitance Microscopy on GaAs Schottky and MOS-Type Junctions

C.Eckhardt, W.Brezna, J.Silvano, O.Bethge, E.Bertagnolli, J.Smoliner
Institut für Festkörperelektronik, TU-Wien
Floragasse 7, A-1040 Wien, Austria

Keywords: SCM, GaAs

In this work, the influence of the tip-geometry in Scanning Capacitance Microscopy is investigated experimentally and theoretically on Metal-Oxide-Semiconductor (MOS) and Schottky type junctions on GaAs. Using a two-dimensional model we find that on Schottky type junctions the electric field around the tip is screened by the surface states and that the essential parameters entering the C(V) characteristics are the doping level and the contact area only. In contrast to that, the electric field from the tip penetrates into the semiconductor on a MOS type junction, and the tip geometry effects are much larger. C(V) spectra are fitted to the experimental data and allowed a quantitative determination of doping levels, oxide thickness, and contact area without further calibration measurements.

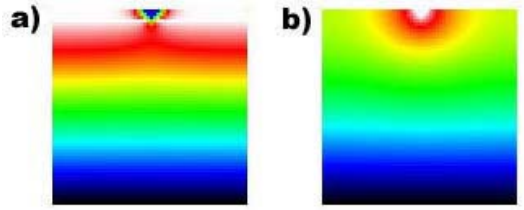

Fig. 1: (a): typical potential distribution of a n-type GaAs Schottky-type contact and (b): a MOS-type contact. The area of this plot is 1 × 1 µm.

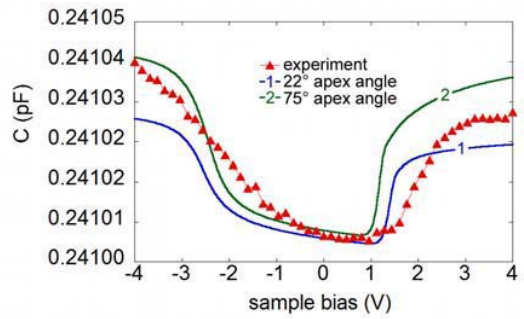

Fig. 2: Calculated C(V) curves of a MOS-type tip-sample contact for various opening angles of the tip apex.

In Fig. 1 we show the two dimensional geometry which was used for our simulations. The lower area (below the tip apex) represents the GaAs substrate. On top we have a layer of Al_2O_3 grown by atomic layer deposition (MOS type contact) or the bare surface (Schottky contact). To determine the potential distribution, a self consistent Poisson Solver employing a Finite Element Method (FEM) was used. The size of the simulation area is 1 µm × 1 µm and the size of the discretization mesh was 400 x 400 points. In Fig.1 (a) the potential distribution is illustrated for a Schottky type contact and shows the corresponding potential distribution in the n-type GaAs substrate (N_D=1 × 10^{16} cm^{-3}). One can see nicely, that due to the chosen boundary conditions, only the area below the tip apex effects the local potential distribution in the semiconductor and that the field arising from sidewalls of the tip are shielded by the surface states. In Fig. 1(b) a MOS type contact with no surface states, no oxide-traps and no oxide-semiconductor interface-traps included was simulated. The potential distribution in the semiconductor is affected by the tip as a whole, either directly in the contact area or indirectly via the ε = 1 environment. In the above figures, a color scheme was used which ranges from $-U_{max}$ (black) through reverse rainbow colors to $+U_{max}$ (white).

Furthermore we discuss the influence of the AFM tip geometry (both for Schottky type and MOS –type) on GaAs with varying parameters like different- opening angles (Fig. 2), doping concentrations, oxide layers and tip apex areas. The frequency behavior up to 20 kHz was also investigated on GaAs MOS junctions.

Interlayer Hall effect of Zero gap conductor

M.Sato*, K.Miura*, S.Sugawara**, N.Tajima***, Y.Nishio*, K.Kajita*,and K.Murata****

* *Department of Physics, Toho University, Funabashi, Chiba, Japan*

** *The Institute for Solid Statephysics, Tokyo University, Kashiwanoha, Kashiwa, Chiba, Japan*

*** *RIKEN(The Institute of Physical and Chemical Research), Hirosawa ,Wako, Saitama, Japan*

**** *Department of Material Science, Fac. Sci. , Osaka City University, Sumiyoshi, Osaka, Japan*

Keywords: α (BEDT-TTF)$_2$I$_3$, zero gap conductor, Interlayer Hall Effect, zero-mode carriers

One of the recent progress in the field of investigation of organic conductors, is a discovery of a zero-gap conductor α-(BEDT-TTF)$_2$I$_3$. Under high pressures, this material exhibits mysterious transport behavior [1]. Those interesting transport phenomena have been an issue to be explained for a long time. A few years ago, this material was found to be a conductor with Dirac cone type energy dispersion [2]. Now, we are in a stage where we can analyze the behavior of α-(BEDT-TTF)$_2$I$_3$ based on the knowledge of zero gap conductors.

This material is the first 1) bulk, 2) two dimensional 3) intrinsic zero gap conductor with layered crystal structure. Since a conductive layer is separated by insulating layers, the electrical transport occurs in each layer, almost independently. Weak but finite electron transfer between layers is important because it opens a way to examine the intra-layer electronic states through the interlayer transport phenomena. It should be emphasized that electrons occupy the energy states below the contact points of Dirac cones at zero temperature and therefore the electron density at low temperatures is very low. For example, it is about 10^8/cm^2/layer at 1.5K. The purpose of this work is to clarify the properties of zero-mode carriers (electrons in the N=0 Landau level) that appears at the contact points when a magnetic field normal to the 2D-layer is applied. To investigate how zero-mode carriers are created, measurement of Hall effect is inevitable since it gives information on the carrier density. In a conventional Hall effect measurement, the electric current is applied in the 2D-layers. Recently, we succeeded in observing the Hall effect for the current normal to the layers. These two types of Hall effect looks very different. In the experiment, magnetic field with a fixed strength was rotated in a plane normal to the current and the Hall resistance was measured as a function of the field direction. We found that as the field is rotated from the in-plane direction to the direction normal to the layers, the conventional Hall resistance first increases and then saturates to a value of the order of h/e^2(/number of layers). The saturation occurs in the field where zero-mode carriers dominate the transport.

On the other hand, the interlayer Hall resistance has a sharp peak when the field is parallel to the layers where the in-plane Hall resistance is zero. We found the envelope of curves in Fig.1 can be fitted to a function $\rho = a\cot(\theta)$ in a wide region of θ. This characteristic behavior can be explained in terms of zero mode carriers. In the vicinity of θ=0, the curves deviate from the above relation. In this region, Landau levels disappear and carriers created by the Zeeman effect gives a dominant contribution on transport .

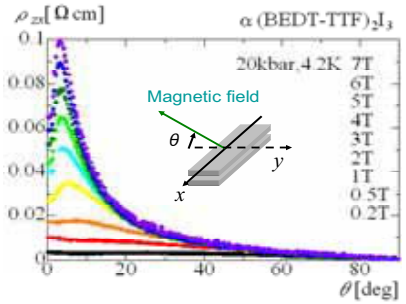

Fig.1 Magnetic angle dependence of Interlayer Hall resistance at high hydrostatic pressure

References

1. N.Tajima et al. , JPSJ **75**, 5, 051010 (2006).
2. S.Katayama et al. , cond-mat 0601068 (2006).

Current counterflow due to hot electron injection in two dimensional electron gas

I. I. Kaya*, E. Karabudak*, M. Hauser**

*Sabanci University, Istanbul,Turkey

** Max-Planck-Institute FKF, Stuttgart, Germany

Keywords: nonequilibrium transport, electron scattering, 2deg,

Nonequilibrium conditions generated by hot electron injection give rise to nonlinear transport in nanodevices with dimensions comparable to intercarrier scattering length scales. In this work, we present the recent experimental results on a three terminal device fabricated on a two dimensional electron gas. High energy electrons (~100 meV) are injected over an electrostatic barrier and the current flow into two leads over adjustable barriers with parallel and perpendicular orientation to the injection direction is measured. The relaxation of the hot electrons via scattering with the cold electron system generates a highly nonequilibrium condition in between the barriers placed with < 1 μm separation. The results provide rich information related to the momentum distribution of the nonequilibrium electron system and the relaxation mechanisms.

It has recently been demonstrated that in a regime of few electron-electron scattering events an analog of classical Bernoulli effect can be observed in a two dimensional electron gas. The effect reveals itself as reversal of current or potential due to hot electron current flow [1]. The strong directionality of electron-electron scattering in two dimensions leads to enhancing of the current flow. In this experimental scheme the relaxation of the electron system via optical [1] and acoustic [2] phonons can also be identified via the energy spectroscopy.

At even higher injection energy levels the ratio of collected and emitted currents, $\alpha = I_C/I_E$, is observed to be wildly modulated by the electrostatic barrier (φ) across the relaxing hot electron stream (Fig. 1). While for lowest gate potentials ($\varphi << E_F$), $0<\alpha<1$ as in the diffusive transport regime and for $\varphi \geq E_F$, $\alpha > 1$; for a range of intermediate φ values, the collector current flow opposes injected current direction ($\alpha < 0$).

The observed unusual electron flow dynamics can be used to analyze the momentum distribution in the electron system bound in between the barriers and to study the details of the electron relaxation maechanisms.

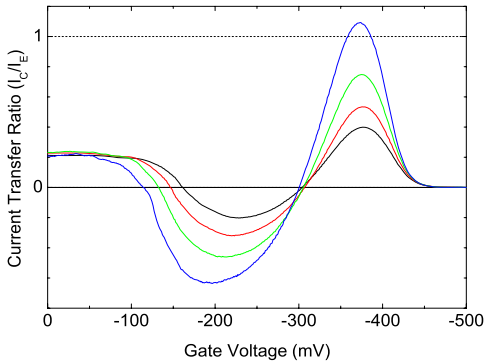

Fig.1 The ratio of collected current to injected current $\alpha = I_C/I_E$ for a three terminal device versus the negative collector gate potential which generates an electrostatic barrier for across the relaxing hot electron stream. $\varphi \sim E_F$ when $V_G = 380$ mV. Each individual trace for V_G offset by -6 mV.

References

1. I. I. Kaya and K. Eberl, Phys. Rev. Lett. 98, 186801 (2007).

2. G. J. Schinner *et. al.* Arxiv, 0901.3520 (2009).

Anisotropic exciton and charged exciton dichroic photoluminescence in undoped ZnSe/BeTe type-II quantum wells in magnetic fields

R. Shen*, E. Kojima*, R. Akimoto** and S. Takeyama*
* *Institute for Solid State Physics, University of Tokyo, 277-8581, Kashiwa, Japan*
** *AIST, Ultrafast Photonics Devices Laboratory, 305-8568, Ibaraki, Japan*

Keywords: photoluminescence, circular dichroism, linear polarization, type-II quantum well

In ZnSe/BeTe quantum wells (QWs), due to the type-II quantum structure, a photoexcitation causes a unique situation where the electrons stay in the ZnSe layer, whereas the holes are injected into the BeTe layer. Since the energy minima for photoexcited electrons and holes lie in different layers, photoluminescence (PL) occurs as a spatially indirect (SID) optical transition. The quantum structure is characterized by a good lattice match (the mismatch less than 0.5%), and a type-II band alignment with a fairly large band-offset (2.3 eV for the conduction band and 0.9 eV for the valence band, respectively). Thus, the electron and hole wavefunction overlap between the adjacent layers is substantially suppressed. In such a case, it has been believed that bright PL can only be allowed through localizations of electrons and holes (or excitons) at the interface. To date localized exciton models have been believed to be realistic for the origin of bright SID PL in these *undoped* systems.

We have studied the SID PL of an *undoped* asymmetrical ZnSe (8 nm) /BeTe (3 nm)/ZnSe (4 nm) quantum layers grown on GaAs substrates. Two major PL peaks appear around 1.91 eV (from the 8-nm ZnSe QW), and 1.94 eV (from the 4-nm ZnSe QW) at 4.2 K, respectively. These PL exhibit high degree of linear polarizations owing to an anisotropy of the interface chemical bonds, which are responsible for the optical transition [1].

Spin degrees of freedom determined from circular polarizations of the PL contains important information for clarifying the origin. However, the circular polarization degree is very much modified by the in-plane anisotropy of the PL.

We have succeeded in extracting intrinsic circular polarization degree by a special combination of a 1/4 wave-plate and a linear polarizer with respect to the in-plane crystal axis. The circular dichrosim of the SID PL from each QW, not affected by the in-plane anisotropy were determined in magnetic fields up to 50 T.

The Zeeman splitting of the PL from the 4-nm ZnSe QW is consistent with the circular polarization degree obtained by the method mentioned above. Thus the SID PL from the 4-nm QW is attributed to a conventional exciton transition at the interface. On the other hand, as for the PL from the 8-nm QW, almost zero Zeeman splitting contradicts with the high value of the circular polarization degree. This phenomenon can only be explained by a charged exciton transition.

Detailed analysis of the optical selection conducted on the SID PL from the 8-nm QW lead us to conclude that a positive charged exciton (a hole bound to an exciton) is majorly involved in the transition. Pump-and-probe absorption spectra in the 8-nm ZnSe QW evidenced the existence of free electrons in the ZnSe well with more than 10^{10} cm^{-2} upon photoexcitation. This fact is also explained by the positive charged excitons occurred as the SID PL. Furthermore, the σ^- polarized PL intensity drastically decreases with increasing magnetic fields. This was quantitatively well described by a crossover of the singlet and the triplet (dark state).

References

[1] A.V. Platonov *et al.*, Phys. Rev. Lett **83**, 3546 (1999).

In search for the geometric potential of curved 2DEGs through coherent electron transport.

A. Bertoni [1], G. Cuoghi [1,2], G. Ferrari [1,3] and G. Goldoni [1,2]

[1] *S3 National Research Center, INFM-CNR, Modena, Italy*

[2] *Dipartimento di Fisica, Università di Modena e Reggio Emilia, Modena, Italy*

[3] *CNISM Unità di Ricerca di Modena, Italy*

Keywords: curved 2DEG, geometric potential, quantum transport, nanowire junction

The 2D quantum equation of motion of a particle constrained on a curved surface has an effective potential term that accounts for its local curvature. This geometric potential (GP), conjectured more than fifty years ago[1], is commonly included in the modelling of curved 2D systems[2], though its direct experimental evidence has not been achieved so far.

In this contribution, we will present our recent theoretical results[3,4] on coherent electron transport in nonplanar 2DEG systems, including a proposal for the experimental detection of the GP[4]. Specifically, we will show that a proper procedure for the reduction of dimensionality from 3D to 2D naturally leads to the GP term and that, with a proper choice of gauge, the effect of external magnetic/electric fields and the effect of the surface curvature can be decoupled. In order to focus on a specific semiconductor system, we apply our formalism to the analysis of charge transport in nonuniform junctions of two and three cylindrical 2DEGs. In fact, a number of nanostructures have recently been realized where carriers are confined in a 2D shell wrapped around a core nanowire via epitaxial overgrown[5], and the controlled growth of branched nanowires has been clearly demonstrated[6]. It is our aim to show how the surface geometry is able to strongly influence the quantum transmission characteristics.

Finally, it will be shown how conductance measurements of a Y-junction three-terminal device can provide a unique signature (see Fig. 1) of the presence of the GP term in the quantum Hamiltonian, this effect being robust against the geometrical details of the junction.

References

1. B.S. DeWitt, Rev. Mod. Phys. **29**, 377 (1957).
2. see e.g. P. Duclos et al., Rev. Math. Phys. **7**, 73 (1995); H. Aoki et al., Phys. Rev. B **65**, 35102 (2001); G. Meyer et al., IEEE Tran. on Nanotech. **6**, 446 (2007).
3. G. Ferrari et al., Phys. Rev. Lett. **100**, 230403 (2008).
4. G. Cuoghi et al., Phys. Rev. B **79**, 73410 (2009).
5. A. Fontcuberta i Morral et al., Small **4**, 899 (2008).
6. D. Wang et al., Nano Lett. **4**, 871 (2004).

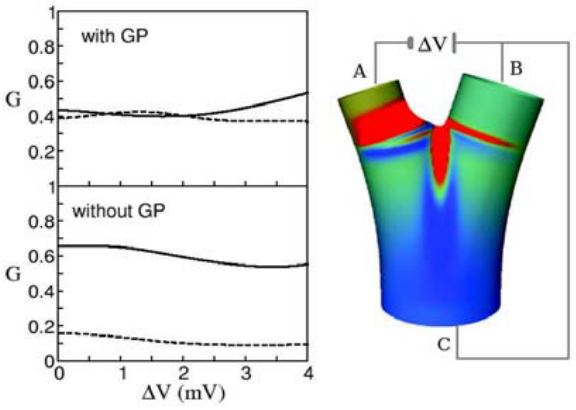

Fig.1 Conductance, calculated through a Landauer-Büttiker approach at 2 K, between two couples of cylindrical leads in the Y junction shown on the right. The solid (dashed) line represents the conductance between A and C (A and B). The three cylindrical surfaces have different radii $R_A<R_B<R_C$. The inclusion of the GP (represented in colour code on the junction) leads to a crossover in the two conductance curves.

Zero-field colossal thermopower in mesoscopic two-dimensional electron systems

Srijit Goswami*, Christoph Siegert*, Arindam Ghosh**, Michael Pepper*, Ian Farrer* and David A. Ritchie*

* Cavendish Laboratory, Cambridge University, J.J. Thomson Avenue, Cambridge CB3 0HE, United Kingdom

**Department of Physics, Indian Institute of Science, Bangalore 560 012, India.

Keywords: thermopower, mesoscopic, 2DEG

High-mobility two-dimensional electron gases (2DEG) have proven to be an excellent platform to study mesoscopic and nanoscale systems. In particular, they may be utilized to fabricate devices in which fundamental electron-electron/electron-spin interactions can be explored in detail. The Kondo effect in single electron transistors and the 0.7 structure in quantum wires are prime examples of such studies. Recently, it has been shown that such correlated states may also exist in 2D mesoscopic systems (2DMS) in the form of a quasi-regular array of localized spins coupled anti-ferromagnetically to the conduction electrons, thus forming a Kondo lattice [1]. As the Fermi level of such a system is tuned, the non-equilibrium conductance characteristics vary in a continuous manner showing two distinct kinds of zero bias anomalies (ZBAs). This variation has been attributed to a competition between Ruderman-Kittel-Kasuya-Yosida (RKKY) exchange interaction and the Kondo effect at low temperatures.

Here, we study similar 2DMS using thermopower measurements at zero magnetic field and milli-kelvin temperatures. The thermopower (TP) of a system depends strongly on the structure of the local density of states in the mesoscopic system. It is also a measure of the entropy per carrier in the system. Thus, TP often yields results that may not be inferred from electrical transport measurements, particularly for spin-correlated systems.

The observed behaviour of TP shows distinct characteristics that cannot be explained within the independent electron framework. (1) The zero field TP in the non-localized regime is almost two orders of magnitude larger than what is predicted. (2) Contrary to what is expected for a degenerate non-interacting electron gas, the magnitude of TP increases with decreasing temperature. However, this is precisely what is expected in traditional Kondo-lattice systems. (3) Variation of the number density of the 2DMS produces reproducible fluctuations in the TP (Fig. 1), which are directly correlated with the variations in the ZBAs. Thus, our studies strongly suggest the existence of correlated states in the 2DMS. Furthermore, we find that TP serves as a powerful tool to study such systems.

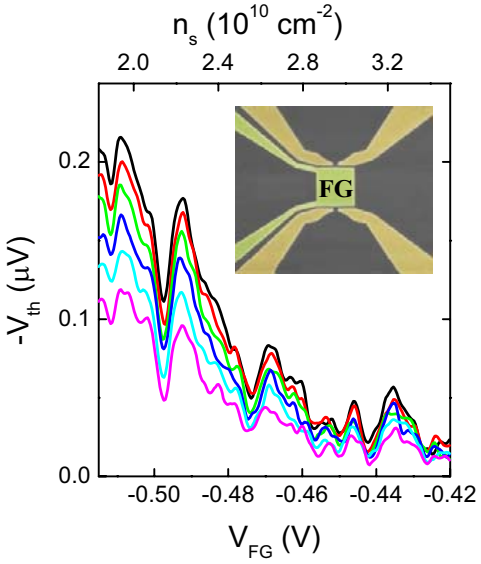

Fig.1 Variation of the longitudinal thermovoltage ($-V_{th}$) with gate voltage ($-V_{FG}$). $-V_{th}$ increases as the temperature difference across the device is increased. The inset shows a micrograph of the 5 μm square device.

References

1. C. Siegert *et al. Nature Phys.* **3**, 315-318 (2007)

Quantum dots around $\nu = 5/2$

A. Harju and E. Tölö
Helsinki Institute of Physics and Department of Applied Physics, Helsinki University of Technology, Espoo, Finland

Keywords: Quantum dots, Pfaffian state

When a gas of electrons is confined to two dimensions, application of a strong magnetic field may lead to startling phenomena such as emergence of interesting topological states. One example of this is the unusual quantum Hall state at half-integer filling $\nu = 5/2$. This state has potential for topological quantum computing [1].

It has been shown that similar filling factor state can be found in quantum dots (QD's) where the gas of electrons is trapped by external electric potentials into small quantum Hall droplets [2]. Taking into account the finite thickness and screening of the electron-electron interaction in the QD's, one can reach as high overlaps as 0.9 between the exact diagonalization and Pfaffian states, for both the lowest and second Landau level [3].

In addition to the overlaps, it is crucial to verify that the state at the angular momentum of the Pfaffian state is energetically favorable. In fact, the Pfaffian state at the lowest Landau level is a possible ground state only at the small and large values of the QD thickness, but not at values of where the overlap is peaked.

A further obstacle for the Pfaffian state in finite-size quantum Hall droplets is that the second Landau level may not attain the high angular momentum and complete spin polarization of the Pfaffian. As Fig. 1 shows, in QD's the degeneracy of Landau levels is lifted when electrons move in external confining potentials, and a compact distribution of electrons on the Landau levels could be energetically more favorable. This leads to a fragmentation of charge and spin densities into incompressible domains and spin-droplet formation [4, 5]. There is also experimental evidence for this, see Fig. 2.

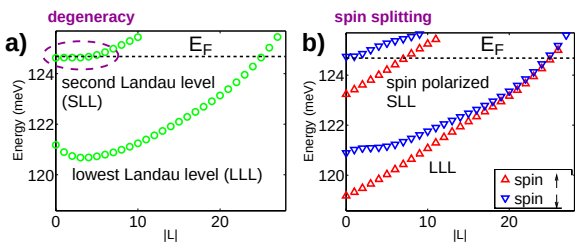

Figure 1: Kohn-Sham energy spectrum as a function of single-particle angular momentum, for (a) spin-compensated solution and (b) spin-polarized solution.

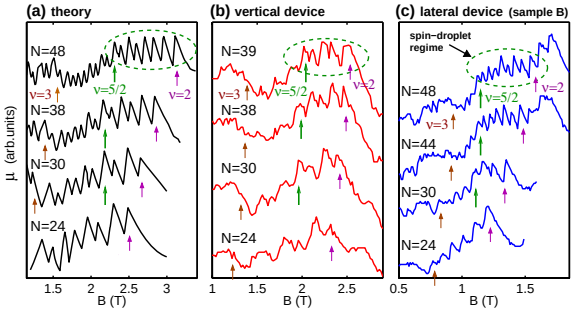

Figure 2: Chemical potentials calculated with the density-functional theory (a) and measured from a vertical (b) and lateral (c) quantum-dot devices for various electron numbers.

The fragmentation of the quantum Hall states could be an issue in the proposed experiments that aim to probe for non-abelian quasi-particle characteristics of the $\nu = 5/2$ quantum Hall state. The possibilites to avoid this by modifying the confinement potential is studied.

References

[1] C. Nayak, S. H. Simon, A. Stern, M. Freedman, and S. Das Sarma, Rev. Mod. Phys. **80**, 1083 (2008).

[2] A. Harju, H. Saarikoski, and E. Räsänen, Phys. Rev. Lett. **96**, 126805 (2006).

[3] E. Tölö and A. Harju, Phys. Rev. B. **79**, 075301 (2009).

[4] E. Räsänen, H. Saarikoski, A. Harju, M. Ciorga, and A. S. Sachrajda, Phys. Rev. B **77**, 041302(R) (2008).

[5] H. Saarikoski, E. Tölö, A. Harju, and E. Räsänen, Phys. Rev. B **78**, 195321 (2008).

Spin selector by hybrid triple barrier resonant tunneling diode

Nammee Kim*, M. K. Li** and T. W. Kang**
*Department of Physics, Soongsil University, Seoul 156-743, Korea
** Quantum-Functional Semiconductor Research Center, Dongguk University, Seoul 100-715, Korea

Keywords: spintronics, ferroelectric, superlattice, non-equilibrium Green's function

A spin light-emitting diode(LED)[1] and voltage controlled spin selection in a magnetic resonant tunneling diode (RTD)[2] have been demonstrated as effective ways of spin injection into a semiconductor structure. However, in order to change the direction of the spin polarization, the direction of external magnetic field should be changed for both cases, which naturally causes complications in device application. Therefore, a different method for controlling the spin polarization without changing the external magnetic field has to be developed. To realize a multi-functional device, people also have tried to control spin through ferroelectric dipole moment[3, 4].

In this work, we propose a spin-selector of ferroelectric triple barrier resonant tunneling diode with diluted magnetic quantum wells as in Figure 1. Spin transport properties of this spin-selector are investigated by non-equilibrium Green's function method. The transmission peak splits into two sub peaks for each spin direction and spin-up and spin down current peaks alternate with the increasing bias voltage. It indicates that the spin polarization of current oscillates with increasing bias voltage. In Figure 2, by reversing the electric dipole direction of ferroelectric barriers, the spin direction of polarized current is reversed simultaneously at a fixed bias voltage. This implies that the spin direction of injected current can be selected through this spin-selector without changing the applied magnetic field.

References

[1] R. Fiederling, M. Keim, G. Reuscher, W. Ossau, G. Schmidt, A. Waag, and L. W. Molenkamp, Nature **402**, 787 (1999).

[2] A. Slobodskyy, C. Gould, T. Slobodskyy, C. R. Becker, G. Schmidt, and L. W. Molenkamp, Phys. Rev. Lett. **90**, 246601 (2003).

[3] C.-W. Nan, M. I. Bichurin, S. Dong, D. Viehland, and G. Srinivasan, Journal of Applied Physics **103**, 031101 (2008).

[4] M. Y. Zhuravlev, S. S. Jaswal, E. Y. Tsymbal, and R. F. Sabirianov, Appl. Phys. Lett. **87**, 222114 (2005).

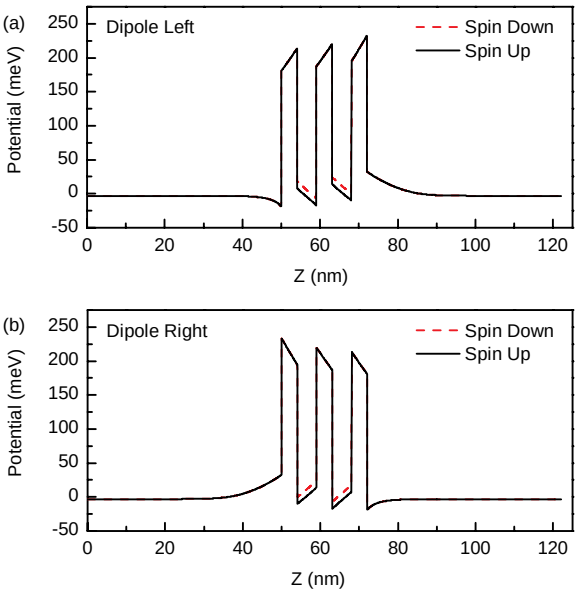

Figure 1: The potentia profiles of the triple barriers RTD for the dipole moment of ferroelectric barriers pointing to the left (a) and the right (b).

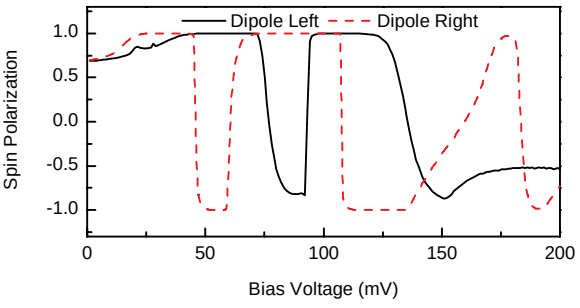

Figure 2: The spin polarization versus bias voltage curves for both dipole directions.

Few hole quantum dot characteristics of gate-all-around PMOS silicon nanowire field effect transistors

B. H. Hong*, L. Choi*, K. H. Song*, S. W. Hwang*, D. Ahn**, K. H. Cho***, K. H. Yeo***, D.-W. Kim***, G. Y. Jin*** and D. Park***

*Research Center for Time domain Nano-functional Devices & School of Electrical Engineering, Korea University, 5-1 Anam, Sungbuk, Seoul 136-701, Korea

**Institute of Quantum Information Processing & Systems, Univ. of Seoul, Dongdaemun, Jeonnong, Seoul 130-743, Korea

***Semiconductor R&D Center, Samsung Electronics Co., Hwaseong-si Gyeonggi-do, 445-701, Korea

Keywords: Few hole quantum dot, Gate-all-around, Silicon nanowire FET, Single-hole-transistor

So far, there has been much progress in the study of few electron physics in various quantum dots (QD) fabricated from GaAs based materials. On the other hand, silicon nanowires have also been providing interesting platforms to study spin transition [1], transport through single dopant states [2]. Recently, single hole transport through a few-electron silicon nanowire QD formed in a VLS synthesized silicon nanowire has been reported [3]. In this study, we report few hole characteristics of a PMOS silicon nanowire field effect transistor (SNWFET) fabricated using top-down VLSI processing techniques.

Figure 1 shows a schematic and cross-sectional transmission electron microscope image of the PMOS SNWFET. The physical channel length and the diameter of the nanowire are 44 and 4 nm, respectively. The nanowire has an almost circular cross-section and it is fully surrounded by 3.5 nm thick gate oxide and TiN gate. The body of the nanowire is etched from the epitaxially grown silicon and it is bridging the p^+ doped source and drain electrodes.

Figure 2 shows the differential conductance dI_{DS}/dV_{DS} measured from the device at the temperature of 4.2 K. The data shows N = 0, 1, and 2 states with several excited states (denoted by the arrows). The turn-on voltage obtained from the extrapolation of the potential barrier vs. gate bias is approximately – 0.42 V, which is consistent with the position of the first peak. The transition energy from G(0) to E(1) is given by 1 meV from the slope analysis of the Coulomb diamond. We will present various other energy scales together with simple calculations.

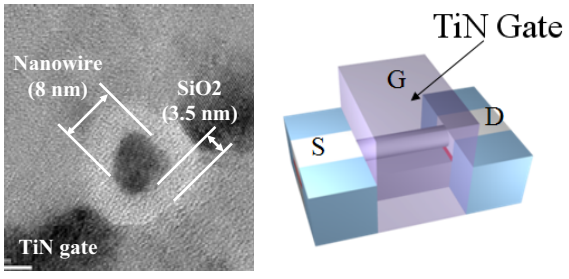

Fig.1 Cross-sectional image and schemetic diagram of gate-all-around silicon nanowire FET [3].

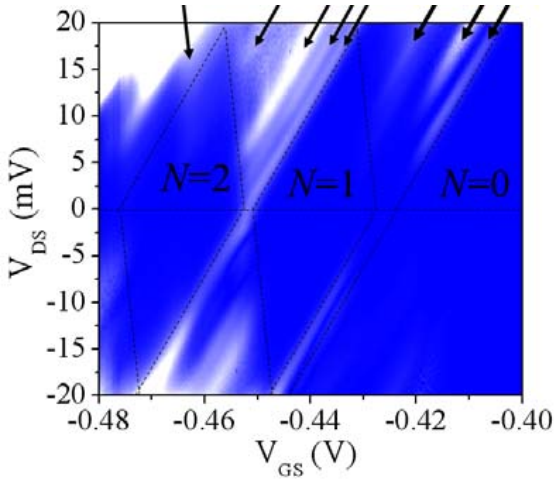

Fig.2 V_{DS} –V_{GS} contour plot of dI_{DS}/dV_{DS}

References

1. L. P. Rokhinson, Phys. Rev. B **63**, 035321 (2001).

2. H. Sellier *et al*., Phys. Rev. Lett., vol. 97, p. 206805, Nov. (2006).

3. K. H. Cho *et al*., *IEEE EDL Vol*. 28, *NO*. 12 pp. 1129 (2007)

Time resolved control of electron tunnelling times and single-shot spin readout in a quantum dot.

L. Gaudreau[*,**], S. Studenikin[*], G. Granger[*], J. Kycia[***], P. Mason[***], A. Kam[*], C.Y. Hsieh*, R. Cheriton*, M. Korkusinski*, P.Hawrylak* and A. Sachrajda[*]

Institute for Microstructural Sciences, National Research Council, Ottawa, Canada, K1A 0R6

** *Physics Department, University of Sherbrooke, Quebec, Canada, J1K 2R1*

*** *Department of Physics and Astronomy, University of Waterloo, Waterloo, Canada, N2L 3G1*

Keywords: Quantum dot, Coulomb blockade, Charge detection, Electron spin relaxation

Since the first report of a few electron lateral quantum dot about 10 years ago [1], there has been much focus on the application of these systems as spin qubits. A crucial technique for read-out of spin qubits has been the time resolved charge detection. In particular, emphasis has been placed on the DiVincenzo criteria and their individual demonstration. A crucial technique for this research has been the time resolved charge detection. This enabled, for example, single-shot single spin read out by Elzerman et al [2]. Surprisingly, to our knowledge, this important scheme has not yet been reproduced.

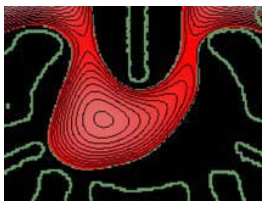

Fig.1 Calculated potential profile of a single quantum dot in a triple quantum dot device.

In this paper we reproduce this Delft protocol for single-shot single spin readout on one quantum dot within a triple quantum dot device (Fig.1) in a GaAs-AlGaAs heterostructure with neighbouring quantum point contacts as charge detectors, and extract the T_1 values at different magnetic fields, e.g., ~300μs at 10T (see Fig. 2).

To enable such investigations, it is important to extract and control the tunnel times for different device gate voltage settings. We achieve this using two techniques : (i) A statistical approach for which the chemical potential of the dot is aligned with the reservoirs and (ii) An averaged gate pulsing scheme in

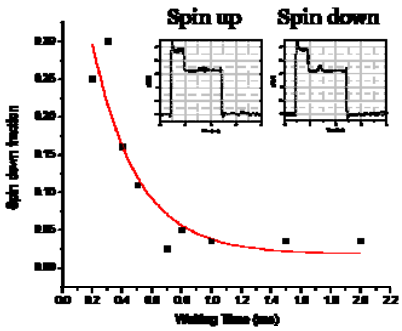

Fig.1 Spin relaxation time extraction from single-shot spin readout experiments as a function of the waiting time in which the electron is held in the dot before measuring its spin state. Each point represents a series of 200 single-shot measurements from which we extract the fraction in which the spin was measured to be down. Inset: two examples of a spin-up and a spin-down measurement.

which the N=0 to N=1 to N=0 transitions are induced by pulses. The first approach results in tunnel in and out times being approximately equal whereas (ii) results in very different times for tunnelling in and out due to the energy dependence of the tunnel barriers. Experimental results are compared with calculated spin relaxation times due to phonons [3], nuclear spins and electrons in leads.

References

1. Ciorga *et al.,* Phys. Rev. B **61**, R16315 (2000).
2. J. M. Elzerman *et al.*, Nature **430**, 431 (2004).
3. M.Florescu *et al.* Physica **E 22**, 41

Fluctuation Theorem in Single-Electron Counting

Y. Utsumi*, D. S. Golubev**, M. Marthaler***, M. Hettler** and G. Schön** ***

** Institute of Solid State Physics, University of Tokyo, Kashiwa, Chiba 277-8581, Japan*
*** Forschungszentrum Karlsruhe, Institut für Nanotechnologie, 76128 Karlsruhe, Germany*
**** Insitut für Theoretische Festkörperphysik, Universität Karlsruhe, 76021 Karlsruhe, Germany*

Keywords: Real-time Electron Counting, Full Counting Statistics, Fluctuation Theorem, Dephasing

In the last fifteen years, a new exact thermodynamic relation valid far from equilibrium, the *fluctuation theorem* (FT), has been established. Although simple in its formulation, it is of fundamental importance and it has proven to be a powerful tool. E.g., in the macroscopic limit it leads to the second law of thermodynamics, and it reproduces Onsager's relations and the fluctuation-dissipation theorem. So far, FT predictions have been tested for biomolecules strongly influenced by thermal fluctuations. However, a full understanding of the FT in the quantum regime, especially its experimental verification, is still missing. Nonequilibrium fluctuations in mesoscopic systems, and specifically quantum shot noise, have been studied intensively since they provide additional information beyond the measurement of the average current. Modern studies of quantum noise concentrate on the probability distribution of transmitted electron number $P(q)$, i.e., the *full counting statistics* (FCS). Recently it has been recognized that the FCS and FT are related [1] and the relation $P(q)/P(-q) = \exp(qV/T)$ is satisfied far from equilibrium. Experimentally it is possible to measure the probability distribution by counting individual electrons in real time using, e.g., a quantum point contact (QPC) charge detector [2].

Motivated by electron counting experiments on a double quantum dot (QD) [2] (Fig. 1), we study the quantum FT for single-electron transport. In particular, we discuss dephasing effects by phonons and the detector backaction. Though the electron-phonon coupling in a GaAs QD is strong, which destroys the coherence of charge quantum states, it does not affect the FT as long as the phonon and electron subsystems are equilibrated. The dephasing caused by the QPC shot noise is more subtle. The large bias voltage applied to QPC, which is needed for the high-speed real-time charge detection, inevitably leads to a high shot noise. Using the real-time diagram technique [3], we show that this noise effectively enhances the QD temperature and leads to deviations from the FT (Fig. 2). Such a heating might have been observed in the experiment [2].

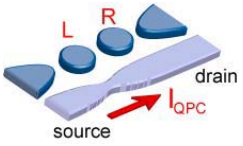

Fig.1: Setup of the real-time electron counting experiment. The tunnel current through the double quantum dot is measured by a nearby quantum point contact, which serves as a high-speed electrometer.

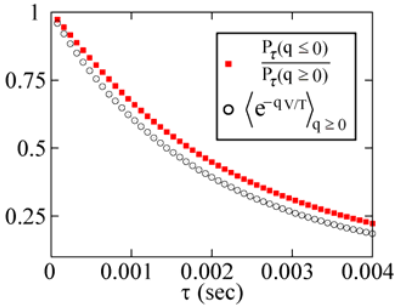

Fig.2: Integrated form of the fluctuation theorem for the probability distribution of the transmitted electron number as a function of the measurement time. Due to the effective heating by the QPC current the two curves do not coincide.

References

1. K. Saito and Y. Utsumi, Phys. Rev. B **78**, 115429 (2008).
2. T. Fujisawa, T. Hayashi, R. Tomita, and Y. Hirayama, Science **312**, 1634 (2006).
3. A. Shnirman and G. Schön, Phys. Rev. B **57**, 15400 (1998).

Single Electron Spin Addressing by Photon-assisted-tunneling for a Double Quantum Dot Integrated with a Micro-magnet

Y.-S. Shin[1], M. Pioro-Ladrière[1,2], T. Obata[1], Y. Tokura[1,3], R. Brunner[1], T. Kubo[1], K. Yoshida[1], S. Tarucha[1,4]

1. Quantum Spin Information Project, ICORP, JST, Atsugi-shi, Kanagawa, 243-0198, Japan
2. Departement de Physique, Universite de Sherbrooke, Sherbrooke, Quebec, J1K-2R1, Canada
3. NTT Basic Research Laboratories, NTT Corporation, Atsugi-shi, Kanagawa, 243-0198, Japan
4. Department of Applied Physics, University of Tokyo, Hongo, Bunkyo-ku, Tokyo, 113-8656, Japan

Keywords: Quantum dots, Micro-magnets, Charge sensing, Spin qubits, Microwaves

Spin-based solid-state quantum computation has been attracting recent research interests [1]. Crucial requirement of the quantum computation is to manipulate and readout electron spins. Spin readout with both spin selectivity and in a non-destructive manner is most ideal. To meet this requirement, a new scheme using a double quantum dot (DQD) with different Zeeman energies E_Z between two dots and photon-assisted-tunneling (PAT) has recently been proposed [2]. We prepared a DQD with a micro-magnet on top to realize the above spin readout scheme. A DQD and a quantum point contact (QPC) flanked with the DQD are defined in a two-dimensional electron gas (2DEG) formed in AlGaAs/GaAs interface by Schottky gates. The two dots are designed to experience a stray magnetic field produced by an on-chip magnet, providing a Zeeman energy difference ΔE_Z(~ 100 MHz) between the two dots. Matching the frequency f_{MW} of an applied microwave (MW) to the energy separation of the states with the same spin between the two dots induces PAT transition of charge state between, for example, (N_1,N_2)=(1,0) and (0,1), where N_1, and N_2 are the number of electrons in the two dots QD1, and QD2, respectively. Suppose the initial charge state is (1,0), then this PAT transition can be detected as a change from (1,0) to (1/2,1/2) using a QPC charge sensor. The MW matching frequency is different between the up and down spin states by the amount of ΔE_Z.

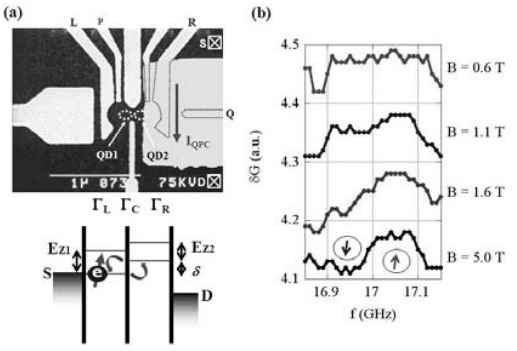

Fig. 1 (a) SEM image without G_{CAP} and schematic energy diagram of the DQD integrated with a micro-magnet of Ni. (b) The MW frequency dependence of transconductance for PAT as a function of external magnetic field. The encircled arrows denote the respective electron spin state.

In this work we investigated to address the spin of a single electron in the DQD with external magnetic field as a key parameter. Suppose the lowest state of QD1 is lower than that of QD2 by energy δ (~hf_{MW}), the Fermi energy E_{F1} of the lead adjacent to QD1 is aligned to the QD1 state, and the Fermi energy E_{F2} of the other lead is lower than both the lowest QD2 state and E_{F1}. In case of E_Z bigger than electron temperature an electron only occupies the up-spin state (ground state) in QD1, otherwise, it can occupy the down-spin state (excited state) as well in QD1. Thus, the PAT peak for the down-spin state disappears with increasing external magnetic field such that $E_z > k_BT$, while that for the up-spin state is always visible independent of external magnetic field (See Fig. 1 (b)).

References

1. D. Loss and D. P. DiVincenzo Phys. Rev. A **57**, 120 (1998).
2. S. D. Barrett and T. M. Stace, Pys. Rev. Lett. **96**, 017405 (2006).

Full control of a flying charge qubit: detection and control of transmission phase shift by Ramsey interference

M. Yamamoto*, **, C. Bäuerle*, *** and S. Tarucha*, ****

* *Department of Applied Physics and QPEC, University of Tokyo, Tokyo, Japan, **ERATO-JST, Saitama, Japan, *** Institut Neel, CNRS, Grenoble, France, **** ICORP-JST, Saitama, Japan*

Keywords: Electron transport, Quantum bit, Transmission phase, Aharonov-Bohm effect

An electron acquires a transmission phase when it coherently travels along a path. The simplest way to make an electron interfere is via a two-path interferometer, i.e. Aharonov-Bohm (AB) ring, in which the relative transmission phase between the two paths can be controlled by an external magnetic field. Although numerous attempts to measure or control the microscopic transmission phase have been made with an AB ring structure, detection of the pure transmission phase of a path has been rather elusive. This is because linear conductance measured in a two-terminal geometry suffers from the phase rigidity resulting from multi-scattering, in which the phase is reconstructed to satisfy the boundary condition imposed by the contacts. Even after pioneering experimental works on multi-terminal devices [1], many discrepancies still remain between experiment and theory, indicating that the boundary condition of the contacts still plays a crucial role on the "observed" phase. Here we present a successful measurement and control of the transmission phase shift of a path, using an original design by combining two coupled quantum wires into an AB ring geometry to form a spatially defined flying charge qubit. The full electrical control of the qubit to address an arbitrary quantum state was realized by the two rotational operations $R_x(\theta)$ and $R_z(\varphi)$, which enables us to measure the transmission phase shift without ambiguity using Ramsey interference.

The structure we employed to define the flying qubit is shown in Fig. 1(A), in which each coherently propagating electron acts as a qubit. The qubit is defined as superposition of two quantum states, $|\uparrow\rangle$ and $|\downarrow\rangle$: an electron existing in either upper or lower wire. The inter-wire tunnel coupling allows flipping between the two quantum states, i.e. rotation $R_x(\theta)$ about the x-axis of the Bloch sphere, and the evolution of AB phase - the relative phase shift between the two states - is translated into rotation $R_z(\varphi)$ about the z-axis. In our experiment, we define the initial qubit state by injecting electrons into only one of the two wires, and detect the output state by measuring the two output currents. Since we have two output contacts, both collecting coherent electrons, our measurement does not suffer from the phase rigidity. We observe Ramsey interference (Fig. 1(B)), in which the output state oscillates as a function of perpendicular magnetic field with the AB oscillation period, whose amplitude becomes maximal when the two tunnel couplings are tuned so that they work as $R_x(\pi/2)$, ideal beam splitters. We also observe that the shift of k-vector in one of the two wires induced by the gate voltage works equivalently as the shift of the perpendicular magnetic field (Fig. 1(C)). This is a direct observation of the phase shift $\Delta\varphi = \Delta k \cdot L$.

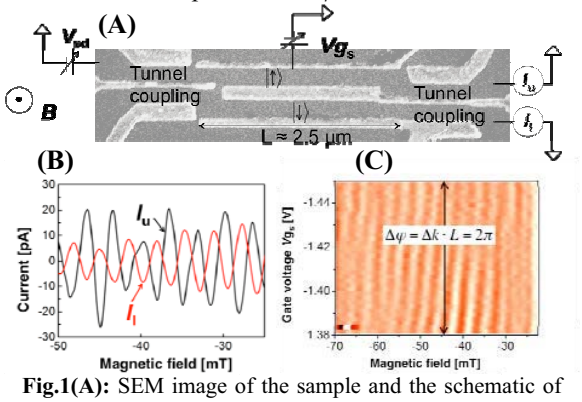

Fig.1(A): SEM image of the sample and the schematic of the measurement setup. **(B):** Oscillatory component of the output currents as a function of B. **(C):** Intensity plot of I_l as a function of B and Vg_S.

References

1. For example, Schuster et al, Nature **385**, 417 (1997)

Observation of the "lobe structure" in the ballistic interferometers

Y. Yamauchi[1], M. Hashisaka[1], S. Nakamura[1], K. Chida[1], S. Kasai[1], T. Ono[1], R. Leturcq[2], K. Ensslin[3], D. C. Driscoll[4], A. C. Gossard[4], and K. Kobayashi[1]

[1]*Institute for Chemical Research, Kyoto University, Uij, Kyoto 611-0011, Japan*
[2]*IEMN - CNRS, Department ISEN Villeneuve d'Ascq, France*
[3]*Solid State Physics Laboratory, ETH Zürich, CH-8093 Zürich, Switzerland*
[4]*Materials Department, University of California, Santa Barbara, California 93106, USA*

Keywords: quantum interference effect, electron Mach-Zehnder interferometer, decoherence, lobe structure

Quantum interference effects have been among the central issues in mesoscopic physics. These days, electronic Mach-Zehnder interferometers (MZI) attract a lot of attention as some of the most ideal electron interferometers [1]. Recent experiments, however, revealed an unexpected phenomenon, the so-called the "lobe structure" [2,3]. At this moment, it is unclear if this lobe structure is specific for the MZI.

To examine the universality of the lobe structure, we performed transport measurements in a ballistic Aharonov-Bohm ring (ABR) (see inset of Fig. 1a) and a Fabry-Pérot type interferometer (FPI) realized in the integer quantum Hall (IQH) regime (see inset of Fig. 1b) [4]. Each of them was fabricated on a GaAs/AlGaAs two-dimensional electron gas and the two-terminal conductance measurement was performed using standard lock-in technique. Samples were cooled by using a dilution refrigerator with a base electron temperature was 125 mK.

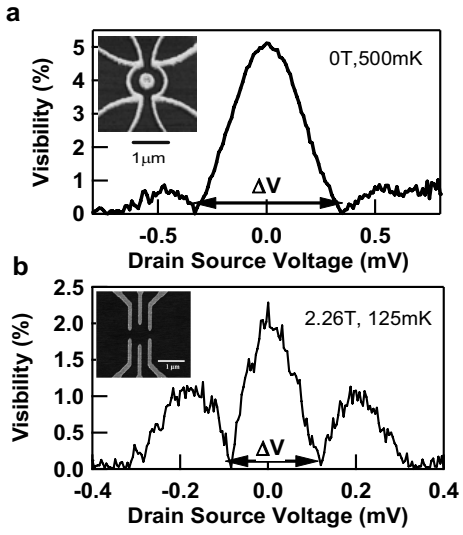

Fig.1 (a) Lobe structure obtained at a AB ring under zero magnetic field (below ±50mT). Visibility is defined as the oscillation amplitude divided by its average. (b) Lobe structure obtained at a FPI in the IQH regime (ν=4).

Figures 1a and 1b show the dependence of the visibility on the drain source bias. The AB amplitude first disappears at a few hundred micro volts and then recovers with an abrupt π phase shift, finally decaying under higher drain source bias, which is in strong analogy with the lobe structure in the MZI. Interestingly, the energy scale to characterize the shape of the lobe (ΔV, see Figures) is much larger than those observed at the MZI. By comparing our data with those reported in previous works, we found that this energy scale is primarily defined by the interferometer arm length, possibly supporting the basic idea proposed in recent theories [5,6]. Our observation of the lobe structure in the ABR and FPI as in the MZI indicates the presence of a universal phenomenon in ballistic interferometers.

References

[1] Y. Ji *et al.*, Nature **422**, 415 (2003).
[2] I. Neder *et al.*, PRL. **96**, 016804 (2006).
[3] L. V. Litvin *et al.*, PRB **75**, 033315 (2007)
[4] B. J. van Wees, *et al.*, PRL **62**, 2523 (1989)
[5] I. Neder and E. Ginossar PRL. **100**, 196806(2008)
[6] S. -C. Youn et *al.*, PRL. **100**, 196807 (2008)

Fluctuation Theorem in a Quantum Dot Aharonov-Bohm Interferometer

Y. Utsumi*, K. Saito** ***

* *Institute of Solid State Physics, University of Tokyo, Kashiwa, Chiba 277-8581, Japan*
** *Graduate School of Science, University of Tokyo, Tokyo 113-0033, Japan*
*** *CREST, Japan Science and Technology (JST), Saitama 332-0012, Japan*

Keywords: Full counting statistics, Magnetic field induced asymmetry in the nonlinear conductance

Microscopic reversibility is a key ingredient in deriving Onsager's relations. It has played a fundamental role in establishing the linear response theory and, recently, a new relationship valid even in the far from equilibrium regime. The relation is known the *fluctuation theorem* (FT), which is able to reproduce both of the second law of thermodynamics and the linear response theory. Recently, based on the theory of the *full counting statistics* (FCS), the FT was generalized to the quantum transport regime in the presence of a magnetic field B. It enables us to derive universal relations among nonlinear transport coefficients beyond Onsager's relations [1]. Precisely, for two terminal systems, the nonlinear transport coefficient $L(B)$ is introduced as follows;

$$\left\langle I^n \right\rangle = \sum_{m=0}^{\infty} \frac{1}{m!} L_m^n(B) \left(\frac{eV}{k_B T} \right)^m ,$$

where V is the source-drain bias voltage and T is the temperature. In the present study, we propose novel relationships, which are related with the nonlinear conductance and the linear response of the current noise, and thus can be measured experimentally [1];

$$L_{2+}^1 = L_{1+}^2, \quad L_{2-}^1 = L_{1-}^2 / 3.$$

Here we defined the symmetrised and anti-symmetrised transport coefficients, $L_{m,\pm}^n = L_m^n(B) \pm L_m^n(-B)$. In order for the theoretical demonstration, we apply the new relationships to a quantum dot (QD) embedded in a two-terminal Aharonov-Bohm interferometer (Fig. 1) [2]. In this setup, because of the lack of the mirror symmetry along the horizontal axis and the Coulomb interaction inside the QD, the asymmetric component of the nonlinear conductance L_{2-}^1 remains finite [2,3]. We

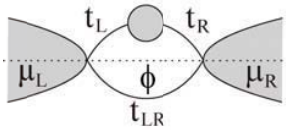

Fig.1: Setup of the Aharonov-Bohm interferometer. A quantum dot is embedded in the upper arm of the ring.

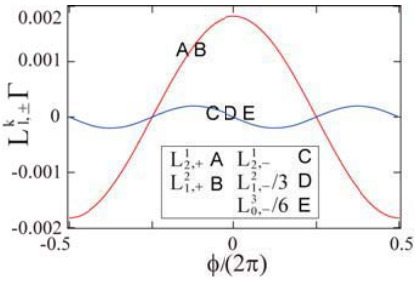

Fig.2: The flux dependence of the nonlinear transport coefficients. The universal relations imposed by the fluctuation theorem are satisfied.

show that the nonlinear transport coefficients satisfy universal relations imposed by the FT (Fig. 2). We also comment on a recent paper, which proposes the universal relationships *not* relying on the micro-reversibility [3]. We point out that they are consistent with the FT for the symmetric component of the nonlinear transport coefficient. However for the asymmetric component, they provide necessary condition of the universal relations imposed by the FT.

References

1. K. Saito and Y. Utsumi, Phys. Rev. B **78**, 115429 (2008).
2. Y Utsumi and K. Saito, arXiv/0810.1113.
3. H. Förster and M. Büttiker, Phys. Rev. Lett. **101**, 136805 (2008).

P12
E1
MoP
E2
E3
E4
TuP
E5
P34
E6
E7
E8
ThP
E9
P56

Electronic states in laterally coupled vertical triple quantum dots

S. Amaha[1], T. Hatano[1], H. Tamura[2], S. Teraoka[1], T. Kubo[1], Y. Tokura[1, 2], D. G. Austing[3] and S. Tarucha[1, 4]

[1] *Quantum Spin Information Project, ICORP-JST, Atsugi, Kanagawa 243-0198, Japan*
[2] *NTT Basic Research Laboratories, NTT Corporation, Atsugi, Kanagawa 243-0198, Japan*
[3] *Institute for Microstructural Sciences M50, NRC, Ottawa, Ontario K1A 0R6, Canada*
[4] *Department of Applied Physics, School of Engineering, University of Tokyo, Bunkyo, Tokyo 133-8656, Japan*

Keywords: Quantum dots, Electronic properties, Coupled quantum dots, Triple quantum dots

Multiple quantum dot (QD) systems are attracting interest due to their enhanced freedom of inter-dot coupling. Recently novel quantum physics in triple QDs has been theoretically investigated such as charge ratchet effect [1], the triplet Nagaoka ground state [2] and a variety of Kondo effects [3]. However experimental reports on few-electron triple QDs (e.g., see Refs. 4-7] are fewer than those for double QDs due to their difficulty of fabrication. Moreover, spin states in triple QDs have not been clearly observed usually due to the limitation of detection of just the charge state.

Here we introduce an experiment to investigate both charge and spin states in three collinear laterally coupled vertical QDs. Our device structure is schematically shown in Fig. 1 (a). The three QDs (Dot 1, Dot 2 and Dot 3) (Fig. 1(b)) are formed inside of three "touching" mesas (mesa 1, mesa 2 and mesa 3). Adjacent dots are sufficiently close that the tunnel coupling is well resolved. The electro-chemical potentials inside the triple QDs can be modulated by applying a gate voltage [V_{g1}, V_{g2} (=V_{g2}'), V_{g3}] to each gate electrode [G_1, G_2, (G_2'), G_3]. We measure the current I flowing from the source, through Dots 1-3 in parallel, to the drain electrode. The total electron number N and the electron numbers on Dot 1, Dot 2 and Dot 3 (N_1, N_2, N_3) can be deduced from Coulomb diamond measurements and by counting Coulomb oscillation lines of the same slope.

Using excitation spectroscopy, we obtain information about the evolution of the N=1, 2 and 3 ground and excited states from the stability diagram. The measured spectra on sweeping V_{g1} and V_{g2} agree well with calculations from a three site Hubbard model. We note that the N=2 singlet state is found to be much more stable than triplet state at an anti-crossing characteristic of a triple QD, because for the triplet states double occupancy in a dot by virtual processes is forbidden. Moreover, only the two doublet states (total spin S=1/2) are identified for the N=3 ground and excited states because the quartet states (S=3/2) are not accessible due to spin blockade. We will also discuss the electronic charge and spin states in the case when an approximately triangular arrangement of the dots (Fig.1 (c)) is induced by gate voltage tuning in the same device.

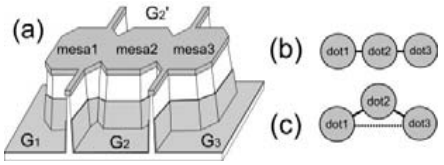

Fig.1 Schematic of (a) our collinear triple QD device, (b) collinear and (c) triangular arrangement.

References

1. M. Stopa, Phys. Rev. Lett. **88**, 146802 (2002).
2. Y. Nagaoka, Phys. Rev. 147, 392 (1966).
3. T. Kuzmenko et al., Phys. Rev. Lett. **96**, 046601 (2006).
4. L. Gaudreau et al., Phys. Rev. Lett. **97**, 036807 (2006).
5. D. Schroer et al., Phys. Rev. B **76**, 75306 (2007).
6. S. Amaha et al., Appl. Phys. Lett. **92**, 202109 (2008).
7. S. Amaha et al., Appl. Phys. Lett. **94,** 092103 (2009).

Scanning gate microscopy on quantum rings: influence of the magnetic field and of charged defects

M. Pala*, F. Martins**, B. Hackens**, S. Baltazar*, H. Sellier***, S. Huant*** and V. Bayot**,***
* *IMEP-LAHC (UMR 5130), INP Grenoble, France*
** *DICE lab, Université catholique de Louvain, Belgium*
*** *Institut Néel, CNRS, and Université Joseph Fourier, Grenoble*

Keywords: scanning gate microscopy, quantum rings, Aharonov-Bohm effect

Scanning tunneling microscopy allows to probe the local density of states (LDOS) of surface electrons. However, in the case of two-dimensional systems buried under an insulator, such a technique is useless, since no direct current can flow between the tip and the electron system. In this case, one can use the biased tip of the scanning probe microscope as a local gate, and record the conductance variations of the electron system as the tip scans over it. Combining experiments and simulations at zero magnetic field B [1], we recently showed that this "scanning gate microscopy" (SGM) allows to probe the LDOS in mesoscopic quantum rings (QRs).

Here, we focus on the correspondance between LDOS and SGM images when a magnetic field is applied to QRs with a more realistic potential landscape (*i.e.* including defects) [2]. The Hamiltonian of the system is described via a tight-binding model, and our simulations are based on the calculations of the relevant Green's functions of the system by a recursive technique. The QR conductance is calculated within the framework of Landauer-Buttiker transport theory. To produce SGM images, we include a lorentzian perturbation potential mimicking the tip-induced perturbation.

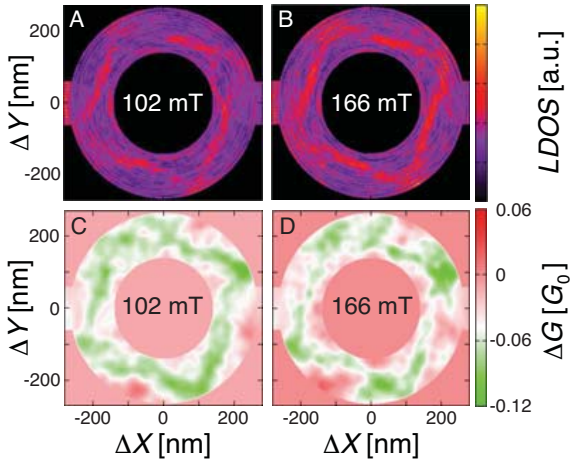

Figure 1: (a-b) Simulated LDOS map in an ideal quantum ring at B=102 mT and 166 mT, respectively (c-d) Simulated SGM conductance maps on the same quantum ring, at B=102 mT and 166 mT, respectively.

Including charged defects in the potential landscape has a strong effect on the LDOS pattern : asymmetric radial fringes appear, with a distribution depending on the Fermi energy. Such fringes originate from internal wavefunction reflections inside the quantum ring. Interestingly, simulations with various defect configurations show that the correspondance between LDOS and SGM maps is maintained even when defects are present. This result therefore explains the presence of radial fringes in experimental SGM data on QR.

When a magnetic field is included in the simulation, recursive orbits scarring the total wave function appear, with the same periodicity as the Aharonov-Bohm effect, as shown in Fig. 1a-b. This phenomenon occurs when a large number of states mimics quasi-classical trajectories inside the QR. The SGM maps simulated using a weak tip perturbation bear the signatures of the same quasi-classical trajectories (Fig. 1c-d). Our results therefore significantly extend the range of situations where the SGM technique can reliably be used to probe the electronic LDOS of mesoscopic devices.

References

[1] B. Hackens et al., Nature Phys. **2**, 826 (2006); F. Martins et al., Phys. Rev. Lett. **99**, 136807 (2007).

[2] M. Pala et al., Phys. Rev. B **77**, 125310 (2008); M. Pala et al., Nanotechnology (submitted).

Differential resistivity noise in low density mesoscopic two-dimensional electron system

R.Koushik[1], Matthias Baenninger[1, 2], Arindam Ghosh[1], H.E.Beere[2], David A.Ritchie[2] and Michael Pepper[2]

[1] *Department of Physics, Indian Institute of Science, Bangalore, India*

[2] *Cavendish Laboratory, University of Cambridge, J.J.Thomson Avenue, Cambridge, UK*

Keywords: Mesoscopic, Differential resistivity noise

Modulation doped heterostructures are ideal candidates to study the effects of disorder on electron-electron interaction in a systematic manner. In these systems the strength of the disorder is determined by an undoped AlGaAS spacer, which separates the charged silicon dopants from the two dimensional electron gas, and can be tuned to atomic precision in molecular beam epitaxy. Several disorder-stabilized strongly interacting many-body phenomena have been either theoretically predicted or experimentally claimed in these systems, ranging from Wigner crystallization, striped or bubble-type charge density waves, or even glassy electron phases. Conventional techniques, based on time averaged resistivity measurements, are however often inconclusive in this regard. In this work, we report the

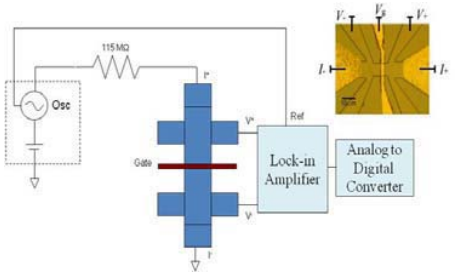

Fig.1 Differential noise measurement in four probe ac+dc mixing geometry. The inset shows the micrograph of a device.

measurements of low-frequency resistivity fluctuations in mesoscopic 2D electron systems in delta-doped GaAs/AlGaAs heterostructures in the strongly interacting regime. Specifically, our experimental technique involves investigation of differential resistivity noise, where the resistivity fluctuations were measured with a small ac modulation across the sample constant (30 μV) at several fixed dc source-drain bias ranging from -400 μV to +400 μV (see figure 1). While the power spectral density varies typically as $S_v \sim 1/f^{\alpha}$,

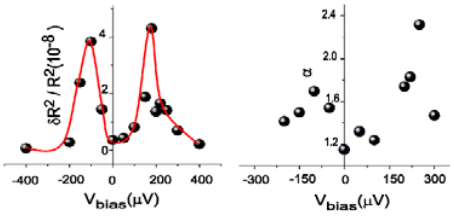

Fig.2 Resistivity fluctuations and Alpha are shown for different source-drain bias at constant ac bias (30 μV) and resistance of 10 kΩ. The red line is a guide to the eye.

where α varies from ~ 1 – 2, our measurements at low temperatures (267 mK) reveal an increase in noise at a critical source-drain field (around 200 μV). We attribute the results to an electrically-driven depinning transition in a many-body quantum electron solid that has been recently claimed in the context of self-localization of interacting electrons or even interaction-driven metallic transport.

References

1. M. Baenninger *et al*., Phys. Rev. Lett. **100**, 016805 (2008).
2. M. Baenninger *et al*., Phys. Rev. B **72**, 241311(R) (2005)

Cooling a 2D electron gas using quantum dots

J. R. Prance, C. G. Smith, J. P. Griffiths, S. J. Chorley, D. Anderson, G. A. C. Jones, I. Farrer and D. A. Ritchie
Cavendish Laboratory, University of Cambridge, UK

Keywords: quantum dots, thermoelectric effects.

Edwards et al.[1, 2] first suggested using energy selective transport through the single-particle states of quantum dots to cool a 2D electron gas (2DEG). Their proposed "Quantum Dot Refrigerator" (QDR) uses two dots: one to remove hot electrons from an isolated 2DEG, the other to remove hot holes. The resulting current extracts heat from the electron gas and dissipates it in the adjacent reservoirs. Because of the weak electron-phonon coupling, they predicted that temperatures below that of the lattice could be reached.

Previously, the superconducting energy gap has been used in a similar way to cool electron gases in metals and heavily doped Silicon (for a review see Giazotto et al.[3]). To our knowledge, however, such a system has not previously been realised using quantum dots.

We will present measurements of a device designed to cool a 6 μm^2 2D electron gas [4]. The measurements reveal a complication not considered in the original proposal: the Coulomb blockade energy of the cooled region itself. We will present a model that accounts for this, and which predicts that the device can still function in this regime. We will also show how the temperature of the cooled region can be inferred from the line-shape of the current through the device. By comparing measured line-shapes with predictions from the model, we find the data to be consistent with cooling of the isolated 2DEG by over 90 mK in the best case.

QDRs could eventually enable the study of very low temperature behaviour of electron gases. It may also be possible to embed large numbers of nanostucture devices within a cooled 2DEG and study their behaviour non-invasively using point-contact detectors or compressibility measurements. We will discuss these possibilities, as well as general techniques to improve QDR performance.

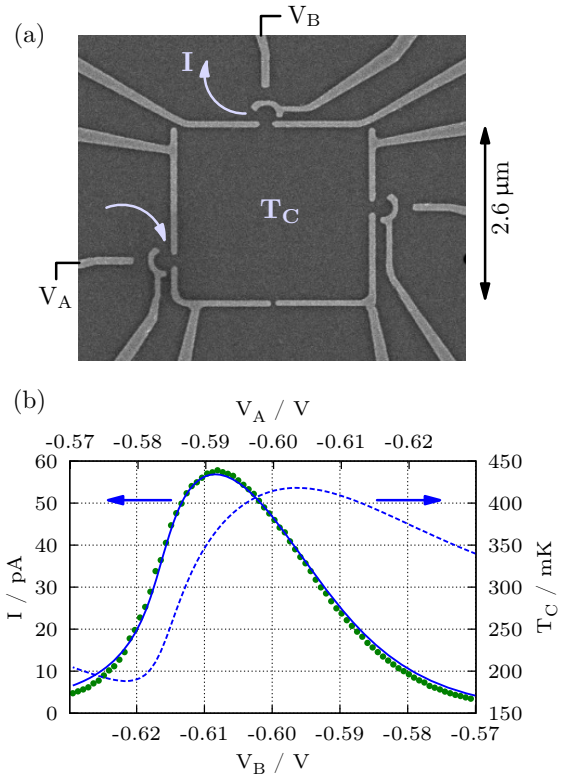

Figure 1: (a) SEM image of a QDR device. (b) Measured current under a small bias (circles), predicted current (solid line), and predicted isolated 2DEG temperature profile (dashed line). The ambient electron temperature in the reservoirs is 280 mK.

References

[1] Edwards et al. Appl. Phys. Lett. **63**, p1815 (1993)

[2] Edwards et al. Phys. Rev. B, **52**, p5714 (1995)

[3] Giazotto et al. Rev. Mod. Phys. **78**, p217 (2006)

[4] Prance et al. Phys. Rev. Lett. (accepted Feb. 2009)

Time-resolved charge detection with cross-correlation techniques

B. Küng*, O. Pfäffli*, S. Gustavsson*, T. Ihn*, M. Reinwald**, W. Wegscheider*, and K. Ensslin*
* *Solid State Physics Laboratory, ETH Zurich, Zurich, Switzerland*
** *Institut für Experimentelle und Angewandte Physik, Universität Regensburg, Regensburg, Germany*

Keywords: electric sensing devices; quantum point contacts; semiconductor quantum dots; time resolved spectra;

The method of charge sensing by quantum point contacts (QPCs) is at present one of the most widely employed tools in the investigation of semiconductor quantum dot circuits and has most recently been used to read out a spin qubit in a single shot [1]. The correlated measurement with two such sensors in a double quantum dot (DQD) is discussed as an approach for the realization of a continuous quantum measurement in nanoelectronics [2]. We present an experimental realization of the classical version of this setup [3]. We show how the cross-correlation can be used to measure tunneling rates in a manner suppressing uncorrelated noise and thus removing the main limitation to the bandwidth and the invasiveness of charge detection with a single sensor.

The measurements presented here were done at a temperature of $80\,\mathrm{mK}$ on a GaAs/AlGaAs based sample consisting of two quantum dots, tunnel-coupled in series and to source and drain contacts, and two proximal QPCs. The currents $I_1(t)$ and $I_2(t)$ flowing through the voltage-biased QPCs have the form of random telegraph signals (RTS) exhibiting steps when tunneling events in the dot take place. A measurement of the frequency of these steps as shown in Fig. 1(a) yields the strength of all three tunnel-couplings defining the DQD.

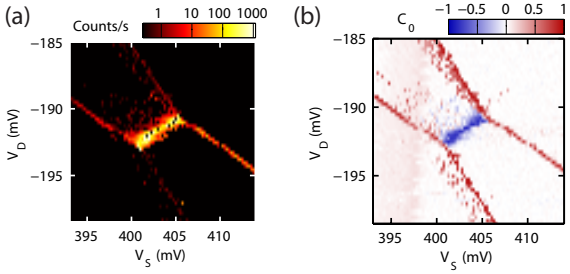

Figure 1: (a) Count rate measured as a function of DQD gate voltages V_S and V_D representing the DQD stability diagram. (b) Correlator C_0 (see text) extracted from the same raw data as used in (a). The sign C_0 is the sign of the correlation between I_1 and I_2.

Due to the asymmetric capacitive coupling between dots and QPCs, the switching directions of I_1 and I_2 for a given event are not necessarily the same. In particular, the normalized correlator $C_0 = (\langle I_1 I_2\rangle - \langle I_1\rangle\langle I_2\rangle)(\langle I_1^2\rangle - \langle I_1\rangle^2)^{-1/2}(\langle I_2^2\rangle - \langle I_2\rangle^2)^{-1/2}$ (angle brackets denote time averaging of the recorded QPC current time traces), reveals positive correlation ($C_0 \approx 1$) for dot-lead tunneling events and negative correlation ($C_0 \approx -1$) for inter-dot events, cf. Fig. 1(b).

The measurement of the tunneling rates with cross-correlation is carried out as follows: calculating the cross-correlation function of I_1 and I_2 filters out uncorrelated noise in the channels and allows to extract a characteristic time scale τ_0 of the RTS transitions. On the other hand, a suitable normalized and noise-insensitive third-order correlator γ obtained from I_1 and I_2 encodes the information on the RTS asymmetry, i.e., the occupation probability of the high- and low-current states of the signal. The two parameters τ_0 and γ are then translated into the transition rates of the RTS. We tested the advantage over the single channel case by reducing the bias voltage across the QPCs and thus the SNR, finding that in the given setup the voltage could be reduced by roughly one order of magnitude. A combination of this method with existing rf impedance-matching technology may allow to increase the (shot-noise limited [4]) bandwidth towards the interesting regime of charge qubit coherence times.

References

[1] C. Barthel *et al.*, arXiv:0902.0227 (2009).

[2] A.N. Jordan and M. Büttiker, Phys. Rev. Lett. **95**, 220401 (2005).

[3] B. Küng *et al.*, Phys. Rev. B **79**, 035314 (2009).

[4] M.C. Cassidy *et al.*, Appl. Phys. Lett. **91**, 222104 (2007).

Enhanced efficiency in natural dye-sensitized solar cells with surface plasmon resonance by incorporating Au nanoparticles

Yi-Feng Lai[1], Yen-Hsun Su[1], Chuan-Pu Liu[1], Yaw-Wen Yang[2] and Liang-Jen Fan[2]

[1] *Department of Materials Science and Engineering and Center for Micro/nano Science and Technology, National Cheng Kung University, Tainan, Taiwan 701*

[2] *National Synchrotron Radiation Research Center, 101 Hsin-Ann Road, Hsinchu, Taiwan 30077*

Keywords: surface plasmon, dye-sensitized, solar cell, Au

Recently, dye-sensitized nanocrystalline TiO_2 solar cells (DSSC) have attracted much attention because of their high conversion efficiency and low cost [1]. Among all dyes used in DSSC, natural dye is a good candidate for use in nontoxic and biologically friendly solar energy devices. But it is still not used widely because of very low conversion efficiency (<1%). A variety of approaches for increasing optical absorption in semiconductor materials based on excitation of surface plasmon polariton resonances in proximate metallic nanoparticles (NPs) have been explored, frequently in the context of photovoltaic applications [2-3].

In this work, an anodic photoelectrode of DSSC loaded with a layer of Au NPs was immersed in a natural dye (Chlorophyll) sensitizer alcohol solution for 2 days. The electrolyte is the water-based solution (35% ethanol and 65% water). The basic device structure employed in these studies is shown in **Fig. 1**

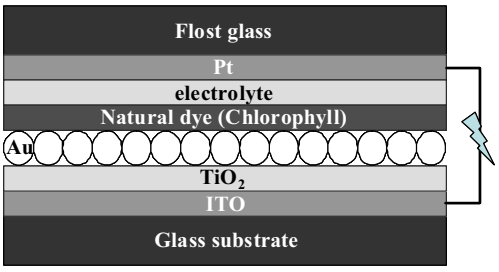

Fig.1 Schematic diagram of the structure of the natural dye-sensitized solar cells.

Fig.2 shows the photocurrent density-voltage characteristics measured with a Keithley 237 source measurement unit under 10 mW/cm2 illumination from an Oriel solar simulator with an AM 1.5 G filter.

Compared to the device without Au NPs, the Au incorporated device shows higher efficiency of 0.705%. We observed that the efficiency is increased more than three times compared to the cell without Au NPs (μ=0.205%). And it is noteworthy that increasing short-circuit current density (J_{sc}) is resulted from an enhanced absorption of the active layer via stronger enhanced local electromagnetic fields from Au NPs, leading to an increase in excition generation.

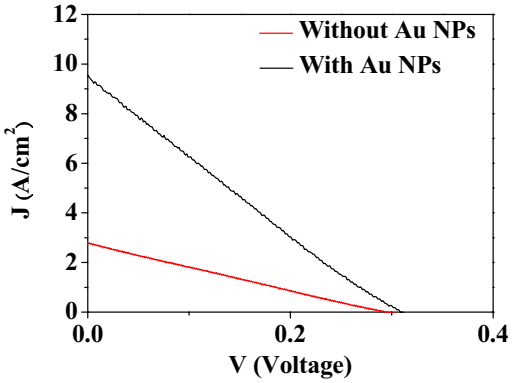

Fig.2 I-V characteristics obtained from natural dye-sensitized solar cell with and without Au nanoparticles.

References

1. B. O'regan, M. Grätzel, Nature 353, 737 (1991).
2. O. Stenzel, S. Wilbrandt, A. Stendal, U. Beckers, K. Voigtsberger, and C.von Borczyskowski, J. Phys. D 28, 2154 (1995).
3. O. Stenzel, A. Stendal, K. Voigtsberger, and C. von Borczyskowski, Sol.Energy Mater. Sol. Cells 37, 337 (1995).

Acknowledgement

The work was supported by Research Grant No. NSC 95-2221-E-006-080-MY3, National Science Council of Taiwan.

Competitive growth mechanisms of the InAs quantum dots on the $In_xGa_{1-x}As$ layer during the post growth interruption

Changjae Yang, Jungsub Kim, Uk Sim, Jaeyel Lee and Euijoon Yoon*

Department of Materials Science and Engineering, Seoul National University, Seoul 151-744, Korea

Keywords: MOCVD, InAs QD, Strained Buffer Layer, Growth interruption

Self-assembled quantum dots (QDs) have been intensively investigated due to their fundamental physics and various potential applications [1]. One of the applications is laser diodes which have the emission wavelength of QDs to 1.3 or 1.55 μm for the optical fiber communication system. In order to tune the emission wavelength and improve the optical efficiency, a Strained Buffer Layer (SBL) which is located below the InAs QD layer and post growth interruption (post GI) are introduced on the growth of QDs [2,3]. However, relatively little attention has been paid to the properties of QDs when SBL and post GI employed simultaneously on the growth of the QDs. The purpose of this paper, therefore, is to investigate the effects of the In contents in InGaAs SBL during the post GI time.

In present work, we grew InAs QDs on InGaAs SBLs by using MOCVD with increasing indium content in SBLs from 5 to 20 %. After the QD growth, one group of samples had post GI steps of 15 seconds and then was cooled down with AsH_3 supply.

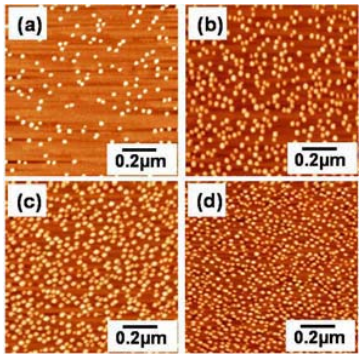

Fig 1. 1.0x 1.0 μ m^2 AFM images of InAs QDs after the post GI on the (a) 5%, (b) 10%, (c) 15% and (d) 20% In contents in SBL

The other, however, was directly cooled down under the AsH_3 ambient. The changes of surface morphologies were observed by atomic force microscopy (AFM). The optical properties were observed by photoluminescence (PL) at 14K without capping layer in order to exclude effects of the capping condition.

Based on the total QD volume which is estimated from the AFM and their optical properties, the volume of QDs is increased with decreasing QD density during the post GI on the 5 and 10% In contents SBL. The ground state emission peak had a red-shift about 50meV as a result of the post GI. As a consequence, an increase of the individual QD volume is occurred by the redistribution of In atoms which are originated from the dissolved QDs and led to the red-shift of the PL emission energy because of increasing QD size with little Ga incorporation. On the other hand, QDs on the 15 and 20% In contents SBL increase their volume during post GI with maintaining high QD density. The total QD volume increases beyond that of QDs which are grown without post GI. Therefore we suggest that the Ga incorporation from the underlying layer plays a key role in the volume increase of the QDs in these cases. The blue-shift of the PL emission energy after the post GI, in spite of increasing each QD volume, can support the QD volume increase by Ga incorporation.

References

1. Y. Arakawa, et al., Appl. Phys. Lett. **40**, 939 (1982)
2. H. Y. Liu, *et al*., J. Appl. Phys. **93**, 2931 (2003)
3. K. Potschke, *et al*, Physica E **21**, 606 (2004)

The influences of the thickness of low temperature Ge layers on a two-step Ge growth on a Si(100) using UHV-CVD

Keun Wook Shin, Hyun-Woo Kim and Euijoon Yoon

Department of Materials Science and Engineering, Seoul National University, 151-744, Republic of Korea

Keywords: Ge, UHV-CVD, two-step growth

The two-step Ge growth is one of the promising techniques to grow a Ge epitaxial layer on a Si substrate for the NIR photodetector applications [1]. This method uses a thin Ge layer grown at low temperature (LT) as a buffer layer. By using a two-step growth, a flat Ge layer with the lower threading dislocation density (TDD) (~10^8 cm^{-2}) is obtained, and the TDD can be reduced to ~10^7 cm^{-2} by combining chemical-mechanical polishing [2]. However, TDD about 10^7 cm^{-2} is still high to manufacture in devices and the optimized growth condition for the higher quality Ge growth is not clear yet. In this study, fully relaxed Ge layers were grown on a Si(100) substrate and we optimized the growth condition of a two-step Ge growth by varying the thickness of LT Ge layers.

The Ge layers were grown on Si(100) substrates by two-step growth in ultrahigh vacuum chemical deposition (UHV-CVD) using GeH_4 gas at the temperature of 320 and 500 ^oC for the two-step Ge growth, respectively. The thickness of LT Ge layer was varied from 20 to 120 nm and that of high temperature (HT) Ge layer was fixed to 900 nm. Although LT Ge layers were used as a buffer layer, the two-step Ge layers were roughened with the high RMS roughness by using the 20 and 40 nm-thick LT Ge layers. However, the LT Ge layers thicker than 50 nm resulted in the flat surfaces of the two-step grown Ge layers with low RMS roughness of about 1 nm due to growth of HT Ge layers on strain-reduced surfaces. In addition, from the HR-XRD results of all samples, the lower FWHM and the higher Ge peak intensity are observed by using 80 nm-thick LT Ge layer. The TDD of two-step grown Ge layers decreased to the minimum value of 1.2 x 10^6 cm^{-2} with increasing the thickness of LT Ge layers up to 80 nm. We speculate that the thicker LT Ge layer has the more point defects which lower the nucleation energy for misfit dislocation and inhibit the propagation of threading dislocations, resulting in the decrease of TDD. However, TDD increases for the two-step Ge layers using LT Ge layers thicker than 80 nm. Therefore, it might be possible to optimize the growth condition of a two-step grown Ge layer by changing the thickness of LT Ge layer.

References

1. J. M. Hartmann, A. Abbadie, A. M. Papon, P. Holliger, G. Rolland, T. Billon, J. M. Fedeli, M. Rouviere, L. Vivien and S. Laval, J. Appl. Phys. **95**, 5905 (2004).

2. Hsin-Chiao Luan, Desmond R. Lim, Kevin K. Lee, Kevin M. Chen, Jessica G. Sandland, Kazumi Wada and Lionel C. Kimerling, Appl. Phys. Lett. **75**, 2909 (1999).

Ring-size dependence of Kondo effect in quantum dot embedded in Aharonov-Bohm ring

R. Yoshii and M. Eto
Faculty of Science and Technology, Keio University, Yokohama, Japan

Keywords: quantum dot, Kondo effect, Aharonov-Bohm ring, scaling method

In a quantum dot embedded in an Aharonov-Bohm (AB) ring, the Fano-Kondo effect is observed which stems from an interplay between the many-body Kondo effect and one-body interference effect [1]. When the AB ring is smaller than the size of the Kondo cloud, the Kondo effect by itself should be influenced by the AB interference effect. In this work, we examine the ring-size dependence of the Kondo effect using the two-stage scaling method.

Our model is shown in the figure. A quantum dot with a single energy level (ϵ_0) is connected to two external leads by tunnel couplings V_L or V_R. Another arm of the AB ring (reference arm) and external leads are represented by a one-dimensional tight-binding model with transfer integral $-t$ and lattice constant a. The reference arm includes a tunnel barrier with transmission probability of $T_{\rm b} = 4x/(1+x)^2$ with $x = (W/t)^2$. ϕ is the AB phase of magnetic flux penetrating the ring. We focus on the Coulomb blockade regime with one electron in the dot: $-\epsilon_0$, $\epsilon_0 + U \gg \Gamma$, where U is the Coulomb interaction in the dot ($U \to \infty$). $\Gamma = \Gamma_L + \Gamma_R$ is the level broadening, where $\Gamma_\alpha = \pi\nu V_\alpha^2$ with $\nu = 1/(\pi t)$ being the local density of states at the end of the leads.

In the small limit of the AB ring ($l = 0$), we have performed the scaling analysis [2]. We begin with the unitary transformation for conduction modes in the outer region of the quantum dot (two leads + reference arm) and obtain a mode which is coupled to the dot by $V = \sqrt{V_L^2 + V_R^2}$. The other mode is completely decoupled from the dot and hence can be neglected. As a result, we obtain an equivalent model in which a quantum dot is coupled to a single lead with flux-dependent density of states

$$\nu(\epsilon) = \bar{\nu}\left[1 + P(\phi)\frac{\epsilon}{D_0}\right],\ P(\phi) = \sqrt{\alpha T_{\rm b}}\cos\phi,$$

where $\bar{\nu} = \nu/(1+x)$, D_0 is half of the bandwidth and $\alpha = 4\Gamma_L\Gamma_R/(\Gamma_L+\Gamma_R)^2$. The Kondo scaling is applied to the reduced model. On the first stage of scaling, we renormalize the energy level ϵ_0 to $\tilde{\epsilon}_0$, taking account of the charge fluctuation in the energy scale D of $|\tilde{\epsilon}_0| \ll D \ll D_0$. We obtain $\tilde{\epsilon}_0(\phi) = \tilde{\epsilon}_0(\pi/2) - 3\bar{\nu}V^2P(\phi)$. On the second stage, we evaluate $T_{\rm K}$ by considering spin fluctuation at $D \ll |\tilde{\epsilon}_0|$:

$$T_{\rm K}(\phi) = T_{\rm K}\,(\pi/2)\exp\left[-3P(\phi)/2\right].$$

Both the renormalized level and $T_{\rm K}$ largely depend on the magnetic flux ϕ [2].

We extend our scaling calculations to the case with finite length of the ring, $L_{\rm r} = (2l+1)a$. By the first stage of scaling, we find that the renormalized level $\tilde{\epsilon}_0$ depends on ϕ when $L_{\rm r} \ll v_{\rm F}\hbar/|\tilde{\epsilon}_0| \equiv L_{\rm c}$. Here, $v_{\rm F}$ is the Fermi velocity. The renormalized level $\tilde{\epsilon}_0$ is almost independent of ϕ when $L_{\rm r} \gg L_{\rm c}$. On the second stage, we evaluate the Kondo temperature. In this case the relevant length scale is the size of the Kondo cloud, $L_{\rm K} = v_{\rm F}\hbar/T_{\rm K}$. $T_{\rm K}$ depends on the flux ϕ significantly when $L_{\rm r} \ll L_{\rm K}$ and hardly when $L_{\rm r} \gg L_{\rm K}$, in accordance with calculated results by the slave-boson mean-field theory [3].

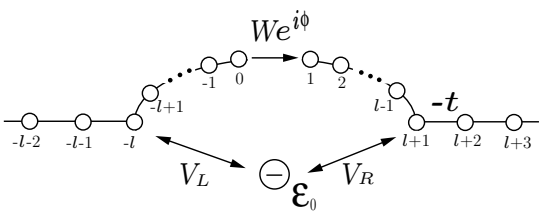

References

[1] W. Hofstetter, J. König and H. Schoeller, Phys. Rev. Lett. **87**, 156803 (2001).

[2] R. Yoshii and M. Eto, J. Phys. Soc. Jpn. **77**, 123714 (2008).

[3] P. Simon, O. Entin-Wohlman and A. Aharony, Phys. Rev. B **72**, 245313 (2005).

Time-dependent DMRG study on nonlinear transport through quantum dot

S. Kirino, T. Fujii and K. Ueda
Institute for Solid State Physics, University of Tokyo, Chiba, Japan

Keywords: quantum dot, Kondo effect, nonequilibrium, time-dependent DMRG

Recently it has been established that the Kondo effect plays an essential role in transport properties of quantum dot systems at low temperatures. An interesting feature of the Kondo effect in quantum dot systems which is not present in the traditional magnetic impurity problems is that nonequilibrium steady states are realized under finite bias voltages.

In order to study the properties of the steady states theoretically, analytical methods based on Keldysh formalism has been employed extensively. On the other hand it seems that only few numerical studies on quantum dot under a finite bias voltage have been done thus far. This is largely due to a lack of reliable numerical techniques for the nonequilibrium problems of the mesoscopic systems. One possible numerical approach to the quantum dot out of equilibrium is the adaptive time-dependent density matrix renormalization group (TdDMRG) method [1], an extension of the DMRG method to time-dependent problems. The TdDMRG allows us to calculate time evolution of a wave function of a one dimensional system accurately.

We investigate the zero temperature transport properties of a quantum dot in a wide range of bias votages by the TdDMRG method. Quantum dot system is modeled by the Anderson Hamiltonian with two 1-D nearest-neighbor tight-binding leads. Initially the ground state wave function is calculated with the usual DMRG algorithm. Then the time evolution of the wave function due to the slowly changing bias voltage between the two leads is calculated by using the TdDMRG technique. Even though the system size is finite, the expectation values of current operator show steady-like behavior for a finite time interval, in which the system is expected to resemble the real nonequilibrium steady state of the infinitely long system.

In our previous study [2] we showed that from the steady-like intervals we can obtain accurate information of the steady state for $1 \leq R_W$(Wilson ratio)≤ 1.71. The limitation of the correlation strength comes from the error-accumulation of the TdDMRG algorithm and the fact that the time scale $1/T_K$ (T_K is the Kondo temperature) to reach the steady state becomes longer as Coulomb interaction increases.

In the presentation we will report rescent progress in our calculation. To improve efficiency and accuracy of the calculation it turns out advantageous to employ the 4th order Suzuki-Trotter decomposition and relatively long time slices rather than the usual 2nd order one. Taking sufficiently long system size, we become capable of treating strongly correlated region up to $R_W \leq 1.97$, close to the strong coupling limit.

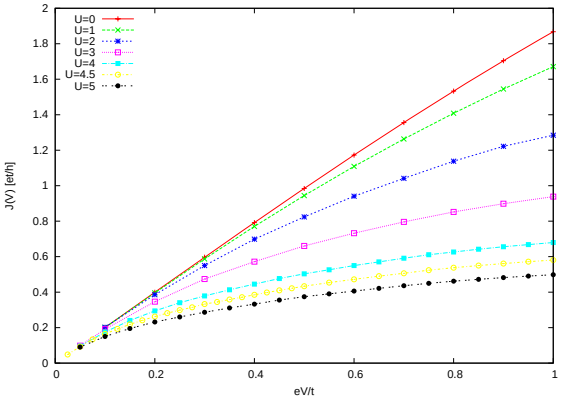

Figure 1: Current through a quantum dot with particle-hole symmetry versus bias voltage eV (divided by the hopping amplitude t in the leads). The linear conductance $\frac{\partial J}{\partial V}|_{V=0}$ shows the unitarity limit value $\frac{2e^2}{h}$ independent of U, as predicted by the Fermi liquid theory.

References

[1] A. J. Daley, C. Kollath, U. Schollwöck and G. Vidal, J. Stat. Mech.: Theor. Exp. (2004) P04005, S. R. White and A. Feiguin, Phys. Rev. Lett. **93** (2004) 076401.

[2] S. Kirino, T. Fujii, J. Zhao and K. Ueda, J. Phys. Soc. Jpn. **77**, 084704 (2008).

Enhanced thermoelectric power of single quantum dot systems at low temperatures: Exact solution analysis

R. Sakano[1], S. Tarucha[1,2] and N. Kawakami[3]
[1] *Department of Applied Physics, University of Tokyo, Tokyo, Japan*
[2] *ICORP JST, Kanagawa, Japan.*
[3] *Department of Physics, Kyoto University, Kyoto, Japan*

Keywords: quantum dot, thermoelectric power, Kondo effect

Recently, thermoelectric properties of various systems have been intensively investigated to explore for new materials with high thermoelectrical effeciency [1, 2]. We especially focus on these in mesoscopic systems and study thermoelectric power (TEP) and some related transport quantities in embedded and T-shaped quantum dot (QD) systems (shown in figure 1 (a), (b)). Making use of the Bethe ansatz exact solution for the impurity Anderson model, the nonequilibrium Green function technique and the Fermi liquid theory, we analyze the TEP of these systems at low temperatures. This enables us to elucidate how electron correlations and interference effects enhance the TEP. We show that QD systems can give high thermoelectrical efficiency and be good candidates of thermoelectric devices.

Computed result of TEP as a function of QD level ε_d is shown in figure 1 (c). Note that the sign of TEP for T-shaped QD is changed to compare the magnitude of the both systems.

For large Coulomb repulsion $U/\Delta = 8$, the shape Kondo tunneling peak emerges around Fermi level, which induces larger TEP around the symmetric point $\varepsilon_d = -U/2$ than noninteracting case $U/\Delta = 0$. Magnetic-fields dependence of TEP is also investigated to make how the Kondo physics works on TEP in the QD systems clear.

In T-shaped quantum dot systems, huge enhancement of TEP is observed (in figure 1 (c)). The conductance suppression due to the Fano interference strongly enhances the TEP due to tunneling resonance asymmetry around the symmetric point $\varepsilon_d = -U/2$ [4].

In addition, to investigate thermoelectrical efficiency of these systems, we discuss the figure of merit for these QD devices.

References

[1] R. Scheubner, H. Buhmann, D. Reuter, M. N. Kiselev, and L. W. Molenkamp, Phys. Rev. Lett. **95**, 176602 (2005).

[2] R. Sakano, T. Kita, and N. Kawakami, J. Phys. Soc. Jpn **76**, 074709 (2007).

[3] T. Usuki, N. Kawakami, and A. Okiji, J. Phys. Soc. Jpn **59**, 1357 (1990).

[4] K. Kang, S. Y. Cho, J.-J. Kim, and S.-C. Shin, Phys. Rev. B **63**, 113304 (2001).

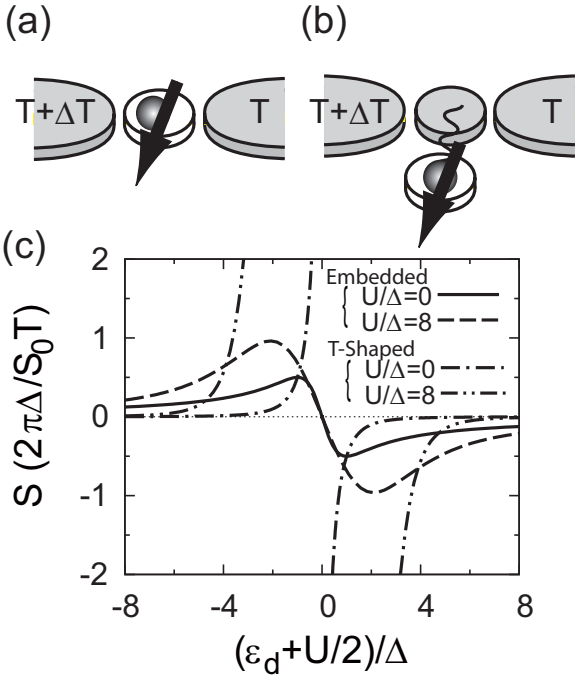

Figure 1: Schematic diagram of (a) embedded QD system and (b) T-shaped QD system. (c)TEP of these QD systems with Coulomb repulsion $U = 0, 8\Delta$ as a function of QD level ε_d. Note that, for comparison, the sign of TEP for T-shaped QD is changed.

Monte Carlo study of resonant tunneling in a Tomonaga-Luttinger liquid

Yuji Hamamoto and Takeo Kato
Institute for Solid State Physics, University of Tokyo, Kashiwa, Japan

Keywords: Tomonaga-Luttinger liquid, quantum dot, quantum phase transition

Quantum transport property of quasi-one-dimensional systems has been studied experimentally in mesoscopic systems such as quantum wires and metallic carbon nanotubes. In these systems, low energy excitations are described by a Tomonaga-Luttinger (TL) liquid, and may affect their transport property. For example, conductance of a quantum dot embedded in a TL liquid shows a peculiar temperature dependence; the width of the conductance peaks shows a power-law behavior as a function of the temperature [1]. Perturbative renormalization group (RG) analysis indicates even a quantum phase transition in this system [2]. When a gate voltage is tuned at the resonant condition, the peak conductance goes to Ke^2/h (zero) for $K < K_c$ ($K > K_c$) with decreasing temperature, where K and K_c are a Luttinger parameter and its critical value, respectively. In general, K_c depends on the barrier height V of the one-body potential forming the quantum dot. The RG analysis predicts that a second-order transition occurs at $K_c = 1/4$ in the small barrier limit ($V \to 0$) while the Kosterlitz-Thouless transition at $K_c = 1/2$ in the large barrier limit ($V \to \infty$). However, since the applicability of the RG analysis is restricted to the small and large barrier limits, it remains an unsolved problem to obtain the whole phase diagram on a K-V plane including a cross of the above two different types of phase transition.

In this talk, we study the quantum phase transition for an intermediate barrier height in the one-dimensional quantum dot system by resorting to the path-integral Monte Carlo (PIMC) method, which is a nonperturbative approach accessible to the region of interest. Hügle and Egger have applied the real-time PIMC simulation to the present system and analyzed the scaling of the resonant peak [3]. However, the real-time formalism is not realistic to investigate the critical region because of the inevitable negative sign problem. The PIMC method we employ is based on the imaginary-time formalism, which is free of the negative sign. To access the critical region at low temperatures, we also adopt an efficient sampling using the cluster algorithm [4]. We demonstrate our PIMC simulation to observe the phase transition by measuring the temperature dependence of the resonant peak (we show an example of our numerical results in Figure 1). Moreover, in the large barrier regime, we see the capacitance of the dot display a non-universal jump at the critical point K_c as a consequence of the Kosterlitz-Thouless transition.

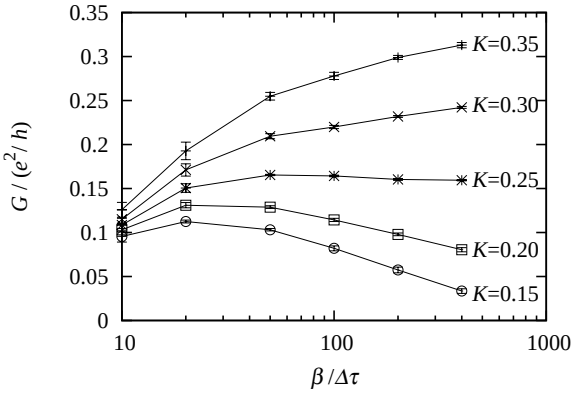

Figure 1: Temperature dependence of the peak conductance through the quantum dot. A quantum phase transition occurs at the critical point $K_c \simeq 0.25$.

References

[1] O. M. Auslaender et al., Phys. Rev. Lett. **84**, 1764 (2000); H. W. Ch. Postma et al., Science 293, **76** (2001).

[2] C. L. Kane and M. P. A. Fisher, Phys. Rev. B **46**, 7268 (1992); C. L. Kane and M. P. A. Fisher, Phys. Rev. B **46**, 15233 (1992); A. Furusaki and N. Nagaosa, Phys Rev. B **47**, 3827 (1993).

[3] S. Hügle and R. Egger, Europhys. Lett. **66**, 565 (2004).

[4] P. Werner and M. Troyer, Phys. Rev. Lett. **95**, 060201 (2005).

Diamagnetic shift of exciton complexes in InAs quantum dots

Y. J. Fu[1], S. D. Lin[1], M. F. Tsai,[1] H. Lin[2], C. H. Lin,[2], S. Y. Wang[2], S. J. Cheng[2], and W. H. Chang[2]
[1]*Department of Electronics Engineering, National Chiao Tung University, Hsinchu 300, Taiwan*
[2]*Department of Electrophysics, National Chiao Tung University, Hsinchu 300, Taiwan*

The measurement and calculation of diamagnetic shift of exciton complexes in single InAs/GaAs quantum dots (QDs) is presented. A clear difference in diamagnetic coefficients of various exciton complexes was observed. The experimental result can be explained with a self-consistent model considering the quantum confinement and Coulomb interaction. Our analysis shows that the strong Coulomb interaction in the small QDs play an important role in their magnetic response.

The μ-PL measurements of several QDs grown by molecular beam epitaxy were performed at 8 K with the magnetic field up to 6 T along the growth direction [1]. Fig. 1 shows the measured PL-spectra from one of the QDs (QD1). The indicated emission peaks of various exciton complexes split into two peaks as the magnetic field due to Zeeman effect. The diamagnetic coefficients (β_{x-}, β_x, β_{xx}, and β_{x+},) of two typical QDs shown in Fig. 2 are obtained accordingly. A clear trend of $\beta_x > \beta_{xx} \cong \beta_{x+} \geq \beta_{x-}$ can be seen.

To simulate the magnetic response, we consider the many-body Schrodinger's equation with Coulomb effect and implement the Hartree-Fock approximation. At first, the ground state wave functions of single electron and hole are solved. The Hartree potential due to Coulomb interaction are evaluated with the solved wave functions. With a self-consistent iteration, the final wave functions of electron and hole are obtained. As we can see in Fig. 2, the calculated diamagnetic coefficients in typical QDs are well consistent with the experimental results. To understand its physical reason, we calculated the relation between the QD's sizes and diamagnetic shift. The size-dependent diamagnetic coefficient of four exciton complexes is shown in Fig. 3a. It is clear that, for large-sized QDs (D>16nm), the diamagnetic coefficients of four exciton complexes are nearly equal and they increase with the QD's sizes, as expected. However, as the size of QD decreases, the difference of diamagnetic shift between β_{x-} and β_x increases while that between β_{xx} and β_{x+} keeps equal. An institute view on this can be learned from the calculated average diameters of X^- and X^+ shown in Fig. 3b. When the sizes of QDs lower, the diameter of electron wave function in its final state raises rapidly and then exceeds the QD's size eventually because of its lighter effective mass, comparing with hole's case.

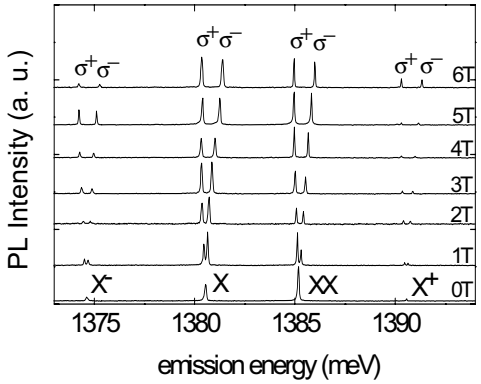

Fig 1: The PL-spectra for QD1 under magnetic field.

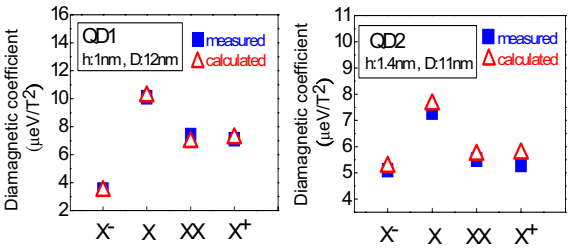

Fig 2: The diamagnetic coefficient of the exciton complexes for the two typical QDs (QD1 and QD2).

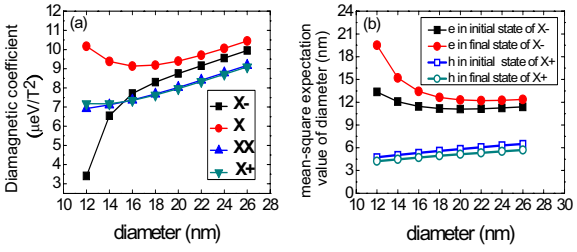

Fig. 3: The simulation for QDs with various diameters.

References

[1] M. F. Tsai, Phys. Rev. Lett. 101, 267402 (2008).
[2] C. E. Pryor, Phys. Review B. 72, 205311 (2005).

Numerical study of quantum Hall effects in two-dimensional multi-band system: single- and multi-layer graphene

Masao Arai* and Yasuhiro Hatsugai**
*Computational Materials Science Center, National Institute for Materials Science, Tsukuba, Japan
** Institute of Physics, University of Tsukuba, Tsukuba, Japan

Keywords: graphene, quantum Hall effects, semi-classical theory

One of the most exciting phenomena in two-dimensional electron system is quantization of Hall conductance, known as integer quantum Hall effects (QHE). The Hall conductance σ_{xy} typically shows plateaux with $\sigma_{xy} = ne^2/h$ where the integer n is theoretically given by a topological number as the Chern number. Recently, graphene, which is a realization of hexagonal lattice system, shed a new light to QHE as anomalous quantization rule of $\sigma_{xy} = (2m+1)e^2/h$, $(m = \ldots, -2, -1, 0, 1, 2, \ldots)$ per spin is observed in this system. The origin of this anomalous quantization is attributed to band dispersions which resemble massless Dirac particles.

The QHE on a graphene sheet has been studied by calculating the Chern numbers of the Berry connection in the magnetic Brillouin zone for single-orbital tight-binding models. From these calculations, it has been predicted that anomalous QHE persists up to van-Hove singularities and conventional QHE will recover near band-edge regions. Thus, peculiar transition in σ_{xy} may be observable if chemical potential can be varied significantly.

To achieve further connections with experiments, it would be necessary to calculate σ_{xy} for realistic band-structure. However, most of theoretical studies about QHE have been limited to simplified tight-binding models. Recently, we demonstrated that σ_{xy} for realistic multi-band models can be calculated numerically if robust formulation of Chern numbers is employed. The magnetic translational symmetry can be also fully utilized to achieve numerical efficiency.

We evaluated the Chern numbers for multi-orbital tight-binding models which describe electrons on graphene [1]. The calculated σ_{xy} shows quantized Hall plateaux in entire energy range. As presented in Fig. 1, several discontinuous jumps appear at van-Hove singularities of energy bands without magnetic fields. We found that the envelope of σ_{xy} coincides with a semi-classical result when magnetic field is sufficiently small. The plateaux of σ_{xy} are explained from semi-classical quantization.

In this paper, we further study multi-layer graphene systems, which have different quantization plateaux with single-layer system. Validity of the semi-classical interpretation is discussed for them.

References

[1] M. Arai and Y. Hatsugai, Phys. Rev. B **79**, 075429 (2009).

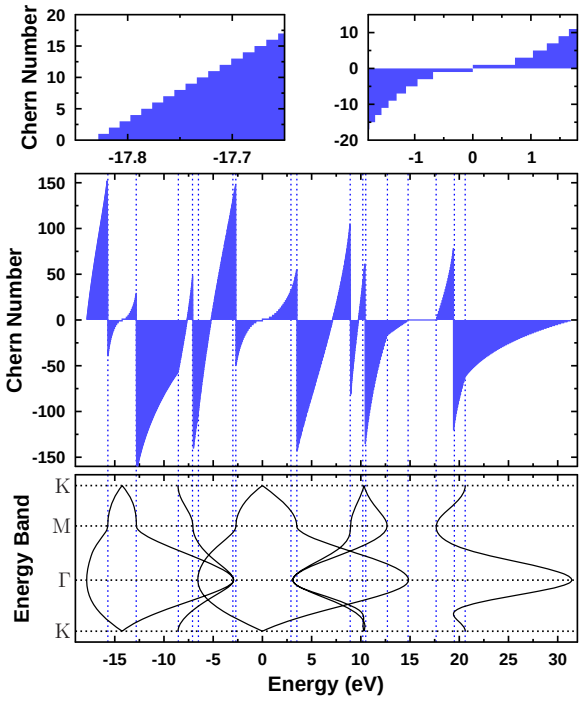

Figure 1: Lower panel shows energy bands of graphene from a multi-band tight-binding model. The calculated Chern number for magnetic flux $\phi = 1/200$ are plotted in middle panel. The dashed lines indicate positions of van-Hove singularities. The upper panels show enlarged figures of Chern numbers near bottom of energy bands (left part) and around massless Dirac region (right part).

Fractional quantum Hall states in single-layer and bilayer graphene

N. Shibata and K. Nomura
Department of Physics, Tohoku University, Sendai, Japan

Keywords: graphene, fractional quantum Hall, valley skyrmion, bilayer

Taking into account the valley degrees of freedom K and K', we study the ground state and low-energy excited states of single-layer graphene (SLG) and bilayer graphene (BLG). The Coulomb interaction between the electrons is projected onto a certain Landau level (LL) and it is exactly diagonalized by the density matrix renormalization group (DMRG) method.

The DMRG method is a real space renormalization group method combined with the exact diagonalization method, which provides the low-energy eigenvalues and corresponding eigenvectors of the Hamiltonian within a restricted number of basis states. The accuracy of the results is systematically controlled by the truncation error, which is smaller than 10^{-4} in the present calculation. We investigate systems of various sizes with up to 40 electrons in the unit cell keeping 1400 basis in each block.[1]

To study the role of valley degrees of freedom in graphene, we calculate the ground state valley polarization at effective filling factors $\nu_n = 1$, 1/3, 2/3 and 2/5 in the $n = 0$ and 1 LLs of SLG and those fillings in the second lowest LL of BLG assuming that the spin degrees of freedom is frozen by the Zeeman splitting. The obtained results show that the ground states at $\nu_n = 1$ and 1/3 in the $n = 0$ LL and at $\nu_n = 1$, 1/3, 2/3, and 2/5 in the $n = 1$ LL of SLG and at those fillings in the second lowest LL of BLG are shown to be valley polarized while the ground states at $\nu_n = 2/3$ and 2/5 in the $n = 0$ LL of SLG are valley unpolarized.

The elementally charge excitations from the above ground states are also studied by the DMRG method and it is shown that at $\nu_n = 1$ and 1/3 in the $n = 0$ and 1 LLs of SLG, the lowest charge excitation is a skyrmion excitation of valley degrees of freedom.[2] This valley-skyrmion excitation has a finite gap Δ_s even in the thermodynamic limit as shown in Fig. 1, which also shows that it is smaller than the valley polarized charge excitation gap Δ_c for the $n = 0$ and 1 LLs of SLG. In the second lowest LL of BLG, however, Δ_s is larger than Δ_c and Δ_s is not presented in the figure.

These results show that for $n = 0$ and 1 LLs of SLG, the valley-skyrmion excitations dominate over the valley polarized excitations at low temperatures. Since Δ_s is larger than Δ_c in the second lowest LL of BLG and Δ_c of BLG is larger then Δ_s of SLG, the most stable fractional quantum Hall state is realized in the second lowest LL of BLG, which is then a good candidate for experimental observations.

References

[1] N. Shibata and D. Yoshioka, Phys. Rev. Lett. **86**, 5755 (2001); N. Shibata, J. Phys. A **36** R381 (2003). ; N. Shibata and D. Yoshioka, J. Phys. Soc. Jpn. **75**, 043712 (2006); N. Shibata and K. Nomura, J. Phys. Soc. Jpn. **76**, 103711 (2007) .

[2] N. Shibata and K. Nomura, Phys. Rev. B **77**, 235426 (2008).

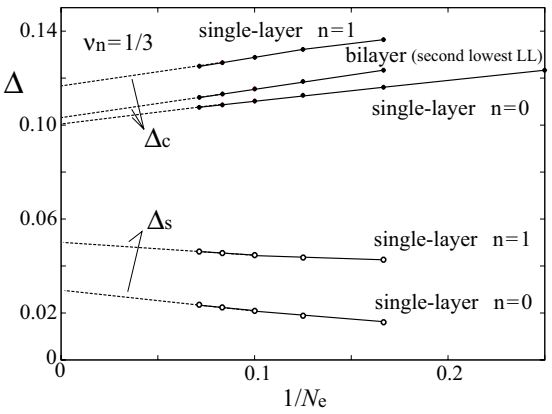

Figure 1: The valley polarized charge excitation gap Δ_c and the valley-skyrmion excitation gap Δ_s at $\nu_n = 1/3$ in the $n = 0$ and 1 LLs of single-layer graphene and in the second lowest LL of bilayer graphene. N_e is the total number of electrons on the sphere geometry. The units of energy gap Δ is $e^2/(\epsilon \ell_B)$.

Cyclotron Resonance in Graphene

E. A. Henriksen*, P. Cadden-Zimansky**†, Z. Jiang‡, L. C. Tung**, M. E. Schwartz†, Y.-J. Wang**, P. Kim†, and H. L. Stormer†§

*California Institute of Technology, Pasadena, California, U.S.A

**National High Magnetic Field Laboratory, Tallahassee, Florida, U.S.A.

†Columbia University, New York, New York, U.S.A.

‡Georgia Institute of Technology, Atlanta, Georgia, U.S.A.

§Bell Labs, Murray Hill, New Jersey, U.S.A.

Keywords: Graphene Quantum Hall Effect

One of the most prominent manifestations of the unusual electronic properties of graphene is the unique Landau Level spectrum that arises in a magnetic field. While first experimentally observed via transport measurements, more recent investigations [1, 2] have directly probed the energy transitions between Landau levels by using infrared spectroscopy to detect cyclotron resonance absorption of graphene in high fields.

By tuning the occupation of the Landau levels via the potential of the graphene substrate, one can observe the resonance transitions at different filling factors, ν, and corroborate the predicted uneven spacing of the Levels (Fig. 1). For high mobility samples the absorption spectrum can also reveal the physics occurring within a four-fold degenerate level. Of particular interest is the unusual $n = 0$ Landau level that forms around graphene's charge-neutral Dirac point, where the carriers switch from holes to electrons. Our recent measurements of cyclotron resonance transitions into and out of this level as the filling factor is tuned through it from $\nu = -2$ to $\nu = +2$ have revealed large, field-dependent shifts in the resonance suggestive of a gap opening at the Dirac point (Fig. 2). Ranging from a few meV at 3 Tesla to nearly 20 meV at 31 Tesla, these shifts raise the possibility of a spontaneous symmetry breaking of the $n = 0$ Level.

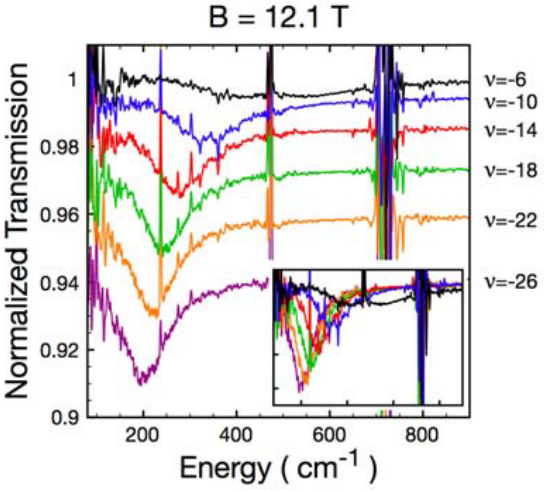

Figure 1: The cyclotron resonance absorption reveals the decreasing energy spacing of Landau Levels in graphene as the filling factor magnitude increases.

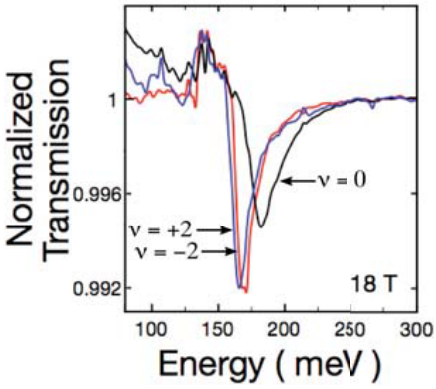

Figure 2: As the filling factor passes through the Dirac point, a higher resonance energy is observed, suggestive of a gap present in the $n = 0$ Landau Level.

References

[1] Z. Jiang *et. al.*, Phys. Rev. Lett **98**, 197403 (2007).

[2] E. A. Henriksen *et. al.*, Phys. Rev. Lett **100**, 087403 (2008).

Spatial distribution of the incompressible strips at Aharonov-Bohm interferometer

Engin Cicek*, Ali Ihsan Mese,* Deniz Eksi*, Mustafa Ulas* and Afif Siddiki**

** Department of Physics, Faculty of Arts and Science, Trakya University, 22030 Edirne, Turkey*

*** Physics Department, Faculty of Arts and Science, Mugla University 48170-Kotekli, Mugla, Turkey*

Keywords: Incompressible strips, Aharonov-Bohm Interferometer

Many recent investigations interested in the quantum information processing, utilizes the quantum Hall based interferometers. In particular, the realization of electron and quasi-particle interference experiments became a paradigm [1,2]. The conventional edge picture is used to explain the observed AB oscillations, however, the actual distribution of the edge-states is still not known for realistic samples, although, several powerful techniques are used [3].

Here, we describe a realistic modelling of AB interferometer described on a 2DEG relies on solving the 3D Poisson equation set by the heterostructure and taking into account the lithographically defined surface patterns to obtain the electron and potential distribution profiles in the absence of an external magnetic field and also under quantized Hall conditions. A fourth order nearest neighbour approximation is used on a square grid with open boundary conditions and 3D fast Fourier transformation method is used to obtain the solution iteratively [4]. Result of this calculation gives the initial condition for the magnetic field dependent calculations. Distinct part of our calculation is that we can handle both gate and etching defined geometries, which essentially is the case for the experiments. Consequently our findings show that the etching defined samples have a sharper potential profile than that of gate defined [5]. In addition we can define the structure with etching and trench gated. Therefore, the formation of the edge-states is strongly influenced. So that these externally defined potential profiles affect the edge physics of the AB interferometers. Figure presents the distribution of the incompressible edge-states, for a selected magnetic field which presumably exhibits clear AB oscillations.

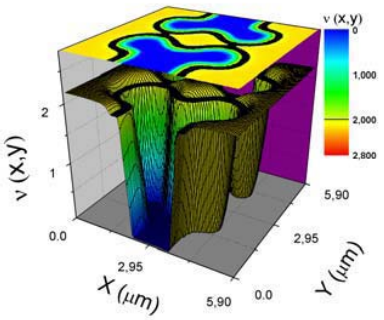

Fig.1 The spatial distribution of the filling factor ν, i.e. the normalized electron density, at 2.0 K for B=8.6 Tesla as a function of lateral coordinates. The blue regions are electron depleted, by applying etching and trench gate with a negative voltage of -1.8 V. The black strips indicate the incompressible edge-states.

References

1. F. E. Camino, W. Zhou, and V. J. Goldman, Phys. Rev. Lett. **95**, 246802 (2005).

2. F. E. Camino, W. Zhou, and V. J. Goldman, Phys. Rev. Lett. **98**, 076805 (2007).

3. S. Ihnatsenka and I. V. Zozoulenko, Phys. Rev. B **76**, 045338 (2007).

4. A. Weichselbaum and S. E. Ulloa, Phys. Rev E **68**, 056707 (2003).

5. S. Arslan, E. Cicek, D. Eksi, S. Aktas, A. Weichselbaum, and A. Siddiki, Phys. Rev. B **78**, 125423(2008).

Selective control of edge channel trajectories by SGM

N. Paradiso*, S. Heun*, S. Roddaro*, L. N. Pfeiffer**, K. W. West** and F. Beltram*

* *NEST, CNR-INFM and Scuola Normale Superiore, Piazza San Silvestro 12, 56127 Pisa, Italy*

** *Bell Laboratories, Alcatel-Lucent, Murray Hill, New Jersey 07974, USA*

Keywords: Quantum Hall Effect, Scanning Gate Microscopy, Edge Channels, Quantum Point Contact

Interference phenomena are a fundamental manifestation of the quantum mechanical nature of electrons and have promising applications in solid-state quantum information technology [1]. Two-dimensional electron systems (2DES) in the quantum Hall (QH) regime are especially suited for this purpose given the large electronic coherence length brought by edge-channel chiral transport. In particular, the realization of electronic Mach–Zehnder (MZ) interferometers in QH systems appears at present a sound technology for the implementation of quantum information schemes. Despite this success, the edge topology of the single-channel MZs limits the complexity of these circuits to a maximum of two interferometers [2]. In order to overcome this constraint, new device architectures were recently proposed, where interference paths are built using two different parallel edge channels [1]. In this configuration, control over the interaction between the different edge channels is very challenging owing to the complex edge structure.

In order to address these issues we are exploring the use of scanning gate microscopy (SGM) to control the trajectory and interaction of edge channels based on our previous results on quantum point contact (QPC) devices in the QH regime [3]. Samples were fabricated starting from high-mobility AlGaAs heterostructures and Schottky split-gate QPCs. SGM experiments were performed at 400mK with magnetic field up to 9T. Figure 1 shows QPC conductance (G) as a function of the position of the biased SGM tip (V_{tip}= -3V). The (bulk) 2DES filling factor is set to $\nu = 6$ (3 spin-degenerate edge channels) while the QPC gates completely deplete the 2DES underneath (gate-region spin-degenerate filling factor $g_1 = g_2 = 0$). When the biased tip is brought close to the QPC, edge channels are backscattered one by one, and the conductance through the QPC decreases in a step-like manner to 0. The split-gate QPC however also allows to bias the individual gates asymmetrically and pre-select edges that can then be manipulated by the SGM tip. For instance in the case $g_1 = 2$, $g_2 = 1$ only the inner edge channel can be backscattered by the local action of the tip, while the others either flow (under the gate) far from the constriction or have no counterpart for the backscattering process to occur. In this latter case, the conductance value remains $G = 4e^2/h$ even when the tip completely pinches off the constriction region (Fig. 1, orange curve).

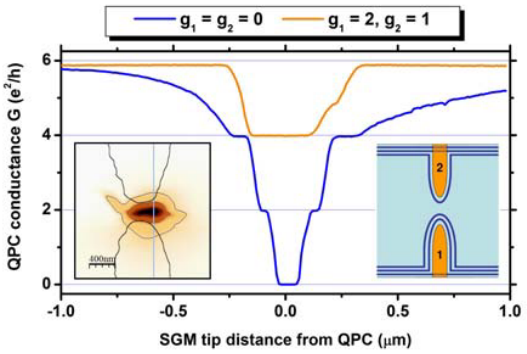

Fig.1 Conductance profile through the QPC as a function of filling factors g under the QPC gates. The left inset shows a two-dimensional SGM map of G vs. tip position for g_1=g_2=0. The vertical line indicates the profile position, the QPC border is outlined. The right inset is a sketch of the edge channels for g_1=2, g_2=1.

We shall show that the SGM tip can be used to selectively control edge trajectories and discuss the impact of our findings as a crucial first step for the implementation of multi-edge beam mixers and interferometers.

References

1. V. Giovannetti et al., Phys. Rev. B **77**, 155320 (2008).
2. I. Neder et al., Nature **448**, 333 (2007).
3. S. Roddaro et al., Phys. Rev. Lett. **95**, 156804 (2005).

Finite bias visibility and phase in an electronic Mach-Zehnder interferometer

A. Helzel*, L.V. Litvin*, H. P. Tranitz*, W. Wegscheider* and C. Strunk*

** Institute for experimental and applied physics, University of Regensburg, Regensburg, Germany*

Keywords: Mach-Zehnder interferometer, phase coherence, quantum interference, lobe structure

We investigate visibility and phase of Aharonov-Bohm interference in an electronic Mach-Zehnder interferometer (MZI) in the integer quantum Hall regime near filling factor 2. Such devices show a lobe structure in the visibility of the oscillations when applying a DC bias voltage. So far, the results of different groups disagree [1] - [3]. In particular, the recent finding, that the visibility can increase with DC bias [4] has renewed the discussion. We have extensively studied the lobe pattern for different settings of incoming biased edge channels (with QPC0) and MZI-QPC's 1 and 2 at filling factor 2.

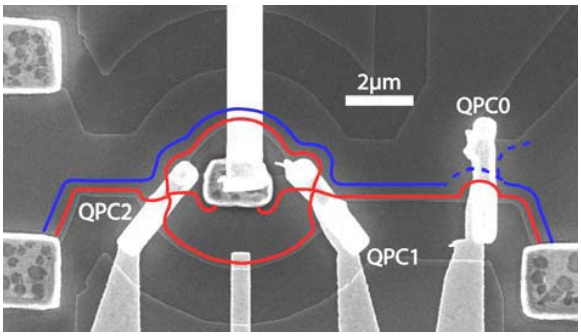

Fig. 1 SEM image of the sample with QPC's 1, 2 and 0 and scetched inner and outer edge channel

In the simplest case, when only one edge channel is biased, one can see the lobe pattern and, depending on magnetic field, one or two side lobes. This observation is unaffected by the transmission of QPCs 1 and 2. The phase of the oscillations is almost rigid inside lobes and has smooth slips of π at nodes.

When opening QPC0 the second edge channel is also biased and participates in the interference. This changes the behaviour of the lobes drastically. When MZI QPC's are tuned to low transmissions (weak tunneling) we see one central lobe with approximately double the width as for one channel bias and one remaining side lobe. If QPCs 1 and 2 are tuned to the weak backscattering regime (large transmission), we see indeed an increase of the visibility with DC bias as reported in [4]. In this case the AB phase is linear with DC bias inside lobes and at nodes one can still see traces of π-jumps.

Using QPC0 not only to reflect the inner edge channel, but also to dilute slowly the outer edge channel dramatically affects the lobe pattern. For high QPC transmissions $T_0 = 1 - 0.5$ side lobes only decrease slowly in height, but widths stay the same. On the other hand, for $T_0 < 0.5$ the second node abruptly disappears and only one wide side lobe remains and the width of the central lobe strongly increases. This effect can be seen as well in the AB-phase.

In summary, we demonstrate the presence of the diverging results in the literature in different parameter regions of a single MZI-device. A consistent explanation of such rich behavior is possible within the frame of the theory of Levkivskyi and Sukhorukov [5].

References

1. I. Neder et al., PRL **96**, 016804 (2006).
2. P. Roulleau et al., PRB **76**, 161309 (2007).
3. L. V. Litvin et al., PRB **78**, 075303 (2008).
4. E. Bieri et al., arXiv:0812.2612.
5. E.V. Sukhorukov and I.P. Levkivskyi, PRB **78**, 045322 (2008).

Finite size scaling analysis of the Chalker-Coddington model

Keith Slevin* and Tomi Ohtsuki**

* *Department of Physics, Graduate School of Science, Osaka University, Osaka, Japan*

** *Department of Physics, Sophia University, Tokyo, Japan*

Keywords: Quantum Hall Effect, Critical Exponent

The quantum Hall effect (QHE) [1] has been the subject of extensive experimental and theoretical study. It is well known that the states at the centre of the Landau level are critical while other states are Anderson localized [2]. The transitions between the quantized values of the Hall resistance occur when the Fermi energy passes through this critical energy. The divergence of the localisation length at the centre of the Landau level is described by a critical exponent ν. A value of 2.35±0.03 was obtained [2] by analyzing the results of simulations of non-interacting electrons using the finite size scaling (FSS) method, a value that is in rough agreement with experiment.

Here, we report an FSS analysis of the Chalker-Coddington model. In this model the motion of the electron in a random potential and quantizing magnetic field is replaced by the transmission of an electron through a network of links and nodes. The links describe electron motion along lines of constant potential and the nodes describe the scattering of electrons at saddle points of the potential. We have used the transfer matrix method to estimate the Lyapunov exponent as a function of the number of nodes N in the cross section and the energy x. The data are shown in Fig. 1 together with a FSS fit to

$$\Gamma = f\left(N^{1/\nu}\psi(x)\right) + N^{y}\phi(x)\,h\left(N^{1/\nu}\psi(x)\right)\log(N/b)$$

We find

$$\nu = 2.58 \pm .01$$

a value that is significantly larger than that reported in [2]. We attribute this discrepancy to the higher precision of our numerical data (0.03%) and a more careful analysis of the corrections to FSS, which appear to be logarithmic rather than power law. For the irrelevant exponent we find y = -0.6±0.06.

Another quantity of interest is the critical value of the MacKinnon-Kramer parameter.

$$\Lambda_c = 1.239 \pm .005$$

Assuming that the, as yet unknown, field theory of the QHE has conformal symmetry, a scaling relation [3] relates this value to the quantity α_0 that is determined in multi-fractal analysis. Our estimate of Λ_c is slightly larger than would be consistent with reported estimates of α_0 [4, 5].

Fig.1 FSS fit to numerical data for the Chalker-Coddinton model. The different lines correspond to numbers of nodes N=8, 12, 16, 24, 32, 48, 64, 96, 128.

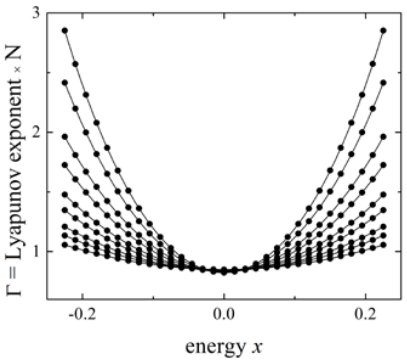

References

1. Klitzing, K.v., *et al*, Phys. Rev. Lett., 1980. **45** 494.
2. Huckestein, B., Rev. Mod. Phys., 1995. **67** 357.
3. Janssen, M., *Fluctuations and localization in mesoscopic electron systems*. World Scientific 2001.
4. Obuse, H., *et al*.,. Phys. Rev. B 2008. **78** 115301.
5. Evers, F., *et al*, Phys. Rev. Lett., 2008. **101** 116803.

Imaging of local filling factor in current flowing ν=1 quantum Hall state by scanning Kerr microscope

K. Oto*, R. Inaba*, T. Yamada*, Y. Saisyu*, T. Matsuda*, K. Muro*, Y. Hirayama**,***, N. Kumada****, and H. Yamaguchi****

* *Graduate School of Science, Chiba University, Inage, Chiba 263-8522, Japan*

** *Graduate School of Science, Tohoku University, Sendai, Miyagi 980-8577, Japan*

*** *ERATO Nuclear Spin Electronics Project, Miyagi 980-8578, Japan*

**** *NTT Basic Research Laboratories, NTT Corporation, Atsugi, Kanagawa 243-0198, Japan*

Keywords: Quantum Hall effect, Spin polarization, Kerr effect, Imaging, Current flow

We obtained the electron spin polarization images in a single layer GaAs/AlGaAs quantum well of the thickness 17 nm at the quantum Hall effect (QHE) regime by means of an optical fiber-based scanning Kerr rotation microscope. By using confocal-like optics, the spot size of photo-excitation for the Kerr measurement can be easily minimize less than a few microns, and the spatial resolution is improved (5 μm) compared with our previous work [1]. At Landau level filling factor ν=1, the spin polarization shows maximum, and the extent of polarization decreases as the filling factor deviates from just one due to the Skyrmion excitation. In this work, the derivative of Kerr rotation by the back-gate voltage $d\theta_K/dV_g$ was measured to detect the very small Kerr rotation ($\leq 10^{-5}$ rad.) by the electron spin polarization. So, the measured signal is to be zero at ν=1, and the small deviation of the filling factor can be detected as positive (ν<1) or negative (ν>1) signal of the $d\theta_K/dV_g$. We can visualize the spatial distribution of the local filling factor through the spin polarization by means of the scanning Kerr microscope.

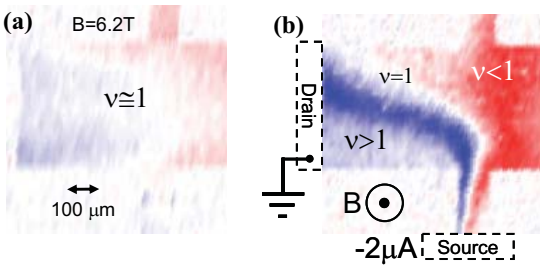

Fig.1 Spin polarization images at ν=1 QHE plateau measured at 4.2 K. (a) The faint contrast measured without current flow is due to the electron density variation less than a few %. (b) Spin polarization measured with external current of -2 μA. The observed Kerr signal $d\theta_K/dV_g$ is negative (ν>1) at the lower left side of the sample, where the electrons are injected from the source electrode.

Without external current flow, the observed Kerr image at ν=1 was almost monotonic, as shown in Fig. 1(a), but the observed faint contrast shows the local filling factor (local electron density) variation only less than 1% in the quantum well. In the current flowing ν=1 QHE state, the spatial distribution of spin polarization drastically changes due to the carrier injection from the source and drain electrodes of the order of only μA, as shown in Fig. 1(b). The Kerr microscope visualized that the injected electrons at the left corner of the source electrode move along the left edge at first, they gradually spread over the bulk region, and finally flowed out to the drain electrode. The spatial distribution pattern of the local filling factor changes if the polarity of the current or magnetic field is reversed. The white strip in the Fig.1(b), where the filling factor is just one, connects between the opposite side of the hot spots at the source and drain electrodes. We demonstrate that the variation of electron distribution in the current flowing ν=1 QHE state by means of the spin polarization mapping.

References

1. K. Oto, *et al.*, Int. J. Modern Phys. (in press)

Voltage controlled group velocity of edge magnetoplasmon in the quantum Hall regime

H. Kamata[1,2], T. Ota[1], K. Muraki[1] and T. Fujisawa[2]

[1] *NTT Basic Research Laboratories, 3-1 Morinosato-Wakamiya, Atsugi, Kanagawa 243-0198, Japan*

[2] *Research Center for Low-Temperature Physics, Tokyo Institute of Technology, 2-12-1 Ookayama, Meguro, Tokyo 152-8551, Japan*

Keywords: quantum Hall effect, edge channel, edge magnetoplasmon

Edge channels in the quantum Hall regime are well recognized as ideal one-dimensional channels without dissipation. Recent experiments of electron interferometer and single-electron injection have motivated us to study dynamics of electrons in edge channels. It has been shown that electrons travel along the edge as an edge magnetoplasmon (EMP) [1]. Here, we demonstrate that the group velocity of EMP can be controlled by the nearby metallic gate electrode via electrostatic and screening effects. This is useful in designing a tunable delay line for EMP.

The experiments were performed on a device fabricated in an AlGaAs/GaAs heterostructure at the bulk filling factor $\nu = 2$ in a dilution refrigerator. As shown in the inset of Fig. 1, an EMP of a pulse shape is generated by applying a short voltage pulse of 0.4 ns to the source, and travels along the edge of the sample to a quantum point contact (QPC) detector, whose gate voltage is pulsed with the width of 0.08 ns. When the pulse hit the EMP, electrons flow to the drain for giving a net current I_{DS}. In this way, we can measure the time-dependent charge distribution of the EMP by changing the delay time of the QPC pulse as shown in Fig. 1.

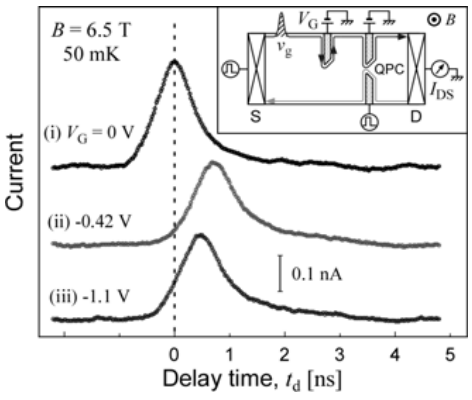

Fig. 1: Charge distribution of the EMP for various gate voltages. Inset: Schematic device structure and experimental setup.

We introduced another gate electrode between the source and the QPC, which adds extra path length by depleting electrons underneath and delays the arrival of the EMP as shown in (ii), (iii). The corresponding group velocity v_{g} changes with the gate voltage V_{G} as shown in Fig. 2. The group velocity depends on the electric field at the edge and strongly influenced by the gate metal (screening effect) [2]. Since the position of the edge channel can be tuned by the gate voltage in our device (inset of Fig. 2), the group velocity can be tuned electrically. The demonstrated voltage-controlled group velocity will be useful in controlling the electron transport dynamically.

This work was partially supported by SCOPE-MIC and KAKENHI-JSPS (19204033).

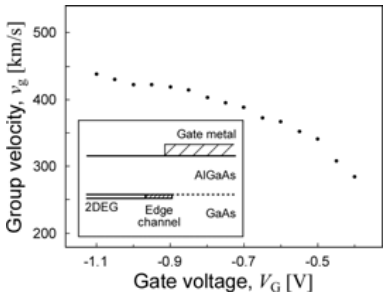

Fig. 2: V_{G} dependence of the group velocity. Inset: Schematic cross-section around the edge channel.

References

[1] R. C. Ashoori *et al.*, Phys. Rev. B **45**, 3894 (1992).

[2] M. D. Johnson and G. Vignale, Phys. Rev. B **67**, 205332 (2003).

Manipulating terahertz photons on a quantum Hall effect device

K. Ikushima[1),2)], D. Asaoka[3)], S. Komiyama[3)], T. Ueda[3)], K. Hirakawa[4)]

[1]*Department of Applied Physics, Tokyo University of A & T, Tokyo, Japan*

[2]*PRESTO, JST, 4-1-8 Honcho Kawaguchi, Saitama, Japan*

[3]*Department of Basic Science, University of Tokyo, Tokyo, Japan*

[4]*Institute of Industrial Science, University of Tokyo, Tokyo, Japan*

Keywords: terahertz, quantum Hall effect, quantum dot, single electron transistor

Individual element technologies for generation, propagation and detection of terahertz (THz) waves are rapidly progressed in recent years. The standard THz measurement system, however, is a composition of the individual element devices configured at separate places. Although an on-chip terahertz device is proposed in a time-domain spectroscopy method, the chip is restricted to a waveform transmission function. Namely, the light generation source and the detection system are independently set up outside the chip. Unlike the above approach, our goal is a completed on-chip THz device: THz waves are locally generated on a chip (driven by a dc-current), transmitted on planar waveguides and finally converted to electric signals via a point detector fabricated on a proper position of the same chip.

In this paper, a first step towards the completed on-chip THz device is implemented at a single photon counting level on a GaAs/AlGaAs single heterostructure crystal (Fig.1). Although an easiest way to generate THz waves is to utilize black body radiation from a heat source, heat diffusion on the chip makes a well localized THz source impossible. Thereby, we use cyclotron emission from edge channels in energy-dissipationless quantum Hall effect (QHE) states [1] as a point light source of THz waves. The emitted THz waves are transmitted via a coplanar waveguide with a length of 0.5 mm to a single photon counter (a quantum-dot detector served as a single electron transistor [2]) fabricated on the same chip.

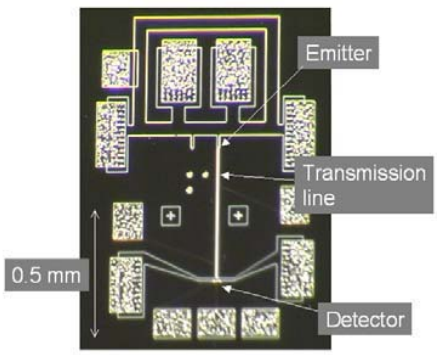

Fig.1 Photograph of on-chip terahertz device fabricated on a GaAs/AlGaAs crystal. The upper and the lower parts serve as a photon emitter and a photon counter, respectively.

In an experimental condition at a Landau-level filling factor ν=3, unequally occupied edge channels encounter at an end of the coplanar waveguide. Consequently, THz waves are emitted and transmitted along the waveguide. We have successfully counted THz photons by the QD detector coupled with another end of the waveguide.

Let us here explain the intention behind. If all efficiencies of photon manipulation processes approach unity, studies of a fundamental issue on the interplay between quantum electronic states and electromagnetic fields may be allowed on a platform of solid state devices. For instance, photon statistics of THz waves driven by a coherent edge channel is one example of interesting targets. Furthermore, because of the long wavelength, a confined electron system strongly coupled with electromagnetic fields may be realized on a solid state device via standard fabrication techniques.

References

1. K. Ikushima et al., Phys. Rev. Lett. **93**, 146804 (2004): K. Ikushima et al., Physica E **40**, 1026 (2008).
2. S. Komiyama et al., Nature. **403**, 405 (2000).

Edge to bulk transition of the IQHE at cleaved edge overgrown samples: an interaction based experimental proposal

U. Erkarslan*, G. Oylumluoglu* and A. Siddiki*

*Mugla University, Physics Department, Faculty of Arts and Sciences, 48170-Kotekli, Mugla, Turkey

Keywords: Incompressible strips, Quantized Hall effect, self-consistent screening, CEO samples

The emergent theories towards explaining the integer quantized Hall effect (IQHE) is still not constituted even twenty seven years after its fascinating discovery [1]. In a first order approximation, two main schools have emerged among others, namely the bulk [2] and the edge [3, 4] pictures, which are thought to be unavoidably in contrast to each other in describing the current distribution. These two main schools are also fractionized in describing the transport properties of the current carrying states namely in between the *compressible* [3, 4] and the *incompressible* [5,6] states, which are like black and white. The cleaved edge overgrown (CEO) samples are known to provide experimentally very sharp edges [7], which we utilize to measure the transition of the IQHE from bulk to edge using the findings of the screening theory [6].

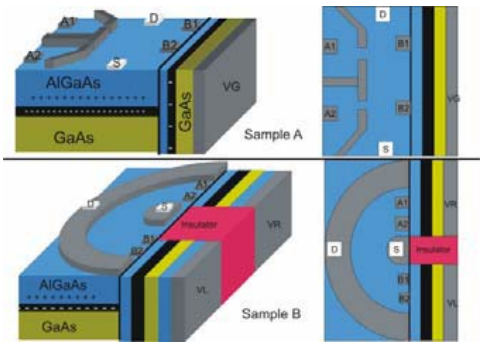

Fig.1: The two sample designs to measure transition of the QHE utilizing the edges. Sample A: Hall bar is defined by top gates which generates a smooth potential profile at the LHS. The sample width should be smaller than the mean free path to avoid the effects imposed by the long-range potential fluctuations. Sample B: Both side CEO design.

We predict that for the, narrow, high mobility CEO samples by changing the steepness of the edge profile using side gates one expects to observe IQHE only if the boundary conditions permit to accumulate at least an incompressible strip. Based on our findings, we proposed two set of experiments (and sample geometries) where the effect of the current induced asymmetry and the transition from bulk to edge IQHE can be controllably measured.

References

1. K. v. Klitzing, G. Dorda, and M. Pepper, Phys. Rev. Lett. 45, 494 (1980).
2. R. B. Laughlin, Phys. Rev. B 23, 5632 (1981).
3. B. I. Halperin, Phys. Rev. B 25, 2185 (1982), M. Büttiker, IBM J. Res. Dev. 32, 317 (1988).
4. D. B. Chklovskii, B. I. Shklovskii, and L. I. Glazman, Phys. Rev. B 46, 4026 (1992).
5. A. M. Chang, Solid State Commun. 74, 871 (1990).
6. A. Siddiki and R. R. Gerhardts, Phys. Rev. B **70**, 195335 (2004).
7. M. Huber, M. Grayson, M. Rother, W. Biberacher, W. Wegscheider, and G. Abstreiter, Phys. Rev. Lett. 94, 016805 (2005).

Calculation of odd integer quantized Hall plateaus due to exchange enhancement of Landé g* factor under experimental conditions

G. Bilgec[1], H. Toffoli [2], A. Siddiki[3] and I. Sokmen[1]
[1]*Dokuz Eylül University, Physics Department, Faculty of Arts and Sciences, 35100 Izmir, Turkey*
[2]*Middle East Technical University, Physics Department, Ankara, 06531, Turkey*
[3]*Mugla University, Physics Department, Faculty of Arts and Sciences, 48170-Kotekli, Mugla, Turkey*

Keywords: Landé g factor, Quantum Hall Effect, Spin-Splitting, DFT

The observation of the odd integer quantized Hall effect is a strong proof of enhanced spin splitting, mediated by exchange interactions, since the bare spin gap is almost two orders of magnitude smaller than the Landau gap [1]. Meanwhile, the inclusion of the exchange interaction alone leads to discrepancies in explaining the experimental data due to underestimation of the correlation effects [2]. Considering both the exchange and correlation interactions are only possible within the direct diagonalization techniques [3] , prohibitively demanding for the systems under investigation [4]. Density functional theory [5] offers an affordable yet accurate description of exchange and correlation [6].

Here, we study the exchange and the correlation interactions in a two dimensional electron gas confined in GaAs/AlGaAs hetero-junction, under the conditions of integer quantized Hall effect, based on self-consistent Thomas-Fermi Poisson Approximation (TFPA). Spin-split incompressible strips (ISs), with integer filling factor are investigated using an empirical effective g factor model and LSDA approximation. We obtain exchange enhanced bulk Landé g-Factor at filling factor $\nu = 1$ and its influence on the quantized Hall plateaus. We show that the enhancement of the g-factor is mainly due to the exchange effects, in the integer quantized Hall effect. Whereas, correlation effects are small compared to exchange effects and are almost unimportant considering odd integer integer plateaus. Our method provides a fully self-consistent calculation scheme to obtain odd integer quantized Hall plateaus and also the transitions in between them, using a local version of the Ohm's law.

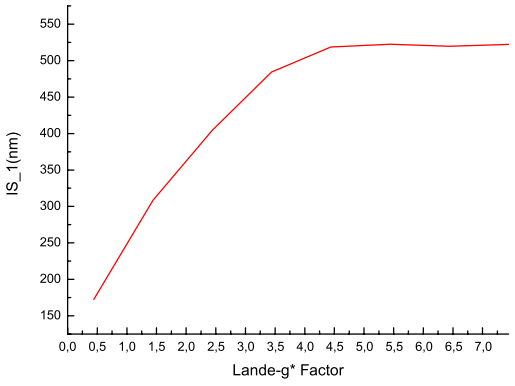

Figure 1: The width of incompressible strip ($\nu = 1$) as a function of bulk Landé g^* factor at T=0.05 K, considering a sample width of 3 μm, and B=7.11 T.

References

[1] A.Manolescu and R.R.Gerhadts, arXiV:cond-mat/9609093v1 (10 Sep 1996)

[2] T. H. Stoof and Gerrit E. W. Bauer, Phy.Rev.B **52**,16(1995)

[3] F. Malet, M. Pi, M. Barranco, L. Serra, E. Lipparini **76**,115306 (2007)

[4] A.Siddiki, Physica E **40**,1124-1126 (2008)

[5] B.Tanatar and D.M.Ceperley, Phys.Rev.B 39, 5005 (1989)

[6] S. Ihnatsenka and I.V. Zozoulenko, Phy.Rev.B **73**,075331 (2006)

Measurement of diffusion thermopower in the quantum Hall systems

K. Fujita, A. Endo, S. Katsumoto and Y. Iye
Institute for Solid State Physics, University of Tokyo, Kashiwa, Japan

Keywords: Diffusion thermopower, Current heating technique, Front gate

The thermopower in two-dimensional electron gases contains contributions from two separate mechanisms: diffusion and phonon drag. It is well known that the latter is by far the dominant contribution in standard experiments using an external heater to introduce temperature gradient [1]. By employing current heating technique that induces gradient only in the electron temperature T_e (leaving the lattice temperature intact), however, the diffusion contribution can be picked out, as demonstrated by Maximov *et al.* in a microfabricated Hall bar [2]. In the present paper, we report our observation of the diffusion thermopower in ordinary-size Hall bar samples applying the current heating technique at low (lattice) temperatures ($T < 100$ mK).

As depicted in Fig. 1, one end of a Hall bar sample is heated by an ac current I ($\sim 50-200$ nA, frequency f), and the longitudinal (Seebeck, S_{xx}) and the transverse (Nernst, S_{yx}) components of the thermopower tensor are detected by probing the corresponding voltage having the frequency $2f$ (note that $\Delta T_e \propto I^2$).

In a low magnetic field regime ($B < \sim 1$ T), we confirmed the generalized Mott relations expected for the diffusion thermopower,

$$S_{xx} = -L_0 eT \frac{d}{d\varepsilon} \ln \sqrt{\sigma_{xx}^2 + \sigma_{yx}^2}$$
$$S_{yx} = -L_0 eT \frac{d}{d\varepsilon} \arctan\left(\frac{\sigma_{yx}}{\sigma_{xx}}\right),$$

by comparing S_{xx} and S_{yx} with σ_{xx} and σ_{yx} measured in the same sample.

In the quantum Hall regime, a complication arises from the large variation with the magnetic field of the resistivity, from ~ 0 at quantum Hall states to $\sim$kΩ in between, that takes place also in the "heater" area of the sample, leading to B-dependent ΔT_e. As shown in Fig. 1, we placed a metallic front gate on the heater area in order to facilitate independent control of the resistivity.

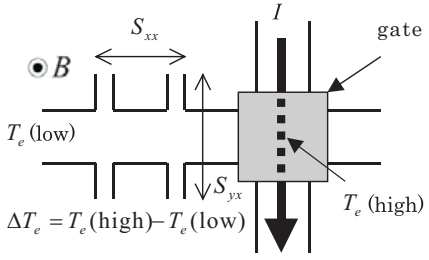

Figure 1: Schematic diagram of the sample.

In Fig. 2b, we plot transverse thermovoltage $V_{yx} = S_{yx}\Delta T_e$ as a function of both B and the gate voltage V_g that controls the filling factor ν_H of the heater area for a fixed B. It can be seen that the signal appears when both the area of the sample to be measured and the heater area are in the resistive (the inter-quantum-Hall transition) region. Interestingly, V_{yx} takes both positive and negative values depending on both ν (the filling factor of the measured area) and ν_H. Therefore traces of magnetic-field sweeps with fixed V_g significantly vary their appearance depending on the value of V_g, as illustrated in Fig. 2a.

References

[1] R. Fletcher, Semicond. Sci. Technol. **14**, R1 (1999).

[2] S. Maximov *et al.*, Phys. Rev. B **70**, 121308 (2004).

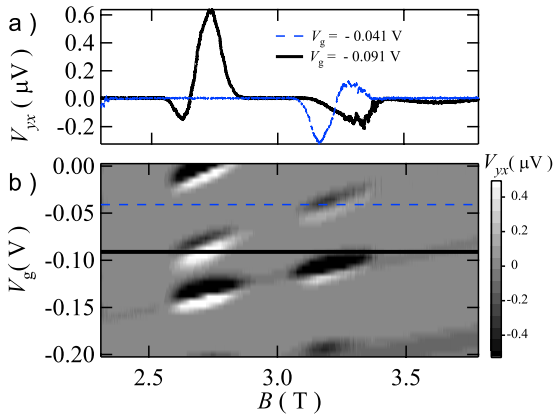

Figure 2: a) Transverse thermovoltage V_{yx} with fixed V_g [cross sections of b) shown by the horizontal lines]. b) Grey-scale plot of V_{yx} as a function of B and V_g.

Importance of interlayer tunneling in Quantum Hall Bilayers at $\nu_T = 1$

Y. Yoon*, L.Tiemann*, S. Schmult*, M. Hauser*, W. Dietsche*, and K. von Klitzing*
*Max-Planck-Institute for Solid State Physics, Heisenbergstr. 1, 70569 Stuttgart, Germany

We have used a counterflow geometry to study transport in correlated bilayer quantum well systems at a total filling factor one ($\nu_T = 1$). We found that at small currents $I < I_C \approx 1.5\ nA$ nearly all the current flows as a tunnel current between the two layers, making the existence of a loop irrelevant. However above the critical value I_C most of the current flows through the loop. Surprisingly, the transport properties are only little affected by the crossover at $I = I_C$.

While the formation and properties of excitonic condensates in bilayer quantum well systems at $\nu_T = 1$ remain a topic of debate, transport experiments in counterflow configuration have been explained as excitonic condensate currents without including interlayer tunneling currents [1, 2]. More recently, it has been shown that a very large interlayer tunneling current exists at least under certain experimental conditions [3, 4].

In this presentation, we demonstrate new results for counterflow experiments [Fig. 1]. It is well known that for the counterflow arrangement both the longitudinal (R_{xx}) and transverse (R_{xy}) resistance at $\nu_T = 1$ [1, 2] tend to zero which may be interpreted as an exciton flow (neutral charge) through the device. Our investigations reveal some new characteristics:

In the $\nu_T = 1$ state, the loop current I_{Loop} (Fig. 1b) is vanishingly small at driving currents (I) below the critical current I_C. This indicates that the interlayer tunneling current (I_{Tunnel}) is nearly identical to that of the total current (I_{Total}) injected into the system. On the other hand, for $I_{Total} > I_C$, about 95 % of I_{Total} flows as I_{Loop} which demonstrates that under this condition the tunneling current is strongly reduced. This result solves the apparent disagreement of published data which show on the one hand a sequential current flow through both layers [1] and on the other hand [3] a very good tunneling between the layers. In summary, it is important whether the total current is below or above the critical value. However the measured R_{xx}, and R_{xy}-data do not show a discontinuity at the critical current I_C.

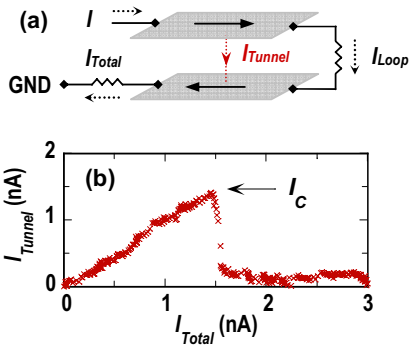

Fig. 1. Measurement set-up (a) and result (b)

Our results therefore provide important evidence that the strongly coupled excitonic quantum Hall state in bilayers at $\nu_T = 1$ can show a large interlayer tunneling current, depending on the magnitude of the injected current in one layer. However, the $\nu_T = 1$ state survives in the breakdown of the large interlayer tunneling.

References

[1] M. Kellogg *et al.*, Phys. Rev. Lett. **93**, 036801 (2004).
[2] E. Tutuc *et al.*, Phys. Rev. Lett. **93**, 036802 (2004).
[3] L. Tiemann *et al.*, New J. Phys. **10**, 045018 (2008).
[4] Jung-Jung Su and A. H. MacDonald, Nature Physics **4**, 799 (2008).

Landau level crossing and pseudospin phase transitions in Si quantum wells

K. Sasaki*, R. Masutomi*, K. Toyama*, K. Sawano**, Y. Shiraki** and T. Okamoto*
*Department of Physics, University of Tokyo, Tokyo, Japan
** Research Center for Silicon Nano-Science, Musashi Institute of Technology, Tokyo, Japan

Keywords: Quantum Hall effect, Landau level crossing

By tilting the magnetic field with respect to the sample normal, the crossing of Landau levels (LLs) with different orbital and spin indices is induced. The two LLs that are nearly degenerate in energy can be relabeled in terms of pseudospin. When the LL filling factor ν is close to an integer, it is believed that electron-electron interaction stabilizes the ferromagnetic alignment of pseudospin with easy-axis (Ising) anisotropy. Resistance spikes and hysteresis have been observed for several two-dimensional electron systems (2DESs) and discussed in association with domain wall resistance in Ising quantum Hall (QH) ferromagnets [1].

Here we extend the study to the intermediate region between QH states with $\nu \neq$ integer [2]. The sample is a very high mobility Si/SiGe quantum well. Magneto-transport measurements are performed in the vicinity of the coincidence of the spin-up LL with an orbital index of $n = 0$ and the spin-down LL with $n = 1$. The Fermi level ε_F lies at these LLs when the Landau level filling factor ν is in the range between 2 and 6, since we have a two-fold valley degeneracy.

In contrast to the QH region where the longitudinal resistivity shows a narrow spike (e.g., $B_\perp \approx 1.87$ T and $B_{\rm tot} = 4.42$ T in Fig. 1(a)), we observe a pronounced dip in the intermediate region (e.g., $B_\perp \approx 2.15$ T and $B_{\rm tot} = 5.23$ T). Together with a Hall resistivity change which exhibits the particle-hole symmetry centered at $\nu = 4$ (see Fig. 1(b)), the dip in the longitudinal resistivity indicates that the electrons or holes in the relevant LLs become localized at the coincidence. Hysteresis loops observed around the dip (both for the higher-$B_{\rm tot}$ and lower-$B_{\rm tot}$ sides) are interpreted as evidence for the first order transition between the pseudospin-unpolarized and pseudospin-polarized states (see Fig. 1(c)). The dip in the longitudinal resistivity disappears as T is raised (see Fig. 1(d)). If we assume an Arrhenius temperature dependence, the energy gap is deduced to be $\Delta \sim 1$ K.

References

[1] K. Toyama *et al.*, Phys. Rev. Lett. **101**, 016805 (2008), and references therein.

[2] T. Okamoto *et al.*, arXiv:0903.0486.

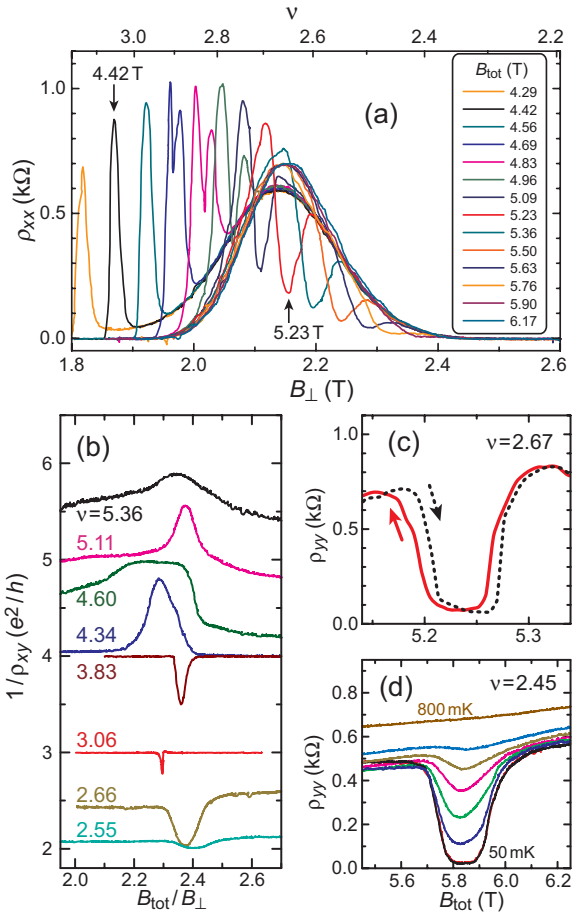

Figure 1: (a) The longitudinal resistivity ρ_{xx} vs the perpendicular component $B_\perp$ of the magnetic field at 70 mK for different fixed values of the total field $B_{\rm tot}$. The in-plane magnetic field is oriented along the x-direction. (b) $B_{\rm tot}$-dependence of the inverse of the Hall resistivity at 70 mK for various fixed values of $B_\perp$, which is proportional to ν. (c) Hysteresis. (d) $B_{\rm tot}$-dependence of ρ_{yy} for $T = 50$, 100, 200, 300, 400, 500, 600, 800 mK.

P12
E1
MoP
E2
E3
E4
TuP
E5
P34
E6
E7
E8
ThP
E9
P56

Spin filtering in Kondo quantum dots and spin-orbit interaction

E. Vernek*, N. Sandler** and S. E. Ulloa**

* *Instituto de Física, Universidade Federal de Uberlândia, Uberlândia, 38400-902, MG - Brazil*

** *Department of Physics and Astronomy, and Nanoscale and Quantum Phenomena Institute, Ohio University, Athens, Ohio 45701-2979 - USA*

Keywords: Kondo effect, quantum dots, spin-orbit interaction, spin transport

Semiconductor quantum dots (QDs) are a promising platform on which to achieve charge and spin control, due to their discrete energy levels, sizable Coulomb interaction and precise level and size manipulation via gate voltages. Moreover, coherent electron propagation at low temperatures and quantum interference may play an essential role in attaining further control of electronic properties in these structures. Control of electronic transport is now systematically achieved by exploiting interference in multiple-path geometries, such as those produced with one or multiple QDs embedded in a ring [1]. In these structures, a few mT magnetic field through a ring produces significant changes in transport properties due to the Aharonov-Bohm (AB) effect. The presence of Rashba spin-orbit (SO) interaction [2], which can be further modulated by applied gate voltages, provides additional dynamical control of charge and spin transport.

The strong Coulomb interaction in these systems may also result in a Kondo state appearing below a characteristic Kondo temperature T_K [3], giving rise to strong antiferromagnetic correlations between localized and itinerant electrons in the leads. This produces an additional transport channel through the system with unique experimental signatures [3].

Several ring geometries have been proposed as *spin polarizers* and their behavior has been analyzed in different regimes, although SO interactions have only been treated perturbatively [4]. The basic physics involved in the spin-filtering effect is the modification of the conductance for different spin species as a result of the AB flux and SO effects that introduce *spin-dependent* dynamical phases for the electrons in the multiply-connected geometry. The correct and complete inclusion of the Kondo physics is crucial in order to provide a proper description of the system, as we describe in this work, especially with respect to its spin transport behavior.

We present here a *numerical renormalization group* study of this system. This approach is capable of addressing the full spin-dependent character of the coupling to the leads and the p-h asymmetry in a non-perturbative fashion [5]. Our analysis demonstrates that the combination of AB and SO effects can strongly suppress the Kondo state, and in fact eliminate the desired spin filtering effect described previously [4]. Most interestingly, we demonstrate that this suppression can be fully compensated by the application of an *in-plane* Zeeman field. Under those conditions, the Kondo screening is restored and the spin filtering effect re-established.

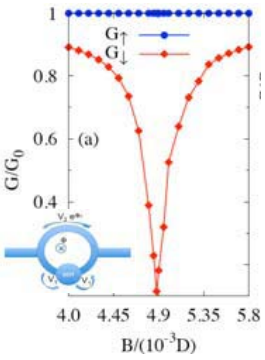

Fig. 1. Spin conductance of QD embedded in ring (see inset) in the presence of SO interaction and AB flux. *In-plane* magnetic field restores Kondo effect and results in perfect spin-filtering

References

1. Y. Ji, *et al.,* Science **290**, 779 (2000).
2. Y. A. Bychkov and E. I. Rashba, J. Phys. C **17**, 6039 (1984).
3. T. Inoshita, Science **281**, 526 (1998), and references therein.
4. Q.-F. Sun, J. Wang and H. Guo, Phys. Rev B **71**, 165310 (2005).
5. R. Bulla, T. Costi, T. Pruschke, Rev. Mod. Phys. **80**, 395 (2008).

Anomalous circular photogalvanic effect in GaAs/AlGaAs two-dimensional electron gas

Y. H. Chen,C. G. Tang, Y. Liu, Z. G. Wang

Key Laboratory of Semiconductor Materials Science, Institute of Semiconductors, Chinese Academy of Sciences, P.O. Box 912, Beijing 100083, P. R. China

Keywords: spin, photogalvanic effect, reciprocal spin Hall effect

The band splitting *k* space due to the spin-orbit interaction in low dimensional structures leads to the so-called circular photogalvanic effect (CPGE): the optical excitation with circularly polarized light induces a spin polarized charge current whose direction and magnitude depend on the degree of circular polarization [1]. For a (001) zinc-blend or a (0001) wurzite quantum structure, the CPGE current vanishes under normal incidence. However, an anomalous CPGE phenomenon in AlGaN/GaN heterostructures has been observed recently, which can be explained by an eddy current induced by a radial spin current via the reciprocal spin Hall effect [2].

Here we report an anomalous CPGE phenomenon in GaAs/AlGaAs two-dimensional electron gas system. The oblique incidence plane of 1064nm laser is perpendicular to electrodes (Y direction), and the CPGE current is measured with the light spot scanning along X axis (Fig.1).

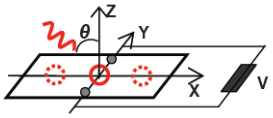

Fig. 1 Schematic of the experiment geometry.

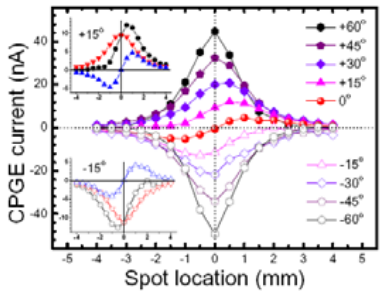

Fig. 2 Total CPGE photocurrent as a function of the light position under different incidence angles.

The CPGE photocurrent (j_C) as a function of the spot position under different incidence angles from -60° to +60° is shown in fig.2, which generally consists of normal CPGE j_n (an even function of x) and anomalous CPGE current j_a (an odd function of x), $j_t(x,\theta) = j_n(x,\theta) + j_a(x,\theta)$,as shown in the insets in Fig.2.

Fig.3 shows the maximum value of normal-and anomalous- CPGE current along X direction as a function of incident angle, which are respectively proportional to $sin\theta$ and $cos^3\theta$. The $cos^3\theta$ dependence of abnormal CPGE currents verifies that it is related to the reciprocal spin Hall effect.

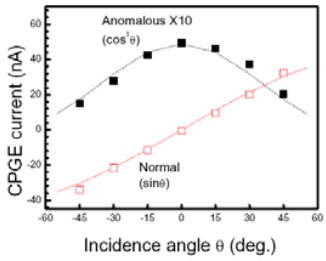

Fig.3 CPGE as a function of incident angle θ. Dotted and dashed lines indicate sine and cubic cosine curves respectively.

The work was supported by NSFC (60625402 and 10804105) and the 973 program (2006CB604908, 2006CB921607).

References

1. S. D. Ganichev and W. Prettl, J. Phys.: Condens. Matter. **15**, R935 (2003).

2. X.W. He, B. Shen, Y. H. Chen, et al., Phys. Rev. Lett. **101**, 147402 (2008)

Electron transport in a Semiconductor-Quantum-Dot Spin Diode

K. Hamaya[1,2,3,4], K. Shibata[1], K. Hirakawa[1,2,5], S. Ishida[6], Y. Arakawa[1,2,6], and T. Machida[1,2,5]

[1]*Institute of Industrial Science, University of Tokyo, Tokyo, Japan*

[2]*Institute for Nano Quantum Information Electronics, University of Tokyo, Tokyo, Japan*

[3]*Department of Electronics, Kyushu University, Fukuoka, Japan*

[4]*Japan Science and Technology Agency, PRESTO, Kawaguchi, Japan*

[5]*Japan Science and Technology Agency, CREST, Kawaguchi, Japan*

[6]*Research Center for Advanced Science and Technology, University of Tokyo, Tokyo, Japan*

Keywords: Coulomb blockade, artificial atom, spin transport

Electron transport properties for a single self-assembled InAs quantum dot (QD) grown on GaAs have been investigated by directly forming nanogap electrodes.[1-6] This technique for nonmagnetic (NM)-Au/Ti electrodes was developed by Jung *et al.*,[1] and artificial atomic nature for such self-assembled InAs QD systems was clearly measured. Recently, we expanded this method into the InAs QD systems with ferromagnetic (FM) electrodes such as Co and Ni.[2] The tunnelling magnetoresistance (TMR) effect and the spin-dependent transport associated with its Coulomb blockade characteristics were observed in the previous reports.[2] Furthermore, the Kondo effect for the strongly coupled NM,[3,6] FM,[5] superconducting[4] metal electrodes was experimentally examined by this technique.

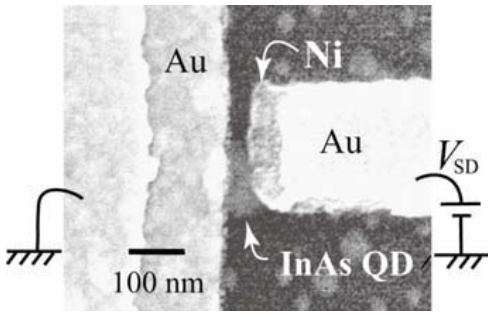

Fig.1 Scanning electron micrograph of a lateral Au/Ti-InAs QD-Ni structure. The InAs QDs were grown on a substrate made of, from the top, 170-nm-thick GaAs layer, 90-nm-thick AlGaAs layer, and n_+-GaAs(001). The n_+-GaAs was used as a backgate electrode.

In this paper, we demonstrate electron transport measurements of NM metal (Au/Ti)-QD-FM metal (Ni) nano-junctions, as shown in Fig. 1, for the first time. This structure is so-called "QD spin diode", fabricated by shadow evaporation techniques and a lift-off method. By a dc method in a dilution refrigerator, Coulomb blockade characteristics and artificial atomic nature can be observed even for the InAs QD spin diode. Also, we can see asymmetric current-voltage characteristics with respect to the polarity of the bias voltage. In particular, we observe anomalous current suppression for the regimes of two-electron tunnelling. We discuss its possible origins in terms of spin blockade and spin accumulation for electron transport in the NM-QD-FM system.

References

1. M. Jung *et al.*, Appl. Phys. Lett. **86**, 033106 (2005); Appl. Phys. Lett **87**, 203109 (2005).
2. K. Hamaya *et al.*, Appl. Phys. Lett. **90**, 053108 (2007); Appl. Phys. Lett. **91**, 022107 (2007); Phys. Rev. B **77**, 081302 (R) (2008); Appl. Phys. Lett. **93**, 222107 (2008).
3. Y. Igarashi *et al.*, Phys. Rev. B **76**, 081303(R) (2007).
4. C. Buizert *et al.*, Phys. Rev. Lett. **99**, 136806 (2007).
5. K. Hamaya *et al.*, Appl. Phys. Lett. **91**, 232105 (2007).
6. K. Shibata and K. Hirakawa, Appl. Phys. Lett. **93**, 062101 (2008).

Suppression of spin relaxation due to dimensional confinement and resonant spin-orbit interaction effect

Y. Kunihashi[1], M. Kohda[1,2] and J. Nitta[1]

[1] *Department of Materials Science, Tohoku University, Sendai, Japan*

[2] *PRESTO Japan Science and Technology Agency, Saitama, Japan*

Keywords: Spin-orbit interaction, Spin relaxation, magneto-conductance, quantum wire

Electrical spin manipulation and long spin relaxation time are required for realizing novel spintronics devices [1]. In semiconductor hetero-structures, an effective magnetic field due to the Rashba spin orbit interaction (SOI) enables the electrical control of spin precession angle [2], whereas it also gives rise to the spin relaxation. Thus, electrical spin manipulation together with long spin relaxation time becomes a great challenge. A semiconductor narrow wire is expected to make spin relaxation time longer since the confinement of electron orbital motion prevents randomization of the spin precession axis [3]. The enhancement of the spin relaxation time in InGaAs narrow wires was observed by lithographically decreasing the wire width [4]. However, the competition between SOI strength and channel width is not yet clarified. In this work, gate voltage dependence of the spin relaxation time is studied from weak antilocalization (WAL) analysis in gate fitted InP / InGaAs / InAlAs narrow wires. We observed the enhancement of the spin relaxation length due to both dimensional confinement effect and approach for the resonant SOI effect which yields momentum-independent effective magnetic fields in equal value of Rashba and Dresslhaus SOIs [1].

An InGaAs inverted HEMT structure was processed into narrow wires with 650-μm long and 766, 861, 1026 and 1263-nm wide by electron beam lithography and reactive ion etching. For minimizing the universal conductance fluctuation, 95 narrow wires were arranged in parallel to the current path. The entire area of the wires was covered with the SiO_2 / Au gate electrode. Gate voltage dependence of the magneto-conductance (MC) was measured at T = 0.3 K. To deduce the spin relaxation length in the narrow wire, we fitted the experimental data with the quantum correction of magneto-transport model developed by Kettemann [5]. Extracted spin relaxation lengths are shown in Fig.1. In lower carrier density region below 1.0 × 10^{12} cm^{-2}, spin relaxation length monotonically increase for all the wires by increasing the carrier density. In addition to that, spin relaxation length is enhanced for the narrower wires. Rapid enhancement of the spin relaxation length was observed for all the wires in high carrier density region above 1.0 × 10^{12} cm^{-2}. Enhanced spin relaxation length becomes more than one order longer than that of two-dimensional electron gas. To confirm the reason for rapid increase of the spin relaxation length, we compared experimental data with Kettemann model. Spin relaxation length calculated by considering the resonant SOI effect shows in good agreements of the experimental result, whereas the calculation with neglecting the resonant SOI effect shows considerable deviation from the experimental result. Therefore, it is found that rapid enhancement of spin relaxation length in high carrier density region is due to approach for the resonant SOI effect. This result is first experimental evidence to observe the suppression of spin relaxation due to the resonant SOI and it provides the possibility of infinite spin lifetime in a specified condition where Rashba SOI equals Dresselhaus SOI.

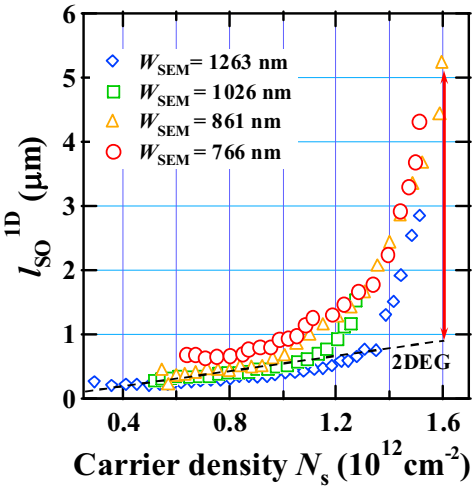

Fig.1 Carrier density dependence of spin relaxation length for the wire structures with different width and two-dimensional electron gas.

References

[1] X. Cartoxiá *et al.*, Appl. Phys. Lett. **83**, 1462 (2003).
[2] T. Bergsten *et al.*, Phys. Rev. Lett. **97**,196803 (2006).
[3] A. A. Kiselev *et al.*, Phys. Rev. B. **61**, 19 (2000).
[4] Th. Schäpers *et. al.*, Phys. Rev. B **74**, 081301(R) (2006).
[5] S. Kettemann, Phys. Rev. Lett. **98**, 176808 (2007).

Anisotropy for spin dephasing in quasi-1D electron ensembles in a GaAs/AlGaAs heterostructure

S. Z. Denega*, T. Last*, J. Liu*, A. Slachter*, P. J. Rizo*, B. J. van Wees*,
D. Reuter**, A. D. Wieck**, P. H. M. van Loosdrecht* and C. H. van der Wal*

** Zernike Institute for Advanced Materials, University of Groningen, The Netherlands*

*** Laboratory for Solid State Physics, Ruhr University, Bochum, Germany*

Keywords: spintronics, spin-orbit fields, spin dephasing, Kerr effect

We report the observation of spin-dephasing anisotropy for electron ensembles in GaAs wires using time-resolved Kerr rotation measurements. For wires along specific crystal directions, spin dephasing is suppressed. These effects result from an anisotropic distribution of spin-orbit fields that occurs when the Rashba and Dresselhaus contributions are of similar magnitude. Such spin-dephasing anisotropy was predicted for quasi-1D ensembles which are realized by patterning two-dimensional electron gas (2DEG) systems [1,2]. Surprisingly, however, our observations show similar spin-dephasing anisotropy for quasi-1D ensembles that reside in deeper bulk layers in our GaAs/AlGaAs heterostructure (Fig. 1).

The wire arrays are fabricated from a GaAs/AlGaAs heterostructure that contains a high-mobility 2DEG. The bulk layer is separated from the 2DEG by a barrier (AlAs/GaAs superlattice). The wires have transverse dimensions below the mean free path and the spin-precession length [2, 3] (in-plane width is 1.4 μm).

The peak values of the spin-dephasing times are found for wires oriented along the [110] direction, and here spin dephasing is strongly suppressed with respect to unpatterned heterostructure areas. The lowest spin-dephasing time is found for orthogonally oriented wires ([-110] direction) [4]. The spin-dephasing anisotropy is most apparent at zero external magnetic fields, but degrades when increasing the external field to values where the spin-precession length becomes shorter than the transverse wire width.

The presented effect is the first direct observation of spin-dephasing anisotropy for electron ensembles in bulk and 2DEG layers in GaAs without full transverse quantum confinement. In addition, it provides evidence that a Rashba contribution to spin-orbit fields can be engineered for ensembles in bulk layers. Further control over these effects can open a way to controlled manipulation of spins in drifting ensembles [1,3].

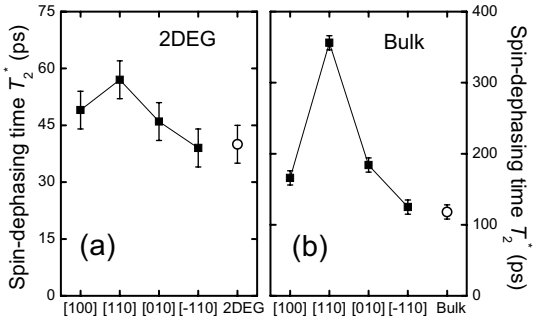

Fig.1 Anisotropy for the spin-dephasing time T_2^* for electron ensembles in wires etched into a GaAs/AlGaAs heterostructure. The spin-dephasing times for ensembles in a quantum well layer (a) and in an underlying bulk GaAs epilayer (b) depend on the crystal orientation in the wire, and can be enhanced with respect to ensembles in unpatterned heterostructure areas. Data taken at the temperature 4.2K and 0T external magnetic field.

References

1. B. Andrei Bernevig, J. Orenstein, and Shou-Cheng Zhang, Phys. Rev. Lett. **97**, 236601 (2006).
2. J. Liu et al., arXiv:0810.1413.
3. A. W. Holleitner, et al., Phys. Rev. Lett. **97**, 036805 (2006).
4. S. Z. Denega, et al., in preparation (2009).

Nuclear spin polarization in the breakdown regimes of integer and fractional quantum Hall states

Minoru Kawamura[1,2,3], Masashi Ono[1], Yoshiaki Hashimoto[4], Shingo Katsumoto[4,5] and Tomoki Machida[1,5]

[1]*Institute of Industrial Science, University of Tokyo, Japan*

[2]*RIKEN, Japan*

[3]*PRESTO, Japan Science and Technology Agency, Japan*

[4]*Institute for Solid State Physics, University of Tokyo, Japan*

[5]*Institute for Nano Quantum Information Electronics, University of Tokyo, Japan*

Keywords: dynamic nuclear polarization, quantum Hall effect, breakdown

Dynamic nuclear polarization (DNP) has been studied in the breakdown regimes of quantum Hall (QH) effect using a two-dimensional electron gas (2DEG) at the interface of GaAs/$Al_{0.3}Ga_{0.7}As$ single heterostructure. We found that nuclear spins are dynamically polaried in breakdown regimes of odd-integer quantum Hall states [1,2]. The experiment was further extended to the breakdown regimes of fractional quantum Hall states and we found that DNPs are also induced even in the breakdown regimes of fractional quantum Hall states with Landau level filling factors ν = 2/3 and 1/3. Results on a pump and probe experiment show that the polarities of the DNPs occuring in the breakdown regime of fractional QH states are opposite to the DNPs induced in the breakdown regimes of odd-integer QH states.

As shown in the main panel of Fig. 1, voltage-current (V_{xx}-I) characteristic curves depend on current sweep rates at ν = 1. The relevance of DNP to the sweep rate dependence was confirmed by nuclear magnetic resonance (NMR) measurements as shown in the inset of Fig. 1. Similar sweep-rate-dependent V_{xx}-I curves and voltage detected NMR spectrum of ^{75}As were also obtained at ν = 2/3 as shown in Fig. 2. The direction of the shift of V_{xx}-I curves at ν = 1 and 2/3 are opposite to each other, suggesting different DNP polarities. We will discuss the polarities of DNPs induced at various conditions referring to the results of a pump and probe experiment.

References

[1] M. Kawamura *et al.,* Appl. Phys. Lett. **90**, 022102 (2007).

[2] M. Kawamura *et al.,* J. Phys. Soc. Jpn. **77**, 023710 (2008).

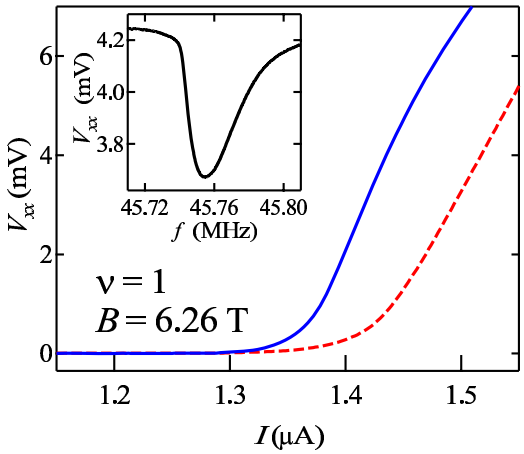

Figure 1: V_{xx}-I curves obtained at ν = 1 and B = 6.26 T. The current sweep rates were 0.4 nA/s (solid) and 6.8 nA/s (dashed). The inset shows NMR spectrum of ^{75}As detected by measuring V_{xx} at ν = 1 and I = 1.4 μA.

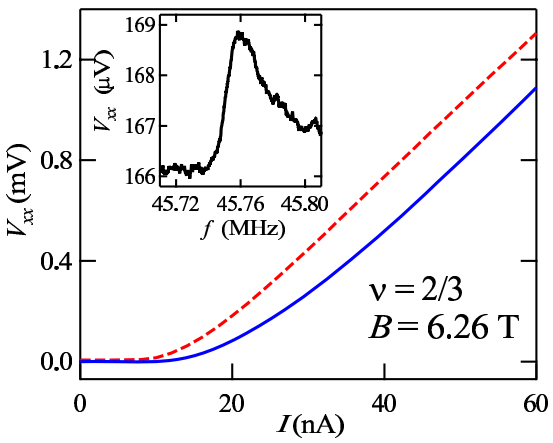

Figure 2: V_{xx}-I curves obtained at ν = 2/3 and B = 6.26 T. The current sweep rates were 0.05 nA/s (solid) and 6.8 nA/s (dashed). The inset shows NMR spectrum of ^{75}As detected by measuring V_{xx} at ν = 2/3 and I = 30 nA.

Charge conservation in dynamic inverse spin Hall effect

K. Hosono, A. Takeuchi and G. Tatara
Department of Physics, Tokyo Metropolitan University, Hachioji, Tokyo 192-0397, Japan

Keywords: Spintronics, Spin Hall effect, Inverse spin Hall effect

Owing to the spin Hall effect discovered in semiconductor systems, transport properties of the flow of the spin degree of freedom in a solids, i.e spin current, were extensively studied in recent years. The spin Hall effect is known as creating method of spin current only by external electric field due to spin dependent scattering arising from the spin-orbit intaraction. Detection of the spin current was carried out first by obtaining the result as spin accumulation at the edge of the sample.

Recently, using the spin dependent scattering from the spin-orbit interaction, electrical detection was observed experimentally which is known the inverse spin Hall effect[1, 2, 3, 4]. They observed that electrical voltage was created in perpendicular both direction to flow of the spin current and spin polarization vector. The relation between the charge current and spin current is speculated as

$$j_\mu = \alpha_{\rm ISH}\epsilon_{\mu l i} j^i_{s,l} \qquad (1)$$

where, j_μ, $j^i_{s,l}$ is the charge current density and the spin current density with the spin polarization (i) and the flow direction(l) respectively, the indexes are $\mu, l, i = x, y, z$ is a complete anti-symmetric tensor.

We study the perturbation theory of conversion from magnetization dynamics to a charge current in metallic systems (dynamic inverse spin Hall effect)[1, 4]. By using non-equilibrium Green function, we calculate the charge current in a perturbative regime with respect to exchange interaction, similarly to the case of a disordered two-dimensional electron gas system with Rashba spin-orbit interaction[5, 6]. Here considering metallic systems, we assume spin-orbit interaction arising from random impurity scattering. The induced charge current is shown diagrammatically in FIG. 1. Especially, we present how the charge conserved relation between the charge density and current is realized in this system[7].

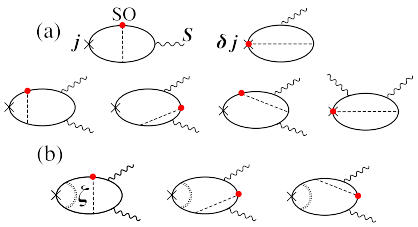

Figure 1: (Color online) Diagrammatic representation of the charge current up to second order in the exchange interaction. Crosses and filled circles represent the current (j) and spin–orbit interaction (SO), respectively. The intersection with a filled circle represents the contribution of the anomalous velocity (δj) from the spin–orbit interaction. Solid and wavy lines denote the impurity-averaged electron Green's function and the exchange interaction $\boldsymbol{S}$, respectively. Dashed lines denote the impurity averaging between the spin–orbit interaction and the impurity scattering.

References

[1] E. Saitoh *et al.*, Appl. Phys. Lett. **88**, 182509 (2006).

[2] T. Kimura *et al.*, Phys. Rev. Lett. **98**, 156601 (2007).

[3] T. Seki *et al.*, Nature Mater. **7**, 125 (2008).

[4] K. Ando *et al.*, Phys. Rev. B **78**, 014413 (2008).

[5] J. Ohe, A.Takeuchi, and G.Tatara, Phys. Rev. Lett.99, 266603 (2007).

[6] A. Takeuchi and G. Tatara, J. Phys. Soc. Jpn. **77**, 074701 (2008).

[7] K. Hosono, A. Takeuchi and G. Tatara, arXiv:0902.3507v1.

Strain-induced enhamcement of electric quadrupole splitting in resistively detected NMR spectrum in quantum Hall systems

Minoru Kawamura[1,2,3], Tatsuya Yamashita[1], Hiroyuki Takahashi[1], Satoru Masubuchi[1], Yoshiaki Hashimoto[4], Shingo Katsumoto[4,5] and Tomoki Machida[1,5]

[1]*Institute of Industrial Science, University of Tokyo, Japan*

[2]*RIKEN, Japan*

[3]*PRESTO, Japan Science and Technology Agency, Japan*

[4]*Institute for Solid State Physics, University of Tokyo, Japan*

[5]*Institute for Nano Quantum Information Electronics, University of Tokyo, Japan*

Keywords: nuclear magnetic resonance, electric quadrupole interaction, integer quantum Hall effect

Electric quadrupole splittings in resistively detected NMR spectra are studied in quantum Hall systems. We demonstrate that the quadrupole splitting can be enhanced intentionally by applying mechanical strain to the Hall-bar devices. The enhancement of the quadrupole splitting enables selective and coherent manipulation of nuclear spin states of the quadrupole-split four-level $I = 3/2$ nuclei.

For the NMR measurements, we used Hall-bar devices fabricated from a wafer of GaAs/$Al_{0.3}Ga_{0.7}As$ single heterostructure with a two-dimensional electron gas at the interface. Nuclear spins in the Hall-bar devices were dynamically polarized by applying bias current in the breakdown regime of odd-integer quantum Hall effect and the NMR spectra are detected by measuring longitudinal voltages [1]. In order to apply mechanical strain to the Hall-bar devices, we coated them with thin films of polyimide. Before the polyimide coating, the spectrum of ^{75}As was single peak as shown in Fig. 1(a). After the polyimide coating, the NMR spectrum of ^{75}As split into three peaks as shown in Fig. 1(b). The splitting of the spectrum demonstrates the enhancement of the electric quadrupole splitting.

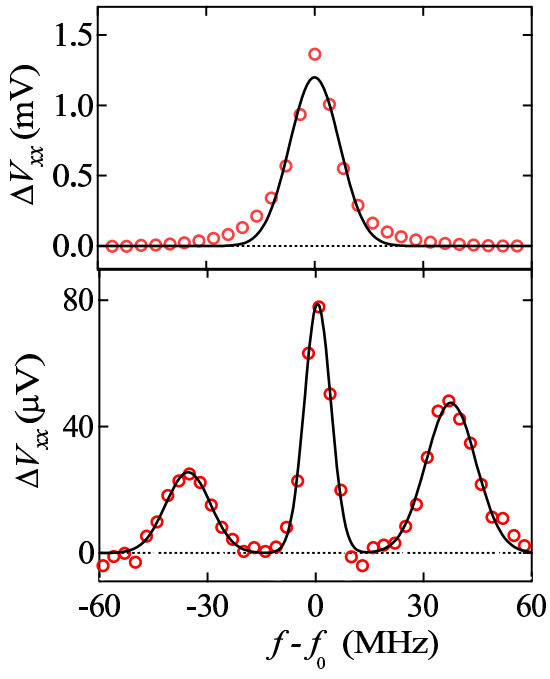

Figure 1: NMR spectrum of ^{75}As (a) before and (b) after polyimide coating taken at $B = 4.92$ T ($f_0 = 35.520$ MHz) and $B = 5.82$ T (f_0 =41.962 MHz), respectively. The solid curves are the fitting results.

Combining with the pulse-NMR techniques [2], coherent oscillations of nuclear spin states were obtained at the three NMR frequencies in Fig. 1. By increasing the amplitude of rf-pulses, additional oscillations corresponding to two-photon absorption (emission) processes were observed. We also performed spin-echo measurements and found that the phase coherent time is considerably extended in the quadrupole-split devices.

References

[1] M. Kawamura *et al.,* Appl. Phys. Lett. **90**, 022102 (2007).

[2] H. Takahashi *et al.,* Appl. Phys. Lett. **91**, 092120 (2007).

Quantum spin transport in magnetic-field-engineered nano-structures

Y. Tokura[1,2], T. Kubo[2], Y. -S. Shin[2], K. Ono[2,3], and S. Tarucha[2,4]
[1] *NTT Basic Research Laboratories, NTT Corporation, Atsugi-shi, Kanagawa 243-0198, Japan*
[2] *Quantum Spin Information Project, ICORP, JST, Atsugi-shi, Kanagawa 243-0198, Japan*
[3] *Low Temperature Physics Laboratory, RIKEN, Wako-shi, Saitama 351-0198, Japan*
[4] *Department of Applied Physics, University of Tokyo, Bunkyo-ku, Tokyo 113-8656, Japan*

Keywords: quantum dots, spin blockade, inhomogenous magnetic field

The electron spins in a quantum dot are gifted a long coherence time since the effect of spin-orbit coupling is strongly suppressed, and are selected candidate for future application of spintronics and quantum information. Spatially dependent spin Zeeman splitting enables individual access to the electron spins, which is recently demonstrated in a coupled dot system with nuclear spin fluctuation[1] or with a closely located micro-magnet[2]. Landé g-factor shows a strong variation in semiconductor materials and its engineering in the nano-structure is another approach. Recently, vertical coupled quantum dot system with different g-factors had been realized[3]. When only one level of the 'probe' dot is below the Fermi level of the source reservoir and the g-factors of the two quantum dots are the same, the resonant current peak as a function of the source-drain bias and the magnetic field shows Fock-Darwin level structure of the 'sample' dot.

Here, we discuss the resonant tunneling transport via such series quantum dots by Bloch equation method when the g-factors of these dots are different. In contrast to the situation with the same g-factors, Coulomb interaction is important and provides intriguing correlation effect (spin blockade).[4] When the effect of electron-phonon scattering is very small, we predict single resonant tunneling peak and its shift toward larger energy when new transport channel by different spin is opened. In contrast, when the phonon assisted tunneling predominates, the peak always appears at one of the two spin resonant tunneling conditions at lower energy.

More intriguing situation appears when the magnetic fields in each dot are non-collinear, or equivalently when the g-factor tensors for the two dots are different. Here we need to consider three parameters, namely, the Zeeman energy in probe (sample) dot, $E_{Zp}(E_{Zs})$ and the relative angle of these fields θ. Since the condition of $\theta = 0$ is considered in the previous paragraph, we concentrate to $\theta \neq 0$. If the effect of Coulomb interaction can be neglected, we expect in total four resonant peaks when $E_{Zp} \neq E_{Zs}$ since the spin eigenstate in one dot has a finite tunnel matrix element with both spin eigenstates in the other dot. However, the Coulomb correlation modifies the result significantly. When $E_{Zp} > E_{Zs}$, we always found single resonant peak as a function of energy offset. The peak current is maximum when $\theta = 0$ and decreases monotonically for larger $\theta \leq \pi/2$. In contract, when $E_{Zp} < E_{Zs}$, we found three peaks as shown in Fig.1 for $\theta < \pi/4$ and two peaks for $\pi/4 < \theta$. We also discuss the effect of microwave irradiated to this system.

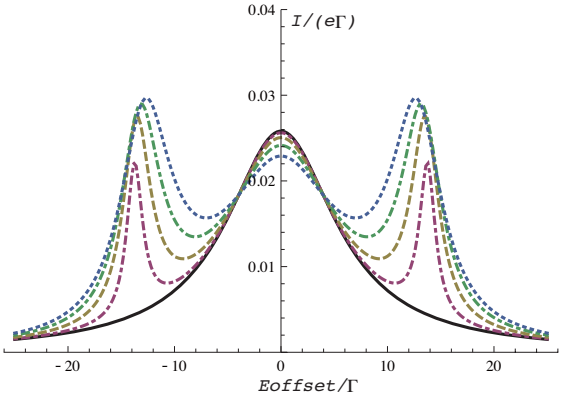

FIG. 1: Resonant current through series double dots as a function of relative energy level offsets E_{offset}. 5 lines from bottom to top correspond to the relative angle of the magnetic field directions, $\theta = 0, \pi/32, \pi/16, 3\pi/32, \pi/8$, respectively. We choose the Zeeman energy for the probe (sample) dot to 8Γ (20Γ) where Γ is the coupling strength to the reservoirs and the inter-dot tunnel coupling is set to Γ.

Acknowledgments

We thank useful discussions with S. M. Huang and S. Amaha.

[1] E. A Laird, *et al.*, 99, 246601 (2007).
[2] M. Pioro-Ladrière, *et al.*, Nature Physics, 4, 776 (2008).
[3] S. M. Huang, *et al.*, unpublished.
[4] Y. Tokura, K. Ono, and S. Tarucha, to appear in phys. stat. solidi B.

Nuclear-spin detection of magnetic-field gradient in nanostructures

S. Watanabe[1], S. Sasaki[2], S. Sato[2], M. Nishimori[2], N. Isogai[3] and Y. Matsumoto[3]

[1]*Centre for Advancement of Higher Education, Tohoku University, Japan*

[2]*Graduate School of Science and Technology, Niigata University, Niigata, Japan*

[3]*Department of Applied Physics and Physico-Informatics, Keio University, Yokohama, Japan*

Keywords: magnetic-field gradient, nanostructure, nuclear spin, quantum computer

To realize solid-state electronic/nuclear-spin-based quantum computers, it is indispensable to produce magnetic-field gradient in nanostructures. Indeed, it is reported that electron spins under a field gradient created by microscopic magnets can be successfully manipulated [1,2]. To the best of our knowledge, however, there have been no reports that the value of a field gradient is evaluated experimentally.

In this paper, we report that, using standard nuclear magnetic resonance (NMR) technique and a well-fabricated sample (Fig. 1), we have succeeded, for the first time, in direct observation of local magnetic field generated by a micromagnet $Ni_{45}Fe_{55}$ (the thickness of 400 nm) which was sputtered on an Al layer of 20-nm thickness. Improved sensitivity of our NMR technique enabled us to clearly observe Al-NMR signals, which are confirmed to come from Al nuclei in the 20-nm layers [3]. In addition, using finite element method, we have succeeded in reproducing the NMR spectra. As a result, the gradient of the local magnetic gradient in the nanostructure is found to be 0.38 T/μm [4]. We would like to stress that no fitting parameters are included in this simulation, and that this value well reproduces the data in electron-spin-resonance experiments [2, 5].

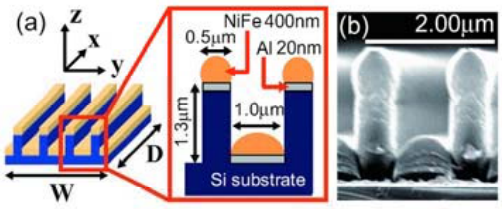

Fig.1 (a) Schematic view of the sample. On the Al layer of 20 nm thickness, Ni45Fe55 alloy is suputtered with the thickness of 400 nm. (b) Scanning electron microscope image of the sample..

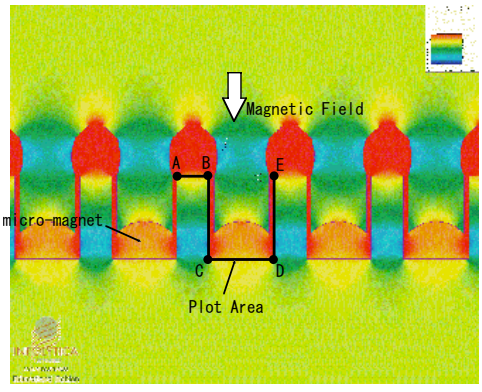

Fig.2 Distribution of the magnetic field in the nano-structured sample simulated by finite element method. This reproduces the Al-NMR spectra without any fitting parameters.

References

1. Y. Tokura, W. G. van der Wiel, T. Obata and S. Tarucha, Phys. Rev. Lett. **96**, 047202 (2006).
2. M. Pioro-Ladriere, T. Obata, Y. Tokura, Y. –S. Shin, T. Kubo, K. Yoshida, T. Taniyama and S. Tarucha, Nature Phys. **4**, 776 (2008).
3. S. Watanabe, S. Sasaki, S. Sato, N. Isogai and Y. Matsumoto, Appl. Phys. Lett. **92**, 253116 (2008).
4. Y. Matsumoto, N. Isogai, S. Sasaki, S. Watanabe and S. Sato, to be submitted.
5. Private communication with S. Tarucha.

Coherent Single Electron Manipulation in a Double Quantum Dot Specially Designed for Scalable Qubits

R. Brunner[1], M. Pioro-Ladrière[1], Y. Tokura[1,2], T. Obata[1], Y.-S. Shin[1], T. Kubo[1], K. Yoshida[1], T. Taniyama[4,5], S. Tarucha[1,6]

1. Quantum Spin Information Project, ICORP, JST, Atsugi-shi, Kanagawa, 243-0198, Japan
2. Departement de Physique, Universite de Sherbrooke, Sherbrooke, Quebec, J1K-2R1, Canada
3. NTT Basic Research Laboratories, NTT Corporation, Atsugi-shi, 243-0198, Japan
4. Materials and Structures Laboratory, Tokyo Institute of Technology, 4259 Nagatsuta, Yokohama, 226-8503, Japan
5. PRESTO, Japan Science and Technology Agency, 4-1-8 Honcho Kawaguchi, Saitama 332-0012, Japan
6. Department of Applied Physics, University of Tokyo, Hongo, Bunkyo-ku, Tokyo, 113-8656, Japan

Keywords: Quantum dots, Micro-magnets, Spin qubits, Quantum information processing, Microwaves

Semiconductor quantum dots provide a promising approach towards the realisation of spin-based solid state quantum computers [1]. A major advantage of solid state quantum computers is the scalability. That is, many of such dots or multiple quantum dots could be implemented in a single chip. Then an important issue is to coherently control a single spin in each quantum dot. Electron spin resonance (ESR) is a basic technique for the coherent spin control, but should be local to each dot. We have recently proposed and demonstrated a new approach to electrically induce ESR in a GaAs/AlGaAs double quantum dot (DQD), namely electrically-driven single spin resonance (EDSR) using a micro-magnet technique [2,3]. In this paper we use a similar double dot but specially designed for the implication in a multiple qubit system to coherently manipulate an electron spin in each dot.

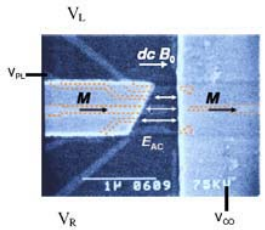

Fig.1 SEM micrograph of the DQD integrating two split micromagnets. The two micromagnets are magnetized M by the external magnetic field B_0.

The device has a split micro-magnet with two dots in between. The split of the micro-magnet is designed to gradually change, so that it is different between the two dots (Fig.1). The stray field produced by such a magnet can firstly shift the Zeeman energy for an electron in each dot and secondly couple the spin and charge degrees of freedom through a slanting magnetic field by electrically oscillating the electron in it [3]. We demonstrate that this device design enables us to detect EDSR, selectively in each dot. Further, we employ a microwave circuit relevant for the pump and probe scheme [2] to perform Rabi and Ramsey experiments for one of the two dots. We find that the obtained results are consistently explained by taking into account nuclear spin effect on the dephasing time T_2^*. Finally we point out, that selective EDSR for more than two dots can be performed just by extending the present device design (Fig.1), i.e. putting more dots in a row.

References

1. D. Loss and D. P. DiVincenzo Phys. Rev. A **57**, 120 (1998) .
2. F. H. L. Koppens et al. Nature **442**, 766 (2006).
3. Y. Tokura et al., PRL **96** 047202 (2006).
4. M. Pioro-Ladrière et al. Nature Physics **4** 776 (2008).

Spin torque shot noise

J. Swiebodzinski*, A. L. Chudnovskiy* and A. Kamenev**
*I. Institut für Theoretische Physik, Universität Hamburg, Jungiusstrasse 9, D-20335 Hamburg, Germany
** Department of Physics, University of Minnesota, Minneapolis, Minnesota 55455, USA

Keywords: Spin torque, spin shot noise, switching rates.

In this contribution we present a general treatment of spin shot noise in magnetic tunnel junctions and investigate its implications on spin torque dynamics. While thermal noise has been studied quite intensively in the context of magnetization dynamics since Brown's pioneering work [1, 2], the role of spin shot noise, though being the dominant contribution to magnetization noise at low temperatures [3] remains largely unexplored yet.

A spin polarized current may transfer angular momentum to a ferromagnet, resulting in the celebrated spin torque phenomenon [4]. The spin shot noise, associated with the discreteness of the spin degree of freedom, leads to a nonequilibrium stochastic force acting on the ferromagnet. We propose a stochastic version of the Landau-Lifshitz-Gilbert equation including both, thermal and nonequilibrium, sources of noise [5]. By means of the Keldysh technique we derive the spin shot noise correlator in the magnetic tunnel junction setup performing a perturbative expansion in terms of the tunneling amplitude and the spin flip processes. The correlator exhibits a dependence on the mutual orientation of the fixed and free layer's magnetizations, thus being fundamentally different from thermal noise. Another peculiarity is its dependence on the spin flip current, counting the total number of spin flips irrespective of their direction, as opposed to the spin current. We solve the corresponding Fokker-Planck equation and show that the spin shot noise leads to the experimentally observed nonmonotonic dependence of the precession spectrum linewidth on the current [6] and to a saturation of the spectral linewidth at small temperatures [7].

Of great interest, not only in the context of technological applications, is the estimation of switching times [8]. We address this question by applying a generalized Fokker-Planck approach [9] that models the alteration in the switching rates by a change of the effective temperature in the Arrhenius factor rather than a change of the potential barrier. We show that the nonequilibrium noise leads to a renormalization of this effective temperature whose details depend on the geometry of the system.

References

[1] W. F. Brown, Phys. Rev. **130**, 1677 (1963).

[2] Z. Li and S. Zhang, Phys. Rev. B **69**, 134416 (2004).

[3] J. Foros, A. Brataas, Y. Tserkovnyak, and G. E. Bauer, Phys. Rev. Lett. **95**, 016601 (2005).

[4] J. C. Slonczewski, J. Magn. Magn. Mater. **159**, L1 (1996).

[5] A. L. Chudnovskiy, J. Swiebodzinski, and A. Kamenev, Phys. Rev. Lett. **101**, 066601 (2008).

[6] W. H. Rippard et al., Phys. Rev. Lett. **92**, 027201 (2004).

[7] J. C. Sankey et al., Phys. Rev. B **72**, 224427 (2005).

[8] I. N. Krivorotov et al., Science **307**, 228 (2005).

[9] D. M. Apalkov and P. B. Visscher, Phys. Rev. B **72**, 180405 (2005).

Graphene-like magneto-oscillations in graphite capacitor

T. Yoshida and K. Oto

Graduate School of Science, Chiba University, Chiba, Japan

Keywords: graphene, graphite, quantum Hall effect, capacitance

Capacitance measurement is known as a useful tool for studying the electron density of state at Fermi energy, the area of compressible state at quantum Hall effect regime, and the very small conductivity such as the hopping conduction regime. We have observed the graphene-like behaviours of magneto-capacitance in the front-gated graphite capacitor.

We made graphite sheets from Kish graphite by using micromechanical cleavage method [1] to get fresh and ultra-smooth surface, and they were transferred to the surface of n-doped Si/SiO_2 substrate, where the thickness of SiO_2 layer was 280 nm. We fabricated NiCr/Au ohmic contact and Al front gate insulated by evaporated 100 nm SiO_x film, as shown Figure 1. The magneto-capacitance was measured at 4.2 K~0.4 K by a LCR meter with 1 kHz~1 MHz AC voltage.

Figure 2 shows the imaginary part of magneto-capacitance measured at 1 MHz and 4.2 K without DC bias, where the background capacitance is subtracted for clarity. The oscillations observed in magneto-capacitance correspond to the Shubnikov-de Haas oscillations of single layer graphene, from the analysis of index plot of the oscillations, as shown in the inset of Fig. 2. The carrier density is 4.5×10^{15} m^{-2} and the estimated filling factors ν = 6, 10, 14 for each minimum of magneto-capacitance (Fig.2). It was reported that the external electric field applied to the surface of layered graphene sheets is strongly screened only in a few graphene sheets [2, 3]. The graphene-like behaviour observed in magneto-capacitance may be attributed to the strong screening effect in surface graphite sheet and the front-gate can modulate the carrier density only in the most surface layer of ultra-planar bulk graphite. In this report, we demonstrate further details of the magneto-capacitance in bulk-graphite sheet, and multilayer graphene sheet.

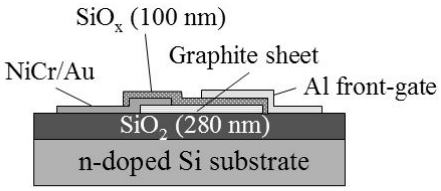

Fig.1: The schematic cross-sectional view of graphite capacitor. Typical area of the capacitor was about 75 μm × 100 μm.

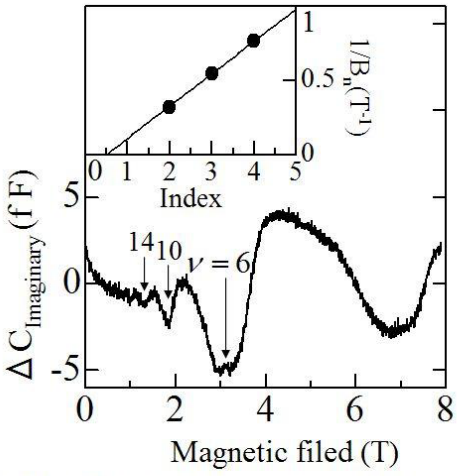

Fig.2 : Imaginary part of magneto-capacitance measured at 1 MHz. The inset shows index plot from capacitance minima in magneto-oscillations.

References

1. K. S. Novoselov *et al.*, Nature **438** (2005) 197.
2. P. B. Visscher and L. M. Falicav, Phys. Rev. B **3** (1971) 2541.
3. K. S. Novoselov *et al.*, Science **306** (2004) 1102896.

Quantum Hall effect in Graphene at large bias current.

K. Bennaceur*, J. Guignard**, F. Schopfer**, W. Poirier**, F. Portier*, P. Roche* and D. C. Glattli*

*Nanoelectronics Group, IRAMIS/SPEC, CEA Saclay F-91192 Gif-sur-Yvette, France

**Quantum Metrology Group, Laboratoire National de Métrologie et d'Essais (LNE), Trappes, France

Keywords: Graphene, Quantum Hall Effect, current breakdown.

Graphene Hall bars prepared from exfoliated natural graphite of large size and high quality have been measured in the quantum Hall regime. We present measurements of the longitudinal resistance of monolayer Graphene under large current. Depending on samples, either variable range hopping or thermal activated law is found.

The samples are made from natural graphite mechanically exfoliated and deposited on a 340nm thick oxidized highly doped Si wafer. Deposition is done on a pirhana cleaned SiO2 surface under dry atmosphere increasing the yield of high quality and often of very large (>1000 µm2) samples. After optical detection of few layer Graphene, Raman scattering is used in order to select pure monolayers. Alignment metallic crosses are then deposited on the substrate closed to the selected sample by e-beam lithography. A second process of electron lithography is then used to deposit 30nm TiAu contacts using electron gun evaporation. Finally a third lithography process is made followed by O2 plasma etching to define the Hall bar shape. Before mounting the sample in the cryostat, it is heated in dry atmosphere for more than 12 hours at 120°C.

All the samples show good quantization of the Hall resistance and very low contact resistance (< 50 Ohms). Measurements are performed at 4.2 K and in magnetic fields up to 17 Tesla. According to ref. [1] for similar studies on GaAs samples, on might expect a variable range hopping law for the dependence of the longitudinal resistance as a function of the Hall voltage, which can be also expressed as the current as long as the Hall quantization persists at large bias. This law of variation is reminiscent from the thermal variable range hopping law where the thermal energy is replaced by the mean electric field times a localization length.

On top of the figure below are displayed an optical picture of a typical Hall bar and a trace of the Hall and longitudinal resistances observed at 16.8 Tesla and plotted as a function of gate voltage around ν=2. Different traces correspond to different large bias. On the bottom of the figure are plotted in logarithmic scale the current times the ratio of the longitudinal resistance normalized to the Hall resistance observed at 16.5 Tesla as a function of inverse square root of the current. On the left, data are for ν around ν=2 and, on the right, for ν=6. The study at ν around 2 shows that the characteristic current I_c is a function of $|\nu - 2|$ [2]. The data suggest variable range hopping regime. A striking point is that we have always observed smooth evolution with the current and no current breakdown as in usual 2DEGs. Further measurements are in progress to firmly establish the universality of the above results and to compare with thermal measurements of the longitudinal resistance.

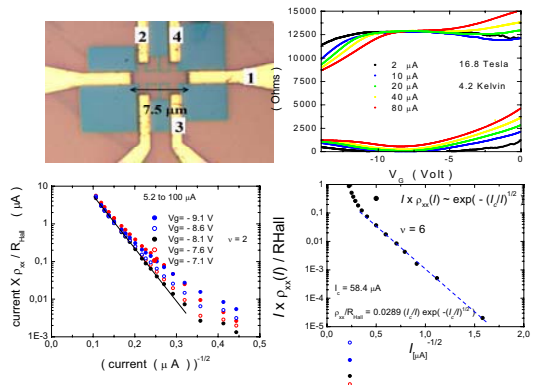

References

1. F. Hohls, U. Zeitler, and R. J. Haug Phys. Rev. Letters **88**, 036802 (2002).
2. B. Jeckelmann et al. IEE Trans. Instrument Meas. 50, 218 (2001).

Weak-field Hall effect in graphene calculated in self-consistent Born approximation

Toshiyuki Fukuzawa, Mikito Koshino, and Tsuneya Ando
Department of Physics, Tokyo Institute of Technology, 2–12–1 Ookayama, Meguro-ku, Tokyo 152-8551, Japan

Keywords: graphene, Hall effect, zero-energy anomaly

One important feature of electronic states of graphene is the presence of a topological singularity at the Dirac point $\mathbf{k} = 0$. The singularity leads to the presence of a Landau level at $\varepsilon = 0$ independent of the magnetic-field strength. This singularity combined with level broadening effects due to impurity scattering or disorder has been known to cause various peculiar behaviors in the transport properties of graphene, such as the universal minimum conductivity in the absence and presence of a magnetic field, the half-integer quantum Hall effect, the characteristic dynamical conductivity, singular diamagnetic susceptibility, etc., [1]. The purpose of this paper is to theoretically explore singular behavior appearing in the weak-field Hall effect.

We calculate the weak-field Hall conductivity proportional to applied magnetic field with the use of a Green's function technique within the self-consistent Born approximation. The strength of impurity scattering is characterized by dimensionless parameter W. The singularity at zero energy can be clarified through the dependence of the Hall conductivity on the Fermi energy and the dependence of the Hall coefficient on the carrier density:

The Hall conductivity sufficiently away from the Dirac point or the charge neutrality point exhibits the energy and electron-concentration dependence qualitatively in agreement with the Boltzmann conductivity. However, the absolute value of the Hall conductivity is smaller and approaches to the Boltzmann result only in the limit of weak scattering $W \ll 1$. The Hall conductivity takes a maximum at $\varepsilon_F \approx -\varepsilon_0$ and a minimum at $\varepsilon_F \approx +\varepsilon_0$, where $\varepsilon_0 = 2W\varepsilon_c \exp(-1/2W)$ where ε_c is the cutoff energy corresponding to the half of the π-band width. Between $\varepsilon \approx \pm\varepsilon_0$, the conductivity varies almost linearly as a function of energy and vanishes at $\varepsilon_F = 0$ (see Fig. 1).

The inverse Hall coefficient takes a minimum at $n_s \approx -n_s^0$ and a maximum at $n_s \approx +n_s^0$ and exhibits divergent behavior $\propto -n_s^{-1}$ in between. The scattering parameter at the Dirac point can be determined by the electron concentrations corresponding to these minimum and maximum. The experimental results of the diagonal conductivity and the Hall effect can be reasonably well understood by assuming W which is inversely proportional to the electron concentration and saturates at the value of $n_s = \pm n_s^0$ for the electron concentration $|n_s| < n_s^0$. This is quite in contrast to results in a simpler model introducing energy-independent broadening or relaxation [2].

References

[1] T. Ando, Physica E **40**, 213 (2007) and references cited therein.
[2] H. Fukuyama, J. Phys. Soc. Jpn. **76**, 043711 (2007).

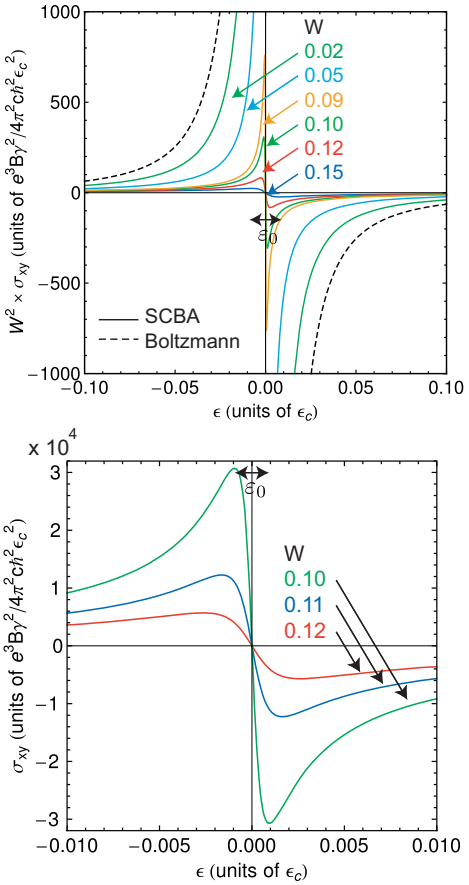

Figure 1: (Top) Some examples of the calculated Hall conductivity. The solid lines represent the results in SCBA and the dashed line represents the Boltzmann result. (Bottom) Expansion of the results in the case of large disorder.

Quantum Hall activation gaps in bilayer graphene

E. V. Kurganova*, A. J. M. Giesbers*, U. Zeitler*, L. A. Ponomarenko**, K. S. Novoselov**, A. K. Geim**, and J. C. Maan*

** High Field Magnet Laboratory, IMM, Radboud University Nijmegen, Nijmegen, the Netherlands*

***Department of Physics, University of Manchester, Manchester, United Kingdom*

Keywords: bilayer graphene, quantum Hall effect

We have performed magneto-transport experiments in a bilayer-graphene ambipolar field-effect transistor. The measurements were done in magnetic fields up to 30 T and a temperature range $T = 0.4 - 220$ K (Fig. 1a). At filling factors $\nu = \pm 4N$ ($N = 1, 2, \ldots$, the sign refers to electrons and holes) the Fermi energy is situated between two Landau levels and quantized Hall plateaus develop. They are accompanied by thermally activated the Shubnikov-de Haas minima. Surprisingly, at $B = 30$ T, this unconventional quantum Hall effect in bilayer graphene [1] remains visible up to 220 K.

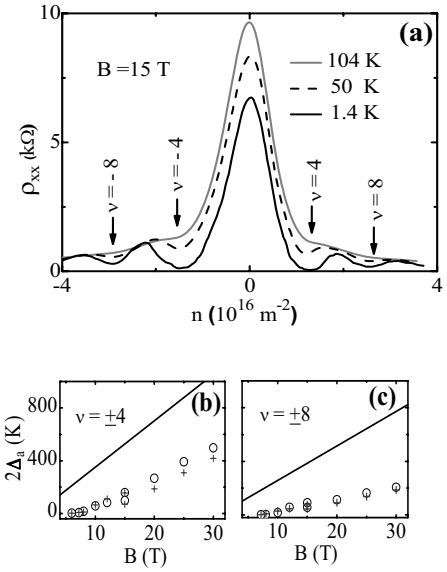

Fig.1 Longitudinal resistivity as a function of the carrier concentration at $B = 15$ T for different temperatures (a). Energy gaps extracted from the temperature dependence of the Shubnikov-de Haas minima as a function of magnetic field for $\nu = \pm 4$ (b) and $\nu = \pm 8$ (c). Circles (crosses) correspond to electrons (holes). The straight lines show theoretically predicted Landau levels splitting for $m_c = 0.054\, m_e$.

The gaps $2\Delta_a$, extracted from the Arrhenius-type behaviour of the Shubnikov-de Haas minima at filling factors $\nu = \pm 4$ and $\nu = \pm 8$, depend linearly on the magnetic field (Fig. 1b and c). The solid lines in the figure show a comparison with the expected Landau level splitting

$$\Delta E_{N,N+1} = \hbar\omega_c\left(\sqrt{N(N+1)} - \sqrt{(N-1)N}\right),$$

where $\hbar\,\omega_c = \hbar\, eB/m_c$ is the cyclotron energy for a mass $m_c = 0.054\, m_e$ [2].

The experimental data follow the theoretical line reasonably with a different slope for the two transitions $\Delta E_{0\to1}$ and $\Delta E_{1\to2}$. The additional offset can be assigned to a finite width of the Landau levels involved and deviations of the slope may be explained by a linear field dependence of the Landau level widths, an effect which is expected for the higher Landau levels and can be tracked down to random fluctuations of the local field orientation caused by the rippled surface of graphene. Additionally, this can also indicate a filling-factor dependent effective cyclotron mass which is consistent with recent cyclotron resonance experiments in bilayer graphene [3].

References

1. K.S. Novoselov et al, Nature Physics **2**, 177 (2006).
2. E. McCann et al, PRL **96**, 086805 (2006).
3. E.A. Henriksen et al, PRL **100**, 087403 (2008).

Approximate validity of Kohn's theorem in cyclotron resonance in graphene

Kenichi Asano* and Tsuneya Ando**
*Department of Physics, Osaka University, Toyonaka, Japan
** Department of Physics, Tokyo Institute of Technology, Tokyo, Japan

Keywords: graphene, many-body effect, cyclotron resonance, Kohn's theorem

Graphene, a monolayer of graphite, have the electrons which behave as Dirac fermions at around K and K' points located at the corners of the Brillouin zone. Since the discovery of an unusual sequence of the quantum Hall effect, its properties under the magnetic fields have been attracting attention both experimentally and theoretically. Quite recently, the cyclotron resonance (CR) spectra were observed in experiments [1, 2, 3], which show some deviation from the one expected from the simple model of the free (non-interacting) Dirac fermions. In this paper, we discuss effects of the electron-electron (e-e) interaction on CR in graphene at absolute zero temperature.

According to Kohn's theorem, the conventional two-dimensional electron systems do not show interaction effects in CR, where the system is homogeneous and all the electrons have the same parabolic energy dispersion. This is because the light couples only with the center-of-mass motion of electrons, which is unaffected by the interaction. This Kohn's theorem is, however, inapplicable for graphene, since the electrons have a linear dispersion. Thus, we can expect enhancement of many-body effects.

We investigate the absorption of a circularly polarized light, which excites a single electron from $n = 0$ to 1 Landau level. We adopt an effective model with only the $n=-1$, 0, and 1 Landau levels. Taking into account the full configuration interactions, we diagonalize the Hamiltonian numerically and obtain all the initial and the final states. Then, the real part of the optical conductivity is calculated via Fermi's golden rule. For simplicity, the spin and the valley degrees of freedom are neglected, and the filling factor for the doped electrons is varied from $\nu=-1/2$ to $1/2$, where $\nu=0$ denotes the case of the half filling of Landau level $n=0$.

The obtained spectra show a double-peak structure, i.e., a dominant peak in the low energy side and a subpeak in the high energy side. This result clearly shows the inapplicability of Kohn's theorem to graphene. The peak splitting is attributed to coupling between two excitation modes; the optically allowed excitation from the $n = 0$ to 1 Landau level and the optically forbidden transition from $n=-1$ to 0 level. The energy splitting of spectra is most enhanced in the limit of $\nu\to-1/2$. With increasing the filling factor, the energy splitting is suppressed, and at $\nu\sim1/2$, the many-body effects are hardly seen in the spectra. In spite of the fact that graphene is in the strong nonparabolicity limit, interaction effects manifest themselves as a surprisingly small modification of the spectra for transitions involving level $n = 0$ in the presence of broadening.

References

[1] M.L. Sadowski et al., Phys. Rev. Lett. **97**, 266405 (2006).
[2] Z. Jiang et al, Phys. Rev. Lett. **98**, 197403 (2007).
[3] R.S. Deacon et al., Phys. Rev. B **76**, 081406 (2007).

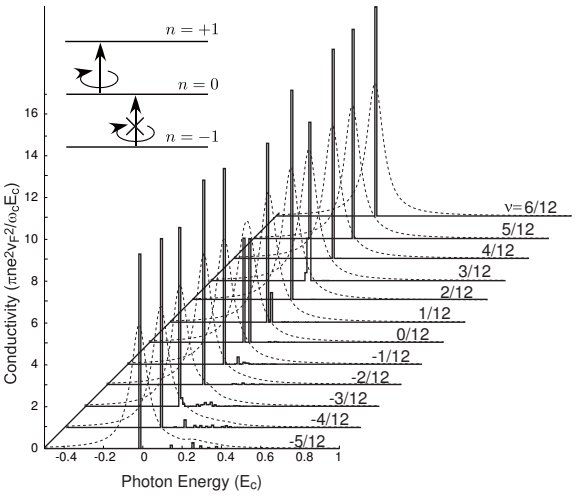

Figure 1: Cyclotron resonance in graphene (without spin and valley). The solid lines show the histogram with width $0.01E_{\rm C}$ and the dotted lines are broadened with a Lorenzian with half-width $0.05E_{\rm C}$, where $E_{\rm C}=e^2/4\pi\epsilon\ell$ is defined with the magnetic length ℓ and the dielectric constant ϵ.

Low temperature magneto-transport in graphite interpreted using the Slonczewski–Weiss–McClure band structure calculations

J. M. Schneider*, M. Orlita*, M. Potemski*, and D. K. Maude*

*Laboratoire National des Champs Magnétiques Intenses, Grenoble High Magnetic Field Laboratory, Centre National de la Recherche Scientifique, 38042 Grenoble, France

Keywords: Graphite Magnetotransport

Historically, graphene forms the starting point for the Slonczewski, Weiss and McClure (SWM) band structure calculations of graphite [1]. In graphite, the Bernal stacked graphene layers are weakly coupled with the form of the in-plane dispersion depending upon the momentum k_z in the direction perpendicular to the layers. The carriers occupy a region along the $H-K-H$ edge of the hexagonal Brillouin zone. At the K point ($k_z = 0$), the dispersion of the electron pocket is parabolic (massive fermions), while at the H point ($k_z = 0.5$) the dispersion of the hole pocket is linear (massless Dirac fermions). The SWM model, provides a remarkably accurate description of the band structure. The observation of massless carriers with a Dirac–like energy spectrum, using magneto-transport measurements [2] remains controversial, since in the SWM model, the electrons and hole carriers at the Fermi level are both massive quasi–particles.

Here we report magnetotransport of natural graphite and highly oriented pyrolytic graphite (HOPG) measured at mK temperatures. Quantum oscillations for both electron and hole carriers are observed with orbital angular momentum quantum number up to $N \approx 90$ (Fig. 1). At high magnetic fields ($B > 2$ T), a significant deviation from 1/B periodicity occurs due to the well documented movement of the Fermi energy as the quantum limit is approached. This seriously questions the validity of using the high field data to extract the phase of the Shubnikov de Haas oscillations, and hence the nature of the charge carriers. A remarkable agreement is obtained when comparing the data and the predictions of the Slonczewski–Weiss–McClure tight binding model for massive fermions [3]. No evidence for Dirac fermions is observed in the transport data which is dominated by the crossing of the Landau bands at the Fermi level, corresponding to $dE/dk_z = 0$, which occurs away from the H point where Dirac fermions are expected.

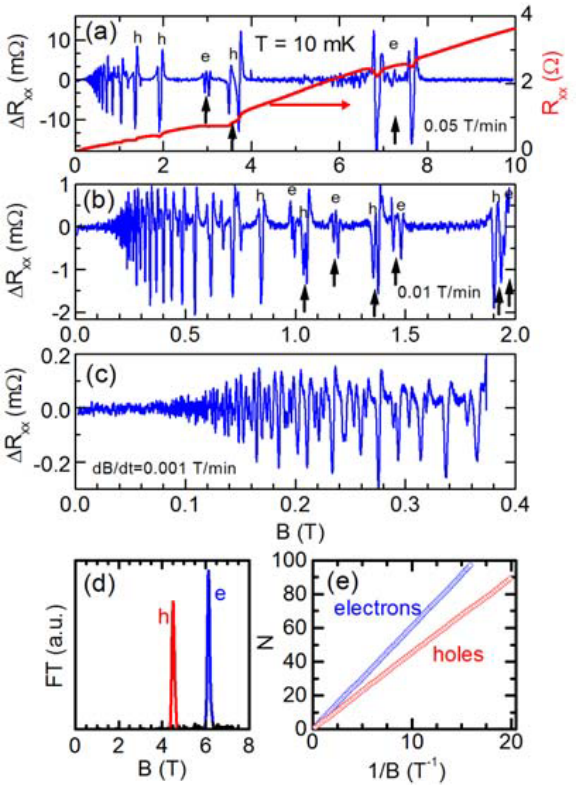

Figure 1: (a) Right axis: Resistance R_{xx} versus B measured at $T = 10$ mK for natural graphite. (a-c) Left axis: Background removed data ΔR_{xx} showing quantum oscillations measured over different magnetic field regions. The vertical arrows indicate spin split electron and hole features. (d) Fourier transform of the low magnetic field $\Delta R_{xx}(1/B)$. (e) Orbital angular momentum quantum number N, as a function of the reciprocal magnetic field positions of the electron and hole features.

References

[1] J. W. McClure, Phys. Rev. **119**, 606 (1960).

[2] I. A. Luk'yanchuk and Y. Kopelevich, Phys. Rev. Lett. 97, 256801 (2006).

[3] J. M. Schneider *et al.* arXiv:0902.1925 (2009).

Towards quantum Hall effect quantization tests in graphene

J. GUIGNARD*, W. POIRIER*, F. SCHOPFER* and D.C. GLATTLI**

** Quantum Metrology Group, Laboratoire National de Métrologie et d'Essais (LNE), Trappes, France*

*** Service de Physique de l'Etat Condensé, CEA, Saclay, France*

Keywords: quantum Hall effect (QHE), graphene, metrology

Due to its electronic properties, graphene exhibits very well quantized Hall resistance plateaus, robust up to the room temperature [1]. This makes graphene particularly interesting for the resistance metrology. However, graphene Hall samples have to fulfil several technical requirements to acquire the status of good (ie accurate) quantum resistance standards: notably, a sufficiently large geometrical width [2] and contact resistances as low as possible.

Here, we report on measurements of the longitudinal resistance R_{xx} and the Hall resistance R_H performed on a graphene Hall bar. The sample is based on a graphene monolayer obtained by mechanical exfoliation of natural graphite, deposited on top of a doped Si substrate covered by 90nm of thermally grown SiO_2 and located by Raman spectroscopy and contrast comparison. The layer is connected with Ti/Au pads. The Hall bar geometry (three pairs of graphene voltage probes) was patterned by Ar:O_2 plasma etching through an electronic beam lithographically defined polymer mask. The doped Si substrate when polarised by the voltage V_g is used as an electrostatic back gate enabling to vary the carrier density n_s as $dn_s/dV_g \approx 2.4.10^{11}$ cm^{-2}/V.

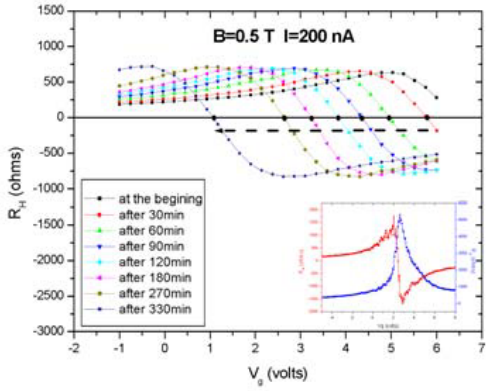

Fig.1 Displacement of the neutrality point during the cleaning process. Insert: R_{xx} and R_H *vs.* V_g. at B=0.5 T and T=1.3 K.

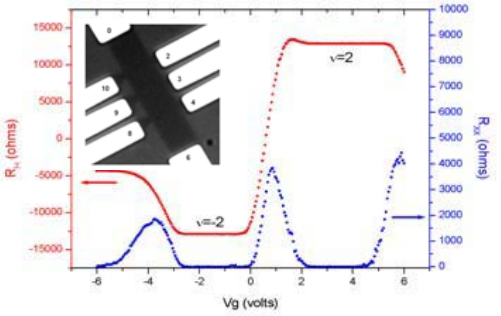

Fig.2 R_{xx} and R_H *vs.* V_g at B=11.7 T and I=200 nA. Insert: optical image of the 13µm long and 3µm wide Hall bar.

Thanks to annealing around 130°C, the graphene layer was progressively cleaned from impurities. Fig. 1 shows the real-time monitored displacement towards small gate voltage V_g of the neutrality point during the heating process. When varying V_g, R_H exhibits half-integer QHE and notably well quantized ν=±2 plateaus for electrons and holes at 1.3 K and a density of magnetic flux B=11.7 T (Fig. 2). The electronic mobility is around 9000 cm^2/(V.s) at n_s=6.10^{11} cm^{-2}. Using a three-terminal measurement technique, the resistance of the contacts was found as low as 10 Ω for electrons doping and 20 Ω for holes doping. The resistance values of the R_{xx} minima measured around ν=2 amount to ≈100 mΩ for a current lower than 1µA: the dissipation level in such a sample is low enough to consider quantization tests using a resistance bridge based on a cryogenic current comparator.

References

1. Novoselov *et al.*, Science **315**, 1379 (2007)
2. Jeckelmann *et al.*, IEEE Trans. Instru. Meas. **50**, 218 (2001)

Ground state phase diagram of graphene in a high Landau level

Tatsuya Higashi and Naokazu Shibata

Department of Physics, Tohoku University, Sendai, 980-8578, Japan

Keywords: graphene, phase diagram, strong magnetic field, DMRG

Graphene, a single atomic layer of graphite, has a honeycomb lattice structure with two carbon atoms in a unit cell. Because carbon atoms form two triangular sublattices, the electron wave function consists of two components. In a perpendicular magnetic field, the wave function in the *N*th Landau level of graphene consists of standard Landau wave functions of a conventional 2D system with Landau index N and $N-1$.

The Landau levels of graphene and the typical energy of the Coulomb interaction between electrons are both proportional to $\sqrt{B}$, where B is the strength of the magnetic field. Thus, the ratio between these energies does not depend on B. In the first few Landau levels, the Landau level separations exceed the typical Coulomb energy, $e^2/\varepsilon l$, where l is the magnetic length. Therefore, one can project the Coulomb interaction between electrons onto the topmost, partially filled, Landau level. Reflecting the form of the eigenfunctions in the $N(\neq 0)$th Landau level of graphene, the effective Coulomb interaction is strongly modified from that of the conventional 2D system, and it is a "mixture" of the effective Coulomb interactions in the *N*th and $N-1$th Landau levels of the conventional 2D system.

In a high Landau level of the conventional 2D system, the charge density waves called stripes and bubbles are realized in the ground state. In the $N=1$ Landau level of the conventional 2D system, it has been suggested that a liquid type ground state is realized at some filling factors.

In the present study, the ground state of graphene in the Landau levels of $N=2$, 3 is examined at various fillings by the density matrix renormalization group (DMRG) method on the torus geometry. In the DMRG method, we can exactly treat the many-body Coulomb interaction. Thus, we can take into account of the effects of quantum fluctuations which are neglected in the HF approximation [1]. Moreover, we can treat large systems beyond the limitation of the exact diagonalization by the restriction of the basis states. By analyzing the pair correlation functions of large systems, we can determine the ground state phase diagram accurately.

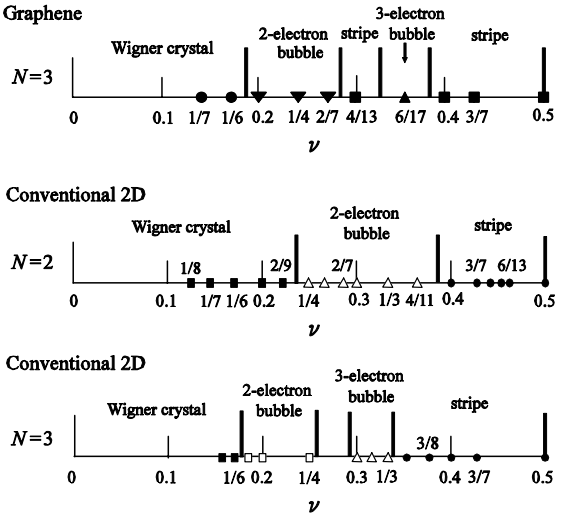

Fig.1 The ground state phase diagram for the N=3 Landau level of graphene (present study) and for the N=2, 3 Landau levels of the conventional 2D system [2].

Reference

1. C. -H. Zhang and Y. N. Joglekar, Phys. Rev. B **75**, 245414 (2007).
2. D. Yoshioka and N. Shibata, Physica E **12**, 43 (2002).

Pseudo-zero-mode Landau levels and pseudospin waves in bilayer graphene

K. Shizuya

Yukawa Institute for Theoretical Physics, Kyoto University, Kyoto 606-8502, Japan

Keywords: Graphene, bilayer, quantum Hall effect, collective excitations

Graphene attracts a great deal of attention, both experimentally and theoretically, for its unusual electronic transport. Of particular interest is bilayer graphene [1], which has a unique property that the energy gap between the conduction and valence bands is controllable [2] by use of external gates or chemical doping.

The presence of the zero(-energy)-mode Landau levels is a feature specific to graphene in a magnetic field. Bilayer graphene supports eight such zero-energy Landau levels, which, as a tunable band gap develops, split into two nearly-degenerate quartets separated by the band gap. The degeneracy of this quartet has a topological origin and derives from a nonzero index of the bilayer Hamiltonian.

At the EP2DS conference I would like to report, on the basis of our recent papers [3,4], some unusual properties of such an isolated quartet of pseudo-zero-mode levels, especially, coherence and collective excitations in the presence of an in-plane electric field and the Coulomb interaction. We focus on revealing further controllable features in bilayer graphene and point out the following:

(1) The pseudo-zero-mode levels, especially at half filling, support, via orbital level mixing, charge carriers with nonzero electric dipole moment. As a result, fine splitting of the pseudo-zero-mode quartet is also externally controlled by an in-plane electric field or by an injected Hall current; see Fig. 1. It will be possible to observe this field-induced level gap via the quantum Hall effect with a suitably strong injected current; one would be able to resolve the $\nu = \pm 2$ Hall plateaus thereby.

(2) The Coulomb interaction enhances the effect of the in-plane field and their interplay leads to rich spectra of collective excitations, pseudospin waves, accessible by microwave experiments. We construct a low-energy effective theory of pseudospin waves, study their microwave response, and note a duality in the excitation spectrum.

A direct experimental study of the excitation gap $M_{\mathbf{p}=0}$ and its field dependence by microwave absorption or reflection would clarify the unique controllable features of the pseudo-zero-mode sector in bilayer graphene,

References

[1] E. McCann and V. I. Fal'ko, Phys. Rev. Lett. **96**, 086805 (2006).

[2] T. Ohta, *et al.*, Science **313**, 951 (2006).
E. McCann, Phys. Rev. B **74**, 161403(R) (2006).
E. V. Castro, *et al.*, Phys. Rev. Lett. **99**, 216802 (2007).

[3] T. Misumi and K. Shizuya, Phys. Rev. B **77**, 195423 (2008).

[4] K. Shizuya, preprint arXiv:0901.2803, to appear in Phys. Rev. B.

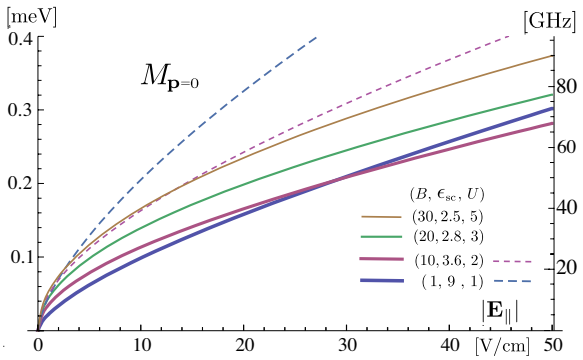

Figure 1: Pseudospin-wave excitation gap $M_{\mathbf{p}=0}$, in units of meV and GHz, plotted as a function of the in-plane field $|E_\parallel|$ for some typical values of magnetic field B[T] and band gap U[meV]. Dashed curves refer to the cases where the screening effect is turned off, $\epsilon_{sc} \to 1$.

Quantum transport of massless Dirac fermions in graphene

Kentaro Nomura[1], Shinsei Ryu[2], Mikito Koshino[3], Christopher Mudry[4], and Akira Furusaki[5]

[1] *Department of Physics, Tohoku University, Japan*

[2] *Department of Physics, University of California, Berkeley, USA*

[3] *Department of Physics, Tokyo Institute of Technology, Japan*

[4] *Condensed Matter Theory Group, Paul Scherrer Institute, Switzerland*

[5] *Condensed Matter Theory Laboratory, RIKEN, Japan*

Keywords: Graphene, Dirac fermion, Localization, Quantum Hall effect

Graphene is a two-dimensional carbon material with a honeycomb lattice structure and a Dirac-like (relativistic) electronic low-energy excitation spectrum. Quantum transport in graphene is exotic in many respects. For example, graphene realizes a relativitic quantum Hall effect. Furthermore, the physics of Anderson localization in graphene is remarkably rich and subtle. We have undertaken numerical studies of the conductivity tensor of disordered two-dimensional massless Dirac fermions.[1,2] When the potential induced by the impurities varies very slowly relative to the lattice spcacing, we observe that the conductivity increases with system size. We argue, based on spectral flows under twisting boundary conditions, the absence of Anderson localization for the stationary states of the massless Dirac equation perturbed by smooth disorder. Correspondingly, in a perpendicular magnetic field, we show that the quantum Hall phases with \sigma_xy=\pm 1/2 [e^2/h] (per valley and per spin) -- the hallmark of the relativistic Dirac spectrum, survive in the limit of weak magnetic fields, provided intra-valley scattering dominates. Conversely, we recover the minimal conductivity at the charge neutral Dirac point that has been observed experimentally, when inter-valley scattering becomes sizable.

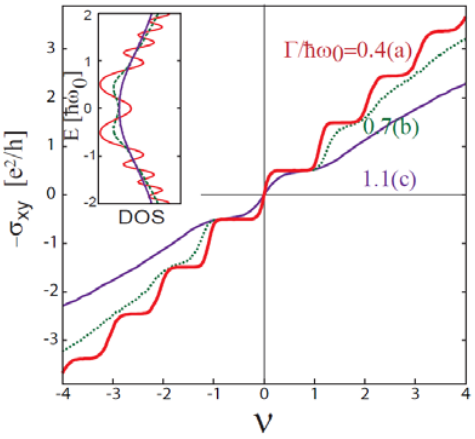

Fig.1 Quantized Hall conductivity of massless Dirac fermions. σxy/[e^2/h]=1/2, and -1/2 plateaus survive even in the strong disorder limit (weak field limit).

[1] K. Nomura, M. Koshino, S. Ryu, Phys. Rev. Lett. 99, 146806 (2007).

[2] K. Nomura, S. Ryu, M. Koshino, C. Mudry, A. Furusaki, Phys. Rev. Lett. 100, 246806 (2008).

Generation and Manipulation of Spin Current in Graphene Nanodisks

Motohiko Ezawa
Department of Applied Physics, University of Tokyo, Tokyo Japan

Keywords: 85.75.-d Magnetoelectronics; spintronics: devices exploiting spin polarized transport or integrated magnetic fields . 81.05.Uw Carbon, diamond, graphite . 73.63.Kv Quantum dots

Graphene nanostructure such as graphene nanoribbons and graphene nanodisks[1, 2, 3] could be basic components of future nanoelectronic and spintronic devices. Nanodisks are nanometer-scale disk-like materials which have closed edges. There are varieties of nanodisks, among which zigzag trigonal nanodisks with size N are prominent because they have N-fold degenerated zero-energy states[1]. It has been shown[1] that spins make a ferromagnetic order and that the relaxation time is finite but quite large even if the size N is very small. This property is referred to as quasi-ferromagnet. Furthermore, a nanodisk behaves as if it were a quantum dot with an internal degree of freedom, where the conductance exhibits a peculiar series of Coulomb blockade peaks[2].

In this work, we make an investigate on the spin-filter effect and its application in the system made of nanodisks and leads[3]. First of all, we can generate a spin current by applying a non-polarized current into a nanodisk due to the spin filter effect. A novel feature of the nanodisk spin filter is that its spin itself can be controlled by the spin current. Namely, it is possible to manupilate the spin current by using nanodisks. We propose some applications for spintronics, such as spin memory, spin amplifier and spin diode.

Spin memory: Since the life time of the nanodisk quasi-ferromagnet is very long compared to the size, we may use the nanodisk spin as an information. We can read-out this information by applying a spin-unpolarized current. The outgoing current from a nanodisk is spin-polarized to the direction of the nanodisk spin. Thus we can obtain the information of the nanodisk spin by observing the outgoing current. Finally, the direction of the nanodisk spin can be controlled by applying a spin-polarized current into the nanodisk. Thus, the nanodisk spin satisfies the conditions as a memory device. The important point is that the size is of the order of nanometer, and it is suitable as a nanodevice.

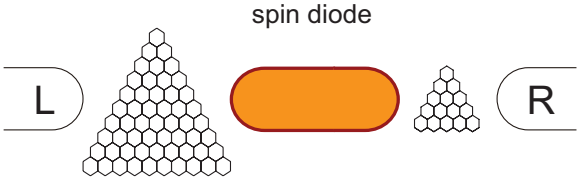

Figure 1: Illustration of spin diode made of two nanodisks with different size. By controlling the bias voltage, the current flows from the left lead to the right lead, or in the opposite way. The incoming current is unpolarized, which is made polarized by the first nanodisk. The electron spin in the central lead is rotated by the Rashba-type interaction.

Spin amiplifier: It is argued that a spin current is reinforced by feeding it into a nanodisk spin amplifier. Spin amplifier is very important because the signal of spin will easily suffer from damping by disturbing noise in leads. By amplifying the signal we can make circuits which are strong against noises.

Spin diode: We can construct the system acts as a rectifier so that the up-spin current flows from the left to the right, or the large nanodisk to the small nanodisk. We may call it ”spin diode”.

We note that spin valve and spin-field-effect transistor are similarly constructed from graphene nanodisks as simple generalization of similar quantum dots. Graphene nanodisk as well as graphene nanoribbon would be a promising candidate of future electronic and spintronic nanodevices.

References

[1] M. Ezawa, Phys. Rev. B 76, 245415 (2007).

[2] M. Ezawa, Phys. Rev. B 77, 155411 (2008).

[3] M. Ezawa, Eur. Phys. J. B 67, 543 (2009).

Coulomb versus spin-orbit interaction in carbon-nanotube quantum dots

Andrea Secchi* and Massimo Rontani**

** CNR-INFM S3 and Dipartimento di Fisica, Università degli Studi di Modena, Modena, Italy*

*** CNR-INFM Research Center S3, Modena, Italy*

Keywords: carbon nanotube, quantum dot, spin-orbit coupling, Wigner molecule

Quantum dots (QDs) in carbon nanotubes (CNs) are promising candidates for the realization of novel spintronics devices. Recent high-resolution tunneling spectra from the Cornell group [1] have shown that QD levels are strongly affected by spin-orbit interaction as well as spin and orbital degrees of freedom are entangled. These relevant findings pave the way to the all-electrical control of spins in CN QDs. Further, on the basis of peculiar features of the spectra, two-electron states were explained entirely in terms of an independent-particle picture [1]. This is intriguing, since other recent experiments [2] have shown the formation of strongly correlated states in CNs, such as the one dimensional Wigner crystal and the Mott insulating state, where the independent-particle model breaks down.

In order to gain insight into the above results, we have performed extensive numerical configuration interaction (CI) calculations [3] for few-electron states in CN QDs. Our model accurately treats Coulomb interaction, taking into account both intra- and inter-valley forward and backward scattering processes, as well as spin-orbit interaction. We are able to quantitatively reproduce the spectra of Ref. [1], e. g. the two-electron ground state transition at a finite value of the axial magnetic field (cf. Fig. 1).

We demonstrate that the two states on both sides of the transition are strongly correlated and are close to the "Wigner molecule" regime of electron localization in space. On the other hand, such states have the same orbital part of the wave function and different isospin projection, where the isospin quantum number is defined by the population of valleys K and K'. This explains the non-interacting feature of the tunneling spectrum, since the energy splitting of the states at zero field is only dictated by spin-orbit interaction. We further predict that the pattern of the spectrum for two electrons is not universal and may be dramatically affected by Coulomb interaction. This may be tested experimentally e.g. by changing the gate potential which defines the QD.

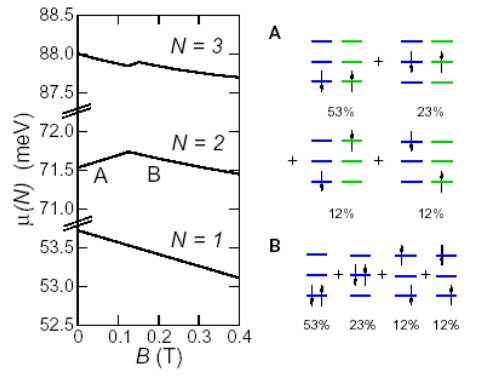

Fig.1 Left: Calculated chemical potential vs *B* up to three electrons. Right: Main configurations contributing to the two-electron states A and B. Blue (green) level ladders are harmonic oscillator states in the K (K') valley. The percentages are the weights of the Slater determinants in the CI expansion of the correlated wave function.

References

1. F. Kuemmeth *et al.*, Nature (London) **452,** 448 (2008).

2. V. V. Deshpande and M. Bockrath, Nature Phys. **4,** 314 (2008); V. V. Deshpande *et al.*, Science **323,** 106 (2009).

3. M. Rontani *et al.*, J. Chem. Phys. **124,** 124102 (2006).

Gate-controlled magnetoresistance effect in graphene spin-valve devices

S. Masubuchi*, M. Ono*, and T. Machida*,**

* *Institute of Industrial Science, University of Tokyo, Japan*

** *Institute for Nano Quantum Information Electronics, University of Tokyo, Japan*

Keywords: graphene, spin transport

We study gate-controlled magnetoresistance (MR) effect in graphene and graphene nanoribbon spin-valve devices. In the earlier works, the origin of the gate dependent MR has been unclear [1,2], which is in contrast to the case of carbon nanotube spin-valve devices [3]. In this work, by comparing the oscillation period of MR effect and that of the conductance due to Fabry-Perot (FP) interference, we will discuss the relation between these two phenomena.

Graphene flakes were fabricated by mechanical exfoliation of Kish graphite. The number of graphene layers was identified by the optical color contrast and the Raman spectrum. Ni ferromagnetic electrodes were defined by using the standard e-beam lithography and lift-off process. By applying an external magnetic field parallel to the easy axis of the electrodes, we measured MR traces for various gate voltages (V_G) at 4.2 K. Clear hysteretic MR curves with a positive sign (Fig. 1a) are observed at V_G = 31.85 V, whereas negative MR curves (Fig. 1b) are observed at V_G = 32.35 V. The amplitude of the MR signal periodically oscillates as a function of V_G. On the other hand, differential conductance dIdV oscillates as a function of V_G and source-drain bias I_{SD}. The oscillation is attributed to FP interference of electronic waves multiply reflected between the two graphene-metal interfaces. We will discuss the correspondence between these two phenomena.

References

1. N. Tombros *et al.*, Nature **448**, 571 (2007).
2. S. Cho *et al.*, Appl. Phys. Lett **91**, 123105 (2007).
3. H. T. Man *et al.*, Phys. Rev. B **73**, 241401 (R) (2006).

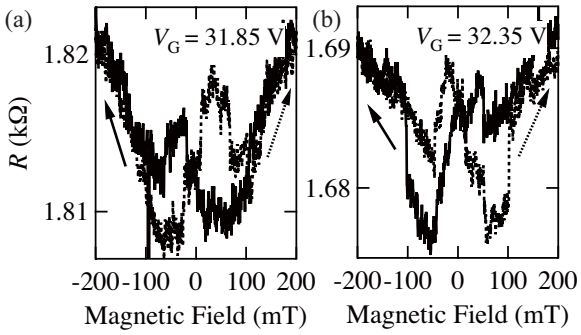

Fig. 1. Magnetoresistance traces measured at V_G = (a) 31.85 V and (b) 32.35 V at T = 4.2 K.

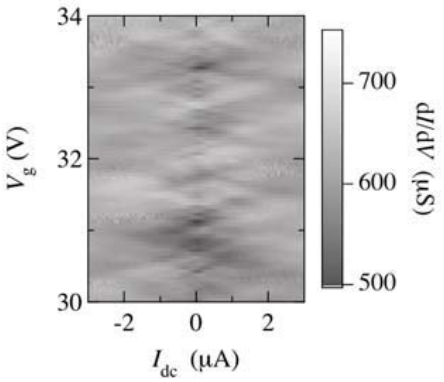

Fig. 2. Gray-scale plot of differential conductance dI/dV as a function of V_G and source-drain bias I_{SD} at T = 20 mK.

Spin-orbit interactions in graphene and zigzag ribbons

M. Zarea* and N. Sandler*

**Dept. of Physics and Astronomy, and Nanoscale and Quantum Phenomena Inst., Ohio University, Athens, OH. USA*

Graphene, Spin-orbit interactions, Graphene zigzag ribbons.

Spin-orbit interactions are expected to introduce new phenomena in the physics of graphene flakes and nanoribbons. In previous works, a new phase of matter, the Quantum Spin Hall (QSH) phase has been predicted as a result of the intrinsic spin-orbit (I-SO) interaction [1]. The phase, characterized by gapped bulk excitations and chiral spin-polarized edge states, is an example of a topological insulating phase. Further analysis of tight-binding models for graphene ribbons with armchair and zigzag terminations produced exact expressions for edge states and band-structures in this regime and allowed for a controlled treatment of unscreened Coulomb interactions[2].

The I-SO interaction is not, however, the only spin-orbit interaction affecting transport properties of graphene. In standard experimental setups, graphene flakes are positioned on top of substrates and the lack of inversion symmetry allows for Rashba spin-orbit (RSO) interactions to be present. As in semiconductors, RSO has the potential to generate spin-polarized currents in a controlled manner by applying external gate voltages. Therefore, it is important to understand its effect on graphene if the material is to be used in device applications.

We investigated the effects of RSO interactions on the electronic band-structure and corresponding wave-functions of graphene. By exactly solving a tight-binding model Hamiltonian we obtain band splittings -due to the $SU(2)$ spin symmetry breaking- that are accompanied by the appearance of *new* Dirac points as shown in Fig.1. These new points are originated by new valence-conduction band crossings and are located respecting the underlying lattice symmetry around the original points.

Zigzag ribbons are a special case of confined geometries because they have non-chiral, quasi-degenerate, low-energy edge states which are absent from graphene's band-structure. The RSO interaction lifts the spin-degeneracy of these bands by shifting the zero energy point and introduces a state-dependent spin separation in real space. A calculation for the average magnetization perpendicular to the ribbon plane suggests that RSO could be used to produce currents that are spin-polarized *on average*. Furthermore, we prove that, despite the unexpected dependence of transport characteristics on ribbon's width[3, 4, 5], the above properties remain valid for all ribbon sizes. These results are in contrast with those obtained with I-SO interactions where the real space spin distribution is not state dependent and the existence of the QSH phase depends on the ribbon width.

References

[1] C. L. Kane and E. J. Mele, Phys. Rev. Lett. **95**, 226801 (2005).

[2] M. Zarea and N. Sandler, Phys. Rev. Lett. **99**, 256804 (2007); M. Zarea, C. Büsser and N. Sandler, Phys. Rev. Lett. **101** , 196804 (2008).

[3] Z. Li et al., Phys. Rev. Lett **100**, 206802 (2008).

[4] A. R. Akhmerov et al., Phys. Rev. B **77**, 205416 (2008).

[5] M. Zarea and N. Sandler. To appear in Phys. Rev. B.

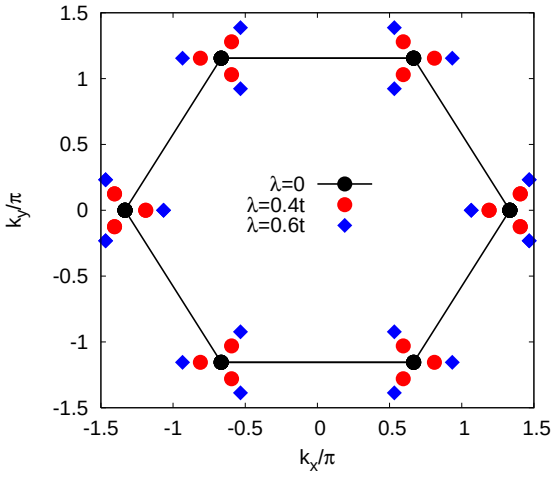

Figure 1: Positions of the new Dirac points for different values of the RSO coupling strength λ_R.

Spin blockade and Kondo physics in a carbon nanotube double quantum dot

S. J. Chorley*, M. R. Buitelaar*, A. L. Cantone*, G. A. C. Jones* and C. G. Smith*
*Department of Physics, Cavendish Laboratory, University of Cambridge, J J Thomson Avenue, Cambridge, CB3 0HE. United Kingdom

Keywords: Quantum dot, Spin blockade, Kondo effect, Carbon nanotube

Spin blockade in double quantum dots (DQDs) is an effect whereby certain transitions between spin states are suppressed by virtue of the Pauli principle. When the DQD contains a single unpaired electron on the right dot, the only (0,2) state available is a singlet (as the triplet is energetically inaccessible). At negative bias both the S(1,1) and T(1,1) states can fill but the T(1,1) state blocks further transport as it cannot transfer to S(0,2) without a spin flip and may not return to the lead, Figure 1(a). In the reversed bias case the dot only fills from the right lead in the S(0,2) state which may freely travel though the DQD via the S(1,1) state, Figure 1(b). Spin blockade has previously been reported and studied in a defect-defined DQD nanotube peapod device [1].

In this work we have fabricated a highly tunable DQD in a CVD grown single-walled carbon nanotube that shows both spin blockade and Kondo effect depending on the coupling to the leads. Gold is evaporated onto each end of the tube to form tunnelling contacts and aluminium-oxide/aluminium gate electrodes patterned near or on the tube to form plungers and the centre barrier. By varying the voltage on the doped silicon back-gate the DQD can be tuned from pinch-off through weak tunnel coupling to strong tunnel coupling. A schematic of the device is shown in the inset of Figure 1.

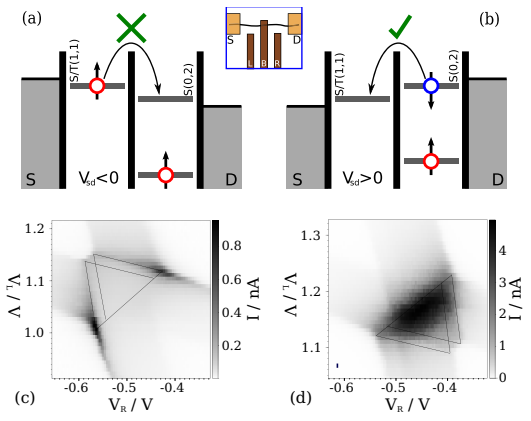

Figure 1: Inset: Device schematic. (a) DQD energy levels for spin blockade at negative bias. (b) No blockade at positive bias. (c) Triple point current for a bias and charge state configuration that leads to spin blockade. (d) The same triple point when not blockaded at positive bias; the total current is much larger.

When the device is tuned close to pinch-off, a DQD forms with a well-defined charge stability honeycomb diagram showing regularly spaced alternately suppressed and high-current triple points. Figure 1(c) shows a typical spin blockade triple point with current inside the bias triangles heavily suppressed, while Figure 1(d) shows the same point with the blockade lifted at positive bias.

The design of our device allows us to control the coupling between the two dots and track evolution of the spin blockade triple points from weak to strong tunnel coupling. We have also investigated how strong magnetic fields change the triplet states and shift spin-blockade from the negative to positive source-drain bias case. The strong co-tunnelling evident in the device allows the DQD detuning versus energy level diagram to be probed. The 'spin-funnel' in direct transport can be measured which shows mixing of singlet and triplet states which may be due to the hyperfine interaction or spin-orbit coupling.

At stronger lead couplings the DQD exhibits the Kondo effect. When there is a single unpaired electron on one dot a single Kondo ridge forms as the dot forms a spin singlet with its lead and the system behaves much like that of a single quantum dot. However, when each dot has an unpaired spin, there is competition between the Kondo effect and singlet-triplet exchange splitting which shows as a double resonance in the $\mathrm{d}I/\mathrm{d}V_{sd}$ curve.

References

[1] M. R. Buitelaar, *et al.* Phys. Rev. B **77**, 245439 (2008).

Dynamical properties of single carbon nanotube transistors

J. Chaste*, G. Fève*, T. Kontos*, J.-M. Berroir*, D. C. Glattli*,**, B. Plaçais*
*Laboratoire Pierre Aigrain, Ecole Normale Supérieure, 24 rue Lhomond, 75005 Paris, France
** Service de Physique de lEtat Condensé, CEA Saclay, F-91191 Gif-sur-Yvette, France

Keywords: MOSFET, carbon nanotube, shot noise, charge detection.

Carbon nanotube transistors constitute a unique model system for the study of quantum transport dynamics and its interplay with interactions. Using ultra small transistors with CVD grown carbon nanotubes, we have directly probed this dynamics with GHz measurements. From these we determine the transconductance and the gate capacitance which is a quantum capacitance in series with the geometrical capacitance. The ratio of the total gate capacitance to quantum capacitance defines the "so-called" Lüttinger parameter g of a quantum wire. In top-gated nanotubes, g can be varied in a broad range $g = 0.1$–1. Another contribution to the dynamics comes from the kinetic inductance of the channel which, in nanotubes, exceeds by three orders of magnitudes the geometrical inductance. Importantly for applications, this inductance, together with channel resistance, controls the transit time of electrons and therefore the transit frequency of transistors. In the one-dimensional nanotube system this contribution is very sensitive to electron-electron interactions which can be in turn controlled by top gate screening measured by the g factor. Multi-GHz dynamical properties combined with nanometer gate size place nanotube transistors in good position for fast charge detectors with a high-frequency sensitivity ultimately limited by shot noise.

The present contribution reviews the experimental results recently obtained in our group on the room temperature GHz properties of carbon nanotube transistors with long (3m) and short (0.3m) gates and a 6nm aluminium oxyde [1]. With these parameters, we estimate a $g \simeq 0.3$ for our devices. From the transconductance and gate capacitance of the diffusive long-gate devices we deduce an electron mobility of $3500\ \mathrm{cm^2V^{-1}s^{-1}}$ and a capacitance of $60\ \mathrm{aF}/\mu\mathrm{m}$ [1]. Correcting for this finite mobility effect, we can conclude that the transconductance of short-gate transistors is limited by time-of-flight effects to a transconductance of $\sim 25\ \mu\mathrm{S}$ in Fig.1. We propose a heuristic model based on the scattering theory approach

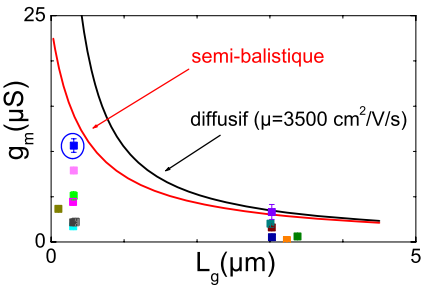

Figure 1: Transconductance of short and long carbon nanotube transistors as function of gate length. Data scattering is attributed to dispersion in the contact resistances. Dashed line is the $\mu = 3500\ \mathrm{cm^2V^{-1}s^{-1}}$ line. Solid line takes into account the time of flight of electrons under the gate.

in [2] adapted for nanotransistors which allows to calculate the transit frequency as function of electronic transmission D and screening (or g). The model predicts a time-of-flight limitation for $g \gtrsim D$ in agreement with our experiment. In addition we present extensive cryogenic measurements, in the 0.1–1 GHz bandwidth, showing the shot noise limitation of nanotube transistors. From the noise, the transconductance and the gate capacitance, we obtain a resolution of $30\ \mu\mathrm{e}/\sqrt{\mathrm{Hz}}$ for the nanotube transistor taken as a charge detector. It is a good premise for nanosecond single electron detection.

References

[1] J. Chaste, L. Lechner, P. Morfin, G. Fève, T. Kontos, J.-M., Berroir, D.C. Glattli, H. Happy, P. Hakonen, and B. Plaçais, Nanoletters **8**, 525 (2008).

[2] J. Gabelli, Fève, T. Kontos, J.-M. Berroir, B. Plaçais, D.C. Glattli, B. Etienne, Y. Jin, M. Büttiker, Phys. Rev. Lett. **98**, 166806 (2007).

Transport properties of guanine nucleotide-conjugated single-wall carbon nanotube field-effect transistor

J. S. Hwang*, H. T. Kim*, D. Ahn** and S. W. Hwang*

** TiNa and School of Electrical Engineering, Korea University, Seoul, Korea*

*** iQUIPS and School of Electrical and Computer Engineering, University of Seoul, Seoul, Korea*

Keywords: DNA, Transport, SWCNT, Transistor

Transport thru DNA molecules has been an interesting topic [1]. Here, we have conjugated guanine nucleotide (poly(dG)) to single-wall carbon nanotube (SWCNT) field-effect transistors (FETs) and investigated the electrical transport properties.

The inset of Fig. 1 shows the schematic structure of poly(dG)-conjugated SWCNT FET. The conjugation process was simply done by applying a drop of poly(dG) (60 bases, Cosmo Genetech) solution on the SWCNT (HiPco, CNI) FET for 1 min and rinsing with deionized water. SEM and TEM images of the SWCNT FET device are shown in the insets of Fig. 2. Figure 1 shows the transport characteristics of the SWCNT FET device before and after poly(dG) conjugation. Both FETs show nonlinear source-drain current (I_{sd}) - source-drain voltage (V_{sd}) characteristics which are originated from the potential barriers between SWCNT and Ti/Au metal electrodes. On the other hand, the zero-bias conductance is decreased dramatically from 75 to 19 nS after conjugation. We have observed such considerable, conjugation-induced decreases (mostly more than 50%) in I_{sd} of several other samples. This observation is similar to our previous results for the conjugation of cytosine nucleotide (poly(dC)) [2]. The decrease of the conductivity by conjugation cannot be explained by simple electrostatics of the negative charged poly(dG). It requires the modulation of the band structure of SWCNT due to surface binding.

Figure 2 shows the I_{sd} - gate voltage (V_g) characteristics of the SWCNT FET before and after poly(dG) conjugation. Both I_{sd}-V_g curves exhibit hole conduction behaviour like usual SWCNT FETs. It is observed that the slope of dI_{sd}/dV_g is decreased after conjugation, suggesting the decrease of the hole mobility. More quantitative analysis regarding the estimation of the hole mobility and detailed comparison with the case of poly(dC) will be presented.

References

1. J. S. Hwang, K. J. Kong, D. Ahn, G. S. Lee, D. J. Ahn, and S. W. Hwang: Appl. Phys. Lett. **81** (2002) 1134.

2. J. S. Hwang, H. T. Kim, M. H. Son, J. H. Oh, S.W. Hwang, and D. Ahn, Physica E **40**, 1115 (2008).

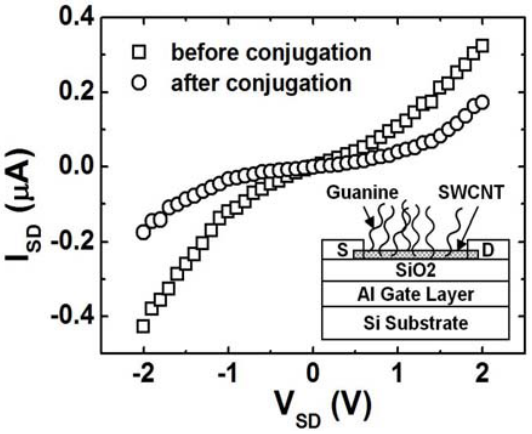

Fig.1 I_{sd}-V_{sd} characteristics of the SWCNT FET before and after conjugation. Inset shows a schematic structure of the SWCNT FET.

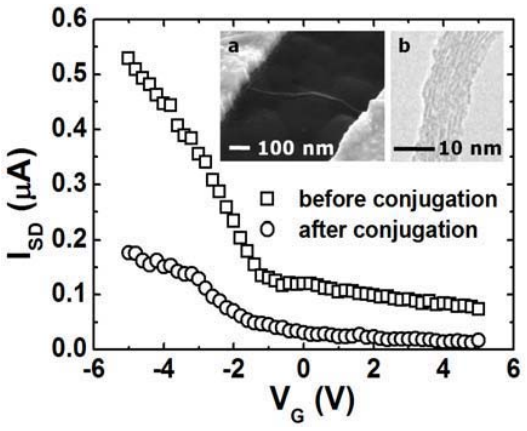

Fig.2 I_{sd}-V_g characteristics of the SWCNT FET before and after conjugation. Insets show (a) SEM and (b) TEM images of the SWCNT FET.

Epitaxial growth of vertically aligned MgZnO nanowire/nanowall network structures by MOCVD

Dong Chan Kim*, Cheol Hyoun Ahn, Bo Hyun Kong, and Hyung Koun Cho

** School of Advanced Materials Science and Engineering, Sungkyunkwan University, Korea*

Keywords: MgZnO nanowires, network structures, MOCVD

Nanostructures have become one of the most intensively studied subjects over the last few decades because of their potential applications to electronic and photonic devices [1,2]. Among the nanostructures, low-dimensional ZnO nanowires have been the subject of intense research for applications in short-wavelength light-emitting devices and ultraviolet field emitters on account of their wide band gap and high exciton binding energy, which can allow the production of devices with a performance relatively unaffected with temperature [3,4]. Studies regarding two-dimensional (2D) ZnO nanostructures including nanowalls and nanosheets are less common compared to the number of reports regarding 1D ZnO nanostructures. The potential of applications in chemical and biological sensors, energy-storage devices, and solar cells is high due to the high surface-to-volume ratio of 2D ZnO nanostructures. Also, the vertically aligned one-dimensional (1D) ZnO nanowires are more suitable structures for the fabrication of electronic devices, considering the interconnection of a metal layer and the feasibility of integration processes. But, the vertically aligned nanowalls or nanowires have a detrimental effect on the performance of field emitters due to the blunt tip shape and electric arcing.

In this work, we investigated epitaxial growth and luminescent properties of vertically aligned MgZnO nanowire/nanowall network structures by catalyst-free metalorganic chemical vapor deposition (MOCVD). Mg was used for decentralization of MgZnO network structures. MgZnO network structure on substrate was dispersed according to Mg introduction as shown Fig. 1. The width in the top region and aspect ratio of the MgZnO nanowires on nanowall were ~ 4 nm and 620, respectively. More importantly, these vertically aligned MgZnO networks have good crystal and optical quality. According to the previous report, the incorporation of small quantity Mg atoms in the ZnO matrix can enhance the emission efficiency and an increase in synthesis temperature can improve the crystalline quality and luminescence intensity. Therefore, it provides the opportunity to study the luminescent properties about each parts of nanowire and nanowall.

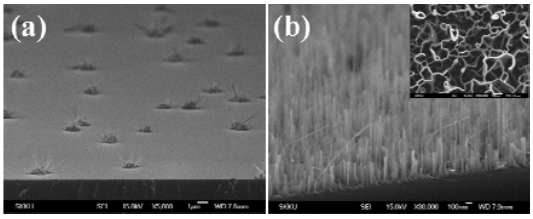

Fig.1 Cross-sectional FESEM images of (a) ZnO and (b) vertically aligned MgZnO nanowire/ nanowall network structure by MOCVD. The inset in (b) shows the plan-view FESEM image of MgZnO network structure.

References

1. L. Pavesi, D. L. Negro, C. Mazzoleni, G. Franzo, and F. Priolo, Nature **408**, 440 (2000).
2. Y. Liu, J. A. Zapien, Y. Y. Shan, C. -Y. Geng, C. S. Lee, and S. -T. Lee, Adv. Mater. **17**, 1372 (2005).
3. W. I. Park and G. -C.Yi, Adv. Mater. **16**, 87 (2004).
4. X. W. Sun, J. Z.Huang, J. X. Wang, and Z. Xu, Nano Lett. **8**, 1219 (2008).

Observation of type II excitons in carbon nanotubes

T. Schuettfort, A.Nish, and R. J. Nicholas

* *Clarendon Laboratory, University of Oxford, Oxford, OX1 3PU, UK,*

Keywords: carbon nanotubes, excitons

We report the study of the excitonic band gaps of carbon nanotube (CNT) polymer composites formed from a number of different polymers which are used to wrap the nanotubes to form soluble nanostructures. We have studied semiconducting polymers such as P3HT which are common building blocks used for the formation of Photovoltaic cells. The combination of polymers with CNT leads to the formation of nanostructures in which the excitonic states are modified by the the polymer semiconductor which is shown to form a nanostructure with typical dimensions of 2-3nm diameter and with lengths of order 1 micron.

By the use of photoluminescence excitation mapping we are able to map both the E11 and E22 band gap energies for many different nanotube species. Previous work using larger band gap polymers with larger work functions has deduced changes to the excitonic band gaps of order 20 meV caused by the dielectric constant of the cladding polymer which has been assumed to act as an electron and hole barrier. In the present case the use of P3HT which has a significantly smaller band gap and higher lying valence band (HOMO level) is thought to lead to the formation of a type II (lowest electron and highest hole levels located in different materials) excitonic structure as predicted by Kanai and Grossman (Nano Lett. **8**, 908 (2008)) in which the hole wavefunction can show significant charge transfer into the cladding layer. As a result of this we observe very large band gap shifts of up to 60 meV for both the E11 and E22 energy band gaps.

The ability to form both type I and type II excitonic structures in polymer CNT composites has significant implications for the production of organic photovoltaic cells and emission devices, since this should enable significant changes in charge separation and recombination to the engineered through the formation of different structures.

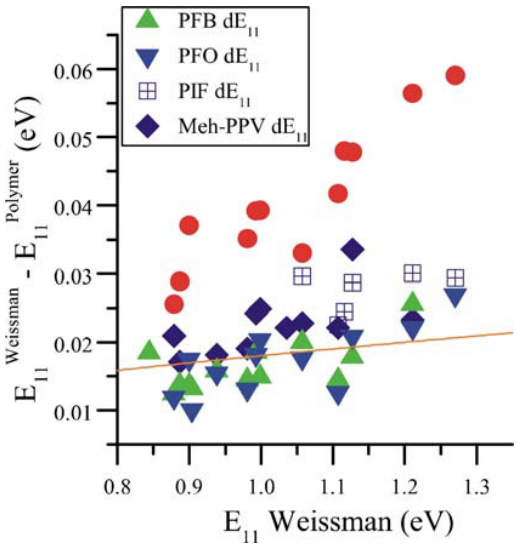

Fig 1. Excitonic band gap shift for a series of carbon nanotube/polymer nanostuctures as a function of the nanotube band gaps for a series of different polymers.

Tunable semiconducting state in bilayer graphene

H. Miyazaki[A,B], K. Tsukagoshi[A,B,C,D], and A. Kanda[B,E]

[A]*AIST,Tsukuba, Japan*

[B]*CREST, JST, Kawaguch, Japan*

[C] *MANA, NIMS, Tsukuba, Japan*

[D]*RIKEN, Wako, Japan*

[E]*Inst. of Physics and TIMS, Univ. of Tsukuba, Tsukuba, Japan*

Keywords: Graphene, band gap, field effect transistor

Inducing band gap in graphene is one of the most important key challenges for graphene electronics. We show an experimental result band gap with several hundreds of meV in bilayer graphene under gate electric field of ~1 V/mn.

We investigate the transport properties of bilayer graphene gated by top and back gate. Highly doped Si substrate is used as the back gate, and Al electrode deposited on graphene is used as the top gate (inset in Fig.1) [1].

The resistance of the bilayer graphene shows ambipolar change with *p*-type and *n*-type conduction depending on the gate voltages. A conductance minimum occurs at the transition from *p*-type to *n*-type conduction. The minimum G_{min} is diminished by a gate electric field which is applied by a bias voltage between the top and the back gate. With the diminishment of the G_{min}, non zero top gate voltage change ΔV_{tg} becomes necessary to switch the graphene channel from *p*-type to *n*-type. This evidences the existence of the band gap, $\Delta_{gap}=e\alpha\Delta V_{tg}$, where α is the gate efficiency factor of the top gate (Fig. 1). Typical value of ΔV_{tg} is 0.5 V at the gate electric field of 1.4 V/nm. The α is given by the ratio of the top gate capacitance C_{tg} to the total capacitance $C_{\Sigma}\sim C_{tg}+C_{bg}$ (C_{bg}: the back gate capacitance) of the channel, $\alpha\sim C_{tg}/(C_{tg}+C_{bg})=0.99$. Thus the corresponding band gap is about 0.5 eV. Such band gap is also supported by the temperature dependence of G_{min}, which is fitted well by the summation of two Arrhenius terms. This suggests that there are two parallel conduction mechanisms with different thermal activation energies. We infer that the each activation energy is related to intrinsic band conduction by thermally exited carriers for the larger one, and hopping conduction via localized states for smaller one [2]. Typical value of the larger activation energy is ~0.1 eV, which supports the existence of the band gap in the order of hundreds of meV. We also found a trend that samples with larger mobility have larger band gap. This suggests that quality of the graphene film is important to induce band gap.

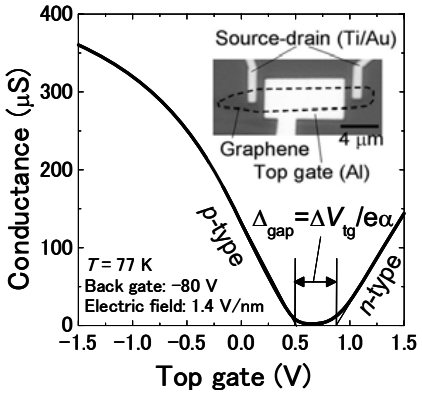

Fig.1 Conductance of a bilayer graphene under the electric field of 1.4 V/nm as a function of the top gate voltage. Inset shows an optical image of a graphene sample with top gate, source, and drain electrodes.

References

1. H. Miyazaki, S. Odaka, T. Sato, S. Tanaka, H. Goto, A. Kanda, K. Tsukagoshi, Y. Ootuka, Y. Aoyagi, *Appl. Phys. Exp.* **1**, 034007 (2008).

2. J. B. Oostinga, H. B. Heersche, X. Liu, A. F. Morpurgo, and L. M. K. Vandersypen, *Nat. Mater.* **7**, 151 (2007).

Low temperature scanning probe imaging of electronic transport in graphene nanostructures

J. Berezovsky* and R. M. Westervelt*

**Department of Physics, and School of Engineering and Applied Sciences, Harvard University, Cambridge, Massachusetts*

Keywords: graphene, transport, scanning probe microscopy

Experiments on the transport properties of graphene over the last several years have revealed numerous unusual and fascinating results. Exploration of these phenomena with high spatial resolution promises to reveal further information about the flow of charge carriers in graphene devices, and the dependence of these effects on microscopic structure. As was previously observed in GaAs two-dimensional electron gas transport[1], the ability to image the flow of charge carriers can provide a window into behavior often unimagined in bulk measurements.

Here we use a similar scanning gate technique to image the transport properties in graphene nanostructures at 4 K with a spatial resolution of $\sim$ 20 nm. For example, Figure 1 shows the fractional change in resistance of a graphene Hall bar as a conducting tip is scanned above it. The Hall bar, defined via electron beam lithography and oxygen plasma etching, is situated between six metal leads indicated by the dashed lines. The close-up region, measured under similar conditions and with the tip $\sim$ 10 nm above the surface, shows fluctuations in the resistance with size scales likely limited by the radius of the tip ($\sim$ 20 nm).

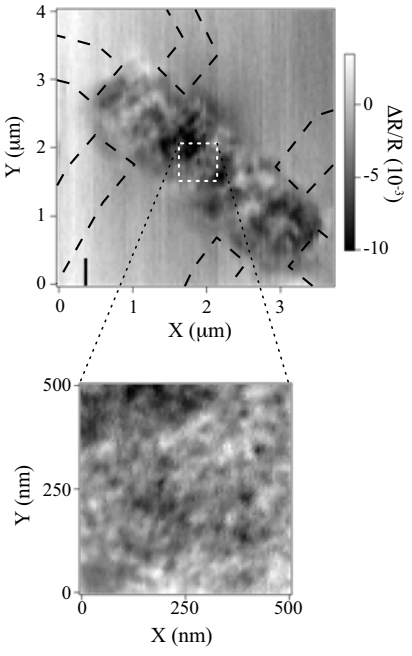

Figure 1: Top: Image of the fractional change in resistance of a graphene Hall bar due to a conductive tip scanned above the surface. Dashed lines indicate the position of metal contacts. Bottom: Zoom in on the indicated region under similar conditions.

This technique allows us to map out the effect of the tip potential on the diffusive transport though graphene. By varying the voltage on the tip, and by sweeping the overall charge density using a back gate, we obtain information about the non-uniform potential seen by the graphene layer due to charged impurities on the surface, in the substrate, or possibly due to strain variations. Additionally, these results can be compared to theory for conduction through this potential landscape, providing information about the mesoscopic transport properties of graphene.

This same measurement may also be performed on a variety of graphene nanostructures, such as nanoribbons or nanoconstrictions. Narrow constrictions in graphene are known to produce a transport gap that depends on the width of the structure, and is predicted to depend on the specific crystal orientation. By investigating such devices with a scanned gate, this transport gap may be probed locally with high spatial resolution, and could also provide a means of imaging the coherent flow of carriers in a graphene structure.

References

[1] M. A. Topinka, Physics Today **56**, 47 (2003).

Picosecond Photocurrent Spectroscopy of Carbon Nanotubes

L. Prechtel*,**, L. Song,**, S. Manus**, D. Schuh***, W. Wegscheider***, and A.W. Holleitner*,**

** Walter Schottky Institut and Physik-Department, Technische Universitaet Muenchen, 85748 Garching, Germany.*

*** Center for NanoScience (CeNS), Ludwig-Maximilians-University, Geschwister-Scholl-Platz 1, 80539 Munich, Germany.*

**** Institut fuer Angewandte und Experimentelle Physik II, University Regensburg, Universitaetsstrasse 31, 93040 Regensburg, Germany.*

Keywords: ultrafast optoelectronics, carbon nanotubes.

Recently, we have demonstrated how to bind carbon nanotubes to photosynthetic proteins [1], to semiconductor nanocrystals [2], and to submicron graphite beads [3]. The exciton dynamics in such carbon nanotube devices can be detected in a time-resolved way by optical techniques such as the transient absorption technique [4] and the time-resolved photoluminescence spectroscopy [5]. Both methods focus mainly on the dynamics of charge carriers within the carbon nanotubes. Many questions remain concerning the separation and the transport of photo-generated charge carriers to source and drain leads. We address these questions by a novel ultrafast photocurrent spectroscopy, which is based on a common pump-probe technique [6]. The experimental setup with a picosecond time-resolution will be introduced, and first results of the time-resolved photocurrent of carbon nanotubes will be shown. We will discuss polarization and charge separation effects within the carbon nanotubes as well as the influence of hot phonons, the bath temperature, and the bias voltage on the photocurrent across carbon nanotubes.

We acknowledge financial support by the DFG excellence initiative “Nanosystems Initiative Munich” (NIM), the DFG project HO 3324/2 and Ho 3324/4, and the Center for NanoScience (CeNS) in Munich.

1. I. Carmeli, M. Mangold, L. Frolov, B. Zebli, C. Carmeli, S. Richter, and A. W. Holleitner, Adv. Mat. 19, 3901 (2007).
2. B. Zebli, H.A. Vieyra, I. Carmeli, A. Hartschuh, J.P. Kotthaus, A.W. Holleitner, arXiv:0807.2111.
3. Li Song, A.W. Holleitner, H. Qian, A. Hartschuh, M. Döblinger, E.M. Weig, J.P. Kotthaus, J. Phys. Chem. C 112, 9644 (2008).
4. Randy J. Ellingson et al., Phys. Rev. B 71, 115444 (2005).
5. A. Hagen et al., PRL. 95, 197401 (2005).
6. D.H. Auston, IEEE J-QE 19, 639 (1983).

Thermal conductivity of a large area graphene membrane

C. Faugeras*, M. Orlita*, M. Potemski*, R.R. Nair** and A.K. Geim**

** LNCMI-CNRS, Grenoble, France*

*** Department of Physics, University of Manchester, Manchester, United Kingdom*

Keywords: Graphene, Raman Scattering, Thermal properties

Graphene, a purely two-dimensional crystal of carbon atoms, has been argued to display an extremely high thermal conductivity, as high or even exceeding the one of diamond [1]. Nevertheless, probing the thermal properties of graphene remains a challenge because of the small size of available specimens.

Following recent report [1] we have further explored the micro-Raman technique to study the thermal conductivity of graphene. The studied sample consists of the graphene membrane, which fully covers the 40 µm diameter pinhole made in the 2mm high plate of copper. Edges of membrane are thermally contacted to cooper plate with silver epoxy. Focusing laser down to 2µm spot, the Raman scattering signal due to G-line of grapheme has been measured as a function of laser power and laser spot position across the membrane diameter, at ambient conditions. Local temperature of the laser spot has been traced by actual energy position of the G-line [2] and more directly by comparing the intensity of Stokes and anti-Stokes components.

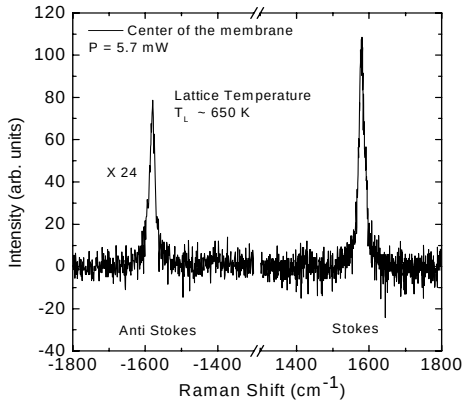

Fig.1 Stokes and Anti-Stokes Raman scattering spectra of graphene G-band measured in the center of the membrane at a power of 5.7 mW.

We present in Fig. 1 characteristic Stokes and anti-Stokes Raman scattering spectra of the G band phonons measured in the center of the membrane with an excitation power of 5.7 mW. This method allows extracting directly the local temperature without any assumption on the absorbed laser power and we find that the local increase in temperature can be as high as 355 K, leading to a lattice temperature of 650 K. This large increase in temperature is mainly due to the fact that heat flow in the present experiment can only occur in two dimensions. When moving the laser spot across the membrane diameter, the induced rise in temperature is then reduced as the excitation laser spot approaches the edge of the membrane which acts as a perfect heat sink at the room temperature (293 K) as no measurable shifts of G band phonons for similar laser powers have been observed outside the suspended regions.

Based on finite elements simulations, we deduce the thermal conductivity of this large graphene membrane considering the temperature profile at constant excitation power. We then discuss the different values for the heat conductivity obtained according to the possible assumptions concerning the laser power absorbed by the membrane in our experimental geometry which only allows a single pass of the laser through the membrane and we compare them to recently reported values [1].

References

1. A.A. Balandin *et al*, Nanoletters **8**, 902, (2007).
2. I. Calizo *et al*, Nanoletters **7,** 2645, (2007)

Photo-excited carriers and optical conductance and transmission in graphene in the presence of phonon scattering

H.M. Dong*, W. Xu*,**, and Z. Zheng*
*Key Laboratory of Materials Physics, Institute of Solid State Physics, Chinese Academy of Sciences, Hefei, China
**Department of Physics, Yunnan University, Kunming, China

Keywords: graphene, optic phonon, photon-excited carriers, optical conductance

Very recently, the study on optoelectronic properties of graphene has become a hot field of research. In particular, it is found that the universal optical conductance $\sigma_0 = e^2/4\hbar$ can be observed in the short wavelength regime ($\lambda < 2\ \mu m$) [1]. An optical absorption window can be observed when $4\ \mu m < \lambda < 50\ \mu m$ [2]. These important experimental discoveries have shed some lights on making better liquid crystal display (LCD) and graphene infrared photodetectors.

In this work, we investigate theoretically the effect of electron-photon-phonon scattering on optoelectronic properties of monolayer graphene. The valence-force-field model is employed to count carrier−LO-phonon interaction in graphene in which the LO-phonon energy is 196 meV [3]. We use the mass- and energy-balance equations derived from the Boltzmann equation to evaluate self-consistently the carrier densities, optical conductance and transmission coefficient in graphene in the presence of the linearly polarized radiation fields. We find the following important features. (1) The infrared radiation is able to vary significantly the carrier densities in graphene (see Fig. 1). The electron density can be increased up to 70%. (2) The universal optical conductance $\sigma_0 = e^2/4\hbar$ is observable when $\lambda < 2\ \mu m$ (see Fig. 2), where the light transmittance is about 0.97 - 0.98 (see insert in Fig. 2). (3) There is an optical absorption window in-between $4 - 100\ \mu$m (see Fig. 2). We find that such absorption window is induced mainly by competing processes of intra- and inter-band optical transitions which require different energies due to the Pauli bloke effect. The depth and the width of the absorption window depend on temperature and electron density (see Fig. 2). The features of (2) and (3) are in line with those obtained experimentally. The results obtained from this study can be applied to understand, reproduce and back-up the recent experimental findings.

References

[1] R.R. Nair *et al*, Science **320**, 1308 (2008).

[2] A.B. Kuzmenko *et al*, Phys. Rev. Lett. **100**, 117401 (2008).

[3] T. Ando, J. Phys. Soc. Jpn. **76**, 024712 (2007).

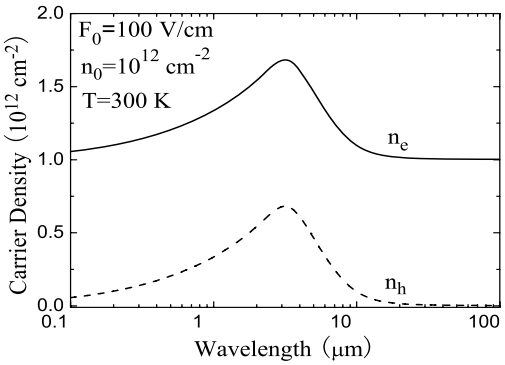

Figure 1: Photo-excited carriers (hole density n_h and electron density n_e) vs radiation wavelength. Here n_0 is the electron density in the absence of a radiation field and F_0 is the electric field strength of the radiation filed.

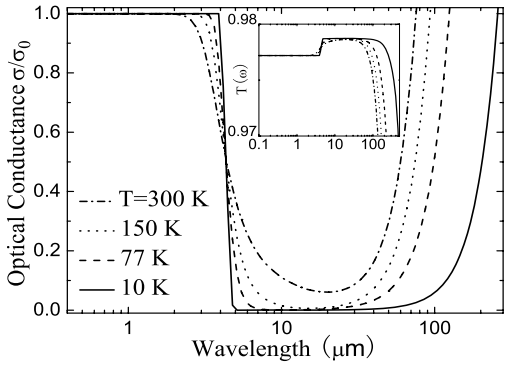

Figure 2: Optical conductance σ as a function of radiation wavelength at a fixed zero-field electron density $n_0 = 10^{12}$ cm^{-2} for different temperatures. Here $\sigma_0 = e^2/4\hbar$ is the universal optical conductance and the insert shows the corresponding transmission coefficient T(ω).

Molecular dynamics study of multi-walled carbon nanotubes under uniaxial loading

Yun-Che Wang*, †, Qu-Yuan Kuo*, Jian-Ming Lu**, Chi-Chuan Hwang***

** Department of Civil Engineering, National Cheng Kung University, Tainan, Taiwan*

*** National Center for High-Performance Computing, Sinshih, Tainan County, Taiwan*

**** Department of Engineering Science, National Cheng Kung University, Tainan, Taiwan*

Keywords: multi-walled carbon nanotube, Young's modulus, molecular dynamics, morphological deformation

The mechanical properties of carbon nanotubes are fundamental to obtain a thorough physical understanding of the nanotubes for future industrial applications. It is known that the Young's modulus of the nanotubes may be different when measured from bending [1], compression [2-3] or tension due to microstructural effects. Multi-walled carbon nanotubes possess another level of complexity due to the interactions between graphene shells [2-3]. In this work, we perform molecular dynamics (MD) simulations to study the mechanical properties of single-, double- and triple-walled carbon nanotubes under uniaxial loading in the MD time scales. A Tersoff-type potential [4] is adopted to describe the carbon-carbon interactions. Through compressive and tensile loading, it is obtained the relationship between strain energy and applied strain in both linear and nonlinear regimes. Hence, the Young's moduli, which are shown in Figure 1, of the nanotubes are determined from the curvature of the energy profile. For a given nanotube, the deviation of the calculated Young's moduli with respect to the pre-chosen strain ranges indicates the anharmonicity of the nanotubes. Theoretically, the Young's modulus is defined with respect to infinitesimal applied strain. The anharmonicity may be responsible for inherent time-dependent properties of the nanotubes. Furthermore, the weak interactions between shells of multi-walled carbon nanotubes are investigated, as well as effects of the number of boundary layers on linear and nonlinear mechanical behavior of the nanotubes. Although defects are not considered in the present study, it has been reported that residual defect-free morphological deformation may be the primary mechanism responsible for the cyclic failure of such nanotubes.

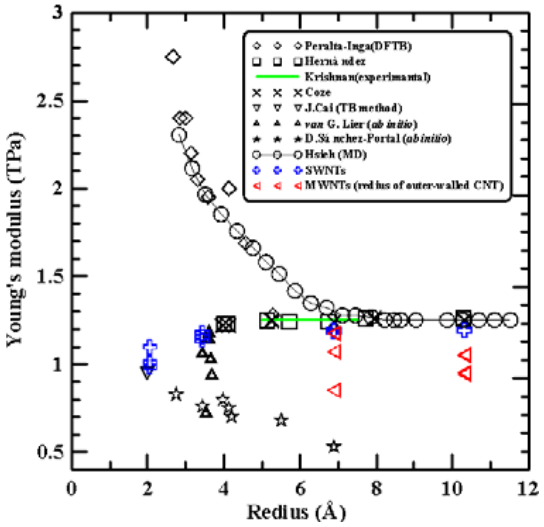

Fig. 1 The Young's modulus of the given carbon nanotube *versus* the radius of that. The present simulation results are indicated by the hollow crosses and the left triangles. Others were calculated by the former researchers.

References

1. J. Y. Hsieh, J. M. Lu, M. Y. Huang, and C. C. Hwang, Nanotechnol. **17**, 3920 (2006).
2. J. M. Lu, C. C. Hwang, Q. Y. Kuo, and Y. C. Wang, Physica E **40**, 1305 (2008).
3. J. M. Lu, Y. C. Wang, J. G. Chang, M. H. Su, and C. C. Hwang, J. Phys. Soc. Jpn. **77**, 044603 (2008).
4. J. Tersoff, Phys. Rev. B **39,** 5566 (1989)

†Corresponding author. E-mail: yunche@mail.ncku.edu.tw

Temperature Dependent Measurements on Two Decoupled Graphene Monolayers

H. Schmidt*, T. Lüdtke*, P. Barthold*, and R. J. Haug*
**Institut für Festkörperphysik, Leibniz Universität Hannover, D-30167 Hannover, Germany*

Keywords: Graphene, Decoupled Monolayers, Magnetotransport

Monolayers of carbon, called graphene, can be used as current-carrying components in field-effect transistors [1]. Using micromechanical cleavage of natural graphite, such samples are deposited on top of a Si/SiO_2 wafer. Among single crystal(SC) mono-, bi- and multilayer graphene, also folded samples are produced. Folding leads to a misorientation in respect to the A-B stacking expected from SC bilayer systems and hence to decoupling of the two stacked layers. Figure 1 shows a drawing of two stacked monolayers of graphene.

We present temperature dependent measurements on such a system of two decoupled monolayers. At fixed backgate voltages, magnetotransport measurements carried out at low temperatures show two very different oscillations, each with a Berry's phase of π [2], verifying a system of stacked monolayers with different carrier concentrations due to screening [3].

Applying backgate voltages up to 60 Volt at zero magnetic field, the typical field effect is observed. With increasing temperature, a decrease in the resistivity close to the neutrality point can been seen. Keeping the carrier concentration fixed at high values, a small contribution of weak localisation is observed at low magnetic fields, also vanishing with increasing temperature.

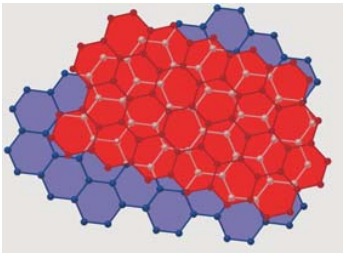

Figure 1: Schematic of two stacked and rotated graphene layers

Figure 2 shows Shubnikov-de Haas oscillations at constant backgate and different temperatures, plotted over the inverse magnetic field. With increasing temperature, both amplitudes of the oscillations corresponding to the two layers decrease. From this damping, the effective masses of charge carriers in both two layers are obtained, being consistent with the different carrier concentrations.

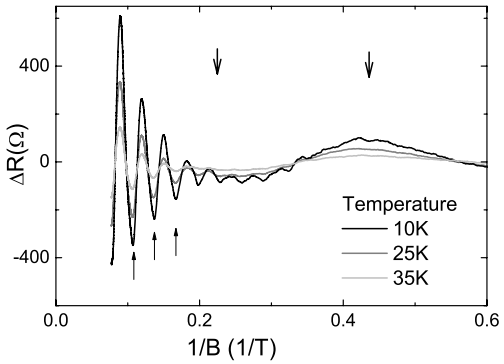

Figure 2: The longitudinal resistance at 60V backgate voltage and a temperature of 10, 25 and 35 Kelvin minus a high temperature background. The arrows at the bottom mark the minima of the oscillation belonging to the bottom layer with a higher carrier concentration, the arrows at the top minimum and maximum of the second one.

References

[1] K. S. Novoselov, A. K. Geim, S. V. Morozov, D. Jiang, Y. Zhang, S. V. Dubonos, I. V. Grigorieva, and A. A. Firsov, Science **306**, 666 (2004).

[2] Y. Zhang, Y. W. Tan, H. L. Stormer, and P. Kim, Nature **438**, 201 (2005).

[3] H. Schmidt, T. Lüdtke, P. Barthold, E. McCann, V. I. Fal'ko, and R. J. Haug, Appl. Phys. Lett. **93**, 172108 (2008).

Local gating of decoupled graphene monolayers

T. Lüdtke and R. J. Haug
Institut für Festkörperphysik, Leibniz Universität Hannover

Keywords: graphene, transport, gate, decoupled

Recently it was shown that it is possible to contact two decoupled monolayers of graphene on top of each other and to control carrier densities in both layers via top and bottom gates [1].

We present measurements on a similar locally gated device containing two decoupled monolayers of graphene. The measurements were done at 300mK and magnetic fields up to 13T were applied perpendicular to the sample. We obtain our samples via micromechanical exfoliation of natural graphite onto a SiO2 substrate. A topgate is fabricated on top of a graphene hall bar separated by a 60nm thick PMMA layer allowing local gating of the device.

By applying a voltage to the global backgate it is possible to change carrier concentration over the whole device. In a four terminal measurement the conductance was measured while tuning the backgate and the topgate independently. Charge neutrality points of both regions are clearly visible, separating the different charge configurations (e.g. p-n-p, n-n-n) of the graphene field effect transistor [2, 3]. Universal conductance fluctuations (UCF) are observed in several measurements as well as a nonlinear behavior in the current voltage characteristics at different gate configurations.

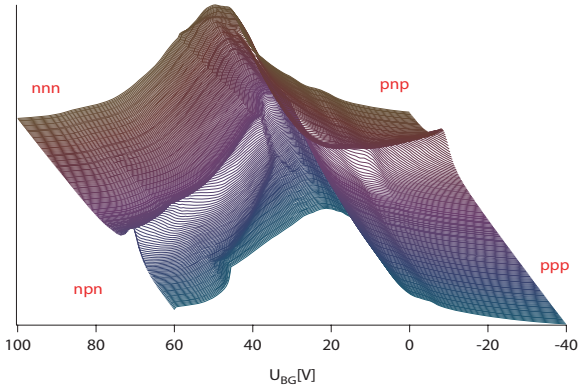

Figure 1: $U_{TG} - U_{BG}$ characteristics of the device showing different charge configurations

The magnetic field dependence of the locally gated sample shows four different oscillations in the Shubnikov-de Haas (SdH) measurement. Two of these oscillations are dependent on the potential of the applied backgate and disappear when tuning the backgate near the charge neutrality point. The other two oscillations changes when tuning the local topgate. SdH oscillation minima are obtained at filling factors of 4(i+1/2) which is equivalent to a Berry phase of Pi. Calculations of the carrier concentrations from SdH measurements as well as a Berry phase of Pi shows the existence of two decoupled monolayers of graphene that can be tuned by gates independently.

References

[1] H. Schmidt, T. Lüdtke, P. Barthold, E. McCann, V. I. Fal'ko, and R. J. Haug, Appl. Phys. Lett. **93**, 172108 (2008).

[2] J. R. Williams, L. DiCarlo, C. M. Marcus, Science **317** 638 - 641 (2007).

[3] Barbaros Özyilmaz, Pablo Jarillo-Herrero, Dmitri Efetov, Dmitry A. Abanin, Leonid S. Levitov, and Philip Kim, Phys. Rev. Lett. **99**, 166804 (2007).

Investigation of the local electronic structure in the vicinity of the graphene edge by means of scanning tunneling microscopy

Ken-ichi Sakai, Kazuyuki Takai, Ken-ichi Fukui and Toshiaki Enoki

Department of Chemistry, Tokyo Institute of Technology, Meguro-ku, Japan

Keywords: graphene edge, superperiodic pattern, edge state, scanning tunnelling microscopy

Graphene edge, which can be obtained by cutting the graphene, is composed of the zigzag and armchair structure. These edge structures are in strong relation with the electronic structure near the Fermi level; a localized electronic states with spin polarization appears in the vicinity of the zigzag edge, meanwhile armchair edge possesses the band structure obtained by the projection of that of the graphene [1]. Graphene edge also plays a role as the potential barrier, therefore electronic interference pattern can be observed near the graphene edge likewise on the metal surface through the scanning tunnelling microscopy (STM). Here we will report about the STM observation near the graphene edge with atomic scale at low temperature (LT).

The graphene edges were fabricated by the heat treatment of a cleaved HOPG surface in an electric furnace at 700-1000 °C under the argon gas flow condition. The heat-treated samples were introduced to UHV-STM chamber of STM equipment and then degassed at 200 °C for several days at 10^{-8} Torr. LT-STM observations were performed under the UHV condition (< 10^{-10} Torr).

On the terrace near the graphene edge, two superperiodic pattens, $(\sqrt{3}\times\sqrt{3})R30^{\circ}$ and honeycomb patterns, were observed [Fig. 1(a)]. Especially, the fine structure with three-fold symmetry was newly discovered on the individual bright spot in the honeycomb pattern. This can be explained on the basis of the spatial distribution of tunnelling current; because the spatial distribution on local density of states (LDOS) in the honeycomb pattern has the three-fold symmetry centered with a bright spot, the tunnelling current also shows the same symmetric spatial distribution as that of the LDOS. Further we succeeded in the observation of the graphene edge with atomic resolution [Fig. 1(b)]. Near the zigzag edges, edge states are observed as the strong bright areas. On the other hand, bight areas also observed near the armchair edge in spite of the absence of the edge state. This can be understood by two considerations. One is the electronic factor; a short zigzag edge embedded in the armchair edge induces LDOS attributed to the edge state. The other is the geometric factor; bulky functional groups attached to the edge-carbon atoms causes the bending of the graphene sheet towards the perpendicular direction near the edge.

References

1. M. Fujita et al., J. Phys. Soc. Jpn **65**, 1920 (1996)

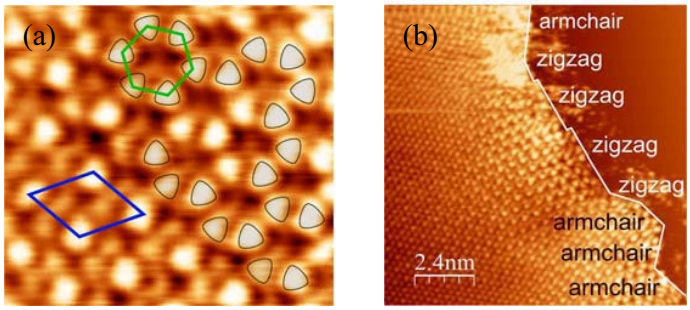

Fig. 1 (a) LT-STM image of a terrace near the edge taken at 9 K. Triangle-like shapes are the fine structures appearing in honeycomb area (1.5 × 1.4 nm^2). (b) LT-STM image of graphene edge obtained at 3.60 K. each edge structure is assigned by the comparison with the atomic image in terrace and the edge direction (12 × 12 nm^2).

A double quantum dot as a magnetic field and spin detector

G. Giavaras*, J. Wabnig*, B. W. Lovett*, J. H. Jefferson** and G. A. D. Briggs*
*Department of Materials, University of Oxford, Parks Road, Oxford OX1 3PH, UK
**QinetiQ, St. Andrews Road, Malvern WR14 3PS, UK

Keywords: double dot, spin detection

In this work we consider a double quantum dot in the Pauli blockade regime [1] weakly coupled to leads and under the application of an oscillating (microwave) magnetic field. When the two dots have a different Zeeman splitting the Pauli blockade can be lifted by applying a resonant microwave field, i.e., when the frequency of the oscillating field matches with a Zeeman frequency [2].

We use a master equation approach to study electrical transport through the double dot system including all the many-body states and taking into account possible spin relaxation. We investigate the dependence of the microwave-induced current on the asymmetry of the Zeeman splitting, δ, and temperature. On resonance and for temperatures smaller than the charging energy the current flows in the regime where $t > \Omega$ with t the interdot coupling and Ω the microwave-induced Rabi frequency which also sets the resonance width. By monitoring the current we are able to probe a δ on the order of t or smaller even at temperatures much higher than the scale set by the Zeeman splitting and with typical dot parameters within the experimental limit. We extend the analysis to temperatures comparable to the charging energy and show the efficacy of the system to detect a local magnetic field inhomogeneity.

We include a nearby target-spin which interacts with the spins on the double dot and show how we can detect its spin state by monitoring the electrical current through the double dot. This can be achieved because the resonance frequencies depend on the state of the target-spin. We examine the efficiency of the method and show that the main limiting factor is the internal spin relaxation on the dots.

The proposed system relies on standard quantum dot technology while oscillating fields can be induced on-chip and electrical currents can be generated and measured with high precision. These make the system a candidate for applications to spintronics, quantum information processing where coherent control and detection of individuals spins are essential and in general for studying spin correlations in solid state systems on the nanometer scale.

References

[1] K. Ono, D. G. Austing, Y. Tokura and S. Tarucha, Science **297**, 1313 (2002).

[2] F. H. L. Koppens, C. Buizert, K. J. Tielrooij, I. T. Vink, K. C. Nowack. T. Meunier, L. P. Kouwenhoven and L. M. K. Vandersypen, Nature **442**, 766 (2006).

Atomic-scale 0-π transition in Josephson junctions through spintronics nano-structures

S. Kawabata*, Y. Asano**, Y. Tanaka*** and S. Kashiwaya*
*National Institute of Advanced Industrial Science and Technology (AIST), Tsukuba, Japan
** Department of Applied Physics, Hokkaido University, Sapporo, Japan
*** Department of Applied Physics, Nagoya University, Nagoya, Japan

Keywords: Quantum computer, Spintronics, Josephson junction, spin filter effect

A superconducting ring with a π-junction made from superconductor/ferromagnetic-metal/superconductor (S /FM/S) hetero-structures exhibits a spontaneous current without an external magnetic field and the corresponding magnetic flux is half a flux quantum in the ground state [1]. Such a π-ring provides so-called *quiet qubit* that can be efficiently decoupled from the fluctuation of the external field [2]. However, the usage of FM gives rise to strong Ohmic dissipation. Therefore, the realization of π–junctions without FM is highly expected for qubit applications.

We theoretically consider the possibility of the π-junction formation in the Josephson junctions through nano-scale *ferromagnetic insulators* by use of the recursive Green's function method [3]. In the case of the fully polarized FIs (FPFIs), e.g., La_2BaCuO_5 and K_2CuF_4 [Fig.1(a)], we found the formation of a π-junction and a novel *atomic-scale 0-π transition* induced by increasing the FI thickness LF [Fig. 2]. More remarkably, in the Josephson junction through the spin-filter materials such as Eu chalcogenides [Fig.1(b)], the orbital hybridization between the conduction d and the localized f electron gives rise to a *hybridization-induced π-junction*. Such FI-based Josephson junctions may become an element in the architecture of future quantum information devices [4].

References

[1] L. N. Bulaevskii, V. V. Kuzii, and A. A. Sobyanin, JETP Lett. **25**, 291 (1977).

[2] L B. Ioffe, V. B. Geshkenbein, M. V. Feigel'man, A. L. Fauchere, and G. Blatter, Nature **398**, 679 (1999).

[3] S. Kawabata, Y. Asano, Y. Tanaka, and S. Kashiwaya, to be submitted (2009).

[4] S. Kawabata, S. Kashiwaya, Y. Asano, Y. Tanaka, and A. A. Golubov, Phys. Rev. B **74** 180502(R) (2006).

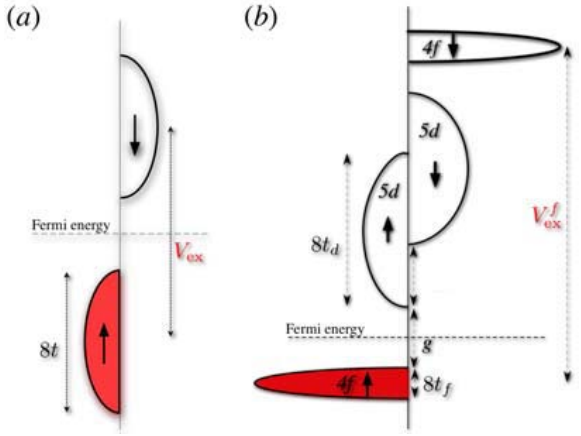

Figure 1: The spin-resolved density of states for (a) fully polarized ferromagnetic insulator (FPFI) and (b) spin filter materials, e.g., Eu-chalcogenides.

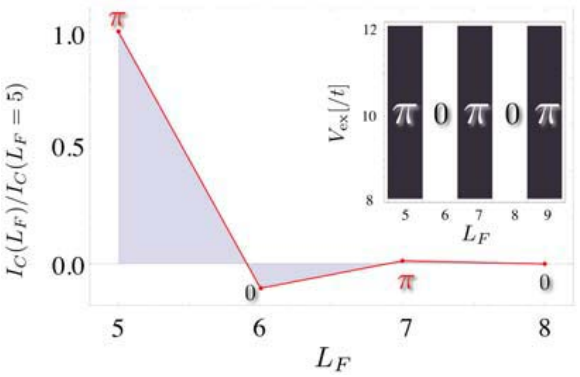

Figure 2: Josephson critical current I_C as a function of the thickness of FPFI layer L_F.

Coherence of single electron and nuclear spins in Diamond

N. Mizuochi,[1,2] P. Neumann,[3] F. Rempp,[3] K. Nakamura,[4] H. Watanabe,[5] S. Yamasaki,[6] F. Jelezko,[3] J. Wrachtrup[3]

[1]*Graduate School of Library, Information and Media Studies, University of Tsukuba, Japan,*
[2]*PRESTO, JST, Japan,*
[3]*Physikalisches Institut, Universität Stuttgart, Germany,*
[4]*Tokyo Gas Co., Ltd., Japan,*
[5]*Diamond Research Center, AIST, Japan,*
[6]*Nanotechnology Research Institute AIST, Japan*

Keywords: Physics and devices for quantum information processing, single spin, entanglement, NV center

Nitrogen-vacancy center (NV center) in diamond, shown in Figure 1, has attracted significant interest in field of quantum information processing. A single electron spin in the NV center can be manipulated and optically read out by means of confocal microscopy. It has extensively long spin coherence time even at room temperature (RT) and can be initialized by light irradiation.

By coupling nuclear spins to the single electron spin of the NV center in diamond, single nuclear spins become addressable and coherently controllable. Recently, we investigate the single NV center which electron spin couples to two ^{13}C nuclear spins. [1] In solid state materials, the entanglement of Bell states was generated among two superconducting qubits at low temperature. In our system, we could generate Bell states and three partite entangled states (GHZ and W states) at room temperature. [1] We also observed several unreported single NV centers which electron spin couples with more than 2 nuclear spins in ^{13}C enriched diamond, [2] which are important from the view point of increasing the number of qubit.

We also investigated the spin dynamics of single electron and nuclear spins in a diamond lattice with different ^{13}C nuclear spin concentration. [2] The ^{13}C concentration dependence of T_2^* is explained by Fermi contact and dipolar interactions with nuclei in the lattice. It has been found that T_2 decreases approximately as $1/n$, where n is ^{13}C concentration, as expected for an electron spin interacting with a nuclear spin bath. Our findings are very important to elucidate the dephasing mechanism and to make T_2 longer for quantum information devices and magnetometry. In ^{12}C enriched diamond, extremely long electron spin T_2 of 1.8 ms was measured at RT. [3]

References

1. P. Neumann, N. Mizuochi, F. Rempp, P. Hemmer, H. Watanabe, S. Yamasaki, V. Jacques, T. Gaebel, F. Jelezko, J. Wrachtrup. Science, **320**, 1326 (2008).
2. N. Mizuochi, P. Neumann, F. Rempp, J. Beck, V. Jacques, P. Siyushev, K. Nakamura, D. Twitchen, H. Watanabe, S. Yamasaki, F. Jelezko, J. Wrachtrup, *submitted* (arXiv:0811.4731).
3. G. Balasubramanian, P. Neumann, D. Twitchen, M. Markham, R. Kolesov, N. Mizuochi, J. Isoya, J. Achard, J. Beck, J. Tissler, V. Jacques, F. Jelezko, J. Wrachtrup, Nature materials, *accepted.*

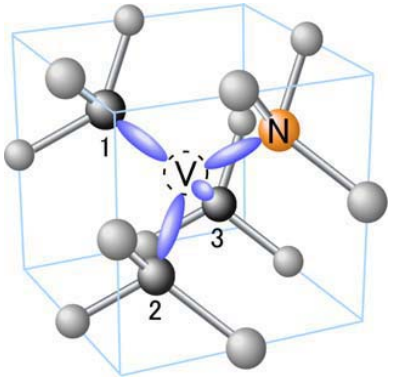

Fig. 1, NV center in diamond. It is the pair of nitrogen atom (N) and vacancy (V). The other atoms are carbon atoms (C). The numbers 1, 2, and 3 mark C in the 1st shell.

Conditional evolution of a charge qubit coupled to a quantum point contact detector

Gyong Luck Khym and Kicheon Kang
Department of Physics, Chonnam National University, Gwangju 500-757, Korea

Keywords: Charge qubit, Quantum measurement, Conditional evolution, Quantum point contact detector

Let us consider a charge qubit coupled to a single channel quantum point contact (QPC) detector at high magnetic field (See Figure 1). The qubit can be realized with double quantum dots or with a two-path interferometer, etc. The edge state electron is either reflected or transmitted at the QPC. Due to the charge sensitivity of the scattering amplitudes at the QPC, the charge state of the qubit can be detected. The charge detection results in dephasing of the qubit. One might assume that the wave function collapse in quantum measurement could be understood in terms of gradual dephasing of the charge state. However, the actual measurement has not been performed for the dephasing process, which only refers to the possibility of measurement and is a result of averaging over all possible measurement outcomes. On the other hand, a quantum measurement performed on the detector brings about a sudden reduction of the charge state (or the "wave function collapse") [1].

There are two possible outcomes of measurement in the QPC detector, that is, transmission and reflection, for each of the detector electrons. We investigate the conditional state of a charge qubit under monitoring only a particular detector output (R or T). This conditional evolution should be distinguished from the stochastic evolution of the charge state under random partitioning of the detector electrons [2, 3]. Continuous measurement on a particular outcome of the detector state results in an evolution of the charge state in a way that depends on the selection of measurement outcome. Our main results are as follows. (1) The initial state given as a coherent superposition of two different charge states is relaxed to the one particular charge state. The direction of the relaxation depends on the choice of measurement on the detector. (2) The relaxation rate is much larger than the current-sensitive part of the dephasing rate. This can be regarded as a manifestation of nonlocality in the measurement process.

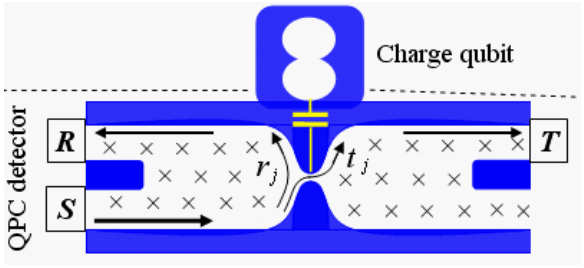

Figure 1: A schematic diagram of a charge qubit coupled to a point contact detector at high magnetic field. The state information is encoded in the charge-dependent reflection and transmission amplitudes, r_j and t_j, respectively, in the detector ($j = 0, 1$). The symbol $\times$ denotes the direction of the magnetic field.

We propose that this conditional evolution can be verified in a two-path interferometer containing a quantum dot capacitively coupled to a QPC [4]. The current-current correlation of the currents between two output leads (one in the interferometer and the other in the detector) selects the conditional state and reveals the characteristic features of the conditional evolution. The modulation of the interference term in the cross correlation is related to the relaxation rate. The magnitude of the interference fringe can be enhanced or reduced, depending on the initial state and the choice of the output lead in the detector.

References

[1] A. Nielson and I. Chuang, *Quantum Computation and Quantum Information* (Cambridge, 2000).

[2] A. Korotkov, Phys. Rev. B **47**, 5737 (1999).

[3] D. Averin, cond-mat/0603802.

[4] G. L. Khym and K. Kang, arXiv:0805.1995

Negative Interlayer Magnetoresistance and Dirac Fermion Nature in an Layered Organic Conductor and Multilayer Graphite

T. Osada, S. Sugawara, D. Nakahara, H. Imamura, T. Konoike, and K. Uchida

Institute for Solid State Physics, University of Tokyo, 5-1-5 Kashiwa, Chiba 277-8581, Japan

Keywords: Dirac fermion, negative magnetoresistance, organic conductor, graphite

Recently, strong negative interlayer magnetoresistance (MR) has been observed experimentally in a layered organic conductor α-(BEDT-TTF)$_2$I$_3$, which has been theoretically suggested to be a multilayer Dirac fermion system [1]. On the other hand, we have measured interlayer MR of well-prepared single crystal graphite, and we have found huge negative MR as shown in Fig.1. In order to clarify the origin of these negative MR phenomena, we have considered interlayer magneto-transport in multilayer Dirac fermion systems which consist of two-dimensional (2D) layers with Dirac-cone dispersion.

Under magnetic fields, because of its massless nature, the Dirac fermion system can easily reach the quantum limit where only the n=0 Landau level (zero-mode) always exists at the Dirac point. At the limit of weak interlayer coupling, single tunnelling event between the zero-modes on neighboring two layers dominates interlayer transport. The increase of degeneracy of the zero-mode causes strong negative MR. The spin splitting of the zero-mode could change the negative MR into positive one in high magnetic fields and low temperatures. These features are in good agreement with the experimental results on α-(BEDT-TTF)$_2$I$_3$ [2].

On the other hand, in the case of strong interlayer coupling, the zero-modes form the n=0 Landau subband with the dispersion along the stacking direction. In this case, interlayer transport is dominated by the subband conduction, but we can also expect negative MR in the quantum limit resulting from the increase of degeneracy of the zero-mode subband.

Multilayer graphite, in which two graphene sheets alternatively stack, is not a simple multilayer Dirac fermion system. In its 3D band dispersion, however, there exists the Dirac-cone dispersion around the H-point in **k**-space. As a result, the H-point hole shows Dirac fermion nature whereas the K-point electron shows conventional fermion nature. So, the H-point hole reaches the quantum limit at the much lower magnetic field than the K-point electron. Therefore, in graphite, negative MR could be expected in the wide field region above the field at which the H-point hole reaches the quantum limit (Fig.2).

References

1. N. Tajima *et al.*, cond-mat 0812.0857.
2. T. Osada, J. Phys. Soc. Jpn. **77**, 084711 (2008).

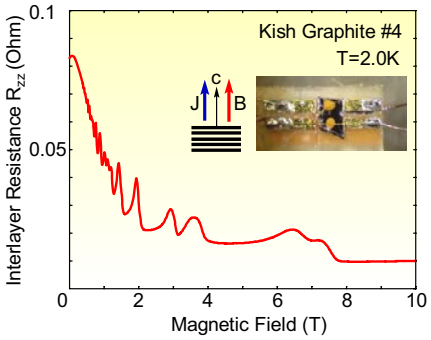

Fig.1 Negative interlayer magnetoresistance observed in multilayer graphite.

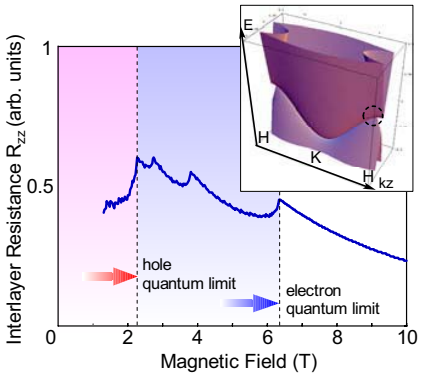

Fig.2 Calculated interlayer magnetoresistance in multilayer graphite.

Indications for a line of continuous phase transitions at finite temperatures connected with the apparent metal-insulator transition in two-dimensional disordered systems

A. Möbius*

**Leibniz Institute for Solid State and Materials Research IFW Dresden, POB 270 116, D-01171 Dresden, Germany*

Keywords: metal-insulator transition, scaling

The question whether electronic conduction in two-dimensional disordered systems is exclusively nonmetallic, so that the resistivity $\rho(T)$ always diverges as temperature $T \to 0$, or whether it can also have metallic character has been under controversial debate for three decades. The existence of a corresponding metal-insulator transition (MIT) was denied by the localization theory of Anderson *et al.* [1], however, it neglects electron-electron interaction. Thus it came as a surprise when Kravchenko *et al.*, who had varied the charge carrier concentration n in high mobility MOSFET samples, first reported a strong decrease of ρ down to 20 mK [2]. They considered the conduction in the respective (T, n) region as metallic.

In a recent experiment, Lai and coworkers studied the apparent MIT of an n-type Si quantum well confined in a $Si_{0.75}Ge_{0.25}$/Si/$Si_{0.75}Ge_{0.25}$ heterostructure [3]. The authors observed the conductivity σ to have nearly linear temperature dependences around the Fermi temperature $T_{\rm F}$, see Fig. 1 of that work. They showed that $\sigma_0(n)$, the $T = 0$ conductivity obtained by linear extrapolation from this T region, exhibits two regimes of different slope. Particularly important, there is a sharp bend at the transition between the two regimes. It coincides with the n value where $\mathrm{d}\sigma/\mathrm{d}T$ changes its sign as $T \to 0$. The authors interpret this finding as an indication of the existence of two different phases.

Lai *et al.* stress the slope of $\sigma(T)$ for $T \sim T_{\rm F}$ to be almost constant within the n region close to the MIT. This statement provokes two questions: Provided, $\sigma_0(n)$ has a knee indeed, and the slope used in extrapolation is roughly constant, should not $\sigma(T = \mathrm{const.}, n)$ exhibit a knee also for finite T? If yes, is the existence of this peculiarity restricted to the region of linear $\sigma(T, n = \mathrm{const.})$ around $T_{\rm F}$, or is it a more general phenomenon?

Here, reconsidering the data published by Lai *et al.*, it is pointed out that the apparent MIT at $T = 0$ may be connected with several peculiarities at finite T: (a) Close to the critical charge carrier concentration $n_{\rm c}$, defined by the sign change of $\mathrm{d}\sigma/\mathrm{d}T$ as $T \to 0$, piecewise linear functions approximate $\sigma(T = \mathrm{const.}, n)$ clearly better than polynomials of third order. This holds for the entire T range from 0.35 to 4.0 K. (b) The knee of the piecewise linear function is always located close to $n_{\rm c}$. (c) In a log-log plot, $\rho(T = \mathrm{const.}, n)$ has a "rounded step" in the immediate vicinity of $n_{\rm c}$, connected with an offset in the curves. Data from two previous experiments seem to exhibit similar features. (d) Scaling of the T dependences of σ for various n is supported by the collapse of the curves for $T = 0.35$ and 0.64 K when plotting σ as function of $(n - n_{\rm c})/T^{0.625}$, utilizing the value of the critical exponent of the characteristic temperature obtained in [4]. (e) The data by Lai *et al.* show sharp peaks in the derivative $\mathrm{d}\log_{10}\sigma/\mathrm{d}n$ at $n_{\rm c}$ for all considered T values.

As a whole, these arguments seem to provide rather convincing evidence for a line of continuous phase transitions at finite T, for details see [5].

References

[1] E. Abrahams, P.W. Anderson, D.C. Licciardello, and T.V. Ramakrishnan, Phys. Rev. Lett. **42**, 673 (1979).

[2] S.V. Kravchenko, G.V. Kravchenko, J.E. Furneaux, V.M. Pudalov, and M. D'Iorio, Phys. Rev. B **50**, 8039 (1994).

[3] K. Lai, W. Pan, D.C. Tsui, S. Lyon, M. Mühlberger, and F. Schäffler, Phys. Rev. B **75**, 033314 (2007).

[4] S.V. Kravchenko, W.E. Mason, G.E. Bowker, J.E. Furneaux, V.M. Pudalov, and M. D'Iorio, Phys. Rev. B **51**, 7038 (1995).

[5] A. Möbius, Phys. Rev. B **77**, 205317 (2008).

Ground-plane screening as a probe of the role of long-range Coulomb interactions in the metallic state of a 2D hole system

A. P. Micolich*, L. H. Ho*, A. R. Hamilton*, W. R. Clarke*, R. Danneau*, O. Klochan*, M. Y. Simmons*, M. Pepper** and D. A. Ritchie**

** School of Physics, University of New South Wales, Sydney NSW 2052, Australia*

*** Cavendish Laboratory, University of Cambridge, Cambridge CB3 0HE, United Kingdom*

Keywords: Metal-insulator transition, 2D hole systems, ground-plane screening, Coulomb interactions

In 2D systems, strong Coulomb interactions can lead to an anomalous metallic state. One route to studying the role played by Coulomb interactions is to limit their length-scale using a metallic ground-plane located close to the 2D system. This approach, originally used to study electrons on the surface of liquid Helium, has recently been employed to study the insulating [1] and metallic [2] regimes of a 2D hole system (2DHS) formed in an AlGaAs/GaAs heterostructure.

When the 2DHS is deep in the insulating regime, it is possible to use a metal surface gate to screen the Coulomb interactions, as in the previous study of electrons on liquid helium. In Ref [1] it was found that the ground plane had a very strong effect on electrical transport in the insulating 2DHS. However to study the effects of screening in the metallic regime is much more challenging, since the hole density is much higher and screening plane needs to be much closer to the 2DHS. Using a novel bilayer 2DHS, where one 2DHS screens the Coulomb interactions in the adjacent layer, it was recently shown that the ground-plane has surprisingly little impact on the metallic behavior in 2DHS [2]. This raises two questions: Firstly one must ask whether a finite thickness 2D system is as effective in the role of ground-plane screening as a metal surface gate. Secondly, if the adjacent ground plane does screen the Coulomb interaction, why does it have such little effect on the metallic behavior in the transport layer?

To answer these questions we present theoretical calculations of the relative effectiveness of a metal and a 2DHS when used for ground-plane screening of a nearby 2DHS [3]. These calculations are performed for three cases: (a) in the Thomas-Fermi approximation with no intralayer screening in the transport layer, (b) in the Thomas-Fermi approximation accounting for intralayer screening in the transport layer, and (c) accounting for intralayer screening in the transport layer, and exchange effects in both the 2DHS ground-plane and transport layer, using the Hubbard approximation. The latter case makes our results relevant for $r_s > 1$, as in the experiments by Huang *et al.* [1] and Ho *et al.* [2].

We show that in the Thomas-Fermi approximation, a 2DHS ground-plane is as effective as a metal gate (to within ~1%) for a ground-plane separation $d \sim 50$ nm, comparable to that considered experimentally [2]. However, more surprisingly, we find that when we account for exchange and finite thickness effects in the 2DHS ground-plane, the 2DHS is actually *more* effective than a metal as a ground-plane.

Finally, our calculations contrasting the presence and absence of intralayer screening in the 2DHS transport layer lead to a possible explanation for why the nearby ground-plane has a significant effect when the transport layer is in the insulating regime [1] and very little effect when it is in the metallic regime [2]. Our results show that bilayer 2D systems may be very useful for studying the breakdown of screening and its role in the 2D metal-insulator transition.

References

1. J. Huang, D.S. Novikov, D.C. Tsui, L.N. Pfeiffer and K.W. West, arXiv:cond-mat/061320.

2. L.H. Ho *et al.*, Phys. Rev. B **77**, 201402(R) (2008).

3. L.H. Ho, A.P. Micolich, A.R. Hamilton and O.P. Sushkov, Manuscript in Preparation

Possible Finite Temperature Phase Transition in Strongly Correlated *GaAs* Two-dimensional Holes in Zero Field

J. Huang*, J. S. Xia**, D. Tsui***, L. Pfeiffer***, and K. West***
* *Department of Physics, Taylor University, Upland, IN 46989, USA*
** *Department of Physics, University of Florida, Gainsville, FL, USA*
*** *Department of Electrical Engineering, Princeton University, Princeton, NJ 08544, USA*

Keywords: electron-electron interaction, phase transition, 2D metal-to-insulator transition, Wigner Crystal

The experimental observation of the Metal-to-Insulator Transition (MIT) in two-dimensional (2D) systems at low temperatures has revealed important aspects of the intriguing nature of the interplay of disorder and electron-electron interaction [1]. Whether the Coulomb force can also, analogous to the Anderson Localization due to random disorder, bring radical change to the electron state (i.e. through Wigner Crystallization) is still an intriguing subject. However, reaching a desired low carrier concentration that provides a dominating interaction effect has proven to be a serious experimental challenge due to the unwanted, hard-to-quench disorder. Experimental results showing activated transport in the insulating side of the MIT are a good indication of such disorder dominance. In recent years, a new type of undoped *GaAs* field-effect transistors (HIGFET) [2-3] has been adopted and an exceedingly low 2D-hole concentration of 6×10^8 cm^{-2} has been achieved. In addition, the exceptional crystal quality is also reflected in the mobility such as 1×10^6 cm^2/Vs for a 2D-hole density of 1×10^{10} cm^{-2}. Such 2D systems allow transport studies of strongly correlated charges of which the Coulomb energy exceeds the nominal Fermi-energy by 100 times if an effective mass of $0.3m_0$ is assumed [2,3].

We present an experimental transport study of high quality dilute 2D holes in (100) *GaAs* HIGFET. The temperature-dependence of the 2D-hole resistivity is measured for a range of charge concentrations from 1×10^{10} cm^{-2} down to 6×10^8 cm^{-2}. For charge densities beyond 4×10^9 cm^{-2} for which the metal-like behavior of MIT is anticipated, the low temperature dependence of the resistivity reveals a turn-around after reaching a minimum around 30 mK [3]. This insulator-like character persists down to 0.5 mK. As the charge concentration is reduced below 4×10^9 cm^{-2} and even into the deep insulating regime of the MIT, the conductivity-T relation resembles a power-law in a temperature window from 30 to 300 mK, instead of the activated conduction. Moreover, for a fixed charge density, a conductivity kink is observed during a slow temperature sweep. An example of this kink feature is shown in Fig.1 (a) for a hole density of 3.8×10^9 cm^{-2} through the leveled $\boldsymbol{\sigma(T)}$ (by subtracting a linear fit), as well as the discontinuity in the temperature derivative $\boldsymbol{d\sigma(T)/dT}$. Such kinks are consistently observed for each fixed hole-density as long as it is below $\sim 7 \times 10^9$ cm^{-2}. The location of the kinks, named T_c, is found to vary, from 220 mK to 430 mK, with increasing density (p) from 0.8 to 7×10^9 cm^{-2}, in two distinctly different fashions: T_c either rises with increasing density for p larger than some characteristic value p_c or shows much weaker change for p less than p_c. Interestingly, p_c agrees with the critical density of the MIT.

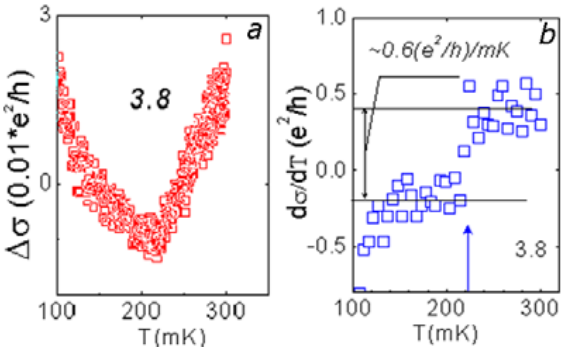

Fig. 1: a. conductivity $\boldsymbol{\sigma(T)}$ leveled by a linear fit. b. kink feature revealed by a discontinuity in $\boldsymbol{d\sigma(T)/dT}$.

References

1. E. Abrahams S.V. Kravchenko, and M.P. Sarachik, Rev. Mod. Phys.**73**, 251(2001).
2. M. P. Lilly, J. L. Reno, J. A. Simmons, I. B. Spielman, J. P. Eisenstein, L. N. Pfeiffer, K.W. West, E. H. Hwang, and S. Das Sarma, Phys. Rev. Lett. **90**, 056806 (2003)
3. Jian Huang, J-S Xia, D.C. Tsui, L. N. Pfeiffer, K. W. West, Phys. Rev. Lett. **98**, 226801 (2007)

Dielectrophoresis-scanning tunneling microscopy method for electron transport measurement of individual nanowires

P. Liu, Z.Z. Wang, W.W. Cai and D.M. Chen
Institute of Physics, Chinese Academy of Sciences, Beijing, China

Keywords: dielectrophoresis, scanning tunneling microscopy, electron transport, nanowires

Since the start of research in semiconductor nanostructures, measuring the electrical properties of individual nano object has been an important issue in the field of nanotechnology. In this abstract, we will present a description on our dielectrophoresis-scanning tunneling microscopy (DEP-STM) joint measurement method [1].

DEP is a phenomenon in which a force is exerted on a dielectric particle when it is subjected to a non-uniform electric field. The strength of the force depends strongly on the medium and particles' electrical properties, shape, size, as well as the frequency of the electrical field. In DEP, nanowires with longer dimension will be attracted and aligned to the probe faster than small particles.

The two terminal transport measurement system is illustrated in Fig.1, where the nanowire forms two contacts with metal probe and Au electrode. The approaching process is similar to a STM servo system, details can be found in ref. [1]. While performing electrical transport measurement, we swept voltage on the probe, and detected the output voltage signal of the pre-amplifier.

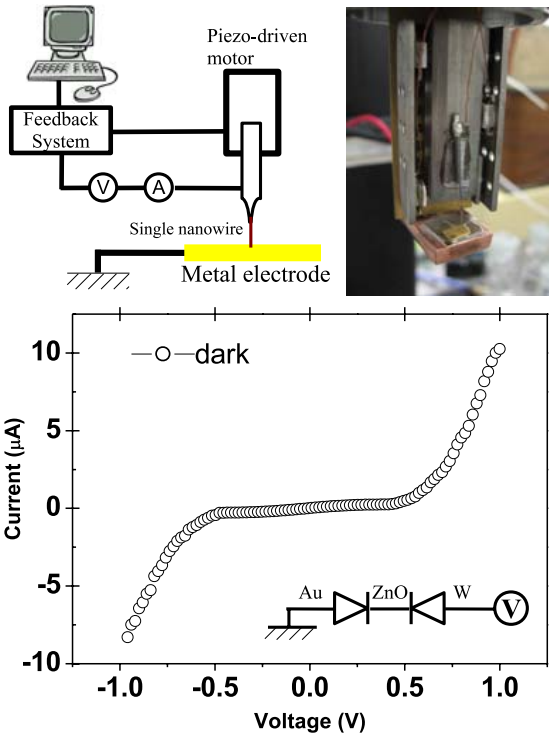

Figure 1: Top left, schematic of two-terminal measurement setup; top right, digital camera image of actual object; bottom, *I-V*characteristics of W-ZnO-Au system.

We have used this method measuring the electron transport properties of individual ZnO nanowire under the condition of darkness, the result is shown in Fig.1. Under dark condition, Au-ZnO-W hybrid structure can be regarded as two back-to-back Schottky barrier diodes (SBD) as illustrated in the inset of Fig.1. The *I-V* characteristics reflect the reverse biased transport behavior of either two SBDs with a small leakage current. With this method and its variation, we have also observed photoconductivity in selenium nanotube [1]; persistent photoconductivity [2] and polarized memory effect in ZnO nanotube.

In conclusion, we have developed a new DEP-STM method for electron transport measurement of nanowires. This versatile technique avoids contact problems often encountered in lithographically patterned devices due to contamination or damage from energetic electron or ion beams. The device made using present technique forms reliable Schottky barrier at the semiconductor-metal contacts. It enables us to investigate novel electrical properties on different kinds of metal-semiconductor contacts.

References

[1] P. Liu, Y. R. Ma, W. W. Cai, Z. Z. Wang, J. Wang, L. M. Qi and D. M. Chen: *Nanotechnology* **18**, 205704 (2007)

[2] P. Liu, GW She, ZL Liao, Y. Wang, ZZ Wang, WS Shi, XH Zhang, ST Lee and DM Chen: *Appl. Phys. Lett.* **94**, 063120 (2009).

Fine structure splitting of quantum dot excitons: role of geometry and environment

M. Abbarchi*,**, T. Kuroda**, C. Mastrandrea*, A. Vinattieri*, S. Sanguinetti***, T. Mano**, N. Koguchi***, K. Sakoda** and M. Gurioli*

**Dipartimento di Fisica, CNISM, Università di Firenze and European Laboratory for Non-Linear Spectroscopy, Via Sansone 1, 50019 Sesto Fiorentino (Firenze), Italy*

***National Institute for Materials Science, 1-1 Namiki, Tsukuba 305-0044, Japan*

****Dipartimento di Scienza dei Materiali, CNISM, Università di Milano-Bicocca, Via Cozzi 53, 20125 Milano, Italy*

Keywords: quantum dot, fine structure splitting, spectral diffusion

The control of fine structure splitting (FSS) quantum dots (QDs) is a relevant issue for quantum information applications because triggered polarization entangled photon pairs could be obtained by the radiative decay of biexcitons provided that FSS is tuned to zero. Generally speaking, the FSS originates, via the exchange interaction, from asymmetries in the QD confinement potential. In epitaxially grown Stransky Krastanov (SK) QDs anisotropies came from several sources, such as shape, strain, and piezoelectricity. In particular claims of the major role of strain induced effects on the FSS have been reported [1]. Taking advantage of the modified droplet epitaxy (MDE) to obtain highly symmetric and strain free GaAs/AlGaAs QDs we realized our sample in order to reduce as much as possible FSS structural-related sources, such as strain, composition, and shape, which affected previous FSS experiments in SK-QDs. High-resolution, PL spectroscopy is employed to characterize the exciton (X), biexciton (XX), and trion (T) lines. The X and XX lines exhibit FSS, which monotonically decreases from 90 to 20 μeV when decreasing the quantum dot size [2]. The FSS decrease closely follows the reduction of [110] shape anisotropy observed in our QDs as the size is reduced. In addition, when the structural asymmetry in our QDs is close to zero, we find that the QD linear polarization axis is significantly distributed along random oriented directions (as shown in Fig.1). These findings highlight the role of extrinsic effects as significant contribution in determining the QD potential anisotropy and we relate them to the presence of charged trap in the QD environment. In fact a rather broad spectral diffusion (SD) is observed in GaAs QDs, as a consequence of the low growth temperature. Moreover, the X, XX and T linewidths show a systematic trend, with (X) typically larger than (XX) and (T). Theoretical simulations of the Stark shift induced by charged traps account for the observed SD-induced linewidth and provide information on the trap type and localization [3]. In order to improve the MDE growth procedure, the growth temperature was increased reducing the defectivity of the QD environment. We demonstrate that the newly developed protocol allows to reduce the QD spectral linewidth by a factor 4 in average, eventually producing QD lines below our instrumental resolution (10 μeV).

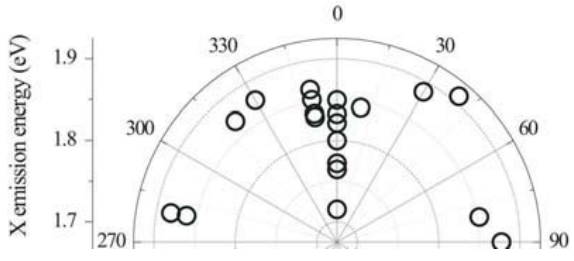

Figure 1: Polar plot of the X emission energy as a function of the polarization axis for different QDs. 0° is the [110] direction.

References

[1] R. Seguin et al., Phys. Rev. Lett. **95**, 257402 (2005).

[2] M. Abbarchi et al., Phys. Rev. B **78**, 125321 (2008).

[3] M. Abbarchi et al., Appl. Phys. Lett. **93**, 162101 (2008).

Skyrmion and Bimeron Excitations in Bilayer Quantum Hall Systems

Z.F. Ezawa* and G.Tsitsishvili**

*Theoretical Physics Laboratory, RIKEN, Saitama 351-0198, Japan

** Department of Theoretical Physics, A. Razmadze Mathematical Institute, Tbilisi, 380093 Georgia

Keywords: Quantum Hall Effects, Bilayer Systems, Topological Excitations, Pseudospin Ferromagnets

Quantum Hall (QH) systems have received a renewed interest owing to the discovery of quantum coherence associated with the spin and layer degrees of freedom. It has also proved to be an ideal system to play with noncommutative geometry. When an electron is confined within the lowest Landau level, its position is described solely by the guiding center, whose X and Y coordinates do not commute with one another. This is the key element of the microscopic theory of QH systems.

One of its consequences is that quantum coherence develops spontaneously in the QH system. Such a system is called the QH ferromagnet. In the spontaneous broken phase of the spin SU(2) symmetry, there arises a topological soliton (skyrmion) flipping several spins coherently. A skyrmion is constructed by dressing a cloud of spins around an electron or a hole. Hence, a skyrmion carries the same charge as an electron or a hole at the filling factor $\nu = 1$.

More remarkable is the bilayer QH system[1], where the layer degree of freedom acts as the pseudospin. In the spontaneously broken phase of the pseudospin SU(2) symmetry, the quasiparticle is a topological soliton to be identified with the pseudospin skyrmion. Furthermore, the parallel magnetic field penetrates between the two layers, and deforms a skyrmion into a bimeron (a pair of merons), as illustrated in Fig.1. Each meron carries a fractional charge. The activation energy is shown to decrease rapidly due to the loss of the exchange energy.

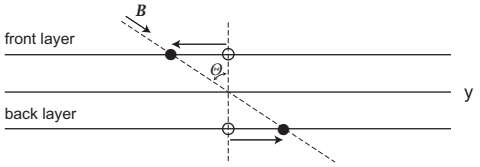

Figure 1: The center of a skyrmion is shifted to the opposite direction along the magnetic field in the front and back layers.

The theoretical result explains the experimental data[3] quite well as in Fig.2. Nevertheless, contrary to a phenomenological analysis made in literature[2], the separation between two merons, being determined uniquely by the noncommutative structure of the geometry, is of the order of the core size. It is hard to say that a bimeron consists of two merons with a string between them. Furthermore, the dominant contribution to the exchange-energy loss comes from the halo region and not from the string region of a bimeron.

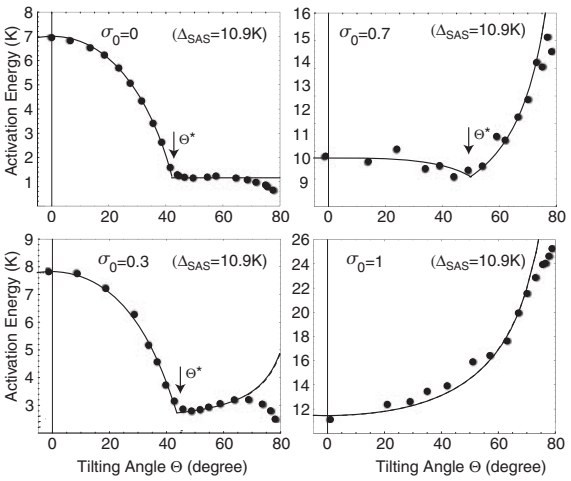

Figure 2: The activation energy at $\nu = 1$ is plotted as a function of the tilting angle Θ in onel sample ($\Delta_{\rm SAS} = 11$ K, $\rho_0 = 0.6 \times 10^{11}$ /cm^2) with different imbalance parameter σ_0. The data are taken from Sawada et al.[**?**, **?**]

References

[1] Z.F. Ezawa, *Quantum Hall Effects* (World Scientific, 2008, 2nd ed.).

[2] K. Moon et al., Phys. Rev. B **51** (1995) 5138.

[3] A. Sawada et al., Physica E **18** (2003) 118; D. Terasawa et al., Physica E **22** (2004) 52.

Fractional quantum Hall effect in trilayer systems in a tilted magnetic field

G. M. Gusev*, S. Wiedmann**, A. K. Bakarov*** and J. C. Portal**,****
* *Instituto de Física da Universidade de São Paulo, São Paulo, SP, Brazil*
**LNCMI-CNRS, BP 166, 38042 Grenoble and INSA, 31077 Toulouse, France*
*** *Institute of Semiconductor Physics, Novosibirsk, Russia*
**** *Institut Universitaire de France, 75005 Paris, France*

Keywords: triple quantum wells, fractional quantum Hall effect

Fabrication of the multiple two-dimensional system in close proximity allows to control interlayer electron - electron interaction and create new correlated states. The important example of the new correlated state in double quantum wells is a spontaneous interlayer phase coherence and the occurrence of the quantum Hall effect at Landau filling factor $\nu = 1$, even in the absence of the interlayer tunneling [1].

The triple quantum well (TQW) system is another semiconductor structure, which is also interesting from both theoretical and experimental point of view. The generalization of the Laughlin state predicts a new incompressible state in a trilayer system. In order to increase the mobility we produce samples with high electron density ($n_s = 9 \times 10^{12}$ cm^{-2}). The density in the central well is 30% smaller than in the lateral well, and the system is slightly imbalanced. The samples are symmetrically doped GaAs triple quantum wells with two barrier thicknesses (14 and 20 Å) and with a mobility $\mu = 500 \times 10^3$ cm^2/Vs. The measurements of the longitudinal and the Hall resistances have been performed in the tilted magnetic field. In a TQW each Landau level consists of 6 sublevels. The tunneling gap oscillates with parallel magnetic field due to the Aharonov Bohm effect [2]. For low Landau level indexes, the tunneling gap decreases with in plane field and no re-entrance behaviour is expected (Figure 1). However, when the tunneling gap at filling factor $\nu = 4$ is collapsed, the novel resistance minima, corresponding to the new fractional filling factors, are developed (Figure 1). Thus, in this work we observe the collapse of the tunneling gap in the presence of the in-plane magnetic field, and emerging of the new resistance minima, associated with anomalous fractional numbers in the Hall plateau quantization. Such anomalous fractional states can not be explained by conventional fractional quantum Hall effect theory.

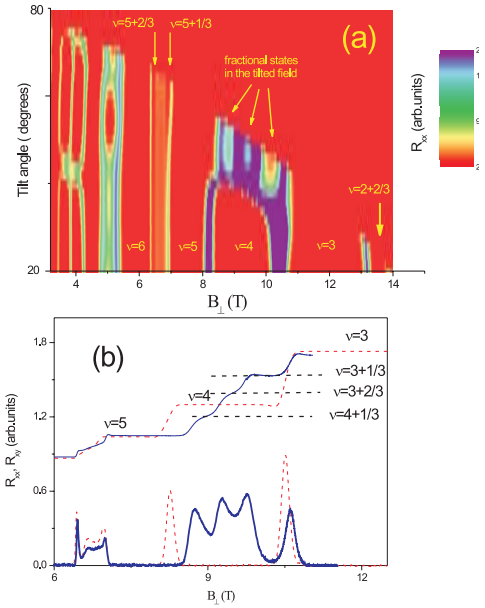

Figure 1: (a) Experimental plot of the resistance in the tilt angle-magnetic field plane for a triple well structure with a barrier thickness 14 Å. Minimum at filling factor $\nu = 4$ is collapsed, and 3 new minima are developed.(b) Longitudinal and Hall resistances as a function of the perpendicular magnetic field for two angles: 0° (red dashes) and 49° (thick blue lines) at T=50 mK.

References

[1] See the review paper J. P. Eisenstein, Superlatt. Microstruct. **12**, 107 (1992) and references therein.

[2] G. M. Gusev, A. K. Bakarov, T. E. Lamas, J. C. Portal, Phys. Rev. Lett. **99**, 126804 (2007). G. M. Gusev, C.A.Duarte, A. K. Bakarov, T. E. Lamas, J. C. Portal, Phys. Rev. B, **78**, 15320 (2008).

Spin-related electron transport in a single type II broken-gap heterojunction doped with Mn

K. Moiseev[1], V. Berezovets[1,2], M. Mikhailova[1], V. Nizhankovskii[2] and R. Parfeniev[1]

[1] *Ioffe Physical-Technical Institute RAS, Saint Petersburg, Russia*

[2] *International Laboratory of High Magnetic Fields and Low Temperatures, Wroclaw, Poland*

Keywords: quantum magnetotransport, spin-dependent current.

We report study of quantum magnetotransport in a 2D electron-hole system situated at a single type II broken-gap InAs/GaInAsSb heterointerface in high magnetic fields up to 35 T at low temperatures T=1.5-4.2 K. Lattice-matched single p-$Ga_{1-x}In_xAs_ySb_{1-y}$/p-InAs heterostructures with planar and abrupt heteroboundary were obtained on p-InAs(100) substrate, doped with Zn or Mn, in a composition range of undoped p-GaInAsSb solid solutions $0.06<x<0.16$ and $y=x+0.06$. Electrons and holes were accumulated and localized in self-consistent quantum wells at the heterointerface forming 2D-semimetal channel [1]. The isotype p-GaInAsSb/p-InAs heterostructures demonstrated high value of Hall mobility (6.0×10^4 $cm^2V^{-1}s^{-1}$) in the semimetal channel containing 1 or 2 electrons subbands with overall concentration up to $n_e=9.2\times10^{11}cm^{-2}$. In a planar magnetotransport, the 2D electron-hole gas exhibited insulating behavior in high magnetic fields (B>20 T) in the extreme quantum limit when the Fermi level is located between the last electron and hole Landau levels. In this insulating state, Quantum Hall Effect becomes symmetric on magnetic field due to the strong rise of R_{xx} contribution, that results in hopping conductivity through totally localized states formed under conditions of a surface potential modulation.

Due to asymmetric potential profile of the InAs/GaInAsSb heterojunction there is Rashba's spin-splitting of electron states near Fermi level in zero magnetic fields [2]. Doping with magnetic impurity of the heterostructure leads to the splitting of Shubnikov-de Haas oscillations of the planar (σ_{xx}) and tunneling (dI/dU) conductance across the sample in magnetic fields B>8T that corresponds to intersection of Fermi level with spin-splintered Landau levels of 2D electrons. This peak splitting non-linearly increases with magnetic field increasing, i.e. with decreasing of Landau level number. That points to a contribution of s-d exchange coupling between localized magnetic moments of Mn ions in the InAs substrate and 2D-electrons states at the interface which can be accelerated by Rashba spin-orbit mechanism. Presence of 0.5 nm-thick Mn δ-layer near the heterojunction, which was deposed on the 0.5 μm-thick p-GaInAsSb epilayer and covered by p-GaSb cap layer, leads to the spin-oriented tunneling of electrons across the heteroboundary. Spin-related structures for the lowest Landau level of 2D-electrons at the interface and magnetic moments of Mn δ-layer were observed as steps in I-V characteristics and spikes in the tunneling conductance measured at quantum Hall regime (B>12 T) at 1.5 K. For filling number of ν=2 the value of dI/dU in co-linear case was higher in an order than for one in non-co-linear case and their ratio increases with magnetic filed increasing. It should be noted that states of Mn ions near the interface have a spin configuration of $3d^5$ (Mn^{2+}) that differs from the configuration of $3d^4$ (Mn^{3+}) for bulk substrate. It results in indirect double interaction between the magnetic ions with different charge states and effects on a spin-splitting of the energy spectrum of the 2D-electron channel. Magneto-tunneling spectroscopy of 2D-electron channel will be discussed.

This work was supported by RBRF grants, by programs of RAS and Scientific School grants.

References

1. M.P. Mikhailova, K.D. Moiseev, Yu.P. Yakovlev, Semicond. Sci. Technol. **19**, R109 (2004).

2. E.I. Rashba, Sov. Phys. Solid State **2**, 1109 (1960).

Spin Hall effect in a curved graphene with spin-orbit interaction

Takashi Kato, Seiichiro Onari and Jun-ichiro Inoue
Department of Applied Physics, Nagoya University, Nagoya 464-8603, Japan

Keywords: Graphene, Spin Hall effect, Spin-orbit interaction

Graphene has attracted much interest due to its striking electronic structure, and many researchers have devoted themselves to elucidate its property. The recently-developed techniques to get high-quality graphene sheets have triggered a new field of graphene-based electronics. Because the low energy band structure near the *K* and *K*' points can be described in the form of Dirac equation, the graphene has been expected to be a stage of novel phenomena, which can not be observed in conventional 2D systems. Actually, an unconventional quantum Hall effect emerges in the graphene. Undoped graphene has a character of a zero-gap semiconductor, because Fermi energy of undoped graphene is located where the valence band and the conduction band meet at two points (Dirac points). When a spin-orbit interaction (SOI) exists, the hybridization of π and σ orbitals at *K* and *K*' points generates an energy gap at the Fermi energy, and the graphene becomes an insulator.

Recently, Kane and Mele have demonstrated that spin Hall effect (SHE), which is a phenomena that a spin current flows perpendicular to an applied electric field, is quantized in the insulating region of graphene [1]. On the other hand, it is reported that the spin Hall conductivity (SHC) calculated using a realistic multi-orbital tight-binding (TB) model is not quantized [2]. These calculations have been carried out for an ideal flat graphene. However, many experimental results suggest that ripples may exist in grapheme sheets. Therefore, it is important to clarify the effect of ripples on the properties of graphene. In this work, we present how ripples in graphene sheets influence the electronic state and SHE.

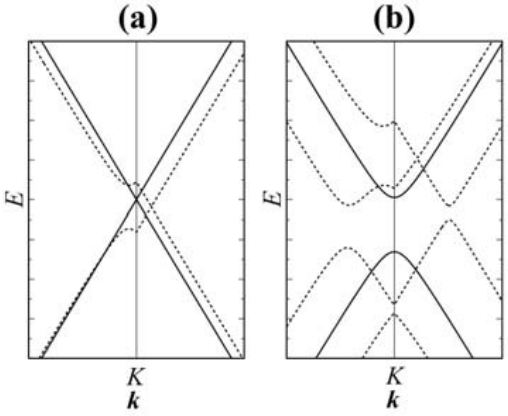

Fig.1 Band structures in the vicinity of *K* point for (a) graphene without SOI and (b) with SOI. Solid lines are for flat graphene and broken lines are for curved one. The left (right) side of *K* point is along Γ (*K*) to *K*(*M*) point.

We employ two models. One is a convenient π orbital TB model, and the other is a realistic π and σ orbital TB model. In the case of flat grapheme without SOI, no hybridization occurs between π and σ orbitals. However the presence of ripples makes these orbitals hybridize and induces an effective SOI. Because actual structures of ripples are very complicated, we design a simplified structure, which has a uniaxial curvature. The SHC is calculated by using Streda formula.

We find the low energy band structure is modified by the curvature. In the absence of SOI, the Dirac points are shifted from *K* and *K*' points by the curvature effect (Fig. 1(a)). This is due to the non-equivalency of three nearest neighbour hoppings among π orbital. In the presence of SOI, the coupling of the curvature and the SOI breaks the spatial inversion symmetry and brings about a SOI of Rashba-type. As a result, the energy bands split laterally as shown in Fig. 1(b). In the conference, we will present the curvature effect on SHC.

References

1. C. L. Kane and E. J. Mele, Phys. Rev. Lett **95**, 226801 (2005).
2. S. Onari, Y. Ishikawa, H. Kontani and J. Inoue, Phys. Rev. B **78**, 121403 (2008)

Optical measurement of electron spin coherence in a semiconductor quantum well

T. Inagaki[1], H. Kosaka[1, 2], Y. Rikitake [3,2], H. Imamura [4,2]
Y. Mitsumori[1, 2], and K. Edamatsu[1]

[1] *Research Institute of Electrical Communication, Tohoku University, Sendai, Japan*
[2] *CREST-JST, Saitama, Japan*
[3] *Department of Information Engineering, Sendai National College of Technology, Sendai, Japan*
[4] *Nanotechnology Research Institute, AIST, Tsukuba, Japan*

Keywords: quantum well, electron spin, coherence, tomography

Read out of the electron spin state is an essential function for spin-based quantum information technology. The traditional spin measurement technique, however, requires an extra step of spin manipulation or precession to measure the electron spin coherence. To measure the electron spin coherence directly, we developed a new scheme, tomographic Kerr rotation, which is based on the magnet-optical Kerr effect and the coherent transfer of light polarization states into the electron spin states [1].

The conventional Kerr rotation technique to measure the electron spin is only possible to deal with the population of spin up and down. This is because electron spins virtually created by the probe light beam conventionally lose the coherence, which is the relative phase information between spin up and down. However, we can prepare coherent superposition of up and down electron spin states by the coherent transfer scheme. By applying this scheme to the probe light beam, we can measure the electron spin coherence.

In this demonstration, we used GaAs/AlGaAs quantum wells in which g-factors are controlled to be able to apply the coherent transfer scheme. When one of two light-hole states is virtually excited by the probe light under an in-plane magnetic field B_x, the tomographic Kerr rotation method is applicable [2]. Here we prepare the electron spins that precess about a static magnetic field B_x by the pump light beam. **Fig.1** shows the result of the tomographic Kerr rotation measurement of the precessing electron spins. We project electron spins on two mutually-orthogonal bases (z-axis and y-axis) in the Bloch sphere. The conventional z-axis projection of electron spins, using the linearly-polarized probe light beam, indicates the population of the spin state $|\uparrow\rangle_e$ (+z) and $|\downarrow\rangle_e$ (-z). In contrast, the y-axis projection of electron spins is measured by the circularly-polarized $\sigma^{\pm}_{ph}$ probe light beam which consists of a linear superposition of two linear polarizations $D^{\pm}_{ph}$. With the coherent transfer scheme, the $D^{\pm}_{ph}$ polarized light beam virtually creates the electron spin states $|\uparrow\rangle_e \pm i|\downarrow\rangle_e$ ($\pm$y). In this situation, the electron spin coherence is measured through the exchange interaction $\mathbf{s}_1 \cdot \mathbf{s}_2$ between the prepared electron spin $\mathbf{s}_1$ by the pump light beam and the virtually created electron spin $\mathbf{s}_2$ by the probe light beam on the y-axis. As a result, we were able to visualize the spin dynamics of precessing electrons as a rotation, not merely as oscillations.

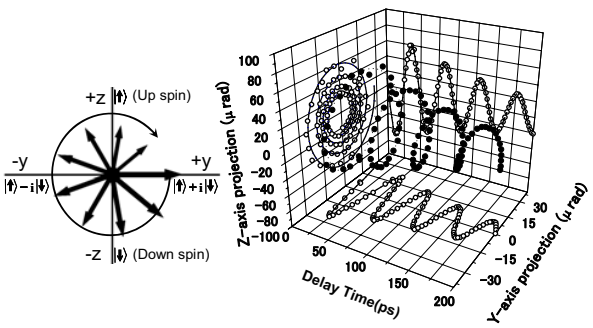

Fig.1 The tomographic Kerr rotation measurement of precessing electron spins. The scale size is corrected for the difference in efficiency between the z-axis and y-axis projection.

This work was supported by CREST-JST, ERATO-JST, SCOPE-MIC, MEXT and NEDO.

References

1. H. Kosaka et al., *Phys. Rev. Lett*. **100**, 096602 (2008).
2. H. Kosaka et al., *Nature* **457**, 702 (2009)

DECOHERENCE IN ADIABATIC PASSAGE

Enav Alcobi and Yuval Oreg

Department of condensed matter physics, Weizmann Institute of Science, Rehovot Israel 76100

Keywords: Quantum dots, Coherence, Qubit, adiabatic processes

Future quantum computers are based on manipulation of quantum bits (qubits), where a qubit is a coherent superposition of states "0" and "1". Researchers suggested to use the electron spin as the basic qubit, since it can be in two definite states, 'up' for "0" and 'down' for "1". For a successful operation of such computers, spins should be manipulated coherently, with a long enough coherence time.

The Coherently Transfer Adiabatic Passage (CTAP) [1] method; embodied by making use of a few quantum dots. In this method, a certain sequence of time dependent adiabatic pulses on the metallic gates defining the quantum dot controls the electron position.

The advantage of the CTAP method is in its ability to transfer an electron between two distant dots so that the probability to find it on its way is minimal. Hence, minimizing decoherence due to interaction with the environment on the way. We describe a novel way to quantify and measure the amount of decoherence in this class of systems using a novel quantum mechanical interferometer

The interferometer is based upon a quantum mechanical phenomenon (the Aharonov-Bohm effect) [2] that leads to oscillations in the quantum dot's occupation as a function of magnetic flux threaded the interferometer. Our theoretical computer simulations of the interferometer find a clear relation between the duration of the adiabatic pulses, decoherence rate, and the amplitude of the oscillations. These findings can be used, in future experiments, to quantify decoherence in this class of devices.

References

1. Andrew D. Greentree et al. *Physical Review B* **70**, 235317 (2004).
2. Y. Aharonov and D. Bohm *Phys. Rev.* **115**: 485 (1959).

Categorization of Resistive Switching of Metal-$Pr_{0.7}Ca_{0.3}MnO_3$-Metal Devices

Z.L.Liao, Z.Z.Wang, and D.M.Chen

** Institute of Physics, Chinese Academy of Sciences*

Keywords: resistive switching, Gibbs free energy of oxidation, oxidation/reduction, oxygen ion migration,

Resistance switching (RS in metal oxides has drawn great attention for its potential application in high-performance non-volatile resistance random access memory (RRAM). However the mechanism for RS has not yet converged. Here report a remarkable trend found in the RS characteristic of $Pr_{0.7}Ca_{0.3}MnO_3$ (PCMO) thin film sandwiched between a Pt bottom electrode and top electrodes (TE) made of various metals.[1] Devices with TE made of Al, Ti and Ta are found to exhibit a large current-voltage (I-V) hysteresis loop and bipolar RS, but those with TE made of Pt, Ag, Au and Cu do not as shown in Fig.1. The Al , Ti,Ta/PCMO/Pt devices show higher resistance than that of devices with TE made of Pt, Ag, Au and Cu. Linear I-V curves for the Pt/PCMO/Pt devices indicate very low resistivity of PCMO (~340Ω. cm) and the high resistance in Al,Ti,Ta/PCMO/Pt devices arise from TE/PCMO interface. Hence we investigated the TE/PCMO interface by HRTEM to find out the difference between different TE/PCMO interface. HRTEM images (not shown here) show that a thin film metal-oxide layer formed at the interface between the group (Al,Ti, Ta) of TE and PCMO but not for the other group (Pt, Ag, Au,Cu) of TE. Interestingly, the analysis shows that the I-V characteristics strongly depend on the Gibbs free energy of oxidation but have no correlation to TE's work function as shown in Fig.2. The distinct I-V characteristics of these two groups can be attributed to the presence/absence of metal oxide layer and a solid state oxidation/reduction process facilitated by a localized electrical field

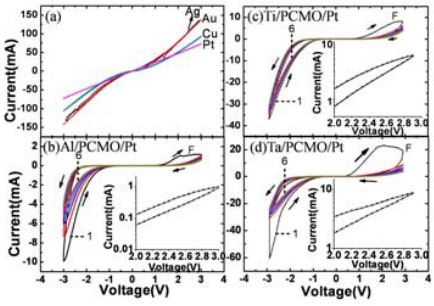

Fig.1 I-V characteristics for a (Ag, Cu Au) Pt/PCMO/Pt devices, (b)Al/PCMO/Pt device (c)Ti/PCMO/Pt device (d)Ta/PCMO/Pt device There are six consecutive loops for (b)(c)(d), the label marks the first loop, and six is the last. The size of the loop reduces progressively from one to six. Label F Marks the forming process. Inset of (b)(c)(d) shows the blow up of hysteresis loop at positive bias.

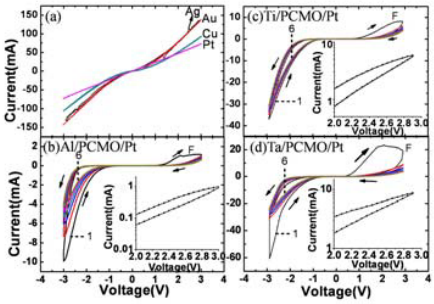

Fig.2 (a)Virgin Resistance vs. work function. The data of each TE materials is an average over 100 devices and small error bars indicate that there devices are quite uniform. The dashed line marks the function of PCMO (b)Virgin resistance vs. metal-oxide formation free energy. The dashed line at -366KJ/mol indicates the oxidation free energy of PCMO.

References

1. Z.L.Liao, et al, Appl.Phys.Lett.94, 253503(2009)

Electron-hole crossover in graphene quantum dots

J. Güttinger*, C. Stampfer*, F. Libisch**, T. Frey*, J. Burgdörfer**, T. Ihn*, and K. Ensslin*
*Solid State Physics Laboratory, ETH Zurich, 8093 Zurich, Switzerland
** Institute for Theoretical Physics, Vienna University of Technology, 1040 Vienna, Austria

Keywords: Graphene, Quantum Dots, Landau Levels

Transport measurements on graphene quantum dots in a perpendicular magnetic fields are performed to investigate the transition from electrons to holes. As the charge neutrality point is approached from both sides, Coulomb blockade peaks covering the regime from hole to electron occupancy can be measured in the investigated sample. In a magnetic field, our measurements reveal signatures of the formation of the graphene specific $n = 0$ Landau level in the center of the transport gap and become manifest in a decrease of the average peak to peak spacing. In this transition regime clear excited states and cotunneling lines [1] are measured, indicating the resolution of quantum confined states (see Fig. 3). Around the crossover no systematic dependence on carrier numbers is observed so far.

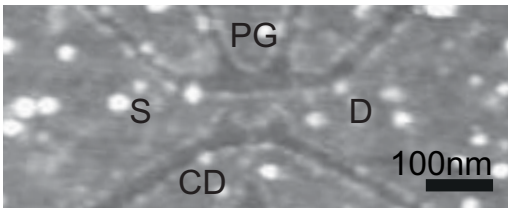

Figure 1: Scanning force microscope image of the sample. The structure consists of a ≈ 50 nm diameter quantum dot connected to source (S) and drain (D) via two ≈ 25 nm wide graphene constrictions. The plunger gate (PG) is used to locally tune the electrochemical potential on the dot.

A scanning force microscopy image of the sample is shown in Fig. 1. The graphene quantum dot is connected to source (S) and drain (D) by two graphene constrictions. A lage scale back gate sweep features electron (hole) conductance for positive (negative) back-gate voltage (see Fig. 2). At the transition point, a transport gap with pinched off conductance resonances opens. The electron-hole crossover in this gap is investigated in more detail by measuring the magnetic field dependence of more than 50 consecutive Coulomb peaks across the transition.

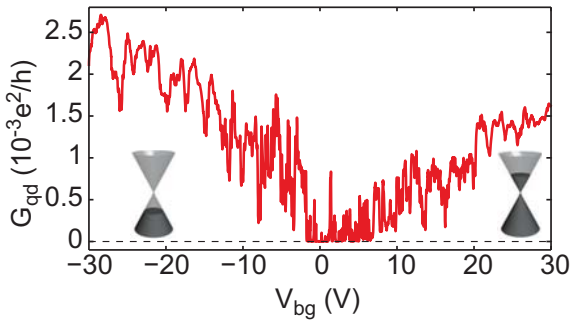

Figure 2: Back-gate characteristics of the graphene quantum dot at $V_{bias} = 8$ mV showing hole and electron transport separated by a transition region of suppressed conductance around $V_{bg} = 2$ V. Measured at $V_{pg} = 2$ V.

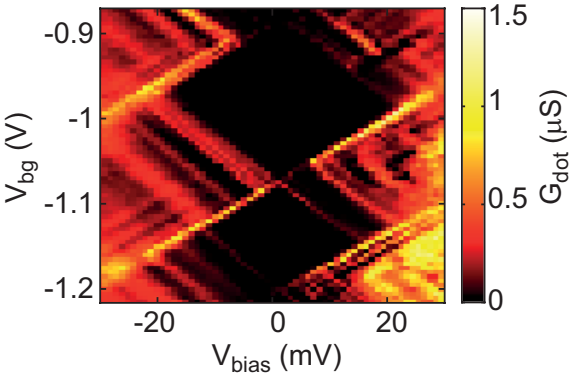

Figure 3: Coulomb diamond measurements in the transition region showing clear excited states. The measurement is taken at $V_{pg} = 5.7$ V.

For increasing magnetic field, the peaks converge towards the lowest Landau level. Crossings with higher Landau levels result in kinks in qualitative agreement with theoretical calculations.

References

[1] S. Schnez, F. Molitor, C. Stampfer, J. Güttinger, I. Shorubalko, T. Ihn, and K. Ensslin, Appl. Phys. Lett., **94**, 012107 (2009)

July 24 (Friday)

9:00 – 10:30

Session E9

Quantum transport

Main Hall

EP2DS-MSS Parallel session

Kobe Chinese food town

Manipulating single electron spins with micro-magnets

M. Pioro-Ladrière[1,2], R. Brunner[1], Y. Tokura[1,3], T. Obata[1], Y.-S. Shin[1], T. Kubo[1], K. Yoshida[1], T. Taniyama[4] and S. Tarucha[5,6]

1. *Quantum Spin Information Project, ICORP, JST, Atsugi-shi, Kanagawa, 243-0198, Japan*
2. *Département de Physique, Université de Sherbrooke, Sherbrooke, Québec, J1K-2R1, Canada*
3. *NTT Basic Research Laboratories, NTT Corporation, Atsugi-shi, 243-0198, Japan*
4. *Materials and Structures Laboratory, Tokyo Institute of Technology, 4259 Nagatsuta, Yokohama, 226-8503, Japan*
5. *PRESTO, Japan Science and Technology Agency, 4-1-8 Honcho Kawaguchi, Saitama 332-0012, Japan*
6. *Department of Applied Physics, University of Tokyo, Hongo, Bunkyo-ku, Tokyo, 113-8656, Japan*

Keywords: Quantum dots, Micro-magnets, Spin qubits, Quantum information processing.

We report on our recent progress in applying semiconductor quantum dots to quantum information processing with electron spins, as initially envisioned by Loss and DiVincenzo. Single spin rotations are performed by displacing, with electric fields, electrons in a magnetic field gradient [1]. The gradient is generated on-chip with micron-size ferromagnets [2] (Figure 1). The method allows for reasonably fast spin rotations using electric dipole induced spin resonance (EDSR), by-passing the need for localized and strong a.c. magnetic fields [3]. In addition, the use of micro-magnets enables the selective manipulation of electron spins [4], which can be done efficiently by shaping the micro-magnets into a split geometry, suitable for multi-qubit systems. The universal set of quantum gates is completed by the spin exchange interaction between neighboring electrons which is shown to be slightly renormalized by the micro-magnets' stray magnetic field.

We demonstrate proper EDSR operation for the split geometry using a GaAs double-quantum-dot device where coherent single spin rotations are observed. Preliminary results on combining single and two-qubits operations are also presented. Based on these results, we discuss the requirements for scaling up the proposed architecture to several quantum dots. The realization of a 10 spin qubits register is readily achievable with gate-defined quantum dots. Since our method is applicable to any material, it should prove very useful once other semiconductors quantum dots are found to solve the decoherence problem caused by the nuclear spin fluctuations in GaAs, for which other electric coupling mechanisms (spin-orbit interaction and g-tensor modulation) might not be as efficient. The micro-magnet design we present has also applications to other kind of spin qubits like paramagnetic defects in silicon and nitrogen vacancies in diamond.

References

[1] Y. Tokura et al., Phys. Rev. Lett. **96** 047202 (2006).

[2] M. Pioro-Ladrière et al., App. Phys. Lett. **90** 024105 (2007).

[3] M. Pioro-Ladrière et al., Nature Physics **4** 776 (2008).

[4] E. A. Laird et al., Phys. Rev. Lett. **99** 246601 (2007).

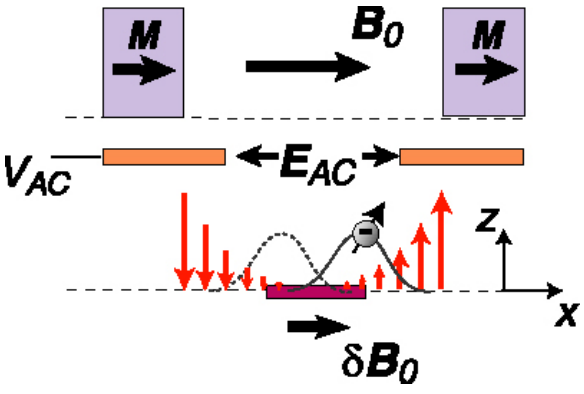

Figure 1: Split micromagnets geometry for single spin manipulation. Two micromagnets are magnetized ($\mathbf{M}$) by the external in-plane magnetic field ($\mathbf{B_0}$) and placed on top of a quantum dot containing a single electon. By shaking back-and-forth the electron's wavefunction (with a.c. electric field $\mathbf{E}_{AC}$) in the magnetic field gradient (vertical arrows), an effective transverse a.c. magnetic field is produced, proportional to the electric driving voltage V_{AC}. Arbitrary single spin operations are performed by tuning the frequency, phase and duration of V_{AC}.

P12
E1
MoP
E2
E3
E4
TuP
E5
P34
E6
E7
E8
ThP
E9
P56

High cumulants in the counting statistics measured for a quantum dot

C. Fricke*, F. Hohls*, C.Flindt** and R. J. Haug*
*Institut für Festkörperphysik, Leibniz Universität Hannover, 30167 Hannover, Germany.
** Department of Physics, Harvard University, 17 Oxford Street, Cambridge, MA 02138, USA .

Keywords: single electron counting, quantum dot, counting statistics

Current fluctuations in mesoscopic conductors can be used to obtain information which is not accessible through dc conductance measurements. The first step beyond the mean current are studies of the shot noise which is equivalent to the second moment of the distribution function. Even more information on the system can be gained when measuring higher moments, going towards a measurement of the full counting statistics of the system introduced by Levitov et al. [1].

Recently an experimental approach to full counting statistics was introduced for semiconductor quantum dots: A quantum point contact near the quantum dot is used to measure the charge on the dot. For sufficiently low tunnelling rates individual tunnelling events onto and off the dot can be resolved. Gustavsson et al. used this technique for a first measurement of a counting distribution function for tunnelling through a quantum dot ground state [2]. This distribution function gives the probability to measure a certain number of electron transitions through the dot in a given time. An alternative description of the system is given by the afore mentioned moments resp. cumulants which are usually calculated in counting theory. The higher the order of cumulants the more detailed is the information gained.

We have measured the cumulants of the counting distribution for tunnelling through a quantum dot for unprecedented high orders up to the 20th using the experimental setup described in Ref. [3]. To determine high order cumulants we have measured up to 850,000 tunnelling events for a single quantum dot setting. The cumulants are determined as function of time, i.e. the length of the counting intervals, and asymmetry of tunnelling rates. For both parameters we observe large oscillations with an amplitude that grows factorially with the order of the cumulants.

The experimentally observed oscillations of the cumulants in this system can be modeled amazingly well by theory. Interestingly they are not a special feature of the quantum dot system but are expected universally for non-trivial counting distributions [4]. To our knowledge these universal oscillations of high cumulants and their growth with order have not been demonstrated experimentally before.

In addition to the results on high cumulants we will discuss our analysis procedure for the raw experimental data and we will examine the influence of the measurement setup and the analysis algorithms. Furthermore we will present an investigation of the statistical uncertainties of the measured moments.

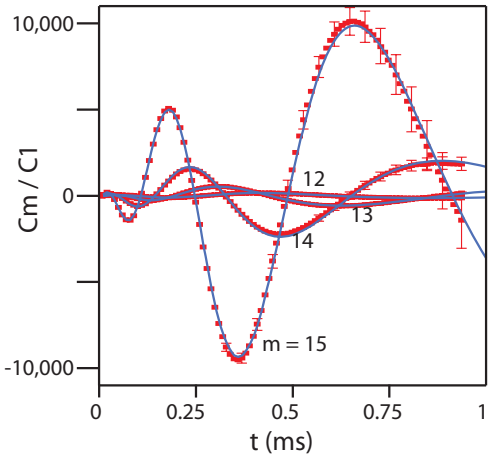

Figure 1: Normalized moments C_m/C_1 for different order m. Symbols show the measured data, lines present the theoretical calculations.

References

[1] Levitov et al., J. Math. Phys. **37**, 4845 (1996).

[2] S. Gustavsson *et al.*, Phys. Rev. Lett. **96**, 076605 (2006).

[3] C. Fricke *et al.*, Phys. Rev. B **75**, 155307 (2007).

[4] C. Flindt *et al.*, arXiv:0901.0832.

Andreev localized states and Kondo effect in InAs quantum dots contacted with superconducting and normal electrodes

R.S. Deacon[α], Y. Tanaka[β], A. Oiwa[α,γ,δ], K. Yoshida[γ], R. Sakano[α], K. Shibata[ϵ], K. Hirakawa[ϵ,δ,ζ] and S. Tarucha[α,γ,ζ]

α Department of Applied Physics and QPEC, University of Tokyo, Japan

β Condensed matter theory lab, RIKEN, Saitama, Japan

γ ICORP JST, Japan

δ JST CREST, Japan

ϵ IIS, University of Tokyo, Japan

ζ INQIE, University of Tokyo, Japan

Keywords: Quantum dot, Transport, Andreev reflection, Kondo singlet state

Coupling of a quantum dot (QD) with a few discrete levels to a superconducting reservoir results in Andreev localized states formed through constructive interference of Andreev reflected electrons and holes. The spectral properties of the Andreev localized states reveal the interplay between proximity effect and correlation effects such as electron-electron interaction and the Kondo effect. We show that in a QD strongly coupled to a superconducting lead and weakly coupled to a normal lead the localized Andreev states can be probed with electron tunneling spectroscopy and that by tuning a gate voltage a phase transition in ground state occurs BCS singlet and degenerate magnetic doublet state where strong electron-electron interaction forces single occupation of the quantum dot. In contrast to more familiar QD Josephson junction system the Andreev localized states are not spectroscopically sharp bound states but broadened through interaction with the normal lead.

Devices are fabricated from single self assembled InAs QDs contacted with one Ti/Au normal metal lead and one Ti/Al superconducting lead using a two step *e*-beam lithography process. When $T < T_c$ the low bias current is carried by Andreev reflection processes. The Andreev transport channel probes the two Andreev localized states producing a subgap transport resonance which we compare with predictions from numerical renormalization group calculations[1]. Crossing of the subgap transport resonances indicates a phase transition in the ground state between BCS-singlet and degenerate (so called magnetic) doublet states. We also identify that for appropriate energy scales the Kondo singlet state enhances the zero bias Andreev conductance in good agreement with recent theoretical treatments[2, 3].

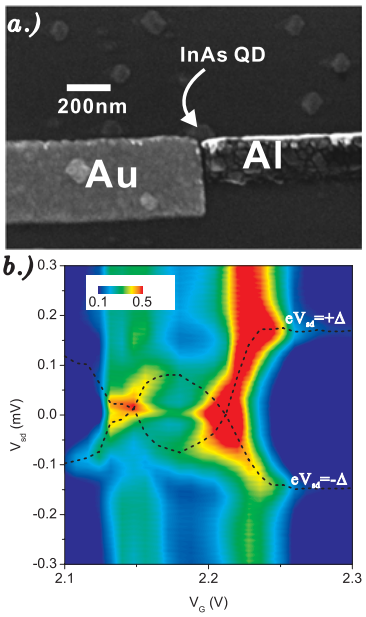

Figure 1: (*a*) Scanning electron microscope image of a typical device. (*b*) Plot of differential conductance ($G = dI/dV_{sd}$) as a function of source-drain bias (V_{sd}) and back gate voltage (V_G) for a odd electron occupation region. Dashed line indicates prominent transport resonances.

References

[1] J. Bauer *et al.*, J. Phys. Cond. Mat. **19**, 486211 (2007).

[2] J. Cuevas *et al.*, Phys. Rev. B **63**, 094515 (2001).

[3] T. Domanski and A. Donabidowicz, Phys. Rev. B **78**, 073105 (2008).

Nonequilibrium Dephasing in an Electronic Mach-Zehnder Interferometer

Seok-Chan Youn*, Hyun-Woo Lee**, and H.-S. Sim*
*Department of Physics, Korea Advanced Institute of Science and Technology, Daejeon 305-701, Korea
** PCTP and Department of Physics, Pohang University of Science and Technology, Pohang, Kyungbuk 790-784, Korea

Keywords: Quantum interference, Decoherence, Shot noise

Electronic Mach-Zehnder Interferometer (EMZI) has been recently realized in the integer quantum Hall (IQH) regime by using quantum Hall edge channels and quantum point contacts which serve as wave guides and beam splitters, respectively[1]. It has attracted considerable attention as it is one of elementary types of interferometry and useful for studying coherence and entanglement effects.

Recent experiments on it have manifested puzzling behavior which is hard to understand within a noninteracting electron model[2]. The interference visibility of differential conductance displays bias-dependent lobe patterns: At certain nonzero bias voltage values, the visibility almost vanishes but between such bias values, the visibility maintains sizable values. There are also abrupt phase jumps of π whenever the visibility vanishes.

We propose an intrinsic mechanism for the puzzling behavior by taking account of the effect of shot noise and electron-electron interaction[3]. When the bias voltage is applied, the shot noise of current occurs at the input beam splitter. The shot noise generates the ensemble of nonequilibrium electron density configuration in the interferometry arms. Electron interaction induces different phase shift to an interferring electron for each density configuration. Ensemble averaging of the phase shifts produces dephasing which shows two characteristic features, a lobe pattern in the visibility and phase jumps of π, which agrees well with experimental results.

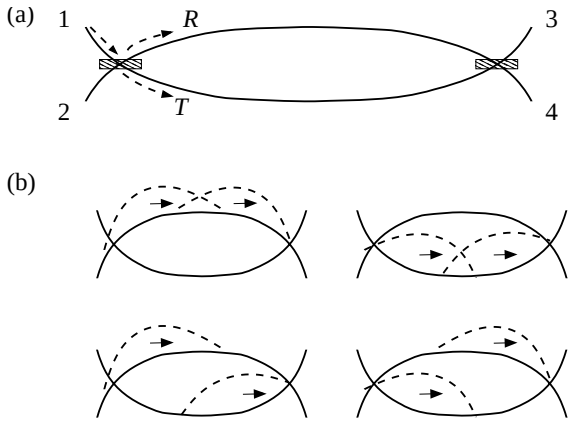

Figure 1: (a) Schematic EMZI setup. It has two beam splitters (gray boxes in the figure), two sources $i = 1, 2$, and two drains $i = 3, 4$. Only the source 1 is biased. Input beam splitter has transmission and reflection probability T and R. (b) Schematic nonequilibrium ensemble of electron density configurations in the two arms resulting from the shot noise at the input beam splitter when the two arms have two nonequilibrium electrons. The configurations can be described by two packets (dashed lines) propagating towards the drains as marked by solid arrows.

References

[1] Yang Ji, Yunchul Chung, D. Sprinzak, M. Heiblum, D. Mahalu, and Hadas Shtrikman, Nature **422**, 415 (2003).

[2] I. Neder, M. Heiblum, Y. Levinson, D. Mahalu, and V. Umansky, Phys. Rev. Lett. **96**, 016804 (2006).

[3] Seok-Chan Youn, Hyun-Woo Lee, and H.-S. Sim, Phys. Rev. Lett. **100**, 196807 (2008).

Fano-Kondo interplay in a side-coupled double quantum dot

S. Sasaki[1], H. Tamura[1], S. Miyashita[2], T. Maruyama[2], T. Akazaki[1] and T. Fujisawa[3]

[1]*NTT Basic Research Laboratories, NTT Corporation*

[2]*NTT Advanced Technology Corporation*

[3]*Tokyo Institute of Technology*

Keywords: Fano resonance, Kondo effect, quantum dot

Large tunability of electronic states in semiconductor quantum dot (QD) systems has unveiled rich quantum transport phenomena such as the Kondo effect and Fano resonances [1]. A QD tunnel-coupled to external reservoirs behaves as an artificial single magnetic impurity when it has an odd number of electrons with spin S=1/2. The Kondo effect drastically modifies the transport characteristics of the QD at low temperature, via spin singlet formation between the localized magnetic moment in the QD and the conduction electrons in the reservoirs. When a second QD (dot 2) is tunnel-coupled to the side of the first QD (dot 1) exhibiting the Kondo effect, as schematically shown in Fig.1, the inter-dot spin singlet formation is expected to suppress the Kondo effect. Although a large number of theoretical studies exist on such a side-coupled double QD, very few experiments have been reported so far. In this work, we measure low temperature transport characteristics of the side-coupled double QD fabricated from GaAs/AlGaAs two dimensional electron system, and discuss novel Fano resonances that arise from interference between discrete levels in dot 2 and the Kondo enhanced conductance (cotunneling) in dot 1.

Figure 2 shows a grey-scale plot of the conductance as a function of the plunger gate voltage, V_1 and V_2, measured with a standard lock-in method at 41mK. Three strong Coulomb peaks are observed when the electron number in dot 1, N_1, changes by one. Conductance between the two Coulomb peaks marked with a triangle is enhanced by the Kondo effect where N_1 is odd. Inter-dot Coulomb interaction is revealed as jumps in the Coulomb peak positions whenever the electron number in dot 2, N_2, changes by one, forming a well-known honeycomb stability diagram. We observe conductance maxima at the upper valley (white arrow) and minima at the lower valley (black circle) when N_2 changes by one. Detailed temperature and magnetic field dependence measurement of these features lead us to conclude that they are Fano resonances where the Kondo effect (cotunneling) in dot 1 plays a role of continuum.

[1] S. Katsumoto, J. Phys.: Condens. Matter **19**, 233201 (2007).

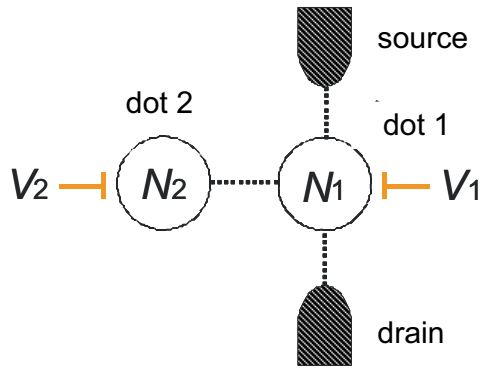

Fig. 1: Schematic diagram of the side-coupled double quantum dot.

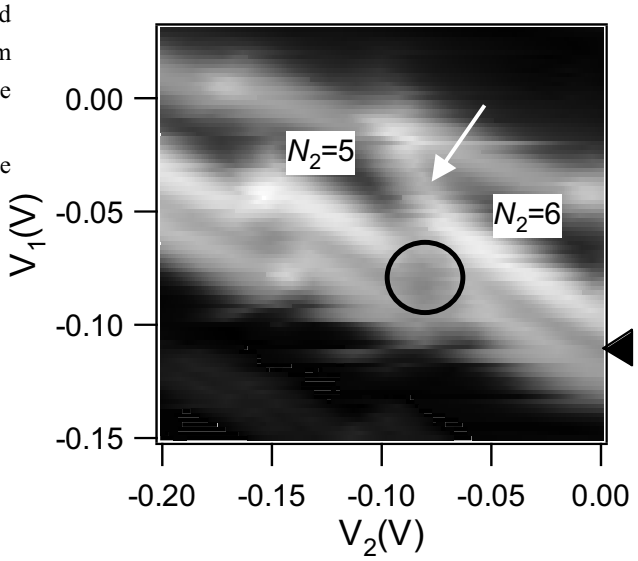

Fig. 2: Observed conductance as a function of the two plunger gate voltages.

July 24 (Friday)

11:00 – 12:30

Plenary Session 5, 6

Main Hall

EP2DS-MSS Joint session

Akashi bridge

Manipulation of Photons by Photonic Crystals

Susumu Noda
Department of Electronic Science and Engineering, Kyoto University, Kyoto 615-8510, Japan
Email: snoda@kuee.kyoto-u.ac.jp

Keywords: Photonic Crystals, Nanocavities and waveguides, Surface-photon physics, Photonic-crystal laser

Photonic crystals, in which the refractive index changes periodically, provide an exciting tool for the manipulation of photons and have made substantial progresses in recent years. In this presentation, I will discuss recent progresses in photonic-crystal researches including (i) two-dimensional photonic-crystal cavities and waveguides, (iii) three-dimensional photonic crystals, and (ii) two-dimensional photonic-crystal lasers.

(i) Two-dimensional photonic-crystal nanocavities and waveguides:

Remarkable progresses in nanocavities and waveguides based on two-dimensional (2D) photonic-crystals have been achieved recently. For example, nanocavity-Q over two millions [1,2] has been successfully achieved while maintaining ultrasmall modal volume based on the concept of Gaussian confinement [3, 4]. The combination of nanocavities and waveguides leads to the realization of photonic nano-devices [5, 6]. Here, if the properties of such photonic-crystal nanocavities and waveguides could be changed or controlled dynamically during their operations, the resulting functionalities would be greatly expanded. In the present talk, I at first discuss the dynamic control of photonic crystals [7,8], where the characteristics of nanocavities and waveguides are dynamically controlled within picosecond time scales, which will contribute to future applications including the stopping/slowing of light, quantum information systems, and next generation ultra-high capacity communications. Then, I will discuss the recent progress of photonic-crystal nanocavities combined with quantum dots, where the stress is on the importance of quantum anti-Zeno effects [9-11] as a third emission mechanism in addition to Purcell effect and vacuum Rabi-oscillation.

(ii) Three-dimensional photonic crystals:

3D photonic crystals with 3D periodic refractive-index distributions are expected to possess the capability of ultimate control of photons, and the manipulation of photons by 3D photonic crystals has so far been carried out by embedding artificial defects and light emitters ‘inside’ crystals [12-14], using 3D directional bandgap effects. In the present talk, I will describe that photons can be manipulated even at the ‘surface’ of 3D photonic crystals, where 3D periodicity is terminated [15]. This phenomenon is of interest because of its relevance to the surface plasmon-polariton effect of metals and the related surface photon physics. We first show that 3D photonic crystals possess surface states and that photons can be confined and propagate through them. Then I will demonstrate that 3D localization of photons at desired surface points is possible by forming a surface-

P12
E1
MoP
E2
E3
E4
TuP
E5
P34
E6
E7
E8
ThP
E9
P56

mode gap and introducing artificial surface-defect structures. Surprisingly, the obtained *Q* factors of the surface-defect mode are the largest reported for 3D photonic crystal nanocavities (up to ~9,000). This represents an important step towards realizing a new route for photon manipulation by 3D photonic crystals, and establishing the surface science of photonic crystals. Furthermore, the absorption-free nature of the 3D photonic-crystal surface could make possible new sensing applications and light-matter interactions.

(ii) Two-dimensional Photonic-Crystal Lasers:

Photonic-crystal surface-emitting lasers [16, 17] have recently attracted much attention because of their perfect, broad-area single-mode surface-emitting operation, their narrow beam divergence angles of < 1°, and the possibility of producing tailored beam patterns by controlling the electric field distribution inside the photonic crystal. These fascinating features arise from the photonic band-edge effect, where the group velocity of light becomes zero and a 2D cavity mode is formed. We will describe the recent progresses in such unique photonic-crystal lasers including the recent achievement in producing tailored beam patterns [18] and lasing oscillation in blue-violet wavelengths [19].

References:

[1] S.Noda, et al. *Nature Photonics*, 1 (2007) 449,
[2] Y. Takahashi, et al. *Optics Express*, 15 (2007) 17206.
[3] Y.Akahane, et al, *Nature*, 425 (2003) 944.
[4] B.S.Song, et al. *Nature Materials*, 4 (2005) 207.
[5] S. Noda, et al. *Nature*, 407 (2000) 608.
[6] B.S.Song, et al, *Science* 300 (2003) 1537.
[7] Y.Tanaka, et al, *Nature Materials*, 6 (2007) 862.
[8] U. Jeremy, et al. *Optics Express*, 16 (2008) 21721.
[9] M.Yamaguchi, et al, *Optics Express*,
[10] M. Yamaguichi, et al, arXiv: 0904.3697 (2009).
[11] S.Noda, *Science*,314 (2006) 260.
[12] S.Noda, et al. *Science*, 289 (2000) 608.
[13] S.Ogawa, et al. *Science*, 305 (2004) 227.
[14] K.Aoki, et al, Nature Photonics, 2 (2008) 688.
[15] Ishizaki and Noda, unpublished.
[16] M.Imada, et al, *Appl.Phys.Lett*., 75 (1999) 316.
[17] S.Noda, et al, *Science*, 293 (2001) 1123.
[18] E.Miyai, et al. *Nature*, 441 (2006) 946.
[19] H. Matsubara, et al, *Scienc*e, 319 (2008) 445.

Physics observed through shot noise measurements

Moty Heiblum

Braun Center for Sub Micron Research, Dept. of Condensed Matter Physic
Weizmann Institute of Science, Rehovot 76100, Israel

Shot noise measurements were proven to be a powerful tool to observe charge, interactions, statistics, and dephasing, as few examples. In this talk I will show new results of shot noise measurements in the fractional quantum Hall effect regime, which points at a more complicated interpretation of fractional charges. I will show results of measurements in a variety of filling factors, being the Laughlin's states (1/3, 2/5, 3/7, 2/3, 7/3) or the even denominator state (5/2), where the deduced charge is highly dependent on the range of measurements, such as the DC current, back-scattering probability of the quasiparticles, and the temperature. If one trusts shot noise measurements to be a good indicator of the charge, the theoretically expected charge seems to exist only under some specific conditions.

Author Index

C

D

E

F

G

H

L

M

N

O

P

T

U

V

W

X

Y

Z